EMERGING MECHANISMS IN NEURONAL SIGNALING: FROM CELL BIOLOGY TO PATHOGENESIS

EDITED BY: Mario Eduardo Guido, Gabriela Alejandra Salvador and Alejandra Alonso

PUBLISHED IN: Frontiers in Cellular Neuroscience, Frontiers in Pharmacology and Frontiers in Neuroscience

frontiers Research Topics

frontiers

ISSN 1664-8714
ISBN 978-2-88966-111-4
DOI 10.3389/978-2-88966-111-4

About Frontiers

Frontiers is more than just an open-access publisher of scholarly articles: it is a pioneering approach to the world of academia, radically improving the way scholarly research is managed. The grand vision of Frontiers is a world where all people have an equal opportunity to seek, share and generate knowledge. Frontiers provides immediate and permanent online open access to all its publications, but this alone is not enough to realize our grand goals.

Frontiers Journal Series

The Frontiers Journal Series is a multi-tier and interdisciplinary set of open-access, online journals, promising a paradigm shift from the current review, selection and dissemination processes in academic publishing. All Frontiers journals are driven by researchers for researchers; therefore, they constitute a service to the scholarly community. At the same time, the Frontiers Journal Series operates on a revolutionary invention, the tiered publishing system, initially addressing specific communities of scholars, and gradually climbing up to broader public understanding, thus serving the interests of the lay society, too.

Dedication to Quality

Each Frontiers article is a landmark of the highest quality, thanks to genuinely collaborative interactions between authors and review editors, who include some of the world's best academicians. Research must be certified by peers before entering a stream of knowledge that may eventually reach the public - and shape society; therefore, Frontiers only applies the most rigorous and unbiased reviews.
Frontiers revolutionizes research publishing by freely delivering the most outstanding research, evaluated with no bias from both the academic and social point of view. By applying the most advanced information technologies, Frontiers is catapulting scholarly publishing into a new generation.

What are Frontiers Research Topics?

Frontiers Research Topics are very popular trademarks of the Frontiers Journals Series: they are collections of at least ten articles, all centered on a particular subject. With their unique mix of varied contributions from Original Research to Review Articles, Frontiers Research Topics unify the most influential researchers, the latest key findings and historical advances in a hot research area! Find out more on how to host your own Frontiers Research Topic or contribute to one as an author by contacting the Frontiers Editorial Office: researchtopics@frontiersin.org

EMERGING MECHANISMS IN NEURONAL SIGNALING: FROM CELL BIOLOGY TO PATHOGENESIS

Topic Editors:
Mario Eduardo Guido, National University of Cordoba(CIQUIBIC), Argentina
Gabriela Alejandra Salvador, National University of the South, Argentina
Alejandra Alonso, College of Staten Island, United States

Citation: Guido, M. E., Salvador, G. A., Alonso A., eds. (2020). Emerging Mechanisms in Neuronal Signaling: From Cell Biology to Pathogenesis. Lausanne: Frontiers Media SA. doi: 10.3389/978-2-88966-111-4

Table of Contents

frontiers in Cellular Neuroscience

EDITORIAL
published: 31 August 2020
doi: 10.3389/fncel.2020.00257

Editorial: Emerging Mechanisms in Neuronal Signaling: From Cell Biology to Pathogenesis

Mario Eduardo Guido[1]*, *Gabriela Alejandra Salvador*[2] and *Alejandra del Carmen Alonso*[3,4]

[1] Departamento de Quimica Biologica "Ranwel Caputto", Facultad de Ciencias Quimicas, CONICET Center for Research in Biological Chemistry, National University of Cordoba (CIQUIBIC), Cordoba, Argentina, [2] Departamento de Biología, Bioquímica y Farmacia, CONICET- Instituto de Investigaciones Bioquímicas de Bahía Blanca, Universidad Nacional del Sur, Bahía Blanca, Argentina, [3] Department of Biology and Center for Developmental Neuroscience, College of Staten Island, Staten Island, NY, United States, [4] Biology Program, Graduate Center, The City University of New York, New York, NY, United States

Keywords: lipid signaling, neurodegeneration, retina, metabolism, cell signaling, oxidative stress, transcription factors, developmental disorders

Editorial on the Research Topic

Emerging Mechanisms in Neuronal Signaling: From Cell Biology to Pathogenesis

Unraveling the molecular processes involved in the genesis, differentiation, and cell death of the nervous system is an intense and continual interest of the neuroscience community. In recent years, the preponderance of research focused upon signal transduction mechanisms relying on protein cascades, but more information is needed on the role and function of other molecular mechanisms. These molecular mechanisms include but not limited to: lipid mediators (sphingolipids, fatty acids, glycerophospholipids, etc.), lipid-binding proteins (ApoD, PPAR, etc.), protein-lipid interactions (c-Fos-lipid synthesizing enzymes), protein misfolding and not fully characterized membrane-protein receptors. Signal transduction events triggered by bioactive lipids and related transcription factors (immediate early genes, metabolic regulators, etc.) now receive special attention as an important nodal regulatory process. Deregulation of lipid-mediated processes is also linked to neurodegenerative diseases [Parkinson (PD), Alzheimer (AD), and retinopathies] and proliferative disorders (brain cancer and diabetic retinopathy). Moreover, the modern lifestyle (hypercaloric diets, continuous artificial light exposure, sedentary life, aging, stress) impacts on lipid signaling and metabolism, and can alter brain function, physiology, and behavior. Focused on this broad spectrum of underlying mechanisms related to molecular and cellular neuroscience, a Research Topic call elicited expansive, research interest and submissions from among international laboratories. As a result of this interest, 33 contributions are accepted and published on the molecular mechanisms as described above. One hundred and fifty-eight authors from research laboratories located in nine countries: North and South America (Argentina, Canada, Chile, and USA), Asia (China), and Europe (France, Poland, Spain, Switzerland), contributed to the accepted, peer-reviewed articles.

GLIA-NEURON CROSSTALK FROM BIOLOGY TO PATHOPHYSIOLOGY

Interesting contributions to this Research Topic includes the characterizations of the glia-neuron communication and interaction that is reported by Pascua-Maestro et al. and Volonté et al. and reviewed by Barber and Raben. Particularly, Pascua-Maestro et al. clearly demonstrated

OPEN ACCESS

Edited and reviewed by:
Dirk M. Hermann, University of Duisburg-Essen, Germany

***Correspondence:**
Mario Eduardo Guido
mguido@fcq.unc.edu.ar

Specialty section:
This article was submitted to Cellular Neuropathology, a section of the journal Frontiers in Cellular Neuroscience

Received: *29 May 2020*
Accepted: *24 July 2020*
Published: *31 August 2020*

Citation:
Guido ME, Salvador GA and Alonso AdC (2020) Editorial: Emerging Mechanisms in Neuronal Signaling: From Cell Biology to Pathogenesis. Front. Cell. Neurosci. 14:257. doi: 10.3389/fncel.2020.00257

that glial cells rescue neurons exposed to cellular stress by astrocyte-secreted extracellular vesicles loaded with the lipid binding protein: ApoD. These observations highlighted the neuro-protective role of ApoD to promote neuronal survival during oxidative stress. In the future, novel therapeutics may involve ApoD-loaded exosomes because these exosomes can cross the blood-brain barrier to treat neurodegenerative diseases. Astroglial cells secrete lipid signals that can modulate functionally both presynaptic and postsynaptic neurotransmissions and consequently brain activity. The lipid compositions of the pre- and post-synaptic membranes of neurons impact functions involving vesicle fusion and receptor mobility, and strongly suggest an essential lipid-mediated communication between glia and neurons. Nevertheless, lipid metabolism controlling the interactions among different cell lineages is a new frontier in neuroscience. Barber and Raben reviewed the published research on neuronal and glial lipid metabolism, and reported mounting evidence that suggests a significant impact of lipid metabolism on neurotransmission.

As part of the central nervous system, the vertebrate retina constitutes a suitable model to investigate the effect of diverse extracellular signals [light, lipopolysaccharide (LPS), oxygen levels, oxidative stress, etc.] under physiological and pathological conditions. A number of papers investigated changes in fatty acid (FA) composition and promotion of oxidative stress might be one of the pathways implicated in retinal degeneration (RD) triggered by continuous LED light exposure of low intensity (Benedetto and Contin). On the contrary, brief pulses of bright blue light cause photic responses in Muller glial cell (MGCs) expressing novel non-visual opsins (Opn3 and Opn5) through intracellular calcium mobilization without affecting cell viability (Rios et al.). This prolonged photosensitivity may play a key role in the retinal physiology presumably regulating cell to cell interaction and glia to neuron communication. In addition, abnormal retina exposure to exogenous LPS administration or high oxygen levels shares a common cellular mechanism of autophagy (Bermúdez et al.; Subirada et al.). Indeed, autophagy mediates retinal pigment epithelium (RPE) cell survival through a pathway modulated by Phospholipase D activity (Bermúdez et al.); whereas, it can also modulate vascular, glial, and neuronal activities in an oxygen-induced retinopathy mouse model (Subirada et al.). Strikingly, the pharmacological regulation of autophagy may offer promising therapeutic strategies to reduce neovascular tufts, persistent gliosis together with the promotion of cell survival in retinal inflammatory and degenerative diseases.

During retina degeneration as in retinitis pigmentosa, photoreceptors may be regenerated by MGCs which acts as stem cells. Demonstrated by Volonté et al., there exists a defective crosstalk between neurons and those MGCs in rd1 retinas that severely impairs the regenerative potential of retinal stem cells. Furthermore, the crosstalk among non-neuronal cells, such as: the RPE cells and retinal neurons, is extensively reviewed by Simón et al. in relation to proliferation, survival, migration, neovascularization, inflammation, and death of retinal cells.

LIPIDS AND BEYOND: NEW INSIGHTS ON FUNCTION AND DYSFUNCTION IN THE NERVOUS SYSTEM

Besides their structural role, lipids have pleiotropic functions in terms of intracellular signaling and metabolism. Insights into lipid metabolism and signaling, lipid-protein interaction, and lipid-binding proteins are topics of many new research papers and reviews. Bioactive lipids inevitably are involved in both physiological and neuropathological processes. FAs have relevant participation as secondary messengers in neuronal signaling. Free FAs are ligands of different types of proteins, such as G-protein coupled receptors, FA-binding proteins, and transcription factors of the Peroxisome Proliferator-Activated Receptors family. The wide variety of signaling molecules modulated by free FAs determine their importance in diverse cellular processes occurring in neurons and glial cells. As new roles for these bioactive compounds are deciphered, new promissory therapeutic targets are under consideration (Falomir-Lockhart et al.). The enzymes catalyzing the elongation of very long chain FAs (ELOV) has been described as new players in neuronal survival and synaptic signaling. ELOV4, one member of this elongase family, expressed in neurons and several mutations in its encoding gene has been associated with different neurological disorders (Stargardt-like macular dystrophy, spinocerebellar ataxia 34, and others) (Deák et al.).

FA-signaling also participates in the sphingolipid rheostat in the retina. Sphingolipids are a complex family of lipids including ceramide, ceramide 1-phosphate, and sphingosine 1-phosphate with relevant roles during development and in the degenerative diseases onsets (Simón et al.). Docosahexaenoic acid, a major n-3 polyunsaturated FA in nervous system, has been shown to protect photoreceptor cells from death through the modulation of the sphingolipid rheostat by decreasing ceramide levels or by enhancing sphingosine 1-phosphate synthesis (Simón et al.).

Phosphatidic acid (PA) is another pleiotropic molecule exhibiting central roles in glycerolipid metabolism and in cellular signaling. Produced by phospholipase D, PA can bind and regulate the activity of an important number of cellular targets such as nucleotide-binding proteins, kinases, and phosphatases. In consequence, deregulation of PA production or catabolism are associated with synaptic dysfunction and several neurological disorder, such as cognitive deficits related to AD, intellectual disability diseases (Fragile-X and Coffin-Lowry syndromes) and fetal alcohol spectrum disorders (Tanguy et al.).

Regarding biological membranes and neurodegenerative diseases such as in AD and PD, a couple of impressive reviews summarizes most of the literature published over the last decades (Alza et al.; Fabiani and Antollini). The article by Fabiani and Antollini highlights the role of different lipids (cholesterol, PA, sphingomyelin, and gangliosides) in nicotinic acetylcholine receptor function, and the crosstalk between amyloid processing, cholinergic signaling and membrane lipid composition, reinforcing the relevance of cholinergic hypothesis for AD. In contrast, lipid-binding properties of α-synuclein, whose pathological aggregation and accumulation are hallmarks

of PD has also been described by Alza et al. highlighting the state of the art of how phospholipids, FAs and their metabolisms participate in the pathological aggregation of this protein.

In the context of lipid biology, a transcription factor, c-FOS, may play a critical role. This intriguing protein belongs to the Immediate Early Gene family and apart from its role as transcription factor, has the unique characteristic of regulating *de novo* biosynthesis of lipids and their enzymes by protein-protein interactions at the endoplasmic reticulum. This novel function is essential for membrane biogenesis, cell proliferation and neurite outgrowth, and involved in pathological conditions such as brain tumors growth and development (Rodríguez-Berdini and Caputto).

NEURODEGENERATIVE DISEASES: UNDERSTANDING NORMAL PHYSIOLOGY GUIDES INTERVENTION INTO PATHOLOGY

To develop therapies and biomarkers for neurodegenerative diseases, one imperative is to understand the normal physiology of the brain during development and aging. Pro-survival and anti-toxic strategies are approaches to protect neurons and prevent neurodegenerative diseases. In this issue, the use of neurotrophins in neuroprotective strategies is reviewed by Saragovi et al.. Gestational, developmental, and nutritional conditions may have permanent effects on the brain physiology. In this issue, the contributions of Adamo et al. revealed the effects of marginal zinc deficiency (MZD) during gestation. The researchers found major alterations in signal transduction pathways in rats kept on an MDZ diet throughout gestation and beyond (i.e., ERK1/2, *Sox2*, etc.), down-regulation of *Pax6*, *Tbr2,* and *Tbr1* expression, a lower density of neurons and a selective decrease of glutamatergic neurons in the young adult brain cortex. Collective changes that can potentially result in behavioral impairment throughout life (Adamo et al.).

Estrogens are characterized as signals involved in the sexual differentiation of the brain. Recently, evidence highlighted the participation of estradiol, not only as a reproductive hormone, but also as a brain derived neuronal, protective factor. The coordination of estradiol signaling protects against neurodegenerative diseases and cognitive decline. The work by Zapata et al. elucidates the mechanism of estradiol to promote axonal growth showing that calcium mobilization from the extracellular space and the endoplasmic reticulum is necessary for the ERK1/2 activation and axogenesis in cultures of hypothalamic neurons.

One interesting aspect of signaling mechanisms is that receptor interactions at the neuronal plasma membrane provide a level of regulation. In the report by Soto et al. measurements of neuronal, plasma-membrane receptors co-localization and expression obtained by immunological pull-down experiments in combination with TIRF microscopy and AFM imaging demonstrated that P2X4/5-HT3A receptor complexes can interact with each other in a 1:1 stoichiometric manner, and preserved after ATP binding. Additional information on the receptor binding interaction and the allosteric regulation of its activity is also provided.

Among the neurodegenerative diseases, prion-like protein aggregation is a typical characteristic of each disease. Protein misfolding and signaling abnormalities is correlated and causally related to neuronal pathology and the progression of neurodegeneration. The mechanisms underlying the retrograde neurodegeneration remains elusive. In a review, Zamponi and Pigino highlighted the involvement of fast axonal transport and CK2 activity in the process of neurodegeneration in AD and prion disease. AD, the most common neurodegenerative disease, is diagnosed by two main histopathological lesions: extracellular amyloid plaques mainly composed by the beta-amyloid peptide (Aβ), and the intra-neuronal, neurofibrillary tangles, mainly composed by hyperphosphorylated tau (HP-tau). In this issue, Lasala et al. demonstrated that the interaction of Aβ directly affects α7 nicotinic receptor by acting as an agonist and a negative modulator. Reduced α7 activity, in the presence of higher Aβ concentrations or its long exposure, contribute to the cholinergic signaling deficit, and may be involved in the initiation and development of AD. Moreover, Morozova et al. presented evidence that the muscarinic cholinergic receptor M1/M3 is linked to the tau uptake by the neurons. The uptake of pathological HP-tau induced neurite breakdown. The release and uptake of HP-tau might participate in the prion-like transmission of the disease to neighboring neurons, and preventing this transmission might provide basis for new therapeutic designs.

CONCLUDING REMARKS

In summary, the accumulation of novel research articles and reviews from this topic call support the further expansion of research into cellular and molecular neurobiological processes. Decoding the puzzle of these processes under physiological and pathological conditions can pave the way to identify potential biomarkers and therapeutic targets and novel treatments. A list of these contributions is appended bellow.

AUTHOR CONTRIBUTIONS

MG and GS wrote Research Topic proposal. MG, GS, and AA wrote the editorial letter, assigned reviewers, edited articles, and reviewed final manuscript. All authors contributed to the article and approved the submitted version.

FUNDING

MG is a professor at the Department of Biological Chemistry "Ranwel Caputto", School of Chemistry, Universidad Nacional de Cordoba, and member of CONICET scientific career, CIQUIBIC, Cordoba, Argentina. Supported by PICT 2016-0187, PIP2014 CONICET and SECyT-UNC (Consolidar 2018). GS is a professor at Departamento de Biología, Bioquímica y Farmacia, Universidad Nacional del Sur and member of CONICET scientific career, INIBIBB, Bahía Blanca, Argentina. Supported by PICT 2017-0224; PGI 24B292, PIP2017 CONICET. AA is a professor and principal investigator at Department of

Biology and Center for Developmental Neuroscience, College of Staten Island and Biology Program, Graduate Center, Staten Island, United States. Supported in part by the private donation by Jeff Lin, as well as grants from the NIH (1R15AG058197-01) and PSC CUNY (60290-00 48).

ACKNOWLEDGMENTS

Authors are grateful to Dr. Robert Marraccino (Staten Island, USA) for critical reading and editing of this article.

Conflict of Interest: The authors declare that the research was conducted in the absence of any commercial or financial relationships that could be construed as a potential conflict of interest.

frontiers in Cellular Neuroscience

ORIGINAL RESEARCH
published: 02 October 2018
doi: 10.3389/fncel.2018.00334

The C-terminus of NMDAR GluN1-1a Subunit Translocates to Nucleus and Regulates Synaptic Function

Liang Zhou[1]* *and Jingjing Duan*[2]

[1] Department of Pharmacology, College of Pharmaceutical Sciences, Soochow University, Jiangsu, China, [2] Department of Anatomy and Neurobiology, Zhongshan School of Medicine, SunYat-sen University, Guangzhou, China

NMDARs, the Ca^{2+} permeable channels, play central roles in synaptic plasticity, brain development, learning, and memory. NMDAR binding partners and associated signaling has been extensively studied in synapse-to-nucleus communications. However, whether NMDARs could directly regulate synapse-to-nucleus communications is largely unknown. Here, we analyze the four alternative splicing of the C-terminus isoforms of GluN1 (1a, 2a, 3a, and 4a), and find that C1 domain of GluN1 is necessary for nuclear localization. Besides, we find that the 10 basic amino acids in C1 domain determine the nuclear localization of GluN1 C-terminus. Further investigating the expression patterns of the full length of GluN1 four isoforms shows that only GluN-1a exhibits the cytoplasmic and nucleus distribution in primary hippocampal neurons. Electrophysiological analyses also show that over-expression of GluN1 C-terminus without C1 domain doesn't affect synaptic transmission, whereas GluN1 C-terminus containing C1 domain potentiates NMDAR-mediated synaptic transmission. Our data suggested that the 10 basic amino acids in C1 domain determine translocation of GluN1 C-terminus into nucleus and regulate synaptic transmission.

Keywords: NMDA receptor, GluN1, synapse-to-nucleus communication, synapse transmission, cLTP

OPEN ACCESS

Edited by:
Mario Eduardo Guido, Center for Research in Biological Chemistry Córdoba (CIQUIBIC), Argentina

Reviewed by:
John J. Woodward, Medical University of South Carolina, United States
Marina Mikhaylova, Universitätsklinikum Hamburg-Eppendorf, Germany

***Correspondence:**
Liang Zhou
liangzhou@suda.edu.cn

Received: *20 June 2018*
Accepted: *12 September 2018*
Published: *02 October 2018*

Citation:
Zhou L and Duan J (2018) The C-terminus of NMDAR GluN1-1a Subunit Translocates to Nucleus and Regulates Synaptic Function. Front. Cell. Neurosci. 12:334. doi: 10.3389/fncel.2018.00334

INTRODUCTION

NMDA receptors (NMDARs) are ionotropic glutamate receptors, which are important for neuronal development, synaptic plasticity, learning, and memory (Tsien et al., 1996). The NMDARs are composed of two GluN1 and two GluN2/3 subunits, which are located at excitatory synapses (Paoletti et al., 2013). The intracellular GluN1 C-terminus contains distinct domains, binds to different proteins, and activates different downstream signaling pathways (Horak and Wenthold, 2009; Gu et al., 2016b). Due to the alternative splicing of the C-terminus, there are four GluN1 isoforms, GluN1-1a, 2a, 3a, 4a (Horak and Wenthold, 2009; Ferreira et al., 2011). The GluN1-1a is the dominant isoform (Laurie and Seeburg, 1994), and the expression levels of GluN1 isoforms are regulated by synaptic activity (Mu et al., 2003; Paoletti et al., 2013).

The synaptic activity modulates the immediate early genes (IEGs) expression in the nucleus (Yang et al., 2014), which is called synapse-to-nucleus communication (Deisseroth et al., 1996, 2003). The synapse-to-nucleus communication is essential for learning and memory (Lim et al., 2017). NMDARs antagonist can block synaptic activation induced IEGs expressions, which demonstrates NMDARs are required for synapse-to-nucleus communication (Mokin and Keifer, 2005; Lonergan et al., 2010). It has been reported that NMDAR associated proteins

(Panayotis et al., 2015; Herbst and Martin, 2017) and Ca^{2+} signaling (Hagenston and Bading, 2011) can lead to the activation of downstream signaling pathways during synaptic activity and regulate synapse-to-nucleus communication (Fainzilber et al., 2011; Lim et al., 2017). NMDAR associated proteins, such as Calmodulin (Deisseroth et al., 1998), Jacob (Dieterich et al., 2008), CRTC1 (Ch'ng et al., 2012), JAKMIP1 (Berg et al., 2015), have been extensively studied in synapse-nucleus communication. Calmodulin could translocate to neuronal nuclei upon synaptic stimulation (Deisseroth et al., 1998), and the translocation of calmodulin from cytoplasm to nucleus is mediated by γCaMKII (Ma et al., 2014). The Jacob translocates to neuronal nuclei through binding to importin α upon NMDARs activation (Dieterich et al., 2008), which could be regulated by ERK activity (Karpova et al., 2013). NMDARs activation also promotes the translocation of CRTC1 to neuronal nuclei, which could selectively increase the CREB-mediated transcription upon synapse activity (Ch'ng et al., 2012, 2015; Nonaka et al., 2014). However, whether NMDAR could directly regulate synapse-to-nucleus communication is largely unknown. Here, we found that the C-terminus of GluN1-1a translocates to neuronal nuclei, regulates synaptic transmission. Furthermore, the translocation of GluN1 C-terminus to nuclei could be regulated by neuronal activity.

MATERIALS AND METHODS

Plasmids

The plasmids of full-length GluN1-1a,-2a,-3a, and -4a were described preciously (Gu et al., 2016b). C2′oligonucleotides (top and bottom strands) are annealed and directly inserted into pEGFP-N3 vector at Nhe I/Sal I sites. The other truncated and full-length plasmids of GluN1 were created by standard PCR methods: PCR products were amplified from pCAGGS-GluN1-1a,−2a,−3a, and−4a using the relative primers, and subsequently inserted into pEGFP-N3 vector at Nhe I/Sal I sites. All GluN1 mutants were generated by overlapping PCR and cloned into pEGFP-N3 vector at Nhe I/Sal I sites. The primers used for the subclones in this study were provided in the **Supplementary Material.**

Cell Culture and Animals

Human embryonic kidney 293A (HEK293A) cells were cultured in DMEM containing 10% FBS (Gibco). For DNA transfection, Effectene Transfection Reagent (QIAGEN) was used in HEK293 cells, DNA-In® Neuro Transfection Reagent (Thermo Fisher Scientific) was used in primary hippocampal neuron. 24–48 h after transfection, the cells were subjected to immunocytochemistry assay. The mice were housed under the standard conditions of temperature and humidity. All animal procedures in this study were approved by Institutional Animal Care and Use Committee of Soochow University.

Primary Hippocampal Neurons Culture

Hippocampal primary dissociated neuronal culture was performed as previously described (Gu et al., 2016b). Briefly, the mouse hippocampi were dissected from E18 mouse embryos, and then digested using papain (Worthington) and DNase I (Worthington) to get individual neurons. After centrifuged at 800 rpm for 5 min, the pellet was resuspended in Hanks solution mixed with trypsin inhibitor (Sigma) and BSA, and then centrifuged at 800 rpm for 10 min. The pellet was resuspended in Neurobasal plating media containing 2% FBS, 2% B27 supplements, and 2 mM L-glutamine. Hippocampal neurons were plated at 200,000 cells/well on coverslips coated with poly-D-lysine in 24-well plates. Neurobasal culture media containing 2% B27 supplements, and 2 mM L-glutamine were used to replaced the culture media each other day.

Organotypic Hippocampal Slice Culture

The mouse hippocampi were dissected from P6–P8 wild-type mice as previously described (Gu et al., 2016a), and transfected biolistically with plasmids in DIV3-4. Slices were cultured for an additional 2 days before recording. For recording evoked EPSCs in slice cultures, the extracellular solution is artificial cerebrospinal fluid (ACSF) containing (in mM) KCl 2.5, $CaCl_2$ 4, $MgCl_2$ 4, NaH_2PO4 1.25, $NaHCO_3$ 25, glucose 7, sucrose 210. 15 μM 2-chloroadenosine and 100 μM picrotoxin were added into ACSF to dampen epileptiform activity and block the $GABA_A$ receptors. The supplier of pharmacological reagents is Abcam.

Neuronal Stimulation

DIV 12–14 dissociated hippocampal neurons were used to perform neuronal stimulation experiments. After bath application of the relative chemicals, all samples were transferred to the solution without the related reagents for 15–20 min, and then the samples were subjected to immunocytochemistry assay. For neuronal membrane depolarization induction, 50 mM KCl was used to treat hippocampal neurons for 5 min. For NMDARs activation induction, 100 μM NMDA (Abcam) and 2 μM glycine was given by bath application for 5 min. For chemical long-term potentiation (cLTP) induction, 200 μM glycine in ACSF was briefly applied for 3 min to stimulate synaptic NMDARs, which is described as previously study (Lu et al., 2001). For chemical long-term depression (cLTD) induction, 50 μM NMDA (Abcam) was given by bath application for 3 min. Ten micromoles MG-132 (Sigma) was used to block the proteasome. Fifty micromoles DHPG (Abcam) was given by bath application for 5 min to induce group 1 metabotropic glutamate receptor-mediated LTD.

Immunocytochemistry Assay

HEK293A cells or hippocampal neurons grown on coverslips were rinsed with PBS twice and fixed in 4% paraformaldehyde (PFA) for 15 min at room temperature, permeabilized with 0.2% TritonX-100 in PBS for 5 min, after blocking with 5% normal goat serum (NGS) in PBS for 1 h, the primary antibodies anti-GluN1 (mouse,1:1,000, NeuroMab, N308/48), anti-GluN1 (rabbit, 1:1,000, Millipore, AB9864) were used at room temperature for 3 h, and then the second antibodies Alexa Fluor 405-conjugated goat anti-mouse and Alexa Fluor 555-conjugated goat anti-rabbit (Invitrogen, Molecular Probes) were incubated for 1 h. Coverslips were mounted with Fluoromont

G (Southern Biotech). Fluorescent images were acquired on a Zeiss510 laser scanning confocal microscope and Olympus IX71 inverted microscope with identical settings for each group. For image quantification analysis, maximal projection images were generated by LSM510 browser software, the integrated fluorescent intensity of GluN1 was measured with ImageJ software (NIH, Bethesda). Statistical analysis was conducted with GraphPad Prism6 software using one-way analysis of variance (ANOVA).

Synaptic Electrophysiology

The AMPA EPSCs and NMDA EPSCs were recorded by stimulating Schaffer collaterals pathway with monopolar glass electrodes filled with ACSF. GFP-positive pyramidal neurons at the CA1 region were visualized with GFP fluorescence. GFP-positive neuron and the neighboring GFP-negative neuron were chose to perform the paired whole-cell recordings. AMPA EPSCs were recorded at −70, and NMDA EPSCs were recorded at +40 mV. The NMDA EPSCs were measured at 100 ms after stimulation. The components of intracellular solution were (in mM) $CsMeSO_4$ 135, NaCl 8, HEPEs 10, Na_3GFP 0.3, MgATP 4, EGTA 0.3, QX-314 5, and spermine 0.1. The 3–5 MΩ borosilicate glass pipettes were used for recording.

Statistics

All data were given as mean ± s.e.m. Statistical significance between means was calculated using Student's *t*-test.

RESULTS

C1 Domain of GluN1 C-terminus Is Necessary for Nuclear Translocation

Our previous study shows the C-terminus of GluN1 play a crucial role in GABAergic synapses formation (Gu et al., 2016b), indicating that the C-terminus of GluN1 is important for NMDARs-mediated biological functions. Due to alternative splicing of the C-terminus, there are four GluN1 isoforms, GluN1-1a, 2a, 3a, and 4a (**Figure 1A**). They are composed of four domains, C0, C1, C2, and C2' (**Figure 1B**). Firstly, we investigated the cellular distribution of these four domains in HEK293A. The results showed that C1-GFP mainly localized in nucleus, while the other domains showed the whole cell diffuse distribution (**Figure 1C**). To verify whether C1 domain is required for nuclear localization, we over expressed 4 isoforms of GluN1 C-terminus in HEK293A cells and primary hippocampal neurons. We found that only the 1a-CT-GFP and 3a-CT-GFP containing the C1 domain showed nuclear localization in HEK293A cells (**Figure 1D**) and primary hippocampal neurons (**Supplementary Figure S1**). Thus, our data demonstrated that C-terminus of GluN1 containing C1 domain was necessary for nuclear translocation.

Ten Basic Amino Acids in C1 Domain Determines the Nuclear Localization of GluN1 C-terminus

Previously, it is suggested that C1 domain contains a bi-particle nuclear localization signal (NLS) by the protein subcellular localization prediction tool (PSORT) (Holmes et al., 2002; Jeffrey et al., 2009) (**Figure 2A**). To verify whether the C1 domain contains NLS, we constructed several mutants of 1a-CT (**Figure 2B**). We found that the bi-particle 7 basic amino acids [1a-CT-GFP(7A)] were not necessary for the nuclear localization of GluN1 C-terminus, but the 10 basic amino acids in the C1 domain 1a-CT-GFP(10A) regulated the nuclear localization of GluN1 C-terminus in HEK293A cells and primary hippocampal neurons (**Figures 2C,D**).

GluN1 C-terminus Translocates to Nucleus in Primary Neurons

To explore the nuclear localization of full-length GluN1, we transfected the full-length four isoforms of GluN1 fused to GFP into cells. Our data showed that the full-length of GluN1 showed diffuse cytoplasmic distribution in HEK293A cells (**Supplementary Figure S2**). In primary hippocampal neurons, we found that the full-length of GluN1-1a exhibited cytoplasmic and nuclear distribution, while the GluN1-2a, GluN1-3a, GluN1-4a, and GluN1-1a(10A) isoforms showed diffuse cytoplasmic distribution (**Figures 3A,B**). Given that single GluN1 subunit could not form the functional NMDARs in HEK293A cells (Cao et al., 2011; Hansen et al., 2014), we transfected GluN1 and GluN2A subunits in HEK293A cells to examine whether GluN2 is required for the translocation of GluN1-1a C terminus, the results showed the full-length GluN1-1a still showed cytoplamic distribution in HEK293A cells (**Supplementary Figure S3**), which suggests that the intrinsic genetic determinants of neuronal form determine the translocation of GluN1 C-terminus to nucleus in primary hippocampal neurons.

There were three possibilities to explain the whole cell diffuse distribution of GluN1-1a-GFP. Firstly, the full-length of GluN1-1a-GFP could translocate to nucleus because of artificial phenomena of over-expression; secondly, the GFP protein can be detached or auto-cleaved from GluN1-1a-GFP in neurons for some unknown reasons; the third possibility is that the C-terminus of GluN1-1a can be detached or cleaved from GluN1-1a-GFP in neurons, so the C-terminus contained GFP fused C1 domain can translocate to nucleus. To test these hypotheses, two commercial antibodies were used (**Figure 3C**). The N-terminus antibody is a mouse antibody that can recognize the N-terminus of GluN1 extracellular domain (amino acids 42–361); the C-terminus antibody is a rabbit antibody that can only recognize the C2 domain part of GluN1 C-terminus (LQNQKDTVLPRRAIEREEGQLQLCSRHRES) (**Figure 3C**). To test the specificity of the antibodies, we over expressed the full-length of GluN1-1a, 2a, 3a, and 4a in HEK293A cells. The results showed that N antibody could recognize all four full-length isoforms, whereas the C antibody could only recognize the full-length GluN1-1a and GluN1-2a containing C2 domain (**Supplementary Figure S4A**). We also used the C-terminus of four isoforms to test these two commercial antibodies. The results showed the N antibody couldn't recognize the C-terminus, while the C antibody could recognize the GluN1-1a-CT and 2a-CT containing C2 domain (**Supplemental Figure S4B**). Therefore,

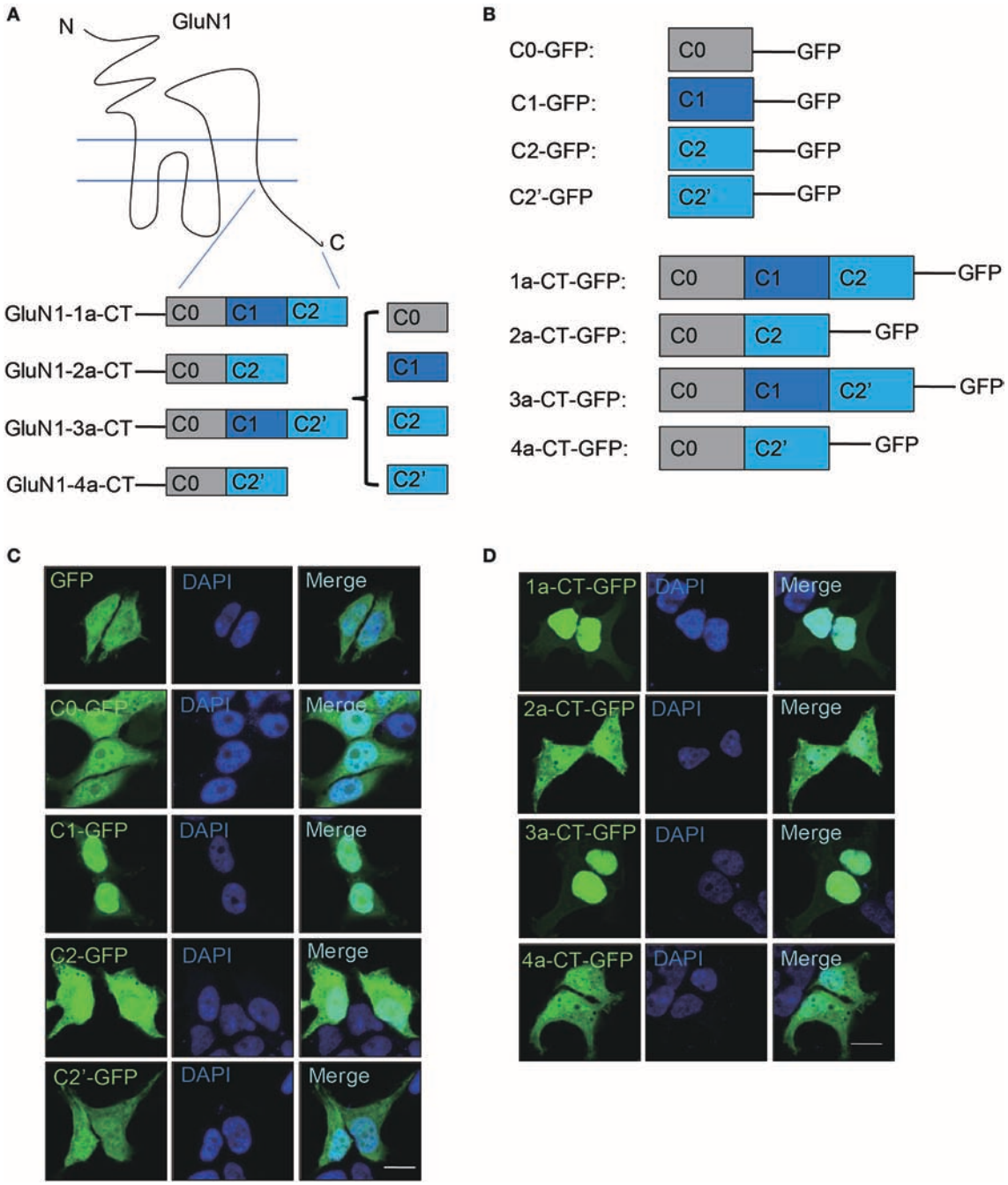

FIGURE 1 | C1 domain determines the nuclear localization of GluN1 C-terminus in HEK293A cells. **(A)** Schematic diagram of GluN1 C-terminus. **(B)** The plasmids of truncated GluN1 C-terminus were used in this study. **(C)** HEK293A cells were transfected with GFP, C0-GFP, C1-GFP, C2-GFP, or C2'-GFP for 24 h, and then the cells were subjected to immunocytochemistry assay. DAPI was used to visualize the cell nuclei. Scale bar: 10 μm. **(D)** The C-terminus of four GluN1 isoforms were transfected in HEK293A cells for 24 h, and then the cells subjected to immunocytochemistry assay. DAPI was used to visualize the cell nuclei. Scale bar: 10 μm.

our data showed the two antibodies could specifically recognize the immunogenic regions.

In cultured hippocampal neurons, the immunocytochemistry assays showed that the nuclear fluorescence of GluN1-1a-GFP could be identified by the C antibody (**Figures 3D–F**). Because the C antibody also recognizes the endogenous GluN1, the red fluorescence in the nucleus is weaker than in the cytoplasm (**Figure 3D**). Thus, our data support the third hypothesis that C-terminus of GluN1-1a can be detached or cleaved from GluN1-1a-GFP in neurons,

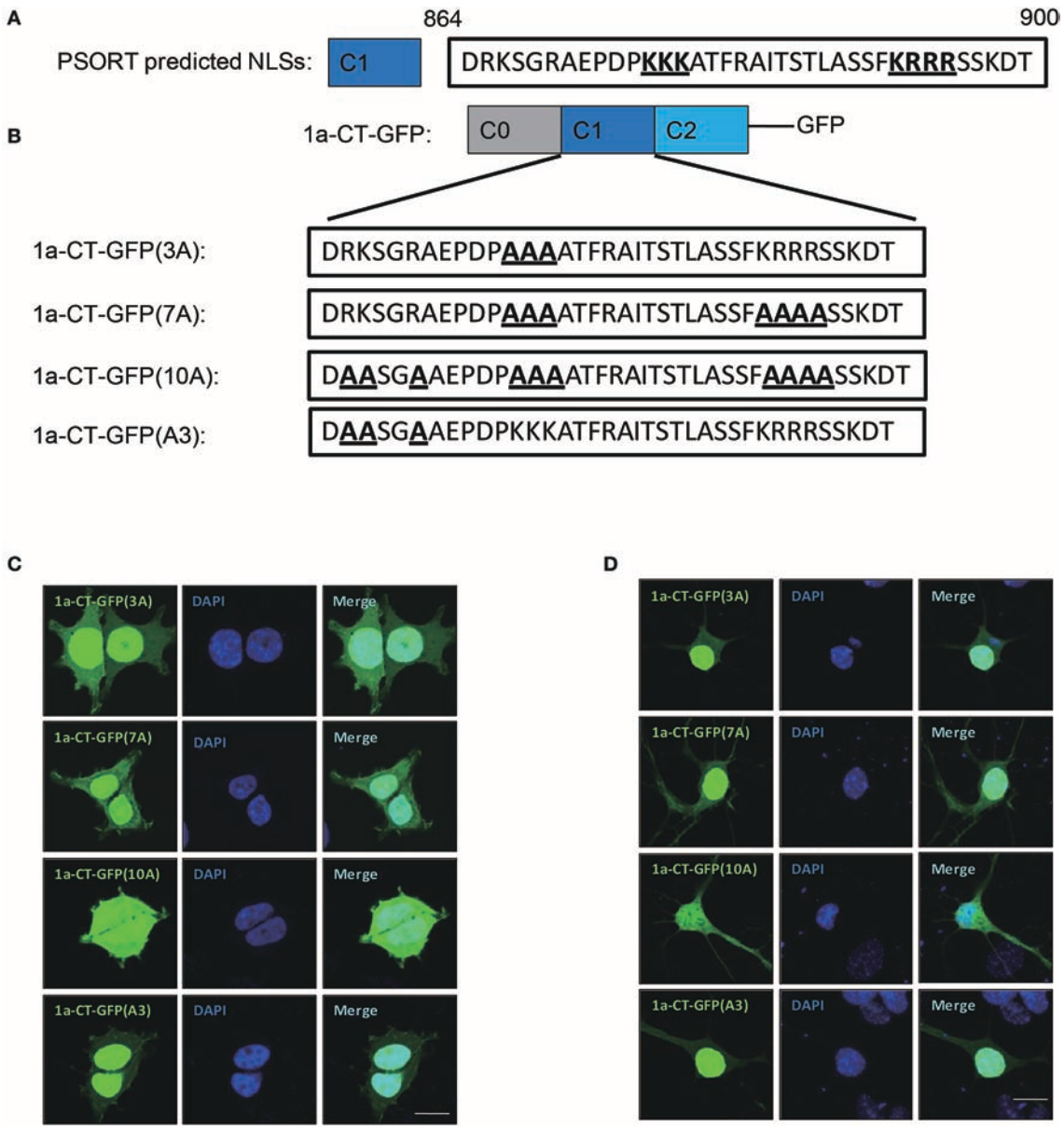

FIGURE 2 | Ten amino acid in C1 domain determines the nuclear localization of GluN1 C-terminus. **(A)** the protein subcellular localization prediction tool (PSORT) predicted nuclear localization signal in C1 domain. **(B)** Indicated mutation for 1a-CT-GFP (3A), 1a-CT-GFP (7A), 1a-CT-GFP (10A), or 1a-CT-GFP (A3). **(C,D)** The HEK293A (**C**) and primary hippocampal neurons **(D)** were transfected with 1a-CT-GFP (3A), 1a-CT-GFP (7A), 1a-CT-GFP (10A), or 1a-CT-GFP (A3) for 24 h, and then the cells were subjected to immunocytochemistry assay. DAPI was used to visualize the cell nuclei. Scale bar: 10 μm.

and the C-terminus including GFP can translocate to nuclei.

Chemical LTP Regulates the Translocation of C-terminus of GluN1 to Nucleus

To explore the relationship of nuclear translocation and neuronal activity, we treated the neurons with KCl to depolarization the neuron, NMDA and glycine to activate NMDARs, glycine to induce chemical LTP (cLTP), NMDA to induce chemical LTD (cLTD), MG-132 to block the proteasome, DHPG to induce group 1 metabotropic glutamate receptor-mediated LTD. Using C antibody to detect C-terminus of GluN1, N antibody to detect total GluN1, we calculated the nuclear fluorescence'ratio of C antibody to N antibody. The results show that the chemical long-term potentiation (cLTP) treatment could significantly decrease the nuclear fluorescence intensity of GluN1 (**Figures 4A,B**).There is no significant difference in the ratios of cytoplasmic and dendritic fluorescence intensity after cLTP treatment (**Figures 4C,D**). Taken together, these data demonstrates that

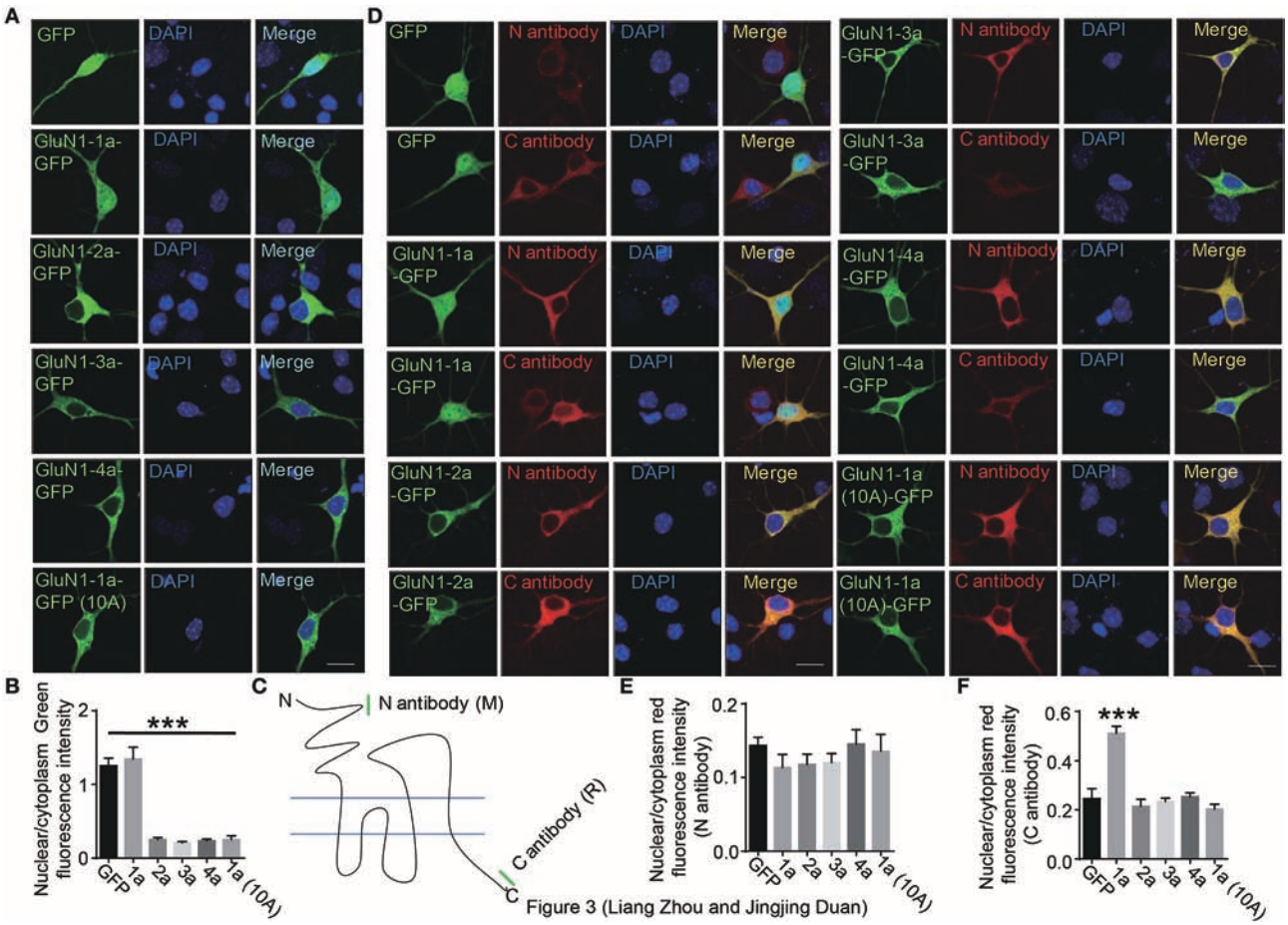

FIGURE 3 | The C-terminus of GluN1-1a translocates to nucleus in primary hippocampal neuron. **(A)** The primary hippocampal neurons were transfected with GFP, GluN1-1a-GFP, GluN1-2a-GFP, GluN1-3a-GFP, GluN1-4a-GFP, or GluN1-1a-GFP (10A) for 24 h, and then the cells were subjected to immunocytochemistry assay. DAPI was used to visualize the cell nuclei. Scale bar: 10 μm. **(B)** Quantitative data (mean ± SEM) of **(A)** from three independent experiments. ***$P < 0.001$, Student's *t*-test. **(C)** Two GluN1 antibodies were used in this study. The mouse N antibody recognizes the N terminus amino acids 42–361 of GluN1 extracellular domain, and the rabbit C antibody recognizes the C2 domain of GluN1. **(D)** The primary hippocampal neurons were transfected with GFP, GluN1-1a-GFP, GluN1-2a-GFP, GluN1-3a-GFP, GluN1-4a-GFP, or GluN1-1a-GFP (10A) for 24 h, and then stained with the N and C antibodies of GluN1 for immunofluorescence measurement. DAPI was used to visualize the nuclei. Scale bar: 10 μm. **(E,F)** Quantitative data (mean ± SEM) of (**D**) from three independent experiments. ***$P < 0.001$, Student's *t*-test.

cLTP could affect the translocation of GluN1 C-terminus to nucleus.

The C-terminus of GluN1-1a Potentiates Glutamate Transmission

Given the crucial role of NMDARs in synaptic functions, we then investigated the regulation of GluN1-1a C terminus on synaptic transmission. We transfected GluN1 C-terminus into neurons, and then did the electrophysiological recording. We found that over-expression of 2a-CT-GFP without C1 domain didn't change AMPA EPSCs or NMDA EPSCs, whereas 1a-CT-GFP containing C1 domain could potentiate NMDAR-mediated synaptic transmission (**Figure 5A**). No change of paired-pulse ratio (PPR) of GluN1-1a-CT-GFP and GluN1-2a-CT-GFP suggested that C1 domain of GluN1 did not affect presynaptic neurotransmitter release probability (**Figure 5B**).

DISCUSSION

NMDARs are widely expressed in neurons throughout the central nervous system with distinct pharmacological and electrophysiological properties because of diversity of subunit composition (Paoletti et al., 2013; Hansen et al., 2014). Once the synaptic plasticity happens, the neuronal nucleus must be informed to activate the IEGs expression, which is mediated by the synapse-to-nucleus signaling pathway (Deisseroth et al., 1996, 2003). Several proteins binding to NMDARs or forming the complex with NMDARs in the postsynaptic density have been reported that can relay the information between synapses and nucleus, such as Calmodulin (Deisseroth et al., 1998), nuclear factor-κB (NF-κB) (Meffert et al., 2003), importins (Ch'ng and Martin, 2011), and Jacob (Dieterich et al., 2008).

Here we found that NMDARs subunit GluN1-1a involved in synapse-to-nucleus communication. Our results showed that the

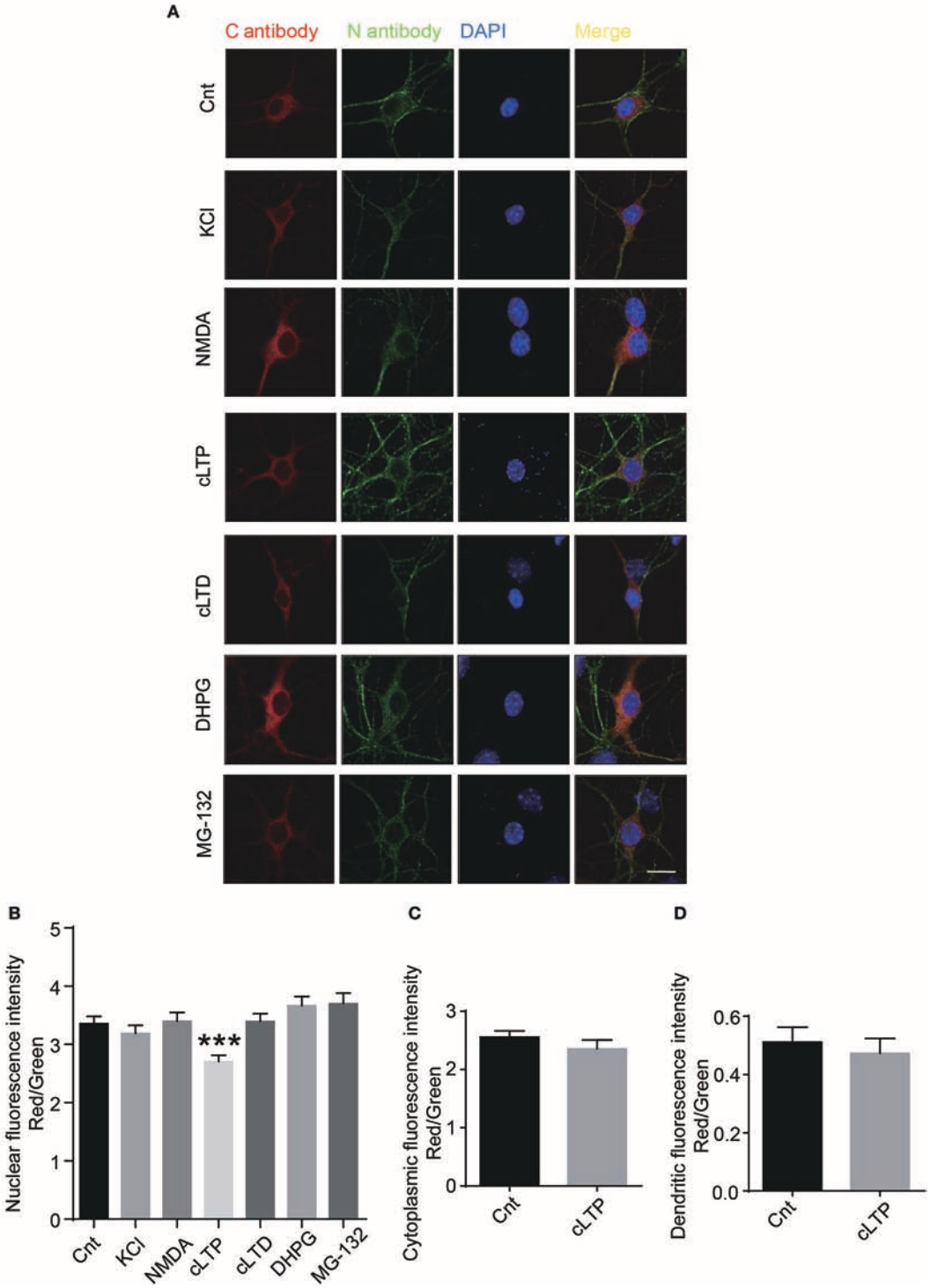

FIGURE 4 | Neuronal activity regulates the cleavage of GluN1. **(A)** The primary hippocampal neurons were treated with several reagents to activate the different signal pathways. 50 mM KCl was used to depolarize the neuronal membrane. One hundred micromoles NMDA (Abcam) and 2 μM glycine was used to activate NMDARs. Two hundred micromoles glycine was used to induce cLTP. Fifty micromoles NMDA was used to induce cLTD. Fifty micromoles DHPG was used to induce group 1 metabotropic glutamate receptor-mediated LTD. Ten micromoles MG-132 was used to block the proteasome. **(B)** The quantitative data were presented with the nuclear fluorescence intensity of GluN1 by measuring ratio of nuclear red fluorescence (rabbit C antibody) to nuclear green fluorescence (mouse N antibody). (Number of neurons in each group: Cnt: $n = 39$, KCl: $n = 38$, NMDA: $n = 36$, cLTP: $n = 42$, cLTD: $n = 41$, DHPG: $n = 48$, MG-132: $n = 35$). Student's t test, $^{***}P < 0.001$. **(C,D)** The quantitative data was presented with the cytoplasmic fluorescence intensity of GluN1 **(C)** or dendritic fluorescence intensity **(D)** by measuring ratio of cytoplamic or dendritic red fluorescence (rabbit C antibody) to cytoplamic or dendritic green fluorescence (mouse N antibody). (Number of neurons in each group: Cnt: $n = 39$, cLTP: $n = 42$). Student's *t*-test, cytoplamic fluorescence $p = 0.2899$, dendritic fluorescence $p = 0.5989$.

C-terminus of GluN1-1a could translocate to neuronal nucleus (**Figures 1**–**3**) and the 10 basic amino acids in C1 domain determined the nuclear localization of GluN1 C terminus. The electrophysiological recording showed that C1 domain of GluN1 affected the NMDAR-mediated synaptic transmission (**Figure 5**). Taken together, these data indicated that the 10 basic amino acids in C1 domain determined the translocation of GluN1 C-terminus into neuronal nucleus, and this translocation is highly related to synaptic transmission (**Figure 5**).

In our study, although the GluN1-1a and GluN1-3a both contained C1 domain in the C-terminus, only the GluN1-1a showed nuclear fluorescence in neurons (**Figure 3**), which suggested that the adjacent alternatively spliced C2'domain affects this process, as the C2' domain can suppresses the function of C1 domain (Standley et al., 2000).

The neuronal activity regulates the localization of NMDARs (Rao and Craig, 1997). Here, we found that cLTP regulated the translocation of C-terminus of GluN1 (**Figure 4**). However, the

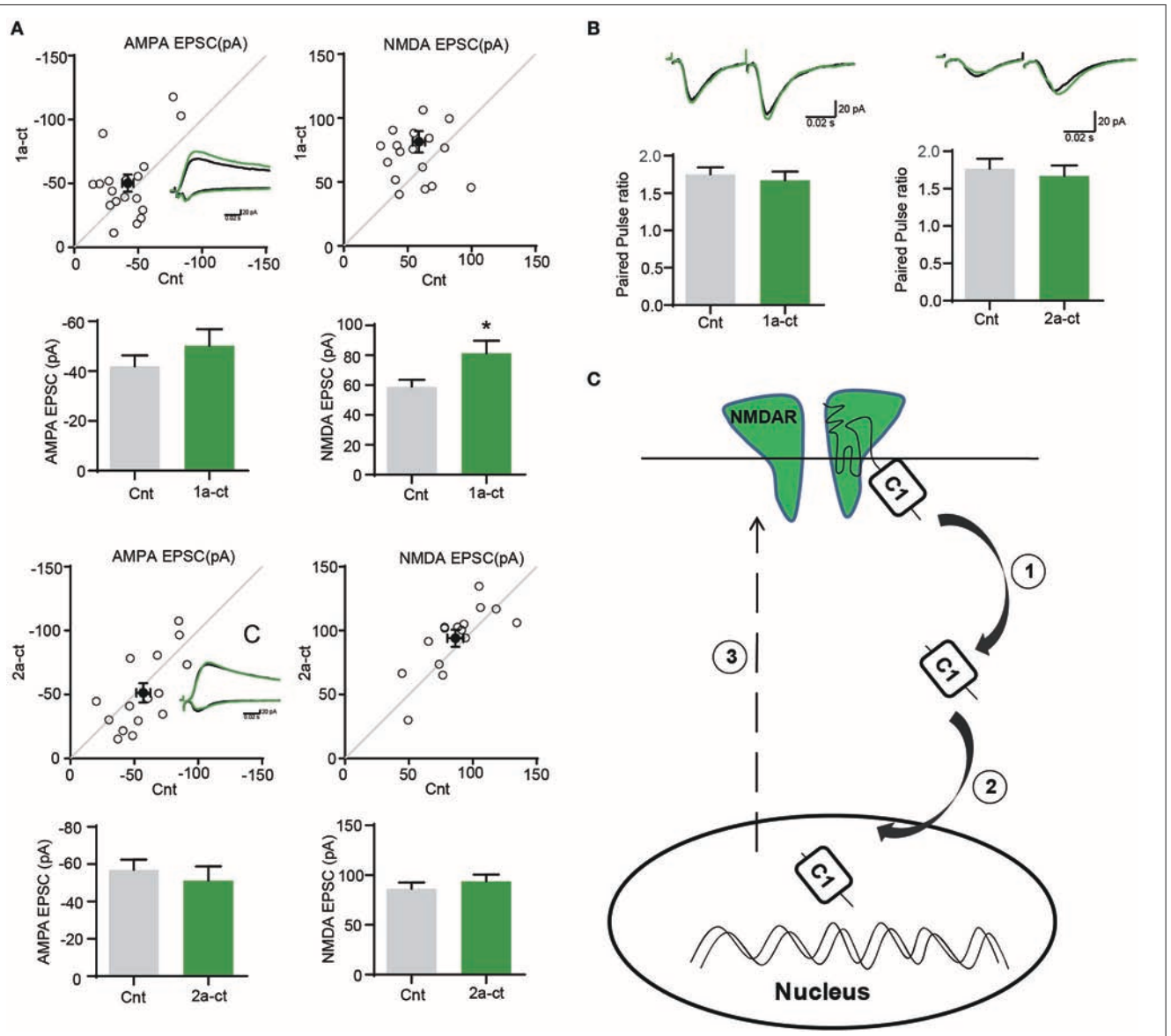

FIGURE 5 | The C terminus of GluN1 regulates synaptic functions. **(A)** The AMPA EPSCs and NMDA EPSCs were recorded after over expressing the 1a-CT-GFP or 2a-CT-GFP. (Amplitude of AMPA EPSCs: Cnt, 41.97 ± 4.403; 1a-CT-GFP, 50.24 ± 6.659, $n = 18$. $p = 0.1911$; Amplitude of NMDA EPSCs: Cnt, 58.84 ± 4.795; 1a-CT-GFP, 81.42 ± 8.345, n = 19. $^*p = 0.0169 < 0.05$; Amplitude of AMPA EPSCs: Cnt, 57.05 ± 5.471; 2a-CT-GFP, 51.26 ± 7.547, $n = 15$. $p = 0.3183$; Amplitude of NMDA EPSCs: Cnt, 86.42 ± 6.226; 2a-CT-GFP, 94.00 ± 6.685, $n = 15$. $p = 0.1146$; Amplitude of AMPA EPSCs: Cnt, 34.38 ± 4.166). **(B)**There were no differences in PPRs after over expressing 1a-CT-GFP or 2a-CT-GFP. (PPR control, 1.750 ± 0.09609 and PPR 1a-CT-GFP, 1.673 ± 0.1146, $n = 14$, $p = 0.3147$; PPR control, 1.767 ± 0.1343 and PPR 2a-CT-GFP, 1.673 ± 0.1380, $n = 13$, $p = 0.4804$). **(C)** A schematic diagram showing the translocation of GluN1 C-terminus to neuronal nucleus. The GluN1-1a C-terminus containing C1 domain could be cleaved by protease ①, and then translocates to neuronal nucleus ②, which eventually potentiates NMDAR-mediated synaptic transmission ③.

proteins that lead to the detachment or cleavage of C-terminus from the full-length of GluN1-1a are needed to be further identified. The calcium-dependent protease calpain could be a candidate, as calpain and NMDARs can regulate the functions of each other (Hell et al., 1996; Wu et al., 2005; Szydlowska and Tymianski, 2010). The LTP coordinates the homeostasis of synapses (Vitureira and Goda, 2013) and normalization of synapses (Hardingham et al., 2007), whether the translocation of GluN1-1a C-terminus to neuronal nuclei mediates the LTP associated these physiological functions, which are needed to be further investigated.

In summary, we found that the C-terminus of GluN1-1a can translocate to neuronal nuclei, and regulate the synaptic activity, which could be affected by cLTP.

AUTHOR CONTRIBUTIONS

LZ supervised the research. LZ and JD performed the experiments. LZ and JD wrote and revised the manuscript.

FUNDING

This work was supported by the National Natural Science Foundation of China (81703535), China Postdoctoral Science Foundation (2017M611895), Jiangsu Province Postdoctoral Science Foundation (1701130C), Natural Science Foundation of Jiangsu Higher Education Institutions of China (17KJD180005).

ACKNOWLEDGMENTS

We are grateful to Dr. Wei Lu from National Institutes of Health (NIH) for generously providing the GluN1 and GluN2A plasmids.

SUPPLEMENTARY MATERIAL

The Supplementary Material for this article can be found online at: https://www.frontiersin.org/articles/10.3389/fncel.2018.00334/full#supplementary-material

REFERENCES

Berg, J. M., Lee, C., Chen, L., Galvan, L., Cepeda, C., Chen, J. Y., et al. (2015). JAKMIP1, a novel regulator of neuronal translation, modulates synaptic function and autistic-like behaviors in mouse. *Neuron* 88, 1173–1191. doi: 10.1016/j.neuron.2015.10.031

Cao, J.-Y., Qiu, S., Zhang, J., Wang, J.-J., Zhang, X.-M., and Luo, J.-H. (2011). Transmembrane region of N-Methyl-D-Aspartate Receptor (NMDAR) subunit is required for receptor subunit assembly. *J. Biol. Chem.* 286, 27698–27705. doi: 10.1074/jbc.M111.235333

Ch'ng, T. H., Desalvo, M., Lin, P., Vashisht, A., Wohlschlegel, J., and Martin, K. (2015). Cell biological mechanisms of activity-dependent synapse to nucleus translocation of CRTC1 in neurons. *Front. Mol. Neurosci.* 8:48. doi: 10.3389/fnmol.2015.00048

Ch'ng, T. H., and Martin, K. C. (2011). Synapse to nucleus signaling. *Curr. Opin. Neurobiol.* 21, 345–352. doi: 10.1016/j.conb.2011.01.011

Ch'ng, T. H., Uzgil, B., Lin, P., Avliyakulov, N. K., O'dell, T. J., and Martin, K. C. (2012). Activity-dependent transport of the transcriptional coactivator CRTC1 from synapse to nucleus. *Cell* 150, 207–221. doi: 10.1016/j.cell.2012.05.027

Deisseroth, K., Bito, H., and Tsien, R. W. (1996). Signaling from synapse to nucleus: postsynaptic CREB phosphorylation during multiple forms of hippocampal synaptic plasticity. *Neuron* 16, 89–101. doi: 10.1016/S0896-6273(00)80026-4

Deisseroth, K., Heist, E. K., and Tsien, R. W. (1998). Translocation of calmodulin to the nucleus supports CREB phosphorylation in hippocampal neurons. *Nature* 392, 198–202. doi: 10.1038/32448

Deisseroth, K., Mermelstein, P. G., Xia, H., and Tsien, R. W. (2003). Signaling from synapse to nucleus: the logic behind the mechanisms. *Curr. Opin. Neurobiol.* 13, 354–365. doi: 10.1016/S0959-4388(03)00076-X

Dieterich, D. C., Karpova, A., Mikhaylova, M., Zdobnova, I., König, I., Landwehr, M., et al. (2008). Caldendrin–Jacob: a protein liaison that couples NMDA receptor signalling to the nucleus. *PLoS Biol.* 6:e34. doi: 10.1371/journal.pbio.0060034

Fainzilber, M., Budnik, V., Segal, R. A., and Kreutz, M. R. (2011). From synapse to nucleus and back again—communication over distance within neurons. *J. Neurosci.* 31, 16045–16048. doi: 10.1523/JNEUROSCI.4006-11.2011

Ferreira, J. S., Rooyakkers, A., She, K., Ribeiro, L., Carvalho, A. L., and Craig, A. M. (2011). Activity and protein kinase C regulate synaptic accumulation of N-Methyl-D-Aspartate (NMDA) receptors independently of GluN1 splice variant. *J. Biol. Chem.* 286, 28331–28342. doi: 10.1074/jbc.M111.222539

Gu, X., Mao, X., Lussier, M. P., Hutchison, M. A., Zhou, L., Hamra, F. K., et al. (2016a). GSG1L suppresses AMPA receptor-mediated synaptic transmission and uniquely modulates AMPA receptor kinetics in hippocampal neurons. *Nat. Commun.* 7:10873. doi: 10.1038/ncomms10873

Gu, X., Zhou, L., and Lu, W. (2016b). An NMDA receptor-dependent mechanism underlies inhibitory synapse development. *Cell Rep.* 14, 471–478. doi: 10.1016/j.celrep.2015.12.061

Hagenston, A. M., and Bading, H. (2011). Calcium signaling in synapse-to-nucleus communication. *Cold Spring Harb. Perspect. Biol.* 3:a004564. doi: 10.1101/cshperspect.a004564

Hansen, K. B., Ogden, K. K., Yuan, H., and Traynelis, S. F. (2014). Distinct functional and pharmacological properties of triheteromeric GluN1/GluN2A/GluN2B NMDA receptors. *Neuron* 81, 1084–1096. doi: 10.1016/j.neuron.2014.01.035

Hardingham, N. R., Hardingham, G. E., Fox, K. D., and Jack, J. J. B. (2007). Presynaptic efficacy directs normalization of synaptic strength in layer 2/3 rat neocortex after paired activity. *J. Neurophysiol.* 97, 2965–2975. doi: 10.1152/jn.01352.2006

Hell, J. W., Westenbroek, R. E., Breeze, L. J., Wang, K. K., Chavkin, C., and Catterall, W. A. (1996). N-methyl-D-aspartate receptor-induced proteolytic conversion of postsynaptic class C L-type calcium channels in hippocampal neurons. *Proc. Nat. Acad. Sci. U.S.A.* 93, 3362–3367. doi: 10.1073/pnas.93.8.3362

Herbst, W. A., and Martin, K. C. (2017). Regulated transport of signaling proteins from synapse to nucleus. *Curr. Opin. Neurobiol.* 45, 78–84. doi: 10.1016/j.conb.2017.04.006

Holmes, K. D., Mattar, P., Marsh, D. R., Jordan, V., Weaver, L. C., and Dekaban, G. A. (2002). The C-terminal C1 cassette of the N-methyl-D-aspartate receptor 1 subunit contains a bi-partite nuclear localization sequence. *J. Neurochem.* 81, 1152–1165. doi: 10.1046/j.1471-4159.2002.00865.x

Horak, M., and Wenthold, R. J. (2009). Different roles of C-terminal cassettes in the trafficking of full-length NR1 subunits to the cell surface. *J. Biol. Chem.* 284, 9683–9691. doi: 10.1074/jbc.M807050200

Jeffrey, R. A., Ch'ng, T. H., O'dell, T. J., and Martin, K. C. (2009). Activity-dependent anchoring of importin alpha at the synapse involves regulated binding to the cytoplasmic tail of the NR1-1a subunit of the NMDA receptor. *J. Neurosci.* 29, 15613–15620. doi: 10.1523/JNEUROSCI.3314-09.2009

Karpova, A., Mikhaylova, M., Bera, S., Bär, J., Reddy, P. P., Behnisch, T., et al. (2013). Encoding and transducing the synaptic or extrasynaptic

origin of NMDA receptor signals to the nucleus. *Cell* 152, 1119–1133. doi: 10.1016/j.cell.2013.02.002

Laurie, D. J., and Seeburg, P. H. (1994). Regional and developmental heterogeneity in splicing of the rat brain NMDAR1 mRNA. *J. Neurosci.* 14, 3180–3194. doi: 10.1523/JNEUROSCI.14-05-03180.1994

Lim, A. F., Lim, W. L., and Ch'ng, T. H. (2017). Activity-dependent synapse to nucleus signaling. *Neurobiol. Learn. Mem.* 138, 78–84. doi: 10.1016/j.nlm.2016.07.024

Lonergan, M. E., Gafford, G. M., Jarome, T. J., and Helmstetter, F. J. (2010). Time-dependent expression of arc and Zif268 after acquisition of fear conditioning. *Neural Plast.* 2010:139891. doi: 10.1155/2010/139891

Lu, W., Man, H., Ju, W., Trimble, W. S., Macdonald, J. F., and Wang, Y. T. (2001). Activation of synaptic NMDA receptors induces membrane insertion of new AMPA receptors and LTP in cultured hippocampal neurons. *Neuron* 29, 243–254. doi: 10.1016/S0896-6273(01)00194-5

Ma, H., Groth, R. D., Cohen, S. M., Emery, J. F., Li, B., Hoedt, E., et al. (2014). gammaCaMKII shuttles Ca^{2+}/CaM to the nucleus to trigger CREB phosphorylation and gene expression. *Cell* 159, 281–294. doi: 10.1016/j.cell.2014.09.019

Meffert, M. K., Chang, J. M., Wiltgen, B. J., Fanselow, M. S., and Baltimore, D. (2003). NF-κB functions in synaptic signaling and behavior. *Nat. Neurosci.* 6, 1072–1078. doi: 10.1038/nn1110

Mokin, M., and Keifer, J. (2005). Expression of the immediate-early gene–encoded protein Egr-1 (zif268) during *in vitro* classical conditioning. *Learn. Mem.* 12, 144–149. doi: 10.1101/lm.87305

Mu, Y., Otsuka, T., Horton, A. C., Scott, D. B., and Ehlers, M. D. (2003). Activity-dependent mRNA splicing controls ER export and synaptic delivery of NMDA receptors. *Neuron* 40, 581–594. doi: 10.1016/S0896-6273(03)00676-7

Nonaka, M., Kim, R., Fukushima, H., Sasaki, K., Suzuki, K., Okamura, M., et al. (2014). Region-specific activation of CRTC1-CREB signaling mediates long-term fear memory. *Neuron* 84, 92–106. doi: 10.1016/j.neuron.2014.08.049

Panayotis, N., Karpova, A., Kreutz, M. R., and Fainzilber, M. (2015). Macromolecular transport in synapse to nucleus communication. *Trends Neurosci.* 38, 108–116. doi: 10.1016/j.tins.2014.12.001

Paoletti, P., Bellone, C., and Zhou, Q. (2013). NMDA receptor subunit diversity: impact on receptor properties, synaptic plasticity and disease. *Nat. Rev. Neurosci.* 14, 383–400. doi: 10.1038/nrn3504

Rao, A., and Craig, A. M. (1997). Activity regulates the synaptic localization of the NMDA receptor in hippocampal neurons. *Neuron* 19, 801–812. doi: 10.1016/S0896-6273(00)80962-9

Standley, S., Roche, K. W., Mccallum, J., Sans, N., and Wenthold, R. J. (2000). PDZ domain suppression of an ER retention signal in NMDA receptor NR1 splice variants. *Neuron* 28, 887–898. doi: 10.1016/S0896-6273(00)00161-6

Szydlowska, K., and Tymianski, M. (2010). Calcium, ischemia and excitotoxicity. *Cell Calcium* 47, 122–129. doi: 10.1016/j.ceca.2010.01.003

Tsien, J. Z., Huerta, P. T., and Tonegawa, S. (1996). The essential role of hippocampal CA1 NMDA receptor–dependent synaptic plasticity in spatial memory. *Cell* 87, 1327–1338. doi: 10.1016/S0092-8674(00)81827-9

Vitureira, N., and Goda, Y. (2013). The interplay between Hebbian and homeostatic synaptic plasticity. *J. Cell Biol.* 203, 175–186. doi: 10.1083/jcb.201306030

Wu, H.-Y., Yuen, E. Y., Lu, Y.-F., Matsushita, M., Matsui, H., Yan, Z., et al. (2005). Regulation of N-methyl-D-aspartate receptors by calpain in cortical neurons. *J. Biol. Chem.* 280, 21588–21593. doi: 10.1074/jbc.M501603200

Yang, J., Ruchti, E., Petit, J.-M., Jourdain, P., Grenningloh, G., Allaman, I., et al. (2014). Lactate promotes plasticity gene expression by potentiating NMDA signaling in neurons. *Proc. Natl. Acad. Sci. U.S.A.* 111, 12228–12233. doi: 10.1073/pnas.1322912111

Conflict of Interest Statement: The authors declare that the research was conducted in the absence of any commercial or financial relationships that could be construed as a potential conflict of interest.

frontiers in Cellular Neuroscience

ORIGINAL RESEARCH
published: 10 January 2019
doi: 10.3389/fncel.2018.00526

Extracellular Vesicles Secreted by Astroglial Cells Transport Apolipoprotein D to Neurons and Mediate Neuronal Survival Upon Oxidative Stress

Raquel Pascua-Maestro[1], Esperanza González[2], Concepción Lillo[3], Maria D. Ganfornina[1], Juan Manuel Falcón-Pérez[2,4†] and Diego Sanchez[1†]*

[1]*Instituto de Biología y Genética Molecular-Departamento de Bioquímica y Biología Molecular y Fisiología, Universidad de Valladolid-CSIC, Valladolid, Spain,* [2]*Exosomes Group, Metabolomics Unit and Platform, CIC bioGUNE, CIBERehd, Technology Park of Bizkaia, Derio, Spain,* [3]*Instituto de Neurociencias de Castilla y León, IBSAL, Universidad de Salamanca, Salamanca, Spain,* [4]*IKERBASQUE, Basque Foundation for Science, Bilbao, Spain*

Extracellular vesicle (EV)-mediated glia-to-neuron communication has been recognized in a growing number of physiological and pathological situations. They transport complex sets of molecules that can be beneficial or detrimental for the receiving cell. As in other areas of biology, their analysis is revolutionizing the field of neuroscience, since fundamental signaling processes are being re-evaluated, and applications for neurodegenerative disease therapies have emerged. Using human astrocytic and differentiated neuronal cell lines, we demonstrate that a classical neuroprotective protein, Apolipoprotein D (ApoD), expressed by glial cells and known to promote functional integrity and survival of neurons, is exclusively transported by EVs from astrocytes to neurons, where it gets internalized. Indeed, we demonstrate that conditioned media derived from ApoD-knock-out (KO) astrocytes exert only a partial autocrine protection from oxidative stress (OS) challenges, and that EVs are required for ApoD-positive astrocytic cell line derived medium to exert full neuroprotection. When subfractionation of EVs is performed, ApoD is revealed as a very specific marker of the exosome-containing fractions. These discoveries help us reframe our understanding of the neuroprotective role of this lipid binding protein and open up new research avenues to explore the use of systemically administered ApoD-loaded exosomes that can cross the blood-brain barrier to treat neurodegenerative diseases.

Keywords: ApoD, exosomes, extracellular vesicles, astrocytes, neurons, oxidative stress, neuroprotection, glia-to-neuron communication

OPEN ACCESS

Edited by:
Gabriela Alejandra Salvador, Universidad Nacional del Sur, Argentina

Reviewed by:
Xiaolu Zhang, Northern Jiangsu People's Hospital, China
Marina Guizzetti, Oregon Health & Science University, United States

****Correspondence:***
Maria D. Ganfornina
opabinia@ibgm.uva.es

†These authors have contributed equally to this work and are senior authors

Received: *03 August 2018*
Accepted: *18 December 2018*
Published: *10 January 2019*

Citation:
Pascua-Maestro R, González E, Lillo C, Ganfornina MD, Falcón-Pérez JM and Sanchez D (2019) Extracellular Vesicles Secreted by Astroglial Cells Transport Apolipoprotein D to Neurons and Mediate Neuronal Survival Upon Oxidative Stress. Front. Cell. Neurosci. 12:526. doi: 10.3389/fncel.2018.00526

INTRODUCTION

Nervous system function relies on a complex set of cell types interacting and communicating among them. Cell contact-dependent interactions underlie cell adhesion processes important for neural circuit construction and plasticity. However, communication can also take place by secretion of signaling molecules and neurotransmitters. In this line, the discovery of extracellular vesicles (EVs) have brought a new format of interactions to an already multifaceted communication network.

EVs produced by most cells, including all nervous system cell types (Frühbeis et al., 2013a; Lopez-Verrilli et al., 2013; Basso and Bonetto, 2016; Guitart et al., 2016; Croese and Furlan, 2018), open up a new mechanism of signal transmission (Valadi et al., 2007; Hervera et al., 2018) that is changing our understanding of how glia and neurons communicate (Frühbeis et al., 2013b; Basso and Bonetto, 2016; Krämer-Albers, 2017).

As the lipid, carbohydrate, protein and nucleic acid composition of EVs (Kalra et al., 2012; Keerthikumar et al., 2015; Kim et al., 2015) is cell type and physiological state-specific (György et al., 2011; Müller, 2012), such feature makes them candidate biomarker tools in many human diseases, including neuronal disorders (Müller, 2012; Cheow et al., 2016). Furthermore, the potential therapeutic use of EVs is particularly important in brain illnesses, given that they can cross the blood-brain barrier (Alvarez-Erviti et al., 2011; Ridder et al., 2014; Krämer-Albers, 2017). In this regard, EVs purposely loaded with neuroprotective molecules are a promising therapy for neurodegenerative disorders (Pandya et al., 2013; Spencer et al., 2014; Rufino-Ramos et al., 2017).

The Lipocalin Apolipoprotein D (ApoD) is mostly expressed in the nervous system and upregulated in response to oxidative stress (OS; Ganfornina et al., 2008; Bhatia et al., 2012, 2013), a challenge that accompanies physiological aging and disease (Ganfornina et al., 2008; Perdomo and Henry Dong, 2009; Bhatia et al., 2012, 2013). Not surprisingly, ApoD is one of the few genes consistently over-expressed in the aging brain of all vertebrate species tested so far (Loerch et al., 2008). Moreover, ApoD expression is boosted in an amazingly wide array of neurodegenerative and psychiatric diseases of diverse etiology (Suresh et al., 1998; Reindl et al., 2001; reviewed by Dassati et al., 2014). ApoD is actively secreted by astrocytes and myelinating glia, and is uptaken by neurons during neural development and differentiation (Sánchez et al., 2002; Ganfornina et al., 2008, 2010; García-Mateo et al., 2014; Pascua-Maestro et al., 2017). At the cellular level, ApoD is found in the endosome-lysosome-autophagosomal compartment (Pascua-Maestro et al., 2017). Such subcellular location is finely regulated, both in glia, that express ApoD, and in neurons that uptake ApoD in a paracrine fashion (Pascua-Maestro et al., 2017). Within the lysosome, ApoD is able to prevent and revert OS-triggered membrane permeabilization (Bhatia et al., 2013; Pascua-Maestro et al., 2017). ApoD has been demonstrated to reduce free radical-generating lipid hydroperoxides to inert lipid hydroxides (Bhatia et al., 2012), a biochemical property that enables the protection and repair of OS-damaged membranes, finally resulting in cell survival. Previous work demonstrate that ApoD pro-survival mechanism is mediated specifically by the control of lipid peroxidation levels both in cultured cells and *in vivo* animal models (Ganfornina et al., 2008; Navarro et al., 2010; Bajo-Grañeras et al., 2011).

ApoD is considered to be secreted through a canonical secretion pathway, and is found associated to serum LDL/HDL (Perdomo and Henry Dong, 2009; Dassati et al., 2014). However, proteomic analyses have identified this Lipocalin in EVs from serum and cerebrospinal fluid (Cheow et al., 2016; Przybycien-Szymanska et al., 2016). Thus, we set up to test whether ApoD is present in glial-derived EVs and contributes, in this cell-cell communication format, to improve neuronal viability and function.

MATERIALS AND METHODS

Animals

ApoD-knock-out (KO) mice were generated by homologous recombination (Ganfornina et al., 2008), and maintained in positive pressure-ventilated racks at 25 ± 1°C with 12 h light/dark cycle, fed *ad libitum* with standard rodent pellet diet (Global Diet 2014; Harlan Inc., Indianapolis, IN, USA), and allowed free access to filtered and UV-irradiated water. To avoid potential maternal effects of ApoD, and to generate wild-type (WT) and ApoD-KO mice of homogeneous genetic background, the experimental cohorts used in this study are the F1 generation of homozygous crosses of $ApoD^{-/-}$ and $ApoD^{+/+}$ littermates born from heterozygous crosses of an ApoD-KO line backcrossed for over 20 generations into the C57BL/6J background.

Mice experimental procedures were approved by the University of Valladolid Animal Care and Use Committee, following the regulations of the Care and the Use of Mammals in Research (European Commission Directive 86/609/CEE, Spanish Royal Decree 1201/2005). No human subject was involved in this study.

Cell Culture and Treatments

The human astrocytoma 1321N1 and neuroblastoma SH-SY5Y cell lines were obtained from ECACC (86030402) and ATCC (CRL-2266) respectively. Cells were grown at 37°C in a humidity-saturated atmosphere containing 5% CO_2. Culture medium was replaced twice a week and cells were subcultured at 90% confluence. Cells were counted with Countess Automated Cell Counter (Invitrogen).

1321N1 cells were cultured in Dulbecco-modified Eagle's medium (DMEM; Lonza) supplemented with heat-inactivated 5% fetal bovine serum (FBS), 1% L-glutamine, and 1% penicillin/streptomycin/amphotericin B (PSA).

SH-SY5Y cells were cultured in DMEM supplemented with 4.5 g/l glucose, heat-inactivated 10% FBS, 1% L-glutamine, 1% PS and 1% nonessential amino acids (Lonza). To subculture, we used 0.25% Trypsin-EDTA (Gibco Life Technologies). SH-SY5Y differentiation was achieved by culturing cells on collagen-treated plates with 3% FBS and 10 μM retinoic acid (Sigma-Aldrich) for 72 h.

Primary astrocytes from WT and ApoD-KO neonatal (0–1 days old) mice were cultured as described (Bajo-Grañeras et al., 2011). Cerebral cortices were quickly dissected, their meninges removed by rolling on filter paper, and pieces of cortex placed in Earle's Balanced Salt Solution (EBSS) with 2.4 mg/ml DNAse I and 0.2 mg/ml bovine serum albumin (BSA). The tissue was minced with a surgical blade, centrifuged (200 *g*, 2 min), incubated with 10 mg/ml trypsin for 15 min at 37°C (incubation terminated by 10% FBS addition), mechanically dissociated with a Pasteur pipette, and centrifuged (200 *g*, 5 min). The resulting

cells were resuspended in DMEM with 10% FBS, 1% L-glutamine, 1% PSA, plated onto cultured flasks, and incubated at 37°C in 5% CO_2 with 90%–95% humidity. Culture medium was replaced after 24 h and weekly thereafter. Cells were used for experiments after two subculture steps, when >99% of cells are astrocytes (Bajo-Grañeras et al., 2011).

Exogenous addition of ApoD: human ApoD purified from breast cystic fluid (Ruiz et al., 2013) was added (10 nM) to the cell cultures for 2 h.

Paraquat (PQ) treatment: cells were cultured in phenol red-free DMEM supplemented with 1% L-glutamine, 1% PS, and 0.2% charcoal stripped FBS. This medium without additives was used as our low-serum (LS) control condition. Cells were treated for 1–24 h with PQ (500 μM) prepared in LS medium.

To label and track the whole population of EVs produced by a cell (including exosomes and shedding vesicles) the membranous organelles were labeled with Vybrant-DiI (V22888). To label organelles of the phagocytic-endocytic pathway [endosomes, lysosomes and multivesicular bodies (MVB)] we used Dextran-Alexa 488 (D22910), following the manufacturer's specifications (Molecular Probes). Cells were incubated with the dye solution for 48 h. After removing the culture medium and performing three 5 min washes with phosphate-buffered saline (PBS), cells were incubated overnight and then subcultured alone or in different co-culture formats (see below).

Cells remained in co-culture during 48 h before performing flow cytometry or fluorescence microscopy analyses to test for transfer of vesicles between astrocytes and neurons. Two types of co-cultures were used: cells were subcultured to experimental plates in a 50:50 proportion (mixed cultures), or separated by a 0.4 μm pore membrane (Transwell plates, Corning Inc.) to avoid direct cell-cell contact.

Conditioned Media Harvesting for EV Preparations

A standard FBS is used for the culture medium used in the maintenance and amplification of each cell type, and for experiments not directed to EV collection. The experiments described below are performed in EV-free media, where FBS was EV-depleted by ultracentrifugation and added (5%) to phenol red-free DMEM with 25 mM HEPES, 4.5 g/l glucose, 1% L-glutamine and 1% PS.

Conditioned media collection: Cells were cultured in EV-free medium and incubated at 37°C in 5% CO_2 with 90%–95% humidity for 72 h before the culture medium was collected. A total of 24 culture dishes (20×10^6 cells/dish) per condition were necessary for EV preparations from 1321N1 cells, and 66 culture flasks (8×10^6 cells/flask) per conditions of primary astrocytes. After centrifugation at 1,500× *g* for 30 min at 4°C, the culture supernatant was filtered through a 0.22 μm membrane to obtain a debris-free conditioned medium (CM). The filtered culture medium was immediately frozen at −80°C. Two independent pools of media from 1321N1 cells and two from primary astrocytes per genotype were prepared for further vesicle isolation by differential ultracentrifugation (see below).

Isolation, Fractionation and Analysis of Astrocyte-Derived EVs

To isolate EVs, the stored debris-free CM samples were centrifuged at 10,000× *g* for 30 min and the supernatant was centrifuged at 100,000× *g* for 75 min. The supernatant of this centrifugation was collected for some experiments as EV-depleted CM. The resulting pellet was washed with an excess of PBS, and centrifuged again at 100,000× *g* for 60 min. The pellet was resuspended in cold PBS and stored at −80°C.

EVs size distribution and concentration were analyzed using a NanoSight LM10 system equipped with a fast video capture and particle-tracking software. Vesicles are visualized by light scattering using a light microscope with a Nanoparticles tracking analysis (NTA) software that tracks Brownian motion of individual vesicles. NTA post-acquisition settings were kept constant for all samples, and each video was analyzed to calculate the median vesicle size and concentration estimates (Dragovic et al., 2011). The starting EV-free culture medium was subject to NTA as control for comparison. We also characterized EVs by Western Blot and Transmission Electron Microscopy (TEM).

Glia-derived EVs (either from the 1321N1 human astrocytic cell line or from mouse primary astrocytes) were fractionated in a continuous 0.25–2 M sucrose density gradient (Taylor, 2015). The EV sample was placed on top of the gradient and centrifuged for 16 h at 210,000× *g*, 4°C, in a SW40 Ti rotor. Fractions (1 ml) were collected from top to bottom by using an autodensity-flow gradient fractionator (Labconco). After mixing by vortex, 20 μl of each fraction were separated for density measures. Subsequently, the rest of the volume was diluted in 20 mM HEPES (pH 7.4), and centrifuged 1 h at 110,000× *g*, 4°C, in a TLA-110 rotor. The pellets were resuspended in PBS and stored at −80°C for subsequent immunoblot analysis. Using the volume set aside, the refractive index of each fraction was measured with a high-resolution refractometer (Abbe 2WAJ, PCE Americans, Inc.). Values are translated into density values by use of equivalence tables.

Immunoblot Analysis

Cell lysates, cultured media (either directly or concentrated 20× by filter centrifugation with 10 KDa cut-off Centricon YM-10; Millipore), isolated EVs, or EV fractions were analyzed by immunoblot. Denaturing and reducing conditions (0.5% SDS, 25 mM DTT) were used to solubilize proteins prior to electrophoresis in order to detect ApoD. Proteins were transferred to PVDF membranes using standard procedures, and exposed to rabbit serum anti-human ApoD (custom made by Abyntek Biopharma against purified ApoD; Ruiz et al., 2013), goat serum anti-mouse ApoD (Santa Cruz Biotechnology), rabbit serum anti-CD81 (GeneTex), mouse anti-flotillin 1 (Becton Dickinson), or rabbit serum anti-BiP (Sigma), and followed by HRP-conjugated secondary antibodies (Santa Cruz Biotechnology). Membranes were developed with ECL reagents (Millipore) and the signal visualized with a digital camera (VersaDoc; BioRad). The integrated optical density of the immunoreactive protein bands was measured in images

taken within the linear range of the camera, avoiding signal saturation.

Electron Microscopy Methods

Primary astrocytes, destined for pre-embedding immunogold labeling of ApoD, were fixed in 4% formaldehyde and 0.3% glutaraldehyde in 0.1 M PB, pH 7.4, for 30 min at 4°C. Following washes in 0.1 M PB, the cells were blocked with 0.1% cold water fish skin gelatin and permeabilized with Tween-20 (0.5%) in Tris-buffered saline (TBS; 20 mM Tris-HCl, 150 mM NaCl). Samples were incubated with rabbit serum anti-human ApoD antibody diluted in blocking solution. After several washes they were incubated with ultra-small gold-conjugated goat anti-rabbit secondary antibodies Electron Microscopy Sciences (EMS) in PBS. After several washes with PBS, samples were post-fixed in 2% glutaraldehyde in PBS for 20 min, washed, and the ultra-small gold particles were silver-enhanced for 20 min at room temperature with AURION R-Gent SE-EM (Silver Enhancement for Electron Microscopy) following the manufacturer indications. Later, samples were post-fixed with 0.5% OsO_4 in PBS for 20 min at 4°C, washed with PBS, dehydrated through a graded series of ethanol and embedded in Epoxy EMbed-812 resin EMS. Ultrathin sections were obtained with an Ultracut E ultramicrotome (Reichert/Leica), contrasted with uranyl acetate and lead citrate, and analyzed using a JEOL JEM-1011 HR electron microscope with a CCD Gatan ES1000W camera with iTEM software.

EV preparations destined to cryo-electron microscopy were directly adsorbed onto glow-discharged holey carbon grids (QUANTIFOIL, Germany). Grids were blotted at 95% humidity and rapidly plunged into liquid ethane with the aid of VITROBOT (Maastricht Instruments BV, Netherlands). Vitrified samples were imaged at liquid nitrogen temperature using a JEM-2200FS/CR transmission electron microscope (JEOL, Japan) equipped with a field emission gun and operated at an acceleration voltage of 200 kV.

Immunocytochemistry

Cells attached to poly-L-lysine (Sigma-Aldrich) treated coverslips were fixed with 4% formaldehyde. Following washes in PBS, cells were blocked and permeabilized with Tween-20 (0.1%) and 1% non-immune (goat or donkey) serum. Cells were incubated with primary antibodies: mouse anti-CD81 (monoclonal JS81), Mouse anti-CD63 (H5C6) or rabbit serum anti-human ApoD. All antibodies were prepared in blocking solution. Cy5, Cy3 (Abcam), Alexa Fluor® 594/488 (Jackson Labs) or DyLight® 405 (Thermo Scientific) conjugated IgGs were used as secondary antibodies. After washes in PBS, cells were mounted in EverBrite™ Mounting Medium with DAPI, and sealed with CoverGrip™ Coverslip Sealant (Biotium).

Image Acquisition and Analysis

Confocal images were obtained with a 63× oil immersion objective (HCX PL Apo CS NA = 1.4; Leica) attached to a confocal DMI 6000B microscope with a TCS SP5 confocal system (Leica) equipped with AOBS and AOTF systems. Fluorophores were excited with WLL laser (Leica) and a 405 line (Leica) controlled by LAS AF software (Leica). Emissions were collected with the AOBS system and three spectral detectors. Laser power and detection gains were set by scanning control samples labeled with secondary antibody alone. We ensured to obtain similar dynamic ranges in our images, and adjusted gain and offset using LUTs. In this manner, bleed through can be neglected. Negative control images showed very weak and homogeneous background. We obtained confocal sections under constant conditions to minimize image acquisition variation. Images were stored as 1,024 × 1,024 pixels and 8-bit TIFF files.

Z-series (xyz scan) were performed in all cases, covering the whole cell *z*-axis dimension. The number of z-stacks was determined by observing the limits of the cell membrane. The focus plane was set to be 3 μm beneath the section surface. The optimal value of the step size was calculated for the wavelength used to fulfill the Nyquist theorem. The optical section thickness was 0.772 μm. Besides, images were taken with a 4× zoom, reducing field size. Pixel size corresponded to 0.06*0.06*0.3777 μm^3. Scanning was performed with a 1.0 Airy unit pinhole size.

Images were processed with a Gaussian Blur filter [Sigma (Radius): 1.00], to facilitate object detection, and analyzed with a Colocalization Indices plug-in (Nakamura et al., 2007) and the 3D Object Counter tool of the FIJI software. To analyze triple-colocalization experiments we used the Image Calculator and 3D Object Counter tools of FIJI. We analyzed 20 cells per condition. Colocalization was quantitated using the intensity correlation quotient (ICQ), as described (Li et al., 2004). A 2 × ICQ was adopted so that colocalization values range from −1 (total exclusion) to +1 (total colocalization), with 0.1 representing the threshold for random association of signals (Pascua-Maestro et al., 2017). The index was referenced either to ApoD signal or to DiI signal.

Flow Cytometry

Cells cultured for 48 h after labeling with Vybrant-DiI or Dextran-Alexa 488 were lifted with 500 μl of Triple (Tryple™ Select, Gibco Life Technologies) after removal of the culture medium and washes with PBS. Suspended cells were analyzed in a FACS Canto II flow cytometer (Beckton Dickinson). DiI signal was collected with the "PE" detector (BP585/42) and Alexa 488 was detected with the "FITC" channel (BP530/30) after excitation with 488 nm laser. Data was processed with Kaluza Analysis software v.1.3 (Beckman Coulter).

MTT-Viability Assay

Cell viability was measured with the 3-(4,5-dimethylthiazol-2-yl)-2,5-diphenyltetrazolium bromide (MTT) colorimetric assay as previously described (Bajo-Grañeras et al., 2011; Pascua-Maestro et al., 2018). After MTT exposure for 3 h, cells were incubated in isopropanol with 10% Triton X-100, and the solubilized formazan was measured by spectrophotometry using the SOFTmax Pro microplate reader (Molecular Devices).

Absorbance was measured at λ = 570 nm after subtracting the λ = 690 nm background.

RT-PCR

RNAs from 1321N1 cells or differentiated SH-SY5Y cells after exposure to 1321N1-derived EVs were extracted with TRIzol (Qiagen). Total RNA (1 μg) was treated with DNaseI and reverse-transcribed with Prime-Script (Takara). The cDNA obtained was used as template for RT-PCR amplifications. To amplify human ApoD and the housekeeping control gene RPL18 we used the following primers: Human ApoD-Forward: 5'-CCACCCCAGTTAACCTCACA; Human ApoD-Reverse: 5'-CCACTGTTTCTGGAGGGAGA; Human RPL18-Forward: 5'-CCATCATGGGAGTGGACAT-3'; Human RPL18-Reverse: 5'-CACGGCCGTCTTGTTTTC.

Statistical Analysis

Statistical analyses were performed with SPSS v.19 (IBM) and SigmaPlot v.11.0 (Systat) software. A p value < 0.05 was used as a threshold for significant changes. The tests used for each experiment are stated in figure legends.

RESULTS

Glia-Neuron Communication *in vitro*

Although extensive data support the role of EVs as mediators of neuron-glia communication *in vivo* (Frühbeis et al., 2013b; Basso and Bonetto, 2016), we tested whether this relationship exists between human astroglial 1321N1 and neuronal SH-SY5Y cells, that have been previously used as a model to unravel the mechanism of action of ApoD (Bajo-Grañeras et al., 2011; Pascua-Maestro et al., 2017). We first studied the possibility of vesicular exchange between these cells by labeling the membranous compartment of 1321N1 astrocytes with the lipophilic compound DiI, and the endo-lysosomal compartment of SH-SY5Y neurons with Dextran-Alexa 488 (see "Material and Methods" section). Co-culturing of labeled cells in EV-free media for 48 h showed colocalization of DiI and Dextran-Alexa 488 in both astrocytes and neurons (**Figures 1C,D**), suggesting an exchange of membranous material among them. In addition, flow cytometry analysis (**Figures 1E–H**) confirms the presence of double-labeled cells (DiI-Dextran co-labeling; **Figure 1H**) and suggests that such transfer of material might be occurring mainly in the astrocyte-to-neuron direction (arrow in **Figure 1H**). However, the pattern of labeled cells observed might also be due to differences in efficiency of the labeling methods.

Analyzing DiI and Dextran-Alexa 488 distribution in 1321N1 and SH-SY5Y respectively by confocal microscopy we found that in both cells some of the labeled organelles colocalize with CD81, a marker of late endocytic compartments (Escola et al., 1998; **Figures 1A,B**). These results suggest that the membranous transfer between cells could be mediated by EVs. Nevertheless, they also could be explained by: (i) a cell-cell direct contact-dependent exchange of material; (ii) endocytosis of cellular debris such as apoptotic bodies generated in the co-cultures; or (iii) endocytosis of EVs produced by either cell type. Thus, to discern between these scenarios we used a Transwell assay, focusing on the transcellular traffic from astrocytes to neurons. Using EV-free media, we cultured DiI-labeled 1321N1 astrocytes as donor cells, on the Transwell insert, and SH-SY5Y neurons as target cells, on the lower compartment. After 48 h of incubation, a DiI positive population of SH-SY5Y recipient cells is detected by flow cytometry (**Figures 2A–C**). These experiments suggest that SH-SY5Y neurons receive and internalize DiI-labeled EVs secreted by 1321N1 astrocytes.

Neurons Uptake Glial-Derived EVs Containing ApoD

As ApoD is secreted by astrocytes and uptaken by neurons (Pascua-Maestro et al., 2017), we wanted to test if EVs play a role in such intracellular communication. In contrast to ApoD-expressing glioma and astrocytic cell lines like 1321N1 cells (Bajo-Grañeras et al., 2011; Pascua-Maestro et al., 2017), no ApoD expression has been detected in SH-SY5Y neuroblastoma cells either by genome-wide transcriptome analyses (e.g., 0.0 FPKM for ApoD in http://systemsbiology.uni.lu/shsy5y/) or by immunodetection of ApoD protein (Pascua-Maestro et al., 2017). We therefore tested whether 1321N1-derived vesicles uptaken by SH-SY5Y neurons contain astrocyte-derived ApoD using the Transwell co-culture system.

When co-cultured with 1321N1 cells in the Transwell insert, we are able to detect ApoD signal in intracellular vesicles of SH-SY5Y (**Figures 2D–F**), with a significant colocalization with the EV markers CD63 (**Figures 2D,G**) and CD81 (**Figures 2E,G**), as well as with the astrocyte-originated DiI signal (**Figures 2F,G**). Although, in general, the detected CD63 and CD81 can be either endogenous (produced by neurons) or transferred in astrocyte-derived EVs, the particular subset of CD63 or CD81-positive organelles that are also ApoD-positive are strong candidates to have an astrocytic origin. Indeed, the high colocalization index ($2 \times ICQ > 0.6$) of CD81 relative to the DiI signal detected in neurons, strongly supports a significant uptake of CD81-DiI-labeled EVs, a fraction of which ($2 \times ICQ > 0.2$), bring ApoD with them (**Figure 2G**). The significant colocalization indexes agree with the high incidence of triple colocalization of ApoD-CD81-DiI (**Figure 2F**).

However, ApoD could be provided externally to neurons as protein or mRNA, or alternatively its expression be induced after treatment with astroglial EVs, since the later have been shown to trigger diverse signaling cascades in cells (e.g., Hervera et al., 2018). To distinguish among these three possibilities we cultured SH-SY5Y neurons with: (1) EV-free standard media (SM); (2) 1321N1-conditioned media (CM); (3) the EV fraction (EVs) obtained by differential centrifugation of CM; and (4) the EV-depleted supernatant (Sup) of CM. We then used immunocytochemistry to detect ApoD protein in neurons, and RT-PCR to monitor *APOD* mRNA expression in the donor and recipient cells involved.

Immunofluorescence analysis of cultured SH-SY5Y showed the absence of ApoD in SM-cultured neurons (**Figure 3A**), thus confirming the absence of endogenous ApoD in control

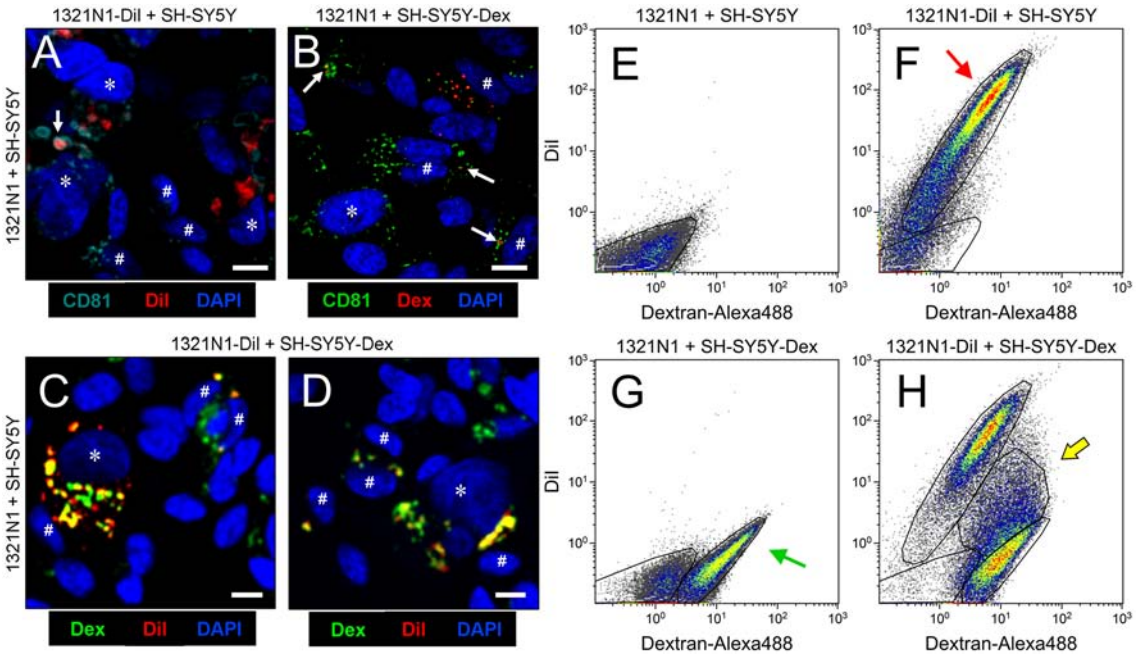

FIGURE 1 | Astrocytes and neurons exchange CD81-positive material. **(A–D)** Single plane confocal microscopy images extracted from Z-stacks obtained from co-cultures of: 1321N1 astrocytes labeled with DiI and unlabeled SHSY5Y neurons **(A)**; unlabeled 1321N1 and SH-SY5Y labeled with Dextran-Alexa 488 **(B)**; 1321N1 labeled with DiI and SH-SY5Y labeled with Dextran-Alexa 488. **(C,D)** Immunocytochemistry with the extracellular vesicle (EV) marker CD81 is shown in **(A,B)**. Arrows point to colocalizing signals. Asterisks and pound signs mark identified nuclei from astrocytes and neurons respectively. *N* = 20 confocal stacks/condition. Calibration bars: 10 μm. **(E–H)** Flow cytometry analyses plotting the DiI and Dextran-Alexa 488 signals in the different co-culture conditions. The red arrow in **(F)** indicates the DiI-1321N1 population, and the green arrow in **(G)** points to the Dextran-Alexa 488-SHSY5Y population. A double labeled cell population appears when both astrocytic and neuronal cells are labeled (**H**, marked with a yellow arrow).

conditions. ApoD protein is observed in CM-cultured neurons (**Figure 3B**), in agreement with our previous reports showing internalization of exogenously added ApoD in neurons (Pascua-Maestro et al., 2017) and with the results obtained in the Transwell experiments (**Figure 2**). Surprisingly, when CM is separated into EVs and EV-depleted supernatant, ApoD is only observed in neurons after addition of the fraction containing EVs (**Figure 3C**) and no ApoD is obtained after exposure to the EV-depleted supernatant (**Figure 3D**).

Additionally, RT-PCR was performed in order to detect *APOD* mRNA expression in 1321N1 donor astrocytes and SH-SY5Y recipient neurons after 48 h exposure to 1321N1 EVs. While the housekeeping ribosomal gene *RPL18* is present in all samples, *APOD* mRNA was only detected in the donor cells (**Figure 3E**), thus discarding a potential induction of endogenous *APOD* expression in SH-SY5Y neurons upon exposure to 1321N1-derived EVs followed by *de novo* synthesis of ApoD protein.

Characterization of ApoD in Glial EVs: ApoD as a Very Specific Marker of Human Astroglial Exosomes

So far, our results show that 1321N1 astroglia express the EV marker CD81 (**Figure 1A**), that colocalizes with DiI-labeled membranous organelles and can be transferred to neurons (**Figures 2**, **3**). Also, MVB can be detected in the cytoplasm of 1321N1 astrocytes by EM (**Figure 4A**). Our previous analysis of intracellular traffic of ApoD (Pascua-Maestro et al., 2017) revealed its presence in the extracellular side of the plasma membrane, and its traffic through the endo-lysosomal and autophagosome compartments. Here, we show by means of immunofluorescence and immunoelectron microscopy that ApoD can also be found both in Lamp2-positive MVBs (**Figure 4B**), and in putative EVs (arrowhead in **Figure 4C**), whose size is in the range of exosomes.

Given the locations of ApoD, would the protein be carried in membrane budding microvesicles (MVs) or in MVB-derived exosomes? When the EV-free medium used to culture cells and the 1321N1-CM collected after 72 h are subjected to NTA (**Figure 4D**), we found that 1321N1 cells secrete several EV populations, absent in the starting culture media, with a group showing a particle size compatible with exosomes (arrow in **Figure 4D**, around 100 nm). Following sucrose gradient fractionation of two independent 1321N1 EV preparations and immunoblot analysis, we uncover that ApoD exclusively partitions in the fractions that contain the known density range for exosomes (1.13–1.20 g/ml; (Salomon et al., 2013; Kharaziha et al., 2015). In the preparation shown (**Figure 4E**), fractions with densities of 1.176 g/ml and 1.232 g/ml are both positive for ApoD and for the exosome marker CD81 (**Figure 4E**). All fractions are negative for other sub-cellular

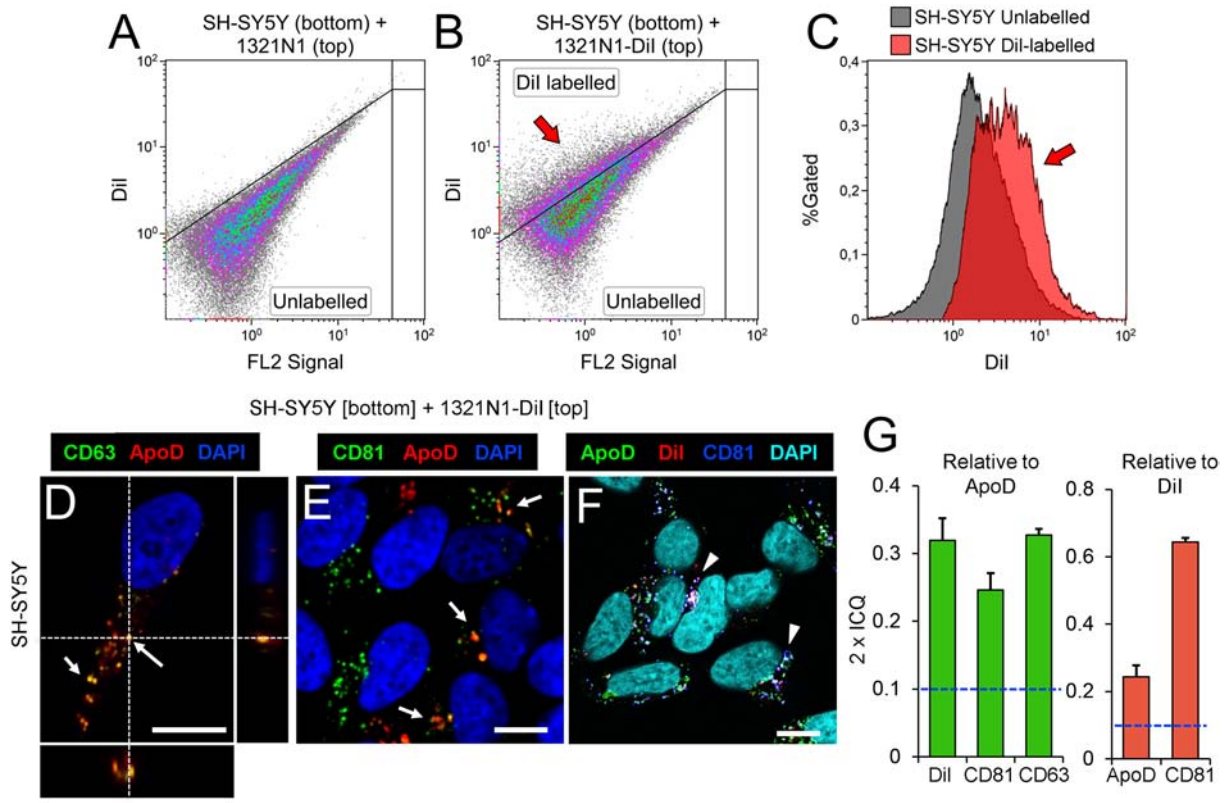

FIGURE 2 | Astrocyte-to-neuron communication is mediated by EVs that carry Apolipoprotein D (ApoD) into neurons. **(A–C)** Flow cytometry analyses of SH-SY5Y cells cultured with 1321N1 cells seeded in a Transwell inset. Astrocytic 1321N1 cells were either unlabeled **(A)** or labeled with DiI. **(B,C)** Dot plots show the existence of a population of DiI-positive SH-SY5Y neurons (arrow in **B**, representing 25.1%) when cultured with labeled 1321N1 astrocytes. The histogram in **(C)** displays the fluorescence increase in DiI-positive neurons (arrow), with median fluorescence increasing from 1.9 to 4.0 (a.u.). **(D–F)** Single plane confocal microscopy images extracted from Z-stacks obtained from unlabeled SH-SY5Y target cells cultured on the lower compartment of a Transwell assay while DiI-labeled 1321N1 donor cells were cultured on the insert. Immunofluorescence with ApoD, CD81 and CD63, and DiI signal are shown with different LUTs to properly display the colocalization of EV markers with ApoD (arrows in **D,E**) or with DiI (arrowheads in F point to triple colocalization DiI-CD81-ApoD). Orthogonal views are shown in **(D)** to visualize the location of vesicular labeling within the cell. *N* = 20 confocal stacks/condition. Calibration bars: 5 μm. **(G)** Average colocalization index (2 × ICQ) referenced either to ApoD signal (green bars) or to DiI signal (red bars) in SH-SY5Y neurons co-cultured in Transwell with DiI-labeled 1321N1 astrocytes. The dotted lines represents the colocalization threshold. Error bars represent SEM (*n* = 20 cells/marker from four independent experiments).

compartment markers (endoplasmic reticulum chaperone BiP; **Figure 4E**). Curiously, the ApoD-containing vesicular fractions present both monomeric and dimeric forms of ApoD (see "Discussion" section). Our results demonstrate that ApoD is specifically enriched in the exosome-containing fractions of 1321N1 astroglial EVs.

ApoD-Containing Exosomes Underlie a Protective Reaction of Glial Cells Against Oxidative Stress and Mediate ApoD-Dependent Neuroprotection

In order to assess whether the presence of ApoD in astrocytic EVs has functional consequences, we tested EV-associated ApoD effect on neuronal viability upon an oxidative insult triggered by the reactive oxygen species (ROS) generator PQ. To address this question we cultured again SH-SY5Y neurons with: (1) EV-free standard media (SM); (2) 1321N1-conditioned media (CM); (3) the EV fraction (EVs) obtained by differential centrifugation of CM; and (4) the EV-depleted supernatant (Sup) of CM.

In the absence of PQ, the exposure of SH-SY5Y neurons to 1321N1 CM or its EVs does not affect their viability (white bars in **Figure 5A**). On the other hand, upon exposure to 2 mM PQ for 2 h (black bars in **Figure 5A**), the decrease observed in SH-SY5Y viability after the OS stimulus is significantly ameliorated after treatment with complete CM or its EV fraction, compared to exposure to PQ in standard medium (SM). Such protection against OS is only partial when the EV-depleted media is used (Sup, black bar, in **Figure 5A**). Since we have demonstrated that ApoD is uptaken by neurons only in EV format (**Figure 3**), these results indicate that a full neuroprotection effect by the 1321N1 secretome can only be achieved when EVs are present in the media. The beneficial effect of EV-associated ApoD is comparable to that obtained with native ApoD purified from human cystic fluid (**Figure 5B**), an effect whose specificity is proven by its reduction when blocking ApoD with a specific antibody.

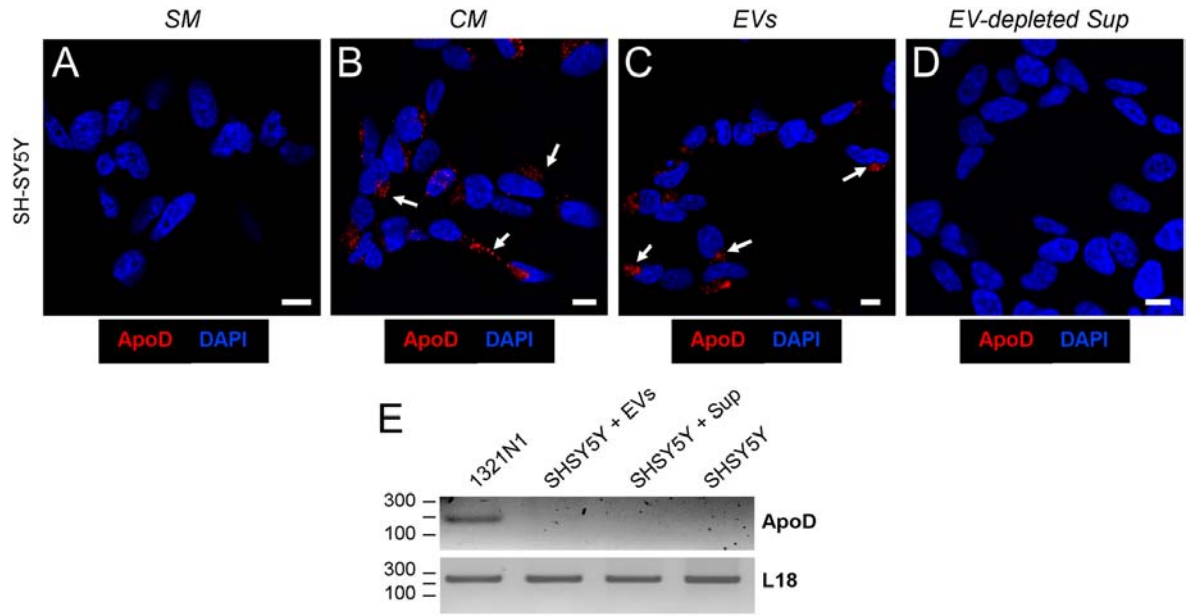

FIGURE 3 | Astrocyte-to-neuron ApoD traffic is exclusively mediated by EVs. **(A–D)** Single plane confocal microscopy images extracted from Z-stacks obtained from SH-SY5Y cells cultured with standard medium (SM; **A**), astrocyte-conditioned medium (CM; **B**), purified astrocyte EVs **(C)**, or EV-depleted astrocyte-derived supernatant, Sup **(D)**. Arrows point to the ApoD vesicular labeling within SH-SY5Y neurons. No signal is detected when SM or EV-depleted Sup is used. Calibration bars: 10 μm. **(E)** RT-PCR analysis of ApoD mRNA expression in the1321N1 donor cells, and in SH-SY5Y differentiated neurons after 48 h exposure to 1321N1-generated EVs. The housekeeping ribosomal gene RPL18 is amplified as control.

In summary, our data demonstrate that a fraction of the ApoD produced by 1321N1 astrocytes is targeted to EVs, and particularly to the fraction displaying exosomal properties. We also show that, surprisingly, it is in this form of cell-cell communication, and not in free soluble form, that ApoD gets internalized by SH-SY5Y neurons, where it is able to protect them from PQ-triggered OS.

A fair amount of data account for the neuroprotective effects of ApoD also on astrocytes themselves (Bajo-Grañeras et al., 2011; Pascua-Maestro et al., 2017). To further contrast this hypothesis and expand the finding to non-immortalized native cells, we used the WT and ApoD-KO mice as experimental model.

First, we performed two additional EV purifications from the culture medium of primary murine cortical astrocytes. Immunoblot analysis (**Figure 6**) demonstrates the presence of ApoD in both the cell homogenate and the EV-enriched fraction from WT primary astrocytes (**Figure 6B**), but not in the ApoD-KO EV preparations (**Figure 6C**), after confirming by EM the presence of EVs in the preparations from both genotypes. As expected, EVs show the markers CD81 and flotillin-1 (also in the whole cell extract) while other subcellular compartment marker (the endoplasmic reticulum chaperon BiP) is absent. Taking into account the starting material for the cell homogenate and the EV-enriched preparations from WT astrocytes (**Figure 6A**), and the relative abundance of ApoD compared with flotillin-1 (**Figure 6B**), we estimate that a significant proportion (around 0.6%) of the ApoD expressed by an astroglial cell is targeted to EVs.

After demonstrating the secretion of ApoD-loaded EVs by primary WT astrocytes, we tested the effect of astrocyte-derived conditioned media on primary astrocytes of WT and ApoD-KO mice exposed to PQ (500 μM, 2 h).

As expected, ApoD-KO astrocytes showed significantly lower viability than WT astrocytes upon exposure to PQ (**Figure 7A**). In both cases, the viability significantly improves after culture with astrocyte-derived conditioned media (collected over a 72 h period), regardless of genotype of the cell originating the conditioned media (**Figure 7B**, gray and black bars). For WT astrocytes, a similar protection effect is attained with media conditioned by either WT or by ApoD-KO cells, which can be explained by the accumulation of various protective factors over time. However, the more vulnerable ApoD-KO astrocytes are significantly better protected when exposed to WT conditioned media (black bar) than when media was conditioned by ApoD-KO astrocytes (gray bar). These results suggest that ApoD, produced by WT astrocytes and present in the extracellular medium, is significantly contributing to protect astrocytes from OS in an autocrine manner.

Together, our results demonstrate that ApoD is present in EVs purified from conditioned media produced by both a human astrocytic cell line and primary murine astrocytes (**Figures 4**, **6**), that ApoD is detected specifically in the exosome-containing fractions of these EVs (**Figure 4**), and that these ApoD-positive EVs become internalized by SH-SY5Y neurons (**Figures 2**, **3**). Moreover, an unexpected result is the absence of detectable ApoD endocytosis into neurons when we use the EV-depleted CM that strongly

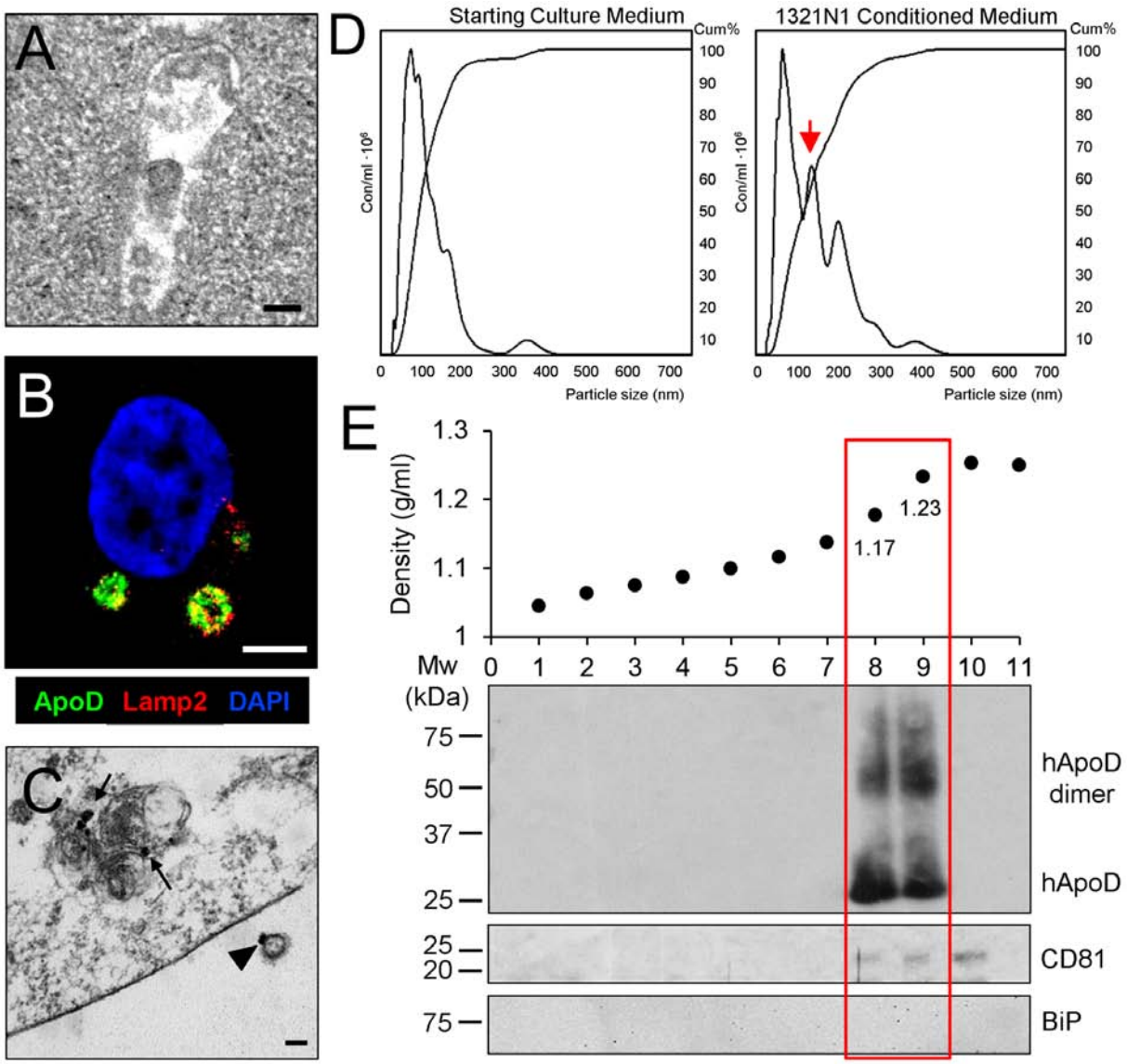

FIGURE 4 | ApoD is specifically found in EV fractions containing astrocyte-derived exosomes. **(A)** Electron microscopy image of a multivesicular body (MVB) in the cytoplasm of a 1321N1 astrocyte. **(B)** Single plane confocal microscopy image extracted from a Z-stack of a 1321N1 astrocyte showing the colocalization of ApoD and Lamp2 in putative MVBs. **(C)** Immunoelectron microscopy image showing ApoD in mature lysosomes of a 1321N1 cell (arrows), and on the external surface of a putative exosome (arrowhead). Calibration bars: **(A,C)**: 100 nm; **(B)**: 5 μm. **(D)** Nanoparticle tracking analysis (NTA) of the starting culture medium or 1321N1-CM shows that 1321N1 astrocytes secrete several EV populations with a group showing particle size compatible with exosomes (red arrow). EV preparations were obtained from two pools of two independent cell culture sets (480 × 10^6 cells/preparation). Particle size: 92 and 97 nm, respectively. Particle concentration: 218 × 10^9 and 222 × 10^9 particles/ml respectively. **(E)** Fractionation of EV preparation from 1321N1 astrocytes by sucrose gradient. The plot shows the fraction density along with the immunoblot analysis of each fraction with ApoD, CD8 and BiP antibodies. Only fractions 8 and 9 are positive for ApoD, while the exosome marker CD81 appears in fractions 8–10.

indicates that the majority of extracellular ApoD produced by 1321N1 astrocytes is associated to EVs and not in a free soluble form, as previously thought. EV-associated ApoD protects both neurons and astrocytes from PQ-induced OS. These results set the stage to study whether we find *in vivo* such an important contribution of exosomes to the ApoD astrocyte-to-neuron traffic both in physiological and pathological situations.

DISCUSSION

Besides a role in cell-cell communication during cellular homeostasis, EVs are shed by cells in response to pathological states (reviewed by Croese and Furlan, 2018; Holm et al., 2018). In the nervous system, glial EVs have been involved both in regulation of neuroinflammation (Dickens et al., 2017; Kumar et al., 2017; Li et al., 2018), and in mechanisms

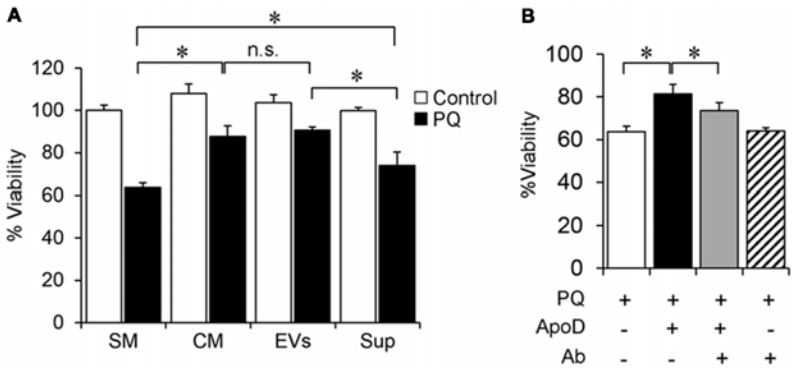

FIGURE 5 | Astroglial EVs promote neuronal survival. **(A)** SH-SY5Y neurons viability in control and oxidative stress (OS) conditions [2 mM paraquat (PQ) for 2 h], measured by the 3-(4,5-dimethylthiazol-2-yl)-2, 5-diphenyltetrazolium bromide (MTT) assay after culture in SM, astrocyte-CM, purified astrocyte EVs, or EV-depleted astrocyte-derived supernatant, Sup. **(B)** Cell viability of PQ-challenged SH-SY5Y neurons (2 mM PQ for 2 h) in the absence or presence of purified native ApoD and/or an equimolar amount of anti-ApoD antibody. Error bars represent SEM ($n = 3$ independent experiments with three technical replicas each). Asterisks represent significant differences ($p < 0.01$) assessed by ANOVA with Holm-Sidak *post hoc* method. (n.s.: non-significant differences) Only the most relevant comparisons are pointed.

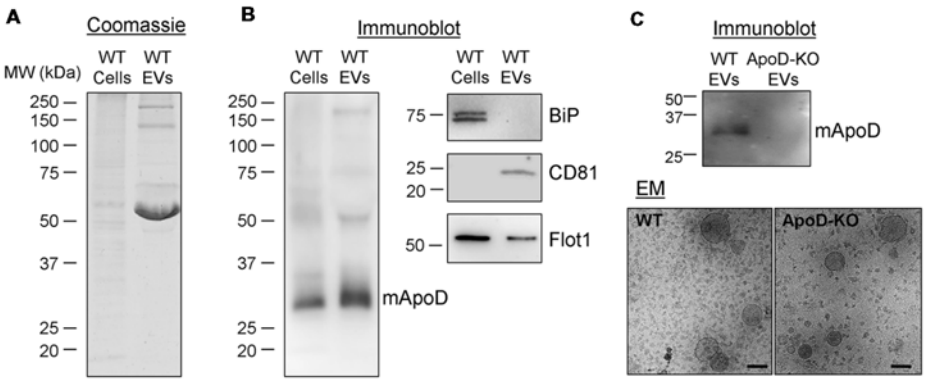

FIGURE 6 | Primary murine astrocytes produce ApoD-positive EVs. **(A)** Coomassie blue staining of whole cell extracts and EV preparation (240 times concentrated, relative to the starting cell culture) from wild-type (WT) primary astrocytes. **(B)** Immunoblot analysis of ApoD, the endoplasmic reticulum marker BiP, and the EV markers CD81 and flotillin-1 in cell lysates and EV preparations from WT primary astrocytes. No signal of BiP is detected in the EV preparation. Intracellular CD81 is not detectable in the cell extract. **(C)** Immunoblot analysis of ApoD in WT and ApoD-knock-out (KO) primary astrocyte EV preparations, confirming the presence of ApoD in WT EVs. Immunoelectron microscopy images of WT and ApoD-KO EVs. Calibration bars: 100 nm.

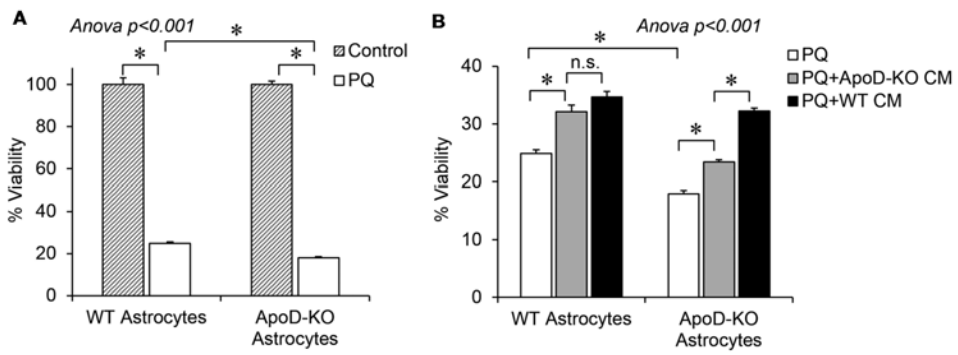

FIGURE 7 | Extracellular ApoD mediates autocrine protection of primary murine astrocytes. **(A)** Percent viability estimated by the MTT assay of WT and ApoD-KO primary astrocytes cultured in SM, in either control or upon an OS challenge with PQ (500 μM, 2 h). ApoD-KO astrocytes are significantly more vulnerable to PQ than WT astrocytes. **(B)** PQ challenge was performed either on SM (white bars), or in astrocyte-CM, either derived from ApoD-KO astrocytes (gray bars) or from WT astrocytes (black bars). Effect of CM on ApoD-KO astrocyte viability is dependent on the genotype of CM origin. Error bars represent SEM ($n = 3$ independent experiments with three technical replicas each). Asterisks point to significant differences ($p < 0.01$) assessed by ANOVA with Holm-Sidak *post hoc* method (n.s.: non-significant differences). Only the most relevant comparisons are pointed.

triggering neuroprotection (Lopez-Verrilli et al., 2013; Guitart et al., 2016).

The production of ROS and a concomitant inflammatory response have been classically considered a negative side-effect of tissue damage that hampers nervous system recovery upon aging and neurodegeneration. Consequently, great efforts have been made to identify antioxidants that can mediate neuroprotection through improvement of neuronal survival and axonal regeneration. However, a recent report has demonstrated that ROS can also play a positive pro-regenerative role upon neural damage by a mechanism based on glia-neuron EV-mediated Nox2-PI3K–pAkt signaling (Hervera et al., 2018). How can a cell control the side effects of ROS, and the levels that can be managed without tilting the equilibrium towards cell-death?

The Lipocalin ApoD has been demonstrated to be a neuroprotectant by controlling the levels of lipid peroxides generated by ROS accumulation with aging or pathological conditions (Ganfornina et al., 2008; Li et al., 2015; Sanchez et al., 2015; Pascua-Maestro et al., 2017). The neuroprotection exerted by ApoD not only influences ApoD-expressing cells such as astrocytes and myelinating glia, but also affects neurons in a paracrine manner (Bajo-Grañeras et al., 2011; Pascua-Maestro et al., 2017). The presence of a signal peptide in the unprocessed protein and the experimentally verified presence of the mature protein in organelles of the canonical secretion pathway and in the extracellular milieu (Pascua-Maestro et al., 2017), result in the annotation of ApoD as a secreted protein (UniProtKB-P51910/P05090). This property was assumed in the interpretation of our previous studies reporting ApoD traffic in astrocytes and neurons under control or OS conditions (Pascua-Maestro et al., 2017).

The results presented in this work link ApoD traffic to the EV compartment of astrocytes, where it appears very specifically in the exosomal subtype of EVs, as determined by the co-expression of classical markers such as CD81 (Tkach et al., 2018). More importantly, the neuroprotective effect that ApoD exerts upon OS-challenged neurons or astrocytes must be entirely based on the protein present in the EVs supplied by reactive astrocytes, since no neuronal ApoD expression is triggered by the EVs, and no incorporation of astrocyte-derived ApoD is detected when EVs have been removed from the astrocyte-CM.

This result agrees with other reports showing that non-neural cells exposed to ROS release EVs that carry OS response proteins and antioxidants (Saeed-Zidane et al., 2017; Chettimada et al., 2018). The fact that EV-associated human ApoD is detected both as monomers and dimers (**Figure 4**), is a readout of its antioxidant activity, since it is known that a consequence of its lipid reducing activity is the formation of stable dimers (Bhatia et al., 2012) that accumulate in advanced stages of Alzheimer's disease patients (Bhatia et al., 2013). Since we know that the1321N1 astrocytic cell line has a basal level of OS (Pascua-Maestro et al., 2017), it is not surprising that they are already targeting the redox pair reduced/oxidized-ApoD to exosomes.

The discovery of ApoD in glia-derived EVs, and particularly in exosome-like fractions, reframes our understanding of the neuroprotective role of this Lipocalin. The capability of EVs to cross the blood-brain barrier (Krämer-Albers, 2017) opens up new research avenues to explore the use of systemically administered ApoD-positive exosomes to treat neurodegenerative diseases.

AUTHOR CONTRIBUTIONS

RP-M, MG, JF-P and DS conceived and designed the project. RP-M, EG, CL and MG designed and performed the experiments. RP, EG, JF-P and DS analyzed the data. DS, MG and JF-P supervised the project. RP-M, EG, CL, JF-P, MG and DS wrote the article.

FUNDING

This work was supported by grants to MG and DS [Ministerio de Ciencia e Innovación (MICINN) grants BFU2011-23978 and BFU2015-68149-R, co-financed by European Regional Development Fund], and by grant to JF-P SAF2015-66312 (Spanish Ministry of Economy and Competitiveness, Ministerio de Economía y Competitividad MINECO). RP-M was supported by a Junta de Castilla y León (JCyL) fellowship to young researchers (call#EDU/1883/2013), financed by the European Social Fund, Operational Programme for Castilla y León and managed by Consejería de Educación (JCyL) and by 1st GEIVEX mobility fellowship. The funders had no role in study design, data collection and analysis, decision to publish, or preparation of the manuscript.

ACKNOWLEDGMENTS

We thank C. Sánchez-Vicente and Y. Noriega at the IBGM Confocal Microscopy Service for technical assistance. C. Pérez-Segurado provided technical support throughout the project. We thank Sergio Diez-Hermano and Miriam Corraliza-Gómez for helpful discussions and inspiring ideas.

REFERENCES

Alvarez-Erviti, L., Seow, Y., Yin, H., Betts, C., Lakhal, S., and Wood, M. J. (2011). Delivery of siRNA to the mouse brain by systemic injection of targeted exosomes. *Nat. Biotechnol.* 29, 341–345. doi: 10.1038/nbt.1807

Bajo-Grañeras, R., Ganfornina, M. D., Martín-Tejedor, E., and Sanchez, D. (2011). Apolipoprotein D mediates autocrine protection of astrocytes and controls their reactivity level, contributing to the functional maintenance of paraquat-challenged dopaminergic systems. *Glia* 59, 1551–1566. doi: 10.1002/glia.21200

Basso, M., and Bonetto, V. (2016). Extracellular vesicles and a novel form of communication in the brain. *Front. Neurosci.* 10:127. doi: 10.3389/fnins.2016.00127

Bhatia, S., Jenner, A. M., Li, H., Ruberu, K., Spiro, A. S., Shepherd, C. E., et al. (2013). Increased apolipoprotein D dimer formation in Alzheimer's disease hippocampus is associated with lipid conjugated diene levels. *J. Alzheimers Dis.* 35, 475–486. doi: 10.3233/JAD-122278

Bhatia, S., Knoch, B., Wong, J., Kim, W. S., Else, P. L., Oakley, A. J., et al. (2012). Selective reduction of hydroperoxyeicosatetraenoic acids to their hydroxy

derivatives by apolipoprotein D: implications for lipid antioxidant activity and Alzheimer's disease. *Biochem. J.* 442, 713–721. doi: 10.1042/BJ20111166

Cheow, E. S., Cheng, W. C., Lee, C. N., de Kleijn, D., Sorokin, V., and Sze, S. K. (2016). Plasma-derived extracellular vesicles contain predictive biomarkers and potential therapeutic targets for myocardial ischemic (MI) injury. *Mol. Cell. Proteomics* 15, 2628–2640. doi: 10.1074/mcp.M115.055731

Chettimada, S., Lorenz, D. R., Misra, V., Dillon, S. T., Reeves, R. K., Manickam, C., et al. (2018). Exosome markers associated with immune activation and oxidative stress in HIV patients on antiretroviral therapy. *Sci. Rep.* 8:7227. doi: 10.1038/s41598-018-25515-4

Croese, T., and Furlan, R. (2018). Extracellular vesicles in neurodegenerative diseases. *Mol. Aspects Med.* 60, 52–61. doi: 10.1016/j.mam.2017.11.006

Dassati, S., Waldner, A., and Schweigreiter, R. (2014). Apolipoprotein D takes center stage in the stress response of the aging and degenerative brain. *Neurobiol. Aging* 35, 1632–1642. doi: 10.1016/j.neurobiolaging.2014.01.148

Dickens, A. M., Tovar-Y-Romo, L. B., Yoo, S. W., Trout, A. L., Bae, M., Kanmogne, M., et al. (2017). Astrocyte-shed extracellular vesicles regulate the peripheral leukocyte response to inflammatory brain lesions. *Sci. Signal.* 10:eaai7696. doi: 10.1126/scisignal.aai7696

Dragovic, R. A., Gardiner, C., Brooks, A. S., Tannetta, D. S., Ferguson, D. J., Hole, P., et al. (2011). Sizing and phenotyping of cellular vesicles using Nanoparticle Tracking Analysis. *Nanomedicine* 7, 780–788. doi: 10.1016/j.nano.2011.04.003

Escola, J. M., Kleijmeer, M. J., Stoorvogel, W., Griffith, J. M., Yoshie, O., and Geuze, H. J. (1998). Selective enrichment of tetraspan proteins on the internal vesicles of multivesicular endosomes and on exosomes secreted by human B-lymphocytes. *J. Biol. Chem.* 273, 20121–20127. doi: 10.1074/jbc.273.32.20121

Frühbeis, C., Fröhlich, D., Kuo, W. P., Amphornrat, J., Thilemann, S., Saab, A. S., et al. (2013a). Neurotransmitter-triggered transfer of exosomes mediates oligodendrocyte-neuron communication. *PLoS Biol.* 11:e1001604. doi: 10.1371/journal.pbio.1001604

Frühbeis, C., Fröhlich, D., Kuo, W. P., and Krämer-Albers, E. M. (2013b). Extracellular vesicles as mediators of neuron-glia communication. *Front. Cell. Neurosci.* 7:182. doi: 10.3389/fncel.2013.00182

Ganfornina, M. D., Do Carmo, S., Lora, J. M., Torres-Schumann, S., Vogel, M., Allhorn, M., et al. (2008). Apolipoprotein D is involved in the mechanisms regulating protection from oxidative stress. *Aging Cell* 7, 506–515. doi: 10.1111/j.1474-9726.2008.00395.x

Ganfornina, M. D., Do Carmo, S., Martinez, E., Tolivia, J., Navarro, A., Rassart, E., et al. (2010). ApoD, a glia-derived apolipoprotein, is required for peripheral nerve functional integrity and a timely response to injury. *Glia* 58, 1320–1334. doi: 10.1002/glia.21010

García-Mateo, N., Ganfornina, M. D., Montero, O., Gijón, M. A., Murphy, R. C., and Sanchez, D. (2014). Schwann cell-derived Apolipoprotein D controls the dynamics of post-injury myelin recognition and degradation. *Front. Cell. Neurosci.* 8:374. doi: 10.3389/fncel.2014.00374

Guitart, K., Loers, G., Buck, F., Bork, U., Schachner, M., and Kleene, R. (2016). Improvement of neuronal cell survival by astrocyte-derived exosomes under hypoxic and ischemic conditions depends on prion protein. *Glia* 64, 896–910. doi: 10.1002/glia.22963

György, B., Szabó, T. G., Pásztói, M., Pál, Z., Misják, P., Aradi, B., et al. (2011). Membrane vesicles, current state-of-the-art: emerging role of extracellular vesicles. *Cell. Mol. Life Sci.* 68, 2667–2688. doi: 10.1007/s00018-011-0689-3

Hervera, A., De Virgiliis, F., Palmisano, I., Zhou, L., Tantardini, E., Kong, G., et al. (2018). Reactive oxygen species regulate axonal regeneration through the release of exosomal NADPH oxidase 2 complexes into injured axons. *Nat. Cell Biol.* 20, 307–319. doi: 10.1038/s41556-018-0039-x

Holm, M. M., Kaiser, J., and Schwab, M. E. (2018). Extracellular vesicles: multimodal envoys in neural maintenance and repair. *Trends Neurosci.* 41, 360–372. doi: 10.1016/j.tins.2018.03.006

Kalra, H., Simpson, R. J., Ji, H., Aikawa, E., Altevogt, P., Askenase, P., et al. (2012). Vesiclepedia: a compendium for extracellular vesicles with continuous community annotation. *PLoS Biol.* 10:e1001450. doi: 10.1371/journal.pbio.1001450

Keerthikumar, S., Chisanga, D., Ariyaratne, D., Al Saffar, H., Anand, S., Zhao, K., et al. (2015). ExoCarta: a web-based compendium of exosomal cargo. *J. Mol. Biol.* 428, 688–692. doi: 10.1016/j.jmb.2015.09.019

Kharaziha, P., Chioureas, D., Rutishauser, D., Baltatzis, G., Lennartsson, L., Fonseca, P., et al. (2015). Molecular profiling of prostate cancer derived exosomes may reveal a predictive signature for response to docetaxel. *Oncotarget* 6, 21740–21754. doi: 10.18632/oncotarget.3226

Kim, D. K., Lee, J., Kim, S. R., Choi, D. S., Yoon, Y. J., Kim, J. H., et al. (2015). EVpedia: a community web portal for extracellular vesicles research. *Bioinformatics* 31, 933–939. doi: 10.1093/bioinformatics/btu741

Krämer-Albers, E. M. (2017). Ticket to ride: targeting proteins to exosomes for brain delivery. *Mol. Ther.* 25, 1264–1266. doi: 10.1016/j.ymthe.2017.05.001

Kumar, A., Stoica, B. A., Loane, D. J., Yang, M., Abulwerdi, G., Khan, N., et al. (2017). Microglial-derived microparticles mediate neuroinflammation after traumatic brain injury. *J. Neuroinflammation* 14:47. doi: 10.1186/s12974-017-0819-4

Li, Q., Lau, A., Morris, T. J., Guo, L., Fordyce, C. B., and Stanley, E. F. (2004). A syntaxin 1, $G\alpha_o$, and N-type calcium channel complex at a presynaptic nerve terminal: analysis by quantitative immunocolocalization. *J. Neurosci.* 24, 4070–4081. doi: 10.1523/JNEUROSCI.0346-04.2004

Li, H., Ruberu, K., Muñoz, S. S., Jenner, A. M., Spiro, A., Zhao, H., et al. (2015). Apolipoprotein D modulates amyloid pathology in APP/PS1 Alzheimer's disease mice. *Neurobiol. Aging* 36, 1820–1833. doi: 10.1016/j.neurobiolaging.2015.02.010

Li, J. J., Wang, B., Kodali, M. C., Chen, C., Kim, E., Patters, B. J., et al. (2018). *In vivo* evidence for the contribution of peripheral circulating inflammatory exosomes to neuroinflammation. *J. Neuroinflammation* 15:8. doi: 10.1186/s12974-017-1038-8

Loerch, P. M., Lu, T., Dakin, K. A., Vann, J. M., Isaacs, A., Geula, C., et al. (2008). Evolution of the aging brain transcriptome and synaptic regulation. *PLoS One* 3:e3329. doi: 10.1371/journal.pone.0003329

Lopez-Verrilli, M. A., Picou, F., and Court, F. A. (2013). Schwann cell-derived exosomes enhance axonal regeneration in the peripheral nervous system. *Glia* 61, 1795–1806. doi: 10.1002/glia.22558

Müller, G. (2012). Microvesicles/exosomes as potential novel biomarkers of metabolic diseases. *Diabetes Metab. Syndr. Obes.* 5, 247–282. doi: 10.2147/DMSO.S32923

Nakamura, K., Watakabe, A., Hioki, H., Fujiyama, F., Tanaka, Y., Yamamori, T., et al. (2007). Transiently increased colocalization of vesicular glutamate transporters 1 and 2 at single axon terminals during postnatal development of mouse neocortex: a quantitative analysis with correlation coefficient. *Eur. J. Neurosci.* 26, 3054–3067. doi: 10.1111/j.1460-9568.2007.05868.x

Navarro, J. A., Ohmann, E., Sanchez, D., Botella, J. A., Liebisch, G., Moltó, M. D., et al. (2010). Altered lipid metabolism in a *Drosophila* model of Friedreich's ataxia. *Hum. Mol. Genet.* 19, 2828–2840. doi: 10.1093/hmg/ddq183

Pandya, R. S., Zhu, H., Li, W., Bowser, R., Friedlander, R. M., and Wang, X. (2013). Therapeutic neuroprotective agents for amyotrophic lateral sclerosis. *Cell. Mol. Life Sci.* 70, 4729–4745. doi: 10.1007/s00018-013-1415-0

Pascua-Maestro, R., Corraliza-Gomez, M., Diez-Hermano, S., Perez-Segurado, C., Ganfornina, M. D., and Sanchez, D. (2018). The MTT-formazan assay: complementary technical approaches and *in vivo* validation in *Drosophila* larvae. *Acta Histochem.* 120, 179–186. doi: 10.1016/j.acthis.2018.01.006

Pascua-Maestro, R., Diez-Hermano, S., Lillo, C., Ganfornina, M. D., and Sanchez, D. (2017). Protecting cells by protecting their vulnerable lysosomes: identification of a new mechanism for preserving lysosomal functional integrity upon oxidative stress. *PLoS Genet.* 13:e1006603. doi: 10.1371/journal.pgen.1006603

Perdomo, G., and Henry Dong, H. (2009). Apolipoprotein D in lipid metabolism and its functional implication in atherosclerosis and aging. *Aging* 1, 17–27. doi: 10.18632/aging.100004

Przybycien-Szymanska, M. M., Yang, Y., and Ashley, W. W. (2016). Microparticle derived proteins as potential biomarkers for cerebral vasospasm post subarachnoid hemorrhage. A preliminary study. *Clin. Neurol. Neurosurg.* 141, 48–55. doi: 10.1016/j.clineuro.2015.12.012

Reindl, M., Knipping, G., Wicher, I., Dilitz, E., Egg, R., Deisenhammer, F., et al. (2001). Increased intrathecal production of apolipoprotein D in multiple sclerosis. *J. Neuroimmunol.* 119, 327–332. doi: 10.1016/s0165-5728(01)00378-2

Ridder, K., Keller, S., Dams, M., Rupp, A.-K., Schlaudraff, J., Del Turco, D., et al. (2014). Extracellular vesicle-mediated transfer of genetic information between the hematopoietic system and the brain in response to inflammation. *PLoS Biol.* 12:e1001874. doi: 10.1371/journal.pbio.1001874

Rufino-Ramos, D., Albuquerque, P. R., Carmona, V., Perfeito, R., Nobre, R. J., and Pereira de Almeida, L. (2017). Extracellular vesicles: novel promising delivery systems for therapy of brain diseases. *J. Control. Release* 262, 247–258. doi: 10.1016/j.jconrel.2017.07.001

Ruiz, M., Ganfornina, M. D., Correnti, C., Strong, R. K., and Sanchez, D. (2013). Ligand binding-dependent functions of the lipocalin NLaz: an *in vivo* study in *Drosophila*. *FASEB J.* 28, 1555–1567. doi: 10.1096/fj.13-240556

Saeed-Zidane, M., Linden, L., Salilew-Wondim, D., Held, E., Neuhoff, C., Tholen, E., et al. (2017). Cellular and exosome mediated molecular defense mechanism in bovine granulosa cells exposed to oxidative stress. *PLoS One* 12:e0187569. doi: 10.1371/journal.pone.0187569

Salomon, C., Kobayashi, M., Ashman, K., Sobrevia, L., Mitchell, M. D., and Rice, G. E. (2013). Hypoxia-induced changes in the bioactivity of cytotrophoblast-derived exosomes. *PLoS One* 8:e79636. doi: 10.1371/journal.pone.0079636

Sanchez, D., Bajo-Grañeras, R., Del Caño-Espinel, M., Garcia-Centeno, R., Garcia-Mateo, N., Pascua-Maestro, R., et al. (2015). Aging without Apolipoprotein D: molecular and cellular modifications in the hippocampus and cortex. *Exp. Gerontol.* 67, 19–47. doi: 10.1016/j.exger.2015.04.003

Sánchez, D., Ganfornina, M. D., and Martínez, S. (2002). Expression pattern of the lipocalin apolipoprotein D during mouse embryogenesis. *Mech. Dev.* 110, 225–229. doi: 10.1016/s0925-4773(01)00578-0

Spencer, B., Verma, I., Desplats, P., Morvinski, D., Rockenstein, E., Adame, A., et al. (2014). A neuroprotective brain-penetrating endopeptidase fusion protein ameliorates Alzheimer disease pathology and restores neurogenesis. *J. Biol. Chem.* 289, 17917–17931. doi: 10.1074/jbc.M114.557439

Suresh, S., Yan, Z., Patel, R. C., Patel, Y. C., and Patel, S. C. (1998). Cellular cholesterol storage in the Niemann-Pick disease type C mouse is associated with increased expression and defective processing of apolipoprotein D. *J. Neurochem.* 70, 242–251. doi: 10.1046/j.1471-4159.1998.70010242.x

Taylor, D. D. (2015). Isolation and molecular characterization of extracellular vesicles. *Methods* 87, 1–2. doi: 10.1016/j.ymeth.2015.08.006

Tkach, M., Kowal, J., and Théry, C. (2018). Why the need and how to approach the functional diversity of extracellular vesicles. *Philos. Trans. R. Soc. Lond. B Biol. Sci.* 373:20160479. doi: 10.1098/rstb.2016.0479

Valadi, H., Ekstrom, K., Bossios, A., Sjostrand, M., Lee, J. J., and Lötvall, J. O. (2007). Exosome-mediated transfer of mRNAs and microRNAs is a novel mechanism of genetic exchange between cells. *Nat. Cell Biol.* 9, 654–659. doi: 10.1038/ncb1596

Conflict of Interest Statement: The authors declare that the research was conducted in the absence of any commercial or financial relationships that could be construed as a potential conflict of interest.

frontiers in Cellular Neuroscience

REVIEW
published: 23 January 2019
doi: 10.3389/fncel.2019.00002

Phosphatidic Acid: From Pleiotropic Functions to Neuronal Pathology

Emeline Tanguy[1], *Qili Wang*[1], *Hervé Moine*[2] *and Nicolas Vitale*[1]*

[1]Institut des Neurosciences Cellulaires et Intégratives (INCI), UPR-3212 Centre National de la Recherche Scientifique & Université de Strasbourg, Strasbourg, France, [2]Institut de Génétique et de Biologie Moléculaire et Cellulaire (IGBMC), CNRS UMR 7104, INSERM U964, Université de Strasbourg, Illkirch-Graffenstaden, France

Among the cellular lipids, phosphatidic acid (PA) is a peculiar one as it is at the same time a key building block of phospholipid synthesis and a major lipid second messenger conveying signaling information. The latter is thought to largely occur through the ability of PA to recruit and/or activate specific proteins in restricted compartments and within those only at defined submembrane areas. Furthermore, with its cone-shaped geometry PA locally changes membrane topology and may thus be a key player in membrane trafficking events, especially in membrane fusion and fission steps, where lipid remodeling is believed to be crucial. These pleiotropic cellular functions of PA, including phospholipid synthesis and homeostasis together with important signaling activity, imply that perturbations of PA metabolism could lead to serious pathological conditions. In this mini-review article, after outlining the main cellular functions of PA, we highlight the different neurological diseases that could, at least in part, be attributed to an alteration in PA synthesis and/or catabolism.

OPEN ACCESS

Edited by:
Gabriela Alejandra Salvador, Universidad Nacional del Sur, Argentina

Reviewed by:
Richard M. Epand, McMaster University, Canada
Daniel M. Raben, Johns Hopkins University, United States

***Correspondence:**
Nicolas Vitale
vitalen@unistra.fr

Received: 22 October 2018
Accepted: 07 January 2019
Published: 23 January 2019

Citation:
Tanguy E, Wang Q, Moine H and Vitale N (2019) Phosphatidic Acid: From Pleiotropic Functions to Neuronal Pathology. Front. Cell. Neurosci. 13:2. doi: 10.3389/fncel.2019.00002

Keywords: lipid signaling, neuron, neuropathology, phosphatidic acid, phospholipase D

INTRODUCTION

Phosphatidic acid (PA) is a low abundant phospholipid of membranes that, nevertheless, constitutes the original building block from which most glycerophospholipids are synthesized, thus plays an important structural task. Interestingly it was later shown that PA also acts to transmit, amplify, and regulate a great number of intracellular signaling pathways and cellular functions. In cells, PA can be synthesized through different enzymatic pathways (Ammar et al., 2014). Structural PA results from two successive acylation reactions (**Figure 1**). Signaling PA instead, results from three biosynthesis alternative pathways. The first pathway includes the phosphorylation of diacylglycerol (DAG) by any of the 10 DAG-kinases (DGKs) in mammals (**Figure 1**). Hydrolysis of the distal phosphodiester bond in phospholipids by phospholipases D (PLD) constitutes the second pathway (**Figure 1**). Although six different PLDs have been identified in mammals, only PLD1/2 and PLD6 have been shown to synthesize PA from phosphatidylcholine (PC) and cardiolipin (CL), respectively (Jang et al., 2012). The third and final biosynthetic pathway involves acylation of lyso-PA by lyso-PA-acyltransferase (LPAAT) enzymes (**Figure 1**).

Chemically, PA is composed of a glycerol backbone esterified with two fatty acyl chains at positions C-1 and C-2, and with a phosphate at position C-3. The latter confers the specific features of PA compared to the other diacyl–glycerophospholipids. Indeed, the small anionic phosphate headgroup provides to PA a combination of unique cone-shaped geometry and negative charge (Jenkins and Frohman, 2005). At the molecular level, these two characteristics enable PA both to

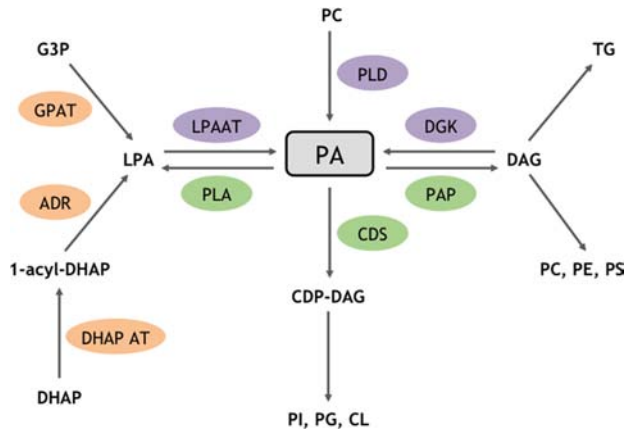

FIGURE 1 | Enzymatic routes for structural and signaling PA metabolism. PA is a major phospholipid for biosynthetic and signaling reactions. Enzymes highlighted in orange are involved in biosynthetic reactions that produce structural PA, whereas enzymes triggering the formation of signaling pools of PA are shown in purple. Enzymes responsible for PA catabolism are shown in green. ADR, Acyldihydroxyacetone-phosphate reductase; CDP, cytidyl phosphatidate; CDS, CDP-diacylglycerol (DAG) synthase; CL, cardiolipin; DHAP, dihydroxyacétone phosphate; DHAP AT, dihydroxyacétone phosphate acyltransferase; G3P, glycerol 3-phosphate; GPAT, glycerol phosphate acyltransferase; PAP, phosphatidic acid phosphatase; PC, phosphatidylcholine; PG, phosphatidylglycerol; PE, phosphatidylethanolamine; PI, phosphatidylinositol; PS, phosphatidylserine; PLA, phospholipase A; TG, triglyceride.

interact with different enzymes to regulate their catalytic activity and/or their association with membrane compartments and also to affect membrane geometry by creating local negative curvatures (Kooijman et al., 2003). As a consequence, PA has been involved in various important cellular functions including membrane trafficking events where membrane rearrangements are necessary (Bader and Vitale, 2009). In this article, we will present some of the most studied PA identified partners, summarize the most well-described cellular processes that require PA and discuss the potential involvement of an alteration in PA synthesis and/or catabolism in different neurological diseases.

PA INTERACTS WITH AND RECRUITS NUMEROUS PROTEINS TO MEMBRANES

Having an overall view of the interaction network of a given molecule is particularly helpful for deciphering the relationships between the constituents of interactomes and characterizing their function in cell signaling. Since the early description of a handful of proteins that bind to PA, at least using the minimal *in vitro* protein-lipid overlay assay, an extensive list of PA interactors has only emerged more recently (Stace and Ktistakis, 2006). For at least some of those, their interaction with PA appears rather specific with little or no interaction with other negatively charged lipids. The position of PA's phosphomonoester headgroup in proximity of the interface of acyl chain headgroup was proposed to be important for binding to specific proteins. Supporting the physiological importance of interactions between PA and proteins, numerous proteins have gained domains that display some level of binding specificity for PA (Jang et al., 2012). Although no clear PA-binding domain can be defined at the three dimensional or secondary structural levels, different factors can influence PA interaction with specific domains in target proteins (Tanguy et al., 2018). For instance, we and others have found that some PA-binding modules possess some levels of specificity for the fatty acyl chains of PA (Kassas et al., 2017). In addition, the local membrane environment surrounding PA also appears to modulate PA binding to these modules (Kassas et al., 2017). Finally, it is most likely that PA-binding domains act first through positively charged residues that initially sample for the negative charge of PA buried within the membrane. This first step is probably followed by a docking state where hydrophobic interaction between hydrophobic residues of the module and the fatty acyl chains of PA stabilize the PA-protein interaction (Potocký et al., 2014; Tanguy et al., 2018). At present, more than 50 different proteins have been shown to directly interact with PA, as extensively reviewed in Jang et al. (2012). Briefly, these PA interactors can be classified in four major families.

Nucleotide-Binding Proteins

Nucleotide (ATP, cAMP, GTP)-binding proteins are important signaling proteins for which the activity is usually regulated by nucleotide binding. Noticeably, the localization and/or activity of many of those proteins are also controlled by PA interaction. This is for instance the case for some of the small GTP-binding proteins of the ADP ribosylation factor (Arf) and Rho (Ras homologous) families that are key players in cytoskeleton remodeling and membrane dynamics. The minimal PA-binding regions of these small GTPases remains however to be defined precisely. Several c-AMP specific phosphodiesterases also interact with PA through their amino-terminal regulatory domains leading to an increase of their enzymatic activity and therefore to a reduction of cAMP levels.

Regulators of GTP-Binding Proteins

The GTPase-activating proteins ArfGAP with GTPase Domain, Ankyrin Repeat and PH domain 1 (AGAP1) and Regulator of G protein Signaling 4 (RGS4) are negative regulators of Arf and Gα GTP-binding proteins, respectively. Intriguingly, while PA stimulates the GTP-hydrolysis activity of AGAP1, it inhibits that of RGS4, highlighting the multiple and sometimes opposite actions of PA on GTP-binding activity. Furthermore, PA has also been shown to recruit and activate different guanine nucleotide-exchange proteins for small GTPases, such as DedicatOr of CytoKinesis 2 (DOCK2) and Son Of Sevenless (SOS), promoting GTP-binding and activation of Rac and Ras, respectively. It is therefore important to have in mind that PA enrichment in particular sub-membrane domains could influence in different and sometimes contradictory manners a given signaling pathway involving GTP-binding proteins by acting at different stages.

Kinases

Protein kinases are among the main signaling regulators with nearly 600 different genes. Among those, protein kinase C (PKC) is one of the largest subgroup and PA modulates the activity of several PKC isoforms. PA also promotes recruitment and activation of the proto-oncogene kinase Raf, acting as a gatekeeper in the ERK1/2 pathway. In addition, PA binding to the FKBP12-rapamycin binding region of mTOR is in competition with FKBP12/rapamycin complex of mTOR and is thus likely to influence nutrient sensing and cell proliferation.

Furthermore, lipid kinases contribute to the great diversity of lipids in cells. Among those, PA is capable to stimulate the action of phosphatidylinositol (PI) 4-phosphate 5-kinase (PI4P5K), to promote the synthesis of PI 4,5-bisphosphate ($PI(4,5)P_2$), a key signaling lipid (Stace and Ktistakis, 2006; Bader and Vitale, 2009). Finally, cytosolic sphingosine kinase that transforms sphingosine into sphingosine-phosphate appears to translocate to the plasma membrane under the control of PA levels, which most likely affects the signaling pathways involving these two lipids. In conclusion, PA binding modules are found in members of the two major kinase families and consequently, the presence of PA in local membrane composition is expected to influence crucial signaling nodes and the various associated key cellular functions.

Phosphatases

In addition to kinases, phosphatases constitute the second important family of signaling proteins that modulate protein activity by removing the phosphate residues added by kinases. The protein-tyrosine phosphatase SHP-1 that negatively modulates signaling pathways involving receptor-tyrosine kinase directly interacts with PA therefore triggering phosphatase activity. Furthermore, PA inhibits the enzymatic activity of protein phosphatase 1 (PP1), involved in many cellular activities such as the metabolism of glycogen, the processing of RNA, and the regulation of cell cycle. In conclusion, although not as well described as for kinases, the regulation of several phosphatases by PA offers the possibility of complex and often paradoxical regulation of signaling pathway by a single lipid family.

THE PLEIOTROPIC CELLULAR FUNCTIONS OF PA

Actin Cytoskeleton Dynamics

Most cellular functions are influenced by precise cell shapes that are under the control of the cytoskeleton proteins network. Among those the dynamics of the cytoskeleton depends on the formation of actin filaments from a pool of cytosolic monomers, and their subsequent association to each other or to cell membranes, pursued by their depolymerization. Most cellular functions actually depend on a permanent remodeling of this actin network and this is orchestrated in large part by actin binding proteins. Interestingly lipids such as phosphoinositides modulate the affinity of these proteins for actin. PA, however, has also been proposed to participate to this regulation (Ammar et al., 2014).

In neurons, the Rho GTPases and related proteins, through the control of the cytoskeleton, modulate various aspects of cell shape including not only neurite outgrowth and differentiation, axonal growth and targeting, but also dendritic spine formation and maintenance (Ammar et al., 2014). As mentioned in the sections "Nucleotide-Binding Proteins" and "Regulators of GTP-Binding Proteins," PA synthesized by either PLD or DGK modulates the activity of some different Rho family of GTPases and their regulators by promoting membrane association and/or through the activation of their regulatory proteins (Chae et al., 2008; Nishikimi et al., 2009; Faugaret et al., 2011; Kurooka et al., 2011; Sanematsu et al., 2013). Alternatively, the p21 activated kinases (PAKs) family that regulates various aspects of neuronal development, through actin cytoskeleton reorganization, is also known for being activated by PA (Daniels et al., 1998; Hayashi et al., 2007). Furthermore, $PI(4,5)P_2$ is a major lipid regulator of the cytoskeleton and PA is an essential building block leading to $PI(4,5)P_2$ synthesis (**Figure 1**). In an alternative pathway, PA stimulates the phospholipid kinase PI4P5K, leading to the phosphorylation of the membrane phospholipid PI(4)P and the formation of $PI(4,5)P_2$ (Honda et al., 1999). In consequence, PA potentially regulates the activity of the three mammalian PI4P5K isozymes that have been described to control actin cytoskeleton reorganization (van den Bout and Divecha, 2009; Roach et al., 2012). Finally, PA levels regulate membrane localization and activity of PKC isoforms α, ε and ζ, all of which are known to affect the morphology of the actin cytoskeleton (Jose Lopez-Andreo et al., 2003).

It is also worth noting that direct interaction of PA with actin-binding proteins has been suggested. Among those potential candidates, the actin-binding protein vinculin known to be involved in neurite outgrowth is a good example (Ito et al., 1982; Johnson and Craig, 1995), but the specificity of these observations remains to be firmly established, since vinculin also binds to other negatively charged lipids, such as $PI(4,5)P_2$.

Membrane Remodeling Events

The secretory pathways have evolved through the establishment of specialized subcellular compartments dedicated to specific biochemical tasks. Membrane trafficking events between these compartments enable particular cells of complex organisms to secrete informative molecules such as hormones, cytokines, and neurotransmitters, for long distance inter-cellular communication. In addition to dedicated and specialized protein machineries, trafficking events of the regulated exocytosis and endocytosis steps also involve remarkable membrane rearrangements that rely on specific lipids (Ammar et al., 2013b). Hence, the first direct molecular data suggesting a role for PLD1-generated PA in hormone release were obtained in chromaffin cells, where overexpression of PLD1, injection of a catalytically-inactive PLD1 mutant (Vitale et al., 2001) or PLD1 silencing (Zeniou-Meyer et al., 2007) affected catecholamine release rates. Using similar approaches, PA synthesized by PLD1 was also shown to govern the regulated secretion of insulin from β-pancreatic cells (Waselle et al., 2005), of von Willebrand factor from endothelial cells (Disse et al., 2009), and acrosomal exocytosis from sperm cells (Lopez et al., 2012; Pelletán et al., 2015). An additional contribution for PA in secretion has been established during the early phase

of azurophilic granules release in neutrophils triggered by anti-neutrophil cytoplasmic antibodies (Williams et al., 2007). Ultimately, different enzymes controlling PA metabolism such as PLDs, LPAATs and DGKs have been proposed to regulate neurotransmission in several neuronal models, suggesting that PA regulates synaptic vesicle release and cycle (Humeau et al., 2001; Schwarz et al., 2011; Tabet et al., 2016a,b; Raben and Barber, 2017).

Intense membrane remodeling also occurs in specialized phagocytic cells, such as in macrophages. Indeed, the ingestion of pathogens, cell debris, or any other solid particle through the formation of phagosomes requires plasma membrane extension and either local lipid synthesis, transfer, or vesicular fusion. PA synthesis by PLD2 has been shown to be important for this early step of phagocytosis, while PA synthesis by PLD1 appears to be also important for the later step of phagosome maturation (Corrotte et al., 2006, 2010). Of note, PA transfer from the ER to plasma membrane during "frustrated phagocytosis," a model where macrophages are plated on IgG-coated plates, has also been suggested to occur from experiments using a combination of lipidomic analysis performed on subcellular fractions and novel PA sensors (Kassas et al., 2017). Furthermore, PA is involved in the invasion and exit of infected cells by apicomplexan parasites (Bullen et al., 2016). It was shown that PA is required for the release of adhesins, perforins and proteases from specialized organelles from these parasites called micronemes (Bullen et al., 2016).

Additional intracellular trafficking events involving intense membrane remodeling have also been shown to require modification in PA levels. To cite only a few, we can also mention that PA critically regulates vesicle budding from the Golgi (Yang et al., 2008), autophagy (Holland et al., 2016), and exosome release (Ghossoub et al., 2014). The mechanisms by which PA promotes membrane rearrangements remain however an unsolved issue (**Figure 2**). The first proposed mode of action of PA in membrane remodeling may depends on its ability to induce membrane curvature and promote fusion, but its ability to specifically regulate the activity of different proteins involved in the vesicle docking and/or recruit crucial fusion proteins has also been proposed (Tanguy et al., 2016, 2018). In a simplified model for membrane fusion a mixture of lipids and proteins appear to be crucial at the fusion site (Tanguy et al., 2016). In principle the intrinsic negative curvatures of accumulating cone-shaped lipids, such as PA in the inner (cis) leaflets of contacting bilayers, should facilitate fusion of merging membranes. But it is worth noting that the promotion of membrane fusion through local modification of membrane curvature also appears to hold true for other cone-shaped lipids such as cholesterol and DAG (Tanguy et al., 2016). Reconstituted membrane fusion assays have been valuable to dissect the role of individual components and on this instance it is important to highlight that PA was observed playing a unique role among cone-shaped lipids in a yeast vacuole fusion assay, suggesting a more complex mode of action of this lipid (Mima and Wickner, 2009). Furthermore, PA could locally accumulate and form microdomains highly negatively charged, which potentially serve as membrane retention sites for several proteins key for exocytosis, such as the SNARE protein syntaxin-1 (Lam et al., 2008), or other membrane remodeling processes (Jenkins and Frohman, 2005). Finally, as a precursor for DAG and PI(4,5)P_2, both known to contribute to numerous membrane remodeling events, PA could also have indirect effects. All these potential contributions of PA in membrane fusion have been reviewed elsewhere (Chasserot-Golaz et al., 2010; Ammar et al., 2013b, 2014; Tanguy et al., 2016), but solving the issue of the mechanistic role of PA in a given membrane remodeling process requires probing these different scenarios (**Figure 2**), which is now in need for novel methods and tools.

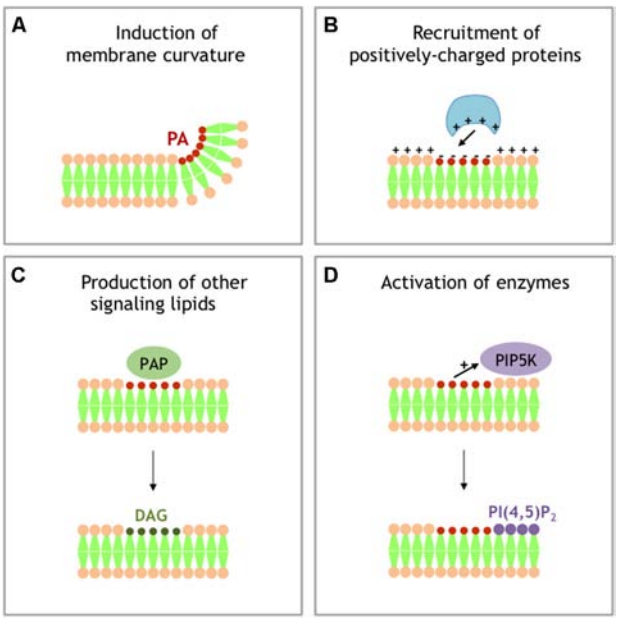

FIGURE 2 | Different models for signaling activity of PA. **(A)** Local accumulation of PA in a single leaflet of membrane generates negative membrane curvature. **(B)** Local accumulation of PA generates local buildup of negative charges that recruit PA effector-containing positively charged domains. **(C)** PAPs transforms PA into DAG, another signaling lipid with specific activity. **(D)** PA stimulates the activity of phosphatidylinositol 4-phosphate 5-kinase (PI4P5K), producing PI 4,5-bisphosphate (PI(4,5)P_2), an additional important signaling lipid.

Apoptosis, Survival, Growth, Proliferation and Migration

Many survival signals including hormones and growth factors activate PA synthesis through the stimulation of PLD activity. Similarly, mitogenic signals trigger cell proliferation, suppression of cell cycle arrest, and prevention of apoptosis. The PLD–PA–Rheb–mTOR and the PLD–PA–MAP kinase pathways are the two main downstream pathways of PLD involved in mitogenic signals and have been described extensively (Foster, 2009). Obviously, future solving of the complex imbrication of these pathways and understanding of the spatiotemporal relationships between PA-generating enzymes, PA-binding partners and PA itself will require development of more specific tools and extensive work.

NEUROLOGICAL DISORDERS POTENTIALLY LINKED TO AN ALTERATION OF PA LEVELS

In all organisms from yeast to mammals, PA was shown to possess signaling activity (Jenkins and Frohman, 2005) and a recent review highlights the apparent mystery of the many roles of PA in plants (Pokotylo et al., 2018). In addition, various PA-generating enzymes were shown to be involved in an increasing number of neuronal pathologies, suggesting a fundamental role of PA in the outcome of these neurodiseases (Tanguy et al., 2018). In the next chapter, we will describe four neuronal pathologies that may be the consequence, at least partially, of an alteration in PA dynamics.

Fetal Alcohol Spectrum Disorders

The damaging effects of alcohol drinking during gestation on the developing fetus are extremely well documented (Ehrhart et al., 2018). Fetal alcohol spectrum disorders (FASDs) is a generic term used to define the birth deficiencies that result from prenatal exposure to alcohol that range from mild to severe. These developmental defects on unborn infants have lifelong physical, behavioral, and cognitive disabilities. As alcohol consumption avoidance during pregnancy is in theory easy to achieve, FASD is in fact considered as one of the largest preventable forms of non-genetic birth disabilities associated with intellectual incapacity.

Although the main effort remains prevention of alcohol consumption during pregnancy, it is also important to understand the underlying pathological mechanisms involved in these effects of ethanol. In addition to the well-recognized ethanol and acetaldehyde toxicity, alcohol intensifies oxidative stress causing consequent effects such as DNA, protein and membrane damages. Additionally, it has been known for over three decades that in the presence of 1%–3% of ethanol, the two best characterized mammalian isoforms PLD1 and PLD2 catalyze a transphosphatidylation reaction. In this case alcohol replaces water during PC hydrolysis, and phosphatidyl alcohols are formed at the expense of PA (Jenkins and Frohman, 2005). Thus, in presence of ethanol, phosphatidylethanol is synthesized while PA is not. Since it is likely that phosphatidylethanol cannot replace PA as a signaling molecule, this was used as a trick to "inhibit" PLD activity (actually prevent PA production), but also in assays to quantify PLD activity (Ammar et al., 2014). It was also shown that ethanol inhibits the mitogenic downstream actions of PA on neuron progenitors (Klein, 2005). Furthermore, it was recently shown that both PLD1 and PLD2 strongly contribute to astroglial proliferation induced by IGF-1 (Burkhardt et al., 2014). Therefore, the perturbation of the IGF1-PLD signaling pathway could, at least in part, explain the teratogenic effects of ethanol observed in FASDs.

Neurological Cancers

Glioblastoma is the most frequent and aggressive brain cancer, with an estimated incidence of near five novel cases per 100,000 persons every year in the USA and Europe. Nearly 200,000 persons die from glioblastoma every year worldwide. It is a relatively difficult cancer to diagnose, as the symptoms are mainly non-specific, including headache and nausea, but leading to alterations of neurological functions such as speech, vision, behavior and memory. Like for many cancer tissues, elevated PLD activity was found in glioblastoma, suggesting that an increase in PA levels is a cause and/or consequence of the pathology (Park et al., 2009). At least part of the survival effect of increased PLD activity on glioblastoma appears to involve the Akt pathway (Bruntz et al., 2014). Interestingly, lipidomic analyses revealed that PA levels are altered in the regions that attract glioblastoma cells, indicating that PA levels control the homing process of glioblastoma (Wildburger et al., 2015). Undoubtedly, a better understanding of the multiple functions of PA in brain tumor development and progression may help to improve treatments and subsequently get a better prognosis for this aggressive cancer.

Intellectual Disability Diseases

Intellectual disability diseases are a common state defined by significant restriction in intellectual capacities and adaptive behavior that happen during childhood, with an overall intelligence quotient bellow 70 together with associated reduction in social, daily living and communication skills. These heterogeneous disease conditions affect 1%–3% of all populations and are thought to result from multiple causes, including environmental, chromosomal and monogenetic alterations. Among the several hundreds of genes involved, some affect brain development, neurogenesis, neuronal migration, or synaptic function (Humeau et al., 2009). Below we will briefly describe the data that support the notion of an alteration of PA levels and/or dynamics in the Fragile-X syndrome (FXS) and the Coffin-Lowry syndrome (CLS).

FXS is a neurodevelopmental pathology accountable for the most common inherited form of intellectual infirmity and autism spectrum disorder. It is generally the consequence of the hypermethylation of CGG expansion repeats (>200) in the 5′ untranslated region of the *FMR1* gene leading to transcription silencing. In a recent study, we pointed DGK kinase-κ (DGKκ) mRNA as the foremost target of Fragile Mental Retardation Protein and found an alteration in PA synthesis in neurons cultured from *Fmr1*-knockout mice after group 1 metabotropic glutamate receptor (mGluRI) stimulation (Tabet et al., 2016a). Silencing DGKκ in CA1 pyramidal neurons modified the immature over mature spine ratio and like in the *Fmr1*-knockout mouse phenotype, reduced LTP and increased LTD (Tabet et al., 2016a). Moreover, the typical *Fmr1*-knockout mouse phenotype on dendritic spine morphology was restored back to normal after overexpression of DGKκ (Tabet et al., 2016a). Finally, DGKκ silencing by shRNA in the mouse reiterated autistic behaviors, such as impaired social interaction, hyperactivity and altered nest-building very much like those seen in the *Fmr1*-knockout mouse model (Tabet et al., 2016a). Based on these observations, it was proposed that a major molecular consequence of the loss of FMRP expression in FXS is to prevent DGKκ translation, leading to an alteration in DAG and PA levels in neurons (Tabet et al., 2016b). A main consequence of this imbalance would be the alteration of the downstream signaling

of DAG and PA required for maturation of dendritic spines and establishment of correct synaptic plasticity (Moine and Vitale, 2018).

Loss of function mutations in the gene encoding Ribosomal S6 Kinase 2 (RSK2) lead to CLS, a rare syndromic form of mental retardation that shows X-linked inheritance. However, the molecular bases of the major neuronal alterations of CLS, such as moderate to severe defect in neurodevelopment, remain indefinable. In agreement with the notion that PLD1-generated PA is key to neurite outgrowth, we observed significant delayed in *Pld1* knockout neuron maturation (Ammar et al., 2013a). These observations were as well found in a mouse model for CLS syndrome since *Rsk2* knockout neurons exhibited developmental delay (Ammar et al., 2013a). Furthermore, RSK2 phosphorylates PLD1 at threonine 147 when exocytosis was triggered (Zeniou-Meyer et al., 2008) or during neurite outgrowth (Ammar et al., 2013a) in PC12 cells. A specific sensor for PA revealed an increase in PA levels at the tips of growing neurites in neurons resulting from PLD1 activation (Ammar et al., 2013a). Interestingly, PLD1 was found to be associated with BDNF positive endosomes (Ammar et al., 2015) and with vesicular structures derived from the trans Golgi, co-labeled by the vesicular SNARE VAMP-7/TiVAMP (Ammar et al., 2013a). The fusion efficiency of these PLD1/VAMP-7 vesicles in the growth cone was severely impaired by RSK2 and PLD1 inhibitors, suggesting that both PLD1 and RSK2 are necessary for membrane provision needed during neurite outgrowth (Ammar et al., 2013a). Accordingly, co-immunoprecipitation and confocal colocalization experiments indicated that RSK2 and PLD1 are found in a complex at the tip end of growing neurites, supporting the observation of an increased PA level at this location (Ammar et al., 2013a). Altogether, these results have highlighted the importance of PA-mediated membrane trafficking in neurite outgrowth and a key role of RSK2 in PA synthesis during this process, by phosphorylation and subsequent activation of PLD1. In consequence, it has been proposed that at least some of the clinical consequences of the CLS might result from an inadequate PA production during neuronal development and function (Zeniou-Meyer et al., 2010).

Neurodegeneration

It is becoming more and more evident that human neurodegenerative diseases such as Alzheimer disease (AD) also have a critical lipidic feature in their outcome. This aspect has been first pointed out by the susceptibility of the ApoE4 allele to AD, but more recently PLDs have also been proposed to contribute to the development of the pathology. It was first shown that PLD1 is involved in the vesicular trafficking of βAPP (Cai et al., 2006) and later that increased expression of APP promoted PLD activity in human astroglioma cells (Jin et al., 2007). Although highly debated, the observation that a rare variant of PLD3 gene confers susceptibility to AD has put PLD and PA on the spotlight (Cruchaga et al., 2014; Heilmann et al., 2015; Lambert et al., 2015; van der Lee et al., 2015). The most compelling evidence that defects in PA production by PLDs are involved in AD comes from an elegant study combining detailed lipidomics with behavioral tests in mouse models. In this study, the authors found that PLD2 knockout fully rescued AD-related synaptic dysfunction and cognitive deficits in a model of AD (Oliveira et al., 2010). The exact nature of the PA imbalance in AD awaits however to be fully defined and the possibility to interfere with AD condition by correcting this imbalance is probably very far from reach.

CONCLUSION

The diversity of mechanisms of PA signaling and physiological functions mostly relies on the fact that PA is synthesized by a complex set of different enzymes involved in diverse array of pathways. PLDs, DGKs, and LPAATs each constitute a big collection of isoenzymes differently localized within cells and displaying cell type specificity. In fact, the specific subcellular distribution, regulation, and/or substrate preferences of these enzymes probably account for the heterogeneity of PA composition in membranes. These aspects, altogether with the capacity of PA-binding modules in proteins to sense the local membrane environment and the type of PA species, offer a hub for the functional diversity of PA from molecular and cellular to physiological functions. There is no doubt that advanced lipidomics in combination with novel imaging tools to follow PA's dynamics will help to gain a better understanding of the apparent paradox of the abundance of function of this simple lipid. Further understanding of the biophysical side of PA's action on membranes is also critically needed to provide novel ideas for the treatment of the growing number of neuronal pathologies linked to the alterations of PA metabolism.

AUTHOR CONTRIBUTIONS

All authors listed have made a substantial, direct and intellectual contribution to the work, and approved it for publication.

FUNDING

This work was supported by Fondation pour la Recherche Médicale and by Fondation Jérôme Lejeune funding to HM.

REFERENCES

Ammar, M. R., Humeau, Y., Hanauer, A., Nieswandt, B., Bader, M. F., and Vitale, N. (2013a). The Coffin-Lowry syndrome-associated protein RSK2 regulates neurite outgrowth through phosphorylation of phospholipase D1 (PLD1) and synthesis of phosphatidic acid. *J. Neurosci.* 33, 19470–19479. doi: 10.1523/JNEUROSCI.2283-13.2013

Ammar, M. R., Kassas, N., Chasserot-Golaz, S., Bader, M. F., and Vitale, N. (2013b). Lipids in regulated exocytosis: what are they doing? *Front. Endocrinol.* 4:125. doi: 10.3389/fendo.2013.00125

Ammar, M. R., Kassas, N., Bader, M. F., and Vitale, N. (2014). Phosphatidic acid in neuronal development: a node for membrane and cytoskeleton rearrangements. *Biochimie* 107, 51–57. doi: 10.1016/j.biochi.2014.07.026

Ammar, M. R., Thahouly, T., Hanauer, A., Stegner, D., Nieswandt, B., and Vitale, N. (2015). PLD1 participates in BDNF-induced signalling in cortical neurons. *Sci. Rep.* 5:14778. doi: 10.1038/srep14778

Bader, M. F., and Vitale, N. (2009). Phospholipase D in calcium-regulated exocytosis: lessons from chromaffin cells. *Biochim. Biophys. Acta* 1791, 936–941. doi: 10.1016/j.bbalip.2009.02.016

Bruntz, R. C., Taylor, H. E., Lindsley, C. W., and Brown, H. A. (2014). Phospholipase D2 mediates survival signaling through direct regulation of Akt in glioblastoma cells. *J. Biol. Chem.* 289, 600–616. doi: 10.1074/jbc.M113.532978

Bullen, H. E., Jia, Y., Yamaryo-Botté, Y., Bisio, H., Zhang, O., Jemelin, N. K., et al. (2016). Phosphatidic acid-mediated signaling regulates microneme secretion in toxoplasma. *Cell Host Microbe* 19, 349–360. doi: 10.1016/j.chom.2016.02.006

Burkhardt, U., Wojcik, B., Zimmermann, M., and Klein, J. (2014). Phospholipase D is a target for inhibition of astroglial proliferation by ethanol. *Neuropharmacology* 79, 1–9. doi: 10.1016/j.neuropharm.2013.11.002

Cai, D., Zhong, M., Wang, R., Netzer, W. J., Shields, D., Zheng, H., et al. (2006). Phospholipase D1 corrects impaired βAPP trafficking and neurite outgrowth in familial Alzheimer's disease-linked presenilin-1 mutant neurons. *Proc. Natl. Acad. Sci. U S A* 103, 1936–1940. doi: 10.1073/pnas.0510710103

Chae, Y. C., Kim, J. H., Kim, K. L., Kim, H. W., Lee, H. Y., Heo, W. D., et al. (2008). Phospholipase D activity regulates integrin-mediated cell spreading and migration by inducing GTP-Rac translocation to the plasma membrane. *Mol. Biol. Cell* 19, 3111–3123. doi: 10.1091/mbc.E07-04-0337

Chasserot-Golaz, S., Coorssen, J. R., Meunier, F. A., and Vitale, N. (2010). Lipid dynamics in exocytosis. *Cell. Mol. Neurobiol.* 30, 1335–1342. doi: 10.1007/s10571-010-9577-x

Corrotte, M., Chasserot-Golaz, S., Huang, P., Du, G., Ktistakis, N. T., Frohman, M. A., et al. (2006). Dynamics and function of phospholipase D and phosphatidic acid during phagocytosis. *Traffic* 7, 365–377. doi: 10.1111/j.1600-0854.2006.00389.x

Corrotte, M., Nyguyen, A. P., Harlay, M. L., Vitale, N., Bader, M. F., and Grant, N. J. (2010). Ral isoforms are implicated in Fcγ R-mediated phagocytosis: activation of phospholipase D by RalA. *J. Immunol.* 185, 2942–2950. doi: 10.4049/jimmunol.0903138

Cruchaga, C., Karch, C. M., Jin, S. C., Benitez, B. A., Cai, Y., Guerreiro, R., et al. (2014). Rare coding variants in the phospholipase D3 gene confer risk for Alzheimer's disease. *Nature* 505, 550–554. doi: 10.1038/nature12825

Daniels, R. H., Hall, P. S., and Bokoch, G. M. (1998). Membrane targeting of p21-activated kinase 1 (PAK1) induces neurite outgrowth from PC12 cells. *EMBO J.* 17, 754–764. doi: 10.1093/emboj/17.3.754

Disse, J., Vitale, N., Bader, M. F., and Gerke, V. (2009). Phospholipase D1 is specifically required for regulated secretion of von Willebrand factor from endothelial cells. *Blood* 113, 973–980. doi: 10.1182/blood-2008-06-165282

Ehrhart, F., Roozen, S., Verbeek, J., Koek, G., Kok, G., van Kranen, H., et al. (2018). Review and gap analysis: molecular pathways leading to fetal alcohol spectrum disorders. *Mol. Psychiatry* 24, 10–17. doi: 10.1038/s41380-018-0095-4

Faugaret, D., Chouinard, F. C., Harbour, D., El azreq, M. A., and Bourgoin, S. G. (2011). An essential role for phospholipase D in the recruitment of vesicle amine transport protein-1 to membranes in human neutrophils. *Biochem. Pharmacol.* 81, 144–156. doi: 10.1016/j.bcp.2010.09.014

Foster, D. A. (2009). Phosphatidic acid signaling to mTOR: signals for the survival of human cancer cells. *Biochim. Biophys. Acta* 1791, 949–949. doi: 10.1016/j.bbalip.2009.02.009

Ghossoub, R., Lembo, F., Rubio, A., Gaillard, C. B., Bouchet, J., Vitale, N., et al. (2014). Syntenin-ALIX exosome biogenesis and budding into multivesicular bodies are controlled by ARF6 and PLD2. *Nat. Commun.* 5:3477. doi: 10.1038/ncomms4477

Hayashi, K., Ohshima, T., Hashimoto, M., and Mikoshiba, K. (2007). Pak1 regulates dendritic branching and spine formation. *Dev. Neurobiol.* 67, 655–669. doi: 10.1002/dneu.20363

Heilmann, S., Drichel, D., Clarimon, J., Fernández, V., Lacour, A., Wagner, H., et al. (2015). PLD3 in non-familial Alzheimer's disease. *Nature* 520, E3–E5. doi: 10.1038/nature14039

Holland, P., Knævelsrud, H., Søreng, K., Mathai, B. J., Lystad, A. H., Pankiv, S., et al. (2016). HS1BP3 negatively regulates autophagy by modulation of phosphatidic acid levels. *Nat. Commun.* 7:13889. doi: 10.1038/ncomms13889

Honda, A., Nogami, M., Yokozeki, T., Yamazaki, M., Nakamura, H., Watanabe, H., et al. (1999). Phosphatidylinositol 4-phosphate 5-kinase α is a downstream effector of the small G protein ARF6 in membrane ruffle formation. *Cell* 99, 521–532. doi: 10.1016/s0092-8674(00)81540-8

Humeau, Y., Gambino, F., Chelly, J., and Vitale, N. (2009). X-linked mental retardation: focus on synaptic function and plasticity. *J. Neurochem.* 109, 1–14. doi: 10.1111/j.1471-4159.2009.05881.x

Humeau, Y., Vitale, N., Chasserot-Golaz, S., Dupont, J. L., Du, G., Frohman, M. A., et al. (2001). A role for phospholipase D1 in neurotransmitter release. *Proc. Natl. Acad. Sci. U S A* 98, 15300–15305. doi: 10.1073/pnas.261358698

Ito, S., Richert, N., and Pastan, I. (1982). Phospholipids stimulate phosphorylation of vinculin by the tyrosine-specific protein kinase of Rous sarcoma virus. *Proc. Natl. Acad. Sci. U S A* 79, 4628–4631. doi: 10.1073/pnas.79.15.4628

Jang, J.-H., Lee, C. S., Hwang, D., and Ryu, S. H. (2012). Understanding of the roles of phospholipase D and phosphatidic acid through their binding partners. *Prog. Lipid Res.* 51, 71–81. doi: 10.1016/j.plipres.2011.12.003

Jenkins, G. M., and Frohman, M. A. (2005). Phospholipase D: a lipid centric review. *Cell. Mol. Life Sci.* 62, 2305–2316. doi: 10.1007/s00018-005-5195-z

Jin, J.-K., Ahn, B.-H., Na, Y.-J., Kim, J.-I., Kim, Y.-S., Choi, E.-K., et al. (2007). Phospholipase D1 is associated with amyloid precursor protein in Alzheimer's disease. *Neurobiol. Aging* 28, 1015–1027. doi: 10.1016/j.neurobiolaging.2006.05.022

Johnson, R. P., and Craig, S. W. (1995). The carboxy-terminal tail domain of vinculin contains a cryptic binding site for acidic phospholipids. *Biochem. Biophys. Res. Commun.* 210, 159–164. doi: 10.1006/bbrc.1995.1641

Jose Lopez-Andreo, M., Gomez-Fernandez, J. C., and Corbalan-Garcia, S. (2003). The simultaneous production of phosphatidic acid and diacylglycerol is essential for the translocation of protein kinase Cε to the plasma membrane in RBL-2H3 cells. *Mol. Biol. Cell* 14, 4885–4895. doi: 10.1091/mbc.e03-05-0295

Kassas, N., Tanguy, E., Thahouly, T., Fouillen, L., Heintz, D., Chasserot-Golaz, S., et al. (2017). Comparative characterization of phosphatidic acid sensors and their localization during frustrated phagocytosis. *J. Biol. Chem.* 292, 4266–4279. doi: 10.1074/jbc.m116.742346

Klein, J. (2005). Functions and pathophysiological roles of phospholipase D in thebrain. *J. Neurochem.* 94, 1473–1487. doi: 10.1111/j.1471-4159.2005.03315.x

Kooijman, E. E., Chupin, V., de Kruijff, B., and Burger, K. N. (2003). Modulation of membrane curvature by phosphatidic acid and lysophosphatidic acid. *Traffic* 4, 162–174. doi: 10.1034/j.1600-0854.2003.00086.x

Kurooka, T., Yamamoto, Y., Takai, Y., and Sakisaka, T. (2011). Dual regulation of RA-RhoGAP activity by phosphatidic acid and Rap1 during neurite outgrowth. *J. Biol. Chem.* 286, 6832–6843. doi: 10.1074/jbc.m110.183772

Lam, A. D., Tryoen-Toth, P., Tsai, B., Vitale, N., and Stuenkel, E. L. (2008). SNARE-catalyzed fusion events are regulated by Syntaxin1A-lipid interactions. *Mol. Biol. Cell* 19, 485–497. doi: 10.1091/mbc.e07-02-0148

Lambert, J. C., Grenier-Boley, B., Bellenguez, C., Pasquier, F., Campion, D., Dartigues, J. F., et al. (2015). PLD3 and sporadic Alzheimer's disease risk. *Nature* 520:E1. doi: 10.1038/nature14036

Lopez, C. I., Pelletán, L. E., Suhaiman, L., De Blas, G. A., Vitale, N., Mayorga, L. S., et al. (2012). Diacylglycerol stimulates acrosomal exocytosis by feeding into a PKC- and PLD1-dependent positive loop that continuously supplies phosphatidylinositol 4,5-bisphosphate. *Biochim. Biophys. Acta* 1821, 1186–1199. doi: 10.1016/j.bbalip.2012.05.001

Mima, J., and Wickner, W. (2009). Complex lipid requirements for SNARE- and SNARE chaperone-dependent membrane fusion. *J. Biol. Chem.* 284, 27114–27122. doi: 10.1074/jbc.m109.010223

Moine, H., and Vitale, N. (2018). Of local translation control and lipid signaling in neurons. *Adv. Biol. Regul.* doi: 10.1016/j.jbior.2018.09.005 [Epub ahead of print].

Nishikimi, A., Fukuhara, H., Su, W., Hongu, T., Takasuga, S., Mihara, H., et al. (2009). Sequential regulation of DOCK2 dynamics by two phospholipids during neutrophil chemotaxis. *Science* 324, 384–387. doi: 10.1126/science.1170179

Oliveira, T. G., Chan, R. B., Tian, H., Laredo, M., Shui, G., Staniszewski, A., et al. (2010). Phospholipase d2 ablation ameliorates Alzheimer's disease-linked synaptic dysfunction and cognitive deficits. *J. Neurosci.* 30, 16419–16428. doi: 10.1523/JNEUROSCI.3317-10.2010

Park, M. H., Ahn, B. H., Hong, Y. K., and Min do, S. (2009). Overexpression of phospholipase D enhances matrix metalloproteinase-2 expression and glioma cell invasion via protein kinase C and protein kinase A/NF-κB/Sp1-mediated signaling pathways. *Carcinogenesis* 30, 356–365. doi: 10.1093/carcin/bgn287

Pelletán, L. E., Suhaiman, L., Vaquer, C. C., Bustos, M. A., De Blas, G. A., Vitale, N., et al. (2015). ADP ribosylation factor 6 (ARF6) promotes acrosomal exocytosis by modulating lipid turnover and Rab3A activation. *J. Biol. Chem.* 290, 9823–9841. doi: 10.1074/jbc.m114.629006

Pokotylo, I., Kravets, V., Martinec, J., and Ruelland, E. (2018). The phosphatidic acid paradox: too many actions for one molecule class? Lessons from plants. *Prog. Lipid Res.* 71, 43–53. doi: 10.1016/j.plipres.2018.05.003

Potocký, M., Pleskot, R., Pejchar, P., Vitale, N., Kost, B., and Zárský, V. (2014). Live-cell imaging of phosphatidic acid dynamics in pollen tubes visualized by Spo20p-derive biosensor. *New Phytol.* 203, 483–494. doi: 10.1111/nph.12814

Raben, D. M., and Barber, C. N. (2017). Phosphatidic acid and neurotransmission. *Adv. Biol. Regul.* 63, 15–21. doi: 10.1016/j.jbior.2016.09.004

Roach, A. N., Wang, Z., Wu, P., Zhang, F., Chan, R. B., Yonekubo, Y., et al. (2012). Phosphatidic acid regulation of PIPKI is critical for actin cytoskeletal reorganization. *J. Lipid Res.* 53, 2598–2609. doi: 10.1194/jlr.m028597

Sanematsu, F., Nishikimi, A., Watanabe, M., Hongu, T., Tanaka, Y., Kanaho, Y., et al. (2013). Phosphatidic acid-dependent recruitment and function of the Rac activator DOCK1 during dorsal ruffle formation. *J. Biol. Chem.* 288, 8092–8100. doi: 10.1074/jbc.m112.410423

Schwarz, K., Natarajan, S., Kassas, N., Vitale, N., and Schmitz, F. (2011). The synaptic ribbon is a site of phosphatidic acid generation in ribbon synapses. *J. Neurosci.* 31, 15996–16011. doi: 10.1523/JNEUROSCI.2965-11.2011

Stace, C. L., and Ktistakis, N. T. (2006). Phosphatidic acid- and phosphatidylserine-binding proteins. *Biochim. Biophys. Acta* 1761, 913–926. doi: 10.1016/j.bbalip.2006.03.006

Tabet, R., Moutin, E., Becker, J. A., Heintz, D., Fouillen, L., Flatter, E., et al. (2016a). Fragile X Mental Retardation Protein (FMRP) controls diacylglycerol kinase activity in neurons. *Proc. Natl. Acad. Sci. U S A* 113, E3619–E3628. doi: 10.1073/pnas.1522631113

Tabet, R., Vitale, N., and Moine, H. (2016b). Fragile X syndrome: are signaling lipids the missing Culprits? *Biochimie* 130, 188–194. doi: 10.1016/j.biochi.2016.09.002

Tanguy, E., Carmon, O., Wang, Q., Jeandel, L., Chasserot-Golaz, S., Montero-Hadjadje, M., et al. (2016). Lipids implicated in the journey of a secretory granule: from biogenesis to fusion. *J. Neurochem.* 137, 904–912. doi: 10.1111/jnc.13577

Tanguy, E., Kassas, N., and Vitale, N. (2018). Protein-phospholipid interaction motifs: a focus on phosphatidic acid. *Biomolecules* 8:E20. doi: 10.3390/biom8020020

van den Bout, I., and Divecha, N. (2009). PIP5K-driven PtdIns(4,5)P2 synthesis: regulation and cellular functions. *J. Cell Sci.* 122, 3837–3850. doi: 10.1242/jcs.056127

van der Lee, S. J., Holstege, H., Wong, T. H., Jakobsdottir, J., Bis, J. C., Chouraki, V., et al. (2015). PLD3 variants in population studies. *Nature* 520, E2–E3. doi: 10.1038/nature14038

Vitale, N., Caumont, A. S., Chasserot-Golaz, S., Du, G., Wu, S., Sciorra, V. A., et al. (2001). Phospholipase D1: a key factor for the exocytotic machinery in neuroendocrine cells. *EMBO J.* 20, 2424–2434. doi: 10.1093/emboj/20.10.2424

Waselle, L., Gerona, R. R., Vitale, N., Martin, T. F., Bader, M. F., and Regazzi, R. (2005). Role of phosphoinositide signaling in the control of insulin exocytosis. *Mol. Endocrinol.* 19, 3097–3106. doi: 10.1210/me.2004-0530

Wildburger, N. C., Wood, P. L., Gumin, J., Lichti, C. F., Emmett, M. R., Lang, F. F., et al. (2015). ESI-MS/MS and MALDI-IMS localization reveal alterations in phosphatidic acid, diacylglycerol, and DHA in glioma stem cell xenografts. *J. Proteome Res.* 14, 2511–2519. doi: 10.1021/acs.jproteome.5b00076

Williams, J. M., Pettitt, T. R., Powell, W., Grove, J., Savage, C. O., and Wakelam, M. J. (2007). Antineutrophil cytoplasm antibody-stimulated neutrophil adhesion depends on diacylglycerol kinase-catalyzed phosphatidic acid formation. *J. Am. Soc. Nephrol.* 18, 1112–1120. doi: 10.1681/asn.2006090973

Yang, J. S., Gad, H., Lee, S. Y., Mironov, A., Zhang, L., Beznoussenko, G. V., et al. (2008). A role for phosphatidic acid in COPI vesicle fission yields insights into Golgi maintenance. *Nat. Cell Biol.* 10, 1146–1153. doi: 10.1038/ncb1774

Zeniou-Meyer, M., Gambino, F., Ammar, M. R., Humeau, Y., and Vitale, N. (2010). The Coffin-Lowry syndrome-associated protein RSK2 and neurosecretion. *Cell. Mol. Neurobiol.* 30, 1401–1406. doi: 10.1007/s10571-010-9578-9

Zeniou-Meyer, M., Liu, Y., Béglé, A., Olanich, M. E., Hanauer, A., Becherer, U., et al. (2008). The Coffin-Lowry syndrome-associated protein RSK2 is implicated in calcium-regulated exocytosis through the regulation of PLD1. *Proc. Natl. Acad. Sci. U S A* 105, 8434–8439. doi: 10.1073/pnas.0710676105

Zeniou-Meyer, M., Zabari, N., Ashery, U., Chasserot-Golaz, S., Haeberlé, A. M., Demais, V., et al. (2007). Phospholipase D1 production of phosphatidic acid at the plasma membrane promotes exocytosis of large dense-core granules at a late stage. *J. Biol. Chem.* 282, 21746–21757. doi: 10.1074/jbc.m702968200

Conflict of Interest Statement: The authors declare that the research was conducted in the absence of any commercial or financial relationships that could be construed as a potential conflict of interest.

frontiers in Cellular Neuroscience

ORIGINAL RESEARCH
published: 08 February 2019
doi: 10.3389/fncel.2019.00037

Molecular Modulation of Human α7 Nicotinic Receptor by Amyloid-β Peptides

*Matías Lasala, Camila Fabiani, Jeremías Corradi, Silvia Antollini and Cecilia Bouzat**

Instituto de Investigaciones Bioquímicas de Bahía Blanca (INIBIBB), Departamento de Biología, Bioquímica y Farmacia, Universidad Nacional del Sur-Consejo Nacional de Investigaciones Científicas y Técnicas (CONICET), Bahía Blanca, Argentina

Amyloid β peptide (Aβ) is a key player in the development of Alzheimer's disease (AD). It is the primary component of senile plaques in AD patients and is also found in soluble forms. Cholinergic activity mediated by α7 nicotinic receptors has been shown to be affected by Aβ soluble forms. To shed light into the molecular mechanism of this effect, we explored the direct actions of oligomeric $A\beta_{1-40}$ and $A\beta_{1-42}$ on human α7 by fluorescence spectroscopy and single-channel recordings. Fluorescence measurements using the conformational sensitive probe crystal violet (CrV) revealed that in the presence of Aβ α7 undergoes concentration-dependent conformational changes. Exposure of α7 to 100 pM Aβ changes CrV K_D towards that of the desensitized state. However, α7 is still reactive to high carbamylcholine (Carb) concentrations. These observations are compatible with the induction of active/desensitized states as well as of a novel conformational state in the presence of both Aβ and Carb. At 100 nM Aβ, α7 adopts a resting-state-like structure which does not respond to Carb, suggesting stabilization of α7 in a blocked state. In real time, we found that Aβ is capable of eliciting α7 channel activity either in the absence or presence of the positive allosteric modulator (PAM) PNU-120596. Activation by Aβ is favored at picomolar or low nanomolar concentrations and is not detected at micromolar concentrations. At high Aβ concentrations, the mean duration of activation episodes elicited by ACh in the presence of PNU-120596 is significantly reduced, an effect compatible with slow open-channel block. We conclude that Aβ directly affects α7 function by acting as an agonist and a negative modulator. Whereas the capability of low concentrations of Aβ to activate α7 could be beneficial, the reduced α7 activity in the presence of higher Aβ concentrations or its long exposure may contribute to the cholinergic signaling deficit and may be involved in the initiation and development of AD.

Keywords: nicotinic receptor, patch-clamp recordings, single-channel currents, Cys-loop receptor, amyloid peptide, crystal violet

OPEN ACCESS

Edited by:
Mario Eduardo Guido, Center for Research in Biological Chemistry Córdoba (CIQUIBIC), Argentina

Reviewed by:
Valentina Echeverria Moran, Bay Pines VA Healthcare System, United States
Marcella Reale, Università degli Studi G. d'Annunzio Chieti e Pescara, Italy

****Correspondence:***
Cecilia Bouzat
inbouzat@criba.edu.ar

Received: *15 November 2018*
Accepted: *23 January 2019*
Published: *08 February 2019*

Citation:
Lasala M, Fabiani C, Corradi J, Antollini S and Bouzat C (2019) Molecular Modulation of Human α7 Nicotinic Receptor by Amyloid-β Peptides. Front. Cell. Neurosci. 13:37. doi: 10.3389/fncel.2019.00037

Abbreviations: ACh, acetylcholine; Carb, carbamylcholine; $A\beta_{1-42}$, amyloid-β_{1-42} peptide; $A\beta_{1-40}$, amyloid-β_{1-40} peptide; nAChR, nicotinic acetylcholine receptor; CrV, crystal violet; NS-1738, N-(5-Chloro-2-hydroxyphenyl)-N′-[2-chloro-5-(trifluoromethyl) phenyl]urea; PNU-120596, [N-(5-Chloro-2,4-dimethoxyphenyl)-N′-(5-methyl-3-isoxazolyl)-urea].

INTRODUCTION

Alzheimer's disease (AD) is a progressive neurodegenerative disease characterized by loss of memory, multiple cognitive impairments and changes in personality and behavior. Memory impairment in AD is associated with neuronal degeneration as well as synaptic damage. Although AD is a multifactorial disease, accumulation of amyloid-β peptides (Aβ) is one of the major pathological factors. Accumulation phase starts with low molecular weight fractions of Aβ (monomers, dimers, or trimers) and continues with larger oligomers or insoluble amyloid fibrils (Sadigh-Eteghad et al., 2014). Although plaques remain the principal identifiers and predictors of Alzheimer's disease, a clear paradigm shift has occurred that emphasizes the primacy of Aβ oligomers in disease causation (Lacor et al., 2004; Shankar et al., 2008; Hayden and Teplow, 2013; Collins-Praino et al., 2014). Despite all research efforts, there are still many unsolved aspects regarding the molecular mechanisms underlying Aβ pathogenic actions. One of these mechanisms involves the interaction of Aβ with synaptic receptors, which consequently emerge as novel druggable sites to restore cognitive functions in AD patients (Kandimalla and Reddy, 2017).

Cholinergic neurons with a pivotal role in learning and memory are mainly involved in the pathogenesis of AD. Indeed, inhibitors of acetylcholinesterase (AChE), which by decreasing ACh breakdown enhance cholinergic neurotransmission, are to date one of the main specific therapeutic drugs, although their efficacy is limited (Kandimalla and Reddy, 2017).

The α7 nicotinic acetylcholine receptor (nAChR) has been shown to be associated with AD. α7 is highly expressed in hippocampus, cortex and several subcortical limbic regions and is involved in cognition, sensory processing information, attention, working memory, and reward pathways (Lendvai et al., 2013). Reduction of α7 in brain, particularly in the hippocampus, has been reported in AD patients (Buckingham et al., 2009; Dineley et al., 2015).

α7 is a pentameric ligand-gated ion channel that responds to ACh by opening an intrinsic channel permeable to cations that triggers rapid membrane depolarization and calcium influx (Wonnacott, 2014). However, α7 also acts as a metabotropic receptor and triggers several signal transduction pathways as well as the release of calcium from intracellular stores (Kabbani et al., 2013; Egea et al., 2015; Guan et al., 2015; Corradi and Bouzat, 2016; Bouzat et al., 2018). This metabotropic activity has been associated to synaptic plasticity and neuroprotection, including against Aβ damage (Buckingham et al., 2009; Inestrosa et al., 2013; Jin et al., 2015).

Enhancement of α7 activity is emerging as a therapeutic strategy for cognitive impairment in AD. Positive allosteric modulators (PAMs) are the most promising therapeutic compounds because they maintain the temporal and spatial characteristics of endogenous activation, are more selective than agonists, and reduce tolerance due to desensitization (Chatzidaki and Millar, 2015; Terry et al., 2015; Corradi and Bouzat, 2016; Echeverria et al., 2016; Yang et al., 2017; Bouzat et al., 2018). Based on their effects on macroscopic currents, PAMs have been classified as type I PAMs, that mainly enhance agonist-induced peak currents, and type II PAMs, that enhance agonist-elicited currents and also decrease desensitization and recover receptors from desensitized states (Bertrand and Gopalakrishnan, 2007; Grønlien et al., 2007; Andersen et al., 2016).

Both α7 agonist- and antagonist-like actions of Aβ have been described in different cells and tissues (Wu et al., 2004; Khan et al., 2010; Li et al., 2011; Parri et al., 2011; Sadigh-Eteghad et al., 2014; Liu et al., 2015; Yan et al., 2015). Studies have been focused mainly on evaluation of the effects of Aβ on α7 metabotropic activity, which includes signaling pathways, such as ERK/MAPK, PI3K/AKT, JAK-2/STAT-3 and intracellular calcium mobilization. The acute effects of Aβ on α7 electrical activity have been explored at the macroscopic current level. Despite problems of comparability and some dissimilar results, probably due to variations on the aggregation state and concentration of amyloid peptides (see Buckingham et al., 2009), the consensus indicates that low concentrations of Aβ (picomolar) activate α7 whereas higher concentrations lead to current inhibition (Liu et al., 2001; Dineley et al., 2002; Grassi et al., 2003; Pym et al., 2005; Parri et al., 2011).

To shed light into the molecular mechanism of the direct action of Aβ on α7, we expressed human α7 on mammalian cells and evaluated functional effects by fluorescence spectroscopic measurements and electrophysiological recordings. We used Aβ preparations enriched in oligomeric forms since these species were shown to be involved in cognitive impairment, inhibition of long-term potentiation, memory loss and α7 modulation (Walsh et al., 2002; Wang et al., 2002; Cleary et al., 2005; Parri et al., 2011). By taking advantage of the potential of single-channel recordings in providing information unattainable by macroscopic measurements, we deciphered the direct molecular effects of oligomeric Aβ as activator and inhibitor of α7 channels. By using a fluorescent conformational probe, we revealed that Aβ elicits different concentration-dependent conformational changes and induces novel conformational states.

MATERIALS AND METHODS

Drugs

Acetylcholine (ACh) and human amyloid-β1–42 ($A\beta_{1-42}$) were purchased from Sigma-Aldrich (St. Louis, MO, USA); NS-1738 N-(5-Chloro-2-hydroxyphenyl)-N′-[2-chloro-5-(trifluoromethyl) phenyl]urea, PNU-120596 [N-(5-Chloro-2,4-dimethoxyphenyl)-N′-(5-methyl-3-isoxazolyl)-urea] and rat amyloid-β1–40 ($A\beta_{1-40}$) were obtained from Tocris Biosciences (Bristol, UK).

Receptor Expression

BOSC-23 cells, derived from HEK 293 cells (Pear et al., 1993), were transfected by calcium phosphate procedure with human α7 cDNA subcloned in pRBG4 vector (Bouzat et al., 1994). Plasmids harboring cDNAs of the α7 chaperone proteins Ric-3 and NACHO were incorporated to favor α7 expression (Bouzat et al., 2008; Andersen et al., 2016; Nielsen et al., 2018). All transfections were carried out for about 12–18 h in Dulbecco's Modified Eagle Medium (DMEM) with 10%

fetal bovine serum and terminated by exchanging the medium. Cells were used for single-channel recordings 2–4 days after transfection. To facilitate identification of transfected cells, a separate plasmid encoding green fluorescent protein was included in all transfections.

Amyloid-β Peptide Preparations

$A\beta_{1-40}$ or $A\beta_{1-42}$ were resuspended in dimethyl sulfoxide at a concentration of 10 mg/ml (peptide stock solution) and stored in aliquots at −80°C. Aβ oligomers were prepared immediately prior to use according to previously published methods (Uranga et al., 2016; Pascual et al., 2017). Briefly, aliquots of peptide stock (10 μl) were added to 280 μl of phosphate buffered saline (PBS; pH 7.4) and stirred continuously (300 rpm) for 120 min and stored at 4°C until use.

Transmission electron microscopy (TEM) studies were carried out according to previously published methods with slight modifications (Uranga et al., 2016; Pascual et al., 2017). Briefly, 10 μl media containing the peptide was placed on a carbon-coated grid and incubated for 60 s. Ten microliters of 0.5% glutaraldehyde was added to the grid followed by incubation for an additional 60 s. The grid was then washed with drops of water and dried. Finally, the grid was stained for 2 min with 2% uranyl acetate and air dried. The grid was subsequently examined under a Jeol 100 Cx II electron microscope (Uranga et al., 2016). TEM photomicrographs showed that Aβ preparations included spheroidal structures individually or in small groups (**Supplementary Figure S1**). These ultrastructural forms were compatible with a heterogeneous array of oligomers, thus discarding the presence of fibrils (Uranga et al., 2016; Pascual et al., 2017).

Single-Channel Recordings

Single-channel recordings were obtained in the cell-attached patch configuration. The bath and pipette solutions contained 142 mM KCl, 5.4 mM NaCl, 1.8 mM $CaCl_2$, 1.7 mM $MgCl_2$ and 10 mM HEPES (pH 7.4). For potentiation, 1 μM PNU-120596 or 10 μM NS-1738 were added to the pipette solution together with ACh.

Single-channel currents were digitized at 5–10 μs intervals, low-pass filtered at a cut-off frequency of 10 kHz using an Axopatch 200B patch-clamp amplifier (Molecular Devices Corp., CA, USA). Single-channel events were idealized by the half amplitude threshold criterion using the program QuB 2.0.0.28 (Qin et al., 1996, 1997; State University of New York at Buffalo) with a digital low-pass filter at 9 kHz. A filter of 3 kHz was used in recordings with PNU-120596 to facilitate the analysis. The open and closed time histograms obtained from idealization were fitted by the maximum interval likelihood (MIL) function in QuB (Qin et al., 1996, 1997), with a dead time of 0.1 ms. This analysis was performed by sequentially adding an open and/or closed state to a starting C ↔ O model in order to properly fit the corresponding histograms (Fabiani et al., 2018; Lasala et al., 2018). Final models contained five-six closed states and three-four open states for α7 in the presence of ACh plus PNU-120596, five-six closed states and three open states for α7 in the presence of ACh plus NS-1738, or three closed states and one-two open states for α7 in the presence of ACh and absence of PAMs.

Clusters were identified as a series of closely separated openings preceded and followed by closings longer than a critical duration. Different critical closed times were calculated by MIL between each closed component. Critical times between the third and fourth closed components for α7 in the presence of PNU-120596 (∼30–60 ms) or NS-1738 (∼2–8 ms) were selected in QuB to chop the idealized data and create a sub-data set that only contained clusters to define mean cluster duration.

Fluorimetric Measurements

Fluorimetric measurements were performed in a SLM model 4800 fluorimeter (SLM Instruments, Urbana, IL, USA) using a vertically polarized light beam from an Hannovia 200-W mercury/xenon arc obtained with a Glan-Thompson polarizer (4 nm excitation and emission slits).

Crystal violet (CrV) was used as a probe to detect conformational changes (Lurtz and Pedersen, 1999; Sun et al., 2017; Fabiani et al., 2018). nAChR-rich membranes were prepared from *Torpedo californica* electric tissue as described previously (Fernández Nievas et al., 2008; Perillo et al., 2012; Fabiani et al., 2018). CrV experiments using *Torpedo* membranes or α7-expressing cells were conducted as described previously for the *Torpedo* nAChR (Fernández Nievas et al., 2008; Perillo et al., 2012; Fabiani et al., 2018). *Torpedo* membranes or BOSC-23 cells expressing α7 were resuspended on phosphate saline buffer with a protein concentration of 100 μg/ml or up to an absorbance value of ∼0.5 at 280 nM measured on a Jasco V-630 spectrophotometer (JASCO Deutschland GmbH), respectively. The suspended cells or membranes were incubated with Aβ oligomers for 20 min. For measurements conducted in the desensitized state, the membrane or cell suspensions were additionally incubated for 15 min with 1 mM or 20 mM carbamylcholine (Carb), respectively. The suspensions were subsequently titrated with increasing concentrations of CrV (in water). After each addition of CrV, the samples were incubated for 15 min before obtaining the fluorescence emission spectra. CrV was excited at 600 nm, and the fluorescence emission spectra were collected from 605 to 700 nm. Before the first addition of CrV, a background fluorescence emission spectrum was obtained for each sample. The spectrum was then subtracted from the emission spectra obtained in the presence of CrV and the maximum intensity (at 623–625 nm) was measured. To determine the CrV dissociation constant (K_D), the value of the CrV maximum fluorescence emission was plotted as a function of the logarithmic CrV concentration (M). The resulting sigmoid curve was fitted by the Boltzmann function and the K_D was calculated using the program Origin 7.0 (OriginLab Corporation).

Statistical Analysis

Intergroup comparisons were carried out using one-way analyses of variance (ANOVA), Dunnett's multiple comparisons

test (Graphpad PRISM software). The values represent the average ± SD of the total number of samples indicated. Statistically significance difference was established at p-values <0.05.

RESULTS

Amyloid β Oligomers Induce Conformational Changes in α7

To examine the potential of oligomeric Aβ peptides to directly affect α7, we first used the conformational-sensitive probe CrV and measured its affinity for the receptor before and after exposure to Aβ by fluorescence spectroscopy.

CrV has been extensively used for studies in the *Torpedo* muscle nAChR where it shows low affinity for the resting state (K_D values ∼400 nM, Fernández Nieves et al., 2008; Perillo et al., 2012) and high affinity for the desensitized state (K_D values ∼60 nM; Fernández Nieves et al., 2008; Perillo et al., 2012; Fabiani et al., 2018; **Figure 1A**).

We first determined if CrV can be used as a conformational probe for the human α7 receptor. Suspensions of BOSC-23 cells expressing α7 were titrated with increasing concentrations of CrV. Saturable CrV binding yielded a K_D value of 492 ± 41 nM for resting α7 receptors, indicating an affinity similar to that for the muscle nAChR in the resting state. Interestingly, measurements in the desensitized state, which was induced by 20-min preincubation with Carb, yielded a K_D value of 680 ± 89 nM for CrV binding (**Figures 1A,B**). The maximal fluorescence intensities of the samples were similar at resting and desensitized conditions, thus discarding that the lower affinity for the desensitized state corresponds to reduced binding of the probe in the latter state. These results indicate that CrV saturates its binding sites at both conditions with different affinities. Thus, opposite to its binding affinity profile for the muscle nAChR, CrV shows higher affinity for resting than for desensitized states in α7.

We next determined the effects of low (0.1 nM) and high (100 nM) $Aβ_{1–40}$ concentrations on α7 conformation by measuring CrV K_D values to resting and desensitized states (**Figure 1B**).

Exposure of α7 in the resting state (in the absence of Carb) to 0.1 nM $Aβ_{1–40}$ increased the CrV K_D towards that of the desensitized state, indicating that amyloid peptides induce conformational changes in α7. Interestingly, subsequent addition of Carb induced a further displacement to higher K_D values, suggesting that the agonist can lead to further conformational changes (**Figure 1B**). K_D values for desensitized conditions were statistically significantly different in the absence and presence of Aβ (**Figure 1B**). Similar results were obtained with 0.1 nM $Aβ_{1–42}$.

On the other hand, incubation of resting α7 receptors with 1,000-fold higher $Aβ_{1–40}$ concentration (100 nM) did not induce statistically significant changes in the CrV K_D value (**Figure 1B**). Furthermore, the K_D value remained constant even after addition of 20 mM Carb, indicating that α7 was not reactive to the agonist. Similar results were obtained with high (100 nM) $Aβ_{1–42}$.

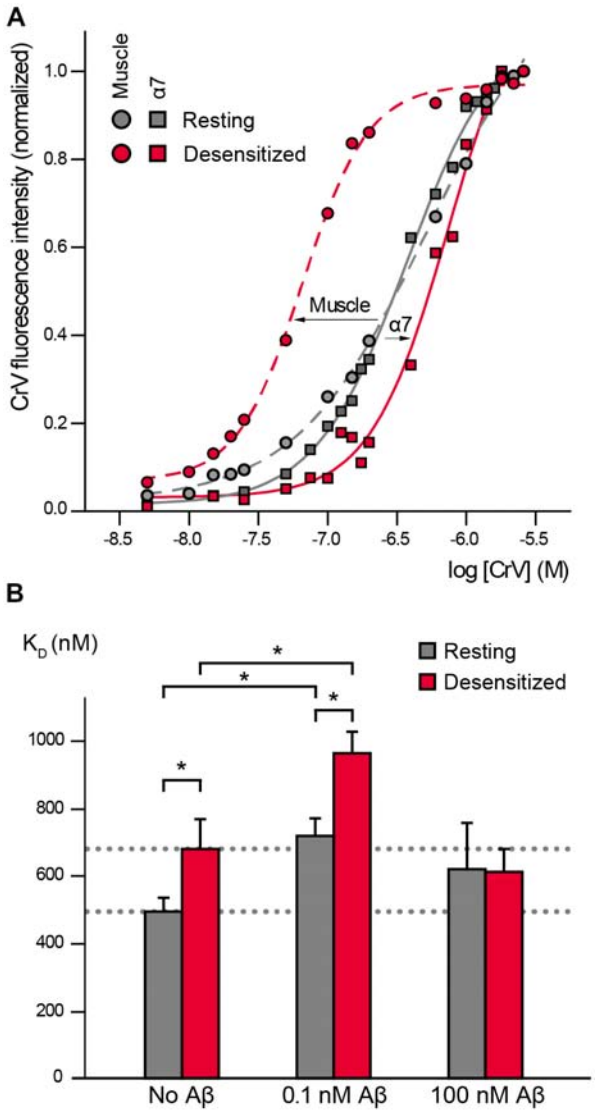

FIGURE 1 | α7 conformational changes depend on Amyloid β peptide (Aβ) concentrations. **(A)** Crystal violet (CrV) titration curves obtained with muscle nicotinic acetylcholine receptor (nAChR) from *T. californica* rich membranes (circles) and with human α7 (squares) in the absence (gray, Resting) and presence of carbamylcholine (Carb; red, desensitized). The arrows indicate the changes from resting to desensitized conditions for each nAChR type. **(B)** Changes in K_D values of CrV by the exposure to low (0.1 nM) and high (100 nM) concentrations of $Aβ_{1–40}$. K_D values of CrV were calculated from the titration curves, in the absence and presence of 20 mM Carb (gray and red columns, respectively). Each column corresponds to the average ± SD of more than four independent experiments. Statistically significant differences are shown by asterisks, $*p < 0.05$.

Oligomeric Amyloid-β Peptides at Low Concentrations Trigger Human α7 Channel Opening

Once established that oligomeric Aβ peptides induce conformational changes that are sensitive to concentration, we took advantage of the potential of single-channel recordings to reveal the mechanistic basis of this modulation.

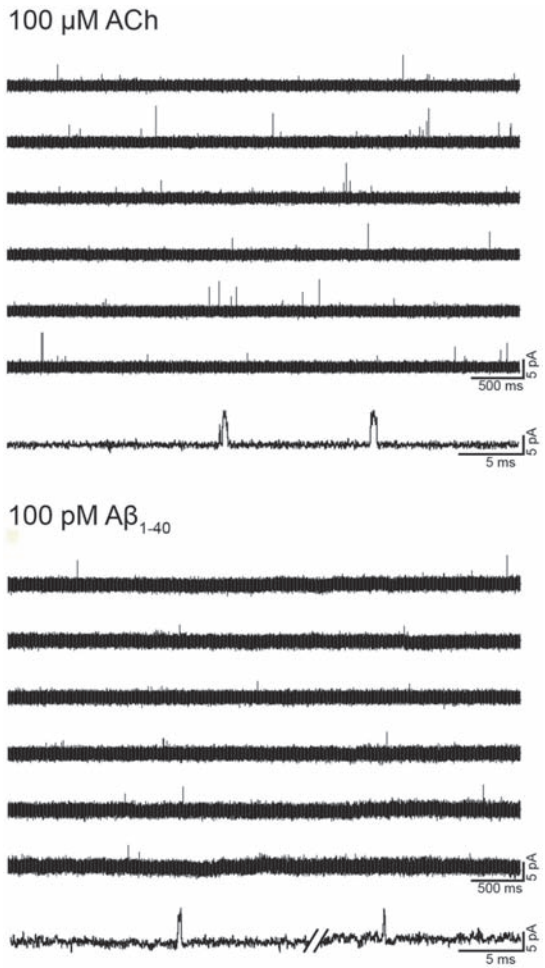

FIGURE 2 | Single-channel activity elicited by Aβ. Single-channel recordings were performed in the cell-attached patch configuration at −70 mV membrane potential. Representative α7 single-channel traces from a continuous recording in the presence of 100 μM acetylcholine (ACh) or 100 pM $A\beta_{1-40}$. For each condition, a trace at higher temporal resolution is shown (bottom traces). Channel openings are shown as upward deflections. Filter: 9 kHz.

To first determine if Aβ can activate human α7, we examined single-channel activity from BOSC-23 cells expressing the receptor (**Figure 2**). In the presence of 100 μM ACh, α7 exhibits single brief openings flanked by long closings, or less often, several openings in quick succession, which are called bursts (Bouzat et al., 2008; Andersen et al., 2016). The mean open duration was 0.36 ± 0.07 ms (n = 3) and the mean burst duration was 0.77 ± 0.21 ms (n = 3; **Figure 2**). No α7 channel activity was detected in the absence of agonist. However, 100 pM $A\beta_{1-40}$ elicited the typical α7 channel openings (**Figure 2**). The number of active patches was lower than in the presence of ACh (28% transfected cells showed channel activity). Channel activity was not detected if $A\beta_{1-40}$ was increased to 10 nM and 100 nM (n = 16 patches of different cells and transfections), indicating that activation is favored at low concentrations. These experiments were performed in parallel with recordings with ACh as the agonist to discard that the lack of channel activity was due to the lack of functional expression.

We next performed recordings in the presence of the type II PAM PNU-120596, which increases the probability of agonist-elicited channel opening and, consequently, favors the detection of infrequent opening events (daCosta et al., 2011; Andersen et al., 2016). By itself, PNU-120596 cannot elicit channel activation (Hurst et al., 2005). In the presence of 1 μM PNU-120596, α7 channel activity elicited by ACh (100 μM) appears in long activation periods of high frequency, named clusters, whose mean duration is about 1–3 s (**Figure 3**, **Table 1**; Andersen et al., 2016).

In the absence of ACh, $A\beta_{1-40}$ or $A\beta_{1-42}$ at a low concentration (100 pM) elicited clusters of PNU-120596-potentiated α7 channels (**Figure 3**). Again, the proportion of active patches was lower than in the presence of ACh. Whereas almost all patches (>90%) showed channel activity with ACh, the percentage of active patches was reduced in the presence of $A\beta_{1-40}$ or $A\beta_{1-42}$ as agonists (**Table 1**). Moreover, as Aβ concentration increased, the number of patches showing α7 activity decreased. As shown in **Table 1**, at 100 pM 43% and 78% of the patches showed clusters elicited by $A\beta_{1-40}$ or $A\beta_{1-42}$, respectively, but no channel activity was detected at 100 nM. Thus, also in the presence of a PAM, activation by Aβ is favored at picomolar or low nanomolar concentrations.

Although the frequency of clusters is usually variable among patches from different cell transfections, it was systematically lower in the presence of Aβ with respect to ACh as illustrated in typical recordings shown in **Figure 3**. For a better comparison, recordings with ACh or Aβ were performed in the same batch of transfected cells.

In the presence of ACh and PNU-120596, each cluster is composed of two or three bursts that contain long-duration openings separated by brief closings (daCosta et al., 2011; Andersen et al., 2016). Clusters elicited by Aβ in the presence of PNU-120596 showed the typical architecture observed with ACh (**Figure 3**). The analysis showed no statistically significant differences in the mean cluster duration at all tested

TABLE 1 | Activation of α7 by Amyloid β peptide (Aβ) in the presence of N-(5-Chloro-2,4-dimethoxyphenyl)-N′-(5-methyl-3-isoxazolyl)-urea (PNU)-120596.

[ACh] (μM)	Aβ	[Aβ] (nM)	% active patches (n)	Mean cluster duration (ms)
100	No	0	100 (6)	2263 ± 990
0	$A\beta_{1-40}$	0.1	42.9 (7)	762 ± 316
0		1	22.2 (18)	2016 ± 1364
0		10	30.0 (10)	5229 ± 1392*
0		100	0 (9)	Nd
0	$A\beta_{1-42}$	0.1	77.8 (9)	1401 ± 805
0		1	46.2 (13)	1208 ± 946
0		10	33.3 (9)	1751 ± 766
0		100	0 (6)	Nd

*Single-channel currents from cells expressing human α7 were recorded in the presence of 1 μM PNU-120596 plus 100 μM acetylcholine (ACh) or Aβ at the indicated concentrations. The mean cluster duration was obtained from the corresponding histograms. Nd: not detected. Statistical comparisons were performed against the corresponding control condition using analyses of variance (ANOVA; Dunnett's multiple comparisons test). *$p < 0.05$.*

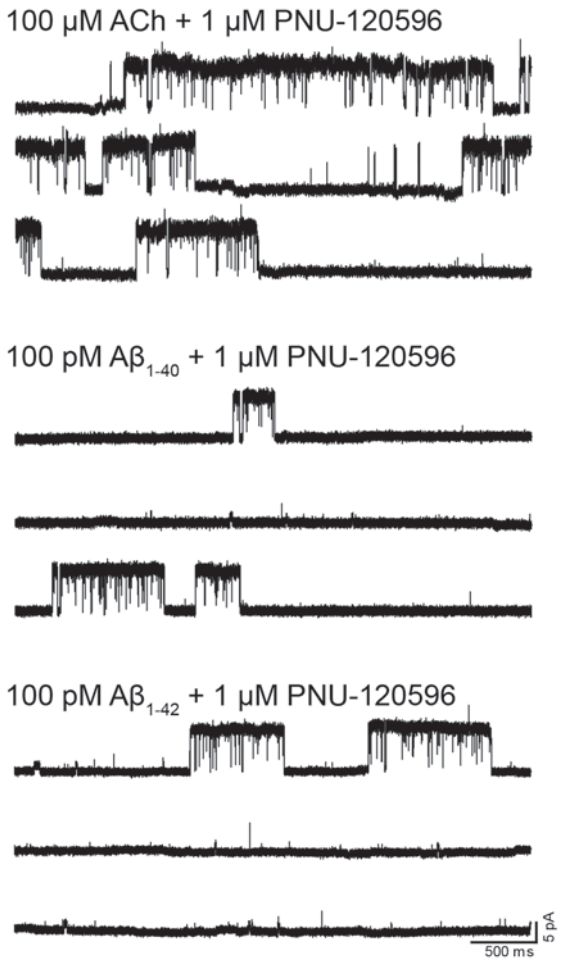

FIGURE 3 | Single-channel activity elicited by Aβ in the presence of N-(5-Chloro-2,4-dimethoxyphenyl)-N′-(5-methyl-3-isoxazolyl)-urea (PNU-120596). Single-channel recordings were performed in the cell-attached patch configuration at −70 mV membrane potential. Representative α7 single-channel traces from a continuous recording in the presence of the type II positive allosteric modulator (PAM) PNU-120596 (1 μM) together with 100 μM ACh, 100 pM $A\beta_{1-40}$ or 100 pM $A\beta_{1-42}$. Channel openings are shown as upward deflections.

concentrations, except for 10 nM $A\beta_{1-40}$ at which clusters were slightly prolonged (**Table 1**).

The results confirm that Aβ at picomolar and low nanomolar concentrations can trigger activation of α7 channels.

Amyloid-β Peptides Decrease the Duration of α7 Activation Episodes

We next explored the effect of Aβ on ACh-elicited channels. To this end, we recorded channels activated by 100 μM ACh in the presence of $A\beta_{1-42}$ (10 and 100 nM). The mean durations of openings and bursts at both Aβ concentrations were slightly briefer than the control but the differences were not statistically significant (**Table 2**). Due to the very brief durations, differences on these values may be inaccurate since they approach the resolution limit of our system. We therefore tested the effect of Aβ (10–1,000 nM) on ACh-activated channels in the presence

TABLE 2 | Effect of Aβ on ACh-elicited channel activity.

PAM	Aβ	Aβ (nM)	*n*	Mean open duration (ms)	Mean cluster/burst duration (ms)
No	No	0	3	0.36 ± 0.07	0.77 ± 0.21
	$A\beta_{1-42}$	10	3	0.26 ± 0.02	0.48 ± 0.06
		100	3	0.27 ± 0.04	0.49 ± 0.11
PNU-120596	No	0	6	159.6 ± 69.6	2263 ± 990
	$A\beta_{1-40}$	50	3	176.7 ± 22.5	2220 ± 256
		100	5	61.6 ± 33.1*	698 ± 409*
		1,000	3	23.4 ± 22.0*	931 ± 303*
	$A\beta_{1-42}$	10	5	61.1 ± 23.8*	888 ± 261*
		100	5	54.7 ± 47.8*	755 ± 560*
		1,000	6	59.6 ± 32.2*	883 ± 289*
NS-1738	No	0	12	4.2 ± 1.8	31.1 ± 8.8
	$A\beta_{1-40}$	100	10	2.7 ± 1.1*	8.4 ± 4.8****
	$A\beta_{1-42}$	100	4	2.1 ± 1.0*	10.7 ± 2.4****

*Single-channel recordings from cells expressing human α7 were recorded in the presence of 100 μM ACh, 100 μM ACh plus 1 μM PNU-120596 or 100 μM ACh plus 10 μM N-(5-Chloro-2-hydroxyphenyl)-N′-[2-chloro-5-(trifluoromethyl) phenyl]urea (NS-1738). The effects of Aβ was evaluated for all conditions. The mean open and cluster durations were obtained from the corresponding histograms. Statistical comparisons were performed against the corresponding control condition using ANOVA (Dunnett's multiple comparisons test). *$p < 0.05$, ****$p < 0.0001$.*

1 μM PNU-120596, which by increasing the duration of the activation episodes allows a better description of the molecular effects.

The presence of $A\beta_{1-40}$ or $A\beta_{1-42}$ reduced the mean duration of openings and clusters elicited by ACh and potentiated by PNU-120596 as a function of concentration (**Figure 4A**). Whereas 50 nM $A\beta_{1-40}$ did not affect open and cluster durations, 10 nM $A\beta_{1-42}$ reduced these durations. The mean open and cluster durations were statistically significantly briefer than the control at concentrations equal and higher than 100 nM for $A\beta_{1-40}$ and 10 nM for $A\beta_{1-42}$ ($p < 0.05$, **Table 2**). At these concentrations, the mean durations were reduced about 3-fold (**Figure 4B**).

To further determine if the effect of Aβ on α7 potentiation is specific for type II PAMs, we evaluated the action on channels activated by ACh and potentiated by NS-1738, which is a type I PAM (Timmermann et al., 2007; Andersen et al., 2016). In the presence of ACh, NS-1738 (10 μM) increased the mean open duration from about 0.3 ms to about 4 ms and opening events appeared grouped in bursts of about 30 ms (**Figure 5**, **Table 2**). In the presence of 100 nM $A\beta_{1-40}$ or $A\beta_{1-42}$, the mean burst duration was reduced to about 3-fold and the mean open duration was also statistically significantly briefer than in the control condition (**Figure 5**, **Table 2**).

Thus, we conclude that episodes elicited by ACh and potentiated by both types of PAMs are reduced by Aβ at high nanomolar concentrations.

DISCUSSION

Low concentrations (picomolar) of soluble Aβ peptides in the brain of healthy people have been reported to play physiological roles whereas in AD patients concentrations increase to the nanomole range and trigger the formation of insoluble plaques,

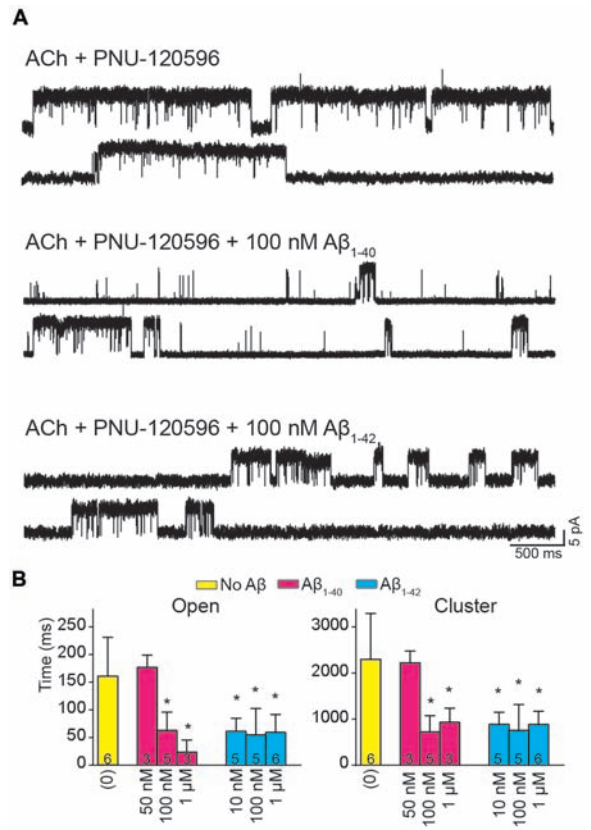

FIGURE 4 | Aβ decreases the duration of activation episodes elicited by ACh and potentiated by PNU-120596. Single-channel recordings were performed in the cell-attached patch configuration at −70 mV membrane potential with 100 μM ACh and 1 μM PNU-120596 and in the absence or presence of Aβ. **(A)** Representative clusters are shown for each condition. Channels are shown as upward deflections. **(B)** Decrease of mean open and cluster durations by Aβ. Each value corresponds to the mean ± SD of different recordings. The number of recordings for each condition is shown in the bars. The cluster and open durations for each recording were obtained from the corresponding histograms and correspond to the slowest open components $^{*}p < 0.05$.

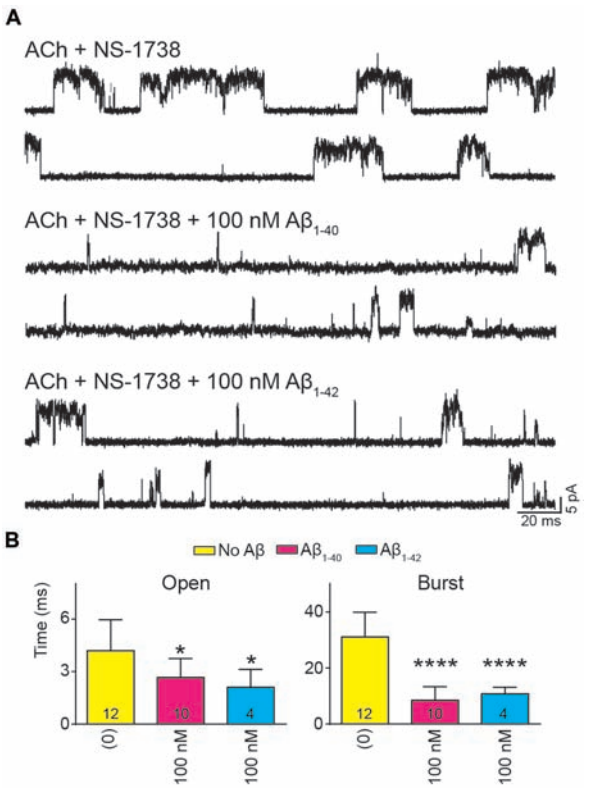

FIGURE 5 | Aβ decreases the duration of events elicited by ACh and potentiated by the type I PAM N-(5-Chloro-2-hydroxyphenyl)-N′-[2-chloro-5-(trifluoromethyl) phenyl]urea (NS-1738). Single-channel recordings were performed in the cell-attached patch configuration at −70 mV membrane potential with100 μM ACh and 10 μM NS-1738 and in the absence or presence of Aβ. **(A)** Representative channel currents are shown for each condition. **(B)** Decrease of mean open and burst durations by Aβ. Each value corresponds to the mean ± SD of *n* different recordings (shown in the bars). The open and burst durations for each recording were obtained from the corresponding histograms and correspond to the slowest open components $^{*}p < 0.05$, $^{****}p < 0.0001$.

a major neuropathologic hallmark of AD (Dineley, 2007; Parihar and Brewer, 2010; Collins-Praino et al., 2014; Puzzo et al., 2015). However, the possibility that Aβ oligomers play an important role in AD progression has gained weight (Miñano-Molina et al., 2011; Puzzo et al., 2015). Moreover, in the absence of plaques, intraneuronal accumulation of Aβ peptide has been shown to correlate with the initial steps in the tau-phosphorylation cascade, alterations in ERK2 signaling and impairment of higher CNS functions in rats (Echeverria et al., 2004a,b). Another feature of AD is the severe cholinergic deficit, which involves mainly α4β2 and α7 receptors. It has been established that α7 exhibits an exceptionally high Aβ affinity, an interaction that may influence synaptic transmission and plasticity and may also contribute to Aβ-mediated synaptic neural network dysfunction and to the severe cholinergic deficit (Wang et al., 2000; Buckingham et al., 2009; Puzzo et al., 2011; Dineley et al., 2015). Several reports have described the intracellular pathways involved in Aβ toxicity as well as crosstalk between Aβ- and α7-triggered signaling pathways (see review in Buckingham et al., 2009; Dougherty et al., 2003; Parri et al., 2011). However, the molecular mechanism by which Aβ affects α7 ionotropic activity is not well understood and has been explored mainly at the macroscopic current level. Thus, we took advantage of two different approaches to decipher the molecular basis of the direct actions of oligomeric Aβ at α7. Our spectroscopic results revealed that α7 adopts distinct stable conformations depending on the Aβ concentration range, and our single-channel recordings revealed that Aβ triggers α7 channel openings at low concentrations (picomolar to low nanomolar range) whereas at high concentrations (nanomolar to low micromolar range) it decreases the duration of ACh-elicited activation episodes. Both results fully support the idea that Aβ can act as an agonist and a negative modulator of α7 at different, physiologically attainable, concentrations.

One of the main concerns of working with Aβ is related to the standardization of the oligomeric preparations since

aggregation is a dynamic and complex process, which is highly sensitive to preparation, experimental and analyzing conditions (Bitan et al., 2005; Buckingham et al., 2009; Hayden and Teplow, 2013; Watt et al., 2013). Thus, preparations are usually heterogenous since many types of soluble species co-exist. However, this scenario mimics the physiological/pathological situations where different oligomeric species and fibrils co-exist in a dynamic equilibrium (Walsh et al., 2000; Shankar et al., 2008; Noguchi et al., 2009; Santos et al., 2012; Esparza et al., 2016). Nevertheless, the results obtained with different Aβ oligomer preparations have yielded rather consistent results (Palop and Mucke, 2010). In particular, the effects exerted by our Aβ preparations, which are compatible with a heterogeneous array of oligomers and the absence of fibrils, are in general agreement with previous reported effects of oligomeric preparations on α7 (Liu et al., 2001; Dineley et al., 2002; Khan et al., 2010; Tong et al., 2011).

α7 ionotropic activity is characterized by very brief, sub-millisecond opening events and rapid desensitization (Bouzat et al., 2008; Corradi and Bouzat, 2016). We found that Aβ is capable of eliciting α7 activity either in the absence or presence of the type II PAM PNU-120596. In both conditions, activation by Aβ was favored at 100 pM or low nanomolar concentrations and was not detected at micromolar concentrations, in close agreement with macroscopic recordings of α7 expressed in oocytes (Dineley et al., 2002, 2015). Channel activity elicited by Aβ was significantly reduced with respect to that elicited by ACh in terms of the number of active patches and frequency of opening events. However, once opened, the mean open duration, cluster architecture and mean cluster duration were similar to those of ACh-elicited channel activity.

Conformational changes of α7 driven by the sole presence of Aβ at a low concentration were sensed by CrV. At 100 pM, oligomeric Aβ drove α7 conformation towards that of desensitized receptors but the subsequent addition of Carb allowed further conformational changes. Although this method senses conformations under equilibrium and cannot provide information about CrV K_D for open channels, the fact that in the presence of Aβ α7 is still responsive to Carb is compatible with the induction of both active and desensitized states. Nevertheless, the conformation of α7 in the presence of low Aβ and high Carb concentrations is different to that of the desensitized state (high Carb alone) as sensed by CrV, thus indicating the induction of a novel conformational state.

The enhancement of α7 activity as a protective role in AD and for the treatment of cognitive and memory impairment associated to neurological disorders appears to be well established (Inestrosa et al., 2013; Lendvai et al., 2013; Wallace and Bertrand, 2013; Uteshev, 2014; Dineley et al., 2015; Corradi and Bouzat, 2016; Yang et al., 2017). Also, a protective, physiological role has been proposed for soluble Aβ at low concentrations in healthy individuals (Giuffrida et al., 2009; Puzzo et al., 2015). Thus, the capability of low concentration Aβ preparations to activate α7 could be related to beneficial physiological effects. However, it would be expected that long-term exposure of an activator would lead to receptor desensitization.

Several reports have shown that high concentrations of Aβ have an inhibitory effect on the amplitude of α7-activated macroscopic currents as well as on signaling pathways (Dineley et al., 2002; Parri et al., 2011). In close agreement, we found that in the presence of PAMs the mean duration of activation episodes (clusters or bursts), which arise from a single receptor molecule, as well as the open channel lifetime are significantly reduced by high concentrations of oligomeric Aβ. There was also a trend of reduced mean durations in the absence of PAMs, but values were not statistically significantly different to the control. However, due to the very brief durations, which are close to the time-resolution limit of our system, such reduction may be underestimated. From a mechanistic point of view, the decreased duration of activation episodes and openings may be compatible with increased desensitization and/or channel block. We can discard fast open-channel blockade since brief closings corresponding to blocked openings (flickering) were not detected. However, enhanced desensitization and slow channel block processes are difficult to distinguish by electrophysiological techniques (Arias et al., 2009; Bouzat and Sine, 2018). CrV experiments showed that at high Aβ concentrations α7 adopts a conformational state which is not different to the resting state in terms of CrV K_D values and from this state α7 is not further reactive to Carb. In agreement with these observations, it was shown for the muscle nAChR that the channel blocker QX-314 does not change the CrV K_D value of the resting state and that this value remains constant even in the presence of Carb (Fabiani et al., 2018). Thus, we can infer that oligomeric Aβ at high concentrations behave as a slow channel blocker of α7. The reduced α7 activity in the presence of Aβ may contribute to the cholinergic signaling deficit and thus may be involved in the initiation and development of AD.

The combined action of PAMs and Aβ suggests that α7 potentiation by PAMs would be probably lower than expected in AD patients. By macroscopic current recordings it has been shown that $Aβ_{1–42}$ inhibits α4β2 and α2β2 receptors and this inhibition is prevented in the presence of a PAM (Pandya and Yakel, 2011). These results are not in full disagreement with ours because, though reduced, we still detected potentiation. The characterization of the influence of Aβ on α7 potentiation contributes to a better extrapolation of the molecular effects of PAMs to their potential therapeutic effects.

A collateral but still important result of our study is the demonstration of different CrV binding profiles between α7 and muscle nAChRs. In the muscle nAChR, the CrV affinity for the desensitized state is greater than for the resting state whereas in α7 it is the other way around. CrV binds to luminal non-competitive antagonist sites which are localized in the channel vestibule (Lurtz and Pedersen, 1999). Our results showed that the conformation of this region is similar for both receptors in the resting state, but it is different in the desensitized state. Thus, the structural arrangements induced by prolonged exposure to Carb are different between muscle and α7 nAChRs. Overall, the use of a conformational probe has proved to be useful for revealing receptor subtype specific structural arrangements associated with functional states and opens doors to further studies in this respect.

The binding site of Aβ remains undefined. Computer docking studies suggested that Aβ may interact with α7 at agonist binding-site interfaces (Espinoza-Fonseca, 2004) and the conserved tyrosine 188 at Loop C of the agonist binding site was proposed to be involved in α7 activation by Aβ (Tong et al., 2011). On the other hand, the transmembrane cavity, a binding site of different allosteric ligands in the Cys-loop receptor family (Gill et al., 2011; Sauguet et al., 2015; Corradi and Bouzat, 2016), was proposed to be involved in the noncompetitive block of Aβ on α4β2 (Pandya and Yakel, 2011). Our spectroscopic results demonstrating that in the presence of low Aβ concentrations α7 is still reactive to Carb suggest that Aβ does not occupy orthosteric agonist binding sites and, in consequence, activation may be mediated by allosteric sites. Allosteric activation of α7 through a transmembrane site has been shown for 4BP-TQS. However, the activity profile is strikingly different to that of ACh, which is not the case of Aβ (Gill et al., 2011; Lasala et al., 2018). Alternatively, Aβ may not occupy the five orthosteric agonist sites but may still be able to induce activation; the remaining sites, subsequently occupied by Carb, may favor activation and desensitization. This possibility is in line with our previous reports showing that occupancy of only one of the five ACh-binding sites is required for α7 activation (Andersen et al., 2013). At high concentrations, Aβ may probably inhibit α7 by acting through an allosteric site, different from that of CrV since it does not interfere with its binding. Dual actions as low-efficacy agonists and channel blockers have been described for several compounds acting at different sites of nAChRs (reviewed in Bouzat and Mukhtasimova, 2018; Bouzat and Sine, 2018).

Overall, our study provides information from a molecular perspective to understand Aβ complex actions at the higher cellular level.

AUTHOR CONTRIBUTIONS

ML, CF, JC, SA and CB contributed to study design, analysis and interpretation of data. ML and CF: acquisition of data. CB and SA contributed to writing.

FUNDING

This work was supported by grants from Universidad Nacional del Sur (UNS) to CB and SA; Agencia Nacional de Promoción Científica y Tecnológica (ANPCYT) to CB and JC; Consejo Nacional de Investigaciones Científicas y Técnicas (CONICET) Argentina to CB and SA.

ACKNOWLEDGMENTS

We are thankful to Drs. Romina Uranga, Gabriela Salvador, Ana Pascual and Susana Pasquare (INIBIBB, Argentina) for help and advice with Aβ preparations.

SUPPLEMENTARY MATERIAL

The Supplementary Material for this article can be found online at: https://www.frontiersin.org/articles/10.3389/fncel.2019.00037/full#supplementary-material

REFERENCES

Andersen, N., Corradi, J., Sine, S. M., and Bouzat, C. (2013). Stoichiometry for activation of neuronal α7 nicotinic receptors. *Proc. Natl. Acad. Sci. U S A* 110, 20819–20824. doi: 10.1073/pnas.1315775110

Andersen, N. D., Nielsen, B. E., Corradi, J., Tolosa, M. F., Feuerbach, D., Arias, H. R., et al. (2016). Exploring the positive allosteric modulation of human α7 nicotinic receptors from a single-channel perspective. *Neuropharmacology* 107, 189–200. doi: 10.1016/j.neuropharm.2016.02.032

Arias, H. R., Gumilar, F., Rosenberg, A., Targowska-Duda, K. M., Feuerbach, D., Jozwiak, K., et al. (2009). Interaction of bupropion with muscle-type nicotinic acetylcholine receptors in different conformational states. *Biochemistry* 48, 4506–4518. doi: 10.1021/bi802206k

Bertrand, D., and Gopalakrishnan, M. (2007). Allosteric modulation of nicotinic acetylcholine receptors. *Biochem. Pharmacol.* 74, 1155–1163. doi: 10.1016/j.bcp.2007.07.011

Bitan, G., Fradinger, E. A., Spring, S. M., and Teplow, D. B. (2005). Neurotoxic protein oligomers—what you see is not always what you get. *Amyloid* 12, 88–95. doi: 10.1080/13506120500106958

Bouzat, C., Bartos, M., Corradi, J., and Sine, S. M. (2008). The interface between extracellular and transmembrane domains of homomeric Cys-loop receptors governs open-channel lifetime and rate of desensitization. *J. Neurosci.* 28, 7808–7819. doi: 10.1523/jneurosci.0448-08.2008

Bouzat, C., Bren, N., and Sine, S. M. (1994). Structural basis of the different gating kinetics of fetal and adult acetylcholine receptors. *Neuron* 13, 1395–1402. doi: 10.1016/0896-6273(94)90424-3

Bouzat, C., Lasala, M., Nielsen, B. E., Corradi, J., and Esandi, M. D. C. (2018). Molecular function of α7 nicotinic receptors as drug targets. *J. Physiol.* 596, 1847–1861. doi: 10.1113/JP275101

Bouzat, C., and Mukhtasimova, N. (2018). The nicotinic acetylcholine receptor as a molecular machine for neuromuscular transmission. *Curr. Opin. Physiol.* 4, 40–48. doi: 10.1016/j.cophys.2018.04.008

Bouzat, C., and Sine, S. M. (2018). Nicotinic acetylcholine receptors at the single-channel level. *Br. J. Pharmacol.* 175, 1789–1804. doi: 10.1111/bph.13770

Buckingham, S. D., Jones, A. K., Brown, L. A., and Sattelle, D. B. (2009). Nicotinic acetylcholine receptor signalling: roles in Alzheimer's disease and amyloid neuroprotection. *Pharmacol. Rev.* 61, 39–61. doi: 10.1124/pr.108.000562

Chatzidaki, A., and Millar, N. S. (2015). Allosteric modulation of nicotinic acetylcholine receptors. *Biochem. Pharmacol.* 97, 408–417. doi: 10.1016/j.bcp.2015.07.028

Cleary, J. P., Walsh, D. M., Hofmeister, J. J., Shankar, G. M., Kuskowski, M. A., Selkoe, D. J., et al. (2005). Natural oligomers of the amyloid-β protein specifically disrupt cognitive function. *Nat. Neurosci.* 8, 79–84. doi: 10.1038/nn1372

Collins-Praino, L. E., Francis, Y. I., Griffith, E. Y., Wiegman, A. F., Urbach, J., Lawton, A., et al. (2014). Soluble amyloid β levels are elevated in the white matter of Alzheimer's patients, independent of cortical plaque severity. *Acta Neuropathol. Commun.* 2:83. doi: 10.1186/s40478-014-0083-0

Corradi, J., and Bouzat, C. (2016). Understanding the bases of function and modulation of 7 nicotinic receptors: implications for drug discovery. *Mol. Pharmacol.* 90, 288–299. doi: 10.1124/mol.116.104240

daCosta, C. J. B., Free, C. R., Corradi, J., Bouzat, C., and Sine, S. M. (2011). Single-channel and structural foundations of neuronal 7 acetylcholine receptor potentiation. *J. Neurosci.* 31, 13870–13879. doi: 10.1523/jneurosci.2652-11.2011

Dineley, K. T. (2007). β-amyloid peptide—nicotinic acetylcholine receptor interaction: the two faces of health and disease. *Front. Biosci.* 12, 5030–5038. doi: 10.2741/2445

Dineley, K. T., Bell, K. A., Bui, D., and Sweatt, J. D. (2002). β-Amyloid peptide activates α 7 nicotinic acetylcholine receptors expressed in *Xenopus* oocytes. *J. Biol. Chem.* 277, 25056–25061. doi: 10.1074/jbc.M200066200

Dineley, K. T., Pandya, A. A., and Yakel, J. L. (2015). Nicotinic ACh receptors as therapeutic targets in CNS disorders. *Trends Pharmacol. Sci.* 36, 96–108. doi: 10.1016/j.tips.2014.12.002

Dougherty, J. J., Wu, J. L., and Nichols, R. A. (2003). β-amyloid regulation of presynaptic nicotinic receptors in rat hippocampus and neocortex. *J. Neurosci.* 23, 6740–6747. doi: 10.1523/jneurosci.23-17-06740.2003

Echeverria, V., Ducatenzeiler, A., Alhonen, L., Janne, J., Grant, S. M., Wandosell, F., et al. (2004a). Rat transgenic models with a phenotype of intracellular Aβ accumulation in hippocampus and cortex. *J. Alzheimers Dis.* 6, 209–219. doi: 10.3233/jad-2004-6301

Echeverria, V., Ducatenzeiler, A., Dowd, E., Jänne, J., Grant, S. M., Szyf, M., et al. (2004b). Altered mitogen-activated protein kinase signaling, tau hyperphosphorylation and mild spatial learning dysfunction in transgenic rats expressing the β-amyloid peptide intracellularly in hippocampal and cortical neurons. *Neuroscience* 129, 583–592. doi: 10.1016/j.neuroscience.2004.07.036

Echeverria, V., Yarkov, A., and Aliev, G. (2016). Positive modulators of the α7 nicotinic receptor against neuroinflammation and cognitive impairment in Alzheimer's disease. *Prog. Neurobiol.* 144, 142–157. doi: 10.1016/j.pneurobio.2016.01.002

Egea, J., Buendia, I., Parada, E., Navarro, E., León, R., and Lopez, M. G. (2015). Anti-inflammatory role of microglial α7 nAChRs and its role in neuroprotection. *Biochem. Pharmacol.* 97, 463–472. doi: 10.1016/j.bcp.2015.07.032

Esparza, T. J., Wildburger, N. C., Jiang, H., Gangolli, M., Cairns, N. J., Bateman, R. J., et al. (2016). Soluble amyloid-β aggregates from human Alzheimer's disease brains. *Sci. Rep.* 6:38187. doi: 10.1038/srep38187

Espinoza-Fonseca, L. M. (2004). Base docking model of the homomeric α7 nicotinic receptor-β-amyloid(1–42) complex. *Biochem. Biophys. Res. Commun.* 320, 587–591. doi: 10.1016/j.bbrc.2004.05.207

Fabiani, C., Murray, A. P., Corradi, J., and Antollini, S. S. (2018). A novel pharmacological activity of caffeine in the cholinergic system. *Neuropharmacology* 135, 464–473. doi: 10.1016/j.neuropharm.2018.03.041

Fernández Nievas, G. A., Barrantes, F. J., and Antollini, S. S. (2008). Modulation of nicotinic acetylcholine receptor conformational state by free fatty acids and steroids. *J. Biol. Chem.* 283, 21478–21486. doi: 10.1074/jbc.M800345200

Gill, J. K., Savolainen, M., Young, G. T., Zwart, R., Sher, E., and Millar, N. S. (2011). Agonist activation of α7 nicotinic acetylcholine receptors *via* an allosteric transmembrane site. *Proc. Natl. Acad. Sci. U S A* 108, 5867–5872. doi: 10.1073/pnas.1017975108

Giuffrida, M. L., Caraci, F., Pignataro, B., Cataldo, S., De Bona, P., Bruno, V., et al. (2009). β-amyloid monomers are neuroprotective. *J. Neurosci.* 29, 10582–10587. doi: 10.1523/JNEUROSCI.1736-09.2009

Grassi, F., Palma, E., Tonini, R., Amici, M., Ballivet, M., and Eusebi, F. (2003). Amyloid β1–42peptide alters the gating of human and mouse α-bungarotoxin-sensitive nicotinic receptors. *J. Physiol.* 547, 147–157. doi: 10.1113/jphysiol.2002.035436

Grønlien, J. H., Håkerud, M., Ween, H., Thorin-hagene, K., Briggs, C. A., Gopalakrishnan, M., et al. (2007). Distinct profiles of α7 nAChR positive allosteric modulation revealed by structurally diverse chemotypes. *Mol. Pharmacol.* 72, 715–724. doi: 10.1124/mol.107.035410

Guan, Y.-Z., Jin, X.-D., Guan, L.-X., Yan, H.-C., Wang, P., Gong, Z., et al. (2015). Nicotine inhibits microglial proliferation and is neuroprotective in global ischemia rats. *Mol. Neurobiol.* 51, 1480–1488. doi: 10.1007/s12035-014-8825-3

Hayden, E. Y., and Teplow, D. B. (2013). Amyloid β-protein oligomers and Alzheimer's disease. *Alzheimers Res. Ther.* 5:60. doi: 10.1186/alzrt226

Hurst, R. S., Hajós, M., Raggenbass, M., Wall, T. M., Higdon, N. R., Lawson, J. A., et al. (2005). A novel positive allosteric modulator of the α7 neuronal nicotinic acetylcholine receptor: *in vitro* and *in vivo* characterization. *J. Neurosci.* 25, 4396–4405. doi: 10.1523/JNEUROSCI.5269-04.2005

Inestrosa, N. C., Godoy, J. A., Vargas, J. Y., Arrazola, M. S., Rios, J. A., Carvajal, F. J., et al. (2013). Nicotine prevents synaptic impairment induced by amyloid-β oligomers through α7-nicotinic acetylcholine receptor activation. *Neuromolecular Med.* 15, 549–569. doi: 10.1007/s12017-013-8242-1

Jin, Y., Tsuchiya, A., Kanno, T., and Nishizaki, T. (2015). Amyloid-β peptide increases cell surface localization of α7 ACh receptor to protect neurons from amyloid β-induced damage. *Biochem. Biophys. Res. Commun.* 468, 157–160. doi: 10.1016/j.bbrc.2015.10.141

Kabbani, N., Nordman, J. C., Corgiat, B. A., Veltri, D. P., Shehu, A., Seymour, V. A., et al. (2013). Are nicotinic acetylcholine receptors coupled to G proteins? *Bioessays* 35, 1025–1034. doi: 10.1002/bies.201300082

Kandimalla, R., and Reddy, P. H. (2017). Therapeutics of neurotransmitters in Alzheimer's disease. *J. Alzheimers Dis.* 57, 1049–1069. doi: 10.3233/JAD-161118

Khan, G. M., Tong, M., Jhun, M., Arora, K., and Nichols, R. A. (2010). β-Amyloid activates presynaptic α7 nicotinic acetylcholine receptors reconstituted into a model nerve cell system: involvement of lipid rafts. *Eur. J. Neurosci.* 31, 788–796. doi: 10.1111/j.1460-9568.2010.07116.x

Lacor, P. N., Buniel, M. C., Chang, L., Fernandez, S. J., Gong, Y., Viola, K. L., et al. (2004). Synaptic targeting by Alzheimer's-related amyloid β oligomers. *J. Neurosci.* 24, 10191–10200. doi: 10.1523/JNEUROSCI.3432-04.2004

Lasala, M., Corradi, J., Bruzzone, A., Esandi, M. D. C., and Bouzat, C. (2018). A human-specific, truncated α7 nicotinic receptor subunit assembles with full-length α7 and forms functional receptors with different stoichiometries. *J. Biol. Chem.* 293, 10707–10717. doi: 10.1074/jbc.RA117.001698

Lendvai, B., Kassai, F., Szájli, A., and Némethy, Z. (2013). α7 nicotinic acetylcholine receptors and their role in cognition. *Brain Res. Bull.* 93, 86–96. doi: 10.1016/j.brainresbull.2012.11.003

Li, S. F., Wu, M. N., Wang, X. H., Yuan, L., Yang, D., and Qi, J. S. (2011). Requirement of α7 nicotinic acetylcholine receptors for amyloid β protein-Induced depression of hippocampal long-term potentiation in CA1 region of rats *in vivo*. *Synapse* 65, 1136–1143. doi: 10.1002/syn.20951

Liu, Q., Kawai, H., and Berg, D. K. (2001). β-Amyloid peptide blocks the response of α 7-containing nicotinic receptors on hippocampal neurons. *Proc. Natl. Acad. Sci. U S A* 98, 4734–4739. doi: 10.1073/pnas.081553598

Liu, Q., Xie, X., Emadi, S., Sierks, M. R., and Wu, J. (2015). A novel nicotinic mechanism underlies β-amyloid-induced neurotoxicity. *Neuropharmacology* 97, 457–463. doi: 10.1016/j.neuropharm.2015.04.025

Lurtz, M. M., and Pedersen, S. E. (1999). Aminotriarylmethane dyes are high-affinity noncompetitive antagonists of the nicotinic acetylcholine receptor. *Mol. Pharmacol.* 55, 159–167. doi: 10.1124/mol.55.1.159

Miñano-Molina, A. J., España, J., Martín, E., Barneda-Zahonero, B., Fadó, R., Solé, M., et al. (2011). Soluble oligomers of amyloid-β peptide disrupt membrane trafficking of α-amino-3-hydroxy-5-methylisoxazole-4-propionic acid receptor contributing to early synapse dysfunction. *J. Biol. Chem.* 286, 27311–27321. doi: 10.1074/jbc.M111.227504

Nielsen, B. E., Minguez, T., Bermudez, I., and Bouzat, C. (2018). Molecular function of the novel α7β2 nicotinic receptor. *Cell. Mol. Life Sci.* 75, 2457–2471. doi: 10.1007/s00018-017-2741-4

Noguchi, A., Matsumura, S., Dezawa, M., Tada, M., Yanazawa, M., Ito, A., et al. (2009). Isolation and characterization of patient-derived, toxic, high mass amyloid β-protein (Aβ) assembly from Alzheimer disease brains. *J. Biol. Chem.* 284, 32895–32905. doi: 10.1074/jbc.M109.000208

Palop, J., and Mucke, L. (2010). Amyloid-β induced neuronal dysfunction in Alzheimer's disease: from synapses toward neural networks. *Nat. Neurosci.* 13, 812–818. doi: 10.1038/nn.2583

Pandya, A., and Yakel, J. L. (2011). Allosteric modulator desformylflustrabromine relieves the inhibition of α2β2 and α4β2 nicotinic acetylcholine receptors by β-amyloid 1–42 peptide. *J. Mol. Neurosci.* 45, 42–47. doi: 10.1007/s12031-011-9509-3

Parihar, M. S., and Brewer, G. J. (2010). Amyloid-β as a modulator of synaptic plasticity. *J. Alzheimers Dis.* 22, 741–763. doi: 10.3233/JAD-2010-101020

Parri, H. R., Hernandez, C. M., and Dineley, K. T. (2011). Research update: α7 nicotinic acetylcholine receptor mechanisms in Alzheimer's disease. *Biochem. Pharmacol.* 82, 931–942. doi: 10.1016/j.bcp.2011.06.039

Pascual, A. C., Gaveglio, V. L., Giusto, N. M., and Pasquaré, S. J. (2017). 2-Arachidonoylglycerol metabolism is differently modulated by oligomeric and fibrillar conformations of amyloid β in synaptic terminals. *Neuroscience* 362, 168–180. doi: 10.1016/j.neuroscience.2017.08.042

Perillo, V. L., Fernández-Nievas, G. A., Vallés, A. S., Barrantes, F. J., and Antollini, S. S. (2012). The position of the double bond in monounsaturated free fatty acids is essential for the inhibition of the nicotinic acetylcholine receptor. *Biochim. Biophys. Acta* 1818, 2511–2520. doi: 10.1016/j.bbamem.2012.06.001

Pear, W. S., Nolan, G. P., Scott, M. L., and Baltimore, D. (1993). Production of high-titer helper-free retroviruses by transient transfection. *Proc. Natl. Acad. Sci. U S A* 90, 8392–8396. doi: 10.1109/ICDMW.2006.113

Puzzo, D., Gulisano, W., Arancio, O., and Palmeri, A. (2015). The keystone of Alzheimer pathogenesis might be sought in Aβ physiology. *Neuroscience* 307, 26–36. doi: 10.1016/j.neuroscience.2015.08.039

Puzzo, D., Privitera, L., Fa', M., Staniszewski, A., Hashimoto, G., Aziz, F., et al. (2011). Endogenous amyloid-β is necessary for hippocampal synaptic plasticity and memory. *Ann. Neurol.* 69, 819–830. doi: 10.1002/ana.22313

Pym, L., Kemp, M., Raymond-Delpech, V., Buckingham, S., Boyd, C. A. R., and Sattelle, D. (2005). Subtype-specific actions of β-amyloid peptides on recombinant human neuronal nicotinic acetylcholine receptors (α7, α4β2, α3β4) expressed in *Xenopus laevis* oocytes. *Br. J. Pharmacol.* 146, 964–971. doi: 10.1038/sj.bjp.0706403

Qin, F., Auerbach, A., and Sachs, F. (1996). Estimating single-channel kinetic parameters from idealized patch-clamp data containing missed events. *Biophys. J.* 70, 264–280. doi: 10.1016/s0006-3495(96)79568-1

Qin, F., Auerbach, A., and Sachs, F. (1997). Maximum likelihood estimation of aggregated Markov processes. *Proc. Biol. Sci.* 264, 375–383. doi: 10.1098/rspb.1997.0054

Sadigh-Eteghad, S., Talebi, M., Farhoudi, M., Golzari, S. E. J., Sabermarouf, B., and Mahmoudi, J. (2014). β-amyloid exhibits antagonistic effects on α 7 nicotinic acetylcholine receptors in orchestrated manner. *J. Med. Hypotheses Ideas* 8, 49–52. doi: 10.1016/j.jmhi.2014.01.001

Santos, A. N., Ewers, M., Minthon, L., Simm, A., Silber, R.-E., Blennow, K., et al. (2012). Amyloid-β oligomers in cerebrospinal fluid are associated with cognitive decline in patients with Alzheimer's disease. *J. Alzheimers Dis.* 29, 171–176. doi: 10.3233/JAD-2012-111361

Sauguet, L., Shahsavar, A., and Delarue, M. (2015). Crystallographic studies of pharmacological sites in pentameric ligand-gated ion channels. *Biochim. Biophys. Acta* 1850, 511–523. doi: 10.1016/j.bbagen.2014.05.007

Shankar, G. M., Li, S., Mehta, T. H., Garcia-Munoz, A., Shepardson, N. E., Smith, I., et al. (2008). Amyloid-β protein dimers isolated directly from Alzheimer's brains impair synaptic plasticity and memory. *Nat. Med.* 14, 837–842. doi: 10.1038/nm1782

Sun, J., Comeau, J. F., and Baenziger, J. E. (2017). Probing the structure of the uncoupled nicotinic acetylcholine receptor. *Biochim. Biophys. Acta Biomembr.* 1859, 146–154. doi: 10.1016/j.bbamem.2016.11.009

Terry, A. V. Jr., Callahan, P. M., and Bertrand, D. (2015). R-(+) and S-(-) isomers of cotinine augment cholinergic responses *in vitro* and *in vivo*. *J. Pharmacol. Exp. Ther.* 352, 405–418. doi: 10.1124/jpet.114.219881

Timmermann, D. B., Grønlien, J. H., Kohlhaas, K. L., Nielsen, E. Ø., Dam, E., Jørgensen, T. D., et al. (2007). An allosteric modulator of the α7 nicotinic acetylcholine receptor possessing cognition-enhancing properties *in vivo*. *J. Pharmacol. Exp. Ther.* 323, 294–307. doi: 10.1124/jpet.107.120436

Tong, M., Arora, K., White, M. M., and Nichols, R. A. (2011). Role of key aromatic residues in the ligand-binding domain of α7 nicotinic receptors in the agonist action of β-amyloid. *J. Biol. Chem.* 286, 34373–34381. doi: 10.1074/jbc.M111.241299

Uranga, R. M., Alza, N. P., Conde, M. A., Antollini, S. S., and Salvador, G. A. (2016). Phosphoinositides: two-path signaling in neuronal response to oligomeric amyloid β peptide. *Mol. Neurobiol.* 54, 3236–3252. doi: 10.1007/s12035-016-9885-3

Uteshev, V. V. (2014). The therapeutic promise of positive allosteric modulation of nicotinic receptors. *Eur. J. Pharmacol.* 727, 181–185. doi: 10.1016/j.ejphar.2014.01.072

Wallace, T. L., and Bertrand, D. (2013). α7 neuronal nicotinic receptors as a drug target in schizophrenia. *Expert Opin. Ther. Targets* 17, 139–155. doi: 10.1517/14728222.2013.736498

Walsh, D. M., Klyubin, I., Fadeeva, J. V., Cullen, W. K., Anwyl, R., Wolfe, M. S., et al. (2002). Naturally secreted oligomers of amyloid β protein potently inhibit hippocampal long-term potentiation *in vivo*. *Nature* 416, 535–539. doi: 10.1038/416535a

Walsh, D. M., Tseng, B. P., Rydel, R. E., Podlisny, M. B., and Selkoe, D. J. (2000). The oligomerization of amyloid β-protein begins intracellularly in cells derived from human brain. *Biochemistry* 39, 10831–10839. doi: 10.1021/bi001048s

Wang, H.-Y., Lee, D. H. S., D'Andrea, M. R., Peterson, P. A., Shank, R. P., and Reitz, A. B. (2000). β-Amyloid1–42 Binds to α 7 nicotinic acetylcholine receptor with high affinity. Implications for Alzheimer's disease pathology. *J. Biol. Chem.* 275, 5626–5632. doi: 10.1074/jbc.275.8.5626

Wang, H. W., Pasternak, J. F., Kuo, H., Ristic, H., Lambert, M. P., Chromy, B., et al. (2002). Soluble oligomers of β amyloid (1–42g) inhibit long-term potentiation but not long-term depression in rat dentate gyrus. *Brain Res.* 924, 133–140. doi: 10.1016/s0006-8993(01)03058-x

Watt, A. D., Perez, K. A., Rembach, A., Sherrat, N. A., Hung, L. W., Johanssen, T., et al. (2013). Oligomers, fact or artefact? SDS-PAGE induces dimerization of β-amyloid in human brain samples. *Acta Neuropathol.* 125, 549–564. doi: 10.1007/s00401-013-1083-z

Wonnacott, S. (2014). Nicotinic ACh receptors. *Tocris Biosci. Sci. Rev. Ser. Nicotinic*, 1–31.

Wu, J., Kuo, Y.-P. P., George, A. A., Xu, L., Hu, J., Lukas, R. J., et al. (2004). β-amyloid directly inhibits human α4β2-nicotinic acetylcholine receptors heterologously expressed in human SH-EP1 cells. *J. Biol. Chem.* 279, 37842–37851. doi: 10.1074/jbc.m400335200

Yan, H., Pan, N., Xue, F., Zheng, Y., Li, C., Chang, Y., et al. (2015). The coupling interface and pore domain codetermine the single-channel activity of theα7 nicotinic receptor. *Neuropharmacology* 95, 448–458. doi: 10.1016/j.neuropharm.2015.04.010

Yang, T., Xiao, T., Sun, Q., and Wang, K. (2017). The current agonists and positive allosteric modulators of α7 nAChR for CNS indications in clinical trials. *Acta Pharm. Sin. B* 7, 611–622. doi: 10.1016/j.apsb.2017.09.001

Conflict of Interest Statement: The authors declare that the research was conducted in the absence of any commercial or financial relationships that could be construed as a potential conflict of interest.

frontiers in Cellular Neuroscience

ORIGINAL RESEARCH
published: 01 March 2019
doi: 10.3389/fncel.2019.00062

Early Developmental Marginal Zinc Deficiency Affects Neurogenesis Decreasing Neuronal Number and Altering Neuronal Specification in the Adult Rat Brain

Ana M. Adamo[1†], *Xiuzhen Liu*[2†], *Patricia Mathieu*[1], *Johnathan R. Nuttall*[2], *Suangsuda Supasai*[2,3] *and Patricia I. Oteiza*[2*]

[1]Department of Biological Chemistry and IQUIFIB (UBA-CONICET), Facultad de Farmacia y Bioquimica, Universidad de Buenos Aires, Buenos Aires, Argentina, [2]Department of Nutrition and Department of Environmental Toxicology, University of California, Davis, Davis, CA, United States, [3]Department of Molecular Tropical Medicine and Genetics, Faculty of Tropical Medicine, Mahidol University, Bangkok, Thailand

OPEN ACCESS

Edited by:
Gabriela Alejandra Salvador, Universidad Nacional del Sur, Argentina

Reviewed by:
Herminia Alicia Brusco, Instituto de Biologia Celular y Neurociencia (UBA-CONICET), Argentina,
João Laranjinha, University of Coimbra, Portugal

***Correspondence:**
Patricia I. Oteiza
poteiza@ucdavis.edu

[†]*These authors have contributed equally to this work*

Received: *21 December 2018*
Accepted: *08 February 2019*
Published: *01 March 2019*

Citation:
Adamo AM, Liu X, Mathieu P, Nuttall JR, Supasai S and Oteiza PI (2019) Early Developmental Marginal Zinc Deficiency Affects Neurogenesis Decreasing Neuronal Number and Altering Neuronal Specification in the Adult Rat Brain. Front. Cell. Neurosci. 13:62. doi: 10.3389/fncel.2019.00062

During pregnancy, a decreased availability of zinc to the fetus can disrupt the development of the central nervous system leading to defects ranging from severe malformations to subtle neurological and cognitive effects. We previously found that marginal zinc deficiency down-regulates the extracellular signal-regulated kinase 1/2 (ERK1/2) signaling pathway and affects neural progenitor cell (NPC) proliferation. This study investigated if marginal zinc deficiency during gestation in rats could disrupt fetal neurogenesis and affect the number and specification of neurons in the adult offspring brain cortex. Rats were fed a marginal zinc deficient or adequate diet throughout gestation and until postnatal day (P) 2, and subsequently the zinc adequate diet until P56. Neurogenesis was evaluated in the offspring at embryonic day (E)14, E19, P2, and P56 measuring parameters of NPC proliferation and differentiation by Western blot and/or immunofluorescence. At E14 and E19, major signals (i.e., ERK1/2, Sox2, and Pax6) that stimulate NPC proliferation and self-renewal were markedly downregulated in the marginal zinc deficient fetal brain. These alterations were associated to a lower number of Ki67 positive cells in the ventricular (VZs) and subventricular zones (SVZs). Following the progression of NPCs into intermediate progenitor cells (IPCs) and into neurons, Pax6, Tbr2 and Tbr1 were affected in the corresponding areas of the brain at E19 and P2. The above signaling alterations led to a lower density of neurons and a selective decrease of glutamatergic neurons in the young adult brain cortex exposed to maternal marginal zinc deficiency from E14 to P2. Current results supports the concept that marginal zinc deficiency during fetal development can disrupt neurogenesis and alter cortical structure potentially leading to irreversible neurobehavioral impairments later in life.

Keywords: zinc, brain development, ERK1/2, Tbr2, zinc deficiency

INTRODUCTION

Prenatal zinc deficiency resulting from insufficient dietary intake, absorption, or transport can compromise development of the central nervous system leading to a spectrum of defects ranging from severe congenital malformations to subtle neurological and cognitive impairments. Severe zinc deficiency during fetal development has been implicated as a mechanism contributing to neural tube defects (NTDs). Severe dietary zinc deficiency in rats during pregnancy leads to NTDs in association with decreased cell proliferation in the ventricular zone (VZ) of the fetal brain (Swenerton et al., 1969). In humans, supplementation with dietary zinc and adequate plasma zinc concentrations are related to a reduced risk of NTDs (Velie et al., 1999; Dey et al., 2010). Although developmental marginal zinc deficiency does not cause gross malformations like NTDs, it is associated with neurological morbidity such as impairments in learning, working memory, and social behavior (Hagmeyer et al., 2015). Similar cognitive defects result from secondary zinc deficiency caused by gestational exposure to infection in rats (Kirsten et al., 2015).

Developmental exposure to a decreased zinc availability could have a long-term and irreversible impact on the offspring's brain leading to neurological and behavioral disorders later in life. In rats, severe postnatal zinc deficiency impairs neurogenesis in the cerebellum (Dvergsten et al., 1983), and decreases the expression of genes related to proliferation and neuronal differentiation in the hippocampus (Gower-Winter et al., 2013). In cultured cells, zinc deficiency impairs human IMR-32 neuroblastoma cell proliferation and induces apoptosis (Adamo et al., 2010), and inhibits retinoic acid-induced neuronal differentiation (Gower-Winter et al., 2013). Furthermore, zinc deficiency alters brain redox regulation and affects signaling pathways involved in neurogenesis (Zago et al., 2005; Aimo et al., 2010a,b; Mackenzie et al., 2011). Thus, we previously observed that gestational marginal zinc deficiency in rats decreases the number of neuronal progenitor cells (NPCs) expressing Ki67 in the VZ at embryonic day (E) 19 (Nuttall et al., 2015). NPCs give rise to all neuronal types present in the brain and play a pivotal role in regulating the balance between cell self-renewal and neurogenesis. Cortical excitatory neurons are directly generated from radial glial progenitors (RGPs) during embryonic neurogenesis or indirectly through intermediate progenitor cells (IPCs) derived from the VZ (Haubensak et al., 2004; Noctor et al., 2004). Radial glia proliferate at the ventricular surface and IPCs divide at a non-surface area in the VZ and subventricular zone (SVZ). The transcription factor cascade involving Pax6, Tbr2 and Tbr1 regulates the different stages of differentiation from NPCs to IPCs to cortical neurons. Tbr1 and Tbr2 are part of the T-box transcription factor subfamily Tbr1, and play key roles in glutamatergic neuron differentiation in the cerebral cortex, olfactory bulbs, hippocampal dentate gyrus, cerebellum and adult SVZ (Mihalas and Hevner, 2017). The extracellular signal-regulated kinase (ERK1/2) pathway is also a key regulator of NPC proliferation and neuronal differentiation (Nuttall and Oteiza, 2012). Marginal zinc deficiency during pregnancy in rats causes a decreased phosphorylation of ERK1/2 in the frontal cortex of the fetal rat brain at E19 (Nuttall et al., 2015) which is associated with a decrease in NPC number. However, it remains unclear if this decrease in NPCs can affect the number of neurons in the adult offspring brain as well as the process of neuronal differentiation and specification.

A complex and tightly regulated cascade of events lead to the differentiation of NPCs into neurons. Our previous results showed impaired NPC proliferation in association with maternal zinc deficiency. Thus, the goal of the present work was to evaluate whether a marginal zinc diet fed throughout gestation and until postnatal day (P) 2 can: (i) affect, in the offspring brain, the transcription factor cascade involved in NPC and IPC proliferation and differentiation into glutamatergic neurons; and (ii) cause long-term effects in the number and specification of cortical neurons in the offspring young adult brain. To such end, the temporal activation/expression of ERK1/2 and transcription factors Sox2, Pax6, Tbr2 and Tbr1 were characterized in the E14, E19 and P2 offspring brain. Alterations in cortical neuronal number and specification to glutamatergic and GABAergic neurons secondary to maternal marginal zinc deficiency were assessed in the adult offspring brain after postnatal repletion of dietary zinc.

MATERIALS AND METHODS

Materials

Primary antibodies for β-actin (#12620), phospho (Thr202/Tyr204) ERK (#4370), and ERK (#9102), were from Cell Signaling Technology (Danvers, MA, USA). Antibodies for glutamic acid decarboxylase 65 (GAD65; SC-377154) and Tbr1 (SC-376258; Western blot) were from Santa Cruz Biotechnology (Santa Cruz, CA, USA). Antibodies for Neu-N (MAB377) and Tbr2 (AB15894) were from Millipore (Burlington, MA, USA). The antibody for Ki67 (550609) was obtained from BD Pharmingen (San José, CA, USA). Antibodies for Sox2 (ab97959), Tbr1 (ab31941; immunofluorescence), vGlut1 (ab77822) and Pax6 (ab5790) were from Abcam Inc. (Cambridge, MA, USA). Secondary fluorescent antibodies were obtained from Jackson ImmunoResearch Co. Laboratories (West Grove, PA, USA). Polyvinylidene difluoride (PVDF), membranes and molecular weight standards for Western blot were obtained from BIO-RAD (Hercules, CA, USA). The enhanced chemiluminescence (ECL) Western blotting system was from Thermo Fisher Scientific Inc. (Piscataway, NJ, USA). Zinquin, the antibody for γ amino butyric acid (GABA; A2052), and all other reagents were of the highest quality available and were purchased from Sigma-Aldrich Co. (St. Louis, MO, USA).

Animals and Animal Care

All procedures were in agreement with standards for the care of laboratory animals as outlined in the National Institutes of Health Guide for the Care and Use of Laboratory Animals. All procedures were administered under the auspices of the Animal Resource Services of the University of California at Davis, which is accredited by the American Association for the Accreditation of Laboratory Animal Care. Experimental protocols were approved before implementation by the University of California at Davis Animal Use and Care Administrative Advisory

Committee and were administered through the Office of the Campus Veterinarian. Adult Sprague-Dawley rats (Charles River, Wilmington, MA, USA; 200–225 g) were housed individually in stainless steel cages in a temperature—(22–23°C) and photoperiod—(12-h light/dark) controlled room. An egg-white protein-based diet with adequate zinc (25 μg zinc/g) was the standard control diet (Keen et al., 1989). Animals were fed the control diet for 1 week before breeding. The overall experimental design is shown in **Figure 1A**. Males and females were caged together overnight and the following morning (E0), after the presence of a sperm plug confirmed a successful breeding, female rats (six animals/group for E14, E19, and P2/P56) were divided into two groups and fed *ad libitum* a control diet (25 μg zinc/g diet, control group) or a diet containing a marginal concentration of zinc (10 μg zinc/g diet; MZD group). Food intake was recorded daily, and body weight was measured at 3-day intervals. On E14 and E19, dams were anesthetized with isoflurane (2 mg/kg body weight) and laparotomies were performed. The gravid uterus was removed and fetuses were weighed. Fetal brains were removed, weighed and immediately either processed for immunohistochemistry, or removed and kept on ice to microdissect regions enriched in cortical tissue (CT), which were then frozen in liquid nitrogen and stored at −80°C. In the E14 offspring, CT included the cortical neuroepithelium with the SVZ and VZ; in E19 offspring, CT included the cortical plate with the SVZ and VZ. At P2, litters were adjusted to eight pups/litter, and brain/brain cortices were dissected from the euthanized pups and processed as described before. Dams from both the control and the MZD groups were subsequently fed the control diet. Pups were weaned at P21 and were all fed the control diet until P56 when euthanized; blood and brain/brain cortex collection was carried out as described before.

With regard to the time of exposure of the offspring to zinc deficiency, it should be considered that milk zinc content does not decrease in conditions of marginal zinc nutrition both in rodents and humans, even when maternal plasma zinc levels are low (Kelleher and Lönnerdal, 2005). Thus, in the current experimental model, it is expected that the offspring would have access to similar amounts of zinc in milk starting at birth in both control and MZD groups.

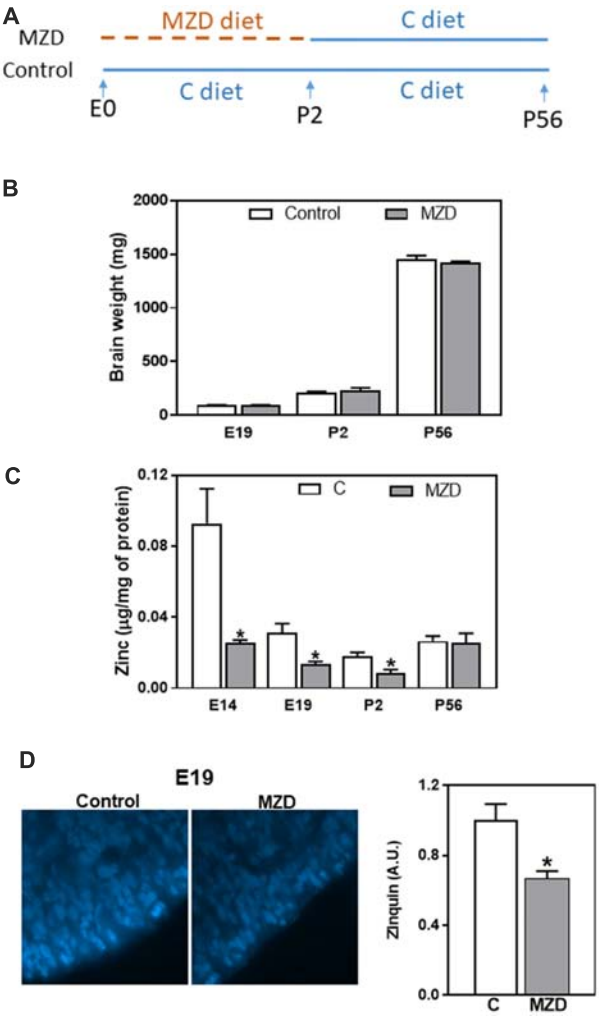

FIGURE 1 | Fetal/offspring brain weight and zinc concentration after maternal consumption of a control or a marginal zinc diet throughout gestation and until postnatal day (P) 2. **(A)** Experimental design. **(B)** Embryonic day (E) 19–P56 offspring brain weight. **(C)** Zinc concentration in fetal/offspring cortical tissue (CT) and brain cortex 100,000× *g* supernatants were measured by atomic emission spectroscopy (AES). **(D)** Labile zinc was measured in the ventricular zone (VZ) at E19 by zinquin staining (blue fluorescence). Micrographs show the VZ of the dorsomedial frontal cortex at 1,000-fold magnification. Fluorescence was quantified as described in "Materials and Methods" section. **(B–D)** Data are shown as mean ± SEM and are the average of 4–6 litters per group. *Significantly different from the control group at the same developmental stage (*t*-test, $p < 0.05$).

Determination of Zinc Concentrations

The concentration of zinc in diets and brain supernatants was measured by inductively coupled plasma atomic emission spectroscopy (ICP-AES) as described by Clegg et al. (2005). E14 and E19 brain CT and P2 and P56 cortices were weighed, homogenized in ice-cold PBS (1:10), and centrifuged for 60 min at 100,000× *g* at 4°C. The supernatant was collected and protein concentration was measured using the Bradford assay (Bradford, 1976). Three milliliter of 16 N HNO_3 were added to the 100,000× *g* supernatants and diet samples and allowed to digest for 72 h. Samples were dried, and resuspended in ultrapure water. Zinc concentration was determined by inductively coupled plasma atomic emission spectroscopy (ICP-AES; Trace Scan; Thermo Elemental, Franklin, MA, USA). Certified reference solutions (QC 21; Spec CentriPrep, Metuchen, NJ, USA) were used to generate standard curves. A sample of a National Bureau of Standards bovine liver (SRM1577; U.S. Department of Commerce, National Bureau of Standards, Washington, DC, USA) was included with the samples to ensure accuracy and reproducibility.

Zinquin Staining

Labile zinc was measured in coronal sections from the fetal rat brain at E19. Slides were overlaid with a solution of 25 μM zinquin in Hank's balanced salt solution (HBSS)

and incubated at 37°C for 40 min. After washing in HBSS, coverslips were mounted with a solution of 90% glycerol and 10% HBSS and imaged on an Olympus BX50 epifluorescence microscope provided with a Cool-Snap digital camera. Image pro software (Rockville, MD, USA) was used to analyze the resulting micrographs. Three randomly selected fields were measured per animal and experimental condition ($n = 3$).

Western Blot Analysis

Extraction of total cellular protein from CT and cortex homogenates was done as previously described (Aimo et al., 2010b). Protein concentration was measured using the Bradford assay (Bradford, 1976), and aliquots containing 25–50 μg of protein were separated by reducing 10% (w/v) SDS-PAGE and electroblotted to PVDF membranes. Colored molecular weight standards were run simultaneously. Membranes were blocked for 1 h in 5% (w/v) nonfat milk and incubated overnight with the corresponding primary antibodies (1:1,000–1:5,000) in 1% (w/v) bovine serum albumin in TBST (20 mM Tris, 150 mM NaCl, pH 7.4, 0.1% Tween 20) at 4°C. After incubation for 1 h at room temperature with the corresponding peroxidase-conjugated secondary antibodies (1:10,000–1:30,000), proteins were visualized by chemiluminescence detection, and subsequently quantified, using a Phosphorimager 840 (Amersham, Piscataway, NJ, USA).

Immunofluorescence

E14, E19, and P2 rat brains were dissected out and fixed in a 4% (w/v) solution of paraformaldehyde in PBS overnight. P56 rats were deeply anesthetized as described above and perfused transcardially with PBS followed by 4% (w/v) solution of paraformaldehyde in PBS, after which brains were collected. In all cases, tissue cryoprotection was subsequently performed in 30% (w/v) sucrose until the tissue sank down, after which, brains were submerged in Cryoplast freezing medium (Biopack, Buenos Aires, Argentina), frozen, cut into 18 μm coronal sections on a Leica CM 1850 cryotome (Leica Microsystems, Nussloch, Germany), and mounted on positively charged microscope slides. Sections were blocked for 45 min in 1% (v/v) donkey serum in 0.1% (v/v) Triton X-100 in PBS, and incubated with the corresponding dilution of primary antibody in blocking solution (1:200 rabbit anti-Sox2, 1:100 rabbit anti-Pax6, 1:200 rabbit anti-Trb1, 1:100 chicken anti-Tbr2, 1:200 mouse anti-NeuN, 1:200 rabbit anti-vGlut1, 1:200 rabbit anti-GABA, 1:100 mouse anti-Ki67) overnight at 4°C. Sections were then washed once in 0.1% (v/v) Triton X-100 in PBS and once in 0.1 M phosphate buffer, pH 7.4, and incubated with the corresponding dilution of secondary antibody (1:500 Cy3-conjugated donkey anti-rabbit, 1:500 Alexa 488 donkey anti-mouse IgG, and 1:500 Alexa 488 donkey anti-chicken) for 2 h at room temperature. After immunostaining, cell nuclei were stained with 1 μg/ml Hoechst 33342 and sections were imaged using an Olympus FV 1000 laser scanning confocal microscope or an Olympus BX50 epifluorescence microscope provided with a Cool-Snap digital camera. Image pro software (Rockville, MD, USA) was used to merge and analyze the resulting micrographs. Marker-positive cells were counted using ImageJ (National Institutes of Health, Bethesda, MD, USA) and results were expressed as the number of positive cells per area. At least 300 cells were counted for each cell marker, analyzed in three independent experiments that were performed in triplicates for four animals per group. Alternatively, fluorescence intensity was measured for vGlut1 and GABA.

Statistical Analysis

Data for the control and MZD groups at each developmental stage were analyzed by Student's t-test using Statview 5.0 (SAS Institute Inc., Cary, NC, USA). The litter was the statistical unit. A p value < 0.05 was considered statistically significant. Data are shown as mean ± SE.

RESULTS

Animal Outcome

Pregnant dams were fed a marginal zinc or a control diet from E0 until P2. Subsequently all dams until P21, and the

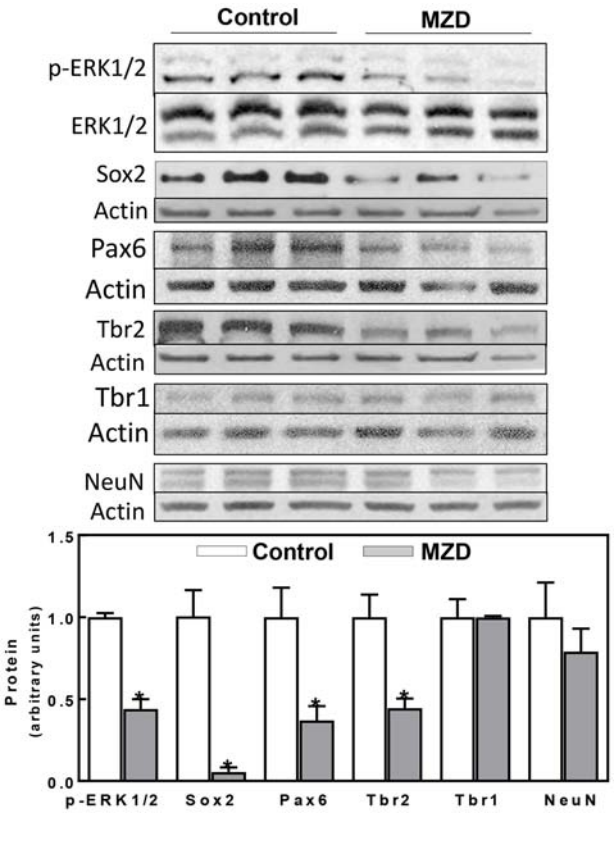

FIGURE 2 | Maternal marginal zinc deficiency affects parameters of neurogenesis in the E14 rat brain. Phospho extracellular signal-regulated kinase 1/2 (ERK1/2), ERK1/2, Sox2, Pax6, Tbr2, Tbr1 and NeuN protein levels were measured by Western blot in E14 brain CT homogenates. After quantification of bands, phospho-ERK1/2 levels were referred to total ERK1/2 content and the other proteins were referred to β-actin levels. Values (arbitrary units, AUs) were normalized to those of the control group (1) Results are shown as mean ± SE of E14 brain cortices from six litters/group. *Significantly different from the control group ($p < 0.05$, Student's t-test).

offspring, until P56, were fed the control diet (**Figure 1A**). As previously described (Aimo et al., 2010b; Nuttall et al., 2015), we observed that a marginal zinc nutrition throughout gestation does not affect overall maternal and fetal outcome (data not shown). Furthermore, consumption of the marginal zinc diet throughout gestational and perinatal period did not affect fetal/offspring brain weight between E19 and P56 (**Figure 1B**). Zinc concentration in E14 and E19 CT and P2 brain cortex 100,000× *g* supernatants was significantly lower (72%, 58% and 56%, respectively) in MZD offspring compared to the control group (**Figure 1C**). Loosely bound zinc in the E19 brain was evaluated by Zinquin staining and subsequent fluorescence microscopy. In the control group, Zinquin fluorescence appeared strongest in the VZ and surrounding blood vessels. In the MZD offspring VZ, the intensity of Zinquin fluorescence was 34% lower than in controls (**Figure 1D**).

Maternal Marginal Zinc Deficiency Affects Markers of Neurogenesis at E14

Given our previous work showing a decrease in ERK1/2 activation together with a reduction in NPC proliferation, we aimed to investigate the impact of these events on cortical excitatory neurons. Signaling cascades involved in NPC proliferation, self-renewal, and progression to differentiation were evaluated at E14 (**Figure 2**). ERK1/2 phosphorylation was 66%, lower in the MZD E14 brain CT compared to controls (**Figure 2**). Maternal marginal zinc nutrition also affected different markers of NPC proliferation and progression to differentiation as evaluated by Western blot (**Figure 2**). Sox2 is a transcription factor that controls the self-renewal of NPCs throughout development. Maternal marginal zinc deficiency caused a 95% decrease in E14 cortical Sox2 levels compared to controls. Pax6, a transcription factor that is central to the development of the brain cortex, showed 63% lower levels in the E14 cortex from MZD compared to the control group (**Figure 2**). Marginal zinc nutrition also affected the abundance of Tbr2, a transcription factor that regulates the specification of the intermediate neural progenitors (INPs) that will differentiate into excitatory neurons. Tbr2 levels were 55% lower in MZD compared to control E14 CT. Protein levels of Tbr1 and of the marker of post-mitotic mature neurons NeuN were similar between groups.

Maternal Marginal Zinc Deficiency Affects Markers of Neurogenesis in the Offspring Brain at E19 and P2

At E19, all measured markers of cortical neurogenesis, from NPC proliferation to fully differentiated neurons, were affected in the MZD embryo brain (**Figure 3**). ERK1/2 phosphorylation was lower (36%) in the E19 CT from MZD compared to controls. Sox2, Pax6, Tbr2, Tbr1 and NeuN protein levels were 57, 37, 57, 43 and 42% lower in MZD compared to control embryo CT as measured by Western blot (**Figure 3A**). Immunofluorescence analysis also showed lower levels of total proliferative cells in the E19 SVZ of MZD compared to control

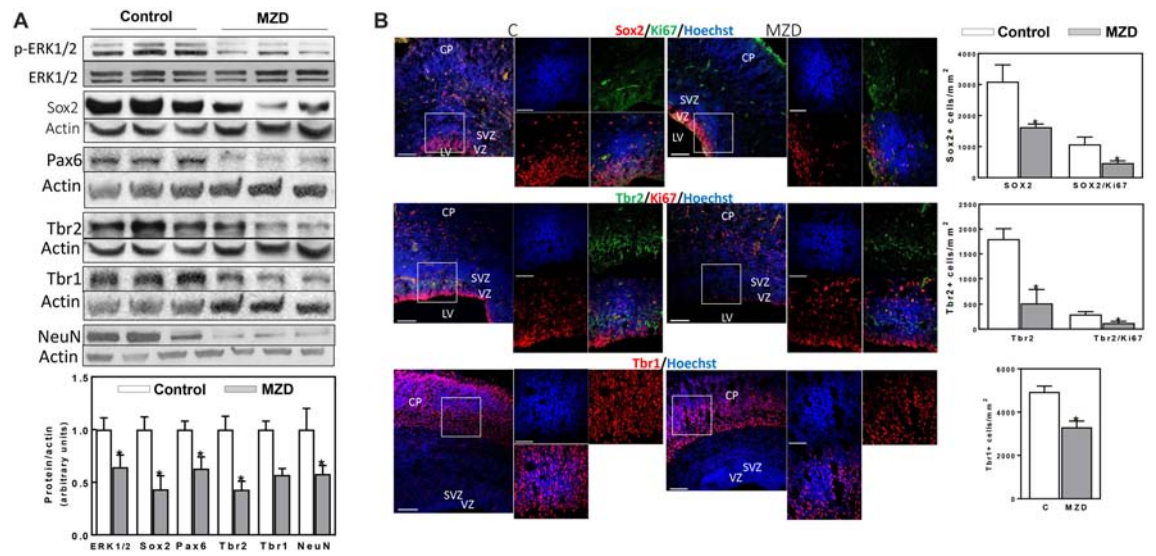

FIGURE 3 | Maternal marginal zinc deficiency affects parameters of neurogenesis in the E19 rat brain. **(A)** Phospho ERK1/2, ERK1/2, Sox2, Pax6, Tbr2, Tbr1 and NeuN protein levels were measured by Western blot in E19 CT homogenates. After quantification of bands, phospho-ERK1/2 levels were referred to total ERK1/2 content and the other proteins were referred to β-actin levels. Values (AUs) were normalized to those of the control group (1) Results are shown as mean ± SE of fetal brain cortices from six litters/group. *Significantly different from the control group ($p < 0.05$, Student's *t*-test). **(B)** Immunofluorescence for Sox2 (red fluorescence) and Ki67 (green fluorescence); Tbr2 (green fluorescence) and Ki67 (red fluorescence); Tbr1 (red fluorescence) and Ki67 (green fluorescence). Nuclei were visualized with Hoechst staining (blue fluorescence; Scale bar, 100 μm). Images in boxes are shown at a higher magnification (Scale bar, 50 μm). Quantifications were done as described in methods. Results are shown as mean ± SE of E19 brains from four litters/group. *Significantly different from the control group ($p < 0.05$, Student's *t*-test).

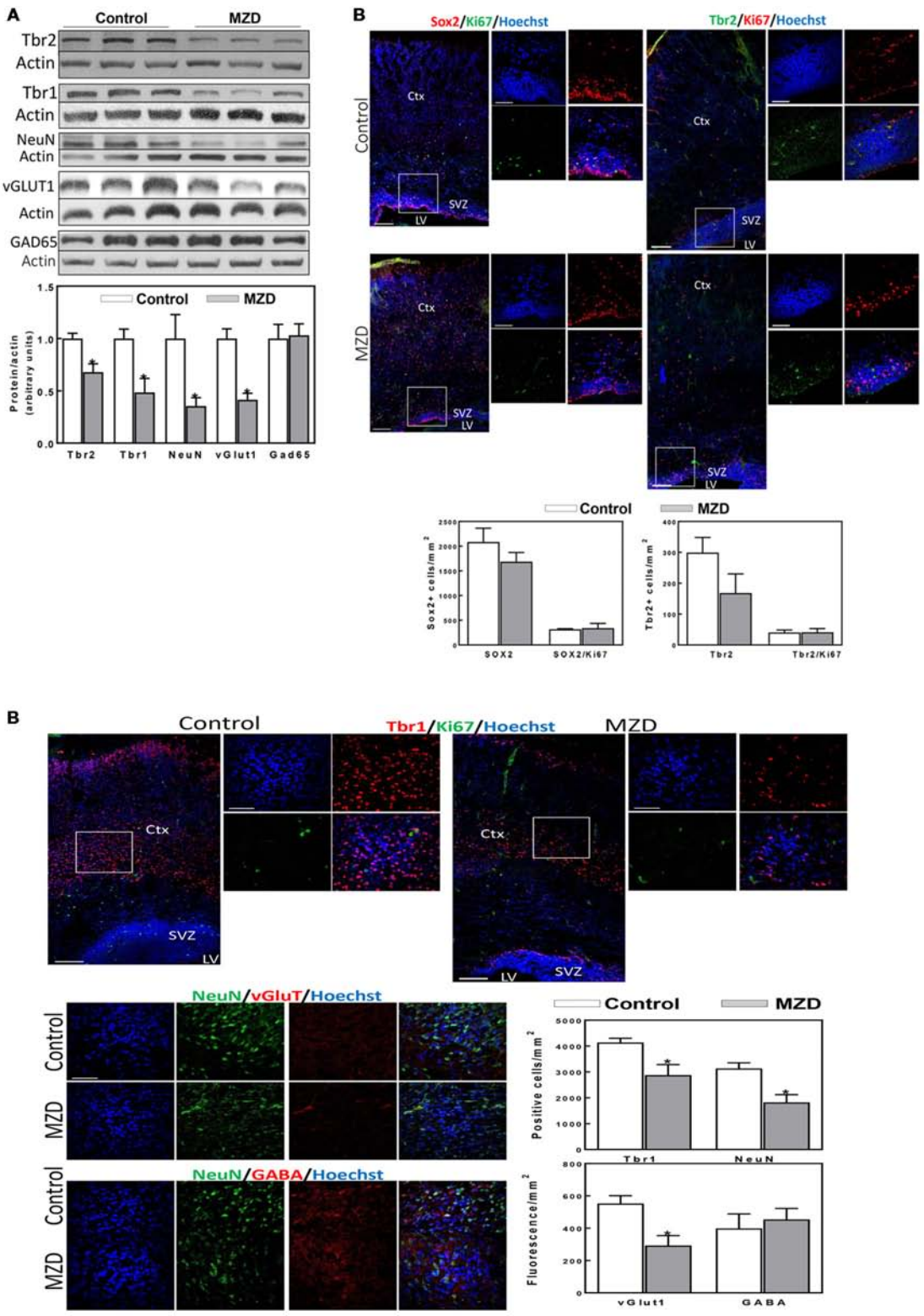

FIGURE 4 | Maternal marginal zinc deficiency affects parameters of neurogenesis in the P2 fetal rat brain. **(A)** Tbr2, Tbr1, NeuN, vGlut1 and glutamic acid decarboxylase 65 (GAD65) protein levels were measured by Western blot in P2 brain cortex homogenates. After quantification of bands, values were referred to β-actin levels and values (AUs) were normalized to those of the control group (1) Results are shown as mean ± SE of fetal brain cortices from six litters/group.

(*Continued*)

FIGURE 4 | Continued
*Significantly different from the control group ($p < 0.05$, Student's *t*-test). **(B)** Immunofluorescence for Sox2 (red fluorescence) and Ki67 (green fluorescence); Tbr2 (green fluorescence) and Ki67 (red fluorescence); Tbr1 (red fluorescence) and Ki67 (green fluorescence); NeuN (green fluorescence) and vGlut1 (red fluorescence); and NeuN (green fluorescence) and γ amino butyric acid (GABA; red fluorescence). Nuclei were visualized with Hoechst staining (blue fluorescence; Scale bar, 100 μm). Images in boxes are shown at a higher magnification (Scale bar, 50 μm). Quantifications were done as described in methods. Results are shown as mean ± SE of offspring brains from four litters/group. *Significantly different from the control group ($p < 0.05$, Student's *t*-test).

offspring (**Figure 3B**). Thus, NPC Sox2 and IPC Tbr2 positive cells in the SVZ of MZD embryos were 47 and 71%, respectively, compared to controls (**Figure 3B**). The ratio Sox2/Ki67 and Tbr2/Ki67 positive cells were 56 and 59% lower, respectively, in MZD than in control embryo SVZ. The number of Tbr1 positive cells in E19 cortices were 33% lower in MZD compared to controls.

Markers of cortical neurogenesis were measured next at P2 by Western blot (**Figure 4A**). Tbr2 and Tbr1 levels were significantly lower in MZD than in control brain cortices (32 and 51%, respectively). A decrease in mature neurons is supported by a 64% decrease in NeuN levels in MZD compared to controls. Furthermore, alterations in neuronal specification were already evident at P2. Thus, a 58% decrease in vGlut1, a glutamate/proton exchanger indicator of glutamatergic neuron abundance, was observed in MZD offspring brain cortices. On the other hand, the protein abundance of Gad65 an enzyme involved in GABA synthesis, was similar between groups. Immunofluorescence analysis (**Figure 4B**) showed no significant differences between groups for Sox2 and Tbr2. Although values were 44% lower for Tbr2, differences were not significant ($p < 0.15$). The number of Tbr1 positive cells was 30% lower in MZD cortices than in controls. The number of NeuN positive cells and of vGlut1 fluorescence intensity were 42 and 47% lower in MZD compared to control P2 offspring brains, while GABA fluorescence intensity was similar between groups.

Early Developmental Marginal Zinc Deficiency Disrupted Neurogenesis Leading to a Decreased Neuronal Number and Altered Neuronal Specification in the Adult Brain (P56)

We next investigated if the effects of gestational marginal zinc deficiency on fetal brain development have long lasting repercussions, even following repletion with a diet containing adequate zinc. The total number of mature neurons (NeuN positive cells) in the brain cortex of the P56 offspring was evaluated by immunohistochemistry. Marginal zinc deficiency from E0-P2 resulted in a 29% decrease in the number of cells expressing NeuN in the offspring frontal cortex (**Figure 5**). While no differences in the fluorescence intensity for GABA was observed between groups, 26% lower levels of fluorescence for vGlut1 were observed in the P56 brain cortex from MZD offspring compared to controls (**Figure 5**).

DISCUSSION

Results from this study demonstrate that a decreased proliferation of NPCs resulting from gestational marginal zinc deficiency leads to the disruption of cortical neurogenesis in the rat offspring brain. This is associated with a decreased number of neurons in the MZD young adult brain cortex, and an altered specification that results in a reduced number of excitatory glutamatergic neurons, not affecting GABAergic neurons.

Severe nutritional zinc deficiency, both due to low zinc content or high content of zinc-binding phytates, during early development causes NTDs and brain/organ teratology (Oteiza et al., 1990; Velie et al., 1999). Also maternal infections, diabetes, and toxicant exposures that stimulate an acute-phase response causes a decreased transport of zinc to the developing fetus (Nuttall et al., 2017), which can lead to increased risk of NTDs (Chua et al., 2006; Uriu-Adams and Keen, 2010). On the other hand, a marginally low dietary zinc intake during pregnancy is associated with decreased fetal heart rate variability, suggesting impaired regulation of the autonomic nervous system (Spann et al., 2015). Accordingly, prenatal zinc supplementation improves the regulation of the autonomic nervous system later in life (Caulfield et al., 2011). Mild developmental zinc deficiency, both in humans and rodents, impairs learning, working memory, and social behavior (Hagmeyer et al., 2015). Similar cognitive defects result from secondary zinc deficiency in a rat model of maternal infection (Kirsten et al., 2015). Importantly, these cognitive defects are consistent with rodent models of autism spectrum disorder, suggesting that disruption of fetal brain development resulting from marginal zinc deficiency could contribute to the risk of developing autism (Grabrucker et al., 2014; Kirsten et al., 2015; Nuttall, 2015). Moreover, reports in humans have established an association between zinc deficiency and Phelan McDermid Syndrome, a genetic disorder characterized by features of autism spectrum disorders (Pfaender et al., 2017). Thus, although not teratogenic, marginal zinc deficiency can have long-lasting effects on the nervous system.

We currently observed that consumption of a marginal zinc deficient diet during pregnancy did not affect the overall pregnancy and fetal/offspring outcome. On the other hand, the concentration of zinc in the offspring brain cytosolic fraction was markedly affected from E14 through P2. This finding stresses the major impact that a mild decrease in zinc availability can have on zinc homeostasis in the developing brain. Cytosolic zinc and Zinquin-reactive zinc largely reflect loosely bound and rapidly available zinc pools, which are highly relevant to the regulation of cell signaling. For example, and stressing the relevance of available zinc pools, both the decrease in ERK1/2 phosphorylation and cell proliferation observed in zinc-deficient IMR-32 cells are rapidly restored upon zinc supplementation and *via* the inhibition of the ERK1/2-directed phosphatase PP2A (Nuttall et al., 2015).

Zinc deficiency affects signaling pathways that can contribute to altered brain development. In this regard, we previously

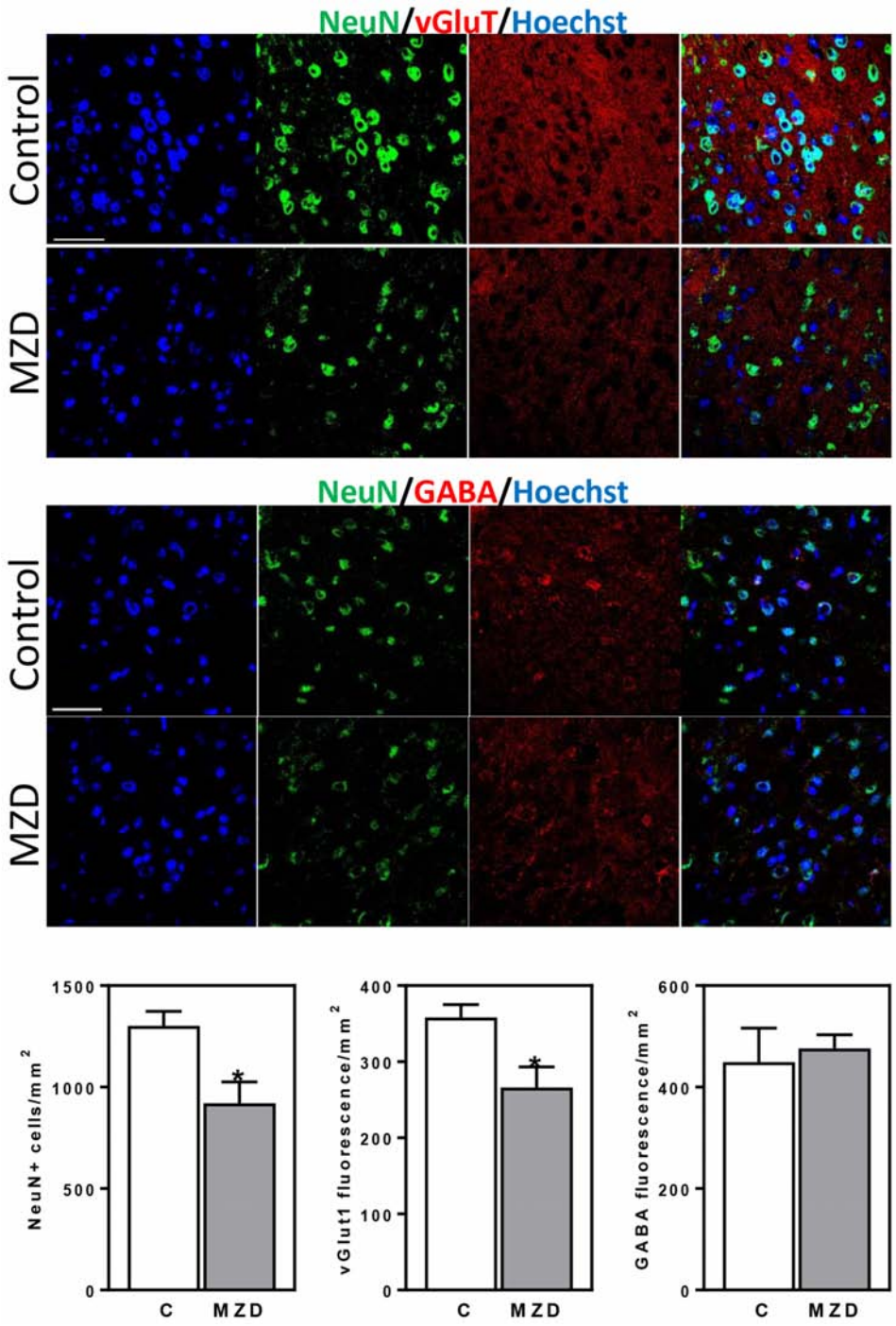

FIGURE 5 | Maternal marginal zinc deficiency from E0 to P2 affects the number and specification of neurons in the young adult brain. NeuN (green fluorescence), vGlut1 (red fluorescence) and GABA (red fluorescence) were measured by immunofluorescence in the frontal cortex at P56. Nuclei were visualized with Hoechst staining (blue fluorescence; Scale bar, 100 μm). Quantifications were done as described in methods. Results are shown as mean ± SE of offspring brain from four litters/group. *Significantly different from the control group ($p < 0.05$, Student's *t*-test).

observed a downregulation of transcription factors NF-κB and NFAT, the activation of MAPKs p38 and JNK, and a downregulation of ERK1/2 both in zinc deficient IMR-32 cells and E19 fetal rat brain (Zago et al., 2005; Aimo et al., 2010b; Nuttall et al., 2015). In particular, ERK1/2 phosphorylation showed a major decrease in the MZD brain CT at E14 and E19. This can in part explain maternal zinc deficiency-associated decrease in VZ NPC number and proliferation and the

observed alterations in neuronal specification. In this regard, ERK1/2 is not only important for NPC proliferation but also for neuronal differentiation (Samuels et al., 2008; Pucilowska et al., 2012). In humans, mutations that disrupt ERK1/2 signaling impair brain development leading to cognitive dysfunction in neuro-cardio-faciocutaneous syndromes and autism spectrum disorders (Samuels et al., 2009; Kalkman, 2012). Mice with a conditional deletion of ERK1/2 in NPCs have decreased NPC proliferation leading to abnormal distribution of neurons in the cortical plate, increased excitability of cortical neurons, increased anxiety-like behavior, reduced memory, and impairments of social behavior (Satoh et al., 2011; Pucilowska et al., 2012). Overall, ERK1/2 can be a key signal underlying the altered neurogenesis and behavior associated with maternal marginal zinc deficiency (Nuttall and Oteiza, 2012).

Transcription factor Sox2 functions by regulating NPC self-renewal in both the developing and mature brain, and inhibiting NPC differentiation (Graham et al., 2003; Favaro et al., 2009). A major decrease of Sox2 was observed in the MZD E14 and E19 embryos, suggesting that Sox2 downregulation can contribute to the observed decrease in NPC proliferation. On the other hand, Sox2 downregulation causes premature neuronal differentiation (Graham et al., 2003), which was not observed in the MZD embryonic brain. Pax6 expression at E14 was also impaired in the MZD group. Pax6, a homeobox and paired domain transcription factor, promotes the expression of Tbr2, inducing the transition of NPC-like RGPs to IPCs (Sansom et al., 2009). Pax6 regulates the proliferation of cortical progenitors being expressed in RGPs at the VZ, but not in IPCs (Manuel et al., 2015). Thus, not only ERK1/2 but also Sox2 and Pax6 downregulation at a period of active progenitor proliferation can contribute to the decrease in the number of fetal brain NPCs as a consequence of maternal marginal zinc deficiency.

We next evaluated the potential disruption of the process of neuronal differentiation and specification that could be associated with an impaired NPC proliferation. Similarly to Sox2 and Pax6, Tbr2 protein levels were markedly low in E14 and E19 MZD brain CT. Tbr2 is expressed in the mouse brain as early as E10.5 in proliferative areas, where neuronal progenitors reside (Kimura et al., 1999). Tbr1 expression is located in the cerebral cortex and other brain areas populated by postmitotic neurons, decreasing the expression postnatally (Bulfone et al., 1995). Tbr2 is a marker of IPCs, being required for the progression of RGPs to IPCs, a process that is in part mediated by the downregulation of Pax6 by Trb2 (Hodge et al., 2012). Most glutamatergic neurons in the brain cortex are originated from a Tbr2 positive lineage (Vasistha et al., 2015). We observed a reduction in the number of Tbr2 positive IPCs in the SVZ and of Tbr1 positive postmitotic neurons in the cortical plate. Thus, while the decrease in NPCs in the MZD embryonic brain may explain a decreased number of neurons, the observed downregulation of Tbr2 during the period of active differentiation suggests that the specification of neurons may also be affected.

As IPCs are necessary to expand the population of cortical glutamatergic neurons, we next analyzed the population of mature NeuN positive neurons and the populations of vGlut1 and GABA positive neurons at P2 and P56. We observed not only a lower number of mature neurons in the MZD mature brain but also, in agreement with alterations in Tbr2 and Tbr1 expression, an impairment in the generation of glutamatergic neurons. Very importantly, even after postnatal zinc repletion, vGlut1 expression in the MZD P56 brain cortex remained markedly affected. The mammalian neocortex has two types of neurons, glutamatergic pyramidal cells and GABAergic non-pyramidal cells (Peters and Jones, 1984; DeFelipe and Fariñas, 1992). Glutamatergic projection neurons give rise from progenitor cells in the VZ of the pallium from where they migrate radially into the neocortex. On the other hand, GABAergic interneurons are born in the subpallium and migrate tangentially into the neocortex (Marin, 2013). They arise from the ventral telencephalon (Anderson et al., 1997), in particular the medial and caudal ganglionic eminences (Wichterle et al., 2001; Wonders and Anderson, 2006; Wonders et al., 2008) from Nkx2.1-expressing progenitors (Butt et al., 2005), in a process modulated by Sonic hedgehog (Hebert and Fishell, 2008). The described diverse origin and regulation of glutamatergic and GABAergic neurons can explain the differential effect of developmental zinc deficiency on these neuronal populations.

The current findings stress the concept that the adverse effects of limited zinc availability during early development can have irreversible consequences in the number and specification of neurons in the mature brain. These results add to previous evidence showing that severe zinc deficiency can disrupt NPC proliferation and neuronal differentiation (Swenerton et al., 1969; Dvergsten et al., 1983; Gower-Winter et al., 2013), but in a condition of marginal zinc availability which can be extrapolated to human populations. The disruption observed in neurogenesis could contribute to the described persistent effects of marginal zinc deficiency on behavior. In this regard, marginal zinc deficiency throughout gestation and lactation decreases working memory in rats after dietary repletion (Halas et al., 1986). In mice, marginal zinc deficiency through gestation leads to increased anxiety-like behavior, abnormal social behavior, and impaired motor learning even after dietary repletion (Grabrucker et al., 2014, 2016). Very relevant to the current results, a dysbalance in excitatory/inhibitory systems has been proposed as a developmental precursor of autism spectrum disorders (Mariani et al., 2015) and a possible target for restoring functional connectivity even in adulthood (Ajram et al., 2017).

In summary, this work demonstrates that gestational marginal zinc deficiency affects neurogenesis in the fetal rat brain leading to a disruption of the cortical excitatory/inhibitory balance that persists into adulthood even after dietary repletion. While earlier studies focused on severely deficient animal models, this is the first study to report disruption of fetal neurogenesis resulting from marginal zinc deficiency that affects the cellularity of the mature brain cortex. These findings stress the relevance of an adequate zinc nutrition during pregnancy to prevent irreversible effects on the offspring cortical structure and ultimately on behavior and cognition.

DATA AVAILABILITY

The datasets generated for this study are available on request to the corresponding author.

AUTHOR CONTRIBUTIONS

PO and AA designed the research. XL, AA, SS, JN and PM performed the research. All authors participated in the analysis and discussion of data. PO, AA and JN wrote the article.

FUNDING

This work was supported by grants from NIFA-USDA (CA-D*-XXX-7244-H) and the Packer-Wentz Endowment to PO, and grants from Universidad de Buenos Aires (20020160100050BA) and CONICET (PIP 0567), Argentina, to AA. SS, JN and XL were recipients of Jastro Shields awards. XL and JN were supported by a National Institute of Environmental Health Sciences funded training program (T32 ES007058-33 and 2T32ES007059-41). SS was a recipient of a Thai Government Scholarship.

REFERENCES

Adamo, A. M., Zago, M. P., Mackenzie, G. G., Aimo, L., Keen, C. L., Keenan, A., et al. (2010). The role of zinc in the modulation of neuronal proliferation and apoptosis. *Neurotox. Res.* 17, 1–14. doi: 10.1007/s12640-009-9067-4

Aimo, L., Cherr, G. N., and Oteiza, P. I. (2010a). Low extracellular zinc increases neuronal oxidant production through nadph oxidase and nitric oxide synthase activation. *Free Radic. Biol. Med.* 48, 1577–1587. doi: 10.1016/j.freeradbiomed.2010.02.040

Aimo, L., Mackenzie, G. G., Keenan, A. H., and Oteiza, P. I. (2010b). Gestational zinc deficiency affects the regulation of transcription factors AP-1, NF-kappaB and NFAT in fetal brain. *J. Nutr. Biochem.* 21, 1069–1075. doi: 10.1016/j.jnutbio.2009.09.003

Ajram, L. A., Horder, J., Mendez, M. A., Galanopoulos, A., Brennan, L. P., Wichers, R. H., et al. (2017). Shifting brain inhibitory balance and connectivity of the prefrontal cortex of adults with autism spectrum disorder. *Transl. Psychiatry* 7:e1137. doi: 10.1038/tp.2017.104

Anderson, S. A., Eisenstat, D. D., Shi, L., and Rubenstein, J. L. (1997). Interneuron migration from basal forebrain to neocortex: dependence on *Dlx* genes. *Science* 278, 474–476. doi: 10.1126/science.278.5337.474

Bradford, M. M. (1976). A rapid and sensitive method for the quantitation of microgram quantities of protein utilizing the principle of protein-dye binding. *Anal. Biochem.* 72, 248–254. doi: 10.1006/abio.1976.9999

Bulfone, A., Smiga, S. M., Shimamura, K., Peterson, A., Puelles, L., and Rubenstein, J. L. (1995). T-brain-1: a homolog of Brachyury whose expression defines molecularly distinct domains within the cerebral cortex. *Neuron* 15, 63–78. doi: 10.1016/0896-6273(95)90065-9

Butt, S. J., Fuccillo, M., Nery, S., Noctor, S., Kriegstein, A., Corbin, J. G., et al. (2005). The temporal and spatial origins of cortical interneurons predict their physiological subtype. *Neuron* 48, 591–604. doi: 10.1016/j.neuron.2005.09.034

Caulfield, L. E., Zavaleta, N., Chen, P., Lazarte, F., Albornoz, C., Putnick, D. L., et al. (2011). Maternal zinc supplementation during pregnancy affects autonomic function of Peruvian children assessed at 54 months of age. *J. Nutr.* 141, 327–332. doi: 10.3945/jn.110.128843

Chua, J. S., Rofe, A. M., and Coyle, P. (2006). Dietary zinc supplementation ameliorates LPS-induced teratogenicity in mice. *Pediatr. Res.* 59, 355–358. doi: 10.1203/01.pdr.0000199906.37619.9c

Clegg, M. S., Hanna, L. A., Niles, B. J., Momma, T. Y., and Keen, C. L. (2005). Zinc deficiency-induced cell death. *IUBMB Life* 57, 661–669. doi: 10.1080/15216540500264554

DeFelipe, J., and Fariñas, I. (1992). The pyramidal neuron of the cerebral cortex: morphological and chemical characteristics of the synaptic inputs. *Prog. Neurobiol.* 39, 563–607. doi: 10.1016/0301-0082(92)90015-7

Dey, A. C., Shahidullah, M., Mannan, M. A., Noor, M. K., Saha, L., and Rahman, S. A. (2010). Maternal and neonatal serum zinc level and its relationship with neural tube defects. *J. Health Popul. Nutr.* 28, 343–350. doi: 10.3329/jhpn.v28i4.6040

Dvergsten, C. L., Fosmire, G. J., Ollerich, D. A., and Sandstead, H. H. (1983). Alterations in the postnatal development of the cerebellar cortex due to zinc deficiency. I. Impaired acquisition of granule cells. *Brain Res.* 271, 217–226. doi: 10.1016/0006-8993(83)90284-6

Favaro, R., Valotta, M., Ferri, A. L., Latorre, E., Mariani, J., Giachino, C., et al. (2009). Hippocampal development and neural stem cell maintenance require Sox2-dependent regulation of *Shh*. *Nat. Neurosci.* 12, 1248–1256. doi: 10.1038/nn.2397

Gower-Winter, S. D., Corniola, R. S., Morgan, T. J. Jr., and Levenson, C. W. (2013). Zinc deficiency regulates hippocampal gene expression and impairs neuronal differentiation. *Nutr. Neurosci.* 16, 174–182. doi: 10.1179/1476830512y.0000000043

Grabrucker, S., Boeckers, T. M., and Grabrucker, A. M. (2016). Gender dependent evaluation of autism like behavior in mice exposed to prenatal zinc deficiency. *Front. Behav. Neurosci.* 3:37. doi: 10.3389/fnbeh.2016.00037

Grabrucker, S., Jannetti, L., Eckert, M., Gaub, S., Chhabra, R., Pfaender, S., et al. (2014). Zinc deficiency dysregulates the synaptic ProSAP/Shank scaffold and might contribute to autism spectrum disorders. *Brain* 137, 137–152. doi: 10.1093/brain/awt303

Graham, V., Khudyakov, J., Ellis, P., and Pevny, L. (2003). SOX2 functions to maintain neural progenitor identity. *Neuron* 39, 749–765. doi: 10.1016/s0896-6273(03)00497-5

Hagmeyer, S., Haderspeck, J. C., and Grabrucker, A. M. (2015). Behavioral impairments in animal models for zinc deficiency. *Front. Behav. Neurosci.* 8:443. doi: 10.3389/fnbeh.2014.00443

Halas, E. S., Hunt, C. D., and Eberhardt, M. J. (1986). Learning and memory disabilities in young adult rats from mildly zinc deficient dams. *Physiol. Behav.* 37, 451–458. doi: 10.1016/0031-9384(86)90205-2

Haubensak, W., Attardo, A., Denk, W., and Huttner, W. B. (2004). Neurons arise in the basal neuroepithelium of the early mammalian telencephalon: a major site of neurogenesis. *Proc. Natl. Acad. Sci. U S A* 101, 3196–3201. doi: 10.1073/pnas.0308600100

Hebert, J. M., and Fishell, G. (2008). The genetics of early telencephalon patterning: some assembly required. *Nat. Rev. Neurosci.* 9, 678–685. doi: 10.1038/nrn2463

Hodge, R. D., Nelson, B. R., Kahoud, R. J., Yang, R., Mussar, K. E., Reiner, S. L., et al. (2012). Tbr2 is essential for hippocampal lineage progression from neural stem cells to intermediate progenitors and neurons. *J. Neurosci.* 32, 6275–6287. doi: 10.1523/JNEUROSCI.0532-12.2012

Kalkman, H. O. (2012). Potential opposite roles of the extracellular signal-regulated kinase (ERK) pathway in autism spectrum and bipolar disorders. *Neurosci. Biobehav. Rev.* 36, 2206–2213. doi: 10.1016/j.neubiorev.2012.07.008

Keen, C. L., Peters, J. M., and Hurley, L. S. (1989). The effect of valproic acid on 65Zn distribution in the pregnant rat. *J. Nutr.* 119, 607–611. doi: 10.1093/jn/119.4.607

Kelleher, S. L., and Lönnerdal, B. (2005). Molecular regulation of milk trace mineral homeostasis. *Mol. Aspects Med.* 26, 328–339. doi: 10.1016/j.mam.2005.07.005

Kimura, N., Nakashima, K., Ueno, M., Kiyama, H., and Taga, T. (1999). A novel mammalian T-box-containing gene, Tbr2, expressed in mouse developing brain. *Dev. Brain Res.* 115, 183–193. doi: 10.1016/s0165-3806(99)00064-4

Kirsten, T. B., Queiroz-Hazarbassanov, N., Bernardi, M. M., and Felicio, L. F. (2015). Prenatal zinc prevents communication impairments and BDNF disturbance in a rat model of autism induced by prenatal lipopolysaccharide exposure. *Life Sci.* 130, 12–17. doi: 10.1016/j.lfs.2015.02.027

Mackenzie, G. G., Salvador, G. A., Romero, C., Keen, C. L., and Oteiza, P. I. (2011). A deficit in zinc availability can cause alterations in tubulin thiol redox status in cultured neurons and in the developing fetal rat brain. *Free Radic. Biol. Med.* 51, 480–489. doi: 10.1016/j.freeradbiomed.2011.04.028

Manuel, M. N., Mi, D., Mason, J. O., and Price, D. J. (2015). Regulation of cerebral cortical neurogenesis by the Pax6 transcription factor. *Front. Cell. Neurosci.* 9:70. doi: 10.3389/fncel.2015.00070

Mariani, J., Coppola, G., Zhang, P., Abyzov, A., Provini, L., Tomasini, L., et al. (2015). FOXG1-dependent dysregulation of GABA/glutamate neuron differentiation in autism spectrum disorders. *Cell* 162, 375–390. doi: 10.1016/j.cell.2015.06.034

Marin, O. (2013). Cellular and molecular mechanisms controlling the migration of neocortical interneurons. *Eur. J. Neurosci.* 38, 2019–2029. doi: 10.1111/ejn.12225

Mihalas, A. B., and Hevner, R. F. (2017). Control of neuronal development by T-box genes in the brain. *Curr. Top. Dev. Biol.* 122, 279–312. doi: 10.1016/bs.ctdb.2016.08.001

Noctor, S. C., Martínez-Cerdeño, V., Ivic, L., and Kriegstein, A. R. (2004). Cortical neurons arise in symmetric and asymmetric division zones and migrate through specific phases. *Nat. Neurosci.* 7, 136–144. doi: 10.1038/nn1172

Nuttall, J. R. (2015). The plausibility of maternal toxicant exposure and nutritional status as contributing factors to the risk of autism spectrum disorders. *Nutr. Neurosci.* 20, 209–218. doi: 10.1080/1028415x.2015.1103437

Nuttall, J. R., Kucera, H. R., Supasai, S., Gaikwad, N. W., and Oteiza, P. I. (2017). Combined effects of gestational phthalate exposure and zinc deficiency on steroid metabolism and growth. *Toxicol. Sci.* 156, 469–479. doi: 10.1093/toxsci/kfx008

Nuttall, J. R., and Oteiza, P. I. (2012). Zinc and the ERK kinases in the developing brain. *Neurotox. Res.* 21, 128–141. doi: 10.1007/s12640-011-9291-6

Nuttall, J. R., Supasai, S., Kha, J., Vaeth, B. M., Mackenzie, G. G., Adamo, A. M., et al. (2015). Gestational marginal zinc deficiency impaired fetal neural progenitor cell proliferation by disrupting the ERK1/2 signaling pathway. *J. Nutr. Biochem.* 26, 1116–1123. doi: 10.1016/j.jnutbio.2015.05.007

Oteiza, P. I., Cuellar, S., Lönnerdal, B., Hurley, L. S., and Keen, C. L. (1990). Influence of maternal dietary zinc intake on *in vitro* tubulin polymerization in fetal rat brain. *Teratology* 41, 97–104. doi: 10.1002/tera.1420410110

Peters, A., and Jones, E. G. (1984). "Classification of cortical neurons," in *Cerebral Cortex, Cellular Components of the Cerebral Cortex*, eds A. Peters and E. G. Jones (New York, NY: Plenum Press), 107–121.

Pfaender, S., Sauer, A. K., Hagmeyer, S., Mangus, K., Linta, L., Liebau, S., et al. (2017). Zinc deficiency and low enterocyte zinc transporter expression in human patients with autism related mutations in SHANK3. *Sci. Rep.* 7:45190. doi: 10.1038/srep45190

Pucilowska, J., Puzerey, P. A., Karlo, J. C., Galán, R. F., and Landreth, G. E. (2012). Disrupted ERK signaling during cortical development leads to abnormal progenitor proliferation, neuronal and network excitability and behavior, modeling human neuro-cardio-facial-cutaneous and related syndromes. *J. Neurosci.* 32, 8663–8677. doi: 10.1523/JNEUROSCI.1107-12.2012

Samuels, I. S., Karlo, J. C., Faruzzi, A. N., Pickering, K., Herrup, K., Sweatt, J. D., et al. (2008). Deletion of ERK2 mitogen-activated protein kinase identifies its key roles in cortical neurogenesis and cognitive function. *J. Neurosci.* 28, 6983–6995. doi: 10.1523/JNEUROSCI.0679-08.2008

Samuels, I. S., Saitta, S. C., and Landreth, G. E. (2009). MAP'ing CNS development and cognition: an ERKsome process. *Neuron* 61, 160–167. doi: 10.1016/j.neuron.2009.01.001

Sansom, S. N., Griffiths, D. S., Faedo, A., Kleinjan, D. J., Ruan, Y., Smith, J., et al. (2009). The level of the transcription factor Pax6 is essential for controlling the balance between neural stem cell self-renewal and neurogenesis. *PLoS Genet.* 5:e1000511. doi: 10.1371/journal.pgen.1000511

Satoh, Y., Endo, S., Nakata, T., Kobayashi, Y., Yamada, K., Ikeda, T., et al. (2011). ERK2 contributes to the control of social behaviors in mice. *J. Neurosci.* 31, 11953–11967. doi: 10.1523/JNEUROSCI.2349-11.2011

Spann, M. N., Smerling, J., Gustafsson, H., Foss, S., Altemus, M., and Monk, C. (2015). Deficient maternal zinc intake-but not folate-is associated with lower fetal heart rate variability. *Early Hum. Dev.* 91, 169–172. doi: 10.1016/j.earlhumdev.2015.01.007

Swenerton, H., Shrader, R., and Hurley, L. S. (1969). Zinc-deficient embryos: reduced thymidine incorporation. *Science* 166, 1014–1015. doi: 10.1126/science.166.3908.1014

Uriu-Adams, J. Y., and Keen, C. L. (2010). Zinc and reproduction: effects of zinc deficiency on prenatal and early postnatal development. *Birth Defects Res. B Dev. Reprod. Toxicol.* 89, 313–325. doi: 10.1002/bdrb.20264

Vasistha, N. A., García-Moreno, F., Arora, S., Cheung, A. F., Arnold, S. J., Robertson, E. J., et al. (2015). Cortical and clonal contribution of Tbr2 expressing progenitors in the developing mouse brain. *Cereb. Cortex* 25, 3290–3302. doi: 10.1093/cercor/bhu125

Velie, E. M., Block, G., Shaw, G. M., Samuels, S. J., Schaffer, D. M., and Kulldorff, M. (1999). Maternal supplemental and dietary zinc intake and the occurrence of neural tube defects in California. *Am. J. Epidemiol.* 150, 605–616. doi: 10.1093/oxfordjournals.aje.a010059

Wichterle, H., Turnbull, D. H., Nery, S., Fishell, G., and Alvarez-Buylla, A. (2001). *In utero* fate mapping reveals distinct migratory pathways and fates of neurons born in the mammalian basal forebrain. *Development* 128, 3759–3771.

Wonders, C. P., and Anderson, S. A. (2006). The origin and specification of cortical interneurons. *Nat. Rev. Neurosci.* 7, 687–696. doi: 10.1038/nrn1954

Wonders, C. P., Taylor, L., Welagen, J., Mbata, I. C., Xiang, J. Z., and Anderson, S. A. (2008). A spatial bias for the origins of interneuron subgroups within the medial ganglionic eminence. *Dev. Biol.* 314, 127–136. doi: 10.1016/j.ydbio.2007.11.018

Zago, M. P., Mackenzie, G. G., Adamo, A. M., Keen, C. L., and Oteiza, P. I. (2005). Differential modulation of MAP kinases by zinc deficiency in IMR-32 cells: role of H_2O_2. *Antioxid. Redox Signal.* 7, 1773–1782. doi: 10.1089/ars.2005.7.1773

Conflict of Interest Statement: The authors declare that the research was conducted in the absence of any commercial or financial relationships that could be construed as a potential conflict of interest.

The reviewer HB declared a shared affiliation, though no other collaboration, with several of the authors AA, PM to the handling Editor.

frontiers in Cellular Neuroscience

PROTOCOLS
published: 19 March 2019
doi: 10.3389/fncel.2019.00095

TF-ChIP Method for Tissue-Specific Gene Targets

Amalia Perna[1]* *and Lavinia Auber Alberi*[1,2]*

[1] Department of Medicine, University of Fribourg, Fribourg, Switzerland, [2] Swiss Integrative Center for Human Health, Fribourg, Switzerland

Chromatin immunoprecipitation (ChIP) is an assay developed in order to define the dynamic nature of transcription processes. This method has been widely employed to identify methylated and acetylated DNA sequences in a variety of organs both in animals and humans. Nevertheless, this technique is significantly less employed to study transcriptional targets of specific nuclear signaling factors (TFs) and the data published so far have mainly used cell culture material and have been hardly reproduced in *ex-vivo* tissue. As nuclear signaling underlies important adaptive and maladaptive responses in chronic conditions such as cancer and neurodegeneration, there is a need for streamlining the upfront workflow of TF-ChIP for subsequent target sequencing. Based on the typical low concentration of the signaling transcriptional complex and the complexity/length of the ChIP Seq protocol, the field of cellular signaling has been confronted with a major roadblock in identifying clinically relevant targets of pathological and physiological signaling pathways. The present protocol offers a standardized procedure for detecting signaling targets in any whole tissue or specific dissected regions. The advantages of the protocol compared to the existing published methods are: (1) the small amount of starting material; appropriate for tissue subregions; (2) the optimization of DNA fragmentation from whole tissue; (3) suitability for sparsely populated tissues (i.e., brain); (4) the specificity of the TF-targeting readout; and (5) high DNA quality for sequencing or hybridization. The present protocol is highly detailed and can be reproduced using both fresh and fresh-frozen tissue. This is particularly relevant in the clinical setting, where specimen integrity is often the limiting step and where transcriptional target profiling is therapeutically relevant. The method is centered on Notch signaling but can be applied to a variety of nuclear signaling pathways as long as specific antibodies are available for pull down. Taken the superior yield/readout of this procedure, ChIP may finally provide relevant information about dynamic downstream gene changes *in vivo* for use in both basic research and clinical applications.

Keywords: ChIP, transcription factor, Notch signaling, brain, low amount DNA, region-specific, gene expression

OPEN ACCESS

Edited by:
Mario Eduardo Guido, Center for Research in Biological Chemistry Córdoba (CIQUIBIC), Argentina

Reviewed by:
Takumi Takizawa, Gunma University, Japan
Terence Hébert, McGill University, Canada

***Correspondence:**
Amalia Perna
amalia.perna@unifr.ch
Lavinia Auber Alberi
lavinia.alberi@unifr.ch

Received: *08 November 2018*
Accepted: *26 February 2019*
Published: *19 March 2019*

Citation:
Perna A and Alberi LA (2019) TF-ChIP Method for Tissue-Specific Gene Targets. Front. Cell. Neurosci. 13:95. doi: 10.3389/fncel.2019.00095

INTRODUCTION

Control of gene expression is essential for a cell to assemble the gene products it needs to regulate cellular homeostasis and communication. Virtually, any step of gene expression can be modulated, from the DNA–RNA transcription step (Genuth and Barna, 2018) to transcripts triaging through miRNA, transcript splicing, protein translation through initiation complex, and

post-translational modification of a protein (Mansuy and Mohanna, 2011). The various checkpoints of gene expression warrant a finely tuned biological repertoire determining the cellular identity in a context-dependent manner. Direct interaction of a protein with DNA is the simplest and the most direct method by which a protein changes transcription levels conferring the appropriate fitness in response to environmental changes (Olfson and Ross, 2017). In the setting of neurons, transcriptional control is often activity dependent and induces the expression of genes regulating synaptic plasticity and neuronal network function (Flavell and Greenberg, 2008; Engelmann and Haenold, 2016). Under this light, the transcription factor (TF) assumes high relevance. By binding to a specific DNA sequence, a TF controls the rate of transcription of genetic information and it represents the last wheel in the gear chain of a signaling pathway, determining the pathways functional outcome. Nonetheless, most TFs do not work alone. Many large TF families form complex homotypic or heterotypic interactions through dimerization and others may recruit intermediary proteins such as cofactors that modulate the effects of TFs by promoting (activator) or blocking (repressor) the recruitment of RNA polymerase to specific genes and their transcription (Vaquerizas et al., 2009).

Furthermore, despite transcriptional processes are highly conserved, human tissues differ from other mammalian species by gene expression patterns thereby adding another layer of complexity (Qian et al., 2005; Huang et al., 2018).

One of the techniques that has best helped understanding transcriptional factors' biological relevance is chromatin immunoprecipitation (ChIP). ChIP is a powerful technique used to detect, map, and quantify the contacts established between the protein of interest and genomic DNA *in vivo*.

As its name suggests, ChIP relies on the use of antibodies to precipitate or pull-down a DNA-binding protein of interest bound to its genomic locus. These DNA fragments are, then, isolated and characterized in order to draw conclusions about a certain transcriptional process.

Despite a simple working principle, ChIP is notoriously technically challenging, highly sensitive to operational errors and artifacts, and often requires a great deal of upfront optimization before reliable results can be obtained. Moreover, it is expensive and time-consuming.

Here, we present a protocol optimized for TF in brain tissues whose extraordinary complexity is thought to rely on refined transcriptional networks and hierarchies.

In particular, we choose to perform this protocol in the Cornus Ammonis (CA) field of the hippocampus (comparing it with cortex) in order to demonstrate the validity of the technique for a little amount of region-specific starting material and provide a best practice TF-ChIP method for researchers working with whole animal and human tissue.

We decided to focus on Notch1 signaling pathway since it provides a good example for low complexity pathway studies. Notch signaling is a well-known player in the embryonic development but increasing evidence points out a critical role in the mature brain of vertebrates and invertebrates. This pathway appears to be involved in neural progenitor regulation, neuronal connectivity, synaptic plasticity, and learning/memory (Alberi et al., 2013). In addition, Notch was also found aberrantly regulated in neurodegenerative diseases, including Alzheimer's disease and ischemic injury both in rodent models and human tissue (Brai et al., 2016; Marathe et al., 2017) but the mechanistic implication of Notch-dependent targets in this setting remains largely unraveled, limiting its clinical relevance. The signaling is composed by a downstream transcriptional factor, recombining binding protein suppressor of hairless (RBPjK) that normally behaves as a repressor and that needs another protein, Notch intracellular domain (NICD), to be activated and transcribe its target genes. Notch1 signaling has a sophisticated program of gene expression orchestrated by the alternating status of RBPjK. Notch1 is a transmembrane receptor scattered across the cell membrane. Ligand proteins bind to the extracellular domain inducing proteolytic cleavage and release the intracellular domain (NICD), which enters in the nucleus and binds RBPjK. This allows transcription and the subsequent cell response (Siebel and Lendahl, 2017).

The ChIP assay executed in this manuscript is performed specifically in the hippocampal CA fields and involves NICD precipitation in order to assess target genes downstream Notch1 canonical activation.

This work aims to explain in detail the critical steps of the procedure which can be further adapted to any experimental setting using *ex-vivo* tissue (tissues with high extracellular matrix density, secondary factor precipitation, low chromatin yield, signaling pathways with few target genes, etc.) in a very short time.

MATERIALS AND EQUIPMENT

Animals

All experiments on mice were performed with permission of the local animal care committee (Canton of Fribourg, Switzerland approved the Protocol no. 2016_32_FR) and according to the present Swiss law and the European Communities Council Directive of 24 November 1986 (86/609/EEC). C57Bl6 male mice were used throughout the experiment. Transgenic Notch Reporter [Tg(C-EGFP) 25 Gaia/Reya; Jax, FL, United States] was used for fluorescent immunohistochemistry (IHC). All animals (3 months of age) were housed on 12 h light–dark cycle with access to food and water *ad libitum*. Mice were euthanized using pentobarbital (120 mg/kg). Once no pinch reflex was assessed, animals were perfused using 0.9% NaCl and either dissected in ice cold saline solution under a stereoscope (Leica, Germany) or immersion fixed using paraformaldehyde (Sigma–Aldrich, United States; P6148).

ChIP Equipment

Glass dish
Razor blades
Pestle
Eppendorf
Pippettor
Rotating wheel
Prism R^{TM} Refrigerated MicroCentrifuge (Labnet, Switzerland; C2500-R)

Vortex-Genie 2 (Scientific Industries, Inc., United States; SI-0236)
Bioruptor Plus (Diagenode, Belgium; B01020001)
1.5 ml Bioruptor® Plus TPX microtubes (Diagenode, Belgium; C30010010-300)
Qubit Fluorometric Quantitation (Thermo Fisher, United States; Q33226)
ThermoMixer® C (Eppendorf, Germany; #5382000015)
Mupid®-One Electrophoresis System (Eurogentec, Germany)
Omega Lum™ W Imaging System (Aplegen, United States; 81-12120-00)
Biometra TRIO Thermal Cycler Series (Analytik Jena, Germany)
Fragment Analyzer (Advanced Analytical AATI, United States)
Mic qPCR Cycler (Bio Molecular Systems, Australia).

ChIP Reagents

Formaldehyde solution, 36.5–38% (Sigma-Aldrich, United States; F8775) !caution formaldehyde is toxic by inhalation, ingestion, or contact with skin.
Phosphate-buffered saline (PBS) (10×) pH 7.4 (Thermo Fisher Scientific, United States; AM9625)
Glycine (Sigma–Aldrich, United States; G8898)
Protease inhibitor (PI) cocktail (Sigma–Aldrich, United States; P8340)
Sodium dodecyl sulfate (SDS) (Roth, Germany; CN30.3) !caution SDS is toxic by inhalation, ingestion, or contact with skin.
Ethylenediaminetetraacetic acid (EDTA) (Sigma–Aldrich, United States; E5134)
Tris (Roth, Germany; 5429.3)
4-(2-hydroxyethyl)-1-piperazineethanesulfonic acid (HEPES) (Sigma–Aldrich, United States; H3375)
NaCl (Roth, Germany; 9265.2)
Sodium deoxycholate (Sigma–Aldrich, United States; 30970)
Triton X-100 (Sigma–Aldrich, United States; 93426)
Tris–HCl (Roth, Germany; 9090)
LiCl (Sigma–Aldrich, United States; L9650)
Nonidet P-40 substitute (Sigma–Aldrich, United States; 74385)
Qubit™ dsDNA HS Assay Kit (Thermo Fisher, United States; Q32851)
Pierce™ Protein A/G Agarose (Thermo Fisher, United States; 20421)
Antibodies: Rabbit anti-NICD (Cell Signaling, United States; #4147); Rabbit IgG (Cell Signaling, United States; #2729); and Rabbit anti-Acetyl-Histone H3 (Lys9) (Cell Signaling, United States; #9649)
RNase A solution (Promega, United States; A7974)
Proteinase K (Roche, Switzerland; 03508838103)
Phenol/chloroform/isoamyl alcohol (Roth, Germany; A156) !Caution chloroform is toxic if absorbed through the skin, inhaled or ingested.
Chloroform/isoamyl alcohol (Roth, Germany; X984) !Caution chloroform is toxic if absorbed through the skin, inhaled or ingested.
Sodium acetate (Merck, Germany; 1.06268.0250)
Glycogen (Roche;10901393001)
Isopropanol (Fisher Chemical, United States; P/7500/15)
Ethanol absolute (Fisher Chemical, United States; E/0650DF/15)
Agarose standard (Roth, Germany; 3810)
SYBR™ Safe DNA Gel Stain (Thermo Fisher, United States; S33102)
GoTaq® Hot Start Green Master Mix (Promega, United States; M5122)
GoTaq PCR Master mix (Promega United States; A6001)
GeneRuler 100 bp DNA Ladder, ready-to-use (Thermo Fisher, United States; SM0243)
DNA Gel Loading Dye (6×) (Thermo Fisher, United States; R0611)
DNF-474 High Sensitivity NGS Fragment Analysis Kit (1–6,000 bp) (Advanced Analytical, United States).

Reagent Setup

Before preparing the final solutions, filter both the water and all the stock solutions. Here volumes are calculated for three precipitations: one for the protein of interest (NICD) plus positive (H3) and negative control (IgG). Scale up if more TFs are planned to be used.

1% FA-PBS (fresh/1 ml for tissue): Mix 972 μl of PBS and 28 μl of FA.

Glycine (2 M stock): Solubilize 1.5 g of glycine in 10 ml of Milli-Q water.

Lysis buffer (fresh/1 ml): Mix 30 μl of SDS [10% (vol/vol) stock solution], 20 μl of EDTA (0.5 M stock solution), 50 μl of Tris pH 8.0 (1 M stock solution), 10 μl of PIs, and fill with filtered Milli-Q water to a final volume of 1 ml. Keep on ice until use. Final concentrations: 0.3% SDS, 10 mM EDTA, 50 mM Tris pH 8.0. ! Critical PI must be added just before use.

IP buffer (10× stock/15 ml): Mix 3 ml of HEPES pH 8.0 (1 M stock solution), 6 ml of NaCl (5 M stock solution), 600 μl of EDTA (0.5 M stock solution), and fill with filtered Milli-Q water to a final volume of 15 ml. Final concentrations: 0.2 M HEPES pH 8.0, 2 M NaCl, 0.02 M EDTA. IP stock solution can be stored in the fridge for several months.

IP buffer (1× fresh/3 ml): Mix 300 μl of high salt IP buffer (10× stock), 30 μl of NaDOC [10% (vol/vol) stock solution], 300 μl of Triton X-100 [10% (vol/vol) stock solution], 30 μl of PIs, and fill with filtered Milli-Q water to a final volume of 3 ml. Keep on ice until use. Final concentrations: 1% high salt IP buffer, 0.1% NaDOC, 1% Triton X-100 ! Critical PI must be added just before use.

Washing buffer – reduced SDS (stock/50 ml): Mix 2.5 ml of HEPES pH 7.6 (1 M stock solution), 1.5 ml of NaCl (5 M stock solution), 5 ml of Triton X-100 [10% (vol/vol) stock solution], 500 μl of NaDOC [10% (vol/vol) stock solution], 250 μl of SDS [20% (vol/vol) stock solution], and fill with filtered Milli-Q water to a final volume of 50 ml. Washing solutions can be stored in the fridge for several months. Final concentrations:

50 mM HEPES pH 7.6, 2 mM NaCl, 1% Triton X-100, 0.1% NaDOC, and 0.1% SDS

Washing buffer – reduced SDS buffer + NaCl (stock/15 ml): Mix 15 ml of reduced SDS buffer and 600 μl of NaCl (5 M stock solution). Washing solutions can be stored in the fridge for several months. Final concentrations: 0.2 M NaCl.

Washing buffer – NP-40 buffer (stock/25 ml): Mix 0.2 ml of Tris–HCl pH 8.0 (1 M stock solution), 0.625 ml of LiCl (8 M stock solution), 40 μl of EDTA (0.5 M stock solution), 1 ml of NP-40 [10% (vol/vol) stock solution], 1 ml of NaDOC [10% (vol/vol) stock solution], and fill with filtered Milli-Q water to a final volume of 25 ml. Washing solutions can be stored in the fridge for several months. Final concentrations: 8 mM Tris–HCl pH 8.0, 2 mM LiCl, 0.8 mM EDTA, 0.4% NP-40, and 0.4% NaDOC.

Washing buffer – TE buffer (stock/50 ml): Mix 0.5 ml of Tris–HCl, pH 8 (1 M stock solution), 100 μl of EDTA (0.5 M stock solution), and fill with filtered Milli-Q water to a final volume of 50 ml. Washing solutions can be stored in the fridge for several months. Final concentrations: 10 mM Tris–HCl, pH 8, 1 mM EDTA.

Elution buffer (fresh/2 ml): Mix 100 μl of Tris, pH 8 (1 M stock solution), 40 μl of EDTA (0.5 M stock solution), 100 μl of SDS [20% (vol/vol) stock solution], and fill with filtered Milli-Q water to a final volume of 2 ml. Elution buffer can be stored in the fridge for several months. Final concentrations: 50 mM Tris pH 8, 10 mM EDTA, and 1% SDS.

Protein A- or protein G-sepharose beads (Pierce™ Protein A/G Agarose; Thermo Fisher, United States; 20421).

Primers List

Primers were obtained from Microsynth, Switzerland.

	Forward	Reverse
Hes5	5′-GGG AAA AGG CAG CAT ATT GAG GCG-3′	5′-CAC GCT AAA TTG CCT GTG AAT TGG CG-3′
DLL1	5′-GTC TCA GGA CCT TCA CAG TAG-3′	5′-GAG CAA CCT TCT CCG TAG TAG-3′
GAPDH	5′-GAT TAC GGG ATG GGT CTG AA-3′	5′-GCT GCA CCT CTG GTA ACT CC-3′

Immunohistochemistry

Floating coronal brain sections from the TNR-EGFP mice, exposed to a novel environment (Alberi et al., 2011), were processed for fluorescent IHC according to the previously published protocols (Marathe et al., 2017) using Rabbit anti-NICD (Cell Signaling, United States; #4147) and goat anti-EGFP (Rockland, United States; #600-102-215). Cy3 donkey anti-rabbit (Jackson Immunoresearch, United Kingdom; #711-165-152) and Cy2 donkey anti-goat (Jackson Immunoresearch, United Kingdom; #705-225-147) were used as secondary antibodies. DAPI (Sigma–Aldrich, United States; D9542) was used for nuclear counterstaining.

Western Blot

Input, unbound, and ChIP-NICD fractions were collected and de-crosslinked by adding 11 μl of 5 M NaCl and 4 μl of RNaseA, and incubating in the thermoshaker for 4 h at 42°C with gentle shaking. Proteins were extracted with Trizol (Trifast; Peqgold, Germany) and resuspended in loading buffer. Twenty-five microliters of protein was loaded onto a 10% polyacrylamide electrophoretic gel. Western blot was conducted as previously described (Marathe et al., 2017) using two primary antibodies: polyclonal goat anti-Notch1 against the c-terminus, 1:1000 (sc-6014; Santa Cruz Biotechnology, United States) and mouse anti-β-actin, 1:2000 (sc-81178; Santa Cruz Biotechnology, United States); and two secondary antibodies diluted 1:2000: Cy3 donkey anti-goat (Jackson Immunoresearch, United Kingdom; # 705-165-147) and Cy2 donkey anti-mouse (Jackson Immunoresearch, United Kingdom; # 715-225-150). Visualization was performed through a fluorescent imager (Omega Lum G from Aplegen).

PROCEDURE

ChIP Protocol Overview

The protocol can be essentially divided into several phases. During the first step, the sample is treated with formaldehyde to cross-link proteins and DNA within ∼2 Å of each other. As a result, proteins are covalently bound to their target sequences on the DNA and provide a snapshot of TF occupancy. Later, the chromatin fraction is released from the nucleus by the mean of a lysis buffer, fragmented into small pieces (ranging from 200 to 500 bp) with a sonicator, and then subjected to immunoprecipitation with chosen antibodies. Once immune complexes are obtained, they are separated from the unbound fraction by using protein A- or protein G-sepharose beads (magnetic protein A/G beads can be used instead of sepharose beads, however, washes are performed using an appropriate magnetic tray). After extensive washing to limit the nonspecific binding, the immune-bound complexes are eluted, decrosslinked by proteinase K digestion, and then purified in order to be analyzed (**Figure 1**).

Protein–DNA interactions can, then, be approached fundamentally in two ways: (i) by looking at the presence of specific sequences in the immunoprecipitated DNA by PCR amplification or (ii) by combining genome-wide approaches culminating in a method for deep protein–DNA interactions analysis: ChIP–Seq.

Considerations Before Starting

- In order to perform a tissue-specific ChIP analysis, it is important to select the specific part of the tissue you are interested in. For peripheral organs, blood could interfere with the purity of your sample, therefore is recommended to transcardially perfuse the animal with saline solution before dissection.

FIGURE 1 | Schematic of the ChIP method and its timing. After tissue processing, DNA and proteins are reversibly crosslinked with short formaldehyde incubation (15 min) to maintain the association of proteins with their target DNA sequence. In our ChIP experiment, NICD and RBPjK are first crosslinked with DNA and then cells lysed with ionic lysis buffer (10 min). Chromatin is later fragmented with ultrasounds (30 min) and precleaned with sepharose beads incubation (1 h 40 min). Once all the unspecific DNA fragments are removed, proteins bound to DNA are ready to be targeted by the selected antibody. After ON incubation, antibody–protein–DNA complexes are precipitated using beads (3 h). Washes and elution (5 h) lead to target genes that once purified (5 h) are ready for further applications.

- The tissue could be made of subregions with different cell populations where the signaling behaves differently. It is worth to study *a priori* your tissue anatomy and composition to reduce the background and obtain unequivocal results. In our case, during hippocampus dissection, we carefully removed the dentate gyrus (composed by neuronal progenitor cells and granule cells) and then we selected just the CA field (Sultan, 2013). For the cortex, we removed the white matter to increase the gray matter content for ChIP analysis.
- While planning the experiment, remember to include always a positive control as a very abundant core histone protein (i.e., H3) and a negative control that is a sample treated in the same way as in the immunoprecipitated samples but without Ab or with a non-specific Ab (i.e., IgG).
- For optimal chromatin yield and ChIP results, it is important to use at least 25 mg of tissue for each immunoprecipitation. The chromatin yield does vary between tissue types and some tissues may require more than 25 mg depending on their cell density. Since positive and negative control must be included, at least 75 mg of tissue is required.

Stepwise Procedure

Crosslinking (timing: ca. 40 min):

Before starting the procedure, prepare all your solutions and keep them refrigerated. Switch on the cold centrifuge and set the Bioruptor sonicator at 4°C. Perform all steps on ice to avoid proteins degradation.

1. After tissue dissection from an anesthetized mouse (**Figure 2A**), snap-freeze the tissue in liquid nitrogen or, if fresh tissue is required, proceed with the protocol.
2. Transfer quickly the tissue in a glass dish already placed in ice.
3. Rapidly put 40 μl of 1% FA-PBS on your tissue piece (this will fix your tissue while it is thawing), start the timer (already set on 15 min), and finely mince the fresh/thawed tissue with two pre-chilled razor blades for 4 min (until it appears slurry and homogeneous).
4. Add 450 μl of 1% FA-PBS in the dish and transfer the tissue to a 1.5 ml tube. Use other 450 μl 1% FA-PBS to harvest tissue residues from the dish and move it into the tube. Incubate for the remaining 10 min at room temperature (RT) on the rotating wheel (make sure to safe-lock the tubes!).
5. Add 63 μl of glycine 2 M to the 940 μl of 1% FA-PBS (final concentration 0.125 M) to terminate cross-linking. Incubate for 10 min at RT on the rotating wheel (make sure to safe-lock the tubes).
6. Wash three times with cold PBS with freshly added PI:

a. Add 500 μl of 1× PBS+PI
b. Invert several times
c. Spin gently at 4°C for 1 min
d. Remove supernatant

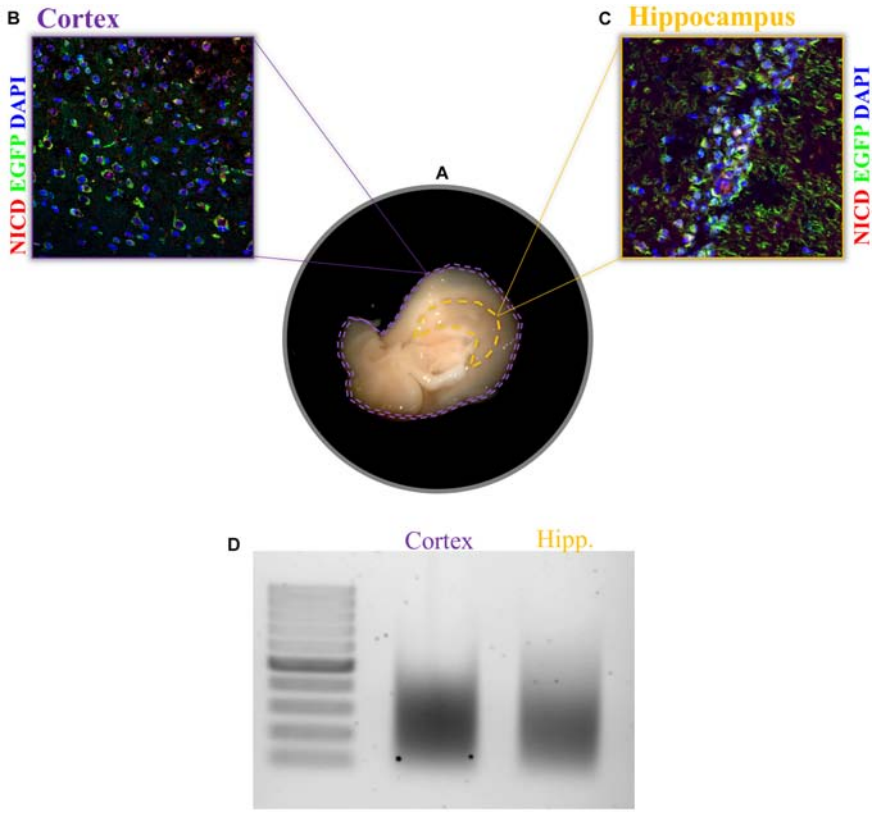

FIGURE 2 | Expression of NICD in cortex and hippocampus and chromatin shearing of the two brain tissues. **(A)** Sagittal brain sections, view from the midline, display the hippocampus and cortex. Example of immunofluorescence for NICD (red) in **(B)** cortex and **(C)** hippocampus of the transgenic mouse line (TNR, for transgenic Notch reporter) expressing enhanced green fluorescent protein (EGFP) in cells with Notch canonical signaling activation. Nuclei are stained in blue. **(D)** CA hippocampal fields and cortical tissue 1% formaldehyde fixed are sonicated for 30 cycles (30″ ON/30″ OFF) with the Bioruptor® PLUS at HIGH power setting. All samples were treated with RNase and Proteinase K prior to gel electrophoresis. Scale bar in **B** and **C** is 25 μm.

7. Resuspend the tissue in 600 μl of ice-cold lysis buffer with freshly added PI (first add 200 μl, start to pestle, then add the remaining 400 μl).
8. Smash the tissue with a pestle by going 50 times up and down until the solution is clear and without clumps.
9. Keep the lysate 10 min on ice.

! Safe stop. Samples can be stored at −20°C at this point.

Chromatin sonication (timing ca. 40 min):
Chromatin needs to be fragmented by sonication into not too short and not too long fragments in order to be precipitated.
Extensive sonication could most likely hit TF-binding sequences and impair them, while long fragments obtained with short sonication are difficult to precipitate.
Sonication conditions should be optimized for your experimental settings (see the section "Anticipated Results"). Avoid foaming as this results in a decrease of energy transfer within the solution and will decrease the sonication efficiency.

10. Transfer the lysate in TPX tubes from Diagenode. Prepare three tubes with 200 μl each.
11. Bioruptor Plus (Diagenode, Belgium):
Power: High
Runs: 3× 10 cycles
Interval: 30″ ON/30″ OFF
Note: Vortex gently and spin down between each run.
During these 30 min, start washing beads.
12. Centrifuge at 13,500 rpm, 4°C for 10 min.
13. Collect the supernatant and transfer all 600 μl in one 2 ml tube.

! Safe stop. Samples can be stored at −20°C at this point.

Determination of DNA fragment size (timing ca. 5 h):
Sonication is the key step for a successful ChIP experiment and the optimal sonication settings should be determinate for each experimental tissue. Therefore is a good practice to check DNA fragments on agarose gel first times ChIP is performed.

14. Prepare a mix with 60 μl of elution buffer, 4.8 μl of 5 M NaCl, 2 μl RNase A (10 mg/ml), and 40 μl of chromatin. Incubate while shaking at 65°C for 1 h.
15. Add 4 μl proteinase K and incubate 3–4 h at 65°C [this incubation could be extended overnight (ON)].

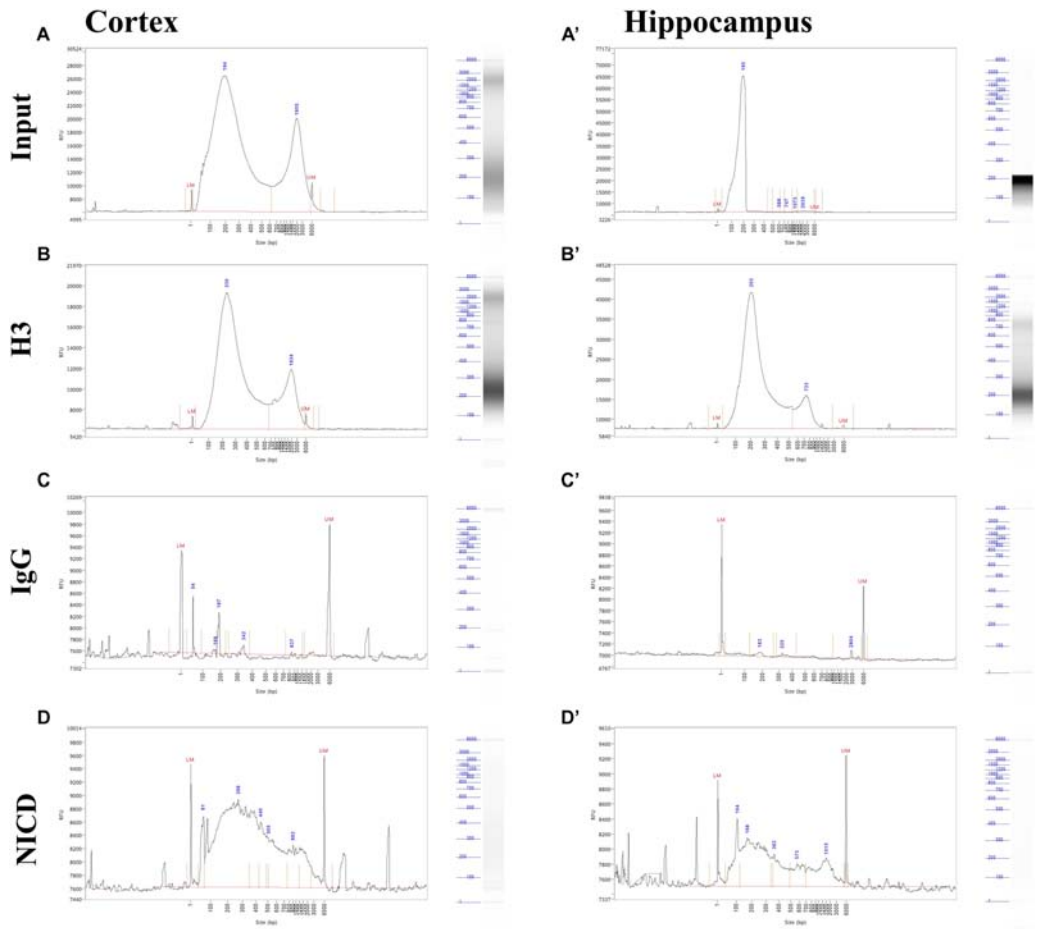

FIGURE 3 | Profiling of ChIP fragments. **(A–D)** Electropherograms of automated capillary gel electrophoresis. Size profiles of purified DNA after immunoprecipitations from cortical and hippocampal CA field lysates **(A'–D')** show the fragment length distribution for **(A, A')** input, **(B, B')** H3, and **(C, C')** NICD showing a bimodal distribution and a major peak around 200 bp. **(D, D')** IgG fragment analysis shows a sparse, mostly background peaks. DNA size (bp) is shown.

16. Add 100 µl of phenol/chloroform (1:1), agitate vigorously.
17. Centrifuge for 10 min at 13,500 rpm, 4°C.
18. Collect the aqueous phase.
19. Add 100 µl chloroform/isoamyl alcohol (1:1).
20. Centrifuge for 10 min at 13,500 rpm, 4°C.
21. Collect the aqueous phase.
22. Add 2 µL of glycogen (20 mg/mL) and 30 µl of $NaCH_3COOH$ (3 M).
23. Flick the tube and add 100 µl of isopropanol.
24. Agitate vigorously the tube several times for 1 min.
25. Leave on ice for 10 min or keep in the freezer for 5 min.
26. Centrifuge 20 min at 13,500 rpm, 4°C.
27. Decant supernatant.
28. Wash by adding 500 µl of 75% EtOH. Spin 5 min at 13,500 rpm, 4°C, and decant the supernatant.
29. Air dry and resuspend in 20 µl of ddH_2O. Incubate several minutes while shaking at 42°C to dissolve DNA.
30. Run purified DNA in a 1.5% agarose gel with a 100 bp DNA marker to determine fragment size.

Beads washing (timing ca. 15 min):

31. Take the IP buffer 10× from the fridge and make 3 ml of IP buffer 1× and add 20 µl of PI.
32. Transfer 20 µl of beads for preclearing and 40 µl for the IPs. Cut the tip used in order to dispense them. You will have in total two 1.5 ml tubes for preclearing and three for IPs.
33. Wash beads three times with 500 µl PBS: At each step spin down the beads shortly with gentle centrifugation so they don't break, wait until they settle down, and then aspirated gently the PBS with a pump using a 10 µl tip and going progressively down with the tip.
34. Wash one time with 500 µl IP buffer with PI. Keep preclearing beads on ice and store IP beads still in IP buffer in the fridge.

Pre-clearing (timing ca. 1 h 40 min):

Pre-clearing is an optional step but is recommended to reduce non-specific binding to the beads.

SDS presence in the lysis buffer is important since it enhances lysis and sonication but it also interferes with

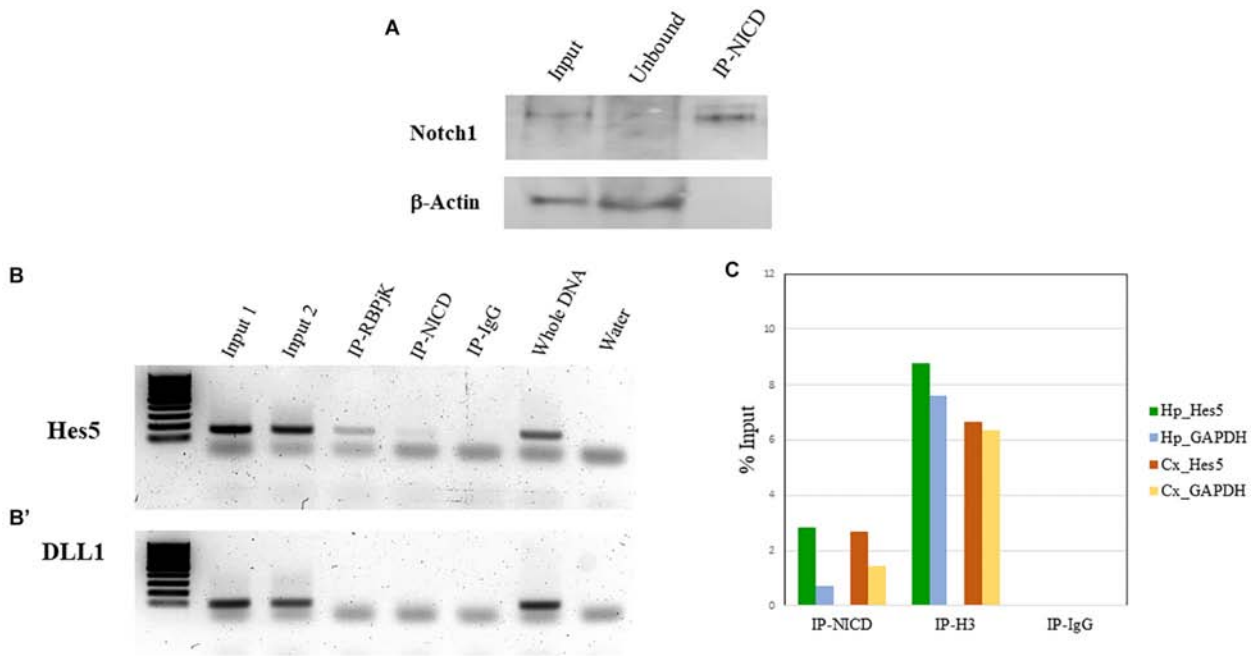

FIGURE 4 | ChIP validation. **(A)** Representative western blot of Notch1 protein present in the input, enriched in the ChIP-NICD sample and absent in the unbound solute. β-Actin is used to detect the housekeeping protein in the input and unbound fractions. **(B, B')** PCR analysis of hippocampus ChIPed with antibodies specific for RBPjK and NICD show an amplicon band for the promoter region of the canonical Notch target, Hes5 **(B)**, but no band for the promoter region of DLL1 **(B')**, chosen as a negative control. Inputs and whole DNA are shown as a positive reference and water controls for contaminants. **(C)** Results from real-time qPCR of ChIPed tissue with the NICD antibody shows a fourfold and twofold enrichment of the specific Notch target, Hes5, compared to the GAPDH promoter region in the hippocampus and cortex, respectively. The ChIPed samples with the antibody against acetyl-histone H3 antibodies show the expected amplification of the Hes5 and the GAPDH promoter in both tissues and there is no amplification in the ChIPed samples with IgG.

protein/antibody and antibody/beads binding. Therefore, it has to be diluted up to 0.1%.

35. Add IP buffer to the chromatin in 3:1 proportion (600 μl chromatin + 1200 μl IP buffer)
36. Split the chromatin over the two pre-clearing tubes and add to the 20 μl beads you kept on ice (900 μl each).
37. Incubate for 1–1.5 h @ 4°C on the rotating wheel (make sure to safe-lock the tubes).
38. Spin down the beads from the pre-cleared chromatin, collect the supernatant, and discard the 20 μl beads.
39. Measure the DNA concentration using Qubit.
40. Take 5% of the total volume of pre-cleared chromatin as input material and freeze it.

! Safe stop. Samples can be stored at −20°C at this point.

Immunoprecipitation and washes (timing ca. 16 h):
The optimal antibody concentration should be calibrated for each antibody as this can improve the signal-to-noise ratio of your experiment (see the section "Anticipated Results").

41. Divide the chromatin into three tubes (600 μl per tube) and add the antibodies to each pre-cleared chromatin: (1) specific for the TF, NICD; (2) negative control, IgG; and (3) positive control, histone H3.
42. Put the chromatin with antibodies on a rotating wheel to mix ON at 4°C (make sure to safe-lock the tubes!).
43. Transfer the chromatin + antibodies to the Eppendorf with the 40 μl beads you kept on ice/on the fridge.
44. Rotate for 3 h at 4°C on the rotating wheel (make sure to safe-lock the tubes).
45. Spin down the beads and discard the supernatant.
46. Wash three times with the reduced SDS buffer: At each step, spin down the beads shortly with gentle centrifugation so they don't break, wait until they settle down and then aspirate the buffer with the sucker using a 10 μl tip and going progressively down with the tip.
47. Wash one time with reduced SDS + NaCl buffer.
48. Wash one time with NP-40 buffer.
49. Wash one time with TE buffer.

Eluting the chromatin (timing ca. 15 min):
Prepare fresh elution buffer.

50. Add 500 μl of elution buffer to the beads and 470 μl to the 5% input.
51. Incubate for 12 min at 65°C while shaking. Flick the tube vigorously once during this incubation and once the incubation is finished.
52. Centrifuge 13,500 rpm, 4°C for 1 min.
53. Transfer the supernatant to a new tube, discard the beads.

Reversing the crosslinking (Input and IP-ed Chromatin) (timing ca.4-5 h):

54. Add 11 μl of 5 M NaCl. Flick tubes briefly.

55. Add 4 µl of RNaseA to the eluted chromatin and incubate in the thermoshaker for 1 h at 65°C with gentle shaking.
56. Add 4 µl of proteinase K to the eluted chromatin and incubate in the thermoshaker for 3–4 h at 65°C with gentle shaking (this incubation could be extended ON).
    Extraction and purification (timing ca. 1.5 h):
    Be careful during the whole extraction and work under a chemical hood.
57. Add 500 µl of phenol/chloroform (1:1), agitate vigorously.
58. Centrifuge for 10 min at 13,500 rpm, 4°C.
59. Collect the aqueous phase.
60. Add 500 µl chloroform/isoamyl alcohol (1:1), agitate vigorously.
61. Centrifuge for 10 min at 13,500 rpm, 4°C.
62. Collect the aqueous phase.
63. Add 50 µl of $NaCH_3COOH$ (3 M).
64. Flick the tube and add 500 µl of isopropanol.
65. Agitate vigorously for 1 min.
66. Keep samples on ice for 10 min or put the samples at −20°C for 5 min.
67. Centrifuge for 20 min at 13,500 rpm, 4°C.
68. Decant the supernatant.
69. Wash by adding 500 µl of 75% EtOH. Spin 5 min at 13,500 rpm, 4°C, and decant the supernatant.
70. Air dry under the hood and resuspend in 10 µl of ddH_2O. Incubate several minutes while shaking at 42°C to dissolve DNA.
71. Measure your DNA concentration using Qubit.

PCR

Primer should be designed bearing in mind that the sequence you precipitated is small and must include the TF-binding sequence. Make sure it is included in your primer design (see the section "Anticipated Results") (**Figure 4B**).

72. Prepare your (Master mix) × *n* samples, using for each sample:

- 7.5 µl hot start GoTaq
- 0.5 µl primers (10 µM)
- ddH_2O up to 15 µl

73. Add at least 1 ng of DNA
74. Use the following ChIP program:

step	°C	H:mm:ss	Go to
1	94.0	0:02:00	
2	94.0	0:00:30	
3	56.5	0:00:30	
4	72.0	0:00:30	29× → Step 2
5	72.0	0:10:00	
6	4.0	inf	

75. Run PCR products in 1.3% agarose gel.

qPCR

Once a specific amplicon is identified by qualitative PCR, the relative efficiency of chromatin pull down should be evaluated via qPCR (**Figure 4C**).

The primers used for qPCR are the same as for the PCR.

76. Prepare your (Master mix) × *n* samples, using for each sample:

- 7.5 µl Promega GoTaq qPCR master mix
- 0.5 µl Primers (10 µM)
- ddH_2O up to 15 µl

77. Add 1 ng of DNA.
78. Run the standard amplification program according to the manufacturer instructions.

ANTICIPATED RESULTS

Starting Material Amount and Crosslinking

Before starting, it is always recommended to check the specificity of the antibody and the activity rate of your TF in the tissue of your interest. One possible way to do this is to perform an IHC of your region of interest. This would help establish the range of starting material to use since this is going to influence the entire experiment. For the experiment we performed in this paper, we found a sparse and nuclear pattern of NICD in cortical tissue as well as in the CA fields of the hippocampus (**Figures 2B,C**). For low concentrations of the TF, as in our case, more chromatin should be used during immunoprecipitation. It is recommended to increase the amount of chromatin rather than the amount of antibody since the latter is going to increase the background. To further confirm the right amount of starting material, it is important to assess the chromatin yield after cell lysis. Each tissue has a different chromatin yield that depends on cell density and tissue composition. Therefore, it is important to measure the DNA concentration with a fluorometric method (Qubit) to evaluate how much tissue and/or lysis buffer is required for the next steps.

Our sample preparation section is well optimized for fresh-frozen samples. In clinical analyses, the vast majority of samples need to be stored at −80°C for later analysis or dispatching to other labs. One of the improvements provided by this protocol is the ongoing fixation while the tissue thaws. This captures chromatin–protein architectural organization in the moment of defrosting and prevents loss of biological content due to cell damage, thus, preserving the integrity of the sample. Furthermore, the mincing step with the razor blades makes fixative penetration uniform and easier and is superior to mechanical treatment that causes cell loss. That said, cross-linking efficiency is empirical and should be tested by modifying either incubation time or formaldehyde concentration prior to performing the whole procedures. Remember that extensive cross-linking may decrease the solubility of any target DNA–protein complex and cause it to be entrapped in the insoluble material removed by sedimentation.

TABLE 1 | Systematic comparisons of ChIP protocols from tissue.

Protocol	ChIP on hippocampus	ChIP on brain tissue	Low-cell ChIP	FastChIP	ChIPmentation	TF-ChIP
Publication title	Chromatin immunoprecipitation in mouse hippocampal cells and tissues.	Chromatin immunoprecipitation technique for study of transcriptional dysregulation in intact mouse brain.	A rapid micro chromatin immunoprecipitation assay (μChIP).	Protocol for the fast chromatin immunoprecipitation (ChIP) method.	ChIPmentation: fast, robust, low-input ChIP-seq for histones and TFs.	TF-ChIP method for tissue-specific gene targets.
Reference	Sailaja et al. (2012)	Braveman et al. (2004)	Dahl and Collas (2008)	Nelson et al. (2006)	Schmidl et al. (2015)	This study.
Starting material used	Mouse whole hippocampus/dissociated hippocampal cells.	One mouse brain hemisphere not perfused.	1K-100 cells and c.ca 1 mm^3 fresh- or frozen-tissue biopsies.	Best results with 2 M cells per IP.	10 K cells for histone markers 100 K for TF.	30 mg of tissue (CA1 fields from two hippocampi or bilateral cortex).
Protocol	General ChIP protocol with Sepharose A/G beads.	Upstate Biotechnology ChIP assay kit for cultured cells adapted to intact mouse brain tissue.	General ChIP protocol using *ab initio* antibody–magnetic bead complexes preparation.	Fast protocol since it shortens two steps: (i) immunoprecipitation time (accelerated by the means of ultrasonic bath) (ii) cross-link reversal and DNA isolation [using a resin-based (Chelex-100)] DNA isolation procedure.	Simple ChIP protocol combined with sequencing library preparation by Tn5 transposase ("tagmentation").	TF-ChIP protocol with Sepharose A/G beads optimized for pure tissue-specific output.
Histone modification tested	Not specified	Not tested	H3K9ac, H3K9m2, H3K9m3, H3K27m3, H3K9m3, H3K4m2, H3K4m3.	H3K9Ac, H3K4me2, H3K4m3, H3K27m3.	H3K4me1, H3K4me3, H3K27ac, H3K27me3, H3K36me3.	Not tested.
TF tested	Not specified	Sp1	RNAPII	RNA polymerase II, hnRNP K, TBP, CREB and CBP.	CTCF, GATA1, PU.1, and REST.	NICD and RBPjK.
Time estimated	3 d	2–3 d	1 d	4–6 h	2–3 d	2 d
Advantages	Optimized for sparsely populated tissues like the brain.	Optimized for sparsely populated tissues like the brain.	(i) Fast procedure; (ii) a small amount of starting material required.	Very fast.	(i) Fast; (ii) low cell numbers for histone marks and relatively low cell numbers for TFs.	(i) Allow detection of dynamic bindings; (ii) tissue-specific; (ii) optimized for low-abundance or not-direct DNA-binding proteins.
Drawbacks	(i) Needs to be optimized depending on applications; (ii) lack of specific information about TF or histone modification.	(i) ChIP kit needs to be used; (ii) uncertain performance for low-abundance or not-direct DNA-binding proteins.	(i) Not tested for sparsely populated tissues like the brain; (ii) uncertain performance for low-abundance or not-direct DNA-binding proteins; (iii) small yield. Not suitable for analysis of more than one genomic locus.	(i) Not tested for sparsely populated tissues like the brain; (ii) uncertain performance for low-abundance or not-direct DNA-binding proteins.	(i) Additional reagent requirements (transposase); (ii) not tested for tissues; (iii) uncertain performance for low-abundance or not-direct DNA-binding proteins.	Optimization required depending on the tissue density and the TF studied.
Advancements with the present protocol.	(i) The antibody for TF has been clearly stated and referenced; (ii) the application has been specified.	(i) Ideally suited for any ChIP-grade antibody, no need for an expensive kit; (ii) designed for co-TF.	(i) Tested and validated for sparsely populated tissue; (ii) designed for co-TF; (iii) high yield from small micro-dissected tissue.	(i) Tested and validated for sparsely populated tissue; (ii) high yield from small micro-dissected tissue.	(i) All reagents are listed; (ii) tested and validated for tissue but also suitable for cell suspension; (iii) high yield from small micro-dissected tissue.	(i) optimized for low expressed-TF-ChIP; (ii) tested and validated to obtain high yields of DNA from sparsely dense tissue; (iii) customizable.

Chromatin Shearing

Sonication is very sensitive to changes, and its efficiency depends on several factors such as temperature, cell type, and density, volume, SDS concentration, and the extent of cross-linking. For reproducible results, these parameters should be kept constant.

We use the Bioruptor Plus sonicator from Diagenode equipped with a cooling water bath and a tray holding up to six samples. To shear DNA, ultrasonic waves are transferred through water generating heat. With this system, the temperature is kept at 4°C preserving sample antigenicity. This system is suitable for shearing up to six sample at a time, assuring reproducibility between replicates. Samples' volume, tissue composition, and density impact the sonication outcome. If new tissues are going to be tested with this protocol and there is no previous knowledge of their sonication settings, several optimization steps are required. Samples volumes should be fixed at the beginning and sonication efficiency calibrated by testing several aliquots of the starting material at increasing dilutions in lysis buffer (es. 1×, 2×, 4×, 6×, 8×, 10×). By keeping settings constants, it is possible to retrieve the optimal conditions for your tissue.

We achieved a nice shearing (**Figure 2D**) using 200 μl of both cortical and hippocampal lysates (0.3% of SDS) with a DNA concentration between 6 and 7 ng/μl performing three runs of 10 cycles each with intervals of 30 s ON and 30 s OFF at high power.

It is important to notice that very low SDS concentration and prolonged crosslinking also impact the shearing efficiency. This should be taken into account if any changes are planned to be made.

Shearing was also tested after ChIP by the mean of Fragment Analyzer. We found some inconsistencies between agarose gel and Fragment Analyzer analysis. In both cortex and hippocampus, it is possible to notice a bimodal distribution in the input as well as in immunoprecipitates (**Figure 3**). This may be due to the higher sensitivity of capillary gel electrophoresis to residual contaminants (ions, SDS, proteins, etc.), due to overloading or to conformation/spatial structure of DNA molecules. However, the low peak is predominant in all sample, and the majority of DNA fragments ranging between 200 and 500 bp (**Figures 3A,B,D**). It is also possible to notice that H3 and NICD antibodies show the same behavior in the two tissues (**Figures 3B,B',D,D'**) whereas the mock precipitated IgG sample (the negative control) has barely precipitate fragments (**Figures 3C,C'**).

PCR Results Analysis

To validate the enrichment of NICD in the ChIP-NICD complex compared to the input and unbound fractions, we performed western blot analysis for Notch1 (c-terminus) and used β-actin as

TABLE 2 | Troubleshooting table.

Problem	Possible reason	Solution
Fragmented chromatin concentration is too low	1. Incomplete tissue lysis. 2. Not enough tissue used for the chromatin preparation.	1. Check for single-cell suspension using a microscope. 2. If incomplete tissue lysis is excluded, try increasing the starting material amount.
Fragments are too large when visualized in Agarose gel.	1. Samples may have been over-crosslinked. 2. Too much input material was processed. 3. Insufficient sonication.	1. Reduce the crosslinking time. 2. Reduce the amount of tissues per sonication or dilute it more in Lysis buffer. 3. Conduct a sonication time course.
Fragments are too short when visualized in Agarose gel.	Samples may have been subjected to excessive shearing by sonication and/or conditions are too harsh.	Conduct a sonication time course. Do not increase the duration of sonication steps, as this could overheat the sample and lead to loss of epitopes.
DNA pellets do not solubilize after extraction.	DNA pellet is overdried.	Heat the pellet at 37°C until it is completely solubilized. Try to avoid excessive drying of the DNA pellet.
No product or a very little band for the input after PCR reactions.	1. DNA added to the PCR reaction was not enough. 2. Conditions are not optimal.	1. Add more DNA to the PCR reaction or increase the number of amplification cycles. 2. Optimize the PCR conditions for experimental primer set using purified DNA from cross-linked and fragmented chromatin.
No product in the positive control after PCR reactions.	1. Not enough chromatin or antibody added to the IP reaction. 2. DNA could have been lost during washes. 3. Incomplete elution of chromatin from beads.	1. Try to add more chromatin or more antibody. 2. Prepare new wash solutions. 3. Try increasing elution time and shake tubes more frequently.
Visible product in the negative control.	1. Insufficient washes. 2. Too much chromatin added to the IP reaction.	1. Increase the number and/or stringency of the washes after immunoprecipitation. 2. Reduce the amount of negative control antibody or the amount of chromatin.
No band for the IP product after PCR reaction.	1. Not enough antibody added to the IP reaction. 2. Not enough DNA added to the PCR reaction. 3. Not enough chromatin added to the IP reaction.	1. Typically a range of 1–5 μg of antibody is added to the IP reaction; however, the exact amount depends greatly on the individual antibody. Try to use ChIP-grade antibodies. 2. Increase the number of amplification cycles or add more DNA to the PCR reaction. 3. Try to add more chromatin or increase the amount of starting tissue.

negative control. The ChIP-NICD fraction is enriched in cleaved Notch1 1.6-fold compared to the input. Precipitation is specific to NICD as indicated by the absence of β-actin, which is instead present in the input and unbound fraction (**Figure 4A**).

Downstream assays to investigate protein–DNA interaction at genomic binding sites are polymerase chain reaction (PCR), quantitative polymerase chain reaction (qPCR), DNA microarray (ChIP-on-chip), and massively parallel DNA sequencing (ChIP-seq).

Normal PCR is the easiest but less reliable approach to analyze a ChIP experiment product. It is a fast and cheap method to assess the quality/purity of the immunoprecipitated chromatin, but it is less employed for detection of potential target genes because it is not quantitative. In that case, it is preferable to use qPCR instead since it provides an accurate determination of levels of specific DNA in ChIP-ed samples. In both cases, primers should be designed for a region the TF binds to, the positive control, and for a region, your TF is supposed not to bind, representing the negative control. If there is previous knowledge, it is recommended to first identify the binding site sequence *in silico* in order to accurately amplify the extracted DNA.

If there are no known sites but candidate target genes are available, it is possible to design primers along the length of potential regulatory regions such as promoters and conserved noncoding sequences within intergenic regions. If candidate target genes or potential sites are not available, ChIP-chip (Buck and Lieb, 2004) or ChIP-seq (Fanelli et al., 2011; Furey, 2012) should be considered instead.

In our case, we know that RBPjK-binding motif is CGTGGGAA (Tun et al., 1994). Therefore, we designed a set of primers looking at the presence of these eight nucleotides strings within the sequence of the Hes5 promoter, a canonical Notch signaling target gene. We also chose Delta-like protein 1 (DLL1) promoter as a negative control region since there are no RBPjK-binding motifs. A good example of purity was achieved as demonstrated by the PCR and qPCR results (**Figure 4**). For Hes5 PCR results, we observe amplification in both RBPjK and NICD samples while there is no amplification in IgG lane suggesting that non-specific binding is absent (**Figure 4B**).

On the other hand, the DLL1 PCR shows no amplification (**Figure 4B'**), indicating the specificity of the ChIP for RBPjK and NICD targets.

Quantitative polymerase chain reaction analysis further confirms the specificity obtained using Hes5 as a positive control and GADPH as a negative control (**Figure 4C**). Binding efficiency is expressed by the percent input method that includes normalization for both background levels and input chromatin (Lacazette, 2016).

This protocol is suitable for sequencing (data not shown). From the ChIPed fragments, a library is prepared according to manufacturer's instruction and loaded into the flow-cell for sequencing; trimmed sequence reads are mapped to a reference genome. Next, peaks are found using peak-calling algorithms (Nakato and Shirahige, 2017). To further analyze the data, differential binding or motif analyses are common endpoints of ChIP-seq workflows. The ChIP-Seq procedure allows to map TF-target sequences and provide a functional readout of gene activation in complex tissues, such as the brain, and under different experimental conditions: i.e., environmental enrichment, aging, neurodegeneration, neuroinflammation, etc. Understanding the downstream targets of signaling pathways critical for plasticity and neurodegeneration will facilitate the discrimination of beneficial versus detrimental genes' products that can be employed for developing therapeutic strategies targeting brain diseases.

Concluding, there are already other protocols describing ChIP procedures (**Table 1**; Braveman et al., 2004; Nelson et al., 2006; Dahl and Collas, 2008; Sailaja et al., 2012; Schmidl et al., 2015). However, all these methods are either centered on abundant histone modification or use cells suspensions as starting material. The added value of this protocol is the possibility to perform all the downstream analyses described (i) from a tissue subregion, (ii) precipitating for a rare transcriptional activator (NICD), and (iii) yielding a sufficient amount of DNA with reduced background. The advantage of performing ChIP for NICD, compared to RBPJK, has undisputed advantages as only activated loci under specific conditions will be captured within the tissue revealing active transcriptional targets.

Troubleshooting

Table 2 indicates issues which can occur during the procedure with a possible reason and suggestions to solve and avoid them.

DATA AVAILABILITY

The datasets generated for this study are available on request to the corresponding author.

ETHICS STATEMENT

Animal protocol n. 2016_32_FR released by the cantonal Veterinary office of Fribourg.

AUTHOR CONTRIBUTIONS

AP conducted the experiments and wrote the manuscript. LA directed the experimentation and co-wrote the manuscript.

FUNDING

The work is supported by funding of the Swiss National Foundation (31003A_163470, LA).

ACKNOWLEDGMENTS

We thank Mr. Simon April and Mr. Daniel Brechtold for dedicating time to establish the first steps of this protocols. We thank the animal caretaker at the University of Fribourg, Simone Eichenberger, for helping us sourcing the mice.

REFERENCES

Alberi, L., Hoey, S. E., Brai, E., Scotti, A. L., and Marathe, S. (2013). Notch signaling in the brain: in good and bad times. *Ageing Res. Rev.* 12, 801–814. doi: 10.1016/j.arr.2013.03.004

Alberi, L., Liu, S., Wang, Y., Badie, R., Smith-Hicks, C., Wu, J., et al. (2011). Activity-induced notch signaling in neurons requires Arc/Arg3.1 and is essential for synaptic plasticity in hippocampal networks. *Neuron* 69, 437–444. doi: 10.1016/j.neuron.2011.01.004

Brai, E., Alina Raio, N., and Alberi, L. (2016). Notch1 hallmarks fibrillary depositions in sporadic alzheimer's disease. *Acta Neuropathol. Commun.* 4:64. doi: 10.1186/s40478-016-0327-2

Braveman, M. W., Chen-Plotkin, A. S., Yohrling, G. J., and Cha, J. H. J. (2004). Chromatin immunoprecipitation technique for study of transcriptional dysregulation in intact mouse brain. *Methods Mol. Biol.* 277, 261–276. doi: 10.1385/1-59259-804-8:261

Buck, M. J., and Lieb, J. D. (2004). ChIP-chip: considerations for the design, analysis, and application of genome-wide chromatin immunoprecipitation experiments. *Genomics* 83, 349–360. doi: 10.1016/j.ygeno.2003.11.004

Dahl, J. A., and Collas, P. (2008). A rapid micro chromatin immunoprecipitation assay (ChIP). *Nat. Protoc.* 3, 1032–1045. doi: 10.1038/nprot.2008.68

Engelmann, C., and Haenold, R. (2016). Transcriptional Control of synaptic plasticity by transcription factor NF-κB. *Neural Plast.* 2016:7027949. doi: 10.1155/2016/7027949

Fanelli, M., Amatori, S., Barozzi, I., and Minucci, S. (2011). Chromatin immunoprecipitation and high-throughput sequencing from paraffin-embedded pathology tissue. *Nat. Protoc.* 6, 1905–1919. doi: 10.1038/nprot.2011.406

Flavell, S. W., and Greenberg, M. E. (2008). Signaling mechanisms linking neuronal activity to gene expression and plasticity of the nervous system. *Annu. Rev. Neurosci.* 31, 563–590. doi: 10.1146/annurev.neuro.31.060407.125631

Furey, T. S. (2012). ChIP–seq and beyond: new and improved methodologies to detect and characterize protein–DNA interactions. *Nat. Rev. Genet.* 13, 840–852. doi: 10.1038/nrg3306

Genuth, N. R., and Barna, M. (2018). Heterogeneity and specialized functions of translation machinery: from genes to organisms. *Nat. Rev. Genet.* 19, 431–452. doi: 10.1038/s41576-018-0008-z

Huang, J., Zheng, J., Yuan, H., and McGinnis, K. (2018). Distinct tissue-specific transcriptional regulation revealed by gene regulatory networks in maize. *BMC Plant Biol.* 18:111. doi: 10.1186/s12870-018-1329-y

Lacazette, E. (2016). A laboratory practical illustrating the use of the ChIP-qPCR method in a robust model: estrogen receptor alpha immunoprecipitation using Mcf-7 culture cells. *Biochem. Mol. Biol. Educ.* 45, 152–160. doi: 10.1002/bmb.20999

Mansuy, I. M., and Mohanna, S. (2011). Epigenetics and the human brain: where nurture meets nature. *Cerebrum* 2011, 1–8.

Marathe, S., Jaquet, M., Annoni, J. -M., and Alberi, L. (2017). Jagged1 is altered in alzheimer's disease and regulates spatial memory processing. *Front. Cell. Neurosci.* 11:220. doi: 10.3389/fncel.2017.00220

Nakato, R., and Shirahige, K. (2017). Recent advances in ChIP-seq analysis: from quality management to whole-genome annotation. *Brief. Bioinform.* 18, 279–290.

Nelson, J. D., Denisenko, O., and Bomsztyk, K. (2006). Protocol for the fast chromatin immunoprecipitation (ChIP) method. *Nat. Protoc.* 1, 179–185. doi: 10.1038/nprot.2006.27

Olfson, E., and Ross, D. A. (2017). Genes orchestrating brain function. *Biol. Psychiatry* 82, e17–e19. doi: 10.1016/j.biopsych.2017.06.003

Qian, J., Esumi, N., Chen, Y., Wang, Q., Chowers, I., and Zack, D. J. (2005). Identification of regulatory targets of tissue-specific transcription factors: application to retina-specific gene regulation. *Nucleic Acids Res.* 33, 3479–3491. doi: 10.1093/nar/gki658

Sailaja, B. S., Takizawa, T., and Meshorer, E. (2012). "Chromatin immunoprecipitation in Mouse hippocampal cells and tissues," in *Transcriptional Regulation: Methods and Protocols*, ed. A. Vancura (New York, NY: Springer New York), 353–364.

Schmidl, C., Rendeiro, A. F., Sheffield, N. C., and Bock, C. (2015). ChIPmentation: fast, robust, low-input ChIP-seq for histones and transcription factors. *Nat. Methods* 12, 963–965. doi: 10.1038/nmeth.3542

Siebel, C., and Lendahl, U. (2017). Notch signaling in development, tissue homeostasis, and disease. *Physiol. Rev.* 97, 1235–1294. doi: 10.1152/physrev.00005.2017

Sultan, F. A. (2013). Dissection of different areas from mouse hippocampus. *Bio Protoc.* 3:e955. doi: 10.21769/BioProtoc.955

Tun, T., Hamaguchi, Y., Matsunami, N., Furukawa, T., Honjo, T., and Kawaichi, M. (1994). Recognition sequence of a highly conserved DNA binding protein RBP-J kappa. *Nucleic Acids Res.* 22, 965–971. doi: 10.1093/nar/22.6.965

Vaquerizas, J. M., Kummerfeld, S. K., Teichmann, S. A., and Luscombe, N. M. (2009). A census of human transcription factors: function, expression and evolution. *Nat. Rev. Genet.* 10, 252–263. doi: 10.1038/nrg2538

Conflict of Interest Statement: The authors declare that the research was conducted in the absence of any commercial or financial relationships that could be construed as a potential conflict of interest.

frontiers in Pharmacology

ORIGINAL RESEARCH
published: 02 April 2019
doi: 10.3389/fphar.2019.00325

Activation of SK/K_{Ca} Channel Attenuates Spinal Cord Ischemia-Reperfusion Injury via Anti-oxidative Activity and Inhibition of Mitochondrial Dysfunction in Rabbits

Jie Zhu†, Li-Kun Yang†, Wei-Liang Chen, Wei Lin, Yu-Hai Wang and Tao Chen**

Department of Neurosurgery, The 101th Hospital of PLA, School of Medicine, Anhui Medical University, Wuxi, China

OPEN ACCESS

Edited by:
Mario Eduardo Guido, Center for Research in Biological Chemistry Córdoba (CIQUIBIC), Argentina

Reviewed by:
Jian Liu, Xijing Hospital, Fourth Military Medical University, China
Damian Dorfman, CONICET Centro de Estudios Farmacológicos y Botánicos (CEFYBO), Argentina

***Correspondence:**
Yu-Hai Wang
prof_wyh101@163.com
Tao Chen
fmmuchentao@163.com

†*These authors have contributed equally to this work*

Specialty section:
This article was submitted to Neuropharmacology, a section of the journal Frontiers in Pharmacology

Received: *13 August 2018*
Accepted: *19 March 2019*
Published: *02 April 2019*

Citation:
Zhu J, Yang L-K, Chen W-L, Lin W, Wang Y-H and Chen T (2019) Activation of SK/K_{Ca} Channel Attenuates Spinal Cord Ischemia-Reperfusion Injury via Anti-oxidative Activity and Inhibition of Mitochondrial Dysfunction in Rabbits. Front. Pharmacol. 10:325. doi: 10.3389/fphar.2019.00325

Spinal cord ischemia-reperfusion injury (SCI/R) is a rare but devastating disorder with a poor prognosis. Small conductance calcium-activated K^+ (SK/K_{Ca}) channels are a family of voltage-independent potassium channels that are shown to participate in the pathological process of several neurological disorders. The aim of this study was to investigate the role of SK/K_{Ca} channels in experimental SCI/R in rabbits. The expression of SK/K_{Ca}1 protein significantly decreased in both cytoplasm and mitochondria in spinal cord tissues after SCI/R. Treatment with 2 mg/kg NS309, a pharmacological activator for SK/K_{Ca} channel, attenuated SCI/R-induced neuronal loss, spinal cord edema and neurological dysfunction. These effects were still observed when the administration was delayed by 6 h after SCI/R initiation. NS309 decreased the levels of oxidative products and promoted activities of antioxidant enzymes in both serum and spinal cord tissues. The results of ELISA assay showed that NS309 markedly decreased levels of pro-inflammatory cytokines while increased anti-inflammatory cytokines levels after SCI/R. In addition, treatment with NS309 was shown to preserve mitochondrial respiratory complexes activities and enhance mitochondrial biogenesis. The results of western blot analysis showed that NS309 differentially regulated the expression of mitochondrial dynamic proteins. In summary, our results demonstrated that the SK/K_{Ca} channel activator NS309 protects against SCI/R via anti-oxidative activity and inhibition of mitochondrial dysfunction, indicating a therapeutic potential of NS309 for SCI/R.

Keywords: SK/K_{Ca} channels, NS309, spinal cord ischemia and reperfusion, mitochondrial dysfunction, mitochondrial dynamic

INTRODUCTION

Spinal cord ischemia-reperfusion injury (SCI/R) is a rare but devastating disorder induced by a period of deterioration of the spinal cord blood supply. SCI/R is associated with several pathophysiological states, while thoracoabdominal surgery and atherosclerotic disease are the most frequent causes (New and McFarlane, 2012). It has been shown that approximately 32% of patients

with thoracic or thoracoabdominal aortic repair surgery suffered from SCI/R, and the incidence of paraplegia was up to 5% (LeMaire et al., 2012; Panthee and Ono, 2015). Many neuroprotective drugs, such as mannitol, corticosteroids and naloxone, have been demonstrated to be beneficial to function recovery in experimental SCI/R models, but none of them was convincingly confirmed in clinical trials (Griepp and Griepp, 2007).

Small conductance calcium-activated K^+ (SK/K_{Ca}) channels are a family of voltage-independent potassium channels that are activated solely by intracellular Ca^{2+}. SK/K_{Ca} channels are extensively expressed throughout the central nervous system, including the brain and spinal cord tissues (Kuiper et al., 2012). They are encoded by the *KCNN* gene family, and three different subtypes of SK/K_{Ca} channels, including SK/K_{Ca}1, SK/K_{Ca}2, and SK/K_{Ca}3, have been cloned in mammals (Stocker, 2004). SK/K_{Ca} channels are activated by increases in intracellular Ca^{2+}, and they not only contribute to the after-hyperpolarization that follows action potentials, but also play key roles in regulating dendritic excitability, synaptic transmission and synaptic plasticity (Faber and Sah, 2007). Three decades of research has shown that SK/K_{Ca} channels are involved in multiple neurological diseases caused by neuronal excitotoxicity and dysfunction of Ca^{2+} homeostasis (Kuiper et al., 2012). By using pharmacological inhibitors and activators, Dolga and colleagues found that SK/K_{Ca} channels participated in the pathological process of stroke, Parkinson's disease (PD), Alzheimer's disease (AD) and schizophrenia (Anderson et al., 2006; Dolga et al., 2011, 2012; Dolga and Culmsee, 2012). A previous study showed that activation of the SK/K_{Ca} channel protected against glutamate-induced oxytosis through inhibiting mitochondrial dysfunction (Dolga et al., 2013). More importantly, activation of the SK/K_{Ca} channel in the spinal cord was shown to reduce the NMDA receptor antagonist dose needed to produce anti-nociception in an inflammatory pain model (Hipolito et al., 2015). In the present study, we investigated the role of SK/K_{Ca} channels in a SCI/R model in rabbits. Previous studies have demonstrated that SK/K_{Ca} channels were also located in mitochondrial-enriched fraction, and this type of subcellular expression of SK/K_{Ca} channels was associated with normal mitochondrial function in dopaminergic neurons (Dolga et al., 2014). Thus, we also determined the underlying mechanism with focus on oxidative stress and mitochondrial function.

MATERIALS AND METHODS

Animals and Agents

Adult New Zealand white rabbits (2.5–3.0 kg) were obtained from the Laboratory Animal Center of Anhui Medical University. All rabbits were kept in standard laboratory conditions with free access to rabbit chow and tap water. All experimental procedures were performed in compliance with the NIH guidelines for the use of experimental animals and approved by the Ethics Review Committee of Anhui Medical University. The mitochondrial isolation kit, malondialdehyde (MDA) assay kit, 8-iso-prostaglandin F2α (8-iso-PGF2α) assay kit, superoxide dismutase (SOD) assay kit and catalase (CAT) assay kit was purchased from Jiancheng Biotech Company (Nanjing, Jiangsu, China). The anti-SK/K_{Ca}1 (ab66624), anti-COX IV (ab66739), and anti-Tubulin (ab56676) antibodies were obtained from abcam (CA, United States). The anti-Opa-1 (sc-30573), anti-Mfn-1 (sc-166644), anti-Drp-1 (sc-101270), anti-Fis-1 (sc-376447), and anti-β-actin (sc-47778) antibodies were purchased from Santa Cruz Biotechnology (Santa Cruz, CA, United States).

SCI/R Model

SCI/R was established by infrarenal aortic occlusion as previously described (Zhou et al., 2013). The animals were anesthetized by intramuscular administration of 25 mg/kg ketamine and 0.10 mg/kg atropine. The right femoral artery was catheterized for measuring distal blood pressure and ear artery was used to collect blood sample. A 5-cm-long midline incision was made to expose abdominal aorta, and aortic clamping was performed using artery clips just below renal artery after administration of 200 units of heparin. After 20 min occlusion, the clips were removed to restore the blood flow. Then, the incision was sutured layer-by-layer, and the rabbits were allowed to recover. During the operation process, the body temperature was maintained close to 38.2°C using a heating lamp.

Experimental Design

Experimental 1

To investigate the effect of SCI/R on the expression of SK/K_{Ca}1 and mitochondrial dynamic proteins, forty animals were randomly divided into sham (n = 8) and SCI/R (n = 32) group. The animals in sham group were given operation without artery occlusion. The animals in SCI/R group were treated with SCI/R and spinal cord tissues were obtained at 3, 6, 12, and 24 h.

Experimental 2

To investigate the protective effect of NS309 against SCI/R, thirty-two animals were randomly divided into vehicle (n = 16) and NS309 (n = 16) group. The animals in NS309 group were treated with 2 mg/kg NS309 by intraperitoneal injection at the time of spinal cord ischemia initiation, and the animals in vehicle group were treated with saline (0.9%) with 1% DMSO. Eight animals in each group were used to measure neurological function and H&E staining, and the other 8 animals were used to measure spinal cord edema.

Experimental 3

To investigate the therapeutic time window of NS309, sixty-four animals were randomly divided into vehicle (n = 16), NS309 at 3 h (n = 16), NS39 at 6 h (n = 16) and NS309 at 9 h (n = 16) group. The animals in vehicle group were treated with saline (0.9%) with 1% DMSO, and the animals in NS309 groups were treated with 2 mg/kg NS309 by intraperitoneal injection at 3, 6, or 9 h after spinal cord ischemia initiation, respectively. Eight animals in each group were used to measure neurological function and H&E staining, and the other 8 animals were used to measure spinal cord edema.

Experimental 4

To investigate the effect of NS309 on oxidative stress, and mitochondrial dysfunction, sixteen animals were randomly divided into vehicle (n = 8) and NS309 (n = 8) group. The animals in NS309 group were treated with 2 mg/kg NS309 by intraperitoneal injection at the time of spinal cord ischemia initiation, and the animals in vehicle group were treated with saline (0.9%) with 1% DMSO. The blood samples were collected at 0, 3, 6, 12, 24, and 48 h after spinal cord ischemia initiation, and the spinal cord tissues were collected at 72 h.

Mitochondrial Isolation

After treatments, the spinal cord tissues were removed and homogenized, and mitochondria was isolated using the mitochondrial isolation kit following the manufacturer's suggested protocol. Mitochondrial pellets were resuspended, and the protein content was quantified using a BCA method. The mitochondrial and cytosolic fractions were used to detect SK/K_{Ca}1 expression, and the total protein was used to detect the expression of mitochondrial dynamic proteins.

Hematoxylin and Eosin (H&E) Staining

After various treatments, the spinal cord tissues were removed, and the paraffin embedded blocks were made. The 5 μm sections from each group was subjected to standard H&E staining and evaluated microscopically. The number of normal motor neurons was counted by an investigator blinded to the grouping.

Spinal Cord Edema Measurement

Spinal cord edema was evaluated by spinal cord water content using the wet-dry method at 72 h after SCI/R. Briefly, after the animals were sacrificed, the spinal cord tissues (L4-6 segments) were quickly removed. Tissue samples were weighed immediately to get wet weight. After drying in an oven for 48 h at 100°C, the tissues were re-weighed to get the dry weight. Spinal cord water content was then calculated using the following formula: % H_2O=(1-dry weight/wet weight) × 100%.

Neurological Function Assay

The hind-limb motor function was determined by the modified Tarlov criteria: no voluntary hind-limb function as score 0; only perceptible joint movement as score 1; active movement but unable to stand as score 2; able to stand but unable to walk as score 3; and complete normal hind-limb motor function as score 4.

Sample Collection

At 0, 3, 6, 12, 24, and 48 after SCI/R, 2 mL of blood was collected from auricular vein, and the serum was separated by centrifugation at 3,000 × g for 15 min at 4°C. At 72 h after reperfusion, the animals were sacrificed, the spinal cord tissues (L4-6 segments) were removed. The spinal cord samples were homogenized in chilled PBS, and then centrifuged at 10,000 × g at 4°C for 10 min. The protein concentration was quantified using a BCA method.

Quantification of Oxidative Products and Antioxidant Enzymes

The levels MDA and 8-iso-PGF2α and the enzymatic activities of SOD and CAT in the serum and spinal cord samples were measured by commercial kits following the manufacturer's suggested protocol.

Quantification of Inflammatory Cytokines

To detect the levels of inflammatory cytokines, animals were sacrificed at 12, 24, or 48 h after SCI/R, and the spinal cord homogenates were obtained. The concentrations of tumor necrosis factor-α (TNF-α), IL-1β, IL-10 and transforming growth factor-β1 (TGF-β1) were measured using specific ELISA kits according to the manufacturers' instructions (Boster Biological Technology, Wuhan, China).

Determination of Mitochondrial Complexes Activities

After treatment with NS309 or vehicle, spinal cord mitochondria were isolated from each group and the enzymatic activities of mitochondrial complexes were assayed using the following methods: NADH dehydrogenase for complex I, succinate dehydrogenase for complex II, ubiquinol cytochrome c oxidase for complex III, and cytochrome c oxidase for complex IV as previously described (Ye et al., 2011).

Real-Time RT-PCR

Total RNA was extracted from the spinal cord tissues using the Trizol reagent (Invitrogen, Carlsbad, CA, United States). Reverse transcription was performed according to the manufacturer's instructions of the real-time PCR kit (BioTNT Co., Ltd., Shanghai, China). The primers sequences used are shown in **Table 1**. The mRNA levels were normalized using GAPDH as an internal control.

Western Blot Analysis

Total proteins from spinal cord tissues were extracted and the protein concentration was determined using a BCA assay kit (Jiancheng Biotech Company, Jiangsu, China). Equivalent proteins (60 μg per sample) were separated using 10 or 12% sodium dodecyl sulfate (SDS)-PAGE, and then electro-transferred onto polyvinylidene fluoride (PVDF) membranes.

TABLE 1 | Primers sequences used in real-time PCR.

Gene	Forward sequences	Reverse sequences
D-loop	5′-AGGCATCTGGTTCTTACTTC-3′	5′-TGACGGCTATGTTGAGGA-3′
ATP8	5′-CTTCCCAAACCTTTCCTG-3′	5′-GGTAATGAAAGAGGCA AATAGA-3′
PGC-1	5′-GTGCAGCCAAGACTCTG TATGG-3′	5′-GTCCAGGTCATTCACAT CAAGTTC-3′
NRF-1	5′-GAGTGACCCAAACCGAACA-3′	5′-GGAGTTGAGTATGTCC GAGT-3′
TFAM	5′-GGTGTATGAAGCGGATTT-3′	5′-CTTTCTTCTTTAGGCGTTT-3′
GAPDH	5′-ATGTATCCGTTGTGGAT CTGAC-3′	5′-CCTGCTTCACCACCTT CTTG-3′

The membranes were incubated with the following primary antibodies: SK/K_{Ca}1 (1:500), COX IV (1:800), Tubulin (1:1000), Opa-1 (1:500), Mfn-1 (1:800), Drp-1 (1:800), Fis-1 (1:500), and β-actin (1:2000). After incubation with secondary antibodies for 1 h, the bands were visualized by using chemiluminescent detection system. Image J (Scion Corporation) was used to quantify the optical density of each band. The expression of each protein was calculated from the optical density of each band normalized against the optical density of β-actin, tubulin or COX IV, and expressed as the fold of control levels.

Statistical Analysis

Each experiment was repeated at least three times. Statistical analysis was performed using SPSS. Statistical evaluation of the data was performed by the Student's *t*-test between two groups. A value of $p < 0.05$ referred to the statistical difference.

RESULTS

SCI/R Decreases the Expression of SK/K_{Ca}1 Subtype

The changes of arterial pH, PaO_2, $PaCO_2$, and blood glucose levels in vehicle or 2 mg/kg NS309 treated rabbits were measured at 10 min before ischemia, 10 min after ischemia initiation and 10 min after reperfusion, respectively. As shown in **Table 2**, no significant differences in blood pH, PaO_2, $PaCO_2$, or glucose were observed among all groups. The results of distal blood pressure (DBP) showed that an approximate 90% reduction in DBP was observed during the time when artery was clamped. The value of DBP was recovered to 90–95% of the baseline within 10 min after reperfusion.

To investigate the effect of SCI/R on SK/K_{Ca} channels expression, western blot analysis was used to detect the changes of SK/K_{Ca}1 subtype at 3, 6, 12, or 24 h after reperfusion (**Figure 1A**). The results showed that the expression of SK/K_{Ca}1 protein significantly decreased at 12 and 24 h after reperfusion. To determine the subcellular localization of SK/K_{Ca}1 after SCI/R, the expression of SK/K_{Ca}1 protein was assayed after mitochondria isolation (**Figure 1B**). The results showed an enrichment of SK/K_{Ca}1 from whole cell extracts to cytoplasm, as well as in mitochondrial fractions, and the decreased expression of SK/K_{Ca}1 protein was also observed in isolated mitochondria after SCI/R (**Figure 1C**).

The SK/K_{Ca} Channel Activator NS309 Protects Against SCI/R

To investigate the effect of SK/K_{Ca} channel activation on SCI/R, rabbits were treated with 2 mg/kg NS309, a pharmacological activator for SK/K_{Ca} channel, at the time of spinal cord ischemia

TABLE 2 | Physiological parameters.

	Rectal temperature (°C)	pH	PaO_2 (mm Hg)	$PaCO_2$ (mm Hg)	Glucose (mg/dl)	DBP (mm Hg)
10 min before ischemia						
Vehicle	38.3 ± 0.2	7.41 ± 0.13	124.2 ± 11.4	34.4 ± 3.8	157 ± 17	106 ± 5.7
NS309 2 mg/kg	38.1 ± 0.2	7.39 ± 0.09	129.5 ± 13.9	31.1 ± 4.6	168 ± 19	104 ± 7.1
10 min after ischemia						
Vehicle	38.3 ± 0.3	7.35 ± 0.19	133.4 ± 15.3	34.3 ± 2.5	154 ± 18	13 ± 2.9*
NS309 2 mg/kg	38.2 ± 0.2	7.38 ± 0.17	127.9 ± 15.2	32.7 ± 4.3	164 ± 23	17 ± 4.3*
10 min after reperfusion						
Vehicle	38.0 ± 0.1	7.37 ± 0.10	125.9 ± 11.4	36.8 ± 3.3	153 ± 19	100 ± 10.4
NS309 2 mg/kg	38.4 ± 0.4	7.41 ± 0.18	131.6 ± 12.3	38.3 ± 3.1	160 ± 22	98 ± 9.3

*Data are presented as mean ± SEM. *$p < 0.05$ vs. 10 min before ischemia.*

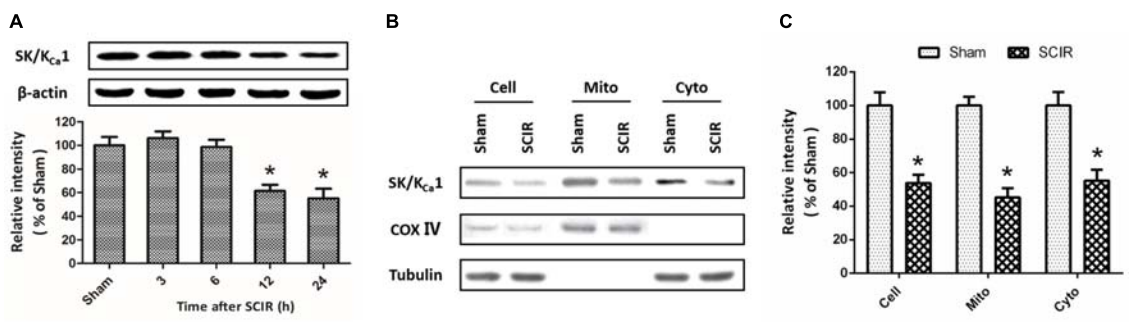

FIGURE 1 | SCI/R decreases the expression of SK/K_{Ca}1 subtypes. The animals were exposed to spinal I/R, and the expression of SK/K_{Ca}1 protein in spinal cord tissues was detected by western blot analysis at 3, 6, 12, or 24 h after reperfusion **(A)**. Immunoblot analysis of whole-cell extract (depicted as "Cell"), cytosol supernatant (depicted as "Cyto") or crude mitochondrial pellets (depicted as "Mito") were also performed **(B)**, and calculated **(C)** to determine subcellular expression of SK/K_{Ca}1 protein. Data are shown as mean ± SEM ($n = 8$). *$p < 0.05$ vs. Sham.

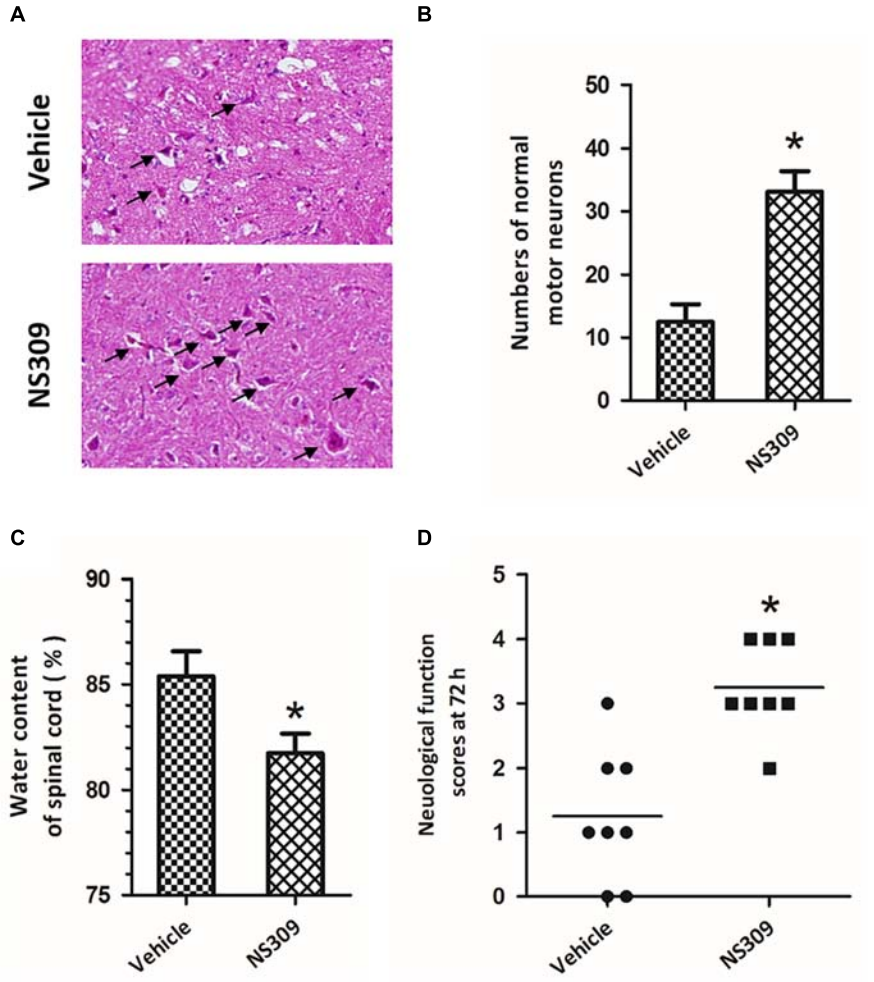

FIGURE 2 | The SK/K_{Ca} channel activator NS309 protects against SCI/R. The animals were treated with 2 mg/kg NS309 or vehicle at the beginning of SCI/R operation. Hematoxylin and eosin staining was performed in the ventral horn of L4 spinal cord segment at 72 h after reperfusion **(A)**, and the number of normal motor neurons was countered **(B)**. The spinal cord edema was assayed by measuring spinal cord water content at 72 h **(C)**. Neurological function scores were assessed at 72 h after reperfusion by an independent observer **(D)**. Arrowheads indicate normal neurons. The data were represented as means ± SEM (n = 8). *$p < 0.05$ vs. Vehicle.

initiation. The representative micrographs of H&E staining in the ventral horn of L4 spinal cord segment at 72 h after reperfusion are shown in **Figure 2A**. The number of normal motor neurons in NS309 group was higher than that in vehicle group (**Figure 2B**). We also determined spinal cord edema by measuring water content of spinal cord tissues at 72 h after injury, and a marked decrease in spinal cord water content was observed in NS309 treated animals as compared with vehicle group (**Figure 2C**). Next, we measured hind-limb motor function scores at 72 h after injury. As shown in **Figure 2D**, treatment with NS309 significantly improved neurological outcome of SCI/R challenged rabbits.

To determine the therapeutic time window of NS309-induced protective effects, the post-injury administration pattern was used, and the rabbits were treated with 2 mg/kg NS309 at different time points (3, 6, or 9 h after ischemia initiation). A significant reduction in spinal cord water content (**Figure 3A**) and increased numbers of normal motor neurons (**Figure 3B**) were observed when NS309 was administrated 3 or 6 h after ischemia initiation but not when the administration was delayed by 9 h. In consistent with these results, a significant improvement of neurologic outcome was still detected when NS309 treatment was started 3 or 6 h, but not 9 h after ischemia initiation (**Figure 3C**).

NS309 Reduces Oxidative Stress and Regulates Inflammation After SCI/R

The levels of MDA and 8-iso-PGF2α, two classic oxidative products, in serum and spinal cord tissues were measured after SCI/R. The results showed that the levels of MDA (**Figure 4A**) and 8-iso-PGF2α (**Figure 4B**) in serum significantly increased after SCI/R in a time-dependent manner, but these increases were attenuated by NS309 treatment. The levels of MDA (**Figure 4C**) and 8-iso-PGF2α (**Figure 4D**) in spinal cord tissues from

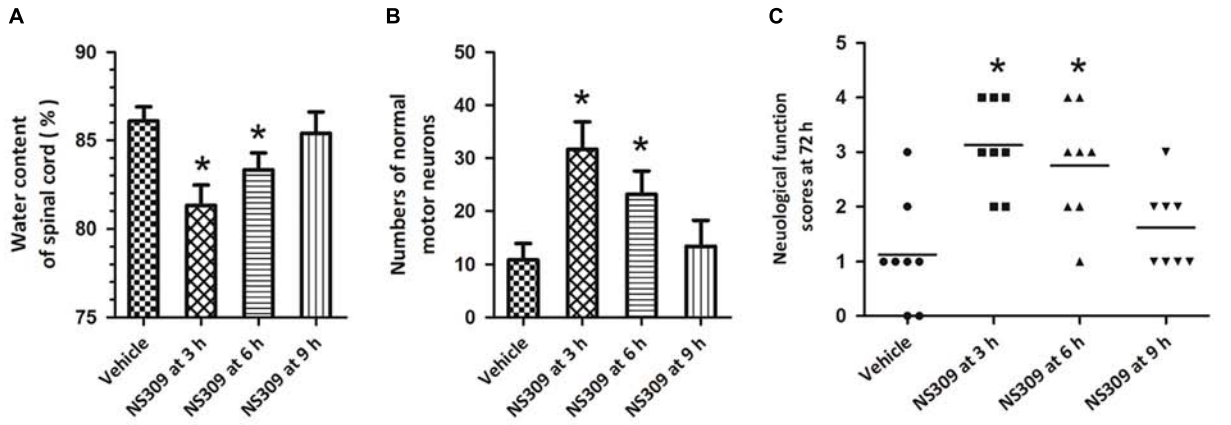

FIGURE 3 | Time window of NS309-induced neuroprotection. The animals were exposed to SCI/R and treated with 2 mg/kg NS309 at different time points (3, 6, or 9 h after SCI/R beginning). The spinal cord water content **(A)**, number of normal motor neurons **(B)** and neurological function scores **(C)** were measured 72 h later. The data were represented as means ± SEM (n = 8). *$p < 0.05$ vs. Vehicle.

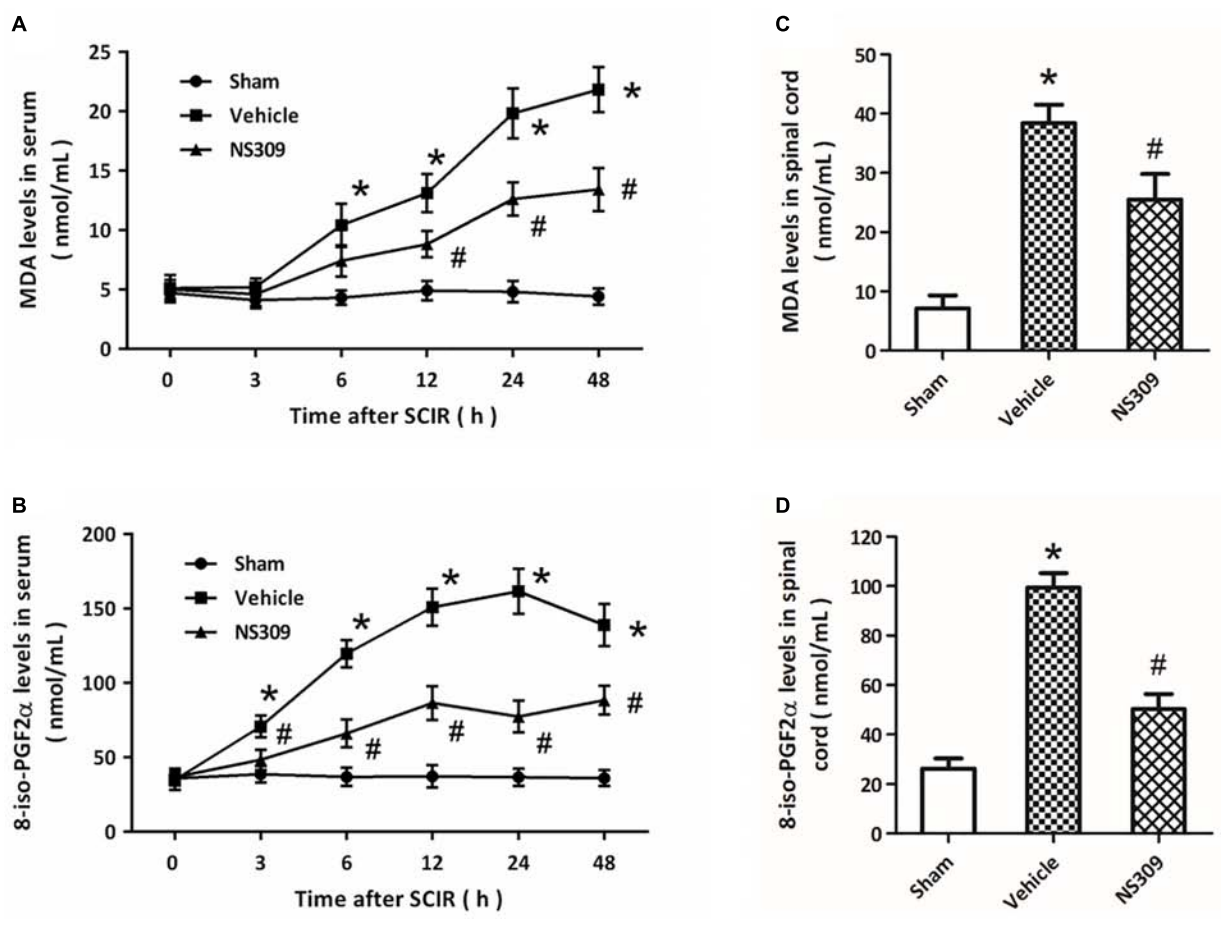

FIGURE 4 | NS309 reduces the expression of oxidative products after SCI/R. The animals were treated with 2 mg/kg NS309 or vehicle at the beginning of SCI/R. The expression levels of MDA **(A)** and 8-iso-PGF2α **(B)** in serum were measured at different time points (0, 3, 6, 12, 24, and 48 h). The expression levels of MDA **(C)** and 8-iso-PGF2α **(D)** in spinal cord tissues were detected at 72 h after reperfusion. The data were represented as means ± SEM (n = 8). *$p < 0.05$ vs. Sham. $^{\#}p < 0.05$ vs. Vehicle.

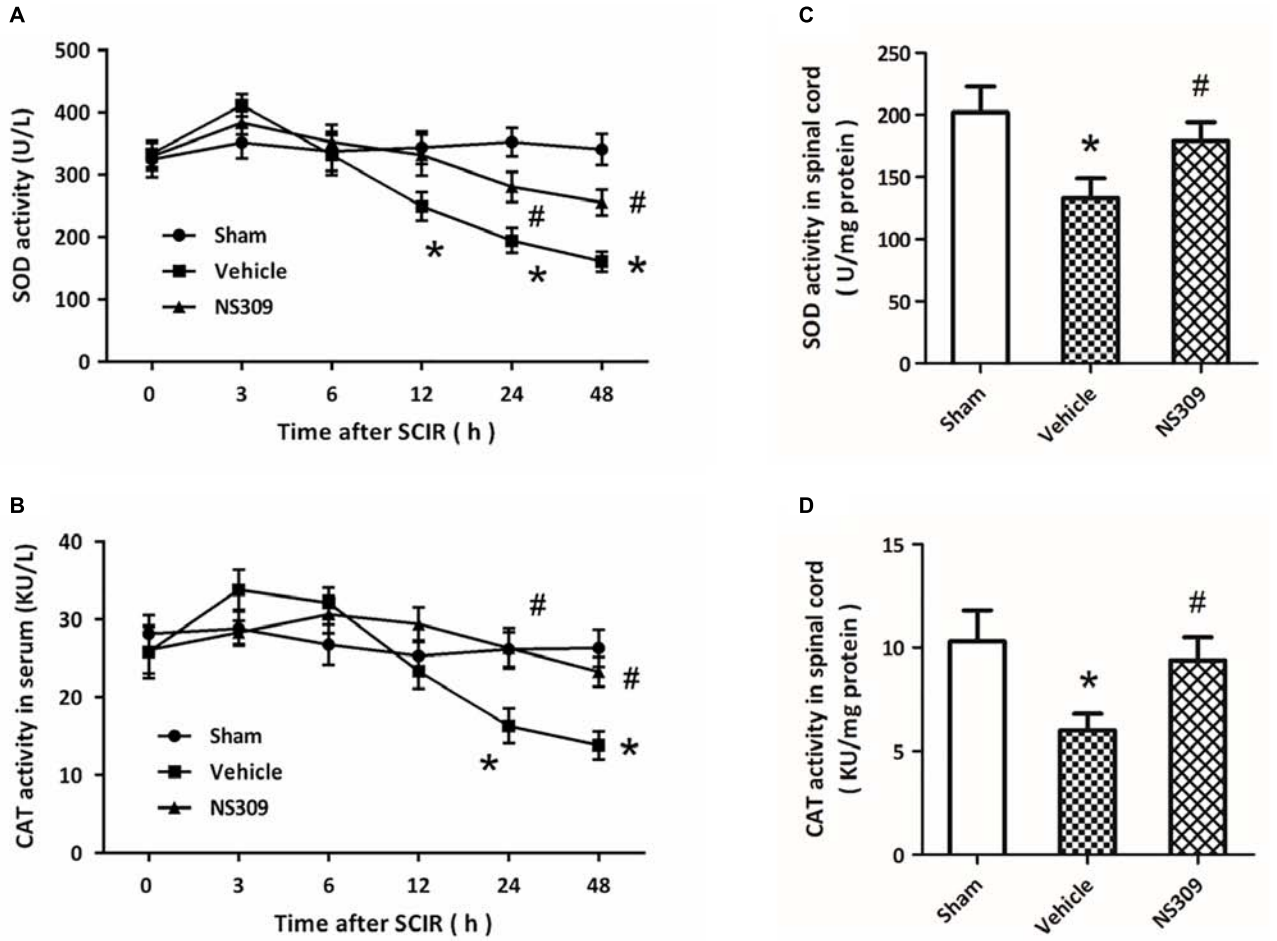

FIGURE 5 | NS309 preserves the activity of antioxidant enzymes after SCI/R. The animals were treated with 2 mg/kg NS309 or vehicle at the beginning of SCI/R. The enzymatic activities of SOD **(A)** and CAT **(B)** in serum were measured at different time points (0, 3, 6, 12, 24, and 48 h). The enzymatic activities of SOD **(C)** and CAT **(D)** in spinal cord tissues were detected at 72 h after reperfusion. The data were represented as means ± SEM (n = 8). $^{*}p < 0.05$ vs. Sham. $^{\#}p < 0.05$ vs. Vehicle.

NS309-treated animals was lower than that in vehicle group. In addition, we also detected the activities of SOD and CAT, two endogenous antioxidant enzymes. The results showed that the activities of SOD (**Figure 5A**) and CAT (**Figure 5B**) in serum from NS309-treated animals was higher than that in vehicle group from 12 to 48 h after SCI/R. As shown in **Figures 5C,D**, NS309 also markedly increased SOD and CAT activities in spinal cord tissues.

To investigate the effect of NS309 on inflammatory responses after SCI/R, the levels of inflammatory cytokines were determined in spinal cord tissues at different time points. The results showed that SCI/R significantly increased the levels of TNF-α (**Figure 6A**) and IL-1β (**Figure 6B**), two pro-inflammatory cytokines. However, application of NS309 significantly reduced the levels of these two cytokines in spinal cord tissues at 12, 24 and 48 h. Furthermore, we also measured the levels of IL-10 and TGF-β1, two anti-inflammatory cytokines. We found that NS309 markedly increased the levels of IL-10 at 24 and 48 h, but not at 12 h after SCI/R (**Figure 6C**). The TGF-β1 levels in NS309-treated group were higher than that in vehicle group at all time points measured (**Figure 6D**).

NS309 Inhibits Mitochondrial Dysfunction After SCI/R

Mitochondrial function plays a key role in regulating oxidative stress under ischemia and reperfusion injury. Thus, we detected the activities of mitochondrial complexes in spinal cord tissues. The results showed that SCI/R significantly decreased the activities of all four mitochondrial complexes, and the activities of complex I (**Figure 7A**), complex III (**Figure 7C**) and complex IV (**Figure 7D**), but not complex II **Figure 7B**), were preserved by NS309 treatment. In addition, we investigated the effect of NS309 on mitochondrial biogenesis. NS309 increased mtDNA levels (**Figure 7E**) and elevated the levels of NRF-1 and PGC-1 mRNA after SCI/R (**Figure 7F**).

Mitochondrial dynamics are also involved in mitochondrial dysfunction under oxidative stress. As shown in **Figure 8A**, we

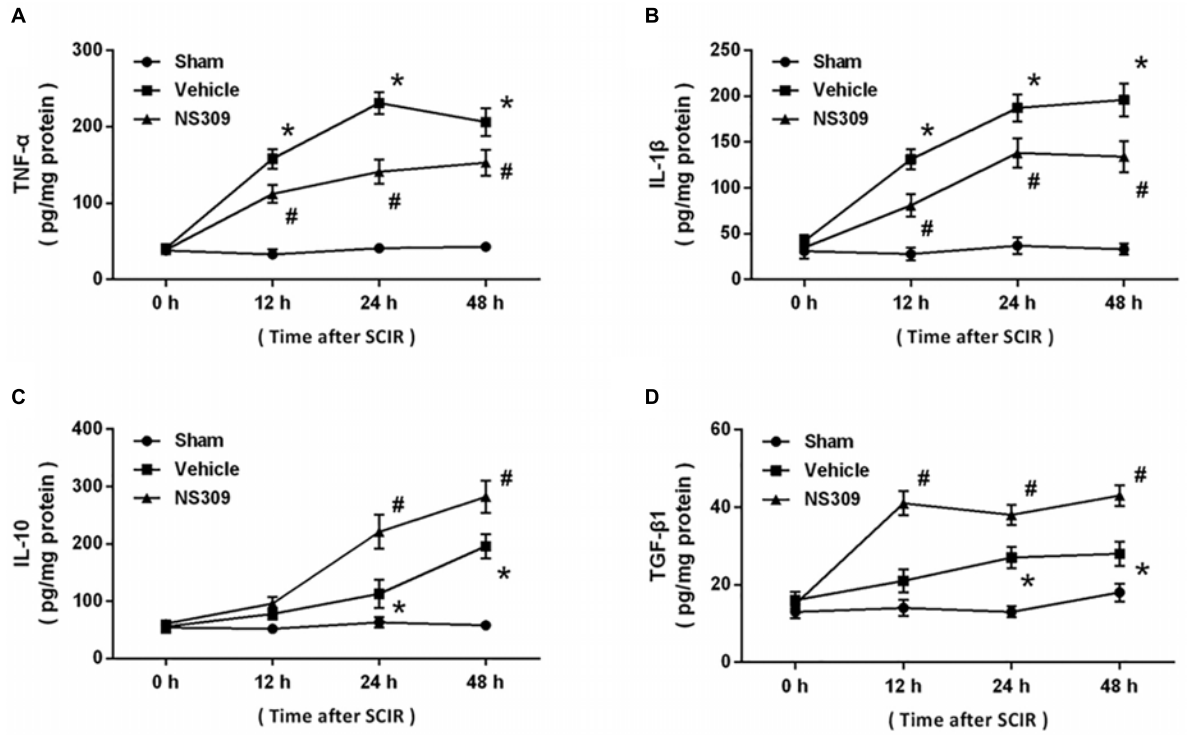

FIGURE 6 | NS309 regulates inflammatory cytokines after SCI/R. The animals were treated with 2 mg/kg NS309 or vehicle at the beginning of SCI/R. The levels of TNF-α **(A)**, IL-1β **(B)**, IL-10 **(C)**, and TGF-β1 **(D)** in spinal cord tissues were determined at different time points (0, 12, 24, and 48 h). The data were represented as means ± SEM ($n = 8$). $^{*}p < 0.05$ vs. Sham. $^{\#}p < 0.05$ vs. Vehicle.

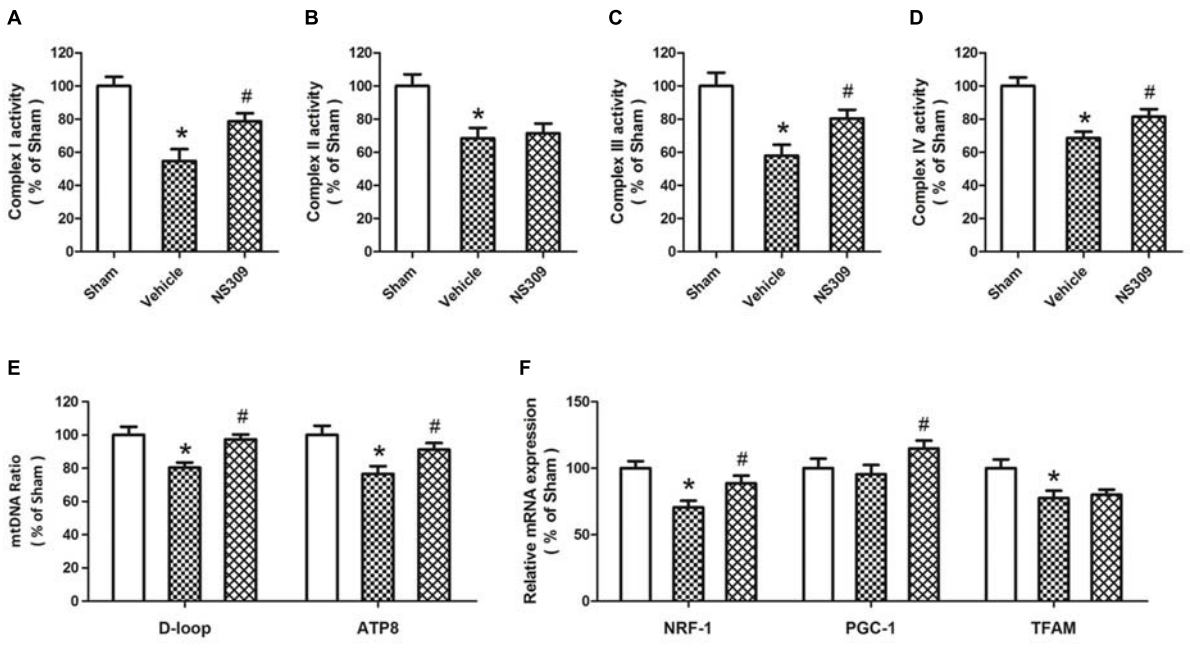

FIGURE 7 | NS309 preserves mitochondrial complex activity and mitochondrial biogenesis after SCI/R. The animals were treated with 2 mg/kg NS309 or vehicle at the beginning of SCI/R. The activities of mitochondrial complex I **(A)**, II **(B)**, III **(C)**, and IV **(D)** were observed in spinal cord, respectively. Real-time RT-PCR was used to detect mtNDA ratio **(E)** and the expression of mitochondrial biogenesis factors **(F)**. The data were represented as means ± SEM ($n = 8$). $^{*}p < 0.05$ vs. Sham. $^{\#}p < 0.05$ vs. Vehicle.

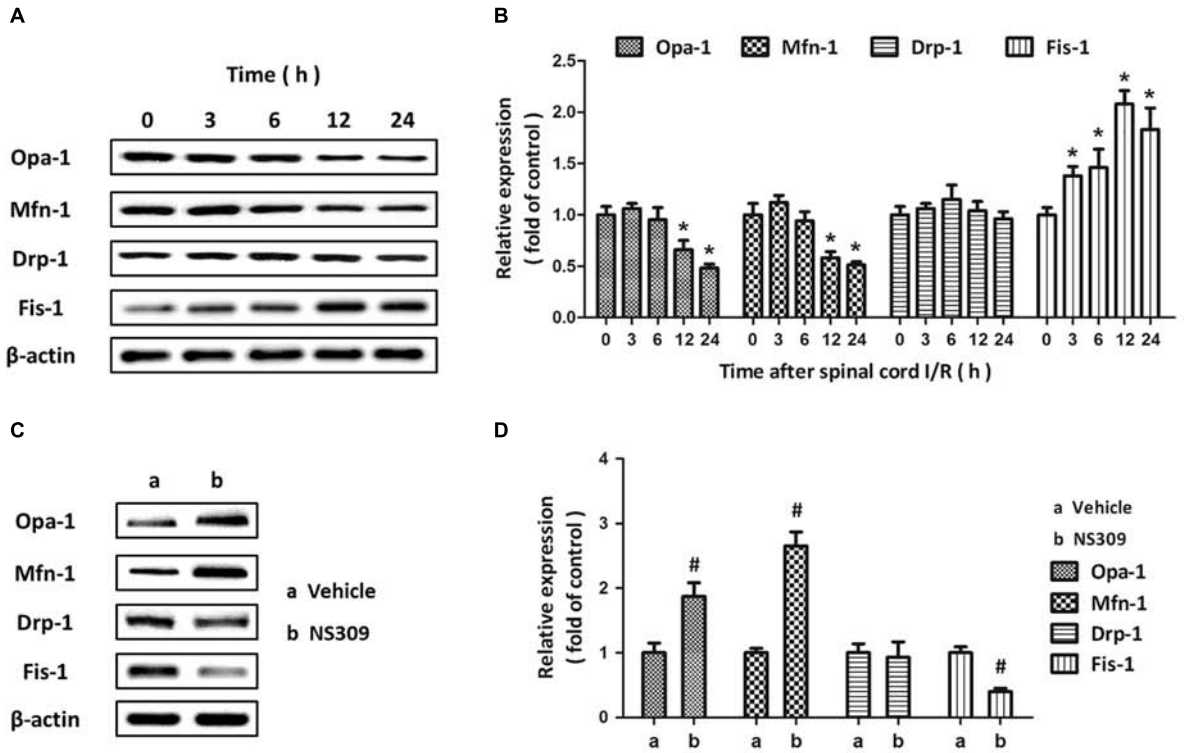

FIGURE 8 | NS309 differently regulates the expression of mitochondrial dynamic proteins. The animals were treated with 2 mg/kg NS309, and the expression of Opa-1, Mfn-1, Drp-1, and Fis-1 at different time points (0, 3, 6, 12, and 24 h) was detected by western blot analysis **(A,B)**. The animals were treated with 2 mg/kg NS309 or vehicle at the beginning of SCI/R. The expression of Opa-1, Mfn-1, Drp-1, and Fis-1 was detected by western blot analysis **(C)** and calculated **(D)**. The data were represented as means ± SEM (n = 8). $^{*}p < 0.05$ vs. Sham. $^{\#}p < 0.05$ vs. Vehicle.

detected the expression of mitochondrial dynamic proteins in spinal cord tissues after SCI/R at different time points. The results showed that SCI/R decreased the expression of Opa-1 and Mfn-1 at 12 and 24 h but increased the expression of Fis-1 from 3 to 24 h, with no effect on Drp-1 expression (**Figure 8B**). Furthermore, we detected the expression of these proteins after NS309 treatment (**Figure 8C**). We found that the decreased expression of Opa-1 and Mfn-1, as well as increased expression of Fis-1 after SCI/R, were all partially prevented by NS309 treatment (**Figure 8D**).

DISCUSSION

Due to the lack of data from randomized controlled clinical trials, contemporary concepts about SCI/R protection are mainly adapted from guidelines for brain ischemia, cardiovascular ischemia and spinal cord trauma (Nardone et al., 2016). This study provides evidence that NS309, a pharmacological activator for SK/K_{Ca} channel, protects against experimental SCI/R in rabbits. Our results showed that (a) SCI/R decreases SK/K_{Ca}1 protein expression in spinal cord tissues; (b) NS309 attenuates neuronal loss and neurological dysfunction after SCI/R; (c) NS309 reduces oxidative stress and regulates the levels of inflammatory cytokines after SCI/R; (d) NS309 preserves mitochondrial function and promotes mitochondrial biogenesis; and (e) NS309 differently regulates mitochondrial dynamic proteins.

The SK/K_{Ca} channels are extensively expressed throughout the central nervous system, but the three subtypes are differentially expressed. SK/K_{Ca}1 can be found in cortex, hippocampus, midbrain, cerebellum and spinal cord; SK/K_{Ca}2 is localized in cortex, amygdala, medial habenula and the inferior olivary complex; SK/K_{Ca}3 is expressed in olfactory bulbs, dentate gyrus thalamus and the locus coeruleus (Sailer et al., 2004). Thus, we detected the expression of SK/K_{Ca}1 protein to investigate the effect of SCI/R on SK/K_{Ca} channels. Significant decrease in SK/K_{Ca}1 expression was observed at 12 and 24 h after SCI/R, and this decrease was detected in both cytosolic and mitochondrial fractions. In neuronal cells, SK/K_{Ca} channels were originally thought to be predominantly presented in the plasma membrane where they regulates K^{+} efflux (Honrath et al., 2017). However, a previous study showed that SK/K_{Ca} channels were also located in the inner mitochondrial membrane of neuronal mitochondria (Dolga et al., 2013). In addition, Dolga et al. demonstrated that the SK/K_{Ca}2 subtype expressed in mitochondrial-enriched fractions and co-localized with the mitochondrial markers in neuronal dopaminergic cells (Dolga et al., 2014). Our results here demonstrated that SK/K_{Ca}1 was also localized in mitochondria in spinal cord, and was downregulated after SCI/R, indicating a potential role in mitochondrial function after SCI/R.

Activation of SK/K_{Ca} channels has been demonstrated to exert protective effects in many *in vitro* neuronal models, and is considered as an emerging therapeutic approach for the treatment of several neurological diseases (Anderson et al., 2006; Dolga et al., 2011, 2012, 2013, 2014; Dolga and Culmsee, 2012). NS309 is a selective and potent SK/K_{Ca} channel opener that activates SK/K_{Ca} channels via increasing their Ca^{2+} sensitivity (Strobaek et al., 2006). The EC_{50} of NS309 to SK/K_{Ca} channels is 30 nM, and it has been demonstrated to be safe and could activate SK/K_{Ca} channels in both *in vitro* and *in vivo* experimental models (Hipolito et al., 2015; Honrath et al., 2017). In this study, we found that NS309 treatment reduced spinal cord edema and spinal cord neuronal loss after SCI/R, which were accompanied by preserved neurological function. Our data extended the neuroprotective effects of SK/K_{Ca} channels activation into SCI/R. Importantly, we found that the protective effects of NS309 were still observed when it was administrated at 6 h after ischemia initiation. One of the serious problems of preclinical experiments is that many neuroprotective agents are administrated prior to injury initiation (Menon, 2009). It is of little clinical relevance due to the difficulty in obtaining informed consent. Our results showed that the therapeutic time window of NS309 was up to 6 h after ischemia initiation, which is useful for future clinical trials. This time window of administration makes it possible to treat SCI/R with NS309 associated neuroprotective agents. Considering the safety of NS309 treatment in previous experimental animal models, NS309 might be an ideal candidate for clinical drug research for SCI/R.

Free radicals-associated oxidative damage is one of the most important mechanisms underlying secondary injury after SCI/R, especially in the reperfusion phase (Chen X.P. et al., 2011). The overproduced ROS causes protein and lipid peroxidation, thereby leading to loss of membrane potential and corruption of membrane fluidity, which eventually results in the release of organelle content. In this study, increased levels of MDA and 8-iso-PGF2α, two oxidative products that correlate with the extent of ROS-mediated damage, was observed in both serum and spinal cord tissues after SCI/R, which were reduced by NS309. Neuronal fate under oxidative stress is dependent on the balance between ROS and the anti-oxidative defense mechanisms within the cell (Jia et al., 2012). SOD and CAT are two endogenous antioxidant enzymes, that can scavenge the superoxide radicals by changing the O_2^- into less damaging species (Rodrigo et al., 2011). At 24 and 48 h after SCI/R, reduced activities of SOD and CAT was found to be preserved by NS309, indicating the anti-oxidative activity of NS309 in our model. Thus, the effects of NS309 on prevention of oxidative stress after SCI/R might be the direct result of the increased activity of antioxidant enzymes, which needs to be further determined in the future. Inflammation is a subsequent event of SCI/R, and inflammatory cell infiltration and release of inflammatory cytokines were observed in spinal cords (Zhu et al., 2013). The pro-inflammatory cytokines, such as TNF-α and IL-1β, and anti-inflammatory cytokines, including IL-10 and TGF-β1, play opposite roles in inflammation regulation (Spitzbarth et al., 2012). Here, NS309 treatment was shown to upregulate anti-inflammatory cytokines but downregulate pro-inflammatory cytokines in the spinal cord tissues. Thus, inhibition of inflammatory responses via differentially regulating inflammatory cytokines might also contribute to NS309-induced protection against SCI/R.

Considering that the SK/K_{Ca}1 subtype was found in spinal cord mitochondria, and that NS309 alleviated oxidative stress after SCI/R, we speculated that activation of SK/K_{Ca} channels could regulate mitochondrial function in the spinal cord. Thus, we further measured mitochondrial complexes activity. It has been demonstrated that dysfunction of mitochondrial complexes occurred within 4–6 h after reperfusion and resulted in permanent mitochondrial damage (Sims and Muyderman, 2010). As expected, we found that the reduced activities of mitochondrial complexes after SCI/R, except for complex II, were all partially prevented by NS309. In addition, these effects were accompanied by the changes in mitochondrial biogenesis factors. Mitochondrial biogenesis is defined as the regulation of mitochondrial mass and turnover, a mechanism aimed to maintain diverse homeostatic demands under physiological and pathological conditions (Chen S.D. et al., 2011). It requires exquisite communication between the mitochondrial genome and the nuclear genome, and can be measured by the copy number and integrity of mtDNA, as well as the levels of many transcription factors, such as NRF-1, PGC-1, and TFAM (Kelly and Scarpulla, 2004). Previous studies have shown that these candidate mitochondrial biogenesis regulatory proteins correlate with mitochondrial respiratory capacity and could augment tolerance to ischemic injury via activating antioxidant system (McLeod et al., 2005). Thus, our results strongly indicate that NS309 might promote mitochondrial biogenesis, leading to inhibition of oxidative stress, and thereby induce protection against SCI/R.

Dynamic structural changes of the mitochondrial network, named as mitochondrial dynamics, are governed by the delicate balance between frequent fusion and fission events, and can adapt mitochondrial function to meet energy demand under stress (Otera et al., 2013). Impaired regulation of mitochondrial dynamic proteins contributes to ischemic injury via reducing energy production and promoting ROS generation (Calo et al., 2013). Multiple mitochondrial guanosine triphosphates hydrolases (GTPases) that regulate mitochondrial networking have been identified, among which DRP-1 and Fis-1 are related to mitochondrial fission, whereas mitochondrial fusion is mediated by Opa-1 and Mfn-1 (Karbowski et al., 2002; Hoppins et al., 2007). We found that SCI/R decreased the expression of Opa-1 and Mfn-1 but increased the levels of Fis-1 rather than Drp-1, indicating the induction of mitochondrial fragmentation in spinal cord after injury. In addition, the changes of these proteins after SCI/R were significantly prevented by NS309 treatment. Previous studies have shown that Opa-1 and Mfn-1 functionally interact to promote mitochondrial

elongation, while Fis-1 was required in the recruitment of Drp-1 to mitochondria during mitochondrial fission (Cipolat et al., 2004; De Palma et al., 2010). However, no significant changes in Drp-1 expression after SCI/R and/or NS309 treatment was observed in this study. Thus, a Drp-1-independent mechanism after SCI/R might exist, which need to be further determined.

In conclusion, our present study demonstrated the neuroprotective effects of NS309, a pharmacological activator for SK/K_{Ca} channel, against SCI/R in rabbits, which may involve an integrated process of the suppression of oxidative stress and the preservation of mitochondrial function.

AUTHOR CONTRIBUTIONS

TC and Y-HW conceived and designed the experiments. JZ, L-KY, and W-LC performed the experiments. WL analyzed the data. TC and JZ wrote the paper.

FUNDING

This work was supported by the National Natural Science Foundation of China (Nos. 81701932, 81601719, and 81871589).

REFERENCES

Anderson, N. J., Slough, S., and Watson, W. P. (2006). In vivo characterisation of the small-conductance KCa (SK) channel activator 1-ethyl-2-benzimidazolinone (1-EBIO) as a potential anticonvulsant. *Eur. J. Pharmacol.* 546, 48–53. doi: 10.1016/j.ejphar.2006.07.007

Calo, L., Dong, Y., Kumar, R., Przyklenk, K., and Sanderson, T. H. (2013). Mitochondrial dynamics: an emerging paradigm in ischemia-reperfusion injury. *Curr. Pharm. Des.* 19, 6848–6857. doi: 10.2174/13816128193931127110701

Chen, S. D., Yang, D. I., Lin, T. K., Shaw, F. Z., Liou, C. W., and Chuang, Y. C. (2011). Roles of oxidative stress, apoptosis, PGC-1alpha and mitochondrial biogenesis in cerebral ischemia. *Int. J. Mol. Sci.* 12, 7199–7215. doi: 10.3390/ijms12107199

Chen, X. P., Fu, W. M., and Gu, W. (2011). Spinal cord stimulation for patients with inoperable chronic critical leg ischemia. *World J. Emerg. Med.* 2, 262–266. doi: 10.5847/wjem.j.1920-8642.2011.04.003

Cipolat, S., Martins de Brito, O., Dal Zilio, B., and Scorrano, L. (2004). OPA1 requires mitofusin 1 to promote mitochondrial fusion. *Proc. Natl. Acad. Sci. U.S.A.* 101, 15927–15932. doi: 10.1073/pnas.0407043101

De Palma, C., Falcone, S., Pisoni, S., Cipolat, S., Panzeri, C., Pambianco, S., et al. (2010). Nitric oxide inhibition of Drp1-mediated mitochondrial fission is critical for myogenic differentiation. *Cell Death Differ.* 17, 1684–1696. doi: 10.1038/cdd.2010.48

Dolga, A. M., and Culmsee, C. (2012). Protective roles for potassium SK/K(Ca)2 channels in microglia and neurons. *Front. Pharmacol.* 3:196. doi: 10.3389/fphar.2012.00196

Dolga, A. M., de Andrade, A., Meissner, L., Knaus, H. G., Hollerhage, M., Christophersen, P., et al. (2014). Subcellular expression and neuroprotective effects of SK channels in human dopaminergic neurons. *Cell Death Dis.* 5:e999. doi: 10.1038/cddis.2013.530

Dolga, A. M., Letsche, T., Gold, M., Doti, N., Bacher, M., Chiamvimonvat, N., et al. (2012). Activation of KCNN3/SK3/K(Ca)2.3 channels attenuates enhanced calcium influx and inflammatory cytokine production in activated microglia. *Glia* 60, 2050–2064. doi: 10.1002/glia.22419

Dolga, A. M., Netter, M. F., Perocchi, F., Doti, N., Meissner, L., Tobaben, S., et al. (2013). Mitochondrial small conductance SK2 channels prevent glutamate-induced oxytosis and mitochondrial dysfunction. *J. Biol. Chem.* 288, 10792–10804. doi: 10.1074/jbc.M113.453522

Dolga, A. M., Terpolilli, N., Kepura, F., Nijholt, I. M., Knaus, H. G., D'Orsi, B., et al. (2011). KCa2 channels activation prevents [Ca2+]i deregulation and reduces neuronal death following glutamate toxicity and cerebral ischemia. *Cell Death Dis.* 2:e147. doi: 10.1038/cddis.2011.30

Faber, E. S., and Sah, P. (2007). Functions of SK channels in central neurons. *Clin. Exp. Pharmacol. Physiol.* 34, 1077–1083. doi: 10.1111/j.1440-1681.2007.04725.x

Griepp, R. B., and Griepp, E. B. (2007). Spinal cord perfusion and protection during descending thoracic and thoracoabdominal aortic surgery: the collateral network concept. *Ann. Thorac. Surg.* 83, S865–S869; discussion S890–S892. doi: 10.1016/j.athoracsur.2006.10.092

Hipolito, L., Fakira, A. K., Cabanero, D., Blandon, R., Carlton, S. M., Moron, J. A., et al. (2015). In vivo activation of the SK channel in the spinal cord reduces the NMDA receptor antagonist dose needed to produce antinociception in an inflammatory pain model. *Pain* 156, 849–858. doi: 10.1097/j.pain.0000000000000124

Honrath, B., Krabbendam, I. E., Culmsee, C., and Dolga, A. M. (2017). Small conductance Ca(2+)-activated K(+) channels in the plasma membrane, mitochondria and the ER: pharmacology and implications in neuronal diseases. *Neurochem. Int.* 109, 13–23. doi: 10.1016/j.neuint.2017.05.005

Hoppins, S., Lackner, L., and Nunnari, J. (2007). The machines that divide and fuse mitochondria. *Annu. Rev. Biochem.* 76, 751–780. doi: 10.1146/annurev.biochem.76.071905.090048

Jia, Z., Zhu, H., Li, J., Wang, X., Misra, H., and Li, Y. (2012). Oxidative stress in spinal cord injury and antioxidant-based intervention. *Spinal Cord* 50, 264–274. doi: 10.1038/sc.2011.111

Karbowski, M., Lee, Y. J., Gaume, B., Jeong, S. Y., Frank, S., Nechushtan, A., et al. (2002). Spatial and temporal association of Bax with mitochondrial fission sites, Drp1, and Mfn2 during apoptosis. *J. Cell Biol.* 159, 931–938. doi: 10.1083/jcb.200209124

Kelly, D. P., and Scarpulla, R. C. (2004). Transcriptional regulatory circuits controlling mitochondrial biogenesis and function. *Genes Dev.* 18, 357–368. doi: 10.1101/gad.1177604

Kuiper, E. F., Nelemans, A., Luiten, P., Nijholt, I., Dolga, A., and Eisel, U. (2012). K(Ca)2 and k(ca)3 channels in learning and memory processes, and neurodegeneration. *Front. Pharmacol.* 3:107. doi: 10.3389/fphar.2012.00107

LeMaire, S. A., Price, M. D., Green, S. Y., Zarda, S., and Coselli, J. S. (2012). Results of open thoracoabdominal aortic aneurysm repair. *Ann. Cardiothorac. Surg.* 1, 286–292. doi: 10.3978/j.issn.2225-319X.2012.08.16

McLeod, C. J., Pagel, I., and Sack, M. N. (2005). The mitochondrial biogenesis regulatory program in cardiac adaptation to ischemia–a putative target for therapeutic intervention. *Trends Cardiovasc. Med.* 15, 118–123. doi: 10.1016/j.tcm.2005.05.001

Menon, D. K. (2009). Unique challenges in clinical trials in traumatic brain injury. *Crit. Care Med.* 37, S129–S135. doi: 10.1097/CCM.0b013e3181921225

Nardone, R., Pikija, S., Mutzenbach, J. S., Seidl, M., Leis, S., Trinka, E., et al. (2016). Current and emerging treatment options for spinal cord ischemia. *Drug Discov. Today* 21, 1632–1641. doi: 10.1016/j.drudis.2016.06.015

New, P. W., and McFarlane, C. L. (2012). Retrospective case series of outcomes following spinal cord infarction. *Eur. J. Neurol.* 19, 1207–1212. doi: 10.1111/j.1468-1331.2012.03702.x

Otera, H., Ishihara, N., and Mihara, K. (2013). New insights into the function and regulation of mitochondrial fission. *Biochim. Biophys. Acta* 1833, 1256–1268. doi: 10.1016/j.bbamcr.2013.02.002

Panthee, N., and Ono, M. (2015). Spinal cord injury following thoracic and thoracoabdominal aortic repairs. *Asian Cardiovasc. Thorac. Ann.* 23, 235–246. doi: 10.1177/0218492314548901

Rodrigo, R., Miranda, A., and Vergara, L. (2011). Modulation of endogenous antioxidant system by wine polyphenols in human disease. *Clin. Chim. Acta* 412, 410–424. doi: 10.1016/j.cca.2010.11.034

Sailer, C. A., Kaufmann, W. A., Marksteiner, J., and Knaus, H. G. (2004). Comparative immunohistochemical distribution of three small-conductance Ca2+-activated potassium channel subunits, SK1, SK2, and SK3 in mouse brain. *Mol. Cell Neurosci.* 26, 458–469. doi: 10.1016/j.mcn.2004.03.002

Sims, N. R., and Muyderman, H. (2010). Mitochondria, oxidative metabolism and cell death in stroke. *Biochim. Biophys. Acta* 1802, 80–91. doi: 10.1016/j.bbadis.2009.09.003

Spitzbarth, I., Baumgartner, W., and Beineke, A. (2012). The role of pro- and anti-inflammatory cytokines in the pathogenesis of spontaneous canine CNS diseases. *Vet. Immunol. Immunopathol.* 147, 6–24. doi: 10.1016/j.vetimm.2012.04.005

Stocker, M. (2004). Ca(2+)-activated K+ channels: molecular determinants and function of the SK family. *Nat. Rev. Neurosci.* 5, 758–770. doi: 10.1038/nrn1516

Strobaek, D., Hougaard, C., Johansen, T. H., Sorensen, U. S., Nielsen, E. O., Nielsen, K. S., et al. (2006). Inhibitory gating modulation of small conductance Ca2+-activated K+ channels by the synthetic compound (R)-N-(benzimidazol-2-yl)-1,2,3,4-tetrahydro-1-naphtylamine (NS8593) reduces afterhyperpolarizing current in hippocampal CA1 neurons. *Mol. Pharmacol.* 70, 1771–1782. doi: 10.1124/mol.106.027110

Ye, R., Zhang, X., Kong, X., Han, J., Yang, Q., Zhang, Y., et al. (2011). Ginsenoside Rd attenuates mitochondrial dysfunction and sequential apoptosis after transient focal ischemia. *Neuroscience* 178, 169–180. doi: 10.1016/j.neuroscience.2011.01.007

Zhou, L., Wang, X., Xue, W., Xie, K., Huang, Y., Chen, H., et al. (2013). Beneficial effects of hydrogen-rich saline against spinal cord ischemia-reperfusion injury in rabbits. *Brain Res.* 1517, 150–160. doi: 10.1016/j.brainres.2013.04.007

Zhu, P., Li, J. X., Fujino, M., Zhuang, J., and Li, X. K. (2013). Development and treatments of inflammatory cells and cytokines in spinal cord ischemia-reperfusion injury. *Med. Inflamm.* 2013:701970. doi: 10.1155/2013/701970

Conflict of Interest Statement: The authors declare that the research was conducted in the absence of any commercial or financial relationships that could be construed as a potential conflict of interest.

frontiers in Cellular Neuroscience

ORIGINAL RESEARCH
published: 02 April 2019
doi: 10.3389/fncel.2019.00122

Estradiol-Mediated Axogenesis of Hypothalamic Neurons Requires ERK1/2 and Ryanodine Receptors-Dependent Intracellular Ca^{2+} Rise in Male Rats

Lucas E. Cabrera Zapata[1], *Mariana Bollo*[1] *and María Julia Cambiasso*[1,2]*

[1]*Instituto de Investigación Médica Mercedes y Martín Ferreyra, INIMEC-CONICET, Universidad Nacional de Córdoba, Córdoba, Argentina,* [2]*Cátedra de Biología Celular, Facultad de Odontología, Universidad Nacional de Córdoba, Córdoba, Argentina*

17β-estradiol (E2) induces axonal growth through extracellular signal-regulated kinase 1 and 2 (ERK1/2)-MAPK cascade in hypothalamic neurons of male rat embryos *in vitro*, but the mechanism that initiates these events is poorly understood. This study reports the intracellular Ca^{2+} increase that participates in the activation of ERK1/2 and axogenesis induced by E2. Hypothalamic neuron cultures were established from 16-day-old male rat embryos and fed with astroglia-conditioned media for 48 h. E2-induced ERK phosphorylation was completely abolished by a ryanodine receptor (RyR) inhibitor (ryanodine) and partially attenuated by an L-type voltage-gated Ca^{2+} channel (L-VGCC) blocker (nifedipine), an inositol-1,4,5-trisphosphate receptor (IP_3R) inhibitor (2-APB), and a phospholipase C (PLC) inhibitor (U-73122). We also conducted Ca^{2+} imaging recording using primary cultured neurons. The results show that E2 rapidly induces an increase in cytosolic Ca^{2+}, which often occurs in repetitive Ca^{2+} oscillations. This response was not observed in the absence of extracellular Ca^{2+} or with inhibitory ryanodine and was markedly reduced by nifedipine. E2-induced axonal growth was completely inhibited by ryanodine. In summary, the results suggest that Ca^{2+} mobilization from extracellular space as well as from the endoplasmic reticulum is necessary for E2-induced ERK1/2 activation and axogenesis. Understanding the mechanisms of brain estrogenic actions might contribute to develop novel estrogen-based therapies for neurodegenerative diseases.

Keywords: hypothalamic neurons, axogenesis, estradiol, ERK1/2, Ca^{2+} signaling, ryanodine receptors

OPEN ACCESS

Edited by:
Gabriela Alejandra Salvador, Universidad Nacional del Sur, Argentina

Reviewed by:
Thomas Behnisch, Institutes of Brain Science, Fudan University, China
Se-Young Choi, Seoul National University, South Korea

***Correspondence:**
María Julia Cambiasso
jcambiasso@immf.uncor.edu

Received: *15 January 2019*
Accepted: *12 March 2019*
Published: *02 April 2019*

Citation:
Cabrera Zapata LE, Bollo M and Cambiasso MJ (2019) Estradiol-Mediated Axogenesis of Hypothalamic Neurons Requires ERK1/2 and Ryanodine Receptors-Dependent Intracellular Ca^{2+} Rise in Male Rats. Front. Cell. Neurosci. 13:122. doi: 10.3389/fncel.2019.00122

INTRODUCTION

For many years, estrogens have been recognized as one of the main orchestrators of the sexual differentiation of the brain, acting during critical periods of development to organize neural circuits in a way that determines the modulatory/activational effects of gonadal hormones in adulthood. Testosterone secreted by male rodent testes during development is aromatized in neurons to 17β-estradiol (E2), which displays multiple cellular processes that finally set the masculine phenotype (McCarthy, 2008; Wright et al., 2010). More recently, accumulating evidence

indicates that E2 is not only a reproductive hormone but also a brain-derived neuroprotective factor, coordinating multiple signaling mechanisms that protect the brain from neurodegenerative diseases, affective disorders and cognitive decline (Arevalo et al., 2015). These beneficial actions in the brain have positioned estrogens as promising therapeutic compounds against different brain pathologies such as Parkinson and Alzheimer diseases, schizophrenia, multiple sclerosis, stroke, neuroinflammation, among others (Dye et al., 2012; Villa et al., 2016; McGregor et al., 2017; Giatti et al., 2018).

Classical estrogenic actions are mediated *via* intracellular estrogen receptors (ERs) that function as ligand-activated transcription factors to regulate the expression of estrogen-responsive genes. Additionally, estrogens generate a wide diversity of rapid "non-classical" effects, which occur in a range from some seconds to a few minutes *via* membrane-initiated mechanisms (Arevalo et al., 2012), including the triggering of Ca^{2+} signals (Beyer and Raab, 1998; Picotto et al., 1999; Wong et al., 2012), and the activation of several signaling pathways, such as phospholipase C (PLC)/inositol 1,4,5-trisphosphate (IP_3) and diacylglycerol (Le Mellay et al., 1997; Chaban et al., 2004), nitric oxide synthase/nitric oxide (Kelly and Levin, 2001), adenylate cyclase/AMPc/protein kinase A (PKA; Beyer and Karolczak, 2000), phosphoinositide-3 kinase (PI3K; Garcia-Segura et al., 2010), PKC, and extracellular signal-regulated kinase 1 and 2 (ERK1/2) cascades (Wu et al., 2005).

Currently, it is known that E2 prevents cell death, promotes neuronal survival, and enhances neuritogenesis and synaptic plasticity in the brain (Carroll and Pike, 2008; Spence et al., 2013; Acaz-Fonseca et al., 2014; Khan et al., 2015; Lai et al., 2017; Céspedes Rubio et al., 2018). The induction of neurite outgrowth by E2 was first demonstrated by Toran-Allerand (1976, 1980) and Toran-Allerand et al. (1983) working with organotypic explant cultures of the preoptic area, hypothalamus, and cerebral cortex. This neuritogenic effect of the hormone was then observed in other brain regions, both directly related and unrelated with reproduction (Nishizuka and Arai, 1981; Reisert et al., 1987; Cambiasso et al., 1995; Murphy and Segal, 1996). Hypothalamic neurons *in vitro* undergo several intermediate stages of development from unpolarized to fully polarized cells (Díaz et al., 1992). Most of the neuritogenic effects of E2 were demonstrated in polarized neurons (stage III of development), which are characterized by the presence of axon (Díaz et al., 1992; Cambiasso et al., 1995). Previous studies from our laboratory have shown that E2 induces axonal growth through ERK1/2 activation in hypothalamic neurons of male embryos *in vitro*. Both axogenesis (Cambiasso and Carrer, 2001) and ERK1/2 activation (Gorosito and Cambiasso, 2008) mediated by the hormone are dependent on a membrane-initiated mechanism since E2-bovine serum albumin (BSA; a membrane-impermeable conjugate of E2) was as effective as free E2. Interestingly, decreasing intracellular Ca^{2+} by the Ca^{2+}-chelator BAPTA-AM or blocking Ca^{2+}-dependent PKC isoforms by Ro 32-0432 significantly decreased these E2 effects (Gorosito and Cambiasso, 2008). These findings strongly suggested an important role for Ca^{2+} in E2-induced ERK1/2 pathway activation and axonal growth; however, the results did not provide the mechanism of E2-induced Ca^{2+} signaling in hypothalamic neurons.

In this study, we found that E2 evoked activation of Ca^{2+} entry *via* L-type voltage-gated Ca^{2+} channels (L-VGCCs) and promoted Ca^{2+} release through ryanodine receptors (RyRs). This early Ca^{2+} response underlies E2-induced ERK1/2 activation and axogenesis in hypothalamic neurons. Altogether, these results bring new insights about the mechanism of brain estrogenic actions and might contribute to developing novel estrogen-based therapies for neurodegenerative diseases.

MATERIALS AND METHODS

Animals and Cell Cultures

Embryos were obtained from pregnant Wistar rats at embryonic day 16 (E16). The day of vaginal plug was set as E0. Experimental procedures for handling and sacrificing animals were approved by the Animal Care and Use Committee at our institution (CICUAL-IMMF, INIMEC-CONICET-UNC; Córdoba, Argentina) and followed the NIH guidelines for care and use of laboratory animals. The minimum number of animals required was used for these experiments and suffering was minimized. Primary neuronal and astroglial cultures were prepared as previously described in Cambiasso et al. (2000). Pregnant rats were sacrificed by cervical dislocation under CO_2 anesthesia, and the fetuses were dissected from the uterus. The male fetuses used for cultures were identified by visualization of the spermatic artery on the developing testes. Ventromedial hypothalamic and mesencephalic regions were dissected out and stripped off the meninges for primary neuronal and glial cultures, respectively. At E16, the axogenic effect of E2 is contingent on the presence of astroglia (Cambiasso et al., 1995) or astroglia-conditioned media from a target region (Cambiasso et al., 2000; Cambiasso and Carrer, 2001; Brito et al., 2004). The basal medium (BM) was (1:1) DMEM:Ham's F12 Nutrient Mixture, supplemented with 0.043% l-alanyl-l-glutamine (GlutaMAX I), 0.15% glucose, 100 U/ml penicillin and 100 μg/ml streptomycin. All cultures were raised under phenol red-free conditions to avoid "estrogen-like effects" (Berthois et al., 1986). For neuronal cultures, the dissociated cell suspension was seeded on different supports pre-coated with 1 mg/ml poly-D-lysine depending on the experiment: 60 mm × 15 mm dishes (Corning Life Science, Tewksbury, MA, USA) for protein assays, 25 mm coverslips (Assistent, Germany) for Ca^{2+} imaging, and 12 mm coverslips (Assistent, Germany) for morphological studies.

Western Blot

Hypothalamic neurons derived from male fetuses plated 1–2 h before were fed with astroglia-conditioned media for 2 days *in vitro* (DIV). After a 2 h washout period using BM, neuronal cultures were treated for 1 h with nifedipine (2 μM; Sigma-Aldrich, St. Louis, MO, USA), inhibitory ryanodine (50 μM; Santa Cruz Biotechnology, Santa Cruz, CA, USA), 2-APB (100 μM; Santa Cruz Biotechnology, Santa Cruz, CA, USA) or U-73122 (10 μM; Sigma-Aldrich, St. Louis, MO, USA), and then pulsed with 100 nM E2 (Sigma-Aldrich, St. Louis, MO, USA)

for 15 min. Hormone concentration used was determined by dose dependence (1–100 nM) experiments previously performed by our group (Gorosito and Cambiasso, 2008; Gorosito et al., 2008). ERK phosphorylation was maximally increased after the application of 100 nM E2. This dose was then used for all further acute stimulation studies. We have used compounds at final concentrations that did not alter cell viability or morphology in control conditions.

After treatment, hypothalamic neurons were washed and harvested at 4°C in RIPA buffer [150 mM NaCl, 0.1% NP40, 0.5% sodium deoxycholate, 0.1% sodium dodecyl sulfate (SDS), 50 mM Tris, pH 7.5] with protease and phosphatase inhibitors (1 μg/ml aprotinin, 1 μg/ml leupeptin, 1 μg/ml pepstatin A, 5 μg/ml chymostatin, 5 μg/ml antipain, 100 μg/ml PMSF, 50 μM NaF, 10 μM $Na_4P_2O_7$, and 1 mM $NaVO_4$). Protein samples (20 μg/lane) were separated by 10% SDS-PAGE and transferred onto polyvinylidene fluoride membrane (Bio-Rad, Hercules, CA, USA). ERK1/2 phosphorylation was detected by using a rabbit monoclonal anti-phospho-p44/42 MAPK (Cell Signaling Technology, Danvers, MA, USA), which specifically detects both Thr202 and Tyr204 ERK phosphorylation forms of ERK [molecular masses (kDa) for ERK1 and ERK2 are 44 and 42, respectively]. Total ERK1/2 was detected by using a mouse anti-p44/42 MAPK (Cell Signaling Technology, Danvers, MA, USA). Secondary antibodies conjugated to horseradish peroxidase (Jackson, West Grove, PA, USA) were used for the detection by enhanced chemiluminescence on X-ray film. After incubation with the antibody against phospho-ERK1/2, blots were stripped and then re-probed with anti-total ERK1/2 to ensure equal protein loading. The resulting film samples were scanned and analyzed with an image analysis program (ImageJ; NIH, Bethesda, MD, USA). Data are presented as a ratio of phospho-ERK1/2/total-ERK1/2 of 3–4 different experiments (independent cultures) performed in duplicate.

Ca^{2+} Imaging

After 2 DIV, hypothalamic neurons were treated (or not) with 50 μM ryanodine or 2 μM nifedipine for 1 h and incubated with 3 μM acetoxymethyl (AM) ester form of the organic Ca^{2+}-dye Cal-520 (AAT Bioquest, Sunnyvale, CA, USA) for 30 min at 37°C in a Ca^{2+}-containing HEPES buffered salt solution (Ca^{2+}-HBSS) composed of (mM): 135 NaCl, 5.4 KCl, 2 $CaCl_2$, 1 $MgCl_2$, 10 HEPES, and 10 glucose; pH = 7.4 set with NaOH at RT. Following loading, neurons were washed twice with warm Ca^{2+}-HBSS and were imaged in the same buffer. To analyze the participation of extracellular Ca^{2+}, the cells were resuspended in an EGTA-containing buffer composed of (mM): 135 NaCl, 5 KCl, 0.5 $CaCl_2$, 1.2 $MgCl_2$, 5 HEPES, 14 $NaHCO_3$, and 1 EGTA; pH = 7.4 set with NaOH at RT.

Imaging of cytosolic Ca^{2+} signals was performed using a 60× oil immersion objective of an Olympus IX81 inverted microscope [equipped with a Disk Spinning Unit (DSU), epifluorescence illumination (150 W Xenon Lamp), and a microprocessor], an ORCA AG (Hamamatsu) CCD camera and OSIS software. Frames were collected at a continuous rate of 2.5 per second during 5 min (790 frames). Cal-520 was excited at a wavelength of 492 nm, and emitted fluorescence was collected at 514 nm. E2 (100 nM) was added 30 s after starting the recording. 10 μM thapsigargin (tg) was added at 3 min of recording as a positive control of normal endoplasmic reticulum Ca^{2+} content. The fluorescence intensity of the Ca^{2+} indicator was analyzed using ImageJ (NIH, Bethesda, MD, USA) software and plotted as the change in fluorescence (ΔF) of 2 × 2 pixels divided by mean resting fluorescence [(Fo; ΔF/Fo)] over time. We measured both the peak fluorescence value and the integrated area under the ΔF/Fo curve with OriginPro 8 SR0 software (OriginLab Corporation, Northampton, MA, USA). The integrated area roughly corresponds to the total amount of Ca^{2+} released over the recording period.

Immunocytochemical Staining

To analyze the effect of ryanodine in E2-stimulated axon growth without affecting the normal polarization of neurons, we performed the experiment after 1 DIV (stage III of development). After 2 h in absence of E2, the cultures were treated for 1 h with 50 μM ryanodine before the addition of 10 nM E2 for an additional 24 h. The hormone concentration used to study the neuritogenic effect of E2 was chosen based on previous studies of our laboratory (Gorosito et al., 2008; Scerbo et al., 2014).

After 2 DIV, neuronal cultures were fixed for 20 min with warm 4% paraformaldehyde in PBS containing 0.12 M sucrose and rinsed in PBS. Neurons were immunocytochemically stained with antibodies against β-tubulin class III (SDL.3D10). The details of the immunocytochemical procedure were as specified by Díaz et al. (1992). Briefly, the fixed cells were permeabilized in 0.2% Triton X-100 for 5 min at RT, preincubated with 5% BSA, incubated in mouse anti-β-tubulin class III (Sigma-Aldrich, St. Louis, MO, USA), rinsed in PBS, and finally incubated with appropriate biotinylated secondary antibody. Incubation with secondary antibody was followed by washing in PBS, incubation for 2 h in VECTASTAIN ABC immunoperoxidase reagent (Vector Laboratories, Burlingame, CA, USA), and a final reaction with 1.4 mM 3,3'-diaminobenzidine in phosphate buffer with H_2O_2. Coverslips were then dehydrated with ethanol, cleared with xylene, and mounted on glass slides for morphometric analysis. No immunostaining was detected when primary antibodies were replaced by 5% BSA.

Morphometric Analysis

The morphometric analysis of stained neuronal cultures was performed on digitized video images using JAVA as an image processor (Jandel Inc., Richmond, CA, USA) controlled by a host computer. Images were acquired through an optic microscope (Carl Zeiss, Germany). Microscope slides were coded, and the person conducting the analysis was blind to the experimental group. All labeled cells that could be identified as one individual neuron were measured in random fields at 40× magnification. Neural processes were classified as minor processes or axons according to accepted morphological criteria (Dotti et al., 1988; Blanco et al., 1990; Díaz et al., 1992). Minor processes are two or three short neurites that emerge from the cell body; axons are much longer, unique, thin, and relatively uniform in diameter. Neurons were considered to have developed an axon

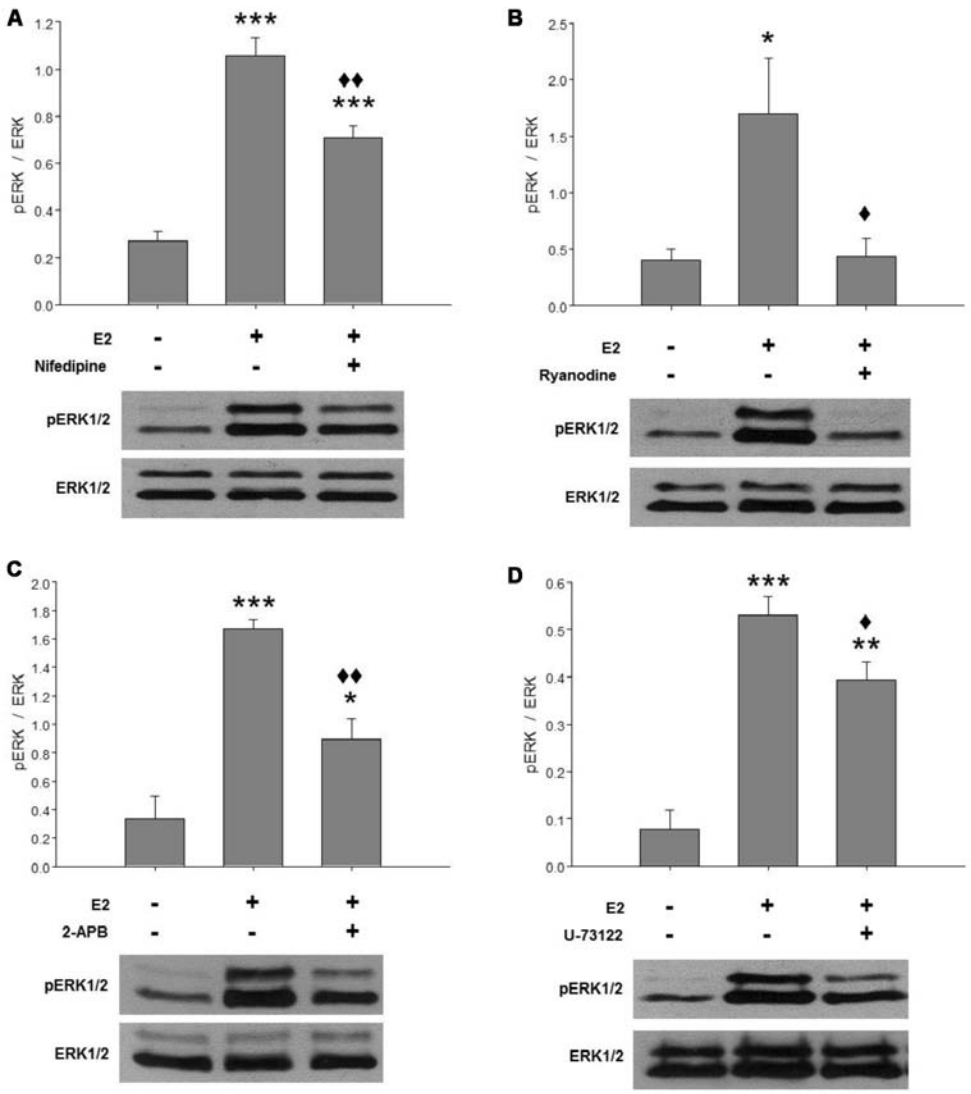

FIGURE 1 | E2-induced extracellular signal-regulated kinase 1 and 2 (ERK1/2) activation depends on cytosolic Ca^{2+} increase mainly mediated by ryanodine receptors (RyRs). Effects of **(A)** 2 μM nifedipine, **(B)** 50 μM ryanodine, **(C)** 100 μM 2-APB or **(D)** 10 μM U-73122 on E2-induced ERK phosphorylation. After washing for 2 h, the cultures were treated with the inhibitors for 1 h and were then pulsed for 15 min with 17β-estradiol (E2) and harvested for Western blotting. Top: ratio of readings for pERK/ERK bands in arbitrary densitometric units. Bottom: examples of immunoblots showing a decrease of hormone-induced ERK phosphorylation in cultures pretreated with the inhibitors. Molecular masses (kDa) for ERK1 and ERK2 are 44 and 42, respectively. Blots shown are representative of the mean ± SEM of 3–4 different cultures. **(A)** Nifedipine: ANOVA $F_{(2,10)} = 52.78$; $p \leq 0.001$. Least significant differences (LSDs) test indicated $^{***}p < 0.001$ vs. control and $^{♦♦}p < 0.01$ vs. E2. **(B)** Ryanodine: ANOVA $F_{(2,6)} = 5.856$; $p = 0.04$. LSDs test indicated $^{*}p = 0.05$ vs. control and $^{♦}p = 0.05$ vs. E2. **(C)** 2-APB: ANOVA $F_{(2,6)} = 27.203$; $p \leq 0.001$. LSDs test indicated $^{***}p < 0.001$ and $^{*}p = 0.05$ vs. control and $^{♦♦}p = 0.01$ vs. E2. **(D)** U-73122: ANOVA $F_{(2,6)} = 34.891$; $p \leq 0.001$. LSDs test indicated $^{***}p < 0.001$ and $^{**}p = 0.01$ vs. control and $^{♦}p \leq 0.05$ vs. E2.

if they showed one neurite three to five times longer than the rest (stage III of development). Soma area, length of minor processes, total axonal length, and the number of neurites per cell were recorded. At least 60 neurons were measured for every experimental condition in each culture; at least three separate cultures were made for every condition.

Statistical Analysis

Data were statistically evaluated by one-way ANOVA, followed by Fisher's Least Significant Difference (LSD) *post hoc* test (Statistica; StatSoft Inc., Tulsa, OK, USA) where $p < 0.05$ was considered statistically significant.

RESULTS

E2-Induced ERK1/2 Activation Is Mainly Mediated by RyRs

Our previous results suggested that E2-induced ERK1/2 phosphorylation is Ca^{2+}-dependent. Here, we further

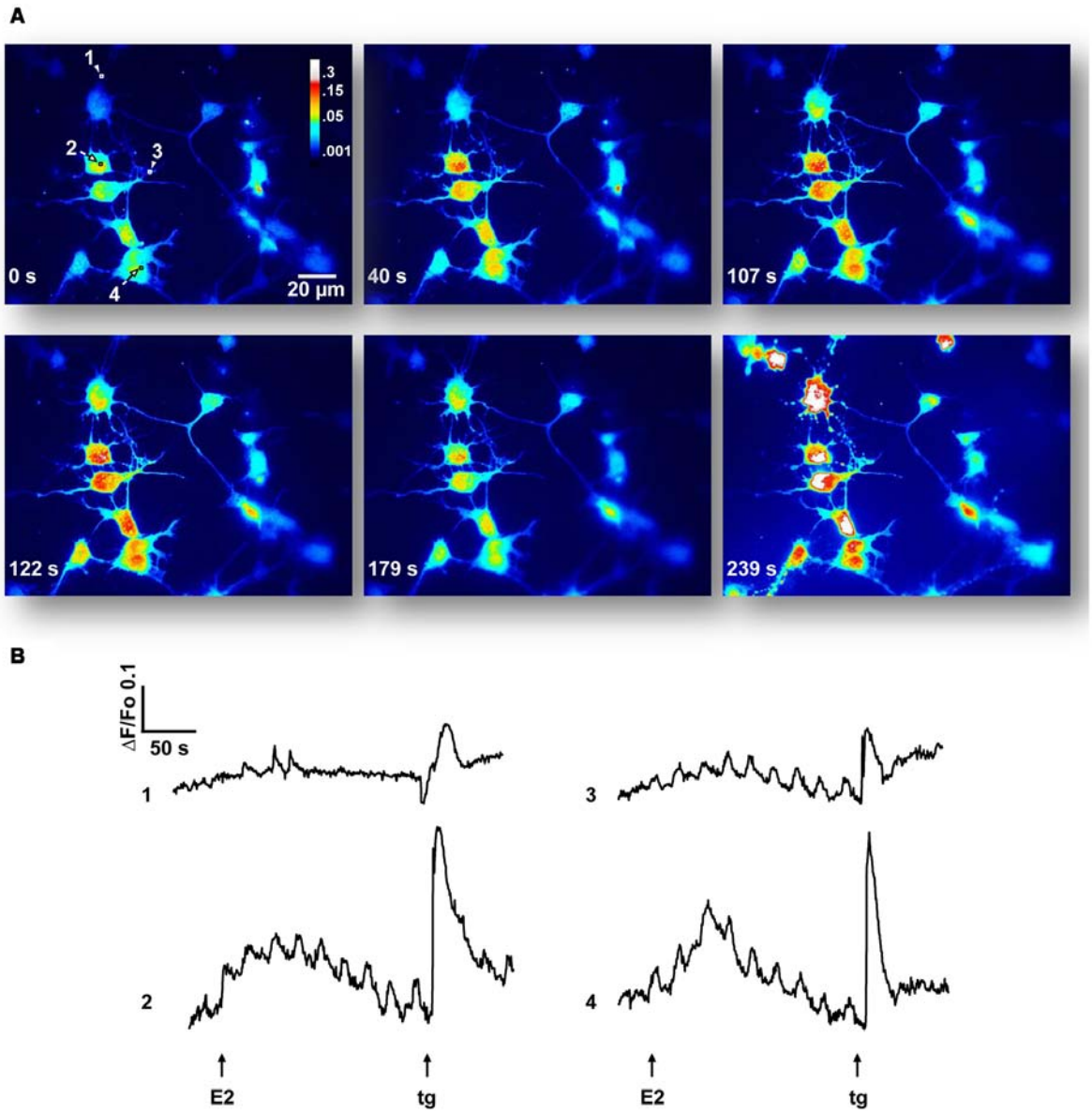

FIGURE 2 | 17β-estradiol (E2) induces Ca^{2+} oscillations. **(A)** Hypothalamic neurons were loaded with Cal-520 AM for 30 min at 37°C, maintained in a Ca^{2+}-containing buffer (Ca^{2+}-HBSS) and changes in cytosolic Ca^{2+} concentration were measured using confocal microscopy [Olympus IX81 inverted microscope equipped with a Disk Spinning Unit (DSU)]. Time series of Cal-520 pseudocolor images is shown, before and after the addition of E2 and thapsigargin (tg). Pseudocolor scale bar: 0.3–0.001 arbitrary units. Length scale bar: 20 µm. **(B)** Representative Ca^{2+} traces [regions of interest labeled 1–4 in **(A)**] plotted as changes over time in fluorescence intensity of the indicator (ΔF) respect to resting values (Fo). Arrows indicate the addition time of E2 (30 s) and tg (3 min). Data are from one representative experiment out of six independent experiments.

investigated the Ca^{2+} response involved in ERK activation mediated by E2. Hypothalamic cultures grown with E2 for 48 h were washed in BM for 2 h and pre-treated with specific compounds for 1 h before a pulse of E2 for 15 min. In agreement with previous reports, E2 induced a strong phosphorylation of ERK at 15 min (**Figure 1**). This effect was completely abolished by inhibitory ryanodine (**Figure 1B**) and partially attenuated by nifedipine (**Figure 1A**), IP_3R inhibitor 2-APB (**Figure 1C**), and a PLC inhibitor U-73122 (**Figure 1D**).

E2 Induces Rapid Ca^{2+} Increase Depending on Ca^{2+} Influx and RyRs

As E2-activation of the ERK1/2 signaling cascade depends on extracellular as well as intracellular Ca^{2+} stores, we decided to characterize the Ca^{2+} signal generated by the hormone. The addition of agonist to cell cultures, loaded with the indicator Cal-520 AM and imaged in a Ca^{2+}-containing buffer, induced fluorescence changes that were observed in neuronal soma as well as in minor processes (**Figure 2**). Seventeen out of

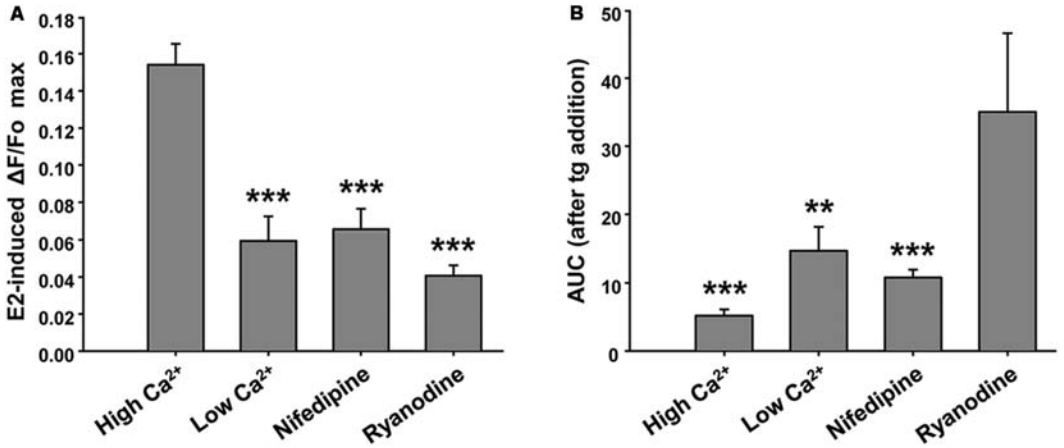

FIGURE 3 | Ryanodine, external Ca^{2+} and nifedipine modulate E2-induced Ca^{2+} increase. **(A)** Mean values of maximal ΔF/Fo for Ca^{2+} mobilized by 17β-estradiol (E2) in hypothalamic neurons recorded either in the presence or absence of extracellular Ca^{2+} (Ca^{2+}-HBSS/EGTA-containing buffer, named High Ca^{2+}/Low Ca^{2+}), or after a pre-incubation period (1 h) with ryanodine or nifedipine. ANOVA $F_{(3,41)} = 22.94$; $p \leq 0.001$. LSDs test indicated $^{***}p < 0.001$ vs. Ca^{2+}-HBSS. **(B)** Mean values of integrated area under ΔF/Fo curve (AUC) after thapsigargin (tg) addition during Ca^{2+} imaging [same conditions as **(A)**]. ANOVA $F_{(3,26)} = 9.18$; $p \leq 0.001$. LSDs test indicated $^{***}p < 0.001$ and $^{**}p = 0.01$ vs. ryanodine. Bars represent mean ± SEM; $n = 4$–6 different cultures.

76 neurons (22.4%) from six independent experiments imaged in Ca^{2+}-HBSS responded to E2 pulses within 15–100 s of treatment (average = 46.8 ± 6.60 s). These Ca^{2+} events often occur in repetitive oscillations, which display interspike intervals of 21.58 ± 8.83 s (9 out of 17 neurons). The amplitude in terms of ΔF/Fo was 0.154 ± 0.01. The total amount of Ca^{2+} mobilized, measured as the integrated area under the curve (AUC) for all E2-generated peaks, was 4.69 ± 1.03, which was 90.6% with respect to the control [remained endoplasmic reticulum Ca^{2+} content released by tg, a sarco/endoplasmic reticulum Ca^{2+}-ATPase (SERCA) inhibitor].

This E2-induced Ca^{2+} signal was not observed in the absence of extracellular Ca^{2+}. Moreover, we found that pre-incubation of neuronal cultures with inhibitory ryanodine suppressed E2-evoked Ca^{2+} release (**Figure 3A**). Importantly, under these conditions, the tg was able to mobilize amounts of Ca^{2+}, measured as AUC, of 14.69 ± 3.45 (EGTA-containing buffer) and 35.05 ± 11.54 (ryanodine pre-incubation), five and nine times greater, respectively, than the amounts of Ca^{2+} mobilized by tg in E2-induced control neurons (**Figure 3B**). Moreover, nifedipine reduced the E2-induced Ca^{2+} increase more than 50% (ΔF/Fo = 0.065 ± 0.011; and AUC = 10.779 ± 1.159, $n = 4$), which strongly suggests the participation of L-VGCCs in this signal (**Figures 3A,B**). Representative Ca^{2+} traces plotted as ΔF/Fo vs. time for EGTA, ryanodine, and nifedipine conditions are provided in **Supplementary Figure S1**.

Taken together, these results indicate that both Ca^{2+} influx and mobilization from intracellular stores contribute to the response.

E2-Induced Axonal Growth Depends on Ca^{2+} Signal Generated by RyRs

Finally, we tested whether the RyR-induced Ca^{2+} response is part of the signaling cascade that mediates the axogenic effect of E2. Neurons grew under the following conditions: in the presence and absence of E2 and pretreated with inhibitory ryanodine. After these treatments, the cells were grown for an additional 24 h period with (E2) or without E2 (control). In agreement with previous results, the morphometric analysis indicated that neurons grown under hormonal treatment show longer axons than neurons in control conditions without E2 (**Figure 4A**). Remarkably, blocking RyRs with ryanodine completely inhibited the E2-induced axogenesis (**Figure 4B**). Moreover, no significant differences were observed in the number of primary neurites, length of minor processes, or soma area per neuron resulting from E2 or ryanodine treatment (**Table 1**), confirming that the hormonal effect is restricted to axonal growth (Díaz et al., 1992; Cambiasso et al., 1995, 2000; Brito et al., 2004).

DISCUSSION

In the present study, results from ERK1/2 phosphorylation, Ca^{2+} imaging and neuronal growth consistently pointed to RyRs as the Ca^{2+} channels necessary to mediate activation of the MAPK/ERK pathway and the final axogenic effect induced by E2. Inhibitory ryanodine completely blocked E2-mediated Ca^{2+} transients, ERK1/2 phosphorylation and axonal outgrowth, which provides valuable evidence to propose that E2 mobilizes endoplasmic reticulum stores of Ca^{2+} through RyRs to activate the signaling cascades that finally affect the axonal elongation of hypothalamic neurons.

In regard to the impact of functional RyRs on cellular response, Dr Hidalgo's group showed that BDNF-induced neural plasticity requires functional RyRs activated by the Ca^{2+}-induced Ca^{2+} release (CICR) mechanism to evoke the larger Ca^{2+} signaling needed to maintain changes during long-term memory storage (Adasme et al., 2011). CICR is a positive

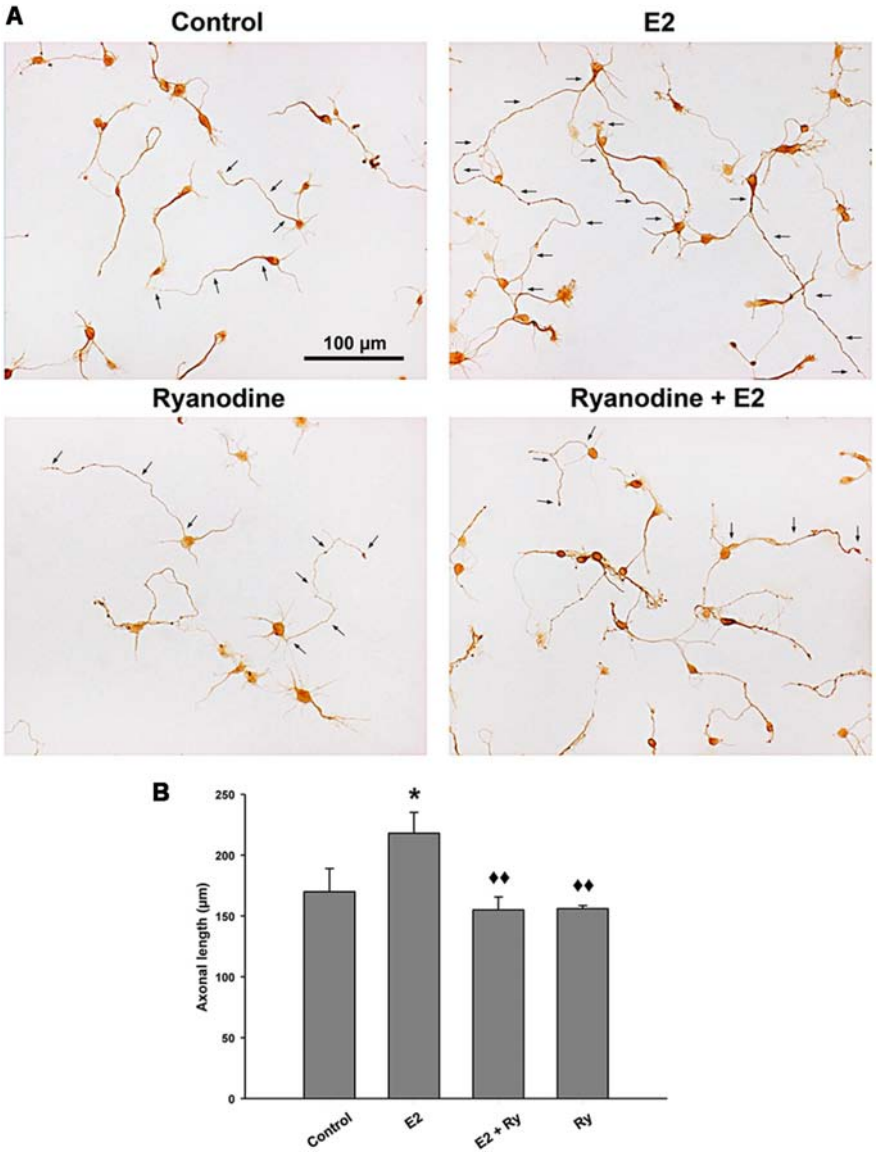

FIGURE 4 | RyR activity is required to the E2-induced axogenesis. **(A)** Representative images of male hypothalamic neurons cultured for 48 h with (E2) or without (control) 10 nM 17β-estradiol in combination or not with 50 µM ryanodine (Ry) for the last 24 h of incubation (arrows indicate the axons of some neurons). **(B)** Mean of axonal length for each condition in **(A)**. ANOVA $F_{(3,12)} = 4.51$; $p = 0.02$. LSDs test indicated $^*p = 0.05$ vs. control and $^{♦♦}p = 0.01$ vs. E2. Data represent the mean ± SEM; $n = 4$ independent cultures. Scale bar: 100 µm.

TABLE 1 | Number of primary neurites, soma area, and length of minor processes of male hypothalamic neurons grown with or without 17β-estradiol (E2) in 3 combination or not with ryanodine.

Variable	Treatment			
	Control	E2	E2 + Ryanodine	Ryanodine
N° of neurites	4.2 ± 0.2	4.4 ± 0.2	4.3 ± 0.4	4.2 ± 0.2
Soma area (µm^2)	118.9 ± 13.2	116.6 ± 4.5	119.5 ± 10.0	126.2 ± 9.0
Minor processes length (µm)	107.2 ± 7.7	115.6 ± 8.9	94.0 ± 11.5	92.6 ± 5.8

Data represent the mean ± SEM; n = 4 independent cultures.

feedback mechanism by which cytoplasmic Ca^{2+} stimulates Ca^{2+} release from the endoplasmic reticulum through RyRs or IP_3Rs (Bezprozvanny et al., 1991; Berridge et al., 2003; Seo et al., 2015). Moreover, several studies have indicated a regulatory role for estrogens on RyRs activity, for instance, in the human eccrine sweat gland cell line NCL-SG3 (Muchekehu and Harvey, 2008),

ventricular myocytes (Yan et al., 2011), detrusor smooth muscle cells (Hristov et al., 2017), and dorsal root ganglion neurons (Ferrari et al., 2016; Khomula et al., 2017). Interestingly, Zhao X. et al. (2005) proposed, in a neuroblastoma cell line, an E2-mediated mechanism starting at the plasma membrane, by which rapid Ca^{2+} signaling potentiates the transcription of genes normally regulated by estrogens; RyRs, IP_3Rs, and N-VGCCs, but not L-VGCCs, were involved in the process. Our results clearly show that RyRs are indispensable Ca^{2+} channels involved in the non-classical signaling events produced by E2 to generate axonal growth in hypothalamic neurons. However, RyRs also require a previous small increase in cytosolic Ca^{2+} from resting levels to activate and release Ca^{2+} by CICR (Hidalgo et al., 2005; Lanner et al., 2010). Since we found that removing extracellular Ca^{2+} or blocking the membrane channels L-VGCCs prevented the Ca^{2+} signaling induced by E2 and that inhibiting L-VGCCs also reduced ERK1/2 phosphorylation modulated by the steroid, we postulate that E2 initially induces a Ca^{2+} influx in hypothalamic neurons *via* L-VGCCs that then enables RyRs opening to generate the final and complete Ca^{2+} signaling event (Hidalgo, 2005; Calin-Jageman and Lee, 2008). Besides L-VGCCs, our results show that the PLC/IP_3Rs system is involved in E2-induced ERK1/2 activation, since both 2-APB and U-73122 used as blockers of IP_3Rs and PLC, respectively, produced a significant reduction in phosphorylation levels of the kinases in the presence of the hormone. The activation of PLC and Ca^{2+} release *via* IP_3Rs induced by estrogens has been previously reported in different cellular systems (Chaban et al., 2004; Fricke et al., 2007).

L-VGCCs are the major route of Ca^{2+} entry into neurons and the most profusely studied and best characterized VGCC type by far, as they play a predominant role in the brain (Striessnig et al., 2014; Vega-Vela et al., 2017). Several studies report that E2 is able to modulate L-VGCCs activity (Bulayeva et al., 2005; Sarkar et al., 2008; Farkas et al., 2012; Feng et al., 2013). Wu et al. (2005) and Zhao L. et al. (2005) indicated that E2 induced rapid Ca^{2+} influx through L-VGCCs, which was required to activate the Src/ERK/CREB/Bcl-2 signaling pathway and finally mediated neuroprotective and neurotrophic responses in rat hippocampal and cortical neurons. The generation of this intracellular Ca^{2+} increase and the downstream activation of ERK depend on the presence of ERs in the membrane of rat hippocampal neurons (Wu et al., 2011). These membrane ER-expressing neurons represented 29% of the cultured cells and all of them co-expressed L-VGCCs. Consistently, our data from Ca^{2+} imaging experiments indicated that approximately 22% of hypothalamic neurons responded to E2.

Although previously it has been reported that E2 induces L-VGCCs-mediated Ca^{2+} influx, the question about how the hormone activates L-VGCCs remains open. Sarkar et al. (2008) reported that E2 potentiated the activity of L-VGCCs by directly binding to specific sites in the channel, independently of ERs. On the other hand, PI3K signaling cascade has been proposed as a candidate to link membrane ER activation with L-VGCCs aperture (Simoncini et al., 2000; Quignard et al., 2001; Wu et al., 2005), although our preceding work blocking PI3K with LY-294,002 did not prevent the axogenic effect of E2 in hypothalamic neurons (Gorosito and Cambiasso, 2008). It is important to note that we have previously reported the expression of ERα on the cell-surface of embryonic hypothalamic neurons (Gorosito et al., 2008), and that the membrane-impermeable E2-albumin construct (E2-BSA) was as effective as free E2 to generate ERK1/2 phosphorylation (Gorosito and Cambiasso, 2008) and axonal elongation (Cambiasso and Carrer, 2001), evidence that altogether indicate these processes respond to a membrane-initiated ERα-mediated mechanism.

Another question that arises is what other elements lead from the RyRs-mediated Ca^{2+} release to ERK1/2 activation. In Gorosito and Cambiasso (2008) we reported that PKC but not PKA nor CaMKII is required in the E2-induced MAPK-ERK pathway activation, since an inhibitor with specificity for the PKC Ca^{2+}-dependent α and βI isoforms, Ro 32-0432, attenuated E2-modulated ERK1/2 phosphorylation and prevented the axogenic effect of the hormone. PKC activation by E2 has been found in different cell types, including breast cancer cells, hepatocytes, and cortical and hypothalamic neurons (Marino et al., 1998; Boyan et al., 2003; Cordey et al., 2003; Qiu et al., 2003). Ca^{2+}-dependent PKC activation can then induce ERK1/2 phosphorylation *via* Src/Ras signaling (Cullen and Lockyer, 2002; Brandt et al., 2003; Roskoski, 2005).

Our results show that E2-induced cytosolic Ca^{2+} often increases as repetitive oscillations. This is in agreement with previous work demonstrating E2-induced intracellular Ca^{2+} oscillations that involved internal stores and PKA and PLC activity in neurons of the arcuate nucleus (Fricke et al., 2007). It is well known that the frequency of Ca^{2+} oscillation may depend on Ca^{2+} influx into the cell (Sneyd et al., 2004), SERCA activity (Falcke et al., 2003) and oscillating cytoplasmic IP_3 concentration (Sneyd et al., 2006). Our data suggest that the frequency of Ca^{2+} oscillations in hypothalamic neurons stimulated by E2 mainly depends on Ca^{2+} entry. Leaving aside its modulation, our results allow us to speculate that the characteristic frequency encodes information to regulate the cellular response (axonal growth) mediated by the hormone (Dolmetsch et al., 1998).

In conclusion, we have provided new insights into the non-classical mechanisms triggered by estrogens and its axogenic effect in male rat hypothalamic neurons. The hormone induces ERK1/2 activation in a Ca^{2+}-dependent manner. RyRs inhibition abolished this activation as well as axonal growth. The oscillatory Ca^{2+} signal generated by E2 required functional RyRs and L-VGCCs. This early Ca^{2+} response that underlies E2-induced RyRs and MAPK/ERK activation may transmit a finely tuned message into a neuronal development program, reflecting the need for tight control of a critical event during sexual differentiation of the male brain. The conjunction of XY genotype with adequate estrogen exposure levels at the time of hypothalamic neuronal differentiation may induce the growth of axons towards their appropriate targets. A complete and detailed understanding of the intracellular signaling mechanisms and neuronal processes mediated by estrogens will allow to

improve current estrogen-based therapies, such as hormone replacement therapy in postmenopausal women, as well as to develop novel treatments to prevent and/or alleviate neurological pathologies based on its widely proven neuritogenic and neuroprotective effects.

AUTHOR CONTRIBUTIONS

LCZ, MB and MC made the conception and design of research, interpreted results of experiments, wrote the manuscript. LCZ performed all experiments and analyzed the data. LCZ and MB prepared the figures. MB and MC edited and revised the manuscript. MC drafted the manuscript.

FUNDING

This study was supported by grants from Consejo Nacional de Investigaciones Científicas y Técnicas (CONICET; PIP 2013-2015), Agencia Nacional de Promoción Científica y Tecnológica (ANPCyT; PICT 2015 N° 1333) and Secretaria de Ciencia y Tecnología (SECyT)-Universidad Nacional de Córdoba (2016-2017), Argentina to MC and from CONICET (PIP 2014-2016) to MB.

ACKNOWLEDGMENTS

We thank for the technical support from INIMEC animal facility and Dr Quassollo for his invaluable help with imaging. Calcium imaging was generated at National Center of Microscopy, Universidad Nacional de Córdoba, Córdoba, Argentina.

SUPPLEMENTARY MATERIAL

The Supplementary Material for this article can be found online at: https://www.frontiersin.org/articles/10.3389/fncel.2019.00122/full#supplementary-material

REFERENCES

Acaz-Fonseca, E., Sanchez-Gonzalez, R., Azcoitia, I., Arevalo, M. A., and Garcia-Segura, L. M. (2014). Role of astrocytes in the neuroprotective actions of 17β-estradiol and selective estrogen receptor modulators. *Mol. Cell. Endocrinol.* 389, 48–57. doi: 10.1016/j.mce.2014.01.009

Adasme, T., Haeger, P., Paula-Lima, A. C., Espinoza, I., Casas-Alarcon, M. M., Carrasco, M. A., et al. (2011). Involvement of ryanodine receptors in neurotrophin-induced hippocampal synaptic plasticity and spatial memory formation. *Proc. Natl. Acad. Sci. U S A* 108, 3029–3034. doi: 10.1073/pnas.1013580108

Arevalo, M. A., Azcoitia, I., and Garcia-Segura, L. M. (2015). The neuroprotective actions of oestradiol and oestrogen receptors. *Nat. Rev. Neurosci.* 16, 17–29. doi: 10.1038/nrn3856

Arevalo, M. A., Ruiz-Palmero, I., Scerbo, M. J., Acaz-Fonseca, E., Cambiasso, M. J., and Garcia-Segura, L. M. (2012). Molecular mechanisms involved in the regulation of neuritogenesis by estradiol: recent advances. *J. Steroid Biochem. Mol. Biol.* 131, 52–56. doi: 10.1016/j.jsbmb.2011.09.004

Berridge, M. J., Bootman, M. D., and Roderick, H. L. (2003). Calcium signalling: dynamics, homeostasis and remodelling. *Nat. Rev. Mol. Cell Biol.* 4, 517–529. doi: 10.1038/nrm1155

Berthois, Y., Katzenellenbogen, J. A., and Katzenellenbogen, B. S. (1986). Phenol red in tissue culture media is a weak estrogen: implications concerning the study of estrogen-responsive cells in culture. *Proc. Natl. Acad. Sci. U S A* 83, 2496–2500. doi: 10.1073/pnas.83.8.2496

Beyer, C., and Karolczak, M. (2000). Estrogenic stimulation of neurite growth in midbrain dopaminergic neurons depends on cAMP/protein kinase A signalling. *J. Neurosci. Res.* 59, 107–116. doi: 10.1002/(sici)1097-4547(20000101)59:1<107::aid-jnr13>3.0.co;2-w

Beyer, C., and Raab, H. (1998). Nongenomic effects of oestrogen: embryonic mouse midbrain neurones respond with a rapid release of calcium from intracellular stores. *Eur. J. Neurosci.* 10, 255–262. doi: 10.1046/j.1460-9568.1998.00045.x

Bezprozvanny, I., Watras, J., and Ehrlich, B. E. (1991). Bell-shaped calcium-response curves of Ins(1,4,5)P3- and calcium-gated channels from endoplasmic reticulum of cerebellum. *Nature* 351, 751–754. doi: 10.1038/351751a0

Blanco, G., Diaz, H., Carrer, H. F., and Beaugé, L. (1990). Differentiation of rat hippocampal neurons induced by estrogen *in vitro*: effects on neuritogenesis and Na, K-ATPase activity. *J. Neurosci. Res.* 27, 47–54. doi: 10.1002/jnr.490270108

Boyan, B. D., Sylvia, V. L., Frambach, T., Lohmann, C. H., Dietl, J., Dean, D. D., et al. (2003). Estrogen-dependent rapid activation of protein kinase C in estrogen receptor-positive MCF-7 breast cancer cells and estrogen receptor-negative HCC38 cells is membrane-mediated and inhibited by tamoxifen. *Endocrinology* 144, 1812–1824. doi: 10.1210/en.2002-221018

Brandt, D. T., Goerke, A., Heuer, M., Gimona, M., Leitges, M., Kremmer, E., et al. (2003). Protein kinase C delta induces Src kinase activity via activation of the protein tyrosine phosphatase PTP α. *J. Biol. Chem.* 278, 34073–34078. doi: 10.1074/jbc.m211650200

Brito, V. I., Carrer, H. F., and Cambiasso, M. J. (2004). Inhibition of tyrosine kinase receptor type B synthesis blocks axogenic effect of estradiol on rat hypothalamic neurones *in vitro*. *Eur. J. Neurosci.* 20, 331–337. doi: 10.1111/j.1460-9568.2004.03485.x

Bulayeva, N. N., Wozniak, A. L., Lash, L. L., and Watson, C. S. (2005). Mechanisms of membrane estrogen receptor-α-mediated rapid stimulation of Ca^{2+} levels and prolactin release in a pituitary cell line. *Am. J. Physiol. Endocrinol. Metab.* 288, E388–E397. doi: 10.1152/ajpendo.00349.2004

Calin-Jageman, I., and Lee, A. (2008). Ca_v1 L-type Ca^{2+} channel signaling complexes in neurons. *J. Neurochem.* 105, 573–583. doi: 10.1111/j.1471-4159.2008.05286.x

Cambiasso, M. J., and Carrer, H. F. (2001). Nongenomic mechanism mediates estradiol stimulation of axon growth in male rat hypothalamic neurons *in vitro*. *J. Neurosci. Res.* 66, 475–481. doi: 10.1002/jnr.1238

Cambiasso, M. J., Colombo, J. A., and Carrer, H. F. (2000). Differential effect of oestradiol and astroglia-conditioned media on the growth of hypothalamic neurons from male and female rat brains. *Eur. J. Neurosci.* 12, 2291–2298. doi: 10.1046/j.1460-9568.2000.00120.x

Cambiasso, M. J., Diaz, H., Cáceres, A., and Carrer, H. F. (1995). Neuritogenic effect of estradiol on rat ventromedial hypothalamic neurons co-cultured with homotopic or heterotopic glia. *J. Neurosci. Res.* 42, 700–709. doi: 10.1002/jnr.490420513

Carroll, J. C., and Pike, C. J. (2008). Selective estrogen receptor modulators differentially regulate Alzheimer-like changes in female 3xTg-AD mice. *Endocrinology* 149, 2607–2611. doi: 10.1210/en.2007-1346

Céspedes Rubio, Á. E., Pérez-Alvarez, M. J., Lapuente Chala, C., and Wandosell, F. (2018). Sex steroid hormones as neuroprotective elements in ischemia models. *J. Endocrinol.* 237, R65–R81. doi: 10.1530/joe-18-0129

Chaban, V. V., Lakhter, A. J., and Micevych, P. (2004). A membrane estrogen receptor mediates intracellular calcium release in astrocytes. *Endocrinology* 145, 3788–3795. doi: 10.1210/en.2004-0149

Cordey, M., Gundimeda, U., Gopalakrishna, R., and Pike, C. J. (2003). Estrogen activates protein kinase C in neurons: role in neuroprotection. *J. Neurochem.* 84, 1340–1348. doi: 10.1046/j.1471-4159.2003.01631.x

Cullen, P. J., and Lockyer, P. J. (2002). Integration of calcium and Ras signalling. *Nat. Rev. Mol. Cell Biol.* 3, 339–348. doi: 10.1038/nrm808

Díaz, H., Lorenzo, A., Carrer, H. F., and Cáceres, A. (1992). Time lapse study of neurite growth in hypothalamic dissociated neurons in culture: sex differences and estrogen effects. *J. Neurosci. Res.* 33, 266–281. doi: 10.1002/jnr.490330210

Dolmetsch, R. E., Xu, K., and Lewis, R. S. (1998). Calcium oscillations increase the efficiency and specificity of gene expression. *Nature* 392, 933–936. doi: 10.1038/31960

Dotti, C. G., Sullivan, C. A., and Banker, G. A. (1988). The establishment of polarity by hippocampal neurons in culture. *J. Neurosci.* 8, 1454–1468. doi: 10.1523/JNEUROSCI.08-04-01454.1988

Dye, R. V., Miller, K. J., Singer, E. J., and Levine, A. J. (2012). Hormone replacement therapy and risk for neurodegenerative diseases. *Int. J. Alzheimers Dis.* 2012:258454. doi: 10.1155/2012/258454

Falcke, M., Li, Y., Lechleiter, J. D., and Camacho, P. (2003). Modeling the dependence of the period of intracellular Ca^{2+} waves on SERCA expression. *Biophys. J.* 85, 1474–1481. doi: 10.1016/s0006-3495(03)74580-9

Farkas, I., Sárvári, M., Aller, M., Okada, N., Okada, H., Likó, I., et al. (2012). Estrogen receptor α and β differentially mediate C5aR agonist evoked Ca^{2+}-influx in neurons through L-type voltage-gated Ca^{2+} channels. *Neurochem. Int.* 60, 631–639. doi: 10.1016/j.neuint.2012.02.024

Feng, Y., Wang, B., Du, F., Li, H., Wang, S., Hu, C., et al. (2013). The involvement of PI3K-mediated and L-VGCC-gated transient Ca^{2+} influx in 17β-estradiol-mediated protection of retinal cells from H_2O_2-induced apoptosis with Ca^{2+} overload. *PLoS One* 8:e77218. doi: 10.1371/journal.pone.0077218

Ferrari, L. F., Khomula, E. V., Araldi, D., and Levine, J. D. (2016). Marked sexual dimorphism in the role of the ryanodine receptor in a model of pain chronification in the rat. *Sci. Rep.* 6:31221. doi: 10.1038/srep31221

Fricke, O., Kow, L. M., Bogun, M., and Pfaff, D. W. (2007). Estrogen evokes a rapid effect on intracellular calcium in neurons characterized by calcium oscillations in the arcuate nucleus. *Endocrine* 31, 279–288. doi: 10.1007/s12020-007-0034-7

Garcia-Segura, L. M., Arévalo, M. A., and Azcoitia, I. (2010). Interactions of estradiol and insulin-like growth factor-I signalling in the nervous system: new advances. *Prog. Brain Res.* 181, 251–272. doi: 10.1016/s0079-6123(08)81014-x

Giatti, S., Garcia-Segura, L. M., Barreto, G. E., and Melcangi, R. C. (2018). Neuroactive steroids, neurosteroidogenesis and sex. *Prog. Neurobiol.* doi: 10.1016/j.pneurobio.2018.06.007 [Epub ahead of print].

Gorosito, S. V., and Cambiasso, M. J. (2008). Axogenic effect of estrogen in male rat hypothalamic neurons involves Ca^{2+}, protein kinase C, and extracellular signal-regulated kinase signaling. *J. Neurosci. Res.* 86, 145–157. doi: 10.1002/jnr.21466

Gorosito, S. V., Lorenzo, A. G., and Cambiasso, M. J. (2008). Estrogen receptor α is expressed on the cell-surface of embryonic hypothalamic neurons. *Neuroscience* 154, 1173–1177. doi: 10.1016/j.neuroscience.2008.05.001

Hidalgo, C. (2005). Cross talk between Ca^{2+} and redox signalling cascades in muscle and neurons through the combined activation of ryanodine receptors/Ca^{2+} release channels. *Philos. Trans. R. Soc. Lond. B Biol. Sci.* 360, 2237–2246. doi: 10.1098/rstb.2005.1759

Hidalgo, C., Donoso, P., and Carrasco, M. A. (2005). The ryanodine receptors Ca^{2+} release channels: cellular redox sensors? *IUBMB Life* 57, 315–322. doi: 10.1080/15216540500092328

Hristov, K. L., Parajuli, S. P., Provence, A., Rovner, E. S., and Petkov, G. V. (2017). Nongenomic modulation of the large conductance voltage- and Ca^{2+}-activated K^+ channels by estrogen: a novel regulatory mechanism in human detrusor smooth muscle. *Physiol. Rep.* 5:e13351. doi: 10.14814/phy2.13351

Kelly, M. J., and Levin, E. R. (2001). Rapid actions of plasma membrane estrogen receptors. *Trends Endocrinol. Metab.* 12, 152–156. doi: 10.1016/s1043-2760(01)00377-0

Khan, M. M., Wakade, C., de Sevilla, L., and Brann, D. W. (2015). Selective estrogen receptor modulators (SERMs) enhance neurogenesis and spine density following focal cerebral ischemia. *J. Steroid Biochem. Mol. Biol.* 146, 38–47. doi: 10.1016/j.jsbmb.2014.05.001

Khomula, E. V., Ferrari, L. F., Araldi, D., and Levine, J. D. (2017). Sexual dimorphism in a reciprocal interaction of ryanodine and IP3 receptors in the induction of hyperalgesic priming. *J. Neurosci.* 37, 2032–2044. doi: 10.1523/JNEUROSCI.2911-16.2017

Lai, Y. J., Yu, D., Zhang, J. H., and Chen, G. J. (2017). Cooperation of genomic and rapid nongenomic actions of estrogens in synaptic plasticity. *Mol. Neurobiol.* 54, 4113–4126. doi: 10.1007/s12035-016-9979-y

Lanner, J. T., Georgiou, D. K., Joshi, A. D., and Hamilton, S. L. (2010). Ryanodine receptors: structure, expression, molecular details, and function in calcium release. *Cold Spring Harb. Perspect. Biol.* 2:a003996. doi: 10.1101/cshperspect.a003996

Le Mellay, V., Grosse, B., and Lieberherr, M. (1997). Phospholipase C β and membrane action of calcitriol and estradiol. *J. Biol. Chem.* 272, 11902–11907. doi: 10.1074/jbc.272.18.11902

Marino, M., Pallottini, V., and Trentalance, A. (1998). Estrogens cause rapid activation of IP3-PKC-α signal transduction pathway in HEPG2 cells. *Biochem. Biophys. Res. Commun.* 245, 254–258. doi: 10.1006/bbrc.1998.8413

McCarthy, M. M. (2008). Estradiol and the developing brain. *Physiol. Rev.* 88, 91–124. doi: 10.1152/physrev.00010.2007

McGregor, C., Riordan, A., and Thornton, J. (2017). Estrogens and the cognitive symptoms of schizophrenia: possible neuroprotective mechanisms. *Front. Neuroendocrinol.* 47, 19–33. doi: 10.1016/j.yfrne.2017.06.003

Muchekehu, R. W., and Harvey, B. J. (2008). 17β-estradiol rapidly mobilizes intracellular calcium from ryanodine-receptor-gated stores via a PKC-PKA-Erk-dependent pathway in the human eccrine sweat gland cell line NCL-SG3. *Cell Calcium* 44, 276–288. doi: 10.1016/j.ceca.2007.12.001

Murphy, D. D., and Segal, M. (1996). Regulation of dendritic spine density in cultured rat hippocampal neurons by steroid hormones. *J. Neurosci.* 16, 4059–4068. doi: 10.1523/JNEUROSCI.16-13-04059.1996

Nishizuka, M., and Arai, Y. (1981). Organizational action of estrogen on synaptic pattern in the amygdala: implications for sexual differentiation of the brain. *Brain Res.* 213, 422–426. doi: 10.1016/0006-8993(81)90247-x

Picotto, G., Vazquez, G., and Boland, R. (1999). 17β-oestradiol increases intracellular Ca^{2+} concentration in rat enterocytes. Potential role of phospholipase C-dependent store-operated Ca^{2+} influx. *Biochem. J.* 339, 71–77. doi: 10.1042/bj3390071

Qiu, J., Bosch, M. A., Tobias, S. C., Grandy, D. K., Scanlan, T. S., Ronnekleiv, O. K., et al. (2003). Rapid signaling of estrogen in hypothalamic neurons involves a novel G-protein-coupled estrogen receptor that activates protein kinase C. *J. Neurosci.* 23, 9529–9540. doi: 10.1523/JNEUROSCI.23-29-09529.2003

Quignard, J. F., Mironneau, J., Carricaburu, V., Fournier, B., Babich, A., Nurnberg, B., et al. (2001). Phosphoinositide 3-kinase γ mediates angiotensin II-induced stimulation of L-type calcium channels in vascular myocytes. *J. Biol. Chem.* 276, 32545–32551. doi: 10.1074/jbc.m102582200

Reisert, I., Han, V., Lieth, E., Toran-Allerand, D., Pilgrim, C., and Lauder, J. (1987). Sex steroids promote neurite growth in mesencephalic tyrosine hydroxylase immunoreactive neurons *in vitro*. *Int. J. Dev. Neurosci.* 5, 91–98. doi: 10.1016/0736-5748(87)90054-2

Roskoski, R. Jr. (2005). Src kinase regulation by phosphorylation and dephosphorylation. *Biochem. Biophys. Res. Commun.* 331, 1–14. doi: 10.1016/j.bbrc.2005.03.012

Sarkar, S. N., Huang, R. Q., Logan, S. M., Yi, K. D., Dillon, G. H., and Simpkins, J. W. (2008). Estrogens directly potentiate neuronal L-type Ca^{2+} channels. *Proc. Natl. Acad. Sci. U S A* 105, 15148–15153. doi: 10.1073/pnas.0802379105

Scerbo, M. J., Freire-Regatillo, A., Cisternas, C. D., Brunotto, M., Arevalo, M. A., Garcia-Segura, L. M., et al. (2014). Neurogenin 3 mediates sex chromosome effects on the generation of sex differences in hypothalamic neuronal development. *Front. Cell. Neurosci.* 8:188. doi: 10.3389/fncel.2014.00188

Seo, M. D., Enomoto, M., Ishiyama, N., Stathopulos, P. B., and Ikura, M. (2015). Structural insights into endoplasmic reticulum stored calcium regulation by inositol 1,4,5-trisphosphate and ryanodine receptors. *Biochim. Biophys. Acta* 1853, 1980–1991. doi: 10.1016/j.bbamcr.2014.11.023

Simoncini, T., Hafezi-Moghadam, A., Brazil, D. P., Ley, K., Chin, W. W., and Liao, J. K. (2000). Interaction of oestrogen receptor with the regulatory subunit of phosphatidylinositol-3-OH kinase. *Nature* 407, 538–541. doi: 10.1038/35035131

Sneyd, J., Tsaneva-Atanasova, K., Reznikov, V., Bai, Y., Sanderson, M. J., and Yule, D. I. (2006). A method for determining the dependence of calcium oscillations on inositol trisphosphate oscillations. *Proc. Natl. Acad. Sci. U S A* 103, 1675–1680. doi: 10.1073/pnas.0506135103

Sneyd, J., Tsaneva-Atanasova, K., Yule, D. I., Thompson, J. L., and Shuttleworth, T. J. (2004). Control of calcium oscillations by membrane

fluxes. *Proc. Natl. Acad. Sci. U S A* 101, 1392–1396. doi: 10.1073/pnas.0303472101

Spence, R. D., Wisdom, A. J., Cao, Y., Hill, H. M., Mongerson, C. R., Stapornkul, B., et al. (2013). Estrogen mediates neuroprotection and anti-inflammatory effects during EAE through ERα signaling on astrocytes but not through ERβ signaling on astrocytes or neurons. *Brain Behav. Evol.* 33, 10924–10933. doi: 10.1523/jneurosci.0886-13.2013

Striessnig, J., Pinggera, A., Kaur, G., Bock, G., and Tuluc, P. (2014). L-type Ca^{2+} channels in heart and brain. *Wiley Interdiscip. Rev. Membr. Transp. Signal.* 3, 15–38. doi: 10.1002/wmts.102

Toran-Allerand, C. D. (1976). Sex steroids and the development of the newborn mouse hypothalamus and preoptic area *in vitro*: implications for sexual differentiation. *Brain Res.* 106, 407–412. doi: 10.1016/0006-8993(76)91038-6

Toran-Allerand, C. D. (1980). Sex steroids and the development of the newborn mouse hypothalamus and preoptic area *in vitro*. II. Morphological correlates and hormonal specificity. *Brain Res.* 189, 413–427. doi: 10.1016/0006-8993(80)90101-8

Toran-Allerand, C. D., Hashimoto, K., Greenough, W. T., and Saltarelli, M. (1983). Sex steroids and the development of the newborn mouse hypothalamus and preoptic area *in vitro*: III. Effects of estrogen on dendritic differentiation. *Brain Res.* 283, 97–101. doi: 10.1016/0165-3806(83)90085-8

Vega-Vela, N. E., Osorio, D., Avila-Rodriguez, M., Gonzalez, J., Garcia-Segura, L. M., Echeverria, V., et al. (2017). L-type calcium channels modulation by estradiol. *Mol. Neurobiol.* 54, 4996–5007. doi: 10.1007/s12035-016-0045-6

Villa, A., Vegeto, E., Poletti, A., and Maggi, A. (2016). Estrogens, neuroinflammation, and neurodegeneration. *Endocr. Rev.* 37, 372–402. doi: 10.1210/er.2016-1007

Wong, C. K., So, W. Y., Law, S. K., Leung, F. P., Yau, K. L., Yao, X., et al. (2012). Estrogen controls embryonic stem cell proliferation via store-operated calcium entry and the nuclear factor of activated T-cells (NFAT). *J. Cell. Physiol.* 227, 2519–2530. doi: 10.1002/jcp.22990

Wright, C. L., Schwarz, J. S., Dean, S. L., and McCarthy, M. M. (2010). Cellular mechanisms of estradiol-mediated sexual differentiation of the brain. *Trends Endocrinol. Metab.* 21, 553–561. doi: 10.1016/j.tem.2010.05.004

Wu, T. W., Chen, S., and Brinton, R. D. (2011). Membrane estrogen receptors mediate calcium signaling and MAP kinase activation in individual hippocampal neurons. *Brain Res.* 1379, 34–43. doi: 10.1016/j.brainres.2011.01.034

Wu, T. W., Wang, J. M., Chen, S., and Brinton, R. D. (2005). 17β-estradiol induced Ca^{2+} influx via L-type calcium channels activates the Src/ERK/cyclic-AMP response element binding protein signal pathway and BCL-2 expression in rat hippocampal neurons: a potential initiation mechanism for estrogen-induced neuroprotection. *Neuroscience* 135, 59–72. doi: 10.1016/j.neuroscience.2004.12.027

Yan, S., Chen, Y., Dong, M., Song, W., Belcher, S. M., and Wang, H. S. (2011). Bisphenol A and 17β-estradiol promote arrhythmia in the female heart via alteration of calcium handling. *PLoS One* 6:e25455. doi: 10.1371/journal.pone.0025455

Zhao, L., Chen, S., Ming Wang, J., and Brinton, R. D. (2005). 17β-estradiol induces Ca^{2+} influx, dendritic and nuclear Ca^{2+} rise and subsequent cyclic AMP response element-binding protein activation in hippocampal neurons: a potential initiation mechanism for estrogen neurotrophism. *Neuroscience* 132, 299–311. doi: 10.1016/j.neuroscience.2004.11.054

Zhao, X., MacBride, M. M., Peterson, B. R., Pfaff, D. W., and Vasudevan, N. (2005). Calcium flux in neuroblastoma cells is a coupling mechanism between non-genomic and genomic modes of estrogens. *Neuroendocrinology* 81, 174–182. doi: 10.1159/000087000

Conflict of Interest Statement: The authors declare that the research was conducted in the absence of any commercial or financial relationships that could be construed as a potential conflict of interest.

frontiers in Cellular Neuroscience

ORIGINAL RESEARCH
published: 11 April 2019
doi: 10.3389/fncel.2019.00139

Oxidative Stress in Retinal Degeneration Promoted by Constant LED Light

Maria M. Benedetto[1,2] *and Maria A. Contin*[1,2]*

[1]*Departamento de Química Biológica Ranwel Caputto, Facultad de Ciencias Químicas, Universidad Nacional de Córdoba, Córdoba, Argentina,* [2]*Centro de Investigaciones en Química Biológica de Córdoba (CIQUIBIC), CONICET, Universidad Nacional de Córdoba, Córdoba, Argentina*

Light pollution by artificial light, might accelerate retinal diseases and circadian asynchrony. The excess of light exposure is a growing problem in societies, so studies on the consequences of long-term exposure to low levels of light are needed to determine the effects on vision. The possibility to understand the molecular mechanisms of light damage will contribute to the knowledge about visual disorders related to defects in the phototransduction. Several animal models have been used to study retinal degeneration (RD) by light; however, some important aspects remain to be established. Previously, we demonstrated that cool white treatment of 200 lux light-emitting diode (LED) induces retinal transformation with rods and cones cell death and significant changes in opsin expression in the inner nuclear layer (INL) and ganglion cell layer (GCL). Therefore, to further develop describing the molecular pathways of RD, we have examined here the oxidative stress and the fatty acid composition in rat retinas maintained at constant light. We demonstrated the existence of oxidative reactions after 5 days in outer nuclear layer (ONL), corresponding to classical photoreceptors; catalase (CAT) enzyme activity did not show significant differences in all times studied and the fatty acid study showed that docosahexaenoic acid decreased after 4 days. Remarkably, the docosahexaenoic acid diminution showed a correlation with the rise in stearic acid indicating a possible association between them. We assumed that the reduction in docosahexaenoic acid may be affected by the oxidative stress in photoreceptors outer segment which in turn affects the stearic acid composition with consequences in the membrane properties. All these miss-regulation affects the photoreceptor survival through unknown mechanisms involved. We consider that oxidative stress might be one of the pathways implicated in RD promoted by light.

Keywords: retinal light damage, LED light, oxidative stress, fatty acid, electroretinogram

OPEN ACCESS

Edited by:
Gabriela Alejandra Salvador, Universidad Nacional del Sur, Argentina

Reviewed by:
Luis Enrique Politi, Instituto de Investigaciones Bioquímicas de Bahía Blanca (INIBIBB), Argentina
Rocío Salceda, National Autonomous University of Mexico, Mexico

***Correspondence:**
Maria A. Contin
mcontin@fcq.unc.edu.ar; maria.ana.contin@unc.edu.ar

Received: *07 December 2018*
Accepted: *20 March 2019*
Published: *11 April 2019*

Citation:
Benedetto MM and Contin MA (2019) Oxidative Stress in Retinal Degeneration Promoted by Constant LED Light. Front. Cell. Neurosci. 13:139. doi: 10.3389/fncel.2019.00139

INTRODUCTION

The disturbance between the amount of reactive oxygen species (ROS) and antioxidants production is defined as oxidative stress. This imbalance produces tissue injury (Halliwell, 1994). The retina carries out the capture of light photons, and for this, it is exposed to suffer oxidative stress. However, it has many mechanisms to counteract these processes through the action of antioxidant enzymes as superoxide dismutase (SOD), catalase (CAT) and glutathione peroxidase (GSHPx) and vitamins as ascorbic acid, vitamin E, melanin (Iusifov et al., 1980; Scibior and Czeczot, 2006; Pavarino et al., 2013). The overexposure to light may

be one of the many factors that can induce the interruption of this homeostasis, promoting the injury of eye tissues, cell death or stimulating simultaneously antioxidant protection by up-regulation of antioxidant enzymes (Yusifov et al., 2000); however, when the equilibrium is broken the consequence is the induction of retinal degeneration (RD). In mammals, in normal light conditions, the retina fulfills two main roles: the vision over rods and cones activity and the non-image forming tasks including circadian entrainment, pupillary response to light, secretion of melatonin and sleep regulation (Berson et al., 2002; Rollag et al., 2003; Guido et al., 2010; Sikka et al., 2014). Light stimulates photoreceptor cells activating the phototransduction cascade which promotes hyperpolarization (Sung and Chuang, 2010). Light overexposure-induced RD might induce retinal task deficits with consequences in the secretion of melatonin, desynchronization of rhythms such as sleep/wake, among others. The use of different sources of artificial light is increasing in actual society but this promotes changes in human behavior. Furthermore, the use of technologies such as light-emitting diode (LED), smart TVs and cell-phones, promote an excess of blue light exposure especially at night. Albeit the effects of artificial illumination are unknown, it may have a strong impact on retinal functions with negative consequences on people's health. Considering that the excess of light exposure constitutes an upcoming polluter, it is clearly an emerging public health issue. Different animal models have been used by researchers in order to study the processes of RD promoted by light exposure. Even though Noell et al. (1966) suggested that exposure to light produces retinal changes, this phenomenon has not been fully clarified yet (Shear et al., 1973; Rapp and Williams, 1979; Sperling et al., 1980; Semple-Rowland and Dawson, 1987; Remé et al., 2000; Organisciak and Vaughan, 2010; Roehlecke et al., 2013; Shang et al., 2014). In retina and retinal pigment epithelium (RPE) cells, the exposure to blue light inhibits the mitochondrial enzymes and cytochrome oxidase expression inducing retinal damage (Chen, 1993; Cai et al., 2000; Roehlecke et al., 2011) suggesting the existence of oxidative stress mechanisms as part of the retinal cell death mechanism induced by light exposure. Recently, Nakamura et al. (2017) established that LED light exposure during 2 h (800 lx) induced retinal damage where oxidative stress was partially involved. However, the consequences of constant low light exposure in which the phototransduction mechanism is constantly activated for long time remain unknown. In this regard, we have established and characterized a model of RD induced by a constant exposure to LED. We have showed that classical photoreceptor cell death without caspase-3 activation and a gradual increase in levels of rhodopsin-phospho-Ser334 as a result of light exposure, suggesting that constant light produces changes in the regulation of phototransduction in rods (Contín et al., 2013).

However, retinal ganglion cells (RGCs) do not die after constant light treatment (LL), suggesting a neuroprotection mechanism also involved in our model (Benedetto et al., 2017). So, the key questions in the present work are: does the overexposure at constant low levels of LED light yield oxidative stress? What is the kinetic of oxidative stress production if the exposure is constant? Therefore, the goals of this work were to investigate the existence of oxidative stress, fatty acid composition and retinal function during the different days of LL stimulation in retinas of Wistar rats.

MATERIALS AND METHODS

Animals

All animal procedures were performed in accordance with the protocol approved by the local animal committee (School of Chemistry, UNC, Exp. 2018-740), in accordance with the ARVO statement for the use of animals in ophthalmic and vision research. Wistar rats from 12 to 15 weeks of age were maintained with food and water *ad libitum* and illumination cycle from 12:12 h (light/dark) with white fluorescent light on (∼50 lux) from Zeitgeber time (ZT) 0–12 from the time they were born, up to the experiment.

Light Damage

Constant Light

RD was induced as described by Contín et al. (2013). Briefly, rats were exposed to constant light in boxes with LED lamps (EVERLIGHT Electronic Co., Ltd. T-13/4 3294-15/T2C9-1HMB, color temperature of 5,500 K) in the inner upper surface and temperature-controlled at 24 ± 1°C. At the level of the rats' eyes, 200 lx were measured with a light meter (model 401036; Extech Instruments Corp., Waltham, MA, USA). After 1 to 8 days of constant light stimulation (LL1–LL8) the animals were killed in a CO_2 chamber at ZT6. Controls in light dark cycle (LD), with LED or fluorescent light (RT) and constant darkness (DD) were exposed for 7 days.

Dark Period Protocol

Animals were subjected to a constant light during 8 days with periods of dark during 2, 4, 6, 10 and 12 h every day at the beginning of the subjective night (ZT6) under identical conditions as animals exposed to LL, in the temperature-controlled stress box at 24 ± 1°C.

Electroretinograms (ERGs)

The methods employed for Scotopic electroretinogram (ERG) were as previously described by Dorfman et al. (2014) using an ERG machine (Akonic BIOPC, Buenos Aires, Argentina). Briefly, first animals were adapted to dark for 20 min. Then, they were anesthetized with an intraperitoneal injection containing a solution of xylazine hydrochloride (2 mg/kg) and ketamine hydrochloride (150 mg/kg). Pupils were dilated with tropicamide (1% Alcon Laboratories) and, in order to prevent eye dehydration and permit electrical contact activity when the electrode is recording, the cornea was irrigated with proparacaine hydrochloride (0.5% Alcon Laboratories). Both eyes were recorded simultaneously applying flashes of white light (5 ms, 0.1 Hz) from a photostimulator set at maximum brightness (3 cd s/m^2 without filter). Then, the recordings were amplified and filtered (1.5 Hz low-pass filter, 300 Hz high-pass filter,

notch filter activated). An average of 10 responses for each eye was measured. Mean "a" and "b" waves peak latencies and amplitudes of the responses from each group of rats were compared.

Outer Nuclear Layer Analysis

The retinal fixation method, sectioning and nuclear quantification were as previously described (Contín et al., 2013). Briefly, rats' eyes were fixed overnight at 4°C in 4% (W/V) paraformaldehyde in 100 mM sodium phosphate buffer (PBS, pH 7.3). Then, they were cryoprotected in sucrose and mounted in an optimal cutting temperature compound (OCT; Tissue-Tek® Sakura). Retinal sections were cut along the horizontal meridian (nasal-temporal). The sections were stained with 1% Hoechst (33258 Sigma Aldrich) for 5 min and photographed using a confocal microscope (Olympus FV1200, Japan) at 40× magnification. The nuclei were counted in "left, middle left, middle right and right" designated areas from five different animals per treatment using the software ImageJ (v. 1.45) and the plugin "Automatic Nuclei Counter".

Superoxide Production

Dihydroethidium [(DHE; sigma 37291-25 mg dihydroethidium at 10-mg/mL stock solution in dimethylsulfoxide)], a redox-sensitive probe, was used to detect superoxide generation as previously described (Peng et al., 2011). Briefly, eyes were removed, washed in PBS solution and then incubated with 1 mM DHE for 12 h at room temperature in PBS. Then the eyes were incubated in paraformaldehyde 4% for 12 h at room temperature, harvested and quikly frozen in liquid nitrogen for cryosection (Leica CM 1950, Leica Microsystems Ltd, Wetzlar, Germany). The cryosections (10 μm) were analyzed by confocal microscopy (Olympus FV300, Japan). The DHE molecules enter the cells and are oxidized by superoxide contained inside cells, to ethidium (Et) which is fluorescent. This product is retained in the cell allowing the estimation of cellular superoxide production.

Oxidative Stress Quantification

ROS molecules were determined by flow cytometry with 2′,7′-dichlorofluorescein diacetate (DCFH-DA) probe (D6883 Sigma). DCFH-DA is sensitive to oxidation and is nonfluorescent, it may be oxidized by ROS and peroxides and become a fluorescent molecule, DCFH (Gomes et al., 2005). Briefly, retinas dissected and dissociated in 0.25% (W/V) trypsin (Life Technology, Inc., Carlsbad, CA, USA) for 7 min at 37°C were centrifuged at 3,000 rpm for 3 min, incubated with 200 μl of trypsin inhibitor (STI) for 3 min and washed twice with PBS 1×. Then, they were suspended in 200 μl of PBS 1×, incubated with DCFH-DA (5 μM) for 60 min at 37°C in dark, washed twice with PBS 1× and analyzed on a Becton-Dickinson FACS flow cytometer; the excitation and emission wavelengths were set at 488 and 525 nm, respectively. Data were analyzed with FlowJo software (LC, Ashland, Ore). Three independent experiments were performed and the results were expressed as mean ± standard error (SE) in arbitrary units of DCFH fluorescence intensity.

Catalase Activity Detection

Catalase (CAT) activity was assessed according to Aebi (1984). Briefly, individual retinas were homogenized in PBS 1×. Then, 1.3 ml of Buffer Phosphate (50 mM, pH 7.4) and 1.25 ml of distilled H_2O were added to 300 μl of previously homogenized sample. Subsequently, 150 μl of H_2O_2 (300 mM) was added and the spectrophotometric changes were detected by measuring the absorbance at 240 nm for 1 min. The protein concentration was determined by Bradford (1976).

Lipid Extraction From Rat Retinas

Lipids were extracted from the samples as Folch' method slightly modified (Folch et al., 1957). Briefly, collected retinas were homogenized in 200 μl of MiliQ H_2O and 3 ml of a combination of Chloroform: methanol [(2:1; v/v)] and 600 μl of MiliQ H_2O were added and vortexed vigorously for 5 min and centrifuged at 2,000 rpm at 15°C for 10 min. The layer containing chloroform was collected and 1.5 ml of a mixture of chloroform: methanol: H_2O [(3:48:47; v/v/v)] was added, mixed gently and centrifuged 10 min at 2,000 rpm. Finally, chloroform was dried under a stream of N_2 and the extracts stored for further experiments.

Fatty Acid Methyl Esters Analysis by Gas Chromatography/Mass Spectrometry With Ion-Trap Detector

Extracted lipids were transmethylated to fatty acid methyl esters (FAMEs) with sodium methoxide and toluene [(2:1; v/v)] overnight at 4°C. FAMEs were then extracted with hexane and analyzed by using a GC/MS (Saturn® 2000 GC/MS, Agilent, Santa Clara, USA) equipped with an ion-trap detector and a fused capillary column (HP-5MS, 30 mm × 0.25 mm i.d × 0.25 μm film thickness, Agilent, Santa Clara, USA). The carrier gas used was Helium (flow rate 1.0 ml/min); the detector and injector temperature were maintained at 150°C and 300°C, respectively. The injection (split-splitless injector) volume of the sample was 1 μl with a split ratio of 1:50. The oven was programmed as follows: 170°C for 3 min—200°C at the rate of 1.2°C/min—10°C/min to 240°C—80°C/min to 280°C and 80°C/min to 300°C with a final hold for 46.7 min.

The column temperature was programmed as follows: 170°C; 1.2°/min to 200°C—10°/min to 240°C—80°/min to 2,800°C—80°/min to 300°C and hold at 300°C for 4 min. Then, FAMEs were identified comparing mass spectra with dates in the library (National Institute of Standards and Technology, Gaithersburg, MD, USA). Furthermore, we compared FAMEs retention times with the commercial standard Supelco 37-Component FAME Mix (Sigma Aldrich, St. Louis, MO, USA).

Statistical Analysis

Statistical analysis was carried out using the Infostat software (Version 2017, InfoStat Group, FCA, National University of Córdoba, Argentina). One-way analysis of variance (ANOVA) was used for statistical comparisons. In the text and figure, data are expressed as mean ± SD or SE. It was considered

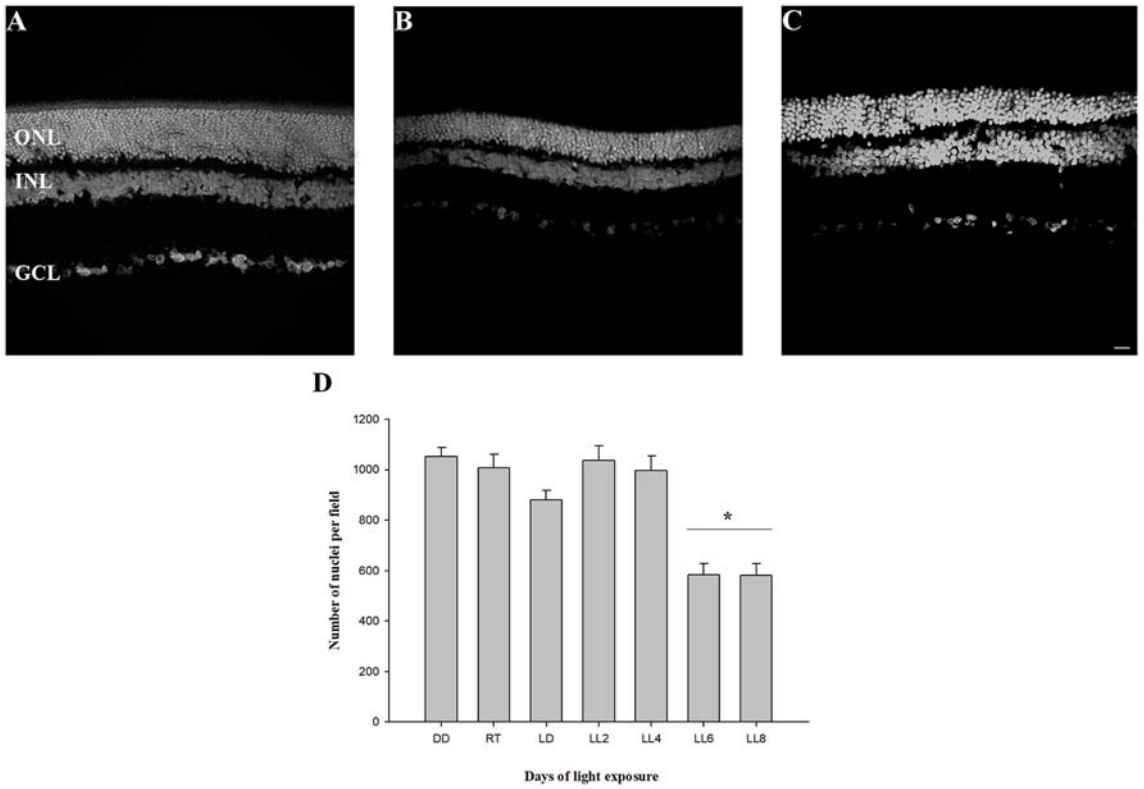

FIGURE 1 | Outer nuclear layer analysis. **(A)** Rat retinas maintained in dark for 7 days (DD). **(B–C)** Retinas from rats exposed 6 (LL6) or 8 (LL8) days to constant light (200 lx). **(D)** Quantification of ONL nuclei; rat retina images corresponding to controls [(LD cycle, RT cycle and non-exposure to light (DD)] or exposure to 200 lx LED light (LL) for 2, 4, 6, and 8 days were analyzed to quantify photoreceptor survival. Data are mean ± standard error (SE), $n = 2$ animals/group from five independent experiments, $^*p < 0.05$ vs. DD and RT by one-way analysis of variance (ANOVA) and Duncan's *post hoc* test. ONL, outer nuclear layer; INL, inner nuclear layer; GCL, ganglion cell layer. Scale bar indicates 30 μm.

statistically significant a p-value < 0.05. The normality and homogeneity of the variance assumptions were proved with Shapiro–Wilks and Levene tests, respectively. Duncan *post hoc* test with a p value < 0.05 were considered statistically significant. A non-parametric Kruskal-Wallis test was performed when the data did not comply with the assumptions of the ANOVA. Spearman correlation coefficients were calculated to determine associations between the content of fatty acids.

RESULTS

Structural Retinal Analysis

In order to know the kinetic of cell death events we analyzed the retinal layers, oxidative stress, CAT activity, fatty acid composition and ERG activity in animals exposed to constant light. The analysis of retinal structure revealed a reduction in outer nuclear layer (ONL) thickness at LL6 and LL8 compared with animals reared in DD (**Figures 1A–C**). The quantification of nuclei in this area showed a significant reduction after 6 and 8 days of constant light (583.04 ± 45.31 and 580.10 ± 45.31 nuclei, respectively) compared with DD and RT [(1052.19 ± 38.41 and 1007.63 ± 54.32 nuclei, respectively, $p < 0.005$, **Figure 1D**)]; indicating that between LL0 to LL6 are being carried out the photoreceptor cell death pathways.

Oxidative Stress Study

DHE Determination

In order to know if retinas from animals exposed to constant light have oxidative stress, DHE was measured in retinal sections as indicated in "Materials and Methods" section. DHE and superoxide anion reaction produces ethidium (E), which binds to DNA rising the fluorescence in the cells (Gomes et al., 2005; Fernandes et al., 2006). Here, we show that retinas from animals exposed for 2 days of LL (LL2) have fluorescent label in few cells in ONL; however, at 8 days of LL (LL8) a significant increment of DHE label was observed (**Figures 2A–C**), correlating with ONL cell reduction (**Figure 1**). Besides the clear staining in ONL, no positive labeled in other retinal layer were observed in any time of LL studied, indicating the existence of oxidized products specifically in this layer.

Reactive Oxygen Species Quantification

To determine the kinetic of oxidative stress events occurred in ONL of retinas exposed to LL, ROS production was determined

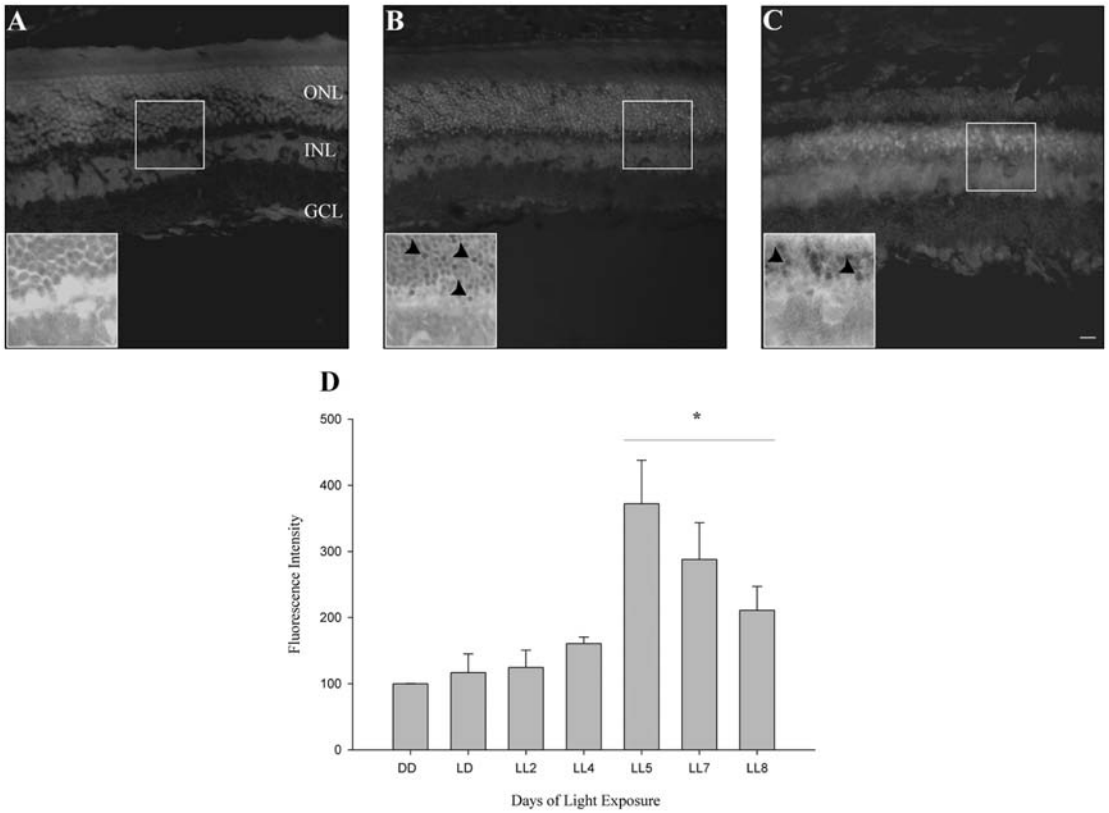

FIGURE 2 | Oxidative stress study. **(A–C)** DHE staining at DD, LL2 and 8 days of light-emitting diode (LED) light exposure. Arrowheads show DHE positive cells in the ONL. **(D)** Reactive oxygen species (ROS) production detection by Flow cytometry using the DCFH-DA probe in controls (DD and LD) and in animals exposed to 2, 4, 5, 7 and 8 days to constant light (LL2–8). Data are mean ± SE, $n = 1$ animal/group from three independent experiments, $^*p < 0.05$ vs. DD by Kruskal Wallis. ONL, outer nuclear layer; INL, inner nuclear layer; GCL, ganglion cell layer. Scale bar indicates 30 μm.

by flow cytometry using the DCFH-DA probe as indicated in "Materials and Methods" section. At 2 and 4 days of LL no significant increases in fluorescence were observed (124.70 ± 44.94 and 160.69 ± 16.9%, respectively). However, constant light treatment increases the levels of fluorescence, showing significant changes after 5 days of LL (LL5) where the production of ROS was maximal (372.16 ± 113.44%) respect to control in DD (100%). Although at 7 and 8 days of LL the fluorescence production decreased in correlation with cell death in the ONL (287.97 ± 221.55 and 211.00 ± 80.80%, respectively), ROS production was greater than in DD (**Figure 2D**).

Catalase Activity Determination

CAT enzyme is known to contribute to H_2O_2 detoxification in the retina and the inhibition of its activity increases H_2O_2 concentration 2.5-fold, which cannot make up for the GPX activity (Ohta et al., 1996) the enzyme being an antioxidant factor in retina. In order to investigate the CAT activity and its association in the prevention of oxidative stress in constant light exposed rats, it was assessed as indicated in "Materials and Methods" section. Although constant light stimuli increased lightly CAT activity at 6 and 8 days of LL (7.22 ± 3.95 and 5.96 ± 3.27, respectively) with respect to LL 2 and 4 (3.38 ± 1.44 and 4.35 ± 2.24, respectively), reaching the levels of DD and RT (5.82 ± 2.55 and 6.96 ± 4.30, respectively) there were no significant differences in any times of LL measured (**Figure 3**), suggesting that CAT is affected by the desynchronization of animals by constant light exposure.

Retinal Fatty Acid

The outer segment membrane of retinal rods and cones contain high polyunsaturated fatty acids (PUFAs) where docosahexaenoic (22–6 n-3, DHA) and arachidonic acid (20:4 n-6, AA) are the major species present. Because PUFAs are a target for oxidation, the analysis by GC-MS in rat retinas from animal exposure to different LL allow us to determine if there are changes in the membrane components during RD as a result of light exposure. Individual fatty acids were identified comparing the mass spectra with those present in the NIST library and their retention time with a commercial standard (see "Materials and Methods"). Representative GC/MS analyses of fatty acids from retinas of control animals and exposed to light (LL) are shown in **Figure 4A**. Palmitic (16:0, PA) and arachidonic acid (20:4 n-6, AA), did not show statistical differences in any times of LL studied (**Figures 4B,D**). However, stearic acid (18:0, EA) shows increased levels with respect to control at LL4, maintaining this higher level at LL6 and LL8 (**Figure 4C**) in association with the DHA decrease which was significant at LL 4 and 8

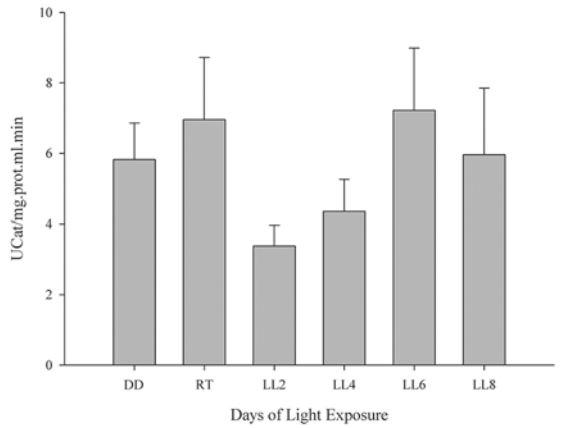

FIGURE 3 | Catalase activity study in retinal light damage. CAT activity expressed as U/mg prot.ml.min in controls (DD and RT) and rats exposed at different days of LL. Data are mean ± SE, n = 1 animal/group from three independent experiments, p = 0.216 by one-way ANOVA and Duncan's *post hoc* test.

(**Figure 4E**). In order to determine if the variations were related, we perform a correlation analysis between EA and DHA in control animals (DD) and animals exposed to 4, 6 and 8 days to LL. **Figures 5A–D** show no correlation in control animals maintained in dark (DD) and in LL6, however, there is a positive correlation in LL4 ($\rho = 1$) and negative correlation in LL8 ($\rho = -0.8$).

Electroretinograms Responses

Previously we demonstrated retinal functional alterations in the scotopic ERG responses, showing that throughout the days of LL, the two principal waves "a" and "b" tend to decrease their amplitudes and increase their latency time, reaching abolished records after LL4, indicating that photoreceptor cells fail between the first 4 days of LL (Quintana et al., 2016). Here, to study the effects of light interruption by darkness, the animals were exposed to constant light with 2, 4, 6, 10 or 12 h of dark during the subjective night as indicated in "Materials and Methods" section. As shown in **Figure 5**, with 2, 4 and 6 h of rest in darkness per day during subjective night, the ERG show abolished records as we described before, however, at 8 and 10 h of dark the ERG began to restore, reaching normal values at 12 h. This result indicates that including hours of rest in darkness during the subjective night the effects of light exposure may be less harmful than constant stimuli.

DISCUSSION

The excess of artificial light exposure constitutes a problem that is emergent worldwide. The behavior of excessive exposure to light might have effects on the vision, promoting RD and circadian asynchrony in healthy population. We have previously characterized a RD model that may provide the possibility to study specific events associated with RD under conditions of low light with LED sources, at constant or long-term periods of exposure (LP context). We demonstrated that photoreceptor cells died along the days of continuous light stimuli through a caspase-3 independent mechanism. Rhodopsin analysis did not show a reduction in protein levels, however, rhodopsin-phospho-Ser334 increased gradually with the days of LL exposure indicating increasing levels in the phosphorylation. The study of rhodopsin allows us to investigate the role of phototransduction mechanism in the RD model suggesting that rhodopsin dysregulation could be involved in one of the ways of RD (Contín et al., 2013). Furthermore, in the inner retina, we demonstrated a relocation of non-visual photopigments (OPN4 and OPN5); however, inner retinal cells survival were not affected, indicating a compensatory mechanism of protection with possible changes in synchronization of circadian rhythms (Benedetto et al., 2017). To further describe the molecular pathways of cell death, in this work, we have examined the oxidative stress involvement in the effects of constant exposure to LED sources. Results from both DHE and DCFH-DA probe analysis demonstrate the existence of oxidative reactions in LL exposed rats (**Figure 2**). The ONL label of DHE indicates the occurrence of oxidative stress only in this layer, discarding stress mechanisms in other cells of the retina, coinciding with cell death study. DCFH-DA analysis shows that the production of ROS increases significantly after LL5 with higher levels at this day of LL (**Figure 2D**) indicating oxidative stress from 5 days of constant light. Powerful defenses against oxidative stress are the effect of Vitamin E, Ascorbic Acid, and melanin as well as the activity of antioxidant enzyme superoxide dismutase (SOD), CAT and GSHPx (Yusifov et al., 2000). Here, we demonstrated that CAT activity does not present significant differences in all times studied (**Figure 3**) showing a light diminution at LL2 to LL4 with respect to controls in DD and LD treatments; however, at LL6 and LL8 the CAT activity increases showing levels similar to the controls. Previous studies have demonstrated that CAT enzyme is finely regulated by the circadian rhythms; CAT bioinformatic and mRNA studies have been shown putative E-box sites in CAT and GPx regulatory regions; furthermore, CAT mRNA expression and enzyme activity shows circadian rhythmicity with higher levels at the end of the day (Navigatore Fonzo et al., 2009; Kharwar and Haldar, 2012; Lacoste et al., 2017). Sani et al. (2006) have demonstrated that CAT activity shows changes across a 24-h period in mouse. Thus, we hypothesize that constant light might produce a complex and multifactorial biological process inducing progressive desynchronization of circadian rhythm with concomitant antioxidant function altered; and therefore, the break of the equilibrium between ROS over-production and antioxidant processes. However, further studies are necessary in order to conclude an association between them.

The vertebrate retina contains high concentration of PUFA; particularly, in the outer segment membrane of retinal rod and cones, the PUFAs DHA and AA are the major species examined (Fliesler and Anderson, 1983; Giusto et al., 2000; SanGiovanni and Chew, 2005). PUFAs are essential for maintaining the appropriate fluidity of the membrane, necessary for efficient phototransduction cascade (Brown, 1994; Gawrisch and Soubias, 2008). The composition of membrane lipids and their direct interaction with proteins

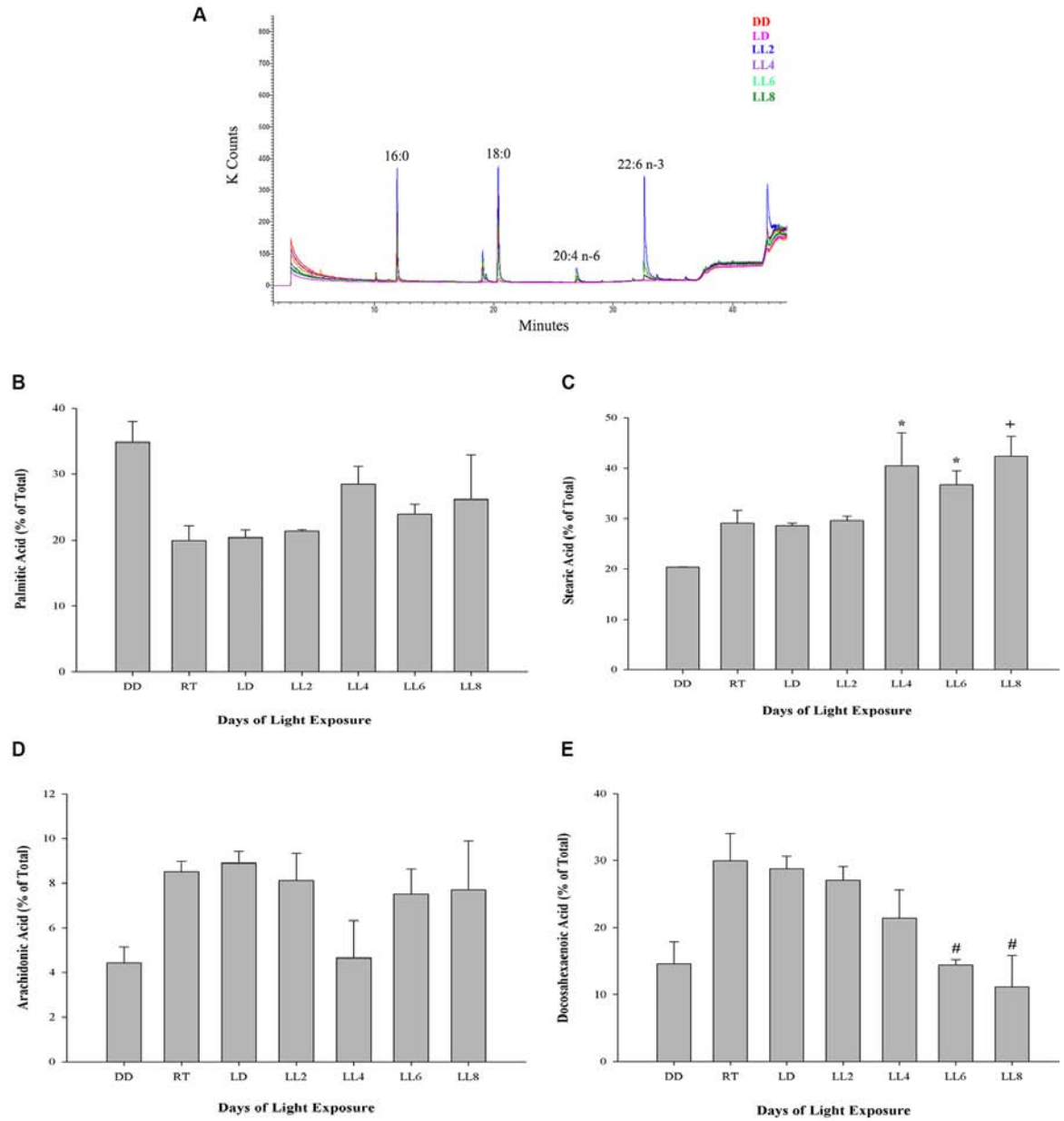

FIGURE 4 | Fatty acid composition in light-treated rat retinas. **(A)** Full scan GC-MS total ion chromatograms of rat retina from controls (DD and LD) and rats exposed to 2, 4, 6 and 8 days of LL. 16:0, palmitic acid; 18:0, stearic acid; 20:4 n-6, arachidonic acid; 22:6 n-3, docosahexaenoic acid. **(B–E)** Quantification of palmitic **(B)**, stearic **(C)**, arachidonic **(D)** and docosahexaenoic acid **(E)** from controls (DD, RT and LD) and animals exposed for 2, 4, 6 and 8 days of constant light (LL), expressed as a percentage of total fatty acids, respectively. Data are mean ± SE, $n = 1$ animal/group from three independent experiments, $^{*}p < 0.05$ vs. DD and LD; $^{+}p < 0.05$ vs. DD; $^{\#}p < 0.05$ vs. RT and LD, by Kruskal-Wallis.

play an important role in the modulation of the rhodopsin function (Salas-Estrada et al., 2018). A good retinal function is subject to adequate membrane structure which contains high levels of DHA. Anderson and Penn (2004) proposed, as neuroprotective adaptive responses, changes in DHA levels at different environmental conditions with the aim to control the number of photons captured by rhodopsin molecule. In the fatty acid n-3-deficient rod outer segment, it has been shown that reduced rhodopsin transducin (Gt) coupling, reduced cGMP phosphodiesterase activity, and slower formation of metarhodopsin II-Gt complex, relative to the animals fed with n-3-adequate diet, explained the reduced activity of rod phototransduction in these animals (Anderson and Penn, 2004). These findings support the so called "photostasis" which infers the morphological and biochemistry adaptation to capture a constant number of photons. The constant light exposure may

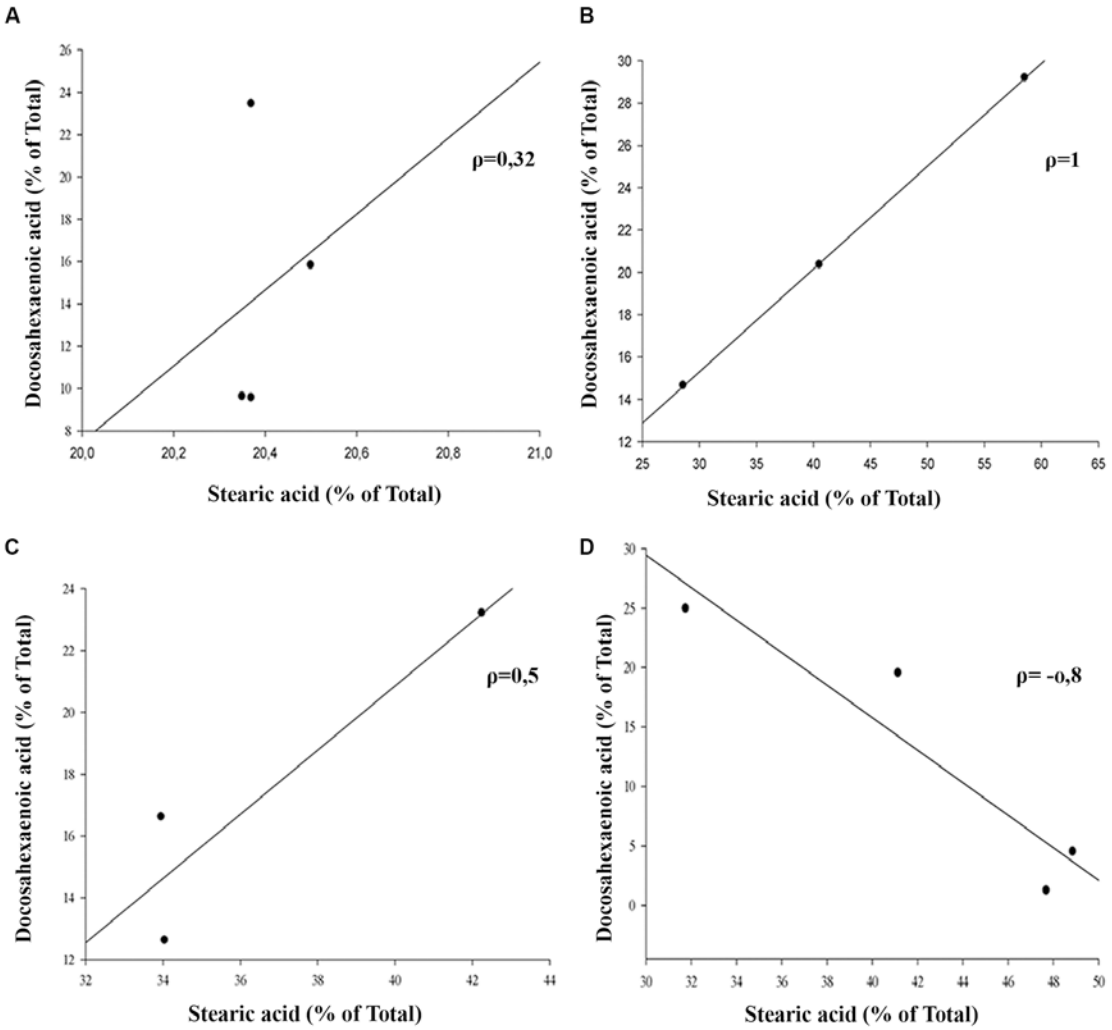

FIGURE 5 | Linear correlation analysis between stearic and docosahexaenoic acid in light-treated retinas. **(A)** Control animals maintained in DD. **(B–D)** Animals maintained for 4, 6 and 8 days at constant light, respectively. ρ: pearson correlation coefficient, *n* = 1 animal/group from three independent experiments.

break the adaptive mechanism and promote several pathways of cell death.

DHA and AA are obtained from two ways: (a) the diet or (b) synthesized from alpha-linolenic (18:3n3) and linoleic acids (18:2n6). DHA is transported from the liver to the RPE cells (Scott and Bazan, 1989). In rat rods, DHA is essential for normal development of function (Benolken et al., 1973; Wheeler et al., 1975) where rat deficient in PUFA showed reduced ERG responses (Jeffrey et al., 2002). DHA located mainly in photoreceptors represents 50% of the total fatty acid and recently it has been demonstrated that the membrane of rod outer segment has higher levels of PUFA and Very Long Chain-PUFA (VLC-PUFA) in rod-dominant rats than cone-dominant, suggesting that rods and cones do not have equal lipid requirements (Agbaga et al., 2018). The cell membranes are susceptible to oxidation due to high level of unsaturation of PUFAs, furthermore, retina membranes exposed to light, elevate the concentration of oxygen with the presence of rhodopsin photo-bleached products that increment the risk (Kagan et al., 1981; Wiegand et al., 1983; Rózanowska and Sarna, 2005; Hunter et al., 2012). Earlier study revealed that lipid peroxidation reactions in light-induced RD induce the specific loss of DHA from rod outer segment membranes during constant illumination with an increase in the production of lipid hydroperoxides. None of the other fatty acids, including the AA, changed significantly over the 3-day time periods; concluding that light mediates the peroxidation of PUFAS in outer segment membrane acids and supporting the hypothesis that peroxidation is involved in retinal light degeneration (Wiegand et al., 1983). So, as we exposed the rat retinas to constant light at 200 lux, and we demonstrated increase in ROS significantly at LL5, we decided to study if fatty acid composition is altered belonging to the days in LL, specially by oxidative stress processes. Results from GC-MS analysis shows that PA (saturated) and AA (unsaturated) do not show statistical changes with the days of LL. However, DHA (unsaturated) decreased with the LL

exposure with statistical significance at LL4, 6 and 8 compared with controls in LD and RT (**Figure 4E**). Remarkably, the decrease of DHA draws a parallel with an SA increase at the same day of LL (**Figure 4C**). The study of the correlation between both fatty acids shows an association between them in LL-treated retinas; instead, we did not find any association in control animals (DD). We assumed that the reduction in DHA may be affected by the oxidative stress in photoreceptor outer segment which in turn affects the photoreceptor survival through unknown different miss-regulation mechanism involved. The hepatic metabolism, through desaturation and elongation steps, influences the fatty acid composition (Engler et al., 2000). Diabetes, atherosclerosis, neurological disorders, cancer and others are enhanced by the disturbances in fatty acid content (see Zolfaghari and Ross, 2003). One fatty acid biosynthesis pathway begins with the desaturation of PA and SA; in this way, delta-9-desaturase (Δ9-desaturase) is the key enzyme necessary for the conversion from palmitic to palmitoleic acid (16:1n-7) and stearic to oleic acid (18:1n-9). Δ6 and Δ5-desaturase enzymes are required for the metabolism of essential fatty acids, linoleic (18:2n-6) and alpha-linolenic (18:3n-3), to long-chain PUFAs (LCP-DHA). Hormonal, dietary factors, peroxisomal proliferators and developmental processes can affect the activity of Δ9-desaturase, which alters monounsaturated and PUFA composition (Ntambi, 1995, 1999). In hypertensive rats, DHA-fed Δ9-desaturase activity decreases at 53% suggesting that dietary DHA influences properties and function of cellular membranes due to changes in fatty acid composition (Engler et al., 2000). Animals with Δ9-desaturase activity dysregulation show changes in the relation of stearic:oleic acid with effects over membrane fluidity and function (Ntambi, 1995, 1999). Lai et al. (2010) saw that patients with BCD (Bietti crystalline dystrophy; a retinal degenerative disease) have higher concentration of stearic acid and lower octadecadienoic acid (18:1n-9) than healthy animals. Furthermore, the activity of Δ9-desaturase and the concentration of monounsaturated fatty acids were lower in BCD animals suggesting abnormalities in lipid metabolism demonstrating a direct relation between rising levels of stearic acid, lowering fatty acid concentration and retinal dysfunction (Lai et al., 2010). We think that reduction of DHA levels by oxidation in LL rats may affect the desaturase activity in retina causing the rising of stearic acid accumulation which might affect the membrane proprieties giving more rigidity to the outer segment. It may explain part of the cell death mechanism induced by oxidative stress. Furthermore, the excess of light may alter the levels of Neuroprotectin D1 (NPD1) due to the DHA oxidation. NPD1 is a biologically active DHA derivative which induces downstream pro-survival pathways such as gene expression, pro-apoptotic gene suppression and pro-inflammatory responses, among others. The diminution of DHA may alter these ways across inducing photoreceptor cell death (see Asatryan and Bazan, 2017). Other studies are required to better understand the effects of DHA reduction; nevertheless, analyzing the time course of oxidative stress, we consider that it is not the only pathway involved, because the production of DHE and ROS have a maximum expression after LL5-6 (**Figure 2**), and the reduction of ONL occurs between LL6 and LL8; however, the two principal waves of ERG, a and b, tend to decrease the amplitudes and increase the latency time during light stimuli, reaching abolished records at LL4 (Quintana et al., 2016). All these results suggest that a dysfunction of retinal electrical activity occurs previously to redox imbalance. It has been demonstrated that low intensities of light stimuli need the activation of photopigments and phototransduction to induce RD (Hao et al., 2002; Grimm and Remé, 2013), suggesting that impairment of the phototransduction mechanism could be responsible for cell death. Besides, previously we demonstrated the existence of more phosphorylated rhodopsin (rhodopsin-phospho-Ser^{334}) after LL2 with a higher level at LL7, supporting the idea that changes in phototransduction cascade are also involved (Contín et al., 2013). Here, we show scotopic ERG responses abolished until 6 h of rest darkness during subjective night; however, after 8 h of dark the activity begin to restore, reaching normal values at 12 h (**Figure 6**). These results suggest that the existence of regulatory mechanisms tend to revert or prevent the process of cell death when the retina is maintained in rest (notice the difference between 10 and 12 h of darkness); nevertheless, when light exposure is prolonged a threshold is exceeded promoting a chain of different cell death pathways. Further studies are necessary to determine the role of opsin-mediated RD processes in this model; however, we think that retinal dysfunction during the 1st days of LL (LL1-LL4) is promoted by phototransduction processes which may induce other pathways of cell death as the oxidative stress occurr. Therefore, prevention therapies with antioxidants would not completely solve RD by LED light.

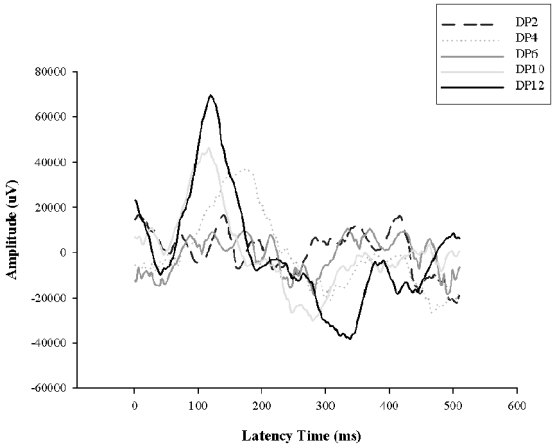

FIGURE 6 | Electroretinogram (ERG) analysis in animals exposed to dark period. Animals exposed for 8 days of constant light with dark periods of 2, 4, 6, 10 and 12 h per day during subjective night (DP 2–8); DD, constant dark. DP, dark period.

ETHICS STATEMENT

Comité Institucional de Cuidado y Uso de Animales de Laboratorio en el ámbito de la Facultad de Ciencias Químicas—CICUAL-FCQ-en los proyectos científicos -fs. 6-EXP-UNC:0007526/201 8 Number 740.

AUTHOR CONTRIBUTIONS

MB has contributed with the hypothesis, has performed the experiments, the analysis of the results and discussion. MC is the corresponding author, and had written the manuscript.

FUNDING

This work has been supported by Consejo Nacional de Investigaciones Científicas y Tecnológicas de la República Argentina (CONICET), Secretaria de Ciencia y Tecnología—Universidad Nacional de Córdoba (SeCyT-UNC) and by Agencia Nacional de Promoción Científica y Técnica (FONCyT, PICT 2012 No. 021).

ACKNOWLEDGMENTS

We are grateful to Dr Pablo Yunes, Dr Carlos R. Mas and Dr Cecilia Sampedro for technical support and Rosa Andrada for animal facility management and to Lucia Carlota Pedraza for doing the language quality check of this manuscript.

REFERENCES

Aebi, H. (1984). Catalase *in vitro*. *Methods Enzymol.* 105, 121–126. doi: 10.1016/S0076-6879(84)05016-3

Agbaga, M. P., Merriman, D. K., Brush, R. S., Lydic, T. A., Conley, S. M., Naash, M. I., et al. (2018). Differential composition of DHA and very-long-chain PUFAs in rod and cone photoreceptors. *J. Lipid Res.* 59, 1586–1596. doi: 10.1194/jlr.M082495

Anderson, R. E., and Penn, J. S. (2004). Environmental light and heredity are associated with adaptive changes in retinal DHA levels that affect retinal functionz. *Lipids* 39, 1121–1124. doi: 10.1007/s11745-004-1338-8

Asatryan, A., and Bazan, N. G. (2017). Molecular mechanisms of signaling via the docosanoid neuroprotectin D1 for cellular homeostasis and neuroprotection. *J. Biol. Chem.* 292, 12390–12397. doi: 10.1074/jbc.r117.783076

Benedetto, M. M., Guido, M. E., and Contin, M. A. (2017). Non-visual photopigments effects of constant light-emitting diode light exposure on the inner retina of Wistar rats. *Front. Neurol.* 8:417. doi: 10.3389/fneur.2017.00417

Benolken, R. M., Anderson, R. E., and Wheeler, T. G. (1973). Membrane fatty acids associated with the electrical response in visual excitation. *Science* 182, 1253–1254. doi: 10.1126/science.182.4118.1253

Berson, D. M., Dunn, F. A., and Takao, M. (2002). Phototransduction by retinal ganglion cells that set the circadian clock. *Science* 295, 1070–1073. doi: 10.1126/science.1067262

Bradford, M. M. (1976). A rapid and sensitive method for the quantitation of microgram quantities of protein utilizing the principle of protein-dye binding. *Anal. Biochem.* 72, 248–254. doi: 10.1006/abio.1976.9999

Brown, M. F. (1994). Modulation of rhodopsin function by properties of the membrane bilayer. *Chem. Phys. Lipids* 73, 159–180. doi: 10.1016/0009-3084(94)90180-5

Cai, J., Nelson, K. C., Wu, M., Sternberg, P. Jr., and Jones, D. P. (2000). Oxidative damage and protection of the RPE. *Prog. Retin. Eye Res.* 19, 205–221. doi: 10.1016/s1350-9462(99)00009-9

Chen, E. (1993). Inhibition of cytochrome oxidase and blue-light damage in rat retina. *Graefes Arch. Clin. Exp. Ophthalmol.* 231, 416–423. doi: 10.1007/bf00919652

Contín, M. A., Arietti, M. M., Benedetto, M. M., Bussi, C., and Guido, M. E. (2013). Photoreceptor damage induced by low-intensity light: model of retinal degeneration in mammals. *Mol. Vis.* 19, 1614–1625.

Dorfman, D., Aranda, M. L., González Fleitas, M. F., Chianelli, M. S., Fernandez, D. C., Sande, P. H., et al. (2014). Environmental enrichment protects the retina from early diabetic damage in adult rats. *PLoS One* 9:e101829. doi: 10.1371/journal.pone.0101829

Engler, M. M., Bellenger-Germain, S. H., Engler, M. B., Narce, M. M., and Poisson, J. P. G. (2000). Dietary docosahexaenoic acid affects stearic acid desaturation in spontaneously hypertensive rats. *Lipids* 35, 1011–1015. doi: 10.1007/s11745-000-0612-0

Fernandes, D. C., Wosniak, J., Pescatore, L. A., Bertoline, M. A., Liberman, M., Laurindo, F. R. M., et al. (2006). Analysis of DHE-derived oxidation products by HPLC in the assessment of superoxide production and NADPH oxidase activity in vascular systems. *Am. J. Physiol. Cell Physiol.* 292, C413–C422. doi: 10.1152/ajpcell.00188.2006

Fliesler, S. J., and Anderson, R. E. (1983). Chemistry and metabolism of lipids in the vertebrate retina. *Prog. Lipid Res.* 22, 79–131. doi: 10.1016/0163-7827(83)90004-8

Folch, J., Lees, M., and Sloane Stanley, G. H. (1957). A simple method for the isolation and purification of total lipides from animal tissues. *J. Biol. Chem.* 226, 497–509.

Gawrisch, K., and Soubias, O. (2008). Structure and dynamics of polyunsaturated hydrocarbon chains in lipid bilayers-significance for GPCR function. *Chem. Phys. Lipids* 153, 64–75. doi: 10.1016/j.chemphyslip.2008.02.016

Giusto, N. M., Pasquaré, S. J., Salvador, G. A., Castagnet, P. I., Roque, M. E., and Ilincheta de Boschero, M. G. (2000). Lipid metabolism in vertebrate retinal rod outer segments. *Prog. Lipid Res.* 39, 315–391. doi: 10.1016/s0163-7827(00)00009-6

Gomes, A., Fernandes, E., and Lima, J. L. (2005). Fluorescence probes used for detection of reactive oxygen species. *J. Biochem. Biophys. Methods* 65, 45–80. doi: 10.1016/j.jbbm.2005.10.003

Grimm, C., and Remé, C. E. (2013). Light damage as a model of retinal degeneration. *Methods Mol. Biol.* 935, 87–97. doi: 10.1007/978-1-62703-080-9_6

Guido, M. E., Garbarino-Pico, E., Contin, M. A., Valdez, D. J., Nieto, P. S., Verra, D. M., et al. (2010). Inner retinal circadian clocks and non-visual photoreceptors: novel players in the circadian system. *Prog. Neurobiol.* 92, 484–504. doi: 10.1016/j.pneurobio.2010.08.005

Halliwell, B. (1994). Free radicals, antioxidants, and human disease: curiosity, cause, or consequence? *Lancet* 344, 721–724. doi: 10.1016/s0140-6736(94)92211-x

Hao, W., Wenzel, A., Obin, M. S., Chen, C. K., Brill, E., Krasnoperova, N. V., et al. (2002). Evidence for two apoptotic pathways in light-induced retinal degeneration. *Nat. Genet.* 32, 254–260. doi: 10.1038/ng984

Hunter, J. J., Morgan, J. I., Merigan, W. H., Sliney, D. H., Sparrow, J. R., and Williams, D. R. (2012). The susceptibility of the retina to photochemical damage from visible light. *Prog. Retin. Eye Res.* 31, 28–42. doi: 10.1016/j.preteyeres.2011.11.001

Iusifov, E. I., Sakina, N. L., and Dontsov, A. E. (1980). Glutathione peroxidase activity of frog eye pigment epithelium. *Biokhimiia* 45, 1470–1475.

Jeffrey, B. G., Mitchell, D. C., Hibbeln, J. R., Gibson, R. A., Chedester, A. L., and Salem, N. (2002). Visual acuity and retinal function in infant monkeys fed long-chain PUFA. *Lipids* 37, 839–848. doi: 10.1007/s11745-002-0969-0

Kagan, V. E., Kuliev, I. Y., Spirichev, V. B., Shvedova, A. A., and Kozlov, Y. P. (1981). Accumulation of lipid peroxidation products and depression of retinal electrical activity in vitamin E-deficient rats exposed to high-intensity light. *Bull. Exp. Biol. Med.* 91, 144–147. doi: 10.1007/bf00835390

Kharwar, R. K., and Haldar, C. (2012). Daily variation in antioxidant enzymes and lipid peroxidation in lungs of a tropical bird Perdicula asiatica: role of melatonin and nuclear receptor RORα. *Comp. Biochem. Physiol. Part A Mol. Integr. Physiol.* 162, 296–302. doi: 10.1016/j.cbpa.2012.01.021

Lacoste, M. G., Ponce, I. T., Golini, R. L., Delgado, S. M., and Anzulovich, A. C. (2017). Aging modifies daily variation of antioxidant enzymes and oxidative status in the hippocampus. *Exp. Gerontol.* 88, 42–50. doi: 10.1016/j.exger.2016.12.002

Lai, T. Y. Y., Chu, K. O., Chan, K. P., Ng, T. K., Yam, G. H. F., Lam, D. S. C., et al. (2010). Alterations in serum fatty acid concentrations and desaturase activities in Bietti crystalline dystrophy unaffected by CYP4V2 genotypes. *Invest. Ophthalmol. Vis. Sci.* 51, 1092–1097. doi: 10.1167/iovs.09-3665

Nakamura, M., Kuse, Y., Tsuruma, K., Shimazawa, M., and Hara, H. (2017). The involvement of the oxidative stress in murine blue LED light-induced

retinal damage model. *Biol. Pharm. Bull.* 40, 1219–1225. doi: 10.1248/bpb.b16-01008

Navigatore Fonzo, L. S., Golini, R. S., Delgado, S. M., Ponce, I. T., Bonomi, M. R., Rezza, I. G., et al. (2009). Temporal patterns of lipoperoxidation and antioxidant enzymes are modified in the hippocampus of vitamin A-deficient rats. *Hippocampus* 19, 869–880. doi: 10.1002/hipo.20571

Noell, W. K., Walker, V. S., Kang, B. S., and Berman, S. (1966). Retinal damage by light in rats. *Invest. Ophthalmol.* 5, 450–473.

Ntambi, J. M. (1995). The regulation of stearoyl-CoA desaturase (SCD). *Prog. Lipid Res.* 34, 139–150. doi: 10.1016/0163-7827(94)00010-j

Ntambi, J. M. (1999). Regulation of stearoyl-CoA desaturase by polyunsaturated fatty acids and cholesterol. *J. Lipid Res.* 40, 1549–1558.

Ohta, Y., Yamasaki, T., Niwa, T., Niimi, K., Majima, Y., and Ishiguro, I. (1996). Role of catalase in retinal antioxidant defence system: its comparative study among rabbits, guinea pigs and rats. *Ophthalmic Res.* 28, 336–342. doi: 10.1159/000267925

Organisciak, D. T., and Vaughan, D. K. (2010). Retinal light damage: mechanisms and protection. *Prog. Retin. Eye Res.* 29, 113–134. doi: 10.1016/j.preteyeres.2009.11.004

Pavarino, É. C., Russo, A., Galbiatti, A. L. S., Almeida, W. P., and Goloni-Bertollo, E. M. (2013). "Glutathione: biosynthesis and mechanism of action," in *Glutathione: Biochemistry, Mechanisms of Action and Biotechnological Implications*, 1st Edn. eds N. Labrou and E. Flemetakis (New York, NY: Nova Science Publishers, Inc.), 1–34.

Peng, Y. W., Zallocchi, M., Wang, W. M., Delimont, D., and Cosgrove, D. (2011). Moderate light-induced degeneration of rod photoreceptors with delayed transducin translocation in shaker1 mice. *Invest. Ophthalmol. Vis. Sci.* 52, 6421–6427. doi: 10.1167/iovs.10-6557

Quintana, Q., Benedetto, M. L., Maldonado, M. M., Vera de Payer, E. A. C., and Contin, M. A. (2016). Electroretinography: a biopotential to assess the function/dysfunction of the retina. *J. Phys. Conf. Ser.* 705:012053. doi: 10.1088/1742-6596/705/1/012053

Rapp, L. M., and Williams, T. P. (1979). Damage to the albino rat retina produced by low intensity light. *Photochem. Photobiol.* 29, 731–733. doi: 10.1111/j.1751-1097.1979.tb07758.x

Remé, C. E., Grimm, C., Hafezi, F., Wenzel, A., and Williams, T. P. (2000). Apoptosis in the retina: the silent death of vision. *News Physiol. Sci.* 15, 120–124. doi: 10.1152/physiologyonline.2000.15.3.120

Roehlecke, C., Schumann, U., Ader, M., Brunssen, C., Bramke, S., Morawietz, H., et al. (2013). Stress reaction in outer segments of photoreceptors after blue light irradiation. *PLoS One* 8:e71570. doi: 10.1371/journal.pone.0071570

Roehlecke, C., Schumann, U., Ader, M., Knels, L., and Funk, R. H. (2011). Influence of blue light on photoreceptors in a live retinal explant system. *Mol. Vis.* 17, 876–884.

Rollag, M. D., Berson, D. M., and Provencio, I. (2003). Melanopsin, ganglion-cell photoreceptors and mammalian photoentrainment. *J. Biol. Rhythm.* 18, 227–234. doi: 10.1177/0748730403018003005

Rózanowska, M., and Sarna, T. (2005). Light-induced damage to the retina: role of rhodopsin chromophore revisited. *Photochem. Photobiol.* 81, 1305–1330. doi: 10.1562/2004-11-13-ir-371

Salas-Estrada, L. A., Leioatts, N., Romo, T. D., and Grossfield, A. (2018). Lipids alter rhodopsin function via ligand-like and solvent-like interactions. *Biophys. J.* 114, 355–367. doi: 10.1016/j.bpj.2017.11.021

SanGiovanni, J. P., and Chew, E. Y. (2005). The role of omega-3 long-chain polyunsaturated fatty acids in health and disease of the retina. *Prog. Retin. Eye Res.* 24, 87–138. doi: 10.1016/j.preteyeres.2004.06.002

Sani, M., Sebaï, H., Gadacha, W., Boughattas, N. A., Reinberg, A., and Mossadok, B. A. (2006). Catalase activity and rhythmic patterns in mouse brain, kidney and liver. *Comp. Biochem. Physiol. B Biochem. Mol. Biol.* 145, 331–337. doi: 10.1016/j.cbpb.2006.08.005

Scibior, D., and Czeczot, H. (2006). [Catalase: structure, properties, functions]. *Postepy Hig. Med. Dosw.* 60, 170–180.

Scott, B. L., and Bazan, N. G. (1989). Membrane docosahexaenoate is supplied to the developing brain and retina by the liver. *Proc. Natl. Acad. Sci. U S A* 86, 2903–2907. doi: 10.1073/pnas.86.8.2903

Semple-Rowland, S. L., and Dawson, W. W. (1987). Retinal cyclic light damage threshold for albino rats. *Lab. Anim. Sci.* 37, 289–298.

Shang, Y. M., Wang, G. S., Sliney, D., Yang, C. H., and Lee, L. L. (2014). White light-emitting diodes (LEDs) at domestic lighting levels and retinal injury in a rat model. *Environ Health Perspect.* 122, 269–276. doi: 10.1289/ehp.1307294

Shear, C. R., O'Steen, W. K., and Anderson, K. V. (1973). Effects of short-term low intensity light on the albino rat retina. An electron microscopic study. *Am. J. Anat.* 138, 127–132. doi: 10.1002/aja.1001380108

Sikka, G., Hussmann, G. P., Pandey, D., Cao, S., Hori, D., Park, J. T., et al. (2014). Melanopsin mediates light-dependent relaxation in blood vessels. *Proc. Natl. Acad. Sci. U S A* 111, 17977–17982. doi: 10.1073/pnas.1420258111

Sperling, H. G., Johnson, C., and Harwerth, R. S. (1980). Differential spectral photic damage to primate cones. *Vis. Res.* 20, 1117–1125. doi: 10.1016/0042-6989(80)90049-8

Sung, C. H., and Chuang, J. Z. (2010). The cell biology of vision. *J. Cell Biol.* 190, 953–963. doi: 10.1083/jcb.201006020

Wheeler, T. G., Benolken, R. M., and Anderson, R. E. (1975). Visual membranes: specificity of fatty acid precursors for the electrical response to illumination. *Science* 188, 1312–1314. doi: 10.1126/science.1145197

Wiegand, R. D., Giusto, N. M., Rapp, L. M., and Anderson, R. E. (1983). Evidence for rod outer segment lipid peroxidation following constant illumination of the rat retina. *Invest. Ophthalmol. Vis. Sci.* 24, 1433–1435.

Yusifov, E. Y., Kerimova, A. A., Atalay, M., and Kerimov, T. M. (2000). Light exposure induces antioxidant enzyme activities in eye tissues of frogs. *Pathophysiology* 7, 203–207. doi: 10.1016/s0928-4680(00)00051-1

Zolfaghari, R., and Ross, A. C. (2003). Recent advances in molecular cloning of fatty acid desaturase genes and the regulation of their expression by dietary vitamin A and retinoic acid. *Prostaglandins Leukot. Essent. Fatty Acids* 68, 171–179. doi: 10.1016/s0952-3278(02)00267-3

Conflict of Interest Statement: The authors declare that the research was conducted in the absence of any commercial or financial relationships that could be construed as a potential conflict of interest.

frontiers in Cellular Neuroscience

ORIGINAL RESEARCH
published: 24 April 2019
doi: 10.3389/fncel.2019.00148

Inhibition of SIRT2 by Targeting GSK3β-Mediated Phosphorylation Alleviates SIRT2 Toxicity in SH-SY5Y Cells

*Shuhu Liu†, Zhihua Zhou†, Ling Zhang, Siying Meng, Shuji Li and Xuemin Wang**

Key Laboratory of Mental Health of the Ministry of Education, Guangdong Province Key Laboratory of Psychiatric Disorders, Department of Neurobiology, School of Basic Medical Sciences, Southern Medical University, Guangzhou, China

Sirtuin 2 (SIRT2) is thought to be important in the pathogenesis of Parkinson's disease (PD), and the inhibition of SIRT2 rescues α-synuclein toxicity in a cellular model of PD. Recent studies have focused on identifying inhibitors of SIRT2, but little is known about the processes that directly regulate its function. GSK3β is a serine/threonine protein kinase that affects a wide range of biological functions, and it is localized in Lewy bodies (LBs). Therefore, we investigated whether SIRT2 is regulated by GSK3β and enhances cell death in PD. In the present study, Western blot showed that total SIRT2 levels did not change noticeably in a cellular model of PD but that SIRT2 phosphorylation was increased, and GSK3β activity was elevated. In addition, mass spectrometry (MS) studies indicated that SIRT2 was phosphorylated by GSK3β at three specific sites. Phospho- or dephospho-mimicking studies demonstrated that this postmodification (phosphorylation) increased SIRT2 toxicity in SH-SY5Y cells. Collectively, our findings identify a posttranslational mechanism that controls SIRT2 function in PD and provide evidence for a novel regulatory pathway involving GSK3β, SIRT2, and α-synuclein.

Keywords: SIRT2, GSK3β, 6-OHDA, PD, neuroprotection

OPEN ACCESS

Edited by:
Gabriela Alejandra Salvador, Universidad Nacional del Sur, Argentina

Reviewed by:
Diego Albani, Istituto Di Ricerche Farmacologiche Mario Negri, Italy
Ulkan Kilic, University of Health Sciences, Turkey

***Correspondence:**
Xuemin Wang
xmwang@fimmu.com

†These authors have contributed equally to this work

Received: *06 October 2018*
Accepted: *08 April 2019*
Published: *24 April 2019*

Citation:
Liu S, Zhou Z, Zhang L, Meng S, Li S and Wang X (2019) Inhibition of SIRT2 by Targeting GSK3β-Mediated Phosphorylation Alleviates SIRT2 Toxicity in SH-SY5Y Cells. Front. Cell. Neurosci. 13:148. doi: 10.3389/fncel.2019.00148

INTRODUCTION

Parkinson's disease (PD) is a long-term neurodegenerative disorder that mainly affects the motor system. Since it was first reported by James Parkinson in 1817 (Lees, 2007), PD has become the second most common neurodegenerative disorder (Dawson and Dawson, 2003). The disease is characterized by the loss of dopaminergic neurons in the substantia nigra, and the pathological hallmark is the accumulation of α-synuclein protein aggregates called Lewy bodies (LBs). It is believed that the number and size of α-synuclein aggregates affect the progression of PD. However, the exact molecular mechanisms that contribute to dopaminergic neuron loss remain to be clarified.

To explore the molecular mechanisms of PD, we focused on sirtuins, a family of class III nicotinamide adenine dinucleotide-dependent deacetylases that deacetylate histone and nonhistone proteins. SIRT2 is one of seven members of the sirtuin family, and it plays diverse roles in cellular metabolism and aging. SIRT2 is highly expressed in the central nervous system (Maxwell et al., 2011; Zhu et al., 2012) and is located in the cytoplasm (North et al., 2003), the nucleus (Dryden et al., 2003; North et al., 2003) and mitochondria (Liu et al., 2017). It has been reported that SIRT2 plays essential roles in PD, and SIRT2 inhibitors rescue α-synuclein-mediated toxicity (Outeiro et al., 2007; Chen et al., 2015). One SIRT2 inhibitor, AK7, even protects against MPTP neurotoxicity in

mice (Chen et al., 2015). The protective effects of SIRT2 inhibition are mediated through a number of pathways. First, SIRT2 can directly deacetylate α-synuclein to exacerbate α-synuclein toxicity *in vivo* (de Oliveira et al., 2017). Second, SIRT2 inhibition achieves neuroprotection by reducing sterol levels *via* the decreased nuclear trafficking of SREBP-2 (Luthi-Carter et al., 2010). Third, SIRT2 inhibition may be neuroprotective in PD by modulating a redox network (Wang et al., 2015; Guan et al., 2016). Although SIRT2 plays a key role in the development of PD, we still do not know how SIRT2 itself is regulated during the development of this disease. It has been reported that SIRT2 is a phosphorylation substrate of CDK5, which modulates the activity of SIRT2 (Pandithage et al., 2008). However, there have been no reports that CDK5 can regulate the activity of SIRT2 in PD. To obtain further insight into the mechanism by which SIRT2 is regulated, we sought to identify novel upstream kinases of SIRT2. GSK3β and CDK5 are two kinases at the center of research on Alzheimer's disease, and they share the same substrate (Wen et al., 2008). Therefore, we hypothesized that SIRT2 may be a substrate of GSK3β.

GSK3β is a serine/threonine protein kinase that is activated by neurotoxins (Hongo et al., 2012; Hernandez-Baltazar et al., 2013; Zhao et al., 2016) and PD-associated gene mutations (Wang et al., 2013; Kawakami et al., 2014). Additionally, in the postmortem PD brain, GSK3β is localized in LBs, as is phosphorylated GSK3β (Ser9; Nagao and Hayashi, 2009). Furthermore, in a study of a group of 251 Spanish patients with PD, Infante et al. (2010) found that a GSK3β (rs6438552) TT genotype, which has been shown to produce a more active isoform (Kwok et al., 2005), is associated with an elevated risk of PD. Thus, GSK3β is important in the development of PD. In accordance with these reports, GSK3β downregulation partially abrogates 6-OHDA-induced SH-SY5Y apoptotic cell death (Li et al., 2011) and MPP (+)-induced neuronal death (Petit-Paitel et al., 2009). These results indicate that GSK3β is a critical mediator of 6-OHDA/MPP (+)-induced neurotoxicity.

Based on the above information, we propose that SIRT2 may be phosphorylated by GSK3β during the development of PD. Here, we provide detailed insight into the mechanism through which GSK3β modulates SIRT2 activity and suggest that the phosphorylation of S327, S331 and S335 may be useful as a target for therapeutic intervention in PD.

MATERIALS AND METHODS

Materials

An MTT assay kit was purchased from Roche. A site-directed mutagenesis kit was purchased from Stratagene. 6-Hydroxydopamine hydrobromide (6-OHDA), DMSO, SB216763 (S3442, an inhibitor of GSK3β) and AGK2 (A8231, an inhibitor of SIRT2) were obtained from Sigma-Aldrich. Antibodies against pGSK3β (Ser9) and GSK3β were purchased from Cell Signaling (Danvers, MA, USA). Antibodies against SIRT2, ace-tubulin, α-tubulin, HA and Flag were purchased from Sigma-Aldrich. Secondary antibodies conjugated to Alexa 488 or Alexa 594 were purchased from Invitrogen. Hoechst 33258 (94403) was purchased from Sigma-Aldrich. Protein A/G-coated Sepharose beads were obtained from Santa Cruz Biotechnology (Dallas, TX, USA). An anti-phosphoserine/threonine/tyrosine antibody was obtained from Abcam (ab15556). Protein kinase CDK5/p25 (cat. 14—516) and GSK3β (cat. 14—306) were purchased from Millipore. Cells were transfected using Lipofectamine 2000 Transfection Reagent (Invitrogen, Thermo Fisher Scientific, Waltham, MA, USA). Other chemicals and reagents were of the highest analytical grade and were purchased from local commercial sources.

Cell Culture

The human neuroblastoma cell line SH-SY5Y was obtained from the American Type Culture Collection. The cells were grown in Dulbecco's modified Eagle's medium (DMEM)/Ham's F12 (1:1 mixture; HyClone) supplemented with 10% fetal bovine serum (GIBCO) in a 5% CO_2 incubator at 37°C. Human embryonic kidney cells (HEK293) were grown in DMEM (HyClone) supplemented with 10% FBS.

Pharmacological Treatments

6-OHDA was dissolved in phosphate-buffered saline (PBS) and used at a final concentration of 100 μM (Ikeda et al., 2008), which was the dose shown to induce 50% cell death within 24 h after 4 h of exposure. SB216763 and AGK2 were dissolved in DMSO. Before adding 6-OHDA, the SH-SY5Y cells were treated with SB216763 (Acevedo et al., 2014) or AGK2 (Outeiro et al., 2007) at a final concentration of 10 μM for 0.5 h (the DMSO content never exceeded 0.1%).

MTT Tests for Cell Viability

Cell viability was measured by a colorimetric MTT [3-(4,5-dimethylthiazol-2-yl)-2,5-diphenyltetrazolium bromide] assay. Briefly, the cells were seeded in a 96-well plate at a density of 5×10^4 cells/well. The cells were then pretreated with SB216763 for 0.5 h. After pretreatment, 6-OHDA was added to the culture medium to reach a final concentration of 100 μM. The control cells were not treated with SB216763 or 6-OHDA. The culture medium was changed after incubation for 4 h. Then, 16 h later, the MTT reagent was added to each well, and the cells were incubated for an additional 4 h. The absorbance of each reaction product was measured with a microplate reader at a wavelength of 595 nm. The results are expressed as a percentage of the MTT absorbance of the control cells, which was set to 100%.

Western Blot Analysis

Whole-cell lysates were prepared by incubating cells in RIPA buffer supplemented with a protease inhibitor cocktail (Selleck) according to the manufacturer's instructions. Briefly, the cells were harvested by centrifugation at 900 rpm for 5 min and washed in PBS (pH 7.2). The pellets were solubilized in the same volume of lysis buffer, kept on ice, vortexed for 5 min, and centrifuged at 13,000× *g* for 20 min at 4°C. Equal amounts of total lysate protein were loaded and separated on a 10% sodium dodecyl sulfate-polyacrylamide

gel electrophoresis (SDS-PAGE) gel. The proteins were electrophoretically transferred to a PVDF membrane, and the membrane was blocked in 5% skim milk in Tris-buffered saline containing 0.1% Tween-20 (TBST) for 1 h. Then, the membranes were incubated at 4°C overnight in the presence of a primary antibody against one of the following proteins: HA, Flag, SIRT2, ace-tubulin, α-tubulin (Sigma), GSK3β or pGSK3β (Ser9). Next, the membranes were washed three times with TBST every 5 min and probed with a corresponding horseradish peroxidase (HRP)-conjugated secondary antibody at room temperature for 1 h. Probe detection was conducted using enhanced ECL Advance Western Blotting Detection Reagents (Perkin Elmer, Waltham, MA, USA) and a ChemiDoc XRS+ system (Bio-Rad, Hercules, CA, USA).

Immunofluorescence Staining

Cultured cells were fixed with PBS containing 4% paraformaldehyde for 15 min, which was followed by washing and permeabilization in PBS with 0.1% Triton X-100 for 5 min. The samples were blocked in PBS with 5% BSA and incubated with primary antibodies overnight at 4°C. The following primary antibodies were used: rabbit anti-SIRT2 (1:100) and mouse anti-acetylated α-tubulin (1:50). Secondary antibodies conjugated to Alexa 488 or Alexa 594 (1:500) were applied for 1 h at room temperature. After washing with PBS and staining with DAPI for 5 min, coverslips were mounted with Mowiol. Images of the cells were acquired at room temperature on a confocal microscope (A1+; Nikon) using either a 40× or a 60× lens. Photoshop CS (Adobe) was used to adjust the contrast and brightness.

Coimmunoprecipitation

Cells were collected and lysed in buffer containing 50 mM Tris-HCl at pH 7.4, 150 mM NaCl, and 1% NP-40. All buffers were supplemented with protease and phosphatase inhibitors. The extracted proteins were precleared by incubating the lysates with Protein A/G-coated Sepharose beads for 1 h at 4°C, and then the supernatants (500 μg, 1 μg/μl) were incubated overnight with an HA or Flag antibody at 4°C. Precipitation of the immune complexes was performed with Protein A/G-coated Sepharose beads for 2 h at 4°C. After immunoprecipitation, the beads were washed five times with lysis buffer at 4°C and suspended in 40 μl of 2× loading buffer. All samples were loaded onto a gel, processed by SDS–PAGE and analyzed by Western blot. To detect SIRT2 phosphorylation, we used an anti-phosphoserine/threonine/tyrosine antibody.

Plasmids and Transfection

GSK3β-HA and SIRT2-flag were obtained from Addgene. PCMV-HA and PCMV-Tag4A are blank plasmids that contain an HA tag and a Flag tag, respectively. A subsequent LR-recombination reaction with PGEX4T3 and phMGFP plasmids resulted in GST-tagged and GFP-tagged expression constructs. Site-directed mutagenesis was performed using a Quick change protocol to generate the S327A, S331A, S335A, S327&331&335A and S327&331&335D mutants. All constructs were verified by DNA sequencing. SIRT2-targeting shRNAs using previously identified sequences (Si et al., 2013) were cloned into a pGPU6/GFP/Neo vector from Genepharma. For transient transfection, cells were transfected using Lipofectamine 2000 Transfection Reagent according to the manufacturer's instructions.

Determining the Survival Rate of Transfected Cells

SH-SY5Y cells were transfected with plasmids (GFP, GFP-SIRT2, GFP-SIRT2SA or GFP-SIRT2SD) for 24 or 48 h to induce the expression of GFP. Chromatin condensation was detected by nuclear staining with Hoechst 33258. Briefly, the cells were fixed with 4% paraformaldehyde for 15 min, stained with PBS/0.1% TritonX-100/10 μM Hoechst 33258 for 5 min, and then visualized by fluorescence microscopy. Apoptotic cells were stained bright blue because of their chromatin condensation. Images were captured from different fields of each well for different groups of cells at 20× magnification using an Olympus fluorescence microscope. The numbers of total and live transfected cells were counted from multiple fields to obtain the percentage of live transfected cells (Dutta et al., 2018).

GST Fusion Protein Purification

The GST-SIRT2 expression plasmid was transformed into competent *Escherichia coli* BL21 cells. A single colony was inoculated in LB medium at 37°C in an orbital shaker incubator until the mid-log phase. IPTG (100 μM) was added to the culture and incubated at 20°C for 8 h. Following the incubation, the culture was centrifuged at 2,500× *g* for 10 min at 4°C, and the resulting pellet was resuspended in binding buffer [50 mM Tris-Cl, pH 8.0, 150 mM NaCl and 1× protease inhibitor cocktail (Biotool)]. The cells were lysed by sonication and centrifuged at 12,000× *g* for 30 min at 4°C. After centrifugation, the supernatant was collected, incubated with GST agarose beads (Novagen) and maintained under agitation overnight at 4°C. After overnight binding, the beads were washed with wash buffer (150 mM NaCl, 50 mM Tris-Cl, pH 7.5 and 1% Triton X-100), and the bead-bound proteins were eluted and stored in 30% glycerol-containing buffer. Other GST fusion proteins were obtained in the same way.

In vitro Kinase Assays

The phosphorylation of GST-SIRT2 was performed in a final volume of 25 μl consisting of 5 mM MOPS, pH 7.2, 0.05 mM DTT, 4 mM $MgCl_2$, 80 μm ATP, 10 μCi of [γ-32P]ATP, 0.4 mM EDTA, 1 mM EGTA, and 2.5 mM β-glycerophosphate for 30 min at 30°C in the presence or absence of CDK5/p25 or GSK3β. The reaction was terminated by the addition of 25 μl of 2× sodium dodecyl sulfate (SDS) loading buffer (187 mm Tris-HCl, pH 6.8, 30% (w/v) glycerol, 6% SDS and 15% β-mercaptoethanol). The samples were then heated at 100°C for 5 min, centrifuged in a microcentrifuge, and loaded on a gel for SDS-PAGE. Following electrophoresis, the proteins were exposed to a Kodak X-ray film for autoradiography at −80°C for 2 or 3 days.

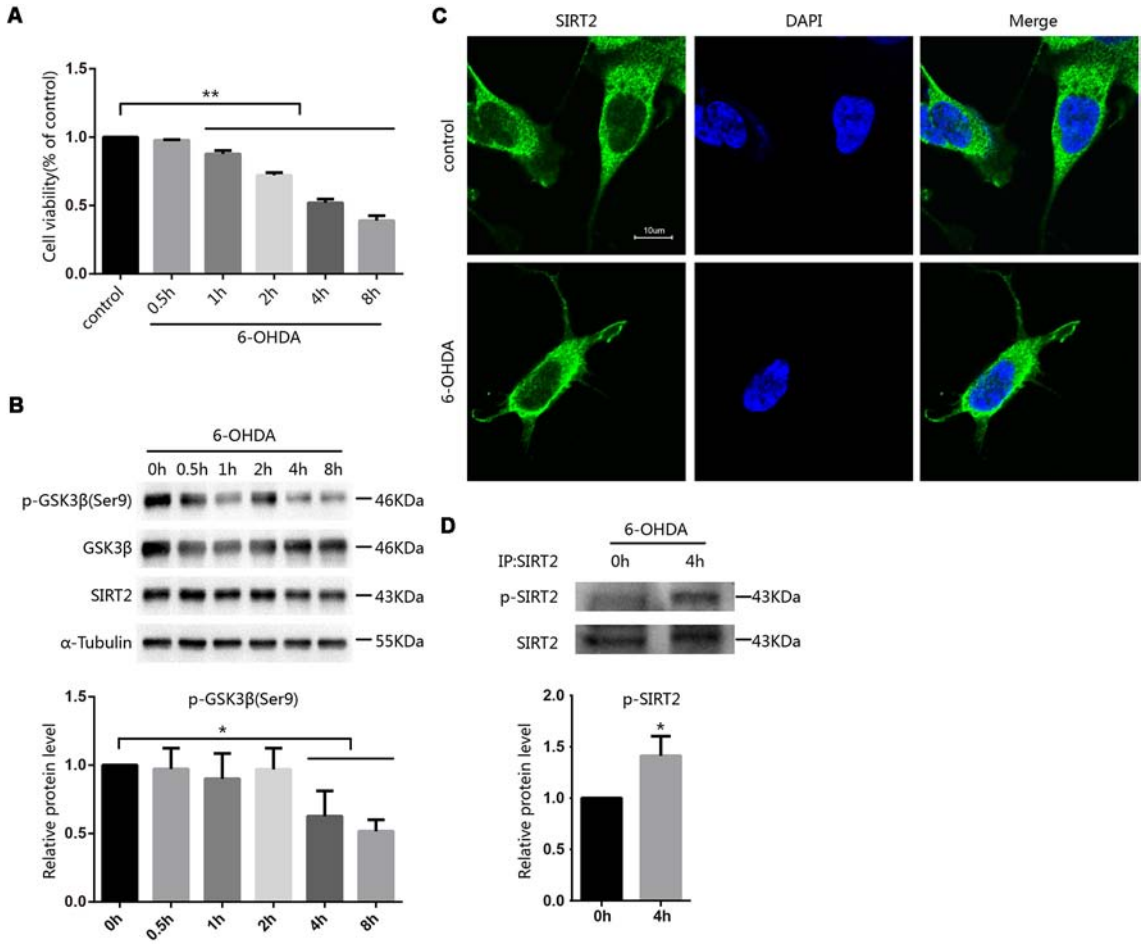

FIGURE 1 | Phosphorylation of SIRT2 increased after treatment with 6-OHDA. **(A)** SH-SY5Y cells were treated with 100 μM 6-OHDA for the indicated time. After 24 h, cell viability was measured by the MTT assay [$^{**}p < 0.01$, one-way analysis of variance (ANOVA) followed by Tukey's *post hoc* test]. **(B)** Western blot analysis showing the phosphorylation of GSK3β at Ser9 and total GSK3β, SIRT2 and α-tubulin levels in SH-SY5Y cells treated with 100 μM 6-OHDA for the indicated time. GSK3β activity was measured by detecting the phosphorylation of GSK3β at Ser9 by Western blot ($^{*}p < 0.05$, one-way ANOVA followed by Tukey's *post hoc* test; **C**). Fluorescence images representing SIRT2 immunofluorescence in phosphate-buffered saline (PBS)/6-OHDA-treated SH-SY5Y cells. Scale bar: 10 μm. **(D)** Western blot analysis showing SIRT2 phosphorylation in cells. Endogenous SIRT2 was immunoprecipitated from SH-SY5Y cells treated with or without 100 μM 6-OHDA for 4 h and probed with an anti-phosphoserine/threonine/tyrosine antibody to detect phosphorylation levels ($^{*}p < 0.05$, $^{**}p < 0.01$, two-tailed Student's *t*-test). The values are expressed as the mean ± SD, $n \geq 3$ for each group.

Phosphopeptide Identification by Mass Spectrometry (MS)

After *in vitro* phosphorylation, GST-SIRT2 was separated *via* SDS-PAGE. The gel was cut out after Coomassie blue staining, and the samples were sent to the Beijing Proteome Research Center (BPRC, China).

Statistics and Reproducibility

Statistical analysis was performed using Student's two-tailed unpaired *t*-tests for two-group comparisons and one-way analysis of variance (ANOVA) or two-way ANOVA for multigroup comparisons. P values < 0.05 were considered statistically significant and are indicated with asterisks ($^{*}P < 0.05$; $^{**}P < 0.01$; $^{***}P < 0.001$; $^{****}P < 0.0001$) in the figure legends. All of the data collected met the normal distribution assumptions of the tests. The data are represented as the mean ± SD. Each experiment was performed at least three times and in duplicate or more.

RESULTS

6-OHDA Elevates the Phosphorylation of SIRT2 in SH-SY5Y Cells

To investigate how toxins regulate SIRT2 function, we first established a cellular model of PD by applying 100 μM 6-OHDA to SH-SY5Y cells at the indicated times and concentrations and then assessed cell viability by the MTT assay. Cell viability decreased in a time-dependent manner following 6-OHDA exposure (**Figure 1A**). Further, we evaluated the expression of SIRT2 in SH-SY5Y cells after treatment with 6-OHDA, and SIRT2 levels showed a slight but not noticeable decrease. Furthermore, the active status of GSK3β was increased

(**Figure 1B**). Because SIRT2 can be distributed in the cytoplasm or nucleus under different conditions (Dryden et al., 2003; North et al., 2003; Liu et al., 2017), we wanted to know where SIRT2 is located under 6-OHDA treatment. We next treated SH-SY5Y cells with PBS as a control or 100 μM 6-OHDA for 4 h; later, the location of endogenous SIRT2 was assessed by immunofluorescence. We observed that SIRT2 resided in the cytoplasm for the duration of the experiment (**Figure 1C**). We next purified endogenous SIRT2 from SH-SY5Y cells treated with or without 6-OHDA and detected SIRT2 phosphorylation using an anti-phosphoserine/threonine/tyrosine antibody. We found that phosphorylated SIRT2 levels were significantly increased after treatment with 6-OHDA (**Figure 1D**).

The Protective Effect of GSK3β Inhibition Occurs Through a Blockade of SIRT2 Phosphorylation

Given that the activity of GSK3β was increased in SH-SY5Y cells treated with 6-OHDA, we blocked the activity of GSK3β in SH-SY5Y cells with SB216763 to determine whether this could protect the cells from 6-OHDA. We pretreated SH-SY5Y cells with different concentrations of SB216763 for 30 min and then applied 100 μM 6-OHDA for 4 h. After that, we measured cell viability and found that SB216763 rescued the SH-SY5Y cells from 6-OHDA (**Figure 2A**). We further analyzed the phosphorylation of endogenous SIRT2 among the control, 6-OHDA and 6-OHDA plus SB216763 groups and found that the phosphorylation of SIRT2 was increased in the 6-OHDA-treated cells, while SB216763 blocked the increase in SIRT2 phosphorylation (**Figure 2B**). These results indicate that GSK3β activation may be responsible for the increased phosphorylation of SIRT2.

SIRT2 is a tubulin deacetylase, and SB216763 increases the acetylation of tubulin (**Figure 2C**), which indicates that the decrease in SIRT2 phosphorylation mediated by SB216763 may reduce SIRT2 deacetylase activity. To further confirm this, we pretreated SH-SY5Y cells with DMSO, SB216763 or AGK2 and monitored the change in acetylated tubulin under 6-OHDA treatment. Acetylated tubulin levels decreased under 6-OHDA treatment, and both SB216763 and AGK2 reversed the decrease in acetylated tubulin levels (**Figure 2D**). To confirm that GSK3β participates in the regulation of SIRT2 deacetylase activity, we overexpressed PCMV-HA or GSK3β-HA in HEK293 cells and treated them with DMSO, SB216763 or AGK2 24 h later. The overexpression of GSK3β resulted in a decrease in acetylated tubulin levels, while SB216763 and AGK2 reversed the decrease in acetylated tubulin levels induced by the overexpression of GSK3β (**Figure 2E**). GSK3β further reduced acetylated tubulin levels relative to SIRT2 overexpression (the acetylated tubulin levels decreased by 23.73% and 40.65% in the absence or presence of GSK3β, respectively; **Figure 2F**). To further confirm that SIRT2 is the downstream target of GSK3β, we used shRNA to knock down endogenous SIRT2 (**Figure 2G**). We found that downregulated SIRT2 could reduce the toxicity of 6-OHDA, while SB216763 could not further improve cell viability after SIRT2 knockdown (**Figure 2H**). These data suggest that SIRT2 is the downstream target of GSK3β under 6-OHDA treatment. Taken together, our data demonstrate that 6-OHDA or the overexpression of GSK3β induces a decrease in acetylated tubulin levels and that inhibiting GSK3β with SB216763 counteracts this effect.

GSK3β Can Phosphorylate SIRT2 at Three Particular Sites

Given that inhibiting GSK3β blocked an increase in SIRT2 activity, we next tested whether SIRT2 interacts with GSK3β by coimmunoprecipitation (**Figures 3A,B**). Our results indicate that GSK3β and SIRT2 may interact in cells.

To test whether GSK3β directly phosphorylates SIRT2, we carried out an *in vitro* kinase assay. We purified GST-SIRT2 from *E. coli* BL21. Because it has been reported that SIRT2 is a phosphorylation substrate for CDK5, we used CDK5/p25 (p25 continues to activate CDK5) as a positive control. We found that GSK3β could phosphorylate SIRT2 (**Figure 3C**). To determine which sites are phosphorylated by GSK3β, we carried out an *in vitro* kinase assay followed by SDS-PAGE and Coomassie blue staining to detect phosphorylated SIRT2, which was later evaluated by MS (**Supplementary Figure S1**). Finally, we identified three sites that could be phosphorylated by GSK3β (**Figure 3D**). To validate the MS results, we mutated these three sites to alanine residues to mimic dephosphorylation. The mutants were purified from *E. coli* and subjected to the kinase assay. We found that each mutant decreased the phosphorylation of SIRT2 by GSK3β (**Figure 3E**). To further test whether the interaction between GSK3β and SIRT2 changes under 6-OHDA stress, we performed a coimmunoprecipitation assay. It was shown that the interaction between GSK3β and SIRT2 was increased under 6-OHDA treatment (**Figure 3F**). In conclusion, we identified S327, S331 and S335 as SIRT2 phosphorylation sites targeted by GSK3β.

SIRT2 Phosphorylation-Resistant Mutants Can Alleviate SIRT2 Toxicity in SH-SY5Y Cells

To further prove that the phosphorylation of SIRT2 by GSK3β does participate in 6-OHDA-induced SH-SY5Y cell death and that overactivated SIRT2 aggravates PD (Outeiro et al., 2007), we constructed two mutants, GFP-SIRT2SA and GFP-SIRT2-SD, to mimic dephosphorylation and phosphorylation, respectively (**Figure 4A**). Given that ace-tubulin is the substrate of SIRT2 (North et al., 2003), we measured the fluorescence intensity of ace-tubulin after the individual overexpression of GFP, GFP-SIRT2, GFP-SIRT2SA or GFP-SIRT2SD, and we found that the mutant that mimicked phosphorylation further decreased the acetylation of α-tubulin, while the mutant that mimicked dephosphorylation did not (**Figures 4B,C**). This result indicates that the phosphorylation-resistant mutant (GFP-SIRT2SA) blocks SIRT2 deacetylation activity. As we showed that GSK3β regulates the phosphorylation of SIRT2 and that the protective effect of blocking GSK3β in the PD cell model occurs through decreased SIRT2 phosphorylation,

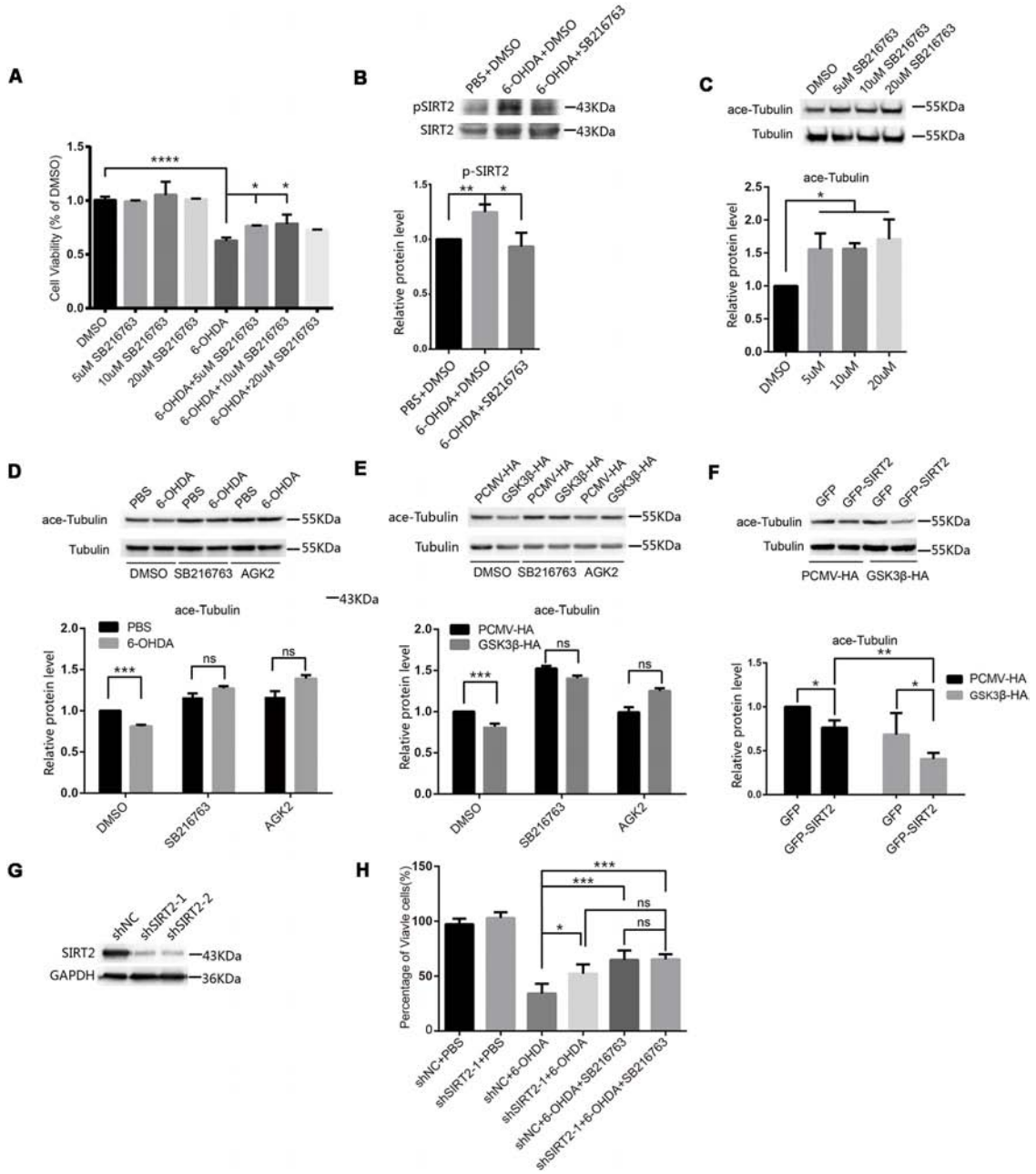

FIGURE 2 | Inhibition of GSK3β protected SH-SY5Y cells from 6-OHDA by decreasing SIRT2 phosphorylation. **(A)** SH-SY5Y cells were pretreated with different concentrations of SB216763 for 30 min and then treated with or without 100 μM 6-OHDA for 4 h. Cell viability was measured by the MTT assay (*$p < 0.05$, ****$p < 0.0001$, one-way ANOVA followed by Dunnett's *post hoc* test). **(B)** Endogenous SIRT2 was immunoprecipitated from whole-cell lysates, and p-SIRT2 was detected by an anti-phosphoserine/threonine/tyrosine antibody (*$p < 0.05$, **$p < 0.01$, one-way ANOVA followed by Tukey's *post hoc* test). **(C)** Western blot analysis showing the acetylation of α-tubulin (ace-tubulin) and total α-tubulin levels in SH-SY5Y cells treated with DMSO or SB216763 at the indicated concentrations (*$p < 0.05$, one-way ANOVA followed by Dunnett's *post hoc* test). **(D)** SH-SY5Y cells were pretreated with DMSO, 10 μM SB216763 or 10 μM AGK2 for 30 min and then treated with or without 100 μM 6-OHDA for 4 h. Ace-tubulin and α-tubulin were detected by Western blotting (***$p < 0.001$, two-way ANOVA followed by Bonferroni's *post hoc* test). **(E)** HEK293 cells were treated with DMSO, 10 μM SB216763 or 10 μM AGK2 for 30 min after transfection with PCMV-HA as a control or GSK3β-HA for 24 h. Ace-tubulin and α-tubulin were detected by Western blotting (***$p < 0.001$, two-way ANOVA followed by Bonferroni's *post hoc* test). **(F)** HEK293 cells were cotransfected with GFP (or GFP-SIRT2) and PCMV-HA (or GSK3β-HA) for 24 h. Ace-tubulin and α-tubulin were detected by Western blotting (*$p < 0.05$, **$p < 0.01$, two-way ANOVA followed by Tukey's *post hoc* test). **(G)** The level of the SIRT2 protein was downregulated in SH-SY5Y cells transfected with SIRT2 shRNA (shSIRT2-1 or shSIRT2-2) compared to cells transfected with the control (shNC). SIRT2 and GAPDH were detected by Western blotting. **(H)** A histogram representing the percentage of viable cells. Cells were transfected with shRNA for 48 h and then treated with 6-OHDA for 4 h. The percentage of viable cells was calculated after 24 h (*$p < 0.05$, **$p < 0.01$, ns, not statistically significant; one-way ANOVA followed by Tukey's *post hoc* test). The values are expressed as the mean ± SD, $n \geq 3$ for each group.

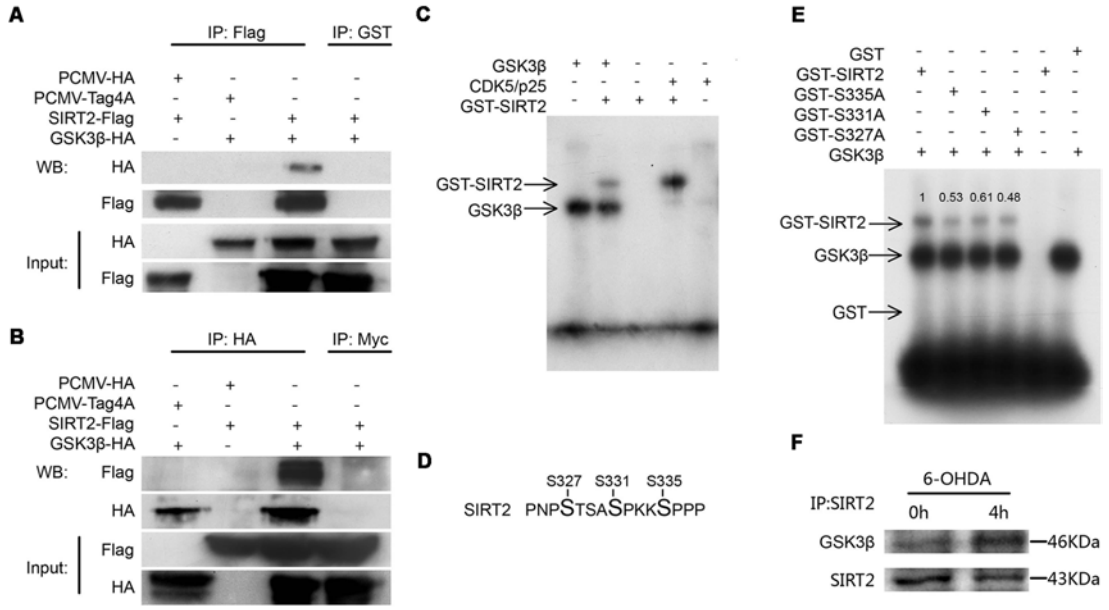

FIGURE 3 | SIRT2 could be phosphorylated by GSK3β *in vitro*. Panels **(A,B)** show the immunoprecipitation and immunoblot analyses of the interaction between SIRT2 and GSK3β in HEK293 cells expressing Flag-tagged SIRT2 or HA-tagged GSK3β. Anti-GST and anti-Myc antibodies were used as the IgG controls. **(C)** GST-SIRT2 was purified from BL21 *E. coli*, and an *in vitro* kinase assay was performed with or without GSK3β or CDK5/p25. GST-SIRT2 phosphorylation was confirmed by autoradiography. Because GSK3β is able to autophosphorylate, GSK3β bands are visible. **(D)** An *in vitro* kinase assay was performed with or without GSK3β. The samples were subjected to mass spectrometry (MS) to detect the phosphorylation of SIRT2. The S327, S331 and S335 sites were phosphorylated. **(E)** Serine was genetically mutated to alanine to mimic the dephosphorylation of the S327, S331 and S335 sites; then, the *in vitro* phosphorylation of these mutants by GSK3β was detected with autoradiography. **(F)** Endogenous SIRT2 was immunoprecipitated from SH-SY5Y cells treated with or without 100 μM 6-OHDA for 4 h. Western blotting analysis showing that the interaction between SIRT2 and GSK3β increased after treatment with 6-OHDA.

we next transfected SH-SY5Y cells with the GFP, GFP-SIRT2, GFP-SIRT2SA, or GFP-SIRT2SD plasmids for 24 h or 48 h. Cell viability was measured by live cell counting, and the data showed a notable increase in the viability of the cells overexpressing GFP-SIRT2SA (the GFP-SIRT2-overexpressing cells relative to the GFP-SIRT2SA-overexpressing cells, $^{*}P < 0.05$, $^{**}P < 0.01$), whereas there was no increase or decrease in the viability of the cells overexpressing GFP-SIRT2SD (the GFP-SIRT2-overexpressing cells relative to the GFP-SIRT2SD-overexpressing cells, $^{*}P < 0.05$, $^{***}P < 0.001$; **Figure 4D**). To assess whether AGK2 is able to block phospho-SIRT2 toxicity, we overexpressed the indicated plasmids and found that AGK2 was able to block GFP-SIRT2 toxicity but not GFP-SIRT2SD toxicity (**Figure 4E**).

These data indicate that the phosphorylation of SIRT2 by GSK3β at S327, S331 and S335 accelerates cell death. All of the data suggest that the dephosphorylation of S327, S331, and S335 decreases the activity of SIRT2, which could slow the cell death induced by SIRT2 (GFP-SIRT2) overexpression in SH-SY5Y cells.

DISCUSSION

SIRT2 appears to play a detrimental role in neurological disorders such as PD (Outeiro et al., 2007; Chen et al., 2015), Huntington's disease (Luthi-Carter et al., 2010) and ischemic stroke (Krey et al., 2015; Xie et al., 2017; She et al., 2018; Wu et al., 2018), and it is important to understand how SIRT2 is regulated since we know little about it. In the present study, we found that SIRT2 phosphorylation was increased in a cellular model of PD and that this change was mediated by the activation of GSK3β. We further identified three phosphorylation sites in SIRT2 that are targeted by GSK3β and found that a genetic mutant that mimics the dephosphorylation of SIRT2 can alleviate cell death induced by SIRT2 overexpression. Several types of evidence support this finding: (i) using Western blot analysis, we found that the phosphorylation of endogenous SIRT2 in SH-SY5Y cells is increased after treatment with 6-OHDA; (ii) SB216763, an inhibitor of GSK3β, reduced the phosphorylation of endogenous SIRT2; (iii) an *in vitro* kinase assay showed that SIRT2 is phosphorylated by GSK3β. Phosphoproteomic analysis of SIRT2 revealed that three particular sites are responsible for this phosphorylation; and (iv) genetic mutants that mimic the phosphorylation or phosphorylation resistance of the three phosphorylation sites aggravates or alleviates SIRT2-induced cell death in SH-SY5Y cells, respectively.

In this study, we first determined the subcellular location of SIRT2 under 6-OHDA treatment and found that it remains in the cytoplasm. SIRT2 regularly localizes to the cytoplasm (North et al., 2003), and it has also been reported to localize to the nucleus during the G2/M phase (Dryden et al., 2003; North et al., 2003). This prompted us to search for an upstream regulator of SIRT2 in the cytoplasm. A previous study showed that the acetylation of GSK3β increases in pathological

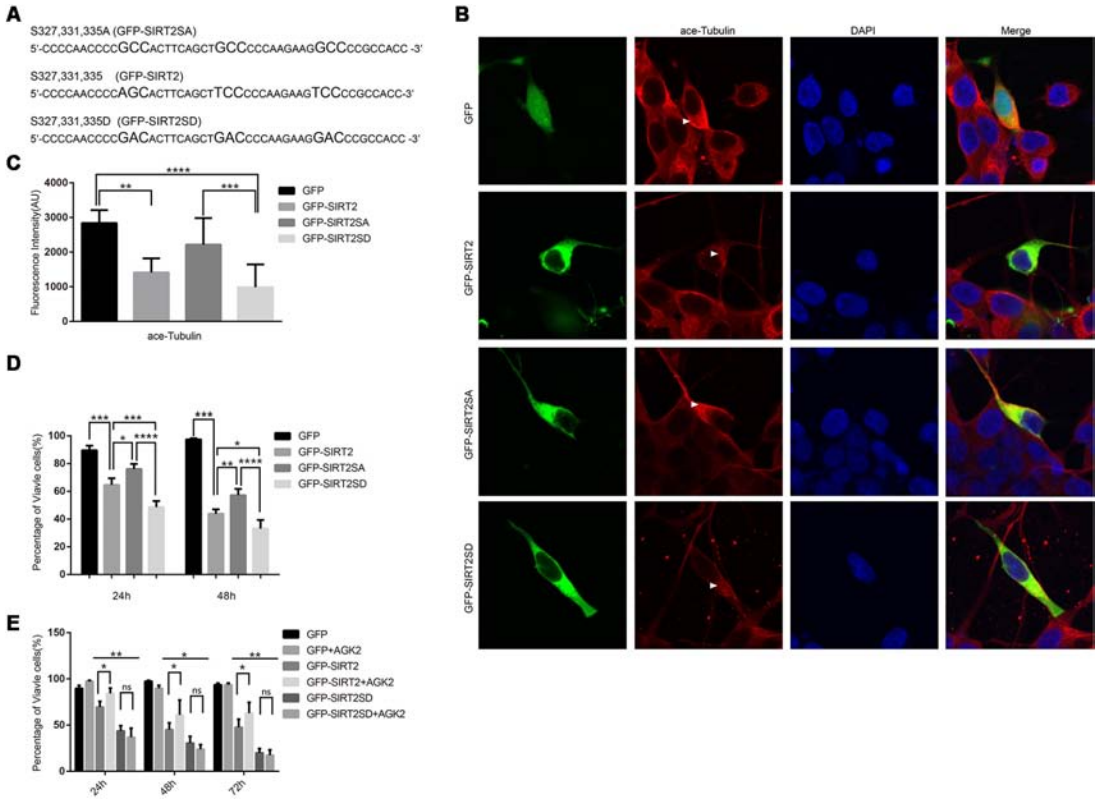

FIGURE 4 | A SIRT2 phosphorylation mimic enhanced SIRT2 cytotoxicity. **(A)** GFP-SIRT2 is the wild-type plasmid DNA sequence, GFP-SIRT2SA is the dephosphorylation mimic sequence, and GFP-SIRT2SD is the phosphorylation mimic sequence. **(B)** Fluorescence images showing ace-tubulin expression in cells transfected with GFP, GFP-SIRT2, GFP-SIRT2SA or GFP-SIRT2SD; the fluorescence intensity of ace-tubulin is shown in red (arrowheads). **(C)** A histogram representing the fluorescence intensity of ace-tubulin immunofluorescence in cells transfected with GFP, GFP-SIRT2, GFP-SIRT2SA or GFP-SIRT2SD (**$p < 0.01$, ***$p < 0.001$, ****$p < 0.0001$, one-way ANOVA followed by Tukey's *post hoc* test). **(D)** A histogram representing the percentage of viable cells. The percentage of viable cells in GFP-, GFP-SIRT2-, GFP-SIRT2SA- or GFP-SIRT2SD-transfected cells was calculated after 24 and 48 h (**$p < 0.01$, ***$p < 0.001$, ****$p < 0.0001$, two-way ANOVA followed by Tukey's *post hoc* test). **(E)** A histogram representing the percentage of viable cells. AGK2 was added after the cells were transfected for 24 h. The percentage of viable cells was calculated 24 h, 48 h and 72 h after the addition of AGK2 (*$p < 0.05$, **$p < 0.01$, two-way ANOVA followed by Tukey's *post hoc* test). The values are expressed as the mean ± SD, $n \geq 3$ for each group (*$p < 0.05$, **$p < 0.01$, ***$p < 0.005$, ns, not statistically significant; two-tailed Student's *t*-test).

cardiac hypertrophy and that SIRT2 binds to, deacetylates and activates GSK3β (Sarikhani et al., 2018). SIRT2 may also act as an upstream regulator of GSK3β to modulate the differentiation of dopaminergic neurons (Szegö et al., 2017). Here, we proposed that the increase in SIRT2 phosphorylation mediated by GSK3β affects SIRT2 catalytic activity as well. To obtain the data presented here, we used a mutant that mimics the dephosphorylation of SIRT2 (GFP-SIRT2SA) and found that it does not decrease α-tubulin acetylation, which is the opposite of what is observed with the mutant that mimics the phosphorylation of SIRT2 (GFP-SIRT2SD). Compared to GFP-SIRT2, GFP-SIRT2SA significantly increased the survival of SH-SY5Y cells. This result coincides with that of a previous study (Outeiro et al., 2007). We showed that SIRT2 phosphorylation increases after exposure to 6-OHDA, and we speculated that SIRT2 phosphorylation accelerates cell death. As expected, cell death worsened in the GFP-SIRT2SD group. Thus, the mutant that mimics the dephosphorylation of SIRT2 (GFP-SIRT2SA) can lessen the cell death induced by SIRT2 overexpression by decreasing SIRT2 deacetylase activity. All of these data suggest that there are complex regulatory relationships between SIRT2 and GSK3β.

We found that AGK2 could not inhibit GFP-SIRT2SD toxicity. This suggests that the phosphorylation sites we found here may be important for the ligand docking of AGK2. In previous studies, decreased enzymatic activity was observed in several C-terminal alanine substitution mutations, such as mutations at S327 or S331 and S335 (Nahhas et al., 2007). Interestingly, S331A and S335A individually did not affect SIRT2 enzymatic activity, but double substitutions elicited a 44% reduction in activity (Nahhas et al., 2007). These reports are consistent with our finding that GFP-SIRT2SA reduces SIRT2 deacetylation activity. In contrast, the phosphorylation of S331 or a phospho-mimicking mutant of this site also inhibits the catalytic activity of SIRT2 (Pandithage et al., 2008). This report differs from our finding that GFP-SIRT2SD does not reduce SIRT2 deacetylation activity. This may be due to the simultaneous substitution of three serine residues in SIRT2.

A preferred site for ligand binding of AGK2 is the "C-pocket" with a hydrogen-bonding pattern that mimics the action of nicotinamide, a known inhibitor of sirtuins (Outeiro et al., 2007). Since S327, S331 and S335 are located outside of the "C-pocket," these serine residues may affect the SIRT2 enzymatic activity by altering the conformation of the protein. In fact, nicotinamide blocks the activity of the phospho-mimicking mutant GST-SIRT-S331D (Pandithage et al., 2008), suggesting that AGK2 also inhibits the activity of GST-SIRT2-S331D. Similarly, we observed that AGK2 does not inhibit GFP-SIRT2SD toxicity, which may be because three simultaneous substitutions alter the conformation of the "C pocket," resulting in the failure of AGK2 docking. Our results indicate that S327, S331 and S335 can be simultaneously phosphorylated by GSK3β *in vitro*, and we are not sure whether this modification occurs *in vivo*. More experiments are needed to study this phenomenon.

Interestingly, it has been reported that CDK5 phosphorylates SIRT2 at S331 (Pandithage et al., 2008), S331 and S335 (Zhang et al., 2018), and we found that S327, S331 and S335 are phosphorylated by GSK3β. Furthermore, the phosphorylation of SIRT2 was found to be stronger after the coapplication of CDK5 and GSK3β (data not shown). These results indicate that there may be crosstalk between the GSK3β and CDK5 pathways. The data we present here suggest that phosphorylation-resistant mutants inhibit the catalytic activity of SIRT2. Nevertheless, phosphorylation by CDK5 inhibits the catalytic activity of SIRT2 (Pandithage et al., 2008). S331 is a common phosphorylation site, and the opposite effect may rely on other phosphorylation sites. Thus, targeting CDK5 and GSK3β at the same time may be a potential direction for the development of therapeutic strategies for PD. One possible approach is to block CDK5 and GSK3β simultaneously with one or two inhibitors. Using this strategy, we can obtain inactivated SIRT2 that is unphosphorylated at S327, S331 and S335. This may be the most effective strategy to suppress SIRT2 expression (Nahhas et al., 2007). There are many inhibitors currently in clinical trials that can block CDK5 and GSK3β simultaneously, such as AZD5438 and brain permeable AZD1080. Roscovitine and CHIR-99021, which are inhibitors of CDK5 and GSK3β, respectively, can also be used together. However, it is worth noting that the activities of CDK5 and GSK3β are related and that crosstalk depends on age (Engmann and Giese, 2009). In young mice, an increase in p25-induced CDK5 activity inhibits GSK3β activity by enhancing inhibitory phosphorylation at Ser-9 of GSK3β (Plattner et al., 2006). However, in older mice, GSK3β activity is enhanced in p25 transgenic mice (Plattner et al., 2006; Wen et al., 2008). Thus, the reaction of young and aged mice to the simultaneous targeting of CDK5 and GSK3β may be different.

As aging is considered a major risk factor for the development of PD, the pathways involved in aging may provide targets for therapeutic interventions for PD. SIRT2 is a member of the sirtuin family of proteins, which participate in a variety of cellular functions and play a role in aging (Maxwell et al., 2011). Outeiro et al. (2007) found that the inhibition of SIRT2 rescues α-synuclein toxicity and modifies inclusion morphology in a cellular model of PD (Dillin and Kelly, 2007; Garske et al., 2007). Later, de Oliveira et al. (2017) showed that α-synuclein is deacetylated by SIRT2 and that α-synuclein acetylation is a key regulatory mechanism governing α-synuclein aggregation and toxicity. Here, we further characterized SIRT2, showing that its activity is activated by its phosphorylation by GSK3β in a cellular model of PD. Based on the above conclusions, we elucidated a complete GSK3β-SIRT2-α-synuclein signaling cascade that participates in the development of PD. Because of the importance of α-synuclein in PD, we believe this cascade may play a vital role in PD. We may find treatments that inhibit the progression of PD by targeting this cascade.

Taken together, the data presented here highlight a previously unexplored cellular pathway that might underlie the impairment of dopaminergic neurons in PD, further underscoring the potential of the GSK3β-SIRT2-α-synuclein signaling cascade as a viable target pathway for neuroprotective therapies.

AUTHOR CONTRIBUTIONS

XW designed the experiments. SL and ZZ performed the enzyme activity assays and the biochemical analysis of the SH-SY5Y cells. LZ, SM and SLi analyzed the data. SL and ZZ wrote the manuscript with help from XW. All authors read and approved the final manuscript.

FUNDING

This work was supported by the Natural Science Foundation of Guangdong (2016A030311009), the National Natural Science Foundation of China (31371184), and the Program for Changjiang Scholars and the Innovative Research Team in University (IRT_16R37).

SUPPLEMENTARY MATERIAL

The Supplementary Material for this article can be found online at: https://www.frontiersin.org/articles/10.3389/fncel.2019.00148/full#supplementary-material

FIGURE S1 | Phosphopeptide identification by mass spectrometry (MS). **(A)** GST-SIRT2 was purified from BL21 *E. coli*, and an *in vitro* kinase assay was performed with or without GSK3β. The samples were separated *via* SDS-PAGE, and then the gel was visualized with Coomassie blue staining. The band in the red rectangle was subjected to MS. **(B)** The serine residues in red are the predicted phosphorylated sites.

REFERENCES

Acevedo, K. M., Opazo, C. M., Norrish, D., Challis, L. M., Li, Q. X., White, A. R., et al. (2014). Phosphorylation of amyloid precursor protein at threonine 668 is essential for its copper-responsive trafficking in SH-SY5Y neuroblastoma cells. *J. Biol. Chem.* 289, 11007–11019. doi: 10.1074/jbc.m113.538710

Chen, X., Wales, P., Quinti, L., Zuo, F., Moniot, S., Herisson, F., et al. (2015). The sirtuin-2 inhibitor AK7 is neuroprotective in models of Parkinson's disease but not amyotrophic lateral sclerosis and

cerebral ischemia. *PLoS One* 10:e0116919. doi: 10.1371/journal.pone.0116919

Dawson, T. M., and Dawson, V. L. (2003). Molecular pathways of neurodegeneration in Parkinson's disease. *Science* 302, 819–822. doi: 10.1126/science.1087753

de Oliveira, R. M., Vicente Miranda, H., Francelle, L., Pinho, R., Szegö, E. M., Martinho, R., et al. (2017). The mechanism of sirtuin 2-mediated exacerbation of α-synuclein toxicity in models of Parkinson disease. *PLoS Biol.* 15:e2000374. doi: 10.1371/journal.pbio.2000374

Dillin, A., and Kelly, J. W. (2007). Medicine. The yin-yang of sirtuins. *Science* 317, 461–462. doi: 10.1126/science.1146585

Dryden, S. C., Nahhas, F. A., Nowak, J. E., Goustin, A. S., and Tainsky, M. A. (2003). Role for human SIRT2 NAD-dependent deacetylase activity in control of mitotic exit in the cell cycle. *Mol. Cell. Biol.* 23, 3173–3185. doi: 10.1128/mcb.23.9.3173-3185.2003

Dutta, D., Ali, N., Banerjee, E., Singh, R., Naskar, A., Paidi, R. K., et al. (2018). Low levels of prohibitin in substantia nigra makes dopaminergic neurons vulnerable in Parkinson's disease. *Mol. Neurobiol.* 55, 804–821. doi: 10.1007/s12035-016-0328-y

Engmann, O., and Giese, K. P. (2009). Crosstalk between Cdk5 and GSK3β: implications for Alzheimer's disease. *Front. Mol. Neurosci.* 2:2. doi: 10.3389/neuro.02.002.2009

Garske, A. L., Smith, B. C., and Denu, J. M. (2007). Linking SIRT2 to Parkinson's disease. *ACS Chem. Biol.* 2, 529–532. doi: 10.1021/cb700160d

Guan, Q., Wang, M., Chen, H., Yang, L., Yan, Z., and Wang, X. (2016). Aging-related 1-methyl-4-phenyl-1,2,3,6-tetrahydropyridine-induced neurochemial and behavioral deficits and redox dysfunction: improvement by AK-7. *Exp. Gerontol.* 82, 19–29. doi: 10.1016/j.exger.2016.05.011

Hernandez-Baltazar, D., Mendoza-Garrido, M. E., and Martinez-Fong, D. (2013). Activation of GSK-3β and caspase-3 occurs in Nigral dopamine neurons during the development of apoptosis activated by a striatal injection of 6-hydroxydopamine. *PLoS One* 8:e70951. doi: 10.1371/journal.pone.0070951

Hongo, H., Kihara, T., Kume, T., Izumi, Y., Niidome, T., Sugimoto, H., et al. (2012). Glycogen synthase kinase-3β activation mediates rotenone-induced cytotoxicity with the involvement of microtubule destabilization. *Biochem. Biophys. Res. Commun.* 426, 94–99. doi: 10.1016/j.bbrc.2012.08.042

Ikeda, Y., Tsuji, S., Satoh, A., Ishikura, M., Shirasawa, T., and Shimizu, T. (2008). Protective effects of astaxanthin on 6-hydroxydopamine-induced apoptosis in human neuroblastoma SH-SY5Y cells. *J. Neurochem.* 107, 1730–1740. doi: 10.1111/j.1471-4159.2008.05743.x

Infante, J., García-Gorostiaga, I., Sánchez-Juan, P., Sierra, M., Martín-Gurpegui, J. L., Terrazas, J., et al. (2010). Synergistic effect of two oxidative stress-related genes (heme oxygenase-1 and GSK3β) on the risk of Parkinson's disease. *Eur. J. Neurol.* 17, 760–762. doi: 10.1111/j.1468-1331.2009.02908.x

Kawakami, F., Shimada, N., Ohta, E., Kagiya, G., Kawashima, R., Maekawa, T., et al. (2014). Leucine-rich repeat kinase 2 regulates tau phosphorylation through direct activation of glycogen synthase kinase-3β. *FEBS J.* 281, 3–13. doi: 10.1111/febs.12579

Krey, L., Lühder, F., Kusch, K., Czech-Zechmeister, B., Könnecke, B., Fleming Outeiro, T., et al. (2015). Knockout of silent information regulator 2 (SIRT2) preserves neurological function after experimental stroke in mice. *J. Cereb. Blood Flow Metab.* 35, 2080–2088. doi: 10.1038/jcbfm.2015.178

Kwok, J. B., Hallupp, M., Loy, C. T., Chan, D. K., Woo, J., Mellick, G. D., et al. (2005). GSK3B polymorphisms alter transcription and splicing in Parkinson's disease. *Ann. Neurol.* 58, 829–839. doi: 10.1002/ana.20691

Lees, A. J. (2007). Unresolved issues relating to the shaking palsy on the celebration of James Parkinson's 250th birthday. *Mov. Disord.* 22, S327–334. doi: 10.1002/mds.21684

Li, Y., Luo, F., Wei, L., Liu, Z., and Xu, P. (2011). Knockdown of glycogen synthase kinase 3 β attenuates 6-hydroxydopamine-induced apoptosis in SH-SY5Y cells. *Neurosci. Lett.* 487, 41–46. doi: 10.1016/j.neulet.2010.09.070

Liu, G., Park, S. H., Imbesi, M., Nathan, W. J., Zou, X., Zhu, Y., et al. (2017). Loss of NAD-dependent protein deacetylase sirtuin-2 alters mitochondrial protein acetylation and dysregulates mitophagy. *Antioxid. Redox Signal.* 26, 849–863. doi: 10.1089/ars.2016.6662

Luthi-Carter, R., Taylor, D. M., Pallos, J., Lambert, E., Amore, A., Parker, A., et al. (2010). SIRT2 inhibition achieves neuroprotection by decreasing sterol biosynthesis. *Proc. Natl. Acad. Sci. U S A* 107, 7927–7932. doi: 10.1073/pnas.1002924107

Maxwell, M. M., Tomkinson, E. M., Nobles, J., Wizeman, J. W., Amore, A. M., Quinti, L., et al. (2011). The Sirtuin 2 microtubule deacetylase is an abundant neuronal protein that accumulates in the aging CNS. *Hum. Mol. Genet.* 20, 3986–3996. doi: 10.1093/hmg/ddr326

Nagao, M., and Hayashi, H. (2009). Glycogen synthase kinase-3β is associated with Parkinson's disease. *Neurosci. Lett.* 449, 103–107. doi: 10.1016/j.neulet.2008.10.104

Nahhas, F., Dryden, S. C., Abrams, J., and Tainsky, M. A. (2007). Mutations in SIRT2 deacetylase which regulate enzymatic activity but not its interaction with HDAC6 and tubulin. *Mol. Cell. Biochem.* 303, 221–230. doi: 10.1007/s11010-007-9478-6

North, B. J., Marshall, B. L., Borra, M. T., Denu, J. M., and Verdin, E. (2003). The human Sir2 ortholog, SIRT2, is an NAD+-dependent tubulin deacetylase. *Mol. Cell* 11, 437–444. doi: 10.1016/s1097-2765(03)00038-8

Outeiro, T. F., Kontopoulos, E., Altmann, S. M., Kufareva, I., Strathearn, K. E., Amore, A. M., et al. (2007). Sirtuin 2 inhibitors rescue α-synuclein-mediated toxicity in models of Parkinson's disease. *Science* 317, 516–519. doi: 10.1126/science.1143780

Pandithage, R., Lilischkis, R., Harting, K., Wolf, A., Jedamzik, B., Lüscher-Firzlaff, J., et al. (2008). The regulation of SIRT2 function by cyclin-dependent kinases affects cell motility. *J. Cell Biol.* 180, 915–929. doi: 10.1083/jcb.200707126

Petit-Paitel, A., Brau, F., Cazareth, J., and Chabry, J. (2009). Involvment of cytosolic and mitochondrial GSK-3β in mitochondrial dysfunction and neuronal cell death of MPTP/MPP-treated neurons. *PLoS One* 4:e5491. doi: 10.1371/journal.pone.0005491

Plattner, F., Angelo, M., and Giese, K. P. (2006). The roles of cyclin-dependent kinase 5 and glycogen synthase kinase 3 in tau hyperphosphorylation. *J. Biol. Chem.* 281, 25457–25465. doi: 10.1074/jbc.M603469200

Sarikhani, M., Mishra, S., Maity, S., Kotyada, C., Wolfgeher, D., Gupta, M. P., et al. (2018). SIRT2 deacetylase regulates the activity of GSK3 isoforms independent of inhibitory phosphorylation. *Elife* 7:e32952. doi: 10.7554/elife.32952

She, D. T., Wong, L. J., Baik, S. H., and Arumugam, T. V. (2018). SIRT2 inhibition confers neuroprotection by downregulation of FOXO3a and MAPK signaling pathways in ischemic stroke. *Mol. Neurobiol.* 55, 9188–9203. doi: 10.1007/s12035-018-1058-0

Si, X., Chen, W., Guo, X., Chen, L., Wang, G., Xu, Y., et al. (2013). Activation of GSK3β by Sirt2 is required for early lineage commitment of mouse embryonic stem cell. *PLoS One* 8:e76699. doi: 10.1371/journal.pone.0076699

Szegö, É. M., Gerhardt, E., and Outeiro, T. F. (2017). Sirtuin 2 enhances dopaminergic differentiation via the AKT/GSK-3β/β-catenin pathway. *Neurobiol. Aging* 56, 7–16. doi: 10.1016/j.neurobiolaging.2017.04.001

Wang, X., Guan, Q., Wang, M., Yang, L., Bai, J., Yan, Z., et al. (2015). Aging-related rotenone-induced neurochemical and behavioral deficits: role of SIRT2 and redox imbalance and neuroprotection by AK-7. *Drug Des. Devel. Ther.* 9, 2553–2563. doi: 10.2147/dddt.s81539

Wang, Y., Liu, W., He, X., and Zhou, F. (2013). Parkinson's disease-associated DJ-1 mutations increase abnormal phosphorylation of tau protein through Akt/GSK-3β pathways. *J. Mol. Neurosci.* 51, 911–918. doi: 10.1007/s12031-013-0099-0

Wen, Y., Planel, E., Herman, M., Figueroa, H. Y., Wang, L., Liu, L., et al. (2008). Interplay between cyclin-dependent kinase 5 and glycogen synthase kinase 3 β mediated by neuregulin signaling leads to differential effects on tau phosphorylation and amyloid precursor protein processing. *J. Neurosci.* 28, 2624–2632. doi: 10.1523/JNEUROSCI.5245-07.2008

Wu, D., Lu, W., Wei, Z., Xu, M., and Liu, X. (2018). Neuroprotective effect of Sirt2-specific inhibitor AK-7 against acute cerebral ischemia is P38 activation-dependent in mice. *Neuroscience* 374, 61–69. doi: 10.1016/j.neuroscience.2018.01.040

Xie, X. Q., Zhang, P., Tian, B., and Chen, X. Q. (2017). Downregulation of NAD-dependent deacetylase SIRT2 protects mouse brain against ischemic stroke. *Mol. Neurobiol.* 54, 7251–7261. doi: 10.1007/s12035-016-0173-z

Zhang, Z., Zhang, P., Qi, G. J., Jiao, F. J., Wang, Q. Z., Yan, J. G., et al. (2018). CDK5-mediated phosphorylation of Sirt2 contributes to depressive-like behavior induced by social defeat stress. *Biochim. Biophys. Acta Mol. Basis Dis.* 1864, 533–541. doi: 10.1016/j.bbadis.2017.11.012

Zhao, Q., Ye, J., Wei, N., Fong, C., and Dong, X. (2016). Protection against MPP^+-induced neurotoxicity in SH-SY5Y cells by tormentic acid via the activation of PI3-K/Akt/GSK3β pathway. *Neurochem. Int.* 97, 117–123. doi: 10.1016/j.neuint.2016.03.010

Zhu, H., Zhao, L., Wang, E., Dimova, N., Liu, G., Feng, Y., et al. (2012). The QKI-PLP pathway controls SIRT2 abundance in CNS myelin. *Glia* 60, 69–82. doi: 10.1002/glia.21248

Conflict of Interest Statement: The authors declare that the research was conducted in the absence of any commercial or financial relationships that could be construed as a potential conflict of interest.

frontiers in Cellular Neuroscience

ORIGINAL RESEARCH
published: 24 April 2019
doi: 10.3389/fncel.2019.00154

Lipopolysaccharide-Induced Autophagy Mediates Retinal Pigment Epithelium Cells Survival. Modulation by the Phospholipase D Pathway

Vicente Bermúdez[1,2], *Paula Estefanía Tenconi*[1,2], *Norma María Giusto*[1,2] *and Melina Valeria Mateos*[1,2]*

[1]*Instituto de Investigaciones Bioquímicas de Bahía Blanca (INIBIBB), Consejo Nacional de Investigaciones Científicas y Técnicas (CONICET), Bahía Blanca, Argentina,* [2]*Departamento de Biología, Bioquímica y Farmacia (DBByF), Universidad Nacional del Sur (UNS), Bahía Blanca, Argentina*

Inflammation and oxidative stress are common factors involved in the pathogenesis of retinal diseases, such as aged-related macular degeneration (AMD) and diabetic retinopathy (DR). Autophagy is a catabolic process essential to cell survival in response to stress. This process is highly active in retinal pigment epithelium (RPE) cells. Our previous findings demonstrated that lipopolysaccharide (LPS) induces an inflammatory response of RPE cells that implies classical phospholipases D (PLD1 and 2) activation, cyclooxygenase-2 (COX-2) expression, prostaglandin E_2 (PGE_2) production and reduced cell viability. In this work, we studied the autophagic process and its modulation by the PLD pathway in D407 and ARPE-19 RPE cells exposed to LPS. LPS (10 μg/ml or 25 μg/ml) exposure for 24 h increased light chain 3B-II (LC3B-II) content (an autophagy marker) and LC3B-positive punctate structures in both RPE cell lines studied. Next, the drug bafilomycin A_1 (BAF, 50 nM) was used to block the autophagic flux. In cells pre-incubated with BAF, LC3B-II and sequestosome 1 (SQSTM1/p62) levels and autophagosome-like structures were increased by LPS, demonstrating that the inflammatory injury increases the autophagic process in RPE cells. To study the role of the PLD pathway, cells were pre-incubated for 1 h with selective PLD1 (VU0359595) or PLD2 (VU0285655-1) inhibitors prior to LPS addition. Under control condition, LC3B-positive punctate structures were increased in cells pre-incubated with PLD2 inhibitor while with PLD1 inhibitor were increased in cells exposed to LPS. MTT reduction assays showed that early autophagy inhibitors, 3-methyladenin (3-MA) or LY294002, enhanced the loss in cell viability induced by LPS exposure for 48 h. On the contrary, the inhibition of PLD1 and PLD2 prevented the loss in cell viability induced by LPS. In conclusion, our results show that even though LPS treatment promotes

OPEN ACCESS

Edited by:
Mario Eduardo Guido, Center for Research in Biological Chemistry Córdoba (CIQUIBIC), Argentina

Reviewed by:
Rafael Linden, Federal University of Rio de Janeiro, Brazil
Maria Del Carmen Fernandez, Universidad de Buenos Aires, Argentina

***Correspondence:**
Melina Valeria Mateos
mvmateos@inibibb-conicet.gob.ar; melinavaleriamateos@gmail.com

Received: *02 January 2019*
Accepted: *08 April 2019*
Published: *24 April 2019*

Citation:
Bermúdez V, Tenconi PE, Giusto NM and Mateos MV (2019) Lipopolysaccharide-Induced Autophagy Mediates Retinal Pigment Epithelium Cells Survival. Modulation by the Phospholipase D Pathway. Front. Cell. Neurosci. 13:154. doi: 10.3389/fncel.2019.00154

Abbreviations: 3-MA, 3-methyladenine; BAF, bafilomycin A_1; BECN1, beclin1; COX-2, cyclooxygenase-2; DAG, diacylglycerol; ERK, extracellular signal-regulated kinase; HRP, horseradish peroxidase; LC3, microtubule-associated protein 1 light chain 3; LPS, lipopolysaccharide; LPPs, lipid phosphate phosphatases; mTOR, mammalian target of rapamycin; NFκB, nuclear factor kappa B; RAP, rapamycin; SQSTM1/p62, sequestosome 1; PA, phosphatidic acid; PC, phosphatidylcholine; PGs, prostaglandins; PKC, protein kinase C; PKD, protein kinases D; PLD, phospholipase D; POS, photoreceptor outer segments; PR, photoreceptor; PVDF, polyvinylidene fluoride; RasGRP, Ras guanine-releasing protein; RPE, retinal pigment epithelium; WB, western blot.

an inflammatory response in RPE cells, it also triggers the activation of the autophagic process which in turn may serve as a protective mechanism for the cells. In addition, we demonstrate that the PLD pathway modulates the autophagic process in RPE cells. Our findings contribute to the knowledge of the molecular basis of retinal inflammatory and degenerative diseases and open new avenues for potential therapeutic exploration.

Keywords: retinal pigment epithelium, lipopolysaccharide, autophagy, inflammation, phospholipase D

INTRODUCTION

The retinal pigment epithelium (RPE) is a monolayer of pigmented epithelial cells located between the retina and the vascular choroid, constituting the outer blood-retinal barrier (BRB). These epithelial cells play various critical roles for the correct function of the neural retina and photoreceptor (PR) survival, such as the secretion of several growth factors and cytokines and the transport of nutrients and water to the retina. Also, they protect against photo-oxidation and mediate the re-isomerization of all-trans-retinal and the renewal of photoreceptor outer segments (POS) by phagocytosis (Strauss, 2005; Strauß, 2016; Carr et al., 2009). Being a fundamental part in the BRB, RPE cells contribute to establishing the immunological privilege of the eye (Simó et al., 2010; Perez et al., 2013; Pavan et al., 2014). Likewise, RPE mediates in the immune response of the retina, by secreting pro- and anti-inflammatory cytokines, chemoattractants proteins, adhesion molecules and complement factors (Strauss, 2005; Strauß, 2016; Simó et al., 2010; Viringipurampeer et al., 2013).

Inflammation is a key factor in the pathogenesis of several retinal diseases such as age-related macular degeneration (AMD), diabetic retinopathy (DR), retinitis pigmentosa and uveitis, ultimately leading to varying degrees of vision loss (Shen et al., 2000; Rodrigues, 2007; Leung et al., 2009; Kauppinen et al., 2016). The inflammatory response is characterized by a series of reactions, including vasodilation and recruitment of immune cells and plasma proteins to the site of infection or tissue injury (Medzhitov, 2008; Ahmed, 2011; Liu et al., 2017). Inflammation can be both a protective and adaptive response while its deregulation can cause excessive or long-lasting tissue damages, contributing to the development of chronic inflammatory diseases (Medzhitov, 2008; Ahmed, 2011; Whitcup et al., 2013; Liu et al., 2017). It has been demonstrated that RPE cells can participate in the inflammatory response observed in several retinal degenerative diseases through the modification of its secretome (Arjamaa et al., 2017; Datta et al., 2017; Willermain et al., 2018). In view of the essential role of the RPE in PR viability and in visual function, elucidating the molecular mechanisms elicited by inflammation in this tissue could provide new insights for the treatment of retinal diseases.

Previous work from our laboratory demonstrated that the human RPE cell line ARPE-19 expresses both classical phospholipase D isoforms (PLD1 and PLD2) and that lipopolysaccharide (LPS) stimulates PLD activity (Mateos et al., 2014). Classical PLDs hydrolyze phosphatidylcholine (PC) to generate the lipid second messenger phosphatidic acid (PA) and choline (Exton, 2002; Foster and Xu, 2003; Peng and Frohman, 2012; Frohman, 2015). PA can be further dephosphorylated by lipid phosphate phosphatases (LPPs) in order to generate diacylglycerol (DAG), another lipid messenger (Brindley, 2004; Brindley et al., 2009). DAG and PA, as bioactive lipids, can modulate the activity of various proteins involved in cell signaling events, such as protein kinases C (PKC), protein kinase D (PKD), and the mammalian target of rapamycin (mTOR) complex, among others (Wang, 2006; Carrasco and Mérida, 2007; Newton, 2010; Foster et al., 2014). Through the modulation of these signaling proteins, DAG and PA participate in various cellular processes, such as vesicular trafficking, endo and exocytosis and cell survival.

Our previous study constituted the first evidence of classical PLDs participation in the LPS-induced inflammatory response of RPE cells through extracellular signal-regulated kinase (ERK1/2) activation and cyclooxygenase-2 (COX-2) expression (Mateos et al., 2014). Furthermore, we showed that PLD1 plays a dual role in LPS-exposed RPE cells, on the one hand by promoting cell damage through COX-2 induction and on the other by preventing LPS-induced apoptotic signals through PKCε modulation (Tenconi et al., 2016).

Autophagy is a conserved lysosomal self-digestion process ubiquitous in eukaryotic cells that respond to stress conditions, allowing them to adapt to environmental and developmental changes (Klionsky, 2007). Autophagy is initiated by the formation of double membrane-bound vesicles, called autophagosomes, which sequester cytoplasmic material. Finally, the fusion of autophagosomes with lysosomes allows the degradation of autophagic cargo and the subsequent recycling of nutrients and membranes (Yang and Klionsky, 2010). Autophagy is highly active in RPE and PR, being responsible for the lysosomal degradation and recycling of proteins and organelles (Wang et al., 2009). As a recycling process, autophagy has been described as a cellular pro-survival process, although other evidence indicates that under certain circumstances it may conduct to programmed cell death (Ferrington et al., 2016; Montagna et al., 2016; Deretic and Klionsky, 2018). Recently, evidences relating autophagy and inflammation have been described that may lead to therapeutic targeting (Netea-Maier et al., 2016), also in the RPE (Liu et al., 2016). Within the kinases that regulate the onset of autophagy, mTOR is the most important since the active mTORC1 complex prevents the formation of autophagosomes (Saxton and Sabatini, 2017).

Taking into account: (i) the participation of classical PLDs in the LPS-induced inflammatory process in RPE cells through ERK1/2 activation; (ii) the role the latter performs in mTOR regulation (Wang et al., 2017); and (iii) the role of PA and DAG signaling in autophagy (Dall'Armi et al., 2013), PLD possible participation in the regulation of the autophagic process in RPE cells exposed to an inflammatory context was further explored in the present work.

In view of the above, this study aims at arriving at a better understanding of the role of PA- and DAG-mediated signaling pathways in RPE cells exposed to inflammatory conditions.

MATERIALS AND METHODS

Reagents

Triton X-100 (octyl phenoxy polyethoxyethanol), dimethyl sulfoxide (DMSO), LPS from *Klebsiella pneumoniae* (LPS, L4268), LY294002 (2-(4-Morpholinyl)-8-phenyl-1(4H)-benzopyran-4-one hydrochloride) and MTT (3-(4,5-dimethylthiazol-2-yl)-2, 5-diphenyltetrazolium bromide) were from Sigma-Aldrich (St. Louis, MO, USA). VU0359595 (PLD1i) and VU0285655-1 (PLD2i) were from Avanti Polar Lipids, Inc. (Alabaster, AL, USA). 4′,6-diamidino-2-phenylindole dihydrochloride (DAPI) was from Life Technologies Corporation (Grand Island, NY, USA). 3-methyladenine (3-MA), rapamycin (RAP) and bafilomycin A_1 (BAF) were from Santa Cruz Biotechnology, Inc. (Santa Cruz, CA, USA). 5(6)-carboxy-2′7′-dichlorodihydrofluorescein diacetate (DCDCDHF), TO-PRO™-3 Iodide and DAPI were from Molecular Probes (Eugene, OR, USA). All other chemicals were of the highest purity available.

Antibodies

Rabbit polyclonal antibody anti-light chain 3B (anti-LC3B; #2775) was from Cell Signaling (Beverly, MA, USA). Mouse monoclonal anti-SQSTM1/p62 (sc-28359) and rabbit polyclonal anti-nuclear factor kappa B (anti-NFκB) p65 (sc-109) antibody were purchased from Santa Cruz Biotechnology, Inc. (Santa Cruz, CA, USA). Mouse monoclonal anti-α Tubulin (DM1-A; CP06) was from EMD/Biosciences-Calbiochem (San Diego, CA, USA). Polyclonal horse radish peroxidase (HRP)-conjugated sheep anti-mouse IgG (NA931V) and polyclonal HRP-conjugated donkey anti-rabbit IgG (NA934V) were purchased from GE Healthcare (Malborough, MA, USA). Alexa Fluor®488 goat anti-rabbit (A11008) and Alexa Fluor®488 goat anti-mouse (A11001) were from Life Technologies Corporation (Grand Island, NY, USA).

Retinal-Pigmented Epithelium Cell Cultures and Treatments

Two human retinal-pigmented epithelium cell lines (ARPE-19 and D407) were used in this work. ARPE-19 cells from the American Type Culture Collection (ATCC, Manassas, VA, USA) were generously donated by Dr. E. Politi and Dr. N. Rotstein (INIBIBB, Bahía Blanca, Argentina). D407 cells were a generous gift from Dr E. Rodriguez-Bouland (Weill Medical College of Cornell University, New York, NY, USA). ARPE-19 cells were maintained in Dulbecco's Modified Eagle's Medium (DMEM) supplemented with 10% fetal bovine serum (FBS, Natocor, Córdoba, Argentina) and antibiotic-antimycotic (Anti-Anti 100×, Gibco by Life Technologies) at 37°C under 5% CO_2. D407 cells were maintained in 5% FBS DMEM. For western blot (WB) assays, cells were grown to 100% confluence on plastic 35 mm diameter culture dishes. Cell cultures were serum-starved for 30 min prior to LPS treatment with different concentrations (10 or 25 μg/ml) in serum-free DMEM or the same volume of sterile ultra pure water (control condition), for 24 or 48 h. LPS stock (4 mg/ml) was prepared in sterile ultra-pure water. Cells were pre-incubated with different concentrations (0.5 or 5 μM) of VU0359595 (PLD1i) to inhibit PLD1 activity or with different concentrations (0.5 or 5 μM) of VU0285655-1 (PLD2i) to inhibit PLD2 activity for 30 min at 37°C prior to cell stimulation with LPS. To inhibit the autophagic process cells were pre-incubated with 3-MA (5 mM) or with LY294002 (10 μM) for 30 min prior to LPS treatment. To block autophagosome fusion with lysosomes cells were pre-incubated with BAF (50 nM) for 30 min at 37°C prior to LPS treatment. As a positive control, cells were treated with the mammalian target of rapamycin complex 1 (mTORC1) inhibitor rapamycin (RAP, 1 μM) for 24 h in order to induce autophagy. DMSO (vehicle of the inhibitors) was added to all conditions to achieve a final concentration of 0.05%.

MTT Reduction Assay

Cell viability was measured in terms of mitochondrial function. D407 cells (1.5×10^4 cells/well) were seeded in 96-well plates. Cells were pre-incubated with different inhibitors as described above and after a 48 h LPS treatment, mitochondrial function was assessed by MTT reduction assay. MTT is reduced by mitochondrial dehydrogenases of metabolically viable cells to a colored, water-insoluble formazan salt. MTT (5 mg/ml) was prepared in phosphate buffer saline (PBS) and was added to the cell culture medium at a final concentration of 0.5 mg/ml. The culture plates were incubated for 1 h at 37°C in a 5% CO_2 atmosphere, cells were then washed twice with PBS and lysed with 100 μl of a buffer containing 10% Triton X-100 and 0.1N HCl in isopropanol. The extent of MTT reduction was measured spectrophotometrically (570 nm absorbance–650 nm absorbance) using a Multiskan™ 60 microplate spectrophotometer (Thermo Fisher Scientific, Waltham, MA, USA). Results are expressed as arbitrary units (AUs) with respect to the control condition.

Western Blot (WB)

WB assays were performed as previously described (Mateos et al., 2014). Briefly, after experimental treatment the medium was removed from confluent 35 mm dishes, cells were washed with PBS and scraped off with 80 μl ice-cold RIPA lysis buffer [10 mM Tris-HCl (pH 7.4), 15 mM NaCl, 1% Triton X-100, 5 mM NaF, 1 mM Na_2VO_4 and the complete protease inhibitor cocktail]. Protein content of total cell lysates was determined by the Bradford method (Bradford, 1976; Bio-Rad Life Science group, Hercules, CA, USA, #500-0006) and samples were denatured with Laemmli sample buffer at

100°C for 5 min (Laemmli, 1970). Thirty micrograms protein were separated by sodium dodecylsulfate polyacrylamide gel electrophoresis (SDS-PAGE) on 10% or 16% polyacrylamide gels and transferred to polyvinylidene fluoride (PVDF) membranes (Millipore, Bedford, MA, USA). Membranes were blocked with 10% bovine serum albumin (BSA) in TTBS buffer [20 mM Tris–HCl (pH 7.4), 100 mM NaCl and 0.1% (w/v) Tween 20] at room temperature for 2 h and subsequently incubated with primary antibodies overnight at 4°C. After three washes with TTBS, membranes were exposed to the appropriate HRP-conjugated secondary antibody for 2 h at room temperature. Immunoreactive bands were detected by enhanced chemiluminescence (Pierce®ECL Western Blotting Substrate, #32209, Thermo scientific) using UltraCruz# Autoradiography Film, Santa Cruz Biotechnology, Inc. (Santa Cruz, CA, USA). Densitometry values of the immunoreactive bands were determined using ImageJ 1.46 software (NIH). The molecular weight of bands was determined using the spectra multicolor broad range protein ladder (26634, Thermo Scientific).

Measurement of Reactive Oxygen Species (ROS) Production

Reactive oxygen species (ROS) production was measured using the probe DCDCDHF (Molecular Probes, Eugene, OR, USA). This probe can cross the membrane and, after oxidation, it is converted into a fluorescent compound. 6×10^4 D407 cells were seeded onto 12 mm coverslips and exposed to LPS (10 μg/ml) or to control condition for 24 h. After the experimental treatment, the cell culture medium was removed and replaced by medium containing 10 μM DCDCDHF and cells were incubated for 30 min at 37°C. Cells were subsequently washed three times with PBS and coverslips were mounted for examination with a Nikon Eclipse TE2000-S microscope coupled to a Nikon DS-Qi2 camera (1,608 × 1,608 pixels) and a 60× Plan Apo (1.4 N.A.) oil-immersion objective. Fluorescence intensity values were determined using ImageJ 1.46 software.

Immunocytochemistry and Fluorescence Microscopy

For immunocytochemistry assays, 6×10^4 cells were seeded onto 12 mm coverslips on 24-well plates. After LPS treatment (10 or 25 μg/ml) for 24 h cells were washed twice with ice-cold PBS and fixed with methanol for 15 min at −20°C. Cells were then blocked with 2% BSA in PBS for 15 min and exposed to primary anti-LC3B antibody (1:200 in blocking solution), anti-p62 (1:100 in blocking solution) or anti-NFκB p65 (1:100 in blocking solution). Cells were then exposed to the appropriate Alexa Fluor®488-conjugated secondary antibodies (1:500 in blocking solution). Finally, nuclei were stained with DAPI or TO-PRO-3 for 10 min at room temperature. The whole immunocytochemical method was performed at room temperature and three washes with ice-cold PBS were performed between each step of the procedure and after nuclear staining. Coverslips were mounted for examination with a Nikon Eclipse TE2000-S microscope coupled to a Nikon DS-Qi2 camera (1,608 × 1,608 pixels) and a 60× Plan Apo (1.4 N.A.) oil-immersion objective or with a TCS-SP2 confocal microscope (Leica Mikrosysteme Vertrieb GmbH, Wetzlar, Germany) equipped with an acousto optical beam splitter using a 63× (1.2 N.A.) objective. Fluorescence intensity values were determined using ImageJ 1.46 software.

Data Quantification and Statistical Analysis

In immunocytochemistry images, the percentage of cells with LC3B- or p62- positive punctate structures was manually scored by a blinded operator. With this aim, at least 100 cells of each condition were counted. Data shown in bar graphs represent the percentage mean value ± SD of four independent experiments (n = 4). Fluorescence intensity values from immunocytochemistry images and densitometry values of the WB immunoreactive bands were determined using ImageJ 1.46 software. WBs shown are representative images of samples from four independent experiments (n = 4).

Statistical analysis of the data was performed using ANOVA followed by Tuckey's test to compare means or Student's t-test when only two conditions were compared. p-values lower than 0.05 were considered statistically significant.

RESULTS

LPS Induces NFκB Nuclear Translocation, ROS Generation and Reduces Cell Viability in D407 RPE Cells

Our previous results demonstrated that the exposure of ARPE-19 cells to LPS induces an inflammatory response that engages NO production, PLD activation, COX-2 expression, prostaglandin E2 (PGE_2) secretion and reduced cell viability (Mateos et al., 2014). To further characterize the inflammatory response of RPE cells induced by LPS, immunocytochemistry assays were performed in order to evaluate NFκB translocation to the nucleus. In addition, ROS generation was evaluated by using the probe DCDCDHF.

In D407 cells exposed to LPS (10 μg/ml) for 24 h epifluorescence microscope images show an increment in NFκB (p65) nuclear translocation (by 60%) and ROS generation (by 220%) with respect to control condition (**Figures 1A,B**). Similar results were obtained when p65 nuclear translocation was observed by confocal microscopy (**Supplementary Figure S1**). Our previous findings in ARPE-19 cells showed that cell viability was affected only after a 48 h exposure to LPS (Mateos et al., 2014). Similar results were obtained in D407 RPE cells, in which cell viability was reduced by 15% and by 27% in cells exposed to 10 and 25 μg/ml for 48 h, respectively (**Figure 1C**). These results together with our previous findings demonstrate that LPS treatment induces a typical inflammatory response of RPE cells. Taking all these data into account, we next used both RPE cell lines (D407 and ARPE-19) to study the role of the autophagic process in the LPS-induced RPE inflammatory response.

LPS Exposure Induces an Increment in LC3-II Content in RPE Cells

To study the effect of LPS on the autophagic process of RPE cells, D407 cells were exposed to LPS (10 or 25 μg/ml) for 24 or

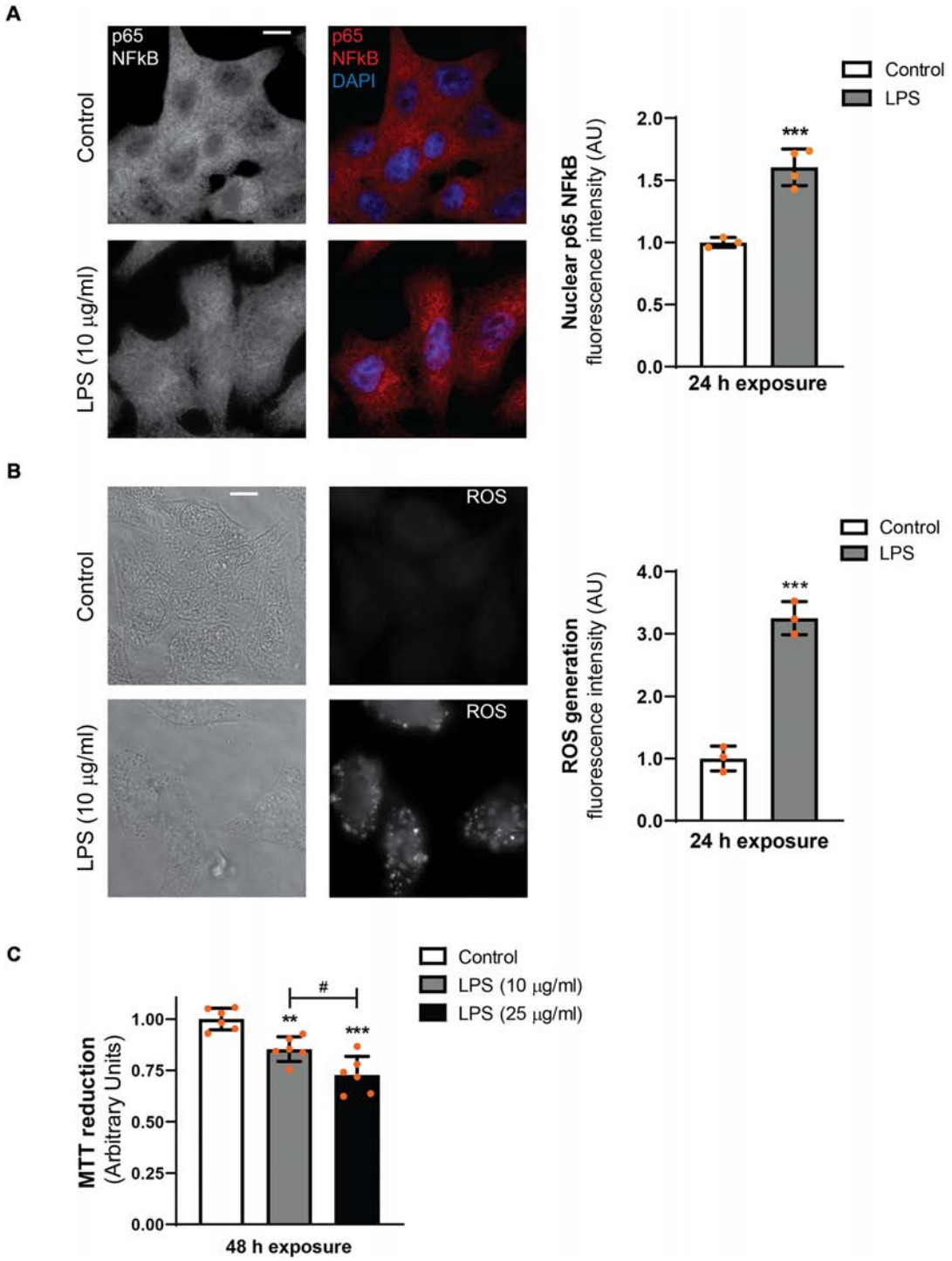

FIGURE 1 | Lipopolysaccharide (LPS) inflammatory model in D407 cells. **(A)** Immunofluorescence assays for analysis of nuclear factor kappa B (NFκB; p65) subcellular distribution were performed as described in "Materials and Methods" section in D407 cells exposed to LPS (10 μg/ml) or to control condition (ultrapure water) for 24 h. Results are expressed as arbitrary units (AU). **(B)** Reactive oxygen species (ROS) generation was analyzed in D407 cells treated with LPS (10 μg/ml) or under control condition (ultrapure water) for 24 h as detailed in "Materials and Methods" section. Left panel show light microscopy images of the cells. For **(A,B)**, bar graph shows fluorescence intensity expressed as arbitrary units with respect to control conditions (mean ± SD). Dots indicate individual values of different experiments ($n \geq 3$). Asterisks (*) indicate significant differences with respect to control condition (***$p < 0.0001$). Scale bar = 10 μm. **(C)** Cell viability was evaluated using the MTT reduction assay in D407 cells treated with LPS (10 or 25 μg/ml) or ultrapure water (control condition) for 48 h. Results are expressed as arbitrary units. Dots indicate individual values from six different experiments ($n = 6$). Asterisks (*) indicate significant differences with respect to control condition (**$p < 0.001$; ***$p < 0.0001$). Number signs (#) indicate significant differences between LPS conditions ($^{\#}p < 0.05$).

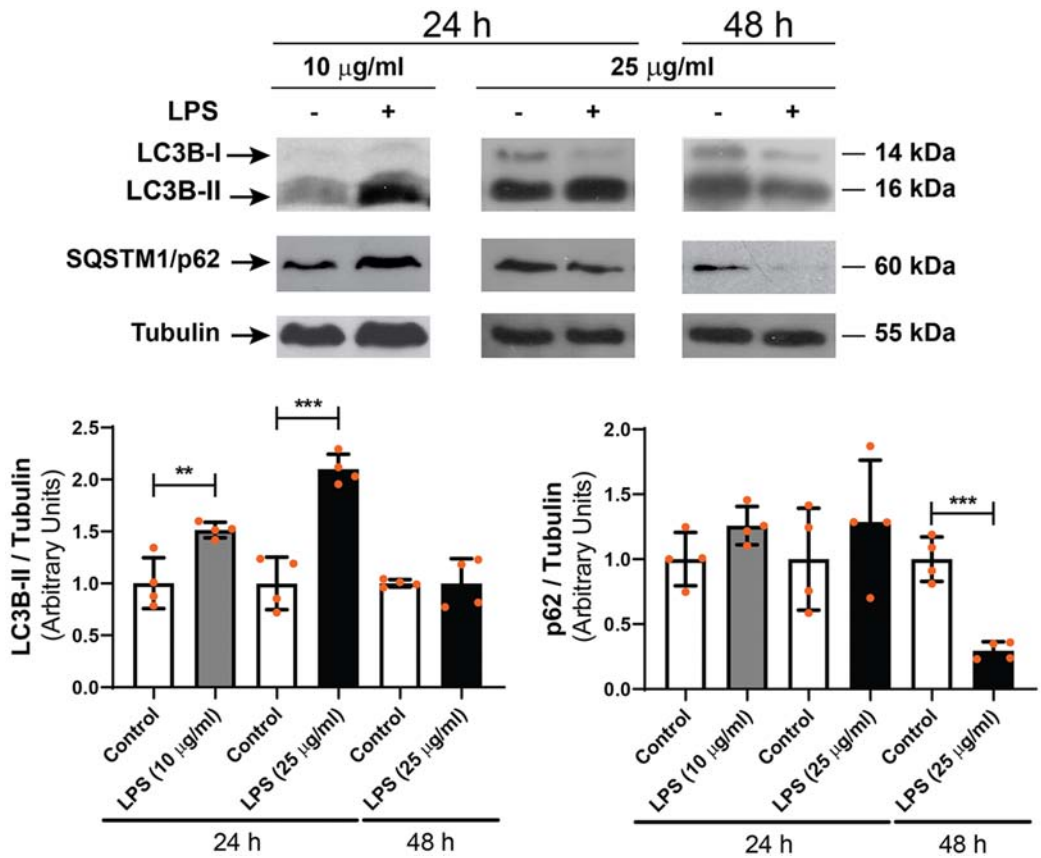

FIGURE 2 | Western blot (WB) assays were performed in order to determine light chain 3B-II (LC3B-II) and p62 levels in D407 cells exposed to LPS (10 or 25 μg/ml) or to control condition (ultrapure water), for 24 or 48 h. Numbers to the right indicate molecular weights designated by standard markers. Bar graphs show the densitometry values of LC3B-II/α-Tubulin or p62/α-Tubulin. Results are expressed as arbitrary units. Dots indicate individual values from four independent experiments ($n = 4$). Asterisks (*) indicate significant differences with respect to each control condition (**$p < 0.01$; ***$p < 0.0001$).

48 h and WB assays were performed in order to determine microtubule-associated protein 1 light chain 3B-II (LC3B-II) and sequestosome 1 (SQSTM1/p62) levels. WB showed that 10 and 25 μg/ml LPS increased LC3B-II content by 51% and by 100% with respect to control condition after 24 h treatment, respectively (**Figure 2**). No changes in LC3B-II content were detected after a 48 h exposure to LPS (25 μg/ml; **Figure 2**). SQSTM1/p62 content was not significantly changed after 24 h treatment with both LPS concentrations but was reduced by 70% after a 48 h LPS exposure (**Figure 2**).

In order to study the subcellular distribution of autophagy markers LC3B and p62, immunocytochemistry assays were performed as described in "Materials and Methods" section. **Figure 3** shows that LPS (10 or 25 μg/ml) treatment for 24 h increased LC3B-positive punctate structures in D407 cells (**Figure 3A**) and similar results were observed in ARPE-19 cells exposed to 25 μg/ml LPS for 24 h (**Supplementary Figure S2**). Under control condition, 22% of D407 cells presented LC3B-positive punctate structures and this percentage raised to 58% in cells treated with 10 μg/ml LPS and to 73% in cells treated with 25 μg/ml LPS (**Figure 3A**). The mTORC1 inhibitor rapamycin (RAP, 1 μM) was used as positive control (**Figure 3A**) and no significant differences were detected in LC3B-punctate structure formation between cells incubated with or without FBS (data not shown). Furthermore, larger LC3B-punctate structures were observed in D407 cells exposed to 25 μg/ml LPS with respect to cells exposed to 10 μg/ml LPS (**Figure 3A**). Although WB assays showed no significant changes in p62 content after a 24 h exposure to LPS (**Figure 2**), immunocytochemistry assays showed that a 24 h LPS (10 μg/ml) treatment increases significantly the percentage of D407 cells with p62-positive punctate structures (**Figure 3B**). These results demonstrate that LPS enhances autophagosome-like structures formation in RPE cells.

In view of our results, most of the following experiments were performed with 10 μg/ml LPS since this concentration induced an inflammatory-like response in RPE cells and increased LC3B-II content and autophagosome-like structures formation with fewer effects on cell metabolic state and viability.

To discern whether LPS treatment induces the autophagic process or blocks the autophagic flux, D407 cells were pre-incubated with BAF (50 nM) in order to block autophagosome fusion with lysosomes and thus, autolysosome formation, prior to LPS (10 μg/ml) treatment for 24 h.

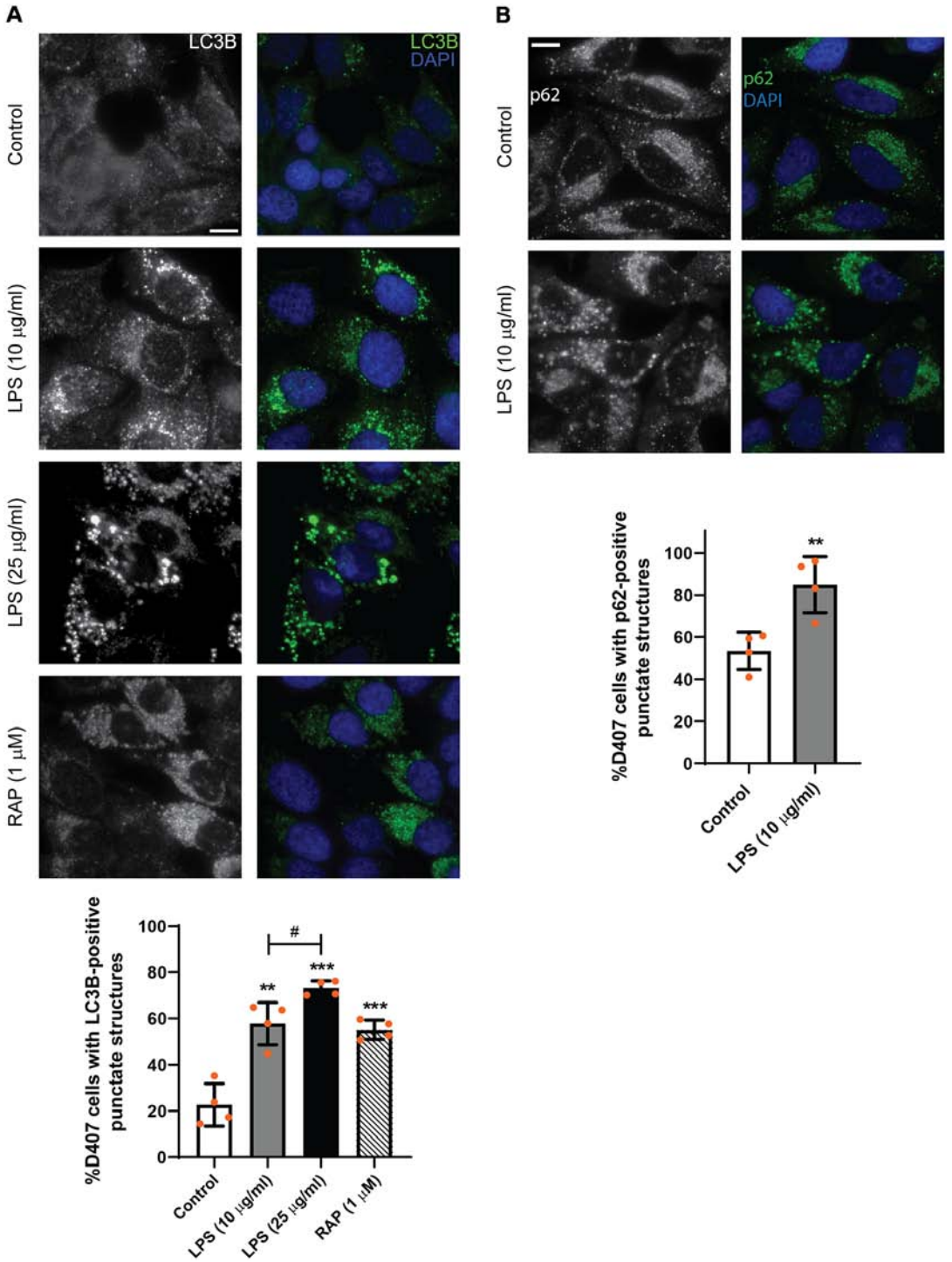

FIGURE 3 | Immunofluorescence assays of D407 cells were performed as described in "Materials and Methods" section. **(A)** LC3B-positive punctate structures were analyzed in D407 cells exposed to LPS (10 or 25 μg/ml) or to control condition (vehicle). The mTORC1 inhibitor rapamycin (RAP, 1 μM) was used as positive control. Bar graph shows the percentage of cells presenting LC3B-positive punctate structures in each condition. Cells showing punctate structures similar or bigger to those observed in RAP condition were considered positives. Graph shows the mean percentage ± SD. Dots indicate individual values from four independent experiments ($n = 4$). **(B)** p62-positive punctate structures were analyzed in D407 cells exposed to LPS (10 μg/ml) or to control condition (ultrapure water) for 24 h. Bar graph shows the % of cells presenting p62-positive punctate structures in each condition. Graph shows the mean percentage ± SD. Dots indicate individual values from four independent experiments ($n = 4$). For **(A,B)**, cells were stained with DAPI to visualize the nuclear structure. Scale bar = 10 μm. Asterisks (*) indicate significant differences with respect to control condition (**$p < 0.01$; ***$p < 0.001$). Number signs (#) indicate significant differences between LPS conditions ($^{\#}p < 0.05$).

In D407 cells, the blockage of the autophagic flux with BAF increased to 86 the percentage of cells with LC3B-positive punctate structures (**Figures 4A,C**) and to 98 the percentage of cells with p62-positive punctate structures under control condition (**Figures 4B,C**). 100% of the cells pre-incubated with BAF and exposed to LPS for 24 h presented LC3B-positive punctae and p62-positive punctae (**Figures 4A–C**). In addition, WBs showed that pre-incubation with BAF induces an increment

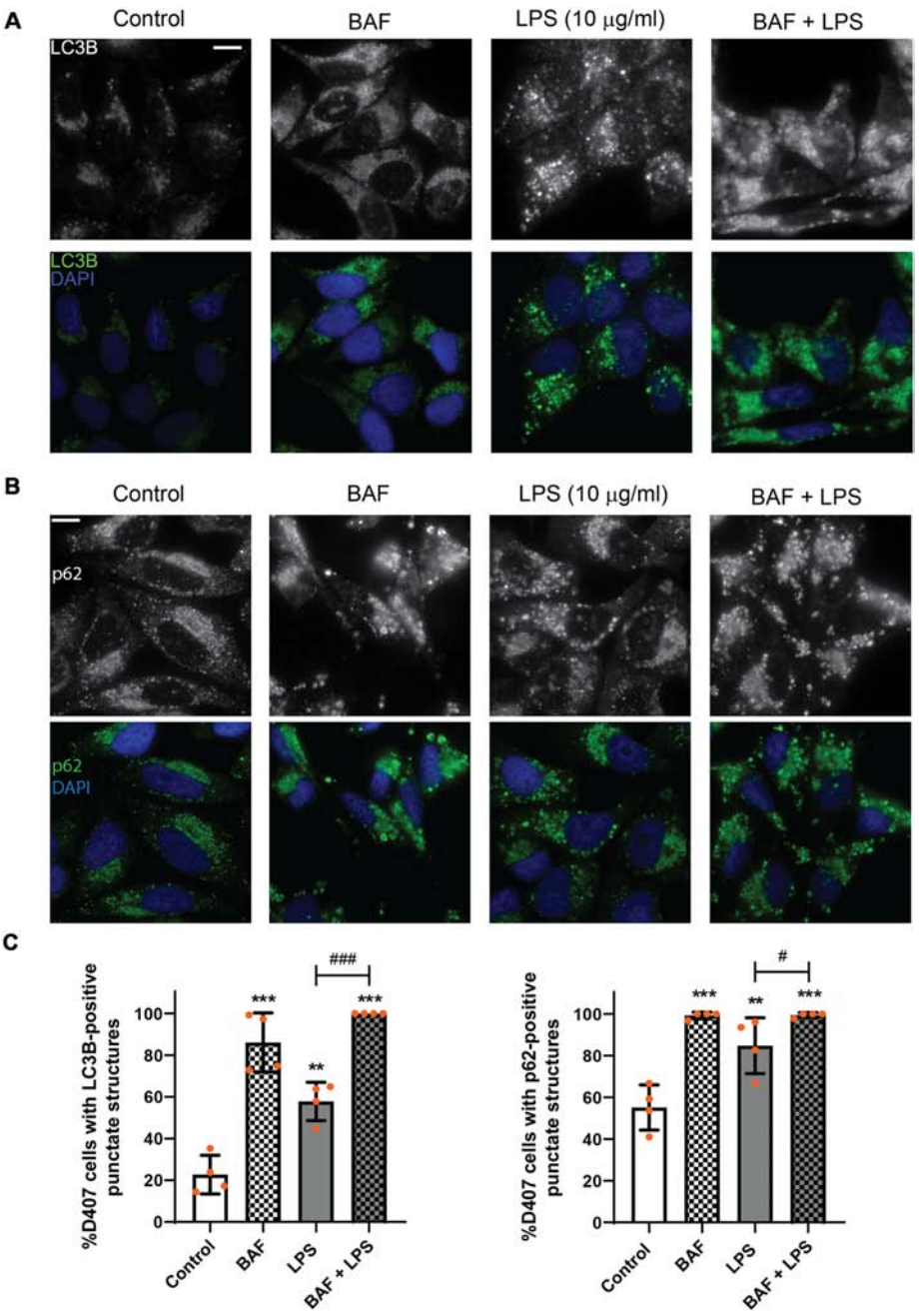

FIGURE 4 | Evaluation of autophagic flux in LPS treated retinal pigment epithelium (RPE) cells. RPE cells were pre-incubated with bafilomycin A_1 (BAF, 50 nM) or with vehicle dimethyl sulfoxide (DMSO) prior to incubation with LPS (10 μg/ml) or under control condition for 24 h. **(A,B)** Immunofluorescence assays were performed in D407 cells as described in "Materials and Methods" section to determine LC3B-positive **(A)** and p62-positive **(B)** punctate structures. Cells were stained with 4′,6-diamidino-2-phenylindole (DAPI) to visualize the nuclear structure. Scale bar = 10 μm. **(C)** Bar graphs show the percentage of cells presenting LC3B- or p62-positive punctate structures in each condition. Graphs show the mean percentage ± SD. Dots indicate individual values from four independent experiments ($n = 4$). Asterisks (*) indicate significant differences with respect to control condition (**$p < 0.01$; ***$p < 0.001$). Number signs (#) indicate significant differences between indicated conditions ($^{\#}p < 0.05$; $^{\#\#\#}p < 0.001$).

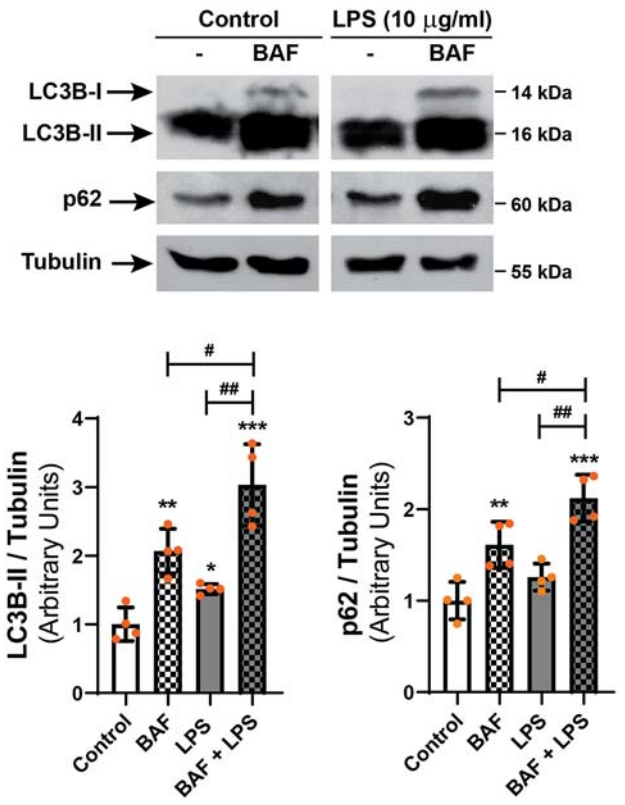

FIGURE 5 | D407 cells were pre-incubated with BAF (50 nM) or with vehicle (DMSO) prior to incubation with LPS (10 μg/ml) or under control condition for 24 h. WBs were performed and analyzed as described in "Materials and Methods" section in order to determine LC3B-II and p62 levels. Numbers to the right indicate molecular weights designated by standard markers. Bar graphs show the densitometry values of LC3B-II/α-Tubulin or p62/α-Tubulin. Dots indicate individual values from four independent experiments ($n = 4$). Results are expressed as arbitrary units. Asterisks (*) indicate significant differences with respect to each control condition ($^{*}p < 0.05$; $^{**}p < 0.01$; $^{***}p < 0.001$). Number signs (#) indicate significant differences between indicated conditions ($^{\#}p < 0.05$; $^{\#\#}p < 0.01$).

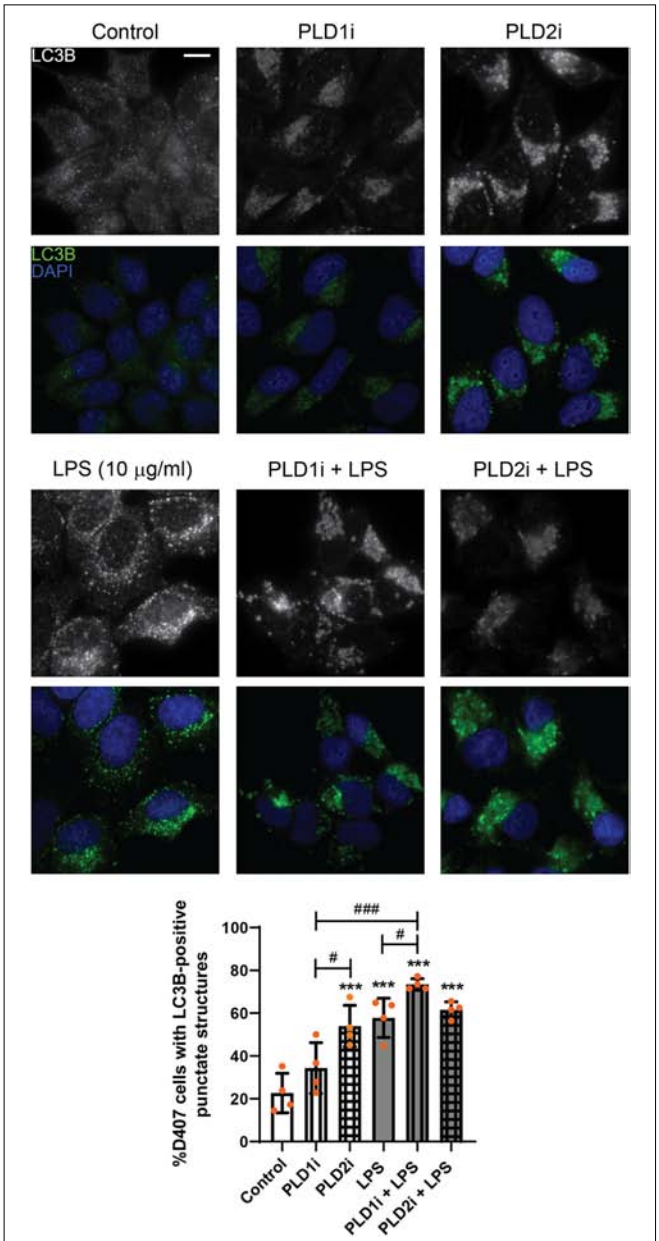

FIGURE 6 | Role of phospholipase D (PLD) isoforms 1 and 2 in the autophagic process of RPE cells. D407 cells were pre-incubated with PLD1 or PLD2 selective inhibitors (PLD1i and PLD2i, 5 μM) or vehicle (DMSO) prior to incubation with LPS (10 μg/ml) or under control condition for 24 h. Immunofluorescence assays were performed to determine LC3B-positive punctate structures. Cells were stained with DAPI to visualize the nuclear structure. Scale bar = 10 μm. Bar graph shows the percentage of cells presenting LC3B-positive punctate structures in each condition. Graph shows the mean percentage ± SD. Dots indicate individual values from four independent experiments ($n = 4$). Asterisks (*) indicate significant differences with respect to control condition ($^{***}p < 0.001$). Number signs (#) indicate significant differences between indicated conditions ($^{\#}p < 0.05$; $^{\#\#\#}p < 0.001$).

in LC3B-II and p62 content under control condition and this increment was higher in cells pre-incubated with BAF and exposed to LPS for 24 h (**Figure 5**). Same results were observed in ARPE-19 cells (Data not shown). These results demonstrate that LPS treatment is not blocking the autophagic flux but is inducing the autophagic process in RPE cells.

PLD1 and PLD2 Inhibition Modulates the Autophagic Process of RPE Cells

As stated above, our previous findings demonstrated the participation of classical PLDs in the LPS-induced inflammatory response of RPE cells (Mateos et al., 2014). To study the role of PLD1 and PLD2 in the LPS-induced autophagic process, D407 cells were pre-incubated with PLD1 or PLD2 selective inhibitors (PLD1i and PLD2i, 5 μM) prior to LPS treatment for 24 h, as described in "Materials and Methods" section. Immunofluorescence assays showed that under control condition the percentage of D407 cells with LC3B-positive punctate structures was increased significantly (to 53%) in cells pre-incubated with PLD2i while PLD1i increased this percentage (to 73%) only in cells exposed to LPS (**Figure 6**). To further support these results, WBs assays show that PLD1 and

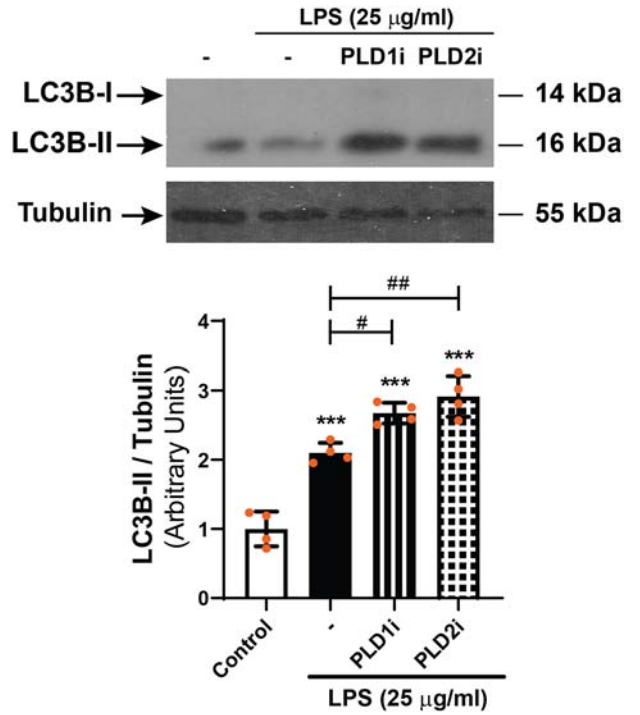

FIGURE 7 | WBs were performed and analyzed as described in "Materials and Methods" section in order to determine LC3B-II levels in D407 cells pre-incubated with PLD1i (0.5 μM), PLD2i (0.5 μM) or vehicle (DMSO) prior to incubation with LPS (25 μg/ml) or under control condition for 24 h. The bar graph shows the densitometry values of LC3B-II/α-Tubulin. Dots indicate individual values from four independent experiments ($n = 4$). Results are expressed as arbitrary units. Asterisks (*) indicate significant differences with respect to control condition (***$p < 0.001$). Number signs (#) indicate significant differences with respect to LPS control condition ($^{\#}p < 0.05$; $^{\#\#}p < 0.01$).

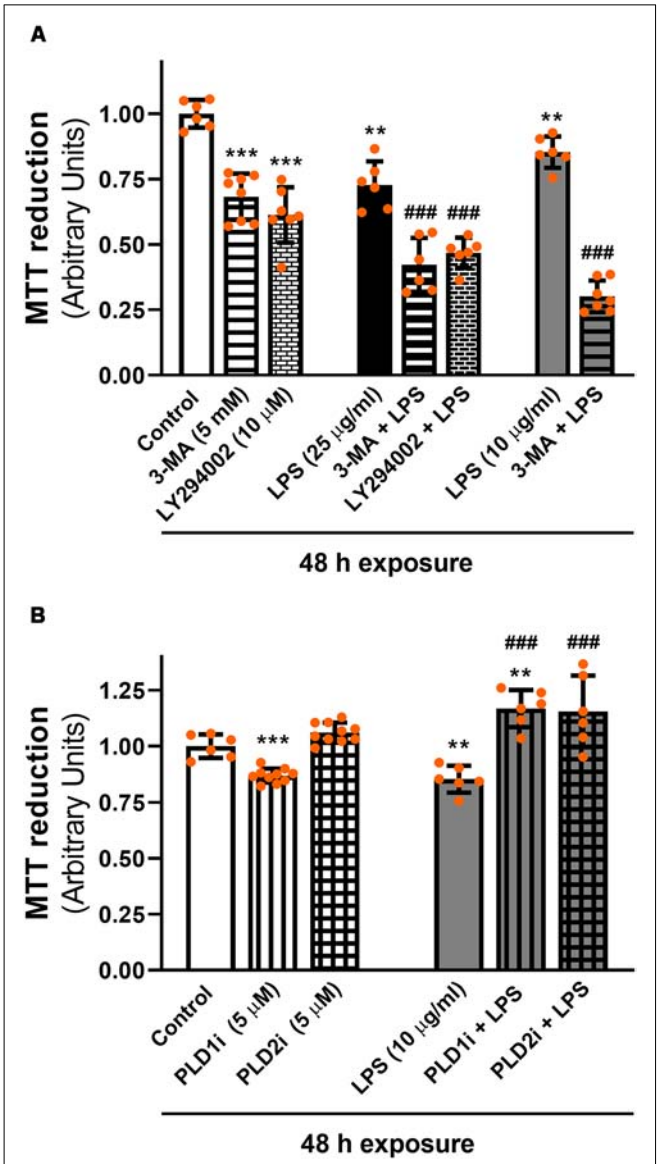

FIGURE 8 | (A) Effect of autophagy inhibitors on cell viability. D407 cells were pre-incubated with autophagy inhibitor 3-methyladenine (3-MA), LY294002 or vehicle (DMSO) prior to LPS (10 or 25 μg/ml) or control condition exposure for 48 h. **(B)** Effect of PLD inhibitors on cell viability. D407 cells were pre-incubated with PLD1i (5 μM), PLD2i (5 μM) or vehicle (DMSO) prior to LPS (10 μg/ml) or control condition exposure for 48 h. For **(A,B)**, cell viability was evaluated using the MTT reduction assay, as described in "Materials and Methods" section expressed as arbitrary units. Dots indicate individual values from different experiments ($n \geq 6$). Asterisks (*) indicate significant differences with respect to control condition (vehicle; **$p < 0.01$; ***$p < 0.0001$). Number signs (#) indicate significant differences with respect to each LPS (vehicle) condition ($^{\#\#\#}p < 0.0001$).

PLD2 inhibition (with lower inhibitor concentrations than those used for immunofluorescence assays, 0,5 μM) also increased LC3B-II content in D407 cells exposed to a higher LPS concentration (25 μg/ml) for 24 h (**Figure 7**). These results suggest that PLD2 modulates basal autophagy under control condition while both PLDs modulate the autophagic process under LPS-induced inflammatory conditions.

The Activation of the Autophagic Process Protects RPE Cells From the Inflammatory Injury

To assess the role of the autophagic process in LPS-induced cell damage, D407 cells were pre-incubated with autophagy inhibitors 3-MA and LY294002 prior to LPS exposure for 48 h since, as stated above, we previously demonstrated that RPE cell viability is not affected after shorter exposures to LPS (Mateos et al., 2014). These inhibitors block autophagy at an early stage by inhibiting class III phosphatidylinositol 3-kinase (PI3K; Klionsky et al., 2016). **Figure 8A** shows that under control condition 3-MA (5 mM) and LY294002 (10 μM) reduced D407 cell viability by 32% and by 39%, respectively. Furthermore, both inhibitors enhanced the cell viability loss induced by LPS since MTT reduction was reduced by 58% and by 54% in cells pre-incubated with 3-MA and LY294002 and exposed to LPS (25 μg/ml) for 48 h, respectively. Cell viability loss was also enhanced by 70% in cells pre-incubated with 3-MA and exposed to a lower LPS concentration (10 μg/ml) for 48 h (**Figure 8A**). On the contrary, the inhibition of PLD1 and PLD2 with 5 μM PLD1i or PLD2i prevented the

loss in cell viability induced by LPS (10 μg/ml) in D407 cells (**Figure 8B**). Lower concentrations (0.5 μM) of PLD1i and PLD2i did not prevent the LPS-induced viability loss of D407 cells (Data not shown). Our results show that the autophagic process is a protective mechanism triggered under LPS-induced inflammation in RPE cells.

DISCUSSION

LPS can reach and directly stimulate RPE cells in situations of acute ocular inflammation, such as bacterial endophthalmitis (posterior segment eye infection) and uveitis (Leung et al., 2009; Pollreisz et al., 2012). Endophthalmitis can arise after an eye surgery, intravitreal injections, trauma and sepsis (endogenous endophthalmitis), the latter mostly seen in immunocompromised patients (Pollreisz et al., 2012; Haddock et al., 2014; Holland et al., 2014). Although bacterial endophthalmitis is an unusual pathology, it is a vital ocular emergency since it usually ends up in vision loss (Haddock et al., 2014; Holland et al., 2014). Additionally, LPS is often used to induce an inflammatory response in cell cultures. In line with this, our previous findings demonstrated that the exposure of ARPE-19 cells to LPS induces a typical inflammatory response which involves PLD and ERK1/2 activation, COX-2 expression, PGE_2 secretion, reduced cell viability and increased caspase-3 cleavage (Mateos et al., 2014; Tenconi et al., 2016). In the present work, we demonstrate that the LPS-induced inflammatory response of RPE cells also involves NFκB nuclear translocation and ROS generation.

Autophagy is a very active catabolic process in RPE cells. It is essential for cell survival in response to stress (Frost et al., 2014; Sinha et al., 2016). Different studies reported that autophagy is selectively dysregulated in the RPE from AMD patients and that downregulation of the autophagic pathway renders the RPE more susceptible to oxidative stress while increased autophagic flux protected the RPE from oxidative damage (Mitter et al., 2014; Golestaneh et al., 2017). In this work, we demonstrate that LPS increases autophagy in RPE cells mediating cell survival. Furthermore, our results show that the PLD pathway can modulate the autophagic process.

Once autophagy is initiated the cytosolic form of LC3 (LC3-I) is processed and transformed by the addition of a group of phosphatidylethanolamine to form LC3-II. This lipidation reaction permits the recruitment of the protein to autophagosome membranes. There are three human isoforms of LC3, LC3A, LC3B, and LC3C. Among the three isoforms, LC3B has been the most studied and has become one of the most reliable markers for characterization of the autophagic process (Klionsky et al., 2016). Similarly, SQSTM1/p62 by interaction with LC3 is associated with the autophagosomal membrane to facilitate the degradation of ubiquitinated protein aggregates (Rubinsztein et al., 2009; Ferrington et al., 2016; Rosa et al., 2016). Finally, p62 is degraded together with ubiquitinated protein in the autolysosome (Rubinsztein et al., 2009; Ferrington et al., 2016; Rosa et al., 2016). Thus, an increase in LC3B-II content and decreased p62 levels are associated with autophagic activation, although p62 changes can be cell type, time and context specific (Klionsky et al., 2016).

The increase in LC3B-II content and in the percentage of cells with LC3B- and p62-positive punctate structures demonstrates that a 24 h LPS exposure induces autophagy in RPE cells. Furthermore, the reduced p62 content observed after a 48 h LPS exposure and the results obtained in the presence of BAF confirm that LPS treatment is inducing the autophagic process in RPE cells rather than blocking its flux. In agreement with our results, Wang and collaborators reported that in ARPE-19 cells LPS plus tetrachlorodibenzo-*p*-dioxin induces the formation of autophagosome-like structures observed by transmission electron microscopy (Wang et al., 2016). The inhibition of autophagy with 3-MA and LY294002, which target early events in the autophagy cycle through irreversible inhibition of class III PI3K, worsened LPS-induced viability loss demonstrating that autophagy is a protective mechanism elicited under LPS condition in RPE cells. Moreover, early autophagy inhibition reduced RPE cell viability in our control condition suggesting that autophagy in a basal context is important for RPE cell maintenance.

The PLD pathway has been postulated both as a positive as well as a negative autophagy modulator (Gomez-Cambronero and Kantonen, 2014). It has been demonstrated that PLD-generated PA induces membrane curvatures necessary for phagocytosis as well as for the formation of the initial autophagosome (Dall'Armi et al., 2010; Holland et al., 2016). On the contrary, PLD-generated PA activates mTORC1, the main inhibitor of the autophagy initiation machinery (Sun and Chen, 2008; Foster et al., 2014; Munson and Ganley, 2015). Moreover, the PLD-mediated autophagic regulation has been proposed as a potential target for cancer therapy (Jang et al., 2014). PA was also shown to bind and activate the mTOR effector S6 kinase (S6K) independently of mTOR (Lehman et al., 2007). An interrelation between PLD2 and mTOR/S6K has been demonstrated in HL-6 leukemia cells, where PLD2 was shown to mediate IL-8-induced mTOR/S6K mRNA up-regulation and, in reverse direction, mTOR and S6K were shown to down-regulate PLD2 activity and gene expression (Tabatabaian et al., 2010). Furthermore, inhibition and genetic knockdown of PLD2 significantly induced autophagy in HT29 and HCT116 colorectal cancer cells (Hwang et al., 2014). However, the role of the PLD pathway in RPE cells autophagic process was a complete unstudied research field. The novelty of our findings is that we show that under control (basal) condition autophagosome-like structures were increased in cells pre-incubated with PLD2i while PLD1i increased autophagosome-like structures in cells exposed to LPS. Our results constitute the first evidence that the PLD pathway is a negative autophagy modulator in RPE cells, possibly through PLD-mediated PA generation and mTORC1 activation. Whereas PLD2 modulates basal autophagy under control condition, both PLDs inhibit the autophagic process under LPS conditions. The PLD2-modulation of basal autophagy in RPE cells is in agreement with the fact that, of both classical PLD isoforms, PLD2 presents higher basal activity.

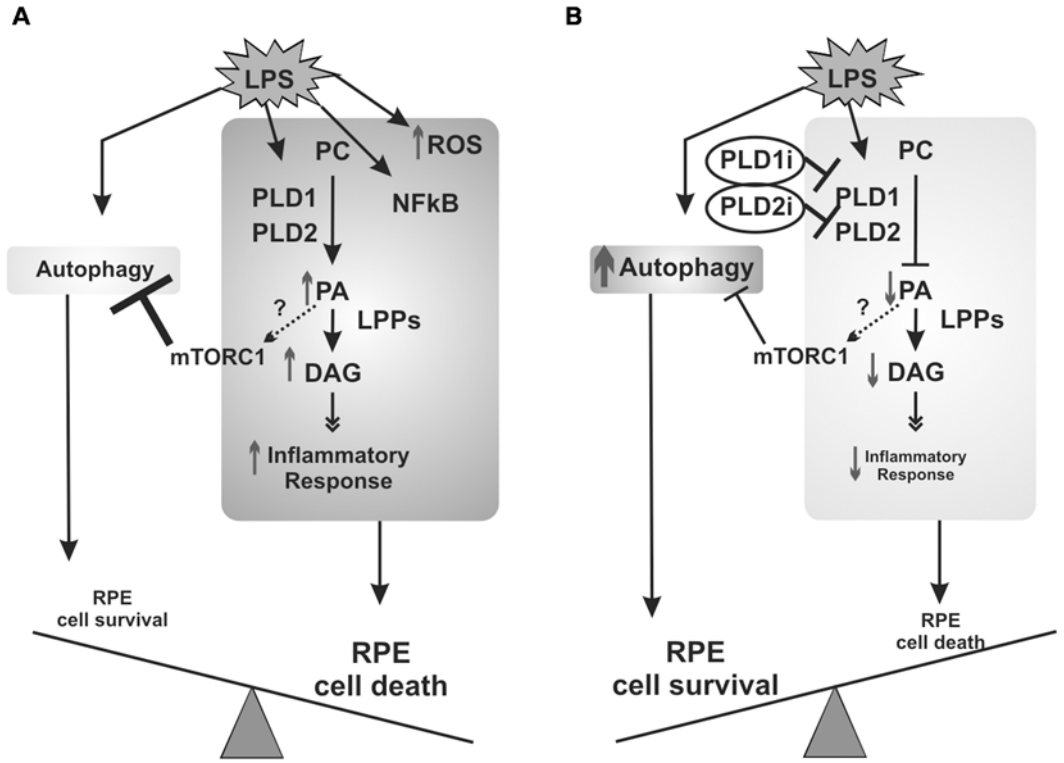

FIGURE 9 | Schematic view of signaling events elicited by LPS in RPE cells. **(A)** PLD activation, ROS generation and NFκB nuclear translocation are part of the inflammatory signaling cascade induced in RPE cells exposed to LPS that ultimately leads to cell viability loss. RPE cells answer to LPS also involves the induction of the autophagic process which mediates cells survival. **(B)** When PLD1 and PLD2 are inhibited, the inflammatory response of RPE cells is reduced and autophagy is enhanced, possibly through a reduced phosphatidic acid (PA)-dependent mTORC1 activation, leading to RPE cell survival. Dashed arrows and question marks indicate possible but unstudied mechanisms.

In agreement with results obtained in RPE cells incubated with early autophagy inhibitors (which worsen cell viability loss), PLD inhibitors (which increase autophagy) prevented LPS-induced viability loss in D407 RPE cells. Together, our findings demonstrate that autophagy is a protective mechanism elicited under the LPS-induced inflammatory response of RPE cells. Certainly, the protective effect of PLD inhibitors does not reside only in the modulation of autophagy since our previous findings demonstrated that the pharmacological inhibition of classical PLDs prevents LPS-induced COX-2 expression and PGE_2 production in ARPE-19 cells (Mateos et al., 2014). To sum up, our previous work and the findings reported herein demonstrate that in RPE cells LPS induces an inflammatory-like response that involves PLD activation, ROS generation and NFκB nuclear translocation, leading to cell viability loss. Furthermore, LPS induces RPE autophagic process which mediates cells survival (**Figure 9A**). The inhibition of the PLD pathway not only reduces the inflammatory response but also enhances autophagy in RPE cells, possibly through a reduced PA-dependent mTORC1 activation, leading to RPE cell survival (**Figure 9B**).

It is well-recognized the role of NFκB in the regulation of inflammatory responses, by mediating the induction of various pro-inflammatory genes, the activation and differentiation of inflammatory T cells and the activation of inflammasomes (Liu et al., 2017). Furthermore, several studies have linked NFκB signaling with autophagy. It has been reported that NFκB is involved in advanced glycation end-products (AGE)-induced autophagy in diverse cell lines (Verma and Manna, 2016, 2017) and in the autophagic process observed in lung tissues from rats with induced pulmonary arterial hypertension (Zhai et al., 2018). Moreover, in several cell lines NFκB (p65) was shown to induce the expression of beclin1 (BECN1), a central protein that assembles the class III PI3K complex to trigger macroautophagy (Copetti et al., 2009; Han et al., 2018). In LPS-primed macrophages, NFκB was shown to upregulate p62 expression (Zhong et al., 2016) and in head and neck squamous cell carcinoma cells the expression of BECN1 and LC3 was also demonstrated to be modulated by NFκB (p65; He et al., 2017). However, the link between NFκB activation and the expression of autophagy-related proteins in the RPE has not been studied yet. Our results demonstrate that in RPE cells NFκB nuclear translocation and autophagy flux are triggered by LPS at the same time frame, opening interesting questions about the role of this transcription factor in RPE autophagic process.

In conclusion, our results showed that LPS treatment enhances autophagy in RPE cells as a protective mechanism triggered under inflammatory conditions. Furthermore, we demonstrated that the PLD pathway modulates the autophagic process in RPE cells. Further experiments are certainly needed to fully elucidate the mechanisms by which classical PLDs modulates autophagy in RPE cells exposed to inflammatory injury. Our findings contribute to the knowledge of the molecular basis of retinal inflammatory and degenerative diseases, such as AMD, DR and endophthalmitis and open possible avenues of therapeutic exploration.

AUTHOR CONTRIBUTIONS

VB and PT performed the experiments. VB and MM designed the experiments and wrote the manuscript. MM supervised the study. NG provided equipment and reagents and revised the manuscript.

FUNDING

This work was supported by grants from Agencia Nacional de Promoción Científica y Tecnológica (ANPCYT; PICTs 2013-2317, 2014-3352 and 2017-0350). MM and NG are research members of CONICET. VB is a postdoctoral fellow. PT is a doctoral fellow from CONICET.

ACKNOWLEDGMENTS

We want to thank Dr. Ana Sofía Vallés (INIBIBB-UNS-CONICET, Bahía Blanca, Argentina) for the critical reading of the manuscript.

SUPPLEMENTARY MATERIAL

The Supplementary Material for this article can be found online at: https://www.frontiersin.org/articles/10.3389/fncel.2019.00154/full#supplementary-material

FIGURE S1 | Confocal images showing NFκB (p65) subcellular distribution in D407 cells exposed to LPS (10 μg/ml) or to control condition (vehicle) for 24 h. Cells were stained with TO-PRO-3 to visualize the nuclear structure. Scale bar = 10 μm.

FIGURE S2 | Immunofluorescence assays of ARPE-19 cells. LC3B-positive punctate structures were analyzed by wide-field fluorescence microscopy in ARPE-19 cells exposed for 24 h to 25 μg/ml LPS or control condition (vehicle), with or without FBS. Cells were stained with DAPI to visualize the nuclear structure. Scale bar = 10 μm.

REFERENCES

Ahmed, A. (2011). An overview of inflammation: mechanism and consequences. *Front. Biol.* 6, 274–281. doi: 10.1007/s11515-011-1123-9

Arjamaa, O., Aaltonen, V., Piippo, N., Csont, T., Petrovski, G., Kaarniranta, K., et al. (2017). Hypoxia and inflammation in the release of VEGF and interleukins from human retinal pigment epithelial cells. *Graefes Arch. Clin. Exp. Ophthalmol.* 255, 1757–1762. doi: 10.1007/s00417-017-3711-0

Bradford, M. M. (1976). A rapid and sensitive method for the quantitation of microgram quantities of protein utilizing the principle of protein-dye binding. *Anal. Biochem.* 72, 248–254. doi: 10.1016/0003-2697(76)90527-3

Brindley, D. N. (2004). Lipid phosphate phosphatases and related proteins: signaling functions in development, cell division and cancer. *J. Cell. Biochem.* 92, 900–912. doi: 10.1002/jcb.20126

Brindley, D. N., Pilquil, C., Sariahmetoglu, M., and Reue, K. (2009). Phosphatidate degradation: phosphatidate phosphatases (lipins) and lipid phosphate phosphatases. *Biochim. Biophys. Acta* 1791, 956–961. doi: 10.1016/j.bbalip.2009.02.007

Carr, A. J., Vugler, A., Lawrence, J., Chen, L. L., Ahmado, A., Chen, F. K., et al. (2009). Molecular characterization and functional analysis of phagocytosis by human embryonic stem cell-derived RPE cells using a novel human retinal assay. *Mol. Vis.* 15, 283–295.

Carrasco, S., and Mérida, I. (2007). Diacylglycerol, when simplicity becomes complex. *Trends Biochem. Sci.* 32, 27–36. doi: 10.1016/j.tibs.2006.11.004

Copetti, T., Bertoli, C., Dalla, E., Demarchi, F., and Schneider, C. (2009). p65/RelA modulates BECN1 transcription and autophagy. *Mol. Cell. Biol.* 29, 2594–2608. doi: 10.1128/MCB.01396-08

Dall'Armi, C., Devereaux, K. A., and Di, P. G. (2013). The role of lipids in the control of autophagy. *Curr. Biol.* 23, R33–R45. doi: 10.1016/j.cub.2012.10.041

Dall'Armi, C., Hurtado-Lorenzo, A., Tian, H., Morel, E., Nezu, A., Chan, R. B., et al. (2010). The phospholipase D1 pathway modulates macroautophagy. *Nat. Commun.* 1:142. doi: 10.1038/ncomms1144

Datta, S., Cano, M., Ebrahimi, K., Wang, L., and Handa, J. T. (2017). The impact of oxidative stress and inflammation on RPE degeneration in non-neovascular AMD. *Prog. Retin. Eye Res.* 60, 201–218. doi: 10.1016/j.preteyeres.2017.03.002

Deretic, V., and Klionsky, D. J. (2018). Autophagy and inflammation: a special review issue. *Autophagy* 14, 179–180. doi: 10.1080/15548627.2017.1412229

Exton, J. H. (2002). Regulation of phospholipase D. *FEBS Lett.* 531, 58–61. doi: 10.1016/S0014-5793(02)03405-1

Ferrington, D. A., Sinha, D., and Kaarniranta, K. (2016). Defects in retinal pigment epithelial cell proteolysis and the pathology associated with age-related macular degeneration. *Prog. Retin. Eye Res.* 51, 69–89. doi: 10.1016/j.preteyeres.2015.09.002

Foster, D. A., Salloum, D., Menon, D., and Frias, M. A. (2014). Phospholipase D and the maintenance of phosphatidic acid levels for regulation of mammalian target of rapamycin (mTOR). *J. Biol. Chem.* 289, 22583–22588. doi: 10.1074/jbc.r114.566091

Foster, D. A., and Xu, L. (2003). Phospholipase D in cell proliferation and cancer. *Mol. Cancer Res.* 1, 789–800.

Frohman, M. A. (2015). The phospholipase D superfamily as therapeutic targets. *Trends Pharmacol. Sci.* 36, 137–144. doi: 10.1016/j.tips.2015.01.001

Frost, L. S., Mitchell, C. H., and Boesze-Battaglia, K. (2014). Autophagy in the eye: implications for ocular cell health. *Exp. Eye Res.* 124, 56–66. doi: 10.1016/j.exer.2014.04.010

Golestaneh, N., Chu, Y., Xiao, Y. Y., Stoleru, G. L., and Theos, A. C. (2017). Dysfunctional autophagy in RPE, a contributing factor in age-related macular degeneration. *Cell Death Dis.* 8:e2537. doi: 10.1038/cddis.2016.453

Gomez-Cambronero, J., and Kantonen, S. (2014). A river runs through it: how autophagy, senescence and phagocytosis could be linked to phospholipase D by Wnt signaling. *J. Leukoc. Biol.* 96, 779–784. doi: 10.1189/jlb.2vmr0214-120RR

Haddock, L. J., Ramsey, D. J., and Young, L. H. (2014). Complications of subspecialty ophthalmic care: endophthalmitis after intravitreal injections of anti-vascular endothelial growth factor medications. *Semin. Ophthalmol.* 29, 257–262. doi: 10.3109/08820538.2014.959616

Han, T., Guo, M., Gan, M., Yu, B., Tian, X., and Wang, J. B. (2018). TRIM59 regulates autophagy through modulating both the transcription and the ubiquitination of BECN1. *Autophagy* 14, 2035–2048. doi: 10.1080/15548627.2018.1491493

He, Z. J., Zhu, F. Y., Li, S. S., Zhong, L., Tan, H. Y., and Wang, K. (2017). Inhibiting ROS-NF-κB-dependent autophagy enhanced brazilin-induced apoptosis in head and neck squamous cell carcinoma. *Food Chem. Toxicol.* 101, 55–66. doi: 10.1016/j.fct.2017.01.002

Holland, P., Knaevelsrud, H., Søreng, K., Mathai, B. J., Lystad, A. H., Pankiv, S., et al. (2016). HS1BP3 negatively regulates autophagy by modulation of phosphatidic acid levels. *Nat. Commun.* 7:13889. doi: 10.1038/ncomms13889

Holland, E. J., McDonald, M. B., Parekh, J. G., and Sheppard, J. D. (2014). Antibiotic resistance in acute postoperative endophthalmitis. *Ophthalmology* 121, S1–S9. doi: 10.1016/j.ophtha.2014.06.049

Hwang, W. C., Kim, M. K., Song, J. H., Choi, K. Y., and Min, D. S. (2014). Inhibition of phospholipase D2 induces autophagy in colorectal cancer cells. *Exp. Mol. Med.* 46:e124. doi: 10.1038/emm.2014.74

Jang, Y. H., Choi, K. Y., and Min, D. S. (2014). Phospholipase D-mediated autophagic regulation is a potential target for cancer therapy. *Cell Death Differ.* 21, 533–546. doi: 10.1038/cdd.2013.174

Kauppinen, A., Paterno, J. J., Blasiak, J., Salminen, A., and Kaarniranta, K. (2016). Inflammation and its role in age-related macular degeneration. *Cell. Mol. Life Sci.* 73, 1765–1786. doi: 10.1007/s00018-016-2147-8

Klionsky, D. J. (2007). Autophagy: from phenomenology to molecular understanding in less than a decade. *Nat. Rev. Mol. Cell Biol.* 8, 931–937. doi: 10.1038/nrm2245

Klionsky, D. J., Abdelmohsen, K., Abe, A., Abedin, M. J., Abeliovich, H., Acevedo, A. A., et al. (2016). Guidelines for the use and interpretation of assays for monitoring autophagy (3rd edition). *Autophagy* 12, 1–222. doi: 10.1080/15548627.2015.1100356

Laemmli, U. K. (1970). Cleavage of structural proteins during the assembly of the head of bacteriophage T4. *Nature* 227, 680–685. doi: 10.1038/227680a0

Lehman, N., Ledford, B., Di, F. M., Frondorf, K., McPhail, L. C., and Gomez-Cambronero, J. (2007). Phospholipase D2-derived phosphatidic acid binds to and activates ribosomal p70 S6 kinase independently of mTOR. *FASEB J.* 21, 1075–1087. doi: 10.1096/fj.06-6652com

Leung, K. W., Barnstable, C. J., and Tombran-Tink, J. (2009). Bacterial endotoxin activates retinal pigment epithelial cells and induces their degeneration through IL-6 and IL-8 autocrine signaling. *Mol. Immunol.* 46, 1374–1386. doi: 10.1016/j.molimm.2008.12.001

Liu, J., Copland, D. A., Theodoropoulou, S., Chiu, H. A., Barba, M. D., Mak, K. W., et al. (2016). Impairing autophagy in retinal pigment epithelium leads to inflammasome activation and enhanced macrophage-mediated angiogenesis. *Sci. Rep.* 6:20639. doi: 10.1038/srep20639

Liu, T., Zhang, L., Joo, D., and Sun, S.-C. (2017). NF-κB signaling in inflammation. *Signal Transduct. Target. Ther.* 2:e17023. doi: 10.1038/sigtrans.2017.23

Mateos, M. V., Kamerbeek, C. B., Giusto, N. M., and Salvador, G. A. (2014). The phospholipase D pathway mediates the inflammatory response of the retinal pigment epithelium. *Int. J. Biochem. Cell Biol.* 55, 119–128. doi: 10.1016/j.biocel.2014.08.016

Medzhitov, R. (2008). Origin and physiological roles of inflammation. *Nature* 454, 428–435. doi: 10.1038/nature07201

Mitter, S. K., Song, C., Qi, X., Mao, H., Rao, H., Akin, D., et al. (2014). Dysregulated autophagy in the RPE is associated with increased susceptibility to oxidative stress and AMD. *Autophagy* 10, 1989–2005. doi: 10.4161/auto.36184

Montagna, C., Rizza, S., Maiani, E., Piredda, L., Filomeni, G., and Cecconi, F. (2016). To eat, or NOt to eat: S-nitrosylation signaling in autophagy. *FEBS J.* 283, 3857–3869. doi: 10.1111/febs.13736

Munson, M. J., and Ganley, I. G. (2015). MTOR, PIK3C3 and autophagy: signaling the beginning from the end. *Autophagy* 11, 2375–2376. doi: 10.1080/15548627.2015.1106668

Netea-Maier, R. T., Plantinga, T. S., van de Veerdonk, F. L., Smit, J. W., and Netea, M. G. (2016). Modulation of inflammation by autophagy: consequences for human disease. *Autophagy* 12, 245–260. doi: 10.1080/15548627.2015.1071759

Newton, A. C. (2010). Protein kinase C: poised to signal. *Am. J. Physiol. Endocrinol. Metab.* 298, E395–E402. doi: 10.1152/ajpendo.00477.2009

Pavan, B., Capuzzo, A., and Forlani, G. (2014). High glucose-induced barrier impairment of human retinal pigment epithelium is ameliorated by treatment with Goji berry extracts through modulation of cAMP levels. *Exp. Eye Res.* 120, 50–54. doi: 10.1016/j.exer.2013.12.006

Peng, X., and Frohman, M. A. (2012). Mammalian phospholipase D physiological and pathological roles. *Acta Physiol.* 204, 219–226. doi: 10.1111/j.1748-1716.2011.02298.x

Perez, V. L., Saeed, A. M., Tan, Y., Urbieta, M., and Cruz-Guilloty, F. (2013). The eye: a window to the soul of the immune system. *J. Autoimmun.* 45, 7–14. doi: 10.1016/j.jaut.2013.06.011

Pollreisz, A., Rafferty, B., Kozarov, E., and Lalla, E. (2012). Klebsiella pneumoniae induces an inflammatory response in human retinal-pigmented epithelial cells. *Biochem. Biophys. Res. Commun.* 418, 33–37. doi: 10.1016/j.bbrc.2011.12.102

Rodrigues, E. B. (2007). Inflammation in dry age-related macular degeneration. *Ophthalmologica* 221, 143–152. doi: 10.1159/000099293

Rosa, M. D., Distefano, G., Gagliano, C., Rusciano, D., and Malaguarnera, L. (2016). Autophagy in diabetic retinopathy. *Curr. Neuropharmacol.* 14, 810–825. doi: 10.2174/1570159x14666160321122900

Rubinsztein, D. C., Cuervo, A. M., Ravikumar, B., Sarkar, S., Korolchuk, V., Kaushik, S., et al. (2009). In search of an "autophagomometer". *Autophagy* 5, 585–589. doi: 10.4161/auto.5.5.8823

Saxton, R. A., and Sabatini, D. M. (2017). mTOR signaling in growth, metabolism and disease. *Cell* 168, 960–976. doi: 10.1016/j.cell.2017.02.004

Shen, D. F., Chang, M. A., Matteson, D. M., Buggage, R., Kozhich, A. T., and Chan, C. C. (2000). Biphasic ocular inflammatory response to endotoxin-induced uveitis in the mouse. *Arch. Ophthalmol.* 118, 521–527. doi: 10.1001/archopht.118.4.521

Simó, R., Villarroel, M., Corraliza, L., Hernandez, C., and Garcia-Ramirez, M. (2010). The retinal pigment epithelium: something more than a constituent of the blood-retinal barrier–implications for the pathogenesis of diabetic retinopathy. *J. Biomed. Biotechnol.* 2010:190724. doi: 10.1155/2010/190724

Sinha, D., Valapala, M., Shang, P., Hose, S., Grebe, R., Lutty, G. A., et al. (2016). Lysosomes: regulators of autophagy in the retinal pigmented epithelium. *Exp. Eye Res.* 144, 46–53. doi: 10.1016/j.exer.2015.08.018

Strauß, O. (2016). Pharmacology of the retinal pigment epithelium, the interface between retina and body system. *Eur. J. Pharmacol.* 787, 84–93. doi: 10.1016/j.ejphar.2016.03.066

Strauss, O. (2005). The retinal pigment epithelium in visual function. *Physiol. Rev.* 85, 845–881. doi: 10.1152/physrev.00021.2004

Sun, Y., and Chen, J. (2008). mTOR signaling: PLD takes center stage. *Cell Cycle* 7, 3118–3123. doi: 10.4161/cc.7.20.6881

Tabatabaian, F., Dougherty, K., Di, F. M., and Gomez-Cambronero, J. (2010). Mammalian target of rapamycin (mTOR) and S6 kinase down-regulate phospholipase D2 basal expression and function. *J. Biol. Chem.* 285, 18991–19001. doi: 10.1074/jbc.M110.111542

Tenconi, P. E., Giusto, N. M., Salvador, G. A., and Mateos, M. V. (2016). Phospholipase D1 modulates protein kinase C-epsilon in retinal pigment epithelium cells during inflammatory response. *Int. J. Biochem. Cell Biol.* 81, 67–75. doi: 10.1016/j.biocel.2016.10.015

Verma, N., and Manna, S. K. (2016). Advanced glycation end products (AGE) potently induce autophagy through activation of raf protein kinase and nuclear factor κB (NF-κB). *J. Biol. Chem.* 291, 1481–1491. doi: 10.1074/jbc.M115.667576

Verma, N., and Manna, S. K. (2017). Advanced glycation end products (AGE) potentiates cell death in p53 negative cells via upregulaion of NF-κ B and impairment of autophagy. *J. Cell. Physiol.* 232, 3598–3610. doi: 10.1002/jcp.25828

Viringipurampeer, I. A., Bashar, A. E., Gregory-Evans, C. Y., Moritz, O. L., and Gregory-Evans, K. (2013). Targeting inflammation in emerging therapies for genetic retinal disease. *Int. J. Inflam.* 2013:581751. doi: 10.1155/2013/581751

Wang, Q. J. (2006). PKD at the crossroads of DAG and PKC signaling. *Trends Pharmacol. Sci.* 27, 317–323. doi: 10.1016/j.tips.2006.04.003

Wang, Y., Hanus, J. W., Abu-Asab, M. S., Shen, D., Ogilvy, A., Ou, J., et al. (2016). NLRP3 upregulation in retinal pigment epithelium in age-related macular degeneration. *Int. J. Mol. Sci.* 17:E73. doi: 10.3390/ijms17010073

Wang, A. L., Lukas, T. J., Yuan, M., Du, N., Tso, M. O., and Neufeld, A. H. (2009). Autophagy and exosomes in the aged retinal pigment epithelium: possible relevance to drusen formation and age-related macular degeneration. *PLoS One* 4:e4160. doi: 10.1371/journal.pone.0004160

Wang, R., Shen, Z., Yang, L., Yin, M., Zheng, W., Wu, B., et al. (2017). Protective effects of heme oxygenase-1-transduced bone marrow-derived mesenchymal stem cells on reducedsize liver transplantation: role of autophagy regulated

by the ERK/mTOR signaling pathway. *Int. J. Mol. Med.* 40, 1537–1548. doi: 10.3892/ijmm.2017.3121

Whitcup, S. M., Nussenblatt, R. B., Lightman, S. L., and Hollander, D. A. (2013). Inflammation in retinal disease. *Int. J. Inflam.* 2013:724648. doi: 10.1155/2013/724648

Willermain, F., Scifo, L., Weber, C., Caspers, L., Perret, J., and Delporte, C. (2018). Potential interplay between hyperosmolarity and inflammation on retinal pigmented epithelium in pathogenesis of diabetic retinopathy. *Int. J. Mol. Sci.* 19:E1056. doi: 10.3390/ijms19041056

Yang, Z., and Klionsky, D. J. (2010). Eaten alive: a history of macroautophagy. *Nat. Cell Biol.* 12, 814–822. doi: 10.1038/ncb0910-814

Zhai, C., Shi, W., Feng, W., Zhu, Y., Wang, J., Li, S., et al. (2018). Activation of AMPK prevents monocrotaline-induced pulmonary arterial hypertension by suppression of NF-κB-mediated autophagy activation. *Life Sci.* 208, 87–95. doi: 10.1016/j.lfs.2018.07.018

Zhong, Z., Umemura, A., Sanchez-Lopez, E., Liang, S., Shalapour, S., Wong, J., et al. (2016). NF-κB restricts inflammasome activation via elimination of damaged mitochondria. *Cell* 164, 896–910. doi: 10.1016/j.cell.2015.12.057

Conflict of Interest Statement: The authors declare that the research was conducted in the absence of any commercial or financial relationships that could be construed as a potential conflict of interest.

frontiers in Cellular Neuroscience

REVIEW
published: 24 April 2019
doi: 10.3389/fncel.2019.00162

Fatty Acid Signaling Mechanisms in Neural Cells: Fatty Acid Receptors

Lisandro Jorge Falomir-Lockhart[1,2], Gian Franco Cavazzutti[1,2], Ezequiel Giménez[1,3] and Andrés Martín Toscani[1,3]*

[1] Instituto de Investigaciones Bioquímicas de La Plata (INIBIOLP), Centro Científico Tecnológico – La Plata, Consejo Nacional de Investigaciones Científicas y Técnicas (CONICET), La Plata, Argentina, [2] Facultad de Ciencias Exactas, Universidad Nacional de La Plata (UNLP), La Plata, Argentina, [3] Facultad de Ciencias Médicas, Universidad Nacional de La Plata (UNLP), La Plata, Argentina

OPEN ACCESS

Edited by:
Gabriela Alejandra Salvador, Universidad Nacional del Sur, Argentina

Reviewed by:
Sharon DeMorrow, The University of Texas at Austin, United States
Tatsuro Mutoh, Fujita Health University, Japan

***Correspondence:**
Lisandro Jorge Falomir-Lockhart
lfalomir@conicet.gov.ar;
ljfalomir@biol.unlp.edu.ar

Specialty section:
This article was submitted to Cellular Neurophysiology, a section of the journal Frontiers in Cellular Neuroscience

Received: *15 January 2019*
Accepted: *08 April 2019*
Published: *24 April 2019*

Citation:
Falomir-Lockhart LJ, Cavazzutti GF, Giménez E and Toscani AM (2019) Fatty Acid Signaling Mechanisms in Neural Cells: Fatty Acid Receptors. Front. Cell. Neurosci. 13:162. doi: 10.3389/fncel.2019.00162

Fatty acids (FAs) are typically associated with structural and metabolic roles, as they can be stored as triglycerides, degraded by β-oxidation or used in phospholipids' synthesis, the main components of biological membranes. It has been shown that these lipids exhibit also regulatory functions in different cell types. FAs can serve as secondary messengers, as well as modulators of enzymatic activities and substrates for cytokines synthesis. More recently, it has been documented a direct activity of free FAs as ligands of membrane, cytosolic, and nuclear receptors, and cumulative evidence has emerged, demonstrating its participation in a wide range of physiological and pathological conditions. It has been long known that the central nervous system is enriched with poly-unsaturated FAs, such as arachidonic (C20:4ω-6) or docosohexaenoic (C22:6ω-3) acids. These lipids participate in the regulation of membrane fluidity, axonal growth, development, memory, and inflammatory response. Furthermore, a whole family of low molecular weight compounds derived from FAs has also gained special attention as the natural ligands for cannabinoid receptors or key cytokines involved in inflammation, largely expanding the role of FAs as precursors of signaling molecules. Nutritional deficiencies, and alterations in lipid metabolism and lipid signaling have been associated with developmental and cognitive problems, as well as with neurodegenerative diseases. The molecular mechanism behind these effects still remains elusive. But in the last two decades, different families of proteins have been characterized as receptors mediating FAs signaling. This review focuses on different receptors sensing and transducing free FAs signals in neural cells: (1) membrane receptors of the family of G Protein Coupled Receptors known as Free Fatty Acid Receptors (FFARs); (2) cytosolic transport Fatty Acid-Binding Proteins (FABPs); and (3) transcription factors Peroxisome Proliferator-Activated Receptors (PPARs). We discuss how these proteins modulate and mediate direct regulatory functions of free FAs in neural cells. Finally, we briefly discuss the advantages of evaluating them as potential targets for drug design in

order to manipulate lipid signaling. A thorough characterization of lipid receptors of the nervous system could provide a framework for a better understanding of their roles in neurophysiology and, potentially, help for the development of novel drugs against aging and neurodegenerative processes.

Keywords: lipid sensing, neuronal differentiation and development, signal transduction, free fatty acid receptor, fatty acid binding protein, peroxisome proliferator activated receptor, docosahexaenoic acid, arachidonic acid

INTRODUCTION

The central nervous system (CNS) is an intricate network of a variety of cell types, with a wide range of distinct properties and functions. Notoriously, lipids represent a larger proportion of mass than in most other tissues, second only after adipose tissue (Etschmaier et al., 2011). The main difference is that, whereas in adipocytes lipids are mainly stored as energy reserve in lipid droplets, in the CNS lipids fulfill multiple functions; such as forming large extensions of membranes necessary for crosstalk between neural cells. This is not limited only to the inner and plasma membranes of neurons, comprising axons, dendrites, and spines; astrocytes, oligodendrocytes, and microglia also have highly complex cellular shapes and, hence, extensive surface areas defined largely by lipids, and their functions in the healthy brain are integrated both physically and metabolically (von Bernhardi et al., 2016). Brain membranes are constituted by proteins, cholesterol (on average, 21.5% mol/mol lipids), sphingomyelin (1.9%), gangliosides (1.4%) and phospholipids (75.1%) (Scandroglio et al., 2008), where the lipids were typically constrained to structural or support functions for the first ones. Lipid distribution is not equivalent for all cell types or brain regions, and neurons are usually enriched in polyunsaturated glycerolipids and cholesterol (Scandroglio et al., 2008; Chan et al., 2012; Arai et al., 2015; Ingolfsson et al., 2017). These lipids are essential for many cellular processes in CNS. For example, the brain is the richest tissue in cholesterol with up to 20 mg/g of tissue, 10-time more than the rest, and it is mainly synthesized *in situ* (Dietschy and Turley, 2001, 2004). Therefore, its levels are independent from circulating cholesterol, highlighting its pivotal role in multiple brain functions such as signal transduction, synaptic transmission, and cell differentiation by modulation of lipid rafts organization and segregation of membrane proteins, as well as in several pathological conditions, either directly by its self or through its metabolism into neurosteroids and oxysterols (Reddy, 2010; Leoni and Caccia, 2011; Orth and Bellosta, 2012; Vance, 2012).

Lipid signaling has attracted increasing attention as different families of lipids have been shown to exhibit important regulatory functions through highly specific receptors (Fernandis and Wenk, 2007; Sunshine and Iruela-Arispe, 2017). Polyunsaturated fatty acids (PUFAs) are of particular relevance because they can also be transformed into much more potent derivatives, such as eicosanoids and docosanoids, from arachidonic (C20:4ω-6, ARA) and docosahexanoic (C22:6ω-3, DHA) acids, respectively (Serhan, 2014; Dennis and Norris, 2015). In the last decades, different families of proteins have been identified and characterized to mediate signaling processes triggered directly by lipids *per se*, including free FAs (Im, 2004; Kostenis, 2004; Wolfrum, 2007). The interest on how these proteins mediate FAs regulatory functions increased as they have been demonstrated to be targets and/or essential carriers for the therapeutic actions of certain drugs (Wolfrum et al., 2001; Landrier et al., 2004; Martin et al., 2013).

Fatty acids regulatory functions are most probably defined by the group of specific receptors expressed in a particular cell-type and, therefore, they are dynamically modulated throughout the cell life-span, the developmental stage, and its differentiation process. This review resumes part of the present understanding on FAs regulatory functions in pathophysiology of neural tissues and three families of proteins involved in these roles. Noteworthy, other proteins involved in lipid signaling with more promiscuous selectivity of ligands, such as FA Translocase (FAT/CD36) or Toll-like Receptor 4 (TLR4), were not included in this manuscript, and their roles could be consulted elsewhere (Pepino et al., 2014; Magnan et al., 2015; Rocha et al., 2016).

PHYSIOLOGICAL FUNCTIONS AND PARTICIPATION OF FATTY ACIDS IN NEURONAL PATHOLOGIES

Fatty acids are typically considered as a source of energy through β-oxidation, and, as part of phospholipids, either as membrane building blocks or reservoir of second messengers and substrates for cytokines synthesis. They can also induce multiple cellular responses, ranging from cell motility and changes in cell morphology (Kamata et al., 2007; Brown et al., 2014), to regulation of gene expression (Kitajka et al., 2004), modulation of hormones secretion or their effects (Wang and Chan, 2015). But several distinctions must be made when referring to FAs in general, because saturated FAs (SFAs) have a clear different origin, metabolism, and functions compared to essential ω-3 and ω-6 PUFAs. Brain SFAs, such as palmitate (16:0, PA) or stearic (18:0, SA), are known to be generated *in situ* as much as being imported into the brain, whereas PUFAs are elongated and further unsaturated mainly in the liver and then transported through the bloodstream and imported into the neural tissue as non-esterified FAs (Edmond et al., 1998; Chen et al., 2008). Only a small fraction of PUFAs is actually synthesized locally from linoleic (C18:2ω-6) and α-linolenic (C18:3ω-3, ALA) acids; and, due to enzymatic restrictions and competition between ω-3 and ω-6 PUFAS for the same enzymes, less than 5% of total ALA assimilated from diet can be transformed into DHA

(Dyall and Michael-Titus, 2008). Both, endogenous and blood-derived PUFAs, accumulate preferentially in neurons as part of phospholipids.

Neurogenesis includes three contiguous phases, namely proliferation, migration and differentiation, and maturation and integration of the precursor cells; with PUFAs having inherence in all of these stages (Chalon, 2006). Therefore, PUFAs are critical for pre- and post-natal brain development, as well as in adulthood or during natural aging (Uauy and Dangour, 2006; Rombaldi Bernardi et al., 2012). For example, ALA maternal restriction during gestation and lactation impairs hippocampal neuronal differentiation, thus compromising neuronal maturation and related brain functions, such as learning and memory (Bhatia et al., 2011; Niculescu et al., 2011). DHA is the most abundant PUFA and accumulates in the immature brain during perinatal life all through the grey matter expansion; and it can reach over 10% of total FAs in human adult brains (McNamara and Carlson, 2006). Actually, preterm-born adolescents, who skipped the fetal DHA accumulation in the CNS during the last weeks of gestation and usually also lactation during the early life, exhibit deficits in cognitive functions associated to attention, including increased risk for attention-deficit/hyperactivity disorder (ADHD) and schizophrenia (McNamara and Carlson, 2006). That is why dietary deficiencies commonly stimulate a more tightened retention of essential FAs in the brain.

Docosahexanoic acid is particularly important for proper neuronal development in cerebral cortex, retina, and hippocampus, where it promotes neurogenesis and neuronal differentiation (Cao et al., 2009; Gharami et al., 2015). It also boosts synaptogenesis by promoting neurite outgrowth and synapsis formation, accompanied by an increase in the expression of neuronal and synaptic proteins. Particularly, in rat neuronal stem cells, DHA stimulates neuronal differentiation by two mechanisms: (1) a decrease in expression levels of basic Helix-loop-Helix transcription factors (NeuroD, Mash1, Hes1, etc.); and (2) an extension of the expression of cyclin-dependent kinase inhibitor p27 (kip1). This results in an increase in the number of positive cells for the neuronal markers TUBB3 and MAP2 and in a reduction of the percentage of cells in S-phase, suggesting an exit from the cell cycle (Katakura et al., 2009). In aged mice, DHA also prevents neuroinflammation and apoptosis, whereas improving memory (Labrousse et al., 2012). DHA can prevent many of the lipopolysaccharide (LPS) deleterious effects on both neurons and microglia, including loss of dendritic spines or production of nitric oxide as biomarkers of neuroinflammation (Chang et al., 2015). Actually, multiple animal and *in vitro* models of neuroinflammation consistently show a marked anti-inflammatory effect of DHA and other ω-3 PUFAs, presumably by reducing the production of proinflammatory cytokines and/or promoting the secretion of anti-inflammatory cytokines (reviewed in Orr et al., 2013). PUFAs can also directly modify neurotransmitter production, accumulation, release, and re-uptake. Dopamine's content, storage in presynaptic vesicles and tyramine-stimulated release, for example, significantly decrease in rat frontal cortex after chronic ω-3 PUFAs deficiency (Delion et al., 1996; Zimmer et al., 1998, 2000). Contrarily, supplementation with ω-3 PUFAs increases dopamine levels in the same area (Chalon et al., 1998).

Fatty acids have been implicated in neuropathological conditions, including neurodegenerative diseases, mental disorders, stroke, and trauma. Severe dietary restriction of essential FAs usually correlates with anxiety-like behavior and deficit in cognitive functions, including memory and learning. However, imbalance between ω-3 and ω-6 PUFAs during gestation also leads to alterations in brain development. In adults, an imbalance in the PUFAs ratio in brain membranes is believed to be a risk factor active during the pathogenesis of neurological and psychiatric disorders (Chalon, 2006). For example, an increase in ARA is known to promote α-Synuclein aggregation. However, it is not clear which is the most relevant cause affecting secretion of dopamine and serotonin, the greater availability of ARA, the deficiency of DHA or the imbalance between them (Chalon, 2006). During normal aging, there is a common cognitive decline and an increasing risk of dementia. High ω-3 PUFAs intake slows down this decline (Johnson and Schaefer, 2006; van Gelder et al., 2007), suggesting that they may have neuroprotective action in the aging brain and even therapeutic potential. Aging is also characterized by increased oxidative stress and neuroinflammation together with altered energy metabolism (reviewed in Prolla and Mattson, 2001). Beside changes in FA composition that favor monounsaturated FAs (MUFAs) over ω-3 and ω-6 PUFAs with time in rodents, the aging brain is also prone to lipid oxidation due to its large content of PUFAs (Favrelere et al., 2000). In humans, the decrease of PUFAs, though subtler during normal aging, is quite evident in neurodegenerative pathologies, including Alzheimer Disease (AD), Parkinson's Disease (PD), Schizophrenia and depression (reviewed in Hussain et al., 2013). Nevertheless, PUFAs are known to promote α-Synuclein pathological aggregation (Yakunin et al., 2012). On the other hand, the anterior cingulate cortex of depressive patients shows reduced quantities of SFAs and PUFAs (Conklin et al., 2010). The deficiency of ω-3 PUFAs also impairs the normal signaling of endocannabinoid in prelimbic prefrontal cortex and accumbens, leading to abnormal emotional behavior (Lafourcade et al., 2011). The reduction in total PUFAs in erythrocyte's membranes of patients with early onset schizophrenia correlates with the degree of demyelination in brain white matter (Peters et al., 2009). Finally, PUFAs also serve as anti-depressants and anti-convulsants, confer protection against traumatic insults, and enhance repairing processes. For example, numerous animal models of epilepsy support the anticonvulsant properties of PUFAs, like the greater resistance to pentylenetetrazol-induced seizures in ω-3 PUFAs fed rats (Taha et al., 2009).

Arachidonic acid is particularly enriched in phosphatidylinositol (PI), whereas DHA is a major component of brain phosphatidylethanolamine (PE) and phosphatidylserine (PS). Both PUFAs are highly enriched in the phospholipids of the synaptic plasma membrane and synaptic vesicles (Glomset, 2006). ARA is also particularly rich in membranes of leukocytes, presumably because it serves as a precursor of a myriad of cytokines (Innes and Calder, 2018). PUFAs are almost exclusively found in position 2 of the glycerol

moiety within any phospholipid and, therefore, their release is catalyzed by phospholipases A_2 (PLA_2). Noteworthy, ARA and eicosapentaenoic acid (20:5ω-3, EPA) are released preferentially by cytoplasmic PLA_2 ($cPLA_2$), whereas DHA is released by Ca^{+2}-independent PLA_2 ($iPLA_2$) (Dyall and Michael-Titus, 2008). These three PUFAs can be converted into more potent cytokines than the free FAs, including prostaglandins, leukotrienes, thromboxanes, protectins and resolvins, and their effects differ from one other (Calder, 2015; Dyall, 2017).

Neuroinflammation is a common denominator for several neuropathologies. SFAs are known to promote the inflammatory phenotype of microglia, stimulating the secretion of TNF-α and IL-6 through TLR4. Furthermore, PA exposure of astrocytes leads to Caspase-3 activation and alters Bax/Bcl-2 ratio, both effects promoting apoptosis (Gupta et al., 2012). On the contrary, ω-3 PUFAs usually have a marked antiinflammatory effect by blocking microglia activation and stimulating the secretion of neurotrophic factors. However, some deleterious effects have also been reported, such as the worsening of neuritic injury and astrocytosis in PD-mice model (Hussain et al., 2013). ARA is the precursor for potent proinflammatory eicosanoids. On the other hand, compounds derived from DHA and EPA, known as resolvins and protectins, show strong anti-inflammatory effects and mediate the end of an ongoing inflammatory response (Hussain et al., 2013). These compounds are just an example of those derived from FAs that have important roles in brain pathophysiology. A special mention should be given to endocannabinoids, such as arachidonoylethanolamine (also known as anandamide), arachidonylglycerol or oleoylethanolamine, just to name a few (Freitas et al., 2017). Nevertheless, the role of free FAs has a renewed interest since the identification of multiple receptors that can couple their signaling to diverse cellular responses. The next section focusses on three families of proteins that recognize FAs and could be modulating FAs regulatory functions.

RECEPTORS FOR FATTY ACIDS SIGNALING

Originally, lipid signaling was limited to steroid hormones and its binding to cytosolic receptors, or to cytokines derived from ARA (leukotrienes and thromboxanes) that bind to specific membrane receptors. As of today, three families of proteins have been identified to be able to sense the presence and type of FAs whether in the extracellular medium, the cytosol or the nuclear matrix. At the plasma membrane, FAs can activate G Protein-coupled receptors known as Free Fatty Acid Receptors (FFARs) (Hara et al., 2013; Offermanns, 2013); while in the cytosol they can be taken by Fatty Acid Binding Proteins (FABPs) and targeted to specific subcellular structures or metabolic pathways (Veerkamp and Zimmerman, 2001; Storch and Corsico, 2008). Finally, nuclear receptors Peroxisome Proliferator-Activated Receptors (PPARs) mediate FAs regulatory functions in the nucleus (Zolezzi et al., 2017). The specific spatio-temporal pattern of expression and the co-expression of more than one isoform from each family of proteins in a single cell suggest a platform for sensing and modulating the cellular response to the bioavailability of the different FAs, for example, adapting the cell to developmental or functional requirements. Therefore, the regulatory and signaling roles of free FAs are gaining importance in physiological and pathological processes as these receptors are better characterized.

We describe bellow some of the known characteristics of each family of FAs receptors selected for this review, including expression patterns, structural features, and specific functions in the CNS. Noteworthy, when the source of expression data is not specified, it was taken from The Human Protein Atlas website[1] (Uhlen et al., 2015), based on Genotype-Tissue Expression (GTEx) project (The GTEx Consortium, 2013), or from the Allen Mouse Brain Atlas[2] (Lein et al., 2007).

Plasma Membrane Receptors

A large number of putative genes coding for GPCRs was identified based on genome sequences, and their deorphanization is still in progress (Civelli, 2005; Diaz et al., 2018; Laschet et al., 2018). Particularly, a cluster of 4 sequences (*GPR40*, *GPR41*, *GPR42* and *GPR43*) was identified in chromosome 19 (Sawzdargo et al., 1997) and FAs were proved to work as their specific endogenous ligands (Briscoe et al., 2003; Brown et al., 2003), dubbing this subfamily of GPCRs as FFARs (Offermanns, 2013). Later on, two other receptors activated by FAs were described, GPR84 and GPR120, located in chromosome 12 and 10, respectively; as well as many others activated by diverse lipids derived from FAs, including lysophosphatidic acid (termed LPARs), endocannabinoids (CBs) and hydroxycarboxylic acids (HCAs) (Offermanns, 2013; Audet and Stevens, 2019).

Within the superfamily of GPCRs, FFARs belong to the largest subfamily of Class A/1 (rhodopsin-like) receptors, constituted by a motif of 7 transmembrane segments (TMs) and at least one longer cytosolic domain that serves as binding site for signaling machinery assembly (Dorsam and Gutkind, 2007; Heldin et al., 2016). The ligand recognition site is defined within the transmembrane helix bundle (**Figure 1A**). The original cluster of FFARs was deorphanized by heterologous expression and ligand screening through monitoring cytosolic Ca^{+2} levels (Briscoe et al., 2003). FAs-triggered Ca^{+2} release from the endoplasmic reticulum is PI3K-dependent. However, some of these receptors can also transduce FAs signal through inhibition of cAMP synthesis, CREB, Akt/PKB, and/or Erk phosphorylation, as well as by β-Arrestin recruitment (Kimura et al., 2011; Zamarbide et al., 2014). Each FFAR shows specific patterns of expression and distinctive ligand selectivity. Their functions have been better studied in peripheral tissues, including the promotion of hormone secretion by the pancreas, lipid taste sensing and the activation of immune cells as a preliminary response toward a putative growing infection. Their participation in the CNS had less attention, although recent results suggest that some isoforms could participate in brain development, neuronal differentiation (Ma et al., 2010) and could be potential drug targets against several neuropathies,

[1] www.proteinatlas.org (accessed January 3, 2019)

[2] http://portal.brain-map.org (accessed January 3, 2019)

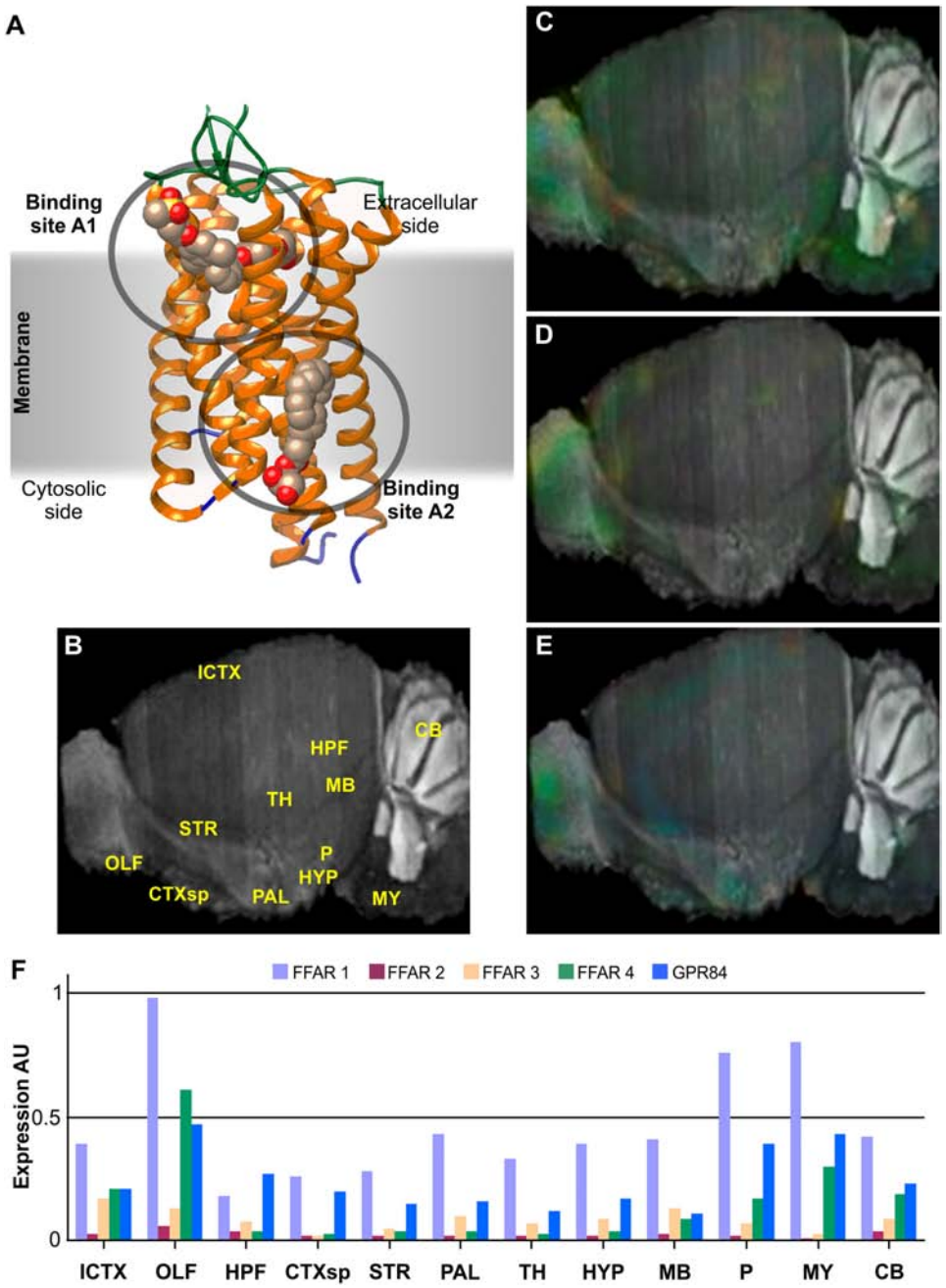

FIGURE 1 | Structure and brain expression patterns of FFARs. **(A)** Cartoon based on FFAR1 crystal structure (PDB-ID: 4PHU) (Srivastava et al., 2014), highlighting membrane orientation and two ligand binding sites in opposite sides of the membrane. **(B)** Central brain section of 8-weeks, male mouse (C57BL/6J) indicating reference regions. **(C–E)** Brain left hemisphere sagittal projection showing expression of FFAR1, FFAR4 and GPR84, respectively, based on *in situ* hybridization (ISH) data. FFAR2 and FFAR3 are not shown due to its lower expression levels. **(F)** Quantification of relative expression from ISH data for all FFARs isoforms. AU: Arbitrary units; ICTX: Isocortex; OLF: Olfactory areas; HPF: Hyppocampal formation; CTXsp: Cortical subplate; STR: Striatum; PAL: Pallidum; TH: Thalamus; HYP: Hypothalamus; MB: Midbrain; P: Pons; MY: Medulla; and CB: Cerebellum. Image credit for panels **C–E**: Allen Institute © 2007 Allen Institute for Brain Science. Allen Mouse Brain Atlas. Available from: http://mouse.brain-map.org/search/. Panels **B** and **F** were constructed from data available through Allen Mouse Brain Atlas website.

such as neuropathic pain and epilepsy (Yoshimura et al., 2015; Yang et al., 2018).

Each isoform presents distinct body expression profiles and different affinity for FAs (Brown et al., 2005; Hara et al., 2013; Offermanns, 2013). There are two FFARs with prominent levels of expression in neural tissues: FFAR1 (also known as GPR40) and FFAR4 (GPR120 or O3FAR). Nevertheless, all isoforms have been detected, though weakly, in some restricted brain region.

We review bellow some of the most recent findings about this novel family of GPCRs activated by FAs.

FFAR1 (GPR40)

The genes that code for FFAR1, FFAR2 and FFAR3, originally named *GPR40*, *GPR43* and *GPR41*, respectively, were identified in 1997 as a group of tandemly encoded genes located on human chromosome 19q13.1. FFAR1 is a 300 amino acids membrane protein of 31.45 kDa. As the product of the single exon gene *GPR40*, it is most abundantly expressed in pancreas and brain of primates (Briscoe et al., 2003; Brown et al., 2005). Other tissues with significant expression include small intestine, spleen, testis, ovaries, and Fallopian tubes. According to GTEx data, within the CNS, higher expression levels of FFAR1 mRNA are found in hippocampus, caudate nucleus, hypothalamus, and cerebral cortex, presumably mainly in neurons but also in glial cells. On the other hand, qPCR targeted experiments showed a wider expression of FFAR1 in neuronal tissues, with higher expression levels in medulla oblongata, *substantia nigra* and spinal cord, followed by putamen, locus cereleus, globus palidus, and amygdala (Briscoe et al., 2003), while western blot analysis showed higher expression in pons, dentate gyrus, pituitary gland, *substantia nigra* and spinal cord, followed by subgranular and subventricular zones, CA1, medulla oblongata, and cerebral cortex, with minor expression in cerebellum (Ma et al., 2007). *In situ* hybridization (ISH) of mice brain sagittal sections indicated discrete preferential FFAR1 expression in olfactory bulb, pons, and medulla (**Figures 1C,F**), while coronal sections highlighted hippocampus and cerebral cortex (Zamarbide et al., 2014). Its levels are weaker than in primates and, hence, it has been suggested that is not essential. Actually, FFAR1-KO mice manifested no evident alteration of social or motor behavior, although they showed a reduction anxiety-like responses (Mancini et al., 2015). An increase in noradrenaline was also observed in FFAR1-KO mice brain regions were the expression of the receptor was shown to be higher, suggesting a role in anxiety and depression symptoms.

This receptor is the only FFAR with solved crystal structures (PDB-ID: 5KW2, 4PHU, 5TZR and 5TZY), as different fusions to Lysozyme, and in complex with different partial and full synthetic agonists, such as TAK-875, MK-8666 or the novel compound (3∼{S})-3-cyclopropyl-3-[2-[1-[2-[2,2-dimethylpropyl-(6-methylpyridin-2-yl) carbamoyl]-5-methoxy-phenyl]piperidin-4-yl]-1-benzofuran-6-yl] propanoic acid (Srivastava et al., 2014; Lu et al., 2017; Ho et al., 2018). Noteworthy, the different structures identified two putative binding sites in opposite sides of the transmembrane region, A1 in the extracellular side and A2 in the cytosolic one (**Figure 1A**). Only the occupancy of the latter by synthetic or natural ligands promotes full agonistic response and structure of intracellular loop IC2 located between transmembrane regions TM3 and TM4, which is believed to be necessary for G-protein interaction. The extracellular loop located between TM4 and TM5 is stabilized by a disulfide bond formed between Cys^{79} and Cys^{170}. Residues participating in ligand recognition have been mapped to include Arg^{183}, Asn^{244} and Arg^{258} that work as anchors for the carboxylic head of the FAs. Residues Tyr^{12}, Tyr^{91}, His^{137}, and Leu^{186} were also identified as relevant for receptor activation; while His^{86}, Tyr^{91}, His^{137} and the anchoring positions seem to be critical for the binding and activation by the synthetic agonist GW9508 (Sum et al., 2007; Tikhonova et al., 2007).

FFAR1 has approximately the same high affinity (EC_{50} 5-60 μM) for medium and long chain saturated FAs ranging from C6 (caproic acid) to C23 (tricosanoic acid), with FAs between C10 to C18 being the preferred endogenous agonists; but it is not active in the presence of acetate, propionate, butyrate, or pentanoate (valerate). It also shows the same range of high affinities for both MUFAs and PUFAs, with ARA (C20:4ω-6), EPA (C22:5ω-3), and DHA (22:6ω-3) exhibiting the highest potencies (Briscoe et al., 2003; Offermanns, 2013). Noteworthy, retinoids can also activate FFAR1 with similar affinities, and, particularly, all-trans-retinoic acid, a well-known factor required for neuronal differentiation (Yu et al., 2012; Janesick et al., 2015), shows one of the highest affinities, $EC_{50} < 5$ μM (Briscoe et al., 2003).

In pancreas, its activation stimulates insulin secretion from β-cells (Itoh et al., 2003), involving signaling by both $G\alpha_{q/11}$ subunit and β-Arrestin2 (Mancini et al., 2015), what does have an impact on systemic metabolism control. Diverse functions have been proposed for FFAR1 in the CNS or the peripheral sensory system. Cartoni et al. (2010) described the expression of FFAR1 in type I cells of the taste buds, along with FFAR4 in type II cells, both participating in the oral perception of fats. FFAR1 has also been associated to neurogenesis and linked to cognitive functions such as memory, space orientation and learning (Ma et al., 2008; Yamashima, 2008; Boneva et al., 2011; Zamarbide et al., 2014). Although these effects are probably mediated mainly by phosphorylation of CREB, its signaling pathway is still not well understood. Since $G\alpha_s$ proteins do not seem to be activated by FFAR1, an alternative phosphorylation of CERB via Erk has been proposed (Yamashima, 2012). Differentiation and maturation of cultures of rat neuronal stem cells overexpressing FFAR1 can be stimulated by DHA, promoting neurite outgrowth and branching, even at concentrations as low as 1,5 μM (Ma et al., 2010). FFAR1 has also been proved to mediate the antinociceptive activities of DHA via induction of secretion of μ and δ opioid peptides, but not κ opioid peptides (Nakamoto et al., 2012). In the hypothalamus FFAR1 is expressed in NPY and POMC expressing neurons linked to satiety and control of food intake, and its activation by its synthetic agonist TUG905 increase POMC (anorexigenic precursor) secretion that leads to body weight loss (Dragano et al., 2017).

High fat diet in mice and PA-albumin complex in neuroblastome derived cells in culture were shown to stimulate synthesis of amyloid precursor protein (APP) and β-site APP cleaving enzyme 1 (BACE1), promoting the release of Aβ peptides in hippocampus and brain cortex, similarly to Akt pathways activation by GW9508 agonist of FFAR1 (Kim et al., 2017). This effect can be blocked in SK-N-MC cells *in vitro* if FFAR1 is pharmacologically inhibited with GW1100, knocked down by siRNA or delocalized from lipid rafts when membranes are depleted from cholesterol with methyl-β-cyclodextrin. However, GW9508 activation of FFAR1 in a mouse model of AD, based on Aβ intracerebroventricular (icv) injection, leads to significant

improvement in cognitive and behavioral tests, what seems to be mediated by CREB phosphorylation and the concomitant increase in expression of NGF and BDNF neurotrophic factors. These effects were not observed when the inhibitor GW1100 was co-administered with the synthetic agonist (Khan et al., 2016). As these opposing effects originate from divergent signaling pathways from a single receptor, exploitation of FFAR1 synthetic agonists or inhibitors for treating neuropathologies may be a task worth pursuing. But first, it is imperative to fully characterize the signal transduction mechanisms active in the CNS, as well as to develop specific drugs that can selectively activate only those promoting neuroprotection, neuronal differentiation, and maturation. During the last decades, an increasing amount of evidence was collected linking the etiology and pathology of AD with Type-2 Diabetes Mellitus (Benedict and Grillo, 2018; Ferreira et al., 2018; Chornenkyy et al., 2019). Considering the wide range of synthetic agonist of FFAR1 being developed to treat Diabetes, it became an interesting possibility to evaluate their repurposing for treating AD as well (Li et al., 2016; Chen et al., 2019). For example, two different mouse models of diabesity (diabetes and obesity), based on high fat diet or db/db mice, present a decrease in FFAR1 and BDNF expression in the hippocampus and brain cortex, that can be reverted by chronic administration of DHA or GW9608 (Sona et al., 2018). Since it can be inhibited by Erk and MAPK inhibitors, BDNF expression depends on FFAR1-pErk pathway.

FFAR2 (GPR43)

Although the gene structure of GPR43 is not yet fully defined, FFAR2 was described to be encoded as a 330 amino acids protein (37.14 kDa) in a single exon. Its structure is predicted to have a topology very similar to FFAR1, where the extra 30 amino acids would correspond mainly to a longer C-terminal tail. However, FFAR2 preferential endogenous ligands are limited to acetate, propionate, butyrate, and pentanoate (with EC_{50} somewhat an order of magnitude larger than those for FFAR1), and this receptor does not respond to ligands with chain length above C6 (Brown et al., 2003; Offermanns, 2013). Its activation has been describe to be coupled both to pertussis toxin sensitive ($G\alpha_i$) and insensitive ($G\alpha_q$) proteins (Brown et al., 2003; Stoddart et al., 2008). In the first pathway, FFAR2 activation leads to a decrease in cAMP production by adenylate cyclase (AC) and, therefore, to a reduction in protein kinase cAMP-activated (PKA) activity. On the other hand, $G\alpha_q$ activates phospholipase C (PLC) that cleaves phosphatidylinositol bisphosphates (PIP_2) into inositol-triphosphate (IP_3) and diacylglycerol. IP_3 binds to IP_3R receptor in the endoplasmic reticulum and induces the internal release of Ca^{+2} to the cytosol, which then activates Ca^{+2}-dependent protein kinase C (PKC). DAG attracts certain PKC isoforms to the plasma membrane and helps to direct its activity to a subset of potential target substrates.

FFAR2 is most abundantly expressed in spleen, bone marrow, and lung, followed by adipose tissue, breast, and all the digestive tract. Its expression is mainly consistent with a leukocyte markers expression pattern, with higher presence in macrophages and leukocyte germ line (Brown et al., 2003). The low level, but widespread FFAR2 expression may be due to its presence in immune cells, such as infiltrating neutrophils and macrophages. Its expression in CNS is rather low compared to other FFARs (**Figure 1F**) and limited to glia and neurons of the caudate, but FFAR2 can also be detected in cortical neurons and pituitary gland. However, the participation of FFAR2 in neuronal processes still needs further analysis.

FFAR3 (GPR41)

FFAR3 is the product of the gene *GPR41*, only 6.62 kb downstream of *GPR40* promoter, but it lacks a formal promoter of its own. Although 3 sites of transcription initiation can be predicted in putative exons upstream *GPR41*, none of them could be confirmed. Contrarily, *GPR41* may be expressed as the result of the skipping of a termination sequence immediately downstream FFAR1 stop codon. Bahar Halpern et al. (2012) demonstrated that *GPR40* and *GPR41* are transcribed as a single bicistronic mRNA thanks to the action of an H2R enhancer, and that a tissue-specific internal ribosome entry site controls the translation of *GPR41* into FFAR3 in pancreatic β-cells. FFAR3 is also coded in a single exon, as a 346 amino acids protein (38.,65 kDa). *GPR40*-common origin is inferred from the relatively high sequence similarity/identity (31/34%), compared to other GPCRs. Like FFAR2, its structure is believed to be similar to FFAR1, with the extra 46 amino acids mainly corresponding to an extension of the cytosolic C-terminal tail; and its activation is mainly due to the binding of the same short chain FAs (Brown et al., 2003). The difference is that pentanoate is more potent than acetate for FFAR3, while it is quite the opposite for FFAR2. FFAR3 activation has been described to be coupled only to Gαi subunits. Its activation by β-hydroxy-butirate negatively regulates the activity of Cav2.2 N-type Ca^{+2} channel (Won et al., 2013; Colina et al., 2018).

High-throughput RNAseq screening analysis of FFAR3 expression indicated a widespread, but weak pattern, with higher levels observed in adipose tissue, breast, spleen, and digestive tract. Neural expression is scarce (**Figure 1F**) and only very weakly detected in the pituitary gland in GTEx (The GTEx Consortium, 2013). A GPR41-mRFP transgenic mice model published by Nohr et al. (2013) showed FFAR3 expression in the digestive tract intimately associated to the enteroendocrine system, mainly in enteric neurons of the submucosal and myenteric ganglia, and in several of the postganglionic sympathetic and sensory neurons, both in autonomic and somatic peripheral nervous system (PNS). But this model showed no expression in the brain or spinal cord. FFAR3 enteroendocrine expression links signaling of short FAs from the microbiota with enteric hormone secretion (Samuel et al., 2008). Its activation by short chain FAs and β-hydroxy-butirate in sympathetic neurons also inhibited $Ca_V2.2$ currents, linking the functions of the PNS to the metabolic state (Won et al., 2013).

FFAR4 (GPR120)

The gene that codes for FFAR4, originally called *GPR120*, was described in 2003 to have four exons that are located on human chromosome 10q23.33 (Fredriksson et al., 2003). It is expressed, at least, as two variants generated by alternative splicing that

leads to exon 3 skipping, *GPR120S* (coding for a 361 amino acids peptide, 40,49 kDa) and *GPR120L* (377 amino acids, 42,24 kDa). Predicted transmembrane regions leave N- and C-terminal segments longer than in previous FFARs, but the most notorious difference is the cytoplasmic loop between TM5 and TM6, where the *GPR120S* lacks 16 amino acids (from 233 to 248) compared to the longer variant *GPR120L*. Activation of FFAR4 signals through $G\alpha_{q/11}$.

Highest expression of FFAR4 includes lower digestive tract, brain, adipose tissue, lung, testis, breast, and adrenal glands. Within the CNS, FFAR4 is found mainly in glial and neuronal cells of hippocampus, cerebral cortex, hypothalamus, and cerebellum (only granular layer and Purkinje cells), with a particularly high expression in pituitary gland (The GTEx Consortium, 2013). ISH of mice brain sections show FFAR4 preferential expression in medulla, pons and olfactory bulb, followed by hypothalamus and cerebellum (**Figures 1D,F**).

FFAR4 natural ligands include saturated FAs of C14, C16 and C18, with affinities around EC_{50} = 30, 52 and 18 μM, respectively. When overexpressed in HEK293 cells, both agonist-stimulated GPR120S and GPR120L receptors recruit β-Arrestin2 and undergo internalization, but the longer variant shows much less Ca^{+2} mobilization and average cellular response (Watson et al., 2012). Two Arg residues on the outer edge of TM2 (Arg^{99}) and TM4 (Arg^{178}) have been mapped to be responsible for FAs binding (Watson et al., 2012), unlike the other FFARs members that have two conserved Arg residues on the outer edge of TM5 and TM7 (Sum et al., 2007; Stoddart et al., 2008), showing once more the evolutionary divergence of FFAR4 from the rest of the GPCRs activated by FAs. Other residues involved in ligand binding and activation of the receptor included four aromatic residues Phe^{115}, Phe^{211}, Trp^{277}, and Phe^{304} that, when mutated, essentially eliminated responsiveness to agonists (Hudson et al., 2014).

FFAR4 has been more thoroughly studied in adipocytes and intestine where it promotes insulin sensitizing and anti-inflammatory effects, respectively (Song et al., 2017). In enteroendocrine cells it helps controlling the secretion of hormones, promoting glucagon-like peptide 1 release but inhibiting ghrelin secretion (Hirasawa et al., 2005; Engelstoft et al., 2013); whereas, in adipocytes, oleic acid stimulates lipid droplet formation by activation of this receptor, which signals through $G\alpha_q$, PI3K-Akt, and PLC pathways (Rohwedder et al., 2014; Villegas-Comonfort et al., 2017). However, it has a greater affinity for PUFAs, particularly those from the ω-3 series. In Caco-2 cells, EPA, DHA, and ARA elicit the same signaling events through FFAR4, but with different kinetics and efficiency (Mobraten et al., 2013). Basal and heterologous phosphorylation of Thr^{347}, Ser^{350}, and Ser^{357} in the C-terminal tail (GPR120S) mediates receptor internalization (Burns et al., 2014; Sanchez-Reyes et al., 2014). Hypothalamic expression of FFAR4 corresponds to microglia and its activation ameliorates neuroinflammatory response by decreasing the production of proinflammatory cytokines (TNFα and IL-1β) and promoting those with anti-inflammatory action (IL-6 and IL-10) (Dragano et al., 2017).

GPR84

This isoform was identified, through an EST library, in B cells encoded in a single exon (exon2) (Wittenberger et al., 2001), but it was the last one to be deorphanized (Wang et al., 2006). Therefore, GPR84 is the least studied isoform of the FFARs and has not yet been assigned with the "FFAR5" name. Its expression was confirmed by Northern-blot in brain, colon, thymus, spleen, kidney, liver, intestine, placenta, lung, leukocytes, heart, and muscle. Regarding CNS expression, it is most abundantly found in medulla and spinal cord, but also significantly in amygdala, *substantia nigra*, thalamus, and *corpus callosum*, whereas only weakly detected in other brain regions such as the cerebellum (Wittenberger et al., 2001) (**Figures 1E,F**). GPR84 is activated only by medium length acyl chain FAs (C9 to C14) and does not recognize longer or shorter chain carboxylic acids, promoting Ca^{+2} mobilization and inhibiting cAMP production, mainly through the activation of $G\alpha_{i/o}$ (Wang et al., 2006). Its expression is augmented in monocytes by incubation with LPS, and its activation by medium chain FAs exacerbates the production of proinflammatory cytokines, highlighting GPR84 role in immune responses (Wang et al., 2006; Muller et al., 2017). Alternatively to endogenous ligands, GPR84 can also be activated by hidroxylated medium chain FAs and synthetic drugs like ZQ16 (2-(hexylthio)pyrimidine-4,6-diol), diindolylmethane or 6-n-octylaminouracil (Suzuki et al., 2013; Nikaido et al., 2015; Zhang et al., 2016).

When activated, GPR84 expressed in mouse primary cultures of microglia stimulates membrane ruffling, modifies its morphology, and promotes motility, but it does not promote an inflammatory response, including the secretion proinflammatory cytokines (Wei et al., 2017). Different FAs are known to be released after diverse brain injuries, from traumatic lesions to neurodegenerative diseases and neuroinflammatory conditions, and they may function as chemo-attractants for microglia, especially short and middle chain FAs that exhibit higher solubility and that can be recognized by FFAR2, FFAR3, and GPR84. This suggests that GPR84 could be a valid therapeutic target in microglia-associated diseases, such as AD or Multiple Sclerosis.

Citosolic Receptors

Due to their low solubility, free FAs need to be bound to proteins in order to diffuse through the aqueous medium of the cytosol. Since the 1970s, the proteins known as FABPs have been studied and proved to help overcome this problem. They are small (15 kDa) intracellular soluble proteins that reversibly bind FAs and other hydrophobic ligands, trafficking them to different intracellular compartments, such as mitochondria, peroxisome, endoplasmic reticulum or the nucleus. Even with as low as 30% identity of amino acids sequence, they share a highly conserved structure (**Figures 2A,B**), consisting in a barrel of 10 β-strands enclosing the binding cavity, and a helix-turn-helix motif capping this barrel. The latter regulates both ligand entry and exit, as well as origin and destiny points of traffic (Banaszak et al., 1994; Thompson et al., 1999; Storch and Corsico, 2008; Storch and Thumser, 2010). These proteins have been

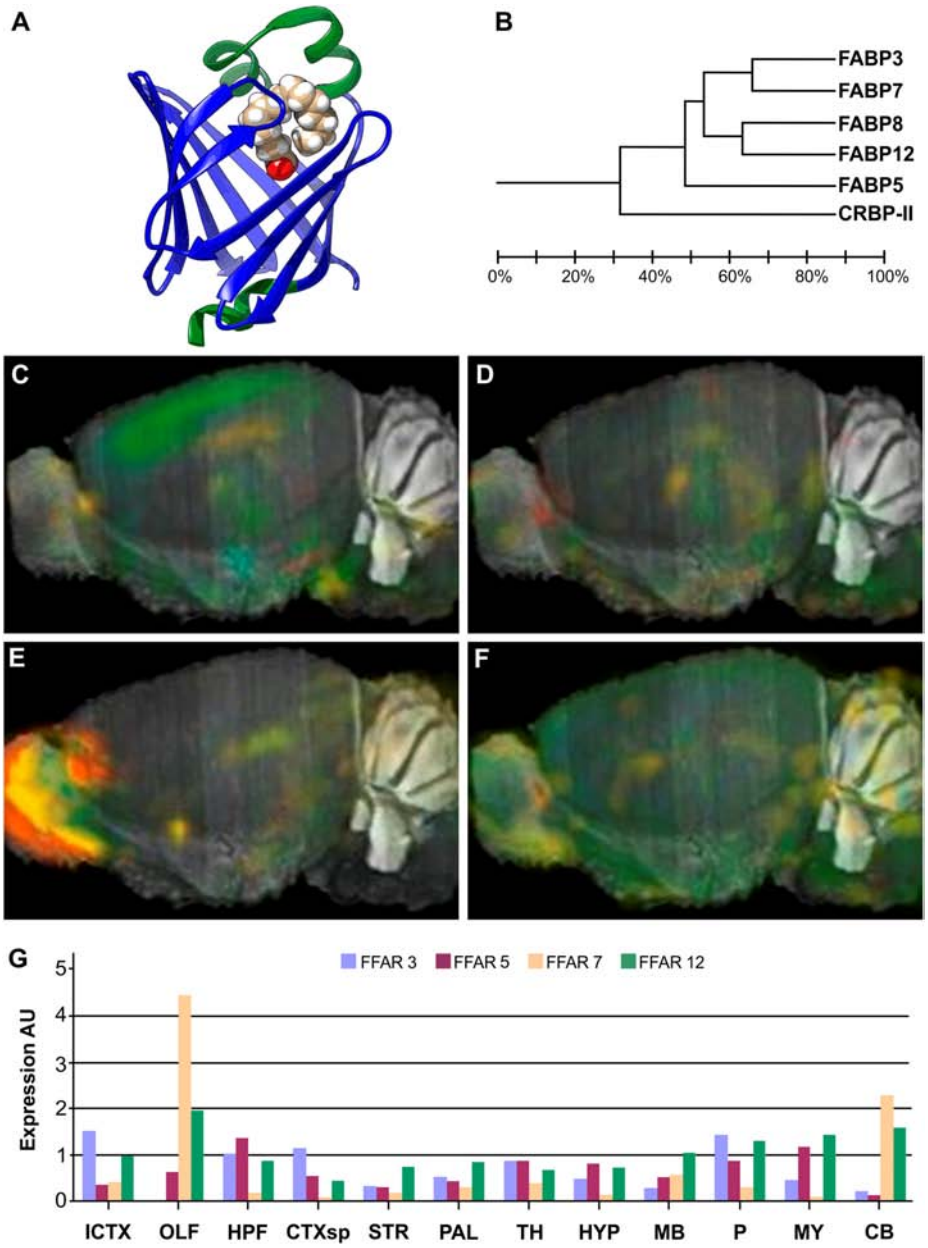

FIGURE 2 | Structure and brain expression patterns of FABPs. **(A)** Cartoon based on crystal structure of human FABP3 complex with palmitic acid (PDB-ID: 6AQ1) (Yan et al., 2018). The β-barrel, array of 10 antiparallel β-strands, is shown in blue, and the helix-tur-helix motif cap is shown in green, with the palmitic acid (in filled-balls model) adopting a U-shaped conformation inside. **(B)** Dendrogram showing relationship between identity of sequence between FABPs expressed in neural tissues. Also belonging to the same folding, CRBP-II was included as and outlier. **(C–F)** Brain left hemisphere sagittal projection showing expression of FABP3, FABP5, FABP7 and FABP12, respectively, based on ISH data. FABP8 expression in mice brain is not significant. **(G)** Quantification of relative brain expression from ISH data for neural FABPs isoforms. AU: Arbitrary units. For brain regions references see legend of **Figure 1**. Image credit for panels **C**–**F**: Allen Institute. © 2007 Allen Institute for Brain Science. Allen Mouse Brain Atlas. Available from: http://mouse.brain-map.org/search/. Panel **G** was constructed from data available through Allen Mouse Brain Atlas website.

extensively characterized *in vitro*, including its three-dimensional structures by NMR and X-ray Crystallography, with and without any cargo, natural or synthetic (Sacchettini et al., 1987; Xu et al., 1991; Ory et al., 1997; Balendiran et al., 2000; Hanhoff et al., 2002; Rademacher et al., 2002; Reese and Banaszak, 2004). They can uptake FAs from model phospholipid vesicles and transfer its cargo to other membranes, according to the properties of each isoform (Herr et al., 1996; Storch and Thumser, 2000; Veerkamp and Zimmerman, 2001; Liou et al., 2002; Storch et al., 2002; Falomir-Lockhart et al., 2006). It has been demonstrated that some isoforms interact better with membranes in the apo-form, presumably looking for ligand uptake; whereas others are

dominated mainly by electrostatic interaction between the holo-protein and the phospholipid's headgroups (Falomir-Lockhart et al., 2006, 2011).

FABPs were originally named after the tissue where each isoform was firstly identified, and intestinal enterocytes were the exception that expressed large quantities of two isoforms, FABP1 and FABP2. Nowadays, the numbered nomenclature is preferred over tissue-related names in order to avoid misinterpretations derived from the fact that most cell types can express more than one member of the FABP family, and their level of expression responds to metabolic conditions, external stimuli, or development stages. Therefore, most FABPs show distinctive expression patterns in different organs and cell types. No isoform shows a high degree of selectivity for a particular FA, although it is usually found a higher affinity for saturated compared to unsaturated FAs (Richieri et al., 2000). The affinity for FAs of each isoform depends on chain length and number of double bonds, but isoforms FABP1 and FABP5 show significant affinity for a wider range of hydrophobic ligands. A total of 9 FABP isoforms with high affinity for long chain FAs (between C12 and C22) are described in mammals, plus 4 more members that show specificity for retinoid ligands (CRBP-I, CRBP-II, CRABP1 and CRABP2) and one extra for bile acids (FABP6, I-BABP or ILBP).

There are five FABP isoforms with relevant levels of expression in neural tissues: FABP3 (commonly known also as Heart-FABP), FABP5 (Epidermal-FABP), FABP7 (Brain-FABP), FABP8 (Myelin-FABP or PMP2), and FABP12 (Retinal-FABP). Each of them presents distinct spatio-temporal expression patterns (Owada et al., 1996; Liu et al., 2000). Many of them are significantly expressed in the brain, whereas FABP8 is apparently exclusive of PNS. Bellow there is a resume of the most prominent information available about each neural isoform.

FABP3

Significant expression of FABP3 is not detected in embryonic stages of rodent or in fetal human brains (Cheon et al., 2003; Saino-Saito et al., 2009). Perinatal FABP3 expression increases gradually, mainly confined to gray matter in rodents. In adult individuals, FABP3 is stably expressed in the neuronal layers of hippocampus, the cerebral neocortex, interneurons of the retina and the olfactory mitral cell layer, particularly in CA1 and CA2 portions (Owada, 2008; Saino-Saito et al., 2009). Its mRNA can also be detected in Purkinje and granulate cells of the cerebellum (Owada, 2008). ISH of mice brain slices localizes FABP3 expression in isocortex, cortex, pons and hippocampus (**Figures 2C,G**).

FABP3 shows somewhat preferential binding of ω-6 PUFAs, but affinities for all FAs range from 0.8 to 5 μM. FABP3 is thought to help to consolidate and maintain the differentiated status of neurons in adult brains through the utilization of PUFAs. Actually, brain ARA assimilation and its incorporation into phospholipids correlate with FABP3 expression levels, which is also necessary to maintain an optimal balance between ω-6 and ω-3 PUFAs in adult neurons (Murphy et al., 2005). FABP3 could also modulate dopamine signaling, since it is highly expressed in acetylcholinergic and terminals of glutamatergic neurons of dorsal *striatum*, and it can interact physically and modulate dopamine D2 receptors (D2R) in mice (Shioda et al., 2010). This was confirmed by dysfunctional response of D2R to amphetamines and to D2R-specific agonist Haloperidol in FABP3$^{-/-}$ mice; whereas response to D1R-specific agonist SCH23390 was not impaired. The expression of FABP3 in dopaminergic neurons is still controversial, even between the same authors (Shioda et al., 2010, 2014). On the other hand, FABP3 can be found in the cochlea, as well as FABP7, not involved in sensing but present in different support cells, suggesting a non-redundant function of these proteins in modulation of the hearing process (Saino-Saito et al., 2010).

Regarding pathological conditions, FABP3 was found to be significantly decreased in frontal, occipital, and parietal cortices of patients suffering Down Syndrome; and it was also elevated in temporal cortex of patients with AD (Cheon et al., 2003; Sanchez-Font et al., 2003; Watanabe et al., 2007). FABP3 expression in dopaminergic neurons may promote MPTP and ARA-induced α-Synuclein aggregation (Shioda et al., 2014), the main component of the characteristic Lewy Bodies present in PD and related neurodegenerative diseases. Furthermore, aberrant expression of FABP3 may affect PUFA enrichment and alter membrane fluidity and signal transduction. Consequently, this deficiency could lead to cellular dysfunction in neurodegenerative disorders.

FABP5

FABP5 is the most ubiquitously expressed FABP. During midterm embryonic stages, it is particularly present in the ventricular germinal zone and the cerebral cortex, as well as in the stem cells differentiating into motor neurons or astrocytes. But its expression progressively decreases after birth until it is only weakly detected in the adult brain (Liu et al., 2010). This moderate expression is shared, with varying intensity in different brain regions, by neurons and glia (**Figures 2D,G**). Regarding mouse retina, FABP5 is found in the retinal ganglion cells, up to E14 strictly localized in the soma, but progressively migrating into axons of optic nerve by E18 and until P10 (Allen et al., 2001; Saino-Saito et al., 2009). This suggests that FABP5 may have a role in neurite outgrowth and axon development by supplying LCFA for phospholipid synthesis. FABP5 also shows high affinity for retinoic acid (RA) and, therefore, it is associated to neuronal survival and differentiation by activation of PPARβ/δ, not only through FAs but RA signaling as well. Actually, the latter depends on the distribution ratio between CRABP2 and FABP5, and it may be as well modulated by displacement from either protein by FAs, and particularly by DHA (Schug et al., 2007, 2008; Yu et al., 2012). Recent publications also link FABP5 to regulatory functions of estrogen receptors (Senga et al., 2018), which could be related to its heterodimerization to Retinoid X Receptors (RXRs), similarly to PPARs.

FABP5 expression is induced under pathological or stress conditions, for example, after axonal injury in peripheral nerves (De Leon et al., 1996), but not in Down Syndrome, AD or Bipolar Disorder (Cheon et al., 2003). Under oxidative stress conditions, FABP5 has been proved to work as a scavenging system of 4-Hydroxynonenal lipid peroxidation subproduct (Bennaars-Eiden et al., 2002). Altogether, we can summarize

that FABP5 is expressed when the fate of the neural cell differentiation must be decided or when it has to adapt to stress or pathological conditions.

FABP7

In embryonic brains, FABP7 is highly expressed in the radial glia, in the ventricular and subventricular zones. After birth, the expression remains strongly positive in gray and white matter (Kurtz et al., 1994). In the neonatal brain, its expression is more evident in the olfactory nerve fiber layers, hippocampal dentate gyrus, and the cerebellar Purkinje cell layer. Finally, in adulthood, the expression decreases although it remains in the Schwann cells of olfactory nerve, in the radial glia of dentate gyrus, and in the glial cells located adjacent to the cerebellar Purkinje cells (Kurtz et al., 1994). Its mRNA expression in 8 weeks-old mice is evident only in olfactory bulb and the cerebellum (**Figures 2E,G**). FABP7 was proposed to be downstream regulator of Pax6 participating in the maintenance of pre-neurogenesis neuroepithelia, while its knock-down promotes neuronal differentiation (Arai et al., 2005). FABP7 and FABP3 are usually expressed in the same regions of the brain, with the later usually showing 10-time higher levels, although local concentration may vary (Pelsers et al., 2004). As mentioned before, both proteins are present in different support cells of the cochlea, suggesting a regulatory function of hearing signals (Saino-Saito et al., 2010). FABP7 is also expressed by glial progenitor cells located in the foregut and midgut during enteric nervous system development (Sasselli et al., 2012).

FABP7 preferentially binds ω-3 PUFAs and oleic acid (18:1n-9, OA) over ω-6 PUFAs, and shows lower affinity for SFAs (Xu et al., 1996; Balendiran et al., 2000; Hanhoff et al., 2002). Therefore, null mice display decreased DHA incorporation into PLs, with an increase in AA and PA instead (Owada, 2008). Its up-regulation during embryonic stages of development (and, probably, FABP5's as well) is likely related to the proliferation and initial differentiation of neural stem cells and progenitorse, with an increasing demand of PUFAs, rather than to their maturation and integration (Liu et al., 2010). Actually, the fluorescent probe CDr3 was identified as a specific ligand for FABP7 in neural stem cells (Yun et al., 2012) and successfully employed for its flow cytometry isolation from both adult and embryonic mouse brains (Leong et al., 2013).

Regarding pathological conditions, FABP7 has been shown to be significantly increased in occipital cortex of patients with Down Syndrome, although no changes were detected in fetal brain (Cheon et al., 2003). Gene allele association studies showed correlation of FABP7 expression with schizophrenia and bipolar disorder (Saino-Saito et al., 2010).

FABP8

FABP8 can be abundantly and exclusively found, although unevenly distributed, in the myelin sheaths and Schwann cells of peripheral nerves, for example, in the human *nervus suralis*. It can represent up to 15% of total protein of bovine PNS myelin (Greenfield et al., 1973). In mice, mRNA levels increase gradually and the protein is detectable after P4 (Zenker et al., 2014). FABP8 is present only in minor amounts in CNS white matter, being more abundant in spinal cord and brain stem myelin. The expression levels of FABP8 vary both in intensity and distribution between different regions of a single nerve as well as between nerves (DeArmond et al., 1980).

FABP8 has a unique function in the organization and stabilization of myelin multilayers as it is capable of stacking phospholipid membranes synergistically with Myelin Basic Protein (Greenfield et al., 1973). Its higher expression during the early postnatal life also suggests a role in FAs uptake and lipid metabolism toward myelination of axons (Zenker et al., 2014). Notably, knock-out of one or both proteins does not affect myelin structure, and its only consequence is a minor retardation in motor nerve conduction (Zenker et al., 2014). However, several point mutations of FABP8 have been associated to the inherited neuropathy known as Charcot-Marie-Tooth disease (Motley et al., 2016; Punetha et al., 2018).

FABP12

The *FABP12* gene was the last one to be identified to code for a member of this family of proteins (Liu et al., 2008) and, hence, has not yet been thoroughly studied like other members. Its mRNA was found at high levels mainly in the retina and testis, and to a lesser extent in the cerebral cortex, kidney and epididymis of rat and mouse tissues (Smathers and Petersen, 2011). ISH of mouse brain sections shows a ubiquitous expression (**Figures 2F,G**). Under oxidative stress conditions, FABP12 protects retinal rod cells from peroxidation mediated by LCFA hydroperoxides (Guajardo et al., 2002).

Nuclear Receptors-Transcription Factors

In many tissues, FAs induce changes in gene expression through nuclear receptors of the PPARs family of transcription factors, ligand-activated nuclear receptors subfamily 1 group C (Capelli et al., 2016). PPARs structure consists of a variable N-terminal region, a conserved DNA binding domain, a variable hinge region, a conserved ligand binding domain, and a variable C-terminal region (Mangelsdorf et al., 1995). Heterodimerization of PPARs with Retinoid-X Receptor (RXR) depends on ligand and DNA binding, being affected also by posttranslational modifications (Berrabah et al., 2011; Anbalagan et al., 2012; Brunmeir and Xu, 2018). The DNA binding domain includes two segments with Zn-fingers motifs, which recognizes its target sequence or Response Element (RE). The N- and C-terminal regions include the Activation-Function 1 (AF1) and 2 (AF2), respectively, essential for interaction with coregulators and transcription modulation functions (**Figure 3A**). PPAR–RXR complexes recognize a direct repeat of the consensus sequence AGGTCA with a single nucleotide in between, also referred to as PPRE: AGGTCA-N_1-AGGTCA. These features have been corroborated by the crystal structures available (PDB-IDs: 3E00, 3DZU, 3DZY) (**Figure 3A**) (Chandra et al., 2008). PPARs are thought to be permanently bound to PPREs as heterodimers with one of the three RXR isoforms (RXRα, RXRβ, or RXRγ). The lack of ligand bound to them promotes their repressor activity through association with corepressors, such as Nuclear Receptor Corepressor (NCoR) or the Silencing Mediator of Retinoid and Thyroid hormone receptor (SMART). Upon ligand binding, corepressors are released and co-activators recruited, including

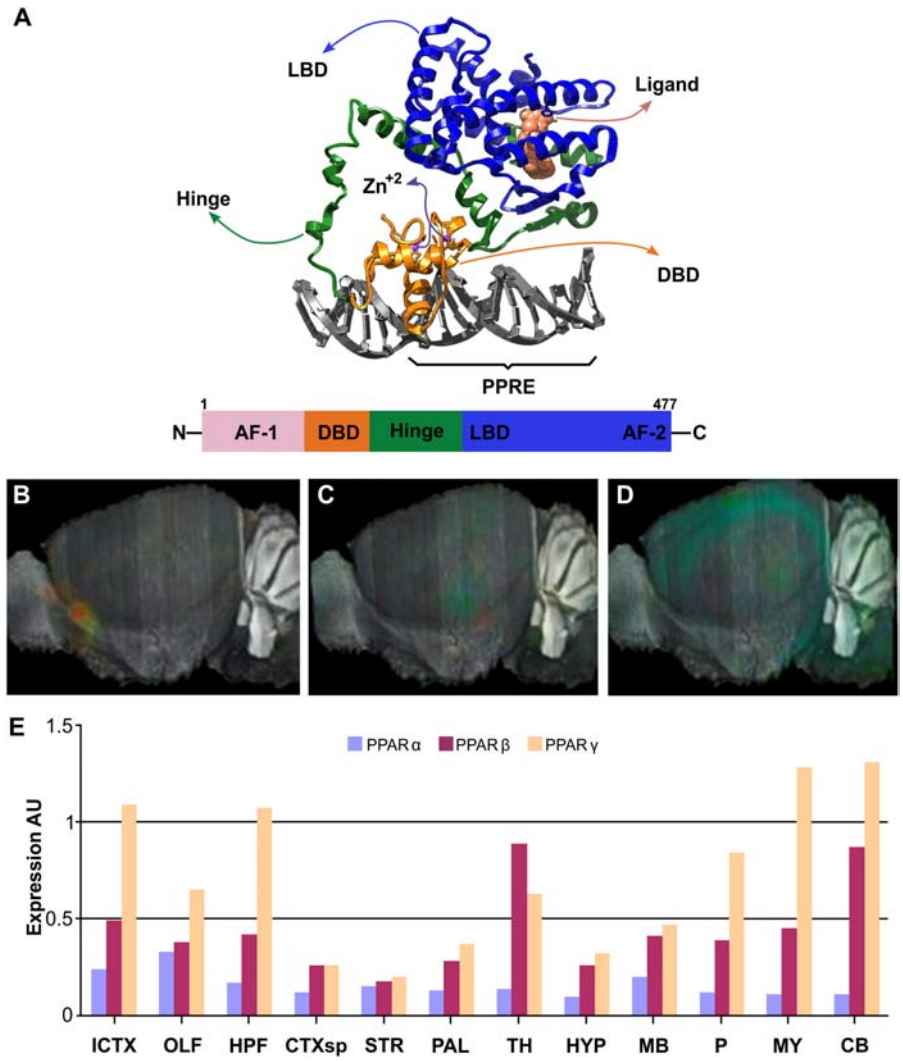

FIGURE 3 | Structure and brain expression patterns of PPARs. **(A)** Cartoon based on crystal structure (PDB-ID: 3DZY) of the full-length PPARγ in a complex with RXRα and two accessory 13-amino acids peptides of Nuclear receptor coactivator 2 and a dsDNA containing the PPRE (Chandra et al., 2008). For clarity, only PPARγ, its synthetic agonist Rosiglitazone and the dsDNA are shown. N-terminal region of PPARγ is not visible because it was not determined due to high flexibility. **(B–D)** Brain left hemisphere sagittal projection showing expression of PPARα, PPARβ and PPARγ, respectively based on ISH data. **(E)** Quantification of relative brain expression from ISH data for neural FABPs isoforms. AU: Arbitrary units. For brain regions references see legend of **Figure 1**. Image credit for panels **B–D**: Allen Institute. © 2007 Allen Institute for Brain Science. Allen Mouse Brain Atlas. Available from: http://mouse.brain-map.org/search/. Panel **E** was constructed from data available through Allen Mouse Brain Atlas website.

p300, CREB-binding protein, or Steroid Receptor Coactivator 1 (SRC1); promoting transcriptional activation of their target genes (Zoete et al., 2007).

PPARα was first identified as a new member of the steroid hormone receptor superfamily and proved to mediate the effects of hypolipidemic drugs commonly used in hyperlipidemias. These drugs were known as peroxisome proliferators, dubbing this receptor PPARs (Issemann and Green, 1990). Parallel identification of multiple isoforms in mammals and *Xenopus* sp. led to some controversy regarding their nomenclature, but nowadays it is accepted that three isoforms are present, comprising PPARα, PPARβ/δ, and PPARγ (Echeverria et al., 2016; Brunmeir and Xu, 2018). Besides FAs, PPARs have also been reported to be activated by other endogenous lipidic compounds, such as endocannabinoids (oleylethanolamide, arachidonylethanolamide, 2-arachidonyl-glycerol, etc.) and by RA (O'Sullivan, 2007; Schug et al., 2007). Unfortunately, little progress has been made identifying natural endogenous ligands which are specific or preferential for any of the PPARs isoforms due to their rather low affinity and similar specificities.

As mentioned above, the activation of PPARs modulates directly the expression of genes near the bound PPER. But a second mechanism of action has been proposed for certain isoforms, blocking or preventing the interaction of other transcription factors. The better studied example corresponds to the ligand-dependent SUMOylation of activated PPARγ that gets

displaced from its PPRE and blocks NFκB interaction with its own response elements and, hence, limiting the inflammatory response (Ricote and Glass, 2007; Glass and Saijo, 2010). This mechanism is known as transrepression and may be a putative target for handling neuroinflmammation.

All PPARs isoforms were detected in the CNS employing multiple techniques, such as reverse transcription-quantitative PCR (RT-qPCR), immunohistochemistry (IHC), and ISH (Kainu et al., 1994; Braissant et al., 1996; Cullingford et al., 1998; Warden et al., 2016). However, despite the vast literature available, there is still some controversy regarding PPARs expression patterns. They are essential for embryonic and fetal development in mammals and, therefore, drug-inducible, tissue specific knockout models have been developed to study their specific roles, particularly for PPARγ null mice which is lethal (Gray et al., 2005; Wang et al., 2013; Rautureau et al., 2017). Double neuronal conditional knockout of PPARβ/δ and PPARγ exacerbates cytotoxicity of 1-methyl-4-phenyl-1,2,3,6-tetrahydropyridine (MPTP) on striatum dopaminergic neurons (Mounsey et al., 2015). Noteworthy, it is not rare to find co-expression of PPARs within a single cell. Some details are offered below about protein expression levels, together with mRNA and protein variants, and the connections of PPARs with brain pathophysiology.

PPARα

Human *PPARA* (or *NR1C1*) gene is located in chromosome 22q12-q13.1 and contains at least 9 exons, with PPARα encoded as a 468 amino acid protein (52.23 kDa). A shorter variant is also described by alternative splicing that introduces an early stop codon after the DNA binding domain and, therefore, is not ligand-sensitive. PPARα shows a wide and similar expression in all tissues, with more prominent levels in liver, intestine, kidney, heart, and skeletal muscle; and its presence is also reported in brown adipose tissue. The higher expression levels of PPARα in these tissues correlate with their high capacities for FAs oxidation, and its main function seems to be related to the control of energy expenditure through lipid catabolism and the adaptation to different nutritional states, such as the postprandial period or fasting. Regarding CNS expression, the GTEx project detected similar levels of *PPARA* mRNA in caudate, pituitary gland, hypothalamus, hippocampus, cerebral cortex, and cerebellum. Furthermore, ISH of brain section showed very similar expression throughout regions and weaker than other isoforms (**Figures 3B,E**). Targeted expression analysis of PPARα reported it in olfactory bulb, retina, cerebellum, and hippocampus (Braissant et al., 1996; Moreno et al., 2004; Rivera et al., 2014). PPARα has been localized in neurons (Cristiano et al., 2001; Santos et al., 2005), oligodendrocytes (Kainu et al., 1994), microglia (Warden et al., 2016), and specially in astrocytes (Cristiano et al., 2001; Chistyakov et al., 2015).

PPARα shows relatively higher affinities for FAs compared to alternative endogenous agonists (eicosanoids and endocannabinoids), and it can be activated also by hypolimidemic drugs, but generally not or only weakly by non-steroidal anti-inflammatory drugs (NSAIDs) and anti-diabetic thiazolidinediones (Corton et al., 2000). PPARα functions in the CNS are still unclear. Its proposed functions include the regulation of sleep process (Murillo-Rodriguez, 2017), also have an impact on learning and memory consolidation. Nevertheless, it has been shown that PPARα agonists such as Wy-14643 reduce Aβ-derived oxidative damage by increasing catalase activity, and activate the Wnt/β-Catenin survival pathway (Santos et al., 2005). Furthermore, PPARα activation by statins is responsible for boosting BDNF production, that mediates cognitive improvement in another mouse mode of AD (Roy and Pahan, 2015).

PPARβ/δ

Gene structure of *PPARD* (*NR1C2*) gene in chromosome 6p21.2-21.1 consists of 11 exons, with the ORF spanning from exon 4 to exon 9 and coding for a 441 amino acids protein termed PPARδ1 (49,09 kDa). Alternative splicing gives rise to shorter isoforms: 80 amino acids shorter isoform 2 (PPARδ2) is the product of an early stop signal due to overtranscription of the 3'-end of exon 8 that introduces an in-frame non-sense codon; variant 4 lacks 98 amino acids (44 to 141) due to exon skipping; while variant 3 is the result of an alternative transcription initiation site with three new N-terminal amino acids instead of the first 43 residues of PPARδ1 (coded by exon 4). Another four alternative transcription initiation sites may be active in *PPARD* downstream to exon 1 and associated to alternative exon 2 (2a′, 2c, 2c′ and 2e) (Lundell et al., 2007). These mRNA 5′-UTR variants do not alter the final ORF but probably are related to translational regulation of PPARβ/δ. The different isoforms are suspected to show distinctive spatio-temporal expression patterns and/or specific functions. For example, PPARδ2 has been proposed to act as a dominant negative form of PPARδ1 (Dickey et al., 2016).

PPARD expression is broad and is particularly high in tissues associated with FAs metabolism, such as the gastrointestinal tract, heart, kidney, skeletal muscle, fat, and skin. Its systemic physiological function is to coordinate and balance the usage levels of FAs and glucose in muscle and liver. However, PPARβ/δ is also the most predominant PPARs isoform in the human CNS and has a ubiquitous expression in the rat brain (**Figures 3C,E**). Despite, all PPARs are co-expressed in developing CNS, PPARβ/δ remains with high expression levels in adult rats (Braissant et al., 1996), suggesting a role in brain development, mielynation, and neuronal function. It was localized in olfactory bulb, cerebral cortex, basal ganglia, hippocampus, hypothalamus, cerebellum, and spinal cord, among others brain areas (Xing et al., 1995; Braissant et al., 1996; Moreno et al., 2004). In mouse models, PPARβ/δ is widely distributed and has been found in neurons of the prefrontal cortex, nucleus accumbens, amydala, cerebellum, hypothalamus, and spinal cord, at mRNA and protein expression levels (Woods et al., 2003; Warden et al., 2016). Regarding cell types, PPARβ/δ is mainly expressed in neurons (Hall et al., 2008), but it has also been found in oligondendrocytes of the corpus callosum (Moreno et al., 2004), and in primary cultures of cortical and cerebral astrocytes (Cristiano et al., 2001). Among the glial cells, PPARβ/δ only co-localized with oligondendrocytes of the corpus callosum (Woods et al., 2003), but no with astrocytes and microglia. *In vitro*, agonists of PPARβ/δ induce the differentiation of SH-SY5Y cells (Di Loreto et al., 2007).

PPARβ/δ shows preferentially affinities for PUFAs, compared to other FAs and eicosanoids, and is selectively activated by bezafibrate (hypolipidemic drug), GW2433 and L-65041 (NSAIDs) among synthetic agonists (Corton et al., 2000). Regarding its pathological links, PPARβ/δ is repressed in patients with Huntington Disease (HD) and its pharmacological activation improves motor function, reduces neurodegeneration, and increases neuronal survival in a HD mice and cellular models (Dickey et al., 2016). The novel PPARβ/δ agonist gemfibrozil is believed to promote oligodentrocyte differentiation by increasing the expression of genes required for myelin formation (Jana et al., 2012) and could potentially be employed against demyelination-related pathologies.

PPARγ

PPARG (*NR1C3*) gene is located in chromosome 3p25. At least four transcriptional start sites actively transcribe different mRNAs with functional cDNAs coding for PPARγ isoforms. While variants 1, 3 and 4 code for the same PPARγ1 isoform (477 amino acids, 54.68 kDa), mRNA variant 2 codes for PPARγ2 which has an additional 28 amino acids at the N-terminus (505 amino acids, 57,62 kDA). PPARγ1 is expressed in a broad variety of cells including immune and brain cells, whereas PPARγ2 is highly abundant in adipose tissue and is considered the master regulator of adipocyte differentiation, where it controls FAs uptake and storage in lipid droplets as triglycerides. Within the CNS, PPARγ was found to show a more discrete pattern of expression than PPARβ/δ, and to be slightly enriched in the hippocampus, being identified both in neurons and glial cells, including microglia, (Bernardo et al., 2000; Roth et al., 2003; Heneka and Landreth, 2007; Sarruf et al., 2009; Warden et al., 2016; Villapol, 2018). Expression analysis in mice brain by ISH showed hippocampus, isocortex, cerebellum and medulla higher levels of *PPARG* mRNAs (**Figures 3D,E**). In the neuroblastome cell line SH-SY5Y, the activation of PPARγ by synthetic agonists promotes neurite outgrowth and neuronal differentiation (Miglio et al., 2009).

PPARγ shows higher affinities for PUFAs than for MUFAs, and it cannot be activated by SFAs, and its response to eicosanoids, hipolipidemic and NSAIDs is diverse, but it is generally activated by thiazolidinediones (Corton et al., 2000). PPARγ is probably the most studied isoform regarding its functions in immune cells, and its interest in neuropathological processes points toward its strong anti-inflammatory effects (Corona and Duchen, 2015). PPARγ activation can induce differentiation of oligodendrocytes and protects them from TNFα toxicity (Bernardo et al., 2009, 2017; De Nuccio et al., 2015). Furthermore, natural and synthetic agonists PPARγ can control brain inflammation processes by shutting-down proinflammatory phenotype of activated microglia, and inhibiting the expression of surface antigens or the synthesis of proinflammatory signals, such as prostaglandins and nitric oxide (Bernardo and Minghetti, 2006). PPARγ can be either positively or negatively modulated by phosphorylation, according to the residue that is modified (Shao et al., 1998; Anbalagan et al., 2012; Brunmeir and Xu, 2018), and can be sent for degradation via the Ubiquitine-Proteasome pathway. PPARγ ability to transrepress NFκB inhibits, or at least limits, the inflammatory response, a regulatory mechanism activated by SUMOylation of its N-terminal region (Ricote and Glass, 2007; Diezko and Suske, 2013; Glass and Saijo, 2010). This could be a putative target for minimizing the neuroinflammatory condition characteristic of many neurodegenerative diseases, such as PAD and AD. Actually, multiple drugs designed as agonist of PPARγ have been and tested in AD models showed to reduce the β-amyloid accumulation, its cytotoxicity and stimulation of inflammatory cytokines (Combs et al., 2000; Sastre et al., 2006; Zolezzi and Inestrosa, 2013; Bonet-Costa et al., 2016).

FUTURE PERSPECTIVES

Fatty acids participate in essential and diverse cellular processes involving neurons and glial cells, ranging from embryonic and perinatal development of tissues, including the CNS, to cognitive functions such as memory and learning. Therefore, they are unavoidably involved in neuropathological processes, including traumatic brain injury and neurodegenerative diseases. But, due to its rather simple chemical structures and low solubility, FAs require specific proteins that could recognize them and mediate its regulatory or signaling functions. Membrane receptors FFARs, cytosolic transport proteins FABPs and nuclear transcription factors PPARs are the preferential mediators of FAs functions. Taken together, and considering that almost all cell types express at least one member of each of these three families of proteins, we could hypothesize that they may be working as a complex, but coordinated sensory system for FAs. Actually, functional interaction of FABPs and PPARs has already been proved in hepatocytes and adipocytes (Smith et al., 2008; Hostetler et al., 2009). The identification of two possible ligand binding sites in FFAR1 structures in opposite sides of the membrane opens the possibility that they could be regulated and/or activated by intracellular lipids as well as by external lipokines, for example released by PLA_2 enzymes, but also by interaction with FABPs. FABP-FFAR interaction, though not yet proved, could be understood either by unloading FAs cargo from the FABPs to activate the FFARs, or as a termination mechanism of FFAR signaling by retrieval of ligands by the FABPs from the FFARs. This is an interesting possibility that would integrate all FAs receptors (**Figure 4**), and its better understanding would definitely help in the design of new drugs with increased specificity and selectivity for its primary targets, avoiding undesired adverse effects.

Fatty acids signaling effects are usually mixed with those displayed by their multiple derivatives, adding a new layer of complexity to distinguish direct cellular responses free FAs signaling. Although specific receptors have been identified for endocannabinoids, eicosanoids, resolvins, protectines, lysophasphatidic acids, monoacylglycerols, N-acylethanolamines, and so on, crosstalk between the different receptors should not be neglected or discarded. Cellular responses are the result of the integration of a myriad of external and internal signals, as evidenced by the convergence of signaling pathways. Particularly, a functional interaction between FFAR2 and FFAR3 to form an heteromeric receptor

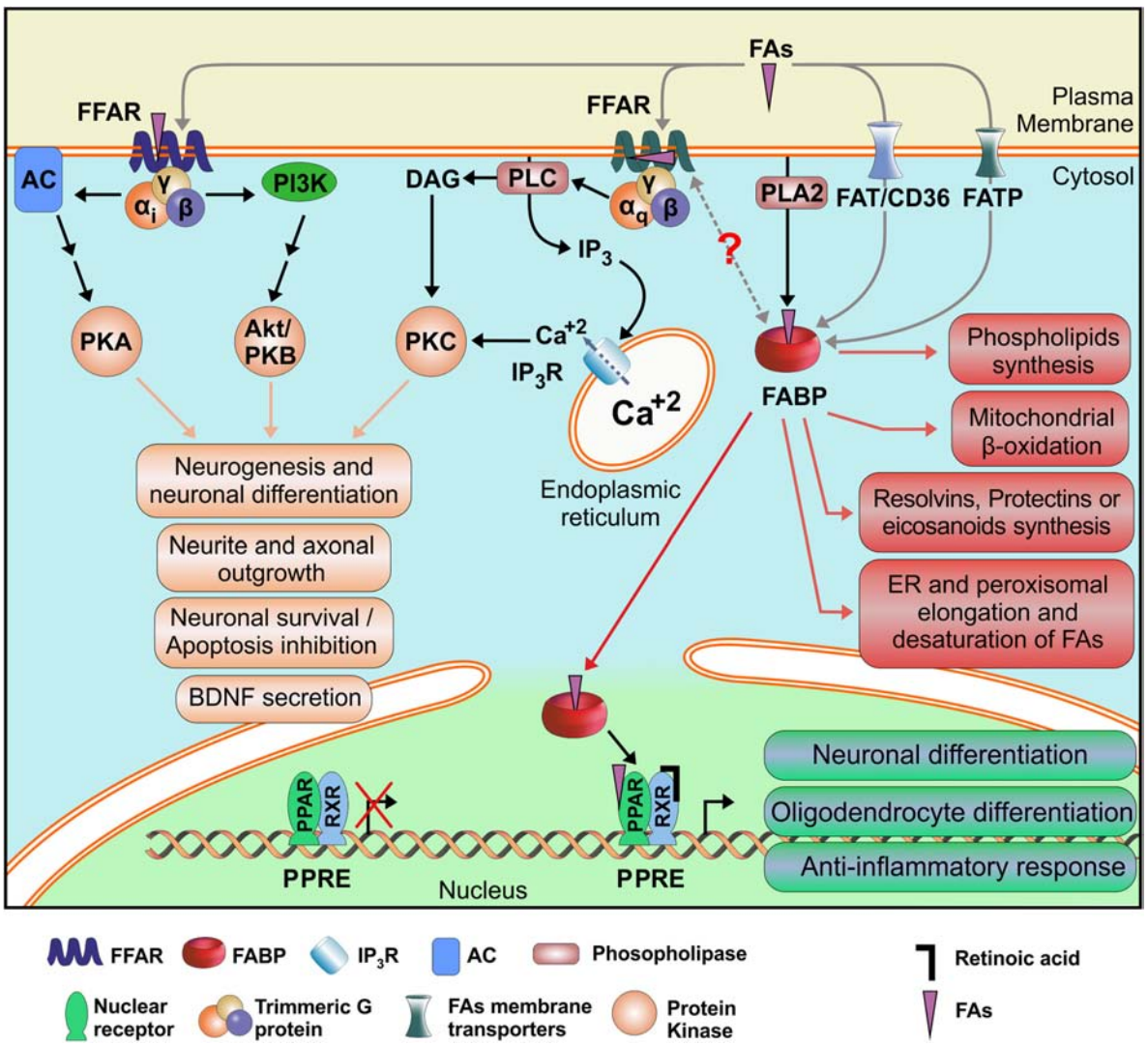

FIGURE 4 | Schematic mechanism proposed for integration of the FAs Receptors System. Alternative FAs receptors are shown along with their demonstrated or putative interactions and their better characterized cellular effects. FFAR: Free Fatty Acid Receptor; FABP: Fatty Acid Binding Protein; PPAR: Peroxisome Proliferator-Activated Receptor; RXR: Retinoid X Receptor; FA: Fatty Acid; PPRE: PPAR Response Element. AC: Adenylate Cyclase; DAG: Diacylglycerol; FATP: FAT/CD36: Fatty Acid Translocase; Fatty Acid Transport Protein; IP3: Inositol (1,4,5)-Trisphosphate; IP_3R: Inositol trisphosphate Receptor; PI3K: Phosphatidyl Inositol (3,4,5)-Trisphosphate Kinase; PLA2: Phospholipase A2; PLC: Phospholipase C; PKA: Protein Kinase A; PKAB/Akt: Protein Kinase B; PKC: Protein Kinase C.

has been proposed in primary monocytes and macrophages, and during heterologous expression in HEK293 cells (Ang et al., 2018). Considering that the origin of the short chain carboxylic acids available in mammals' bloodstream is exclusive from the microbiota colonizing their body, FFAR2 and FFAR3 may act as a remote sensory system to prevent infections, activating the proliferation and modulating the reactivity of immune cells in preparation against a growing focus of bacteria (Ulven, 2012).

Signaling of PUFAs is intimately related to RA signaling, as mentioned above by the similar activation of FFAR1. Furthermore, and similarly to what happens with FABP5 and CRABP2, PPARγ has been described to be activated by RA, as well as RXRs by DHA. In this case, FABP5 translocate its ligand, either DHA or RA, to the nucleus and unload it to the PPARβ/δ (Noy, 2016). Similarly, CRABP2 would do the same to RXR. Therefore, FABP/CRABP2 biological interaction with PPAR/RXXR is not only direct but they also compete for the same ligands, increasing the possibilities of diverse responses mounted and the subset of target genes affected. Regarding this, one must remember that many nuclear receptors heterodimerize with RXRs and, therefore the final cellular response observed is also affected by their presence and ligands (Zhang et al., 2015).

Another utility for FABPs is their detection as early biomarkers of tissue injuries, and increasing evidence is being recorded for the early or differential diagnosis of diverse pathologies (Pelsers et al., 2004, 2005; Wunderlich et al., 2005). Their main advantages are related to their fast release, as close as 30 min to the injurious event, and their relatively fast clearance. Consequently,

FABPs presence in plasma or cephaloraquidean liquid reports for recent trauma, allowing for the differentiation of consecutive events separated by less than 24 h. Neural FABPs detection has been correlated with traumatic brain injury and certain gliomas overexpressing FABP5 or FABP7 (De Rosa et al., 2012; Walder et al., 2013).

Finally, the increasing complexity of the lipid-sensing system available in humans raises the question if the regulatory and signaling functions of FAs can be individually discriminated and specifically targeted for the treatment of pathological conditions. Significant effort is being invested in the development of new drugs that would allow for their precise manipulation and the better treatment of brain injuries, neurological or neurodegenerative diseases by taking advantage of the neuroprotective and anti-inflammatory properties, particularly of PUFAs, employing either FFARs, FABPs, or PPARs as drug targets (Holliday et al., 2012; Wang et al., 2016; Zhou et al., 2016; Li et al., 2018a,b,c, 2019; Shang et al., 2018). Specificity will come together with our better understanding of how these proteins work. For example, an important step forward in this direction is the recent variation analysis of the PPRE sequence for PPARα/RXRα complex that resulted in the ideal sequence WAWVT-RGGBBA-H-RGKTYA (where W = A or T; V = not T; R = A or G; B = not A; H = not G; K = G or T; Y = T or C) as an optimized DNA sequence for PPARα (underlined) and RXRα binding (not underlined) (Tzeng et al., 2015). Noteworthy, although stronger DNA binding of RXRα to PPRE led to higher transcription rates, this is not always the case for PPARα. New candidate target genes have been identified employing this optimized sequence to screen genomic databases as being regulated by PPARα, and that could not be recognized by the consensus sequence for PPRE, improving our understanding of PPARs isoform specific functions. This could also help to development of drugs that could selectively affect only one PPAR isoform and/or only its functions regarding a certain subset of genes under its control.

Another elements that must be considered are non-coding microRNAs (miRs), which act usually as negative regulators of gene expression in the CNS, and several of them have been reported to participate in the regulation exhibited by lipids (Wnuk and Kajta, 2017). For example, the expression levels of miR-21 are decreased by DHA treatment of SH-SY5Y neuroblastome cells, showing an inverse correlation with PPARα levels (Fu et al., 2017). The miR-21 is thought to destabilize PPARα mRNAs and reduce its translation (Chen et al., 2017). Treatment with DHA plus salicylic acid promotes PPARα-RXRα heterodimer formation that correlates with a reduction of miR-21. Together, they promote PSD-95, BDNF and GDNF neuronal differentiation markers and reduce NFκB, COX-2, caspase 3 levels proinflammatory markers (Fu et al., 2017). Similarly, miR-499a negatively regulates the level of expression of PPARγ in microglia cells, promoting the expression of proinflammatory markers, such as iba-1, TNFα and IL-1β (Yu et al., 2018). Finally, PPARs can be activated by valproic acid and its short/medium-chain derivatives, a long time used family of anticonvulsants to treat epilepsy, that has also showed beneficial effects against autism, maniac and bipolar disorders (Lampen et al., 2001; Hunsberger et al., 2013; Hirsch et al., 2018). Its beneficial effects as a promoter of neuroregeneration, neurodifferentiation and neuroprotection (Liu et al., 2012; Foti et al., 2013; Oikawa and Sng, 2016) may come from the modulation of the expression of multiple miRs through PPARs, either by their transrepression or transactivation (Dharap et al., 2015). FFARs may also participate of miRs expression, such as miR-143 that is controlled in adipocytes by both PPARγ and FFAR4 activation (Bae et al., 2017). These line of evidence has recently pushed miRs to be evaluated as novel therapeutic targets against neurodegenerative diseases, such as PD o AD.

Drug discovery strategies focused on FFARs, FABPs and PPARs have already started aiming at neurological and also other pathologies like diabetes, obesity, leukemia, cancer, and so on (Kaczocha et al., 2014; Nikaido et al., 2015; Corona and Duchen, 2016; Wang et al., 2016; Cheng et al., 2019), paving the way for new developments and facilitating drug repurposing, what may save years of research and development. Noteworthy, in the case of FFARs with multiple signal transduction pathways, the concept of biased signaling is of particular interest, where a partial agonistic ligand may only and selectively activate a single pathway over the others available for that receptor. For example, FFARs partial agonist could activate β-Arrestin-mediated but not G protein-mediated signaling (Mancini et al., 2015). This kind of developments has attracted substantial attention for its potential to model molecular differences in receptors functionality that could yield enhanced therapeutic strategies, with improved efficacy and reduced adverse effects (Whalen et al., 2011; Kenakin and Christopoulos, 2013; Correll and McKittrick, 2014).

AUTHOR CONTRIBUTIONS

All authors listed have made a substantial, direct and intellectual contribution to the work, and approved it for publication.

FUNDING

This work was supported by funds from the Consejo Nacional de Investigaciones Científicas y Tecnológicas (CONICET, Argentina, grant PIP2014-618), Agencia Nacional de Promoción Científica y Tecnológica (ANPCyT, Argentina, grants PICT2014-2019 and PICT2016-3776) to LJF-L. AMT was recipient of CONICET postdoctoral fellowship. EG was recipient of CONICET doctoral fellowship and of Bunge & Born Foundation-Max Planck Society-Williams Foundations doctoral research fellowship. GFC was recipient of Consejo Interuniversitario Nacional (CIN, Argentina) undergraduate and of Universidad Nacional de La Plata (UNLP, Argentina) doctoral fellowships.

ACKNOWLEDGMENTS

We are grateful with Rosana del Cid for use-of-English revision, and with Mario R. Ramos for graphic design support. We apologize to all researchers whose work is also relevant to this manuscript but, in interest of space, was not included.

REFERENCES

Allen, G. W., Liu, J., Kirby, M. A., and De Leon, M. (2001). Induction and axonal localization of epithelial/epidermal fatty acid-binding protein in retinal ganglion cells are associated with axon development and regeneration. *J. Neurosci. Res.* 66, 396–405. doi: 10.1002/jnr.1232

Anbalagan, M., Huderson, B., Murphy, L., and Rowan, B. G. (2012). Post-translational modifications of nuclear receptors and human disease. *Nucl. Recept. Signal.* 10:e001. doi: 10.1621/nrs.10001

Ang, Z., Xiong, D., Wu, M., and Ding, J. L. (2018). FFAR2-FFAR3 receptor heteromerization modulates short-chain fatty acid sensing. *FASEB J.* 32, 289–303. doi: 10.1096/fj.201700252RR

Arai, Y., Funatsu, N., Numayama-Tsuruta, K., Nomura, T., Nakamura, S., and Osumi, N. (2005). Role of Fabp7, a downstream gene of Pax6, in the maintenance of neuroepithelial cells during early embryonic development of the rat cortex. *J. Neurosci.* 25, 9752–9761. doi: 10.1523/JNEUROSCI.2512-05.2005

Arai, Y., Sampaio, J. L., Wilsch-Brauninger, M., Ettinger, A. W., Haffner, C., and Huttner, W. B. (2015). Lipidome of midbody released from neural stem and progenitor cells during mammalian cortical neurogenesis. *Front. Cell. Neurosci.* 9:325. doi: 10.3389/fncel.2015.00325

Audet, M., and Stevens, R. C. (2019). Emerging structural biology of lipid G protein-coupled receptors. *Protein Sci.* 28, 292–304. doi: 10.1002/pro.3509

Bae, I.-S., Park, P. J., Lee, J. H., Cho, E.-G., Lee, T. R., and Kim, S. H. (2017). PPARgamma-mediated G-protein coupled receptor 120 signaling pathway promotes transcriptional activation of miR-143 in adipocytes. *Gene* 626, 64–69. doi: 10.1016/j.gene.2017.05.016

Bahar Halpern, K., Veprik, A., Rubins, N., Naaman, O., and Walker, M. D. (2012). GPR41 gene expression is mediated by internal ribosome entry site (IRES)-dependent translation of bicistronic mRNA encoding GPR40 and GPR41 proteins. *J. Biol. Chem.* 287, 20154–20163. doi: 10.1074/jbc.M112.358887

Balendiran, G. K., Schnutgen, F., Scapin, G., Borchers, T., Xhong, N., Lim, K., et al. (2000). Crystal structure and thermodynamic analysis of human brain fatty acid-binding protein. *J. Biol. Chem.* 275, 27045–27054. doi: 10.1074/jbc.M003001200

Banaszak, L., Winter, N., Xu, Z. H., Bernlohr, D. A., Cowan, S., and Jones, T. A. (1994). Lipid-binding proteins - a family of fatty-acid and retinoid transport proteins. *Adv. Protein Chem.* 45, 89–151. doi: 10.1016/S0065-3233(08)60639-7

Benedict, C., and Grillo, C. A. (2018). Insulin resistance as a therapeutic target in the treatment of Alzheimer's disease: a state-of-the-art review. *Front. Neurosci.* 12:215. doi: 10.3389/fnins.2018.00215

Bennaars-Eiden, A., Higgins, L., Hertzel, A. V., Kapphahn, R. J., Ferrington, D. A., and Bernlohr, D. A. (2002). Covalent modification of epithelial fatty acid-binding protein by 4-hydroxynonenal in vitro and in vivo. Evidence for a role in antioxidant biology. *J. Biol. Chem.* 277, 50693–50702. doi: 10.1074/jbc.M209493200

Bernardo, A., Bianchi, D., Magnaghi, V., and Minghetti, L. (2009). Peroxisome proliferator-activated receptor-gamma agonists promote differentiation and antioxidant defenses of oligodendrocyte progenitor cells. *J. Neuropathol. Exp. Neurol.* 68, 797–808. doi: 10.1097/NEN.0b013e3181aba2c1

Bernardo, A., Giammarco, M. L., De Nuccio, C., Ajmone-Cat, M. A., Visentin, S., De Simone, R., et al. (2017). Docosahexaenoic acid promotes oligodendrocyte differentiation via PPAR-gamma signalling and prevents tumor necrosis factor-alpha-dependent maturational arrest. *Biochim. Biophys. Acta* 1862, 1013–1023. doi: 10.1016/j.bbalip.2017.06.014

Bernardo, A., Levi, G., and Minghetti, L. (2000). Role of the peroxisome proliferator-activated receptor-gamma (PPAR-gamma) and its natural ligand 15-deoxy-Delta12, 14-prostaglandin J2 in the regulation of microglial functions. *Eur. J. Neurosci.* 12, 2215–2223. doi: 10.1046/j.1460-9568.2000.00110.x

Bernardo, A., and Minghetti, L. (2006). PPAR-gamma agonists as regulators of microglial activation and brain inflammation. *Curr. Pharm. Des.* 12, 93–109. doi: 10.2174/138161206780574579

Berrabah, W., Aumercier, P., Lefebvre, P., and Staels, B. (2011). Control of nuclear receptor activities in metabolism by post-translational modifications. *FEBS Lett.* 585, 1640–1650. doi: 10.1016/j.febslet.2011.03.066

Bhatia, H. S., Agrawal, R., Sharma, S., Huo, Y.-X., Ying, Z., and Gomez-Pinilla, F. (2011). Omega-3 fatty acid deficiency during brain maturation reduces neuronal and behavioral plasticity in adulthood. *PLoS One* 6:e28451. doi: 10.1371/journal.pone.0028451

Bonet-Costa, V., Herranz-Perez, V., Blanco-Gandia, M., Mas-Bargues, C., Ingles, M., Garcia-Tarraga, P., et al. (2016). Clearing amyloid-beta through PPARgamma/ApoE activation by Genistein is a treatment of experimental Alzheimer's disease. *J. Alzheimers Dis.* 51, 701–711. doi: 10.3233/JAD-151020

Boneva, N. B., Kaplamadzhiev, D. B., Sahara, S., Kikuchi, H., Pyko, I. V., Kikuchi, M., et al. (2011). Expression of fatty acid-binding proteins in adult hippocampal neurogenic niche of postischemic monkeys. *Hippocampus* 21, 162–171. doi: 10.1002/hipo.20732

Braissant, O., Foufelle, F., Scotto, C., Dauca, M., and Wahli, W. (1996). Differential expression of peroxisome proliferator-activated receptors (PPARs): tissue distribution of PPAR-alpha, -beta, and -gamma in the adult rat. *Endocrinology* 137, 354–366. doi: 10.1210/endo.137.1.8536636

Briscoe, C. P., Tadayyon, M., Andrews, J. L., Benson, W. G., Chambers, J. K., Eilert, M. M., et al. (2003). The orphan G protein-coupled receptor GPR40 is activated by medium and long chain fatty acids. *J. Biol. Chem.* 278, 11303–11311. doi: 10.1074/jbc.M211495200

Brown, A. J., Goldsworthy, S. M., Barnes, A. A., Eilert, M. M., Tcheang, L., Daniels, D., et al. (2003). The Orphan G protein-coupled receptors GPR41 and GPR43 are activated by propionate and other short chain carboxylic acids. *J. Biol. Chem.* 278, 11312–11319. doi: 10.1074/jbc.M211609200

Brown, A. J., Jupe, S., and Briscoe, C. P. (2005). A family of fatty acid binding receptors. *DNA Cell Biol.* 24, 54–61. doi: 10.1089/dna.2005.24.54

Brown, M., Roulson, J.-A., Hart, C. A., Tawadros, T., and Clarke, N. W. (2014). Arachidonic acid induction of Rho-mediated transendothelial migration in prostate cancer. *Br. J. Cancer* 110, 2099–2108. doi: 10.1038/bjc.2014.99

Brunmeir, R., and Xu, F. (2018). Functional regulation of PPARs through post-translational modifications. *Int. J. Mol. Sci.* 19:E1738. doi: 10.3390/ijms19061738

Burns, R. N., Singh, M., Senatorov, I. S., and Moniri, N. H. (2014). Mechanisms of homologous and heterologous phosphorylation of FFA receptor 4 (GPR120): GRK6 and PKC mediate phosphorylation of Thr(3)(4)(7), Ser(3)(5)(0), and Ser(3)(5)(7) in the C-terminal tail. *Biochem. Pharmacol.* 87, 650–659. doi: 10.1016/j.bcp.2013.12.016

Calder, P. C. (2015). Marine omega-3 fatty acids and inflammatory processes: effects, mechanisms and clinical relevance. *Biochim. Biophys. Acta* 1851, 469–484. doi: 10.1016/j.bbalip.2014.08.010

Cao, D., Kevala, K., Kim, J., Moon, H.-S., Jun, S. B., Lovinger, D., et al. (2009). Docosahexaenoic acid promotes hippocampal neuronal development and synaptic function. *J. Neurochem.* 111, 510–521. doi: 10.1111/j.1471-4159.2009.06335.x

Capelli, D., Cerchia, C., Montanari, R., Loiodice, F., Tortorella, P., Laghezza, A., et al. (2016). Structural basis for PPAR partial or full activation revealed by a novel ligand binding mode. *Sci. Rep.* 6:34792. doi: 10.1038/srep34792

Cartoni, C., Yasumatsu, K., Ohkuri, T., Shigemura, N., Yoshida, R., Godinot, N., et al. (2010). Taste preference for fatty acids is mediated by GPR40 and GPR120. *J. Neurosci.* 30, 8376–8382. doi: 10.1523/JNEUROSCI.0496-10.2010

Chalon, S. (2006). Omega-3 fatty acids and monoamine neurotransmission. *Prostaglandins Leukot. Essent. Fatty Acids* 75, 259–269. doi: 10.1016/j.plefa.2006.07.005

Chalon, S., Delion-Vancassel, S., Belzung, C., Guilloteau, D., Leguisquet, A. M., Besnard, J. C., et al. (1998). Dietary fish oil affects monoaminergic neurotransmission and behavior in rats. *J. Nutr.* 128, 2512–2519. doi: 10.1093/jn/128.12.2512

Chan, R. B., Oliveira, T. G., Cortes, E. P., Honig, L. S., Duff, K. E., Small, S. A., et al. (2012). Comparative lipidomic analysis of mouse and human brain with Alzheimer disease. *J. Biol. Chem.* 287, 2678–2688. doi: 10.1074/jbc.M111.274142

Chandra, V., Huang, P., Hamuro, Y., Raghuram, S., Wang, Y., Burris, T. P., et al. (2008). Structure of the intact PPAR-gamma-RXR- nuclear receptor complex on DNA. *Nature* 456, 350–356. doi: 10.1038/nature07413

Chang, P. K.-Y., Khatchadourian, A., McKinney, R. A., and Maysinger, D. (2015). Docosahexaenoic acid (DHA): a modulator of microglia activity and dendritic spine morphology. *J. Neuroinflammation* 12:34. doi: 10.1186/s12974-015-0244-5

Chen, C. T., Green, J. T., Orr, S. K., and Bazinet, R. P. (2008). Regulation of brain polyunsaturated fatty acid uptake and turnover. *Prostaglandins Leukot. Essent. Fatty Acids* 79, 85–91. doi: 10.1016/j.plefa.2008.09.003

Chen, J.-J., Gong, Y.-H., and He, L. (2019). Role of GPR40 in pathogenesis and treatment of Alzheimer's disease and type 2 diabetic dementia. *J. Drug Target.* 27, 347–354. doi: 10.1080/1061186X.2018.1491979

Chen, Q., Qiu, F., Zhou, K., Matlock, H. G., Takahashi, Y., Rajala, R. V. S., et al. (2017). Pathogenic role of microRNA-21 in diabetic retinopathy through downregulation of PPARalpha. *Diabetes* 66, 1671–1682. doi: 10.2337/db16-1246

Cheng, A., Shinoda, Y., Yamamoto, T., Miyachi, H., and Fukunaga, K. (2019). Development of FABP3 ligands that inhibit arachidonic acid-induced alpha-synuclein oligomerization. *Brain Res.* 1707, 190–197. doi: 10.1016/j.brainres.2018.11.036

Cheon, M. S., Kim, S. H., Fountoulakis, M., and Lubec, G. (2003). "Heart type fatty acid binding protein (H-FABP) is decreased in brains of patients with Down syndrome and Alzheimer's disease," in *Advances in Down Syndrome Research. Journal of Neural Transmission Supplement 67*, ed. G. Lubec (Vienna: Springer), 225–234. doi: 10.1007/978-3-7091-6721-2_20

Chistyakov, D. V., Aleshin, S. E., Astakhova, A. A., Sergeeva, M. G., and Reiser, G. (2015). Regulation of peroxisome proliferator-activated receptors (PPAR) α and -γ Of rat brain astrocytes in the course of activation by toll-like receptor agonists. *J. Neurochem.* 134, 113–124. doi: 10.1111/jnc.13101

Chornenkyy, Y., Wang, W.-X., Wei, A., and Nelson, P. T. (2019). Alzheimer's disease and type 2 diabetes mellitus are distinct diseases with potential overlapping metabolic dysfunction upstream of observed cognitive decline. *Brain Pathol.* 29, 3–17. doi: 10.1111/bpa.12655

Civelli, O. (2005). GPCR deorphanizations: the novel, the known and the unexpected transmitters. *Trends Pharmacol. Sci.* 26, 15–19. doi: 10.1016/j.tips.2004.11.005

Colina, C., Puhl, H. L. III, and Ikeda, S. R. (2018). Selective tracking of FFAR3-expressing neurons supports receptor coupling to N-type calcium channels in mouse sympathetic neurons. *Sci. Rep.* 8:17379. doi: 10.1038/s41598-018-35690-z

Combs, C. K., Johnson, D. E., Karlo, J. C., Cannady, S. B., and Landreth, G. E. (2000). Inflammatory mechanisms in Alzheimer's disease: inhibition of beta-amyloid-stimulated proinflammatory responses and neurotoxicity by PPARgamma agonists. *J. Neurosci.* 20, 558–567. doi: 10.1523/JNEUROSCI.20-02-00558.2000

Conklin, S. M., Runyan, C. A., Leonard, S., Reddy, R. D., Muldoon, M. F., and Yao, J. K. (2010). Age-related changes of n-3 and n-6 polyunsaturated fatty acids in the anterior cingulate cortex of individuals with major depressive disorder. *Prostaglandins Leukot. Essent. Fatty Acids* 82, 111–119. doi: 10.1016/j.plefa.2009.12.002

Corona, J. C., and Duchen, M. R. (2015). PPAR c and PGC-1 a as Therapeutic Targets in Parkinson ' s. *Neurochem. Res.* 40, 308–316. doi: 10.1007/s11064-014-1377-0

Corona, J. C., and Duchen, M. R. (2016). PPARgamma as a therapeutic target to rescue mitochondrial function in neurological disease. *Free Radic. Biol. Med.* 100, 153–163. doi: 10.1016/j.freeradbiomed.2016.06.023

Correll, C. C., and McKittrick, B. A. (2014). Biased ligand modulation of seven transmembrane receptors (7TMRs): functional implications for drug discovery. *J. Med. Chem.* 57, 6887–6896. doi: 10.1021/jm401677g

Corton, J. C., Anderson, S. P., and Stauber, A. (2000). Central role of peroxisome proliferator-activated receptors in the actions of peroxisome proliferators. *Annu. Rev. Pharmacol. Toxicol.* 40, 491–518. doi: 10.1146/annurev.pharmtox.40.1.491

Cristiano, L., Bernardo, A., and Cerù, M. P. (2001). Peroxisome proliferator-activated receptors (PPARs) and peroxisomes in rat cortical and cerebellar astrocytes. *J. Neurocytol.* 30, 671–683. doi: 10.1023/A:1016525716209

Cullingford, T. E., Bhakoo, K., Peuchen, S., Dolphin, C. T., Patel, R., and Clark, J. B. (1998). Distribution of mRNAs encoding the peroxisome proliferator-activated receptor alpha, beta, and gamma and the retinoid X receptor α, β, and γ in rat central nervous system. *J. Neurochem.* 70, 1366–1375. doi: 10.1046/j.1471-4159.1998.70041366.x

De Leon, M., Welcher, A. A., Nahin, R. H., Liu, Y., Ruda, M. A., Shooter, E. M., et al. (1996). Fatty acid binding protein is induced in neurons of the dorsal root ganglia after peripheral nerve injury. *J. Neurosci. Res.* 44, 283–292. doi: 10.1002/(sici)1097-4547(19960501)44:3<283::aid-jnr9>3.0.co;2-c

De Nuccio, C., Bernardo, A., Cruciani, C., De Simone, R., Visentin, S., and Minghetti, L. (2015). Peroxisome proliferator activated receptor-gamma agonists protect oligodendrocyte progenitors against tumor necrosis factor-alpha-induced damage: effects on mitochondrial functions and differentiation. *Exp. Neurol.* 271, 506–514. doi: 10.1016/j.expneurol.2015.07.014

De Rosa, A., Pellegatta, S., Rossi, M., Tunici, P., Magnoni, L., Speranza, M. C., et al. (2012). A radial glia gene marker, fatty acid binding protein 7 (FABP7), is involved in proliferation and invasion of glioblastoma cells. *PLoS One* 7:e52113. doi: 10.1371/journal.pone.0052113PONE-D-12-11234

DeArmond, S. J., Deibler, G. E., Bacon, M., Kies, M. W., and Eng, L. F. (1980). A neurochemical and immunocytochemical study of P2 protein in human and bovine nervous systems. *J. Histochem. Cytochem.* 28, 1275–1285. doi: 10.1177/28.12.6785343

Delion, S., Chalon, S., Guilloteau, D., Besnard, J. C., and Durand, G. (1996). alpha-Linolenic acid dietary deficiency alters age-related changes of dopaminergic and serotoninergic neurotransmission in the rat frontal cortex. *J. Neurochem.* 66, 1582–1591. doi: 10.1046/j.1471-4159.1996.66041582.x

Dennis, E. A., and Norris, P. C. (2015). Eicosanoid storm in infection and inflammation. *Nat. Rev. Immunol.* 15, 511–523. doi: 10.1038/nri3859

Dharap, A., Pokrzywa, C., Murali, S., Kaimal, B., and Vemuganti, R. (2015). Mutual induction of transcription factor PPARgamma and microRNAs miR-145 and miR-329. *J. Neurochem.* 135, 139–146. doi: 10.1111/jnc.13220

Di Loreto, S., D'Angelo, B., D'Amico, M. A., Benedetti, E., Cristiano, L., Cinque, B., et al. (2007). PPARbeta agonists trigger neuronal differentiation in the human neuroblastoma cell line SH-SY5Y. *J. Cell. Physiol.* 211, 837–847. doi: 10.1002/jcp.20996

Diaz, C., Angelloz-Nicoud, P., and Pihan, E. (2018). Modeling and Deorphanization of Orphan GPCRs. *Methods Mol. Biol.* 1705, 413–429. doi: 10.1007/978-1-4939-7465-8_21

Dickey, A. S., Pineda, V. V., Tsunemi, T., Liu, P. P., Miranda, H. C., Gilmore-Hall, S. K., et al. (2016). PPAR-delta is repressed in Huntington's disease, is required for normal neuronal function and can be targeted therapeutically. *Nat. Med.* 22, 37–45. doi: 10.1038/nm.4003

Dietschy, J. M., and Turley, S. D. (2001). Cholesterol metabolism in the brain. *Curr. Opin. Lipidol.* 12, 105–112.

Dietschy, J. M., and Turley, S. D. (2004). Thematic review series: brain Lipids. Cholesterol metabolism in the central nervous system during early development and in the mature animal. *J. Lipid Res.* 45, 1375–1397. doi: 10.1194/jlr.R400004-JLR200

Diezko, R., and Suske, G. (2013). Ligand binding reduces SUMOylation of the peroxisome proliferator-activated receptor gamma (PPARgamma) activation function 1 (AF1) domain. *PLoS One* 8:e66947. doi: 10.1371/journal.pone.0066947

Dorsam, R. T., and Gutkind, J. S. (2007). G-protein-coupled receptors and cancer. *Nat. Rev. Cancer* 7, 79–94. doi: 10.1038/nrc2069

Dragano, N. R. V., Solon, C., Ramalho, A. F., de Moura, R. F., Razolli, D. S., Christiansen, E., et al. (2017). Polyunsaturated fatty acid receptors, GPR40 and GPR120, are expressed in the hypothalamus and control energy homeostasis and inflammation. *J. Neuroinflammation* 14:91. doi: 10.1186/s12974-017-0869-7

Dyall, S. C. (2017). Interplay between n-3 and n-6 long-chain polyunsaturated fatty acids and the endocannabinoid system in brain protection and repair. *Lipids* 52, 885–900. doi: 10.1007/s11745-017-4292-8

Dyall, S. C., and Michael-Titus, A. T. (2008). Neurological benefits of omega-3 fatty acids. *Neuromolecular Med.* 10, 219–235. doi: 10.1007/s12017-008-8036-z

Echeverria, F., Ortiz, M., Valenzuela, R., and Videla, L. A. (2016). Long-chain polyunsaturated fatty acids regulation of PPARs, signaling: Relationship to tissue development and aging. *Prostaglandins Leukot. Essent. Fatty Acids* 114, 28–34. doi: 10.1016/j.plefa.2016.10.001

Edmond, J., Higa, T. A., Korsak, R. A., Bergner, E. A., and Lee, W. N. (1998). Fatty acid transport and utilization for the developing brain. *J. Neurochem.* 70, 1227–1234. doi: 10.1046/j.1471-4159.1998.70031227.x

Engelstoft, M. S., Park, W.-M., Sakata, I., Kristensen, L. V., Husted, A. S., Osborne-Lawrence, S., et al. (2013). Seven transmembrane G protein-coupled receptor repertoire of gastric ghrelin cells. *Mol. Metab.* 2, 376–392. doi: 10.1016/j.molmet.2013.08.006

Etschmaier, K., Becker, T., Eichmann, T. O., Schweinzer, C., Scholler, M., Tam-Amersdorfer, C., et al. (2011). Adipose triglyceride lipase affects triacylglycerol metabolism at brain barriers. *J. Neurochem.* 119, 1016–1028. doi: 10.1111/j.1471-4159.2011.07498.x

Falomir-Lockhart, L. J., Franchini, G. R., Guerbi, M. X., Storch, J., and Córsico, B. (2011). Interaction of enterocyte FABPs with phospholipid membranes: clues for specific physiological roles. *Biochim. Biophys. Acta* 1811, 452–459. doi: 10.1016/j.bbalip.2011.04.005

Falomir-Lockhart, L. J., Laborde, L., Kahn, P. C., Storch, J., Córsico, B., Falomir Lockhart, L. J., et al. (2006). Protein-membrane interaction and fatty acid transfer from intestinal fatty acid-binding protein to membranes. Support for a multistep process. *J. Biol. Chem.* 281, 13979–13989. doi: 10.1074/jbc.M511943200

Favrelere, S., Stadelmann-Ingrand, S., Huguet, F., De Javel, D., Piriou, A., Tallineau, C., et al. (2000). Age-related changes in ethanolamine glycerophospholipid fatty acid levels in rat frontal cortex and hippocampus. *Neurobiol. Aging* 21, 653–660. doi: 10.1016/S0197-4580(00)00170-6

Fernandis, A. Z., and Wenk, M. R. (2007). Membrane lipids as signaling molecules. *Curr. Opin. Lipidol.* 18, 121–128. doi: 10.1097/MOL.0b013e328082e4d5

Ferreira, L. S. S., Fernandes, C. S., Vieira, M. N. N., and De Felice, F. G. (2018). Insulin Resistance in Alzheimer's Disease. *Front. Neurosci.* 12:830. doi: 10.3389/fnins.2018.00830

Foti, S. B., Chou, A., Moll, A. D., and Roskams, A. J. (2013). HDAC inhibitors dysregulate neural stem cell activity in the postnatal mouse brain. *Int. J. Dev. Neurosci.* 31, 434–447. doi: 10.1016/j.ijdevneu.2013.03.008

Fredriksson, R., Höglund, P. J., Gloriam, D. E., Lagerström, M. C., and Schiöth, H. B. (2003). Seven evolutionarily conserved human rhodopsin G protein-coupled receptors lacking close relatives. *FEBS Lett.* 554, 381–388. doi: 10.1016/S0014-5793(03)01196-7

Freitas, H. R., Isaac, A. R., Malcher-Lopes, R., Diaz, B. L., Trevenzoli, I. H., and De Melo Reis, R. A. (2017). Polyunsaturated fatty acids and endocannabinoids in health and disease. *Nutr. Neurosci.* 21, 695–714. doi: 10.1080/1028415X.2017.1347373

Fu, Y., Zhen, J., and Lu, Z. (2017). Synergetic neuroprotective effect of docosahexaenoic acid and aspirin in SH-Y5Y by inhibiting miR-21 and activating RXRalpha and PPARalpha. *DNA Cell Biol.* 36, 482–489. doi: 10.1089/dna.2017.3643

Gharami, K., Das, M., and Das, S. (2015). Essential role of docosahexaenoic acid towards development of a smarter brain. *Neurochem. Int.* 89, 51–62. doi: 10.1016/j.neuint.2015.08.014

Glass, C. K., and Saijo, K. (2010). Nuclear receptor transrepression pathways that regulate inflammation in macrophages and T cells. *Nat. Rev. Immunol.* 10, 365–376. doi: 10.1038/nri2748

Glomset, J. A. (2006). Role of docosahexaenoic acid in neuronal plasma membranes. *Sci. STKE* 2006:pe6. doi: 10.1126/stke.3212006pe6

Gray, S. L., Dalla Nora, E., and Vidal-Puig, A. J. (2005). Mouse models of PPAR-gamma deficiency: dissecting PPAR-gamma's role in metabolic homoeostasis. *Biochem. Soc. Trans.* 33, 1053–1058. doi: 10.1042/BST20051053

Greenfield, S., Brostoff, S., Eylar, E. H., and Morell, P. (1973). Protein composition of myelin of the peripheral nervous system. *J. Neurochem.* 20, 1207–1216. doi: 10.1111/j.1471-4159.1973.tb00089.x

Guajardo, M. H., Terrasa, A. M., and Catala, A. (2002). Retinal fatty acid binding protein reduce lipid peroxidation stimulated by long-chain fatty acid hydroperoxides on rod outer segments. *Biochim. Biophys. Acta* 1581, 65–74. doi: 10.1016/S1388-1981(02)00121-X

Gupta, S., Knight, A. G., Gupta, S., Keller, J. N., and Bruce-Keller, A. J. (2012). Saturated long-chain fatty acids activate inflammatory signaling in astrocytes. *J. Neurochem.* 120, 1060–1071. doi: 10.1111/j.1471-4159.2012.07660.x

Hall, M. G., Quignodon, L., and Desvergne, B. (2008). Peroxisome proliferator-activated receptor β/δ in the brain: Facts and hypothesis. *PPAR Res.* 2008:780452. doi: 10.1155/2008/780452

Hanhoff, T., Lücke, C., and Spener, F. (2002). Insights into binding of fatty acids by fatty acid binding proteins. *Mol. Cell. Biochem.* 239, 45–54. doi: 10.1023/A:1020502624234

Hara, T., Kimura, I., Inoue, D., Ichimura, A., and Hirasawa, A. (2013). Free fatty acid receptors and their role in regulation of energy metabolism. *Rev. Physiol. Biochem. Pharmacol.* 164, 77–116. doi: 10.1007/112_2013_13

Heldin, C., Lu, B., Evans, R., and Gutkind, J. S. (2016). Signals and receptors. *Cold Spring Harb. Perspect. Biol.* 8:a005900. doi: 10.1101/cshperspect.a005900

Heneka, M. T., and Landreth, G. E. (2007). PPARs in the brain. *Biochim. Biophys. Acta* 1771, 1031–1045. doi: 10.1016/j.bbalip.2007.04.016

Herr, F. M., Aronson, J., and Storch, J. (1996). Role of portal region lysine residues in electrostatic interactions between heart fatty acid binding protein and phospholipid membranes. *Biochemistry* 35, 1296–1303. doi: 10.1021/bi952204b

Hirasawa, A., Tsumaya, K., Awaji, T., Katsuma, S., Adachi, T., Yamada, M., et al. (2005). Free fatty acids regulate gut incretin glucagon-like peptide-1 secretion through GPR120. *Nat. Med.* 11, 90–94. doi: 10.1038/nm1168

Hirsch, M. M., Deckmann, I., Fontes-Dutra, M., Bauer-Negrini, G., Della-Flora Nunes, G., Nunes, W., et al. (2018). Behavioral alterations in autism model induced by valproic acid and translational analysis of circulating microRNA. *Food Chem. Toxicol.* 115, 336–343. doi: 10.1016/j.fct.2018.02.061

Ho, J. D., Chau, B., Rodgers, L., Lu, F., Wilbur, K. L., Otto, K. A., et al. (2018). Structural basis for GPR40 allosteric agonism and incretin stimulation. *Nat. Commun.* 9:1645. doi: 10.1038/s41467-017-01240-w

Holliday, N. D., Watson, S.-J., and Brown, A. J. H. (2012). Drug discovery opportunities and challenges at g protein coupled receptors for long chain free fatty acids. *Front. Endocrinol.* 2:112. doi: 10.3389/fendo.2011.00112

Hostetler, H. A., McIntosh, A. L., Atshaves, B. P., Storey, S. M., Payne, H. R., Kier, A. B., et al. (2009). L-FABP directly interacts with PPAR alpha in cultured primary hepatocytes. *J. Lipid Res.* 50, 1663–1675. doi: 10.1194/jlr.M900058-JLR200

Hudson, B. D., Shimpukade, B., Milligan, G., and Ulven, T. (2014). The molecular basis of ligand interaction at free fatty acid receptor 4 (FFA4/GPR120). *J. Biol. Chem.* 289, 20345–20358. doi: 10.1074/jbc.M114.561449

Hunsberger, J. G., Fessler, E. B., Chibane, F. L., Leng, Y., Maric, D., Elkahloun, A. G., et al. (2013). Mood stabilizer-regulated miRNAs in neuropsychiatric and neurodegenerative diseases: identifying associations and functions. *Am. J. Transl. Res.* 5, 450–464.

Hussain, G., Schmitt, F., Loeffler, J.-P., and de Aguilar, J.-L. G. (2013). Fatting the brain: a brief of recent research. *Front. Cell. Neurosci.* 7:144. doi: 10.3389/fncel.2013.00144

Im, D.-S. (2004). Discovery of new G protein-coupled receptors for lipid mediators. *J. Lipid Res.* 45, 410–418. doi: 10.1194/jlr.R300006-JLR200

Ingolfsson, H. I., Carpenter, T. S., Bhatia, H., Bremer, P.-T., Marrink, S. J., and Lightstone, F. C. (2017). Computational lipidomics of the neuronal plasma membrane. *Biophys. J.* 113, 2271–2280. doi: 10.1016/j.bpj.2017.10.017

Innes, J. K., and Calder, P. C. (2018). Omega-6 fatty acids and inflammation. *Prostaglandins Leukot. Essent. Fatty Acids* 132, 41–48. doi: 10.1016/j.plefa.2018.03.004

Issemann, I., and Green, S. (1990). Activation of a member of the steroid hormone receptor superfamily by peroxisome proliferators. *Nature* 347, 645–650. doi: 10.1038/347645a0

Itoh, Y., Kawamata, Y., Harada, M., Kobayashi, M., Fujii, R., Fukusumi, S., et al. (2003). Free fatty acids regulate insulin secretion from pancreatic beta cells through GPR40. *Nature* 422, 173–176. doi: 10.1038/nature01478

Jana, M., Mondal, S., Gonzalez, F. J., and Pahan, K. (2012). Gemfibrozil, a lipid-lowering drug, increases myelin genes in human oligodendrocytes via peroxisome proliferator-activated receptor-beta. *J. Biol. Chem.* 287, 34134–34148. doi: 10.1074/jbc.M112.398552

Janesick, A., Wu, S. C., and Blumberg, B. (2015). Retinoic acid signaling and neuronal differentiation. *Cell. Mol. Life Sci.* 72, 1559–1576. doi: 10.1007/s00018-014-1815-9

Johnson, E. J., and Schaefer, E. J. (2006). Potential role of dietary n-3 fatty acids in the prevention of dementia and macular degeneration. *Am. J. Clin. Nutr.* 83, 1494S–1498S. doi: 10.1093/ajcn/83.6.1494S

Kaczocha, M., Rebecchi, M. J., Ralph, B. P., Teng, Y.-H. G., Berger, W. T., Galbavy, W., et al. (2014). Inhibition of fatty acid binding proteins elevates brain anandamide levels and produces analgesia. *PLoS One* 9:e94200. doi: 10.1371/journal.pone.0094200

Kainu, T., Wikstrom, A. C., Gustafsson, J. A., and Pelto-Huikko, M. (1994). Localization of the peroxisome proliferator-activated receptor in the brain. *Neuroreport* 5, 2481–2485.

Kamata, Y., Shiraga, H., Tai, A., Kawamoto, Y., and Gohda, E. (2007). Induction of neurite outgrowth in PC12 cells by the medium-chain fatty acid octanoic acid. *Neuroscience* 146, 1073–1081. doi: 10.1016/j.neuroscience.2007.03.001

Katakura, M., Hashimoto, M., Shahdat, H. M., Gamoh, S., Okui, T., Matsuzaki, K., et al. (2009). Docosahexaenoic acid promotes neuronal differentiation by regulating basic helix-loop-helix transcription factors and cell cycle in neural stem cells. *Neuroscience* 160, 651–660. doi: 10.1016/j.neuroscience.2009.02.057

Kenakin, T., and Christopoulos, A. (2013). Signalling bias in new drug discovery: detection, quantification and therapeutic impact. *Nat. Rev. Drug Discov.* 12, 205–216. doi: 10.1038/nrd3954

Khan, M. Z., Zhuang, X., and He, L. (2016). GPR40 receptor activation leads to CREB phosphorylation and improves cognitive performance in an Alzheimer's disease mouse model. *Neurobiol. Learn. Mem.* 131, 46–55. doi: 10.1016/j.nlm.2016.03.006

Kim, J. Y., Lee, H. J., Lee, S.-J., Jung, Y. H., Yoo, D. Y., Hwang, I. K., et al. (2017). Palmitic acid-BSA enhances amyloid-beta production through GPR40-mediated dual pathways in neuronal cells: Involvement of the Akt/mTOR/HIF-1alpha and Akt/NF-kappaB pathways. *Sci. Rep.* 7:4335. doi: 10.1038/s41598-017-04175-w

Kimura, I., Inoue, D., Maeda, T., Hara, T., Ichimura, A., Miyauchi, S., et al. (2011). Short-chain fatty acids and ketones directly regulate sympathetic nervous system via G protein-coupled receptor 41 (GPR41). *Proc. Natl. Acad. Sci. U.S.A.* 108, 8030–8035. doi: 10.1073/pnas.1016088108

Kitajka, K., Sinclair, A. J., Weisinger, R. S., Weisinger, H. S., Mathai, M., Jayasooriya, A. P., et al. (2004). Effects of dietary omega-3 polyunsaturated fatty acids on brain gene expression. *Proc. Natl. Acad. Sci. U.S.A.* 101, 10931–10936. doi: 10.1073/pnas.0402342101

Kostenis, E. (2004). A glance at G-protein-coupled receptors for lipid mediators: a growing receptor family with remarkably diverse ligands. *Pharmacol. Ther.* 102, 243–257. doi: 10.1016/j.pharmthera.2004.04.005

Kurtz, A., Zimmer, A., Schnutgen, F., Bruning, G., Spener, F., and Muller, T. (1994). The expression pattern of a novel gene encoding brain-fatty acid binding protein correlates with neuronal and glial cell development. *Development* 120, 2637–2649.

Labrousse, V. F., Nadjar, A., Joffre, C., Costes, L., Aubert, A., Gregoire, S., et al. (2012). Short-term long chain omega3 diet protects from neuroinflammatory processes and memory impairment in aged mice. *PLoS One* 7:e36861. doi: 10.1371/journal.pone.0036861

Lafourcade, M., Larrieu, T., Mato, S., Duffaud, A., Sepers, M., Matias, I., et al. (2011). Nutritional omega-3 deficiency abolishes endocannabinoid-mediated neuronal functions. *Nat. Neurosci.* 14, 345–350. doi: 10.1038/nn.2736

Lampen, A., Carlberg, C., and Nau, H. (2001). Peroxisome proliferator-activated receptor delta is a specific sensor for teratogenic valproic acid derivatives. *Eur. J. Pharmacol.* 431, 25–33. doi: 10.1016/s0014-2999(01)01423-6

Landrier, J.-F., Thomas, C., Grober, J., Duez, H., Percevault, F., Souidi, M., et al. (2004). Statin induction of liver fatty acid-binding protein (L-FABP) gene expression is peroxisome proliferator-activated receptor-alpha-dependent. *J. Biol. Chem.* 279, 45512–45518. doi: 10.1074/jbc.M407461200

Laschet, C., Dupuis, N., and Hanson, J. (2018). The G protein-coupled receptors deorphanization landscape. *Biochem. Pharmacol.* 153, 62–74. doi: 10.1016/j.bcp.2018.02.016

Lein, E. S., Hawrylycz, M. J., Ao, N., Ayres, M., Bensinger, A., Bernard, A., et al. (2007). Genome-wide atlas of gene expression in the adult mouse brain. *Nature* 445, 168–176. doi: 10.1038/nature05453

Leong, C., Zhai, D., Kim, B., Yun, S.-W., and Chang, Y.-T. (2013). Neural stem cell isolation from the whole mouse brain using the novel FABP7-binding fluorescent dye, CDr3. *Stem Cell Res.* 11, 1314–1322. doi: 10.1016/j.scr.2013.09.002

Leoni, V., and Caccia, C. (2011). Oxysterols as biomarkers in neurodegenerative diseases. *Chem. Phys. Lipids* 164, 515–524. doi: 10.1016/j.chemphyslip.2011.04.002

Li, Z., Chen, Y., Zhang, Y., Jiang, H., Liu, Y., Chen, Y., et al. (2018a). Structure-based design of free fatty acid receptor 1 agonists bearing non-biphenyl scaffold. *Bioorg. Chem.* 80, 296–302. doi: 10.1016/j.bioorg.2018.06.039

Li, Z., Chen, Y., Zhou, Z., Deng, L., Xu, Y., Hu, L., et al. (2019). Discovery of first-in-class thiazole-based dual FFA1/PPARdelta agonists as potential anti-diabetic agents. *Eur. J. Med. Chem.* 164, 352–365. doi: 10.1016/j.ejmech.2018.12.069

Li, Z., Qiu, Q., Geng, X., Yang, J., Huang, W., and Qian, H. (2016). Free fatty acid receptor agonists for the treatment of type 2 diabetes: drugs in preclinical to phase II clinical development. *Expert Opin. Investig. Drugs* 25, 871–890. doi: 10.1080/13543784.2016.1189530

Li, Z., Xu, X., Hou, J., Wang, S., Jiang, H., and Zhang, L. (2018b). Structure-based optimization of free fatty acid receptor 1 agonists bearing thiazole scaffold. *Bioorg. Chem.* 77, 429–435. doi: 10.1016/j.bioorg.2018.01.039

Li, Z., Zhou, Z., Deng, F., Li, Y., Zhang, D., and Zhang, L. (2018c). Design, synthesis, and biological evaluation of novel pan agonists of FFA1, PPARgamma and PPARdelta. *Eur. J. Med. Chem.* 159, 267–276. doi: 10.1016/j.ejmech.2018.09.071

Liou, H. L., Kahn, P. C., and Storch, J. (2002). Role of the helical domain in fatty acid transfer from adipocyte and heart fatty acid-binding proteins to membranes - Analysis of chimeric proteins. *J. Biol. Chem.* 277, 1806–1815. doi: 10.1074/jbc.M107987200

Liu, R.-Z., Li, X., and Godbout, R. (2008). A novel fatty acid-binding protein (FABP) gene resulting from tandem gene duplication in mammals: transcription in rat retina and testis. *Genomics* 92, 436–445. doi: 10.1016/j.ygeno.2008.08.003

Liu, R. Z., Mita, R., Beaulieu, M., Gao, Z., and Godbout, R. (2010). Fatty acid binding proteins in brain development and disease. *Int. J. Dev. Biol.* 54, 1229–1239. doi: 10.1387/ijdb.092976rl092976rl

Liu, X. S., Chopp, M., Kassis, H., Jia, L. F., Hozeska-Solgot, A., Zhang, R. L., et al. (2012). Valproic acid increases white matter repair and neurogenesis after stroke. *Neuroscience* 220, 313–321. doi: 10.1016/j.neuroscience.2012.06.012

Liu, Y., Longo, L. D., and De Leon, M. (2000). In situ and immunocytochemical localization of E-FABP mRNA and protein during neuronal migration and differentiation in the rat brain. *Brain Res.* 852, 16–27. doi: 10.1016/s0006-8993(99)02158-7

Lu, J., Byrne, N., Wang, J., Bricogne, G., Brown, F. K., Chobanian, H. R., et al. (2017). Structural basis for the cooperative allosteric activation of the free fatty acid receptor GPR40. *Nat. Struct. Mol. Biol.* 24, 570–577. doi: 10.1038/nsmb.3417

Lundell, K., Thulin, P., Hamsten, A., and Ehrenborg, E. (2007). Alternative splicing of human peroxisome proliferator-activated receptor delta (PPAR delta): effects on translation efficiency and trans-activation ability. *BMC Mol. Biol.* 8:70. doi: 10.1186/1471-2199-8-70

Ma, D., Lu, L., Boneva, N. B., Warashina, S., Kaplamadzhiev, D. B., Mori, Y., et al. (2008). Expression of free fatty acid receptor GPR40 in the neurogenic niche of adult monkey hippocampus. *Hippocampus* 18, 326–333. doi: 10.1002/hipo.20393

Ma, D., Tao, B., Warashina, S., Kotani, S., Lu, L., Kaplamadzhiev, D. B., et al. (2007). Expression of free fatty acid receptor GPR40 in the central nervous system of adult monkeys. *Neurosci. Res.* 58, 394–401. doi: 10.1016/j.neures.2007.05.001

Ma, D., Zhang, M., Larsen, C. P., Xu, F., Hua, W., Yamashima, T., et al. (2010). DHA promotes the neuronal differentiation of rat neural stem cells transfected with GPR40 gene. *Brain Res.* 1330, 1–8. doi: 10.1016/j.brainres.2010.03.002

Magnan, C., Levin, B. E., and Luquet, S. (2015). Brain lipid sensing and the neural control of energy balance. *Mol. Cell. Endocrinol.* 418(Pt. 1), 3–8. doi: 10.1016/j.mce.2015.09.019

Mancini, A. D., Bertrand, G., Vivot, K., Carpentier, E., Tremblay, C., Ghislain, J., et al. (2015). beta-Arrestin recruitment and biased agonism at free fatty acid receptor 1. *J. Biol. Chem.* 290, 21131–21140. doi: 10.1074/jbc.M115.644450

Mangelsdorf, D. J., Thummel, C., Beato, M., Herrlich, P., Schutz, G., Umesono, K., et al. (1995). The nuclear receptor superfamily: the second decade. *Cell* 83, 835–839. doi: 10.1016/0092-8674(95)90199-X

Martin, G. G., McIntosh, A. L., Huang, H., Gupta, S., Atshaves, B. P., Landrock, K. K., et al. (2013). The human liver fatty acid binding protein T94A variant alters the structure, stability, and interaction with fibrates. *Biochemistry* 52, 9347–9357. doi: 10.1021/bi401014k

McNamara, R. K., and Carlson, S. E. (2006). Role of omega-3 fatty acids in brain development and function: potential implications for the pathogenesis and prevention of psychopathology. *Prostaglandins Leukot. Essent. Fatty Acids* 75, 329–349. doi: 10.1016/j.plefa.2006.07.010

Miglio, G., Rattazzi, L., Rosa, A. C., and Fantozzi, R. (2009). PPARgamma stimulation promotes neurite outgrowth in SH-SY5Y human neuroblastoma cells. *Neurosci. Lett.* 454, 134–138. doi: 10.1016/j.neulet.2009.03.014

Mobraten, K., Haug, T. M., Kleiveland, C. R., and Lea, T. (2013). Omega-3 and omega-6 PUFAs induce the same GPR120-mediated signalling events, but

with different kinetics and intensity in Caco-2 cells. *Lipids Health Dis.* 12:101. doi: 10.1186/1476-511X-12-101

Moreno, S., Farioli-vecchioli, S., and Cerù, M. P. (2004). Immunolocalization of peroxisome proliferator-activated receptors and retinoid X receptors in the adult rat CNS. *Neuroscience* 123, 131–145. doi: 10.1016/j.neuroscience.2003.08.064

Motley, W. W., Palaima, P., Yum, S. W., Gonzalez, M. A., Tao, F., Wanschitz, J. V., et al. (2016). De novo PMP2 mutations in families with type 1 Charcot-Marie-Tooth disease. *Brain* 139, 1649–1656. doi: 10.1093/brain/aww055

Mounsey, R. B., Martin, H. L., Nelson, M. C., Evans, R. M., and Teismann, P. (2015). The effect of neuronal conditional knock-out of peroxisome proliferator-activated receptors in the MPTP mouse model of Parkinson's disease. *Neuroscience* 300, 576–584. doi: 10.1016/j.neuroscience.2015.05.048

Muller, M. M., Lehmann, R., Klassert, T. E., Reifenstein, S., Conrad, T., Moore, C., et al. (2017). Global analysis of glycoproteins identifies markers of endotoxin tolerant monocytes and GPR84 as a modulator of TNFalpha expression. *Sci. Rep.* 7:838. doi: 10.1038/s41598-017-00828-y

Murillo-Rodriguez, E. (2017). The role of nuclear receptor pparalpha in the sleep-wake cycle modulation. A tentative approach for treatment of sleep disorders. *Curr. Drug Deliv.* 14, 473–482. doi: 10.2174/1567201814666161109123803

Murphy, E. J., Owada, Y., Kitanaka, N., Kondo, H., and Glatz, J. F. C. (2005). Brain arachidonic acid incorporation is decreased in heart fatty acid binding protein gene-ablated mice. *Biochemistry* 44, 6350–6360. doi: 10.1021/bi047292r

Nakamoto, K., Nishinaka, T., Matsumoto, K., Kasuya, F., Mankura, M., Koyama, Y., et al. (2012). Involvement of the long-chain fatty acid receptor GPR40 as a novel pain regulatory system. *Brain Res.* 1432, 74–83. doi: 10.1016/j.brainres.2011.11.012

Niculescu, M. D., Lupu, D. S., and Craciunescu, C. N. (2011). Maternal alpha-linolenic acid availability during gestation and lactation alters the postnatal hippocampal development in the mouse offspring. *Int. J. Dev. Neurosci.* 29, 795–802. doi: 10.1016/j.ijdevneu.2011.09.006

Nikaido, Y., Koyama, Y., Yoshikawa, Y., Furuya, T., and Takeda, S. (2015). Mutation analysis and molecular modeling for the investigation of ligand-binding modes of GPR84. *J. Biochem.* 157, 311–320. doi: 10.1093/jb/mvu075

Nohr, M. K., Pedersen, M. H., Gille, A., Egerod, K. L., Engelstoft, M. S., Husted, A. S., et al. (2013). GPR41/FFAR3 and GPR43/FFAR2 as cosensors for short-chain fatty acids in enteroendocrine cells vs FFAR3 in enteric neurons and FFAR2 in enteric leukocytes. *Endocrinology* 154, 3552–3564. doi: 10.1210/en.2013-1142

Noy, N. (2016). Non-classical transcriptional activity of retinoic acid. *Subcell. Biochem.* 81, 179–199. doi: 10.1007/978-94-024-0945-1_7

Offermanns, S. (2013). Free fatty acid (FFA) and hydroxy carboxylic acid (HCA) receptors. *Annu. Rev. Pharmacol. Toxicol.* 54, 407–434. doi: 10.1146/annurev-pharmtox-011613-135945

Oikawa, H., and Sng, J. C. G. (2016). Valproic acid as a microRNA modulator to promote neurite outgrowth. *Neural Regen. Res.* 11, 1564–1565. doi: 10.4103/1673-5374.193227

Orr, S. K., Trepanier, M. O., and Bazinet, R. P. (2013). n-3 Polyunsaturated fatty acids in animal models with neuroinflammation. *Prostaglandins Leukot. Essent. Fatty Acids* 88, 97–103. doi: 10.1016/j.plefa.2012.05.008

Orth, M., and Bellosta, S. (2012). Cholesterol: its regulation and role in central nervous system disorders. *Cholesterol* 2012:292598. doi: 10.1155/2012/292598

Ory, J., Kane, C. D., Simpson, M. A., Banaszak, L. J., and Bernlohr, D. A. (1997). Biochemical and crystallographic analyses of a portal mutant of the adipocyte lipid-binding protein. *J. Biol. Chem.* 272, 9793–9801. doi: 10.1074/jbc.272.15.9793

O'Sullivan, S. E. (2007). Cannabinoids go nuclear: evidence for activation of peroxisome proliferator-activated receptors. *Br. J. Pharmacol.* 152, 576–582. doi: 10.1038/sj.bjp.0707423

Owada, Y. (2008). Fatty acid binding protein: localization and functional significance in the brain. *Tohoku J. Exp. Med.* 214, 213–220. doi: 10.1620/tjem.214.213

Owada, Y., Yoshimoto, T., and Kondo, H. (1996). Spatio-temporally differential expression of genes for three members of fatty acid binding proteins in developing and mature rat brains. *J. Chem. Neuroanat.* 12, 113–122. doi: 10.1016/s0891-0618(96)00192-5

Pelsers, M. M., Hanhoff, T., Van Der Voort, D., Arts, B., Peters, M., Ponds, R., et al. (2004). Brain- and heart-type fatty acid-binding proteins in the brain: Tissue distribution and clinical utility. *Clin. Chem.* 50, 1568–1575. doi: 10.1373/clinchem.2003.030361

Pelsers, M. M., Hermens, W. T., and Glatz, J. F. C. (2005). Fatty acid-binding proteins as plasma markers of tissue injury. *Clin. Chim. Acta* 352, 15–35. doi: 10.1016/j.cccn.2004.09.001

Pepino, M. Y., Kuda, O., Samovski, D., and Abumrad, N. A. (2014). Structure-function of CD36 and importance of fatty acid signal transduction in fat metabolism. *Annu. Rev. Nutr.* 34, 281–303. doi: 10.1146/annurev-nutr-071812-161220

Peters, B. D., Duran, M., Vlieger, E. J., Majoie, C. B., den Heeten, G. J., Linszen, D. H., et al. (2009). Polyunsaturated fatty acids and brain white matter anisotropy in recent-onset schizophrenia: a preliminary study. *Prostaglandins Leukot. Essent. Fatty Acids* 81, 61–63. doi: 10.1016/j.plefa.2009.04.007

Prolla, T. A., and Mattson, M. P. (2001). Molecular mechanisms of brain aging and neurodegenerative disorders: lessons from dietary restriction. *Trends Neurosci.* 24, S21–S31. doi: 10.1016/S0166-2236(01)00005-4

Punetha, J., Mackay-Loder, L., Harel, T., Coban-Akdemir, Z., Jhangiani, S. N., Gibbs, R. A., et al. (2018). Identification of a pathogenic PMP2 variant in a multi-generational family with CMT type 1: clinical gene panels versus genome-wide approaches to molecular diagnosis. *Mol. Genet. Metab.* 125, 302–304. doi: 10.1016/j.ymgme.2018.08.005

Rademacher, M., Zimmerman, A. W., Ruterjans, H., Veerkamp, J. H., and Lucke, C. (2002). Solution structure of fatty acid-binding protein from human brain. *Mol. Cell. Biochem.* 239, 61–68. doi: 10.1023/A:1020566909213

Rautureau, Y., Paradis, P., and Schiffrin, E. L. (2017). Generation of a mouse model with smooth muscle cell specific loss of the expression of PPARgamma. *Methods Mol. Biol.* 1527, 381–407. doi: 10.1007/978-1-4939-6625-7_30

Reddy, D. S. (2010). Neurosteroids: endogenous role in the human brain and therapeutic potentials. *Prog. Brain Res.* 186, 113–137. doi: 10.1016/B978-0-444-53630-3.00008-7

Reese, A. J., and Banaszak, L. J. (2004). Specificity determinants for lipids bound to beta-barrel proteins. *J. Lipid Res.* 45, 232–243. doi: 10.1194/jlr.M300113-JLR200

Richieri, G. V., Ogata, R. T., Zimmerman, A. W., Veerkamp, J. H., and Kleinfeld, A. M. (2000). Fatty acid binding proteins from different tissues show distinct patterns of fatty acid interactions. *Biochemistry* 39, 7197–7204. doi: 10.1021/bi000314z

Ricote, M., and Glass, C. K. (2007). PPARs and molecular mechanisms of transrepression. *Biochim. Biophys. Acta* 1771, 926–935. doi: 10.1016/j.bbalip.2007.02.013

Rivera, P., Arrabal, S., Vargas, A., Blanco, E., Serrano, A., Pavon, F. J., et al. (2014). Localization of peroxisome proliferator-activated receptor alpha (PPARα) and N-acyl phosphatidylethanolamine phospholipase D (NAPE-PLD) in cells expressing the Ca^{2+}-binding proteins calbindin, calretinin, and parvalbumin in the adult rat hippocampus. *Front. Neuroanat.* 8:12. doi: 10.3389/fnana.2014.00012

Rocha, D. M., Caldas, A. P., Oliveira, L. L., Bressan, J., and Hermsdorff, H. H. (2016). Saturated fatty acids trigger TLR4-mediated inflammatory response. *Atherosclerosis* 244, 211–215. doi: 10.1016/j.atherosclerosis.2015.11.015

Rohwedder, A., Zhang, Q., Rudge, S. A., and Wakelam, M. J. O. (2014). Lipid droplet formation in response to oleic acid in Huh-7 cells is mediated by the fatty acid receptor FFAR4. *J. Cell Sci.* 127, 3104–3115. doi: 10.1242/jcs.145854

Rombaldi Bernardi, J., de Souza Escobar, R., Ferreira, C. F., and Pelufo Silveira, P. (2012). Fetal and neonatal levels of omega-3: effects on neurodevelopment, nutrition, and growth. *ScientificWorldJournal* 2012:202473. doi: 10.1100/2012/202473

Roth, A. D., Leisewitz, A. V., Jung, J. E., Cassina, P., Barbeito, L., Inestrosa, N. C., et al. (2003). PPAR γ activators induce growth arrest and process extension in B12 oligodendrocyte-like cells and terminal differentiation of cultured oligodendrocytes. *J. Neurosci. Res.* 72, 425–435. doi: 10.1002/jnr.10596

Roy, A., and Pahan, K. (2015). PPARalpha signaling in the hippocampus: crosstalk between fat and memory. *J. Neuroimmune Pharmacol.* 10, 30–34. doi: 10.1007/s11481-014-9582-9

Sacchettini, J. C., Meininger, T. A., Lowe, J. B., Gordon, J. I., and Banaszak, L. J. (1987). Crystallization of rat intestinal fatty-acid binding protein - preliminary-x-ray data obtained from protein expressed in *Escherichia*-coli. *J. Biol. Chem.* 262, 5428–5430.

Saino-Saito, S., Nourani, R. M., Iwasa, H., Kondo, H., and Owada, Y. (2009). Discrete localization of various fatty-acid-binding proteins in various cell populations of mouse retina. *Cell Tissue Res.* 338, 191–201. doi: 10.1007/s00441-009-0862-2

Saino-Saito, S., Suzuki, R., Tokuda, N., Abe, H., Kondo, H., and Owada, Y. (2010). Localization of fatty acid binding proteins (FABPs) in the cochlea of mice. *Ann. Anat.* 192, 210–214. doi: 10.1016/j.aanat.2010.06.007

Samuel, B. S., Shaito, A., Motoike, T., Rey, F. E., Backhed, F., Manchester, J. K., et al. (2008). Effects of the gut microbiota on host adiposity are modulated by the short-chain fatty-acid binding G protein-coupled receptor, Gpr41. *Proc. Natl. Acad. Sci. U.S.A.* 105, 16767–16772. doi: 10.1073/pnas.0808567105

Sanchez-Font, M. F., Bosch-Comas, A., Gonzalez-Duarte, R., and Marfany, G. (2003). Overexpression of FABP7 in Down syndrome fetal brains is associated with PKNOX1 gene-dosage imbalance. *Nucleic Acids Res.* 31, 2769–2777. doi: 10.1093/nar/gkg396

Sanchez-Reyes, O. B., Romero-Avila, M. T., Castillo-Badillo, J. A., Takei, Y., Hirasawa, A., Tsujimoto, G., et al. (2014). Free fatty acids and protein kinase C activation induce GPR120 (free fatty acid receptor 4) phosphorylation. *Eur. J. Pharmacol.* 723, 368–374. doi: 10.1016/j.ejphar.2013.11.003

Santos, M. J., Quintanilla, R. A., Toro, A., Grandy, R., Dinamarca, M. C., Godoy, J. A., et al. (2005). Peroxisomal proliferation protects from beta-amyloid neurodegeneration. *J. Biol. Chem.* 280, 41057–41068. doi: 10.1074/jbc.M505160200

Sarruf, D. A., Yu, F., Nguyen, H. T., Williams, D. L., Printz, R. L., Niswender, K. D., et al. (2009). Expression of peroxisome proliferator-activated receptor-γ in key neuronal subsets regulating glucose metabolism and energy homeostasis. *Endocrinology* 150, 707–712. doi: 10.1210/en.2008-0899

Sasselli, V., Pachnis, V., and Burns, A. J. (2012). The enteric nervous system. *Dev. Biol.* 366, 64–73. doi: 10.1016/j.ydbio.2012.01.012

Sastre, M., Klockgether, T., and Heneka, M. T. (2006). Contribution of inflammatory processes to Alzheimer's disease: molecular mechanisms. *Int. J. Dev. Neurosci.* 24, 167–176. doi: 10.1016/j.ijdevneu.2005.11.014

Sawzdargo, M., George, S. R., Nguyen, T., Xu, S., Kolakowski, L. F., and O'dowd, B. F. (1997). A cluster of four novel human g protein-coupled receptor genes occurring in close proximity to CD22 gene on chromosome 19q13.1. *Biochem. Biophys. Res. Commun.* 239, 543–547. doi: 10.1006/bbrc.1997.7513

Scandroglio, F., Venkata, J. K., Loberto, N., Prioni, S., Schuchman, E. H., Chigorno, V., et al. (2008). Lipid content of brain, brain membrane lipid domains, and neurons from acid sphingomyelinase deficient mice. *J. Neurochem.* 107, 329–338. doi: 10.1111/j.1471-4159.2008.05591.x

Schug, T. T., Berry, D. C., Shaw, N. S., Travis, S. N., and Noy, N. (2007). Opposing effects of retinoic acid on cell growth result from alternate activation of two different nuclear receptors. *Cell* 129, 723–733. doi: 10.1016/j.cell.2007.02.050

Schug, T. T., Berry, D. C., Toshkov, I. A., Cheng, L., Nikitin, A. Y., and Noy, N. (2008). Overcoming retinoic acid-resistance of mammary carcinomas by diverting retinoic acid from PPARbeta/delta to RAR. *Proc. Natl. Acad. Sci. U.S.A.* 105, 7546–7551. doi: 10.1073/pnas.0709981105

Senga, S., Kawaguchi, K., Kobayashi, N., Ando, A., and Fujii, H. (2018). A novel fatty acid-binding protein 5-estrogen-related receptor alpha signaling pathway promotes cell growth and energy metabolism in prostate cancer cells. *Oncotarget* 9, 31753–31770. doi: 10.18632/oncotarget.25878

Serhan, C. N. (2014). Pro-resolving lipid mediators are leads for resolution physiology. *Nature* 510, 92–101. doi: 10.1038/nature13479

Shang, J., Brust, R., Mosure, S. A., Bass, J., Munoz-Tello, P., Lin, H., et al. (2018). Cooperative cobinding of synthetic and natural ligands to the nuclear receptor PPARgamma. *eLife* 7:e43320. doi: 10.7554/eLife.43320

Shao, D., Rangwala, S. M., Bailey, S. T., Krakow, S. L., Reginato, M. J., and Lazar, M. A. (1998). Interdomain communication regulating ligand binding by PPAR-gamma. *Nature* 396, 377–380. doi: 10.1038/24634

Shioda, N., Yabuki, Y., Kobayashi, Y., Onozato, M., Owada, Y., and Fukunaga, K. (2014). FABP3 protein promotes alpha-synuclein oligomerization associated with 1-methyl-1,2,3,6-tetrahydropiridine-induced neurotoxicity. *J. Biol. Chem.* 289, 18957–18965. doi: 10.1074/jbc.M113.527341

Shioda, N., Yamamoto, Y., Watanabe, M., Binas, B., Owada, Y., and Fukunaga, K. (2010). Heart-type fatty acid binding protein regulates dopamine D2 receptor function in mouse brain. *J. Neurosci.* 30, 3146–3155. doi: 10.1523/JNEUROSCI.4140-09.2010

Smathers, R. L., and Petersen, D. R. (2011). The human fatty acid-binding protein family: evolutionary divergences and functions. *Hum. Genomics* 5, 170–191.

Smith, A. J., Sanders, M. A., Juhlmann, B. E., Hertzel, A. V., and Bernlohr, D. A. (2008). Mapping of the hormone-sensitive lipase binding site on the adipocyte fatty acid-binding protein (AFABP). Identification of the charge quartet on the AFABP/aP2 helix-turn-helix domain. *J. Biol. Chem.* 283, 33536–33543. doi: 10.1074/jbc.M806732200

Sona, C., Kumar, A., Dogra, S., Kumar, B. A., Umrao, D., and Yadav, P. N. (2018). Docosahexaenoic acid modulates brain-derived neurotrophic factor via GPR40 in the brain and alleviates diabesity-associated learning and memory deficits in mice. *Neurobiol. Dis.* 118, 94–107. doi: 10.1016/j.nbd.2018.07.002

Song, T., Yang, Y., Zhou, Y., Wei, H., and Peng, J. (2017). GPR120: a critical role in adipogenesis, inflammation, and energy metabolism in adipose tissue. *Cell. Mol. Life Sci.* 74, 2723–2733. doi: 10.1007/s00018-017-2492-2

Srivastava, A., Yano, J., Hirozane, Y., Kefala, G., Gruswitz, F., Snell, G., et al. (2014). High-resolution structure of the human GPR40 receptor bound to allosteric agonist TAK-875. *Nature* 513, 124–127. doi: 10.1038/nature13494

Stoddart, L. A., Smith, N. J., Jenkins, L., Brown, A. J., and Milligan, G. (2008). Conserved polar residues in transmembrane domains V, VI, and VII of free fatty acid receptor 2 and free fatty acid receptor 3 are required for the binding and function of short chain fatty acids. *J. Biol. Chem.* 283, 32913–32924. doi: 10.1074/jbc.M805601200

Storch, J., and Corsico, B. (2008). The emerging functions and mechanisms of mammalian fatty acid-binding proteins. *Annu. Rev. Nutr.* 28, 73–95. doi: 10.1146/annurev.nutr.27.061406.093710

Storch, J., and Thumser, A. E. (2010). Tissue-specific functions in the fatty acid-binding protein family. *J. Biol. Chem.* 285, 32679–32683. doi: 10.1074/jbc.R110.135210

Storch, J., and Thumser, A. E. A. (2000). The fatty acid transport function of fatty acid-binding proteins. *Biochim. Biophys. Acta* 1486, 28–44. doi: 10.1016/S1388-1981(00)00046-9

Storch, J., Veerkamp, J. H., and Hsu, K. T. (2002). Similar mechanisms of fatty acid transfer from human anal rodent fatty acid-binding proteins to membranes: liver, intestine, heart muscle, and adipose tissue FABPs. *Mol. Cell. Biochem.* 239, 25–33. doi: 10.1023/A:1020546321508

Sum, C. S., Tikhonova, I. G., Neumann, S., Engel, S., Raaka, B. M., Costanzi, S., et al. (2007). Identification of residues important for agonist recognition and activation in GPR40. *J. Biol. Chem.* 282, 29248–29255. doi: 10.1074/jbc.M705077200

Sunshine, H., and Iruela-Arispe, M. L. (2017). Membrane lipids and cell signaling. *Curr. Opin. Lipidol.* 28, 408–413. doi: 10.1097/MOL.0000000000000443

Suzuki, M., Takaishi, S., Nagasaki, M., Onozawa, Y., Iino, I., Maeda, H., et al. (2013). Medium-chain fatty acid-sensing receptor, GPR84, is a proinflammatory receptor. *J. Biol. Chem.* 288, 10684–10691. doi: 10.1074/jbc.M112.420042

Taha, A. Y., Filo, E., Ma, D. W. L., and McIntyre Burnham, W. (2009). Dose-dependent anticonvulsant effects of linoleic and alpha-linolenic polyunsaturated fatty acids on pentylenetetrazol induced seizures in rats. *Epilepsia* 50, 72–82. doi: 10.1111/j.1528-1167.2008.01731.x

The GTEx Consortium (2013). The genotype-tissue expression (GTEx) project. *Nat. Genet.* 45, 580–585. doi: 10.1038/ng.2653

Thompson, J., Reese-Wagoner, A., and Banaszak, L. (1999). Liver fatty acid binding protein: species variation and the accommodation of different ligands. *Biochim. Biophys. Acta* 1441, 117–130. doi: 10.1016/S1388-1981(99)00146-8

Tikhonova, I. G., Sum, C. S., Neumann, S., Thomas, C. J., Raaka, B. M., Costanzi, S., et al. (2007). Bidirectional, iterative approach to the structural delineation of the functional "chemoprint" in GPR40 for agonist recognition. *J. Med. Chem.* 50, 2981–2989. doi: 10.1021/jm0614782

Tzeng, J., Byun, J., Park, J. Y., Yamamoto, T., Schesing, K., Tian, B., et al. (2015). An Ideal PPAR response element bound to and activated by PPARalpha. *PLoS One* 10:e0134996. doi: 10.1371/journal.pone.0134996

Uauy, R., and Dangour, A. D. (2006). Nutrition in brain development and aging: role of essential fatty acids. *Nutr. Rev.* 64, S24–S33. doi: 10.1111/j.1753-4887.2006.tb00242.x

Uhlen, M., Fagerberg, L., Hallstrom, B. M., Lindskog, C., Oksvold, P., Mardinoglu, A., et al. (2015). Proteomics. Tissue-based map of the human proteome. *Science* 347:1260419. doi: 10.1126/science.1260419

Ulven, T. (2012). Short-chain free fatty acid receptors FFA2/GPR43 and FFA3/GPR41 as new potential therapeutic targets. *Front. Endocrinol.* 3:111. doi: 10.3389/fendo.2012.00111

van Gelder, B. M., Tijhuis, M., Kalmijn, S., and Kromhout, D. (2007). Fish consumption, n-3 fatty acids, and subsequent 5-y cognitive decline in elderly men: the Zutphen Elderly Study. *Am. J. Clin. Nutr.* 85, 1142–1147. doi: 10.1093/ajcn/85.4.1142

Vance, J. E. (2012). Dysregulation of cholesterol balance in the brain: contribution to neurodegenerative diseases. *Dis. Model. Mech.* 5, 746–755. doi: 10.1242/dmm.010124

Veerkamp, J. H., and Zimmerman, A. W. (2001). Fatty acid-binding proteins of nervous tissue. *J. Mol. Neurosci.* 16, 133–137.

Villapol, S. (2018). Roles of peroxisome proliferator-activated receptor gamma on brain and peripheral inflammation. *Cell. Mol. Neurobiol.* 38, 121–132. doi: 10.1007/s10571-017-0554-5

Villegas-Comonfort, S., Takei, Y., Tsujimoto, G., Hirasawa, A., and García-Sáinz, J. A. (2017). Effects of arachidonic acid on FFA4 receptor: signaling, phosphorylation and internalization. *Prostaglandins Leukot. Essent. Fat. Acids* 117, 1–10. doi: 10.1016/j.plefa.2017.01.013

von Bernhardi, R., Eugenin-von Bernhardi, J., Flores, B., and Eugenin Leon, J. (2016). Glial cells and integrity of the nervous system. *Adv. Exp. Med. Biol.* 949, 1–24. doi: 10.1007/978-3-319-40764-7_1

Walder, B., Robin, X., Rebetez, M. M. L., Copin, J.-C., Gasche, Y., Sanchez, J.-C., et al. (2013). The prognostic significance of the serum biomarker heart-fatty acidic binding protein in comparison with s100b in severe traumatic brain injury. *J. Neurotrauma* 30, 1631–1637. doi: 10.1089/neu.2012.2791

Wang, F., Mullican, S. E., DiSpirito, J. R., Peed, L. C., and Lazar, M. A. (2013). Lipoatrophy and severe metabolic disturbance in mice with fat-specific deletion of PPARgamma. *Proc. Natl. Acad. Sci. U.S.A.* 110, 18656–18661. doi: 10.1073/pnas.1314863110

Wang, J., Wu, X., Simonavicius, N., Tian, H., and Ling, L. (2006). Medium-chain fatty acids as ligands for orphan G protein-coupled receptor GPR84. *J. Biol. Chem.* 281, 34457–34464. doi: 10.1074/jbc.M608019200

Wang, X., and Chan, C. B. (2015). n-3 polyunsaturated fatty acids and insulin secretion. *J. Endocrinol.* 224, R97–R106. doi: 10.1530/JOE-14-0581

Wang, Y.-T., Liu, C.-H., and Zhu, H.-L. (2016). Fatty acid binding protein (FABP) inhibitors: a patent review (2012-2015). *Expert Opin. Ther. Pat.* 26, 767–776. doi: 10.1080/13543776.2016.1182500

Warden, A., Truitt, J., Merriman, M., Ponomareva, O., Jameson, K., Ferguson, L. B., et al. (2016). Localization of PPAR isotypes in the adult mouse and human brain. *Sci. Rep.* 6:27618. doi: 10.1038/srep27618

Watanabe, A., Toyota, T., Owada, Y., Hayashi, T., Iwayama, Y., Matsumata, M., et al. (2007). Fabp7 maps to a quantitative trait locus for a schizophrenia endophenotype. *PLoS Biol.* 5:e297. doi: 10.1371/journal.pbio.0050297

Watson, S.-J., Brown, A. J. H., and Holliday, N. D. (2012). Differential signaling by splice variants of the human free fatty acid receptor GPR120. *Mol. Pharmacol.* 81, 631–642. doi: 10.1124/mol.111.077388

Wei, L., Tokizane, K., Konishi, H., Yu, H.-R., and Kiyama, H. (2017). Agonists for G-protein-coupled receptor 84 (GPR84) alter cellular morphology and motility but do not induce pro-inflammatory responses in microglia. *J. Neuroinflammation* 14:198. doi: 10.1186/s12974-017-0970-y

Whalen, E. J., Rajagopal, S., and Lefkowitz, R. J. (2011). Therapeutic potential of beta-arrestin- and G protein-biased agonists. *Trends Mol. Med.* 17, 126–139. doi: 10.1016/j.molmed.2010.11.004

Wittenberger, T., Schaller, H. C., and Hellebrand, S. (2001). An expressed sequence tag (EST) data mining strategy succeeding in the discovery of new G-protein coupled receptors. *J. Mol. Biol.* 307, 799–813. doi: 10.1006/jmbi.2001.4520

Wnuk, A., and Kajta, M. (2017). Steroid and xenobiotic receptor signalling in apoptosis and autophagy of the nervous system. *Int. J. Mol. Sci.* 18:E2394. doi: 10.3390/ijms18112394

Wolfrum, C. (2007). Cytoplasmic fatty acid binding protein sensing fatty acids for peroxisome proliferator activated receptor activation. *Cell. Mol. Life Sci.* 64, 2465–2476. doi: 10.1007/s00018-007-7279-4

Wolfrum, C., Borrmann, C. M., Borchers, T., and Spener, F. (2001). Fatty acids and hypolipidemic drugs regulate peroxisome proliferator-activated receptors alpha - and gamma-mediated gene expression via liver fatty acid binding protein: a signaling path to the nucleus. *Proc. Natl. Acad. Sci. U.S.A.* 98, 2323–2328. doi: 10.1073/pnas.051619898

Won, Y.-J., Lu, V. B., Puhl, H. L. III, and Ikeda, S. R. (2013). beta-Hydroxybutyrate modulates N-type calcium channels in rat sympathetic neurons by acting as an agonist for the G-protein-coupled receptor FFA3. *J. Neurosci.* 33, 19314–19325. doi: 10.1523/JNEUROSCI.3102-13.2013

Woods, J. W., Tanen, M., Figueroa, D. J., Biswas, C., Zycband, E., Moller, D. E., et al. (2003). Localization of PPARδ in murine central nervous system: expression in oligodendrocytes and neurons. *Brain Res.* 975, 10–21. doi: 10.1016/S0006-8993(03)02515-0

Wunderlich, M. T., Hanhoff, T., Goertler, M., Spener, F., Glatz, J. F. C., Wallesch, C. W., et al. (2005). Release of brain-type and heart-type fatty acid-binding proteins in serum after acute ischaemic stroke. *J. Neurol.* 252, 718–724. doi: 10.1007/s00415-005-0725-z

Xing, G., Zhang, L., Zhang, L., Heynen, T., Yoshikawa, T., Smith, M., et al. (1995). Rat PPARgama contains A CGG triplet repeat and is prminently expressed in the thalamic nuclei. *Biochem. Biophys. Res. Commun.* 217, 1015–1025. doi: 10.1006/bbrc.1995.2871

Xu, L. Z., Sanchez, R., Sali, A., and Heintz, N. (1996). Ligand specificity of brain lipid-binding protein. *J. Biol. Chem.* 271, 24711–24719. doi: 10.1074/jbc.271.40.24711

Xu, Z. H., Buelt, M. K., Banaszak, L. J., and Bernlohr, D. A. (1991). Expression, purification, and crystallization of the adipocyte lipid-binding protein. *J. Biol. Chem.* 266, 14367–14370.

Yakunin, E., Loeb, V., Kisos, H., Biala, Y., Yehuda, S., Yaari, Y., et al. (2012). Alpha-synuclein neuropathology is controlled by nuclear hormone receptors and enhanced by docosahexaenoic acid in a mouse model for Parkinson's disease. *Brain Pathol.* 22, 280–294. doi: 10.1111/j.1750-3639.2011.00530.x

Yamashima, T. (2008). A putative link of PUFA, GPR40 and adult-born hippocampal neurons for memory. *Prog. Neurobiol.* 84, 105–115. doi: 10.1016/j.pneurobio.2007.11.002

Yamashima, T. (2012). PUFA-GPR40-CREB signaling hypothesis for the adult primate neurogenesis. *Prog. Lipid Res.* 51, 221–231. doi: 10.1016/j.plipres.2012.02.001

Yan, S., Elmes, M. W., Tong, S., Hu, K., Awwa, M., Teng, G. Y. H., et al. (2018). SAR studies on truxillic acid mono esters as a new class of antinociceptive agents targeting fatty acid binding proteins. *Eur. J. Med. Chem.* 154, 233–252. doi: 10.1016/j.ejmech.2018.04.050

Yang, Y., Tian, X., Xu, D., Zheng, F., Lu, X., Zhang, Y., et al. (2018). GPR40 modulates epileptic seizure and NMDA receptor function. *Sci. Adv.* 4:eaau2357. doi: 10.1126/sciadv.aau2357

Yoshimura, M., Miyata, A., Arita, K., Kurihara, T., Shioda, S., Oyoshi, T., et al. (2015). Attenuation of inflammatory and neuropathic pain behaviors in mice through activation of free fatty acid receptor GPR40. *Mol. Pain* 11:6. doi: 10.1186/s12990-015-0003-8

Yu, S., Levi, L., Siegel, R., and Noy, N. (2012). Retinoic acid induces neurogenesis by activating both retinoic acid receptors (RARs) and peroxisome proliferator-activated receptor beta/delta (PPARbeta/delta). *J. Biol. Chem.* 287, 42195–42205. doi: 10.1074/jbc.M112.410381

Yu, Y., Zhu, M., Zhao, Y., Xu, M., and Qiu, M. (2018). Overexpression of TUSC7 inhibits the inflammation caused by microglia activation via regulating miR-449a/PPAR-gamma. *Biochem. Biophys. Res. Commun.* 503, 1020–1026. doi: 10.1016/j.bbrc.2018.06.111

Yun, S. W., Leong, C., Zhai, D., Tan, Y. L., Lim, L., Bi, X., et al. (2012). Neural stem cell specific fluorescent chemical probe binding to FABP7. *Proc. Natl. Acad. Sci. U.S.A.* 109, 10214–10217. doi: 10.1073/pnas.1200817109120081 7109

Zamarbide, M., Etayo-Labiano, I., Ricobaraza, A., Martinez-Pinilla, E., Aymerich, M. S., Lanciego, J. L., et al. (2014). GPR40 activation leads to CREB and ERK phosphorylation in primary cultures of neurons from the mouse CNS and in human neuroblastoma cells. *Hippocampus* 24, 733–739. doi: 10.1002/hipo.22263

Zenker, J., Stettner, M., Ruskamo, S., Domenech-Estevez, E., Baloui, H., Medard, J.-J., et al. (2014). A role of peripheral myelin protein 2 in lipid homeostasis of myelinating Schwann cells. *Glia* 62, 1502–1512. doi: 10.1002/glia.22696

Zhang, Q., Yang, H., Li, J., and Xie, X. (2016). Discovery and characterization of a novel small-molecule agonist for medium-chain free fatty acid receptor G protein-coupled receptor 84. *J. Pharmacol. Exp. Ther.* 357, 337–344. doi: 10.1124/jpet.116.232033

Zhang, R., Wang, Y., Li, R., and Chen, G. (2015). Transcriptional factors mediating retinoic acid signals in the control of energy metabolism. *Int. J. Mol. Sci.* 16, 14210–14244. doi: 10.3390/ijms160614210

Zhou, Y., Nie, T., Zhang, Y., Song, M., Li, K., Ding, M., et al. (2016). The discovery of novel and selective fatty acid binding protein 4 inhibitors by virtual screening and biological evaluation. *Bioorg. Med. Chem.* 24, 4310–4317. doi: 10.1016/j.bmc.2016.07.022

Zimmer, L., Delpal, S., Guilloteau, D., Aioun, J., Durand, G., and Chalon, S. (2000). Chronic n-3 polyunsaturated fatty acid deficiency alters dopamine vesicle density in the rat frontal cortex. *Neurosci. Lett.* 284, 25–28. doi: 10.1016/s0304-3940(00)00950-2

Zimmer, L., Hembert, S., Durand, G., Breton, P., Guilloteau, D., Besnard, J. C., et al. (1998). Chronic n-3 polyunsaturated fatty acid diet-deficiency acts on dopamine metabolism in the rat frontal cortex: a microdialysis study. *Neurosci. Lett.* 240, 177–181. doi: 10.1016/s0304-3940(97)00938-5

Zoete, V., Grosdidier, A., and Michielin, O. (2007). Peroxisome proliferator-activated receptor structures: ligand specificity, molecular switch and interactions with regulators. *Biochim. Biophys. Acta* 1771, 915–925. doi: 10.1016/j.bbalip.2007.01.007

Zolezzi, J. M., and Inestrosa, N. C. (2013). Peroxisome proliferator-activated receptors and Alzheimer's disease: hitting the blood-brain barrier. *Mol. Neurobiol.* 48, 438–451. doi: 10.1007/s12035-013-8435-5

Zolezzi, J. M., Santos, M. J., Bastías-Candia, S., Pinto, C., Godoy, J. A., and Inestrosa, N. C. (2017). PPARs in the central nervous system: roles in neurodegeneration and neuroinflammation. *Biol. Rev. Camb. Philos. Soc.* 92, 2046–2069. doi: 10.1111/brv.12320

Conflict of Interest Statement: The authors declare that the research was conducted in the absence of any commercial or financial relationships that could be construed as a potential conflict of interest.

frontiers in Cellular Neuroscience

REVIEW
published: 01 May 2019
doi: 10.3389/fncel.2019.00175

Lipids at the Crossroad of α-Synuclein Function and Dysfunction: Biological and Pathological Implications

*Natalia P. Alza[1,2], Pablo A. Iglesias González[1†], Melisa A. Conde[1,3†], Romina M. Uranga[1,3] and Gabriela A. Salvador[1,3]**

[1] Instituto de Investigaciones Bioquímicas de Bahía Blanca, Consejo Nacional de Investigaciones Científicas y Técnicas, Universidad Nacional del Sur, Bahía Blanca, Argentina, [2] Departamento de Química, Universidad Nacional del Sur, Bahía Blanca, Argentina, [3] Departamento de Biología, Bioquímica y Farmacia, Universidad Nacional del Sur, Bahía Blanca, Argentina

OPEN ACCESS

Edited by:
Lavinia Alberi,
SICHH, Switzerland

Reviewed by:
Luigi Bubacco,
University of Padova, Italy
Natalia Ninkina,
Cardiff University, United Kingdom
Jean-Christophe Rochet,
Purdue University, United States

***Correspondence:**
Gabriela A. Salvador
salvador@inibibb-conicet.gob.ar;
salvador@criba.edu.ar

[†]These authors have contributed equally to this work

Specialty section:
This article was submitted to Cellular Neuropathology, a section of the journal Frontiers in Cellular Neuroscience

Received: 21 December 2018
Accepted: 11 April 2019
Published: 01 May 2019

Citation:
Alza NP, Iglesias González PA, Conde MA, Uranga RM and Salvador GA (2019) Lipids at the Crossroad of α-Synuclein Function and Dysfunction: Biological and Pathological Implications. Front. Cell. Neurosci. 13:175. doi: 10.3389/fncel.2019.00175

Since its discovery, the study of the biological role of α-synuclein and its pathological implications has been the subject of increasing interest. The propensity to adopt different conformational states governing its aggregation and fibrillation makes this small 14-kDa cytosolic protein one of the main etiologic factors associated with degenerative disorders known as synucleinopathies. The structure, function, and toxicity of α-synuclein and the possibility of different therapeutic approaches to target the protein have been extensively investigated and reviewed. One intriguing characteristic of α-synuclein is the different ways in which it interacts with lipids. Though in-depth studies have been carried out in this field, the information they have produced is puzzling and the precise role of lipids in α-synuclein biology and pathology and *vice versa* is still largely unknown. Here we provide an overview and discussion of the main findings relating to α-synuclein/lipid interaction and its involvement in the modulation of lipid metabolism and signaling.

Keywords: α–synuclein, lipids, lipid metabolism, lipid signal transduction, membrane lipids

INTRODUCTION

α-Synuclein is a cytosolic protein of 140 amino acids which was discovered in 1988 together with β- and γ-synucleins by Maroteaux et al. (1988). The name α-synuclein derives from the fact that it was originally described as being located in presynaptic endings and also as being associated with nuclear envelopes. In the central nervous system, α-synuclein is abundantly expressed in neurons of different brain areas such as the neocortex, hippocampus, SN, thalamus, and cerebellum (Iwai et al., 1995; Asi et al., 2014). α-Synuclein is also present in the peripheral nervous system, muscle, liver, heart, lungs, kidney, hematopoietic cells of the bone marrow, and circulating blood cells

Abbreviations: AA, arachidonic acid; Chol, cholesterol; DHA, docosahexaenoic acid; FFA, free fatty acids; HMG-CoA, 3-hydroxy-3-methylglutaryl coenzyme A; LB, Lewy bodies; LD, lipid droplet; PA, phosphatidic acid; PC, phosphatidylcholine; PD, Parkinson's disease; PE, phosphatidylethanolamine; PI, phosphatidylinositol; PL, phospholipid; PLA2, phospholipases A2; PLC, phospholipase C; PLD, phospholipase D; PS, phosphatidylserine; PUFA, polyunsaturated fatty acids; SN, *substantia nigra pars compacta*; TAGs, triacylglycerols.

(Gardai et al., 2013; Burré et al., 2018; Mohamed Badawy et al., 2018). β-Synuclein is also located at presynaptic terminals in the central nervous system (Jakes et al., 1994; Wilhelm et al., 2014) while γ-synuclein is primarily expressed in the peripheral nervous system, and the ocular and adipose tissues (Buchman et al., 1998; Surguchov et al., 2001). It has been reported that γ-synuclein is overexpressed in different human tumors (Bruening et al., 2000; Guo et al., 2007; Hibi et al., 2009).

Though numerous studies have been carried out on the biology of α-synuclein, its physiological function remains a matter of debate. The search for a fuller understanding of this function is driven by the fact that it has been linked with several devastating diseases known as synucleinopathies, including neurodegenerative disorders such as: PD, Lewy body dementia, neurodegeneration with brain iron accumulation, Krabbe disease, dementia with LB, diffuse Lewy body disease, Lewy body variant of Alzheimer's disease, among others (Burré, 2015; Burré et al., 2018).

Parkinson's disease is the second most prevalent neurodegenerative age-associated disorder after Alzheimer's disease and is mainly characterized by movement impairments such as resting tremor, bradykinesia, and rigidity. The loss of dopaminergic neurons in the SN has been identified as the cause of the typical motor disablement (Dunnett and Björklund, 1999). Current therapies focus on the reestablishment of the neurotransmitter dopamine for controlling motor symptoms, but specific treatments are still not available owing mainly to a lack of knowledge of the molecular mechanisms that trigger neuronal degeneration and death (Oertel and Schulz, 2016). Since diagnosis occurs when the loss of dopaminergic neurons is massive, a better understanding of the molecular events involved in the neurodegenerative process would undoubtedly help in the discovery of specific treatments.

Parkinson's disease is a multifactorial neurodegenerative disorder whose etiopathogenesis is still largely unknown, though a common finding in patients' brain is the abnormal accumulation, and aggregation of α-synuclein. Intracellular aggregates of α-synuclein, named LB, constitute the histological hallmark of the PD brain. LB are also the main histopathological findings in the above-mentioned synucleinopathies. The role of α-synuclein as one of the leading causes of dopaminergic cell death was described after the identification of the first missense mutations (A30P, E46K, and A53T) in the SNCA gene (Polymeropoulos et al., 1997; Krüger et al., 1998; Zarranz et al., 2004). The involvement of α-synuclein mutants in familial inherited PD has been confirmed by genome-wide association studies (Chang et al., 2017). In addition, SNCA duplication and triplication causing elevated levels of the protein are associated with early-onset PD (Singleton et al., 2003; Chartier-Harlin et al., 2004). Although the α-synuclein protein does not display any mutations in sporadic PD and LB dementia, its involvement in neuronal damage is widely recognized. Of the several mechanisms that could be responsible for the association of α-synuclein with PD pathogenesis, there is an overall consensus that its aggregation leading to the formation of oligomers is a central event related to neuronal dysfunction (Ingelsson, 2016; Bengoa-Vergniory et al., 2017). These α-synuclein oligomeric forms are considered the most toxic species, disrupting cellular homeostasis and triggering neuronal death. Moreover, α-synuclein can exert a deleterious effect by spreading from cell to cell and thus contributing to progressive neurodegeneration (Desplats et al., 2009). Identification of the factors promoting the toxic conversion of mutated or wild-type forms of α-synuclein is a topic of intense interest. Deeper insight into the physiological function and pathological features of α-synuclein would not only contribute toward a better understanding of the pathogenesis but also help to develop biomarkers for early disease detection and progression and to design specific disease-modifying therapies for synucleinopathies.

The α-synuclein protein is composed of three well-described regions that confer the biological and functional characteristics that implicate it in PD pathology. The N-terminal domain comprises residues 1–60 and bestows lipid binding properties on the protein, in particular, the ability to interact with membranes and lipid micelles. This distinctive feature of α-synuclein is explained by the presence of amphipathic repeats of 11 amino acids, predominantly with the highly conserved KTKEGV motif, similar to that present in apolipoprotein domains (Bussell and Eliezer, 2003). This structural characteristic is shared with β- and γ-synucleins (Clayton and George, 1998). The missense mutations A53T, A30P, H50Q, G51D, A53E, and E46K reside in the N-terminal domain of α-synuclein (Polymeropoulos et al., 1997; Krüger et al., 1998; Zarranz et al., 2004; Flagmeier et al., 2016). The central hydrophobic region (residues 61–95) called NAC (non-amyloid β component) is essential for the conformational change of α-synuclein from random coil to β-sheets, leading to aggregation, and fibrillation (El-Agnaf et al., 1998; Rodriguez et al., 2015). Giasson et al. (2001) demonstrated through different assays that amino acids 71–82 represent the specific sequence of the NAC core which is necessarily involved in α-synuclein fibrillation. Biophysical studies using methods like nuclear magnetic resonance, electron paramagnetic resonance, circular dichroism and transmission electron microscopy,with recombinant proteins of α-synuclein and synthetic fragments of NAC were the first and are still used to demonstrate the importance of this region in the fibrillation pathway (El-Agnaf et al., 1998; Giasson et al., 2001; Der-Sarkissiant et al., 2003; Tashiro et al., 2008; Waxman et al., 2009; Shaltiel-Karyo et al., 2010). The elimination of the NAC region or its targeting with antibodies showed to inhibit aggregation and toxicity in cell culture (Lynch et al., 2008; Luk et al., 2009). *In vivo* models were also used to evaluate the pathological effects of this region. For instance, the deletion of amino acids 71–82 in *Drosophila* prevents α-synuclein aggregation and neurotoxicity, thus testifying to the importance of this region in the pathogenicity of the protein (Periquet et al., 2007). Differences in the amino acid sequence of the NAC region have been attributed to be responsible for the non-fibrillation feature of β-synuclein (Uversky and Fink, 2002). The third region of α-synuclein, enriched in glutamate, aspartate, and proline residues, is the acidic C-terminal domain (residues 96–140). It constitutes the main site of post-translational modifications, such as phosphorylation and nitration, although other modifications (ubiquitination, glycation, and methionine

oxidation) also occur in the N-terminal domain (Chen et al., 2019). These modifications alter α-synuclein structure and provoke changes in hydrophobicity and protein-protein and protein-lipid interactions (Burré et al., 2018). Oxidation, nitration and phosphorylation are thought to contribute to different extents to α-synuclein aggregation and fibrillation (Barrett and Timothy Greenamyre, 2015). Phosphorylation is the most relevant post-translational modification related to synucleinopathies. Increased levels of the phosphorylated protein at serine 87 have been found in human brains from LB dementia patients (Paleologou et al., 2010) and at serine 129 in LB from PD patients (Fujiwara et al., 2002). Although this latter has been widely investigated, its role on the pathogenesis of PD has not been determined yet. Some authors propose that it is implicated in α-synuclein pathological aggregation (Fujiwara et al., 2002) whereas others suggest that it has a protective role on the aggregation and toxicity (Oueslati et al., 2010; Chen et al., 2019). The protein also suffers C-terminal truncation linked to an increase of α-synuclein aggregation *in vitro* (Murray et al., 2003); the loss of SN neurons in transgenic mice overexpressing this form has been reported (Wakamatsu et al., 2008). Both the N- and C-terminal domains have also been involved in the interaction with proteins and metal ions (Miotto et al., 2014; Carboni and Lingor, 2015; Billings et al., 2016).

From a conformational point of view, under physiological conditions α-synuclein is considered to be an intrinsically unstructured protein. The soluble α-synuclein in the cytosol is natively unfolded (Burré et al., 2013). Conformational flexibility is largely attributed to the α-synuclein structure because it can adopt a range of conformations depending on its interactions with membranes or proteins (Lashuel et al., 2013). When α-synuclein/PL interaction occurs, the N-terminal domain takes on an α-helical configuration that occurs physiologically in a dynamic equilibrium with the soluble state (Eliezer et al., 2001). An α-helical homo-tetramer of the protein has recently been identified in neurons and other cells (Bartels et al., 2011; Wang et al., 2011; Fanning et al., 2018), occurring in equilibrium with α-synuclein monomers. As the tetramer is resistant to pathological aggregation, the promotion of its formation could be protective against α-synuclein oligomerization (Bartels et al., 2011; Dettmer et al., 2013, 2015a,b, 2017). Moreover, under pathological conditions, the induction of α-synuclein aggregation results in the formation of an initial population of oligomers enriched in insoluble cross-β-sheets (Conway et al., 2000; Pineda and Burré, 2017). These species may act as nuclei for the next steps of elongation and assembly into fibrils, which are finally deposited in LB (Wood et al., 1999; Lashuel et al., 2013). Another proposed mechanism for the formation of fibrillar aggregates is the lateral association of the oligomeric granules without nuclei formation (Bhak et al., 2009; Makwana and Sundd, 2016). Oxidative stress, post-translational modifications, accumulation of α-synuclein and changes in the levels of metal ions, PL, and fatty acids have been proposed as modulators of the aggregation process (Ruipérez et al., 2010; Lashuel et al., 2013; Galvagnion, 2017).

This review focuses on the intriguing characteristic of α-synuclein to pleiotropically interact with and modulate a variety of lipids and on how these interactions participate in the protein's biological and pathological functions.

FUNCTIONS OF α-SYNUCLEIN

The physiological cellular functions of α-synuclein are still a matter of intense debate, despite continuous efforts over the last 30 years to clarify the issue. Since it is highly concentrated in presynaptic terminals, where it is associated with synaptic vesicles (Maroteaux et al., 1988), the involvement of α-synuclein in neurotransmission, and synaptic plasticity has been extensively investigated (Burré, 2015; Zaltieri et al., 2015). Although there is disagreement as to whether it promotes or inhibits neurotransmitter release, it is well-established that α-synuclein mediates this process by regulating the availability of synaptic vesicles in different pools, facilitating their clustering, recycling, and docking to the cell membrane (Chandra et al., 2005; Burré et al., 2010; Zaltieri et al., 2015; Miraglia et al., 2018). The involvement of α-synuclein in synaptic vesicle endocytosis has been demonstrated (Vargas et al., 2014). In addition, α-synuclein can act as a chaperone molecule thus contributing to the assembly of the SNARE complex (Bonini and Giasson, 2005; Diao et al., 2013; Burré et al., 2014). The modulation of dopamine levels by α-synuclein has been demonstrated as a consequence of the inhibition of the neurotransmitter synthesis through the regulation of tyrosine hydroxylase activity (Abeliovich et al., 2000; Peng, 2005) and the inhibition of the vesicular monoamine transporter-2 (Guo et al., 2008). It also has a regulatory effect on the targeting and activity of the dopamine transporter DAT (Swant et al., 2011; Oaks et al., 2013; Butler et al., 2015).

α-Synuclein also has roles which are unrelated to synaptic functions. Surguchev and Surguchov have reviewed recent findings focused on its implication in the regulation of gene expression (Surguchev and Surguchov, 2017). A plethora of other biological functions have been attributed to α-synuclein such as regulation of apoptosis, modulation of glucose and calmodulin levels, and neuronal differentiation (Emamzadeh, 2016). Even though these latter functions have not been explored in depth, they provide evidence for proposing α-synuclein as a pleiotropic molecule.

β- and γ-synucleins have not been linked to the pathogenesis of PD. However, several reports have shown that β-synuclein has an inhibitory effect on the aggregation of α-synuclein (Brown et al., 2016) suggesting a neuroprotective role against synucleinopathies. Otherwise, it has been proposed that γ-synuclein is involved in cancer progression and metastasis (Hibi et al., 2009; Hua et al., 2009; Dunn et al., 2015).

α-SYNUCLEIN AND MEMBRANE LIPIDS

Although the native α-synuclein three-dimensional conformation is still under discussion, differential folding states for physiological and pathological conditions have been assigned.

One of the cutting-edge questions is the role of membrane lipids in α-synuclein conformation since protein-membrane binding has been associated with both normal and pathological functions. It has been reported that the α-synuclein/membrane interaction induces different α-helix states that could participate in protein function or drive aggregation (Bodner et al., 2010; Dikiy and Eliezer, 2012; Fares et al., 2014; Ysselstein et al., 2015; Burré et al., 2018; O'Leary et al., 2018). At the same time, the targeting of α-synuclein in its different conformations at the membrane surface can alter lipid composition, thus promoting pathological effects (van Rooijen et al., 2009; Reynolds et al., 2011; Tosatto et al., 2012; Hellstrand et al., 2013). A significant body of experimental evidence reinforces the hypothesis that oligomers, the initial state of protein aggregation, are the most neurotoxic species because of their ability, after interaction, to disrupt biological membranes (Danzer et al., 2007; Winner et al., 2011; Fusco et al., 2017; Galvagnion, 2017).

The nature of the interactions between α-synuclein and PLs has been extensively reviewed in several papers that mainly address this topic through biophysical studies (Dikiy and Eliezer, 2012; Pineda and Burré, 2017; Burré et al., 2018; O'Leary and Lee, 2018). Here we will discuss the most biologically relevant findings. One of the points included in this section is how specific PLs participate in the induction of conformational changes of α-synuclein and how this affects its biological and/or pathological functions.

After adipose tissue, the brain is the organ with the highest lipid content. PL content in the brain is approximately 6% of dry weight and is represented by two main classes of molecules: glycerophospholipids and sphingolipids (Lahiri and Futerman, 2007). A glycerophospholipid molecule consists of two fatty acids, one saturated and one unsaturated, esterified in sn-1 and sn-2 of the glycerol backbone, respectively. The brain is particularly enriched in two PUFA: arachidonic acid (AA, 20:4-ω-6) and docosahexaenoic acid (DHA, 22:6-ω-3) (Chen et al., 2008). PLs are the main constituents of cellular membranes and because of their amphipathic nature, they provide the necessary biophysical environment for ensuring the proper functioning of structural proteins, receptors, enzymes, and ion channels located at the cell surface or in intracellular membranes.

The plasma and organelle membranes are asymmetric; this characteristic determines specific and differential lipid composition in the inner and the outer leaflets. PC, PE, sphingomyelin, and Chol are the most abundant lipids in the outer hemimembranes. PS and PI are acidic PLs and are predominantly located in the inner hemimembranes. This particular lipid composition is determinant for the formation of lipid rafts, specific membrane liquid-ordered microdomains that govern protein recruitment (van Meer et al., 2008; Marquardt et al., 2015).

In native conditions, α-synuclein can be mainly found in two states: a soluble unfolded monomeric form or a membrane-associated multimeric form. The pathological state of the protein is composed of predominantly β-sheet oligomers and amyloid fibrils (Burré, 2015). PLs have been reported to participate in and modulate the different states of α-synuclein. Originally, α-synuclein was described as a monomer in equilibrium between the cytosol and the membrane fraction (i.e., plasma membrane or vesicles). The occurrence of these two physiological states has generated some controversy, but consensus has now been reached that α-synuclein mainly occurs as an intrinsically disordered monomer (Burré et al., 2013). Very recently, a helically folded tetramer of the soluble protein has been described in equilibrium with the monomer (Bartels et al., 2011; Wang et al., 2011; Fanning et al., 2018). Soluble α-synuclein exists as a random coil three dimensional structure that increases α-helical conformation after interacting with membrane PLs, suggesting that protein/PL interaction triggers structural changes that could modulate biological function (Davidson et al., 1998; Zhu et al., 2003). Furthermore, biophysical studies using tryptophan- and spin-labeled determinations demonstrated that the portion of the protein that interacts with the membrane adopts an α-helix conformation which is entirely buried within the depth of the membrane whereas the rest of the segments present lower membrane penetration and higher flexibility (Bussell, 2005; Wietek et al., 2013).

The preferred PLs for α-synuclein membrane binding are those with an acidic head group such as PS and PI (Shvadchak et al., 2011). The charged nature of these PLs makes lysine residues candidates for α-synuclein binding sites (Jo et al., 2000; Perrin et al., 2000). The interaction between the N-terminal of α-synuclein and PS seems to be critical for C-terminal SNARE-dependent vesicle docking (Lou et al., 2017). Since SNARE-dependent vesicle docking is necessary for calcium-mediated neurotransmitter release, it is reasonable to assume that α-synuclein/PS interaction is critical to the neurotransmission process at the synapse. Indeed, as previously mentioned, one of the best characterized biological functions of α-synuclein is its participation in vesicle recycling (Scott and Roy, 2012; Wang et al., 2014). Experiments performed in giant unilamellar vesicles composed of different proportions of dioleoyl-PC and several anionic PLs demonstrated that wild-type α-synuclein binding is dependent on the presence of negatively charged head groups. Binding to anionic PLs is also dependent of the liquid-ordered state of the vesicles, thus indicating that protein/membrane interactions are governed not only by electrostatic forces but also by lipid packaging and hydrophobic forces (O'Leary and Lee, 2018). The interaction of β- and γ-synucleins with membranes depends on the presence of PL acidic head group and is also determined by the curvature of the binding surface (Ducas and Rhoades, 2012).

A fact that argues in favor of the role of α-synuclein/lipid interaction in the etiopathogenesis of synucleinopathies is that all missense mutations responsible for familial PD are localized in the 11-residue repeat domain that has membrane-binding properties; indeed, these mutations alter the lipid binding properties (Jo et al., 2002; Fares et al., 2014; Ghosh et al., 2014; Robotta et al., 2017). A30P and E46K mutants display altered binding to anionic PLs, thus suggesting that membrane interaction could be disrupted in the familial forms of PD (Stöckl et al., 2008).

Binding to PS has been shown to induce an increase in α-synuclein oligomerization, thus providing evidence of the role of protein/PL interaction in the modulation of the pathological

aggregation of the protein (Hu et al., 2016). After interacting with PLs, the impairing effects of α-synuclein on biological membranes could be explained by the increase in membrane tension and lipid extraction that promote pore formation and membrane lysis (Jo et al., 2000; Zhu et al., 2003; Tosatto et al., 2012; Braun and Sachs, 2015; Pan et al., 2018). In line with this, it has been proposed that the interaction between acidic PLs and α-synuclein plays a role during nuclear extrusion in erythroblast differentiation (Araki et al., 2018).

Phosphatidic acid (PA), another anionic PL, differs from PS, and PI mainly in terms of the small size of its head group; this particular characteristic allows its localization very close to the hydrophobic core of the lipid bilayer. PA is also an α-synuclein partner for membrane targeting (Perrin et al., 2000). Specifically, PA esterified with saturated/monounsaturated fatty acids is the preferred molecular species for α-synuclein binding and also induces an enhancement in protein aggregation through the induction of changes in the secondary structure (Mizuno et al., 2017). It has been reported that α-synuclein overexpression is also able to modulate enzyme pathways that produce PA (Dikiy and Eliezer, 2012) (see the section "α-Synuclein and Lipid Signaling").

α-Synuclein has also been shown to be associated with mitochondrial membranes (Ghio et al., 2016). Binding of α-synuclein to mitochondrial membranes has been detected in SN dopaminergic neurons from mice and human brain (Li et al., 2007; Devi et al., 2008). The nature of protein association with mitochondria was determined by using liquid-disordered membranes enriched in cardiolipin, an essential PL very abundant in the inner mitochondrial membrane and also essential for organelle function. Cardiolipin-mediated binding of α-synuclein could represent a mechanism by which the cytosolic protein is targeted to mitochondria (Ghio et al., 2016). Once attached to the membrane surface, the protein is also able to extract lipids, which could explain the loss of mitochondrial integrity during dopaminergic neuronal degeneration (Pozo Devoto and Falzone, 2017).

The structural changes that α-synuclein undergoes after interacting with PLs in membranes and how these changes contribute to amyloidogenesis is nevertheless still under debate. There is agreement that acidic PLs are the preferred lipids for membrane targeting and that the protein/lipid ratio could be determinant for both biological function and amyloidogenic propensity. Very recently, it has been shown that the conformational state of α-synuclein depends on the protein/lipid ratio. A high α-synuclein/lipid ratio would promote protein/protein interaction and in consequence increase the propensity to form oligomers enriched in β-sheet conformation which in turn could also fibrillate and induce amyloid aggregation (Powers et al., 2017; Terakawa et al., 2018). A low α-synuclein/lipid ratio, on the other hand, would establish a condition of protein dilution, thus blocking amyloid fibrillation, and indeed maintaining physiological interactions with the membrane (Terakawa et al., 2018). Previously mentioned evidence describes the interaction of α-synuclein with membranes in the absence of post-translational modifications; however, it has been shown that post-translational modifications such as phosphorylated or acetylated forms of the protein would interact in a different way (Burré et al., 2018). One of the physiologically relevant post-translational modifications of α-synuclein is its acetylation in the N-terminal, which enhances binding to PC, a zwitterionic PL presented in micelles and small unilamellar vesicles with high curvature (r∼16–20 nm). Chol, another important membrane constituent, has been shown to reduce N-acetylated α-synuclein-PC binding. These *in vitro* results reported by O'Leary and coworkers suggest that N-acetylation promotes the binding of α-synuclein to highly curved membranes and that Chol interferes with this interaction (O'Leary et al., 2018). Moreover, N-acetylated α-synuclein has been shown to diminish the aggregation propensity triggered by ganglioside GM1 binding (Bartels et al., 2014). Phosphorylated α-synuclein in serine 129 has been studied in depth in the last decade, with disparate data being reported in relation to membrane interaction. However, the most accepted theory to emerge from *in vitro* and *in vivo* experiments is that the phosphorylated form has an inhibitory effect on α-synuclein association with the membrane (Fiske et al., 2011; Kuwahara et al., 2012; Nübling et al., 2014; Oueslati, 2016).

Phospholipids also participate in the spreading of α-synuclein, mainly attributed to exosomes, and are thus involved in synucleinopathy propagation. Mass spectrometry studies show the presence of PC, PE, PI, PS, and the gangliosides GM2 and GM3 in exosomes isolated from neuroblastoma cells (Marie et al., 2015). Moreover, experiments carried out on small unilamellar vesicles to ascertain the role of gangliosides in α-synuclein conformation demonstrated that GM1 and GM3, as well as exosomes, are able to accelerate the aggregation of the protein (Marie et al., 2015).

Despite the mounting evidence mentioned above, the question of how PL interaction intervenes in α-synuclein physiological and pathological function remains unanswered (**Figure 1**). In order to shed further light on the specific role of lipid interactions in α-synuclein biology and pathology and how these interactions occur *in vivo*, it is necessary to carry out additional experiments using models that mimic living cell lipid composition, membrane asymmetry, and the intracellular environment.

α-SYNUCLEIN AND LIPID DROPLETS

Neutral lipids are part of a large, heterogeneous family of compounds with the distinctive characteristic of being hydrophobic molecules. Another of their particular features is the lack of charged groups. The two main classes of neutral lipids in mammals are TAGs and Chol esters, both of which reside in the cytosol, contained in a simple membrane-surrounded organelle, the LD (Welte, 2015). LD membranes contain PLs, unesterified Chol, and specific anchored proteins with signaling and lipolytic functions (Gao et al., 2017; Sztalryd and Brasaemle, 2017); as highly dynamic storage organelles, they provide a rapidly mobilizable TAG pool to act as an energy source or as a fatty acid donor for lipid remodeling processes.

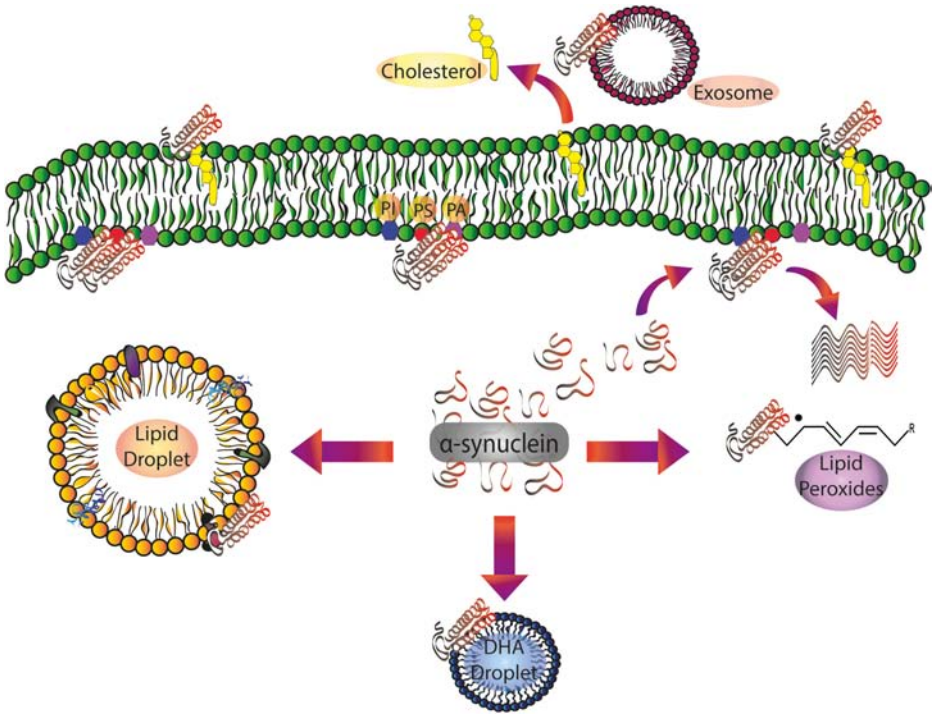

FIGURE 1 | α-Synuclein/lipid interactions: from the plasma membrane to intracellular compartments and extracellular vesicles. Soluble α-synuclein exists as a random coil three-dimensional structure. Membrane targeting with acidic PLs (PS and PI) triggers α-helical folding at the N-terminal domain. Protein pathological conformation is predominantly represented by β-sheet oligomers and amyloid fibrils. α-Synuclein pathological aggregation is dependent on the protein/lipid ratio. Spreading of α-synuclein, largely attributed to exosomes, is also regulated by its interaction with the PLs of the extracellular vesicles. Free fatty acids, mainly DHA, are able to induce α-synuclein oligomerization. After the interaction with lipid peroxidation products, α-synuclein is prone to the formation of toxic stable oligomers. α-Synuclein also regulates Chol efflux via ABCA1 transporter. DHA, docosahexaenoic acid; PA: phosphatidic acid; PI, phosphatidylinositol; PS, phosphatidylserine.

Though LDs are present in almost all cell types, their major occurrence is in adipocytes and hepatocytes. They also serve as cellular stress indicators and are associated with pathological states including starvation, infection, cancer, and liver steatosis (Gluchowski et al., 2017; Tirinato et al., 2017). Scarce information on the precise function of LDs on the nervous system is available in the literature. However, recent works correlate the appearance of LDs with pathological situations in neurodegenerative disorders. Glial cells were reported to be LD-positive cells that accumulate neutral lipids in response to the injury of neighbor neurons in several neurodegenerative conditions (Liu et al., 2015; Cabirol-Pol et al., 2018). LDs were detected in Aplysia axons and neuronal primary cultures and neurons of Huntington's disease models (Savage et al., 1987; Martinez-Vicente et al., 2010; Welte, 2015). In addition, iron accumulation, an event intensively described in several neurodegenerative processes and also in PD, has been shown to increase LD formation in dopaminergic neurons (Salvador, 2010; Schneider and Bhatia, 2012; Sánchez Campos et al., 2015).

A large body of evidence points to α-synuclein/LD interaction. Experiments performed *in vitro* demonstrate that α-synuclein binds to artificial 60 nm diameter LDs (Thiam et al., 2013). Moreover, it has been shown that in HeLa cells incubated with a high concentration of fatty acid, wild-type α-synuclein translocates from the cytosol to the surface of LDs (Colebc et al., 2002). α-Synuclein mutants display a different behavior: whereas A53T strongly associates with LDs, A30P remains cytosolic. These findings were corroborated by the heterologous expression of human α-synuclein in *Saccharomyces cerevisiae* (Sere et al., 2010). The biological significance of the α-synuclein-induced increase in LDs observed in yeasts was addressed in a mutant strain unable to synthesize neutral lipids and more tolerant to α-synuclein overexpression (Sere et al., 2010). In line with these findings, we recently reported that A53T α-synuclein overexpression in dopaminergic neurons induces an increase in TAG production and LD accumulation (Sánchez Campos et al., 2018). Fe exposure in A53T α-synuclein-overexpressing neurons increases protein aggregation, thus also augmenting TAG and LD content (Sánchez Campos et al., 2018). The nature of the α-synuclein/LD interaction has been shown to depend on PL packing at the LD membrane, being not fully packed monolayers the preferred surface for protein binding (Thiam et al., 2013). LD surface has been described as a higher hydrophobic environment than the PL bilayer (Thiam et al., 2013; Kory et al., 2016). The need for this highly hydrophobic organelle has been reported in other biological processes such as protein viral assembly (Ogawa et al., 2009; Welte and Gould, 2017).

The relevance of the biological interaction between α-synuclein/LD has not been explored *in vivo*, but it can be proposed that LDs are early markers of neurodegenerative

processes and the characteristic of these vesicles make them good candidates for the modulation of α-synuclein conformational changes and pathological aggregation. Further research is required for a deeper understanding of these phenomena and their implications in synucleinopathies (**Figure 1**).

α-SYNUCLEIN AND FATTY ACIDS

Another interesting discussion is the role of FFA in α-synuclein biology. Brain membranes exclusively contain a high concentration of PUFA, DHA, and AA being the most abundant. DHA is an essential fatty acid that needs to be incorporated from the diet, and disturbances in its metabolism have been reported to be associated with both neurodevelopment and neurodegenerative disorders (Chen et al., 2008). Some years ago, several *in vitro* observations proposed that α-synuclein could act as a fatty acid binding protein in the brain (Sharon et al., 2001). Soon afterward, PUFA were shown to promote the assembly of α-synuclein soluble oligomers (Sharon et al., 2003a; Karube et al., 2008). Both DHA and to a lesser extent AA are able to induce α-synuclein oligomerization as demonstrated by transmission electron microscopy, electrophoresis of native gels, and fluorescence assays with thioflavin T (Broersen et al., 2006). Relative concentrations of α-synuclein and DHA appear to govern the free and bound states of the protein and also its conformational changes, by increasing its α-helix structure (Sharon et al., 2001; Fecchio et al., 2018). Moreover, prolonged exposure to PUFA triggers the formation of α-synuclein fibrils. The establishment of oligomeric or fibrillar conformations in the presence of DHA depends on the protein/FFA ratio. Whereas fibril formation is favored by a 1:10 molar ratio, oligomeric species characterized by lack of seeding properties for fibrillation are stabilized by a 1:50 ratio (De Franceschi et al., 2011). The general consensus among the broad range of studies on the effect of fatty acids on α-synuclein biology is that PUFA elicit the formation of diverse oligomeric forms with differential structural and biological properties (Perrin et al., 2001; Fecchio et al., 2013). Oligomeric species generated *in vitro* by DHA exposure showed a partial α-helical structure, with the capacity to alter the membrane permeability and thus to trigger cytotoxicity (Fecchio et al., 2013). β- and γ-synucleins are also able to interact with PUFA trough their lipid binding domain (Perrin et al., 2001).

A rise in free DHA levels in cytosolic fractions has already been found in brains of patients with PD and LB dementia, and this could be responsible for the oligomerization of α-synuclein and the underlying neuronal damage (Sharon et al., 2003b). Biophysical studies combined with transmission electron microscopy demonstrated that DHA in solution is able to form oil droplets. These oil droplets can be remodeled by α-synuclein, reducing their size and fatty acid concentration (Broersen et al., 2006; De Franceschi et al., 2009; **Figure 1**). In addition, the interaction with DHA droplets promotes differential susceptibility of proteolytic degradation (De Franceschi et al., 2009).

α-Synuclein has been shown not only to form covalent bonds with DHA but also to act as a scavenger of the oxidation products of DHA, mainly through its histidine residue in position 50 (De Franceschi et al., 2017). Moreover, it has been observed that lysine residues, acting as nucleophiles, are able to interact with electrophilic products of lipid peroxidation and that this protective effect is weakened after lysine acetylation. Additionally, α-synuclein binding to liposomes containing PC and PA enriched with PUFA has been reported to have a protective effect against nitration and oxidation (Trostchansky et al., 2006). The interaction of α-synuclein with 4-hydroxy-2-nonenal, one of the main products of PUFA peroxidation, is able to promote the formation of toxic stable oligomers, and also prevent the passage toward the final state of fibrils (Qin et al., 2007; Puspita et al., 2017; Shamoto-Nagai et al., 2018). Furthermore, dopaminergic cells incubated with free PUFA showed decreased viability associated with the presence of oligomeric α-synuclein (Assayag et al., 2007).

The reported findings highlight the connection between oligomeric α-synuclein and fatty acid oxidation in dopaminergic toxicity, suggesting the existence of a positive loop of increased damage when α-synuclein is allowed to interact with PUFA and their oxidation products. One of the most accepted theories for the onset of neurodegenerative diseases associated with aging postulates the increase in oxidative stress as one of the main gating factors. Since the well-described decrease in antioxidant defenses associated with the aging process increases oxidative stress, it is arguable that lipid peroxides could be available for the interaction with α-synuclein thus triggering the generation of toxic oligomeric forms. Moreover, the extensively documented decrease in brain PUFA content during aging could also be responsible for an increase in saturated PLs at the membranes that in turn could decrease the association with α-synuclein and augment the cytosolic levels of the protein available for binding with lipid peroxides (López et al., 1995; Giusto et al., 2002; Mateos et al., 2010; Ledesma et al., 2012). Studies on oligodendroglial cells overexpressing the A53T mutant have shown that oxidative stress exposure after supplementation with DHA is able to promote the genesis of inclusion bodies whose composition includes phosphorylated α-synuclein (serine 129) and ubiquitinated and SUMOylated proteins, all reported to be aggregation inducers (Riedel et al., 2011).

A number of PD animal models have been used to corroborate some of the above-discussed *in vitro* results. The use of transgenic mice overexpressing different α-synuclein forms and subjected to high-DHA diet has served to support some of the earlier findings. Yakunin et al. (2012) showed increased accumulation of soluble and insoluble α-synuclein forms accompanied by astrocytosis and neuritic defects in an A53T transgenic mouse model fed a DHA-enriched diet. Experiments *in vivo* with transgenic mice expressing the A53T α-synuclein mutant demonstrated that a diet with high DHA content reduces lipoxidative damage (Muntané et al., 2010). A very recent report demonstrated that a diet supplemented with n-3 PUFA promotes the accumulation of a 42-kDa oligomeric form of the protein (Yakunin et al., 2012; Coulombe et al., 2018). Analysis of *post-mortem* human brains corroborates some of the previous *in vitro* and *in vivo* experimental findings. Protein profile of synucleinopathy patients was enriched with

both soluble and insoluble oligomers and a positive correlation between the accumulation of α-synuclein oligomers and cytosolic DHA content was reported (Sharon et al., 2003a,b).

All these findings postulate DHA in soluble and esterified forms as an important candidate for modulating both the targeting and the biological function of α-synuclein. Thus, the regulation of DHA availability under pathological conditions could be an important event for regulating α-synuclein oligomerization and aggregation processes. In this sense, lipid pathways involved in DHA acylation, and deacylation could constitute a promising strategy for new therapeutic approaches in synucleinopathies (see section "α-Synuclein and Lipid Signaling") (**Figures 1**, **3**).

α-SYNUCLEIN AND LIPID METABOLISM

The clear involvement of a crosstalk between α-synuclein and lipid metabolism was investigated by Murphy's group using protein knock-out mice (Castagnet et al., 2005; Golovko et al., 2006, 2007, 2009; Barceló-Coblijn et al., 2007; Golovko and Murphy, 2008). SNCA (−/−) mice oppositely metabolize the two main brain PUFA, AA, and DHA. The lower intake of AA reported both in neurons and astrocytes from SNCA (−/−) mice was reverted by exogenous wild-type α-synuclein through the modulation of acyl-CoA synthetase activity (Golovko et al., 2006). However, DHA turnover and acylation in PE, PI, and PS was found to be increased in SNCA (−/−) mice when compared with SNCA (+/+) mice (Golovko et al., 2007). This differential effect in AA and DHA metabolism as a consequence of the silencing of α-synuclein argues in favor of compensatory mechanisms associated with PUFA content in brain membranes (**Figure 2**).

Several experimental evidences have demonstrated that both the absence and the overexpression of α-synuclein are able to disturb lipid homeostasis by increasing neutral lipid storage. In astrocytes and whole brain, the absence of α-synuclein switches the distribution of fatty acids to neutral lipid reserves and also increases neutral lipid mass (Castagnet et al., 2005; Barceló-Coblijn et al., 2007). Surprisingly, α-synuclein overexpression gives rise to abnormal lipid metabolism in yeasts, characterized by an increase in LD content (Outeiro and Lindquist, 2003; Su et al., 2010). In line with this, overexpression of wild-type and mutant forms of α-synuclein triggers the accumulation of LDs in HeLa cells, and in human-induced pluripotent stem cell (Colebc et al., 2002; Fanning et al., 2018). Regarding these findings, it can be suggested that physiological levels of α-synuclein are necessary for lipid homeostasis. γ-Synuclein, another member of the synuclein family, has also been implicated in the maintenance of LD formation and in the modulation of lipid composition in adipocytes and the nervous system in mice (Guschina et al., 2011; Voshol et al., 2012).

In harmony with these results, a recent study in our laboratory showed that the overexpression of A53T α-synuclein induces an increase in TAG content and the accumulation of LDs in N27 dopaminergic neurons (Sánchez Campos et al., 2018). The rise in neuronal TAG content was associated with increased fatty acid synthase expression and Acyl-CoA synthetase activity, with no variations in TAG lipase activity or in fatty acid β-oxidation, thus demonstrating that the overexpression of A53T α-synuclein triggers a lipid metabolic switch in dopaminergic neurons. Pharmacological blockage of TAG *de novo* synthesis renders the neurons more susceptible to iron-induced oxidative stress (Sánchez Campos et al., 2018).

α-Synuclein biology and Chol metabolism have been shown to interact in many different ways. Such intersections regulate

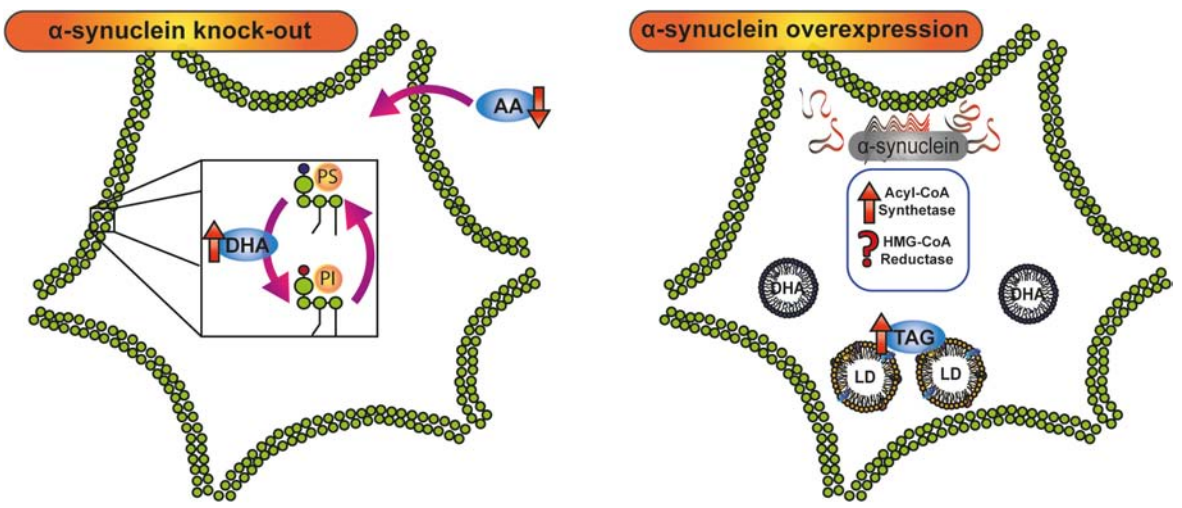

FIGURE 2 | Crosstalk between α-synuclein and lipid metabolism. Knock-down and overexpression of α-synuclein have demonstrated the involvement of the protein in lipid metabolism. In α-synuclein knock-out mice, AA and DHA, the main polyunsaturated fatty acids in the brain, are oppositely metabolized: whereas AA intake is diminished, DHA turnover and acylation in PI and PS are increased. α-Synuclein overexpression triggers an increase in TAG content and LD accumulation by stimulation of acyl-CoA synthetase activity and probably the modulation of HMG-CoA reductase. AA, arachidonic acid; DHA, docosahexaenoic acid; HMG-CoA, 3-Hydroxy-3-methyl glutaryl coenzyme A; LD, lipid droplet; PI, phosphatidylinositol; PS, phosphatidylserine; TAG, triacylglycerol.

one another in a complex and not yet fully understood manner (Yeger-Lotem et al., 2009; Galvagnion, 2017). Controversial information coexists regarding plasma Chol level since it has been considered as either positive or negative risk factor for PD, or even not being linked at all to PD (Galvagnion, 2017). More concrete evidence links oxidized Chol derivatives with the onset and progression of PD (Bosco et al., 2006; Marwarha and Ghribi, 2015). In this regard, 27-hydroxycholesterol, a product of Chol oxidation, has been found to be increased in the brain, cortex and plasma, of PD patients (Lee et al., 2009; Seet et al., 2010; Cheng et al., 2011). Moreover, exogenous 27-hydroxycholesterol is able to induce the expression and accumulation of α-synuclein in human dopaminergic neurons through a transcriptional mechanism mediated by the transcription factor LXRβ (Marwarha et al., 2011). A possible mechanism that supports these findings could be the regulation of Chol efflux from neuronal cultures via ABCA1 transporter associated with the increased levels of oxidative stress reported in PD (Hsiao et al., 2017).

Regarding Chol biosynthesis, *in silico* analysis from the Yeger-Lotem laboratory identified the ergosterol-mevalonate pathway as a candidate for the cellular response to α-synuclein toxicity. One of the identified genes is Hrd1, a ubiquitin protein ligase related with the regulation of HMG-CoA reductase, the rate-limiting enzyme for the *de novo* Chol synthesis (Yeger-Lotem et al., 2009). They also found that pharmacological inhibition of HMG-CoA reductase by statins makes yeasts more vulnerable to α-synuclein toxicity (Yeger-Lotem et al., 2009).

Our results in dopaminergic neurons and those obtained in yeasts suggest a protective role of neutral lipids (TAG and Chol) during α-synuclein overexpression either against proteotoxicity or against oxidative stress (Yeger-Lotem et al., 2009; Auluck et al., 2010; Sánchez Campos et al., 2018). However, contrasting effects have been reported in primary human neurons treated with statins (Bar-On et al., 2008; Roy and Pahan, 2011). In view of the above, additional studies are needed to understand the biological significance of these controversial experimental evidences. Concerning this matter, the clinical relevance of statins is still under debate and is currently being addressed in a trial with PD patients treated with simvastatin which ends in 2020 (Carroll and Wyse, 2017).

The accumulated data allows us to propose a biological function for α-synuclein as a lipid metabolism modulator. Both at physiological levels and when overexpressed, α-synuclein is able to trigger a metabolic switch involving several aspects of lipid biology (**Figure 2**). The main biological response to α-synuclein overexpression is an increase in neutral lipid content that could be related to a neuroprotective strategy, whereas under physiological conditions the modulation of AA levels by the protein appears to be associated with prostaglandin generation and thus with a role in the inflammatory cascade (Golovko et al., 2007).

The open question is how α-synuclein triggers the above-mentioned metabolic changes. One possibility is that the switch in neutral lipid metabolism in terms of LD accumulation could be a consequence of endoplasmic reticulum stress and autophagy impairment, triggered by proteotoxicity due to the overexpression of α-synuclein (Velázquez et al., 2016; Garcia et al., 2018; Pitcairn et al., 2018). The other possibility is that α-synuclein could be involved in the regulation of gene expression associated with lipid metabolism. This latter possibility relates to the high DNA affinity of amyloidogenic proteins, the nuclear localization of α-synuclein, and its participation in epigenetic modifications through histone acetylation (Ma et al., 2014; Surguchev and Surguchov, 2017). Specifically, it has been described that α-synuclein modulates gene expression related with cell survival by decreasing H3 acetylation (Pavlou et al., 2017) and with ubiquitination (Martins et al., 2011). Additional studies will be required to ascertain which of the above-mentioned mechanisms are biologically and pathologically involved and their link with lipid metabolism.

α-SYNUCLEIN AND LIPID SIGNALING

Apart from their structural and biophysical role in biological membranes, lipids also serve as reservoirs of intracellular and extracellular messengers. One of the most investigated events in lipid signaling is the action of phospholipases and PL kinases and phosphatases that produce different lipid and non-lipid messengers from membrane PLs.

Phospholipases catalyze the hydrolysis of acyl and phosphate esters and are named according to their hydrolyzed position on the PL molecule. Among them, PLA2 and phospholipases C and D (PLC and PLD) are widely studied and many of them have been implicated in neurodegenerative processes.

Phospholipases A2 catalyzes the hydrolysis of the fatty acid esterified in the sn-2 of the glycerol backbone of PL moieties and releases FFA and a lysophospholipid. There are currently six different known types of PLA2: secreted (groups I, II, III, V, IX, X, XI, XII, XIII, and XIV), cytosolic (cPLA2, group IV), calcium-independent (iPLA2, group VI), lipoprotein (groups VII and VIII), adipose (group XVI) and lysosomal (group XV), together constituting an enzyme superfamily (Dennis et al., 2011; Vasquez et al., 2018). In terms of neurodegenerative processes, and specifically PD, the most studied PLA2 isotypes are cPLA2 and iPLA2. The classical role assigned to iPLA2 enzymes is their active participation in membrane homeostasis through PL remodeling in Lands cycle where phospholipase activity operates coordinately with PL-acyltransferases. Later findings postulate other important functions for iPLA2s: while lysophosphatidyl moieties have been shown to modulate store-operated calcium entry, the released fatty acid, mostly DHA, has been described as the preferred substrate for the production of resolvins, lipid mediators involved in the resolution of inflammatory processes (Bazan, 2005; Serhan and Petasis, 2011). iPLA2 are mainly encoded by the PLA2G6 gene. In the nervous system, iPLA2β has been shown to be essential for remodeling membrane PLs in axons and synapses. Mutations in PLA2G6 have been associated with several neurodegenerative disorders, including adult-onset dystonia-parkinsonism, PARK14. In this regard, PLA2G6 knock-out mice have been widely used for the study of neuronal membrane-associated degeneration (Sumi-Akamaru et al., 2016). Indeed, increased expression of α-synuclein has

been associated with mitochondrial injury triggered by iPLA2 dysfunction in PLA2G6 knock-out animals (Sumi-Akamaru et al., 2016). Moreover, the impairment of iPLA2-dependent calcium signaling has recently been implicated in neuronal loss through autophagic dysfunction in dopaminergic neurons derived from fibroblasts from PD patients and PLA2G6 knock-out animals (Zhou et al., 2016).

cPLA2 is mainly associated with the release of AA, the obligate substrate for prostaglandins generation catalyzed by cyclooxygenase-2, which is considered one of the main pathways mediating inflammatory response. Though neuroinflammation is a hallmark of PD, the specific PLA2 isoforms that are activated in dopaminergic neuronal damage have not been fully described. Besides the classical inflammatory process, the exposure to extracellular α-synuclein is able to activate cPLA2 and to promote synapse damage induced by phospholipase-dependent activity (Bate and Williams, 2015).

Upon PLA2 activation, it is important that fatty acid release be properly coupled to PL acylation activity; impairment of the Lands cycle could be responsible for an increase in FFA availability (DHA, AA). This increase in FFA availability, could in turn, be associated with α-synuclein and promote its oligomerization. The rise in cytosolic/soluble DHA content reported by Sharon and coworkers in *post-mortem* brains in PD and LB dementia patients is in agreement with the activation of any specific PLA2 that could consecutively induce α-synuclein oligomerization and aggregation (Sharon et al., 2003a). The workings of this mechanism still lack clarity.

The fact that SNCA knock-out mice present enhanced prostaglandin generation during neuronal injury argues in favor of a biological role for α-synuclein in the regulation of the inflammatory cascade (Golovko and Murphy, 2008). It has been demonstrated that DHA, mainly released from PLs by iPLA2 action, has a long half-life compared with other fatty acids and that its free form is the preferred substrate for neuroprotectin synthesis, and the resolution of the inflammatory process (Murphy, 2013). An important question is whether the dyshomeostasis between cPLA2 and iPLA2 triggered by α-synuclein overexpression could be responsible for a differential AA/DHA ratio and availability, thus modulating the balance between inflammation and resolution processes and promoting the neuroinflammatory phenotype in PD (**Figure 3**).

Among the classical signaling pathways associated with G-protein-coupled receptors is PI-specific PLC. Upon receptor activation, PLC hydrolyzes PI 4,5-bisphosphate to produce the lipid messenger diacylglycerol and the soluble inositol triphosphate. There are now six different families of PLC (β, γ, δ, ε, ζ, and η) described in different tissues, with pleiotropic functions associated with the membrane receptor to which they are coupled (Kadamur and Ross, 2013). It has recently been shown that α-synuclein overexpression interferes with Gq/PLC-β signaling by preventing the rise in cytosolic calcium and ERK 1/2 activation (Volta et al., 2017). α-Synuclein is also able to trigger the impairment of G-protein signaling associated with sphingosine-1-phosphate by promoting the exclusion of the receptor from lipid rafts (Mohamed Badawy et al., 2018).

Phospholipase D signaling impairment has been reported in Alzheimer's disease and the signaling pathway is, therefore, an emerging therapeutic target for this neurodegenerative disorder (Brown et al., 2017). The role of PLD in α-synuclein-associated pathologies, however, still lacks clarity. Classical PLDs, PLD1 and PLD2, catalyze the hydrolysis of the PC head group in order to produce PA. PA has pleiotropic functions both as a lipid messenger, regulating the activity of signaling proteins, and as an important modulator of membrane curvature. Whereas neuronal PLD1 has been associated with cytoskeleton architecture, PLD2 activity is linked to molecular events triggered by the activation of membrane receptors (Watanabe et al., 2011; Comoglio et al., 2014). Both PLD1 and PLD2 have been reported to participate in astroglial differentiation (Burkhardt et al., 2015). Genetic deletion of PLD1 or PLD2 in transgenic mice demonstrates that both

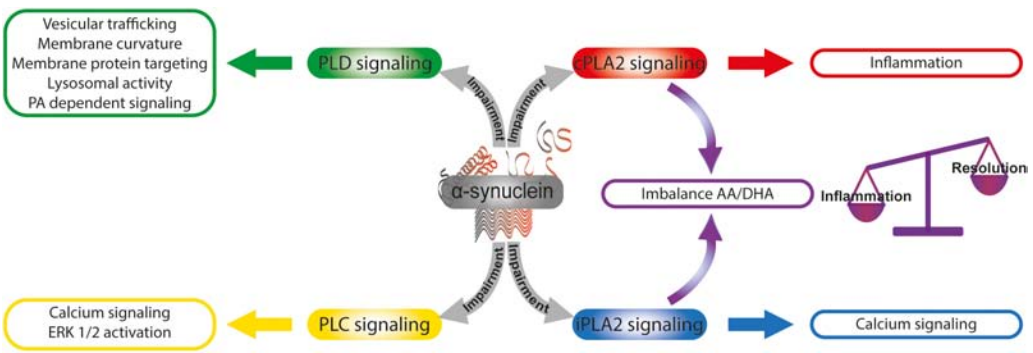

FIGURE 3 | α-Synuclein and the modulation of lipid signaling. α-Synuclein is able to intervene lipid signaling by the modulation of phospholipase activities. The α-synuclein -induced impairment of cPLA2 and iPLA2 signaling triggers an imbalance in the AA/DHA ratio that finally could affect the balance of inflammation and resolution processes. Calcium signaling and ERK 1/2 activation are modulated by α-synuclein through PLC pathway impairment. α-Synuclein intervention in PLD signaling impacts on diverse cellular functions as vesicular trafficking, membrane curvature, and membrane protein targeting, lysosomal activity and PA-dependent signaling. AA, arachidonic acid; DHA, docosahexaenoic acid; PA, phosphatidic acid; cPLA2, calcium-sensitive cytosolic phospholipase A2; iPLA2, calcium-independent phospholipase A2; PLC, phospholipase C; PLD, phospholipase D.

enzymes participate in brain development and cognitive function (Burkhardt et al., 2014).

The role of classical PLDs in the several processes of the nervous system has been well-established, but their participation in neurodegenerative processes associated with synucleinopathies is not clear. *In vitro* and *in vivo* assays have given rise to a number of divergent reports of the role of α-synuclein in PLD signaling. *In vivo* experiments have demonstrated that α-synuclein-induced PLD2 inhibition is able to prevent dopaminergic neurodegeneration (Gorbatyuk et al., 2010), whereas *in vitro* assays using recombinant α-synuclein and purified PLD1 and PLD2 have shown no inhibition of PLD activity (Rappley et al., 2009). However, protein profile studies in *post-mortem* brains from PD patients display diminished PLD1 expression (Bae et al., 2014). In yeast, it has been demonstrated that PLD inhibition elicited by α-synuclein was related to dysregulation of lipid metabolism and trafficking (Outeiro and Lindquist, 2003). In line with this, our laboratory has recently described that the overexpression of human α-synuclein in neuroblastoma cells is able to induce a decrease in PLD1 mRNA and protein levels and to impair ERK1/2 signaling (Conde et al., 2018). In this cellular model of synucleinopathy, we demonstrated that the inhibition of PLD1 expression and the impairment of ERK1/2 signaling triggered by α-synuclein overexpression are associated with a decrease in neurofilament light chain expression and in consequence with alteration of the neuronal cytoskeleton. The reported findings highlight the biological significance of PLD regulation exerted by α-synuclein that could modulate PA levels in a compartment-specific manner, thus impacting on different cellular functions: (i) vesicular trafficking, (ii) membrane curvature and membrane protein targeting, (iii) lysosomal activity, and (iv) PA-dependent signaling, among others (**Figure 3**).

It is clear from the above that α-synuclein, mainly when it is overexpressed, is able to disturb lipid signaling. The plethora of lipid messengers (PA, AA, DHA, and diacylglycerol) able to be produced due to α-synuclein could have different impacts on important cellular processes in the nervous system such as vesicular trafficking, autophagy, cytoskeleton architecture, and neuroinflammation. Dissecting the signaling pathways responsible for the production of each lipid messenger and the specific cellular compartment where they work, could contribute to the development of new strategic therapies for synucleinopathies.

CONCLUDING REMARKS

This review covers the diversity of ways in which α-synuclein interacts and connects with lipid biology. Much of the experimental evidences dealing with the physical interaction of the protein with different lipid moieties derive from biophysical studies performed on artificial membranes. It is clear that the α-synuclein N-terminal domain is able to interact with the majority of PLs and with Chol with different affinities. Further research is required in order to shed more light on precisely which of these α-synuclein/lipid interactions occur *in vivo*; clear findings will undoubtedly contribute to a fuller understanding of both the biological and pathological implications of α-synuclein.

Efforts toward a more detailed characterization of α-synuclein interventions in lipid metabolism and signaling will open the way to a more in-depth assessment of the protein's implications for therapeutic purposes. One hypothesis to be tested is whether α-synuclein pleiotropic properties are able to trigger a lipid metabolic and signaling switch, creating a propensity to interact and aggregate thus establishing a positive feedback. Unraveling this paradigm could provide not only new insights into the biological role of α-synuclein but also innovative ways of devising strategies for the treatment of synucleinopathies.

AUTHOR CONTRIBUTIONS

GS contributed to conception and design of the study. GS, NA, and PIG organized the database and wrote the sections of the manuscript. MC designed and performed the figures. RU performed the critical reading and editing. All authors contributed to manuscript revision, read, and approved the submitted version.

FUNDING

GS, NA, and RU are research members of the CONICET. MC and PIG are research fellows of the CONICET. Articles from our laboratory that have been cited in this review were granted by ANPCyT (PICT 2013-0987 and PICT 2017-0224), CONICET (PIP 11220120100251), and UNS (PGI 24/B226).

REFERENCES

Abeliovich, A., Schmitz, Y., Fariñas, I., Choi-Lundberg, D., Ho, W. H., Castillo, P. E., et al. (2000). Mice lacking α-synuclein display functional deficits in the nigrostriatal dopamine system. *Neuron* 25, 239–252. doi: 10.1016/S0896-6273(00)80886-7

Araki, K., Sugawara, K., Hayakawa, E. H., Ubukawa, K., Kobayashi, I., Wakui, H., et al. (2018). The localization of α-synuclein in the process of differentiation of human erythroid cells. *Int. J. Hematol.* 108, 130–138. doi: 10.1007/s12185-018-2457-8

Asi, Y. T., Simpson, J. E., Heath, P. R., Wharton, S. B., Lees, A. J., Revesz, T., et al. (2014). Alpha-synuclein mRNA expression in oligodendrocytes in MSA. *Glia* 62, 964–970. doi: 10.1002/glia.22653

Assayag, K., Yakunin, E., Loeb, V., Selkoe, D. J., and Sharon, R. (2007). Polyunsaturated fatty acids induce α-synuclein-related pathogenic changes in neuronal cells. *Am. J. Pathol.* 171, 2000–2011. doi: 10.2353/ajpath.2007.070373

Auluck, P. K., Caraveo, G., and Lindquist, S. (2010). α-Synuclein: membrane interactions and toxicity in Parkinson's disease. *Annu. Rev. Cell Dev. Biol.* 26, 211–233. doi: 10.1146/annurev.cellbio.042308.113313

Bae, E. J., Lee, H. J., Jang, Y. H., Michael, S., Masliah, E., Min, D. S., et al. (2014). Phospholipase D1 regulates autophagic flux and clearance of α-synuclein aggregates. *Cell Death Differ.* 21, 1132–1141. doi: 10.1038/cdd.2014.30

Barceló-Coblijn, G., Golovko, M. Y., Weinhofer, I., Berger, J., and Murphy, E. J. (2007). Brain neutral lipids mass is increased in α-synuclein gene-ablated mice. *J. Neurochem.* 101, 132–141. doi: 10.1111/j.1471-4159.2006.04348.x

Bar-On, P., Crews, L., Koob, A. O., Mizuno, H., Adame, A., Spencer, B., et al. (2008). Statins reduce neuronal α-synuclein aggregation in in vitro models of Parkinson's disease. *J. Neurochem.* 105, 1656–1667. doi: 10.1111/j.1471-4159.2008.05254.x

Barrett, P. J., and Timothy Greenamyre, J. (2015). Post-translational modification of α-synuclein in Parkinson's disease. *Brain Res.* 1628(Pt B), 247–253. doi: 10.1016/j.brainres.2015.06.002

Bartels, T., Choi, J. G., and Selkoe, D. J. (2011). α-Synuclein occurs physiologically as a helically folded tetramer that resists aggregation. *Nature* 477, 107–110. doi: 10.1038/nature10324

Bartels, T., Kim, N. C., Luth, E. S., and Selkoe, D. J. (2014). N-alpha-acetylation of α-synuclein increases its helical folding propensity, GM1 binding specificity and resistance to aggregation. *PLoS One* 9:e103727. doi: 10.1371/journal.pone.0103727

Bate, C., and Williams, A. (2015). cAMP-inhibits cytoplasmic phospholipase A2 and protects neurons against amyloid-β-induced synapse damage. *Biology* 4, 591–606. doi: 10.3390/biology4030591

Bazan, N. G. (2005). Neuroprotectin D1 (NPD1): a DHA-derived mediator that protects brain and retina against cell injury-induced oxidative stress. *Brain Pathol.* 15, 159–166. doi: 10.1111/j.1750-3639.2005.tb00513.x

Bengoa-Vergniory, N., Roberts, R. F., Wade-Martins, R., and Alegre-Abarrategui, J. (2017). Alpha-synuclein oligomers: a new hope. *Acta Neuropathol.* 134, 819–838. doi: 10.1007/s00401-017-1755-1

Bhak, G., Lee, J. H., Hahn, J. S., and Paik, S. R. (2009). Granular assembly of α-synuclein leading to the accelerated amyloid fibril formation with shear stress. *PLoS One* 4:e4177. doi: 10.1371/journal.pone.0004177

Billings, J. L., Hare, D. J., Nurjono, M., Volitakis, I., Cherny, R. A., Bush, A. I., et al. (2016). Effects of neonatal iron feeding and chronic clioquinol administration on the Parkinsonian human A53T transgenic mouse. *ACS Chem. Neurosci.* 7, 360–366. doi: 10.1021/acschemneuro.5b00305

Bodner, C. R., Maltsev, A. S., Dobson, C. M., and Bax, A. (2010). Differential phospholipid binding of α-synuclein variants implicated in Parkinson's disease revealed by solution NMR spectroscopy. *Biochemistry* 49, 862–871. doi: 10.1021/bi901723p

Bonini, N., and Giasson, B. (2005). Snaring the function of alpha-synuclein. *Cell* 123, 359–361. doi: 10.1016/j.cell.2005.10.017

Bosco, D. A., Fowler, D. M., Zhang, Q., Nieva, J., Powers, E. T., Wentworth, P., et al. (2006). Elevated levels of oxidized cholesterol metabolites in Lewy body disease brains accelerate α-synuclein fibrilization. *Nat. Chem. Biol.* 2, 249–253. doi: 10.1038/nchembio782

Braun, A. R., and Sachs, J. N. (2015). α-synuclein reduces tension and increases undulations in simulations of small unilamellar vesicles. *Biophys. J.* 108, 1848–1851. doi: 10.1016/j.bpj.2015.03.029

Broersen, K., van den Brink, D., Fraser, G., Goedert, M., and Davletov, B. (2006). Alpha-synuclein adopts an alpha-helical conformation in the presence of polyunsaturated fatty acids to hinder micelle formation. *Biochemistry* 45, 15610–15616. doi: 10.1021/bi061743l

Brown, H. A., Thomas, P. G., and Lindsley, C. W. (2017). Targeting phospholipase D in cancer, infection and neurodegenerative disorders. *Nat. Rev. Drug Discov.* 16, 351–367. doi: 10.1038/nrd.2016.252

Brown, J. W. P., Buell, A. K., Michaels, T. C. T., Meisl, G., Carozza, J., Flagmeier, P., et al. (2016). β-Synuclein suppresses both the initiation and amplification steps of α-synuclein aggregation via competitive binding to surfaces. *Sci. Rep.* 6:36010. doi: 10.1038/srep36010

Bruening, W., Giasson, B. I., Klein-Szanto, A. J. P., Lee, V. M. Y., Trojanowski, J. Q., and Godwin, A. K. (2000). Synucleins are expressed in the majority of breast and ovarian carcinomas and in preneoplastic lesions of the ovary. *Cancer* 88, 2154–2163. doi: 10.1002/(sici)1097-0142(20000501)88%3A9%3C2154%3A%3Aaid-cncr23%3E3.0.co%3B2-9

Buchman, V. L., Hunter, H. J., Pinõn, L. G., Thompson, J., Privalova, E. M., Ninkina, N. N., et al. (1998). Persyn, a member of the synuclein family, has a distinct pattern of expression in the developing nervous system. *J. Neurosci.* 18, 9335–9341. doi: 10.1523/JNEUROSCI.18-22-09335.1998

Burkhardt, U., Beyer, S., and Klein, J. (2015). Role of phospholipases D1 and 2 in astroglial proliferation: effects of specific inhibitors and genetic deletion. *Eur. J. Pharmacol.* 761, 398–404. doi: 10.1016/j.ejphar.2015.05.004

Burkhardt, U., Stegner, D., Hattingen, E., Beyer, S., Nieswandt, B., and Klein, J. (2014). Impaired brain development and reduced cognitive function in phospholipase D-deficient mice. *Neurosci. Lett.* 572, 48–52. doi: 10.1016/j.neulet.2014.04.052

Burré, J. (2015). The synaptic function of α-synuclein. *J. Parkinsons Dis.* 5, 699–713. doi: 10.3233/JPD-150642

Burré, J., Sharma, M., and Südhof, T. C. (2014). α-Synuclein assembles into higher-order multimers upon membrane binding to promote SNARE complex formation. *Proc. Natl. Acad. Sci. U.S.A.* 111, E4274–E4283. doi: 10.1073/pnas.1416598111

Burré, J., Sharma, M., and Südhof, T. C. (2018). Cell biology and pathophysiology of α-synuclein. *Cold Spring Harb. Perspect. Med.* 8:a024091. doi: 10.1101/cshperspect.a024091

Burré, J., Sharma, M., Tsetsenis, T., Buchman, V., Etherton, M. R., and Südhof, T. C. (2010). α-Synuclein promotes SNARE-complex assembly in vivo and in vitro. *Science* 329, 1663–1667. doi: 10.1126/science.1195227

Burré, J., Vivona, S., Diao, J., Sharma, M., Brunger, A. T., and Südhof, T. C. (2013). Properties of native brain α-synuclein. *Nature* 498, E4–E6. doi: 10.1038/nature12125

Bussell, R. (2005). Helix periodicity, topology, and dynamics of membrane-associated α-Synuclein. *Protein Sci.* 14, 862–872. doi: 10.1110/ps.041255905

Bussell, R., and Eliezer, D. (2003). A structural and functional role for 11-mer repeats in α-synuclein and other exchangeable lipid binding proteins. *J. Mol. Biol.* 329, 763–778. doi: 10.1016/S0022-2836(03)00520-5

Butler, B., Saha, K., Rana, T., Becker, J. P., Sambo, D., Davari, P., et al. (2015). Dopamine transporter activity is modulated by α-synuclein. *J. Biol. Chem.* 290, 29542–29554. doi: 10.1074/jbc.M115.691592

Cabirol-Pol, M. J., Khalil, B., Rival, T., Faivre-Sarrailh, C., and Besson, M. T. (2018). Glial lipid droplets and neurodegeneration in a *Drosophila* model of complex I deficiency. *Glia* 66, 874–888. doi: 10.1002/glia.23290

Carboni, E., and Lingor, P. (2015). Insights on the interaction of alpha-synuclein and metals in the pathophysiology of Parkinson's disease. *Metallomics* 7, 395–404. doi: 10.1039/c4mt00339j

Carroll, C. B., and Wyse, R. K. H. (2017). Simvastatin as a potential disease-modifying therapy for patients with Parkinson's disease: rationale for clinical trial, and current progress. *J. Parkinsons Dis.* 7, 545–568. doi: 10.3233/JPD-171203

Castagnet, P. I., Golovko, M. Y., Barceló-Coblijn, G. C., Nussbaum, R. L., and Murphy, E. J. (2005). Fatty acid incorporation is decreased in astrocytes cultured from α-synuclein gene-ablated mice. *J. Neurochem.* 94, 839–849. doi: 10.1111/j.1471-4159.2005.03247.x

Chandra, S., Gallardo, G., Fernández-Chacón, R., Schlüter, O. M., and Südhof, T. C. (2005). α-Synuclein cooperates with CSPα in preventing neurodegeneration. *Cell* 123, 383–396. doi: 10.1016/j.cell.2005.09.028

Chang, D., Nalls, M. A., Hallgrímsdottir, I. B., Hunkapiller, J., Van Der Brug, M., Cai, F., et al. (2017). A meta-analysis of genome-wide association studies identifies 17 new Parkinson's disease risk loci. *Nat. Genet.* 49, 1511–1516. doi: 10.1038/ng.3955

Chartier-Harlin, M. C., Kachergus, J., Roumier, C., Mouroux, V., Douay, X., Lincoln, S., et al. (2004). α-synuclein locus duplication as a cause of familial Parkinson's disease. *Lancet* 364, 1167–1169. doi: 10.1016/S0140-6736(04)17103-1

Chen, C. T., Green, J. T., Orr, S. K., and Bazinet, R. P. (2008). Regulation of brain polyunsaturated fatty acid uptake and turnover. *Prostaglandins Leukot. Essent. Fatty Acids* 79, 85–91. doi: 10.1016/j.plefa.2008.09.003

Chen, H., Zhao, Y.-F., Chen, Y.-X., and Li, Y.-M. (2019). Exploring the roles of post-translational modifications in the pathogenesis of Parkinson's disease using synthetic and semisynthetic modified α-synuclein. *ACS Chem. Neurosci.* 10, 910–921. doi: 10.1021/acschemneuro.8b00447

Cheng, D., Jenner, A. M., Shui, G., Cheong, W. F., Mitchell, T. W., Nealon, J. R., et al. (2011). Lipid pathway alterations in Parkinson's disease primary visual cortex. *PLoS One* 6:e17299. doi: 10.1371/journal.pone.0017299

Clayton, D. F., and George, J. M. (1998). The synucleins: a family of proteins involved in synaptic function, plasticity, neurodegeneration and disease. *Trends Neurosci.* 21, 249–254. doi: 10.1016/S0166-2236(97)01213-7

Colebc, N. B., Murphy, D. D., Grider, T., Rueter, S., Brasaemle, D., and Nussbaum, R. L. (2002). Lipid droplet binding and oligomerization properties of the Parkinson's disease protein α-synuclein. *J. Biol. Chem.* 277, 6344–6352. doi: 10.1074/jbc.M108414200

Comoglio, Y., Levitz, J., Kienzler, M. A., Lesage, F., Isacoff, E. Y., and Sandoz, G. (2014). Phospholipase D2 specifically regulates TREK potassium channels via direct interaction and local production of phosphatidic acid. *Proc. Natl. Acad. Sci. U.S.A.* 111, 13547–13552. doi: 10.1073/pnas.1407160111

Conde, M. A., Alza, N. P., Iglesias González, P. A., Scodelaro Bilbao, P. G., Sánchez Campos, S., Uranga, R. M., et al. (2018). Phospholipase D1 downregulation by α-synuclein: implications for neurodegeneration in Parkinson's disease. *Biochim. Biophys. Acta Mol. Cell Biol. Lipids* 1863, 639–650. doi: 10.1016/j.bbalip.2018.03.006

Conway, K. A., Harper, J. D., and Lansbury, P. T. (2000). Fibrils formed in vitro from α-synuclein and two mutant forms linked to Parkinson's disease are typical amyloid. *Biochemistry* 39, 2552–2563. doi: 10.1021/bi991447r

Coulombe, K., Kerdiles, O., Tremblay, C., Emond, V., Lebel, M., Boulianne, A. S., et al. (2018). Impact of DHA intake in a mouse model of synucleinopathy. *Exp. Neurol.* 301(Pt A), 39–49. doi: 10.1016/j.expneurol.2017.12.002

Danzer, K. M., Haasen, D., Karow, A. R., Moussaud, S., Habeck, M., Giese, A., et al. (2007). Different species of a-synuclein oligomers induce calcium influx and seeding. *J. Neurosci.* 27, 9220–9232. doi: 10.1523/JNEUROSCI.2617-07.2007

Davidson, W. S., Jonas, A., Clayton, D. F., and George, J. M. (1998). Stabilization of α-Synuclein secondary structure upon binding to synthetic membranes. *J. Biol. Chem.* 273, 9443–9449. doi: 10.1074/jbc.273.16.9443

De Franceschi, G., Fecchio, C., Sharon, R., Schapira, A. H. V., Proukakis, C., Bellotti, V., et al. (2017). α-Synuclein structural features inhibit harmful polyunsaturated fatty acid oxidation, suggesting roles in neuroprotection. *J. Biol. Chem.* 292, 6927–6937. doi: 10.1074/jbc.M116.765149

De Franceschi, G., Frare, E., Bubacco, L., Mammi, S., Fontana, A., and de Laureto, P. P. (2009). Molecular insights into the interaction between α-synuclein and docosahexaenoic acid. *J. Mol. Biol.* 394, 94–107. doi: 10.1016/j.jmb.2009.09.008

De Franceschi, G., Frare, E., Pivato, M., Relini, A., Penco, A., Greggio, E., et al. (2011). Structural and morphological characterization of aggregated species of α-synuclein induced by docosahexaenoic acid. *J. Biol. Chem.* 286, 22262–22274. doi: 10.1074/jbc.M110.202937

Dennis, E. A., Cao, J., Hsu, Y. H., Magrioti, V., and Kokotos, G. (2011). Phospholipase A2 enzymes: physical structure, biological function, disease implication, chemical inhibition, and therapeutic intervention. *Chem. Rev.* 111, 6130–6185. doi: 10.1021/cr200085w

Der-Sarkissiant, A., Jao, C. C., Chen, J., and Langen, R. (2003). Structural organization of α-synuclein fibrils studied by site-directed spin labeling. *J. Biol. Chem.* 278, 37530–37535. doi: 10.1074/jbc.M305266200

Desplats, P., Lee, H.-J., Bae, E.-J., Patrick, C., Rockenstein, E., Crews, L., et al. (2009). Inclusion formation and neuronal cell death through neuron-to-neuron transmission of alpha-synuclein. *Proc. Natl. Acad. Sci. U.S.A.* 106, 13010–13015. doi: 10.1073/pnas.0903691106

Dettmer, U., Newman, A. J., Luth, E. S., Bartels, T., and Selkoe, D. (2013). In vivo cross-linking reveals principally oligomeric forms of α-synuclein and β-synuclein in neurons and non-neural cells. *J. Biol. Chem.* 288, 6371–6385. doi: 10.1074/jbc.M112.403311

Dettmer, U., Newman, A. J., Soldner, F., Luth, E. S., Kim, N. C., Von Saucken, V. E., et al. (2015a). Parkinson-causing α-synuclein missense mutations shift native tetramers to monomers as a mechanism for disease initiation. *Nat. Commun.* 6:7314. doi: 10.1038/ncomms8314

Dettmer, U., Newman, A. J., von Saucken, V. E., Bartels, T., and Selkoe, D. J. (2015b). KTKEGV repeat motifs are key mediators of normal α-synuclein tetramerization: their mutation causes excess monomers and neurotoxicity. *Proc. Natl. Acad. Sci. U.S.A.* 112, 9596–9601. doi: 10.1073/pnas.1505953112

Dettmer, U., Ramalingam, N., von Saucken, V. E., Kim, T. E., Newman, A. J., Terry-Kantor, E., et al. (2017). Loss of native α-synuclein multimerization by strategically mutating its amphipathic helix causes abnormal vesicle interactions in neuronal cells. *Hum. Mol. Genet.* 26, 3466–3481. doi: 10.1093/HMG/DDX227

Devi, L., Raghavendran, V., Prabhu, B. M., Avadhani, N. G., and Anandatheerthavarada, H. K. (2008). Mitochondrial import and accumulation of α-synuclein impair complex I in human dopaminergic neuronal cultures and Parkinson disease brain. *J. Biol. Chem.* 283, 9089–9100. doi: 10.1074/jbc.M710012200

Diao, J., Burré, J., Vivona, S., Cipriano, D. J., Sharma, M., Kyoung, M., et al. (2013). Native α-synuclein induces clustering of synaptic-vesicle mimics via binding to phospholipids and synaptobrevin-2/VAMP2. *eLife* 2:e00592. doi: 10.7554/eLife.00592

Dikiy, I., and Eliezer, D. (2012). Folding and misfolding of alpha-synuclein on membranes. *Biochim. Biophys. Acta* 1818, 1013–1018. doi: 10.1016/j.bbamem.2011.09.008

Ducas, V. C., and Rhoades, E. (2012). Quantifying interactions of β-synuclein and γ-synuclein with model membranes. *J. Mol. Biol.* 423, 528–539. doi: 10.1016/j.jmb.2012.08.008

Dunn, T. N., Akiyama, T., Lee, H. W., Kim, J. B., Knotts, T. A., Smith, S. R., et al. (2015). Evaluation of the synuclein-γ (sncg) gene as a PPARγ target in murine adipocytes, dorsal root ganglia somatosensory neurons, and human adipose tissue. *PLoS One* 10:e0115830. doi: 10.1371/journal.pone.0115830

Dunnett, S. B., and Björklund, A. (1999). Prospects for new restorative and neuroprotective treatments in Parkinson's disease. *Nature* 399(Suppl. 6738), A32–A39. doi: 10.1038/399a032

El-Agnaf, O. M. A., Jakes, R., Curran, M. D., Middleton, D., Ingenito, R., Bianchi, E., et al. (1998). Aggregates from mutant and wild-type α-synuclein proteins and NAC peptide induce apoptotic cell death in human neuroblastoma cells by formation of β-sheet and amyloid-like filaments. *FEBS Lett.* 440, 71–75. doi: 10.1016/S0014-5793(98)01418-5

Eliezer, D., Kutluay, E., Bussell, R., and Browne, G. (2001). Conformational properties of α-synuclein in its free and lipid-associated states. *J. Mol. Biol.* 307, 1061–1073. doi: 10.1006/jmbi.2001.4538

Emamzadeh, F. N. (2016). Alpha-synuclein structure, functions, and interactions. *J. Res. Med. Sci.* 21:29. doi: 10.4103/1735-1995.181989

Fanning, S., Haque, A., Imberdis, T., Baru, V., Barrasa, M. I., Nuber, S., et al. (2018). Lipidomic analysis of α-synuclein neurotoxicity identifies stearoyl CoA desaturase as a target for Parkinson treatment. *Mol. Cell* 73, 1001–1014.e8. doi: 10.1016/J.MOLCEL.2018.11.028

Fares, M. B., Ait-Bouziad, N., Dikiy, I., Mbefo, M. K., Jovičić, A., Kiely, A., et al. (2014). The novel Parkinson's disease linked mutation G51D attenuates in vitro aggregation and membrane binding of α-synuclein, and enhances its secretion and nuclear localization in cells. *Hum. Mol. Genet.* 23, 4491–4509. doi: 10.1093/hmg/ddu165

Fecchio, C., De Franceschi, G., Relini, A., Greggio, E., Dalla Serra, M., Bubacco, L., et al. (2013). α-synuclein oligomers induced by docosahexaenoic acid affect membrane integrity. *PLoS One* 8:e82732. doi: 10.1371/journal.pone.0082732

Fecchio, C., Palazzi, L., and Polverino de Laureto, P. (2018). α-Synuclein and polyunsaturated fatty acids: molecular basis of the interaction and implication in neurodegeneration. *Molecules* 23:E1531. doi: 10.3390/molecules23071531

Fiske, M., Valtierra, S., Solvang, K., Zorniak, M., White, M., Herrera, S., et al. (2011). Contribution of alanine-76 and serine phosphorylation in α-synuclein membrane association and aggregation in yeasts. *Parkinsons Dis.* 2011:392180. doi: 10.4061/2011/392180

Flagmeier, P., Meisl, G., Vendruscolo, M., Knowles, T. P. J., Dobson, C. M., Buell, A. K., et al. (2016). Mutations associated with familial Parkinson's disease alter the initiation and amplification steps of α-synuclein aggregation. *Proc. Natl. Acad. Sci. U.S.A.* 113, 10328–10333. doi: 10.1073/pnas.1604645113

Fujiwara, H., Hasegawa, M., Dohmae, N., Kawashima, A., Masliah, E., Goldberg, M. S., et al. (2002). α-synuclein is phosphorylated in synucleinopathy lesions. *Nat. Cell Biol.* 4, 160–164. doi: 10.1038/ncb748

Fusco, G., Chen, S. W., Williamson, P. T. F., Cascella, R., Perni, M., Jarvis, J. A., et al. (2017). Structural basis of membrane disruption and cellular toxicity by α-synuclein oligomers. *Science* 358, 1440–1443. doi: 10.1126/science.aan6160

Galvagnion, C. (2017). The role of lipids interacting with α-synuclein in the pathogenesis of Parkinson's disease. *J. Parkinsons Dis.* 7, 433–450. doi: 10.3233/JPD-171103

Gao, Q., Binns, D. D., Kinch, L. N., Grishin, N. V., Ortiz, N., Chen, X., et al. (2017). Pet10p is a yeast perilipin that stabilizes lipid droplets and promotes their assembly. *J. Cell Biol.* 216, 3199–3217. doi: 10.1083/jcb.201610013

Garcia, E. J., Vevea, J. D., and Pon, L. A. (2018). Lipid droplet autophagy during energy mobilization, lipid homeostasis and protein quality control. *Front. Biosci.* 23, 1552–1563. doi: 10.2741/4660

Gardai, S. J., Mao, W., Schüle, B., Babcock, M., Schoebel, S., Lorenzana, C., et al. (2013). Elevated alpha-synuclein impairs innate immune cell function and

provides a potential peripheral biomarker for Parkinson's disease. *PLoS One* 8:e71634. doi: 10.1371/journal.pone.0071634

Ghio, S., Kamp, F., Cauchi, R., Giese, A., and Vassallo, N. (2016). Interaction of α-synuclein with biomembranes in Parkinson's disease - Role of cardiolipin. *Prog. Lipid Res.* 61, 73–82. doi: 10.1016/j.plipres.2015.10.005

Ghosh, D., Sahay, S., Ranjan, P., Salot, S., Mohite, G. M., Singh, P. K., et al. (2014). The newly discovered Parkinsons disease associated finnish mutation (A53E) attenuates α-synuclein aggregation and membrane binding. *Biochemistry* 53, 6419–6421. doi: 10.1021/bi5010365

Giasson, B. I., Murray, I. V. J., Trojanowski, J. Q., and Lee, V. M. Y. (2001). A hydrophobic stretch of 12 amino acid residues in the middle of α-synuclein is essential for filament assembly. *J. Biol. Chem.* 276, 2380–2386. doi: 10.1074/jbc.M008919200

Giusto, N. M., Salvador, G. A., Castagnet, P. I., Pasquaré, S. J., and Ilincheta de Boschero, M. G. (2002). Age-associated changes in central nervous system glycerolipid composition and metabolism. *Neurochem. Res.* 27, 1513–1523. doi: 10.1023/A:1021604623208

Gluchowski, N. L., Becuwe, M., Walther, T. C., and Farese, R. V. (2017). Lipid droplets and liver disease: from basic biology to clinical implications. *Nat. Rev. Gastroenterol. Hepatol.* 14, 343–355. doi: 10.1038/nrgastro.2017.32

Golovko, M. Y., Barceló-Coblijn, G., Castagnet, P. I., Austin, S., Combs, C. K., and Murphy, E. J. (2009). The role of α-synuclein in brain lipid metabolism: a downstream impact on brain inflammatory response. *Mol. Cell. Biochem.* 326, 55–66. doi: 10.1007/s11010-008-0008-y

Golovko, M. Y., and Murphy, E. J. (2008). Brain prostaglandin formation is increased by α-synuclein gene-ablation during global ischemia. *Neurosci. Lett.* 432, 243–247. doi: 10.1016/j.neulet.2007.12.031

Golovko, M. Y., Rosenberger, T. A., Faergeman, N. J., Feddersen, S., Cole, N. B., Pribill, I., et al. (2006). Acyl-CoA synthetase activity links wild-type but not mutant alpha-synuclein to brain arachidonate metabolism. *Biochemistry* 45, 6956–6966. doi: 10.1021/bi0600289

Golovko, M. Y., Rosenberger, T. A., Feddersen, S., Færgeman, N. J., and Murphy, E. J. (2007). α-Synuclein gene ablation increases docosahexaenoic acid incorporation and turnover in brain phospholipids. *J. Neurochem.* 101, 201–211. doi: 10.1111/j.1471-4159.2006.04357.x

Gorbatyuk, O. S., Li, S., Nha Nguyen, F., Manfredsson, F. P., Kondrikova, G., Sullivan, L. F., et al. (2010). α-synuclein expression in rat substantia nigra suppresses phospholipase D2 toxicity and nigral neurodegeneration. *Mol. Ther.* 18, 1758–1768. doi: 10.1038/mt.2010.137

Guo, J., Shou, C., Meng, L., Jiang, B., Dong, B., Yao, L., et al. (2007). Neuronal protein synuclein γ predicts poor clinical outcome in breast cancer. *Int. J. Cancer* 121, 1296–1305. doi: 10.1002/ijc.22763

Guo, J. T., Chen, A. Q., Kong, Q., Zhu, H., Ma, C. M., and Qin, C. (2008). Inhibition of vesicular monoamine transporter-2 activity in α-synuclein stably transfected SH-SY5Y cells. *Cell. Mol. Neurobiol.* 28, 35–47. doi: 10.1007/s10571-007-9227-0

Guschina, I., Millership, S., O'Donnell, V., Ninkina, N., Harwood, J., and Buchman, V. (2011). Lipid classes and fatty acid patterns are altered in the brain of γ-synuclein null mutant mice. *Lipids* 46, 121–130. doi: 10.1007/s11745-010-3486-0

Hellstrand, E., Grey, M., Ainalem, M. L., Ankner, J., Forsyth, V. T., Fragneto, G., et al. (2013). Adsorption of α-synuclein to supported lipid bilayers: positioning and role of electrostatics. *ACS Chem. Neurosci.* 4, 1339–1351. doi: 10.1021/cn400066t

Hibi, T., Mori, T., Fukuma, M., Yamazaki, K., Hashiguchi, A., Yamada, T., et al. (2009). Synuclein-γ is closely involved in perineural invasion and distant metastasis in mouse models and is a novel prognostic factor in pancreatic cancer. *Clin. Cancer Res.* 15, 2864–2871. doi: 10.1158/1078-0432.CCR-08-2946

Hsiao, J. H. T., Halliday, G. M., and Kim, W. S. (2017). α-Synuclein regulates neuronal cholesterol efflux. *Molecules* 22:E1769. doi: 10.3390/molecules22101769

Hu, R., Diao, J., Li, J., Tang, Z., Li, X., Leitz, J., et al. (2016). Intrinsic and membrane-facilitated α-synuclein oligomerization revealed by label-free detection through solid-state nanopores. *Sci. Rep.* 6:20776. doi: 10.1038/srep20776

Hua, H., Xu, L., Wang, J., Jing, J., Luo, T., and Jiang, Y. (2009). Up-regulation of gamma-synuclein contributes to cancer cell survival under endoplasmic reticulum stress. *J. Pathol.* 217, 507–515. doi: 10.1002/path.2465

Ingelsson, M. (2016). Alpha-synuclein oligomers-neurotoxic molecules in Parkinson's disease and other lewy body disorders. *Front. Neurosci.* 10:408. doi: 10.3389/fnins.2016.00408

Iwai, A., Masliah, E., Yoshimoto, M., Ge, N., Flanagan, L., Rohan de Silva, H. A., et al. (1995). The precursor protein of non-Aβ component of Alzheimer's disease amyloid is a presynaptic protein of the central nervous system. *Neuron* 14, 467–475. doi: 10.1016/0896-6273(95)90302-X

Jakes, R., Spillantini, M. G., and Goedert, M. (1994). Identification of two distinct synucleins from human brain. *FEBS Lett.* 345, 27–32. doi: 10.1016/0014-5793(94)00395-5

Jo, E., Fuller, N., Rand, R. P., St George-Hyslop, P., and Fraser, P. E. (2002). Defective membrane interactions of familial Parkinson's disease mutant A30P α-Synuclein. *J. Mol. Biol.* 315, 799–807. doi: 10.1006/jmbi.2001.5269

Jo, E., McLaurin, J. A., Yip, C. M., St George-Hyslop, and Fraser, P. E. (2000). α-Synuclein membrane interactions and lipid specificity. *J. Biol. Chem.* 275, 34328–34334. doi: 10.1074/jbc.M004345200

Kadamur, G., and Ross, E. M. (2013). Mammalian phospholipase C. *Annu. Rev. Physiol.* 75, 127–154. doi: 10.1146/annurev-physiol-030212-183750

Karube, H., Sakamoto, M., Arawaka, S., Hara, S., Sato, H., Ren, C. H., et al. (2008). N-terminal region of α-synuclein is essential for the fatty acid-induced oligomerization of the molecules. *FEBS Lett.* 582, 3693–3700. doi: 10.1016/j.febslet.2008.10.001

Kory, N., Farese, R. V., and Walther, T. C. (2016). Targeting fat: mechanisms of protein localization to lipid droplets. *Trends Cell Biol.* 26, 535–546. doi: 10.1016/j.tcb.2016.02.007

Krüger, R., Kuhn, W., Müller, T., Woitalla, D., Graeber, M., Kösel, S., et al. (1998). Ala30Pro mutation in the gene encoding α-synuclein in Parkinson's disease. *Nat. Genet.* 18, 106–108. doi: 10.1038/ng0298-106

Kuwahara, T., Tonegawa, R., Ito, G., Mitani, S., and Iwatsubo, T. (2012). Phosphorylation of α-synuclein protein at ser-129 reduces neuronal dysfunction by lowering its membrane binding property in *Caenorhabditis elegans*. *J. Biol. Chem.* 287, 7098–7109. doi: 10.1074/jbc.M111.237131

Lahiri, S., and Futerman, A. H. (2007). The metabolism and function of sphingolipids and glycosphingolipids. *Cell. Mol. Life Sci.* 64, 2270–2284. doi: 10.1007/s00018-007-7076-0

Lashuel, H. A., Overk, C. R., Oueslati, A., and Masliah, E. (2013). The many faces of α-synuclein: from structure and toxicity to therapeutic target. *Nat. Rev. Neurosci.* 14, 38–48. doi: 10.1038/nrn3406

Ledesma, M. D., Martin, M. G., and Dotti, C. G. (2012). Lipid changes in the aged brain: effect on synaptic function and neuronal survival. *Prog. Lipid Res.* 51, 23–35. doi: 10.1016/j.plipres.2011.11.004

Lee, C.-Y. J., Seet, R. C. S., Huang, S. H., Long, L. H., and Halliwell, B. (2009). Different patterns of oxidized lipid products in plasma and urine of dengue fever, stroke, and Parkinson's disease patients: cautions in the use of biomarkers of oxidative stress. *Antioxid. Redox Signal.* 11, 407–420. doi: 10.1089/ars.2008.2179

Li, W. W., Yang, R., Guo, J. C., Ren, H. M., Zha, X. L., Cheng, J. S., et al. (2007). Localization of α-synuclein to mitochondria within midbrain of mice. *Neuroreport* 18, 1543–1546. doi: 10.1097/WNR.0b013e3282f03db4

Liu, L., Zhang, K., Sandoval, H., Yamamoto, S., Jaiswal, M., Sanz, E., et al. (2015). Glial lipid droplets and ROS induced by mitochondrial defects promote neurodegeneration. *Cell* 160, 177–190. doi: 10.1016/j.cell.2014.12.019

López, G. H., Ilincheta de Boschero, M. G., Castagnet, P. I., and Giusto, N. M. (1995). Age-associated changes in the content and fatty acid composition of brain glycerophospholipids. *Comp. Biochem. Physiol. Part B Biochem.* 112, 331–343. doi: 10.1016/0305-0491(95)00079-8

Lou, X., Kim, J., Hawk, B. J., and Shin, Y.-K. (2017). α-Synuclein may cross-bridge v-SNARE and acidic phospholipids to facilitate SNARE-dependent vesicle docking. *Biochem. J.* 474, 2039–2049. doi: 10.1042/BCJ20170200

Luk, K. C., Branch, J. R., Brunden, K. R., Trojanowski, J. Q., O'Brien, P., Lee, V. M.-Y., et al. (2009). Exogenous α-synuclein fibrils seed the formation of Lewy body-like intracellular inclusions in cultured cells. *Proc. Natl. Acad. Sci. U.S.A.* 106, 20051–20056. doi: 10.1073/pnas.0908005106

Lynch, S. M., Zhou, C., and Messer, A. (2008). An scFv intrabody against the nonamyloid component of α-synuclein reduces intracellular aggregation

and toxicity. *J. Mol. Biol.* 377, 136–147. doi: 10.1016/j.jmb.2007.11.096

Ma, K. L., Song, L. K., Yuan, Y. H., Zhang, Y., Yang, J. L., Zhu, P., et al. (2014). α-synuclein is prone to interaction with the GC-box-like sequence in vitro. *Cell. Mol. Neurobiol.* 34, 603–609. doi: 10.1007/s10571-014-0046-9

Makwana, P. K., and Sundd, M. (2016). Alpha-synuclein structure, aggregation and modulators. *J. Proteins Proteom*. 7, 83–100.

Marie, G., Dunning, C. J., Gaspar, R., Grey, C., Brundin, P., Sparr, E., et al. (2015). Acceleration of α-synuclein aggregation by exosomes. *J. Biol. Chem.* 290, 2969–2982. doi: 10.1074/jbc.M114.585703

Maroteaux, L., Campanelli, J. T., and Scheller, R. H. (1988). Synuclein: a neuron-specific protein localized to the nucleus and presynaptic nerve terminal. *J. Neurosci.* 8, 2804–2815. doi: 10.1523/JNEUROSCI.08-08-02804.1988

Marquardt, D., Geier, B., and Pabst, G. (2015). Asymmetric lipid membranes: towards more realistic model systems. *Membranes* 5, 180–196. doi: 10.3390/membranes5020180

Martinez-Vicente, M., Talloczy, Z., Wong, E., Tang, G., Koga, H., Kaushik, S., et al. (2010). Cargo recognition failure is responsible for inefficient autophagy in Huntington's disease. *Nat. Neurosci.* 13, 567–576. doi: 10.1038/nn.2528

Martins, M., Rosa, A., Guedes, L. C., Fonseca, B. V., Gotovac, K., Violante, S., et al. (2011). Convergence of miRNA expression profiling, α-synuclein interaction and GWAS in Parkinson's disease. *PLoS One* 6:e25443. doi: 10.1371/journal.pone.0025443

Marwarha, G., and Ghribi, O. (2015). Does the oxysterol 27-hydroxycholesterol underlie Alzheimer's disease-Parkinson's disease overlap? *Exp. Gerontol.* 68, 13–18. doi: 10.1016/j.exger.2014.09.013

Marwarha, G., Rhen, T., Schommer, T., and Ghribi, O. (2011). The oxysterol 27-hydroxycholesterol regulatesα-synuclein and tyrosine hydroxylase expression levels in human neuroblastoma cells through modulation of liver X receptors and estrogen receptors-relevance to Parkinson's disease. *J. Neurochem.* 119, 1119–1136. doi: 10.1111/j.1471-4159.2011.07497.x

Mateos, M. V., Salvador, G. A., and Giusto, N. M. (2010). Selective localization of phosphatidylcholine-derived signaling in detergent-resistant membranes from synaptic endings. *Biochim. Biophys. Acta* 1798, 624–636. doi: 10.1016/j.bbamem.2009.12.008

Miotto, M. C., Rodriguez, E. E., Valiente-Gabioud, A. A., Torres-Monserrat, V., Binolfi, A., Quintanar, L., et al. (2014). Site-specific copper-catalyzed oxidation of α-synuclein: tightening the link between metal binding and protein oxidative damage in Parkinson's disease. *Inorg. Chem.* 53, 4350–4358. doi: 10.1021/ic4031377

Miraglia, F., Ricci, A., Rota, L., and Colla, E. (2018). Subcellular localization of alpha-synuclein aggregates and their interaction with membranes. *Neural Regen. Res.* 13, 1136–1144. doi: 10.4103/1673-5374.235013

Mizuno, S., Sasai, H., Kume, A., Takahashi, D., Satoh, M., Kado, S., et al. (2017). Dioleoyl-phosphatidic acid selectively binds to α-synuclein and strongly induces its aggregation. *FEBS Lett.* 591, 784–791. doi: 10.1002/1873-3468.12592

Mohamed Badawy, S. M., Okada, T., Kajimoto, T., Hirase, M., Matovelo, S. A., Nakamura, S., et al. (2018). Extracellular α-synuclein drives sphingosine 1-phosphate receptor subtype 1 out of lipid rafts, leading to impaired inhibitory G-protein signaling. *J. Biol. Chem.* 293, 8208–8216. doi: 10.1074/jbc.RA118.001986

Muntané, G., Janué, A., Fernandez, N., Odena, M. A., Oliveira, E., Boluda, S., et al. (2010). Modification of brain lipids but not phenotype in α-synucleinopathy transgenic mice by long-term dietary n-3 fatty acids. *Neurochem. Int.* 56, 318–328. doi: 10.1016/j.neuint.2009.10.015

Murphy, E. J. (2013). A lipid neurochemist's siren: docosahexaenoic acid and its elusive function in the central nervous system. *J. Neurochem.* 127, 299–302. doi: 10.1111/jnc.12439

Murray, I. V. J., Giasson, B. I., Quinn, S. M., Koppaka, V., Axelsen, P. H., Ischiropoulos, H., et al. (2003). Role of α-synuclein carboxy-terminus on fibril formation in vitro. *Biochemistry* 22, 8530–8540. doi: 10.1021/bi027363r

Nübling, G. S., Levin, J., Bader, B., Lorenzl, S., Hillmer, A., Högen, T., et al. (2014). Modelling Ser129 phosphorylation inhibits membrane binding of pore-forming alpha-synuclein oligomers. *PLoS One* 9:e98906. doi: 10.1371/journal.pone.0098906

Oaks, A. W., Frankfurt, M., Finkelstein, D. I., and Sidhu, A. (2013). Age-dependent effects of A53T alpha-synuclein on behavior and dopaminergic function. *PLoS One* 8:e60378. doi: 10.1371/journal.pone.0060378

Oertel, W., and Schulz, J. B. (2016). Current and experimental treatments of Parkinson disease: a guide for neuroscientists. *J. Neurochem.* 139(Suppl. 1), 325–337. doi: 10.1111/jnc.13750

Ogawa, K., Hishiki, T., Shimizu, Y., Funami, K., Sugiyama, K., Miyanari, Y., et al. (2009). Hepatitis C virus utilizes lipid droplet for production of infectious virus. *Proc. Jpn. Acad. Ser. B Phys. Biol. Sci.* 85, 217–228. doi: 10.2183/pjab.85.217

O'Leary, E. I., Jiang, Z., Strub, M. P., and Lee, J. C. (2018). Effects of phosphatidylcholine membrane fluidity on the conformation and aggregation of N-terminally acetylated α-Synuclein. *J. Biol. Chem.* 293, 11195–11205. doi: 10.1074/jbc.RA118.002780

O'Leary, E. I., and Lee, J. C. (2018). Interplay between α-synuclein amyloid formation and membrane structure. *Biochim. Biophys. Acta Proteins Proteom.* 1867, 483–491. doi: 10.1016/j.bbapap.2018.09.012

Oueslati, A. (2016). Implication of alpha-synuclein phosphorylation at S129 in synucleinopathies: what have we learned in the last decade? *J. Parkinsons Dis.* 6, 39–51. doi: 10.3233/JPD-160779

Oueslati, A., Fournier, M., and Lashuel, H. A. (2010). Role of post-translational modifications in modulating the structure, function and toxicity of α-synuclein. Implications for Parkinson's disease pathogenesis and therapies. *Prog. Brain Res.* 183, 115–145. doi: 10.1016/S0079-6123(10)83007-9

Outeiro, T. F., and Lindquist, S. (2003). Yeast cells provide insight into alpha-synuclein biology and pathobiology. *Science* 302, 1772–1775. doi: 10.1126/science.1090439

Paleologou, K. E., Oueslati, A., Shakked, G., Rospigliosi, C. C., Kim, H.-Y., Lamberto, G. R., et al. (2010). Phosphorylation at S87 is enhanced in synucleinopathies, inhibits alpha-synuclein oligomerization, and influences synuclein-membrane interactions. *J. Neurosci.* 30, 3184–3198. doi: 10.1523/JNEUROSCI.5922-09.2010

Pan, J., Dalzini, A., Khadka, N. K., Aryal, C. M., and Song, L. (2018). Lipid extraction by α-synuclein generates semi-transmembrane defects and lipoprotein nanoparticles. *ACS Omega* 3, 9586–9597. doi: 10.1021/acsomega.8b01462

Pavlou, M. A. S., Pinho, R., Paiva, I., and Outeiro, T. F. (2017). The yin and yang of α-synuclein-associated epigenetics in Parkinson's disease. *Brain* 140, 878–886. doi: 10.1093/brain/aww227

Peng, X. M. (2005). Alpha-Synuclein activation of protein phosphatase 2A reduces tyrosine hydroxylase phosphorylation in dopaminergic cells. *J. Cell Sci.* 118(Pt 15), 3523–3530. doi: 10.1242/jcs.02481

Periquet, M., Fulga, T., Myllykangas, L., Schlossmacher, M. G., and Feany, M. B. (2007). Aggregated alpha-synuclein mediates dopaminergic neurotoxicity in vivo. *J. Neurosci.* 27, 3338–3346. doi: 10.1523/JNEUROSCI.0285-07.2007

Perrin, R. J., Woods, W. S., Clayton, D. F., and George, J. M. (2000). Interaction of human α-synuclein and Parkinson's disease variants with phospholipids: structural analysis using site-directed mutagenesis. *J. Biol. Chem.* 275, 34393–34398. doi: 10.1074/jbc.M004851200

Perrin, R. J., Woods, W. S., Clayton, D. F., and George, J. M. (2001). Exposure to long chain polyunsaturated fatty acids triggers rapid multimerization of synucleins. *J. Biol. Chem.* 276, 41958–41962. doi: 10.1074/jbc.M105022200

Pineda, A., and Burré, J. (2017). Modulating membrane binding of α-synuclein as a therapeutic strategy. *Proc. Natl. Acad. Sci. U.S.A.* 114, 1223–1225. doi: 10.1073/pnas.1620159114

Pitcairn, C., Wani, W. Y., and Mazzulli, J. R. (2018). Dysregulation of the autophagic-lysosomal pathway in Gaucher and Parkinson's disease. *Neurobiol. Dis.* 122, 72–82. doi: 10.1016/j.nbd.2018.03.008

Polymeropoulos, M. H., Lavedan, C., Leroy, E., Ide, S. E., Dehejia, A., Dutra, A., et al. (1997). Mutation in the α-synuclein gene identified in families with Parkinson's disease. *Science* 276, 2045–2047. doi: 10.1126/science.276.5321.2045

Powers, R., Lei, S., Anandhan, A., Marshall, D. D., Worley, B., Cerny, R. L., et al. (2017). Metabolic investigations of the molecular mechanisms associated with Parkinson's disease. *Metabolites* 7:E22. doi: 10.3390/metabo7020022

Pozo Devoto, V. M., and Falzone, T. L. (2017). Mitochondrial dynamics in Parkinson's disease: a role for α-synuclein? *Dis. Model. Mech.* 10, 1075–1087. doi: 10.1242/dmm.026294

Puspita, L., Chung, S. Y., and Shim, J. W. (2017). Oxidative stress and cellular pathologies in Parkinson's disease. *Mol. Brain* 10:53. doi: 10.1186/s13041-017-0340-9

Qin, Z., Hu, D., Han, S., Reaney, S. H., Di Monte, D. A., and Fink, A. L. (2007). Effect of 4-hydroxy-2-nonenal modification on alpha-synuclein aggregation. *J. Biol. Chem.* 282, 5862–5870. doi: 10.1074/jbc.M608126200

Rappley, I., Gitler, A. D., Selvy, P. E., LaVoie, M. J., Levy, B. D., Brown, H. A., et al. (2009). Evidence that α-synuclein does not inhibit phospholipase D. *Biochemistry* 48, 1077–1083. doi: 10.1021/bi801871h

Reynolds, N. P., Soragni, A., Rabe, M., Verdes, D., Liverani, E., Handschin, S., et al. (2011). Mechanism of membrane interaction and disruption by α-synuclein. *J. Am. Chem. Soc.* 133, 19366–19375. doi: 10.1021/ja2029848

Riedel, M., Goldbaum, O., Wille, M., and Richter-Landsberg, C. (2011). Membrane lipid modification by docosahexaenoic acid (DHA) promotes the formation of alpha-synuclein inclusion bodies immunopositive for SUMO-1 in oligodendroglial cells after oxidative stress. *J. Mol. Neurosci.* 43, 290–302. doi: 10.1007/s12031-010-9439-5

Robotta, M., Cattani, J., Martins, J. C., Subramaniam, V., and Drescher, M. (2017). Alpha-synuclein disease mutations are structurally defective and locally affect membrane binding. *J. Am. Chem. Soc.* 139, 4254–4257. doi: 10.1021/jacs.6b05335

Rodriguez, J. A., Ivanova, M. I., Sawaya, M. R., Cascio, D., Reyes, F. E., Shi, D., et al. (2015). Structure of the toxic core of α-synuclein from invisible crystals. *Nature* 525, 486–490. doi: 10.1038/nature15368

Roy, A., and Pahan, K. (2011). Prospects of statins in Parkinson disease. *Neuroscientist* 17, 244–255. doi: 10.1177/1073858410385006

Ruipérez, V., Darios, F., and Davletov, B. (2010). Alpha-synuclein, lipids and Parkinson's disease. *Prog. Lipid Res.* 49, 420–428. doi: 10.1016/j.plipres.2010.05.004

Salvador, G. A. (2010). Iron in neuronal function and dysfunction. *Biofactors* 36, 103–110. doi: 10.1002/biof.80

Sánchez Campos, S., Alza, N. P., and Salvador, G. A. (2018). Lipid metabolism alterations in the neuronal response to A53T α-synuclein and Fe-induced injury. *Arch. Biochem. Biophys.* 655, 43–54. doi: 10.1016/j.abb.2018.08.007

Sánchez Campos, S., Diez, G. R., Oresti, G. M., and Salvador, G. A. (2015). Dopaminergic neurons respond to iron-induced oxidative stress by modulating lipid acylation and deacylation cycles. *PLoS One* 10:e0130726. doi: 10.1371/journal.pone.0130726

Savage, M. J., Goldberg, D. J., and Schacher, S. (1987). Absolute specificity for retrograde fast axonal transport displayed by lipid droplets originating in the axon of an identified Aplysia neuron in vitro. *Brain Res.* 406, 215–223. doi: 10.1016/0006-8993(87)90785-2

Schneider, S. A., and Bhatia, K. P. (2012). Syndromes of neurodegeneration with brain iron accumulation. *Semin. Pediatr. Neurol.* 19, 57–66. doi: 10.1016/j.spen.2012.03.005

Scott, D., and Roy, S. (2012). α-synuclein inhibits intersynaptic vesicle mobility and maintains recycling-pool homeostasis. *J. Neurosci.* 32, 10129–10135. doi: 10.1523/JNEUROSCI.0535-12.2012

Seet, R. C. S., Lee, C. Y. J., Lim, E. C. H., Tan, J. J. H., Quek, A. M. L., Chong, W. L., et al. (2010). Oxidative damage in Parkinson disease: measurement using accurate biomarkers. *Free Radic. Biol. Med.* 48, 560–566. doi: 10.1016/j.freeradbiomed.2009.11.026

Sere, Y. Y., Regnacq, M., Colas, J., and Berges, T. (2010). A *Saccharomyces cerevisiae* strain unable to store neutral lipids is tolerant to oxidative stress induced by α-synuclein. *Free Radic. Biol. Med.* 49, 1755–1764. doi: 10.1016/j.freeradbiomed.2010.09.007

Serhan, C. N., and Petasis, N. A. (2011). Resolvins and protectins in inflammation resolution. *Chem. Rev.* 111, 5922–5943. doi: 10.1021/cr100396c

Shaltiel-Karyo, R., Frenkel-Pinter, M., Egoz-Matia, N., Frydman-Marom, A., Shalev, D. E., Segal, D., et al. (2010). Inhibiting α-synuclein oligomerization by stable cell-penetrating β-synuclein fragments recovers phenotype of Parkinson's disease model flies. *PLoS One* 5:e13863. doi: 10.1371/journal.pone.0013863

Shamoto-Nagai, M., Hisaka, S., Naoi, M., and Maruyama, W. (2018). Modification of α-synuclein by lipid peroxidation products derived from polyunsaturated fatty acids promotes toxic oligomerization: its relevance to Parkinson disease. *J. Clin. Biochem. Nutr.* 62, 207–212. doi: 10.3164/jcbn.18-25

Sharon, R., Bar-Joseph, I., Frosch, M. P., Walsh, D. M., Hamilton, J. A., Selkoe, D. J., et al. (2003a). The formation of highly soluble oligomers of alpha-synuclein is regulated by fatty acids and enhanced in Parkinson's disease. *Neuron* 37, 583–595. doi: 10.1016/s0896-6273(03)00024-2

Sharon, R., Bar-Joseph, I., Mirick, G. E., Serhan, C. N., and Selkoe, D. J. (2003b). Altered fatty acid composition of dopaminergic neurons expressing α-synuclein and human brains with α-synucleinopathies. *J. Biol. Chem.* 278, 49874–49881. doi: 10.1074/jbc.M309127200

Sharon, R., Goldberg, M. S., Bar-Josef, I., Betensky, R. A., Shen, J., Selkoe, D. J., et al. (2001). α-Synuclein occurs in lipid-rich high molecular weight complexes, binds fatty acids, and shows homology to the fatty acid-binding proteins. *Proc. Natl. Acad. Sci. U.S.A.* 98, 9110–9115. doi: 10.1073/pnas.171300598

Shvadchak, V. V., Falomir-Lockhart, L. J., Yushchenko, D. A., and Jovin, T. M. (2011). Specificity and kinetics of alpha-synuclein binding to model membranes determined with fluorescent excited state intramolecular proton transfer (ESIPT) probe. *J. Biol. Chem.* 286, 13023–13032. doi: 10.1074/jbc.M110.204776

Singleton, A. B., Farrer, M., Johnson, J., Singleton, A., Hague, S., Kachergus, J., et al. (2003). α-synuclein locus triplication causes Parkinson's disease. *Science* 302:841. doi: 10.1126/science.1090278

Stöckl, M., Fischer, P., Wanker, E., and Herrmann, A. (2008). α-synuclein selectively binds to anionic phospholipids embedded in liquid-disordered domains. *J. Mol. Biol.* 375, 1394–1404. doi: 10.1016/j.jmb.2007.11.051

Su, L. J., Auluck, P. K., Outeiro, T. F., Yeger-Lotem, E., Kritzer, J. A., Tardiff, D. F., et al. (2010). Compounds from an unbiased chemical screen reverse both ER-to-Golgi trafficking defects and mitochondrial dysfunction in Parkinson's disease models. *Dis. Model. Mech.* 3, 194–208. doi: 10.1242/dmm.004267

Sumi-Akamaru, H., Beck, G., Shinzawa, K., Kato, S., Riku, Y., Yoshida, M., et al. (2016). High expression of α-synuclein in damaged mitochondria with PLA2G6 dysfunction. *Acta Neuropathol. Commun.* 4:27. doi: 10.1186/s40478-016-0298-3

Surguchev, A. A., and Surguchov, A. (2017). Synucleins and gene expression: ramblers in a crowd or cops regulating traffic? *Front. Mol. Neurosci.* 10:224. doi: 10.3389/fnmol.2017.00224

Surguchov, A., Palazzo, R. E., and Surgucheva, I. (2001). Gamma synuclein: subcellular localization in neuronal and non-neuronal cells and effect on signal transduction. *Cell Motil. Cytoskeleton* 49, 218–228. doi: 10.1002/cm.1035

Swant, J., Goodwin, J. S., North, A., Ali, A. A., Gamble-George, J., Chirwa, S., et al. (2011). α-synuclein stimulates a dopamine transporter-dependent chloride current and modulates the activity of the transporter. *J. Biol. Chem.* 286, 43933–43943. doi: 10.1074/jbc.M111.241232

Sztalryd, C., and Brasaemle, D. L. (2017). The perilipin family of lipid droplet proteins: gatekeepers of intracellular lipolysis. *Biochim. Biophys. Acta Mol. Cell Biol. Lipids* 1862(10 Pt B), 1221–1232. doi: 10.1016/j.bbalip.2017.07.009

Tashiro, M., Kojima, M., Kihara, H., Kasai, K., Kamiyoshihara, T., Uéda, K., et al. (2008). Characterization of fibrillation process of α-synuclein at the initial stage. *Biochem. Biophys. Res. Commun.* 369, 910–914. doi: 10.1016/j.bbrc.2008.02.127

Terakawa, M. S., Lee, Y. H., Kinoshita, M., Lin, Y., Sugiki, T., Fukui, N., et al. (2018). Membrane-induced initial structure of α-synuclein control its amyloidogenesis on model membranes. *Biochim. Biophys. Acta* 1860, 757–766. doi: 10.1016/j.bbamem.2017.12.011

Thiam, A. R., Antonny, B., Wang, J., Delacotte, J., Wilfling, F., Walther, T. C., et al. (2013). COPI buds 60-nm lipid droplets from reconstituted water-phospholipid-triacylglyceride interfaces, suggesting a tension clamp function. *Proc. Natl. Acad. Sci. U.S.A.* 110, 13244–13249. doi: 10.1073/pnas.1307685110

Tirinato, L., Pagliari, F., Limongi, T., Marini, M., Falqui, A., Seco, J., et al. (2017). An overview of lipid droplets in cancer and cancer stem cells. *Stem Cells Int.* 2017:1656053. doi: 10.1155/2017/1656053

Tosatto, L., Andrighetti, A. O., Plotegher, N., Antonini, V., Tessari, I., Ricci, L., et al. (2012). Alpha-synuclein pore forming activity upon membrane association. *Biochim. Biophys. Acta* 1818, 2876–2883. doi: 10.1016/j.bbamem.2012.07.007

Trostchansky, A., Lind, S., Hodara, R., Oe, T., Blair, I. A., Ischiropoulos, H., et al. (2006). Interaction with phospholipids modulates α-synuclein nitration and

lipid–protein adduct formation. *Biochem. J.* 393(Pt 1), 343–349. doi: 10.1016/B978-0-12-409547-2.12460-6

Uversky, V. N., and Fink, A. L. (2002). Amino acid determinants of α-synuclein aggregation: putting together pieces of the puzzle. *FEBS Lett.* 522, 9–13. doi: 10.1016/S0014-5793(02)02883-1

van Meer, G., Voelker, D. R., and Feigenson, G. W. (2008). Membrane lipids: where they are and how they behave. *Nat. Rev. Mol. Cell Biol.* 9, 112–124. doi: 10.1038/nrm2330

van Rooijen, B. D., Claessens, M. M., and Subramaniam, V. (2009). Lipid bilayer disruption by oligomeric α-synuclein depends on bilayer charge and accessibility of the hydrophobic core. *Biochim. Biophys. Acta* 1788, 1271–1278. doi: 10.1016/j.bbamem.2009.03.010

Vargas, K. J., Makani, S., Davis, T., Westphal, C. H., Castillo, P. E., and Chandra, S. S. (2014). Synucleins regulate the kinetics of synaptic vesicle endocytosis. *J. Neurosci.* 34, 9364–9376. doi: 10.1523/JNEUROSCI.4787-13.2014

Vasquez, A. M., Mouchlis, V. D., and Dennis, E. A. (2018). Review of four major distinct types of human phospholipase A2. *Adv. Biol. Regul.* 67, 212–218. doi: 10.1016/j.jbior.2017.10.009

Velázquez, A. P., Tatsuta, T., Ghillebert, R., Drescher, I., and Graef, M. (2016). Lipid droplet-mediated ER homeostasis regulates autophagy and cell survival during starvation. *J. Cell Biol.* 212, 621–631. doi: 10.1083/jcb.201508102

Volta, M., Lavdas, A. A., Obergasteiger, J., Überbacher, C., Picard, A., Pramstaller, P. P., et al. (2017). Elevated levels of alpha-synuclein blunt cellular signal transduction downstream of Gq protein-coupled receptors. *Cell. Signal.* 30, 82–91. doi: 10.1016/j.cellsig.2016.11.012

Voshol, P. J., Dennis, R. J., Buchman, V. L., Oort, P. J., Ninkina, N., Guschina, I. A., et al. (2012). Increased lipolysis and altered lipid homeostasis protect γ-synuclein-null mutant mice from diet-induced obesity. *Proc. Natl. Acad. Sci. U.S.A.* 109, 20943–20948. doi: 10.1073/pnas.1210022110

Wakamatsu, M., Ishii, A., Iwata, S., Sakagami, J., Ukai, Y., Ono, M., et al. (2008). Selective loss of nigral dopamine neurons induced by overexpression of truncated human α-synuclein in mice. *Neurobiol. Aging* 29, 574–585. doi: 10.1016/j.neurobiolaging.2006.11.017

Wang, L., Das, U., Scott, D. A., Tang, Y., McLean, P. J., and Roy, S. (2014). α-Synuclein multimers cluster synaptic vesicles and attenuate recycling. *Curr. Biol.* 24, 2319–2326. doi: 10.1016/j.cub.2014.08.027

Wang, W., Perovic, I., Chittuluru, J., Kaganovich, A., Nguyen, L. T. T., Liao, J., et al. (2011). A soluble α-synuclein construct forms a dynamic tetramer. *Proc. Natl. Acad. Sci. U.S.A.* 108, 17797–17802. doi: 10.1073/pnas.1113260108

Watanabe, H., Hongu, T., Yamazaki, M., and Kanaho, Y. (2011). Phospholipase D2 activation by p38 MAP kinase is involved in neurite outgrowth. *Biochem. Biophys. Res. Commun.* 413, 288–293. doi: 10.1016/j.bbrc.2011.08.088

Waxman, E. A., Mazzulli, J. R., and Giasson, B. I. (2009). Characterization of hydrophobic residue requirements for α-synuclein fibrillization. *Biochemistry* 48, 9427–9436. doi: 10.1021/bi900539p

Welte, M. A. (2015). Expanding roles for lipid droplets. *Curr. Biol.* 25, R470–R481. doi: 10.1016/j.cub.2015.04.004

Welte, M. A., and Gould, A. P. (2017). Lipid droplet functions beyond energy storage. *Biochim. Biophys. Acta Mol. Cell Biol. Lipids* 1862(10 Pt B), 1260–1272. doi: 10.1016/j.bbalip.2017.07.006

Wietek, J., Haralampiev, I., Amoussouvi, A., Herrmann, A., and Stöckl, M. (2013). Membrane bound α-synuclein is fully embedded in the lipid bilayer while segments with higher flexibility remain. *FEBS Lett.* 587, 2572–2577. doi: 10.1016/j.febslet.2013.06.034

Wilhelm, B. G., Mandad, S., Truckenbrodt, S., Kröhnert, K., Schäfer, C., Rammner, B., et al. (2014). Composition of isolated synaptic boutons reveals the amounts of vesicle trafficking proteins. *Science* 344, 1023–1028. doi: 10.1126/science.1252884

Winner, B., Jappelli, R., Maji, S. K., Desplats, P. A., Boyer, L., Aigner, S., et al. (2011). In vivo demonstration that α-synuclein oligomers are toxic. *Proc. Natl. Acad. Sci. U.S.A.* 108, 4194–4199. doi: 10.1073/pnas.1100976108

Wood, S. J., Wypych, J., Steavenson, S., Louis, J. C., Citron, M., and Biere, A. L. (1999). α-Synuclein fibrillogenesis is nucleation-dependent. Implications for the pathogenesis of Parkinson's disease. *J. Biol. Chem.* 274, 19509–19512. doi: 10.1074/jbc.274.28.19509

Yakunin, E., Loeb, V., Kisos, H., Biala, Y., Yehuda, S., Yaari, Y., et al. (2012). α-Synuclein neuropathology is controlled by nuclear hormone receptors and enhanced by docosahexaenoic acid in a mouse model for Parkinson's disease. *Brain Pathol.* 22, 280–294. doi: 10.1111/j.1750-3639.2011.00530.x

Yeger-Lotem, E., Riva, L., Su, L. J., Gitler, A. D., Cashikar, A. G., King, O. D., et al. (2009). Bridging high-throughput genetic and transcriptional data reveals cellular responses to alpha-synuclein toxicity. *Nat. Genet.* 41, 316–323. doi: 10.1038/ng.337

Ysselstein, D., Joshi, M., Mishra, V., Griggs, A. M., Asiago, J. M., McCabe, G. P., et al. (2015). Effects of impaired membrane interactions on α-synuclein aggregation and neurotoxicity. *Neurobiol. Dis.* 79, 150–163. doi: 10.1016/j.nbd.2015.04.007

Zaltieri, M., Grigoletto, J., Longhena, F., Navarria, L., Favero, G., Castrezzati, S., et al. (2015). α-synuclein and synapsin III cooperatively regulate synaptic function in dopamine neurons. *J. Cell Sci.* 128, 2231–2243. doi: 10.1242/jcs.157867

Zarranz, J. J., Alegre, J., Gómez-Esteban, J. C., Lezcano, E., Ros, R., Ampuero, I., et al. (2004). The new mutation, E46K, of α-synuclein causes Parkinson and lewy body dementia. *Ann. Neurol.* 55, 164–173. doi: 10.1002/ana.10795

Zhou, Q., Yen, A., Rymarczyk, G., Asai, H., Trengrove, C., Aziz, N., et al. (2016). Impairment of PARK14-dependent Ca2+ signalling is a novel determinant of Parkinson's disease. *Nat. Commun.* 7:10332. doi: 10.1038/ncomms10332

Zhu, M., Li, J., and Fink, A. L. (2003). The association of α-synuclein with membranes affects bilayer structure, stability, and fibril formation. *J. Biol. Chem.* 278, 40186–40197. doi: 10.1074/jbc.M305326200

Conflict of Interest Statement: The authors declare that the research was conducted in the absence of any commercial or financial relationships that could be construed as a potential conflict of interest.

frontiers in Neuroscience

ORIGINAL RESEARCH
published: 03 May 2019
doi: 10.3389/fnins.2019.00429

Effects of FGF2/FGFR1 Pathway on Expression of A1 Astrocytes After Infrasound Exposure

Lin-Hui Zou[1,2†], Ya-Jun Shi[1†], Hua He[3†], Shi-Mei Jiang[4], Fang-Fang Huo[5], Xiao-Mu Wang[1], Fan Wu[1] and Lei Ma[1]*

[1] Department of Neurology, Xijing Hospital, Fourth Military Medical University, Xi'an, China, [2] Frontier Medical Training Brigade, Army Medical University, Changji, China, [3] Department of Specific Diagnosis, PLA 986 Hospital, Xi'an, China, [4] Department of Acu-Moxibustion and Tuina, Henan University of Traditional Chinese Medicine, Zhengzhou, China, [5] Department of Medicine, Yulin Yuyang District Hospital of Traditional Chinese Medicine, Yulin, China

Two types of reactive astrocytes, A1 and A2 astrocytes, are induced following neuroinflammation and ischemia. In this study, we evaluated the effects of the fibroblast growth factor (FGF)2/FGF receptor (FGFR)1 pathway on A1 and A2 astrocytes in the rat hippocampus using double-labeling immunofluorescence following infrasound exposure. A1 astrocytes were induced in the CA1 region of the hippocampus after exposure to infrasound for 3 days. The number of microglial cells was also increased, and we investigated if these might be responsible for the reactivity of A1 astrocytes. Accordingly, expression levels of C3 and Iba-1, as markers of A1 astrocytes and microglial cells, respectively, were both up-regulated in rat hippocampus following infrasound exposure, as demonstrated by western blot. We also explored the effect of the FGF2/FGFR1 pathway on A1 astrocyte reactivity by pretreating rats with FGF2 or the specific FGFR1 antagonist, PD173074. A1 astrocytes were gradually down-regulated by activation of the FGF2/FGFR1 pathway and were up-regulated by inhibition of the FGF2/FGFR1 pathway after infrasound damage. These results further our understanding of the role of reactive astrocytes in infrasound-induced central nervous system injury and will thus facilitate the development of new treatments for these injuries.

Keywords: infrasound, hippocampus, A1 astrocyte, microglial cell, FGF2/FGFR1 pathway

OPEN ACCESS

Edited by:
Mario Eduardo Guido, Center for Research in Biological Chemistry Córdoba (CIQUIBIC), Argentina

Reviewed by:
Hirokazu Ohtaki, Showa University, Japan
Tullio Florio, University of Genoa, Italy

***Correspondence:**
Lei Ma
malei@fmmu.edu.cn

† These authors have contributed equally to this work

Specialty section:
This article was submitted to Neuroendocrine Science, a section of the journal Frontiers in Neuroscience

Received: *23 December 2018*
Accepted: *15 April 2019*
Published: *03 May 2019*

Citation:
Zou L-H, Shi Y-J, He H, Jiang S-M, Huo F-F, Wang X-M, Wu F and Ma L (2019) Effects of FGF2/FGFR1 Pathway on Expression of A1 Astrocytes After Infrasound Exposure. Front. Neurosci. 13:429. doi: 10.3389/fnins.2019.00429

INTRODUCTION

Sound waves <20 Hz are referred to as infrasound. Infrasound is generated by numerous environmental factors, including agricultural machinery and industrial processes (Backteman et al., 1983; Bilski, 2017), and has been implicated in various kinds of health damage. For example, infrasound exposure is noted to be harmful in pregnant women (Castelo-Branco and Rodriguez, 1999). Furthermore, human and animal experiments have suggested that prolonged infrasound exposure can damage the central nervous system (CNS), including the hippocampus, cerebellum, limbic-corticular complex, hypothalamus, and cortex (Izmerov et al., 1997; Fei et al., 2000; Yuan et al., 2009; Shi et al., 2013; Cai et al., 2014; Ma et al., 2015). We previously confirmed that infrasound exposure activated astrocytes and induced neuronal apoptosis in the CNS, which subsequently impaired spatial learning and memory abilities (Shi et al., 2013, 2018).

Neuroinflammation and ischemia have been reported to induce two different types of reactive astrocytes, A1 and A2 astrocytes (Zamanian et al., 2012). A1 astrocytes are induced by activated microglia and gain a neurotoxic function, resulting in neuron killing (Liddelow et al., 2017), while A2 astrocytes upregulate many neurotrophic factors and strongly promote neuronal survival and tissue repair (Bush et al., 1999). Double-immunofluorescence labeling with complement component 3 (C3) and glial fibrillary acidic protein (GFAP) had been used to label A1 astrocytes, and double-immunofluorescence labeling with S100a10 and GFAP had been used to label A2 astrocytes (Liddelow et al., 2017).

In this study, we investigated the effects of infrasound on the induction of A1 and A2 astrocytes in the rat hippocampus by double-immunofluorescence labeling with C3 and GFAP, or S100a10 and GFAP, respectively. We also detected microglial cells by immunofluorescence labeling with Iba-1, to investigate their role in the effects of infrasound exposure. We verified the immunofluorescence results by measuring expression levels of C3 and Iba-1 in rat hippocampus.

We previously showed that the fibroblast growth factor (FGF)2/FGF receptor (FGFR)1 pathway inhibited astrocyte-mediated neuroinflammation *in vitro* and *in vivo* after infrasound exposure (Shi et al., 2018), suggesting that the reactivity of A1 astrocytes was related to activation of this pathway. We therefore investigated the role of the FGF2/FGFR1 pathway in infrasound-induced changes of A1 astrocytes in rats pretreated with FGF2 or the selective FGFR1 inhibitor, PD173074 (Mohammadi et al., 1998).

MATERIALS AND METHODS

Infrasound Device

The infrasound radiation laboratory was located at the Center for Radiation, the Fourth Military Medical University, Xi'an, China. The infrasound device included an infrasound chamber and infrasonic signal detection system. Infrasound with a frequency of 16 Hz and a pressure level of 150 dB was used in this study. The frequency and pressure of the infrasound were kept steady during 2 h of animal exposure and monitored using the infrasonic signal detection system.

Animals

Male Sprague-Dawley rats, weighing 220–250 g, were obtained from the Center of Experimental Animals, Fourth Military Medical University. The rats were maintained in an animal laboratory under controlled conditions at 20–25°C, humidity 50–60%, and a 12-h light/dark cycle, and were provided with free access to rodent chow and water.

The rats were divided randomly into groups as described previously (Shi et al., 2018): control group (no infrasound exposure, $n = 6$), infrasound (IS) exposure groups (exposed to 16 Hz, 150 dB of infrasound for 1, 3, 5, or 7 days, $n = 6$ per group), FGF2 groups (treated with FGF2 for 1, 3, 5, or 7 days, $n = 6$ per group), PD groups (treated with PD173074 for 1, 3, 5, or 7 days, $n = 6$ per group), FGF2+IS groups (infrasound-exposed rats treated with FGF2, $n = 6$ per group), and PD + IS groups (infrasound-exposed rats treated with PD173074, $n = 6$ per group). For FGF2 administration, rats were injected intraperitoneally (i.p.) with 0.1 mg/kg FGF2. For PD173074 administration, rats were injected i.p. with 1.5 mg/kg PD173074. FGF2 was dissolved in saline (Graham and Richardson, 2009) and PD173074 was dissolved in saline containing 12.5% Cremophor EL and 2.5% dimethylsulfoxide (Di Marco et al., 2014). FGF2 and PD173074 were injected everyday. The rats were exposed to infrasound of 16 Hz and 150 dB for 2 h a day.

Tissue Preparation

Brain slices were obtained as described previously (Melvin and Sutherland, 2010). After infrasound exposure, the rats were anesthetized with 10% chloral hydrate and then perfused sequentially with 200 ml ice-cold saline via a perfusion pump at 30 rpm, 200 ml 4% ice-cold paraformaldehyde (PFA) at 30 rpm, and 200 ml 4% PFA at 4 rpm. The brains were removed, fixed in 4% PFA for 12 h, dehydrated in 30% sucrose solution, embedded in OCT compound, and sectioned transversely into 35 μm-thick slices using a Leica CM 1900 cryostat. These sections were stored in 60% glycerine at −20°C and used for immunofluorescence.

Primary Astrocyte Culture

Primary cultures of rat hippocampus astrocytes were prepared from neonatal rats. Briefly, hippocampus tissue was minced with forceps and digested with 0.05% trypsin for 5 min. DMEM (Corning, New York, NY, United States) containing 10% fetal bovine serum, 1% glutamine, and 1% penicillin was added to stop the digestion and the supernatant was filtered. After centrifugation at 1000 rpm for 5 min, the cell mass was resuspended in DMEM and streptomycin at 37°C. The culture medium was replaced every 3 days. The purity of the astrocytes was determined by immunostaining with GFAP antibody, as described below. For the experiments, the astrocytes were exposed to infrasound of 16 Hz and 150 dB for 2 h, fixed with 4% PFA for 20 min, and stored for immunofluorescence staining.

Immunofluorescence

Brain sections or cultured astrocytes on coverslips were blocked with 3% bovine serum albumin (BSA) in PBS containing 0.3% Triton X-100 for 1 h at room temperature (RT). The sections or cells were then incubated with primary antibodies overnight at 4°C. Two antibodies were added simultaneously for double-immunofluorescence staining. The following antibodies were used: rabbit anti-S100a10 (1:100; Novus, Colorado Springs, CO, United States), mouse anti-C3 (1:100; Santa Cruz Biotechnology, Santa Cruz, CA, United States), rabbit anti-Iba-1 (1:800; Sigma, United States), mouse anti-GFAP (1:500; Abcam, Cambridge, United Kingdom), and rabbit anti-GFAP (1:500; Abcam). The samples were then incubated with species-specific secondary antibodies conjugated with Alexa Fluor (1:200; Zhuangzhi, Beijing, China) for 2 h at RT, and nuclei were stained with Hoechst-33342 (1:10000, GeneCopoeia, United States). Fluorescent signals were visualized under a confocal laser microscope.

Western Blotting

Rats were killed after each treatment, the hippocampus was collected, and total proteins were extracted using radioimmunoprecipitation assay lysis buffer (Beyotime Biotechnology, China). Protein concentrations were determined by BCA protein assay (Beyotime Biotechnology). Brain tissue extracts from each group were boiled for 5 min and the denatured proteins (40 μg) were separated by 10% sodium dodecyl sulfate-polyacrylamide gel electrophoresis and transferred onto nitrocellulose membranes (Bio-Rad, Hercules, CA, United States). After incubation in blocking buffer (0.1% Tween-20 and 5% non-fat-dried milk in Tris-buffered saline) at RT for 1 h, the membranes were incubated with anti-C3 antibody (1:500; Santa Cruz Biotechnology), anti-Iba-1 antibody (1:1000; Sigma), or anti-β-actin antibody (1:2000; Zhuangzhi). Semi-quantitative analysis of protein expression was carried out using horseradish peroxidase-conjugated secondary antibodies (1:5000; Zhuangzhi) and an electrochemiluminescence system (Bio-Rad).

Statistical Analysis

Fluorescent areas were measured using Image-Pro Plus 6.0 software. All statistical analyses were carried out using SPSS17.0 software and presented as mean ± standard deviation (SD) using GraphPad Prism 6.0 software. Data were analyzed by one-way ANOVA, followed by least significant difference tests for comparisons of three or more samples. Statistical significance was set at $P < 0.05$.

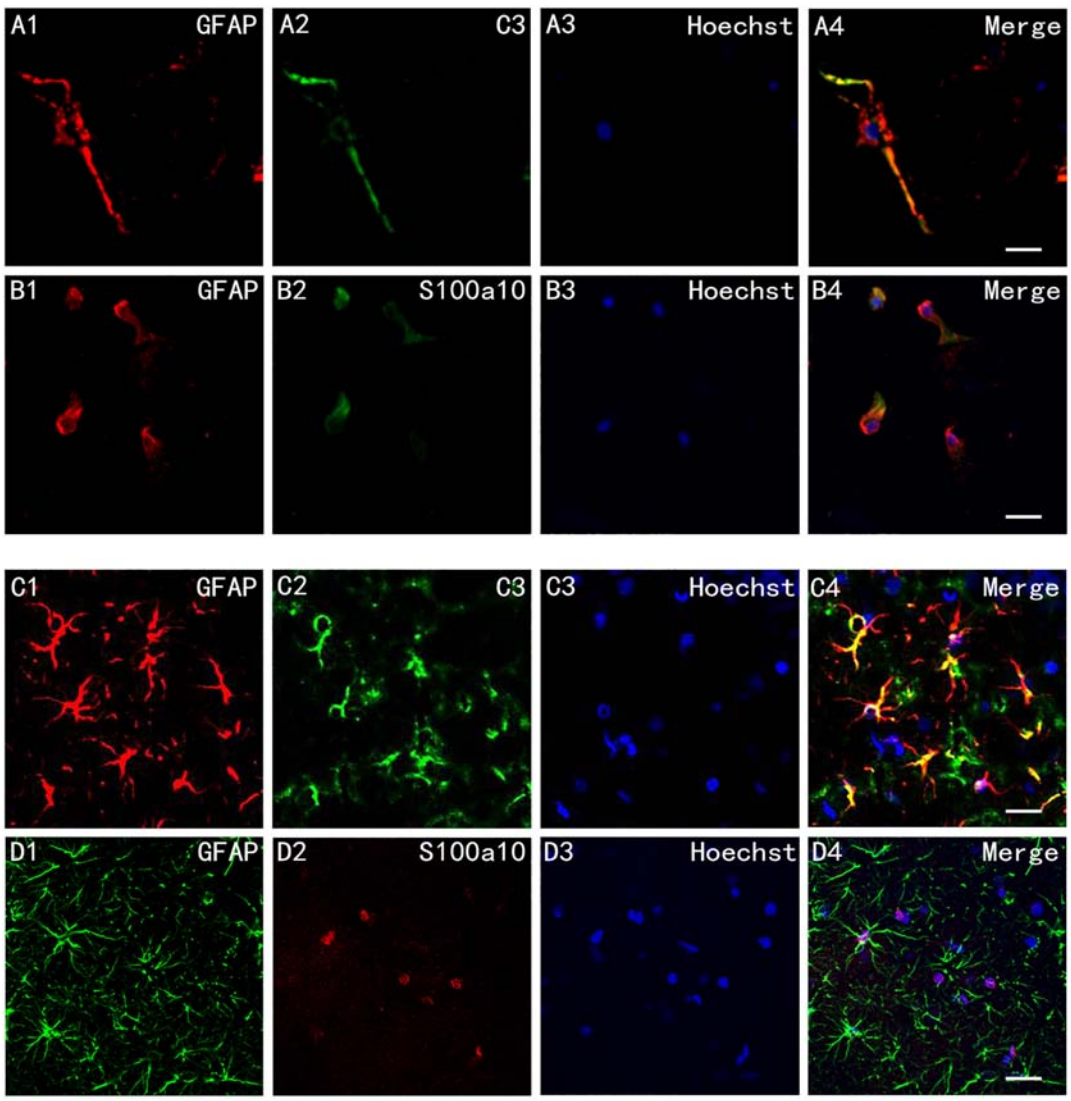

FIGURE 1 | Cell morphology of A1 and A2 astrocytes *in vitro* and *in vivo*. **(A1–A4)** Immunofluorescence staining of cultured astrocytes *in vitro* after exposure to infrasound for 2 h with glial fibrillary acidic protein (GFAP) and component 3 (C3), and **(B1–B4)** with GFAP and S100a10. **(C1–C4)** Immunofluorescence staining of astrocytes in the CA1 region in rats after exposure to infrasound for 3 days with GFAP and C3, and **(D1–D4)** with GFAP and S100a10. Nuclei stained with Hoechst. Scale bar: 25 μm.

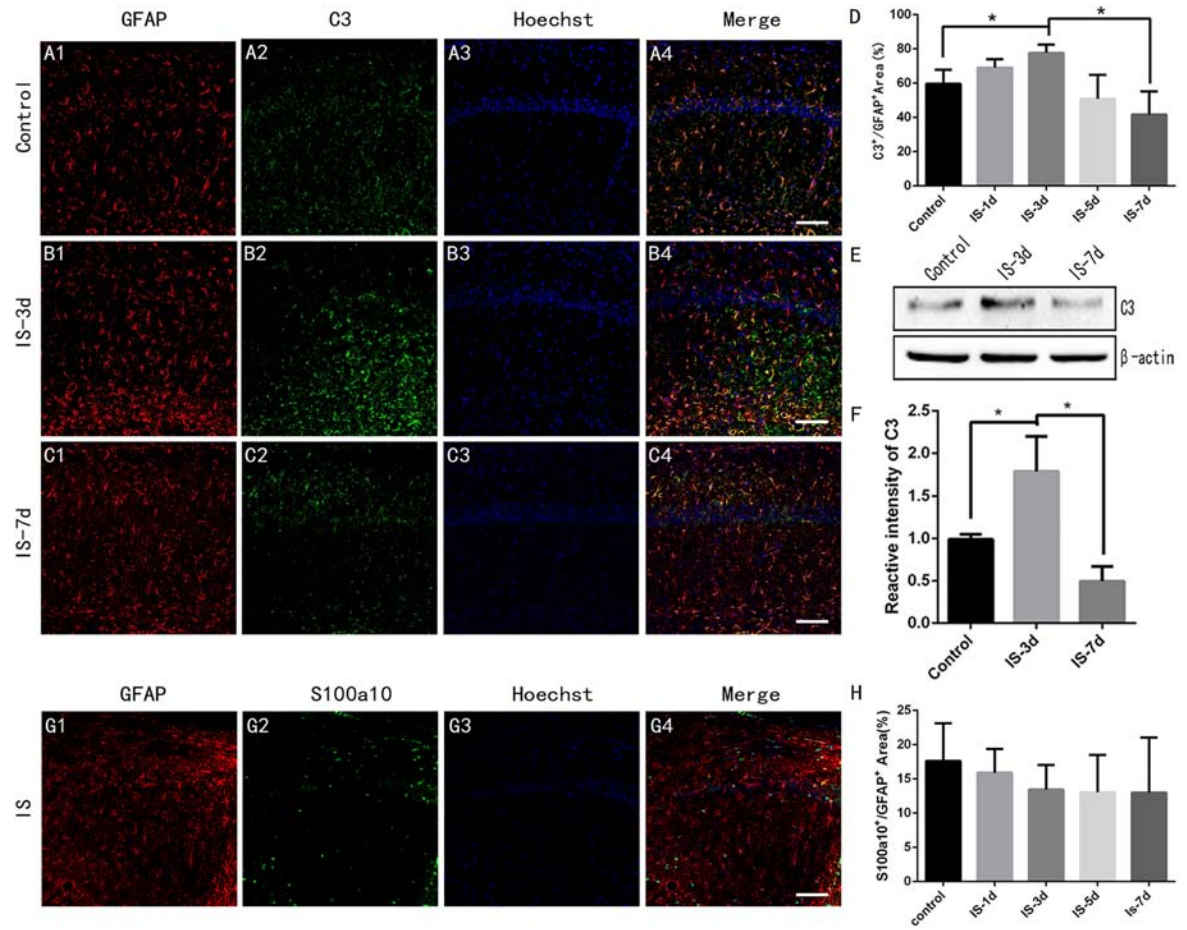

FIGURE 2 | A1 astrocytes were induced in rat hippocampus after 3 days of infrasound exposure. **(A1–A4)** A1 astrocytes in the CA1 region of the rat hippocampus double-labeled by C3 and GFAP in the control group without infrasound exposure, **(B1–B4)** in the group exposed to infrasound (IS) for 3 days (IS-3d), and **(C1–C4)** in the group exposed to infrasound for 7 days (IS-7d). **(D)** Quantitative analysis of percentage of $C3^+/GFAP^+$ area in the CA1 region of rat hippocampus. **(E)** C3 expression in rat hippocampus in control group, IS-3d group, and IS-7d group, by western blotting. **(F)** Semi-quantitative analysis of C3 expression in rat hippocampus in control group, IS-3d group, and IS-7d group. **(G1–G4)** A2 astrocytes in the CA1 region of rat hippocampus double-labeled by S100a10 and GFAP. **(H)** Quantitative analysis of percentage of $S100a10^+/GFAP^+$ area in the CA1 region of rat hippocampus. Nuclei stained with Hoechst. Scale bar: 100 μm. $N = 6–8$ for each experiment. One-way ANOVA. Values are all expressed as mean ± SD. $^*P < 0.05$.

RESULTS

Cell Morphology of A1 and A2 Astrocytes

We cultured rat hippocampus astrocytes *in vitro* and exposed them to infrasound of 16 Hz and 150 dB for 2 h, followed by immunofluorescence staining with S100a10, C3, and GFAP. Fluorescence microscopy showed that $C3^+$ A1 astrocytes had obvious long dendrites (**Figure 1A**), while $S100a10^+$ A2 astrocytes had hypertrophic cell bodies with few dendrites (**Figure 1B**).

In vivo, we pretreated rat by infrasound with a frequency of 16 Hz and a pressure level of 150 dB. Double-immunofluorescence labeling with S100a10, C3, and GFAP was also carried out on brain slices of the rat. Immunofluorescent staining with C3 and GFAP highlighted both the cell bodies and slender processes of A1 astrocytes (**Figure 1C**). But immunofluorescent staining with S100a10 only highlighted the cell bodies of astrocytes (**Figure 1D**).

Infrasound Induced A1 Astrocytes

Then, we used double-immunofluorescent labeling to investigate the effects of infrasound on the activation states of the two types of astrocytes in the CA1 region of the rat hippocampus. The percentage of $C3^+/GFAP^+$ area increased after exposure to infrasound for 3 days ($P < 0.05$) (**Figures 2A–D**). Previous studies demonstrated that GFAP expression increased after infrasound damage (Shi et al., 2013, 2018), and we therefore concluded that A1 astrocytes were activated by infrasound exposure. We also analyzed C3 protein expression levels in rat hippocampus semi-quantitatively by western blotting and confirmed that C3 protein expression levels in the hippocampus were up-regulated after 3 days of infrasound exposure ($P < 0.05$) (**Figures 2E,F**).

There were no significant differences in the percentage of $S100A10^+/GFAP^+$ area between control rats and rats exposed to infrasound for 1, 3, 5, or 7 days ($P > 0.05$) (**Figures 2G,H**).

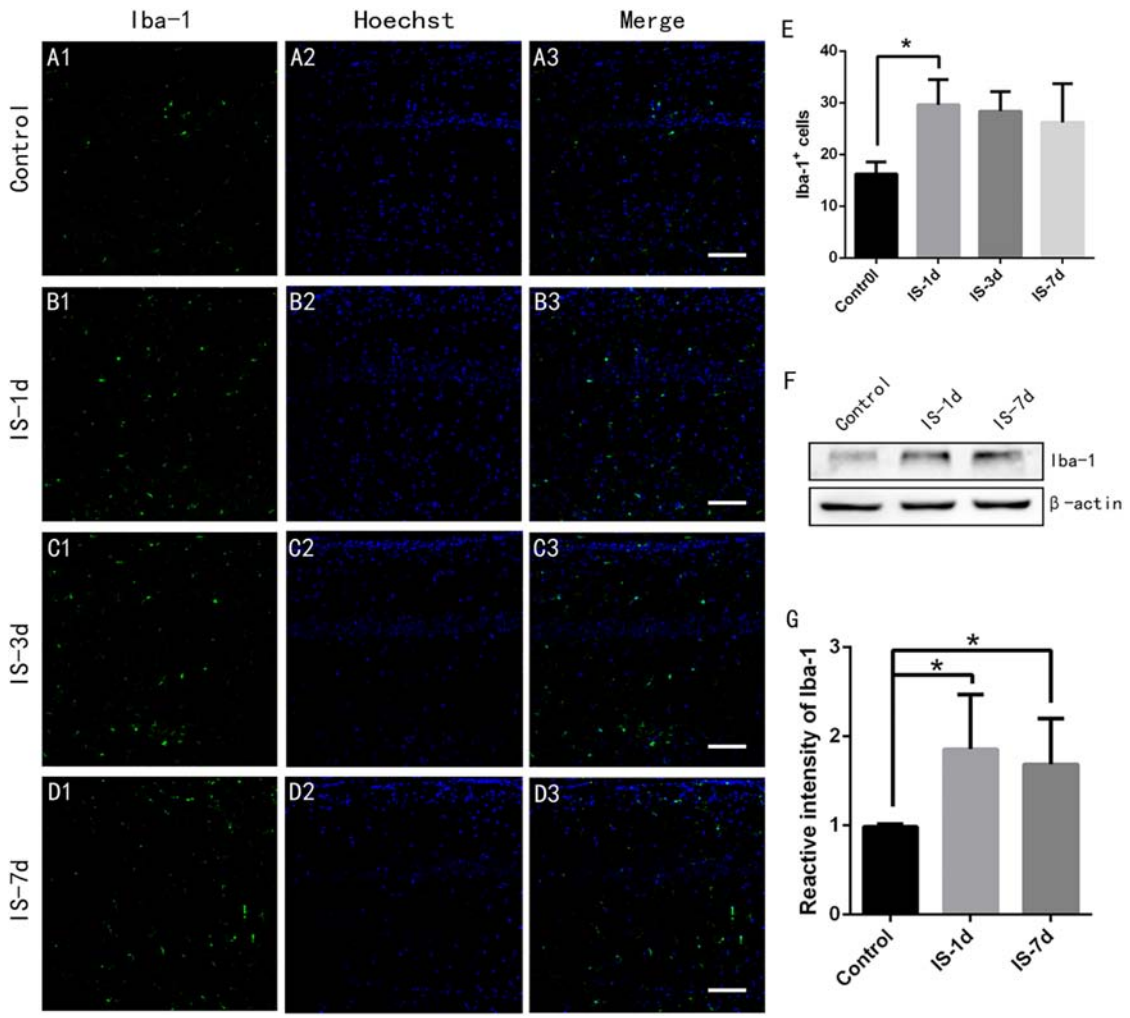

FIGURE 3 | Microglial cells in rat hippocampus increased after 1 day of infrasound exposure. **(A1–A3)** Microglial cells in the CA1 region of the rat hippocampus labeled with Iba-1 in the control group without infrasound exposure, **(B1–B3)** in the IS-1d group (1 day infrasound exposure), **(C1–C3)** IS-3d group (3 days infrasound exposure), and **(D1–D3)** in the IS-7d group (7 days infrasound exposure). **(E)** Quantitative analysis of Iba-1$^+$ cells per 625 μm × 625 μm in the CA1 region of the rat hippocampus by immunofluorescence staining. **(F)** Iba-1 expression in rat hippocampus in the control group, IS-1d group, and IS-7d group by western blotting. **(G)** Semi-quantitative analysis of Iba-1 expression in rat hippocampus in the control group, IS-1d group, and IS-7d group by western blotting. Nuclei stained with Hoechst. Scale bar: 100 μm. N = 6–8 for each experiment. One-way ANOVA. Values are all expressed as mean ± SD. *P < 0.05.

These results suggested that infrasound induced A1 astrocytes, but not A2 astrocytes.

Microglial Cells Were Reactive Following Infrasound Exposure

Liddelow et al. (2017) demonstrated that reactive microglia induced A1 astrocytes, and we therefore determined if microglial cells were activated by infrasound. We labeled microglial cells by Iba-1 immunofluorescence. The results showed that the number of Iba-1$^+$ microglial cells in the CA1 region of the rat hippocampus increased after 1 day of infrasound exposure (P < 0.05) (**Figures 3A–E**), consistent with the results of a previous study (Xu et al., 2008). Western blotting confirmed that Iba-1 expression in the rat hippocampus increased after 1 day of infrasound exposure. Microglial cells decreased slightly during 1 day and 7 days, but the result was not significant (P > 0.05) (**Figures 3E–G**). These results suggested that infrasound exposure for 1 day activated microglial cells in the rat hippocampus.

A1 Astrocytes Were Regulated by the FGF2/FGFR1 Pathway

We initially investigated the role of the FGF2/FGFR1 pathway in A1 astrocyte reactivity by pretreating rats with FGF2 and then exposing them to infrasound. Double-immunofluorescent labeling revealed that the percentage of C3$^+$/GFAP$^+$ area in the CA1 region of the rat hippocampus were decreased during 1 and 7 days of FGF2 treatment and infrasound exposure (P < 0.05) (**Figure 4A**). Expression levels of C3 in the rat hippocampus also decreased during 1 and 7 days of treatment, as demonstrated by western blotting (P < 0.05) (**Figures 4B,C**).

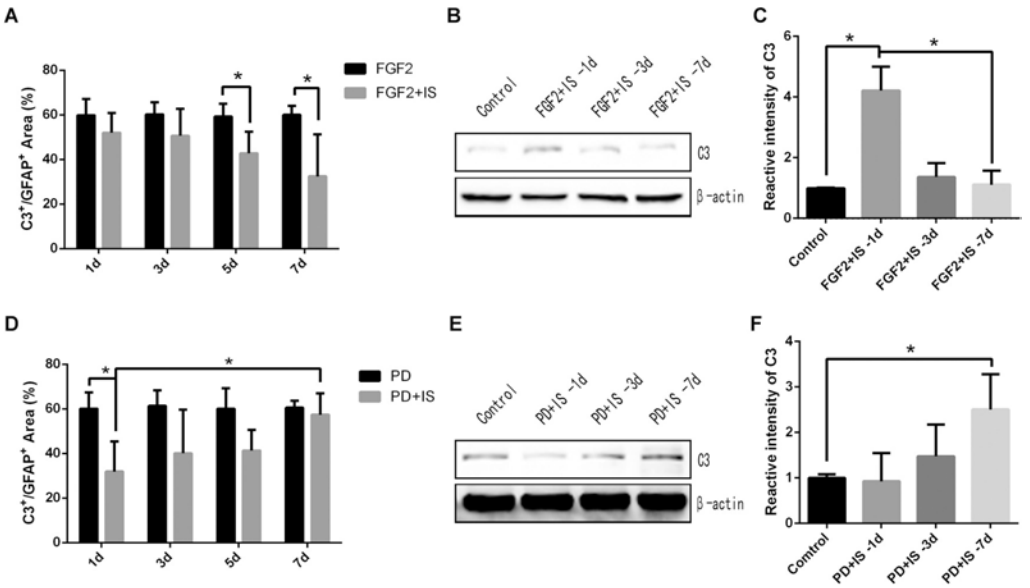

FIGURE 4 | A1 astrocytes were gradually down-regulated by activation of the FGF2/FGFR1 pathway and were up-regulated by inhibition of the FGF2/FGFR1 pathway. **(A,D)** Quantitative analysis of percentage of $C3^+/GFAP^+$ area in the CA1 region of rat hippocampus in different groups, by immunofluorescence staining. **(B,E)** C3 expression in rat hippocampus in different groups by western blotting. **(C,F)** Semi-quantitative analysis of C3 expression in rat hippocampus in different groups. $N = 6–8$ for each experiment. One-way ANOVA. Values expressed as mean ± SD. $^*P < 0.05$.

We then pretreated rats with PD173074 to inhibit activation of the FGF2/FGFR1 pathway. In the CA1 region of the rat hippocampus, the percentage of $C3^+/GFAP^+$ area was increased during 1 and 7 days of PD173074 treatment and infrasound exposure ($P < 0.05$) (**Figure 4D**). C3 expression levels increased gradually as well ($P < 0.05$) (**Figures 4E,F**). In our previous research (Shi et al., 2018), GFAP positive cells were not affected by the FGF2 or PD173074 treatment. Overall, these results suggested that A1 astrocytes were gradually down-regulated by activation of the FGF2/FGFR1 pathway and were up-regulated by inhibition of the FGF2/FGFR1 pathway after infrasound damage.

DISCUSSION

Astrocytes are the main type of glial cells in the brain and spinal cord. Astrocytes undergo astrogliosis during CNS injury and eventually transform into reactive astrocytes (Zamanian et al., 2012; Anderson et al., 2014), as demonstrated for A1 astrocytes in spinal cord injury, CNS brain trauma, and neuroinflammatory and neurodegenerative diseases (Liddelow et al., 2017). Furthermore, we previously demonstrated that infrasound exposure also induced astrocyte and microglial activation (Shi et al., 2013; Cai et al., 2014).

In this study, we examined the activation of microglia and astrocytes to investigate the mechanisms responsible for infrasound-induced neuronal apoptosis in the hippocampus. $C3^+$ and $GFAP^+$ A1 astrocytes in the CA1 region of the rat hippocampus were activated after 3 days of exposure to infrasound, while Iba-1^+ microglial cells were activated after 1 day of exposure, suggesting that microglial cells were activated before A1 astrocyte reactivity. Infrasound-activated microglia have previously been shown to produce a wide range of proinflammatory cytokines, including interleukin (IL)-1β, IL-6, IL-18, and tumor necrosis factor (TNF)-α (Cai et al., 2014). Furthermore, Liddelow et al. (2017) indicated that microglia-derived IL-1α, TNF, and C1q worked together to mediate A1 astrocyte reactivity, while A1 astrocytes exerted powerful neurotoxic effects that killed CNS neurons. Overall, these findings suggest that infrasound exposure initially activated microglial cells in the hippocampus, with subsequent induction of A1 astrocytes and neuronal cell apoptosis, resulting in learning and memory impairments.

The current results also found that FGF2 could restrain the reactivity of A1 astrocytes in the hippocampus after infrasound exposure. This neuroprotective effect of FGF2 against infrasound damage was in accord with previous studies showing that FGF2 could regulate the ability of the newborn hippocampal dentate gyrus, the formation of functional circuits, and the structural plasticity of neurons (Kirby et al., 2013; Pollak et al., 2014). Given that FGF2 could trigger FGFR1 signaling (Sutthiwarotamakun, 2011) and the FGF2/FGFR1 pathway may exert an inhibitory effect on astrocyte-mediated inflammation (Shi et al., 2018), we deduced that the neuroprotective effect involved the inhibition of astrocyte-mediated inflammation via the FGF2/FGFR1 pathway. In contrast, we observed that A1 astrocytes gradually increased in the hippocampus during 7 days of infrasound exposure with PD173074 treatment, thus confirming that inhibition of the FGF2/FGFR1 passageway caused reactivity of A1 astrocytes.

This study had several limitations. We used the method of Liddelow et al. (2017) in the immunofluorescence experiment,

but we could not provide enough evidence to verify Liddelow et al.'s (2017) conclusion that the A2-specific marker S100a10 did not co-localize with C3 positive A1 astrocytes. In our experimental results, we found C3 existed in most of astrocytes which were labeled by GFAP (**Figures 2A–C**). It is possible that C3 exist in brain of normal animals (Rong et al., 2007; Fonseca et al., 2011). C3-positive astrocytes is expressed at a low level in normal physiological state, and some brain injury factors may lead to increased pathological expression, thus resulting in neurotoxic effects (Liddelow et al., 2017). We focused on the neurotoxic function of A1 astrocytes in infrasound damage; however, infrasound is a type of noise and might thus also have psychological effects. Furthermore, it is possible that pathways other than the FGF2/FGFR1 pathway might be involved in regulating the reactivity of A1 astrocytes. Further research is therefore needed to identify other potential mechanisms involved in the neurotoxic function of A1 astrocytes in infrasound damage.

In summary, our results demonstrated that A1 astrocytes were induced by microglia in the CA1 region of the rat hippocampus after infrasound exposure, and that these A1 astrocytes were regulated by the FGF2/FGFR1 pathway. Inhibiting A1 astrocytes or activating the FGF2/FGFR1 pathway may thus represent promising targets for the treatment of infrasound-induced CNS injury.

ETHICS STATEMENT

All procedures used in this study were approved by the Institutional Review Board and were performed according to the Guidelines of Institutional Animal Care and Use Committee at the Fourth Military Medical University.

AUTHOR CONTRIBUTIONS

All authors contributed substantially to this work. LM conceived and designed the experiments. L-HZ performed the experiments and drew the figures. Y-JS and HH analyzed the data. S-MJ reviewed the language and grammar and provided reference materials. F-FH contributed reagents and analysis tools. X-MW and FW searched and provided material for writing the manuscript, and arranged the manuscript in accordance with the journal specifications. L-HZ, Y-JS, and HH wrote the manuscript.

FUNDING

This work was supported by grants from the Natural Science Foundation of China (Grant No. 31570848).

ACKNOWLEDGMENTS

We thank Dr. Ming Shi and Dongyun Feng (Department of Neurology, Xijing Hospital, Fourth Military Medical University) for their technical assistance and valuable suggestions. We also thank International Science Editing (http://www.internationalscienceediting.com) for editing a draft of this manuscript.

REFERENCES

Anderson, M., Ao, Y., and Sofroniew, M. (2014). Heterogeneity of reactive astrocytes. *Neurosci. Lett.* 565, 23–29. doi: 10.1016/j.neulet.2013.12.030

Backteman, O., Köhler, J., and Sjöberg, L. (1983). Infrasound-tutorial and review: Part 1.O. Backteman. *J. Low Frequency Noise Vib. Active Control* 3, 1–31.

Bilski, B. (2017). Exposure to infrasonic noise in agriculture. *Ann. Agric. Environ. Med.* 1, 86–89.

Bush, T., Puvanachandra, N., Homer, C., Polito, A., Ostenfeld, T., Svendsen, C., et al. (1999). Leukocyte infiltration, neuronal degeneration, and neurite outgrowth after ablation of scar-forming, reactive astrocytes in adult transgenic mice. *Neuron* 2, 297–308.

Cai, J., Jing, D., Shi, M., Liu, Y., Lin, T., Xie, Z., et al. (2014). Epigallocatechin gallate (EGCG) attenuates infrasound-induced neuronal impairment by inhibiting microglia-mediated inflammation. *J. Nutr. Biochem.* 25, 716–725. doi: 10.1016/j.jnutbio.2014.02.012

Castelo-Branco, N., and Rodriguez, E. (1999). The vibroacoustic disease–an emerging pathology. *Aviat. Space Environ. Med.* 70, 1–6.

Di Marco, S., Reuter, S., Kentrup, D., Grabner, A., Amaral, A., and Fobker, M. (2014). Treatment of established left ventricular hypertrophy with fibroblast growth factor receptor blockade in an animal model of CKD. *Nephrol. Dial. Transplant.* 29, 2028–2035. doi: 10.1093/ndt/gfu190

Fei, Z., Zhang, X., Wang, X., Li, Z., Lu, P., Liu, X., et al. (2000). The changes of rat blood-brain barrier permeability and expression of heat shock protein 70 after infrasonic damage. *J. Low Frequency Noise Vib. Active Control* 2, 93–99.

Fonseca, M., Chu, S., Berci, A., Benoit, M., Peters, D., Kimura, Y., et al. (2011). Contribution of complement activation pathways to neuropathology differs among mouse models of Alzheimer's disease. *J. Neuroinflammation* 8, 4–16.

Graham, B., and Richardson, R. (2009). Acute systemic fibroblast growth factor-2 enhances long-term extinction of fear and reduces reinstatement in rats. *Neuropsychopharmacology* 34, 1875–1882. doi: 10.1038/npp.2009.14

Izmerov, N., Suvorov, G., Kuralesin, N., and Ovakimov, V. (1997). Infrasound: body's effects and hygienic regulation. *Vestn. Ross. Akad. Med. Nauk* 7, 39–46.

Kirby, E., Muroy, S., Sun, W., Covarrubias, D., Leong, M., Barchas, L., et al. (2013). Acute stress enhances adult rat hippocampal neurogenesis and activation of newborn neurons via secreted astrocytic FGF2. *eLife* 2:362. doi: 10.7554/eLife.00362

Liddelow, S., Guttenplan, K., Clarke, L., Bennett, F., Bohlen, C., Schirmer, L., et al. (2017). Neurotoxic reactive astrocytes are induced by activated microglia. *Nature* 541, 481–487. doi: 10.1038/nature21029

Ma, L., He, H., Liu, X., Zhang, G., Li, L., Yan, S., et al. (2015). Involvement of cannabinoid receptors in infrasonic noise-induced neuronal impairment. *Acta Biochim. Biophys. Sin.* 8, 647–653. doi: 10.1093/abbs/gmv049

Melvin, N., and Sutherland, R. (2010). Quantitative caveats of standard immunohistochemical procedures: implications for optical disector-based designs. *J. Histochem. Cytochem.* 58, 577–584. doi: 10.1369/jhc.2009.954164

Mohammadi, M., Froum, S., Hamby, J., Schroeder, M., Panek, R., Lu, G., et al. (1998). Crystal structure of an angiogenesis inhibitor bound to the FGF receptor tyrosine kinase domain. *EMBO J.* 20, 5896–5904.

Pollak, D., Minh, B., Cicvaric, A., and Monje, F. (2014). A novel fibroblast growth factor receptor family member promotes neuronal outgrowth and synaptic plasticity in Aplysia. *Amino Acids* 11, 2477–2488. doi: 10.1007/s00726-014-1803-2

Rong, F., Kelly, D., and William, E. (2007). Induction of complement proteins in a mouse model for cerebral microvascular Aβ deposition. *J. Neuroinflammation* 4, 22–30.

Shi, M., Du, F., Liu, Y., Li, L., Cai, J., Zhang, G., et al. (2013). Glial cell-expressed mechanosensitive channel TRPV4 mediates infrasound-induced

neuronal impairment. *Acta Neuropathol.* 5, 725–739. doi: 10.1007/s00401-013-1166-x

Shi, Y., Shi, M., Xiao, L., Zou, L., Li, C., Zhang, Q., et al. (2018). Inhibitive effects of FGF2/FGFR1 pathway on astrocyte-mediated inflammation in vivo and in vitro after infrasound exposure. *Front. Neurosci.* 12:582. doi: 10.3389/fnins.2018.00582

Sutthiwarotamakun, R. (2011). *Perpheral Autoimmunity Induces Central Neuro-Inflammation and Hippocampal Neurogenesis Impairment in a Murine Model of Collagen Induced Rheumatoid Arthritis*. .

Xu, X., Zhao, G., Rao, Z., Du, F., Shi, J., and Liu, J. (2008). The response of microglia in the hypothalamic paraventricular nucleus of rats to infrasound. *Chin. J. Neurosurg. Dis. Res.* 7, 513–516.

Yuan, H., Long, H., Liu, J., Qu, L., Chen, J., and Mou, X. (2009). Effects of infrasound on hippocampus-dependent learning and memory in rats and some underlying mechanisms. *Environ. Toxicol. Pharmacol.* 2, 243–247. doi: 10.1016/j.etap.2009.04.011

Zamanian, J. L., Xu, L., Foo, L., Nouri, N., Zhou, L., Giffard, R., et al. (2012). Genomic analysis of reactive astrogliosis. *J. Neurosci.* 32, 6391–6410. doi: 10.1523/JNEUROSCI.6221-11.2012

Conflict of Interest Statement: The authors declare that the research was conducted in the absence of any commercial or financial relationships that could be construed as a potential conflict of interest.

frontiers in Cellular Neuroscience

REVIEW
published: 07 May 2019
doi: 10.3389/fncel.2019.00198

Lipid Metabolism in Neurons: A Brief Story of a Novel c-Fos-Dependent Mechanism for the Regulation of Their Synthesis

*Lucia Rodríguez-Berdini and Beatriz L. Caputto**

Centro de Investigaciones en Química Biológica de Córdoba (Consejo Nacional de Investigaciones Científicas y Técnicas), Departamento de Química Biológica "Ranwel Caputto", Facultad de Ciencias Químicas, Universidad Nacional de Córdoba, Córdoba, Argentina

The mechanisms that coordinately regulate lipid synthesis in the nervous system together with the high rates of membrane biogenesis needed to support cell growth are largely unknown as are their subcellular site of synthesis. c-Fos, a well-known AP-1 transcription factor, has emerged as a unique protein with the capacity to associate to specific enzymes of the pathway of synthesis of phospholipids at the endoplasmic reticulum and activate their synthesis to accompany genomic decisions of growth. Herein, we discuss this effect of c-Fos in the context of neuronal differentiation and also with respect to pathologies of the nervous system such as the development and growth of tumors. We also provide insights into the sub-cellular sites where this regulation occurs at the endoplasmic reticulum membranes and the molecular mechanism by which c-Fos exerts this activity.

Keywords: nervous system phospholipid synthesis regulation, membrane biogenesis, proliferation and differentiation, brain tumors, endomembrane compartments

OPEN ACCESS

Edited by:
Gabriela Alejandra Salvador, Universidad Nacional del Sur, Argentina

Reviewed by:
Norma María Giusto, National Council for Scientific and Technical Research (CONICET), Argentina
Hermona Soreq, Hebrew University of Jerusalem, Israel

***Correspondence:**
Beatriz L. Caputto
bcaputto@fcq.unc.edu.ar

Specialty section:
This article was submitted to Cellular Neurophysiology, a section of the journal Frontiers in Cellular Neuroscience

Received: *20 February 2019*
Accepted: *18 April 2019*
Published: *07 May 2019*

Citation:
Rodríguez-Berdini L and Caputto BL (2019) Lipid Metabolism in Neurons: A Brief Story of a Novel c-Fos-Dependent Mechanism for the Regulation of Their Synthesis. Front. Cell. Neurosci. 13:198. doi: 10.3389/fncel.2019.00198

INTRODUCTION

Lipids, essential constituent molecules of all organisms, participate in a broad range of cellular processes. Their importance is highlighted by the fact that almost 5% of the human genes are related to their synthesis (van Meer et al., 2008). Particularly, the nervous system has a rich lipid composition, being the brain the second tissue in humans with both the highest lipid content and the highest diversity in their composition (Sastry, 1985; Hamilton et al., 2007; Bozek et al., 2015). Some authors have related this diversity to the cognitive abilities acquired by humans through their evolutionary lineage (Bozek et al., 2015). Among the main functions of lipids in the nervous system, of undoubtable importance is their structural role in biological membranes, their participation as bioactive messengers involved in cell signaling and their contribution to energy supply (Tracey et al., 2018).

The homeostasis of the lipid content of the nervous system is of vital importance, since several neuropathologies have been associated to their abnormal metabolism (Ahmed et al., 2017; Gaspar et al., 2018; Valadas et al., 2018; Yu et al., 2018). Evidence has linked disturbances in cholesterol metabolism to the progressive neurodegeneration observed in Alzheimer patients (Chang et al., 2017; Habchi et al., 2018; Penke et al., 2018) and also to autism spectrum disorders, possibly through lipid rafts disarrangements and the consequent alteration of synaptic

functions (Wang, 2014). Elevated ganglioside levels have been related to Parkinson's disease, probably through their influence on α-synuclein aggregation kinetics (Gaspar et al., 2018). Abnormalities in the metabolism of polyphosphoinositides also underlie nervous system diseases such as schizophrenia, bipolar disorder, Friedrich's ataxia, Parkinson's and Down syndrome (Lauwers et al., 2016).

An unbalanced content of fatty acids in the nervous system has also been associated to neurodegenerative diseases. Docosahexaenoic acid (DHA) and arachidonic acid (AA) are the most abundant and biologically active essential fatty acids in brain phospholipids (Sanchez-Mejia and Mucke, 2010). DHA and its derivatives, the docosanoids, are involved in neuronal survival signaling pathways that resolve inflammation and reduce oxidative stress (Farooqui, 2012; Bazan, 2014; Tayebati, 2018). A significant decrease in DHA levels has been observed in cognitive impairment and Alzheimer's disease (AD) (Bazan et al., 2011; Bazan, 2014; Kim et al., 2014). In fact, DHA enriched diets have been proven to be efficient against neurodegeneration and able to prevent AD symptoms (Strokin et al., 2006; Hooijmans et al., 2009; Oster and Pillot, 2010; Tayebati, 2018). In retina neurons, DHA protects cells against oxidative stress and promotes photoreceptor differentiation (Simon et al., 2016). On the other hand, an activated metabolism of AA and its derivatives, the eicosanoids, has been associated to different pathologies, such as multiple sclerosis or AD, probably through the promotion of neuroinflammation and of an increase in neuronal activity and excitotoxicity (Lukiw and Bazan, 2000; Sanchez-Mejia and Mucke, 2010; Palumbo, 2017).

Brain choline metabolism has received much attention due to the important role of acetylcholine transmission in neuronal functions, especially those involved in cognitive abilities (Ferreira-Vieira et al., 2016). Abnormalities in the brain cholinergic system have been observed in AD, Lewy Bodies Dementia, Parkinson's disease and Huntington, among other pathologies (Pepeu and Grazia Giovannini, 2017).

In the case of the neuronal membrane, its lipid composition varies according to the neuronal type and the structural compartment of the neuron (Vance et al., 2000). The first results obtained after addressing the subcellular localization of lipid synthesis in neurons indicated that it was carried out in the neuronal soma (Weiss and Hiscoe, 1948), from where these components were transported by anterograde transport to the growing dendrites and axons during differentiation (Ledeen, 1985). However, it was later suggested that axonal transport was neither fast nor abundant enough to supply the necessary amounts of lipids to support axonal membrane expansion, an event that can reach an increment of up to 20% per day during the peak of neuronal growth (Pfenninger, 2009). So, given the size and architecture of neurons, it seemed reasonable to imagine the existence of a temporal and domain-specific organization. This could regulate lipid synthesis at distal sites of the neuron so as to avoid the sole dependence on axonal transport of these compounds from the soma.

Several reports have demonstrated the presence in axons of endoplasmic reticulum (ER) membranes, the main organelle for lipid synthesis, suggesting that the axon could contain a local functional biosynthetic machinery (Palay, 1958; Tsukita and Ishikawa, 1976; Rambourg and Droz, 1980; Lindsey and Ellisman, 1985; Gonzalez and Couve, 2014; Luarte et al., 2018; Terasaki, 2018). In fact, this seems to be the case: several enzymes of the pathway of lipid synthesis have been shown to be present in axons where they are capable of locally synthetizing phosphatidylcholine, phosphatidylethanolamine, phosphatidylserine, phosphatidylinositol, sphingomyelin and fatty acids (Vance et al., 1991, 1994). For example, 50% of the phosphatidylcholine required for normal axonal elongation has been shown to be locally synthetized in the axonal ER (Posse de Chaves et al., 1995).

These observations posed questions regarding the mechanisms that determine which lipids are synthetized in the axon, the quantitative extent of the domain-specific synthesis of lipids and the regulatory constraints driving this phenomenon. In this regard, many aspects of this metabolism remain unanswered, especially if its influence on neuronal plasticity is considered.

c-FOS: ONE PROTEIN LEADING TO AT LEAST TWO ROADS

The oncogene *fos* codifies for a protein of 380 amino acids called c-Fos that belongs to the *Immediate Early Genes* (IEGs) family (Angel and Karin, 1991). Five different proteins form the Fos family: c-Fos, Fos-B, ΔFos-B, Fra-1, and Fra-2 (Tulchinsky, 2000; Raivich and Behrens, 2006), all of which heterodimerize mainly with proteins of the Jun family thus forming the well-known AP-1 family of transcription factors (Angel and Karin, 1991). c-Fos heterodimerizes with Jun through a leucine zipper domain (LZ) and the resulting heterodimer interacts with a DNA consensus sequence through the basic domains (BD) of both proteins (Glover and Harrison, 1995).

It has been established that AP-1 activity is induced under a wide range of physiological and pathological stimuli including cytokines, growth factors, stress signals, infections and upon oncogenic transformation (Shaulian and Karin, 2001). It has also been proposed that its activity can be regulated through multiple pathways: (a)- via the transcriptional regulation of the proteins that compose each AP-1 dimer; (b)- through the stability of their mRNAs; (c)- via post-transductional modifications; (d)- by regulating the turnover of pre-existing molecules of the proteins or of the newly synthetized ones; (e)- through specific interactions between the different AP-1 subunits; (f)- through interactions with other transcription factors and co-factors (Hess et al., 2004).

Under certain circumstances, c-Fos is capable of inducing cellular transformation (Miller et al., 1984), a role that is usually associated to its function as an AP-1 transcription factor. Evidence has been provided that demonstrates its main role in cell growth and in neoplastic transformation (Tulchinsky, 2000; Shaulian and Karin, 2001; Hess et al., 2004; Milde-Langosch, 2005). Surprisingly, it was shown that, unlike other oncogenes studied, its oncogenic activity does not rely on mutations of its sequence but is rather dependent only on

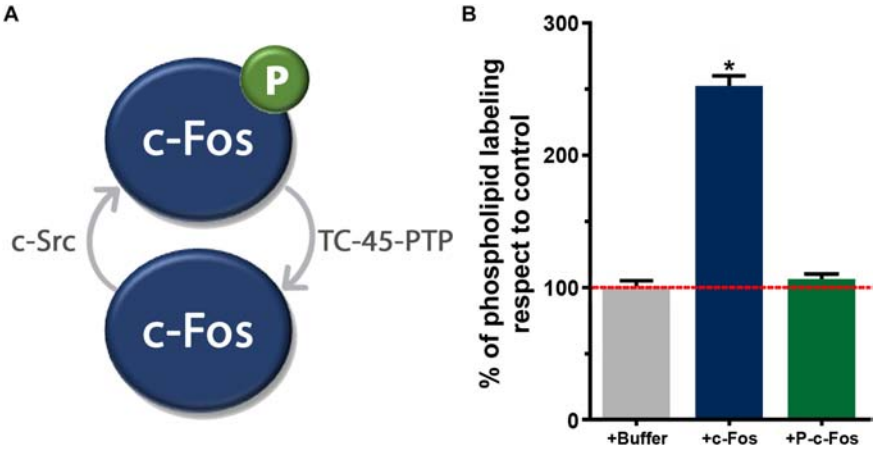

FIGURE 1 | (A) Schematic representation of the phosphorylation/dephosphorylation cycle of the tyrosine residues of c-Fos by the kinase c-Src and the phosphatase TC-45-PTP. Dephosphorylated c-Fos is able to associate to ER membranes whereas phosphorylated c-Fos is not. **(B)** Labeling of total phospholipids in T98G cells homogenates in the presence of recombinant dephosphorylated c-Fos and phosphorylated c-Fos (obtained after incubation with recombinant c-Src). The capacity to incorporate [^{32}P] to phospholipids from [^{32}P]-ATP was measured *in vitro*. The results are the mean ± SD of two experiments performed in triplicate. *$p < 0.002$ with respect to the control, as determined by Student's two-tailed *t*-test. Adapted from Ferrero et al., 2012 (ownership of copyright in original Springer Nature research articles remains with the Author, and provided that, when reproducing the contribution or extracts from it or from the Supplementary Information, the author acknowledges first and reference publication in the Journal).

its over-expression (Miller et al., 1984). In addition, different stress signals such as UV exposure or alkylating agents, that normally provoke cell cycle arrest or cell death, also induce its expression (Buscher et al., 1988; Curran and Franza, 1988; Piechaczyk and Blanchard, 1994; Shaulian and Karin, 2001). Even more, numerous studies pointed out that the outcome of AP-1 activity seems to be cell-type specific: whereas in some cells it promotes apoptosis, in others it is required for survival (Hess et al., 2004). Hence, although the different functions of AP-1 have been exhaustively studied, the complete scenario resulting from its expression/overexpression is complex due to its capacity to exert completely antagonizing functions. This duality can be particularly distinguished in the nervous system where AP-1 is involved in both degenerative and regenerative processes, as a degeneration effector or as a physiological neuroprotective player (Herdegen and Waetzig, 2001).

In the nervous system, c-Fos expression has also been related to processes involving memory and learning (Dragunow, 1996; Grimm and Tischmeyer, 1997; Rosen et al., 1998; Minatohara et al., 2015; Gallo et al., 2018). These findings transformed this protein into a marker of plastic changes that favor the establishment of long term memory and the maintenance of specific neuronal populations (Rosen et al., 1998; Minatohara et al., 2015). In fact, AP-1 inhibition negatively affects memory formation and physiological adaptive processes such as the synchronization of the endogenous clock (Wollnik et al., 1995; Grimm and Tischmeyer, 1997). While all this evidence has reliably demonstrated the importance of c-Fos and the functional consequences of its induction, surely other cellular mechanisms in which this protein participates, remain unknown.

During the last 20 years, our laboratory has accumulated evidence that demonstrates that c-Fos is a moonlighting protein: it is capable of performing two different, apparently autonomous, unrelated functions. In addition to its well-known function as an AP-1 transcription factor, c-Fos associates to the ER where it activates lipid synthetizing enzymes independently of

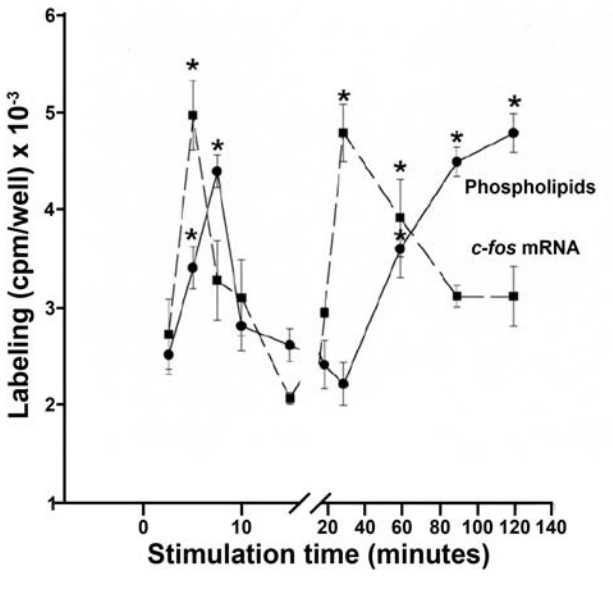

FIGURE 2 | Time curves of phospholipid metabolic labeling (circles, full line) and c-Fos mRNA expression (squares, dashed line) in NIH-3T3 cells stimulated to re-enter cell cycle after quiescence. In all the conditions, phospholipid labeling was determined by pulsing cells with ^{32}P-orthophosphate during 15 min, irrespective of the stimulation status. The results are the mean ± SD of six independent experiments performed in duplicate. *$p < 0.025$ with respect to time 0 of stimulation. Adapted from Bussolino et al., 2001 (the Copyright Clearance Center, Inc. grants authors rights to reproduce figures or tables from their own works free of charge).

its nuclear function (Guido et al., 1996; Bussolino et al., 1998, 2001; Gil et al., 2004; Crespo et al., 2008; Alfonso Pecchio et al., 2011; Caputto et al., 2014; Cardozo Gizzi et al., 2015). This phenomenon has been observed in animal models with nervous system tumors, in cultured cells derived from the nervous system (PC12 cells, the neuronal tumor cell lines T98G, U87MG, NB41A3, C6, among others) and in non-nervous cells such as breast cancer cells (Gil et al., 2004; Motrich et al., 2013). The association of c-Fos to the ER is essential for lipid synthesis activation to occur and it is regulated by a phosphorylation/dephosphorylation cycle exerted by the enzymes c-Src and TC45-PTP. c-Src phosphorylates the tyrosine residues 10 and 30 of c-Fos determining its dissociation from the ER. By contrast, TC45-PTP is the phosphatase that removes the phosphate groups allowing c-Fos to associate to membranes in its dephosphorylated form (**Figure 1**; Ferrero et al., 2012).

Using different types of cells in culture, we showed that the expression of c-Fos mRNA exhibits two peaks, each of them concordant with a significant increase in the metabolic labeling of lipids (**Figure 2**; Bussolino et al., 2001). Specifically blocking c-Fos expression also blocks activation of lipid synthesis. Even more, in order to obtain an insight on the mechanism for enzyme activation, we performed biochemical assays. We found that at the ER, c-Fos is capable of activating only some particular enzymes of the different lipid synthetizing pathways: CDP-diacylglycerolsynthase-1 (CDS1), Phosphatidylinositol-4-kinase type II α (PI4KIIα) and Lipin-1 are activated by c-Fos, whereas Phosphatidylinositol synthase (PIS1) and Phosphatidylinositol-4-kinase type II β (PI4KIIβ) are not (Alfonso Pecchio et al., 2011; Cardozo Gizzi et al., 2015). As can be seen in the activity assays shown in **Figure 3B**, activation is achieved by increasing their V_{max} without affecting their K_m. Furthermore, for activation to occur, c-Fos interacts with the enzymes it activates but not with those it does not regulate (see FRET experiments in **Figure 3A**). Interestingly, this physical interaction is achieved by the N-terminal domain of c-Fos, where a stretch enriched in basic amino acids (BD domain, 139–159) is of fundamental importance for enzyme activation (Alfonso Pecchio et al., 2011). Surprisingly, c-Fos can also perform this activity in the nucleus, where it promotes transcriptional changes in genes lacking an AP-1 consensus sequence in their promoters by increasing the nuclear content of phosphatidylinositol-4,5-bisphosphate (Ferrero et al., 2014). These findings provide an even more complex scenario regarding the cellular consequences of inducing c-Fos expression and allowed us to propose an additional role for c-Fos as a transcriptional regulator but in an AP-1-independent manner.

A great effort was destined to study this function in the nervous system, where c-Fos-dependent lipid activation has been consistently confirmed. In fact, the first studies that gave the initial evidence of this phenomena in the nervous system were performed in the chicken retina, where we found that during sensory stimulation, the transcription and transduction of c-Fos

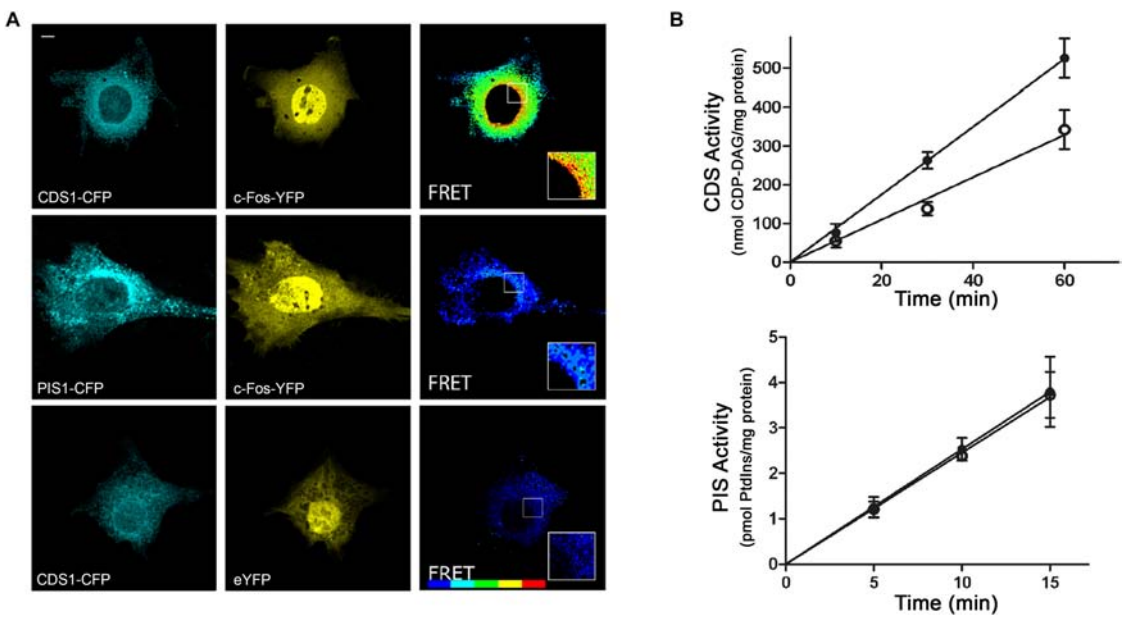

FIGURE 3 | The enzyme CDP-diacylglycerol synthase (CDS) interacts with and is activated by c-Fos, while the enzyme phosphatidylinositol synthase (PIS) neither interacts nor is activated by c-Fos. **(A)** FRET experiments of cells co-transfected to express c-Fos-YFP and CDS1-CFP (first row) or PIS1-CFP (second row) were examined by confocal microscopy using filters for eCFP (left) or for eYFP (middle). FRET efficiency images were obtained and pseudocolored (right). The last row shows control cells co-expressing CDS1-CFP and eYFP. FRET scale goes from no FRET (blue) to maximum FRET (red). Scale bar: 5 μm. **(B)** Effect of c-Fos on CDS and PIS activities. Assays were performed in the presence (black circles) or the absence (open circles) of recombinant c-Fos. Formation of CDP-diacylglycerol (CDP-DAG) was measured in the case of determining CDS activity and phosphatidylinositol (PtdIns) in the case of examining PIS activity. Results are the mean ± SD of at least two experiments performed in triplicate. Adapted from Alfonso Pecchio et al., 2011 (article available to the public under an Attribution–Noncommercial–Share Alike 3.0 Unported Creative Commons License - http://creativecommons.org/licenses/by-nc-sa/3.0).

participate in the regulation of glycerophospholipids synthesis: if c-Fos expression is specifically inhibited in photoreceptors and ganglion cells, the differences usually observed in lipid synthesis after the exposure of the animals to light or dark cycles are abolished (Guido et al., 1996; Bussolino et al., 1998).

Later studies showed that this c-Fos-dependent lipid synthesis activation was also present in T98G cells, cells derived from a malignant human glioblastoma: blocking c-Fos expression in these cells promotes a decrease in the metabolic labeling of phospholipids and an impairment in cell proliferation (Portal et al., 2007; Ferrero et al., 2012). Results obtained in PC12 cells, which derive from a pheochromocytoma of the rat adrenal medulla, highlighted the existence of the dual functions of c-Fos as an AP-1 transcription factor and as an activator of lipid synthesis. Normally, the addition of nerve growth factor (NGF) to the cell culture media triggers a genomic differentiation program that drives these cells towards a sympathetic neuron phenotype, a process that is accompanied by an induction of c-Fos expression (Gil et al., 2004). If, together with NGF treatment, the entrance of c-Fos to the nucleus is impaired by blocking AP-1 importation, neuritogenesis and differentiation are inhibited even when c-Fos expression remains at its normal levels. However, if the import of c-Fos into the nucleus is blocked 16 hours after NGF induction, differentiation is normal. This implies that c-Fos is required at early stages of differentiation in the nucleus as AP-1 to trigger the differentiation program. However, once the cells have been induced to differentiate, when c-Fos expression is blocked, there is a decrease in lipid synthesis and neurites not only stop growing, they also begin to retract, a process that can be reverted by the over-expression of only c-Fos even in the absence of NGF. This indicates that c-Fos is no longer required in the nucleus at advanced times of differentiation but is rather required in the cytoplasm activating lipid synthesis at the ER to sustain neurite outgrowth (Gil et al., 2004).

To advance in the understanding of the role of c-Fos on brain development, studies were performed using transgenic *fos* (-/-) mice. These animals show a significant reduction in the thickness of the developing neocortex respect to wild type animals, a phenotype that is still observed at the adult stage (**Figure 4**; Velazquez et al., 2015a,b). This reduction correlates with a decrease in the number of differentiating cells and an increase in apoptosis levels at the ventricular zone. No differences are observed in the number of cells going through mitosis although the mitotic angle found is mainly vertical, suggesting a decreased tendency for the progenitor cells to differentiate. These results probably reflect the initial dependence of c-Fos AP-1 activity for neuronal development to occur.

As c-Fos has been shown to be a potent oncoprotein that induces cell transformation when deregulated (Piechaczyk and Blanchard, 1994; Tulchinsky, 2000), we evaluated if this role could be due to its cytoplasmic lipid-synthetizing function. We found a strong expression of cytoplasmic c-Fos co-localizing with ER markers in 100% of the more than 200 human malignant brain tumor samples examined. This strongly contrasted with the lack of detectable expression of this protein in normal, paired biopsies (Silvestre et al., 2010). In a human glioblastoma multiforme sample, in addition to the increased expression of c-Fos, a > 100% activation of lipid synthesis was observed when assayed *in vitro*, with respect to a paired non-pathological sample. Furthermore, elimination from the assay media of endogenous c-Fos (using high ionic strength followed by centrifugation) reduced the activated levels of lipid synthesis, whereas addition

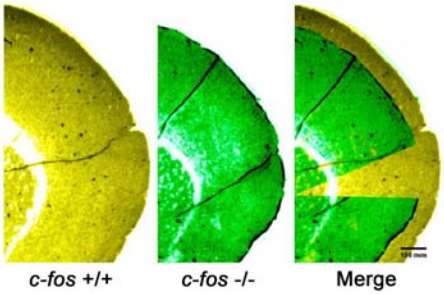

FIGURE 4 | Representative images of brain cortical slices from *fos* (+/+) mice (left, pseudo colored yellow), *fos* (–/–) mice (middle, pseudo colored green) and the merged image (right). Note that in the merged image, part of the *fos* (–/–) image was cropped to better show the superposition of both images. Adapted from Velazquez et al., 2015b (this is an open-access article distributed under the terms of the Creative Commons Attribution License, which permits unrestricted use, distribution, and reproduction in any medium, provided the original author and source are credited).

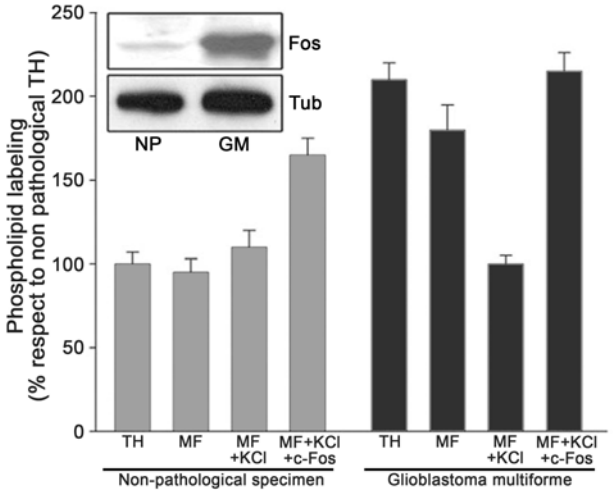

FIGURE 5 | Activation of phospholipid synthesis in membranes from a human glioblastoma multiforme (GM). Homogenates were obtained from a human GM and from adjacent non pathological tissue (NP) excised from the same patient. TH: total homogenate; MF: microsomal membrane fraction; MF+KCl: 1M KCl stripped microsomal membrane fraction; MF+KCl+c-Fos: stripped MF plus recombinant c-Fos. Results are the mean ± SD of three experiments performed in triplicate; non-pathological TH values were taken as 100%. Inset: Western Blot for c-Fos content in the samples assayed; Tubulin staining is used as a loading control. Note the high content of c-Fos in the GM sample as compared to the almost undetectable levels in the NP sample. Adapted from Silvestre et al., 2010 (this is an open-access article distributed under the terms of the Creative Commons Attribution License, which permits unrestricted use, distribution, and reproduction in any medium, provided the original author and source are credited).

of recombinant c-Fos to the c-Fos-devoid assay media re-established lipid synthesis levels (**Figure 5**).

Confirmation of the dependence of tumor growth on c-Fos expression was obtained in NPcis mice, a mouse model of the human disease Neurofibromatosis Type 1. These animals spontaneously develop central and peripheral nervous system tumors. In these mice, tumor progression is slowed down or even stopped by blocking c-Fos expression, in concordance with an abrogation of phospholipid synthesis activation in spite that AP-1 content is not substantially affected (Silvestre et al., 2010). Strikingly, NPcis *fos* (−/−) mice do not develop tumors in contrast to their *fos* (+/−) or *fos* (+/+) littermates, in which tumor development was observed in 71% of the animals (Silvestre et al., 2010). These *in vivo* examples of the dependence on c-Fos for nervous system tumors to grow disclose c-Fos as a potential target to control brain cancer.

FINAL COMMENTS

All the above-mentioned results highlight the relevance of c-Fos for the development of the nervous system. The emergence of an AP-1-independent function that relies on the capacity of c-Fos to activate lipid synthesis provides an explanation for many results observed upon the induction of c-Fos expression that remained obscure even though almost 35 years have passed since the first description of this protein. To the best of our knowledge, c-Fos is the first transcription factor with the capacity to regulate lipid synthesis independently of its canonical transcriptional function. The SREBPs transcription factors, for example, are tightly linked to fatty acid and cholesterol synthesis but only through their genomic activity in the nucleus (Eberle et al., 2004; Cheng et al., 2018).

Many questions regarding the cytoplasmic function of c-Fos remain to be elucidated. Clearly, c-Fos expression is related to changes in cell cycle and morphology, controlling different aspects of development (Hess et al., 2004). The fact that c-Fos can act in two different ways, either as an AP-1 transcription factor or activating lipid synthesis, raises the interrogation about how these two functions are coordinated or which are the signals that trigger one or the other function to exert a physiological/pathological role. It has been proposed that AP-1 fulfills a homeostatic role in cells in response to changes in their environment and growth conditions, adjusting gene expression so as to allow the cell to adapt to those changes (Shaulian and Karin, 2001). If we now consider the function of c-Fos as a lipid synthesis activator, the perspective must necessarily be deepened. It seems reasonable to think that the elicited function will depend on the triggering stimulus. In any case, studies must be extended in order to further elucidate this novel mechanism.

c-Fos was the first transcription factor whose induction was shown to be dependent on neuronal activity (Morgan and Curran, 1988; Sagar et al., 1988). As stated previously, this attribute rapidly transformed c-Fos into a marker for neuronal activity. The increase in its expression was observed in the central nervous system after applying learning and memory recovery protocols (Gallo et al., 2018). Interestingly, these changes in c-Fos expression were observed mainly during the first training sessions, indicating that this is probably an adaptive response. Consequently, it seems reasonable to propose that, in light of the above mentioned evidence, this adaptive response might be entailed with neuronal and synaptic plasticity processes that involve the cytoplasmic function of c-Fos: once all the new circuits related to a specific training are formed and established, the cells require a lower amount of lipids just to maintain all the pre-formed contacts. In fact, a reduction in synaptic plasticity mechanisms was found in the hippocampus of a selective *fos* knock-out mouse (Fleischmann et al., 2003).

In any case, all the background information described in the literature regarding the role of c-Fos in the physiology of the nervous system consistently confirmed its importance for cellular plasticity although they have always been associated to changes in gene expression. But, could they be related to changes in lipid homeostasis? This hypothesis seems reasonable given the evidence underlined herein. In this regard, we are currently finishing additional studies on the role of c-Fos in neuronal differentiation, using primary cultures as development models. This will allow us to unravel the mechanisms through which c-Fos participates in normal brain development.

The apparently unrelated functions of c-Fos as a transcription factor or as an activator of lipid synthesis may be related to its structural plasticity given its nature as an Intrinsically Disordered Protein (IDP), a characteristic already described for other proteins (Tompa, 2005). IDPs do not have a tridimensional defined structure in their native states (Dyson and Wright, 2005). This feature gives them the advantage of having conformational plasticity and allows them to recognize and associate with multiple, different targets (Wright and Dyson, 2009). Even though we have described that the N-terminal of c-Fos together with its BD are responsible for its association with different enzymes and their subsequent activation, it is yet to be determined if c-Fos suffers a conformational change to an ordered structure during this process.

It is promising to consider the reaches of this new role of c-Fos in physiological and pathological aspects of the nervous system. It could be involved in controlling neuronal development and in the establishment of correct neuronal circuits, or in regeneration events that require high amounts of lipid synthesis for membrane biogenesis. More importantly, the possible participation of c-Fos in lipid homeostasis in the neurobiology of disease should be approached. Highlighting the importance of lipid synthesis activation by c-Fos is the observation that, by specifically blocking its expression, proliferation and growth of tumor cells of the nervous system are slowed or halted. This discloses the cytoplasmic activity of c-Fos as a potential target for controlling growth of brain carcinomas. Future studies are being driven through this exciting road.

AUTHOR CONTRIBUTIONS

Both authors participated in the preparation of the manuscript.

FUNDING

The authors thank the financial support of the following institutions: the Secretaría de Ciencia y Técnica, Universidad Nacional de Córdoba; the Fondo para la Investigación Científica y Tecnológica, Secretaría de Ciencia, Tecnología e Innovación Productiva, Argentina; and the Instituto Nacional del Cáncer, Ministerio de Salud y Desarrollo Social, Argentina. BC is a member of and LB a fellow of CONICET (Consejo Nacional de Investigaciones Científicas y Tecnológicas), Secretaría de Ciencia, Tecnología e Innovación Productiva, Argentina.

REFERENCES

Ahmed, M. Y., Al-Khayat, A., Al-Murshedi, F., Al-Futaisi, A., Chioza, B. A., Pedro Fernandez-Murray, J., et al. (2017). A mutation of EPT1 (SELENOI) underlies a new disorder of Kennedy pathway phospholipid biosynthesis. *Brain* 140, 547–554. doi: 10.1093/brain/aww318

Alfonso Pecchio, A. R., Cardozo Gizzi, A. M., Renner, M. L., Molina-Calavita, M., and Caputto, B. L. (2011). c-Fos activates and physically interacts with specific enzymes of the pathway of synthesis of polyphosphoinositides. *Mol. Biol. Cell* 22, 4716–4725. doi: 10.1091/mbc.E11-03-0259

Angel, P., and Karin, M. (1991). The role of Jun, Fos and the AP-1 complex in cell-proliferation and transformation. *Biochim. Biophys. Acta* 1072, 129–157. doi: 10.1016/0304-419x(91)90011-9

Bazan, N. G. (2014). Is there a molecular logic that sustains neuronal functional integrity and survival? Lipid signaling is necessary for neuroprotective neuronal transcriptional programs. *Mol. Neurobiol.* 50, 1–5. doi: 10.1007/s12035-014-8897-0

Bazan, N. G., Molina, M. F., and Gordon, W. C. (2011). Docosahexaenoic acid signalolipidomics in nutrition: significance in aging, neuroinflammation, macular degeneration, Alzheimer's, and other neurodegenerative diseases. *Annu. Rev. Nutr.* 31, 321–351. doi: 10.1146/annurev.nutr.012809.104635

Bozek, K., Wei, Y., Yan, Z., Liu, X., Xiong, J., Sugimoto, M., et al. (2015). Organization and evolution of brain lipidome revealed by large-scale analysis of human, chimpanzee, macaque, and mouse tissues. *Neuron* 85, 695–702. doi: 10.1016/j.neuron.2015.01.003

Buscher, M., Rahmsdorf, H. J., Litfin, M., Karin, M., and Herrlich, P. (1988). Activation of the c-fos gene by UV and phorbol ester: different signal transduction pathways converge to the same enhancer element. *Oncogene* 3, 301–311.

Bussolino, D. F., De Arriba Zerpa, G. A., Grabois, V. R., Conde, C. B., Guido, M. E., and Caputto, B. L. (1998). Light affects c-fos expression and phospholipid synthesis in both retinal ganglion cells and photoreceptor cells in an opposite way for each cell type. *Brain Res. Mol. Brain Res.* 58, 10–15. doi: 10.1016/s0169-328x(98)00065-5

Bussolino, D. F., Guido, M. E., Gil, G. A., Borioli, G. A., Renner, M. L., Grabois, V. R., et al. (2001). c-Fos associates with the endoplasmic reticulum and activates phospholipid metabolism. *FASEB J.* 15, 556–558. doi: 10.1096/fj.00-0446fje

Caputto, B. L., Cardozo Gizzi, A. M., and Gil, G. A. (2014). c-Fos: an AP-1 transcription factor with an additional cytoplasmic, non-genomic lipid synthesis activation capacity. *Biochim. Biophys. Acta* 1841, 1241–1246. doi: 10.1016/j.bbalip.2014.05.007

Cardozo Gizzi, A. M., Prucca, C. G., Gaveglio, V. L., Renner, M. L., Pasquare, S. J., and Caputto, B. L. (2015). The catalytic efficiency of lipin 1beta increases by physically interacting with the proto-oncoprotein c-Fos. *J. Biol. Chem.* 290, 29578–29592. doi: 10.1074/jbc.M115.678821

Chang, T. Y., Yamauchi, Y., Hasan, M. T., and Chang, C. (2017). Cellular cholesterol homeostasis and Alzheimer's disease. *J. Lipid Res.* 58, 2239–2254. doi: 10.1194/jlr.R075630

Cheng, C., Geng, F., Cheng, X., and Guo, D. (2018). Lipid metabolism reprogramming and its potential targets in cancer. *Cancer Commun.* 38:27.

Crespo, P. M., Silvestre, D. C., Gil, G. A., Maccioni, H. J., Daniotti, J. L., and Caputto, B. L. (2008). c-Fos activates glucosylceramide synthase and glycolipid synthesis in PC12 cells. *J. Biol. Chem.* 283, 31163–31171. doi: 10.1074/jbc.M709257200

Curran, T., and Franza, B. R. (1988). Fos and Jun: the AP-1 connection. *Cell* 55, 395–397. doi: 10.1016/0092-8674(88)90024-4

Dragunow, M. (1996). A role for immediate-early transcription factors in learning and memory. *Behav. Genet.* 26, 293–299. doi: 10.1007/bf02359385

Dyson, H. J., and Wright, P. E. (2005). Intrinsically unstructured proteins and their functions. *Nat. Rev. Mol. Cell. Biol.* 6, 197–208. doi: 10.1038/nrm1589

Eberle, D., Hegarty, B., Bossard, P., Ferre, P., and Foufelle, F. (2004). SREBP transcription factors: master regulators of lipid homeostasis. *Biochimie* 86, 839–848. doi: 10.1016/j.biochi.2004.09.018

Farooqui, A. A. (2012). Lipid mediators and their metabolism in the nucleous: implications for Alzheimer's disease. *J. Alzheimers Dis.* 30(Suppl. 2), S163–S178. doi: 10.3233/JAD-2011-111085

Ferreira-Vieira, T. H., Guimaraes, I. M., Silva, F. R., and Ribeiro, F. M. (2016). Alzheimer's disease: targeting the cholinergic system. *Curr. Neuropharmacol.* 14, 101–115.

Ferrero, G. O., Renner, M. L., Gil, G. A., Rodriguez-Berdini, L., and Caputto, B. L. (2014). c-Fos-activated synthesis of nuclear phosphatidylinositol 4,5-bisphosphate [PtdIns(4,5)P(2)] promotes global transcriptional changes. *Biochem. J.* 461, 521–530. doi: 10.1042/bj20131376

Ferrero, G. O., Velazquez, F. N., and Caputto, B. L. (2012). The kinase c-Src and the phosphatase TC45 coordinately regulate c-Fos tyrosine phosphorylation and c-Fos phospholipid synthesis activation capacity. *Oncogene* 31, 3381–3391. doi: 10.1038/onc.2011.510

Fleischmann, A., Hvalby, O., Jensen, V., Strekalova, T., Zacher, C., Layer, L. E., et al. (2003). Impaired long-term memory and NR2A-type NMDA receptor-dependent synaptic plasticity in mice lacking c-Fos in the CNS. *J. Neurosci.* 23, 9116–9122. doi: 10.1523/jneurosci.23-27-09116.2003

Gallo, F. T., Katche, C., Morici, J. F., Medina, J. H., and Weisstaub, N. V. (2018). Immediate early genes, memory and psychiatric disorders: focus on c-Fos, Egr1 and Arc. *Front. Behav. Neurosci.* 12:79. doi: 10.3389/fnbeh.2018.00079

Gaspar, R., Pallbo, J., Weininger, U., Linse, S., and Sparr, E. (2018). Ganglioside lipids accelerate alpha-synuclein amyloid formation. *Biochim. Biophys. Acta Proteins Proteom*. doi: 10.1016/j.bbapap.2018.07.004 [Epub ahead of print].

Gil, G. A., Bussolino, D. F., Portal, M. M., Alfonso Pecchio, A., Renner, M. L., Borioli, G. A., et al. (2004). c-Fos activated phospholipid synthesis is required for neurite elongation in differentiating PC12 cells. *Mol. Biol. Cell* 15, 1881–1894. doi: 10.1091/mbc.e03-09-0705

Glover, J. N., and Harrison, S. C. (1995). Crystal structure of the heterodimeric bZIP transcription factor c-Fos-c-Jun bound to DNA. *Nature* 373, 257–261. doi: 10.1038/373257a0

Gonzalez, C., and Couve, A. (2014). The axonal endoplasmic reticulum and protein trafficking: cellular bootlegging south of the soma. *Semin. Cell Dev. Biol.* 27, 23–31. doi: 10.1016/j.semcdb.2013.12.004

Grimm, R., and Tischmeyer, W. (1997). Complex patterns of immediate early gene induction in rat brain following brightness discrimination training and pseudotraining. *Behav. Brain Res.* 84, 109–116. doi: 10.1016/s0166-4328(97)83330-x

Guido, M. E., De Arriba Zerpa, G. A., Bussolino, D. F., and Caputto, B. L. (1996). Immediate early gene c-fos regulates the synthesis of phospholipids but not of gangliosides. *J. Neurosci. Res.* 43, 93–98. doi: 10.1002/jnr.490430112

Habchi, J., Chia, S., Galvagnion, C., Michaels, T. C. T., Bellaiche, M. M. J., Ruggeri, F. S., et al. (2018). Cholesterol catalyses Abeta42 aggregation through a heterogeneous nucleation pathway in the presence of lipid membranes. *Nat. Chem.* 10, 673–683. doi: 10.1038/s41557-018-0031-x

Hamilton, J. A., Hillard, C. J., Spector, A. A., and Watkins, P. A. (2007). Brain uptake and utilization of fatty acids, lipids and lipoproteins: application to neurological disorders. *J. Mol. Neurosci.* 33, 2–11. doi: 10.1007/s12031-007-0060-1

Herdegen, T., and Waetzig, V. (2001). AP-1 proteins in the adult brain: facts and fiction about effectors of neuroprotection and neurodegeneration. *Oncogene* 20, 2424–2437. doi: 10.1038/sj.onc.1204387

Hess, J., Angel, P., and Schorpp-Kistner, M. (2004). AP-1 subunits: quarrel and harmony among siblings. *J. Cell Sci.* 117, 5965–5973. doi: 10.1242/jcs.01589

Hooijmans, C. R., Van Der Zee, C. E., Dederen, P. J., Brouwer, K. M., Reijmer, Y. D., Van Groen, T., et al. (2009). DHA and cholesterol containing diets influence Alzheimer-like pathology, cognition and cerebral vasculature in APPswe/PS1dE9 mice. *Neurobiol. Dis.* 33, 482–498. doi: 10.1016/j.nbd.2008.12.002

Kim, H. Y., Huang, B. X., and Spector, A. A. (2014). Phosphatidylserine in the brain: metabolism and function. *Prog. Lipid Res.* 56, 1–18. doi: 10.1016/j.plipres.2014.06.002

Lauwers, E., Goodchild, R., and Verstreken, P. (2016). Membrane lipids in presynaptic function and disease. *Neuron* 90, 11–25. doi: 10.1016/j.neuron.2016.02.033

Ledeen, R. W. (1985). *Transport, Exchange, and Transfer of Phospholipids in the Nervous System*. New York, NY: John Wiley & Sons Inc.

Lindsey, J. D., and Ellisman, M. H. (1985). The neuronal endomembrane system. III. The origins of the axoplasmic reticulum and discrete axonal cisternae at the axon hillock. *J. Neurosci.* 5, 3135–3144. doi: 10.1523/jneurosci.05-12-03135.1985

Luarte, A., Cornejo, V. H., Bertin, F., Gallardo, J., and Couve, A. (2018). The axonal endoplasmic reticulum: one organelle-many functions in development, maintenance, and plasticity. *Dev. Neurobiol.* 78, 181–208. doi: 10.1002/dneu.22560

Lukiw, W. J., and Bazan, N. G. (2000). Neuroinflammatory signaling upregulation in Alzheimer's disease. *Neurochem. Res.* 25, 1173–1184.

Milde-Langosch, K. (2005). The Fos family of transcription factors and their role in tumourigenesis. *Eur. J. Cancer* 41, 2449–2461. doi: 10.1016/j.ejca.2005.08.008

Miller, A. D., Curran, T., and Verma, I. M. (1984). c-fos protein can induce cellular transformation: a novel mechanism of activation of a cellular oncogene. *Cell* 36, 51–60. doi: 10.1016/0092-8674(84)90073-4

Minatohara, K., Akiyoshi, M., and Okuno, H. (2015). Role of immediate-early genes in synaptic plasticity and neuronal ensembles underlying the memory trace. *Front. Mol. Neurosci.* 8:78. doi: 10.3389/fnmol.2015.00078

Morgan, J. I., and Curran, T. (1988). Calcium as a modulator of the immediate-early gene cascade in neurons. *Cell Calcium* 9, 303–311. doi: 10.1016/0143-4160(88)90011-5

Motrich, R. D., Castro, G. M., and Caputto, B. L. (2013). Old players with a newly defined function: Fra-1 and c-Fos support growth of human malignant breast tumors by activating membrane biogenesis at the cytoplasm. *PLoS One* 8:e53211. doi: 10.1371/journal.pone.0053211

Oster, T., and Pillot, T. (2010). Docosahexaenoic acid and synaptic protection in Alzheimer's disease mice. *Biochim. Biophys. Acta* 1801, 791–798. doi: 10.1016/j.bbalip.2010.02.011

Palay, S. L. (1958). The morphology of synapses in the central nervous system. *Exp Cell Res* 14, 275–293.

Palumbo, S. (2017). "Pathogenesis and progression of multiple sclerosis: the role of arachidonic acid-mediated neuroinflammation," in *Multiple Sclerosis: Perspectives in Treatment and Pathogenesis*, eds I. S. Zagon and P. J. Mclaughlin (Brisbane: Codon Publications).

Penke, B., Paragi, G., Gera, J., Berkecz, R., Kovacs, Z., Crul, T., et al. (2018). The role of lipids and membranes in the pathogenesis of Alzheimer's disease: a comprehensive view. *Curr. Alzheimer Res.* 15, 1191–1212. doi: 10.2174/1567205015666180911151716

Pepeu, G., and Grazia Giovannini, M. (2017). The fate of the brain cholinergic neurons in neurodegenerative diseases. *Brain Res.* 1670, 173–184. doi: 10.1016/j.brainres.2017.06.023

Pfenninger, K. H. (2009). Plasma membrane expansion: a neuron's Herculean task. *Nat. Rev. Neurosci.* 10, 251–261. doi: 10.1038/nrn2593

Piechaczyk, M., and Blanchard, J. M. (1994). c-fos proto-oncogene regulation and function. *Crit. Rev. Oncol. Hematol.* 17, 93–131. doi: 10.1016/1040-8428(94)90021-3

Portal, M. M., Ferrero, G. O., and Caputto, B. L. (2007). N-Terminal c-Fos tyrosine phosphorylation regulates c-Fos/ER association and c-Fos-dependent phospholipid synthesis activation. *Oncogene* 26, 3551–3558. doi: 10.1038/sj.onc.1210137

Posse de Chaves, E., Vance, D. E., Campenot, R. B., and Vance, J. E. (1995). Axonal synthesis of phosphatidylcholine is required for normal axonal growth in rat sympathetic neurons. *J. Cell Biol.* 128, 913–918. doi: 10.1083/jcb.128.5.913

Raivich, G., and Behrens, A. (2006). Role of the AP-1 transcription factor c-Jun in developing, adult and injured brain. *Prog. Neurobiol.* 78, 347–363. doi: 10.1016/j.pneurobio.2006.03.006

Rambourg, A., and Droz, B. (1980). Smooth endoplasmic reticulum and axonal transport. *J. Neurochem.* 35, 16–25. doi: 10.1111/j.1471-4159.1980.tb12484.x

Rosen, J. B., Fanselow, M. S., Young, S. L., Sitcoske, M., and Maren, S. (1998). Immediate-early gene expression in the amygdala following footshock stress and contextual fear conditioning. *Brain Res.* 796, 132–142. doi: 10.1016/s0006-8993(98)00294-7

Sagar, S. M., Sharp, F. R., and Curran, T. (1988). Expression of c-fos protein in brain: metabolic mapping at the cellular level. *Science* 240, 1328–1331. doi: 10.1126/science.3131879

Sanchez-Mejia, R. O., and Mucke, L. (2010). Phospholipase A2 and arachidonic acid in Alzheimer's disease. *Biochim. Biophys. Acta* 1801, 784–790. doi: 10.1016/j.bbalip.2010.05.013

Sastry, P. S. (1985). Lipids of nervous tissue: composition and metabolism. *Prog. Lipid Res.* 24, 69–176. doi: 10.1016/0163-7827(85)90011-6

Shaulian, E., and Karin, M. (2001). AP-1 in cell proliferation and survival. *Oncogene* 20, 2390–2400. doi: 10.1038/sj.onc.1204383

Silvestre, D. C., Gil, G. A., Tomasini, N., Bussolino, D. F., and Caputto, B. L. (2010). Growth of peripheral and central nervous system tumors is supported by cytoplasmic c-Fos in humans and mice. *PLoS One* 5:e9544. doi: 10.1371/journal.pone.0009544

Simon, M. V., Agnolazza, D. L., German, O. L., Garelli, A., Politi, L. E., Agbaga, M. P., et al. (2016). Synthesis of docosahexaenoic acid from eicosapentaenoic acid in retina neurons protects photoreceptors from oxidative stress. *J. Neurochem.* 136, 931–946. doi: 10.1111/jnc.13487

Strokin, M., Chechneva, O., Reymann, K. G., and Reiser, G. (2006). Neuroprotection of rat hippocampal slices exposed to oxygen-glucose deprivation by enrichment with docosahexaenoic acid and by inhibition of hydrolysis of docosahexaenoic acid-containing phospholipids by calcium independent phospholipase A2. *Neuroscience* 140, 547–553. doi: 10.1016/j.neuroscience.2006.02.026

Tayebati, S. K. (2018). Phospholipid and Lipid Derivatives as Potential Neuroprotective Compounds. *Molecules* 23:E2257. doi: 10.3390/molecules23092257

Terasaki, M. (2018). Axonal endoplasmic reticulum is very narrow. *J. Cell Sci.* 131:jcs210450. doi: 10.1242/jcs.210450

Tompa, P. (2005). The interplay between structure and function in intrinsically unstructured proteins. *FEBS Lett.* 579, 3346–3354. doi: 10.1016/j.febslet.2005.03.072

Tracey, T. J., Steyn, F. J., Wolvetang, E. J., and Ngo, S. T. (2018). Neuronal lipid metabolism: multiple pathways driving functional outcomes in health and disease. *Front. Mol. Neurosci.* 11:10. doi: 10.3389/fnmol.2018.00010

Tsukita, S., and Ishikawa, H. (1976). Three-dimensional distribution of smooth endoplasmic reticulum in myelinated axons. *J. Electron. Microsc.* 25, 141–149.

Tulchinsky, E. (2000). Fos family members: regulation, structure and role in oncogenic transformation. *Histol. Histopathol.* 15, 921–928. doi: 10.14670/HH-15.921

Valadas, J. S., Esposito, G., Vandekerkhove, D., Miskiewicz, K., Deaulmerie, L., Raitano, S., et al. (2018). ER lipid defects in neuropeptidergic neurons impair sleep patterns in Parkinson's disease. *Neuron* 98, 1155–1169.e6. doi: 10.1016/j.neuron.2018.05.022

van Meer, G., Voelker, D. R., and Feigenson, G. W. (2008). Membrane lipids: where they are and how they behave. *Nat. Rev. Mol. Cell. Biol.* 9, 112–124. doi: 10.1038/nrm2330

Vance, J. E., Campenot, R. B., and Vance, D. E. (2000). The synthesis and transport of lipids for axonal growth and nerve regeneration. *Biochim. Biophys. Acta* 1486, 84–96. doi: 10.1016/s1388-1981(00)00050-0

Vance, J. E., Pan, D., Campenot, R. B., Bussiere, M., and Vance, D. E. (1994). Evidence that the major membrane lipids, except cholesterol, are made in axons of cultured rat sympathetic neurons. *J. Neurochem.* 62, 329–337. doi: 10.1046/j.1471-4159.1994.62010329.x

Vance, J. E., Pan, D., Vance, D. E., and Campenot, R. B. (1991). Biosynthesis of membrane lipids in rat axons. *J. Cell Biol.* 115, 1061–1068. doi: 10.1083/jcb.115.4.1061

Velazquez, F. N., Caputto, B. L., and Boussin, F. D. (2015a). c-Fos importance for brain development. *Aging* 7, 1028–1029. doi: 10.18632/aging.100862

Velazquez, F. N., Prucca, C. G., Etienne, O., D'astolfo, D. S., Silvestre, D. C., Boussin, F. D., et al. (2015b). Brain development is impaired in c-fos -/- mice. *Oncotarget* 6, 16883–16901.

Wang, H. (2014). Lipid rafts: a signaling platform linking cholesterol metabolism to synaptic deficits in autism spectrum disorders. *Front. Behav. Neurosci.* 8:104. doi: 10.3389/fnbeh.2014.00104

Weiss, P., and Hiscoe, H. B. (1948). Experiments on the mechanism of nerve growth. *J. Exp. Zool.* 107, 315–395. doi: 10.1002/jez.1401070302

Wollnik, F., Brysch, W., Uhlmann, E., Gillardon, F., Bravo, R., Zimmermann, M., et al. (1995). Block of c-Fos and JunB expression by antisense oligonucleotides inhibits light-induced phase shifts of the mammalian circadian clock. *Eur. J. Neurosci.* 7, 388–393. doi: 10.1111/j.1460-9568.1995.tb00334.x

Wright, P. E., and Dyson, H. J. (2009). Linking folding and binding. *Curr. Opin. Struct. Biol.* 19, 31–38. doi: 10.1016/j.sbi.2008.12.003

Yu, Q., He, Z., Zubkov, D., Huang, S., Kurochkin, I., Yang, X., et al. (2018). Lipidome alterations in human prefrontal cortex during development, aging, and cognitive disorders. *Mol. Psychiatry* doi: 10.1038/s41380-018-0200-8 [Epub ahead of print].

Conflict of Interest Statement: The authors declare that the research was conducted in the absence of any commercial or financial relationships that could be construed as a potential conflict of interest.

frontiers in Cellular Neuroscience

MINI REVIEW
published: 21 May 2019
doi: 10.3389/fncel.2019.00212

Lipid Metabolism Crosstalk in the Brain: Glia and Neurons

*Casey N. Barber and Daniel M. Raben**

Department of Biological Chemistry, The Johns Hopkins University School of Medicine, Baltimore, MD, United States

Until recently, glial cells have been considered mainly support cells for neurons in the mammalian brain. However, many studies have unveiled a variety of glial functions including electrolyte homeostasis, inflammation, synapse formation, metabolism, and the regulation of neurotransmission. The importance of these functions illuminates significant crosstalk between glial and neuronal cells. Importantly, it is known that astrocytes secrete signals that can modulate both presynaptic and postsynaptic function. It is also known that the lipid compositions of the pre- and post-synaptic membranes of neurons greatly impact functions such as vesicle fusion and receptor mobility. These data suggest an essential lipid-mediated communication between glial cells and neurons. Little is known, however, about how the lipid metabolism of both cell types may interact. In this review, we discuss neuronal and glial lipid metabolism and suggest how they might interact to impact neurotransmission.

Keywords: neurons, lipids, glial, CNS, communication

OPEN ACCESS

Edited by:
Gabriela Alejandra Salvador, Universidad Nacional del Sur, Argentina

Reviewed by:
Randy Franklin Stout, New York Institute of Technology, United States
Arturo Ortega, Centro de Investigación y de Estudios Avanzados (CINVESTAV), Mexico

****Correspondence:***
Daniel M. Raben
draben@jhmi.edu

Specialty section:
This article was submitted to Cellular Neurophysiology, a section of the journal Frontiers in Cellular Neuroscience

Received: *01 February 2019*
Accepted: *26 April 2019*
Published: *21 May 2019*

Citation:
Barber CN and Raben DM (2019) Lipid Metabolism Crosstalk in the Brain: Glia and Neurons. Front. Cell. Neurosci. 13:212. doi: 10.3389/fncel.2019.00212

Research on glial cells began in 1846, when Rudolf Virchow described a "substance" in which the various parts of the nervous system were embedded. In subsequent years, different kinds of glial cells were discovered and classified. Even though Santiago Ramon y Cajal was the first to propose a wide and diverse list of the functions of glia, these cells were viewed as simple neuronal support cells (García-Marín et al., 2007). In the last 20 years, however, studies have illuminated many functions of glia, highlighting their significance within the nervous system. In addition to providing many homeostatic functions to neurons, glial cells play a large role in regulating neurotransmission. Currently, much is known about lipid metabolism within neurons and glia separately, but little is known about potential lipid metabolic crosstalk between the two cell types. Here, we propose that lipid metabolism specifically from glial cells affects neurotransmission by regulating the rates of synaptic vesicle exo- and endocytosis. We will describe the known functions of glia and their lipid metabolism and then describe how glial lipid metabolism can possibly interact with neuronal lipid metabolism to regulate neurotransmission within the mammalian central nervous system.

Glial cells are the predominant cell type in the mammalian brain. They can contribute to 33–66% of the brain's total mass. Glial cells are segregated into three main classifications: astrocytes, microglia, and oligodendrocytes. Importantly, each cell type performs critical functions that sustain the health and function of the surrounding neurons. Astrocytes have many functions, among them are regulating water transport and ion levels in neurons, maintaining the blood brain barrier, and clearing glutamate from synapses to prevent neurotoxicity (Jäkel and Dimou, 2017). Microglia act as neuroprotectors by engulfing debris and cells in the process of apoptosis. Microglia actively surveil and respond to the state of functional synapses, such that they can sense dysfunctional synapses and influence information circuitry by either contributing to the repair or removal

of a cell (Graeber and Streit, 2010). In the developing brain, microglia actively phagocytose some synaptic material and have a critical role in synaptic pruning during maturation (Paolicelli et al., 2011). Oligodendrocytes are well-known as the myelin-producing glial cells that insulate axons to ensure rapid electrical conduction and also provide trophic support to neurons (Simons and Trajkovic, 2006). Together glial cells provide an abundance of support to neurons, and defects in glial cells are implicated in many neurological diseases such as Alzheimer's disease, amyotrophic lateral sclerosis, and herpes encephalitis (Tracey et al., 2018).

As mentioned above, much is known about the variety of functions performed by these non-neuronal cells within the mammalian brain. Specifically, there is a wealth of information regarding the brain's energy utilization and how glial cells and neurons work together to support the brain's energy demands (Pellerin et al., 2007; Bélanger et al., 2011; Bruce et al., 2017; Tracey et al., 2018). This is crucial, as 20% of the body's total ATP consumption occurs in the brain, primarily for restoring ion gradients and motor-driven transport, as well as other functions (Bélanger et al., 2011). However, not nearly as much is known about lipid metabolism within glial cells and its potential neuronal implications. Here, we would like to propose that there is significant lipid metabolic crosstalk between glia and neurons that could influence neuronal function and neurotransmission. This could be yet another example of how glial cells regulate synaptic transmission and brain function overall.

Lipid molecules are key components of the brain's complex structure and function, with lipids comprising around 50% of the brain's dry weight. The lipid composition of neuronal and glial cell membranes has been shown to affect cell function and neurotransmission (O'Brien and Sampson, 1965; Puchkov and Haucke, 2013). The brain is mainly comprised of long-chain polyunsaturated fatty acids (LC-PUFAs) such as eicosapentaenoic acid, docosahexaenoic acid, and arachidonic acid. Importantly, several recent studies provide evidence that fatty acids, including essential fatty acids which must be obtained from the diet, can cross the blood-brain barrier (BBB) and be taken up by neurons via fatty acid transporters. Both neurons and astrocytes express several fatty acid transporters such as FATP1, FATP4, and CD36. It was recently shown that fatty acid binding protein 7 (FABP7) knockout mice exhibit schizophrenic phenotypes, such as deficits in prepulse inhibition, related to mutated spine morphology. Neurons from these mice had a reduction in dendritic complexity, spine density, and maturity of spines of pyramidal neurons (Watanabe et al., 2007; Ebrahimi et al., 2016; Bruce et al., 2017).

It is also widely thought that neurons receive metabolic support from astrocytes in a number of ways, one of which being that fatty acid oxidation primarily occurs in astrocytes. After which, the metabolites (ketones, NADH, acetyl CoA, $FADH_2$) are taken up and utilized by neurons. Neurons are not energy-storing cells and do not normally contain a significant pool of lipid droplets or glycogen. Therefore, the available energy is depleted rapidly. This is one factor that makes them especially sensitive to stressful conditions such as continued stimulation. This is because the consumption of glycogen or fatty acids from lipid droplets is used in many other cell types as energy reserves. Periods of such high stimulation lead to increased reactive oxygen species (ROS) levels, which causes a buildup of peroxidated fatty acids. This is extremely harmful to neurons and must be prevented by removing or destroying the peroxidated fatty acids. In contrast to neurons, astrocytes store energy in the form of lipid droplets and act as a buffer to periods of toxic stimulation to neurons. Studies have shown that periods of high stress in neurons induce the formation of lipid droplets in nearby astrocytes, implying that overstimulated neurons may shuttle their peroxidated fatty acids to neighboring astrocytes (Bailey et al., 2015; Liu et al., 2015). This effect was found to be dependent on lipoproteins, the proteins responsible for trafficking fatty acids. In support of these studies, Ioannou et al. (2018) found that stressed neurons release peroxidated fatty acids bound to lipoproteins that are secreted by astrocytes or neurons. Neighboring astrocytes endocytose these lipoprotein-fatty acid particles and store the fatty acids in their lipid droplets. Astrocytes also react to overstimulated neurons by breaking down their lipid droplets and shuttling them to their own mitochondria for oxidative phosphorylation. Taken together, these data support the notion that astrocytes provide defense for overstimulated neurons by preventing fatty acid toxicity (Ioannou et al., 2018).

In addition to the metabolism of peroxidated lipids by astrocytes, most of the research regarding astrocytic lipid metabolism has been conducted specifically on cholesterol, and further research is required to study the metabolism of other lipids within astrocytes. Astrocytes and neurons both make cholesterol *de novo* but differ greatly in the pathways of cholesterol homeostasis and trafficking. Currently cholesterol metabolism within astrocytes serves as a model to illustrate the differences within neurons and astrocytes in pathways of synthesis, utilization, and efflux. Chen et al. (2013) found that astrocytes expel cholesterol with both lipid-free apolipoproteins and lipoproteins, while cholesterol efflux from neurons is induced only by lipoproteins. Lipoproteins are synthesized specifically by astrocytes and not neurons. While these proteins take cholesterol from neurons, they are also able to bind lipoprotein receptors within neuronal membranes that induce synaptogenesis (Chen et al., 2013).

Cholesterol is particularly enriched in synaptic membranes and affects a number of properties including endo- and exocytosis, lipid raft formation, and membrane fluidity, all of which greatly regulate neurotransmission. Therefore, the synthesis and transport of cholesterol is a modulating factor of synaptic signaling. Camargo et al. (2012) found that the synthesis of cholesterol, as well as fatty acids, within astrocytes is dependent on sterol regulatory element binding proteins (SREBPs). It was later found that components of the SREBP pathway are most highly expressed in hippocampal astrocytes. Importantly, a decrease in SREBP activity in astrocytes leads to a defect in synaptic function and plasticity. Mutated proteins within the astrocyte SREBP pathway caused a defect in synaptic structure, vesicle populations, and presynaptic function. Specifically, synapses in mice in which the SREBP cleavage-activating protein (SCAP) was deleted from GFAP-expressing

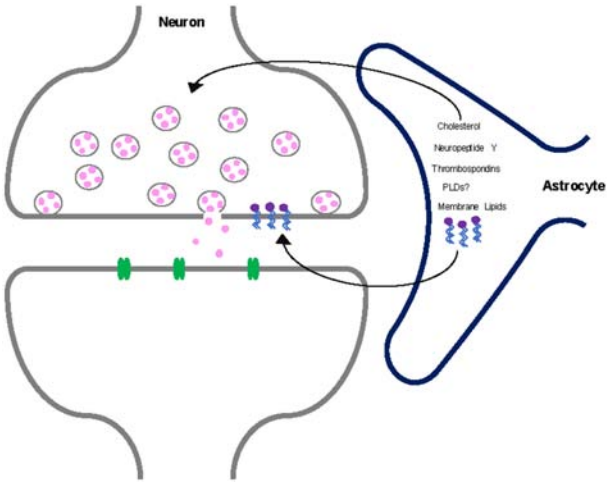

FIGURE 1 | Astrocytes secrete many factors that are critical to neuron function such as cholesterol, neuropeptide Y, thrombospondins, and other metabolic intermediates. We hypothesize that membrane lipids are also secreted by astrocytes and taken up by neurons to regulate neurotransmission. Additionally, PLDs selectively expressed within astrocytes may contribute to this astrocytic lipid metabolism.

cells were found to have lower levels of SNAP-25, a crucial SNARE protein involved in vesicle fusion with the presynaptic membrane (van Deijk et al., 2017). This is a critical example of how elements produced within glial cells can be transferred to neurons to affect synaptic transmission.

The phospholipid composition of presynaptic membranes contributes to the regulation of the rates of synaptic vesicle exo- and endocytosis. The shapes of particular lipids affect the membrane curvature and make the architecture more or less susceptible to vesicle fusion. Cholesterol, diacylglycerol, and phosphatidic acid are cone-shaped lipids and induce negative membrane curvature, promoting membrane fusion (Ammar et al., 2013). In addition to affecting membrane curvature, these lipids also bind important protein regulators of vesicle fusion, such as syntaxin-1A, NSF, and small GTPases (Jang et al., 2012). Therefore, portions of the membrane that are more highly enriched in these cone-shaped lipids are potentially more likely to undergo vesicle fusion, highlighting the phospholipid composition of synaptic membranes as a regulating factor of synaptic vesicle cycling.

So how is the lipid composition of membranes determined? What factors play a role in regulating the relative amounts of lipids within membranes? One of the most important factors are lipid-metabolizing enzymes, such as diacylglycerol kinases (DGKs) and phospholipases, that catalyze the conversion of these lipids. For example, DGKs and phospholipases D (PLDs) both produce phosphatidic acid from different substrates (Puchkov and Haucke, 2013). As phosphatidic acid is highly implicated in vesicle fusion, these enzymes are thought to be regulators of the synaptic vesicle cycle. In 2016, Goldschmidt et al. found that knockout of a particular DGK, DGKθ, in neurons resulted in significantly decreased rates of endocytosis after stimulation, in comparison to wildtype neurons. This is just one study, in addition to many others, that has discovered proteins with a regulatory role in the synaptic vesicle cycle (Rosahl et al., 1995; Südhof and Rizo, 1996; Wang et al., 1997; Turner et al., 1999; Reim et al., 2001; Pechstein et al., 2010; Lai et al., 2017). Many of these characterized proteins can be categorized by their mechanism of action on the SV cycle: regulation of calcium influx, regulation of SNARE dynamics, changes in membrane curvature, or synaptic vesicle priming. However, in some cases, the exact molecular actions of regulatory proteins have not been discovered. Being that the lipid membrane is the physical barrier between an intact synaptic vesicle and the synaptic cleft, it is not hard to imagine that the last regulatory step of vesicle fusion could be the lipid composition of the presynaptic membrane. This being so, the hypothesis that many SV regulatory proteins are lipid-metabolizing proteins is not inconceivable.

In addition to proteins, other factors influence the phospholipid composition of membranes. As discussed above, astrocytes synthesize lipids, and traffic them to neurons, offering another point of regulation by astrocytes. Also, they secrete signals that can influence synaptic transmission. These are often signaling factors that have downstream effects that influence synaptic vesicle fusion (Jäkel and Dimou, 2017). What about astrocytic factors that have a more direct impact on the synaptic vesicle cycle? We hypothesize that astrocytes have a direct role in regulating synaptic transmission via astrocyte lipid metabolism followed by transport to neurons. We suggest that astrocytes might be responsible for making some of the lipids that are directly inserted into the presynaptic plasma membrane. Other proteins, such as flippases, are likely involved that flip lipids into the inner membrane leaflet and sort these lipids into microdomains that make certain areas of the membrane susceptible for fusing with synaptic vesicles (Andersen et al., 2016). Astrocytes are involved in the transportation of several molecules and proteins to neurons, so membrane lipids such as phosphatidic acid could feasibly be transferred directly or indirectly from astrocytes to neurons. In fact, Tabernero et al. (2001) found that astrocytes secrete oleic acid and suggested that this is taken up by neurons for the process of phospholipid synthesis during neuronal differentiation. In addition to lipids, studies have also found that astrocytes secrete or release: large vesicles containing functional mitochondria, ATP, and lipid droplets (Falchi et al., 2013); dense-core vesicles containing neuropeptide Y (Ramamoorthy and Whim, 2008); glucose, lactate, glutamine, and glutamate through gap junctions connecting astrocytes (Giaume et al., 1997; Gandhi et al., 2009); thrombospondins and hevin, which act on neurons to promote synaptogenesis (Christopherson et al., 2005; Kucukdereli et al., 2011); and many other molecules and proteins such as glypicans, Wnts, and tumor necrosis factor α (TNFα) (Allen, 2014). Therefore, there is much evidence that astrocytes release many factors that affect neurons, and we propose that lipids are also an important astrocyte-secreted factor.

Astrocytic processes are intimately involved with synapses, comprising the tripartite synapse. Astrocytes have a wide, radial branching morphology, allowing them to physically protrude into the synaptic cleft between pre- and postsynaptic boutons

and exchange information with these elements, contributing to synaptic physiology (Perea et al., 2009). Therefore, it is conceivable that lipids may be transferred within the synaptic region of the neuron because of how closely related neurons and astrocytes are in physical space. In support of this hypothesis, Zhu et al. (2016) found that phosphatidic acid produced specifically from astrocytes regulates neurite outgrowth and dendritic branching in neurons. This study found that knockdown of PLD1 only in astrocytes led to a reduction in secretion of phosphatidic acid and a decrease in dendritic branching of neurons. Furthermore, neurons grown in the presence of conditioned media from astrocytes with PLD1 knockdown had significantly decreased dendritic branching. This study is an example of how secreted lipids from astrocytes can affect functional aspects of neurons.

Astrocytes could also synthesize other proteins that have regulatory roles in the synaptic vesicle cycle, thereby having a more indirect effect on neurotransmission. For instance, it is possible that specific lipid-metabolizing enzymes could be expressed only within glial cells and that mechanisms transfer the products of the reactions they catalyze from glial cells to neurons to affect membrane architecture. We hypothesize that PLD may be implicated in synaptic vesicle exocytosis. The localization and expression of PLD is currently unclear (Saito et al., 2000; Ammar et al., 2015; Vermeren et al., 2016), although some studies suggest that PLDs are localized within glial cells (Jin et al., 2002; Zhang et al., 2004; Zhu et al., 2016). The localization and expression pattern of PLDs in the brain needs to be clarified, but it is possible that PLDs are selectively expressed in astrocytes. If this is the case, astrocytes could produce phosphatidic acid by PLD that is trafficked to or taken up by neurons to influence the dynamics of synaptic vesicle fusion (**Figure 1**).

In conclusion, we believe that glial cells have a specific role in regulating synaptic transmission in neurons via lipid metabolism. The relative amount of certain lipids within neuronal membranes impacts the efficiency of endo- and exocytosis, and this could be developed by lipid synthesis or metabolism within glial cells. Further research is required to determine the expression of lipid-metabolizing enzymes within glial cells and pathways of lipid metabolism and trafficking. Regardless, astrocytes, microglia, and oligodendrocytes are vital components of the nervous system that contribute to regulating many neuronal functions, including synaptic transmission.

AUTHOR CONTRIBUTIONS

All authors listed have made a substantial, direct and intellectual contribution to the work, and approved it for publication.

FUNDING

This work was supported by grant from the National Institutes of Health (R01NS077923, DR).

REFERENCES

Allen, N. J. (2014). Astrocyte regulation of synaptic behavior. *Cell Dev. Biol.* 30, 439–463. doi: 10.1146/annurev-cellbio-100913-013053

Ammar, M., Kassas, N., Chasserot-Golaz, S., Bader, M. F., and Vitale, N. (2013). Lipids in regulated exocytosis: what are they doing? *Front. Endocrinol.* 4:125. doi: 10.3389/fendo.2013.00125

Ammar, M. R., Thahouly, T., Hanauer, A., Stegner, D., Nieswandt, B., and Vitale, N. (2015). PLD1 participates in BDNF-induced signalling in cortical neurons. *Sci. Rep.* 5:14778. doi: 10.1038/srep14778

Andersen, J. P., Vestergaard, A. L., Mikkelsen, S. A., Mogensen, L. S., Chalat, M., and Molday, R. S. (2016). P4-ATPases as phospholipid flippases—structure, function, and enigmas. *Front. Physiol.* 7:275. doi: 10.3389/fphys.2016.00275

Bailey, A. P., Koster, G., Guillermier, C., Hirst, E. M., MacRae, J. I., Lechene, C. P., et al. (2015). Antioxidant role for lipid droplets in a stem cell niche of drosophila. *Cell* 163, 340–353. doi: 10.1016/j.cell.2015.09.020

Bélanger, M., Allaman, I., and Magistretti, P. J. (2011). Brain Energy metabolism: focus on astrocyte-neuron metabolic cooperation. *Cell Metab.* 14, 724–738. doi: 10.1016/j.cmet.2011.08.016

Bruce, K. D., Zsombok, A., and Eckel, R. H. (2017). Lipid processing in the brain: a key regulator of systemic metabolism. *Front. Endocrinol.* 8:60. doi: 10.3389/fendo.2017.00060

Camargo, N., Brouwers, J. F., Loos, M., Gutmann, D. H., Smit, A. B., and Verheijen, M. H. (2012). High-fat diet ameliorates neurological deficits caused by defective astrocyte lipid metabolism. *FASEB J.* 26, 4302–4315. doi: 10.1096/fj.12-205807

Chen, J., Zhang, X., Kusumo, H., Costa, L. G., and Guizzetti, M. (2013). Cholesterol efflux is differentially regulated in neurons and astrocytes: implications for brain cholesterol homeostasis. *Biochim. Biophys. Acta Mol. Cell. Biol. Lipids* 1831, 263–275. doi: 10.1016/j.bbalip.2012.09.007

Christopherson, K. S., Ullian, E. M., Stokes, C. C., Mullowney, C. E., Hell, J. W., Agah, A., et al. (2005). Thrombospondins are astrocyte secreted proteins that promote CNS synaptogenesis. *Cell* 120, 421–433. doi: 10.1016/j.cell.2004.12.020

Ebrahimi, M., Yamamoto, Y., Sharifi, K., Kida, H., Kagawa, Y., Yasumoto, Y., et al. (2016). Astrocyte-expressed FABP7 regulates dendritic morphology and excitatory synaptic function of cortical neurons. *Glia* 64, 48–62. doi: 10.1002/glia.22902

Falchi, A. M., Sogos, V., Saba, F., Piras, M., Congiu, T., and Piludu, M. (2013). Astrocytes shed large membrane vesicles that contain mitochondria, lipid droplets and ATP. *Histochem. Cell Biol.* 139, 221–231. doi: 10.1007/s00418-012-1045-x

Gandhi, G. K., Cruz, N. F., Ball, K. K., Theus, S. A., and Dienel, G. A. (2009). Selective astrocytic gap junctional trafficking of molecules involved in the glycolytic pathway: impact on cellular brain imaging. *J. Neurochem.* 110, 857–869. doi: 10.1111/j.1471-4159.2009.06173.x

García-Marín, V., García-López, P., and Freire, M. (2007). Cajal's contributions to glia research. *Trends Neurosci.* 30, 479–487. doi: 10.1016/j.tins.2007.06.008

Giaume, C., Tabernero, A., and Medina, J. M. (1997). Metabolic trafficking through astrocytic gap junctions. *Glia* 21, 114–123. doi: 10.1002/(SICI)1098-1136(199709)21:1<114::AID-GLIA13>3.0.CO;2-V

Graeber, M. B., and Streit, W. J. (2010). Microglia: biology and pathology. *Acta Neuropathol.* 119, 89–105. doi: 10.1007/s00401-009-0622-0

Ioannou, M., Jackson, J., Sheu, S.-H., Chang, C.-L., Weigel, A. V., Liu, H., et al. (2018). Neuron-astrocyte metabolic coupling during neuronal stimulation protects against fatty acid toxicity. *Biorxiv* 465237. doi: 10.1101/465237

Jäkel, S., and Dimou, L. (2017). Glial cells and their function in the adult brain: a journey through the history of their ablation. *Front. Cell Neurosci.* 11:24. doi: 10.3389/fncel.2017.00024

Jang, J. H., Lee, C. S., Hwang, D., and Ryu, S. H. (2012). Understanding of the roles of phospholipase D and phosphatidic acid through their binding partners. *Prog. Lipid Res.* 51, 71–81. doi: 10.1016/j.plipres.2011.12.003

Jin, S., Schatter, B., Weichel, O., Walev, I., Ryu, S., and Klein, J. (2002). Stability of phospholipase D in primary astrocytes. *Biochem. Biophys. Res. Co* 297, 545–551. doi: 10.1016/S0006-291X(02)02231-3

Kucukdereli, H., Allen, N. J., Lee, A. T., Feng, A., Ozlu, M. I., Conatser, L. M., et al. (2011). Control of excitatory CNS synaptogenesis by astrocyte-secreted proteins Hevin and SPARC. *Proc. Natl. Acad. Sci. USA.* 108, E440–E49. doi: 10.1073/pnas.1104977108

Lai, Y., Choi, U. B., Leitz, J., Rhee, H. J., Lee, C., Altas, B., et al. (2017). Molecular mechanisms of synaptic vesicle priming by Munc13 and Munc18. *Neuron* 95, 591–607.e10. doi: 10.1016/j.neuron.2017.07.004

Liu, L., Zhang, K., Sandoval, H., Yamamoto, S., Jaiswal, M., Sanz, E., et al. (2015). Glial lipid droplets and ROS induced by mitochondrial defects promote neurodegeneration. *Cell* 160, 177–190. doi: 10.1016/j.cell.2014.12.019

O'Brien, J. S., and Sampson, E. L. (1965). Lipid composition of the normal human brain: gray matter, white matter, and myelin. *J. Lipid Res.* 6, 537–544.

Paolicelli, R. C., Bolasco, G., Pagani, F., Maggi, L., Scianni, M., Panzanelli, P., et al. (2011). Synaptic pruning by microglia is necessary for normal brain development. *Science* 333, 1456–1458. doi: 10.1126/science.1202529

Pechstein, A., Shupliakov, O., and Haucke, V. (2010). Intersectin 1: a versatile actor in the synaptic vesicle cycle. *Biochem. Soc. T* 38, 181–186. doi: 10.1042/BST0380181

Pellerin, L., Bouzier-Sore, A. K., Aubert, A., Serres, S., Merle, M., Costalat, R., et al. (2007). Activity-dependent regulation of energy metabolism by astrocytes: an update. *Glia* 55, 1251–1262. doi: 10.1002/glia.20528

Perea, G., Navarrete, M., and Araque, A. (2009). Tripartite synapses: astrocytes process and control synaptic information. *Trends Neurosci.* 32, 421–431. doi: 10.1016/j.tins.2009.05.001

Puchkov, D., and Haucke, V. (2013). Greasing the synaptic vesicle cycle by membrane lipids.*Trends Cell Biol.* 23, 493–503. doi: 10.1016/j.tcb.2013.05.002

Ramamoorthy, P., and Whim, M. D. (2008). Trafficking and fusion of neuropeptide Y-containing dense-core granules in astrocytes. *J. Neurosci.* 28, 13815–13827. doi: 10.1523/JNEUROSCI.5361-07.2008

Reim, K., Mansour, M., Varoqueaux, F., McMahon, H. T., Südhof, T. C., Brose, N., et al. (2001). Complexins regulate a late step in Ca2+-dependent neurotransmitter release. *Cell* 104, 71–81. doi: 10.1016/S0092-8674(01)0 0192-1

Rosahl, T. W., Spillane, D., Missler, M., Herz, J., Selig, D. K., Wolff, J. R., et al. (1995). Essential functions of synapsins I and II in synaptic vesicle regulation. *Nature* 375, 488–493. doi: 10.1038/375488a0

Saito, S., Sakagami, H., and Kondo, H. (2000). Localization of mRNAs for phospholipase D (PLD) type 1 and 2 in the brain of developing and mature rat. *Dev. Brain Res.* 120, 41–47. doi: 10.1016/S0165-3806(99)0 0189-3

Simons, M., and Trajkovic, K. (2006). Neuron-glia communication in the control of oligodendrocyte function and myelin biogenesis. *J. Cell Sci.* 119, 4381–4389. doi: 10.1242/jcs.03242

Südhof, T. C., and Rizo, J. (1996). Synaptotagmins: C2-domain proteins that regulate membrane traffic. *Neuron* 17, 379–388. doi: 10.1016/S0896-6273(00)80171-3

Tabernero, A., Lavado, E. M., Granda, B., Velasco, A., and Medina, J. M. (2001). Neuronal differentiation is triggered by oleic acid synthesized and released by astrocytes. *J. Neurochem.* 79, 606–616. doi: 10.1046/j.1471-4159.2001.00598.x

Tracey, T. J., Steyn, F. J., Wolvetang, E. J., and Ngo, S. T. (2018). Neuronal lipid metabolism: multiple pathways driving functional outcomes in health and disease. *Front. Mol. Neurosci.* 11:10. doi: 10.3389/fnmol.2018.00010

Turner, K. M., Burgoyne, R. D., and Morgan, A. (1999). Protein phosphorylation and the regulation of synaptic membrane traffic.*Trends Neurosci.* 22, 459–464. doi: 10.1016/S0166-2236(99)01436-8

van Deijk, A. F., Camargo, N., Timmerman, J., Heistek, T., Brouwers, J. F., Mogavero, F., et al. (2017). Astrocyte lipid metabolism is critical for synapse development and function *in vivo*. *Glia* 65, 670–682. doi: 10.1002/glia.23120

Vermeren, M. M., Zhang, Q., Smethurst, E., Segonds-Pichon, A., Schrewe, H., and Wakelam, M. J. (2016). The phospholipase D2 knock out mouse has ectopic purkinje cells and suffers from early adult-onset anosmia. *PLoS ONE* 11:e0162814. doi: 10.1371/journal.pone.0162814

Wang, Y., Okamoto, M., Schmitz, F., Hofmann, K., and Südhof, T. C. (1997). Rim is a putative Rab3 effector in regulating synaptic-vesicle fusion. *Nature* 388, 593–598. doi: 10.1038/41580

Watanabe, A., Toyota, T., Owada, Y., Hayashi, T., Iwayama, Y., Matsumata, M., et al. (2007). Fabp7 maps to a quantitative trait locus for a schizophrenia endophenotype. *PLoS Biol.* 5:e297. doi: 10.1371/journal.pbio.0050297

Zhang, Y., Huang, P., Du, G., Kanaho, Y., Frohman, M. A., and Tsirka, S. E. (2004). Increased expression of two phospholipase D isoforms during experimentally induced hippocampal mossy fiber outgrowth. *Glia* 46, 74–83. doi: 10.1002/glia.10322

Zhu, Y. B., Gao, W., Zhang, Y., Jia, F., Zhang, H. L., Liu, Y. Z., et al. (2016). Astrocyte-derived phosphatidic acid promotes dendritic branching. *Sci. Rep.* 6:21096. doi: 10.1038/srep21096

Conflict of Interest Statement: The authors declare that the research was conducted in the absence of any commercial or financial relationships that could be construed as a potential conflict of interest.

frontiers in Neuroscience

REVIEW
published: 24 May 2019
doi: 10.3389/fnins.2019.00513

The Complex Interactions Between Obesity, Metabolism and the Brain

Romina María Uranga[1,2]* *and Jeffrey Neil Keller*[3]*

[1] Instituto de Investigaciones Bioquímicas de Bahía Blanca, Universidad Nacional del Sur-Consejo Nacional de Investigaciones Científicas y Técnicas, Bahía Blanca, Argentina, [2] Departamento de Biología, Bioquímica y Farmacia, Universidad Nacional del Sur, Bahía Blanca, Argentina, [3] Pennington Biomedical Research Center, Louisiana State University System, Baton Rouge, LA, United States

Obesity is increasing at unprecedented levels globally, and the overall impact of obesity on the various organ systems of the body is only beginning to be fully appreciated. Because of the myriad of direct and indirect effects of obesity causing dysfunction of multiple tissues and organs, it is likely that there will be heterogeneity in the presentation of obesity effects in any given population. Taken together, these realities make it increasingly difficult to understand the complex interplay between obesity effects on different organs, including the brain. The focus of this review is to provide a comprehensive view of metabolic disturbances present in obesity, their direct and indirect effects on the different organ systems of the body, and to discuss the interaction of these effects in the context of brain aging and the development of neurodegenerative diseases.

Keywords: obesity, overweight, metabolic dysfunction, brain, weight loss

OPEN ACCESS

Edited by:
Mario Eduardo Guido, Center for Research in Biological Chemistry Córdoba (CIQUIBIC), Argentina

Reviewed by:
Russell H. Swerdlow, The University of Kansas, United States
Qingchun Tong, The University of Texas Health Science Center at Houston, United States

***Correspondence:**
Romina María Uranga
ruranga@inibibb-conicet.gob.ar; ruranga@criba.edu.ar
Jeffrey Neil Keller
jeffrey.keller@pbrc.edu

Specialty section:
This article was submitted to Neuroendocrine Science, a section of the journal Frontiers in Neuroscience

Received: *09 January 2019*
Accepted: *06 May 2019*
Published: *24 May 2019*

Citation:
Uranga RM and Keller JN (2019) The Complex Interactions Between Obesity, Metabolism and the Brain. Front. Neurosci. 13:513. doi: 10.3389/fnins.2019.00513

OBESITY

Obesity is often considered to result from excessive calorie consumption (food intake) and/or insufficient or inadequate calorie expenditure (metabolic and physical activity) (**Figure 1**). Obesity is a complex and chronic non-communicable disease that affects more than a third of the world's population (Hruby and Hu, 2015). It has been shown that obesity in middle age is able to shorten life expectancy by 4–7 years (Peeters et al., 2003). A major problem with obesity is the diverse set of health associated complications it promotes including hypertension, diabetes, increased cardiovascular risk, and cancer (Calle et al., 2003). The most commonly utilized tool used for measuring obesity today is the body mass index (BMI), defined as a person's weight in kilograms divided by his or her height in meters squared. By convention, a person with a BMI of less than 25.0 is considered non-obese or "normal," a person with a BMI between 25.0 and 29.9 is defined as overweight, and a person with a BMI of 30 or more is considered obese. A BMI of more than 40.0 deserves particular attention since it represents morbid obesity (also known as severe or extreme obesity). This index provides a reasonable estimate of body fat, and it is more accurate than skinfold measurements. However, the use of BMI has certain limitations, because it does not distinguish between lean and fat mass, nor does it indicate anything about fat distribution. In this sense, computed tomography or magnetic resonance imaging are the most accurate methods to measure the amount of visceral fat. Unfortunately, these tests are expensive and require sophisticated equipment. Waist circumference, a more straightforward but more reliable method to measure abdominal adiposity, has become an increasingly important tool for classifying obesity (Hu, 2007). Numerous studies have shown that many obesity-related risk factors depend mainly on fat body

distribution rather than excess weight *per se*. Hence, it is important to take into account how body fat is distributed in an individual, for example, between subcutaneous versus visceral (or intra-abdominal) fat. It is important to note that visceral fat, but not subcutaneous fat, is more associated with metabolic syndrome, which is further discussed below.

Adipose Deposition

Adipose tissue is a complex, specialized, multicellular organ able to influence the function of almost all other organs. It is a loose connective tissue composed mostly of adipocytes, but which also contains the stromal-vascular fraction of cells (vascular endothelial cells, preadipocytes, and fibroblasts) as well as macrophages. Adipose tissue is very heterogeneous and, anatomically, consists of different fat depots with unique characteristics. This mentioned heterogeneity in adipose tissue is not only from an anatomical point of view but also from the characteristics of the tissue expansion, the regulation of lipid metabolism and also the pattern of secreted factors (collectively called "adipokines") in a particular fat depot. All these characteristics bring with them metabolic consequences that impact the whole body, including the brain. It is known that each anatomical fat depot has a particular physiological role, which implies having specific metabolic and hormonal characteristics. As aforementioned, there is strong evidence showing that some fat depots are more robustly associated with disease development and outcomes.

In mammals, adipose tissue forms *in utero* just before birth and throughout life. Moreover, the continuous generation of new adipocytes has been shown in adult humans (Spalding et al., 2008). Unfortunately, little is known about adipocyte development. However, the study of adipose stem cell biology results extremely important for understanding adipose tissue development, expansion, migration, and maintenance. Adipose tissue is classified as white adipose tissue (WAT) and brown adipose tissue (BAT). These two main classes are molecularly and functionally different. WAT serves majorly as an energy store whereas BAT dissipates energy generating heat. WAT is spread throughout the body as subcutaneous and visceral fat. Subcutaneous WAT (sWAT) is a fat layer under the skin, with major depots in the upper and lower body. The upper body subcutaneous fat consists of superficial and deep abdominal fat, extremity fat, and, in the case of females, breast fat, whereas the lower body subcutaneous fat is mainly in the gluteofemoral region (Jensen, 2008; Kwok et al., 2016). Visceral WAT (vWAT) is around vital organs within the abdominal cavity and rib cage. Its major depots are the omental, mesenteric, epicardial, and mediastinal (Kwok et al., 2016). Numerous differences between sWAT and vWAT have been reported. For example, sWAT is heterogeneous and is composed mainly of unilocular adipocytes together with small multilocular adipocytes whereas vWAT looks more uniform and is composed mainly of large unilocular adipocytes (Tchernof et al., 2006; Tchkonia et al., 2007). It is believed that while increased sWAT deposition (known as a pear-shaped fat distribution) might protect against metabolic dysfunction, the increase in vWAT (known as an apple-shaped fat distribution) might increase the risk of metabolic disease (Grauer et al., 1984; Snijder et al., 2003a,b). Indeed, vWAT has been demonstrated to expand majorly by hypertrophy of preexisting adipocytes while sWAT expands by hyperplasia, i.e., the increase of the number of progenitor cells and subsequent differentiation. It is important to highlight that bigger hypertrophic adipocytes are usually associated with metabolic dysfunction. In line with this, very important in terms of metabolic disease is the fact that vWAT adipocytes are metabolically (i.e., lipolytically) more active than sWAT adipocytes, thus releasing more free fatty acids to the bloodstream (Wajchenberg, 2000; Hajer et al., 2008). vWAT is also associated with the release of pro-inflammatory adipokines (Fontana et al., 2007) and this would explain, at least partially, why central obesity is strongly linked with metabolic complications such as type-2 diabetes mellitus and cardiovascular disease, and many others caused by elevated free fatty acids (Jensen, 2008). Indeed, this characteristic of being metabolically less active than vWAT makes of sWAT a very important source of free fatty acids during food deprivation. It is important to highlight at this point that vWAT mass but not sWAT mass correlates with the development of insulin resistance (Chowdhury et al., 1994; Wajchenberg, 2000; Hoffstedt et al., 2018). A plethora of studies argue in favor of women better distributing fat in the periphery (compared to men having more central obesity) and thus having better metabolic health (Kwok et al., 2016).

Interesting experiments with transplantation of adipose tissue have been performed in animals, and they have been very useful for assessing the different functions and metabolic properties of the different fat depots. For example, transplantation of subcutaneous fat from donor mice into visceral fat site of recipient mice has shown to confer metabolic benefits in the latter, namely decrease in body weight and total fat, improvement of insulin sensitivity, and lowering of both insulinemia and glycemia (Tran et al., 2008). Unexpectedly, intraperitoneal transplantation of visceral fat from lean mice showed to improve insulin sensitivity, suggesting that the metabolic performance of a certain fat depot is more important as a metabolic risk factor than the anatomical location or the amount of fat itself (Konrad et al., 2007; Kwok et al., 2016). On the other hand, transplantation of visceral fat or subcutaneous fat into subcutaneous fat site has not shown to cause any alterations in body weight or metabolic profile, so it seems there are both donor and recipient site-specific factors that intervene in the final outcome (Tran et al., 2008). Other experiments have shown similar results in both autologous as well as heterotransplantation of subcutaneous fat into the intraabdominal cavity of diet-induced obese animals. In both cases, transplanted adipocytes showed to diminish their size, and insulin sensitivity, as well as serum lipid profile, showed to be improved, correcting almost all the metabolic parameters altered by obesity (Foster et al., 2013; Torres-Villalobos et al., 2016). Interestingly, transplantation of brown adipose tissue to the visceral cavity has also demonstrated to prevent weight gain and improve carbohydrate metabolism in high-fat diet-induced obese animals (Townsend and Tseng, 2012). All this evidence strongly suggests that fat cells from different depots do have different characteristics and thus can play protective or detrimental roles in metabolism.

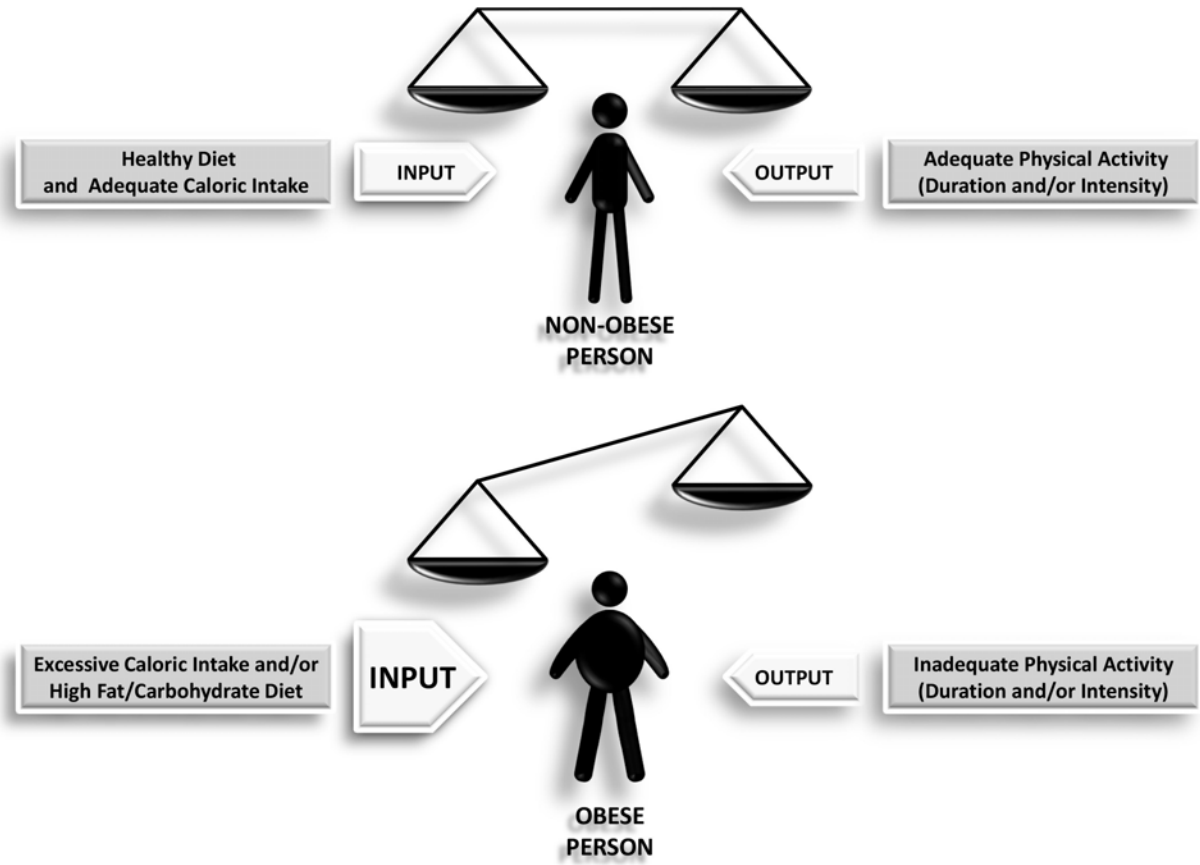

FIGURE 1 | Scheme depicting how the imbalance between the input and the output leads to obesity as a final outcome.

Obesity and Peripheral Health

Obesity is known as a chronic low-grade inflammatory disorder that results a triggering factor for many other metabolic and inflammatory disturbances. The obesity-linked inflammatory response includes many components of the classical inflammatory response, namely augmented secretion of circulating inflammatory factors, recruitment of leukocytes to inflamed tissues and organs, and activation of these leukocytes. However, the metainflammation observed in obesity has distinctive characteristics. For example, it is known that the chronic low-grade inflammation ends affecting the metabolic homeostasis in the long-term. Also, the multi-organ affection observed as the result of obesity-associated inflammation results to be unique (Lumeng and Saltiel, 2011). Adipose tissue, which was primarily thought to be a mere storage depot for triglycerides, is now considered an immune organ playing a vital role as a primary *in vivo* site of inflammation in obesity. Indeed, adipose tissue also plays a critical endocrine role due to the ever-increasing number of adipocyte-derived secretory factors that have been described.

Obesity, Adipokines, and Peripheral Inflammation

Substantial evidence supports that many of the circulating adipokines might be responsible for the peripheral inflammation observed in obese patients, including tumor necrosis factor α (TNFα), leptin, and various interleukins, among others. Importantly, the dysregulation of the adipokine secretion pattern has been linked to obesity and all the obesity-related metabolic disturbances such as cardiovascular disease, hypertension, type-2 diabetes, etc. Moreover, changes in either the amount or the quantity of the secreted adipokines are able to affect the various organ systems of the body vital for energy homeostasis. It is important to note that the weight loss-associated normalization of the adipokine secretion pattern is linked to the consequent normalization of different metabolic parameters, reinforcing the idea that adipokines are critical for the whole body metabolic homeostasis.

It is important to highlight that although secreted by adipose tissue, adipokines (except for leptin) are not solely secreted by adipocytes. Leukocytes, almost half of the non-adipocytes cell fraction in adipose tissue, are the source of classic adipokines such as IL-1, TNFα, visfatin, and resistin. Many other adipokines are produced and secreted by both adipocytes and leukocytes, such as adiponectin and IL-6. All fat depots are able to release adipose hormones, but visceral fat is considered to be the primary source of them. It has also been demonstrated that each fat depot has a particular pattern of adipokine expression (Dodson et al., 2014; Zhang et al., 2014). Interestingly, it has been shown

that adipokines are also released by some particular places of the central nervous system where adipokine receptors are also expressed. Nonetheless, alterations of adipokine release during obesity and aging are attributed almost exclusively to changes in the structure and function of the adipose tissue (Kiliaan et al., 2014). A detailed description of each adipokine is beyond the scope of this review, but a few generalizations of the most important ones deserve mention.

Leptin is probably the most studied adipokine. It positively correlates with BMI (Friedman and Halaas, 1998; Lissner et al., 1999); however, obesity is considered a state of reduced leptin function. It is produced peripherally by WAT but exerts the bulk of its metabolic functions centrally, after crossing the blood brain barrier (BBB). However, it has been shown to be produced both in rodent and human brains (Morash et al., 1999; Wiesner et al., 1999; Brown et al., 2007; Wilkinson et al., 2007). It is well known that leptin action in the hypothalamus maintains body weight homeostasis in response to changes in the nutritional status. Leptin is considered the principal regulator of the "brain-gut-axis," which provides a satiety signal through its action on hypothalamic leptin receptors (Konturek et al., 2004). Activation of these receptors suppresses food intake and promotes energy expenditure pathways (Tilg and Moschen, 2006; Simerly, 2008). It is worth highlighting that several hypothalamic neuropeptides have been shown to be produced by leptin-sensitive neurons and to act as neurotransmitters mediating leptin action (Xu and Tong, 2011). However, the specific neurotransmitter responsible for midbrain leptin action on feeding remains elusive. It has also been shown that leptin is able to regulate numerous inflammatory and immune processes, including cytokine expression and cell proliferation and death (O'Rourke, 2010). Very importantly, experiments of leptin receptor restoration in the brain of mice which completely lack the receptor function have shown the normalization of the metabolic parameters (de Luca et al., 2005). Interestingly, leptin signaling has also been suggested to be one of the circulating factors connecting obesity and the consequent reproductive dysfunction, being the reproduction defects reverted by pharmacological administration of leptin (Tong and Xu, 2012).

Adiponectin is an adipokine with insulin-sensitizing and anti-inflammatory effects produced exclusively by adipose tissue and suggested to be a visceral adiposity marker, due to the fact that several studies in humans have shown that visceral adipocytes secret more adiponectin than subcutaneous adipocytes (Lenchik et al., 2003; Ryan et al., 2003; Matsuzawa, 2007; Drolet et al., 2009). It exists as trimers, hexamers, and high-molecular-weight (HMW) multimeric complexes (Rutkowski and Scherer, 2014). Recent data indicate that the HMW complexes have predominant action in metabolic tissues (Achari and Jain, 2017). Unlike the majority of adipokines, adiponectin plasma levels correlate inversely with obesity, insulin resistance, and type-2 diabetes mellitus (Hotta et al., 2001; Kondo et al., 2002; Deng and Scherer, 2010). However, the decreased level of adiponectin in obesity is not clear yet. Physiological functions of adiponectin in the brain have been related majorly to food intake, energy expenditure, lipid and glucose metabolism, and body weight control (Kubota et al., 2007; Wen et al., 2010; Park et al., 2011). Interestingly, adiponectin physiological levels are generally higher in females than in males and decrease in both sexes as age increases (Ng and Chan, 2017). It should be mentioned that several studies have shown that the pharmacological reconstitution of adiponectin levels through drugs targeting adiponectin synthesis would help in the treatment of obesity and the associated diabetes and cardiovascular disease (Achari and Jain, 2017).

Resistin was first discovered to be secreted by adipocytes in rodents. However, in humans, it is predominantly expressed and secreted by macrophages. It is known that increased resistin levels are linked to the development of insulin resistance, diabetes mellitus, and cardiovascular disease. Moreover, resistin would promote endothelial dysfunction, vascular smooth muscle cell proliferation, arterial inflammation, and the generation of foam cells, thus contributing to the pathogenesis of atherosclerosis (Park et al., 2017). Circulating levels of resistin correlate directly with inflammatory markers such as C-reactive protein, TNFα, and IL-6 in patients with different metabolic disturbances (Park and Ahima, 2013).

Visfatin is also known as pre-B cell colony-enhancing factor (PBEF) or nicotinamide phosphoribosyltransferase (NAMPT), the latter due to the fact that it is the limiting enzyme in nicotinamide adenine dinucleotide (NAD) biosynthesis. This adipokine is expressed by different types of cells, including adipocytes, hepatocytes, and myocytes. However, in adipose tissue, it has been shown to be secreted majorly by infiltrating macrophages (Deng and Scherer, 2010). Visfatin is produced by visceral adipose tissue, and thus its production is increased in abdominal obesity. Interestingly, visfatin has been demonstrated to bind to insulin receptor and mimic insulin hypoglycemic effects, i.e., decreasing glucose release from the liver and increasing glucose uptake and utilization by peripheral tissues (Singla et al., 2010).

Apelin has been relatively recently classified as an adipokine since although it is produced and secreted by adipocytes, it is also expressed (together with its receptor) in the central nervous system and the cardiovascular system. Apelin has been related to the regulation of blood pressure, food intake, cell proliferation, and angiogenesis (Castan-Laurell et al., 2011). *In vitro* as well as *in vivo* studies have shown a strong relationship between apelin and insulin (Boucher et al., 2005). Moreover, apelin has been suggested to be the last protection before the appearance of obesity-associated metabolic disorders such as insulin resistance, type-2 diabetes, or cardiovascular disease (Castan-Laurell et al., 2005).

IL-6 is a pro-inflammatory cytokine synthesized and secreted by several cell types, including adipocytes and immune cells. Not only does IL-6 participate in inflammatory responses but it also controls feeding behavior at a hypothalamic level (Stenlöf et al., 2003). IL-6 circulating levels have been systematically reported to be augmented in obesity, being visceral fat secretion an important source of IL-6 thus linking the enlarged visceral fat with the existence of systemic inflammation in obese patients (Fontana et al., 2007). Importantly, IL-6 levels have been reported to normalize in morbidly obese patients who underwent bariatric surgery (Illán-Gómez et al., 2012).

TNFα is an inflammatory adipokine whose levels are increased in adipose tissue and plasma of both obese rodents and humans (O'Rourke, 2010). It was the first inflammatory adipokine associated with the onset and progression of insulin resistance (Hotamisligil and Spiegelman, 1994). It was first thought to be secreted by adipocytes, but today it is accepted that the bulk of TNFα is secreted by adipose tissue-resident macrophages. It has been shown that high levels of TNFα and IL-6 suppress the transcription of adiponectin thus connecting the role of visceral fat accumulation in adiponectin decreased secretion in obesity (Suganami et al., 2005).

In summary, adipose tissue, as an immune and endocrine organ, produces a wide variety of soluble factors collectively called adipokines. These molecules were initially associated uniquely to metabolic activities, but today it is known that they regulate numerous physiological and physiopathological events. Adipokines have pro- and anti-inflammatory properties and are considered fundamental circulating factors mediating the cross-talk between different organs and metabolic systems, thus integrating the systemic metabolism with immunity.

Before leaving the topic of adipokines, it is important to note that while adipokines have been primarily studied in terms of their links to adipose tissue, it is well established that non-adipose tissues produce and release adipokines. For example, muscle is known to produce and release several cytokines which are also produced and released by adipose tissue (Trayhurn et al., 2011; Görgens et al., 2015; Leal et al., 2018). Similarly, the liver is known to be an organ that is very much involved in the contribution of overall circulating adipokine levels. For example, leptin, adiponectin, and resistin have been shown to be locally produced by the liver (Marra et al., 2005). It is therefore important to understand that even circulating adipokine levels, in obese and non-obese individuals, is the result of the shared contributions of adipokine production from multiple tissues.

Obesity and Peripheral Metabolic Changes

As mentioned, the obesity-associated increase in the adipose tissue mass is linked to a change in the adipokine secretion pattern, thus causing what is known as "metainflammation," which affects systemic metabolism. A common consequence of obesity is metabolic syndrome, a condition which is associated with pro-inflammatory states and which is considered to be a compilation of risk factors that predispose individuals to the development of cardiovascular disease and type-2 diabetes. The diagnosis of metabolic syndrome is made when any 3 of the 5 following risk factors are present: central obesity (enlarged waist circumference, defined according population-specific and country-specific criteria), high blood pressure (defined as systolic blood pressure $\geq$ 130 mm Hg or diastolic blood pressure $\geq$ 85 mm Hg), loss of glycemic control (elevated fasting glucose, defined as blood glucose $>$ 100 mg/dl), low serum high-density lipoprotein (HDL) (defined as $<$ 40 mg/dl in men and $<$50 mg/dl in women), and high serum triglycerides (defined as $\geq$ 150 mg/dl) (Lam and LeRoith, 2000). The existence of metabolic syndrome is well known to predispose an individual to diabetes and cardiovascular disease. It is important to know that metabolic syndrome also predisposes individuals to a number of other severe conditions including non-alcoholic fatty liver disease, non-alcoholic steatohepatitis, obstructive sleep apnea, and cancer, among others. Indeed, hyperleptinemia, hypoadiponectinemia, and insulin resistance are also widely linked to features of the metabolic syndrome.

Insulin resistance and type-2 diabetes mellitus are typical metabolic changes observed in obese patients. Insulin resistance implies impaired insulin-induced glucose uptake and metabolism in adipocytes and skeletal muscle, and impaired suppression of hepatic glucose production (Reaven, 1995). Insulin resistance is a key etiologic factor of type-2 diabetes but is also associated with a plethora of other pathophysiologic disorders including hypertension, hyperlipidemia, and atherosclerosis. Although several hypotheses about factors influencing insulin resistance coexist (including inflammation, mitochondrial dysfunction, hyperinsulinemia, lipotoxicity, oxidative stress, and endoplasmic reticulum stress), there is no consensus about a unifying mechanism for insulin resistance etiology (Ye, 2013). It is generally accepted that insulin resistance occurs first, with hyperinsulinemia as a pancreatic compensatory response, and after pancreatic failure to meet metabolic demands, hyperglycemia with hypoinsulinemia occurs. Importantly, central obesity precedes the development of insulin resistance, thus reinforcing the idea of visceral fat and its pro-inflammatory adipokines playing a key role in the pathophysiology of insulin resistance.

It is worth mentioning that although obesity is commonly associated with different metabolic abnormalities, 2–50% of obese adults are "metabolically healthy or metabolically normal" (the wide range is due to different criteria in the classification and also to the population studied) (Tiemann Luecking et al., 2015). The concept of "metabolically healthy obese" refers to obese people with normal metabolic risk profile (Karelis et al., 2005; Stefan et al., 2008). However, studies have previously shown that "metabolically healthy obese" individuals do have increased cardiovascular risk (Ärnloöv et al., 2010).

Effect of weight loss on metabolic endpoints of obesity

Reducing the amount of total body fat has been thought of as a strategy to diminish the impact of obesity and comorbidities on health. Weight loss interventions such as low-fat diets have been demonstrated to reduce many of the risk factors associated with obesity (Lee et al., 2011), as well as decrease all-cause mortality in obese adults. It is important to note that each reference to weight loss in this review is "intentional weight loss" and not involuntary weight loss. It is important to note that intentional weight reducing diets are routinely shown to be more effective in reducing blood pressure and improving dyslipidemia when combined with exercise (Schwingshackl et al., 2014). Interestingly, low-carbohydrate diets have been found to be more effective for reducing body weight than low-fat diets (Tobias et al., 2015). However, evidence supported by randomized controlled trials shows that most adults are unable to maintain weight loss (Wing and Phelan, 2005; Wadden et al., 2011; Ross et al., 2012). From this perspective, alternative approaches to diet-induced weight loss are needed, including the establishment of

healthy eating and physical activity habits that may be more sustained over time. Bariatric surgery, also known as metabolic surgery, is associated with sustained weight loss, decreased cardiovascular risk factors and events, diminution in diabetes-linked microvascular complications, and improvement of obesity-associated comorbidities and overall survival (Christou et al., 2004; Sjöström et al., 2007; Sowemimo et al., 2007; Buchwald et al., 2009; Cummings and Rubino, 2018). Moreover, bariatric surgery has been shown to be superior to other weight loss-associated interventions in normalizing almost all the metabolic endpoints. However, studies with longer follow-up time (>5 years) are still needed, including studies that identify any potential long-term adverse effects following bariatric surgery (Busetto, 2014; Cummings and Rubino, 2018). Liposuction, which is mainly thought to remove subcutaneous fat without affecting visceral abdominal fat depot, is another common weight loss procedure. However, there is controversy about the impact of liposuction on obesity endpoints like insulin sensitivity. This controversy may be due in part to the fact that lipectomy of sWAT has been linked to the enlargement of vWAT (Benatti et al., 2012).

The complexity of weight loss in the elderly. As mentioned, there is a strong obesity-mortality association during adulthood. However, this association diminishes with age, and weight loss in older adults is not as beneficial as one might expect. Surprisingly, unintentional weight loss (more than 5% of body weight reduction in a year) in older adults is associated with increased morbidity and mortality (Gaddey and Holder, 2014). Although cachexia, i.e., the loss of muscle mass with or without fat loss, is thought to be the main responsible for these negative effects, the pathophysiology of unintentional weight loss remains unclear. It is well known that body composition changes with age, with fat mass gains until 65–70 years old, a characteristic peak in body weight around 60 years old, and gradual small decreases thereafter (Wallace and Schwartz, 2002). The ideal BMI in the elderly is considered (from a mortality point of view) to be of 25–30. At this point, it is worth to have in mind that although BMI in younger adults correlates quite well with total body fat, it does not in older adults and this might be an appropriate explication for the so-called "obesity paradox," according to which obese old individuals have lower mortality than lean. The main reason is that not only there is a continuous loss of body muscle with age (without loss in body fat), but also the height is reduced due to spine-shortening as a consequence of age-related bone disease. In this sense, as mentioned before, waist circumference is a better index of adiposity, mainly because it correlates with abdominal body fat, which is the main contributor to metabolic disorders. Moreover, inactivity in older adults is usually accompanied by a loss in body muscle mass, a condition which may go unnoticed but which brings several functional consequences in the long-term period. This condition is known as sarcopenic obesity, and together with degenerative joint disease, it leads to the incapability to perform activities of daily living. Thus the impairment in daily function finally causes the development of frailty phenotype (which is generally present in the elderly but is greatly increased with obesity) with disability as a final outcome (Han et al., 2011).

Many observational studies have linked weight loss with increased risk of mortality (Yaari and Goldbourt, 1998; Knudtson et al., 2005; Sørensen et al., 2005; Shea et al., 2011). There are several causes of unintentional weight loss in the elderly (Gaddey and Holder, 2014). Only intentional weight loss in older people seems to lead to some clinical benefits, mainly due to the fact that unintentional weight loss is often associated with underlying subclinical illnesses. However, since intentional weight loss is linked to muscle mass loss and decreased bone mass (Waters et al., 2013), it appears that diet-induced weight loss should be accompanied by a program of physical activity which can potentially inhibit the muscle and bone loss associated with diet-induced weight loss (Shea et al., 2011). Lifestyle interventions that include diet plus exercise components have been shown to lead to a 10% weight loss with changes in physical function and metabolism (Waters et al., 2013). However, the clinical significance of these observations as well as long-term consequences of weight loss remains unclear.

Obesity and Peripheral Lipid Changes

Dyslipidemia is very common in obesity, reaching almost 70% of obese patients. The lipid abnormalities usually observed in obese patients are high levels of serum triglycerides, free fatty acids, very low-density lipoproteins (VLDL), Apo B, and non-HDL cholesterol (Franssen et al., 2011; Bays et al., 2013). HDL-cholesterol levels are typically found to be low together with HDL dysfunction. Regarding LDL-cholesterol, although in the normal range, the size of LDL particles is unbalanced, with more small pro-atherogenic LDL particles rather than large ones. Lipid changes in obesity have been shown to be strongly dependent on body fat distribution. For example, visceral adipose tissue and upper body subcutaneous adipose tissue have been related to high triglyceride and HDL cholesterol levels and insulin resistance, whereas lower body subcutaneous adipose tissue has been related to a healthier lipid profile (Feingold and Grunfeld, 2018).

All these obesity-related lipid abnormalities are frequent observations in metabolic syndrome and typically associated with the pro-inflammatory state described before. An important link between obesity, metabolic syndrome, and dyslipidemia appears to be insulin resistance in peripheral tissues. It has been shown that the increase in circulating free fatty acids associated with obesity contributes to several metabolic disturbances being insulin resistance probably the most important (Karpe et al., 2011). It is important to highlight, however, that the increase in free fatty acids is not only a consequence of insulin resistance but also contributes to its development (Lam and LeRoith, 2000). There are several reasons for increased free fatty acids in obesity: (1) enlarged adipose tissue resistant to the antilipolytic effect of insulin; (2) increased liver fatty acid *de novo* synthesis (Jacome-Sosa and Parks, 2014; Björnson et al., 2016; Xiao et al., 2016); (3) increased uptake of triglyceride-rich lipoproteins by the liver (Yu and Ginsberg, 2005; Dash et al., 2015; Björnson et al., 2016; Xiao et al., 2016). This increased free fatty acid

flux finally exceeds adipose tissue lipid storage capacity, and free fatty acids begin to accumulate in the liver, pancreas, skeletal muscle, and heart, a condition known as "ectopic lipid deposition" which has several pathologic consequences. Lipids result cytotoxic to cells other than adipocytes. For example, lipid deposition in the pancreas has been involved in the development of diabetes whereas lipid deposition in the skeletal muscle has been associated with insulin resistance. Moreover, lipid accumulation in the liver defines steatosis. The hypothesis of adipose tissue protecting against ectopic accumulation of lipids (working as a metabolic sink) has been supported by observations in animals and humans with lipodystrophy, where the absence of adipose tissue is associated with generalized lipid ectopic deposition and insulin resistance (O'Rourke, 2010).

Effect of weight loss on peripheral lipids

The effect of weight loss on peripheral lipid profile has been extensively assessed. Serum fasting and non-fasting triglyceride levels have been demonstrated to be reduced by weight loss (Chan et al., 2002; James et al., 2003). On average, a 3-kg weight loss represents a reduction of 15 mg/dl in triglyceride levels. Indeed, LDL levels are also usually decreased by weight loss, and HDL levels are usually increased: a 5- to 8-kg weight loss is associated with a decrease of 5 mg/dl in LDL and an increase of 2–3 mg/dl of HDL (Ebbert et al., 2014). However, considerable variability in the results has been observed, and the improvement of dyslipidemia is not always the final outcome. On the other hand, the type of weight-loss diet followed does impact on lipid profiles. It is still unclear which factors associated with weight loss are predictive of the change in lipid profile. Several studies have shown a poor correlation between lipid profile improvement and the degree of weight loss, and a threshold effect has been suggested when the lipid profile resulted improved with a minimal weight loss but when no further effects were observed with a larger weight loss (Kelly and Jones, 1986; Busetto et al., 2000).

Interestingly, metabolic surgery impacts positively on serum lipid levels as a consequence of weight loss. Normalization of serum lipid profile is a common observation after gastric bypass surgery. In a meta-analysis of 11 randomized clinical trials comparing surgical versus non-surgical treatment of morbid obesity, bariatric surgery was found to be associated with more significant weight loss, remission of metabolic syndrome, and improvement in lipid profiles with the consequent decrease in medication requirements (Gloy et al., 2013; Koliaki et al., 2017). A 5-year follow-up study compared patients who received medical therapy alone with patients who underwent surgical therapy. Surgical patients were found to achieve the greatest health benefits, with a more significant reduction in triglyceride levels and a more considerable increase in HDL with respect to patients who received medical treatment alone (Schauer et al., 2017). It is worth mentioning that the beneficial effects of bariatric surgery have been analyzed in the short-term period and up to 5 years after the intervention; however, the long-term effects remain elusive.

EFFECTS OF OBESITY-ASSOCIATED FAT DEPOSITION AND CIRCULATING FACTORS ON THE VARIOUS NON-CNS ORGANS OF THE BODY

Although the cause of obesity is mainly attributed to energy imbalance, the etiology of obesity is multifactorial, including genetic, psychological, economic, environmental, social, and physiological factors, only to cite some (Wright and Aronne, 2012). Whatever etiopathogenesis of obesity is considered, several organs are damaged as a consequence of the development of obesity, including the pancreas, liver, muscle, and the cardiovascular system. A brief outline of how ectopic fat deposition and the concomitant obesity-related circulating factors contribute to disease of each organ is provided (**Figure 2**).

Pancreas

The ectopic fat accumulation in the pancreatic gland is usually referred to as pancreatic steatosis. Intra- and interlobular adipocytes, acinar cell fat, as well as islet fat content have been found to be augmented in obesity (Pinnick et al., 2008; Lee et al., 2010). A close relationship between insulin resistance and pancreatic steatosis has been described. As it is known, pancreatic β-cells usually produce and release insulin to control glucose homeostasis. Under the condition of insulin resistance, pancreatic β-cells increase the production and release of insulin to maintain the normal glycemia. However, patients predisposed to type-2 diabetes fail to secrete enough insulin to meet the metabolic demand (due to insulin resistance in several tissues) and type-2 diabetes occurs (Poitout, 2004). Different stages in the development of type-2 diabetes have been well characterized. In the first stage, there is insulin hypersecretion, which allows for normal glycemic control. In contrast, during the second stage of type-2 diabetes, there is a failure of β-cells to secrete sufficient insulin for glycemic control, and thus hyperglycemia is manifest. However, it is a matter of debate whether dysfunction precedes or follows the loss of β-cells in obesity-linked diabetes mellitus (Alarcon et al., 2016). Whatever the origin of obesity-associated diabetes, there is a failure in insulin production and/or the secretory capacity of β-cells. Interestingly, *in vitro* studies have shown that β-cells have an exceptional capacity to synthesize significant amounts of insulin even in obesity-like conditions, and that this insulin is readily available for secretion. It is believed that fat accumulation in the pancreatic islets would be responsible for, at least in part, the decreased insulin secretion of the second stage of type-2 diabetes, since ectopic fat deposits in the pancreas have been reported to cause β-cell dysfunction, both directly through lipotoxicity exerted by free fatty acids and indirectly through activation of inflammatory pathways (Le et al., 2011; Pezzilli and Calculli, 2014). Moreover, evidence suggests that lipid toxicity to pancreatic β-cells is a long-term process and it takes around a decade before diabetes is diagnosed (Oakes et al., 1997). On the other hand, studies performed in morbidly obese humans have shown that obesity and peripheral insulin resistance are also associated with substantial changes in pancreatic metabolism and pancreatic blood flow, together

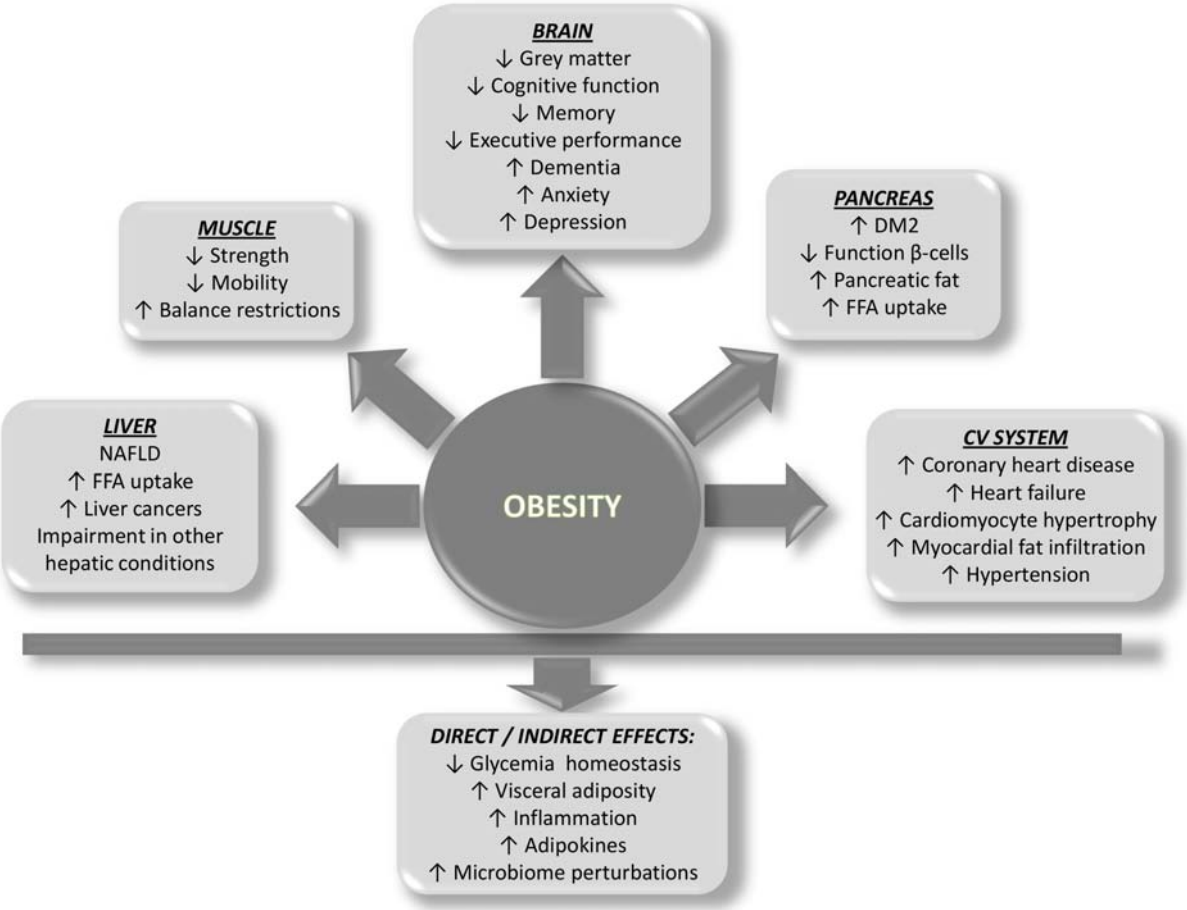

FIGURE 2 | Scheme showing the predicted impact of obesity on organ systems and the direct and indirect effects on health.

with β-cell dysfunction. Interestingly, as a consequence of insulin resistance in adipose tissue, increased free fatty acids have been shown to be delivered from the bloodstream in morbidly obese individuals, and these people clearly show a shift in the preferred pancreatic energy substrate, with lipid usage being predominant over glucose usage (Honka et al., 2014). The possibility of these observations (pancreatic metabolic shift and defect in blood flow) to be reverted by weight loss is still unclear.

In addition, the changes in circulating adipokines constitute an important link between the excessive adiposity in obesity, insulin resistance, and β-cell failure, mainly due to the fact that several adipokines have demonstrated to affect both the function and survival of β-cells thus deteriorating the function of the pancreas and contributing to acute and chronic pancreatitis as well as pancreatic cancer (Zhao et al., 2006; Gumbs, 2008). Leptin, adiponectin, resistin, and visfatin are the most important adipokines that would participate in the pathogenesis of pancreatic diseases (Biernacka and Małecka-Panas, 2015). Beyond the previously mentioned physiological roles of leptin, this adipokine has also been shown to reduce insulin secretion. It has also been demonstrated to regulate the inflammatory response, thus protecting the pancreas from some kinds of damage by reducing TNFα and increasing IL-4 production (Jaworek et al., 2002). Indeed, adiponectin has been shown to play anti-diabetic and anti-inflammatory roles. Regarding the role of adipokines and pancreatic disease, it is thought that the higher risk of acute pancreatitis in obese people would come from the increased adipokine-producer visceral fat in the surroundings of the pancreas (Biernacka and Małecka-Panas, 2015). However, the precise role of adipokines in acute and chronic pancreatitis, as well as in pancreatic cancer, is unclear yet and needs to be further investigated. Controversial results regarding the functions of leptin, visfatin, adiponectin, and resistin have been found.

In summary, obesity-linked type-2 diabetes is characterized by the decreased number and function of pancreatic β-cells. The impairment in β-cell function, as well as the number of β-cells, has been related to lipotoxicity (with the concomitant increased oxidative and endoplasmic reticulum stress) and the adipokine-induced inflammation processes (Halban et al., 2014).

Liver

Obesity has been involved as a risk factor at different stages of liver disease (Manne and Saab, 2014), not only causing non-alcoholic fatty liver disease (NAFLD) but also impairing the

general state of patients with other preexisting conditions such as viral hepatitis. NAFLD is an important metabolic risk factor defined as a higher than 5% intracytoplasmic fat deposition in the hepatocyte in the absence of alcohol consumption, toxin exposure or viral disease (Tiniakos et al., 2010; Calvo et al., 2015). However, fat deposition is not the only observation of NAFLD, an inflammatory process coexists, with hepatocellular ballooning injury that can lead to fibrosis and cirrhosis (Brunt et al., 1999). Since triglycerides have been shown to accumulate in the liver through different manners, there is not a unique mechanism by which obesity could lead to NAFLD. Moreover, beyond the role of triglycerides, insulin resistance does have an important role in the development of fatty liver (Marchesini et al., 1999; Sanyal et al., 2001; Willner et al., 2001; Pagano et al., 2002). Free fatty acid uptake by the liver not only leads to hepatic steatosis but also produces hepatic toxicity by oxidative stress-dependent mechanisms (Manne and Saab, 2014). In this connection, it is thought that hepatic accumulation of triglycerides occurs first (hepatic steatosis or fatty liver) and then, since fatty liver is more prone to suffer oxidative injury, it evolves to steatohepatitis (Qureshi and Abrams, 2007).

The link between obesity and NAFLD has been explained by different hypotheses which take into consideration the portal hypothesis, the endocrine role of adipokines, and many observations from lipodystrophic states. It has been mentioned that visceral adipocytes constitute an important source of fatty acids and other factors entering the portal circulation (Qureshi and Abrams, 2007). The portal hypothesis supports the idea that the increased hepatic uptake of fatty acids coming from an enlarged visceral adipose tissue leads to decreased hepatic insulin clearance and thus increased circulating insulin. Indeed, fatty acids stimulate hepatic gluconeogenesis, triglyceride synthesis, and hepatic glucose output (by altering insulin signaling) (Kahn and Flier, 2000). On the other hand, adipokines are also involved in the development of NAFLD during obesity. For example, in addition to all the general effects of leptin, this adipokine has been shown to better liver enzymes and hepatic fat content, thus attenuating different manifestations of fatty liver in patients with lipoatrophy and metabolic syndrome (Lee et al., 2006). In obese NAFLD patients, leptin levels correlate with the severity of fatty liver, thus suggesting the presence of leptin resistance, probably due to a failure in leptin signaling. Low levels of adiponectin have been found in NAFLD patients, probably due to the concomitant high levels of IL-6 and TNFα found, both of which inhibit adiponectin expression. Therapy with adiponectin administration has shown to improve insulin resistance in animal models of obesity; however, in lipodystrophic animal cases, the complete reversal of insulin resistance requires the co-administration of leptin. Adipose tissue-derived TNFα and IL-6 cause the activation of Kupffer cells which leads to hepatic fibrogenesis. Moreover, TNFα has been shown to be also produced by the Kupffer cells, playing a key role in the pathogenesis of NAFLD (Qureshi and Abrams, 2007). Additionally, fatty liver, accompanied by insulin resistance and diabetes, is usually observed in lipodystrophic patients, where the fatty liver usually progresses to cirrhosis. Among different explanations proposed, reduced adiponectin and leptin levels are thought to be responsible for the presence of NAFLD in lipodystrophic individuals.

Not only has obesity been related to the development and progression of NAFLD, but also with the impairment of other hepatic conditions, being obesity considered as a strong risk factor for different liver cancers. Very interestingly, the mere losing weight of obese patients has been shown to be sufficient not only to improve the results of several hepatic treatments (Nobili et al., 2011) but also to increase insulin sensitivity and decrease hepatic triglyceride and free fatty acid uptake by liver (Viljanen et al., 2009; Manne and Saab, 2014).

Muscle

As a general picture, obesity is linked to functional limitations in muscle performance and increased probability of developing a functional disability related to strength, mobility, postural, and dynamic balance restrictions. It is known that obese people, regardless of age, have greater absolute maximum muscle strength in anti-gravity muscles compared to non-obese counterparts (this is valid only for lower limbs, since upper limb strength reveals no statistical difference between obese and normal-weight people) (Maffiuletti et al., 2007, 2008; Delmonico et al., 2009; Abdelmoula et al., 2012; Tomlinson et al., 2016). This observation has been interpreted as adiposity being a chronic overload stimulus for muscles, thus making muscles stronger and bigger. However, it is noteworthy that when muscular strength is normalized to total body mass, the obese people seem to be overall weaker than their lean control individuals. Notwithstanding, the existing literature shows considerable controversy on this matter (Tomlinson et al., 2016). For this reason, the real effect of obesity on skeletal muscle size, structure, and function remains elusive. Although there is no consensus regarding accurate measures of obesity-associated muscle damage or quality, it is worth mentioning that obesity does have been shown to generate a negative impact on skeletal musculature through adolescence to young and old adulthood (Blimkie et al., 1990; Rolland et al., 2004; Zoico et al., 2004; Maffiuletti et al., 2007, 2008). Obviously, the relevance for reduced muscle performance is higher for older people, as they are generally affected by reduced functional capacity. This includes impairments in walking, impaired ability to go up and downstairs, and difficulty with rising from chair or bed. Similarly, there is an augmented risk to suffer joint pathologies, such as knee osteoarthritis, due to joint overload and reduced muscle strength (Cooper et al., 1998; Rolland et al., 2009; LaRoche et al., 2011; Maden-Wilkinson et al., 2015). All these conditions represent a clear sign of poor quality of life for older people, which is worsened by obesity. Further work is needed to systematically investigate whether body fat percentage *per se* may be related to agonist muscle activation and antagonist co-activation and/or morphological and architectural muscle characteristics.

In connection to ectopic fat deposition, the accumulation of triglycerides intra-myocellularly and inter-myocellularly is known to cause lipotoxicity, insulin resistance, and impaired glucose metabolism. The increased flux of fatty acids to the myocyte appears to be the link between muscle fat infiltration and insulin resistance and altered glucose metabolism. It has been

shown that when mitochondrial β-oxidation is overwhelmed due to an excess of free fatty acids entering the myocyte, metabolic intermediaries of fatty acids accumulate and finally impair insulin signaling (Moro et al., 2008; Ghosh, 2014). It has been shown that skeletal muscle fat infiltration, together with sarcopenia, is able to have not only metabolic consequences but also to impair the daily living, by diminishing mobility (Katsanos and Mandarino, 2011).

The effect of adipokines on the skeletal muscle has emerged as an important area of research. It has been shown that adipokines including leptin, adiponectin, visfatin, and resistin are able to affect muscle insulin sensitivity (Nicholson et al., 2018). There are several *in vitro* studies about the role of adipokines in the skeletal muscle metabolism and insulin sensitivity. However, those studies have been carried out mainly using rodent skeletal muscle cells that are known to have different fiber composition and different metabolic characteristics than human skeletal muscle cells. This may be the reason why reports about the role of adipokines in muscle function and insulin resistance result controversial.

Beyond the effect of inflammation-associated adipokines on skeletal muscle, it is worth mentioning that under obesity conditions, the muscle becomes an inflammatory organ itself, able to secrete several circulating factors (known as myokines) that can act in either autocrine, paracrine or endocrine manner, thus affecting the metabolism of both muscle and other organs. The muscle is able to secrete several hundred of factors in response to contraction, which became a whole new paradigm for understanding the communication between muscles and the various organ systems, including adipose tissue, liver, pancreas, and brain. It is worth to mention that some myokines exert their functions in the muscle itself and have been suggested to regulate skeletal muscle growth, repair, maintenance, and regeneration, in addition to mediating the health benefits of exercise (for review see Pedersen, 2013).

Cardiovascular System

Obesity, at the population level, has been considered as a risk factor for the development of cardiovascular diseases such as coronary heart disease and heart failure. Obesity-associated transition from asymptomatic subclinical left ventricle changes to overt dilated cardiomyopathy, irrespective of the coexistence of hypertension or diabetes mellitus, has been shown (Wong and Marwick, 2007). Importantly, body fat distribution has been found to be more important than total fat composition on left ventricle adaptations to obesity, with excessive visceral fat causing adverse hemodynamics, concentric left ventricle remodeling, lower cardiac output, and higher systemic vascular resistance. Lower-body subcutaneous fat has been found to cause eccentric left ventricle remodeling, higher cardiac output, and lower systemic vascular resistance, thus suggesting a protective role for subcutaneous adipose tissue, highlighting the importance of adipose tissue quality and function more than just the amount of body fat *per se* (Kim et al., 2016). In this regard, one hypothesis holds that the presence of insulin-sensitive subcutaneous adipose tissue protects the individual from ectopic accumulation of lipids and the development of metabolic syndrome (Kim et al., 2016). Cardiomyocyte hypertrophy and myocardial fat infiltration have also been demonstrated in obesity (Ommen and Lopez-Jimenez, 2013; Samanta et al., 2015). In this sense, obesity-triggered ectopic fat deposition is considered as a predictive risk factor for cardiovascular disease. The above mentioned ectopic fat accumulation in the liver and muscle (together with the associated inflammation) in particular constitutes a cardiovascular risk due to the associated insulin resistance and altered lipid and glucose metabolism. Fat surrounding the heart and blood vessels and within the renal sinus has been linked to local toxic effects by several lines of evidence. The damaging effect of ectopic fat in the cardiovascular system has been attributed to two main mechanisms: (1) fat deposition around the heart (pericardial or epicardial fat) and coronary arteries, (2) lipid accumulation within the cardiomyocyte. Pericardial, perivascular, pericoronary, and myocardial fat accumulation may lead to injury in blood vessels and heart directly by lipotoxicity and indirectly by cytokine secretion (Lim and Meigs, 2014). Fat in the neck is the only fat depot in the upper-body that is considered as an additional cardiovascular risk, and it has been found to positively correlate with insulin resistance, visceral fat content, and metabolic syndrome (Ben-Noun and Laor, 2003; Preis et al., 2010). Interestingly, pericardial fat has been proposed to play roles in support and mechanical purpose (for example, attenuation of vascular tension and torsion). However, this fat depot, when gets considerably enlarged in obesity conditions, represents a mechanical hindrance for the beating heart, thus altering cardiac size and performance (Iacobellis, 2009). In this connection, according to the Framingham Heart Study, pericardial fat is associated with coronary artery calcification and impaired cardiac function and conduction (Rosito et al., 2008). Accumulated fat around the coronary arteries and the heart appears to promote the atherosclerosis process, being associated with oxidative stress-related mechanisms. Myocardial fat accumulation has been associated with increased left ventricle mass, myocardiopathy and heart failure, mainly due to lipid-caused apoptosis of cardiomyocytes and the consequent cardiac dysfunction (Szczepaniak et al., 2003; Lim and Meigs, 2014).

A vast body of experimental, epidemiological, and clinical evidence supports the idea that obesity results harmful for both cardiovascular structure and function, mainly due to increased inflammation caused by deregulated adipokine production by a dysfunctional adipose tissue. In line with this, active endocrine and paracrine activity of cardiac ectopic fat depots within the cardiovascular system may be greatly responsible for insulin resistance and the atherosclerosis process. Moreover, leptin, adiponectin, resistin, visfatin, omentin, IL-1, IL-6, plasminogen activator inhibitor-1, and TNFα, among several other circulating factors, have been reported to signal to the myocardium through either paracrine or autocrine pathways (Iacobellis, 2015). Also, some anti-inflammatory factors secreted from perivascular fat (adiponectin, adrenomedullin, and omentin) have been demonstrated to play a key protective role in the regulation of the arterial vascular tone (vasodilation), decreasing oxidative stress, improving endothelial function, and increasing insulin sensitivity (Sacks and Fain, 2007; Piché and Poirier, 2018). It is important to highlight that secretion of pro-inflammatory adipokines is not

only due to adipocyte secretion but also to secretion coming from adipose tissue-infiltrated macrophages (Chatterjee et al., 2009).

In summary, beyond the contribution of visceral fat-secreted adipokines to cardiovascular disease, the presence of cardiac ectopic fat does also contribute: firstly, due to mechanical functions, and secondly, due to cardiac ectopic fat-released adipokines which would link the ectopic cardiac fat depot, the vasculature, and the myocardium, thus playing key roles in the pathogenesis of cardiovascular disease.

THE "OBESE" BRAIN

This section of the review is dedicated exclusively to the brain in the context of obesity. We will approach this topic from a variety of perspectives, including the anatomical and functional changes observed in the brain of obese individuals, the effects of obesity-associated circulating factors on the brain, the effects of obesity-associated morbidities on the brain and, last but not least, the effects of obesity-associated inflammation on the brain.

Anatomical Aspects

Differences in both gray and white matter have been reported in obese individuals compared to their normal-weight counterparts. Regarding the gray matter, it has been shown that it is reduced in brain regions such as the hippocampus, prefrontal cortex, and other subcortical regions in the context of obesity (Stillman et al., 2017). Interestingly, these differences have been attributed exclusively to excessive adiposity, since they have been shown to be still present even after controlling obesity-associated conditions, including diabetes (Raji et al., 2009). Hippocampal atrophy is of particular importance since it has been related to Alzheimer's disease (AD) (Elias et al., 2000). Reduction in the volume of gray matter has been quite well established in several other brain regions of obese individuals using a variety of methodologies (Pannacciulli et al., 2006; Raji et al., 2009; Medic et al., 2016). There are studies reporting both obesity-associated reductions, as well as increases, in white matter in the context of obesity (Pannacciulli et al., 2006; Raji et al., 2009; Debette et al., 2010; Driscoll et al., 2012; van Bloemendaal et al., 2016).

Cognitive Function

Obesity and metabolic syndrome have undoubtedly been linked to deterioration in cognitive function. Moreover, clinical data have shown that obesity and diabetes mellitus are linked not only to cognitive decline but also to other brain disorders such as dementia, anxiety, and depression (Simon et al., 2006; Riederer et al., 2017; Sanderlin et al., 2017). Due to the difficulty to dissect the impact of each component of the obesity-associated altered metabolism on neuronal performance, it is assumed that brain structural changes, as well as the consequent cognitive impairment, are the result of the synergistic interplay between the different obesity-induced risk factors (Yaffe, 2007; Yates et al., 2012). Several models have been proposed that include the involvement of oxidative stress, inflammation, and abnormal brain lipid metabolism (Yates et al., 2012). Peripheral insulin resistance has been shown to be accompanied with cognitive decline, mainly in memory and executive performance (Heni et al., 2015; Mainardi et al., 2015; Cheke et al., 2017).

Several studies have reported that obesity in midlife is associated with increased risk of mild cognitive impairment, altered executive functioning and short-term memory, and dementia (Kivipelto et al., 2005; Cournot et al., 2006; Whitmer et al., 2008; Sabia et al., 2009; Nguyen et al., 2014). Similar results have been shown in studies carried out in animal models of high-fat diet-induced obesity (Murray et al., 2009; McNeilly et al., 2011; Nguyen et al., 2014). In contrast, the association between obesity late in life and cognitive function is less clear. A recent and important study of more than 10000 men and women, followed for up to 28 years, has examined the link between obesity and cognitive change. In this study, participants were assessed for BMI, waist circumference, signs of dementia, as well as cognitive decline (Singh-Manoux et al., 2018). This study identified that obesity (BMI $>$ 30) at age 50 years is a risk factor for dementia, whereas obesity was not a dementia risk factor at ages 60 and 70 years. This difference may be due to the fact that BMI starts to decline several years before the diagnosis of dementia (Singh-Manoux et al., 2018). These findings could explain, at least in part, the situation known as "obesity paradox" in which underweight older people consistently show an increased risk of dementia while people having normal BMI or even being overweight in the elderly do not.

Effects of Obesity-Associated Circulating Factors on the Brain

Vast epidemiological evidence supports a link between diabetes mellitus and cognitive dysfunction (Gudala et al., 2013; Koekkoek et al., 2015; Zhao et al., 2018). However, it should be mentioned that this association, as well as the severity of cognitive decline, may vary according to the type of diabetes and the age diabetes starts. Loss in glycemic control, evidenced by increased circulating HbA1c levels, has been found to be a risk factor for cognitive dysfunction, with behavioral and psychological manifestations (Sakurai et al., 2014). However, the Leiden 85-plus Study, which prospectively evaluated 599 individuals of ∼85 years of age, reported that HbA1c concentrations were not associated with cognitive dysfunction (van den Berg et al., 2006). Clinical evidence has suggested that the duration of diabetes alone may not influence cognitive performance if glycemia is properly controlled over time (West et al., 2014). Interestingly, beyond the chronically high glucose levels, blood glucose peaks have been related to both cognitive impairment and increased risk of dementia (Geijselaers et al., 2015; Rawlings et al., 2017). Additionally, observational studies have shown beneficial effects of some glucose-lowering treatments on cognitive performance. For example, metformin has been shown to improve cognitive performance in US diabetic veterans (Orkaby et al., 2017).

Leptin deficiency has been linked to alterations in brain volume and structure, and these alterations have been shown to be reversed by external leptin administration (Matochik et al., 2005; London et al., 2011). Leptin has been shown to have a direct impact on the hypothalamic nuclei which are responsible for the production of both orexigenic and anorexigenic peptides

(Qi et al., 2004; Kishi and Elmquist, 2005). Indeed, leptin has been demonstrated to exert neurotrophic actions during the development of the hypothalamus, stimulating the growth of axons from the arcuate nucleus to other regions that control energy homeostasis, thus participating in the development of feeding circuits. Interestingly, this developmental activity of leptin has been shown to depend on timing and duration of leptin exposure (Bouret et al., 2004, 2012; Bouyer and Simerly, 2013; Kamitakahara et al., 2018). Leptin has also been related to presynaptic neurotransmitter release and postsynaptic neurotransmitter sensitivity, and to the processes of memory and cognition, especially to hypothalamic and hippocampal functions (Fewlass et al., 2004; Davidson et al., 2005; Harvey et al., 2005; Oomura et al., 2010). Alterations in hippocampal structure and function have been reported in animals with congenital leptin deficit, supporting a role for leptin in hippocampal development and function (Li et al., 2002; Dhar et al., 2014). Neurodegeneration, neurogenesis, synaptic plasticity as well as memory consolidation have been shown to be influenced by leptin action on the hippocampus (Doherty, 2011). Also, leptin has been shown to enhance cognition through the regulation of hippocampal function. Both *in vivo* and *in vitro* studies (the latter in hippocampal slices) have shown that exogenous leptin is able to induce long-term potentiation (Shanley et al., 2001; Wayner et al., 2004; Luo et al., 2015). Other *in vitro* studies have shown that leptin is able to induce synapse formation in cultured hippocampal neurons, thus providing a possible explanation for the long-term potentiation observed after leptin administration. Studies in humans have shown that high leptin levels are negatively correlated with late-in-life dementia risk (Harvey et al., 2005; Lieb et al., 2009). Moreover, leptin has been shown to reduce extracellular levels of amyloid beta peptide (Aβ; whose deposition is pathognomonic of AD) both *in vivo* and *in vitro* (Fewlass et al., 2004). For these reasons, the elevation of leptin has been suggested as a therapeutic alternative for dementia (Fewlass et al., 2004; Harvey et al., 2005; Irving and Harvey, 2013; McGregor and Harvey, 2018). Although animal studies are promising, further research is needed to assess whether these findings apply to human beings.

Due to undetectable levels of adiponectin in the cerebrospinal fluid (CSF), it was first thought that this hormone was not able to cross the BBB (Pan et al., 2006; Spranger et al., 2006). However, several studies have shown that intravenous injection of adiponectin leads to detectable levels of the hormone in the CSF of patients with unspecified neurological disorders (Kos et al., 2007; Kusminski et al., 2007; Neumeier et al., 2007). Indeed, as no HMW adiponectin has been detected in the CSF, it is now believed that only smaller forms of the adiponectin hormone can cross the BBB (Kusminski et al., 2007; Schulz et al., 2011). Thus, the origin of brain associated adiponectin is still a matter of debate. Adiponectin plasma levels correlate inversely with obesity, insulin resistance and type-2 diabetes mellitus (Hotta et al., 2001; Kondo et al., 2002), with adiponectin levels in the CSF being 1000-fold lower than the plasma levels (Kos et al., 2007; Kusminski et al., 2007). Adiponectin has been shown to regulate proliferation, neurogenesis, and branching of hippocampal neural stem cells (Zhang et al., 2011, 2016; Yau et al., 2014). Also, it has been shown to exert a neuroprotective role against Aβ-induced oxidative stress *in vitro* (Ng and Chan, 2017). Adiponectin deficiency in mice has shown to cause memory and spatial learning impairment, anxiety, and impaired fear conditioning, symptoms that are probably associated to the decreased synaptic protein levels, increased neuronal apoptosis and impaired insulin signaling found in those animals (Ng et al., 2016). Also, adiponectin-deficient mice have shown to suffer larger brain infarctions after ischemia and reperfusion compared with control animals, and adiponectin administration has shown to reduce the infarction size. Thus neuroprotective effects have been attributed to this adipokine (Nishimura et al., 2008). Adiponectin physiological levels are generally higher in females than in males and decrease in both sexes as age increases (Ng and Chan, 2017). However, among women, those with higher plasma levels of adiponectin have shown to exhibit poorer performance in language and global cognition and to coincide with greater mild cognitive impairment diagnosis (Wennberg et al., 2016). Nevertheless, more studies are necessary to conclusively affirm that higher adiponectin plasma level is a trustable predictor of cognitive decline. Patients with AD have been observed to have decreased levels of adiponectin in CSF, compared to those found in healthy controls or even to patients with mild cognitive impairment. However, adiponectin levels have been found to be increased in plasma of patients with mild cognitive impairment and AD, compared to that in controls. Thus, a loss of function of adiponectin signaling has been suggested to occur in the pathogenesis of AD (Waragai et al., 2017).

As mentioned before, the increased circulating levels of pro-inflammatory cytokines participate in obesity-induced systemic inflammation. This systemic inflammation may participate in the development of cognitive decline and dementia. For example, IL-1β and IL-6 have been shown to disrupt cognition- and memory-related neuronal circuits (Gemma and Bickford, 2007). Increased plasma levels of C-reactive protein and IL-6 have been identified in a meta-analysis performed by Koyama et al. (2013). Peripheral cytokines have been shown to induce local production of cytokines in the brain (Dantzer et al., 2008).

Effects of Obesity-Associated Morbidities on the Brain

It is important to highlight that all the obesity-associated morbidities mentioned before (cardiovascular disease, diabetes, atherosclerosis, etc.) do impact on brain health. Obesity-derived vascular problems, such as atherosclerosis and arteriosclerosis, which are systemic diseases, are known to affect the steady blood flow of vessels that feed the brain, thus contributing to cognitive impairment or even stroke, where large areas of the brain die due to the stop in the blood flow of a major brain artery caused by a blood clot. Vascular dementia has been shown to be caused by cerebrovascular disease, and compelling evidence has shown that cerebrovascular disease may be initiated by obesity (Gorelick et al., 2011; Zlokovic, 2011). However, many aspects of the association between obesity and cerebrovascular disease are still poorly defined. Also, epidemiological studies have shown that cardiovascular risk factors such as obesity, hypertension, diabetes,

and low physical activity negatively affect brain performance (Wolf, 2012; Yano et al., 2014). A longitudinal study from Gustafson and coworkers has shown lower BBB integrity in overweight or obese individuals, compared to normal-weight controls (Gustafson et al., 2007). Similar evidence has been presented from rodent studies (Kanoski et al., 2010; Davidson et al., 2012). Indeed, irregular heartbeat conditions such as arrhythmia or atrial fibrillation, as well as obstructive sleep apnea (both highly prevalent in obese individuals), have been linked to increased risk of ischemic stroke and dementia development (Zhang et al., 2015). Interestingly, several studies have reported that obese people who survive to a first stroke event usually have improved subsequent cerebrovascular disease and mortality, as part of the previously mentioned "obesity paradox." This could come in line with the fact that obese people tend to suffer more lacunar-type of stroke, which is generally of faster recovery and better prognosis (Letra and Seiça, 2017).

Epidemiological studies have linked type-2 diabetes mellitus with cognitive impairment and dementia, with insulin resistance and hyperglycemia as the probable mechanistic links (Ott et al., 1996; Peila et al., 2002). Similarly, several cross-sectional studies have confirmed the association between insulin resistance and cognitive decline (van den Berg et al., 2006; Young et al., 2006; Ekblad et al., 2017). Hyperglycemia has been associated with poor cognitive outcomes both in cross-sectional studies (Yaffe et al., 2012) as well as in prospective studies (Prickett et al., 2015). A very recent 6-year follow-up study from Hong and coworkers has found that insulin resistance is associated with diminished cognitive performance in older individuals (Kong et al., 2018). Also, data from prospective studies have shown that individuals with type-2 diabetes exhibit poorer performance in information-processing speed, memory, attention, and executive function compared to controls (Hassing et al., 2004; van den Berg et al., 2010; Moheet et al., 2015). Longitudinal and cross-sectional studies have undoubtedly demonstrated a relationship between diabetes and mild/moderate cognitive dysfunction in type-2 diabetes, but less is known about the strength of association between diabetes and dementia. Systematic review and meta-analysis performed by Biessels and coworkers have shown an increase of 50–100% in the risk of dementia in people with type-2 diabetes, compared with people without diabetes (Biessels et al., 2006). However, the evidence is controversial, and further interventional studies are needed to evaluate the effect of controlling insulin resistance and diabetes on cognitive dysfunction.

Interestingly, obesity comorbidities have been shown to participate in the onset and progression of neurodegenerative diseases such as AD. The complete mechanisms by which obesity influences the risk of AD is not entirely clear yet. However, epidemiological studies have demonstrated that type-2 diabetes increases the risk of AD (Profenno et al., 2010). It is assumed that insulin resistance is a key causative factor for diabetes and it has been demonstrated that individuals with peripheral insulin resistance are more prone to develop AD and related pathologies (Sims-Robinson et al., 2010; Rasgon et al., 2011). Moreover, at the cellular and molecular level, insulin signaling has been demonstrated to interfere with Aβ degradation and deposition (Carro et al., 2002; Farris et al., 2003). Further, insulin deficiency has also been shown to promote tau phosphorylation, leading to the accumulation of neurofibrillary tangles (Schubert et al., 2003). Accumulating evidence has shown that the brain itself develops insulin resistance due to the impairment in the insulin pathway (Moloney et al., 2010; Talbot and Wang, 2014; Su et al., 2017). In line with this, *in vivo* experimental data have shown that insulin resistance modifies cognitive performance even in the absence of diabetes (Su et al., 2017). Moreover, insulin signaling impairment has been found in brains from AD patients (Talbot et al., 2012). Increased levels of amyloid proteins have been found in the plasma of obese individuals (Lee et al., 2009; Jahangiri et al., 2013). Also, higher expression levels of beta-amyloid precursor protein and tau, two pathognomonic features of AD, have been found in the hippocampus of morbidly obese patients, compared to non-obese controls (Mrak, 2009; Nguyen et al., 2014). On the other hand, numerous studies have demonstrated that high-fat diets contribute to the higher expression of AD markers in rodents (Studzinski et al., 2009; Puig et al., 2012; Koga et al., 2014). Indeed, uncontrolled diabetes has also been linked to the risk of developing AD (Xu et al., 2009).

Effects of Obesity-Associated Inflammation Within the Brain

Several aspects of brain function result affected by obesity-triggered inflammation. Periodic neuroinflammation is a necessary defense for the brain. However, when neuroinflammation becomes prolonged or uncontrolled (chronic neuroinflammation), it disrupts the normal protective barriers and leads to maladaptive synaptic plasticity and the development of different neurodegenerative disorders (Purkayastha and Cai, 2013). It has long been accepted that the BBB keeps blood inflammatory cells (monocytes and neutrophils) from getting into the brain. Therefore, microglia would be the only cells that mediate brain inflammation. However, it has become known that neutrophils and monocytes are able to infiltrate the injured brain and contribute to inflammation (Jeong et al., 2013). Astrocytes are known to produce anti-inflammatory factors that recruit monocytes, and neurons are able to both positively or negatively modulate anti-inflammatory response (Kim et al., 2010; Jeong et al., 2013). Thus, brain inflammation involves the coordinated efforts of several types of cells including microglia neutrophils, monocytes, astrocytes, and neurons.

Chronic neuroinflammation has been shown to impair adult hippocampal neurogenesis, and the blockade of neuroinflammation has demonstrated to restore it (Ekdahl et al., 2003; Monje et al., 2003). Also, impaired neurogenesis has been found in the hypothalamus of high-fat diet-fed rodents, probably due to the chronic neuroinflammatory response (Li et al., 2012). The complete mechanism is not fully understood, but stimulation of immune cells with the concomitant activation of the NF-kB pathway, and the release of interleukins and nitric oxide are thought to be involved (Purkayastha and Cai, 2013).

On the other hand, brain inflammation, mediated by inflammatory cells such as microglia and astrocytes, plays pivotal roles in regulating synaptic structure and function

(Mottahedin et al., 2017). Synaptic disorganization is an integral part of several neurological disorders (Ebrahimi-Fakhari and Sahin, 2015). Glial cells are thought to play a vital role in synaptic architecture and hence neuronal connectivity. For this reason, factors that affect glial cells during development may also have long-term consequences on the synapse performance. Accordingly, an interaction between synaptic disorganization and immune function has been linked with cognitive weakness (Delpech et al., 2015). The BBB is known to actively participate in the inflammatory events and, conversely, the obesity-associated chronic inflammation also influences the BBB. It has been suggested that the BBB disruption occurs well before the infiltration of immune cells to the site of inflammation. Once within the brain, these effector cells and their secreted factors act upon microglia, astrocytes, and pericytes, which are important components of the BBB, and collaborate to a further BBB disruption thus leading to neuronal damage (Sonar and Lal, 2018).

Chronic brain inflammation also has been linked to neurodegenerative disorders such as AD. Aβ peptide accumulation in the brain parenchyma and blood vessels has been shown to promote both acute and chronic inflammatory responses which are mediated by astrocytes and microglia and which may finally cause neurodegeneration. However, the role of inflammation in AD is controversial, because inflammation has been found to have a beneficial role in the early stages of the disease. Nevertheless, the chronic activation of the microglia has been linked to the increased generation of Aβ and also with tau phosphorylation (Meraz-Ríos et al., 2013). Overall, the inflammatory process in AD is characterized by changes in microglial morphology together with astrogliosis (increased number, size, and motility of astrocytes). Studies in rodent models have shown that neuroinflammation is linked to early stages in tauopathies, even preceding tangle formation (Yoshiyama et al., 2007). Although the neuronal death associated with inflammation makes it a potential risk factor in the pathogenesis of AD, whether brain inflammation is the cause of or a secondary phenomenon to this disorder is unclear yet. Obesity may serve as an amplifier or initiator of the chronic inflammation observed in AD patients, although further research is needed to clarify the specific contribution of obesity to the chronic brain inflammation observed at the onset and progression of AD.

CONCLUDING REMARKS

The causes and impact of obesity on overall health are far from linear and point to a complex set of interactions. The ultimate impact of obesity on an individual appears to be the summation of the effects of adipose-derived factors (adipokines, triglycerides, etc.) and indirect obesity effects (hypertension, glycemic dysregulation, etc.) and the physiology of the various organ systems of the body. Environmental factors and aging can accelerate or inhibit the effects of obesity on the various organ systems and tissues of the body, and this is an area of research that is rapidly expanding and identifying exciting results. Given the rapid increase in both obesity and aging in the populations of most Western societies, it will be critical to move obesity research into the realm of translational interventions, whereby the negative impacts of obesity on health are delayed or prevented in an increasingly elderly population.

AUTHOR CONTRIBUTIONS

RU and JK contributed to conception and design of the review and wrote the manuscript.

REFERENCES

Abdelmoula, A., Martin, V., Bouchant, A., Walrand, S., Lavet, C., Taillardat, M., et al. (2012). Knee extension strength in obese and nonobese male adolescents. *Appl. Physiol. Nutr. Metab.* 37, 269–275. doi: 10.1139/h2012-010

Achari, A. E., and Jain, S. K. (2017). Adiponectin, a therapeutic target for obesity, diabetes, and endothelial dysfunction. *Int. J. Mol. Sci.* 18:E1321. doi: 10.3390/ijms18061321

Alarcon, C., Boland, B. B., Uchizono, Y., Moore, P. C., Peterson, B., Rajan, S., et al. (2016). Pancreatic β-cell adaptive plasticity in obesity increases insulin production but adversely affects secretory function. *Diabetes* 65, 438–450. doi: 10.2337/db15-0792

Ärnlöov, J., Ingelsson, E., Sundstroöm, J., and Lind, L. (2010). Impact of body mass index and the metabolic syndrome on the risk of cardiovascular disease and death in middle-aged men. *Circulation* 121, 230–236. doi: 10.1161/CIRCULATIONAHA.109.887521

Bays, H. E., Toth, P. P., Kris-Etherton, P. M., Abate, N., Aronne, L. J., Brown, W. V., et al. (2013). Obesity, adiposity, and dyslipidemia: a consensus statement from the National Lipid Association. *J. Clin. Lipidol.* 7, 304–383. doi: 10.1016/j.jacl.2013.04.001

Benatti, F., Solis, M., Artioli, G., Montag, E., Painelli, V., Saito, F., et al. (2012). Liposuction induces a compensatory increase of visceral fat which is effectively counteracted by physical activity: a randomized trial. *J. Clin. Endocrinol. Metab.* 97, 2388–2395. doi: 10.1210/jc.2012-1012

Ben-Noun, L. L., and Laor, A. (2003). Relationship of neck circumference to cardiovascular risk factors. *Obes. Res.* 11, 226–231. doi: 10.1038/oby.2003.35

Biernacka, K., and Małecka-Panas, E. (2015). *Adipokines in Pancreatic Diseases*. Available at: http://www.pnmedycznych.pl/wp-content/uploads/2016/01/pnm_2015_8b_011-015.pdf (accessed April 15, 2015).

Biessels, G. J., Staekenborg, S., Brunner, E., Brayne, C., and Scheltens, P. (2006). Risk of dementia in diabetes mellitus: a systematic review. *Lancet Neurol.* 5, 64–74. doi: 10.1016/S1474-4422(05)70284-2

Björnson, E., Adiels, M., Taskinen, M.-R., and Borén, J. (2016). Kinetics of plasma triglycerides in abdominal obesity. *Curr. Opin. Lipidol.* 28, 11–18. doi: 10.1097/MOL.0000000000000375

Blimkie, C. J., Sale, D. G., and Bar-Or, O. (1990). Voluntary strength, evoked twitch contractile properties and motor unit activation of knee extensors in obese and non-obese adolescent males. *Eur. J. Appl. Physiol. Occup. Physiol.* 61, 313–318.

Boucher, J., Masri, B., Daviaud, D., Gesta, S., Guigné, C., Mazzucotelli, A., et al. (2005). Apelin, a newly identified adipokine up-regulated by insulin and obesity. *Endocrinology* 146, 1764–1771. doi: 10.1210/en.2004-1427

Bouret, S. G., Bates, S. H., Chen, S., Myers, M. G., and Simerly, R. B. (2012). Distinct roles for specific leptin receptor signals in the development of hypothalamic feeding circuits. *J. Neurosci.* 32, 1244–1252. doi: 10.1523/jneurosci.2277-11.2012

Bouret, S. G., Draper, S. J., and Simerly, R. B. (2004). Trophic action of leptin on hypothalamic neurons that regulate feeding. *Science* 304, 108–110. doi: 10.1126/science.1095004

Bouyer, K., and Simerly, R. B. (2013). Neonatal leptin exposure specifies innervation of presympathetic hypothalamic neurons and improves the metabolic status of leptin-deficient mice. *J. Neurosci.* 33, 840–851. doi: 10.1523/jneurosci.3215-12.2013

Brown, R., Imran, S. A., Belsham, D. D., Ur, E., and Wilkinson, M. (2007). Adipokine gene expression in a novel hypothalamic neuronal cell line: resistin-dependent regulation of fasting-induced adipose factor and SOCS-3. *Neuroendocrinology* 85, 232–241. doi: 10.1159/000104248

Brunt, E. M., Janney, C. G., Bisceglie, A. M., Neuschwander-Tetri, B. A., and Bacon, B. R. (1999). Nonalcoholic steatohepatitis: a proposal for grading and staging the histological lesions. *Am. J. Gastroenterol.* 94, 2467–2474. doi: 10.1111/j.1572-0241.1999.01377.x

Buchwald, H., Estok, R., Fahrbach, K., Banel, D., Jensen, M. D., Pories, W. J., et al. (2009). Weight and type 2 diabetes after bariatric surgery: systematic review and meta-analysis. *Am. J. Med.* 122, 248.e–256.e. doi: 10.1016/j.amjmed.2008.09.041

Busetto, L. (2014). Bariatric/metabolic surgery for the obese with Type 2 diabetes with BMI < 35 kg/m2: why caution is required. *Diabetes Manag.* 4, 123–130. doi: 10.2217/dmt.13.76

Busetto, L., Pisent, C., Rinaldi, D., Longhin, P. L., Segato, G., De Marchi, F., et al. (2000). Variation in lipid levels in morbidly obese patients operated with the LAP-BAND adjustable gastric banding system: effects of different levels of weight loss. *Obes. Surg.* 10, 569–577.

Calle, E. E., Rodriguez, C., Walker-Thurmond, K., and Thun, M. J. (2003). Overweight, obesity, and mortality from cancer in a prospectively studied cohort of U.S. adults. *N. Engl. J. Med.* 348, 1625–1638. doi: 10.1056/NEJMoa021423

Calvo, N., Beltrán-Debón, R., Rodríguez-Gallego, E., Hernández-Aguilera, A., Guirro, M., Mariné-Casadó, R., et al. (2015). Liver fat deposition and mitochondrial dysfunction in morbid obesity: an approach combining metabolomics with liver imaging and histology. *World J. Gastroenterol.* 21, 7529–7544. doi: 10.3748/wjg.v21.i24.7529

Carro, E., Trejo, J. L., Gomez-Isla, T., LeRoith, D., and Torres-Aleman, I. (2002). Serum insulin-like growth factor I regulates brain amyloid-β levels. *Nat. Med.* 8, 1390–1397. doi: 10.1038/nm793

Castan-Laurell, I., Boucher, J., Dray, C., Daviaud, D., Guigné, C., and Valet, P. (2005). Apelin, a novel adipokine over-produced in obesity: Friend or foe? *Mol. Cell. Endocrinol.* 245, 7–9. doi: 10.1016/J.MCE.2005.09.012

Castan-Laurell, I., Dray, C., Attané, C., Duparc, T., Knauf, C., and Valet, P. (2011). Apelin, diabetes, and obesity. *Endocrine* 40, 1–9. doi: 10.1007/s12020-011-9507-9

Chan, D. C., Watts, G. F., Barrett, P. H., Mamo, J. C. L., and Redgrave, T. G. (2002). *Markers of Triglyceride-Rich Lipoprotein Remnant Metabolism in Visceral Obesity*. Available at: https://pdfs.semanticscholar.org/f2a7/60b5c3b24a0cfec2e3e6ffc1188b70f7ef1c.pdf (accessed April 17, 2019).

Chatterjee, T. K., Stoll, L. L., Denning, G. M., Harrelson, A., Blomkalns, A. L., Idelman, G., et al. (2009). Proinflammatory phenotype of perivascular adipocytes: influence of high-fat feeding. *Circ. Res.* 104, 541–549. doi: 10.1161/CIRCRESAHA.108.182998

Cheke, L. G., Bonnici, H. M., Clayton, N. S., and Simons, J. S. (2017). Obesity and insulin resistance are associated with reduced activity in core memory regions of the brain. *Neuropsychologia* 96, 137–149. doi: 10.1016/j.neuropsychologia.2017.01.013

Chowdhury, B., Sjöström, L., Alpsten, M., Kostanty, J., Kvist, H., and Löfgren, R. (1994). A multicompartment body composition technique based on computerized tomography. *Int. J. Obes. Relat. Metab. Disord.* 18, 219–234.

Christou, N. V., Sampalis, J. S., Liberman, M., Look, D., Auger, S., McLean, A. P. H., et al. (2004). Surgery decreases long-term mortality, morbidity, and health care use in morbidly obese patients. *Ann. Surg.* 240, 416–423.

Cooper, C., Inskip, H., Croft, P., Campbell, L., Smith, G., McLaren, M., et al. (1998). Individual risk factors for hip osteoarthritis: obesity, hip injury, and physical activity. *Am. J. Epidemiol.* 147, 516–522.

Cournot, M., Marquie, J. C., Ansiau, D., Martinaud, C., Fonds, H., Ferrieres, J., et al. (2006). Relation between body mass index and cognitive function in healthy middle-aged men and women. *Neurology* 67, 1208–1214. doi: 10.1212/01.wnl.0000238082.13860.50

Cummings, D. E., and Rubino, F. (2018). Metabolic surgery for the treatment of type 2 diabetes in obese individuals LAGB Laparoscopic adjustable gastric banding NIH National Institutes of Health QALY Quality-adjusted life-year. *Diabetologia* 61, 257–264. doi: 10.1007/s00125-017-4513-y

Dantzer, R., O'Connor, J. C., Freund, G. G., Johnson, R. W., and Kelley, K. W. (2008). From inflammation to sickness and depression: when the immune system subjugates the brain. *Nat. Rev. Neurosci.* 9, 46–56. doi: 10.1038/nrn2297

Dash, S., Xiao, C., Morgantini, C., and Lewis, G. F. (2015). New insights into the regulation of chylomicron production. *Annu. Rev. Nutr.* 35, 265–294. doi: 10.1146/annurev-nutr-071714-034338

Davidson, T., Kanoski, S., Walls, E., and Jarrard, L. (2005). Memory inhibition and energy regulation. *Physiol. Behav.* 86, 731–746. doi: 10.1016/j.physbeh.2005.09.004

Davidson, T. L., Monnot, A., Neal, A. U., Martin, A. A., Horton, J. J., and Zheng, W. (2012). The effects of a high-energy diet on hippocampal-dependent discrimination performance and blood–brain barrier integrity differ for diet-induced obese and diet-resistant rats. *Physiol. Behav.* 107, 26–33. doi: 10.1016/j.physbeh.2012.05.015

de Luca, C., Kowalski, T. J., Zhang, Y., Elmquist, J. K., Lee, C., Kilimann, M. W., et al. (2005). Complete rescue of obesity, diabetes, and infertility in db/db mice by neuron-specific LEPR-B transgenes. *J. Clin. Invest.* 115, 3484–3493. doi: 10.1172/JCI24059

Debette, S., Beiser, A., Hoffmann, U., DeCarli, C., O'Donnell, C. J., Massaro, J. M., et al. (2010). Visceral fat is associated with lower brain volume in healthy middle-aged adults. *Ann. Neurol.* 68, 136–144. doi: 10.1002/ana.22062

Delmonico, M. J., Harris, T. B., Visser, M., Park, S. W., Conroy, M. B., Velasquez-Mieyer, P., et al. (2009). Longitudinal study of muscle strength, quality, and adipose tissue infiltration. *Am. J. Clin. Nutr.* 90, 1579–1585. doi: 10.3945/ajcn.2009.28047

Delpech, J.-C., Madore, C., Nadjar, A., Joffre, C., Wohleb, E. S., and Layé, S. (2015). Microglia in neuronal plasticity: Influence of stress. *Neuropharmacology* 96, 19–28. doi: 10.1016/j.neuropharm.2014.12.034

Deng, Y., and Scherer, P. E. (2010). Adipokines as novel biomarkers and regulators of the metabolic syndrome. *Ann. N. Y. Acad. Sci.* 1212, E1–E19. doi: 10.1111/j.1749-6632.2010.05875.x

Dhar, M., Wayman, G. A., Zhu, M., Lambert, T. J., Davare, M. A., and Appleyard, S. M. (2014). Leptin-induced spine formation requires TrpC channels and the CaM kinase cascade in the hippocampus. *J. Neurosci.* 34, 10022–10033. doi: 10.1523/JNEUROSCI.2868-13.2014

Dodson, M. V., Du, M., Wang, S., Bergen, W. G., Fernyhough-Culver, M., Basu, U., et al. (2014). Adipose depots differ in cellularity, adipokines produced, gene expression, and cell systems. *Adipocyte* 3, 236–241. doi: 10.4161/adip.28321

Doherty, G. H. (2011). Obesity and the ageing brain: could leptin play a role in neurodegeneration? *Curr. Gerontol. Geriatr. Res.* 2011:708154. doi: 10.1155/2011/708154

Driscoll, I., Beydoun, M. A., An, Y., Davatzikos, C., Ferrucci, L., Zonderman, A. B., et al. (2012). Midlife obesity and trajectories of brain volume changes in older adults. *Hum. Brain Mapp.* 33, 2204–2210. doi: 10.1002/hbm.21353

Drolet, R., Bélanger, C., Fortier, M., Huot, C., Mailloux, J., Légaré, D., et al. (2009). Fat depot-specific impact of visceral obesity on adipocyte adiponectin release in women. *Obesity* 17, 424–430. doi: 10.1038/oby.2008.555

Ebbert, J. O., Elrashidi, M. Y., and Jensen, M. D. (2014). Managing overweight and obesity in adults to reduce cardiovascular disease risk. *Curr. Atheroscler. Rep.* 16:445. doi: 10.1007/s11883-014-0445-x

Ebrahimi-Fakhari, D., and Sahin, M. (2015). Autism and the synapse. *Curr. Opin. Neurol.* 28, 91–102. doi: 10.1097/WCO.0000000000000186

Ekblad, L. L., Rinne, J. O., Puukka, P., Laine, H., Ahtiluoto, S., Sulkava, R., et al. (2017). Insulin resistance predicts cognitive decline: an 11-year follow-up of a nationally representative adult population sample. *Diabetes Care* 40, 751–758. doi: 10.2337/dc16-2001

Ekdahl, C. T., Claasen, J.-H., Bonde, S., Kokaia, Z., and Lindvall, O. (2003). Inflammation is detrimental for neurogenesis in adult brain. *Proc. Natl. Acad. Sci. U.S.A.* 100, 13632–13637. doi: 10.1073/pnas.2234031100

Elias, M. F., Beiser, A., Wolf, P. A., Au, R., White, R. F., and D'Agostino, R. B. (2000). The preclinical phase of alzheimer disease: a 22-year prospective study of the Framingham Cohort. *Arch. Neurol.* 57, 808–813.

Farris, W., Mansourian, S., Chang, Y., Lindsley, L., Eckman, E. A., Frosch, M. P., et al. (2003). Insulin-degrading enzyme regulates the levels of insulin, amyloid -protein, and the -amyloid precursor protein intracellular domain in vivo. *Proc. Natl. Acad. Sci. U.S.A.* 100, 4162–4167. doi: 10.1073/pnas.0230450100

Feingold, K. R., and Grunfeld, C. (2018). *Obesity and Dyslipidemia*. Available at: http://www.ncbi.nlm.nih.gov/pubmed/26247088 (accessed April 17, 2019).

Fewlass, D. C., Noboa, K., Pi-Sunyer, F. X., Johnston, J. M., Yan, S. D., and Tezapsidis, N. (2004). Obesity-related leptin regulates Alzheimer's Aβ. *FASEB J.* 18, 1870–1878. doi: 10.1096/fj.04-2572com

Fontana, L., Eagon, J. C., Trujillo, M. E., Scherer, P. E., and Klein, S. (2007). Visceral fat adipokine secretion is associated with systemic inflammation in obese humans. *Diabetes* 56, 1010–1013. doi: 10.2337/db06-1656

Foster, M. T., Softic, S., Caldwell, J., Kohli, R., DeKloet, A. D., and Seeley, R. J. (2013). Subcutaneous adipose tissue transplantation in diet-induced obese mice attenuates metabolic dysregulation while removal exacerbates it. *Physiol. Rep.* 1:e00015. doi: 10.1002/phy2.15

Franssen, R., Monajemi, H., Stroes, E. S. G., and Kastelein, J. J. P. (2011). Obesity and Dyslipidemia. *Med. Clin. North Am.* 95, 893–902. doi: 10.1016/j.mcna.2011.06.003

Friedman, J. M., and Halaas, J. L. (1998). Leptin and the regulation of body weight in mammals. *Nature* 395, 763–770. doi: 10.1038/27376

Gaddey, H. L., and Holder, K. (2014). Unintentional weight loss in older adults. *Am. Fam. Physician* 89, 718–722.

Geijselaers, S. L. C., Sep, S. J. S., Stehouwer, C. D. A., and Biessels, G. J. (2015). Glucose regulation, cognition, and brain MRI in type 2 diabetes: a systematic review. *Lancet Diabetes Endocrinol.* 3, 75–89. doi: 10.1016/S2213-8587(14)70148-2

Gemma, C., and Bickford, P. C. (2007). Interleukin-1beta and caspase-1: players in the regulation of age-related cognitive dysfunction. *Rev. Neurosci.* 18, 137–148.

Ghosh, S. (2014). Ectopic fat: the potential target for obesity management. *J. Obes. Metab. Res.* 1, 30–38. doi: 10.4103/2347-9906.123883

Gloy, V. L., Briel, M., Bhatt, D. L., Kashyap, S. R., Schauer, P. R., Mingrone, G., et al. (2013). Bariatric surgery versus non-surgical treatment for obesity: a systematic review and meta-analysis of randomised controlled trials. *BMJ* 347, f5934–f5934. doi: 10.1136/bmj.f5934

Gorelick, P. B., Scuteri, A., Black, S. E., DeCarli, C., Greenberg, S. M., Iadecola, C., et al. (2011). Vascular contributions to cognitive impairment and dementia. *Stroke* 42, 2672–2713. doi: 10.1161/STR.0b013e3182299496

Görgens, S. W., Eckardt, K., Jensen, J., Drevon, C. A., and Eckel, J. (2015). Exercise and regulation of adipokine and myokine production. *Prog. Mol. Biol. Transl. Sci.* 135, 313–336. doi: 10.1016/bs.pmbts.2015.07.002

Grauer, W. O., Moss, A. A., Cann, C. E., and Goldberg, H. I. (1984). Quantification of body fat distribution in the abdomen using computed tomography. *Am. J. Clin. Nutr.* 39, 631–637. doi: 10.1093/ajcn/39.4.631

Gudala, K., Bansal, D., Schifano, F., and Bhansali, A. (2013). Diabetes mellitus and risk of dementia: a meta-analysis of prospective observational studies. *J. Diabetes Investig.* 4, 640–650. doi: 10.1111/jdi.12087

Gumbs, A. A. (2008). Obesity, pancreatitis, and pancreatic cancer. *Obes. Surg.* 18, 1183–1187. doi: 10.1007/s11695-008-9599-3

Gustafson, D. R., Karlsson, C., Skoog, I., Rosengren, L., Lissner, L., and Blennow, K. (2007). Mid-life adiposity factors relate to blood-brain barrier integrity in late life. *J. Intern. Med.* 262, 643–650. doi: 10.1111/j.1365-2796.2007.01869.x

Hajer, G. R., van Haeften, T. W., and Visseren, F. L. J. (2008). Adipose tissue dysfunction in obesity, diabetes, and vascular diseases. *Eur. Heart J.* 29, 2959–2971. doi: 10.1093/eurheartj/ehn387

Halban, P. A., Polonsky, K. S., Bowden, D. W., Hawkins, M. A., Ling, C., Mather, K. J., et al. (2014). β-cell failure in type 2 diabetes: postulated mechanisms and prospects for prevention and treatment. *J. Clin. Endocrinol. Metab.* 99, 1983–1992. doi: 10.1210/jc.2014-1425

Han, T. S., Tajar, A., and Lean, M. E. J. (2011). Obesity and weight management in the elderly. *Br. Med. Bull.* 97, 169–196. doi: 10.1093/bmb/ldr002

Harvey, J., Shanley, L. J., O'Malley, D., and Irving, A. J. (2005). Leptin: a potential cognitive enhancer? *Biochem. Soc. Trans.* 33, 1029–1032. doi: 10.1042/BST20051029

Hassing, L. B., Grant, M. D., Hofer, S. M., Pedersen, N. L., Nilsson, S. E., Berg, S., et al. (2004). Type 2 diabetes mellitus contributes to cognitive decline in old age: a longitudinal population-based study. *J. Int. Neuropsychol. Soc.* 10, 599–607. doi: 10.1017/S1355617704104165

Heni, M., Kullmann, S., Preissl, H., Fritsche, A., and Häring, H.-U. (2015). Impaired insulin action in the human brain: causes and metabolic consequences. *Nat. Rev. Endocrinol.* 11, 701–711. doi: 10.1038/nrendo.2015.173

Hoffstedt, J., Amer, P., Hellers, G., and Lonnqvist', F. (2018). *Variation in Adrenergic Regulation of Lipolysis between Omental and Subcutaneous Adipocytes from Obese and Non-Obese Men*. Available at: www.jlr.org (accessed December 6, 2018).

Honka, H., Hannukainen, J. C., Tarkia, M., Karlsson, H., Saunavaara, V., Salminen, P., et al. (2014). Pancreatic metabolism, blood flow, and β-Cell function in obese humans. *J. Clin. Endocrinol. Metab.* 99, 981–990. doi: 10.1210/jc.2013-4369

Hotamisligil, G. S., and Spiegelman, B. M. (1994). Tumor necrosis factor alpha: a key component of the obesity-diabetes link. *Diabetes* 43, 1271–1278.

Hotta, K., Funahashi, T., Bodkin, N. L., Ortmeyer, H. K., Arita, Y., Hansen, B. C., et al. (2001). Circulating concentrations of the adipocyte protein adiponectin are decreased in parallel with reduced insulin sensitivity during the progression to type 2 diabetes in rhesus monkeys. *Diabetes* 50, 1126–1133.

Hruby, A., and Hu, F. B. (2015). The epidemiology of obesity: a big picture. *Pharmacoeconomics* 33, 673–689. doi: 10.1007/s40273-014-0243-x

Hu, F. B. (2007). Obesity and mortality: watch your waist, not just your weight. *Arch. Intern. Med.* 167, 875–876. doi: 10.1001/archinte.167.9.875

Iacobellis, G. (2009). Epicardial and pericardial fat: close, but very different. *Obesity* 17, 625–625. doi: 10.1038/oby.2008.575

Iacobellis, G. (2015). Local and systemic effects of the multifaceted epicardial adipose tissue depot. *Nat. Rev. Endocrinol.* 11, 363–371. doi: 10.1038/nrendo.2015.58

Illán-Gómez, F., Gonzálvez-Ortega, M., Orea-Soler, I., Alcaraz-Tafalla, M. S., Aragón-Alonso, A., Pascual-Díaz, M., et al. (2012). Obesity and inflammation: change in adiponectin, C-reactive protein, tumour necrosis factor-alpha and interleukin-6 after bariatric surgery. *Obes. Surg.* 22, 950–955. doi: 10.1007/s11695-012-0643-y

Irving, A. J., and Harvey, J. (2013). Leptin regulation of hippocampal synaptic function in health and disease. *Philos. Trans. R. Soc. B Biol. Sci.* 369:20130155. doi: 10.1098/rstb.2013.0155

Jacome-Sosa, M. M., and Parks, E. J. (2014). Fatty acid sources and their fluxes as they contribute to plasma triglyceride concentrations and fatty liver in humans. *Curr. Opin. Lipidol.* 25, 213–220. doi: 10.1097/MOL.0000000000000080

Jahangiri, A., Wilson, P. G., Hou, T., Brown, A., King, V. L., and Tannock, L. R. (2013). Serum amyloid A is found on ApoB-containing lipoproteins in obese humans with diabetes. *Obesity* 21, 993–996. doi: 10.1002/oby.20126

James, A. P., Watts, G., Barrett, H., Smith, D., Pal, S., Chan, D., et al. (2003). Effect of weight loss on postprandial lipemia and low density lipoprotein receptor binding in overweight men. *Metabolism* 52, 136–141. doi: 10.1053/META.2003.50032

Jaworek, J., Bonior, J., Pierzchalski, P., Tomaszewska, R., Stachura, J., Sendur, R., et al. (2002). Leptin protects the pancreas from damage induced by caerulein overstimulation by modulating cytokine production. *Pancreatology* 2, 89–99. doi: 10.1159/000055897

Jensen, M. D. (2008). Role of body fat distribution and the metabolic complications of obesity. *J. Clin. Endocrinol. Metab.* 93, 57–63. doi: 10.1210/jc.2008-1585

Jeong, H.-K., Ji, K., Min, K., and Joe, E.-H. (2013). Brain inflammation and microglia: facts and misconceptions. *Exp. Neurobiol.* 22, 59–67. doi: 10.5607/en.2013.22.2.59

Kahn, B. B., and Flier, J. S. (2000). Obesity and insulin resistance. *J. Clin. Invest.* 106, 473–481. doi: 10.1172/JCI10842

Kamitakahara, A., Bouyer, K., Wang, C. H., and Simerly, R. (2018). A critical period for the trophic actions of leptin on AgRP neurons in the arcuate nucleus of the hypothalamus. *J. Comp. Neurol.* 526, 133–145. doi: 10.1002/cne.24327

Kanoski, S. E., Zhang, Y., Zheng, W., and Davidson, T. L. (2010). The effects of a high-energy diet on hippocampal function and blood-brain barrier integrity in the rat. *J. Alzheimers Dis.* 21, 207–219. doi: 10.3233/JAD-2010-091414

Karelis, A. D., Faraj, M., Bastard, J.-P., St-Pierre, D. H., Brochu, M., Prud'homme, D., et al. (2005). The metabolically healthy but obese individual presents a favorable inflammation profile. *J. Clin. Endocrinol. Metab.* 90, 4145–4150. doi: 10.1210/jc.2005-0482

Karpe, F., Dickmann, J. R., and Frayn, K. N. (2011). Fatty acids, obesity, and insulin resistance: time for a reevaluation. *Diabetes* 60, 2441–2449. doi: 10.2337/db11-0425

Katsanos, C. S., and Mandarino, L. J. (2011). Protein metabolism in human obesity: a shift in focus from whole-body to skeletal muscle. *Obesity* 19, 469–475. doi: 10.1038/oby.2010.290

Kelly, T. M., and Jones, S. B. (1986). Changes in serum lipids after gastric bypass surgery. Lack of a relationship to weight loss. *Int. J. Obes.* 10, 443–452.

Kiliaan, A. J., Arnoldussen, I. A. C., and Gustafson, D. R. (2014). Adipokines: a link between obesity and dementia? *Lancet Neurol.* 13, 913–923. doi: 10.1016/S1474-4422(14)70085-7

Kim, J., Min, K.-J., Seol, W., Jou, I., and Joe, E. (2010). Astrocytes in injury states rapidly produce anti-inflammatory factors and attenuate microglial inflammatory responses. *J. Neurochem.* 115, 1161–1171. doi: 10.1111/j.1471-4159.2010.07004.x

Kim, S. H., Després, J. P., and Koh, K. K. (2016). Obesity and cardiovascular disease: friend or foe? *Eur. Heart J.* 37, 3560–3568. doi: 10.1093/eurheartj/ehv509

Kishi, T., and Elmquist, J. K. (2005). Body weight is regulated by the brain: a link between feeding and emotion. *Mol. Psychiatry* 10, 132–146. doi: 10.1038/sj.mp.4001638

Kivipelto, M., Ngandu, T., Fratiglioni, L., Viitanen, M., Kåreholt, I., Winblad, B., et al. (2005). Obesity and vascular risk factors at midlife and the risk of dementia and Alzheimer disease. *Arch. Neurol.* 62, 1556–1560. doi: 10.1001/archneur.62.10.1556

Knudtson, M. D., Klein, B. E. K., Klein, R., and Shankar, A. (2005). Associations with weight loss and subsequent mortality risk. *Ann. Epidemiol.* 15, 483–491. doi: 10.1016/j.annepidem.2004.12.003

Koekkoek, P. S., Kappelle, L. J., van den Berg, E., Rutten, G. E., and Biessels, G. J. (2015). Cognitive function in patients with diabetes mellitus: guidance for daily care. *Lancet Neurol.* 14, 329–340. doi: 10.1016/S1474-4422(14)70249-2

Koga, S., Kojima, A., Kuwabara, S., and Yoshiyama, Y. (2014). Immunohistochemical analysis of tau phosphorylation and astroglial activation with enhanced leptin receptor expression in diet-induced obesity mouse hippocampus. *Neurosci. Lett.* 571, 11–16. doi: 10.1016/j.neulet.2014.04.028

Koliaki, C., Liatis, S., le Roux, C. W., and Kokkinos, A. (2017). The role of bariatric surgery to treat diabetes: current challenges and perspectives. *BMC Endocr. Disord.* 17:50. doi: 10.1186/s12902-017-0202-6

Kondo, H., Shimomura, I., Matsukawa, Y., Kumada, M., Takahashi, M., Matsuda, M., et al. (2002). Association of adiponectin mutation with type 2 diabetes: a candidate gene for the insulin resistance syndrome. *Diabetes* 51, 2325–2328.

Kong, S. H., Park, Y. J., Lee, J.-Y., Cho, N. H., and Moon, M. K. (2018). Insulin resistance is associated with cognitive decline among older Koreans with normal baseline cognitive function: a prospective community-based cohort study. *Sci. Rep.* 8:650. doi: 10.1038/s41598-017-18998-0

Konrad, D., Rudich, A., and Schoenle, E. J. (2007). Improved glucose tolerance in mice receiving intraperitoneal transplantation of normal fat tissue. *Diabetologia* 50, 833–839. doi: 10.1007/s00125-007-0596-1

Konturek, S. J., Konturek, J. W., Pawlik, T., and Brzozowki, T. (2004). Brain-gut axis and its role in the control of food intake. *J. Physiol. Pharmacol.* 55(1 Pt 2), 137–154.

Kos, K., Harte, A. L., da Silva, N. F., Tonchev, A., Chaldakov, G., James, S., et al. (2007). Adiponectin and resistin in human cerebrospinal fluid and expression of adiponectin receptors in the human hypothalamus. *J. Clin. Endocrinol. Metab.* 92, 1129–1136. doi: 10.1210/jc.2006-1841

Koyama, A., O'Brien, J., Weuve, J., Blacker, D., Metti, A. L., and Yaffe, K. (2013). The role of peripheral inflammatory markers in dementia and Alzheimer's disease: a meta-analysis. *J. Gerontol. A Biol. Sci. Med. Sci.* 68, 433–440. doi: 10.1093/gerona/gls187

Kubota, N., Yano, W., Kubota, T., Yamauchi, T., Itoh, S., Kumagai, H., et al. (2007). Adiponectin stimulates AMP-activated protein kinase in the hypothalamus and increases food intake. *Cell Metab.* 6, 55–68. doi: 10.1016/j.cmet.2007.06.003

Kusminski, C. M., McTernan, P. G., Schraw, T., Kos, K., O'Hare, J. P., Ahima, R., et al. (2007). Adiponectin complexes in human cerebrospinal fluid: distinct complex distribution from serum. *Diabetologia* 50, 634–642. doi: 10.1007/s00125-006-0577-9

Kwok, K. H. M., Lam, K. S. L., and Xu, A. (2016). Heterogeneity of white adipose tissue: molecular basis and clinical implications. *Exp. Mol. Med.* 48:e215. doi: 10.1038/emm.2016.5

Lam, D. W., and LeRoith, D. (2000). *Metabolic Syndrome*. Available at: http://www.ncbi.nlm.nih.gov/pubmed/25905173 (accessed April 16, 2019).

LaRoche, D. P., Kralian, R. J., and Millett, E. D. (2011). Fat mass limits lower-extremity relative strength and maximal walking performance in older women. *J. Electromyogr. Kinesiol.* 21, 754–761. doi: 10.1016/j.jelekin.2011.07.006

Le, K.-A., Ventura, E. E., Fisher, J. Q., Davis, J. N., Weigensberg, M. J., Punyanitya, M., et al. (2011). Ethnic differences in pancreatic fat accumulation and its relationship with other fat depots and inflammatory markers. *Diabetes Care* 34, 485–490. doi: 10.2337/dc10-0760

Leal, L. G., Lopes, M. A., and Batista, M. L. Jr. (2018). Physical exercise-induced myokines and muscle-adipose tissue crosstalk: a review of current knowledge and the implications for health and metabolic diseases. *Front. Physiol.* 9:1307. doi: 10.3389/fphys.2018.01307

Lee, D., Sui, X., Artero, E. G., Lee, I.-M., Church, T. S., McAuley, P. A., et al. (2011). Long-term effects of changes in cardiorespiratory fitness and body mass index on all-cause and cardiovascular disease mortality in men. *Circulation* 124, 2483–2490. doi: 10.1161/CIRCULATIONAHA.111.038422

Lee, J. H., Chan, J. L., Sourlas, E., Raptopoulos, V., and Mantzoros, C. S. (2006). Recombinant methionyl human leptin therapy in replacement doses improves insulin resistance and metabolic profile in patients with lipoatrophy and metabolic syndrome induced by the highly active antiretroviral therapy. *J. Clin. Endocrinol. Metab.* 91, 2605–2611. doi: 10.1210/jc.2005-1545

Lee, Y., Lingvay, I., Szczepaniak, L. S., Ravazzola, M., Orci, L., and Unger, R. H. (2010). Pancreatic steatosis: harbinger of type 2 diabetes in obese rodents. *Int. J. Obes.* 34, 396–400. doi: 10.1038/ijo.2009.245

Lee, Y.-H., Martin, J. M., Maple, R. L., Tharp, W. G., and Pratley, R. E. (2009). Plasma Amyloid-β peptide levels correlate with adipocyte amyloid precursor protein gene expression in obese individuals. *Neuroendocrinology* 90, 383–390. doi: 10.1159/000235555

Lenchik, L., Register, T. C., Hsu, F. C., Lohman, K., Nicklas, B. J., Freedman, B. I., et al. (2003). Adiponectin as a novel determinant of bone mineral density and visceral fat. *Bone* 33, 646–651.

Letra, L., and Seiça, R. (eds) (2017). *Obesity and Brain Function*. Cham: Springer International Publishing.

Li, J., Tang, Y., and Cai, D. (2012). IKKβ/NF-κB disrupts adult hypothalamic neural stem cells to mediate a neurodegenerative mechanism of dietary obesity and pre-diabetes. *Nat. Cell Biol.* 14, 999–1012. doi: 10.1038/ncb2562

Li, X.-L., Aou, S., Oomura, Y., Hori, N., Fukunaga, K., and Hori, T. (2002). Impairment of long-term potentiation and spatial memory in leptin receptor-deficient rodents. *Neuroscience* 113, 607–615.

Lieb, W., Beiser, A. S., Vasan, R. S., Tan, Z. S., Au, R., Harris, T. B., et al. (2009). Association of plasma leptin levels with incident Alzheimer disease and MRI measures of brain aging. *JAMA* 302, 2565–2572. doi: 10.1001/jama.2009.1836

Lim, S., and Meigs, J. B. (2014). Links between ectopic fat and vascular disease in humans. *Arterioscler. Thromb. Vasc. Biol.* 34, 1820–1826. doi: 10.1161/ATVBAHA.114.303035

Lissner, L., Karlsson, C., Lindroos, A. K., Sjöström, L., Carlsson, B., Carlsson, L., et al. (1999). Birth weight, adulthood BMI, and subsequent weight gain in relation to leptin levels in Swedish women. *Obes. Res.* 7, 150–154.

London, E. D., Berman, S. M., Chakrapani, S., Delibasi, T., Monterosso, J., Erol, H. K., et al. (2011). Short-term plasticity of gray matter associated with leptin deficiency and replacement. *J. Clin. Endocrinol. Metab.* 96, E1212–E1220. doi: 10.1210/jc.2011-0314

Lumeng, C. N., and Saltiel, A. R. (2011). Inflammatory links between obesity and metabolic disease. *J. Clin. Invest.* 121, 2111–2117. doi: 10.1172/JCI57132

Luo, X., McGregor, G., Irving, A. J., and Harvey, J. (2015). Leptin induces a novel form of NMDA receptor-dependent LTP at hippocampal temporoammonic-CA1 synapses. *eNeuro* 2:ENEURO.0007-15.2015. doi: 10.1523/ENEURO.0007-15.2015

Maden-Wilkinson, T. M., McPhee, J. S., Jones, D. A., and Degens, H. (2015). Age-related loss of muscle mass, strength, and power and their association with mobility in recreationally-active older adults in the United Kingdom. *J. Aging Phys. Act.* 23, 352–360. doi: 10.1123/japa.2013-0219

Maffiuletti, N. A., Jubeau, M., Agosti, F., De Col, A., and Sartorio, A. (2008). Quadriceps muscle function characteristics in severely obese and nonobese adolescents. *Eur. J. Appl. Physiol.* 103, 481–484. doi: 10.1007/s00421-008-0737-3

Maffiuletti, N. A., Jubeau, M., Munzinger, U., Bizzini, M., Agosti, F., De Col, A., et al. (2007). Differences in quadriceps muscle strength and fatigue between lean and obese subjects. *Eur. J. Appl. Physiol.* 101, 51–59. doi: 10.1007/s00421-007-0471-2

Mainardi, M., Fusco, S., and Grassi, C. (2015). Modulation of hippocampal neural plasticity by glucose-related signaling. *Neural Plast.* 2015, 1–10. doi: 10.1155/2015/657928

Manne, V., and Saab, S. (2014). Impact of nutrition and obesity on chronic liver disease. *Clin. Liver Dis.* 18, 205–218. doi: 10.1016/j.cld.2013.09.008

Marchesini, G., Brizi, M., Morselli-Labate, A. M., Bianchi, G., Bugianesi, E., McCullough, A. J., et al. (1999). Association of nonalcoholic fatty liver disease with insulin resistance. *Am. J. Med.* 107, 450–455. doi: 10.1016/S0002-9343(99)00271-5

Marra, F., Aleffi, S., Bertolani, C., Petrai, I., and Vizzutti, F. (2005). Adipokines and liver fibrosis. *Eur. Rev. Med. Pharmacol. Sci.* 9, 279–284.

Matochik, J. A., London, E. D., Yildiz, B. O., Ozata, M., Caglayan, S., DePaoli, A. M., et al. (2005). Effect of leptin replacement on brain structure in genetically leptin-deficient adults. *J. Clin. Endocrinol. Metab.* 90, 2851–2854. doi: 10.1210/jc.2004-1979

Matsuzawa, Y. (2007). The metabolic syndrome and adipocytokines. *Expert Rev. Clin. Immunol.* 580, 2917–2921. doi: 10.1586/1744666X.3.1.39

McGregor, G., and Harvey, J. (2018). Food for thought: leptin regulation of hippocampal function and its role in Alzheimer's disease. *Neuropharmacology* 136, 298–306. doi: 10.1016/j.neuropharm.2017.09.038

McNeilly, A. D., Williamson, R., Sutherland, C., Balfour, D. J. K., and Stewart, C. A. (2011). High fat feeding promotes simultaneous decline in insulin sensitivity and cognitive performance in a delayed matching and non-matching to position task. *Behav. Brain Res.* 217, 134–141. doi: 10.1016/j.bbr.2010.10.017

Medic, N., Ziauddeen, H., Ersche, K. D., Farooqi, I. S., Bullmore, E. T., Nathan, P. J., et al. (2016). Increased body mass index is associated with specific regional alterations in brain structure. *Int. J. Obes.* 40, 1177–1182. doi: 10.1038/ijo.2016.42

Meraz-Ríos, M. A., Toral-Rios, D., Franco-Bocanegra, D., Villeda-Hernández, J., and Campos-Peña, V. (2013). Inflammatory process in Alzheimer's disease. *Front. Integr. Neurosci.* 7:59. doi: 10.3389/fnint.2013.00059

Moheet, A., Mangia, S., and Seaquist, E. (2015). Impact of diabetes on cognitive function and brain structure. *Ann. N. Y. Acad. Sci.* 1353, 60–71. doi: 10.1111/NYAS.12807

Moloney, A. M., Griffin, R. J., Timmons, S., O'Connor, R., Ravid, R., and O'Neill, C. (2010). Defects in IGF-1 receptor, insulin receptor and IRS-1/2 in Alzheimer's disease indicate possible resistance to IGF-1 and insulin signalling. *Neurobiol. Aging* 31, 224–243. doi: 10.1016/J.NEUROBIOLAGING.2008.04.002

Monje, M. L., Toda, H., and Palmer, T. D. (2003). Inflammatory blockade restores adult hippocampal neurogenesis. *Science* 302, 1760–1765. doi: 10.1126/science.1088417

Morash, B., Li, A., Murphy, P. R., Wilkinson, M., and Ur, E. (1999). Leptin gene expression in the brain and pituitary gland. *Endocrinology* 140, 5995–5998. doi: 10.1210/endo.140.12.7288

Moro, C., Bajpeyi, S., and Smith, S. R. (2008). Determinants of intramyocellular triglyceride turnover: implications for insulin sensitivity. *Am. J. Physiol. Metab.* 294, E203–E213. doi: 10.1152/ajpendo.00624.2007

Mottahedin, A., Ardalan, M., Chumak, T., Riebe, I., Ek, J., and Mallard, C. (2017). Effect of neuroinflammation on synaptic organization and function in the developing brain: implications for neurodevelopmental and neurodegenerative disorders. *Front. Cell. Neurosci.* 11:190. doi: 10.3389/fncel.2017.00190

Mrak, R. E. (2009). Alzheimer-type neuropathological changes in morbidly obese elderly individuals. *Clin. Neuropathol.* 28, 40–45.

Murray, A. J., Knight, N. S., Cochlin, L. E., McAleese, S., Deacon, R. M. J., Rawlins, J. N. P., et al. (2009). Deterioration of physical performance and cognitive function in rats with short-term high-fat feeding. *FASEB J.* 23, 4353–4360. doi: 10.1096/fj.09-139691

Neumeier, M., Weigert, J., Buettner, R., Wanninger, J., Schäffler, A., Mü, A. M., et al. (2007). Detection of adiponectin in cerebrospinal fluid in humans Downloaded from. *Am. J. Physiol. Endocrinol. Metab.* 293, 965–969. doi: 10.1152/ajpendo.00119.2007

Ng, R. C.-L., and Chan, K.-H. (2017). Potential neuroprotective effects of adiponectin in Alzheimer's disease. *Int. J. Mol. Sci.* 18:E592. doi: 10.3390/ijms18030592

Ng, R. C.-L., Cheng, O.-Y., Jian, M., Kwan, J. S.-C., Ho, P. W.-L., Cheng, K. K.-Y., et al. (2016). Chronic adiponectin deficiency leads to Alzheimer's disease-like cognitive impairments and pathologies through AMPK inactivation and cerebral insulin resistance in aged mice. *Mol. Neurodegener.* 11:71. doi: 10.1186/s13024-016-0136-x

Nguyen, J. C. D., Killcross, A. S., and Jenkins, T. A. (2014). Obesity and cognitive decline: role of inflammation and vascular changes. *Front. Neurosci.* 8:375. doi: 10.3389/fnins.2014.00375

Nicholson, T., Church, C., Baker, D. J., and Jones, S. W. (2018). The role of adipokines in skeletal muscle inflammation and insulin sensitivity. *J. Inflamm.* 15:9. doi: 10.1186/s12950-018-0185-8

Nishimura, M., Izumiya, Y., Higuchi, A., Shibata, R., Qiu, J., Kudo, C., et al. (2008). Adiponectin prevents cerebral ischemic injury through endothelial nitric oxide synthase–dependent mechanisms. *Circulation* 117, 216–223. doi: 10.1161/CIRCULATIONAHA.107.725044

Nobili, V., Carter-Kent, C., and Feldstein, A. E. (2011). The role of lifestyle changes in the management of chronic liver disease. *BMC Med.* 9:70. doi: 10.1186/1741-7015-9-70

Oakes, N. D., Bell, K. S., Furler, S. M., Camilleri, S., Saha, A. K., Ruderman, N. B., et al. (1997). Diet-induced muscle insulin resistance in rats is ameliorated by acute dietary lipid withdrawal or a single bout of exercise: parallel relationship between insulin stimulation of glucose uptake and suppression of long-chain fatty acyl-CoA. *Diabetes* 46, 2022–2028.

Ommen, S. R., and Lopez-Jimenez, F. (2013). Obesity and hypertrophic cardiomyopathy. *J. Am. Coll. Cardiol.* 62, 458–459. doi: 10.1016/j.jacc.2013.03.063

Oomura, Y., Aou, S., and Fukunaga, K. (2010). Prandial increase of leptin in the brain activates spatial learning and memory. *Pathophysiology* 17, 119–127. doi: 10.1016/j.pathophys.2009.04.004

Orkaby, A. R., Cho, K., Cormack, J., Gagnon, D. R., and Driver, J. A. (2017). Metformin vs sulfonylurea use and risk of dementia in US veterans aged=65 years with diabetes. *Neurology* 89, 1877–1885. doi: 10.1212/WNL.0000000000004586

O'Rourke, R. W. (2010). Inflammation in obesity-related disease. *Surgery* 145, 255–259. doi: 10.1016/j.surg.2008.08.038

Ott, A., Stolk, R. P., Hofman, A., Van Harskamp, F., Grobbee, D. E., and Breteler, M. M. B. (1996). *Association of Diabetes Mellitus and Dementia: The Rotterdam Study*. Available at: https://core.ac.uk/download/pdf/43310876.pdf (accessed April 19, 2019).

Pagano, G., Pacini, G., Musso, G., Gambino, R., Mecca, F., Depetris, N., et al. (2002). Nonalcoholic steatohepatitis, insulin resistance, and metabolic syndrome: Further evidence for an etiologic association. *Hepatology* 35, 367–372. doi: 10.1053/JHEP.2002.30690

Pan, W., Tu, H., and Kastin, A. J. (2006). Differential BBB interactions of three ingestive peptides: obestatin, ghrelin, and adiponectin. *Peptides* 27, 911–916. doi: 10.1016/j.peptides.2005.12.014

Pannacciulli, N., Del Parigi, A., Chen, K., Le, D. S., Reiman, E. M., and Tataranni, P. A. (2006). Brain abnormalities in human obesity: a voxel-based morphometric study. *Neuroimage* 31, 1419–1425. doi: 10.1016/j.neuroimage.2006.01.047

Park, H. K., and Ahima, R. S. (2013). Resistin in rodents and humans. *Diabetes Metab. J.* 37, 404–414. doi: 10.4093/dmj.2013.37.6.404

Park, H. K., Kwak, M. K., Kim, H. J., and Ahima, R. S. (2017). Linking resistin, inflammation, and cardiometabolic diseases. *Korean J. Intern. Med.* 32, 239–247. doi: 10.3904/kjim.2016.229

Park, S., Kim, D. S., Kwon, D. Y., and Yang, H. J. (2011). Long-term central infusion of adiponectin improves energy and glucose homeostasis by decreasing fat storage and suppressing hepatic gluconeogenesis without changing food intake. *J. Neuroendocrinol.* 23, 687–698. doi: 10.1111/j.1365-2826.2011.02165.x

Pedersen, B. K. (2013). Muscle as a secretory organ. *Compr. Physiol.* 3, 1337–1362. doi: 10.1002/cphy.c120033

Peeters, A., Barendregt, J. J., Willekens, F., Mackenbach, J. P., Al Mamun, A., Bonneux, L., et al. (2003). Obesity in adulthood and its consequences for life expectancy: a life-table analysis. *Ann. Intern. Med.* 138, 24–32.

Peila, R., Rodriguez, B. L., Launer, L. J., and Honolulu-Asia Aging Study. (2002). Type 2 diabetes, APOE gene, and the risk for dementia and related pathologies. *Diabetes* 51, 1256–1262. doi: 10.2337/DIABETES.51.4.1256

Pezzilli, R., and Calculli, L. (2014). Pancreatic steatosis: Is it related to either obesity or diabetes mellitus? *World J. Diabetes* 5, 415–419. doi: 10.4239/wjd.v5.i4.415

Piché, M.-E., and Poirier, P. (2018). Obesity, ectopic fat and cardiac metabolism. *Expert Rev. Endocrinol. Metab.* 13, 213–221. doi: 10.1080/17446651.2018.1500894

Pinnick, K. E., Collins, S. C., Londos, C., Gauguier, D., Clark, A., and Fielding, B. A. (2008). Pancreatic ectopic fat is characterized by adipocyte infiltration and altered lipid composition. *Obesity* 16, 522–530. doi: 10.1038/oby.2007.110

Poitout, V. (2004). β-cell lipotoxicity: burning fat into heat? *Endocrinology* 145, 3563–3565. doi: 10.1210/en.2004-0479

Preis, S. R., Massaro, J. M., Hoffmann, U., D'Agostino, R. B., Levy, D., Robins, S. J., et al. (2010). Neck circumference as a novel measure of cardiometabolic risk: the framingham heart study. *J. Clin. Endocrinol. Metab.* 95, 3701–3710. doi: 10.1210/jc.2009-1779

Prickett, C., Brennan, L., and Stolwyk, R. (2015). Examining the relationship between obesity and cognitive function: a systematic literature review. *Obes. Res. Clin. Pract.* 9, 93–113. doi: 10.1016/j.orcp.2014.05.001

Profenno, L. A., Porsteinsson, A. P., and Faraone, S. V. (2010). Meta-analysis of Alzheimer's disease risk with obesity. *Diabetes Relat. Disord. Biol. Psychiatry* 67, 505–512. doi: 10.1016/J.BIOPSYCH.2009.02.013

Puig, K. L., Floden, A. M., Adhikari, R., Golovko, M. Y., and Combs, C. K. (2012). Amyloid precursor protein and proinflammatory changes are regulated in brain and adipose tissue in a murine model of high fat diet-induced obesity. *PLoS One* 7:e30378. doi: 10.1371/journal.pone.0030378

Purkayastha, S., and Cai, D. (2013). Disruption of neurogenesis by hypothalamic inflammation in obesity or aging. *Rev. Endocr. Metab. Disord.* 14, 351–356. doi: 10.1007/s11154-013-9279-z

Qi, Y., Takahashi, N., Hileman, S. M., Patel, H. R., Berg, A. H., Pajvani, U. B., et al. (2004). Adiponectin acts in the brain to decrease body weight. *Nat. Med.* 10, 524–529. doi: 10.1038/nm1029

Qureshi, K., and Abrams, G. A. (2007). Metabolic liver disease of obesity and role of adipose tissue in the pathogenesis of nonalcoholic fatty liver disease. *World J. Gastroenterol.* 13, 3540–3553. doi: 10.3748/wjg.v13.i26.3540

Raji, C. A., Ho, A. J., Parikshak, N. N., Becker, J. T., Lopez, O. L., Kuller, L. H., et al. (2009). Brain structure and obesity. *Hum. Brain Mapp.* 31, 353–364. doi: 10.1002/hbm.20870

Rasgon, N. L., Kenna, H. A., Wroolie, T. E., Kelley, R., Silverman, D., Brooks, J., et al. (2011). Insulin resistance and hippocampal volume in women at risk for Alzheimer's disease. *Neurobiol. Aging* 32, 1942–1948. doi: 10.1016/J.NEUROBIOLAGING.2009.12.005

Rawlings, A. M., Sharrett, A. R., Mosley, T. H., Ballew, S. H., Deal, J. A., and Selvin, E. (2017). Glucose peaks and the risk of dementia and 20-year cognitive decline. *Diabetes Care* 40, 879–886. doi: 10.2337/dc16-2203

Reaven, G. M. (1995). Pathophysiology of insulin resistance in human disease. *Physiol. Rev.* 75, 473–486. doi: 10.1152/physrev.1995.75.3.473

Riederer, P., Korczyn, A. D., Ali, S. S., Bajenaru, O., Choi, M. S., Chopp, M., et al. (2017). The diabetic brain and cognition. *J. Neural Transm.* 124, 1431–1454. doi: 10.1007/s00702-017-1763-2

Rolland, Y., Lauwers-Cances, V., Cristini, C., van Kan, G. A., Janssen, I., Morley, J. E., et al. (2009). Difficulties with physical function associated with obesity, sarcopenia, and sarcopenic-obesity in community-dwelling elderly women: the EPIDOS (EPIDemiologie de l'OSteoporose) Study. *Am. J. Clin. Nutr.* 89, 1895–1900. doi: 10.3945/ajcn.2008.26950

Rolland, Y., Lauwers-Cances, V., Pahor, M., Fillaux, J., Grandjean, H., and Vellas, B. (2004). Muscle strength in obese elderly women: effect of recreational physical activity in a cross-sectional study. *Am. J. Clin. Nutr.* 79, 552–557. doi: 10.1093/ajcn/79.4.552

Rosito, G. A., Massaro, J. M., Hoffmann, U., Ruberg, F. L., Mahabadi, A. A., Vasan, R. S., et al. (2008). Pericardial fat, visceral abdominal fat, cardiovascular disease risk factors, and vascular calcification in a community-based sample. *Circulation* 117, 605–613. doi: 10.1161/CIRCULATIONAHA.107.743062

Ross, R., Lam, M., Blair, S. N., Church, T. S., Godwin, M., Hotz, S. B., et al. (2012). Trial of prevention and reduction of obesity through active living in clinical settings. *Arch. Intern. Med.* 172, 414–424. doi: 10.1001/archinternmed.2011.1972

Rutkowski, J. M., and Scherer, P. E. (2014). Isolation and quantitation of adiponectin higher order complexes. *Methods Enzymol.* 537, 243–259. doi: 10.1016/B978-0-12-411619-1.00013-6

Ryan, A. S., Berman, D. M., Nicklas, B. J., Sinha, M., Gingerich, R. L., Meneilly, G. S., et al. (2003). Plasma adiponectin and leptin levels, body composition, and glucose utilization in adult women with wide ranges of age and obesity. *Diabetes Care* 26, 2383–2388. doi: 10.2337/DIACARE.26.8.2383

Sabia, S., Kivimaki, M., Shipley, M. J., Marmot, M. G., and Singh-Manoux, A. (2009). Body mass index over the adult life course and cognition in late midlife: the Whitehall II Cohort Study. *Am. J. Clin. Nutr.* 89, 601–607. doi: 10.3945/ajcn.2008.26482

Sacks, H. S., and Fain, J. N. (2007). Human epicardial adipose tissue: a review. *Am. Heart J.* 153, 907–917. doi: 10.1016/j.ahj.2007.03.019

Sakurai, T., Kawashima, S., Satake, S., Miura, H., Tokuda, H., and Toba, K. (2014). Differential subtypes of diabetic older adults diagnosed with Alzheimer's disease. *Geriatr. Gerontol. Int.* 14, 62–70. doi: 10.1111/ggi.12250

Samanta, R., Pouliopoulos, J., Thiagalingam, A., Kovoor, P., and Bs, M. B. (2015). Role of adipose tissue in the pathogenesis of cardiac arrhythmias. *Heart Rhythm* 13, 311–320. doi: 10.1016/j.hrthm.2015.08.016

Sanderlin, A. H., Todem, D., and Bozoki, A. C. (2017). Obesity and Co-morbid conditions are associated with specific neuropsychiatric symptoms in mild cognitive impairment. *Front. Aging Neurosci.* 9:164. doi: 10.3389/fnagi.2017.00164

Sanyal, A. J., Campbell-Sargent, C., Mirshahi, F., Rizzo, W. B., Contos, M. J., Sterling, R. K., et al. (2001). Nonalcoholic steatohepatitis: association of insulin resistance and mitochondrial abnormalities. *Gastroenterology* 120, 1183–1192. doi: 10.1053/GAST.2001.23256

Schauer, P. R., Bhatt, D. L., Kirwan, J. P., Wolski, K., Aminian, A., Brethauer, S. A., et al. (2017). Bariatric surgery versus intensive medical therapy for diabetes — 5-year outcomes. *N. Engl. J. Med.* 376, 641–651. doi: 10.1056/NEJMoa1600869

Schubert, M., Brazil, D. P., Burks, D. J., Kushner, J. A., Ye, J., Flint, C. L., et al. (2003). Insulin receptor substrate-2 deficiency impairs brain growth and promotes tau phosphorylation. *J. Neurosci.* 23, 7084–7092.

Schulz, C., Paulus, K., and Lehnert, H. (2011). Adipocyte–brain: crosstalk. *Results Probl. Cell Differ.* 52, 189–201. doi: 10.1007/978-3-642-14426-4_16

Schwingshackl, L., Dias, S., and Hoffmann, G. (2014). Impact of long-term lifestyle programmes on weight loss and cardiovascular risk factors in overweight/obese participants: a systematic review and network meta-analysis. *Syst. Rev.* 3:130.

Shanley, L. J., Irving, A. J., and Harvey, J. (2001). Leptin enhances NMDA receptor function and modulates hippocampal synaptic plasticity. *J. Neurosci.* 21:RC186.

Shea, M. K., Nicklas, B. J., Houston, D. K., Miller, M. E., Davis, C. C., Kitzman, D. W., et al. (2011). The effect of intentional weight loss on all-cause mortality in older adults: results of a randomized controlled weight-loss trial. *Am. J. Clin. Nutr.* 94, 839–846. doi: 10.3945/ajcn.110.006379

Simerly, R. B. (2008). Hypothalamic substrates of metabolic imprinting. *Physiol. Behav.* 94, 79–89. doi: 10.1016/j.physbeh.2007.11.023

Simon, G. E., Von Korff, M., Saunders, K., Miglioretti, D. L., Crane, P. K., van Belle, G., et al. (2006). Association between obesity and psychiatric disorders in the US adult population. *Arch. Gen. Psychiatry* 63, 824–830. doi: 10.1001/archpsyc.63.7.824

Sims-Robinson, C., Kim, B., Rosko, A., and Feldman, E. L. (2010). How does diabetes accelerate Alzheimer disease pathology? *Nat. Rev. Neurol.* 6, 551–559. doi: 10.1038/nrneurol.2010.130

Singh-Manoux, A., Dugravot, A., Shipley, M., Brunner, E. J., Elbaz, A., Sabia, S., et al. (2018). Obesity trajectories and risk of dementia: 28 years of follow-up in the Whitehall II Study. *Alzheimers Dement.* 14, 178–186. doi: 10.1016/j.jalz.2017.06.2637

Singla, P., Bardoloi, A., and Parkash, A. A. (2010). Metabolic effects of obesity: a review. *World J. Diabetes* 1, 76–88. doi: 10.4239/wjd.v1.i3.76

Sjöström, L., Narbro, K., Sjöström, C. D., Karason, K., Larsson, B., Wedel, H., et al. (2007). Effects of bariatric surgery on mortality in swedish obese subjects. *N. Engl. J. Med.* 357, 741–752. doi: 10.1056/NEJMoa066254

Snijder, M. B., Dekker, J. M., Visser, M., Bouter, L. M., Stehouwer, C. D. A., Kostense, P. J., et al. (2003a). Associations of hip and thigh circumferences independent of waist circumference with the incidence of type 2 diabetes: the Hoorn study. *Am. J. Clin. Nutr.* 77, 1192–1197.

Snijder, M. B., Dekker, J. M., Visser, M., Yudkin, J. S., Stehouwer, C. D. A., Bouter, L. M., et al. (2003b). Larger thigh and hip circumferences are associated with better glucose tolerance: the Hoorn study. *Obes. Res.* 11, 104–111. doi: 10.1038/oby.2003.18

Sonar, S. A., and Lal, G. (2018). Blood-brain barrier and its function during inflammation and autoimmunity. *J. Leukoc. Biol.* 103, 839–853. doi: 10.1002/JLB.1RU1117-428R

Sørensen, T. I., Rissanen, A., Korkeila, M., and Kaprio, J. (2005). Intention to lose weight, weight changes, and 18-y mortality in overweight individuals without co-morbidities. *PLoS Med.* 2:e171. doi: 10.1371/journal.pmed.0020171

Sowemimo, O. A., Yood, S. M., Courtney, J., Moore, J., Huang, M., Ross, R., et al. (2007). Natural history of morbid obesity without surgical intervention. *Surg. Obes. Relat. Dis.* 3, 73–77. doi: 10.1016/j.soard.2006.10.017

Spalding, K. L., Arner, E., Westermark, P. O., Bernard, S., Buchholz, B. A., Bergmann, O., et al. (2008). Dynamics of fat cell turnover in humans. *Nature* 453, 783–787. doi: 10.1038/nature06902

Spranger, J., Verma, S., Göhring, I., Bobbert, T., Seifert, J., Sindler, A. L., et al. (2006). Adiponectin does not cross the blood-brain barrier but modifies cytokine expression of brain endothelial cells. *Diabetes* 55, 141–147.

Stefan, N., Kantartzis, K., Machann, J., Schick, F., Thamer, C., Rittig, K., et al. (2008). Identification and characterization of metabolically benign obesity in humans. *Arch. Intern. Med.* 168, 1609–1616. doi: 10.1001/archinte.168.15.1609

Stenlöf, K., Wernstedt, I., Fjällman, T., Wallenius, V., Wallenius, K., and Jansson, J.-O. (2003). Interleukin-6 levels in the central nervous system are negatively correlated with fat mass in overweight/obese subjects. *J. Clin. Endocrinol. Metab.* 88, 4379–4383. doi: 10.1210/jc.2002-021733

Stillman, C. M., Weinstein, A. M., Marsland, A. L., Gianaros, P. J., and Erickson, K. I. (2017). Body-brain connections: the effects of obesity and behavioral interventions on neurocognitive aging. *Front. Aging Neurosci.* 9:115. doi: 10.3389/fnagi.2017.00115

Studzinski, C. M., Li, F., Bruce-Keller, A. J., Fernandez-Kim, S. O., Zhang, L., Weidner, A. M., et al. (2009). Effects of short-term Western diet on cerebral oxidative stress and diabetes related factors in APP × PS1 knock-in mice. *J. Neurochem.* 108, 860–866. doi: 10.1111/j.1471-4159.2008.05798.x

Su, F., Shu, H., Ye, Q., Wang, Z., Xie, C., Yuan, B., et al. (2017). Brain insulin resistance deteriorates cognition by altering the topological features of brain networks. *Neuroimage Clin.* 13, 280–287. doi: 10.1016/J.NICL.2016.12.009

Suganami, T., Nishida, J., and Ogawa, Y. (2005). A paracrine loop between adipocytes and macrophages aggravates inflammatory changes. *Arterioscler. Thromb. Vasc. Biol.* 25, 2062–2068. doi: 10.1161/01.ATV.0000183883.72263.13

Szczepaniak, L. S., Dobbins, R. L., Metzger, G. J., Sartoni-D'Ambrosia, G., Arbique, D., Vongpatanasin, W., et al. (2003). Myocardial triglycerides and systolic function in humans: in vivo evaluation by localized proton spectroscopy and cardiac imaging. *Magn. Reson. Med.* 49, 417–423. doi: 10.1002/mrm.10372

Talbot, K., and Wang, H.-Y. (2014). The nature, significance, and glucagon-like peptide-1 analog treatment of brain insulin resistance in Alzheimer's disease. *Alzheimers Dement.* 10, S12–S25. doi: 10.1016/J.JALZ.2013.12.007

Talbot, K., Wang, H.-Y., Kazi, H., Han, L.-Y., Bakshi, K. P., Stucky, A., et al. (2012). Demonstrated brain insulin resistance in Alzheimer's disease patients is associated with IGF-1 resistance, IRS-1 dysregulation, and cognitive decline. *J. Clin. Invest.* 122, 1316–1338. doi: 10.1172/JCI59903

Tchernof, A., Bélanger, C., Morisset, A. S., Richard, C., Mailloux, J., Laberge, P., et al. (2006). Regional differences in adipose tissue metabolism in women: minor effect of obesity and body fat distribution. *Diabetes* 55, 1353–1360. doi: 10.2337/db05-1439

Tchkonia, T., Lenburg, M., Thomou, T., Giorgadze, N., Frampton, G., Pirtskhalava, T., et al. (2007). Identification of depot-specific human fat cell progenitors through distinct expression profiles and developmental gene patterns. *Am. J. Physiol. Metab.* 292, E298–E307. doi: 10.1152/ajpendo.00202.2006

Tiemann Luecking, C., Yoshino, M., Klein, S., Samovski, D., Magkos, F., Okunade, A. L., et al. (2015). Metabolically normal obese people are protected from adverse effects following weight gain. *J. Clin. Invest.* 125, 787–795. doi: 10.1172/jci78425

Tilg, H., and Moschen, A. R. (2006). Adipocytokines: mediators linking adipose tissue, inflammation and immunity. *Nat. Rev. Immunol.* 6, 772–783. doi: 10.1038/nri1937

Tiniakos, D. G., Vos, M. B., and Brunt, E. M. (2010). Nonalcoholic fatty liver disease: pathology and pathogenesis. *Annu. Rev. Pathol. Mech. Dis.* 5, 145–171. doi: 10.1146/annurev-pathol-121808-102132

Tobias, D. K., Chen, M., Manson, J. E., Ludwig, D. S., Willett, W., and Hu, F. B. (2015). Effect of low-fat diet interventions versus other diet interventions on long-term weight change in adults: a systematic review and meta-analysis. *Lancet Diabetes Endocrinol.* 3, 968–979. doi: 10.1016/S2213-8587(15)00367-8

Tomlinson, D. J., Erskine, R. M., Morse, C. I., Winwood, K., and Onambélé-Pearson, G. (2016). The impact of obesity on skeletal muscle strength and structure through adolescence to old age. *Biogerontology* 17, 467–483. doi: 10.1007/s10522-015-9626-4

Tong, Q., and Xu, Y. (2012). Central leptin regulation of obesity and fertility. *Curr. Obes. Rep.* 1, 236–244. doi: 10.1007/s13679-012-0025-8

Torres-Villalobos, G., Hamdan-Pérez, N., Díaz-Villaseñor, A., Tovar, A. R., Torre-Villalvazo, I., Ordaz-Nava, G., et al. (2016). Autologous subcutaneous adipose tissue transplants improve adipose tissue metabolism and reduce insulin resistance and fatty liver in diet-induced obesity rats. *Physiol. Rep.* 4:e12909. doi: 10.14814/phy2.12909

Townsend, K., and Tseng, Y.-H. (2012). Brown adipose tissue. *Adipocyte* 1, 13–24. doi: 10.4161/adip.18951

Tran, T. T., Yamamoto, Y., Gesta, S., and Kahn, C. R. (2008). Beneficial effects of subcutaneous fat transplantation on metabolism. *Cell Metab.* 7, 410–420. doi: 10.1016/j.cmet.2008.04.004

Trayhurn, P., Drevon, C. A., and Eckel, J. (2011). Secreted proteins from adipose tissue and skeletal muscle – adipokines, myokines and adipose/muscle cross-talk. *Arch. Physiol. Biochem.* 117, 47–56. doi: 10.3109/13813455.2010.535835

van Bloemendaal, L., Ijzerman, R. G., Ten Kulve, J. S., Barkhof, F., Diamant, M., Veltman, D. J., et al. (2016). Alterations in white matter volume and integrity in obesity and type 2 diabetes. *Metab. Brain Dis.* 31, 621–629. doi: 10.1007/s11011-016-9792-3

van den Berg, E., de Craen, A. J. M., Biessels, G. J., Gussekloo, J., and Westendorp, R. G. J. (2006). The impact of diabetes mellitus on cognitive decline in the oldest of the old: a prospective population-based study. *Diabetologia* 49, 2015–2023.

van den Berg, E., Reijmer, Y. D., de Bresser, J., Kessels, R. P. C., Kappelle, L. J., Biessels, G. J., et al. (2010). A 4 year follow-up study of cognitive functioning in patients with type 2 diabetes mellitus. *Diabetologia* 53, 58–65. doi: 10.1007/S00125-009-1571-9

Viljanen, A. P. M., Iozzo, P., Borra, R., Kankaanpää, M., Karmi, A., Lautamäki, R., et al. (2009). Effect of weight loss on liver free fatty acid uptake and hepatic insulin resistance. *J. Clin. Endocrinol. Metab.* 94, 50–55. doi: 10.1210/jc.2008-1689

Wadden, T. A., Volger, S., Sarwer, D. B., Vetter, M. L., Tsai, A. G., Berkowitz, R. I., et al. (2011). A two-year randomized trial of obesity treatment in primary care practice. *N. Engl. J. Med.* 365, 1969–1979. doi: 10.1056/NEJMoa1109220

Wajchenberg, B. L. (2000). Subcutaneous and visceral adipose tissue: their relation to the metabolic syndrome. *Endocr. Rev.* 21, 697–738. doi: 10.1210/edrv.21.6.0415

Wallace, J. I., and Schwartz, R. S. (2002). Epidemiology of weight loss in humans with special reference to wasting in the elderly. *Int. J. Cardiol.* 85, 15–21.

Waragai, M., Ho, G., Takamatsu, Y., Sekiyama, K., Sugama, S., Takenouchi, T., et al. (2017). Importance of adiponectin activity in the pathogenesis of Alzheimer's disease. *Ann. Clin. Transl. Neurol.* 4, 591–600. doi: 10.1002/acn3.436

Waters, D. L., Ward, A. L., and Villareal, D. T. (2013). Weight loss in obese adults 65years and older: a review of the controversy. *Exp. Gerontol.* 48, 1054–1061. doi: 10.1016/j.exger.2013.02.005

Wayner, M., Armstrong, D., Phelix, C., and Oomura, Y. (2004). Orexin-A (Hypocretin-1) and leptin enhance LTP in the dentate gyrus of rats in vivo. *Peptides* 25, 991–996. doi: 10.1016/j.peptides.2004.03.018

Wen, J.-P., Liu, C., Hu, Y.-T., Chen, G., and Lin, L. (2010). Globular adiponectin regulates energy homeostasis through AMP-activated protein kinase–acetyl-CoA carboxylase (AMPK/ACC) pathway in the hypothalamus. *Mol. Cell. Biochem.* 344, 109–115. doi: 10.1007/s11010-010-0534-2

Wennberg, A. M. V., Gustafson, D., Hagen, C. E., Roberts, R. O., Knopman, D., Jack, C., et al. (2016). Serum adiponectin levels, neuroimaging, and cognition in the mayo clinic study of aging. *J. Alzheimers Dis.* 53, 573–581. doi: 10.3233/JAD-151201

West, R. K., Ravona-Springer, R., Schmeidler, J., Leroith, D., Koifman, K., Guerrero-Berroa, E., et al. (2014). The association of duration of type 2 diabetes with cognitive performance is modulated by long-term glycemic control. *Am. J. Geriatr. Psychiatry* 22, 1055–1059. doi: 10.1016/j.jagp.2014.01.010

Whitmer, R. A., Gustafson, D. R., Barrett-Connor, E., Haan, M. N., Gunderson, E. P., and Yaffe, K. (2008). Central obesity and increased risk of dementia more than three decades later. *Neurology* 71, 1057–1064. doi: 10.1212/01.wnl.0000306313.89165.ef

Wiesner, G., Vaz, M., Collier, G., Seals, D., Kaye, D., Jennings, G., et al. (1999). Leptin is released from the human brain: influence of adiposity and gender 1. *J. Clin. Endocrinol. Metab.* 84, 2270–2274. doi: 10.1210/jcem.84.7.5854

Wilkinson, M., Brown, R., Imran, S. A., and Ur, E. (2007). Adipokine gene expression in brain and pituitary gland. *Neuroendocrinology* 86, 191–209. doi: 10.1159/000108635

Willner, I. R., Waters, B., Patil, S. R., Reuben, A., Morelli, J., and Riely, C. A. (2001). Ninety patients with nonalcoholic steatohepatitis: insulin resistance, familial tendency, and severity of disease. *Am. J. Gastroenterol.* 96, 2957–2961. doi: 10.1111/j.1572-0241.2001.04667.x

Wing, R. R., and Phelan, S. (2005). Long-term weight loss maintenance. *Am. J. Clin. Nutr.* 82, 222S–225S. doi: 10.1093/ajcn/82.1.222S

Wolf, P. A. (2012). Contributions of the framingham heart study to stroke and dementia epidemiologic research at 60 years. *Arch. Neurol.* 69, 567. doi: 10.1001/archneurol.2011.977

Wong, C., and Marwick, T. H. (2007). Obesity cardiomyopathy: diagnosis and therapeutic implications. *Nat. Clin. Pract. Cardiovasc. Med.* 4, 480–490. doi: 10.1038/ncpcardio0964

Wright, S. M., and Aronne, L. J. (2012). Causes of obesity. *Abdom. Imaging* 37, 730–732. doi: 10.1007/s00261-012-9862-x

Xiao, C., Dash, S., Morgantini, C., Hegele, R. A., and Lewis, G. F. (2016). Pharmacological targeting of the atherogenic dyslipidemia complex: the next frontier in CVD prevention beyond lowering LDL cholesterol. *Diabetes* 65, 1767–1778. doi: 10.2337/db16-0046

Xu, W. L., von Strauss, E., Qiu, C. X., Winblad, B., and Fratiglioni, L. (2009). Uncontrolled diabetes increases the risk of Alzheimer's disease: a population-based cohort study. *Diabetologia* 52, 1031–1039. doi: 10.1007/s00125-009-1323-x

Xu, Y., and Tong, Q. (2011). Expanding neurotransmitters in the hypothalamic neurocircuitry for energy balance regulation. *Protein Cell* 2, 800–813. doi: 10.1007/s13238-011-1112-4

Yaari, S., and Goldbourt, U. (1998). Voluntary and involuntary weight loss: associations with long term mortality in 9,228 middle-aged and elderly men. *Am. J. Epidemiol.* 148, 546–555.

Yaffe, K. (2007). Metabolic syndrome and cognitive decline. *Curr. Alzheimer Res.* 4, 123–126.

Yaffe, K., Falvey, C., Hamilton, N., Schwartz, A. V., Simonsick, E. M., Satterfield, S., et al. (2012). Diabetes, glucose control, and 9-year cognitive decline among older adults without dementia. *Arch. Neurol.* 69, 1170–1175. doi: 10.1001/archneurol.2012.1117

Yano, Y., Bakris, G. L., Inokuchi, T., Ohba, Y., Tamaki, N., Nagata, M., et al. (2014). Association of cognitive dysfunction with cardiovascular disease events in elderly hypertensive patients. *J. Hypertens.* 32, 423–431. doi: 10.1097/HJH.0000000000000025

Yates, K. F., Sweat, V., Yau, P. L., Turchiano, M. M., and Convit, A. (2012). Impact of metabolic syndrome on cognition and brain. *Arterioscler. Thromb. Vasc. Biol.* 32, 2060–2067. doi: 10.1161/ATVBAHA.112.252759

Yau, S. Y., Li, A., Hoo, R. L. C., Ching, Y. P., Christie, B. R., Lee, T. M. C., et al. (2014). Physical exercise-induced hippocampal neurogenesis and antidepressant effects are mediated by the adipocyte hormone adiponectin. *Proc. Natl. Acad. Sci. U.S.A.* 111, 15810–15815. doi: 10.1073/pnas.1415219111

Ye, J. (2013). Mechanisms of insulin resistance in obesity. *Front. Med.* 7, 14–24. doi: 10.1007/s11684-013-0262-6

Yoshiyama, Y., Higuchi, M., Zhang, B., Huang, S.-M., Iwata, N., Saido, T. C., et al. (2007). Synapse loss and microglial activation precede tangles in a p301s tauopathy mouse model. *Neuron* 53, 337–351. doi: 10.1016/j.neuron.2007.01.010

Young, S. E., Mainous, A. G., and Carnemolla, M. (2006). Hyperinsulinemia and cognitive decline in a middle-aged cohort. *Diabetes Care* 29, 2688–2693. doi: 10.2337/DC06-0915

Yu, Y.-H., and Ginsberg, H. N. (2005). Adipocyte signaling and lipid homeostasis. *Circ. Res.* 96, 1042–1052. doi: 10.1161/01.RES.0000165803.47776.38

Zhang, D., Guo, M., Zhang, W., and Lu, X.-Y. (2011). Adiponectin Stimulates Proliferation of Adult Hippocampal Neural Stem/Progenitor Cells through Activation of p38 Mitogen-activated Protein Kinase (p38MAPK)/Glycogen Synthase Kinase 3β (GSK-3β)/β-Catenin Signaling Cascade. *J. Biol. Chem.* 286, 44913–44920. doi: 10.1074/jbc.M111.310052

Zhang, D., Wang, X., and Lu, X.-Y. (2016). Adiponectin exerts neurotrophic effects on dendritic arborization, spinogenesis, and neurogenesis of the dentate gyrus of male mice. *Endocrinology* 157, 2853–2869. doi: 10.1210/en.2015-2078

Zhang, L., Hou, Y., and Po, S. S. (2015). Obstructive sleep apnoea and atrial fibrillation. *Arrhythmia Electrophysiol. Rev.* 4, 14–18. doi: 10.15420/aer.2015.4.1.14

Zhang, Y., Zitsman, J. L., Hou, J., Fennoy, I., Guo, K., Feinberg, J., et al. (2014). Fat cell size and adipokine expression in relation to gender, depot, and metabolic risk factors in morbidly obese adolescents. *Obesity* 22, 691–697. doi: 10.1002/oby.20528

Zhao, X., Han, Q., Lv, Y., Sun, L., Gang, X., and Wang, G. (2018). Biomarkers for cognitive decline in patients with diabetes mellitus: evidence from clinical studies. *Oncotarget* 9, 7710–7726. doi: 10.18632/oncotarget.23284

Zhao, Y.-F., Feng, D. D., and Chen, C. (2006). Contribution of adipocyte-derived factors to beta-cell dysfunction in diabetes. *Int. J. Biochem. Cell Biol.* 38, 804–819. doi: 10.1016/j.biocel.2005.11.008

Zlokovic, B. V. (2011). Neurovascular pathways to neurodegeneration in Alzheimer's disease and other disorders. *Nat. Rev. Neurosci.* 12, 723–738. doi: 10.1038/nrn3114

Zoico, E., Di Francesco, V., Guralnik, J. M., Mazzali, G., Bortolani, A., Guariento, S., et al. (2004). Physical disability and muscular strength in relation to obesity and different body composition indexes in a sample of healthy elderly women. *Int. J. Obes.* Relat. Metab. Disord. 28, 234–241. doi: 10.1038/sj.ijo.0802552

Conflict of Interest Statement: The authors declare that the research was conducted in the absence of any commercial or financial relationships that could be construed as a potential conflict of interest.

frontiers in Cellular Neuroscience

REVIEW
published: 06 June 2019
doi: 10.3389/fncel.2019.00231

Neuroprotection: Pro-survival and Anti-neurotoxic Mechanisms as Therapeutic Strategies in Neurodegeneration

Horacio Uri Saragovi[1,2,3], Alba Galan[1,2] and Leonard A. Levin[3,4,5]*

[1] Lady Davis Institute, Montreal, QC, Canada, [2] Jewish General Hospital, Montreal, QC, Canada, [3] Department of Ophthalmology and Visual Sciences, McGill University, Montreal, QC, Canada, [4] McGill University Health Centre, Montreal, QC, Canada, [5] Montreal Neurological Institute, Mcgill University, Montreal, QC, Canada

Neurotrophins (NTs) are a subset of the neurotrophic factor family. These growth factors were originally named based on the nerve growth functional assays used to identify them. NTs act as paracrine or autocrine factors for cells expressing NT receptors. The receptors and their function have been studied primarily in cells of the nervous system, but are also present in the cardiovascular, endocrine, and immune systems, as well as in many neoplastic cells. The signals activated by NTs can be varied, depending on cellular stage and context, healthy or disease states, and depending on whether the specific NTs and their receptors are expressed in the relevant cells. In the healthy central and peripheral adult nervous systems, NTs drive neuronal survival, phenotype, synaptic maintenance, and function. Deficiencies of the NT/NT receptor axis are causally associated with disease onset or disease progression. Paradoxically, NTs can also drive synaptic loss and neuronal death. In the embryonic stage this activity is essential for proper developmental pruning of the nervous system, but in the adult it can be associated with neurodegenerative disease. Given their key role in neuronal survival and death, NTs and NT receptors have long been considered therapeutic targets to achieve neuroprotection. The first neuroprotective approaches consisted of enhancing neuronal survival signals using NTs. Later strategies selectively targeted receptors to induce survival signals specifically, while avoiding activation of death signals. Recently, the concept of selectively targeting receptors to reduce neuronal death signals has emerged. Here, we review the rationale of each neuroprotective strategy with respect to the complex cell biology and pharmacology of each target receptor.

Keywords: small molecule, mimetic, antibody, growth factor, neurotrophin, receptor, neurodegeneration, therapy

OPEN ACCESS

Edited by:
Mario Eduardo Guido, Center for Research in Biological Chemistry Córdoba (CIQUIBIC), Argentina

Reviewed by:
Christopher von Bartheld, University of Nevada, Reno, United States
Carlos Bas Orth, Universität Heidelberg, Germany

****Correspondence:***
Horacio Uri Saragovi
uri.saragovi@mcgill.ca

Specialty section:
This article was submitted to Cellular Neuropathology, a section of the journal Frontiers in Cellular Neuroscience

Received: *31 January 2019*
Accepted: *08 May 2019*
Published: *06 June 2019*

Citation:
Saragovi HU, Galan A and Levin LA (2019) Neuroprotection: Pro-survival and Anti-neurotoxic Mechanisms as Therapeutic Strategies in Neurodegeneration. Front. Cell. Neurosci. 13:231. doi: 10.3389/fncel.2019.00231

INTRODUCTION

Neurotrophins (NTs) are a family of growth factors that include nerve growth factor (NGF), brain-derived neurotrophic factor (BDNF), neurotrophin-3 (NT-3), and neurotrophin 4/5 (NT-4/5). Neurotrophin mRNAs are translated into larger precursors named pro-NTs, which are then processed into mature NTs by enzymatic cleavage. The pro-NTs and the mature NTs activate

different and sometimes opposing signals and physiological pathways, acting through different receptors (Teng , and Hempstead, 2004).

Mature NTs preferentially activate Trk receptors, which are generally associated with survival signals, whereas pro-NTs activate p75 receptors, which are generally associated with death signals (Chao et al., 2006). Neurodegenerative diseases often exhibit imbalances either in NT (e.g., poor processing of pro-NTs to the mature state or poor transport of NTs to the site, where they are needed) or imbalances in NT receptors (e.g., decreases in pro-survival Trks and increases in pro-death p75). This summary is a simplification, and there are additional issues, such as positive and negative functional cross-regulation of Trks and p75, when these receptors are co-expressed. In certain cellular contexts the receptors may also have altered functions, for example in neoplasia.

Clinical trials using NTs as drugs to promote neuroprotection have consistently failed, in large part due to poor receptor selectivity (e.g., binding to Trks and p75), their pleiotropic pro-survival and pro-death activities, short half-lives, poor pharmacokinetics and bioavailability (Yuen and Mobley, 1996; Thoenen and Sendtner, 2002), or because pro-death p75 receptors may be up-regulated in disease (Rudzinski et al., 2004; Ibanez and Simi, 2012), thus negating the full benefit of Trk activation (Josephy-Hernandez et al., 2017). In addition, in some cases Trk receptors can also promote neuronal death (Tauszig-Delamasure et al., 2007), resulting in a confusing pattern of *in vivo* physiology and hard-to-predict pharmacology.

Many excellent reviews of the NT field discuss the biology and physiology of each factor and receptor (Ibanez and Simi, 2012; Bothwell, 2016), and postulate reasons to explain clinical failures (Yuen and Mobley, 1996; Thoenen and Sendtner, 2002). Other comprehensive reviews describe compounds reported to activate/inactivate Trks and p75 receptors, some of which were used as proof-of-concept therapeutics [reviewed in (Longo and Massa, 2004; Josephy-Hernandez et al., 2017)].

Here, we present a reassessment of neuroprotection strategies and their challenges, focusing on the paradoxes of receptor pharmacology and signals. We distinguish strategies that promote survival and strategies that reduce neurotoxicity, as separate but complementary approaches. Each strategy faces challenges which must be addressed for successful translation into clinically effective neuroprotective therapies.

NEUROTROPHIN RECEPTORS AND ROLES IN DISEASE

Neurotrophins (NTs) act through two distinct receptor families: three receptor tyrosine kinases named TrkA TrkB and TrkC, and a receptor named p75. NGF binds TrkA, BDNF and NT-4 bind TrkB, and NT-3 prefers TrkC but also can bind TrkA and TrkB (**Figure 1**).

Ligands binding to Trks drive the activation of the receptor tyrosine kinase enzymatic activity and the tyrosine phosphorylation of intracellular proteins (e.g., PLCγ, PI3K, Ras and Raf/MEK/Erk1) to initiate signaling pathways (Saragovi and Gehring, 2000; Miller and Kaplan, 2001). These intracellular signaling pathways are usually associated with neuronal survival, maintenance and function in the peripheral and central nervous systems (CNS), and the survival of stressed neurons (Huang and Reichardt, 2003). Therefore, activation of Trks or their signaling cascades has been sought as a mechanism to thwart neuronal degeneration (Saragovi and Gehring, 2000; Saragovi et al., 2009).

All NTs, including the pro-NTs, also bind to p75, a member of the Tumor Necrosis Factor-α (TNFα) receptor superfamily. NTs binding to p75 lead to the activation of complex cascades that are stage- or tissue-specific. Generally, p75 is believed to signal neuronal atrophy, synaptic loss, loss of function, and cell death (Zaccaro et al., 2001; Hempstead, 2002, 2006; Saragovi and Zaccaro, 2002; Ivanisevic et al., 2003; Chao et al., 2006; Saragovi et al., 2009), and is commonly upregulated in neurodegenerative diseases. In pathological states (**Table 1**), pro-NTs binding to p75 promotes the production of inflammatory cytokines TNFα and α2 Macroglobulin (α2M) by glial cells, and increase levels of pro-NGF itself, thus perpetuating the deleterious activation of p75. All of these factors are neurotoxic at increased levels, and result in a vicious cycle of neurotoxic events (Barcelona and Saragovi, 2015).

Adding another layer of complexity to this signaling axis, the biological function of p75 depends on several factors. The p75 receptor cooperates with other proteins, such as the sortilin family of receptors, which are integral to p75 signaling (Vaegter et al., 2011; Skeldal et al., 2012). Additionally, co-expression of Trks can influence p75 biology, as can the type of cell and its stage of maturation/differentiation. As mentioned above, the p75 receptor also has multiple ligands (all NTs as well as all pro-NTs) (Dechant and Barde, 2002; Nykjaer et al., 2005; Al-Shawi et al., 2007), and co-expression of p75 and Trks regulates ligand binding and affinity (Hempstead and Chao, 1997), as well as functional signaling (Zaccaro et al., 2001; Saragovi and Zaccaro, 2002) in a positive or negative manner (**Figure 1**). Due to the complexity of the signaling pathways, the consequences of pharmacological modulation of p75 *in vivo* are difficult to predict.

Yet another level of complexity in Trk receptor signaling emerges from the presence of Trk receptor isoforms. Trks can be expressed as full-length Trk tyrosine kinase receptors (Trk-FL) or as truncated isoforms without a kinase domain. The truncated isoforms are generated by alternative mRNA splicing, gaining a new and distinct intracellular sequence while lacking intrinsic tyrosine kinase activity (Brahimi et al., 2016). Both truncated TrkB.T1 and TrkC.T1 are able to mediate signals, either by inhibiting full-length tyrosine kinase as a dominant-negative mechanism (Valenzuela et al., 1993; Palko et al., 1999; Das et al., 2000) or by being activated in a ligand-dependent manner (Baxter et al., 1997; Esteban et al., 2006). Pathological upregulation of TrkC.T1 induces neuronal cell death through activation of Rac1 GTPase and pERK signaling pathways, with subsequent increase of TNFα production to toxic levels (Esteban et al., 2006; Galán et al., 2017b). Expression of TrkB.T1 and TrkC.T1 receptors increases in many neurodegenerative diseases (**Table 1**; Bai et al., 2010b; Yanpallewar et al., 2012; Galán et al., 2017b).

TABLE 1 | Experimental (and in some cases clinical) validation of the indicated receptor targets as "proof-of-concept" in neurodegenerative diseases affecting the CNS.

	TrkC	TrkC.T1	p75	TrkA	TrkB	TrkB.T1	RET
Brain / Spinal Cord							
Alzheimer's/memory			Antag.	Agonist	Agonist	Prevent splicing*	
Parkinson's			?		Agonist		Agonist
ALS	Agonist	Antag. or prevent splicing*	Antag.		Agonist	Prevent splicing*	Agonist
Huntington's			Antag.		Agonist		Agonist
Cochlea							
Hearing loss	Agonist	Antag. or prevent splicing*	?		Agonist		Agonist
Retina							
Retinitis pigmentosa		Antag.	Antag.				Agonist
Glaucoma		Antag. or prevent splicing*	Antag.	Agonist	Agonist		Agonist
Diabetic retinopathy			Antag.				
Optic nerve injury			Antag.	Agonist	Agonist		Agonist
Retinal angiogenesis		Antag.	Antag.				

*Antag = antagonist. ALS = amyotrophic lateral sclerosis. *Prevention of TrkB or TrkC mRNA splicing to their truncated isoforms was achieved by an engineered mutation of the splicing site in transgenic mice. ? = unclear or contradictory data.*

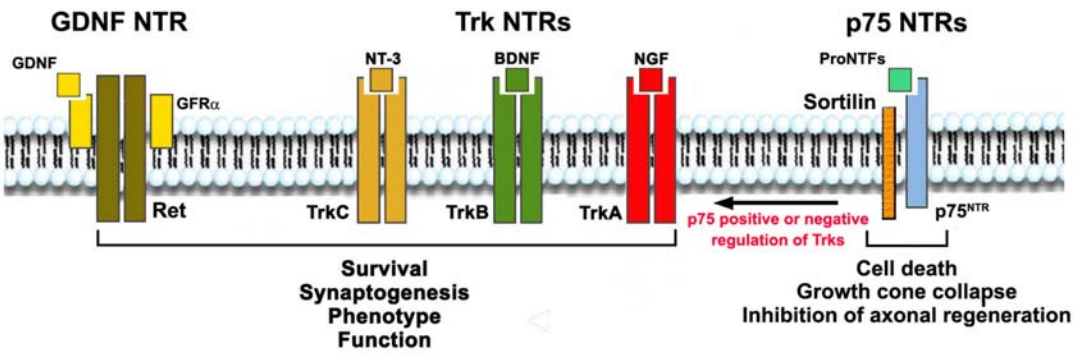

FIGURE 1 | Neurotrophic Factors, their receptors (NTRs) and functions. NTs activate signaling receptors TrkA, TrkB, TrkC, and $p75^{NTR}$. Each NT receptor (NTR) can act alone, and all Trks can also cooperate positively or negatively with $p75^{NTR}$. GDNF acts through RET but binds the glycosyl-phosphatidylinositol-anchored co-receptor (GFRα1–4) subunits. Mature NTs (NGF, BDNF, NT-3) bind, respectively, TrkA, TrkB and TrkC with some selectivity. All NTs and the precursor pro-neurotrophin proteins bind to $p75^{NTR}$. Growth factor activation of Trks or RET promote survival, growth, differentiation and synaptogenesis. Trk receptors may be present in truncated forms that are not protective (not shown). Growth factor activation of $p75^{NTR}$/sortilin complex in neurons leads to apoptosis, growth cone collapse, and inhibition of axonal regeneration; and in glia, activation of $p75^{NTR}$ leads to production of pro-inflammatory and neurotoxic factors. $p75^{NTR}$ can also regulate the action of Trk receptors positively or negatively, depending on its binding partners and other factors.

Given that truncated isoforms are increased in disease and can be activated by NTs to cause toxicity, it would seem counterintuitive to use NTs as therapeutic agents in these conditions.

NEUROTROPHIC FACTORS IN CLINICAL DEVELOPMENT

Neurotrophins (NTs) are part of a larger family of neurotrophic factors (NTFs). Among the NTFs, glial-derived neurotrophic factor (GDNF), ciliary-derived neurotrophic factor (CNTF), and insulin-like growth factor-1 (IGF-1) are key determinants of neuronal health (Sakowski et al., 2009; Pasquin et al., 2015) and were tested for clinical efficacy (Yuen and Mobley, 1996; Thoenen and Sendtner, 2002).

Glial-derived neurotrophic factor (GDNF) signals by binding to a co-receptor known as GFRα1, leading to the activation of the tyrosine kinase Ret. Similarly to its counterparts in the Trk family, Ret induces survival through the PI3K/Akt, Ras/Erk, Src and PLCγ signaling pathways (Ibanez, 2013). The absolute requirement of GFRα co-receptors for GDNF activation of Ret limits the number of neurons targeted by GDNF.

THE EVOLUTION OF THE CONCEPT OF NT-BASED NEUROPROTECTION

The translational potential of NTs as drugs and NT receptors as targets for neuroprotection has long been recognized, and several clinical trials were carried out in the 1990's, none resulting in regulatory approval, the main problems attributed to lack of specific targeting, not achieving an effective dose, and failure to avoid side effects (Thoenen and Sendtner, 2002). The failure of these

trials to achieve their endpoints led to a re-evaluation of the validity and druggability of these targets in disease, and particularly the scrutiny of the physiological basis for their pharmacology.

Below we present evolving concepts of NT receptor biology and receptor physiology relevant to their roles in disease. We discuss 4 generations of neuroprotection strategies. Neuroprotection strategy 1.0 refers to the use of NTs or NT-inducing agents regardless of receptor selectivity, pharmacokinetics, or receptor expression patterns. Neuroprotection strategy 2.0 refers to the selective activation of Trk receptors without p75 binding and activation, particularly in diseases, where p75 is upregulated. Neuroprotection strategy 3.0 refers to inhibition of p75-mediated signals, which are pro-inflammatory and neurotoxic. Neuroprotection strategy 4.0 refers to improved Trk-activation in a selective manner, not only circumventing p75 activation but also the activation of truncated Trk isoforms that mediate neurotoxicity (**Figure 2**). Conceivably, these 4 strategies may be combined to achieve synergy, given that they have different mechanisms of action.

NEUROPROTECTION STRATEGY 1.0: ACTIVATING NT RECEPTORS

Neurotrophins (NTs) normally drive neuronal survival, maintenance of phenotype and synapses, and function. Ligand-dependent activation of the Trk receptors is associated with those survival signals (Sendtner et al., 1996; Bechade et al., 2002; Wan et al., 2014; Brahimi et al., 2016). As mentioned earlier, deficits in the activation of Trk receptor tyrosine kinases (for instance, impaired cellular transport, decreased receptor expression, or agonist deficiency) are linked to early stages of neurodegeneration, and precede neuronal death and symptoms. These data supported the rationale that Trk-agonism may be therapeutic, and NTs were evaluated in multiple experimental models with the expectation that they would solely act as Trk agonists.

Nerve growth factor (NGF) was studied therapeutically to activate TrkA in models of Alzheimer disease (AD) (Schindowski et al., 2008; Cuello et al., 2010), and ageing (Mufson et al., 2000; Bruno et al., 2004; Saragovi, 2005), or Down syndrome (Sendera et al., 2000; Dorsey et al., 2006), models with cholinergic deficits and memory impairment. BDNF and GDNF were studied therapeutically in models of Parkinson disease (PD) (Rangasamy et al., 2010) and Huntington disease (HD) (Alberch et al., 2004), with loss of neurons that express TrkB and RET. NT-3 was studied therapeutically in models of amyotrophic lateral sclerosis (ALS) with loss of spinal cord motor neurons that express TrkC (Ekestern, 2004). Ophthalmic neurodegenerative diseases such as glaucoma (Rudzinski et al., 2004; Nafissi and Foldvari, 2016), retinitis pigmentosa (RP) (Thanos and Emerich, 2005), and diabetic retinopathy (DR) (Bikbova et al., 2014) were studied using NTs as therapeutic agents. In most of these diseases, growth factors other than NTs were explored, including GDNF, CNTF, and IGF-1 (Kaspar et al., 2003; Dupraz et al., 2013; Bassil et al., 2014; Ma et al., 2015; Agostinone et al., 2018) [reviewed in (Gould and Oppenheim, 2011)].

Clinical trials using exogenous delivery of these factors or cells secreting these factors, designed to agonize Trk or RET or IGF-1 receptors, have been consistently unsuccessful. Reasons include the poor pharmacokinetics and pharmacodynamics of NTs, short half-lives, undesirable high potency and pleiotropic effects, inability to penetrate tissue barriers, and difficulty in delivery of these large proteins across the BBB, requiring increasingly sophisticated and risky methods of administration (Weissmiller and Wu, 2012; Rafii et al., 2018), with consequent limitations in reaching the relatively high doses required for efficacy in experimental studies.

Notably, the reasons thought to be responsible for failure are not exclusive to NTs: they generally affect most protein-based therapies, and the issues are resolvable. But there are problems specific to NTs. These include poor receptor selectivity and unpredictable *in vivo* pharmacology, particularly off-target effects on unintended activation of p75 or truncated Trk receptors (Saragovi and Gehring, 2000; Josephy-Hernandez et al., 2017). The expression and activity of these receptors are increased in neurodegenerative states, and given that they are neurotoxic, they invalidate the benefit of Trk activation, decrease the therapeutic effect, and create a poor risk/benefit ratio (**Figure 2A**; Peleshok and Saragovi, 2006; Josephy-Hernandez et al., 2017).

NEUROPROTECTION STRATEGY 2.0: TARGETING FULL LENGTH Trk RECEPTORS AND AVOIDING p75 ACTIVATION

Based on the many failures of neuroprotection strategy 1.0, we hypothesized that selective Trk-activating agents which circumvent p75 binding and activation would be neuroprotective. To test this idea, we produced a wide range of TrkA-, TrkB-, and TrkC-selective agonists and tested them in different neurodegenerative pathologies (**Figure 2B**). GDNF agonists are also briefly summarized.

TrkA-, TrkB-, or TrkC-Selective Agonists

We generated small molecule mimetics of NTs (LeSauteur et al., 1995, 1996a; Debeir et al., 1999; Maliartchouk et al., 2000a,b; Pattarawarapan et al., 2002; Zaccaro et al., 2005; Chen et al., 2009), agonistic mAbs (LeSauteur et al., 1996b, Saragovi et al., 1998; Bai et al., 2010c; Guillemard et al., 2010), small molecule mimetics of the mAbs (Brahimi et al., 2009, 2010, 2014; Chen et al., 2009), and mutant NTs (Saragovi et al., 1998; Ivanisevic et al., 2007; Bai et al., 2010a; Aboulkassim et al., 2011). We then tested them in animal models of neurodegenerative disease, demonstrating effectiveness *in vivo*.

For instance, a TrkA-selective NGF mutant that does not activate p75 (Bai et al., 2010a) and the selective small molecule

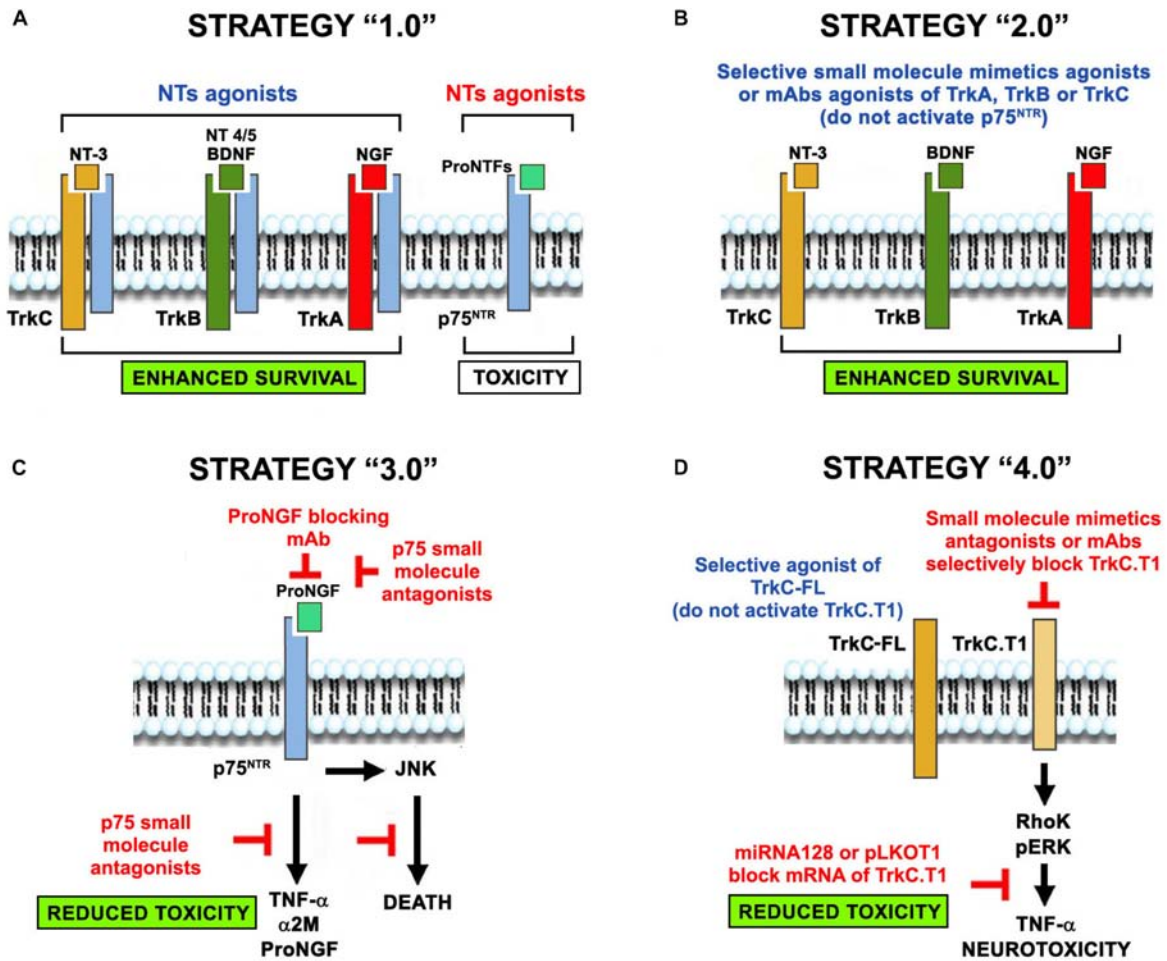

FIGURE 2 | The evolution of the concept of NT-based neuroprotection. Four neuroprotective strategies evolved from the use of NTs-based therapies in neurodegenerative diseases. **(A)** Neuroprotection strategy 1.0 was the original use of NTs regardless of receptor selectivity, causing unintended signaling through $p75^{NTR}$ or truncated Trk isoforms that are up-regulated in neurodegenerative pathologies. **(B)** Neuroprotection strategy 2.0 overcomes some of the drawbacks by using selective agonists of Trk receptors (small molecules, mAbs, and mutant NTs that do not bind p75), circumventing $p75^{NTR}$ activation. **(C)** Neuroprotection strategy 3.0 addresses $p75^{NTR}$ neurotoxicity using selective blocking antibodies and small molecules antagonists. **(D)** Neuroprotection strategy 4.0 addresses the toxic function of truncated Trk isoforms by using selective Trk full-length agonists (that do not activate the truncated forms) or selective antagonists of truncated isoforms (small molecules, mAbs, miRNAs and shRNA vectors). Co-expression of p75 and TrkC.T1 in glia may exacerbate neurotoxicity. We predict that combinations of these strategies (e.g., strategy 2 + strategy 3) may be synergistic because of their complementary mechanisms of action.

TrkA agonist D3 (Shi et al., 2007) rescued retinal ganglion cells (RGCs) in glaucoma and optic nerve axotomy models. A selective agonistic mAb that binds TrkB delayed RGC death and preserved the structure of retinal layers from degenerating in optic nerve axotomy and glaucoma (Bai et al., 2010c). A mutant NT-3 selective for TrkC, and an agonistic mAb that activates TrkC (Guillemard et al., 2010) selectively protected motor neurons in an ALS model (Enomoto et al., 2013; Brahimi et al., 2016). None of these ligands bind or activate p75. Many of these agents were very effective *in vivo* in disease states and paradigms, where the native NTs were ineffective unless p75 was concomitantly silenced or neutralized (Bruno et al., 2004; Shi et al., 2007; Lebrun-Julien et al., 2009b, 2010).

Later, other groups validated the concept by generating TrkB small molecule agonists and TrkB and TrkC agonistic mAbs that were protective in the MPTP neurotoxicity mouse model of PD (Berezov et al., 2002; Jang et al., 2010; Devi and Ohno, 2012; Bollen et al., 2013; Coles et al., 2014; Chitranshi et al., 2015; Nie et al., 2015), HD (Jiang et al., 2013; Simmons et al., 2013), and ALS. These agents were effective in experimental paradigms, where the wild type NTs were ineffective, whether endogenously produced or added as therapeutic agents. Yet the wild type NTs became effective when p75 expression was concomitantly silenced or inhibited [reviewed in Josephy-Hernandez et al. (2017)].

With respect to translation to clinical use, one of our TrkA-selective small molecule agonists is currently in Phase 3 clinical trials for an ophthalmic indication, a TrkC-selective mAb agonist is in pre-clinical studies for ALS, and Trk-selective agonistic mAbs and NT mutants are under investigation for

neurosensory hearing loss. Other translational efforts with Trk-selective agonists are in progress in PD, ALS, AD, and HD.

GDNF/Ret Agonists

The GDNF/Ret/GFRα1 axis plays an important neuroprotective role in the retina and other anatomical sites. GDNF causes upregulation of the glutamate aspartate transporter in glial cells, and therefore counteracts the excitotoxic environment in the degenerating retina (Delyfer et al., 2005). GDNF also stimulates the secretion of osteopontin and basic fibroblast growth factor (bFGF), which have been shown to prolong rod survival (Hauck et al., 2006; Del Rio et al., 2011). Following the initial evaluation of GDNF therapies (Strategy 1.0), new efforts have led to the generation of small-molecule agonists with GDNF-like activity or Ret modulatory activity (Sidorova et al., 2017).

Norgestrel is a small molecule related to progesterone that has been demonstrated to be neuroprotective in the rd10 model of RP (Doonan et al., 2011), possibly through the upregulation of bFGF. XIB4035t is a small molecule with effects on GFRα1/Ret signaling. Originally, it was inappropriately characterized as a GFRα1 agonist (Tokugawa et al., 2003), but is nowadays considered to be a GFRα1 modulator, able to potentiate signaling in the presence of GDNF (Hedstrom et al., 2014; Sidorova et al., 2017; Ivanova et al., 2018).

NEUROPROTECTION STRATEGY 3.0: INHIBITING p75 RECEPTORS

In the adult, the p75 receptor is expressed at low levels in healthy states (Tomellini et al., 2014), but is upregulated in disease. This injury-induced expression recapitulates the role of p75 in development (Ibanez and Simi, 2012), where p75 is expressed at high levels and modulates synaptic pruning and the death of unwanted neurons (Lebrun-Julien et al., 2009b; Bai et al., 2010b). The upregulated p75 receptor is generally associated with neuronal death and is activated primarily by proNGF (**Figure 2C**; Teng et al., 2005).

In neurons, activation of p75 by proNGF triggers apoptotic death, decreases synaptic function (Jansen et al., 2007), and reduces the neuroprotective effect associated with agonists of full-length Trk receptors (Zaccaro et al., 2001; Saragovi and Zaccaro, 2002; Ivanisevic et al., 2003; Saragovi et al., 2009).

In the vasculature, p75 activation causes pericyte dysfunction (Siao et al., 2013; Barcelona et al., 2016) and breakdown of blood–tissue barriers, causing vascular permeability and edema, and leading to vascular endothelial cell death and hypoxia (Shanab et al., 2015). Consequent vaso-obliteration and hypoxia induce VEGF, angiogenic remodeling, and pathological neovascularization (Siao et al., 2013; Barcelona et al., 2016). Thus, p75 on pericytes is relevant to deficits after cardiac hypoxia associated with cardiac injury, retinal neovascularization in DR, and choroidal neovascularization in the wet form of age-related macular degeneration.

In glia, p75 enhances production of the inflammatory mediators TNFα (Srinivasan et al., 2004; Nakazawa et al., 2006; Lebrun-Julien et al., 2009a, Lebrun-Julien et al., 2010; Bai et al., 2010b; Barcelona et al., 2016; Galan et al., 2017a; Platon-Corchado et al., 2017), proNGF (Srinivasan et al., 2004; Lim et al., 2008; Lebrun-Julien et al., 2009b, 2010; Xu et al., 2009; Barcelona et al., 2016), and α2M (Shi et al., 2008; Bai et al., 2010a,b; Barcelona et al., 2016; Galan et al., 2017a; Platon-Corchado et al., 2017). Each of these factors is neurotoxic, and they cooperate to synergistically worsen pathology (Mysona et al., 2013; Barcelona and Saragovi, 2015). Mechanistically, α2M extends the half-lives of TNFα and proNGF (Barcelona and Saragovi, 2015), and p75-driven production of proNGF generates an autocrine loop, resulting in its persistent activation.

Notably, TNFα, proNGF, and α2M are each validated therapeutic targets. Inhibition of TNFα (Nakazawa et al., 2006; Roh et al., 2012), proNGF (Barcelona et al., 2013; Barcelona and Saragovi, 2015), or α2M (Shi et al., 2008; Bai et al., 2010a,b) as monotherapy affords moderate efficacy in retinal neurodegeneration, and other pathologies. Thus, p75 overexpression in disease creates an unfavorable environment by driving at least three neurotoxic proteins, which then feeds back in an autocrine-mediated vicious cycle. Expression and activity of p75 in disease disrupts neuro-glia-vascular homeostasis, with progressive pathology, whereby inflammation causes neuronal death, and neuronal death causes more inflammation and vascular pathology.

These observations in animal models are relevant to human neurodegenerative and vascular diseases because increased levels of p75, TNFα, proNGF, and α2M, alone or in combination, have been documented in ALS, cardiac hypoxia, RP, DR, and others. Inhibition of p75 should also prevent direct neuronal death, vascular deficits, acute inflammation, and chronic production of TNFα, proNGF, and α2M.

We developed a family of drug-like agents that selectively inhibit p75 activity (Bai et al., 2010a; Josephy-Hernandez et al., 2017). These p75 antagonists were therapeutic in models of glaucoma and optic nerve injury (Bai et al., 2010a), RP (Galán et al., 2017b; Platon-Corchado et al., 2017), and neovascularization in DR (Barcelona et al., 2016; Galan et al., 2017a), even when applied as monotherapy after disease onset. Other small p75 ligands reduced tau-related pathology in AD (Massa et al., 2002; Nguyen et al., 2014) and p75-induced motor neuron cell death in ALS (Pehar et al., 2006).

NEUROPROTECTION STRATEGY 4.0: INHIBITING TRUNCATED Trk RECEPTORS

As described above, the full length Trk receptors have a tyrosine kinase intracellular domain that phosphorylates and activates survival signals such as Akt or PLCɤ pathways in a ligand-dependent manner. The "full length" (FL) receptor activity is critical to the survival and function of neurons, where they are expressed. For instance, TrkC-FL is necessary for the physiology of motor neurons and cochlear neurons (Sendtner et al., 1996; Bechade et al., 2002; Mellado Lagarde et al., 2014; Wan et al., 2014; Wan and Corfas, 2015; Brahimi et al., 2016;

Suzuki et al., 2016), whereas TrkB-FL is necessary for brain dopaminergic neurons (Nie et al., 2015).

However, there are truncated Trk receptors which arise from alternative mRNA splicing of Trk-FL mRNAs. The resulting truncated isoforms lack the kinase domain, and signal differently. The most common truncated TrkC and TrkB isoforms in humans and rodents are TrkC.T1 (Tessarollo, 1998; Palko et al., 1999) and TrkB.T1, respectively, (**Figure 2D**; Yanpallewar et al., 2012).

Truncated TrkC Isoform (TrkC.T1)

TrkC.T1 arises from alternative mRNA splicing of TrkC-FL mRNA, resulting in deletion of the kinase domain, and gain of a new intracellular domain with a unique sequence from a spliced-in exon. For this reason, the TrkC-FL and TrkC.T1 isoforms only differ at the intracellular domain primary sequences, but retain the same extracellular primary sequence. Both TrkC-FL and TrkC.T1 bind NT-3 equally well and both signal in an NT-3–dependent manner (Esteban et al., 2006).

TrkC.T1 acts by activation of Rho kinase-Erk pathways (Esteban et al., 2006; Galán et al., 2017b), and via tamalin (Esteban et al., 2006). One physiological consequence of TrkC.T1 activity is an NT-3–dependent increase in TNFα, which is neurotoxic (Bai et al., 2010b; Brahimi et al., 2016; Galán et al., 2017b). Hence there must be a balance of TrkC-FL and TrkC.T1 signals in health and disease. In healthy adult tissue TrkC.T1 is low or undetectable, but it is significantly upregulated shortly after injury, but before degeneration and detectable symptoms, in neurodegenerative diseases such as glaucoma, RP, and ALS (Bai et al., 2010b; Brahimi et al., 2016; Galán et al., 2017b), as well as in noise-induced hearing loss (Saragovi, unpublished).

TrkC.T1 mRNA is produced constitutively and is immediately degraded by miRNA128. miRNA128 is reduced and TrkC.T1 mRNA is increased in neurodegenerative diseases (Brahimi et al., 2016). Hence, at the onset of neurodegenerative diseases TrkC.T1 protein is upregulated, but without a decrease in TrkC-FL until very late in disease, when neurons die (Bai et al., 2010b; Brahimi et al., 2016; Galán et al., 2017b).

TrkC-FL is present mainly in neurons, whereas in disease states TrkC.T1 is mainly in glia and astrocytes. Hence the TrkC.FL/TrkC.T1 ratio is reduced in diseased tissues with a difference in cellular distribution that is relevant to the mechanisms of action. In glia, TrkC.T1 activity promotes TNFα production in a pErk–dependent manner, and *in vivo* all TrkC.T1 mRNA co-localizes in cells expressing TNFα mRNA (Brahimi et al., 2016; Galan et al., 2017a; Galán et al., 2017b). The TrkC.T1–dependent increase in TNFα is neurotoxic and neurodegenerative, and relevant to the etiology of glaucoma and RP (Bai et al., 2010b; Galán et al., 2017b).

NT-3 binds TrkC-FL and TrkC.T1, and therefore paradoxically activates both neuroprotective and neurodegenerative signals. In this context, we postulated that NT-3 would be therapeutically useful if administered before disease onset (e.g., before TrkC.T1 upregulation), whereas neurotoxicity would predominate when NT-3 was applied after disease onset (e.g., after TrkC.T1 upregulation) (Corse et al., 1999; Park et al., 2009; Wyatt et al., 2011; Suzuki et al., 2016). Indeed, this paradox has been reported in motor neuron degeneration (such as SOD1 mutant rodent models of ALS) (Brahimi et al., 2016), in the death of retinal ganglion cell neurons in a model of RP (Galán et al., 2017b), and may be germane to the death of spiral ganglion neurons in a noise-induced hearing loss model (NIHL).

To directly test the hypothesis that the therapeutic failure of NT-3 is due in part to the unintended activation of TrkC.T1, we developed selective agonists of TrkC-FL. These agents activate TrkC-FL but do not bind or activate TrkC.T1, and therefore do not stimulate TNFα production (Guillemard et al., 2010; Brahimi et al., 2016). In an animal model of ALS these selective TrkC-FL agonists protect motor neuron health and significantly prolong life-span, even when injected after disease onset (Brahimi et al., 2016).

Additionally, we validated this concept by showing that in disease models of neurodegeneration (glaucoma causing RGC neuronal death (Bai et al., 2010b) and a genetically driven model of RP causing photoreceptor neuronal death (Galán et al., 2017b), reduced TrkC.T1 expression had significantly reduced disease progression. reduced levels of TNFα, lower activation of pErk in glia, and reduced neuronal death and neurodegeneration.

With respect to pharmacological inhibition, we have also developed highly selective inhibitors of TrkC.T1 expression (miRNA128 and shRNA vectors) which silence or inhibit TrkC.T1 and prevent induction of TNFα by NT-3 *in vitro* (Brahimi et al., 2016) and *ex vivo* in organotypic cultures (Galán et al., 2017b). Published small molecule inhibitors of TrkC (Brahimi et al., 2010, Brahimi et al., 2014, 2016; Liu et al., 2010) are non-selective between TrkC-FL and TrkC.T1, but significantly decrease TNFα levels and neuronal cell death in a mouse model of glaucoma (Bai et al., 2010b). The non-selective TrkC antagonists used in glaucoma were useful because virtually all the TrkC in the glaucomatous retina is TrkC.T1. However, selective TrkC.T1 inhibitors would be preferable, and we have developed and evaluated such agents (Brahimi et al., 2009, Brahimi et al., 2016).

Truncated TrkB Isoform (TrkB.T1)

TrkB.T1 (T1) is the main TrkB isoform in the mature brain (Dorsey et al., 2006) and its function was studied *in vivo* (Ferrer et al., 1999). Similar to TrkC.T1, TrkB.T1 inhibits TrkB.FL signaling acting as a dominant-negative receptor, thereby decreasing the effects of BDNF on neuronal survival, differentiation, and plasticity. TrkB.T1 also has BDNF-independent functions and regulates Rho GTPase activity (Ohira et al., 2006) and may stimulate PLCγ and MAPK signaling (Ohira et al., 2007).

TrkB.T1 is upregulated in neurodegenerative diseases such as AD (Ferrer et al., 1999) and ALS (Yanpallewar et al., 2012). Genetic deletion of TrkB.T1 in the SOD mouse model of ALS significantly delayed the onset of motor neuron degeneration (Yanpallewar et al., 2012) and restored cognitive abnormalities (Quarta et al., 2018).

In summary, TrkC.T1 (along with p75, TNFα, proNGF, and α2M) and TrkB.T1 are upregulated in animal and in human

diseases (Sanchez et al., 2007; Bai et al., 2011; Roh et al., 2012; Yanpallewar et al., 2012; Siao et al., 2013; Shepheard et al., 2014) and are relevant to pathophysiology, making them excellent therapeutic targets.

CONCLUSION

It has been 25 years since the first clinical trials of NTs in CNS neurodegenerative disorders. These and subsequent studies failed, due not only to poor pharmacokinetics, short half-lives and/or poor bioavailability of the drugs, but also due to the complex biology of NTs and their receptors. Our understanding of the finely tuned physiology of NT receptors is critical to developing strategies for selectively restoring the balance between neuroprotective and neurotoxic signals. Over the years, we have learned that failures of NTs (neuroprotection strategy 1.0) were related to their pleiotropic effects, poor selectivity and off-target effects on unintended p75 or truncated Trk isoforms. More specific and successful strategies were developed using specific Trk-activating agents that circumvented p75 (neuroprotection strategy 2.0) and therefore potentiated neuroprotection, or by specifically inhibiting p75 receptors (neuroprotection strategy 3.0) or truncated Trk isoforms (neuroprotection strategy 4.0), both signaling neurotoxicity.

NT-based neuroprotection is still an evolving concept, and we can expect the development of even more focused strategies in coming years, which should deal with the complex nature of NT receptor physiology. We envision a future neuroprotection strategy 5.0 based on combining strategies, for example a synergistic neuroprotective and anti-neurotoxic combination, which might finally provide successful translation for treatment of chronic neurodegenerative diseases.

AUTHOR CONTRIBUTIONS

All authors listed have made a substantial, direct and intellectual contribution to the work, and approved it for publication.

FUNDING

This work was supported by grants from the Canadian Institutes of Health Research (HS and LL), NIH (LL), and Canada Research Chairs (LL). HS has licensed products for neuroprotection, and is a consultant to Otonomy Inc. LL is a consultant to Aerie, Eyevensys, Galimedix, Prilenia, Quark, and Regenera on neuroprotection.

REFERENCES

Aboulkassim, T., Tong, X. K., Chung Tse, Y., Wong, T. P., Woo, S. B., Neet, K. E., et al. (2011). Ligand-dependent TrkA activity in brain differentially affects spatial learning and long-term memory. *Mol. Pharmacol.* 80, 498–508. doi: 10.1124/mol.111.071332

Agostinone, J., Alarcon-Martinez, L., Gamlin, C., Yu, W. Q., Wong, R. O. L., and Di Polo, A. (2018). Insulin signalling promotes dendrite and synapse regeneration and restores circuit function after axonal injury. *Brain* 141, 1963–1980. doi: 10.1093/brain/awy142

Alberch, J., Perez-Navarro, E, and Canals, J. M. (2004). Neurotrophic factors in Huntington's disease. *Prog. Brain Res.* 146, 195–229.

Al-Shawi, R., Hafner, A., Chun, S., Raza, S., Crutcher, K., Thrasivoulou, C., et al. (2007). ProNGF, sortilin, and age-related neurodegeneration. *Ann. N. Y. Acad. Sci.* 1119, 208–215. doi: 10.1196/annals.1404.024

Bai, Y., Dergham, P., Nedev, H., Xu, J., Galan, A., Rivera, J. C., et al. (2010a). Chronic and acute models of retinal neurodegeneration TrkA activity are neuroprotective whereas p75NTR activity is neurotoxic through a paracrine mechanism. *J. Biol. Chem.* 285, 39392–39400. doi: 10.1074/jbc.M110.147801

Bai, Y., Shi, Z., Zhuo, Y., Liu, J., Malakhov, A., Ko, E., et al. (2010b). In glaucoma the upregulated truncated TrkC.T1 receptor isoform in glia causes increased TNF-alpha production, leading to retinal ganglion cell death. *Invest. Ophthalmol. Vis. Sci.* 51, 6639–6651. doi: 10.1167/iovs.10-5431

Bai, Y., Sivori, D., Woo, S. B., Neet, K. E., Lerner, S. F., Saragovi, H. U. et al. (2011). During glaucoma, alpha2-macroglobulin accumulates in aqueous humor and binds to nerve growth factor, neutralizing neuroprotection. *Invest. Ophthalmol. Vis. Sci.* 52, 5260–5265. doi: 10.1167/iovs.10-6691

Bai, Y., Xu, J., Brahimi, F., Zhuo, Y., Marinko Sarunic, V., and Saragovi, H. U. et al. (2010c). An agonistic anti-TrkB mAb, but not BDNF, causes sustained TrkB activation, delays RGC death, and protects the retinal structure in optic nerve axotomy and in glaucoma. *Invest. Ophthalmol. Vis. Sci.* 51, 4722–4731.

Barcelona, P. F., Ortiz, S. G., Chiabrando, G. A., and Sanchez, M. C. (2013). alpha2-Macroglobulin induces glial fibrillary acidic protein expression mediated by low-density lipoprotein receptor-related protein 1 in Muller cells. *Invest. Ophthalmol. Vis. Sci.* 52, 778–786. doi: 10.1167/iovs.10-5759

Barcelona, P. F., Sitaras, N., Galan, A., Esquiva, G., Jmaeff, S., Jian, Y., et al. (2016). p75NTR and its ligand ProNGF activate paracrine mechanisms etiological to the vascular, inflammatory, and neurodegenerative pathologies of diabetic retinopathy. *J. Neurosci.* 36, 8826–8841. doi: 10.1523/JNEUROSCI.4278-15.2016

Barcelona, P. F and Saragovi, H. U. (2015). A pro-nerve growth factor (proNGF) and NGF binding protein, alpha2-macroglobulin, differentially regulates p75 and TrkA receptors and is relevant to neurodegeneration *ex vivo* and *in vivo*. *Mol. Cell. Biol.* 35, 3396–3408. doi: 10.1128/mcb.00544-15

Bassil, F., Fernagut, P. O., Bezard, E., and Meissner, W. G. (2014). Insulin, IGF-1 and GLP-1 signaling in neurodegenerative disorders: targets for disease modification? *Prog. Neurobiol.* 118, 1–18. doi: 10.1016/j.pneurobio.2014.02.005

Baxter, G. T., Radeke, M. J., Kuo, R. C., Makrides, V., Hinkle, B., Hoang, R., et al. (1997). Signal transduction mediated by the truncated trkB receptor isoforms, trkB.T1 and trkB.T2. *J. Neurosci.* 17, 2683–2690. doi: 10.1523/jneurosci.17-08-02683.1997

Bechade, C., Mallecourt, C., Sedel, F., Vyas, S., and Triller, A. (2002). Motoneuron-derived neurotrophin-3 is a survival factor for PAX2-expressing spinal interneurons. *J. Neurosci.* 22, 8779–8784. doi: 10.1523/jneurosci.22-20-08779.2002

Berezov, A., Chen, J., Liu, Q., Zhang, H. T., Greene, M. I., Murali, R. et al. (2002). Disabling receptor ensembles with rationally designed interface peptidomimetics. *J. Biol. Chem.* 277, 28330–28339. doi: 10.1074/jbc.m202880200

Bikbova, G., Oshitari, T., Baba, T., and Yamamoto, S. (2014). Neurotrophic factors for retinal ganglion cell neuropathy - with a special reference to diabetic neuropathy in the retina. *Curr. Diabetes Rev.* 10, 166–176. doi: 10.2174/1573399810666140508121927

Bollen, E., Vanmierlo, T., Akkerman, S., Wouters, C., Steinbusch, H. M., Prickaerts, J. et al. (2013). 7,8-Dihydroxyflavone improves memory consolidation processes in rats and mice. *Behav. Brain Res.* 257, 8–12. doi: 10.1016/j.bbr.2013.09.029

Bothwell, M. (2016). Recent advances in understanding neurotrophin signaling. *F1000Res.* 5:F1000 Faculty Rev-1885.

Brahimi, F., Ko, E., Malakhov, A., Burgess, K., and Saragovi, H. U. (2014). Combinatorial assembly of small molecules into bivalent antagonists of TrkC or TrkA receptors. *PLoS One* 9:e89617. doi: 10.1371/journal.pone.0089617

Brahimi, F., Liu, J., Malakhov, A., Chowdhury, S., Purisima, E. O., Ivanisevic, L., et al. (2010). A monovalent agonist of TrkA tyrosine kinase receptors can be converted into a bivalent antagonist. *Biochim. Biophys. Acta* 1800, 1018–1026. doi: 10.1016/j.bbagen.2010.06.007

Brahimi, F., Maira, M., Barcelona, P. F., Galan, A., Aboulkassim, T., Teske, K., et al. (2016). The Paradoxical Signals of Two TrkC Receptor Isoforms Supports a Rationale for Novel Therapeutic Strategies in ALS. *PLoS One* 11:e0162307. doi: 10.1371/journal.pone.0162307

Brahimi, F., Malakhov, A., Lee, H. B., Pattarawarapan, M., Ivanisevic, L., Burgess, K., et al. (2009). A peptidomimetic of NT-3 acts as a TrkC antagonist. *Peptides* 30, 1833–1839. doi: 10.1016/j.peptides.2009.07.015

Bruno, M. A., Clarke, P. B., Seltzer, A., Quirion, R., Burgess, K., Cuello, A. C., et al. (2004). Long-lasting rescue of age-associated deficits in cognition and the CNS cholinergic phenotype by a partial agonist peptidomimetic ligand of TrkA. *J. Neurosci.* 24, 8009–8018. doi: 10.1523/jneurosci.1508-04.2004

Chao, M. V., Rajagopal, R., and Lee, F. S. (2006). Neurotrophin signalling in health and disease. *Clin. Sci.* 110, 167–173. doi: 10.1042/cs20050163

Chen, D., Brahimi, F., Angell, Y., Li, Y. C., Moscowicz, J., Saragovi, H. U., et al. (2009). Bivalent peptidomimetic ligands of TrkC are biased agonists and selectively induce neuritogenesis or potentiate neurotrophin-3 trophic signals. *ACS Chem. Biol.* 4, 769–781. doi: 10.1021/cb9001415

Chitranshi, N., Gupta, V., Kumar, S., and Graham, S. L. (2015). Exploring the molecular interactions of 7,8-dihydroxyflavone and its derivatives with TrkB and VEGFR2 proteins. *Int. J. Mol. Sci.* 16, 21087–21108. doi: 10.3390/ijms160921087

Coles, C. H., Mitakidis, N., Zhang, P., Elegheert, J., Lu, W., Stoker, A. W., et al. (2014). Structural basis for extracellular cis and trans RPTPsigma signal competition in synaptogenesis. *Nat. Commun.* 5:5209. doi: 10.1038/ncomms6209

Corse, A. M., Bilak, M. M., Bilak, S. R., Lehar, M., Rothstein, J. D., Kuncl, R. W. et al. (1999). Preclinical testing of neuroprotective neurotrophic factors in a model of chronic motor neuron degeneration. *Neurobiol. Dis.* 6, 335–346. doi: 10.1006/nbdi.1999.0253

Cuello, A. C., Bruno, M. A., Allard, S., Leon, W., and Iulita, M. F. (2010). Cholinergic involvement in Alzheimer's disease. A link with NGF maturation and degradation. *J. Mol. Neurosci.* 40, 230–235. doi: 10.1007/s12031-009-9238-z

Das, I., Sparrow, J. R., Lin, M. I., Shih, E., Mikawa, T., Hempstead BL. (2000). Trk C signaling is required for retinal progenitor cell proliferation [published erratum appears. *J. Neurosci.* 20, 2887–2895. doi: 10.1523/jneurosci.20-08-02887.2000

Debeir, T., Saragovi, H. U., and Cuello, A. C. (1999). A nerve growth factor mimetic TrkA antagonist causes withdrawal of cortical cholinergic boutons in the adult rat. *Proc. Natl. Acad. Sci. U.S.A.* 96, 4067–4072. doi: 10.1073/pnas.96.7.4067

Dechant, G., and Barde, Y. A. (2002). The neurotrophin receptor p75(NTR): novel functions and implications for diseases of the nervous system. *Nat. Neurosci.*refvol5, 1131–1136. doi: 10.1038/nn1102-1131

Del Rio, P., Irmler, M., Arango-Gonzalez, B., Favor, J., Bobe, C., Bartsch, U., et al. (2011). GDNF-induced osteopontin from Muller glial cells promotes photoreceptor survival in the Pde6brd1 mouse model of retinal degeneration. *Glia* 59, 821–832. doi: 10.1002/glia.21155

Delyfer, M. N., Forster, V., Neveux, N., Picaud, S., Leveillard, T., Sahel, J. A. et al. (2005). Evidence for glutamate-mediated excitotoxic mechanisms during photoreceptor degeneration in the rd1 mouse retina. *Mol. Vis.* 11, 688–696.

Devi, L, and Ohno, M. (2012). 7,8-dihydroxyflavone, a small-molecule TrkB agonist, reverses memory deficits and BACE1 elevation in a mouse model of Alzheimer's disease. *Neuropsychopharmacology* 37, 434–444. doi: 10.1038/npp.2011.191

Doonan, F., O'Driscoll, C., Kenna, P., and Cotter, T. G. (2011). Enhancing survival of photoreceptor cells in vivo using the synthetic progestin Norgestrel. *J. Neurochem.* 118, 915–927. doi: 10.1111/j.1471-4159.2011.07354.x

Dorsey, S. G., Renn, C. L., Carim-Todd, L. Barrick, C. A., Bambrick, L., Krueger, B. K., et al. (2006). In vivo restoration of physiological levels of truncated TrkB.T1 receptor rescues neuronal cell death in a trisomic mouse model. *Neuron* 51, 21–28. doi: 10.1016/j.neuron.2006.06.009

Dupraz, S., Grassi, D., Karnas, D., Nieto, A. F., Guil, D., Hicks, D et al. (2013). The insulin-like growth factor 1 receptor is essential for axonal regeneration in adult central nervous system neurons. *PLoS One* 8:e54462. doi: 10.1371/journal.pone.0054462

Ekestern, E. (2004). Neurotrophic factors and amyotrophic lateral sclerosis. *Neurodegener. Dis.* 1, 88–100. doi: 10.1159/000080049

Enomoto, M., Bunge, M. B., and Tsoulfas, P. (2013). A multifunctional neurotrophin with reduced affinity to p75NTR enhances transplanted Schwann cell survival and axon growth after spinal cord injury. *Exp. Neurol.* 248, 170–182. doi: 10.1016/j.expneurol.2013.06.013

Esteban, P. F., Yoon, H. Y., Becker, J., Dorsey, S. G., Caprari, P., Palko, M. E., et al. (2006). A kinase-deficient TrkC receptor isoform activates Arf6-Rac1 signaling through the scaffold protein tamalin. *J. Cell Biol.* 173, 291–299. doi: 10.1083/jcb.200512013

Ferrer, I., Marin, C., Rey, M. J., Ribalta, T., Goutan, E., Blanco, R., et al. (1999). BDNF and full-length and truncated TrkB expression in Alzheimer disease. Implications in therapeutic strategies. *J. Neuropathol. Exp. Neurol.* 58, 729–739. doi: 10.1097/00005072-199907000-00007

Galan, A., Barcelona, P. F., Nedev, H., Sarunic, M. V., Jian, Y., Saragovi, H. U., et al. (2017a). Subconjunctival delivery of p75NTR antagonists reduces the inflammatory, vascular, and neurodegenerative pathologies of diabetic retinopathy. *Invest. Ophthalmol. Vis. Sci.* 58, 2852–2862. doi: 10.1167/iovs.16-20988

Galán, A., Jmaeff, S., Barcelona, P. F., Brahimi, F., Sarunic, M. V., and Saragovi, H. U. (2017b). In retinitis pigmentosa TrkC.T1-dependent vectorial Erk activity upregulates glial TNF-alpha, causing selective neuronal death. *Cell Death Dis.* 8, 3222. doi: 10.1038/s41419-017-0074-8

Gould, T. W, and Oppenheim, R. W. (2011). Motor neuron trophic factors: therapeutic use in ALS? *Brain Res. Rev.* 67, 1–39. doi: 10.1016/j.brainresrev.2010.10.003

Guillemard, V., Ivanisevic, L., Garcia, A. G., Scholten, V., Lazo, O. M., Bronfman, F. C., et al. (2010). An agonistic mAb directed to the TrkC receptor juxtamembrane region defines a trophic hot spot and interactions with p75 coreceptors. *Dev. Neurobiol.* 70, 150–164. doi: 10.1002/dneu.20776

Hauck, S. M., Kinkl, N., Deeg, C. A., Swiatek-de Lange, M., Schoffmann, S., and Ueffing, M. (2006). GDNF family ligands trigger indirect neuroprotective signaling in retinal glial cells. *Mol. Cell. Biol.* 26, 2746–2757. doi: 10.1128/mcb.26.7.2746-2757.2006

Hedstrom, K. L., Murtie, J. C., Albers, K., Calcutt, N. A., and Corfas, G. (2014). Treating small fiber neuropathy by topical application of a small molecule modulator of ligand-induced GFRalpha/RET receptor signaling. *Proc. Natl. Acad. Sci. U.S.A.* 111, 2325–2330. doi: 10.1073/pnas.1308889111

Hempstead, B. L. (2002). The many faces of p75NTR. *Curr. Opin. Neurobiol.* 12, 260–267. doi: 10.1016/s0959-4388(02)00321-5

Hempstead, B. L. (2006). Dissecting the diverse actions of pro- and mature neurotrophins. *Curr. Alzheimer Res.* 3, 19–24. doi: 10.2174/156720506775697061

Hempstead, B. L, and Chao, M. V. (1997). Entering the domain of neurotrophin binding. *Nat. Biotechnol.* 15, 623–624. doi: 10.1038/nbt0797-623

Huang, E. J, and Reichardt, L. F. (2003). Trk receptors: roles in neuronal signal transduction. *Annu. Rev. Biochem.* 72, 609–642. doi: 10.1146/annurev.biochem.72.121801.161629

Ibanez, C. F. (2013). Structure and physiology of the RET receptor tyrosine kinase. *Cold Spring Harb. Perspect. Biol.* 5:a009134. doi: 10.1101/cshperspect.a009134

Ibanez, C. F, and Simi, A. (2012). p75 neurotrophin receptor signaling in nervous system injury and degeneration: paradox and opportunity. *Trends Neurosci.* 35, 431–440. doi: 10.1016/j.tins.2012.03.007

Ivanisevic, L., Banerjee, K., and Saragovi, H. U. (2003). Differential cross-regulation of TrkA and TrkC tyrosine kinase receptors with p75. *Oncogene* 22, 5677–5685. doi: 10.1038/sj.onc.1206864

Ivanisevic, L., Zheng, W., Woo, S. B., Neet, K. E., Saragovi, H. U. (2007). TrkA receptor hot spots for binding of NT-3 as a heterologous ligand. *J. Biol. Chem.* 282, 16754–16763. doi: 10.1074/jbc.m701996200

Ivanova, L., Tammiku-Taul, J., Garcia-Sosa, A. T., Sidorova, Y., Saarma, M., and Karelson, M. (2018). Molecular Dynamics Simulations of the Interactions between Glial Cell Line-Derived Neurotrophic Factor Family Receptor GFRalpha1 and Small-Molecule Ligands. *ACS Omega* 3, 11407–11414. doi: 10.1021/acsomega.8b01524

Jang, S. W., Liu, X., Yepes, M., Shepherd, K. R., Miller, G. W., Liu, Y., et al. (2010). A selective TrkB agonist with potent neurotrophic activities by 7,8-dihydroxyflavone. *Proc. Natl. Acad. Sci. U.S.A.* 107, 2687–2692. doi: 10.1073/pnas.0913572107

Jansen, P., Giehl, K., Nyengaard, J. R., Teng, K., Lioubinski, O., Sjoegaard, S. S., et al. (2007). Roles for the pro-neurotrophin receptor sortilin in neuronal development, aging and brain injury. *Nat. Neurosci.* 10, 1449–1457. doi: 10.1038/nn2000

Jiang, M., Peng, Q., Liu, X., Jin, J., Hou, Z., Zhang, J., et al. (2013). Small-molecule TrkB receptor agonists improve motor function and extend survival in a mouse model of Huntington's disease. *Hum. Mol. Genet.* 22, 2462–2470. doi: 10.1093/hmg/ddt098

Josephy-Hernandez, S., Jmaeff, S., Pirvulescu, I., Aboulkassim, T., and Saragovi, H. U. (2017). Neurotrophin receptor agonists and antagonists as therapeutic agents: an evolving paradigm. *Neurobiol. Dis.* 97(Pt. B), 139–155. doi: 10.1016/j.nbd.2016.08.004

Kaspar, B. K., Llado, J., Sherkat, N., Rothstein, J. D., and Gage, F. H. (2003). Retrograde viral delivery of IGF-1 prolongs survival in a mouse ALS model. *Science* 301, 839–842. doi: 10.1126/science.1086137

Lebrun-Julien, F., Bertrand, M. J., De Backer, O., Stellwagen, D., Morales, C. R., Di Polo, A, and Barker, P. A. (2010). ProNGF induces TNFalpha-dependent death of retinal ganglion cells through a p75NTR non-cell-autonomous signaling pathway. *Proc. Natl. Acad. Sci. U.S.A.* 107, 3817–3822. doi: 10.1073/pnas.0909276107

Lebrun-Julien, F., Duplan, L., Pernet, V., Osswald, I., Sapieha, P., Bourgeois, P., et al. (2009a). Excitotoxic death of retinal neurons in vivo occurs via a non-cell-autonomous mechanism. *J. Neurosci.* 29, 5536–5545. doi: 10.1523/JNEUROSCI.0831-09.2009

Lebrun-Julien, F., Morquette, B., Douillette, A., Saragovi, H. U., and Di Polo, A. (2009b). Inhibition of p75(NTR) in glia potentiates TrkA-mediated survival of injured retinal ganglion cells. *Mol. Cell. Neurosci.* 40, 410–420. doi: 10.1016/j.mcn.2008.12.005

LeSauteur, L., Cheung, N. K., Lisbona, R., and Saragovi, H. U. (1996a). Small molecule nerve growth factor analogs image receptors *in vivo*. *Nat. Biotechnol.* 14, 1120–1122.

LeSauteur, L., Maliartchouk, S., Le Jeune, H., Quirion, R., and Saragovi, H. U. (1996b). Potent human p140-TrkA agonists derived from an anti-receptor monoclonal antibody. *J. Neurosci.* 16, 1308–1316. doi: 10.1523/jneurosci.16-04-01308.1996

LeSauteur, L., Wei, L., Gibbs, B. F., and Saragovi, H. U. (1995). Small peptide mimics of nerve growth factor bind TrkA receptors and affect biological responses. *J. Biol. Chem.* 270, 6564–6569. doi: 10.1074/jbc.270.12.6564

Lim, Y. S., McLaughlin, T., Sung, T. C., Santiago, A., Lee, K. F., and O'Leary, D. D. (2008). p75(NTR) mediates ephrin-A reverse signaling required for axon repulsion and mapping. *Neuron* 59, 746–758. doi: 10.1016/j.neuron.2008.07.032

Liu, J., Brahimi, F., Saragovi, H. U., and Burgess, K. (2010). Bivalent diketopiperazine-based tropomysin receptor kinase C (TrkC) antagonists. *J. Med. Chem.* 53, 5044–5048. doi: 10.1021/jm100148d

Longo, F. M, and Massa, S. M. (2004). Neurotrophin-based strategies for neuroprotection. *J. Alzheimers Dis.* 6:S13–S17.

Ma, J., Guo, C., Guo, C., Sun, Y., Liao, T., Beattie, U., et al. (2015). Transplantation of human neural progenitor cells expressing IGF-1 enhances retinal ganglion cell survival. *PLoS One* 10:e0125695. doi: 10.1371/journal.pone.0125695

Maliartchouk, S., Debeir, T., Beglova, N., Cuello, A. C., Gehring, K., and Saragovi, H. U. (2000a). Genuine monovalent ligands of TrkA nerve growth factor receptors reveal a novel pharmacological mechanism of action. *J. Biol. Chem.* 275, 9946–9956. doi: 10.1074/jbc.275.14.9946

Maliartchouk, S., Feng, Y., Ivanisevic, L., Debeir, T., Cuello, A. C., Burgess, K., et al. (2000b). A designed peptidomimetic agonistic ligand of TrkA nerve growth factor receptors. *Mol. Pharmacol.* 57, 385–391.

Massa, S. M., Xie, Y., and Longo, F. M. (2002). Alzheimer's therapeutics: neurotrophin small molecule mimetics. *J. Mol. Neurosci.* 19, 107–111. doi: 10.1007/s12031-002-0019-1

Mellado Lagarde, M. M., Wan, G., Zhang, L., Gigliello, A. R., McInnis, J. J., Zhang, Y., et al. (2014). Spontaneous regeneration of cochlear supporting cells after neonatal ablation ensures hearing in the adult mouse. *Proc. Natl. Acad. Sci. U.S.A.* 111, 16919–16924. doi: 10.1073/pnas.1408064111

Miller, F. D, and Kaplan, D. R. (2001). Neurotrophin signalling pathways regulating neuronal apoptosis. *Cell. Mol. Life Sci.* 58, 1045–1053. doi: 10.1007/pl00000919

Mufson, E. J., Ma, S. Y., Cochran, E. J., Bennett, D. A., Beckett, L. A., Jaffar, S., et al. (2000). Loss of nucleus basalis neurons containing trkA immunoreactivity in individuals with mild cognitive impairment and early Alzheimer's disease. *J. Comp. Neurol.* 427, 19–30. doi: 10.1002/1096-9861(20001106)427:1<19::aid-cne2>3.0.co;2-a

Mysona, B. A., Al-Gayyar, M. M., Matragoon, S., Abdelsaid, M. A., El-Azab, M. F., Saragovi, H. U., et al. (2013). Modulation of p75(NTR) prevents diabetes- and proNGF-induced retinal inflammation and blood-retina barrier breakdown in mice and rats. *Diabetologia* 56, 2329–2339. doi: 10.1007/s00125-013-2998-6

Nafissi, N., and Foldvari, M. (2016). Neurotrophin signalling pathways regulating neuronal apoptosis. *Wiley Interdiscip. Rev. Nanomed. Nanobiotechnol.* 8, 240–254.

Nakazawa, T., Nakazawa, C., Matsubara, A., Noda, K., Hisatomi, T., She, H., et al. (2006). Tumor necrosis factor-alpha mediates oligodendrocyte death and delayed retinal ganglion cell loss in a mouse model of glaucoma. *J. Neurosci.* 26, 12633–12641. doi: 10.1523/jneurosci.2801-06.2006

Nguyen, T. V., Shen, L., Vander Griend, L., Quach, L. N., Belichenko, N. P., Saw, N., et al. (2014). Small molecule p75^{NTR} ligands reduce pathological phosphorylation and misfolding of tau, inflammatory changes, cholinergic degeneration, and cognitive deficits in AbetaPP$^{L/S}$ transgenic mice. *J. Alzheimers Dis.* 42, 459–483. doi: 10.3233/JAD-140036

Nie, S., Xu, Y., Chen, G., Ma, K., Han, C., Guo, Z., et al. (2015). Small molecule TrkB agonist deoxygedunin protects nigrostriatal dopaminergic neurons from 6-OHDA and MPTP induced neurotoxicity in rodents. *Neuropharmacology* 99, 448–458. doi: 10.1016/j.neuropharm.2015.08.016

Nykjaer, A., Willnow, T. E., and Petersen, C. M. (2005). p75NTR–live or let die. *Curr. Opin. Neurobiol.* 15, 49–57. doi: 10.1016/j.conb.2005.01.004

Ohira, K., Funatsu, N., Homma, K. J., Sahara, Y., Hayashi, M., Kaneko, T., et al. (2007). Truncated TrkB-T1 regulates the morphology of neocortical layer I astrocytes in adult rat brain slices. *Eur. J. Neurosci.* 25, 406–416. doi: 10.1111/j.1460-9568.2007.05282.x

Ohira, K., Homma, K. J., Hirai, H., Nakamura, S., and Hayashi, M. (2006). TrkB-T1 regulates the RhoA signaling and actin cytoskeleton in glioma cells. *Biochem. Biophys. Res. Commun.* 342, 867–874. doi: 10.1016/j.bbrc.2006.02.033

Palko, M. E., Coppola, V., and Tessarollo, L. (1999). Evidence for a role of truncated trkC receptor isoforms in mouse development. *Neurosci. J.* 19, 775–782. doi: 10.1523/jneurosci.19-02-00775.1999

Park, S., Kim, H. T., Yun, S., Kim, I. S., Lee, J., Lee, I. S., et al. (2009). Growth factor-expressing human neural progenitor cell grafts protect motor neurons but do not ameliorate motor performance and survival in ALS mice. *Exp. Mol. Med.* 41, 487–500. doi: 10.3858/emm.2009.41.7.054

Pasquin, S., Sharma, M., and Gauchat, J. F. (2015). Ciliary neurotrophic factor (CNTF): new facets of an old molecule for treating neurodegenerative and metabolic syndrome pathologies. *Cytokine Growth Factor Rev.* 26, 507–515. doi: 10.1016/j.cytogfr.2015.07.007

Pattarawarapan, M., Zaccaro, M. C., Saragovi, U. H., and Burgess, K. (2002). New templates for syntheses of ring-fused, C(10) beta-turn peptidomimetics leading to the first reported small-molecule mimic of neurotrophin-3. *J. Med. Chem.* 45, 4387–4390. doi: 10.1021/jm0255421

Pehar, M., Cassina, P., Vargas, M. R., Xie, Y., Beckman, J. S., Massa, S. M., et al. (2006). Modulation of p75-dependent motor neuron death by a small non-peptidyl mimetic of the neurotrophin loop 1 domain. *Eur. J. Neurosci.* 24, 1575–1580. doi: 10.1111/j.1460-9568.2006.05040.x

Peleshok, J., and Saragovi, H. U. (2006). Functional mimetics of neurotrophins and their receptors. *Biochem. Soc. Trans.* 34(Pt. 4), 612–617. doi: 10.1042/bst0340612

Platon-Corchado, M., Barcelona, P. F., Jmaeff, S., Marchena, M., Hernandez-Pinto, A. M., Hernandez- Sanchez, C., et al. (2017). p75NTR antagonists attenuate photoreceptor cell loss in murine models of retinitis pigmentosa. *Cell Death Dis.* 8:e2922. doi: 10.1038/cddis.2017.306

Quarta, E., Fulgenzi, G., Bravi, R., Cohen, E. J., Yanpallewar, S., Tessarollo, L., et al. (2018). Deletion of the endogenous TrkB.T1 receptor isoform restores the number of hippocampal CA1 parvalbumin-positive neurons and rescues long-term potentiation in pre-symptomatic mSOD1(G93A) ALS mice. *Mol. Cell. Neurosci.* 89, 33–41. doi: 10.1016/j.mcn.2018.03.010

Rafii, M. S., Tuszynski, M. H., Thomas, R. G., Barba, D., Brewer, J. B., Rissman, R. A., et al. (2018). Adeno-associated viral vector (Serotype 2)-nerve growth factor for patients with Alzheimer disease: a randomized clinical trial. *JAMA Neurol.* 75, 834–841. doi: 10.1001/jamaneurol.2018.0233

Rangasamy, S. B., Soderstrom, K., Bakay, R. A., and Kordower, J. H. (2010). Neurotrophic factor therapy for Parkinson's disease. *Prog. Brain Res.* 184, 237–264. doi: 10.1016/S0079-6123(10)84013-0

Roh, M., Zhang, Y., Murakami, Y., Thanos, A., Lee, S. C., Vavvas, D. G., et al. (2012). Etanercept, a widely used inhibitor of tumor necrosis factor-alpha (TNF-alpha), prevents retinal ganglion cell loss in a rat model of glaucoma. *PLoS One* 7:e40065. doi: 10.1371/journal.pone.0040065

Rudzinski, M., Wong, T. P., and Saragovi, H. U. (2004). Changes in retinal expression of neurotrophins and neurotrophin receptors induced by ocular hypertension. *J. Neurobiol.* 58, 341–354. doi: 10.1002/neu.10293

Sakowski, S. A., Schuyler, A. D., and Feldman, E. L. (2009). Insulin-like growth factor-I for the treatment of amyotrophic lateral sclerosis. *Amyotroph. Lateral Scler.* 10, 63–73. doi: 10.1080/17482960802160370

Sanchez, M. C., Luna, J. D., Barcelona, P. F., Gramajo, A. L., Juarez, P. C., Riera, C. M., et al. (2007). Effect of retinal laser photocoagulation on the activity of metalloproteinases and the alpha(2)-macroglobulin proteolytic state in the vitreous of eyes with proliferative diabetic retinopathy. *Exp. Eye Res.* 85, 644–650. doi: 10.1016/j.exer.2007.07.018

Saragovi, H. U. (2005). Progression of age-associated cognitive impairment correlates with quantitative and qualitative loss of TrkA receptor protein in nucleus basalis and cortex. *J. Neurochem.* 95, 1472–1480. doi: 10.1111/j.1471-4159.2005.03479.x

Saragovi, H. U., Hamel, E., and Di Polo A. (2009). A neurotrophic rationale for the therapy of neurodegenerative disorders. *Curr. Alzheimer Res.* 6, 419–423. doi: 10.2174/156720509789207912

Saragovi, H. U., Zheng, W., Maliartchouk, S., DiGugliemo, G. M., Mawal, Y. R., Kamen, A., et al. (1998). A TrkA-selective, fast internalizing nerve growth factor-antibody complex induces trophic but not neuritogenic signals. *Biol. J. Chem.* 273, 34933–34940. doi: 10.1074/jbc.273.52.34933

Saragovi, H. U, and Zaccaro, M. C. (2002). Small molecule peptidomimetic ligands of neurotrophin receptors, identifying binding sites, activation sites and regulatory sites. *Curr. Pharm. Des.* 8, 2201–2216. doi: 10.2174/1381612023393215

Saragovi, H. U., and Gehring, K. (2000). Development of pharmacological agents for targeting neurotrophins and their receptors. *Trends Pharmacol. Sci.*refvol 21, 93–98. doi: 10.1016/s0165-6147(99)01444-3

Schindowski, K., Belarbi, K., and Buee, L. (2008). Neurotrophic factors in Alzheimer's disease: role of axonal transport. *Genes Brain Behav.* 7, 43–56. doi: 10.1111/j.1601-183X.2007.00378.x

Sendera, T. J., Ma, S. Y., Jaffar, S., Kozlowski, P. B., Kordower, J. H., Mawal, Y., et al. (2000). Reduction in TrkA-immunoreactive neurons is not associated with an overexpression of galaninergic fibers within the nucleus basalis in Down's syndrome. *Neurochem. J.* 74, 1185–1196. doi: 10.1046/j.1471-4159.2000.741185.x

Sendtner, M., Holtmann, B., and Hughes, R. A. (1996). The response of motoneurons to neurotrophins. *Neurochem. Res.* 21, 831–841. doi: 10.1007/bf02532307

Shanab, A. Y., Mysona, B. A., Matragoon, S., and El-Remessy, A. B. (2015). Silencing p75(NTR) prevents proNGF-induced endothelial cell death and development of acellular capillaries in rat retina. *Mol. Ther. Methods Clin. Dev.* 2:15013. doi: 10.1038/mtm.2015.13

Shepheard, S. R., Chataway, T., Schultz, D. W., Rush, R. A., and Rogers, M. L. (2014). The extracellular domain of neurotrophin receptor p75 as a candidate biomarker for amyotrophic lateral sclerosis. *PLoS One* 9:e87398. doi: 10.1371/journal.pone.0087398

Shi, Z., Birman, E., and Saragovi, H. U. (2007). Neurotrophic rationale in glaucoma: a TrkA agonist, but not NGF or a p75 antagonist, protects retinal ganglion cells in vivo. *Dev. Neurobiol.* 67, 884–894. doi: 10.1002/dneu.20360

Shi, Z., Rudzinski, M., Meerovitch, K., Lebrun-Julien, F., Birman, E., Di, A., et al. (2008). Alpha2-macroglobulin is a mediator of retinal ganglion cell death in glaucoma. *J. Biol. Chem.* 283, 29156–29165. doi: 10.1074/jbc.M802365200

Siao, C. J., Lorentz, C. U., Kermani, P., Marinic, T., Carter, J., McGrath, K., et al. (2013). ProNGF, a cytokine induced after myocardial infarction in humans, targets pericytes to promote microvascular damage and activation. *J. Exp. Med.* 209, 2291–2305. doi: 10.1084/jem.20111749

Sidorova, Y. A., Bespalov, M. M., Wong, A. W., Kambur, O., Jokinen, V., Lilius, T. O., et al. (2017). A novel small molecule GDNF receptor RET agonist, BT13, promotes neurite growth from sensory neurons *in vitro* and attenuates experimental neuropathy in the rat. *Front. Pharmacol.* 8:365. doi: 10.3389/fphar.2017.00365

Simmons, D. A., Belichenko, N. P., Yang, T., Condon, C., Monbureau, M., Shamloo, M., et al. (2013). A small molecule TrkB ligand reduces motor impairment and neuropathology in R6/2 and BACHD mouse models of Huntington's disease. *J. Neurosci.* 33, 18712–18727. doi: 10.1523/JNEUROSCI.1310-13.2013

Skeldal, S., Sykes, A. M., Glerup, S., Matusica, D., Palstra, N., Autio, H., et al. (2012). Mapping of the interaction site between sortilin and the p75 neurotrophin receptor reveals a regulatory role for the sortilin intracellular domain in p75 neurotrophin receptor shedding and apoptosis. *J. Biol. Chem.* 287, 43798–43809. doi: 10.1074/jbc.M112.374710

Srinivasan, B., Roque, C. H., Hempstead, B. L., Al-Ubaidi, M. R., and Roque, R. S. (2004). Microglia-derived pronerve growth factor promotes photoreceptor cell death via p75 neurotrophin receptor. *J. Biol. Chem.*refvol 279, 41839–41845. doi: 10.1074/jbc.m402872200

Suzuki, J., Corfas, G., and Liberman, M. C. (2016). Round-window delivery of neurotrophin 3 regenerates cochlear synapses after acoustic overexposure. *Sci. Rep.* 6:24907. doi: 10.1038/srep24907

Tauszig-Delamasure, S., Yu, L. Y., Cabrera, J. R., Bouzas-Rodriguez, J., Mermet-Bouvier, C., Guix, C., et al. (2007). The TrkC receptor induces apoptosis when the dependence receptor notion meets the neurotrophin paradigm. *Proc. Natl. Acad. Sci. U.S.A.* 104, 13361–13366. doi: 10.1073/pnas.0701243104

Teng, H. K., Teng, K. K., Lee, R., Wright, S., Tevar, S., Almeida, R. D., et al. (2005). ProBDNF induces neuronal apoptosis via activation of a receptor complex of p75NTR and sortilin. *J. Neurosci.* 25, 5455–5463. doi: 10.1523/jneurosci.5123-04.2005

Teng K. K., and Hempstead, B. L. (2004). Neurotrophins and their receptors: signaling trios in complex biological systems. *Cel Mol. Life Sci.* 61, 35–48. doi: 10.1007/s00018-003-3099-3

Tessarollo, L. (1998). Pleiotropic functions of neurotrophins in development. *Cytokine Growth Factor Rev.* 9, 125–137. doi: 10.1016/s1359-6101(98)00003-3

Thanos C. and Emerich, D. (2005). Delivery of neurotrophic factors and therapeutic proteins for retinal diseases. *Expert Opin. Biol. Ther.*refvol 5, 1443–1452. doi: 10.1517/14712598.5.11.1443

Thoenen H. and Sendtner, M. (2002). Neurotrophins: from enthusiastic expectations through sobering experiences to rational therapeutic approaches. *Nat. Neurosci.*refvol 5 1046–1050. doi: 10.1038/nn938

Tokugawa, K., Yamamoto, K., Nishiguchi, M., Sekine, T., Sakai, M., Ueki, T., et al. (2003). XIB4035, a novel nonpeptidyl small molecule agonist for GFRalpha-1. *Neurochem. Int.* 42, 81–86. doi: 10.1016/s0197-0186(02)00053-0

Tomellini, E., Lagadec, C., Polakowska, R., and Le Bourhis, X. (2014). Role of p75 neurotrophin receptor in stem cell biology: more than just a marker. *Cell. Mol. Life Sci.* 71, 2467–2481. doi: 10.1007/s00018-014-1564-9

Vaegter, C. B., Jansen, P., Fjorback, A. W., Glerup, S., Skeldal, S., Kjolby, M., et al. (2011). Sortilin associates with Trk receptors to enhance anterograde transport and neurotrophin signaling. *Nat. Neurosci.* 14, 54–61. doi: 10.1038/nn.2689

Valenzuela, D. M., Maisonpierre, P. C., Glass, D. J., Rojas, E., Nunez, L., Kong, Y., et al. (1993). Alternative forms of rat TrkC with different functional capabilities. *Neuron* 10, 963–974. doi: 10.1016/0896-6273(93)90211-9

Wan, G., and Corfas, G. (2015). No longer falling on deaf ears: mechanisms of degeneration and regeneration of cochlear ribbon synapses. *Hear. Res.* 329, 1–10. doi: 10.1016/j.heares.2015.04.008

Wan, G., Gomez-Casati, M. E., Gigliello, A. R., Liberman, M. C., and Corfas, G. (2014). Neurotrophin-3 regulates ribbon synapse density in the cochlea and induces synapse regeneration after acoustic trauma. *eLife* 3:e03564.

Weissmiller, A. M, and Wu, C. (2012). Current advances in using neurotrophic factors to treat neurodegenerative disorders. *Transl. Neurodegener.* 1:14. doi: 10.1186/2047-9158-1-14

Wyatt, T. J., Rossi, S. L., Siegenthaler, M. M., Frame, J., Robles, R., Nistor, G., et al. (2011). Human motor neuron progenitor transplantation leads to endogenous neuronal sparing in 3 models of motor neuron loss. *Stem Cells Int.* 2011:207230. doi: 10.4061/2011/207230

Xu, F., Wei, Y., Lu, Q., Zheng, D., Zhang, F., Gao, E., et al. (2009). Immunohistochemical localization of sortilin and p75(NTR) in normal and ischemic rat retina. *Neurosci. Lett.* 454, 81–85. doi: 10.1016/j.neulet.2009.02.036

Yanpallewar, S. U., Barrick, C. A., Buckley, H., Becker, J., and Tessarollo, L. (2012). Deletion of the BDNF truncated receptor TrkB.T1 delays disease onset in a mouse model of amyotrophic lateral sclerosis. *PLoS One* 7:e39946. doi: 10.1371/journal.pone.0039946

Yuen, E. C, and Mobley, W. C. (1996). Therapeutic potential of neurotrophic factors for neurological disorders. *Ann. Neurol.* 40, 346–354. doi: 10.1002/ana.410400304

Zaccaro, M. C., Ivanisevic, L., Perez, P., Meakin, S. O., and Saragovi, H. U. (2001). p75 Co-receptors regulate ligand-dependent and ligand-independent Trk receptor activation, in part by altering Trk docking subdomains. *J. Biol. Chem.* 276, 31023–31029. doi: 10.1074/jbc.m104630200

Zaccaro, M. C., Lee, H. B., Pattarawarapan, M., Xia, Z., Caron, A., L'Heureux, P. J., et al. (2005). Selective small molecule peptidomimetic ligands of TrkC and TrkA receptors afford discrete or complete neurotrophic activities. *Chem. Biol.* 12, 1015–1028. doi: 10.1016/j.chembiol.2005.06.015

Conflict of Interest Statement: The authors declare that the research was conducted in the absence of any commercial or financial relationships that could be construed as a potential conflict of interest.

frontiers in Cellular Neuroscience

REVIEW
published: 11 June 2019
doi: 10.3389/fncel.2019.00246

Sphingolipids as Emerging Mediators in Retina Degeneration

*M. Victoria Simón, Facundo H. Prado Spalm, Marcela S. Vera and Nora P. Rotstein**

Instituto de Investigaciones Bioquímicas de Bahía Blanca (INIBIBB), Departamento De Biología, Bioquímica y Farmacia, Universidad Nacional del Sur (UNS), Argentine National Research Council (CONICET), Bahía Blanca, Argentina

The sphingolipids ceramide (Cer), sphingosine-1-phosphate (S1P), sphingosine (Sph), and ceramide-1-phosphate (C1P) are key signaling molecules that regulate major cellular functions. Their roles in the retina have gained increasing attention during the last decade since they emerge as mediators of proliferation, survival, migration, neovascularization, inflammation and death in retina cells. As exacerbation of these processes is central to retina degenerative diseases, they appear as crucial players in their progression. This review analyzes the functions of these sphingolipids in retina cell types and their possible pathological roles. Cer appears as a key arbitrator in diverse retinal pathologies; it promotes inflammation in endothelial and retina pigment epithelium (RPE) cells and its increase is a common feature in photoreceptor death *in vitro* and in animal models of retina degeneration; noteworthy, inhibiting Cer synthesis preserves photoreceptor viability and functionality. In turn, S1P acts as a double edge sword in the retina. It is essential for retina development, promoting the survival of photoreceptors and ganglion cells and regulating proliferation and differentiation of photoreceptor progenitors. However, S1P has also deleterious effects, stimulating migration of Müller glial cells, angiogenesis and fibrosis, contributing to the inflammatory scenario of proliferative retinopathies and age related macular degeneration (AMD). C1P, as S1P, promotes photoreceptor survival and differentiation. Collectively, the expanding role for these sphingolipids in the regulation of critical processes in retina cell types and in their dysregulation in retina degenerations makes them attractive targets for treating these diseases.

Keywords: ceramide, sphingosine-1-phosphate, sphingosine, ceramide-1-phosphate, photoreceptor, glia, pigmented epithelium

OPEN ACCESS

Edited by:
Mario Eduardo Guido, Center for Research in Biological Chemistry Córdoba (CIQUIBIC), Argentina

Reviewed by:
Antonio Gomez-Muñoz, University of the Basque Country, Spain
Elisabetta Catalani, Università degli Studi della Tuscia, Italy

****Correspondence:***
Nora P. Rotstein
inrotste@criba.edu.ar

Specialty section:
This article was submitted to Cellular Neuropathology, a section of the journal Frontiers in Cellular Neuroscience

Received: *25 February 2019*
Accepted: *17 May 2019*
Published: *11 June 2019*

Citation:
Simón MV, Prado Spalm FH, Vera MS and Rotstein NP (2019) Sphingolipids as Emerging Mediators in Retina Degeneration. Front. Cell. Neurosci. 13:246. doi: 10.3389/fncel.2019.00246

Abbreviations: AMD, age related macular degeneration; C1P, ceramide-1-phosphate; Cer, ceramide; CerK, ceramide kinase; CerKL, Cer kinase-like; CerS, Cer synthase; CERT, Cer transport protein; DAMP, damage associated molecular pattern; DHA, docosahexaenoic acid; DHCer, dihydroceramide; ER, endoplasmic reticulum; GDNF, glial derived neurotrophic factor; GlucoCer, glucosylceramide; OS, outer segments; PARP1, poly ADP-ribose-polymerase 1; PUFA, polyunsaturated fatty acids; ROS, reactive oxygen species; RPE, retinal pigment epithelium; S1P, sphingosine-1-phosphate; S1PR, S1P receptor; SM, sphingomyelin; SMase, sphingomyelinase; Sph, sphingosine; SphK, sphingosine kinase; SPP, S1P phosphatases; SPT, serine palmitoyltransferase; TNF, tumor necrosis factor; VLCPUFA, very long chain polyunsaturated fatty acids.

INTRODUCTION

Sphingolipids entered the group of Bioactive Lipids about three decades ago; however, they are still regarded by many as newcomers, less familiar than the phosphatidylinositol phosphates, prostaglandins or leukotrienes. Yet, the overwhelming amount of literature accumulated evidences that simple sphingolipids such as Cer, Sph, and their phosphorylated derivatives, S1P and C1P (**Figure 1**) have taken centre stage in controlling normal and pathological cellular processes throughout the organism.

First identified in the brain by Thudichum in the late 19th century, for virtually another century their functions remained as enigmatic as the Sphinx their name honors. Being lipid molecules, they were considered as ubiquitous membrane components both in animal and plant cells for several decades. Even just as such, they have multiple and relevant roles. They are crucial constituents of lipid rafts and regulate their formation and expansion, essential for building signaling platforms (Grassme et al., 2001); they are also critical for receptor function, membrane conductance and cell–cell interactions, and play key roles in pathogen internalization (Huwiler et al., 2000; Gulbins and Kolesnick, 2003; Hannun and Luberto, 2004). The pioneer work from both Hannun and Kolesnick laboratories three decades ago added an additional dimension to their biological relevance; the groundbreaking findings that Sph inhibits protein kinase C and Cer is a "potential second messenger" in the signaling cascade activated by TNF-α provided the first data as to their role as bioactive lipids (Hannun et al., 1986; Kolesnick, 1987; Dressler et al., 1992; Obeid et al., 1993). Sph and Cer were then established to inhibit cell growth and promote cell death upon different cell stressors. The family of bioactive sphingolipids gained in complexity when their phosphorylated counterparts, S1P and C1P were shown to control the opposing processes, proliferation and cell survival. The sphingolipid family also includes GlucoCer, lactosylceramide, several gangliosides and DHCer.

These bioactive lipids respond to a diversity of cell stimuli by modifying their intracellular levels, thus regulating multiple signaling pathways that finally induce major changes in cell fate. Their roles have strikingly extended to include virtually every aspect of cell biology, from cell cycle, differentiation, endosome and exosome formation, adhesion and migration to angiogenesis, immune response, inflammation and cell death, including autophagy and apoptosis. Recent advances have revealed that sphingolipid mediators play important roles in human disease.

This Review focuses on the functions played by simple sphingolipids in the retina during development and particularly in the onset of retina pathologies. Lipids have long been known to be essential for maintaining both the structure and functionality of the visual system. Docosahexaenoic acid (DHA) has been shown to promote photoreceptor survival and differentiation, and docosanoids, such as Neuroprotectin D1, and elovanoids have relevant neuroprotective roles in the retina (Rotstein et al., 1996, 1997; Jun et al., 2017; Bazan, 2018). Conversely, mutations of lipid metabolizing proteins and chronic misregulation of retinal lipid metabolism have been linked to retinal degeneration (Fliesler and Bretillon, 2010; Friedman et al., 2010; Yu et al., 2011). During the last decade, understanding on the relevance of lipids in the retina has expanded to reveal the involvement of sphingolipids in numerous ocular diseases. Here, we briefly present the structural characteristics and metabolism of sphingolipids and a concise description of the physiological and pathophysiological roles of simple sphingolipids as Cer, Sph, S1P, C1P, and DHCer. We then focus on the information that points to both their deleterious and protective functions in the retina and in retina pathologies, supporting the emerging roles of sphingolipids as novel mediators in retina degenerative diseases.

Structure and Metabolism of Sphingolipids

The sphingolipid family encompasses a huge diversity of molecular species that place them among the major lipid classes in eukaryotic cells. Sph, a straight, long chain (18–20 carbon atoms) aminoalcohol, is the common backbone shared by all these species (**Figure 1**). Attachment of a fatty acid to Sph through an amide bond gives rise to Cer, the central molecule in sphingolipid metabolism (Fahy et al., 2005). Further attachment of hundreds of diverse headgroups at the C-1 position of Cer originates the more complex sphingolipids (**Figure 1**). Taking into account than in addition to these huge number of headgroups, sphingolipids are formed by at least sixty different long-chain bases and dozens of fatty acids varying from twelve to over thirty carbons in length, the number of sphingolipid molecular species is likely in the tens of thousands (Merrill et al., 1993). If we add this up to their complex metabolism, and their ability to interconvert upon different and even opposing cell stimuli, we can start to grasp their extraordinary flexibility for modulating an ample range of cell responses.

A key to the multiplicity and diversity of the signaling roles of sphingolipids is in their intricate and highly interconnected metabolism, their constant cross-conversions that modify their levels upon changes in the environment (**Figure 2**). Cer is the central hub among these metabolic pathways and can be synthesized by different pathways, *de novo* synthesis, degradation of sphingomyelin (*sphingomyelinase pathway*) and recycling of Sph and complex sphingolipids (*salvage pathway*). *De novo* synthesis begins in the ER (Mandon et al., 1992) with the condensation of L-serine and palmitoyl CoA, catalyzed by SPT; the resulting 3-ketosphinganine is reduced to sphinganine, which is amino-acylated with a chain of 14 to 32 carbons to form diverse DHCer species; finally, the insertion of a *trans* double bond at the C4 position of the sphingoid base backbone by DHCer desaturase gives rise to Cer. SPT, a heteromeric complex, is responsible for opening the entrance to the sphingolipid network. Interestingly, recent evidence has uncovered that subunit mutations causing hereditary sensory and autonomic neuropathy type 1 (HSAN1) shift SPT preference to use alanine and glycine instead of serine (Penno et al., 2010; Bode et al., 2016). This gives rise to a class of atypical 1-deoxysphingolipids, such as deoxy(dihydro)ceramides and 1-deoxysphingosine, shown to induce cell death in various cell types. When elevated, as in HSAN1, they are neurotoxic and contribute to sensory and autonomic neuropathies affecting both cytoskeletal stability, NMDA receptor signaling and membrane

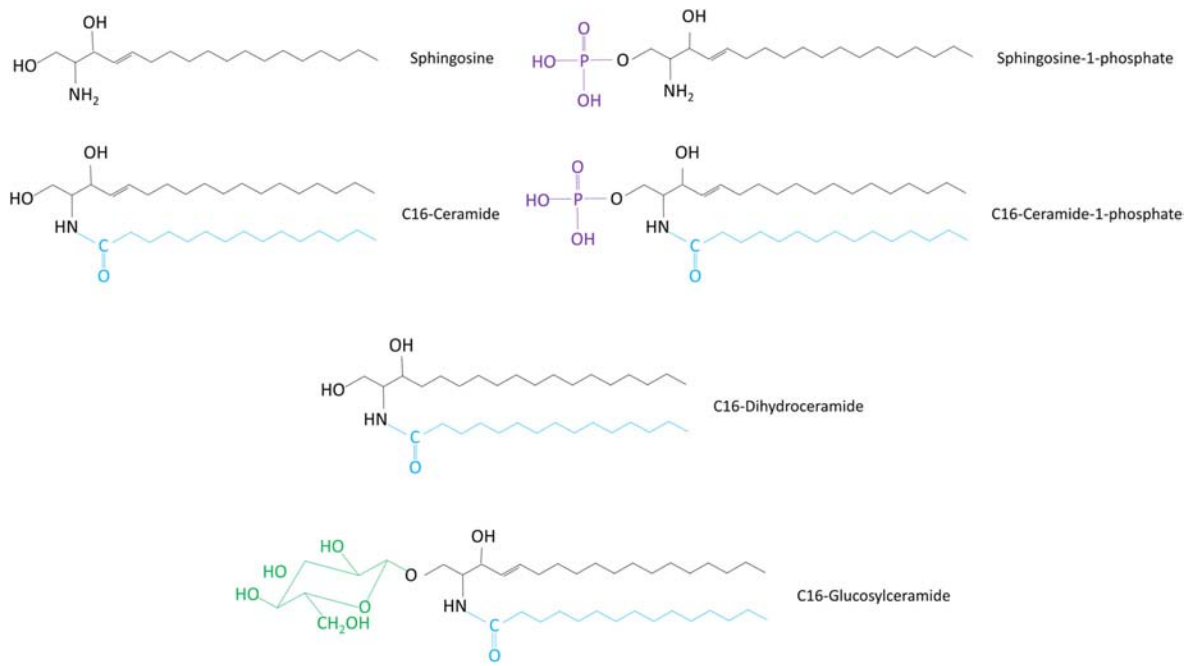

FIGURE 1 | Chemical structures of sphingolipid molecules. The structures of different sphingolipid types are shown. All sphingolipids share a sphingosine backbone (black). This sphingoid backbone is amide-linked to a fatty acid moiety (blue).

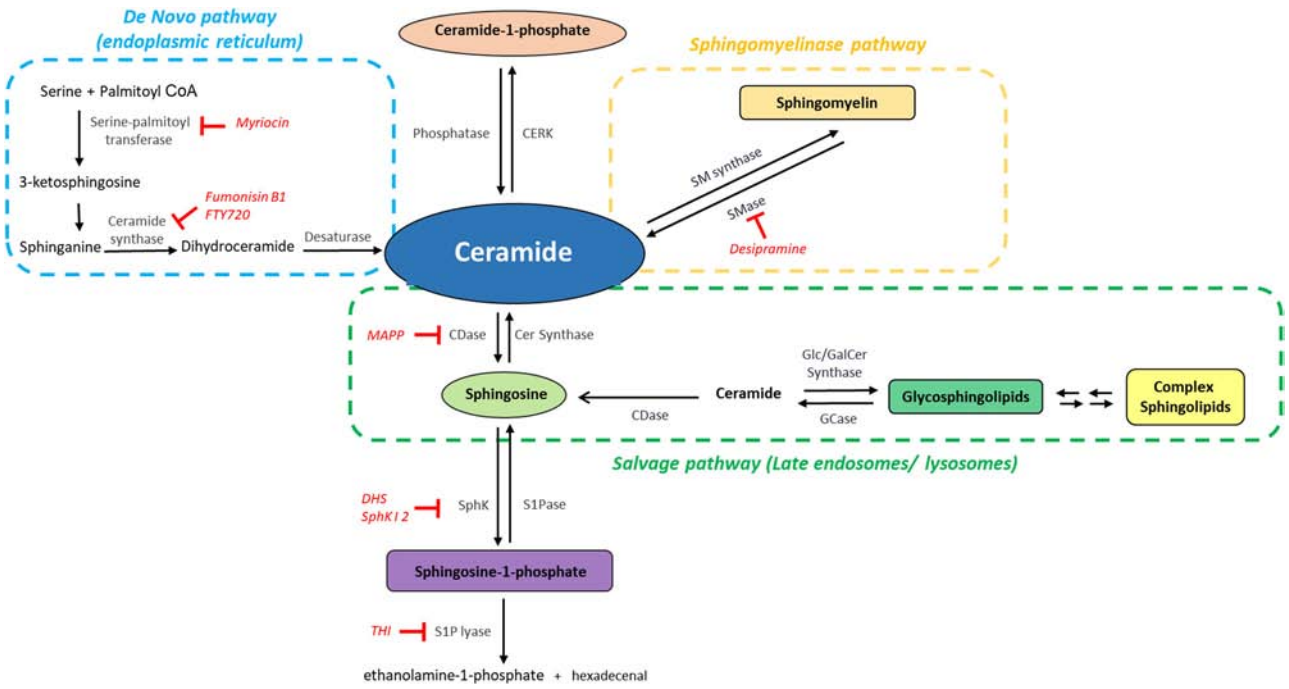

FIGURE 2 | The sphingolipid network: metabolic interconnection between bioactive sphingolipids. Ceramide, the central hub of sphingolipid metabolism, is synthesized by the *de novo* pathway (light blue), from serine and palmitoyl CoA, by the sphingomyelinase pathway, i.e., through hydrolysis of sphingomyelin mediated by sphingomyelinases (SMase) (orange) or by the salvage pathway (green). Ceramide can then be phosphorylated to generate Ceramide-1-phosphate and/or deacylated to form sphingosine, which is then phosphorylated to generate sphingosine-1-phosphate (S1P). The catabolism of S1P mediated by S1P lyase provides the only exit route from the sphingolipid network. CDase, ceramidase; CERK, ceramide kinase; GCase, glucosylceramidase; SMase, sphingomyelinase; SM synthase, sphingomyelin synthase; SphK, sphingosine kinase; SPPase, sphingosine phosphate phosphatase. The inhibitors mentioned in this Review are indicated in red.

properties (Jiménez-Rojo et al., 2014; Güntert et al., 2016). SPT can also change its selectivity for palmitate, using myristate or stearate as substrates (Hornemann et al., 2009; Harmon et al., 2013), further increasing the diversity of sphingolipid molecules.

The newly synthesized Cer can be glycosylated by GlucoCer synthase on the cytoplasmic surface of the Golgi, to render GlucoCer, the precursor of glycosphingolipids, or galactosylated by galactosyl Ceramide synthase in the ER (**Figure 2**; Raas-Rothschild et al., 2004). It can also receive a phosphocholine head group from phosphatidylcholine and thus generate sphingomyelin (SM), a reaction mediated by SM synthases (Tafesse et al., 2006). In turn, these complex sphingolipids can generate Cer through basal or signal-mediated catabolic pathways. The hydrolysis of the phosphodiester bonds in SM, catalyzed by at least five different SMases, renders Cer through the so-called *sphingomyelinase pathway* (**Figure 2**). These enzymes present several isoforms differing in subcellular localization, optimal pH range and cation dependence. A prominent example is neutral SMase; a Mg^{2+} -dependent form is localized in the plasma membrane whereas a cation-independent form is found in cytosol (Marchesini and Hannun, 2004); a mitochondrial neutral SMase has also been identified (Wu et al., 2010; Rajagopalan et al., 2015). The acid SMase gene can also generate, through differential trafficking, a cation-independent acid SMase, found in the endosomal-lysosomal compartment and an acid SMase that is secreted extracellularly and is responsible for hydrolyzing SM in the outer leaflet of the plasma membrane in addition to that present in plasma lipoproteins (Jenkins et al., 2009). Activation of SMases in response to diverse stimuli in different compartments provides the means for a rapid Cer generation, crucial for signal transduction.

A third pathway for Cer generation relies on the breakdown of complex sphingolipids in the lysosomal or late endosomal compartment through the reverse activity of different hydrolases, such as specific β-glucosidases and galactosidases, to form Cer, which cannot be released from this compartment. The subsequent activity of at least five different ceramidases generates Sph and its recycling in the ER and reacylation by CerSs yields Cer; this "salvage pathway" (**Figure 2**) is involved in inflammatory processes (Kitatani et al., 2008; Canals et al., 2018). Finally, exogenous Cer can also be recycled and generate endogenous Cer by the reverse action of ceramidases (Kitatani et al., 2008; Novgorodov et al., 2011).

Cer is phosphorylated by a specific kinase, CerK to form C1P (Wijesinghe et al., 2005). As stated above, deacylation of Cer by ceramidases renders Sph, the phosphorylation of which by one of the two existing SphKs, SphK1 and SphK2, generates S1P (Hait et al., 2006; **Figure 2**). The irreversible degradation of S1P by S1P lyase, at the cytoplasmic side of the ER, yields ethanolamine-1-phosphate and hexadecenal, providing the only release gate from the complex sphingolipid metabolic cycle (Bandhuvula and Saba, 2007). Comprehensive and detailed accounts of sphingolipid molecular diversity and metabolism can be found in excellent previous reviews (Lahiri and Futerman, 2007; Kitatani et al., 2008; Hannun and Obeid, 2011; Canals et al., 2018).

To Be or Not to Be. . ., a Decision for the Sphingolipid Rheostat

By 1995, several seminal findings evidenced that Cer and S1P had opposing cellular roles; whereas growth and survival factors increase S1P levels to stimulate proliferation and survival, different cell stressors promote an intracellular accumulation of Cer, which arrests the cell cycle or induces cell death. The ready interconversion of S1P, Sph, and Cer (**Figure 2**), prompted by numerous cues that stimulate or inhibit the activities of the enzymes involved, provides a significant tool for determining the patterns of intracellular signaling and deciding the physiological outcome. This understanding led to the proposal that the opposite functions of S1P and Cer transform their signal-mediated interconversion in a sensor of intracellular conditions, and the consequent rapid alteration of the balance between their levels in a key switch in the control of cell fate, later termed as the "sphingolipid rheostat" (Gómez-Muñoz et al., 1995; Cuvillier et al., 1996).

Since then, the collective effort of numerous laboratories has shed new light on the molecular actors and the signaling pathways involved in the intricate cross-reactions of these sphingolipids, included new sphingolipid molecules such as C1P and DHCer, and shown that this rheostat is involved in the induction of multiple pathologies, including neurodegeneration (Taha et al., 2006; Hannun and Obeid, 2008; Young et al., 2013; Newton et al., 2015; Wang and Bieberich, 2018). The extensive available data provides us with an optimal position to complete the unraveling of the sphingolipid universe. The subcellular compartmentalization of their metabolic pathways has been established and the major enzymes giving rise to this diversity of sphingolipids have been identified and cloned during the past three decades. New evidence suggests that different Cer molecular species, generated by different pathways in different compartments might differ in their intracellular roles (Hannun and Obeid, 2011; Hernández-Corbacho et al., 2015). Hence, the relevance of the sphingolipids involved in the rheostat model extends beyond their relative levels and the tightly regulated enzymes involved in their synthesis and degradation to encompass the innumerable and frequently opposite signaling pathways they control, their site of biosynthesis and their release to the extracellular milieu, to finely tune the sphingolipid rheostat.

Sphingolipids in Eye Pathology

The last 15 years have seen the buildup of a body of evidence pointing to a role for sphingolipids in normal development and function of the retina and in the pathogenesis of ocular diseases. The first link between alterations in sphingolipid metabolism and eye disease originated from lysosomal storage diseases, collectively denominated sphingolipidoses, which arise in mutations in the enzymes or cofactors involved in sphingolipid degradation. These diseases share an early neurodegeneration and visual impairment, with ocular manifestations including retinal vascular abnormalities, degeneration of ganglion cells, and even blindness (Harcourt and Ashton, 1973; Brownstein et al., 1978; Brownstein et al., 1980; Chen et al., 2014).

In Farbert's disease, Cer accumulation in the retina brings on visual dysfunction, with ganglion cells being the most affected (Zarbin et al., 1988). Brain accumulation of Cer occurs in the juvenile form of Batten disease, in which retina neurodegeneration and blindness are early events (Puranam et al., 1997). These early reports underscored the relevance of sphingolipid metabolism in eye pathogenesis; however, few clues existed on how this accumulation led to ocular manifestations. Thrillingly, work from many laboratories over the last decade has implicated sphingolipids such as Cer, S1P, Sph, and C1P in the progression of ocular diseases, including diabetic retinopathy, retinitis pigmentosa, AMD and other neuronal degenerative diseases. We will first summarize the sphingolipid species present in the eye and then review their roles in retinal cells and in the pathogenesis of these diseases.

Sphingolipid Presence in the Eye

Due to their high complexity, detailed composition analysis of retina sphingolipids is quite recent. Sphingolipids amount to about 11–13 (mole) % of both rat and bovine retinal lipids (Brush et al., 2010). SM is the most abundant species, amounting to 2.4–2.5% of total retinal lipids, whereas Cer and GlucoCer amount to less than 1%. Retinal sphingolipids have abundant (nearly 90%) of saturated, and particularly very long chain saturated fatty acids, with 18:0 and 16:0 being the most abundant fatty acid species. They contain about 2–3% of DHA, 22:6 n–3, the most abundant PUFA, but no VLCPUFA longer than 24 carbons are present (Brush et al., 2010); this is intriguing since the retina is characterized for the abundance of PUFA and VLCPUFA, which are enriched in sphingolipids in other tissues (Aveldaño and Sprecher, 1987; Oresti et al., 2011). In mice retina, almost 80% of Cer contains 16:0 and 18:0, with 21% having 20:0 or longer chain fatty acids (Fox et al., 2006). Bovine rod OS have lower levels of sphingolipids than the whole retina, varying from 3.4 to 6.4 mole % (Brush et al., 2010). SM and Cer from detergent resistant membranes obtained from rod OS are enriched in saturated fatty acids (Martin et al., 2005).

Diverse studies confirm the earlier observations that the sphingolipid profile is modified in retinal pathologies. Cer mass content decreases in retinas from diabetic mice compared to normal retinas, without modifying its fatty acid composition, with a concomitant increase in GlucoCer, and no changes in Sph and SM (Fox et al., 2006). The relevance of particular Cer molecular species in preserving retinal functions has been emphasized by recent findings from the Busik laboratory, demonstrating that overexpression of elongation of very long-chain fatty acids protein 4 (ELOVL4), whose presence is significantly reduced in the diabetic retina, preserves tight junctions and prevents retinal vascular permeability; this effect is parallel to an increase in the levels of Cer having 16 and 24 carbons, and very long chain fatty acids, which localize in and might stabilize tight junctions (Kady et al., 2018). In a retinitis pigmentosa model, the 23H-1 rat, photoreceptor degeneration starts at the beginning of light responsiveness; Cer, S1P and SM increase in the retina early during degeneration, with a reduction in shorter-chain species and an increase in longer-chain species (Stiles et al., 2016).

The fact that sphingolipids are affected during the course of degeneration intuitively makes them likely candidates to have a role in retinal diseases. A combination of studies *in vivo* and *in vitro* has contributed to our understanding of these roles. *In vivo* studies with animal models have provided comprehension on the biological functions of sphingolipids and allowed to test the physiological effects of modulating its levels. Research *in vitro* has allowed dissecting their specific effects on particular cell types and the biochemical pathways involved in these effects. We will now highlight the findings that support that significance of sphingolipids during normal development and in pathologies affecting the retina.

CERAMIDE, A CRUCIAL EXECUTIONER IN RETINAL DEGENERATION

Cer Metabolism

Cer has a central role in the sphingolipid family, both structural and metabolic. Consisting in a Sph molecule bound to a fatty acid of 16 to 24 carbons length (Fahy et al., 2005), these long acyl chains confer Cer its high hydrophobic properties; unable to exist in a free-solution form in the cytoplasm, it is the most hydrophobic lipid in biological membranes (Castro et al., 2014). This apparently static, membrane-confined location of Cer does not preclude it from having key intracellular actions, as the regulation of cell cycle and cell death.

As Cer is synthesized in the ER, its hydrophobic nature demands a transport mechanism to reach its diverse cellular destinations. Cer transport to the *trans* Golgi region, to generate SM, involves a CERT, which carries it in a non-vesicular manner (Hanada et al., 2009). Cer has very different patterns of tissue distribution and functions (Bartke and Hannun, 2009; Kurz et al., 2018). Interestingly, six specific types of CerSs (CerS 1–6) have been identified, each of them attaching acylCoAs differing in their chain length to the sphingoid backbone, thus generating different molecular species of Cer, with distinct cellular effects (Levy and Futerman, 2010; Park and Pewzner-Jung, 2013; Wegner et al., 2016). The distribution of these CerSs differs between organs and even between cell types in the same organ, contributing to a characteristic Cer composition (Laviad et al., 2008; Kremser et al., 2013).

Ceramide Biological Functions

Numerous cellular stressors, such as oxidative stress, absence of trophic factors, chemotherapy, and UV radiation, activate the synthesis of Cer; the consequent increase in Cer levels mediates many cell-stress responses, including the regulation of cell growth, differentiation (Okazaki et al., 1989), senescence (Trayssac et al., 2018), proliferation, necrosis, apoptosis and autophagy (Obeid et al., 1993; Hannun and Obeid, 2008; Scarlatti et al., 2004). These multiple roles of Cer result from its ability to act both at membrane level and as an intracellular messenger. Cer is a key modulator of membrane dynamics; as a cone-shaped lipid, it readily forms non-lamellar phases with increased negative spontaneous curvature, thus promoting membrane invagination, budding and fusion

(Holopainen et al., 2000; Stancevic and Kolesnick, 2010). Cer initiates multiple signaling pathways through the rapid formation or expansion of Cer-enriched microdomains in the plasma or outer mitochondrial membrane. These microdomains allow for the interaction and/or oligomerization of different proteins, such as death receptors in the former or Bax in the later that then signal the activation of diverse death programs (Grassmé et al., 2001; Ganesan et al., 2010).

In addition, Cer triggers many of its effects by acting as a lipid second messenger, through the activation of several intracellular targets. Cer activates protein phosphatase PP1A and PP2A (Chalfant et al., 1999) and regulates protein kinase C zeta (PKCζ) and Akt activity (Wang et al., 2005; Canals et al., 2018; Hannun and Obeid, 2018) as well as raf-1 and the kinase-suppressor of Ras, significantly changing the level of phosphorylation of various key substrates (Ruvolo, 2003).

Among the multifaceted roles of Cer, autophagy and cell death have been those that have drawn more attention. Cer controls both autophagy-mediated cell survival and cell death by regulating nutrient transport, ER stress and mitophagy (Dany and Ogretmen, 2015). Still, Cer has been more frequently identified as a key cell death player (Galadari et al., 2015), activating both the intrinsic and extrinsic pathways of apoptosis. Although its actual contribution to the apoptotic response in living cells has been unclear, multiple *in vitro* studies suggest that Cer might initiate cell death by acting directly on mitochondria. In an interesting recent work, a diverting CERT-mediated Cer transport to mitochondria has been shown to trigger Bax-dependent apoptosis (Jain et al., 2017).

Knowledge on the role of Cer in different pathological processes is vast and constantly expanding, and there are excellent reviews covering its functions (Canals et al., 2018; Hannun and Obeid, 2018; Kurz et al., 2018). We will here focus on Cer functions in retinal physiology and pathologies.

Ceramide in the Retina

Cer and Retina Degeneration

Acharya's group provided the first direct link between Cer and the death of retinal neurons in a *Drosophila* model of retinal degeneration. Using photo-transduction mutants, they demonstrated Cer has a crucial role in photoreceptor fate; keeping Cer levels low by preventing its *de novo* synthesis or by targeting neutral ceramidase suppresses photoreceptor death in the *Drosophila* mutants (Acharya et al., 2003). In functional null mutants of *Drosophila* ceramidase, photoreceptors degenerate in a light-dependent manner, do not respond to light stimulus and have no effective turnover of rhodopsin; in turn, overexpression of ceramidase, even in tissues distant from photoreceptors, suppresses their degeneration in arrestin mutants and facilitates membrane turnover in a rhodopsin null mutant (Acharya et al., 2008). Furthermore, a *Drosophila* mutant in the CerK shows increased Cer levels leading to the loss of phospholipase C activity and inhibition of phototransduction, ultimately accompanied by photoreceptor degeneration (Dasgupta et al., 2009).

Along the last decade, increasing evidence points to a key involvement of Cer in the onset of retina degeneration in mammals (**Table 1**). The gradual loss of photoreceptors observed in a rabbit model of retinal detachment correlates with the

TABLE 1 | Ceramide and sphingosine functions in the retina.

Sphingolipid	Retinal Process
Ceramide (Cer)	**Photoreceptor death**
	↓ Cer levels rescues photoreceptors from death in *Drosophila* RP models (Acharya et al., 2003)
	↑ Cer levels induces photoreceptor loss of function and death in *Drosophila* (Dasgupta et al., 2009)
	Photoreceptor death induced by retinal detachment correlated with ↑ Cer levels in rabbits (Ranty et al., 2009)
	↓ Cer levels by Myoricin treatment (*de novo* Cer synthesis inhibitor) rescue photoreceptors in a *rd10* mouse model (Strettoi et al., 2010)
	↓ Cer levels by inhibiting *de novo* synthesis with FTY720 delays retinal degeneration in P23H-1 rats (Stiles et al., 2016)
	↓expression of acid SMase protects the retina and preserves its function after ischemic injury in an acidic SMase +/− mice model (Fan et al., 2016)
	Intra-vitreal C2Cer injection causes vision loss in rats (Lou et al., 2017)
	C2Cer treatment induces photoreceptor and amacrine cell death in rat retinal neuronal cultures (German et al., 2006)
	Oxidative stress ↑ Cer levels and leads to cone cell death in 661W cell line (Sanvicens and Cotter, 2006)
	Brief C2Cer treatment induces photoreceptor death by activating parthanatos in rat retinal cultures (Prado Spalm et al., 2018)
	Retinal Pigment Epithelium (RPE) dystrophy
	C2Cer induces caspase-dependent death in rat RPE cells (Tomita et al., 2000)
	Oxidative stress ↑ Cer levels and activates cell death in ARPE-19 cells (Sugano et al., 2018)
	C2Cer treatment induces apoptosis in non-polarized, but not in polarized RPE cells (Zhu et al., 2010)
Sphingosine (Sph)	**Photoreceptor death**
	Oxidative stress ↑ Sph synthesis, preceding the onset of photoreceptor death *in vitro* (Abrahan et al., 2010)
	Addition of exogenous Sph induces mitochondrial-dependent photoreceptor death (Abrahan et al., 2010)
	RPE alterations
	Increased levels of Sph in SMase knockout mice match with age-dependent retina degeneration and RPE alterations, and an impaired autophagic flux (Wu et al., 2015)
	Overexpression of acid ceramidase in ARPE19 cells ↑ Sph levels and protects these cells from oxidative stress (Sugano et al., 2018).

production of Cer (Ranty et al., 2009). Intra-vitreal C2-Cer injection causes vision loss in rats, increasing apoptosis and expression of glial fibrillary acidic protein, a marker of gliosis (Lou et al., 2017). A recent work in a mouse model of Farber disease, with a deficiency in acid ceramidase activity, provides direct evidence of accumulation of Cer in the retina, associated to inflammation and severe visual loss (Yu et al., 2018). Ischemia increases the expression of acid SMase, increasing Cer levels and leading to retinal degeneration in wild type mice; reduction of this expression in an acid SMase +/− mouse model decreases Cer levels, protects retina structure and preserves its function after ischemic injury (Fan et al., 2016). However, the maintenance of a basal acid SMase activity is necessary for preserving normal retina structure and function; a total deficiency in acid SMase, as occurs in acid SMase knockout mice, leads to the disruption in lysosomal function and prominent photoreceptor degeneration (Wu et al., 2015). Mandalt's group showed alterations in the sphingolipid profile in P23H-1 rat retinas during degeneration, with an increase in neutral SMase activity leading to higher Cer levels at PN22. Treatment with FTY720, an established CerS inhibitor, partly decreases neutral SMase activity and delays the alterations in retina structure and functionality, granting partial neuronal protection. However, this treatment also leads to a stimulation of acid SMase activity and the consequent increase in Cer levels, which might explain why FTY720 does not fully prevent degeneration (Stiles et al., 2016). This underscores the relevance of establishing not only the pathways leading to Cer increase in each retinopathy but also whether inhibition of a major pathway promotes the activation of further biosynthetic paths, to identify the targets to effectively promote photoreceptor survival.

Diabetic retinopathy is the major cause of blindness among working age adults; increased Cer levels have been associated to reduction of insulin action (Chaurasia and Summers, 2015) and recent research establishes Cer as a relevant player in the progression of this retinopathy. Acid SMase is highly activated in the diabetic retina, particularly in retinal endothelium, elevating Cer levels and contributing to the pro-inflammatory changes in this tissue; noteworthy, DHA, which is decreased in the diabetic retina (Tikhonenko et al., 2010), downregulates the expression of acid SMase in human retinal endothelial cells (Opreanu et al., 2010; Busik et al., 2012; Hammer and Busik, 2017). Acid SMase vascular isoform specifically increases in the retinas of diabetic animal models at the vasodegenerative stage, whereas its absence or downregulation with DHA prevents capillary formation and cytokine production (Opreanu et al., 2010, 2011; Busik et al., 2012; Chakravarthy et al., 2016). Activation of acid SMase and the consequent Cer increase appear as relevant contributors to the pathogenesis of diverse retina degenerations, and reestablishing an adequate balance in sphingolipid levels emerges as essential to maintain retina functionality.

Ceramide and Photoreceptor Death

The work of several groups, including ours, has provided direct links between Cer increase and the onset of photoreceptor death. This death is the hallmark of most retinal degenerative diseases with very diverse etiologies (Chang et al., 1993; Portera-Cailliau et al., 1994; Sancho-Pelluz et al., 2008); hence, uncovering common molecular mechanisms and mediators is essential to identify new therapeutic targets. *In vitro* studies have been fundamental to establish Cer as a mediator of photoreceptor death. Our group demonstrated that oxidative stress increases the *de novo* synthesis of Cer preceding photoreceptor death in rat retina cultured neurons, whereas inhibiting this synthesis with fumonisin B1, a CerS inhibitor, prevents this death (German et al., 2006). These neurons present low levels of DHA, which has been shown to be neuroprotective for photoreceptors (Rotstein et al., 1996, 1997). DHA supplementation protects photoreceptors from C2-Cer and oxidative stress-induced death, promoting the synthesis of GlucoCer (German et al., 2006). Cotter's group extended Cer role in oxidative stress-induced death of photoreceptors; they showed that treatment of 661W cells, a cone cell line, with a nitric oxide donor increases Cer levels by activating acid SMase; inhibition of Cer synthesis by an acid SMase inhibitor (Desipramine) prevents cone cell death (Sanvicens and Cotter, 2006). Interestingly, induction of oxidative stress with H_2O_2 also raises Cer levels and promotes cell death in 661W cells, whereas inhibiting *de novo* synthesis of Cer with Myriocin, a serine palmitoyl transferase inhibitor, prevents Cer increase preserving cell viability (Fabiani et al., 2017). The buildup of Cer, arising from the activation of different biosynthetic pathways in rod and cone photoreceptors, emerges as a death arbitrator in photoreceptors, suggesting that pharmacological prevention of this increase might have therapeutic potential (**Figures 3**, **4**).

In vivo studies have supported this hypothesis. Cer levels increase during the peak of photoreceptor degeneration in the *rd10* mouse, a mouse model of Retinitis Pigmentosa, and treatment with Myriocin noticeably prevents photoreceptor loss and preserves both photoreceptor morphology and retina functionality (Strettoi et al., 2010). Although the genetic mutations in Retinitis pigmentosa and in animal models of this disease affect mostly rods, their death is eventually followed by the death of cones; noteworthy, Myriocin was also effective as a strategy to promote cone survival in the same *rd10* model, even after rod death (Piano et al., 2013).

Increasing evidence suggests that Cer activates death pathways alternative to those of canonical apoptosis to induce photoreceptor demise. Cer increase triggers several pathways in 661W cells subjected to oxidative stress; it not only induces the mitochondrial pathway and subsequent activation of caspases, but also promotes Ca^{2+} increases in both mitochondria and cytosol that precede the activation of calpain-mediated death and activates cathepsin D pathway as well (Sanvicens and Cotter, 2006).

We have recently established that Cer activates PARP-1 to induce photoreceptor death. Cer induces photoreceptor death in cultured rat retina neurons in a caspase-independent process, involving generation of ROS, increase in mitochondrial permeability, activation of PARP-1 and calpain, accumulation of poly ADP-ribose polymers and nuclear translocation of AIF (Prado Spalm et al., 2018), which are features of a recently unveiled death process named Parthanatos (David et al., 2009). Notably, inhibition of both PARP-1 and calpain

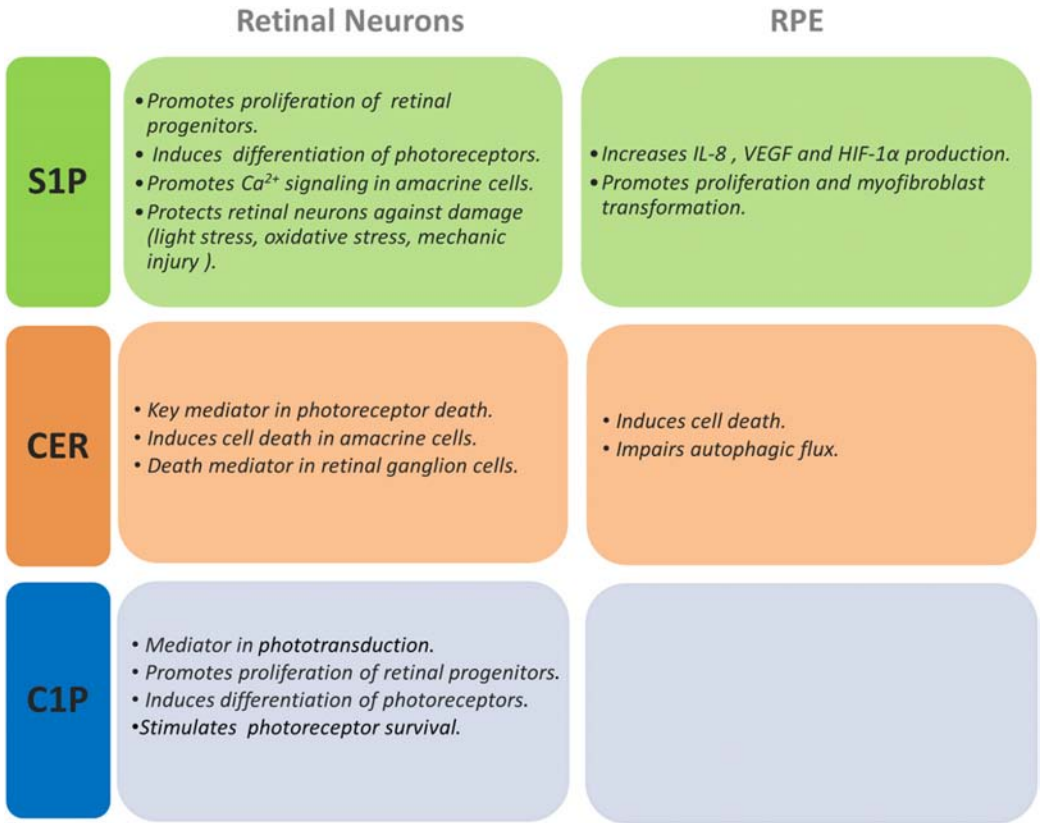

FIGURE 3 | Actions of S1P, Cer, and C1P on retinal neurons and RPE cells. This figure summarizes the effects shown for S1P, Cer, and C1P on different retinal neurons and RPE cells.

activity rescues photoreceptors from Cer-induced death (Prado Spalm et al., 2018). Paquet-Durandt's group established PARP-1 activation as a common non-apoptotic mechanism involved in retinal neurodegeneration in animal models encompassing the major groups of inherited human blindness (Arango-Gonzalez et al., 2014). PARP-1 activity is crucial in the induction of photoreceptor death in the *rd1* and *rd2* mouse models (Sahaboglu et al., 2017). Activation of PARP-1 has only been associated with Cer-induced death in neuroblastoma cells (Czubowicz and Strosznajder, 2014); hence, these findings not only link for the first time Parthanatos with Cer-induced photoreceptor death but support Parthanatos as a novel cell death routine triggered by Cer. Although different retinal neurodegenerative diseases may have particular cell death mechanisms, taking together these studies Parthanatos appears as a central, shared photoreceptor death-process with Cer as a crucial mediator in these degenerations. Targeting Cer overproduction or Parthanatos key molecular actors might provide enticing strategies for novel, disease-independent treatments for retina neurodegenerations.

Cer as a Death Mediator in Other Neuronal Types in the Retina

Cer role as a mediator in the induction of cell damage is not confined to photoreceptors. A 24 h treatment with C2-Cer induces death of amacrine neurons in retina neuronal cultures (German et al., 2006). Optic nerve crush, which triggers the injury to retinal ganglion cells in the rat retina, increases the expression of enzymes involved in Cer biosynthesis (Agudo-Barriuso et al., 2013). Gene expression profiling in injured retinal ganglion cells following overexpression of the *Sox11 transcription factor* revealed that genes associated with Cer biosynthetic and metabolic processes are upregulated, suggesting the activation of a Cer-induced cell death pathway (Norsworthy et al., 2017).

Cer and RPE Degeneration

Cer also plays a pivotal role in diseases affecting RPE function, such as AMD and Stargardt disease. Atrophy of RPE cells followed or accompanied by photoreceptor cell death is usually the final outcome of all forms of retinitis pigmentosa, despite their different etiologies. RPE atrophy, i.e., RPE cell death, in the macular region is the primary event in dry AMD and a common event in early stage wet AMD (Al-Zamil and Yassin, 2017). C2-Cer induces death of human and rat RPE cultured cells, which involves caspase activation and is partially prevented by antioxidants and growth factors (Tomita et al., 2000; Kannan et al., 2004; Sreekumar et al., 2009). Oxidative stress increases Cer levels and induces apoptosis in human RPE cells and this was replicated by using C2- and C6-Cer (Barak et al., 2001). Oxidative stress increases both Cer and hexosyl-Cer

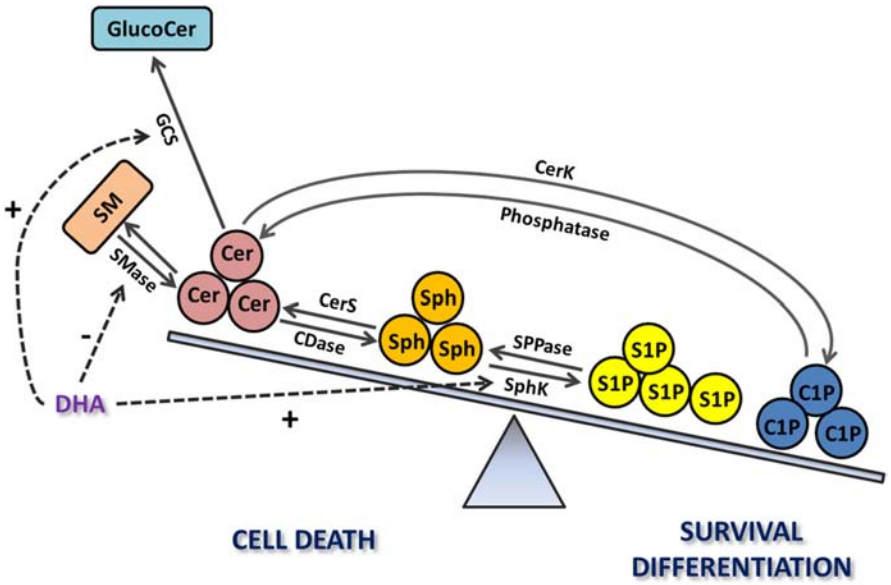

FIGURE 4 | The relevance of the sphingolipid rheostat in retina photoreceptors. Increases in Cer levels through the activation of its *de novo* synthesis or the SMase pathway trigger photoreceptor death; this death is also induced after Cer hydrolysis to increase Sph levels, mediated by ceramidase (CDase). In turn, S1P and C1P promote photoreceptor survival and differentiation. Docosahexaenoic acid (DHA) promotes survival by regulating the sphingolipid rheostat, inhibiting SMase or stimulating the synthesis of glucosylceramide (GlucoCer) to decrease Cer levels or enhancing the synthesis of S1P. Exogenous addition of C1P also promotes photoreceptor survival and differentiation.

levels in ARPE-19 cells, a human RPE cell line, promoting cell death; this death is prevented by over-expression of acid ceramidase, which increases Sph levels but not those of S1P (Sugano et al., 2018). Interestingly, increased serum levels of hexosyl-Cer have been reported in patients with late stage AMD (Pujol-Lereis et al., 2018). Noteworthy, oxidative stress leads to increased S1P levels in control RPE cells, which might reflect an attempt to counteract Cer action toward cell death (Sugano et al., 2018). Laser exposure, a frequent treatment for retina neovascularization, induces human RPE cell death concomitant with Cer overproduction (Barak et al., 2005).

Cer significance as a mediator of RPE cell death is also evidenced by the induction of cell death in ARPE19 cells overexpressing neutral SMase3. Intracellular Cer increase and cell death are proportional to the amount of the transfected enzyme and SMase3 overexpression also inhibits proliferation in ARPE19 cells (Zhu et al., 2010). Intriguingly, C2-Cer treatment induces apoptosis in non-polarized RPE cells but does not affect differentiated and polarized RPE cells (Zhu et al., 2010). This differential susceptibility suggests that while healthy, polarized cells forming the RPE monolayer *in vivo* may be resistant to injures leading to an eventual Cer increase, non-polarized, activated RPE cells, frequent in late AMD lesions and in proliferative vitreoretinopathies, might be more susceptible to increased Cer levels resulting from chronic retina injuries (**Figure 3**).

Cer increase is common to several diseases affecting RPE cells. Excessive acid SMase activation and the subsequent Cer accumulation have been related to the pathogenic changes of RPE cells in diabetic retinopathy. High glucose enhances acid SMase expression, increasing Cer levels in ARPE19 cells. Interestingly, microRNAs (miR) appear as novel players in the modulation of sphingolipid metabolic enzymes. Work from the Busik laboratory showed miR-15a participates in the regulation of Cer levels; its expression is decreased by high glucose whereas its overexpression downregulates acid SMase expression in human RPE cells, restoring normal Cer levels (Wang et al., 2016). This adds an additional complexity to the intricate regulation of sphingolipid metabolism and underscores the usefulness of its modulation in disease treatment.

Acid SMase activation has been shown in aged RPE and in a Stargardt disease mouse model, and the consequent Cer increase impairs autophagic flux, which is crucial for preserving functional RPE and photoreceptor cells (Toops et al., 2015). Efficient endolysosome function in RPE is essential for its phagocytic role and autophagic clearance of cellular debris, and endolysosomal dysfunction is characteristic of neurodegenerative diseases. Recent findings show acid SMase-derived Cer increase and subsequent endolysosomal dysfunction contribute to internalization of the complement protein C3, abnormal levels of which have been implicated in AMD; inhibiting Cer synthesis with desipramine decreases this dysfunction and C3 internalization (Kaur et al., 2018). Significantly, epidemiological studies indicate that the use of tricyclic antidepressants, like desipramine, is associated with a statistically significant protective effect against developing early AMD (Klein et al., 2001), emphasizing the significance of Cer increase in RPE cell dysfunction and AMD progression (**Figure 3**).

Several signaling pathways participate in Cer-induced RPE cell death. C2-Cer induces the over-production of ROS, activating the intrinsic apoptotic pathway, with a subsequent increase in mitochondrial membrane permeability and caspase-3 activation (Kannan et al., 2004). Both H_2O_2 and UV radiation induce ER and stress-activated protein kinase (AMPK) axis, which promote RPE cell death (Yao et al., 2013). Tunicamycin treatment of cultured RPE cells induces NF-κB nuclear translocation, increases in nitric oxide synthase 2 expression and nitrotyrosine formation leading to cell death, which is prevented with a neutral SMase inhibitor, implying Cer generation is involved in this death (Kucuksayan et al., 2014). These data suggest a key role for ER-stress induced by Cer in RPE cell death and a disease-specific activation of SMases.

Taking together the above studies, Cer distinctly emerges as a common pathological mediator in numerous retinopathies of diverse etiologies, activating multiple downstream pathways that induce both the degeneration of rod and cone photoreceptors and RPE dysfunction and death. Pharmacological interventions to prevent Cer increase might provide useful tools for treating multiple retinopathies, in a disease-independent mode. The preservation of retina morphology and functionality by the inhibition of Cer synthesis (Strettoi et al., 2010; Stiles et al., 2016) sustains this proposal. In addition, DHA provides an exciting "proof of concept," emerging as a modulator of several enzymes of sphingolipid metabolism in order to prevent Cer accumulation, thus tilting the sphingolipid rheostat toward cell survival (**Figure 4**).

SPHINGOSINE, A DEADLY MESSENGER IN THE RETINA?

Sph Biological Functions

The finding that Sph inhibits protein kinase C was one of the first supporting a role for sphingolipids in cell signaling (Hannun and Bell, 1989; Merrill et al., 1989). Later work demonstrated that in addition to this modulatory function, Sph, as its precursor Cer, is a crucial signal for cell death. Sph levels increase during the early stages of cell death, and its addition can trigger this death (Cuvillier, 2002). Oxidative stress, radiation and chemotherapy enhance Cer and Sph generation promoting senescence, cell cycle arrest or cell death (Ogretmen and Hannun, 2004; Hannun and Obeid, 2018). Although Sph increase might result from a decreased SphK activity, as occurs in radiation-resistant prostate cancer cells (Nava et al., 2000), the rapid deacylation of Cer is the main source of Sph increase. The increase in Cer usually precedes that of Sph, suggesting that Cer hydrolysis by ceramidases gives rise to this increase (Ohta et al., 1995; Cuvillier et al., 2000). Precisely, the fact that Cer can be hydrolyzed to Sph, and Sph reacylated to generate Cer made it difficult initially to discern their effects. However, exogenous Sph induces apoptosis in cell lines such as Jurkat cells and rhabdomyosarcoma cell lines even when its conversion to Cer is inhibited (Cuvillier et al., 2000; Phillips et al., 2007) and Sph has been shown to act independently from Cer and at an earlier step in the apoptotic pathway in human leukemic cells (Sweeney et al., 1996). Conversely, inhibiting the synthesis of Sph reduces the induction of apoptosis by different stimuli (Lépine et al., 2004; Suzuki et al., 2004). Sph is now an established second messenger, rapidly generated by different apoptotic stimuli to induce cell death. Sph signals this death through mitochondrial membrane permeabilization, formation of ROS, cytochrome c release, and caspase-3 activation (Sweeney et al., 1996; García-Ruiz et al., 1997; Cuvillier et al., 2000, 2001). Mitochondrial permeabilization is crucial for Sph induction of cell death; Sph induces the downregulation of Bcl-2 levels (Sweeney et al., 1996) whereas Bcl-xl overexpression prevents the onset of apoptosis in spite of the increase in Sph levels (Cuvillier et al., 2001).

Sph Functions in the Retina

Scarce information exists regarding Sph roles in the eye (**Table 1**). Initial data in *Drosophila* mutants showed that expression of ceramidase suppresses retinal degeneration in arrestin mutant flies, in parallel to a decrease in Cer levels; however, these mutants show enhanced degeneration of photoreceptors when they are raised with a Sph-enriched diet, suggesting that Sph is not involved in preventing degeneration (Acharya et al., 2003).

Sph functions in mammalian retina are still ill-defined. Sph induces cell death in amacrine and photoreceptor neurons in culture (Abrahan et al., 2010); oxidative stress rapidly enhances Sph synthesis, preceding the onset of photoreceptor death *in vitro*. In turn, inhibition of Sph synthesis by blocking Cer breakdown with an alkaline ceramidase inhibitor, MAPP, markedly decreases oxidative stress-induced photoreceptor death. Moreover, exogenous Sph promotes photoreceptor death, even when Cer synthesis is inhibited, implying that Sph is responsible for this death. As reported in different cell types, Sph promotes apoptotic death by inducing mitochondrial permeabilization in photoreceptors, increasing ROS formation and cytochrome c release, whereas inhibiting Sph synthesis prevents mitochondrial permeabilization (Abrahan et al., 2010).

As occurs with Cer (German et al., 2006), DHA prevents Sph-induced apoptosis, enhancing the expression of SphK1 and its translocation to the plasma membrane (Miranda et al., 2009; Abrahan et al., 2010). Noteworthy, inhibition of SphK1 activity with DHS blocks DHA protection, implying that the decrease in the levels of Sph and/or the generation of S1P are required for DHA protective effect (Abrahan et al., 2010). As a whole, these findings suggest that oxidative stress increases the generation of Cer and Sph in retina photoreceptors, which act as second messengers, inducing mitochondrial dysfunction and increased generation of ROS (Rotstein et al., 2010), to activate cell death. Lowering Sph levels, by preventing its synthesis or promoting its phosphorylation to S1P effectively prevents photoreceptor death, accentuating the relevance of manipulating sphingolipid metabolism in photoreceptor survival.

Whether Sph acts as a deadly messenger promoting degenerative changes in other retinal cell types is still unclear.

In acid SMase knockout mice, increased levels of Sph and normal levels of Cer are found in the retina (Wu et al., 2015), probably due to compensatory changes in the activities of other sphingolipid enzymes, aimed at maintaining Cer levels constant. These mice show age-dependent retina degeneration and RPE alterations, with an impaired autophagic flux (Wu et al., 2015); it still remains to be defined whether Sph increase leads to these changes. Puzzlingly, overexpression of acid ceramidase in ARPE19 cells increases their Sph levels, and protects these cells from oxidative stress, with no concomitant increase in S1P levels (Sugano et al., 2018). Hence, much remains to be investigated regarding Sph actions in the retina in order to design new therapies through the adequately modulation of sphingolipid levels.

SPHINGOSINE-1-PHOSPHATE, A FORMIDABLE DOUBLE-EDGED SWORD IN THE RETINA

S1P Synthesis

Sphingosine-1-phosphate is a crucial lipid intermediate in the complex sphingolipid metabolism. It has a polar head group (phosphate), and a long-chain sphingoid base backbone (Sph) (Saba and Hla, 2004; **Figure 1**). Sph is phosphorylated to generate S1P by two different SphKs, SphK1 and SphK2 (Maceyka et al., 2005; **Figure 2**). SphK1 is found mainly in the cytosol, close to the cell membrane, in nearly every cell type. When activated, it translocates to the plasma membrane, where Sph is localized. Its structure, functions and roles in disease are widely identified. Much less is known on SphK2; predominantly localized in nuclei and mitochondria, its expression is tissue and time of development dependent (Hait et al., 2009; Strub et al., 2011). Its structure, functions and the processes in which it is involved are poorly understood. Its most recognized function is its ability to phosphorylate FTY720/Fingolimod, a Sph analog and the first oral pro-drug to be approved for the treatment of multiple sclerosis by the FDA.

S1P as an Intracellular and an Extracellular Messenger

Notably, in spite of being chemically identical, S1P molecules from nuclei or cytoplasm perform different functions. While nuclear S1P works as a histone deacetylase (HDAC) inhibitor to epigenetically regulate gene transcription (Hait et al., 2009), cytoplasmic S1P acts as a second messenger or as an extracellular ligand. To function as an extracellular ligand, the S1P produced inside the cell is exported by specific transporters, such as Spinster 2 (Spns2) (Osborne et al., 2008; Kawahara et al., 2009; Spiegel et al., 2019) or ABCA1 (Sato et al., 2007), ABCC1 (Mitra et al., 2006), and ABCG2 (Takabe et al., 2010). Once outside the cell, S1P acts in a paracrine or autocrine fashion, a process known as "inside-out signaling" (Takabe et al., 2008). As an extracellular ligand, S1P interacts with five S1P G protein-coupled membrane receptors (S1PRs), termed $S1P_{1-5}$. Most cells express one or more subtypes of S1PRs, and depending on the G-protein they are coupled with, S1PRs exhibit unique properties and regulate different cellular processes. Downstream effectors of S1PRs include adenylate cyclase, PI3-kinase, phospholipase C, protein kinase C and intracellular calcium (Hla et al., 2001; Spiegel and Milstien, 2002). In addition, S1P has been proposed to signal through S1PRs, in a paracrine fashion, upregulating the transcription of SphK1 and thus activating the S1P/SphK1 axis; this "outside-in" signaling pathway has been shown to contribute to the progression of diabetic retinopathy (Huang et al., 2014).

Sphingosine-1-phosphate is a pleiotropic bioactive lipid mediator; its cellular concentration responds to different stimuli and is tightly regulated. Concentrations of S1P in blood and lymph are actually higher than in tissues (Cyster and Schwab, 2012; Olivera et al., 2013; Nagahashi et al., 2016). The final concentration of S1P in any tissue depends on the balance between its synthesis and its degradation, with S1P degrading enzymes playing an important role in maintaining the low tissue levels of S1P. The main enzymes that degrade S1P are S1P lyases and SPP. SPP has two isoforms, SPP1 and SPP2, which catalyze the reversible dephosphorylation of S1P, generating Sph that it is then converted to Cer by CerS (Mandala, 2001; Pyne et al., 2009). S1P lyases are responsible for irreversibly degrading S1P to hexadecenal and ethanolamine-1-phosphate, removing S1P from the sphingolipid metabolic routes and providing the only escape path from this complex metabolism (Bandhuvula and Saba, 2007).

Sphingosine-1-phosphate induces a wide spectrum of cellular effects, including proliferation, differentiation, survival, migration, angiogenesis and immune responses (Tabasinezhad et al., 2013). These pleiotropic effects grant S1P a key role in several diseases, including cancer, inflammation, autoimmunity, atherosclerosis and fibrotic disorders (Knapp, 2011; Maceyka et al., 2012; Takuwa et al., 2013). The highly conserved relevance of S1P and its regulation of important biological functions in organisms ranging from yeast and plants to flies and vertebrates highlight its significance in cell signaling.

The role of S1P in immune functions is well demonstrated, being involved in infections, allergy and chronic inflammation (Aoki et al., 2016). Its key role in neuroinflammation is evident in the successful use of FTY720 in the treatment of multiple sclerosis. S1P acts as an "extracellular siren song," its high plasma concentrations stimulating pathogenic lymphocyte migration and promoting their egress from lymph nodes to blood vessels (Bandhuvula and Saba, 2007). FTY720, and more precisely its phosphorylated form, is a functional antagonist of almost all S1PRs, excepting S1P2, and prevents S1P activation of S1P1 by binding and promoting its internalization and further degradation, thus decreasing S1P1 membrane levels and retaining lymphocytes in the lymph nodes (Paugh et al., 2003; Brinkmann et al., 2010; Chun and Hartung, 2010). In addition, FTY720 has been shown to inhibit *de novo* synthesis of Cer (Berdyshev et al., 2009) and histone deacetylases (Hait et al., 2014). Its efficacy in the treatment of multiple sclerosis has led to an accelerated research on its therapeutic effects in other inflammatory diseases.

Glial cells are key players in neuroinflammation and S1P induces this inflammation in the different glial types (microglia,

astrocytes, and oligodendrocytes). S1P has been linked to microglial activation; S1P addition to cultured microglial cell lines increases the release of pro- inflammatory cytokines whereas microglial activation *in vivo* increases SphK1 activity (Nayak et al., 2010; Lv et al., 2016). Astrocytes, which are involved in many central nervous system pathologies, respond to and release inflammatory mediators, and an active crosstalk exists between S1P and these mediators; S1P induces astrogliosis, whereas IL-1 induces SphK1 expression (Sorensen et al., 2003; Paugh et al., 2009). S1P1 expression in astrocytes is critical in the development of animal models of multiple sclerosis, as shown by the protective effect of FTY720 (Choi et al., 2011).

Inflammation, angiogenesis, proliferation and migration are common features in most retinopathies; hence, S1P signaling of these processes makes it an ideal candidate to regulate the onset and progression of these diseases. We will here discuss current knowledge regarding the role of S1P in eye and retina development and during retina pathological disorders, particularly the opposing functions of S1P in both neuronal survival and inflammation and fibrosis in the retina.

S1P, Dr. Jekill or Mr. Hyde in the Retina?

Numerous findings during the last decade have shed new light on S1P functions in the retina (**Table 2**). SphK1 is expressed in photoreceptors whereas SphK1 and SphK2 are expressed both in ARPE19 and in human fetal RPE cells, implying these cells have the molecular machinery required for S1P synthesis (Abrahan et al., 2010; Zhu et al., 2010). A recent work has dissected the distribution of SphKs and S1PRs in mouse retina (Porter et al., 2018). *SphK1* is low in most mouse ocular tissues and highest in the retina and optic nerve, whereas higher levels of *SphK2* are observed in all mouse eye tissues. Interestingly, both SphK2 and SphK1 increase in the retina during early development, peaking at adulthood. *S1p1* and *S1p3* are expressed in the retina, while expression of *S1p2* and *S1p5* is minimal; S1P3 expression remains high and constant during retina development, whereas S1P1 increases gradually. Photoreceptors express both S1P1 and S1P3; S1P1 is highly expressed in RPE cells while S1P3 is localized in ganglion cells (Porter et al., 2018). Müller glial cells also show expression of SphK1 and S1P3 (Simón et al., 2015). Hence, the enzymes and receptors that take part in S1P signaling pathway are present in most retina cell types.

S1P in Eye Development and Neuronal Survival

Sphingosine-1-phosphate has essential functions during normal eye development. Mutations in *Spns2* cause the abnormal fusion of eyelids during rat embryogenesis, which can be reversed by treatment with S1P (Bian et al., 2018). Functional SPNS2 is crucial for retinal morphogenesis, since dysfunctional SPNS2 causes delayed cell-cycle exit of retinal progenitors and retinal laminar disorganization (Fang et al., 2018). A role for S1P signaling in axon guidance has also been reported; S1P promotes repulsive turning and collapse of growth cones from ganglion cell axons in the Xenopus retina, through activation of the S1P5 and RhoA whereas loss of S1P function results in target recognition errors (Strochlic et al., 2008). S1P is also involved in signaling in inner retina cells; S1P increases cytosolic Ca^{2+} levels in cultured amacrine cells, through the activation of S1P1 and S1P3 (Crousillac et al., 2009).

Sphingosine-1-phosphate displays a vital function in preventing neuronal death during retinal injuries. S1P1 contributes to survival and axonal sprout of injured retinal ganglion cells after damage to the optic nerve (Joly and Pernet, 2016) and FTY720 has neuroprotective effects in experimental glaucoma in rats (You et al., 2014). Moreover, the expression of SphK1, S1P2, and S1P3 immediately increases in light-stressed retinas, with S1PRs localizing to the pyknotic nuclei, suggesting the up-regulation of a cytoprotective S1P signaling to counteract the onset of apoptosis (Porter et al., 2018).

S1P as a Mediator in Photoreceptor Survival and Differentiation

Sphingosine-1-phosphate emerges as a pleiotropic mediator for development and survival of photoreceptors. Our group established that 1 μM S1P promotes the proliferation of retinal progenitors and their later differentiation into photoreceptors; S1P increases the expression of specific photoreceptor proteins, and advances the development of rudimentary OS (Miranda et al., 2009). We also evidenced that S1P is a key mediator in photoreceptor survival, preventing photoreceptor death during development *in vitro* and when exposed to oxidative stress (Miranda et al., 2009; Rotstein et al., 2010).

An increase in S1P intracellular levels protects 661W cells from oxidative stress; exogenous addition of S1P or inhibiting S1P lyase with THI preserves viability in these cells when treated with H_2O_2, by decreasing Cer levels, activating the Nrf-regulated antioxidant pathway and increasing the Bcl-2/Bax ratio (Fabiani et al., 2017). Further evidence supports the proposal that S1P is an intracellular second messenger, the synthesis of which is promoted by photoreceptor trophic factors to exert its actions. GDNF promotes the proliferation of photoreceptor progenitors (Politi et al., 2001; Insua et al., 2003), as S1P does, and inhibiting SphK1 with DHS blocks GDNF mitogenic effect (Miranda et al., 2009). Inhibition of SphK1 abolishes DHA neuroprotection of photoreceptors during oxidative stress-induced apoptosis and DHA enhancement of photoreceptor differentiation (Miranda et al., 2009; Abrahan et al., 2010). Cytokines and growth factors, such as Transforming growth factor β and Nerve growth factor (NGF), enhance the expression of SphK1 and promote its rapid translocation and activation to increase the synthesis of S1P, which then acts as a second messenger to exert their effects (Toman et al., 2004; Yamanaka et al., 2004; Wattenberg et al., 2006). Noteworthy, both GDNF and DHA upregulate the expression of SphK1 and promote its translocation to the plasma membrane (Abrahan et al., 2010). Thus, GDNF and DHA might elicit their biological effects on photoreceptors by promoting SphK1 activity and increasing the synthesis of S1P, which then acts as a second messenger, essential for proper development and survival of photoreceptors. As described above, DHA prevents photoreceptor death by promoting Cer glucosylation (German et al., 2006). As a whole, these findings highlight the importance of the "sphingolipid rheostat" and of manipulating sphingolipid metabolism to promote photoreceptor survival in retinal degenerations (**Figure 4**).

TABLE 2 | Functions of Sphingosine-1-phosphate and Ceramide-1-phosphate in the retina.

Sphingolipid	Retinal Process
Sphingosine-1- phosphate (S1P)	**Normal Eye development and function**
	↓ in *Spns2* expression causes abnormal eyelid fusion (Bian et al., 2018), alterations in retinal progenitors cell cycle and laminar disorganization (Fang et al., 2018)
	↑S1P promotes proliferation of retinal progenitors and their later differentiation into photoreceptors (Miranda et al., 2009)
	↑ S1P promotes Ca^{2+} signaling in amacrine cells in the inner retina via S1P1 and S1P3 (Crousillac et al., 2009)
	Protection against Retinal injuries
	↑ S1P through S1P1 promotes neuronal survival and axonal sprouting after optic nerve damage (Joly and Pernet, 2016)
	FTY720 has neuroprotective effects in rat models of glaucoma (You et al., 2014)
	↓ S1P abolishes DHA–mediated protection of cultured photoreceptors from oxidative stress (Abrahan et al., 2010)
	Light- stressed retinas ↑ expression of SphK1, S1P2 and S1P3 (Porter et al., 2018)
	Eye inflammation
	↑ S1P promotes retinal angiogenesis and neovascularization (Eresch et al., 2018)
	↑ S1P increases IL-8 secretion in RPE (Qiao et al., 2012)
	TNF-α promotes ↑ S1P and IL-8 and IL-6 production (Qiao et al., 2012)
	↑ S1P promotes VEGF and HIF-1α production in RPE (Terao et al., 2017)
	↑ levels of S1P1 and S1P lyase in vitreous of patients with proliferative diabetic retinopathy (Abu El-Asrar et al., 2014)
	Retinal fibrosis
	S1P promotes proliferation, myofibroblast transformation and formation of pro- fibrotic proteins in RPE cells (Swaney et al., 2008)
	S1P promotes glial migration (Simón et al., 2015)
	Blockade of S1P with monoclonal antibodies reduces angiogenesis and sub-retinal fibrosis (Caballero et al., 2009) and prevents excessive scarring in animal models of glaucoma (Lukowski et al., 2013)
Cer-1- phosphate (C1P)	**Signaling in photoreceptors**
	C1P regulates lipid metabolism in photoreceptor outer segments (Pasquaré and Giusto, 2008; Pasquaré et al., 2008)
	C1P increases the proliferation of photoreceptor progenitors in retina neuronal cultures (Miranda et al., 2011)
	C1P promotes differentiation and prevents apoptosis in cultured rat retina photoreceptors (Miranda et al., 2011)
	↑ C1P levels in uveitis (Wang et al., 2018)
	Phototransduction
	CerK regulation of Cer levels required for phospholipase C activity and PIP2 production during phototransduction (Dasgupta et al., 2009)

S1P Signaling in Retina Inflammation and Neovascularization

Sphingosine-1-phosphate is a potent mediator in the modulation of inflammatory responses and angiogenesis. It is crucial in the regulation of lymphocyte traffic, an essential step in the pathology of inflammation (Aarthi et al., 2011; Aoki et al., 2016). Several cytokines and chemokines, including TNF-α and interleukin 1-beta (IL1-β), activate SphK1 to produce S1P, which later induces cyclo-oxygenase 2 activity (Snider et al., 2010).

Collective evidence supports the relevance of S1P in retina inflammatory and vascular diseases. Abnormal retina blood vessel growth and macular edema are major complications leading to vision loss in diabetes retinopathy and S1P emerges as a key signal in the induction of neovascularization and in the preservation of retina endothelial barrier integrity (Allende and Proia, 2002; McGuire et al., 2011). In transgenic mice that overexpress SphK2, higher retinal S1P concentration accelerates retinal angiogenesis and increases neovascularization (Eresch et al., 2018). In turn, downregulation of S1P signaling with anti-S1P monoclonal antibodies and in S1P2 null mice in an ischemia-driven retinopathy markedly reduces pathologic neovascularization (Skoura et al., 2007; Caballero et al., 2009). RPE cells express the five S1PRs, and exogenous S1P induces the secretion of Interleukin-8 (IL-8); interestingly, supplementation with TNF-α enhances S1P3 expression, with a subsequent increase in S1P-induced IL-8 and IL-6 production (Zhu et al., 2010; Qiao et al., 2012). S1P also promotes the expression of vascular endothelial growth factor (VEGF) and hypoxia inducible factor-1α in RPE cells, which are crucial angiogenic factors (Terao et al., 2017). A significant increase in the expression of S1P1 and S1P lyase is detected in the vitreous of patients with proliferative diabetic retinopathy (Abu El-Asrar et al., 2014) whereas S1P signaling through S1P1/S1P3 promotes angiogenesis *in vitro*, participating in the changes affecting pericytes and endothelial cells (Durham et al., 2015). Hence, S1P signaling through S1PRs is a driving force in the onset and progression of inflammatory and angiogenic responses in retina inflammatory diseases (**Figure 3**).

S1P and Retinal Fibrosis

Fibrosis is a pathological process characterized by the deregulation of production and deposition of extracellular matrix components, leading to the destruction of normal tissue function and architecture (Wynn, 2007). Initiated by an acute injury or a vascular damage that leads to the recruitment of inflammatory cells, subsequent secretion of pro-inflammatory

cytokines, as tumor growth factor (TGF)-β, platelet derived growth factor (PDGF), connective tissue growth factor, IL-3 and also S1P conducts to the excessive production and deposition of extracellular matrix components (Kisseleva and Brenner, 2008). Although the initial damage promotes a physiological fibrotic response to accomplish tissue repair, the chronic exposure to irritation and/ or inflammation leads to the formation of a fibrotic scar that impairs functionality. Many reports establish the role of S1P in fibrotic disorders in lung (Kono et al., 2007; Milara et al., 2012), kidney (Geoffroy et al., 2005; Awad et al., 2011), liver (Davaille et al., 2002; Li et al., 2011; Liu et al., 2011) and heart (Gellings Lowe et al., 2009; Pchejetski et al., 2012). However, S1P involvement in retinal fibrosis is poorly understood.

Many retinal diseases, including AMD, diabetic retinopathy and proliferative vitreoretinopathy, have a common underlying etiology of pathological scar tissue production and the role of TGF-β and PDGF in the development of eye fibrosis is well-known (Connor et al., 1989; Gamulescu et al., 2006; Saika, 2006; Lei et al., 2007). Recent data indicate a crosstalk between S1P and TGF-β in human corneas and orbital connective tissues and suggest that S1P anti- or pro-fibrotic functions in the eye are tissue-specific (Ko et al., 2017; Nicholas et al., 2017).

The available evidence suggests that S1P is involved in retina fibrotic disorders. A monoclonal anti-S1P strategy reduces sub-retinal fibrosis in a mouse model of choroidal neovascularization and prevents the formation of excessive scarring after surgery in animal models of glaucoma (Caballero et al., 2009; Lukowski et al., 2013). Müller glial cells and RPE cells, the two main cell types that support normal retinal function, have protagonic roles in the development of retinal fibrosis (Saika et al., 2008; Bringmann and Wiedemann, 2009). S1P promotes proliferation, myofibroblast transformation, collagen production and pro-fibrotic protein expression in human RPE cells (Swaney et al., 2008). We have shown that S1P has a key role in the regulation of Müller glial cell motility; 5 μM S1P promotes the migration of cultured rat Müller glial cells through activation of S1P3 while inhibiting S1P synthesis using SphK inhibitor 2 (SphKI 2) completely blocks this migration (Simón et al., 2015). We have proposed that Müller glial cells release S1P, which signals through S1P3 and activates the PI3K and the ERK/MAPK pathway to enhance migration (Simón et al., 2015). Taking into account that the deregulation of glial migration is involved in proliferative retinopathies, the S1P/SphK1/S1P3 axis emerges as a key target for controlling these diseases.

The above findings position S1P as a real Jekill and Hyde in the retina. S1P is indispensable for establishing retina structure, regulating proliferation of retinal progenitors and their later laminar distribution in the retina (Miranda et al., 2009; Fang et al., 2018). It is also a pro-survival factor for neurons, promoting their differentiation, preserving normal functioning and granting neuroprotection (Crousillac et al., 2009; Miranda et al., 2009; Abrahan et al., 2010; Joly and Pernet, 2016; Porter et al., 2018). On the other hand, S1P unleashes threatening processes in Müller glial cells and RPE cells, such as secretion of pro- inflammatory cytokines, proliferation, migration and transdifferentiation that promote and/or enhance inflammation and fibrosis (Swaney et al., 2008; Qiao et al., 2012; Simón et al., 2015; Terao et al., 2017). Thus, S1P facilitates the formation of gliotic scars that alter retinal structure and enhance visual dysfunction instead of preventing it.

The central role of S1P in the regulation of the crucial cellular processes that are altered in retinal pathologies turns it into an exceptional therapeutic target for treating these diseases. In order to accomplish this goal, several questions remain to be answered. How to take advantage of S1P protective role on photoreceptors and simultaneously elude the potentially risks for visual function derived from its effects on glial and epithelial cells? The S1P concentration might provide a clue, since the concentration that protects photoreceptors is 5-fold lower than that enhancing glial migration; promoting a controlled intracellular synthesis of S1P and preventing its release might preclude S1P deleterious effects.

Whether S1P dual roles depend on the signaling pathways it activates in each cell type and whether they respond to the microenvironment and/ or the type of injury cells are exposed to are pending questions as well. An attractive hypothesis for the dual role of S1P in retina degeneration is its function as a DAMP, signals that are exposed or released from stressed cells and recognized by and mobilize the immune system. S1P and Cer have been proposed as DAMPs in cancer cells; treating squamous carcinoma cells by photodynamic therapy results in Cer and S1P increases on the cell surface and in S1P release, and both sphingolipids trigger NFκB signaling in macrophages in co-culture (Korbelik et al., 2014). The ubiquitous expression of S1PRs in macrophages supports this proposal (Fischer et al., 2007). Recent research has shown that apoptotic cells release exosome-like vesicles, the biogenesis of which depends on S1P/S1PRs signaling; these vesicles have S1P, S1P1, and S1P3 and induce genes of proinflammatory cytokines and chemokines (Park et al., 2018), highlighting a new pathway for S1P in the pathogenesis of inflammatory diseases. Microglia, as resident retinal macrophages, has a detrimental role and contributes to retinal degeneration; microglia release of harmful factors contributes to Müller glial cell reactivity in *rd10* mice (Peng et al., 2014; Zhao et al., 2015). DAMPs have dual roles in the retina; e.g., fractalkine, which has been reported as a DAMP, is neuroprotective in *rd10* retinas by signaling through its CX3CR1 receptor, preventing microglia-induced damage (Roche et al., 2016). Stressed photoreceptors release DAMPs early in degeneration to induce neuroprotective responses in retinal glial cells by interacting with receptors as Toll-like receptor 2, a DAMP receptor that increases in Müller glial cells during degeneration (Hooper et al., 2018). S1P promotes migration in Müller glial cells and RPE cells (Swaney et al., 2008; Simón et al., 2015), which might release it to the retina milieu to act as an autocrine signal and promote a fibrotic process and/or to act as a paracrine signal in photoreceptors, promoting neuroprotection. Whether S1P is a DAMP released by retinal cells to either promote inflammation or neuroprotection is an exciting question to be explored in the sphingolipid field.

Finding answers to these questions would provide crucial understanding of the puzzling behavior of S1P and new insight to design effective therapeutic for the treatment of retinopathies.

SEARCHING FOR CERAMIDE-1-PHOSPHATE FUNCTIONS IN THE RETINA

C1P Synthesis and Functions

Ceramide-1-phosphate is a later incorporation to the sphingolipid family, now established as a pleiotropic bioactive sphingolipid with multiple cellular roles. CerK was first identified in brain synaptic vesicles and shown to synthesize a molecule identified as C1P (Bajjalieh et al., 1989). C1P existence and its synthesis from Cer were then demonstrated in the human pro-myelocytic leukemia cell line HL-60 (Dressler et al., 1992). Cer phosphorylation by CerK is the only mechanism for C1P generation established in mammals, although the presence of a small pool of C1P in CerK-/CerK- mutants suggests an alternative biosynthetic mechanism must exist (Bornancin, 2011). C1P is synthesized in the *trans* Golgi and a specific C1P transfer protein transports it to the plasma membrane, where it can be released for autocrine or paracrine signaling (Lamour et al., 2007; Simanshu et al., 2013). CerK is present in the brain and brain synaptic vesicles (Bajjalieh et al., 1989; Bajjalieh and Batchelor, 2000; Hannun et al., 2001) whereas cerebellar granule cells generate C1P from newly synthesized Cer, formed through SM degradation and Sph recycling (Riboni et al., 2002).

First thought as an intermediate in the complex sphingolipid metabolism, C1P functions began to be unraveled when it was shown to promote proliferation, in fibroblasts and macrophages (Gomez-Muñoz et al., 1995, 1997; Gangoiti et al., 2008), myoblasts and cancer cells (Mitra et al., 2007; Gangoiti et al., 2008). C1P is now known to be antiapoptotic (Gómez-Muñoz et al., 2004; Granado et al., 2009), to promote cell migration in different cell types (Granado et al., 2009; Arana et al., 2012), and to regulate the production of TNF-α (Lamour et al., 2011). Although mostly known for its pro-inflammatory actions, both C1P and CerK have been shown to exert either pro- or anti-inflammatory actions depending on the cell type (Presa et al., 2016). C1P has been proposed to be relevant for cancer progression, promoting tumor cell survival, growth and migration (Mitra et al., 2007; Rivera et al., 2016).

Ceramide-1-phosphate is also an intracellular and an extracellular messenger. In most cases, it acts as an intracellular signal, but it can be released to the extracellular milieu in specific circumstances or upon cell damage (Boath et al., 2008; Kim et al., 2012; Schneider et al., 2013). The Gomez-Muñoz laboratory demonstrated that exogenous C1P stimulates migration of macrophages independently of intracellular C1P synthesis by activating a G-protein coupled membrane receptor for C1P, partially identified and different from S1PRs (Granado et al., 2009). In contrast, C1P mitogenic effect on macrophages depends on its action as an intracellular messenger, as C1P effect can be mimicked by a photolabile caged-C1P analog, which activates cPLA2, PKCα and NADPH oxidase, generating ROS that promote proliferation (Arana et al., 2012).

Ceramide-1-phosphate activates multiple signaling pathways. To enhance proliferation, C1P activates the PI3K and the ERK/MAPK pathways, Jun N terminal kinase (JNK), nuclear factor NF-κB (NF-κB) and glucogen synthase kinase 3 (GSK3) (Gangoiti et al., 2010). C1P promotes survival of macrophages in the absence of trophic factors by inhibiting caspases and blocking Cer synthesis (Gómez-Muñoz et al., 2004; Granado et al., 2009). Activation of PI3K, NF-κB, increases in Bcl-2, decreases in Bax levels and inhibition of caspases 9 and 3 also participate in its survival effects (Gómez-Muñoz et al., 2005; Gomez-Muñoz, 2018). The findings by the Chalfant laboratory that C1P is a direct activator of cPLA2 provided the link between this sphingolipid and inflammation (Pettus et al., 2004). C1P interacts with cPLA2, promoting its translocation and association to membranes, and its subsequent activation, producing inflammatory mediators such as eicosanoids (Lamour et al., 2009; Hoeferlin et al., 2013; Simanshu et al., 2013).

Mounting evidence points to different roles for C1P in the nervous system. A 5-fold increase in C1P levels in the subventricular zone in Huntington disease patients has been reported, with no associated changes in Cer levels; this increase might represent a response to the chronic brain damage in these patients and might either reflect an attempt at neuroprotection and enhanced neurogenesis or contribute to neuroinflammation and neurodegeneration (Hunter et al., 2018). C1P has neuroprotective effects in the nervous system. Upregulation of CerK by Peroxisome proliferator-activated receptors protects neurons and astrocytes against Cer-induced death (Aleshin and Reiser, 2014) and promotes survival of cochlear hair cells during ototoxicity (Tabuchi and Hara, 2018). C1P might also be involved in neurotransmitter release; C1P promotes dopamine release from PC12 cells (Jeon et al., 2005), which is consistent with the ability of C1P to promote phagolysosome formation and with CerK presence in synaptic vesicles (Bajjalieh et al., 1989; Hinkovska-Galcheva et al., 1998).

C1P in the Retina

Little is known regarding C1P and CerK roles in the eye (**Table 2**). Pioneer work from Acharya's group in *Drosophila* eye revealed an indirect effect of *Drosophila* ceramide kinase (DCerK) in phototransduction. DCerK is an integral membrane protein that phosphorylates Cer, thus decreasing its levels (Dasgupta et al., 2009). DCerK mutants show severe photoreceptor degeneration and do not respond to light. The absence of DCerK increases Cer levels, and leads to proteolysis of NORPA, a critical effector of phototransduction. The degradation of this phospholipase C homolog leads to a consequent loss of activity, and failure in light signal transduction (Dasgupta et al., 2009). Thus, modulation of Cer levels by DCerK is essential for phototransduction. Noteworthy, C1P is involved in light-dependent regulation of other enzymes of lipid metabolism, such as diacylglycerol lipase and lipid phosphatases, in photoreceptor rod OS (Pasquaré and Giusto, 2008; Pasquaré et al., 2008),

suggesting its role in phototransduction might also extend to the mammalian retina.

The finding that mutations in a CerKL gene are associated to a variant of autosomal recessive retinitis pigmentosa (Tuson et al., 2004), and to Cone-rod dystrophy (Littink et al., 2010; Birtel et al., 2018) brought huge expectations to the field, as it associated sphingolipid metabolism and retinal degeneration. CerKL has been further connected with retinitis pigmentosa in numerous studies (Auslender et al., 2007; Avila-Fernandez et al., 2008; Avela et al., 2018). However, the physiological functions of CerKL and its contribution to degeneration are still unclear. CerKL has no kinase activity neither on lipids nor on proteins in spite of having a diacylglycerol kinase domain (Tuson et al., 2004, 2009; Bornancin et al., 2005) and it interacts with several calcium sensor proteins in the retina (Nevet et al., 2012). A targeted deletion of CerKL in mouse leads to a mild retinal phenotype, with increased gliosis and mild functional alterations of the ganglion cell layer but no gross morphological alterations (Garanto et al., 2012). In contrast, CerKL knockdown causes retinal degeneration in zebrafish, with failure in the development of photoreceptor OS and increased apoptosis (Riera et al., 2013). CerKL might have antioxidant functions in the retina. Its overexpression protects retinal cells from oxidative stress-induced death, whereas its downregulation renders cells sensitive to this damage; CerKL deficiency causes zebrafish retinal degeneration and photoreceptor apoptosis through increased oxidative damage (Tuson et al., 2009; Li et al., 2014). CerKL is prominently localized in RPE cells, ganglion cells, inner nuclear layer and photoreceptor inner segments and its expression increases in light-stressed retinas (Mandal et al., 2013). An alteration in OS phagocytosis in a zebrafish CerKL knockout suggests a role for CerKL in RPE cell phagocytosis, leading to rod-cone dystrophy (Yu et al., 2017). Recent miRNA analysis of RPE cells exposed to oxidative stress shows that CerKL is a target of five altered miRNA (Donato et al., 2018). Existing evidence thus points to a role for CerKL in retina protection from oxidative stress-induced damage, and not related to Cer phosphorylation.

Ceramide kinase is ubiquitously and highly expressed in the retina (Mandal et al., 2013). CerK^{-}/− retinas show decreased C1P and increased Cer; on the contrary, CerKL−/− retinas have normal C1P and Cer levels, supporting CerK as the major and probably unique responsible for C1P synthesis in the retina (Graf et al., 2008). RPE cells express CerK, among other enzymes involved in sphingolipid metabolism (Zhu et al., 2010) and no C1P is detected in these cells in CerK^{-}/− retinas (Graf et al., 2008). Our group has shown that exogenous C1P promotes the proliferation of cultured photoreceptor progenitors and advances their differentiation as photoreceptors, enhancing the expression of opsin and peripherin and promoting the formation of rudimentary OS (Miranda et al., 2011). Notably, overexpression of CerK inhibits all-trans retinoic acid (ATRA)-induced differentiation of a human neuroblastoma cell line, SH-SY5Y (Murakami et al., 2010), suggesting that the effect of C1P on differentiation might be cell or context dependent. C1P also stimulates the survival of cultured photoreceptors, preventing their degeneration; this protection involves the preservation of mitochondrial potential, suggesting that C1P activates pathways upstream of mitochondrial depolarization (Miranda et al., 2011). Consistently, whereas a pan-caspase inhibitor decreases photoreceptor death in controls, it promotes no further reduction in photoreceptor death in C1P-supplemented cultures, suggesting C1P might prevent caspase activation (Miranda et al., 2011). Inhibiting the *de novo* synthesis of Cer prevents photoreceptor cell death in culture (German et al., 2006). Since C1P prevents macrophage apoptosis by impeding Cer accumulation, either by inhibiting its *de novo* synthesis or acid SMase activity (Gómez-Muñoz et al., 2004; Granado et al., 2009), C1P might also block Cer synthesis in photoreceptors, thus promoting their survival (**Figures 3**, **4**).

Higher levels of C12-, C16- and C24-C1P, and of C16- and C18-Cer have been found in retinas in a rat model of endotoxin-induced uveitis, together with increases in TNF-α and IL-6 levels, suggesting these sphingolipids might participate in the inflammation process (Wang and Bieberich, 2018). Ongoing work in our laboratory suggests that C1P might promote the migration of retina Müller glial cells *in vitro*, which, together with glial proliferation, contributes to the progression of proliferative retinopathies (Vera et al., unpublished data).

Ceramide-1-phosphate functions in the retina are just starting to be uncovered. Existing evidence points to a crucial role of C1P in photoreceptor functionality, promoting their proliferation, survival and advancing differentiation. It might also be involved in modulation of phototransduction. Its contribution to inflammatory and proliferative pathologies of the retina has to be further explored.

DIHYDROCERAMIDE, A NEWCOMER PLAYER IN RETINA CELL DEATH?

Dihydroceramide, the immediate precursor of Cer in the *de novo* synthetic pathway, had long been considered as an inactive sphingolipid, since its exogenous addition had little effect on cell death (Ahn and Schroeder, 2010). However, cumulative evidence during the last decade supports a signaling role for endogenous DHCer and for other dihydrosphingolipids as well. Its accumulation has been implicated in autophagy regulation. Noteworthy, DHCer increase has been shown to induce cytotoxic autophagy in cancer cells and an impairment of autophagic flux and increase in fibrosis markers in liver cells (Hernández-Tiedra et al., 2016; Lee et al., 2017). DHCer also triggers cell cycle arrest and cell death (reviewed in Siddique et al., 2015). Therefore, it is now thought that DHCer is the principal Cer-mediated autophagy regulator (Siddique et al., 2015; Hannun and Obeid, 2018).

In the eye, early work showed distinct effects between Cer and DHCer. Cer induces cell death in cultured rat photoreceptors and amacrine neurons, in human RPE cells, in human corneal stromal fibroblasts and in lens epithelial cells, whereas addition of DHCer has no deleterious effect in these cell types (Barak et al., 2001; German et al., 2006; Samadi, 2007; Rizvi et al., 2011). However, recent evidence suggests a noxious role for

DHCer in the eye. DHCer content increases during aging in human lens and might be related to changes in the permeability barrier properties (Deeley et al., 2010). Both Cer and DHCer content increase in light-induced photoreceptor degeneration in albino rats, and preventing these increases protects retinal function and structure (Chen et al., 2013; Huang et al., 2014). DHCer desaturase catalyzes the conversion of DHCer to Cer and its modulation is crucial for the signaling pathways regulated by both sphingolipids. Loss of DHCer desaturase in *Drosophila* eye leads to DHCer accumulation, increased ROS production and loss of photoreceptor functionality and viability; in turn, blocking DHCer synthesis preserves their viability (Jung et al., 2017). Further work will establish whether DHCer is a member of the club of deadly sphingolipid messengers and whether it contributes to retinal pathologies.

Unraveling the Sphingolipid Network in the Retina

Sphingolipids emerge as crucial mediators in the activation of numerous pathways that might either activate neuroprotective mechanisms or whose dysregulation might lead to retina dysfunction. Cer stands out as a key messenger in the onset of degeneration in photoreceptors induced by oxidative stress and in numerous models of retina neurodegeneration; its increase through *de novo* synthesis or by SM breakdown activates different downstream pathways leading to cell death. Cer buildup, due to an activation or increased expression of SMases is also crucial in the onset of RPE cell death and inflammation. Preventing Cer increase through the inhibition or modulation of different enzymes of its intricate metabolism has been shown to effectively prevent photoreceptor and RPE cell death, both *in vivo* and *in vitro*, and preserve visual function. These findings underscore both the relevance of imbalances in Cer levels as inducers of RPE and photoreceptor cell death and the significance of modulation of the sphingolipid metabolism as a therapeutic strategy for the treatment of retina neurodegenerations. Having an integral picture of the functions of Cer in the retina and of the effects of preventing its accretion demands establishing the processes regulated by Cer in glial cells and its potential role in their gliotic response. Several questions remain to be answered in order to accomplish the fine tuning of the highly interconnected sphingolipid metabolism, which is crucial for the development of new treatments for retinal pathologies. The complexity of this metabolism makes its modulation a powerful approach for preserving vision function but might also be an Achilles' heel, jeopardizing strategies based on the inhibition of one of the metabolic pathways leading to Cer synthesis. Being Cer the central molecule in sphingolipid metabolism, the effects of blocking a single pathway established as crucial in generating Cer accumulation in a particular pathological circumstance should be explored. This inhibition might efficiently reduce cell death but impair other key, Cer-dependent, retinal processes or affect them indirectly, through the increase in bioactive sphingolipid metabolites. As blocking a certain biosynthetic pathway for Cer has been shown to provide a transient protection, it is critical to explore whether altering the flux through the network activates alternative Cer biosynthetic pathways and/or leads to the accumulation of bioactive sphingolipids, such as Sph or DHCer, which might trigger cell death. Further research aimed at understanding these balances and connections in a comprehensive molecular way might contribute to devising successful treatments based in new or already established drugs or suggest the necessity of combining different drugs in order to simultaneously modulate these metabolic processes.

Modulation of the sphingolipid rheostat might provide clues for preventing the death of photoreceptors (**Figure 4**). Nevertheless, S1P functions remain enigmatic. S1P, either exogenous or generated intracellularly, promotes survival of these cells; notably, photoreceptor trophic factors enhance S1P synthesis to exert their functions. A pending question is determining whether increasing S1P intracellular levels, either by promoting its synthesis and/or or blocking its degradation can prevent degeneration of photoreceptors and preserve their functionality in diseased retinas. Even if this is the case, taking advantage of S1P neuroprotective effect on photoreceptors still requires uncovering the clues to prevent or overcome S1P deleterious effects on other retinal cells, as glial, epithelial and endothelial cells, that may turn on fibrosis, neovascularization and inflammation. Similarly, the actions of S1P and Cer are critical for the pathogeneses of proliferative diseases, such as diabetic retinopathy and AMD. Both sphingolipids drive forward the crucial events leading to the progression of these diseases, with S1P inducing fibrosis and pro-inflammatory changes and Cer triggering cell death. Given the cross-conversions of sphingolipids, it is necessary to find out how to simultaneously balance their levels to avoid the onset of lethal processes in the retina. As stated above, this requires unraveling the intricate network of metabolic and signaling pathways to obtain the cues for refining the adjustment of the sphingolipid network. At least part of these cues might lie in the differential cellular expression of S1PRs and/or the molecular pathways activated by S1P. Uncovering the myriad of potential combinations of S1PRs and downstream signaling pathways, either activatory or inhibitory, might explain the variety of the responses triggered by S1P in different retinal cell types. In order to make use of the S1P axis as a tool for the treatment of retinal diseases, the precise mechanisms by which S1P achieves its effects should be clarified. Current evidence suggests that the expression pattern of S1PRs in the retina is modified in particular pathologies. Further studies are now required to establish whether photoreceptors, glial and epithelial cells differ in their S1PR expression pattern, and if and how are these patterns differentially modulated in each cell type by the environmental context, i.e., healthy or diseased retina and by extracellular cues, such as starvation, light damage, or oxidative stress. In addition, it is essential to understand the roles of S1P, and also establish those of C1P, in controlling neovascularization and fibrotic changes and whether they exhibit pro or anti-inflammatory actions in different pathological environments. Advancing our understanding of the multiple roles of sphingolipids and of the fine detail and regulation of their complex metabolic network will contribute to achieve much-needed therapies for retina pathologies.

AUTHOR CONTRIBUTIONS

MS wrote and edited the manuscript and contributed to the design of the figures. FPS wrote and edited the manuscript and contributed to the design of the figures. MV wrote the manuscript. NR designed the manuscript and figures and wrote and edited the manuscript.

FUNDING

Funding from the National Agency for Science and Technology (ANPCYT) (PICT-2015-0284 to NR); National Research Council of Argentina (CONICET) (PIP 11220-1101–00827, to NR); and PGI 24/B254 from the Secretary of Science and Technology, Universidad Nacional del Sur (to NR).

ACKNOWLEDGMENTS

NR is a principal researcher from the National Research Council of Argentina (CONICET), and Professor of Biological Chemistry from the Universidad Nacional del Sur (UNS). MS is an Assistant Researcher from CONICET and a Teaching Assistant from UNS. FPS is a Teaching Assistant from UNS and MV is a CONICET Doctoral Research fellow.

REFERENCES

Aarthi, J. J., Darendeliler, M. A., and Pushparaj, P. N. (2011). Dissecting the role of the S1P/S1PR axis in health and disease. *J. Dent. Res.* 90, 841–854. doi: 10.1177/0022034510389178

Abrahan, C. E., Miranda, G. E., Agnolazza, D. L., Politi, L. E., and Rotstein, N. P. (2010). Synthesis of sphingosine is essential for oxidative stress-induced apoptosis of photoreceptors. *Invest. Ophthalmol. Vis. Sci.* 51, 1171–1180. doi: 10.1167/iovs.09-3909

Abu El-Asrar, A. M., Nawaz, M. I., Mohammad, G., Siddiquei, M. M., Alam, K., Mousa, A., et al. (2014). Expression of bioactive lysophospholipids and processing enzymes in the vitreous from patients with proliferative diabetic retinopathy. *Lipids Health Dis.* 13:187. doi: 10.1186/1476-511X-13-187

Acharya, J. K., Dasgupta, U., Rawat, S. S., Yuan, C., Sanxaridis, P. D., Yonamine, I., et al. (2008). Cell-nonautonomous function of ceramidase in photoreceptor homeostasis. *Neuron* 57, 69–79. doi: 10.1016/j.neuron.2007.10.041

Acharya, U., Patel, S., Koundakjian, E., Nagashima, K., Han, X., and Acharya, J. K. (2003). Modulating sphingolipid biosynthetic pathway rescues photoreceptor degeneration. *Science* 299, 1740–1743. doi: 10.1126/science.1080549

Agudo-Barriuso, M., Lahoz, A., Nadal-Nicolás, F. M., Sobrado-Calvo, P., Piquer-Gil, M., Díaz-Llopis, M., et al. (2013). Metabolomic changes in the rat retina after optic nerve crush. *Invest. Ophthalmol. Vis. Sci.* 54, 4249–4259. doi: 10.1167/iovs.12-11451

Ahn, E. H., and Schroeder, J. J. (2010). Induction of apoptosis by sphingosine, sphinganine, and C(2)-ceramide in human colon cancer cells, but not by C(2)-dihydroceramide. *Anticancer Res.* 30, 2881–2884.

Aleshin, S., and Reiser, G. (2014). Peroxisome proliferator-activated receptor β/δ (PPARβ/δ) protects against ceramide-induced cellular toxicity in rat brain astrocytes and neurons by activation of ceramide kinase. *Mol. Cell. Neurosci.* 59, 127–134. doi: 10.1016/j.mcn.2014.01.008

Allende, M. L., and Proia, R. L. (2002). Sphingosine-1-phosphate receptors and the development of the vascular system. *Biochim. Biophys. Acta* 1582, 222–227. doi: 10.1016/s1388-1981(02)00175-0

Al-Zamil, W., and Yassin, S. (2017). Recent developments in age-related macular degeneration: a review. *Clin. Interv. Aging* 12, 1313–1330. doi: 10.2147/CIA.S143508

Aoki, M., Aoki, H., Ramanathan, R., Hait, N. C., and Takabe, K. (2016). Sphingosine-1-phosphate signaling in immune cells and inflammation: roles and therapeutic potential. *Mediators Inflamm.* 2016:8606878. doi: 10.1155/2016/8606878

Arana, L., Gangoiti, P., Ouro, A., Rivera, I.-G., Ordoñez, M., Trueba, M., et al. (2012). Generation of reactive oxygen species (ROS) is a key factor for stimulation of macrophage proliferation by ceramide 1-phosphate. *Exp. Cell Res.* 318, 350–360. doi: 10.1016/j.yexcr.2011.11.013

Arango-Gonzalez, B., Trifunović, D., Sahaboglu, A., Kranz, K., Michalakis, S., Farinelli, P., et al. (2014). Identification of a common non-apoptotic cell death mechanism in hereditary retinal degeneration. *PLoS One* 9:e112142. doi: 10.1371/journal.pone.0112142

Auslender, N., Sharon, D., Abbasi, A. H., Garzozi, H. J., Banin, E., and Ben-Yosef, T. (2007). A common founder mutation of CERKL underlies autosomal recessive retinal degeneration with early macular involvement among Yemenite Jews. *Invest. Ophthalmol. Vis. Sci.* 48, 5431–5438. doi: 10.1167/iovs.07-0736

Avela, K., Sankila, E.-M., Seitsonen, S., Kuuluvainen, L., Barton, S., Gillies, S., et al. (2018). A founder mutation in CERKL is a major cause of retinal dystrophy in Finland. *Acta Ophthalmol.* 96, 183–191. doi: 10.1111/aos.13551

Aveldaño, M. I., and Sprecher, H. (1987). Very long chain (C24 to C36) polyenoic fatty acids of the n-3 and n-6 series in dipolyunsaturated phosphatidylcholines from bovine retina. *J. Biol. Chem.* 262, 1180–1186.

Avila-Fernandez, A., Riveiro-Alvarez, R., Vallespin, E., Wilke, R., Tapias, I., Cantalapiedra, D., et al. (2008). CERKL mutations and associated phenotypes in seven Spanish families with autosomal recessive retinitis pigmentosa. *Invest. Ophthalmol. Vis. Sci.* 49, 2709–2713. doi: 10.1167/iovs.07-0865

Awad, A. S., Rouse, M. D., Khutsishvili, K., Huang, L., Bolton, W. K., Lynch, K. R., et al. (2011). Chronic sphingosine 1-phosphate 1 receptor activation attenuates early-stage diabetic nephropathy independent of lymphocytes. *Kidney Int.* 79, 1090–1098. doi: 10.1038/ki.2010.544

Bajjalieh, S., and Batchelor, R. (2000). Ceramide kinase. *Methods Enzymol.* 311, 207–215.

Bajjalieh, S. M., Martin, T. F., and Floor, E. (1989). Synaptic vesicle ceramide kinase. A calcium-stimulated lipid kinase that co-purifies with brain synaptic vesicles. *J. Biol. Chem.* 264, 14354–14360.

Bandhuvula, P., and Saba, J. D. (2007). Sphingosine-1-phosphate lyase in immunity and cancer: silencing the siren. *Trends Mol. Med.* 13, 210–217. doi: 10.1016/j.molmed.2007.03.005

Barak, A., Goldkorn, T., and Morse, L. S. (2005). Laser induces apoptosis and ceramide production in human retinal pigment epithelial cells. *Investig. Opthalmol. Vis. Sci.* 46, 2587. doi: 10.1167/iovs.04-0920

Barak, A., Morse, L. S., and Goldkorn, T. (2001). Ceramide: a potential mediator of apoptosis in human retinal pigment epithelial cells. *Invest. Ophthalmol. Vis. Sci.* 42, 247–254.

Bartke, N., and Hannun, Y. A. (2009). Bioactive sphingolipids: metabolism and function. *J. Lipid Res.* 50, S91–S96. doi: 10.1194/jlr.R800080-JLR200

Bazan, N. G. (2018). Docosanoids and elovanoids from omega-3 fatty acids are pro-homeostatic modulators of inflammatory responses, cell damage and neuroprotection. *Mol. Aspects Med.* 64, 18–33. doi: 10.1016/j.mam.2018.09.003

Berdyshev, E. V., Gorshkova, I., Skobeleva, A., Bittman, R., Lu, X., Dudek, S. M., et al. (2009). FTY720 inhibits ceramide synthases and up-regulates dihydrosphingosine 1-phosphate formation in human lung endothelial cells. *J. Biol. Chem.* 284, 5467–5477. doi: 10.1074/jbc.M805186200

Bian, G., Yu, C., Liu, L., Fang, C., Chen, K., Ren, P., et al. (2018). Sphingosine 1-phosphate stimulates eyelid closure in the developing rat by stimulating EGFR signaling. *Sci. Signal.* 11:eaat1470. doi: 10.1126/scisignal.aat1470

Birtel, J., Eisenberger, T., Gliem, M., Müller, P. L., Herrmann, P., Betz, C., et al. (2018). Clinical and genetic characteristics of 251 consecutive patients with macular and cone/cone-rod dystrophy. *Sci. Rep.* 8:4824. doi: 10.1038/s41598-018-22096-0

Boath, A., Graf, C., Lidome, E., Ullrich, T., Nussbaumer, P., and Bornancin, F. (2008). Regulation and traffic of ceramide 1-phosphate produced by ceramide kinase: comparative analysis to glucosylceramide and sphingomyelin. *J. Biol. Chem.* 283, 8517–8526. doi: 10.1074/jbc.M707107200

Bode, H., Bourquin, F., Suriyanarayanan, S., Wei, Y., Alecu, I., Othman, A., et al. (2016). HSAN1 mutations in serine palmitoyltransferase reveal a close structure-function-phenotype relationship. *Hum. Mol. Genet.* 25, 853–865. doi: 10.1093/hmg/ddv611

Bornancin, F. (2011). Ceramide kinase: the first decade. *Cell. Signal.* 23, 999–1008. doi: 10.1016/j.cellsig.2010.11.012

Bornancin, F., Mechtcheriakova, D., Stora, S., Graf, C., Wlachos, A., Dévay, P., et al. (2005). Characterization of a ceramide kinase-like protein. *Biochim. Biophys. Acta* 1687, 31–43. doi: 10.1016/j.bbalip.2004.11.012

Bringmann, A., and Wiedemann, P. (2009). Involvement of Müller glial cells in epiretinal membrane formation. *Graefes Arch. Clin. Exp. Ophthalmol.* 247, 865–883. doi: 10.1007/s00417-009-1082-x

Brinkmann, V., Billich, A., Baumruker, T., Heining, P., Schmouder, R., Francis, G., et al. (2010). Fingolimod (FTY720): discovery and development of an oral drug to treat multiple sclerosis. *Nat. Rev. Drug Discov.* 9, 883–897. doi: 10.1038/nrd3248

Brownstein, S., Carpenter, S., Polomeno, R. C., and Little, J. M. (1980). Sandhoff's disease (GM2 gangliosidosis type 2). Histopathology and ultrastructure of the eye. *Arch. Ophthalmol.* 98, 1089–1097.

Brownstein, S., Meagher-Villemure, K., Polomeno, R. C., and Little, J. M. (1978). Optic nerve in globoid leukodystrophy (Krabbe's disease). Ultrastructural changes. *Arch. Ophthalmol.* 96, 864–870.

Brush, R. S., Tran, J.-T. A., Henry, K. R., McClellan, M. E., Elliott, M. H., and Mandal, M. N. A. (2010). Retinal sphingolipids and their very-long-chain fatty acid–containing species. *Investig. Opthalmol. Vis. Sci.* 51, 4422. doi: 10.1167/iovs.09-5134

Busik, J. V., Esselman, W. J., and Reid, G. E. (2012). Examining the role of lipid mediators in diabetic retinopathy. *Clin. Lipidol.* 7, 661–675. doi: 10.2217/clp.12.68

Caballero, S., Swaney, J., Moreno, K., Afzal, A., Kielczewski, J., Stoller, G., et al. (2009). Anti-sphingosine-1-phosphate monoclonal antibodies inhibit angiogenesis and sub-retinal fibrosis in a murine model of laser-induced choroidal neovascularization. *Exp. Eye Res.* 88, 367–377. doi: 10.1016/j.exer.2008.07.012

Canals, D., Salamone, S., and Hannun, Y. A. (2018). Visualizing bioactive ceramides. *Chem. Phys. Lipids* 216, 142–151. doi: 10.1016/j.chemphyslip.2018.09.013

Castro, B. M., Prieto, M., and Silva, L. C. (2014). Ceramide: a simple sphingolipid with unique biophysical properties. *Prog. Lipid Res.* 54, 53–67. doi: 10.1016/j.plipres.2014.01.004

Chakravarthy, H., Navitskaya, S., O'Reilly, S., Gallimore, J., Mize, H., Beli, E., et al. (2016). Role of acid sphingomyelinase in shifting the balance between proinflammatory and reparative bone marrow cells in diabetic retinopathy. *Stem Cells* 34, 972–983. doi: 10.1002/stem.2259

Chalfant, C. E., Kishikawa, K., Mumby, M. C., Kamibayashi, C., Bielawska, A., and Hannun, Y. A. (1999). Long chain ceramides activate protein phosphatase-1 and protein phosphatase-2A. *J. Biol. Chem.* 274, 20313–20317. doi: 10.1074/jbc.274.29.20313

Chang, G. Q., Hao, Y., and Wong, F. (1993). Apoptosis: final common pathway of photoreceptor death in rd, rds, and rhodopsin mutant mice. *Neuron* 11, 595–605. doi: 10.1016/0896-6273(93)90072-y

Chaurasia, B., and Summers, S. A. (2015). Ceramides – lipotoxic inducers of metabolic disorders. *Trends Endocrinol. Metab.* 26, 538–550. doi: 10.1016/j.tem.2015.07.006

Chen, H., Chan, A. Y., Stone, D. U., and Mandal, N. A. (2014). Beyond the cherry-red spot: Ocular manifestations of sphingolipid-mediated neurodegenerative and inflammatory disorders. *Surv. Ophthalmol.* 59, 64–76. doi: 10.1016/j.survophthal.2013.02.005

Chen, H., Tran, J.-T. A., Eckerd, A., Huynh, T.-P., Elliott, M. H., Brush, R. S., et al. (2013). Inhibition of de novo ceramide biosynthesis by FTY720 protects rat retina from light-induced degeneration. *J. Lipid Res.* 54, 1616–1629. doi: 10.1194/jlr.M035048

Choi, J. W., Gardell, S. E., Herr, D. R., Rivera, R., Lee, C.-W., Noguchi, K., et al. (2011). FTY720 (fingolimod) efficacy in an animal model of multiple sclerosis requires astrocyte sphingosine 1-phosphate receptor 1 (S1P1) modulation. *Proc. Natl. Acad. Sci. U.S.A.* 108, 751–756. doi: 10.1073/pnas.1014154108

Chun, J., and Hartung, H.-P. (2010). Mechanism of action of oral fingolimod (FTY720) in multiple sclerosis. *Clin. Neuropharmacol.* 33, 91–101. doi: 10.1097/WNF.0b013e3181cbf825

Connor, T. B., Roberts, A. B., Sporn, M. B., Danielpour, D., Dart, L. L., Michels, R. G., et al. (1989). Correlation of fibrosis and transforming growth factor-beta type 2 levels in the eye. *J. Clin. Invest.* 83, 1661–1666. doi: 10.1172/JCI114065

Crousillac, S., Colonna, J., McMains, E., Dewey, J. S., and Gleason, E. (2009). Sphingosine-1-phosphate elicits receptor-dependent calcium signaling in retinal amacrine cells. *J. Neurophysiol.* 102, 3295–3309. doi: 10.1152/jn.00119.2009

Cuvillier, O. (2002). Sphingosine in apoptosis signaling. *Biochim. Biophys. Acta* 1585, 153–162. doi: 10.1016/s1388-1981(02)00336-0

Cuvillier, O., Edsall, L., and Spiegel, S. (2000). Involvement of sphingosine in mitochondria-dependent Fas-induced apoptosis of type II Jurkat T cells. *J. Biol. Chem.* 275, 15691–15700. doi: 10.1074/jbc.M000280200

Cuvillier, O., Nava, V. E., Murthy, S. K., Edsall, L. C., Levade, T., Milstien, S., et al. (2001). Sphingosine generation, cytochrome c release, and activation of caspase-7 in doxorubicin-induced apoptosis of MCF7 breast adenocarcinoma cells. *Cell Death Differ.* 8, 162–171. doi: 10.1038/sj.cdd.4400793

Cuvillier, O., Pirianov, G., Kleuser, B., Vanek, P. G., Cosot, O. A., Gutkind, J. S., et al. (1996). Suppression of ceramide-mediated programmed cell death by sphingosine- 1-phosphate. *Nature* 381, 800–803. doi: 10.1038/381800a0

Cyster, J. G., and Schwab, S. R. (2012). Sphingosine-1-phosphate and lymphocyte egress from lymphoid organs. *Annu. Rev. Immunol.* 30, 69–94. doi: 10.1146/annurev-immunol-020711-075011

Czubowicz, K., and Strosznajder, R. (2014). Ceramide in the molecular mechanisms of neuronal cell death. The role of sphingosine-1-phosphate. *Mol. Neurobiol.* 50, 26–37. doi: 10.1007/s12035-013-8606-4

Dany, M., and Ogretmen, B. (2015). Ceramide induced mitophagy and tumor suppression. *Biochim. Biophys. Acta* 1853, 2834–2845. doi: 10.1016/j.bbamcr.2014.12.039

Dasgupta, U., Bamba, T., Chiantia, S., Karim, P., Tayoun, A. N. A., Yonamine, I., et al. (2009). Ceramide kinase regulates phospholipase C and phosphatidylinositol 4, 5, bisphosphate in phototransduction. *Proc. Natl. Acad. Sci. U.S.A.* 106, 20063–20068. doi: 10.1073/pnas.0911028106

Davaille, J., Li, L., Mallat, A., and Lotersztajn, S. (2002). Sphingosine 1-phosphate triggers both apoptotic and survival signals for human hepatic myofibroblasts. *J. Biol. Chem.* 277, 37323–37330. doi: 10.1074/jbc.M202798200

David, K. K., Andrabi, S. A., Dawson, T. M., and Dawson, V. L. (2009). Parthanatos, a messenger of death. *Front. Biosci.* 14, 1116–1128.

Deeley, J. M., Hankin, J. A., Friedrich, M. G., Murphy, R. C., Truscott, R. J. W., Mitchell, T. W., et al. (2010). Sphingolipid distribution changes with age in the human lens. *J. Lipid Res.* 51, 2753–2760. doi: 10.1194/jlr.M007716

Donato, L., Bramanti, P., Scimone, C., Rinaldi, C., D'Angelo, R., and Sidoti, A. (2018). miRNAexpression profile of retinal pigment epithelial cells under oxidative stress conditions. *FEBS Open Biol.* 8, 219–233. doi: 10.1002/2211-5463.12360

Dressler, K. A., Mathias, S., and Kolesnick, R. N. (1992). Tumor necrosis factor-alpha activates the sphingomyelin signal transduction pathway in a cell-free system. *Science* 255, 1715–1718. doi: 10.1126/science.1313189

Durham, J. T., Dulmovits, B. M., Cronk, S. M., Sheets, A. R., and Herman, I. M. (2015). Pericyte chemomechanics and the angiogenic switch: insights into the pathogenesis of proliferative diabetic retinopathy? *Invest. Ophthalmol. Vis. Sci.* 56, 3441–3459. doi: 10.1167/iovs.14-13945

Eresch, J., Stumpf, M., Koch, A., Vutukuri, R., Ferreirós, N., Schreiber, Y., et al. (2018). Sphingosine kinase 2 modulates retinal neovascularization in the mouse model of oxygen-induced retinopathy. *Invest. Ophthalmol. Vis. Sci.* 59, 653–661. doi: 10.1167/iovs.17-22544

Fabiani, C., Zulueta, A., Bonezzi, F., Casas, J., Ghidoni, R., Signorelli, P., et al. (2017). 2-Acetyl-5-tetrahydroxybutyl imidazole (THI) protects 661W cells against oxidative stress. *Naunyn. Schmiedebergs Arch. Pharmacol.* 390, 741–751. doi: 10.1007/s00210-017-1374-3

Fahy, E., Subramaniam, S., Brown, H. A., Glass, C. K., Merrill, A. H., Murphy, R. C., et al. (2005). A comprehensive classification system for lipids. *J. Lipid Res.* 46, 839–862. doi: 10.1194/jlr.E400004-JLR200

Fan, J., Wu, B. X., and Crosson, C. E. (2016). Suppression of acid sphingomyelinase protects the retina from ischemic injury. *Investig. Opthalmol. Vis. Sci.* 57, 4476. doi: 10.1167/iovs.16-19717

Fang, C., Bian, G., Ren, P., Xiang, J., Song, J., Yu, C., et al. (2018). S1p transporter spns2 regulates proper postnatal retinal morphogenesis. *FASEB J.* 32, 3597–3613. doi: 10.1096/fj.201701116R

Fischer, H., Ellström, P., Ekström, K., Gustafsson, L., Gustafsson, M., and Svanborg, C. (2007). Ceramide as a TLR4 agonist; a putative signalling intermediate between sphingolipid receptors for microbial ligands and TLR4. *Cell. Microbiol.* 9, 1239–1251. doi: 10.1111/j.1462-5822.2006.00867.x

Fliesler, S. J., and Bretillon, L. (2010). The ins and outs of cholesterol in the vertebrate retina. *J. Lipid Res.* 51, 3399–3413. doi: 10.1194/jlr.R010538

Fox, T. E., Han, X., Kelly, S., Merrill, A. H., Martin, R. E., Anderson, R. E., et al. (2006). Diabetes alters sphingolipid metabolism in the retina: a potential mechanism of cell death in diabetic retinopathy. *Diabetes* 55, 3573–3580. doi: 10.2337/db06-0539

Friedman, J. S., Chang, B., Krauth, D. S., Lopez, I., Waseem, N. H., Hurd, R. E., et al. (2010). Loss of lysophosphatidylcholine acyltransferase 1 leads to photoreceptor degeneration in rd11 mice. *Proc. Natl. Acad. Sci. U.S.A.* 107, 15523–15528. doi: 10.1073/pnas.1002897107

Galadari, S., Rahman, A., Pallichankandy, S., and Thayyullathil, F. (2015). Tumor suppressive functions of ceramide: evidence and mechanisms. *Apoptosis* 20, 689–711. doi: 10.1007/s10495-015-1109-1

Gamulescu, M.-A., Chen, Y., He, S., Spee, C., Jin, M., Ryan, S. J., et al. (2006). Transforming growth factor beta2-induced myofibroblastic differentiation of human retinal pigment epithelial cells: regulation by extracellular matrix proteins and hepatocyte growth factor. *Exp. Eye Res.* 83, 212–222. doi: 10.1016/j.exer.2005.12.007

Ganesan, V., Perera, M. N., Colombini, D., Datskovskiy, D., Chadha, K., and Colombini, M. (2010). Ceramide and activated Bax act synergistically to permeabilize the mitochondrial outer membrane. *Apoptosis* 15, 553–562. doi: 10.1007/s10495-009-0449-0

Gangoiti, P., Granado, M. H., Arana, L., Ouro, A., and Gomez-Muñoz, A. (2010). Activation of protein kinase C-α is essential for stimulation of cell proliferation by ceramide 1-phosphate. *FEBS Lett.* 584, 517–524. doi: 10.1016/j.febslet.2009.11.086

Gangoiti, P., Granado, M. H., Wang, S. W., Kong, J. Y., Steinbrecher, U. P., and Gómez-Muñoz, A. (2008). Ceramide 1-phosphate stimulates macrophage proliferation through activation of the PI3-kinase/PKB, JNK and ERK1/2 pathways. *Cell. Signal.* 20, 726–736. doi: 10.1016/j.cellsig.2007.12.008

Garanto, A., Vicente-Tejedor, J., Riera, M., de la Villa, P., Gonzàlez-Duarte, R., Blanco, R., et al. (2012). Targeted knockdown of Cerkl, a retinal dystrophy gene, causes mild affectation of the retinal ganglion cell layer. *Biochim. Biophys. Acta* 1822, 1258–1269. doi: 10.1016/j.bbadis.2012.04.004

García-Ruiz, C., Colell, A., Marí, M., Morales, A., and Fernández-Checa, J. C. (1997). Direct effect of ceramide on the mitochondrial electron transport chain leads to generation of reactive oxygen species. Role of mitochondrial glutathione. *J. Biol. Chem.* 272, 11369–11377. doi: 10.1074/jbc.272.17.11369

Gellings Lowe, N., Swaney, J. S., Moreno, K. M., and Sabbadini, R. A. (2009). Sphingosine-1-phosphate and sphingosine kinase are critical for transforming growth factor-beta-stimulated collagen production by cardiac fibroblasts. *Cardiovasc. Res.* 82, 303–312. doi: 10.1093/cvr/cvp056

Geoffroy, K., Troncy, L., Wiernsperger, N., Lagarde, M., and El Bawab, S. (2005). Glomerular proliferation during early stages of diabetic nephropathy is associated with local increase of sphingosine-1-phosphate levels. *FEBS Lett.* 579, 1249–1254. doi: 10.1016/j.febslet.2004.12.094

German, O. L., Miranda, G. E., Abrahan, C. E., and Rotstein, N. P. (2006). Ceramide is a mediator of apoptosis in retina photoreceptors. *Invest. Ophthalmol. Vis. Sci.* 47, 1658–1668. doi: 10.1167/iovs.05-1310

Gomez-Muñoz, A. (2018). "The role of ceramide 1-phosphate in tumor cell survival and dissemination," in *Advances in Cancer Research*, eds C. E. Chalfant and P. Fisher (Cambridge, MA: Academic Press), 217–234. doi: 10.1016/bs.acr.2018.04.012

Gomez-Muñoz, A., Duffy, P. A., Martin, A., O'Brien, L., Byun, H. S., Bittman, R., et al. (1995). Short-chain ceramide-1-phosphates are novel stimulators of DNA synthesis and cell division: antagonism by cell-permeable ceramides. *Mol. Pharmacol.* 47, 833–839.

Gomez-Muñoz, A., Frago, L. M., Alvarez, L., and Varela-Nieto, I. (1997). Stimulation of DNA synthesis by natural ceramide 1-phosphate. *Biochem. J.* 325(Pt 2), 435–440. doi: 10.1042/bj3250435

Gómez-Muñoz, A., Kong, J. Y., Parhar, K., Wang, S. W., Gangoiti, P., González, M., et al. (2005). Ceramide-1-phosphate promotes cell survival through activation of the phosphatidylinositol 3-kinase/protein kinase B pathway. *FEBS Lett.* 579, 3744–3750. doi: 10.1016/j.febslet.2005.05.067

Gómez-Muñoz, A., Kong, J. Y., Salh, B., and Steinbrecher, U. P. (2004). Ceramide-1-phosphate blocks apoptosis through inhibition of acid sphingomyelinase in macrophages. *J. Lipid Res.* 45, 99–105. doi: 10.1194/jlr.M300158-JLR200

Gómez-Muñoz, A., Waggoner, D. W., O'Brien, L., and Brindley, D. N. (1995). Interaction of ceramides, sphingosine, and sphingosine 1-phosphate in regulating DNA synthesis and phospholipase D activity. *J. Biol. Chem.* 270, 26318–26325. doi: 10.1074/jbc.270.44.26318

Graf, C., Niwa, S., Müller, M., Kinzel, B., and Bornancin, F. (2008). Wild-type levels of ceramide and ceramide-1-phosphate in the retina of ceramide kinase-like-deficient mice. *Biochem. Biophys. Res. Commun.* 373, 159–163. doi: 10.1016/j.bbrc.2008.06.002

Granado, M. H., Gangoiti, P., Ouro, A., Arana, L., González, M., Trueba, M., et al. (2009). Ceramide 1-phosphate (C1P) promotes cell migration. *Cell. Signal.* 21, 405–412. doi: 10.1016/j.cellsig.2008.11.003

Grassme, H., Jekle, A., Riehle, A., Schwarz, H., Berger, J., Sandhoff, K., et al. (2001). CD95 signaling via ceramide-rich membrane rafts. *J. Biol. Chem.* 276, 20589–20596. doi: 10.1074/jbc.M101207200

Grassmé, H., Schwarz, H., and Gulbins, E. (2001). Molecular mechanisms of ceramide-mediated CD95 clustering. *Biochem. Biophys. Res. Commun.* 284, 1016–1030. doi: 10.1006/bbrc.2001.5045

Gulbins, E., and Kolesnick, R. (2003). Raft ceramide in molecular medicine. *Oncogene* 22, 7070–7077. doi: 10.1038/sj.onc.1207146

Güntert, T., Hänggi, P., Othman, A., Suriyanarayanan, S., Sonda, S., Zuellig, R. A., et al. (2016). 1-Deoxysphingolipid-induced neurotoxicity involves N-methyl- d -aspartate receptor signaling. *Neuropharmacology* 110, 211–222. doi: 10.1016/j.neuropharm.2016.03.033

Hait, N. C., Allegood, J., Maceyka, M., Strub, G. M., Harikumar, K. B., Singh, S. K., et al. (2009). Regulation of histone acetylation in the nucleus by sphingosine-1-phosphate. *Science* 325, 1254–1257. doi: 10.1126/science.1176709

Hait, N. C., Oskeritzian, C. A., Paugh, S. W., Milstien, S., and Spiegel, S. (2006). Sphingosine kinases, sphingosine 1-phosphate, apoptosis and diseases. *Biochim. Biophys. Acta* 1758, 2016–2026. doi: 10.1016/j.bbamem.2006.08.007

Hait, N. C., Wise, L. E., Allegood, J. C., O'Brien, M., Avni, D., Reeves, T. M., et al. (2014). Active, phosphorylated fingolimod inhibits histone deacetylases and facilitates fear extinction memory. *Nat. Neurosci.* 17, 971–980. doi: 10.1038/nn.3728

Hammer, S. S., and Busik, J. V. (2017). The role of dyslipidemia in diabetic retinopathy. *Vision Res.* 139, 228–236. doi: 10.1016/j.visres.2017.04.010

Hanada, K., Kumagai, K., Tomishige, N., and Yamaji, T. (2009). CERT-mediated trafficking of ceramide. *Biochim. Biophys. Acta* 1791, 684–691. doi: 10.1016/j.bbalip.2009.01.006

Hannun, Y. A., and Bell, R. M. (1989). Functions of sphingolipids and sphingolipid breakdown products in cellular regulation. *Science* 243, 500–507. doi: 10.1126/science.2643164

Hannun, Y. A., Loomis, C. R., Merrill, A. H., and Bell, R. M. (1986). Sphingosine inhibition of protein kinase C activity and of phorbol dibutyrate binding in vitro and in human platelets. *J. Biol. Chem.* 261, 12604–12609.

Hannun, Y. A., and Luberto, C. (2004). Lipid metabolism: ceramide transfer protein adds a new dimension. *Curr. Biol.* 14, R163–R165.

Hannun, Y. A., Luberto, C., and Argraves, K. M. (2001). Enzymes of sphingolipid metabolism: from modular to integrative signaling. *Biochemistry* 40, 4893–4903. doi: 10.1021/bi002836k

Hannun, Y. A., and Obeid, L. M. (2008). Principles of bioactive lipid signalling: lessons from sphingolipids. *Nat. Rev. Mol. Cell Biol.* 9, 139–150. doi: 10.1038/nrm2329

Hannun, Y. A., and Obeid, L. M. (2011). Many ceramides. *J. Biol. Chem.* 286, 27855–27862. doi: 10.1074/jbc.R111.254359

Hannun, Y. A., and Obeid, L. M. (2018). Sphingolipids and their metabolism in physiology and disease. *Nat. Rev. Mol. Cell Biol.* 19, 175–191. doi: 10.1038/nrm.2017.107

Harcourt, B., and Ashton, N. (1973). Ultrastructure of the optic nerve in Krabbe's leucodystrophy. *Br. J. Ophthalmol.* 57, 885–891. doi: 10.1136/bjo.57.12.885

Harmon, J. M., Bacikova, D., Gable, K., Gupta, S. D., Han, G., Sengupta, N., et al. (2013). Topological and functional characterization of the ssSPTs, small activating subunits of serine palmitoyltransferase. *J. Biol. Chem.* 288, 10144–10153. doi: 10.1074/jbc.M113.451526

Hernández-Corbacho, M. J., Canals, D., Adada, M. M., Liu, M., Senkal, C. E., Yi, J. K., et al. (2015). Tumor necrosis factor-α (TNFα)-induced ceramide generation via ceramide synthases regulates loss of focal adhesion kinase (FAK) and programmed cell death. *J. Biol. Chem.* 290, 25356–25373. doi: 10.1074/jbc.M115.658658

Hernández-Tiedra, S., Fabriàs, G., Dávila, D., Salanueva, ÍJ., Casas, J., Montes, L. R., et al. (2016). Dihydroceramide accumulation mediates cytotoxic autophagy of cancer cells via autolysosome destabilization. *Autophagy* 12, 2213–2229. doi: 10.1080/15548627.2016.1213927

Hinkovska-Galcheva, V. T., Boxer, L. A., Mansfield, P. J., Harsh, D., Blackwood, A., and Shayman, J. A. (1998). The formation of ceramide-1-phosphate during neutrophil phagocytosis and its role in liposome fusion. *J. Biol. Chem.* 273, 33203–33209. doi: 10.1074/jbc.273.50.33203

Hla, T., Lee, M. J., Ancellin, N., Paik, J. H., and Kluk, M. J. (2001). Lysophospholipids - receptor revelations. *Science* 294, 1875–1878. doi: 10.1126/science.1065323

Hoeferlin, L. A., Wijesinghe, D. S., and Chalfant, C. E. (2013). The role of ceramide-1-phosphate in biological functions. *Handb. Exp. Pharmacol* 215, 153–166. doi: 10.1007/978-3-7091-1368-4_8

Holopainen, J. M., Angelova, M. I., and Kinnunen, P. K. (2000). Vectorial budding of vesicles by asymmetrical enzymatic formation of ceramide in giant liposomes. *Biophys. J.* 78, 830–838. doi: 10.1016/S0006-3495(00)76640-9

Hooper, M. J., Wang, J., Browning, R., and Ash, J. D. (2018). Damage-associated molecular pattern recognition is required for induction of retinal neuroprotective pathways in a sex-dependent manner. *Sci. Rep.* 8:9115. doi: 10.1038/s41598-018-27479-x

Hornemann, T., Penno, A., Rütti, M. F., Ernst, D., Kivrak-Pfiffner, F., Rohrer, L., et al. (2009). The SPTLC3 subunit of serine palmitoyltransferase generates short chain sphingoid bases. *J. Biol. Chem.* 284, 26322–26330. doi: 10.1074/jbc.M109.023192

Huang, K., Huang, J., Chen, C., Hao, J., Wang, S., Huang, J., et al. (2014). AP-1 regulates sphingosine kinase 1 expression in a positive feedback manner in glomerular mesangial cells exposed to high glucose. *Cell. Signal.* 26, 629–638. doi: 10.1016/j.cellsig.2013.12.002

Hunter, M., Demarais, N. J., Faull, R. L. M., Grey, A. C., and Curtis, M. A. (2018). Subventricular zone lipidomic architecture loss in Huntington's disease. *J. Neurochem.* 146, 613–630. doi: 10.1111/jnc.14468

Huwiler, A., Kolter, T., Pfeilschifter, J., and Sandhoff, K. (2000). Physiology and pathophysiology of sphingolipid metabolism and signaling. *Biochim. Biophys. Acta* 1485, 63–99.

Insua, M. F., Garelli, A., Rotstein, N. P., German, O. L., Arias, A., and Politi, L. E. (2003). Cell cycle regulation in retinal progenitors by glia-derived neurotrophic factor and docosahexaenoic acid. *Investig. Ophthalmol. Vis. Sci.* 44, 2235–2244.

Jain, A., Beutel, O., Ebell, K., Korneev, S., and Holthuis, J. C. M. (2017). Diverting CERT-mediated ceramide transport to mitochondria triggers Bax-dependent apoptosis. *J. Cell Sci.* 130, 360–371. doi: 10.1242/jcs.194191

Jenkins, R. W., Canals, D., and Hannun, Y. A. (2009). Roles and regulation of secretory and lysosomal acid sphingomyelinase. *Cell. Signal.* 21, 836–846. doi: 10.1016/j.cellsig.2009.01.026

Jeon, H. J., Lee, D. H., Kang, M. S., Lee, M.-O., Jung, K. M., Jung, S. Y., et al. (2005). Dopamine release in PC12 cells is mediated by Ca^{2+}-dependent production of ceramide via sphingomyelin pathway. *J. Neurochem.* 95, 811–820. doi: 10.1111/j.1471-4159.2005.03403.x

Jiménez-Rojo, N., Sot, J., Busto, J. V., Shaw, W. A., Duan, J., Merrill, A. H., et al. (2014). Biophysical properties of novel 1-deoxy-(dihydro)ceramides occurring in mammalian cells. *Biophys. J.* 107, 2850–2859. doi: 10.1016/j.bpj.2014.10.010

Joly, S., and Pernet, V. (2016). Sphingosine 1-phosphate receptor 1 is required for retinal ganglion cell survival after optic nerve trauma. *J. Neurochem.* 138, 571–586. doi: 10.1111/jnc.13701

Jun, B., Mukherjee, P. K., Asatryan, A., Kautzmann, M.-A., Heap, J., Gordon, W. C., et al. (2017). Elovanoids are novel cell-specific lipid mediators necessary for neuroprotective signaling for photoreceptor cell integrity. *Sci. Rep.* 7:5279. doi: 10.1038/s41598-017-05433-7

Jung, W.-H., Liu, C.-C., Yu, Y.-L., Chang, Y.-C., Lien, W.-Y., Chao, H.-C., et al. (2017). Lipophagy prevents activity-dependent neurodegeneration due to dihydroceramide accumulation in vivo. *EMBO Rep.* 18, 1150–1165. doi: 10.15252/embr.201643480

Kady, N. M., Liu, X., Lydic, T. A., Syed, M. H., Navitskaya, S., Wang, Q., et al. (2018). ELOVL4-mediated production of very long-chain ceramides stabilizes tight junctions and prevents diabetes-induced retinal vascular permeability. *Diabetes* 67, 769–781. doi: 10.2337/db17-1034

Kannan, R., Jin, M., Gamulescu, M.-A., and Hinton, D. R. (2004). Ceramide-induced apoptosis: role of catalase and hepatocyte growth factor. *Free Radic. Biol. Med.* 37, 166–175. doi: 10.1016/j.freeradbiomed.2004.04.011

Kaur, G., Tan, L. X., Rathnasamy, G., La Cunza, N., Germer, C. J., Toops, K. A., et al. (2018). Aberrant early endosome biogenesis mediates complement activation in the retinal pigment epithelium in modelsof macular degeneration. *Proc. Natl. Acad. Sci. U.S.A* 115, 9014–9019. doi: 10.1073/pnas.1805039115

Kawahara, A., Nishi, T., Hisano, Y., Fukui, H., Yamaguchi, A., and Mochizuki, N. (2009). The sphingolipid transporter Spns2 functions in migration of zebrafish myocardial precursors. *Science* 323, 524–527. doi: 10.1126/science.1167449

Kim, C. H., Wu, W., Wysoczynski, M., Abdel-Latif, A., Sunkara, M., Morris, A., et al. (2012). Conditioning for hematopoietic transplantation activates the complement cascade and induces a proteolytic environment in bone marrow: a novel role for bioactive lipids and soluble C5b-C9 as homing factors. *Leukemia* 26, 106–116. doi: 10.1038/leu.2011.185

Kisseleva, T., and Brenner, D. A. (2008). Mechanisms of Fibrogenesis. *Exp. Biol. Med.* 233, 109–122. doi: 10.3181/0707-MR-190

Kitatani, K., Idkowiak-Baldys, J., and Hannun, Y. A. (2008). The sphingolipid salvage pathway in ceramide metabolism and signaling. *Cell. Signal.* 20, 1010–1018. doi: 10.1016/j.cellsig.2007.12.006

Klein, R., Klein, B. E., Jensen, S. C., Cruickshanks, K. J., Lee, K. E., Danforth, L. G., et al. (2001). Medication use and the 5-year incidence of early age-related maculopathy: the Beaver Dam Eye Study. *Arch. Ophthalmol.* 119, 1354–1359.

Knapp, M. (2011). Cardioprotective role of sphingosine-1-phosphate. *J. Physiol. Pharmacol.* 62, 601–607. doi: 10.1016/S0040-4020(99)00597-9

Ko, J., Chae, M. K., Lee, J. H., Lee, E. J., and Yoon, J. S. (2017). Sphingosine-1-phosphate mediates fibrosis in orbital fibroblasts in Graves' Orbitopathy. *Investig. Opthalmol. Vis. Sci.* 58, 2544. doi: 10.1167/iovs.16-20684

Kolesnick, R. N. (1987). 1,2-Diacylglycerols but not phorbol esters stimulate sphingomyelin hydrolysis in GH3 pituitary cells. *J. Biol. Chem.* 262, 16759–16762.

Kono, Y., Nishiuma, T., Nishimura, Y., Kotani, Y., Okada, T., Nakamura, S.-I., et al. (2007). Sphingosine kinase 1 regulates differentiation of human and mouse lung fibroblasts mediated by TGF-beta1. *Am. J. Respir. Cell Mol. Biol.* 37, 395–404. doi: 10.1165/rcmb.2007-0065OC

Korbelik, M., Banáth, J., Sun, J., Canals, D., Hannun, Y. A., and Separovic, D. (2014). Ceramide and sphingosine-1-phosphate act as photodynamic therapy-elicited damage-associated molecular patterns: cell surface exposure. *Int. Immunopharmacol.* 20, 359–365. doi: 10.1016/j.intimp.2014.03.016

Kremser, C., Klemm, A.-L., van Uelft, M., Imgrund, S., Ginkel, C., Hartmann, D., et al. (2013). Cell-type-specific expression pattern of ceramide synthase 2 protein in mouse tissues. *Histochem. Cell Biol.* 140, 533–547. doi: 10.1007/s00418-013-1091-z

Kucuksayan, E., Konuk, E. K., Demir, N., Mutus, B., and Aslan, M. (2014). Neutral sphingomyelinase inhibition decreases ER stress-mediated apoptosis and inducible nitric oxide synthase in retinal pigment epithelial cells. *Free Radic. Biol. Med.* 72, 113–123. doi: 10.1016/j.freeradbiomed.2014.04.013

Kurz, J., Parnham, M. J., Geisslinger, G., and Schiffmann, S. (2018). Ceramides as novel disease biomarkers. *Trends Mol. Med.* 52, 20–32. doi: 10.1016/j.molmed.2018.10.009

Lahiri, S., and Futerman, A. H. (2007). The metabolism and function of sphingolipids and glycosphingolipids. *Cell. Mol. Life Sci.* 64, 2270–2284. doi: 10.1007/s00018-007-7076-0

Lamour, N. F., Stahelin, R. V., Wijesinghe, D. S., Maceyka, M., Wang, E., Allegood, J. C., et al. (2007). Ceramide kinase uses ceramide provided by ceramide transport protein: localization to organelles of eicosanoid synthesis. *J. Lipid Res.* 48, 1293–1304. doi: 10.1194/jlr.M700083-JLR200

Lamour, N. F., Subramanian, P., Wijesinghe, D. S., Stahelin, R. V., Bonventre, J. V., and Chalfant, C. E. (2009). Ceramide 1-phosphate is required for the

translocation of group IVA cytosolic phospholipase A2 and prostaglandin synthesis. *J. Biol. Chem.* 284, 26897–26907. doi: 10.1074/jbc.M109.001677

Lamour, N. F., Wijesinghe, D. S., Mietla, J. A., Ward, K. E., Stahelin, R. V., and Chalfant, C. E. (2011). Ceramide kinase regulates the production of tumor necrosis factor α (TNFα) via inhibition of TNFα-converting enzyme. *J. Biol. Chem.* 286, 42808–42817. doi: 10.1074/jbc.M111.310169

Laviad, E. L., Albee, L., Pankova-Kholmyansky, I., Epstein, S., Park, H., Merrill, A. H., et al. (2008). Characterization of ceramide synthase 2: tissue distribution, substrate specificity, and inhibition by sphingosine 1-phosphate. *J. Biol. Chem.* 283, 5677–5684. doi: 10.1074/jbc.M707386200

Lee, A. Y., Lee, J. W., Kim, J.-E., Mock, H. J., Park, S., Kim, S., et al. (2017). Dihydroceramide is a key metabolite that regulates autophagy and promotes fibrosis in hepatic steatosis model. *Biochem. Biophys. Res. Commun.* 494, 460–469. doi: 10.1016/j.bbrc.2017.10.110

Lei, H., Hovland, P., Velez, G., Haran, A., Gilbertson, D., Hirose, T., et al. (2007). A potential role for PDGF-C in experimental and clinical proliferative vitreoretinopathy. *Invest. Ophthalmol. Vis. Sci.* 48, 2335–2342. doi: 10.1167/iovs.06-0965

Lépine, S., Lakatos, B., Courageot, M.-P., Le Stunff, H., Sulpice, J.-C., and Giraud, F. (2004). Sphingosine contributes to glucocorticoid-induced apoptosis of thymocytes independently of the mitochondrial pathway. *J. Immunol.* 173, 3783–3790. doi: 10.4049/jimmunol.173.6.3783

Levy, M., and Futerman, A. H. (2010). Mammalian ceramide synthases. *IUBMB Life* 62, 347–356. doi: 10.1002/iub.319

Li, C., Wang, L., Zhang, J., Huang, M., Wong, F., Liu, X., et al. (2014). CERKL interacts with mitochondrial TRX2 and protects retinal cells from oxidative stress-induced apoptosis. *Biochim. Biophys. Acta* 1842, 1121–1129. doi: 10.1016/j.bbadis.2014.04.009

Li, C., Zheng, S., You, H., Liu, X., Lin, M., Yang, L., et al. (2011). Sphingosine 1-phosphate (S1P)/S1P receptors are involved in human liver fibrosis by action on hepatic myofibroblasts motility. *J. Hepatol.* 54, 1205–1213. doi: 10.1016/j.jhep.2010.08.028

Littink, K. W., Koenekoop, R. K., van den Born, L. I., Collin, R. W. J., Moruz, L., Veltman, J. A., et al. (2010). Homozygosity mapping in patients with cone-rod dystrophy: novel mutations and clinical characterizations. *Invest. Ophthalmol. Vis. Sci.* 51, 5943–5951. doi: 10.1167/iovs.10-5797

Liu, X., Yue, S., Li, C., Yang, L., You, H., and Li, L. (2011). Essential roles of sphingosine 1-phosphate receptor types 1 and 3 in human hepatic stellate cells motility and activation. *J. Cell. Physiol.* 226, 2370–2377. doi: 10.1002/jcp.22572

Lou, H., Kang, D., Yang, Q., Lian, C., Zhang, C., Li, Z., et al. (2017). Erythropoietin protects retina against ceramide 2-induced damage in rat. *Curr. Mol. Med.* 17, 699–706. doi: 10.2174/1566524018666180322161252

Lukowski, Z. L., Min, J., Beattie, A. R., Meyers, C. A., Levine, M. A., Stoller, G., et al. (2013). Prevention of ocular scarring after glaucoma filtering surgery using the monoclonal antibody LT1009 (Sonepcizumab) in a rabbit model. *J. Glaucoma* 22, 145–151. doi: 10.1097/IJG.0b013e31822e8c83

Lv, M., Zhang, D., Dai, D., Zhang, W., and Zhang, L. (2016). Sphingosine kinase 1/sphingosine-1-phosphate regulates the expression of interleukin-17A in activated microglia in cerebral ischemia/reperfusion. *Inflamm. Res.* 65, 551–562. doi: 10.1007/s00011-016-0939-9

Maceyka, M., Harikumar, K. B., Milstien, S., and Spiegel, S. (2012). Sphingosine-1-phosphate signaling and its role in disease. *Trends Cell Biol.* 22, 50–60. doi: 10.1016/j.tcb.2011.09.003

Maceyka, M., Sankala, H., Hait, N. C., Le Stunff, H., Liu, H., Toman, R., et al. (2005). SphK1 and SphK2, sphingosine kinase isoenzymes with opposing functions in sphingolipid metabolism. *J. Biol. Chem.* 280, 37118–37129. doi: 10.1074/jbc.M502207200

Mandal, N. A., Tran, J.-T. A., Saadi, A., Rahman, A. K., Huynh, T.-P., Klein, W. H., et al. (2013). Expression and localization of CERKL in the mammalian retina, its response to light-stress, and relationship with NeuroD1 gene. *Exp. Eye Res.* 106, 24–33. doi: 10.1016/j.exer.2012.10.014

Mandala, S. M. (2001). Sphingosine-1-phosphate phosphatases. *Prostaglandins Other Lipid Mediat.* 64, 143–156. doi: 10.1016/S0090-6980(01)00111-3

Mandon, E. C., Ehses, I., Rother, J., van Echten, G., and Sandhoff, K. (1992). Subcellular localization and membrane topology of serine palmitoyltransferase, 3-dehydrosphinganine reductase, and sphinganine N-acyltransferase in mouse liver. *J. Biol. Chem.* 267, 11144–11148.

Marchesini, N., and Hannun, Y. A. (2004). Acid and neutral sphingomyelinases: roles and mechanisms of regulation. *Biochem. Cell Biol.* 82, 27–44. doi: 10.1139/o03-091

Martin, R. E., Elliott, M. H., Brush, R. S., and Anderson, R. E. (2005). Detailed characterization of the lipid composition of detergent-resistant membranes from photoreceptor rod outer segment membranes. *Invest. Ophthalmol. Vis. Sci.* 46, 1147–1154. doi: 10.1167/iovs.04-1207

McGuire, P. G., Rangasamy, S., Maestas, J., and Das, A. (2011). Pericyte-derived sphingosine 1-phosphate induces the expression of adhesion proteins and modulates the retinal endothelial cell barrier. *Arterioscler. Thromb. Vasc. Biol.* 31, e107–e115. doi: 10.1161/ATVBAHA.111.235408

Merrill, A. H., Hannun, Y. A., and Bell, R. M. (1993). Introduction: sphingolipids and their metabolites in cell regulation. *Adv. Lipid Res.* 25, 1–24.

Merrill, A. H., Nimkar, S., Menaldino, D., Hannun, Y. A., Loomis, C., Bell, R. M., et al. (1989). Structural requirements for long-chain (sphingoid) base inhibition of protein kinase C in vitro and for the cellular effects of these compounds. *Biochemistry* 28, 3138–3145. doi: 10.1021/bi00434a004

Milara, J., Navarro, R., Juan, G., Peiró, T., Serrano, A., Ramón, M., et al. (2012). Sphingosine-1-phosphate is increased in patients with idiopathic pulmonary fibrosis and mediates epithelial to mesenchymal transition. *Thorax* 67, 147–156. doi: 10.1136/thoraxjnl-2011-200026

Miranda, G. E., Abrahan, C. E., Agnolazza, D. L., Politi, L. E., and Rotstein, N. P. (2011). Ceramide-1-phosphate, a new mediator of development and survival in retina photoreceptors. *Invest. Ophthalmol. Vis. Sci.* 52, 6580–6588. doi: 10.1167/iovs.10-7065

Miranda, G. E., Abrahan, C. E., Politi, L. E., and Rotstein, N. P. (2009). Sphingosine-1-phosphate is a key regulator of proliferation and differentiation in retina photoreceptors. *Investig. Ophthalmol. Vis. Sci.* 50, 4416–4428. doi: 10.1167/iovs.09-3388

Mitra, P., Maceyka, M., Payne, S. G., Lamour, N., Milstien, S., Chalfant, C. E., et al. (2007). Ceramide kinase regulates growth and survival of A549 human lung adenocarcinoma cells. *FEBS Lett.* 581, 735–740. doi: 10.1016/j.febslet.2007.01.041

Mitra, P., Oskeritzian, C. A., Payne, S. G., Beaven, M. A., Milstien, S., and Spiegel, S. (2006). Role of ABCC1 in export of sphingosine-1-phosphate from mast cells. *Proc. Natl. Acad. Sci. U.S.A.* 103, 16394–16399. doi: 10.1073/pnas.0603734103

Murakami, M., Ito, H., Hagiwara, K., Yoshida, K., Sobue, S., Ichihara, M., et al. (2010). ATRA inhibits ceramide kinase transcription in a human neuroblastoma cell line, SH-SY5Y cells: the role of COUP-TFI. *J. Neurochem.* 112, 511–520. doi: 10.1111/j.1471-4159.2009.06486.x

Nagahashi, M., Yamada, A., Aoyagi, T., Allegood, J., Wakai, T., Spiegel, S., et al. (2016). Sphingosine-1-phosphate in the lymphatic fluid determined by novel methods. *Heliyon* 2:e00219. doi: 10.1016/j.heliyon.2016.e00219

Nava, V. E., Cuvillier, O., Edsall, L. C., Kimura, K., Milstien, S., Gelmann, E. P., et al. (2000). Sphingosine enhances apoptosis of radiation-resistant prostate cancer cells. *Cancer Res.* 60, 4468–4474.

Nayak, D., Huo, Y., Kwang, W. X. T., Pushparaj, P. N., Kumar, S. D., Ling, E.-A., et al. (2010). Sphingosine kinase 1 regulates the expression of proinflammatory cytokines and nitric oxide in activated microglia. *Neuroscience* 166, 132–144. doi: 10.1016/j.neuroscience.2009.12.020

Nevet, M. J., Vekslin, S., Dizhoor, A. M., Olshevskaya, E. V., Tidhar, R., Futerman, A. H., et al. (2012). Ceramide kinase-like (CERKL) interacts with neuronal calcium sensor proteins in the retina in a cation-dependent manner. *Invest. Ophthalmol. Vis. Sci* 53, 4565–4574. doi: 10.1167/iovs.12-9770

Newton, J., Lima, S., Maceyka, M., and Spiegel, S. (2015). Revisiting the sphingolipid rheostat: Evolving concepts in cancer therapy. *Exp. Cell Res.* 333, 195–200. doi: 10.1016/j.yexcr.2015.02.025

Nicholas, S. E., Rowsey, T. G., Priyadarsini, S., Mandal, N. A., and Karamichos, D. (2017). Unravelling the interplay of sphingolipids and TGF-β signaling in the human corneal stroma. *PLoS One* 12:e0182390. doi: 10.1371/journal.pone.0182390

Norsworthy, M. W., Bei, F., Kawaguchi, R., Wang, Q., Tran, N. M., Li, Y., et al. (2017). Sox11 expression promotes regeneration of some retinal ganglion cell types but kills others. *Neuron* 94, 1112–1120.e4. doi: 10.1016/j.neuron.2017.05.035

Novgorodov, S. A., Wu, B. X., Gudz, T. I., Bielawski, J., Ovchinnikova, T. V., Hannun, Y. A., et al. (2011). Novel pathway of ceramide production in

mitochondria: thioesterase and neutral ceramidase produce ceramide from sphingosine and acyl-CoA. *J. Biol. Chem.* 286, 25352–25362. doi: 10.1074/jbc.M110.214866

Obeid, L. M., Linardic, C. M., Karolak, L. A., and Hannun, Y. A. (1993). Programmed cell death induced by ceramide. *Science* 259, 1769–1771. doi: 10.1126/science.8456305

Ogretmen, B., and Hannun, Y. A. (2004). Biologically active sphingolipids in cancer pathogenesis and treatment. *Nat. Rev. Cancer* 4, 604–616. doi: 10.1038/nrc1411

Ohta, H., Sweeney, E. A., Masamune, A., Yatomi, Y., Hakomori, S., and Igarashi, Y. (1995). Induction of apoptosis by sphingosine in human leukemic HL-60 cells: a possible endogenous modulator of apoptotic DNA fragmentation occurring during phorbol ester-induced differentiation. *Cancer Res.* 55, 691–697.

Okazaki, T., Bell, R. M., and Hannun, Y. A. (1989). Sphingomyelin turnover induced by vitamin D3 in HL-60 cells. Role in cell differentiation. *J. Biol. Chem.* 264, 19076–19080.

Olivera, A., Allende, M. L., and Proia, R. L. (2013). Shaping the landscape: Metabolic regulation of S1P gradients. *Biochim. Biophys. Acta* 1831, 193–202. doi: 10.1016/j.bbalip.2012.06.007

Opreanu, M., Lydic, T. A., Reid, G. E., McSorley, K. M., Esselman, W. J., and Busik, J. V. (2010). Inhibition of cytokine signaling in human retinal endothelial cells through downregulation of sphingomyelinases by docosahexaenoic acid. *Invest. Ophthalmol. Vis. Sci.* 51, 3253–3263. doi: 10.1167/iovs.09-4731

Opreanu, M., Tikhonenko, M., Bozack, S., Lydic, T. A., Reid, G. E., McSorley, K. M., et al. (2011). The unconventional role of acid sphingomyelinase in regulation of retinal microangiopathy in diabetic human and animal models. *Diabetes* 60, 2370–2378. doi: 10.2337/db10-0550

Oresti, G. M., Luquez, J. M., Furland, N. E., and Aveldaño, M. I. (2011). Uneven distribution of ceramides, sphingomyelins and glycerophospholipids between heads and tails of rat spermatozoa. *Lipids* 46, 1081–1090. doi: 10.1007/s11745-011-3601-x

Osborne, N., Brand-Arzamendi, K., Ober, E. A., Jin, S. W., Verkade, H., Holtzman, N. G., et al. (2008). The spinster homolog, two of hearts, is required for sphingosine 1-phosphate signaling in zebrafish. *Curr. Biol.* 18, 1882–1888. doi: 10.1016/j.cub.2008.10.061

Park, J.-W., and Pewzner-Jung, Y. (2013). Ceramide synthases: reexamining longevity. *Handb. Exp. Pharmacol.* 215, 89–107. doi: 10.1007/978-3-7091-1368-4_5

Park, S. J., Kim, J. M., Kim, J., Hur, J., Park, S., Kim, K., et al. (2018). Molecular mechanisms of biogenesis of apoptotic exosome-like vesicles and their roles as damage-associated molecular patterns. *Proc. Natl. Acad. Sci. U.S.A.* 115, E11721–E11730. doi: 10.1073/pnas.1811432115

Pasquaré, S. J., and Giusto, N. M. (2008). Diacylglyceride lipase activity in rod outer segments depends on the illumination state of the retina. *Neurochem. Int.* 53, 382–388. doi: 10.1016/j.neuint.2008.09.007

Pasquaré, S. J., Salvador, G. A., and Giusto, N. M. (2008). Involvement of lysophosphatidic acid, sphingosine 1-phosphate and ceramide 1-phosphate in the metabolization of phosphatidic acid by lipid phosphate phosphatases in bovine rod outer segments. *Neurochem. Res.* 33, 1205–1215. doi: 10.1007/s11064-007-9569-5

Paugh, B. S., Bryan, L., Paugh, S. W., Wilczynska, K. M., Alvarez, S. M., Singh, S. K., et al. (2009). Interleukin-1 regulates the expression of sphingosine kinase 1 in glioblastoma cells. *J. Biol. Chem.* 284, 3408–3417. doi: 10.1074/jbc.M807170200

Paugh, S. W., Payne, S. G., Barbour, S. E., Milstien, S., and Spiegel, S. (2003). The immunosuppressant FTY720 is phosphorylated by sphingosine kinase type 2. *FEBS Lett.* 554, 189–193. doi: 10.1016/s0014-5793(03)01168-2

Pchejetski, D., Foussal, C., Alfarano, C., Lairez, O., Calise, D., Guilbeau-Frugier, C., et al. (2012). Apelin prevents cardiac fibroblast activation and collagen production through inhibition of sphingosine kinase 1. *Eur. Heart J.* 33, 2360–2369. doi: 10.1093/eurheartj/ehr389

Peng, B., Xiao, J., Wang, K., So, K.-F., Tipoe, G. L., and Lin, B. (2014). Suppression of microglial activation is neuroprotective in a mouse model of human retinitis pigmentosa. *J. Neurosci.* 34, 8139–8150. doi: 10.1523/JNEUROSCI.5200-13.2014

Penno, A., Reilly, M. M., Houlden, H., Laurá, M., Rentsch, K., Niederkofler, V., et al. (2010). Hereditary sensory neuropathy type 1 is caused by the accumulation of two neurotoxic sphingolipids. *J. Biol. Chem.* 285, 11178–11187. doi: 10.1074/jbc.M109.092973

Pettus, B. J., Bielawska, A., Subramanian, P., Wijesinghe, D. S., Maceyka, M., Leslie, C. C., et al. (2004). Ceramide 1-phosphate is a direct activator of cytosolic phospholipase A2. *J. Biol. Chem.* 279, 11320–11326. doi: 10.1074/jbc.M309262200

Phillips, D. C., Martin, S., Doyle, B. T., and Houghton, J. A. (2007). Sphingosine-induced apoptosis in rhabdomyosarcoma cell lines is dependent on pre-mitochondrial Bax activation and post-mitochondrial caspases. *Cancer Res.* 67, 756–764. doi: 10.1158/0008-5472.can-06-2374

Piano, I., Novelli, E., Gasco, P., Ghidoni, R., Strettoi, E., and Gargini, C. (2013). Cone survival and preservation of visual acuity in an animal model of retinal degeneration. *Eur. J. Neurosci.* 37, 1853–1862. doi: 10.1111/ejn.12196

Politi, L. E., Rotstein, N. P., and Carri, N. G. (2001). Effect of GDNF on neuroblast proliferation and photoreceptor survival: additive protection with docosahexaenoic acid. *Investig. Ophthalmol. Vis. Sci.* 42, 3008–3015.

Porter, H., Qi, H., Prabhu, N., Grambergs, R., McRae, J., Hopiavuori, B., et al. (2018). Characterizing sphingosine kinases and sphingosine 1-phosphate receptors in the mammalian eye and retina. *Int. J. Mol. Sci.* 19:E3885. doi: 10.3390/ijms19123885

Portera-Cailliau, C., Sung, C. H., Nathans, J., and Adler, R. (1994). Apoptotic photoreceptor cell death in mouse models of retinitis pigmentosa. *Proc. Natl. Acad. Sci. U.S.A.* 91, 974–978. doi: 10.1073/pnas.91.3.974

Prado Spalm, F. H., Vera, M. S., Dibo, M. J., Simón, M. V., Politi, L. E., and Rotstein, N. P. (2018). Ceramide induces the death of retina photoreceptors through activation of parthanatos. *Mol. Neurobiol.* doi: 10.1007/s12035-018-1402-4 [Epub ahead of print].

Presa, N., Gomez-Larrauri, A., Rivera, I.-G., Ordoñez, M., Trueba, M., and Gomez-Muñoz, A. (2016). Regulation of cell migration and inflammation by ceramide 1-phosphate. *Biochim. Biophys. Acta-Mol. Cell Biol. Lipids* 1861, 402–409. doi: 10.1016/j.bbalip.2016.02.007

Pujol-Lereis, L. M., Liebisch, G., Schick, T., Lin, Y., Grassmann, F., Uchida, K., et al. (2018). Evaluation of serum sphingolipids and the influence of genetic risk factors in age-related macular degeneration. *PLoS One* 13:e0200739. doi: 10.1371/journal.pone.0200739

Puranam, K., Qian, W. H., Nikbakht, K., Venable, M., Obeid, L., Hannun, Y., et al. (1997). Upregulation of Bcl-2 and elevation of ceramide in Batten disease. *Neuropediatrics* 28, 37–41. doi: 10.1055/s-2007-973664

Pyne, S., Lee, S. C., Long, J., and Pyne, N. J. (2009). Role of sphingosine kinases and lipid phosphate phosphatases in regulating spatial sphingosine 1-phosphate signalling in health and disease. *Cell. Signal.* 21, 14–21. doi: 10.1016/j.cellsig.2008.08.008

Qiao, Y., Hu, R., Wang, Q., Qi, J., Yang, Y., Kijlstra, A., et al. (2012). Sphingosine 1-phosphate elicits proinflammatory responses in ARPE-19 cells. *Invest. Ophthalmol. Vis. Sci.* 53, 8200–8207. doi: 10.1167/iovs.12-10965

Raas-Rothschild, A., Pankova-Kholmyansky, I., Kacher, Y., and Futerman, A. H. (2004). Glycosphingolipidoses: beyond the enzymatic defect. *Glycoconj. J.* 21, 295–304. doi: 10.1023/B:GLYC.0000046272.38480.ef

Rajagopalan, V., Canals, D., Luberto, C., Snider, J., Voelkel-Johnson, C., Obeid, L. M., et al. (2015). Critical determinants of mitochondria-associated neutral sphingomyelinase (MA-nSMase) for mitochondrial localization. *Biochim. Biophys. Acta* 1850, 628–639. doi: 10.1016/j.bbagen.2014.11.019

Ranty, M.-L., Carpentier, S., Cournot, M., Rico-Lattes, I., Malecaze, F., Levade, T., et al. (2009). Ceramide production associated with retinal apoptosis after retinal detachment. *Graefes Arch. Clin. Exp. Ophthalmol.* 247, 215–224. doi: 10.1007/s00417-008-0957-6

Riboni, L., Bassi, R., Anelli, V., and Viani, P. (2002). Metabolic formation of ceramide-1-phosphate in cerebellar granule cells: evidence for the phosphorylation of ceramide by different metabolic pathways. *Neurochem. Res.* 27, 711–716.

Riera, M., Burguera, D., Garcia-Fernàndez, J., and Gonzàlez-Duarte, R. (2013). CERKL knockdown causes retinal degeneration in zebrafish. *PLoS One* 8:e64048. doi: 10.1371/journal.pone.0064048

Rivera, I.-G., Ordoñez, M., Presa, N., Gangoiti, P., Gomez-Larrauri, A., Trueba, M., et al. (2016). Ceramide 1-phosphate regulates cell migration and invasion of human pancreatic cancer cells. *Biochem. Pharmacol.* 102, 107–119. doi: 10.1016/j.bcp.2015.12.009

Rizvi, F., Heimann, T., Herrnreiter, A., and O'Brien, W. J. (2011). Mitochondrial dysfunction links ceramide activated HRK expression and cell death. *PLoS One* 6:e18137. doi: 10.1371/journal.pone.0018137

Roche, S. L., Wyse-Jackson, A. C., Gómez-Vicente, V., Lax, P., Ruiz-Lopez, A. M., Byrne, A. M., et al. (2016). Progesterone attenuates microglial-driven retinal degeneration and stimulates protective fractalkine-CX3CR1 signaling. *PLoS One* 11:e0165197. doi: 10.1371/journal.pone.0165197

Rotstein, N. P., Aveldaño, M. I., Barrantes, F. J., and Politi, L. E. (1996). Docosahexaenoic acid is required for the survival of rat retinal photoreceptors in vitro. *J. Neurochem.* 66, 1851–1859. doi: 10.1046/j.1471-4159.1996.66051851.x

Rotstein, N. P., Aveldaño, M. I., Barrantes, F. J., Roccamo, A. M., and Politi, L. E. (1997). Apoptosis of retinal photoreceptors during development in vitro: protective effect of docosahexaenoic acid. *J. Neurochem.* 69, 504–513. doi: 10.1046/j.1471-4159.1997.69020504.x

Rotstein, N. P., Miranda, G. E., Abrahan, C. E., and German, O. L. (2010). Regulating survival and development in the retina: key roles for simple sphingolipids. *J. Lipid Res.* 51, 1247–1262. doi: 10.1194/jlr.R003442

Ruvolo, P. P. (2003). Intracellular signal transduction pathways activated by ceramide and its metabolites. *Pharmacol. Res.* 47, 383–392. doi: 10.1016/s1043-6618(03)00050-1

Saba, J. D., and Hla, T. (2004). Point-counterpoint of sphingosine 1-phosphate metabolism. *Circ. Res.* 94, 724–734. doi: 10.1161/01.RES.0000122383.60368.24

Sahaboglu, A., Sharif, A., Feng, L., Secer, E., Zrenner, E., and Paquet-Durand, F. (2017). Temporal progression of PARP activity in the Prph2 mutant rd2 mouse: neuroprotective effects of the PARP inhibitor PJ34. *PLoS One* 12:e0181374. doi: 10.1371/journal.pone.0181374

Saika, S. (2006). TGFbeta pathobiology in the eye. *Lab. Invest.* 86, 106–115. doi: 10.1038/labinvest.3700375

Saika, S., Yamanaka, O., Sumioka, T., Miyamoto, T., Miyazaki, K., Okada, Y., et al. (2008). Fibrotic disorders in the eye: targets of gene therapy. *Prog. Retin. Eye Res.* 27, 177–196. doi: 10.1016/j.preteyeres.2007.12.002

Samadi, A. (2007). Ceramide-induced cell death in lens epithelial cells. *Mol. Vis.* 13, 1618–1626.

Sancho-Pelluz, J., Arango-Gonzalez, B., Kustermann, S., Romero, F. J., Van Veen, T., Zrenner, E., et al. (2008). Photoreceptor cell death mechanisms in inherited retinal degeneration. *Mol. Neurobiol.* 38, 253–269. doi: 10.1007/s12035-008-8045-9

Sanvicens, N., and Cotter, T. G. (2006). Ceramide is the key mediator of oxidative stress-induced apoptosis in retinal photoreceptor cells. *J. Neurochem.* 98, 1432–1444. doi: 10.1111/j.1471-4159.2006.03977.x

Sato, K., Malchinkhuu, E., Horiuchi, Y., Mogi, C., Tomura, H., Tosaka, M., et al. (2007). Critical role of ABCA1 transporter in sphingosine 1-phosphate release from astrocytes. *J. Neurochem.* 103, 2610–2619. doi: 10.1111/j.1471-4159.2007.04958.x

Scarlatti, F., Bauvy, C., Ventruti, A., Sala, G., Cluzeaud, F., Vandewalle, A., et al. (2004). Ceramide-mediated macroautophagy involves inhibition of protein kinase B and up-regulation of beclin 1. *J. Biol. Chem.* 279, 18384–18391. doi: 10.1074/jbc.M313561200

Schneider, G., Bryndza, E., Abdel-Latif, A., Ratajczak, J., Maj, M., Tarnowski, M., et al. (2013). Bioactive lipids S1P and C1P are prometastatic factors in human rhabdomyosarcoma, and their tissue levels increase in response to radio/chemotherapy. *Mol. Cancer Res.* 11, 793–807. doi: 10.1158/1541-7786.MCR-12-0600

Siddique, M. M., Li, Y., Chaurasia, B., Kaddai, V. A., and Summers, S. A. (2015). Dihydroceramides: from bit players to lead actors. *J. Biol. Chem.* 290, 15371–15379. doi: 10.1074/jbc.R115.653204

Simanshu, D. K., Kamlekar, R. K., Wijesinghe, D. S., Zou, X., Zhai, X., Mishra, S. K., et al. (2013). Non-vesicular trafficking by a ceramide-1-phosphate transfer protein regulates eicosanoids. *Nature* 500, 463–467. doi: 10.1038/nature12332

Simón, M. V., Prado Spalm, F. H., Politi, L. E., and Rotstein, N. P. (2015). Sphingosine-1-phosphate is a crucial signal for migration of retina Müller Glial cells. *Invest. Ophthalmol. Vis. Sci.* 56, 5808–5815. doi: 10.1167/iovs.14-16195

Skoura, A., Sanchez, T., Claffey, K., Mandala, S. M., Proia, R. L., and Hla, T. (2007). Essential role of sphingosine 1-phosphate receptor 2 in pathological angiogenesis of the mouse retina. *J. Clin. Invest.* 117, 2506–2516. doi: 10.1172/JCI31123

Snider, A. J., Orr Gandy, K. A., and Obeid, L. M. (2010). Sphingosine kinase: role in regulation of bioactive sphingolipid mediators in inflammation. *Biochimie* 92, 707–715. doi: 10.1016/j.biochi.2010.02.008

Sorensen, S. D., Nicole, O., Peavy, R. D., Montoya, L. M., Lee, C. J., Murphy, T. J., et al. (2003). Common signaling pathways link activation of murine PAR-1, LPA, and S1P receptors to proliferation of astrocytes. *Mol. Pharmacol.* 64, 1199–1209. doi: 10.1124/mol.64.5.1199

Spiegel, S., and Milstien, S. (2002). Sphingosine 1-phosphate, a key cell signaling molecule. *J. Biol. Chem.* 277, 25851–25854. doi: 10.1074/jbc.R200007200

Spiegel, S., Maczis, M. A., Maceyka, M., and Milstien, S. (2019). New insights into functions of the sphingosine-1-phosphate transporter SPNS2. *J. Lipid Res.* 60, 484–489. doi: 10.1194/jlr.S091959

Sreekumar, P. G., Ding, Y., Ryan, S. J., Kannan, R., and Hinton, D. R. (2009). Regulation of thioredoxin by ceramide in retinal pigment epithelial cells. *Exp. Eye Res.* 88, 410–417. doi: 10.1016/j.exer.2008.10.009

Stancevic, B., and Kolesnick, R. (2010). Ceramide-rich platforms in transmembrane signaling. *FEBS Lett.* 584, 1728–1740. doi: 10.1016/j.febslet.2010.02.026

Stiles, M., Qi, H., Sun, E., Tan, J., Porter, H., Allegood, J., et al. (2016). Sphingolipid profile alters in retinal dystrophic P23H-1 rats and systemic FTY720 can delay retinal degeneration. *J. Lipid Res.* 57, 818–831. doi: 10.1194/jlr.M063719

Strettoi, E., Gargini, C., Novelli, E., Sala, G., Piano, I., Gasco, P., et al. (2010). Inhibition of ceramide biosynthesis preserves photoreceptor structure and function in a mouse model of retinitis pigmentosa. *Proc. Natl. Acad. Sci. U.S.A.* 107, 18706–18711. doi: 10.1073/pnas.1007644107

Strochlic, L., Dwivedy, A., van Horck, F. P. G., Falk, J., and Holt, C. E. (2008). A role for S1P signalling in axon guidance in the Xenopus visual system. *Development* 135, 333–342. doi: 10.1242/dev.009563

Strub, G. M., Paillard, M., Liang, J., Gomez, L., Allegood, J. C., Hait, N. C., et al. (2011). Sphingosine-1-phosphate produced by sphingosine kinase 2 in mitochondria interacts with prohibitin 2 to regulate complex IV assembly and respiration. *FASEB J.* 25, 600–612. doi: 10.1096/fj.10-167502

Sugano, E., Edwards, G., Saha, S., Wilmott, L., Grambergs, R. C., Mondal, K., et al. (2018). Overexpression of acid-Ceramidase (ASAH1) Protects Retinal Cells (ARPE19) from Oxidative Stress. *J. Lipid Res.* 60, 30–43. doi: 10.1194/jlr.M082198

Suzuki, E., Handa, K., Toledo, M. S., and Hakomori, S. (2004). Sphingosine-dependent apoptosis: a unified concept based on multiple mechanisms operating in concert. *Proc. Natl. Acad. Sci. U.S.A.* 101, 14788–14793. doi: 10.1073/pnas.0406536101

Swaney, J. S., Moreno, K. M., Gentile, A. M., Sabbadini, R. A., and Stoller, G. L. (2008). Sphingosine-1-phosphate (S1P) is a novel fibrotic mediator in the eye. *Exp. Eye Res.* 87, 367–375. doi: 10.1016/j.exer.2008.07.005

Sweeney, E. A., Sakakura, C., Shirahama, T., Masamune, A., Ohta, H., Hakomori, S., et al. (1996). Sphingosine and its methylated derivative N,N-dimethylsphingosine (DMS) induce apoptosis in a variety of human cancer cell lines. *Int. J. Cancer* 66, 358–366. doi: 10.1002/(sici)1097-0215(19960503)66%3A3%3C358%3A%3Aaid-ijc16%3E3.0.co%3B2-7

Tabasinezhad, M., Samadi, N., Ghanbari, P., Mohseni, M., Saei, A. A., Sharifi, S., et al. (2013). Sphingosin 1-phosphate contributes in tumor progression. *J. Cancer Res. Ther.* 9, 556–563. doi: 10.4103/0973-1482.126446

Tabuchi, K., and Hara, A. (2018). Impact of sphingolipid mediators on the determination of cochlear survival in ototoxicity. *Curr. Mol. Pharmacol.* 11, 279–284. doi: 10.2174/1874467211666180516101111

Tafesse, F. G., Ternes, P., and Holthuis, J. C. M. (2006). The multigenic sphingomyelin synthase family. *J. Biol. Chem.* 281, 29421–29425. doi: 10.1074/jbc.R600021200

Taha, T. A., Hannun, Y. A., and Obeid, L. M. (2006). Sphingosine kinase: biochemical and cellular regulation and role in disease. *J. Biochem. Mol. Biol.* 39, 113–131. doi: 10.5483/bmbrep.2006.39.2.113

Takabe, K., Kim, R. H., Allegood, J. C., Mitra, P., Ramachandran, S., Nagahashi, M., et al. (2010). Estradiol induces export of sphingosine 1-phosphate from breast cancer cells via ABCC1 and ABCG2. *J. Biol. Chem.* 285, 10477–10486. doi: 10.1074/jbc.M109.064162

Takabe, K., Paugh, S. W., Milstien, S., and Spiegel, S. (2008). Inside-Out" signaling of sphingosine-1-phosphate: therapeutic targets. *Pharmacol. Rev.* 60, 181–195. doi: 10.1124/pr.107.07113

Takuwa, Y., Ikeda, H., Okamoto, Y., Takuwa, N., and Yoshioka, K. (2013). Sphingosine-1-phosphate as a mediator involved in development of fibrotic diseases. *Biochim. Biophys. Acta* 1831, 185–192. doi: 10.1016/j.bbalip.2012.06.008

Terao, R., Honjo, M., and Aihara, M. (2017). Apolipoprotein M inhibits angiogenic and inflammatory response by sphingosine 1-phosphate on retinal pigment epithelium cells. *Int. J. Mol. Sci.* 19:112. doi: 10.3390/ijms19010112

Tikhonenko, M., Lydic, T. A., Wang, Y., Chen, W., Opreanu, M., Sochacki, A., et al. (2010). Remodeling of retinal fatty acids in an animal model of diabetes: a decrease in long-chain polyunsaturated fatty acids is associated with a decrease in fatty acid Elongases Elovl2 and Elovl4. *Diabetes* 59, 219–227. doi: 10.2337/db09-0728

Toman, R. E., Payne, S. G., Watterson, K. R., Maceyka, M., Lee, N. H., Milstien, S., et al. (2004). Differential transactivation of sphingosine-1-phosphate receptors modulates NGF-induced neurite extension. *J. Cell Biol.* 166, 381–392. doi: 10.1083/jcb.200402016

Tomita, H., Abe, T., and Tamai, M. (2000). Ceramide-induced cell death in cultured rat retinal pigment epithelial cells. *Tohoku J. Exp. Med.* 190, 223–229. doi: 10.1620/tjem.190.223

Toops, K. A., Tan, L. X., Jiang, Z., Radu, R. A., and Lakkaraju, A. (2015). Cholesterol-mediated activation of acid sphingomyelinase disrupts autophagy in the retinal pigment epithelium. *Mol. Biol. Cell* 26, 1–14. doi: 10.1091/mbc.e14-05-1028

Trayssac, M., Hannun, Y. A., and Obeid, L. M. (2018). Role of sphingolipids in senescence: implication in aging and age-related diseases. *J. Clin. Invest.* 128, 2702–2712. doi: 10.1172/JCI97949

Tuson, M., Garanto, A., Gonzàlez-Duarte, R., and Marfany, G. (2009). Overexpression of CERKL, a gene responsible for retinitis pigmentosa in humans, protects cells from apoptosis induced by oxidative stress. *Mol. Vis.* 15, 168–180.

Tuson, M., Marfany, G., and Gonzàlez-Duarte, R. (2004). Mutation of CERKL, a novel human ceramide kinase gene, causes autosomal recessive retinitis pigmentosa (RP26). *Am. J. Hum. Genet.* 74, 128–138. doi: 10.1086/381055

Wang, G., and Bieberich, E. (2018). Sphingolipids in neurodegeneration (with focus on ceramide and S1P). *Adv. Biol. Regul.* 70, 51–64. doi: 10.1016/j.jbior.2018.09.013

Wang, G., Silva, J., Krishnamurthy, K., Tran, E., Condie, B. G., and Bieberich, E. (2005). Direct binding to ceramide activates protein kinase C Cζ before the formation of a pro-apoptotic complex with PAR-4 in differentiating stem cells. *J. Biol. Chem.* 280, 26415–26424. doi: 10.1074/jbc.M501492200

Wang, Q., Navitskaya, S., Chakravarthy, H., Huang, C., Kady, N., Lydic, T. A., et al. (2016). Dual anti-inflammatory and anti-angiogenic action of miR-15a in diabetic retinopathy. *EBioMedicine* 11, 138–150. doi: 10.1016/j.ebiom.2016.08.013

Wang, H.-Y., Wang, Y., Zhang, Y., Wang, J., Xiong, S.-Y., and Sun, Q. (2018). Crosslink between lipids and acute uveitis: a lipidomic analysis. *Int. J. Ophthalmol.* 11, 736–746. doi: 10.18240/ijo.2018.05.05

Wattenberg, B. W., Pitson, S. M., and Raben, D. M. (2006). The sphingosine and diacylglycerol kinase superfamily of signaling kinases: localization as a key to signaling function. *J. Lipid Res.* 47, 1128–1139. doi: 10.1194/jlr.R600003-JLR200

Wegner, M.-S., Schiffmann, S., Parnham, M. J., Geisslinger, G., and Grösch, S. (2016). The enigma of ceramide synthase regulation in mammalian cells. *Prog. Lipid Res.* 63, 93–119. doi: 10.1016/j.plipres.2016.03.006

Wijesinghe, D. S., Massiello, A., Subramanian, P., Szulc, Z., Bielawska, A., and Chalfant, C. E. (2005). Substrate specificity of human ceramide kinase. *J. Lipid Res.* 46, 2706–2716. doi: 10.1194/jlr.M500313-JLR200

Wu, B. X., Clarke, C. J., and Hannun, Y. A. (2010). Mammalian neutral sphingomyelinases: regulation and roles in cell signaling responses. *Neuromolecular Med.* 12, 320–330. doi: 10.1007/s12017-010-8120-z

Wu, B. X., Fan, J., Boyer, N. P., Jenkins, R. W., Koutalos, Y., Hannun, Y. A., et al. (2015). Lack of acid sphingomyelinase induces age-related retinal degeneration. *PLoS One* 10:e0133032. doi: 10.1371/journal.pone.0133032

Wynn, T. A. (2007). Common and unique mechanisms regulate fibrosis in various fibroproliferative diseases. *J. Clin. Invest.* 117, 524–529. doi: 10.1172/JCI31487

Yamanaka, M., Shegogue, D., Pei, H., Bu, S., Bielawska, A., Bielawski, J., et al. (2004). Sphingosine kinase 1 (SPHK1) is induced by transforming growth factor-beta and mediates TIMP-1 up-regulation. *J. Biol. Chem.* 279, 53994–54001. doi: 10.1074/jbc.M410144200

Yao, J., Bi, H.-E., Sheng, Y., Cheng, L.-B., Wendu, R.-L., Wang, C.-H., et al. (2013). Ultraviolet (UV) and hydrogen peroxide activate ceramide-ER stress-AMPK signaling axis to promote retinal pigment epithelium (RPE) cell apoptosis. *Int. J. Mol. Sci.* 14, 10355–10368. doi: 10.3390/ijms140510355

You, Y., Gupta, V. K., Li, J. C., Al-Adawy, N., Klistorner, A., and Graham, S. L. (2014). FTY720 protects retinal ganglion cells in experimental glaucoma. *Investig. Ophthalmol. Vis. Sci.* 55, 3060–3066. doi: 10.1167/iovs.13-13262

Young, M. M., Kester, M., and Wang, H.-G. (2013). Sphingolipids: regulators of crosstalk between apoptosis and autophagy. *J. Lipid Res.* 54, 5–19. doi: 10.1194/jlr.R031278

Yu, F. P., Sajdak, B., Sikora, J., Salmon, A. E., Nagree, M. S., Gurka, J., et al. (2018). Acid ceramidase deficiency in mice leads to severe ocular pathology and visual impairment. *Am. J. Pathol.* 189, 320–338. doi: 10.1016/j.ajpath.2018.10.018

Yu, S., Li, C., Biswas, L., Hu, X., Liu, F., Reilly, J., et al. (2017). CERKL gene knockout disturbs photoreceptor outer segment phagocytosis and causes rod-cone dystrophy in zebrafish. *Hum. Mol. Genet.* 26, 2335–2345. doi: 10.1093/hmg/ddx137

Yu, Y., Reynolds, R., Fagerness, J., Rosner, B., Daly, M. J., and Seddon, J. M. (2011). Association of variants in the LIPC and ABCA1 genes with intermediate and large drusen and advanced age-related macular degeneration. *Invest. Ophthalmol. Vis. Sci.* 52, 4663–4670. doi: 10.1167/iovs.10-7070

Zarbin, M. A., Green, W. R., Moser, A. B., and Tiffany, C. (1988). Increased levels of ceramide in the retina of a patient with Farber's disease. *Arch. Ophthalmol.* 106:1163. doi: 10.1001/archopht.1988.01060140323008

Zhao, L., Zabel, M. K., Wang, X., Ma, W., Shah, P., Fariss, R. N., et al. (2015). Microglial phagocytosis of living photoreceptors contributes to inherited retinal degeneration. *EMBO Mol. Med.* 7, 1179–1197. doi: 10.15252/emmm.201505298

Zhu, D., Sreekumar, P. G., Hinton, D. R., and Kannan, R. (2010). Expression and regulation of enzymes in the ceramide metabolic pathway in human retinal pigment epithelial cells and their relevance to retinal degeneration. *Vision Res.* 50, 643–651. doi: 10.1016/j.visres.2009.09.002

Conflict of Interest Statement: The authors declare that the research was conducted in the absence of any commercial or financial relationships that could be construed as a potential conflict of interest.

frontiers in Cellular Neuroscience

ORIGINAL RESEARCH
published: 26 June 2019
doi: 10.3389/fncel.2019.00279

Effect of Autophagy Modulators on Vascular, Glial, and Neuronal Alterations in the Oxygen-Induced Retinopathy Mouse Model

*Paula V. Subirada[1,2], María C. Paz[1,2], Magali E. Ridano[1,2], Valeria E. Lorenc[3], Claudio M. Fader[4,5], Gustavo A. Chiabrando[1,2] and María C. Sánchez[1,2]**

[1] Departamento de Bioquímica Clínica, Facultad de Ciencias Químicas, Universidad Nacional de Córdoba, Córdoba, Argentina, [2] Consejo Nacional de Investigaciones Científicas y Técnicas (CONICET), Centro de Investigaciones en Bioquímica Clínica e Inmunología (CIBICI), Córdoba, Argentina, [3] Nanomedicine and Vision Group, Facultad de Ciencias Biomédicas, Instituto de Investigaciones en Medicina Traslacional, Universidad Austral, Consejo Nacional de Investigaciones en Ciencia y Tecnología (CONICET), Pilar, Argentina, [4] Facultad de Odontología Mendoza, Universidad Nacional de Cuyo, Mendoza, Argentina, [5] Instituto de Histología y Embriología (IHEM), Facultad de Ciencias Médicas, Universidad Nacional de Cuyo, Consejo Nacional de Investigaciones Científicas y Técnicas (CONICET), Mendoza, Argentina

OPEN ACCESS

Edited by:
Gabriela Alejandra Salvador, Universidad Nacional del Sur, Argentina

Reviewed by:
Elisabetta Catalani, Università degli Studi della Tuscia, Italy
Sheng Zhang, University of Texas Health Science Center at Houston, United States

***Correspondence:**
María C. Sánchez
csanchez@fcq.unc.edu.ar

Specialty section:
This article was submitted to Cellular Neurophysiology, a section of the journal Frontiers in Cellular Neuroscience

Received: *14 January 2019*
Accepted: *11 June 2019*
Published: *26 June 2019*

Citation:
Subirada PV, Paz MC, Ridano ME, Lorenc VE, Fader CM, Chiabrando GA and Sánchez MC (2019) Effect of Autophagy Modulators on Vascular, Glial, and Neuronal Alterations in the Oxygen-Induced Retinopathy Mouse Model. Front. Cell. Neurosci. 13:279. doi: 10.3389/fncel.2019.00279

Hypoxia is one of the main insults in proliferative retinopathies, leading to neovascularization and neurodegeneration. To maintain homeostasis, neurons require efficient degradation and recycling systems. Autophagy participates in retinal cell death, but it is also a cell survival mechanism. Here, we analyzed the role of autophagy at the three characteristic time periods in the oxygen-induced retinopathy (OIR) mouse model and determined if its modulation can improve vascular and non-vascular alterations. Experiments were performed with chloroquine (CQ) in order to monitor autophagosome accumulation by lysosomal blockade. Post natal day (P)17 OIR mouse retinas showed a significant increase in autophagy flux. In particular, an intense LC3B and p62 staining was observed in inner layers of the retina, mainly proliferating endothelial cells. After a single intraocular injection of Rapamycin at P12 OIR, a decreased neovascular area and vascular endothelial growth factor (VEGF) protein expression were observed at P17 OIR. In addition, whereas the increased expression of glial fibrillary acidic protein (GFAP) was reversed at P26 OIR, the functional alterations persisted. Using a similar therapeutic schedule, we analyzed the effect of anti-VEGF therapy on autophagy flux. Like Rapamycin, VEGF inhibitor treatment not only reduced the amount of neovascular tufts, but also activated autophagy flux at P17 OIR, mainly in ganglion cell layer and inner nuclear layer. Finally, the effects of the disruption of autophagy by Spautin-1, were evaluated at vascular, glial, and neuronal levels. After a single dose of Spautin-1, Western blot analysis showed a significant decrease in LC3B II and p62 protein expression at P13 OIR, returning both autophagy markers to OIR control levels at P17. In addition, neither gliosis nor functional alterations were attenuated. In line with these results, TUNEL staining showed a slight increase in the number of positive cells in the outer nuclear layer at P17 OIR. Overall, our results demonstrate that all treatments of induction or

inhibition of the autophagic flux reduced neovascular area but were unable to completely reverse the neuronal damage. Besides, compared to current treatments, rapamycin provides a more promising therapeutic strategy as it reduces both neovascular tufts and persistent gliosis.

Keywords: autophagy, hypoxia, proliferative retinopathies, vascular endothelial growth factor, retinal functionality, gliosis, neurodegeneration

INTRODUCTION

Retinal neovascular pathologies are still leading causes of blindness worldwide in middle age (DR) and pediatric [retinopathy of prematurity (ROP)] population (Campochiaro, 2015; Rubio and Adamis, 2016). Currently, there is a wide spectrum of treatments available for these diseases including laser photocoagulation and, more recently the intraocular injections of anti-VEGF agents (Evans et al., 2014; Diabetic Retinopathy Clinical Research Network et al., 2015; Tah et al., 2015). Independently of the etiology, retinal neovascular pathologies are characterized by an increase in cytoplasmic HIF-1α levels, a subsequent dimerization with HIF-1β and translocation to the nucleus (Semenza, 2012). Vascular endothelial growth factor is one of the most critical target genes of HIF, and a well-known key player in neovascularization (NV) (Nagy et al., 2008). This trophic factor has pleiotropic functions over neurons and ECs in health and disease (Saint-Geniez et al., 2008; Zhang et al., 2009). In hypoxic environment VEGF levels largely increase and is the main responsible of ECs survival, migration, and proliferation (Gerhardt, 2008). Nowadays, anti-VEGF therapies are the most recommended treatment for retinal NV as they have proved high efficacy in animal models and clinical trials (Tah et al., 2015). Although anti-VEGF treatment has shown better outcomes than alternative treatments, ophthalmologists have detected unequal response of patients to the same administration scheme. Moreover, they have observed that some patients lost visual acuity after the chronic treatment (Osaadon et al., 2014; Yang et al., 2016). There are two main explanations that shed light on these events. On one hand, other proteins involved in NV, inflammation, vascular tone and metabolism have critical roles, whereby, VEGF inhibition would result insufficient to restore retinal homeostasis and regresses NV in the hypoxic milieu. On the other hand, VEGF is also a neuroprotective factor and its further depletion has deleterious effects over neuronal survival.

Consequently, many researchers have designed new pharmacological strategies to cope with NV through the modulation of different proteins or molecular pathways. Based on multiple studies carried out in the field of cancer angiogenesis, recently, it has been proposed that autophagy flux would have an important role as a potential therapeutic tool in clinical medicine (Mizushima and Komatsu, 2011). Autophagy is a catabolic intracellular mechanism that provides recycling of its components through the engulfment of damaged proteins and organelles in a double membrane vesicle (Levine et al., 2015). As it participates in retinal cell death but it is also a cell survival mechanism, its modulation may be either beneficial or deleterious depending on the retinal cell type involved or the disease context (Boya et al., 2016; Chai et al., 2016; Rosa et al., 2016; Amato et al., 2018). In this work, we intend to unravel the role of autophagy on retinal pathological NV and neurodegeneration in mice with oxygen-induced retinopathy (OIR), an animal model of proliferative ischemic retinopathy, and determine if its modulation can improve retinal functionality, gliosis, and avoid neuronal cell death.

Abbreviations: CQ, chloroquine; DR, diabetic retinopathy; ECs, endothelial cells; ERG, electroretinogram; GCL, ganglion cell layer; GFAP, glial fibrilar acid protein; GS, glutamine synthase; HIF, hypoxia inducible factor; ILM, inner limitant membrane; INL, inner nuclear layer; LAMP1, lysosomal-associated membrane protein 1; LC3B, microtubule-associated proteins 1A/1B light chain 3B; MGCs, Muller glial cells; NG-2, neuron-glial 2; NV, neovascularization; OIR, oxygen induced retinopathy; ONL, outer nuclear layer; P, post natal day; RA, room air; ROP, retinopathy of prematurity; VEGF, vascular endothelial growth factor; VO, vaso-obliteration.

MATERIALS AND METHODS

C57BL/6J mice were handled according to guidelines of the ARVO Statement for the Use of Animals in Ophthalmic and Vision Research. Experimental procedures were designed and approved by the Institutional Animal Care and Use Committee (CICUAL) of the Faculty of Chemical Sciences, National University of Córdoba (Res. HCD 1216/18). All efforts were made to reduce the number of animals used.

Oxygen-Induced Retinopathy (OIR) Mouse Model

In the OIR mouse model (Smith et al., 1994), litters of mice pups and their mothers were exposed to high oxygen concentration (75 ± 2%) from P7 to P12 (hyperoxic period) in an incubator chamber. Oxygen was checked twice daily with an oxygen analyzer (Teledyne Analytical Instruments, Industry, CA, United States). Then, mice were brought to room air (RA) for additional 5 or 14 days. Age-matched control C57BL/6 mice were kept continuously at RA. Animals were maintained in clear plastic cages with standard light cycles (12 h light/12 h dark). At P12, OIR mice were intravitreally injected with a 1.0 μl of solution containing a specific treatment: (a) Rapamycin: 0.5 μg/ml (R0395 Sigma Aldrich, St. Louis, MO, United States); (b) Anti-VEGF mAb: 1.25 μg anti-VEGF diluted 1/20 with phosphate buffered saline (PBS) (Bevacizumab; Genentech, San Francisco, CA, United States) as previously reported (Ridano et al., 2017); (c) Spautin-1 200 μM (SML0440, Sigma Aldrich, St. Louis, MO, United States). Vehicle (DMSO/PBS or PBS)/-injected mice were used as controls. Rapamycin and Spautin-1 concentrations were selected according to *in vitro* assays

(Chen et al., 2014; Russo et al., 2018) and concentrations 10 folds higher than in cell cultures were used (taking in account the dilution of the drug in the vitreous cavity). Briefly, pups were locally anesthetized with one drop of proparacaine hydrochloride 0.5% (Anestalcon, Alcon), exophthalmia was induced with one drop of tropicamide 1% (Midril, Alcon, Buenos Aires, Argentina) and eyes were injected at the upper nasal limbus as described previously (Barcelona et al., 2011). Some mice were sacrificed at three typical times in the OIR mouse model: P12 (maximum vaso-obliteration, VO), P17 (maximum NV) and P26 (vascular alteration resolution) (Smith et al., 1994). To evaluate the effect of Rapamycin or Spautin-1 mice were sacrificed 24 h after the injection (P13). In order to analyze the autophagy flux, some mice received an intraperitoneal (i.p.) injection of chloroquine (CQ) 60 mg/kg (Sigma Aldrich, St. Louis, MO, United States) diluted in sterile PBS 4 h before sacrifice. Eyes or retinas of sacrificed mice with CQ pre-treatment were collected and processed for Western blot and immunofluorescence assays and without CQ pre-treatment for quantitative real-time PCR (qRT-PCR), immunohistochemistry, or flat-mount assays. At least six mice per group were used for each condition at each survival time examined. Data were collected from both males and females as there were no apparent sex differences. All mice were sacrificed at the same time of day in order to avoid the circadian effects and to reduce the mouse-to-mouse variability in autophagy markers and flux. Lysosomal analyses were carried out with intraocular injection of 1 μl of red DQ-BSA (1 mg/ml dissolved in PBS pH 7.2; D12051, Invitrogen). The reagent is taken up by every cell and then the red dye is detected in acidic compartments, where DQ is hydrolyzed from albumin. Mice were sacrificed 4 h after DQ injection (without CQ pre-treatment), fixed with 4% paraformaldehyde (PFA) and dehydrated by sucrose gradient for further cryosection.

Electroretinography (ERG)

Electroretinographic activity was assessed as previously described (Ridano et al., 2017). Briefly, after overnight (ON) dark adaptation and under dim red illumination, mice were anesthetized via i.p. injections with a solution containing ketamine (90 mg/kg)/xilacine (8 mg/kg). The pupils were dilated with 1% tropicamide and the cornea was lubricated with gel drops of 0.4% polyethyleneglycol 400 and 0.3% propylene glycol (Systane, Alcon, Buenos Aires, Argentina) to prevent damage. Mice were exposed to stimuli at a distance of 20 cm. A reference electrode was inserted on the back in the neck, a grounding electrode was attached to the tail, and a gold electrode was placed in contact with the central cornea. Electroretinograms were simultaneously recorded from both eyes and 10 responses to flashes of unattenuated white light (5 cd.s/m^2, 0.2 Hz) from a photic stimulator (light-emitting diodes) set at maximum brightness were amplified, filtered (1.5-Hz low-pass filter, 1000 high-pass filter, notch activated) and averaged (Akonic BIO-PC, Argentina). The a-wave was measured as the difference in amplitude between the recording at onset and trough of the negative deflection, and the b-wave amplitude was measured from the trough of the a-wave to the peak of the b-wave. The latencies of the a- and b-waves were measured from the time of flash presentation to the trough of the a-wave or the peak of the b-wave, respectively. Responses were averaged across the two eyes for each mouse.

Labeling of Flat-Mount Retinas

Mice were euthanized at P17 and eyes were enucleated and fixed with freshly prepared 4% PFA for 1–2 h at room temperature (RT). Corneas were removed with scissors along the limbus and the whole retinas were dissected. Then, they were blocked and permeabilized in Tris-buffered saline (TBS) containing 5% Bovine Serum Albumin (BSA) and 0.1% Triton-X-100 during6 h at 4°C. After that, retinas were incubated ON with 0.01 μg/μl of Isolectin IB4 Alexa fluor-488 conjugate (GSA-IB4) from Molecular Probes, Inc. (Eugene, OR, United States) and anti-GFAP (1/200; Dako, Carpinteria, CA, United States) or anti-microtubule-associated protein-1 light-chain 3 (LC3) B (1:100; L7543, Sigma). Retinas were then washed with TBS containing 0.1% Triton-X-100, stored in PBS at 4°C and examined by confocal laser-scanning microscopy (Olympus FluoView FV1200; Olympus, Corp., New York, NY, United States).

Retinal Cryosection, Protein Extract, and RNA Sample Preparation

For cryosection, enucleated eyes were fixed during 2 h with 4% PFA at RT, and incubated ON in 10, 20, and 30% of sucrose in PBS at 4°C. Then, they were embedded in optimum cutting temperature (OCT) (Tissue-TEK, Sakura) compound, and 10 μm-thick radial sections were obtained by using a cryostat, as described (Sanchez et al., 2006). Retinal cryosections were stored at −20°C under dry conditions until immunohistochemical analysis.

Neural retinas were dissected from RPE/choroid layers for Western blot and qRT-PCR analysis. Protein extracts were obtained from retinas after homogenization with a lysis buffer containing 20 mM Tris-HCl pH 7.5, 137 mM NaCl, 2 mM EDTA pH 8, 1% Nonidet P40, 1 mM phenylmethylsulfonyl fluoride (PMSF), 2 mM sodium ortovanadate and protease inhibitor cocktail (Sigma Aldrich, St. Louis, MO, United States) (Sanchez et al., 2006), and were sonicated during 20 s at 40% amplitude. In addition, some neural retinas were disrupted in 500 μL Trizol (Invitrogen) and were stored at −80°C until RNA extraction. All the assays were performed in triplicate and results are representative of at least three independent experiments (animals in each group).

Immunofluorescence

Immunostaining was performed as described previously (Ridano et al., 2017). Briefly, mouse cryosections were washed in PBS, blocked with 2% of BSA in PBS containing 0.1% Tween-20, for 1 h and then incubated ON at 4°C with the following primary antibodies, respectively: rabbit polyclonal anti-LC3B (1/100; L7543, Sigma Aldrich), mouse monoclonal anti-p62 (1/100; ab56416, Abcam), rabbit polyclonal anti- GS (1/100; ab16802, Abcam), rat monoclonal anti- LAMP1 (1/350; ab25245, Abcam), mouse monoclonal anti- GS (1/100; MAB 302, Millipore), mouse monoclonal anti-CD31 (1/50; Abcam, Inc., Cambridge, MA,

United States) and rabbit polyclonal anti-NG-2 (1/100; AB5320, Millipore). Then, sections were washed with TBS 0.1% Triton-X-100 and incubated with secondary antibodies including goat against rabbit or mouse IgG conjugated with Alexa Fluor 488 and 594 (1/250; Molecular Probes, Eugene, OR, United States) and goat anti rat IgG conjugated with Alexa Fluor 594 (1/200; ab150160, Abcam), during 1 h at RT. The sections were also counterstained with Hoechst 33258 (1:3000; Molecular Probes) for 7 min. After a thorough rinse, the sections were mounted with Fluor Save (Calbiochem, La Jolla, CA, United States) and cover slipped. The labeling was visualized using a confocal laser-scanning microscope (Olympus Fluvial FV300 or FV1200; Olympus, Corp., New York, NY, United States). Finally, images were processed with Image J 2 software (National Institutes of Health, Bethesda, MD, United States), including spatial deconvolution, vesicle quantification and colocalization. Negative controls without incubation with primary antibody were carried out to detect unspecific staining (data not shown).

Western Blot

Protein concentration of retinal extracts were determined by a BCA kit (Pierce, Buenos Aires, Argentina) and 10–20 μg of proteins were electrophoresed in 15% SDS-PAGE. After electrophoresis, proteins were transferred to nitrocellulose membranes (Amersham Hybond ECL; GE Healthcare Bio-Sciences AB, Uppsala, Sweden). To prevent non-specific binding, membranes were blocked with 5% milk in TBS containing 0.1% Tween-20 (TBST) during at least 1 h at RT. Then, blots were incubated with primary antibodies diluted in TBST or 5% BSA in TBST for 1 h at RT or overnight at 4°C, according to the antibody. The following antibodies were used: rabbit polyclonal anti-LC3 (1/1000; L7543, Sigma Aldrich), mouse monoclonal anti p62 (1/1000; ab56416, Abcam) mouse monoclonal anti- VEGF (1/500; R&D system), rabbit polyclonal anti-GFAP (1/1000; Dako, Carpinteria, CA, United States), mouse monoclonal anti-GS (1/500; MAB 302, Millipore Corporation MA, United States), rabbit polyclonal anti-caspase 3 (1/300; HPA 002643, Sigma Aldrich) and mouse monoclonal anti-β-actin (1/2000; ab8226, Abcam). Blots were incubated with IRDye 800 CW donkey anti-rabbit Ig, or IRDye 800 CW donkey anti-mouse IgG antibodies (1/15000 in TBS with 5% BSA) for 1 h, protected from light. After washing with TBST, membranes were visualized and quantified using the Odyssey Infrared Imaging System (LI-COR, Inc., Lincoln, NE, United States).

Quantitative Real-Time Polymerase Chain Reaction

Total RNA was extracted from neural retinas using Trizol (Invitrogen), according to the manufacturer's instructions and was processed as previously reported (Ridano et al., 2017). Briefly, 1 μg of total RNA was reverse-transcribed in a total volume of 20 μl using random primers (Invitrogen, Buenos Aires, Argentina) and 50 U of M-MLV reverse transcriptase (Promega, Corp.). Then, cDNA was mixed with 1x SYBR Green PCR Master Mix (Applied Biosystems) and forward and reverse primers: Beclin1 forward: ATGGAGGGGTCTAAGGCGTC/ Beclin 1 reverse: TGGGCTGTGGTAAGTAATGGA; ATG5 forward: TGTGCTTCGAGATGTGTGGTT/ ATG5 reverse: GTCAAATAGCTGACTCTTGGCAA; MAPLC3 forward: CGCTTGCAGCTCAATGCTAAC/ MAPLC3 reverse: TCG TACACTTCGGAGATGGG; P62 forward: TGTGGAACAT GGAGGGAAGAG/ P62 reverse: TGTGCCTGTGCTGGAA CTTTC. qPCR were carried out on an Applied Biosystems 7500 Real-Time PCR System with Sequence Detection Software v1.4. The cycling conditions included a hot start at 95°C for 10 min, followed by 40 cycles at 95°C for 15 s and 60°C for 1 min. Specificity was verified by melting curve analysis. Results were normalized to β-actin (Forward: GGCTGTATTCCCCTCCATCG/ Reverse: CCAGTTGGTAACAATGCCATGT). Relative gene expression was calculated according to the 2-ΔΔCt method. Each sample was analyzed in triplicate. No amplification was observed in PCRs using as template water during the cDNA synthesis (data not shown).

TUNEL Assay

Cell death was examined by terminal deoxynucleotidyltransferase biotin dUTP nick end labeling (TUNEL) assay (Roche, Mannheim, Germany), which contain an anti-dUTP antibody labeled with peroxidase (POD), according to manufacturer's instructions. Slides were counterstained with methyl green to visualize total nuclei and then mounted with DPX Mounting Media (Sigma Aldrich, St. Louis, MO, United States). Negative controls without enzyme were processed in order to avoid false positive results (data not shown). Images were obtained under a light microscope (Nikon Eclipse TE2000-E, United States).

Statistical Analysis

Statistical analysis was performed using the GraphPad Prism 5.0 software. A p-value < 0.05 was considered statistically significant. Parametric or non-parametric tests were used according to variance homogeneity evaluated by F or Barlett's tests. Two-tailed unpaired t or Mann–Whitney tests were used in analysis of two groups. One-way analysis of variance (ANOVA) followed by Dunnett´s multiple comparison post-test or Kruskal–Wallis followed by Dunn's multiple comparison post-test were used to determine statistical significance among more than two different groups. Two-way ANOVA followed by Bonferroni post-test was used in comparisons between groups when two variables were affecting the dependent variable. Mean ± standard error (SEM) are shown in graphs analyzed with parametric tests and median with interquartile range are shown when data were analyzed with non-parametric test.

RESULTS

Hypoxia Induced Autophagy During Neovascular Stage in the OIR Mouse Model

Autophagy is a strictly regulated process that plays a vital role in cell growth, transition, and death (Kimura et al., 2017). In

the nervous system it is a matter of intense investigation as these pathways are often missregulated during neovascular and neurodegenerative conditions (Harris and Rubinsztein, 2011; Du et al., 2012; Liu et al., 2016). In this regard, the mouse model of OIR offers an opportunity to examine the role of hypoxia in the pathogenesis of retinal NV, neuroinflammation, oxidative stress, and neurovascular cross-talk (Kim et al., 2016). Thus, in order to study autophagy flux, we determined the expression of classical autophagy markers at the three relevant time points in the OIR mouse model (**Figure 1A**). As we expected, GSA-IB4 lectin-labeled blood vessels in flat-mount retinas showed, at P17 OIR, a central zone of VO in addition to the characteristic vitreoretinal neovascular tufts, which were not observed in P17 RA controls (**Figure 1B**). Post-mitotic cells, especially neurons, are highly dependent on intracellular degradation systems because they provide adequate waste products elimination. The retina is known to have a fast autophagy flux due to the constant exposure to light and increased production of reactive oxygen species (Trachsel-Moncho et al., 2018). Therefore, we decided to block the autophagosome fusion with lysosomes and degradation with an i.p. injection of CQ to evaluate the accumulation of autophagosomes. Retinal levels for LC3B and p62 protein expression, at each temporal point, were measured in both RA and OIR mice by Western blot assays (**Figure 1C**). Quantitative analysis revealed a slight increase in LC3B II protein expression level at P12 in OIR mice, which was markedly upregulated in P17, returning to baseline levels at P26. In our experimental conditions, upregulation of LC3B II in retinal extracts at P17 OIR was associated with an increase, although not statistically significant, in p62 protein expression (**Figure 1D**). To gain more insight into autophagy regulation at the time point where most changes have been observed (P17), additional Western blot assays in mice injected with vehicle or CQ were performed (**Figure 1E**). Quantitative analysis showed an increase, although not statistically significant, in both LC3B II and p62 levels at P17 OIR compared to RA mice retinas injected with vehicle, which were further enhanced after CQ treatment (**Figure 1F**). Our data showed that the augmentation of LC3B II by hypoxic injury is due to the enhancement of autophagic flux rather than impaired clearance of autophagosomes.

Next, we examined the transcript expression of molecules involved in nucleation (Beclin-1), elongation (ATG-5), and structure (LC3) of the autophagosome (Yin et al., 2016), and also the autophagy substrate p62 at the peak of NV. Beclin-1, ATG-5 and LC3 mRNA levels did not showed changes at P17, whereas expression of p62 mRNA was increased ∼1.8−fold at this time point (**Figure 1G**).

By immunostaining of retinal cryosections we confirmed the increase in LC3B and p62 protein expression at P17 OIR (**Figure 1H**). Given that there is a tissue gradient of hypoxia in OIR retinas (Rodrigues et al., 2013), we decided to evaluate whether variations in autophagy flux were similar in every retinal layer. The analysis revealed an intense LC3B and p62 signal in the inner limiting membrane (ILM) at P17 OIR (**Figure 1I**). As neurons in the INL and GCL are severely affected by hypoxia (Ridano et al., 2017), quantification evidenced an increase in LC3B puncta mainly in these areas. At the same time, no modification in the autophagy marker puncta was observed in the ONL (**Figures 1I,J**).

Finally, we explored in more detail the presence of autophagosomes in the ILM, a region where vascular and macroglial cells actively interact. In cryosections, we identified Müller glial cells (MGCs) and vascular cells by staining with GS and CD31 respectively, whereas in retinal flat-mounts ECs were isolectin IB4^{+} cells (**Figure 2**, upper panel). Both macroglial and ECs showed, at P17 OIR, a slight increase in LC3B vesicles within the cells (**Figures 2A,B**). However, in neovascular tufts, ECs showed the great number of autophagic vesicles (**Figure 2C**).

In order to determine if the degradative pathway is activated at P17 OIR, we performed immunofluorescence assays using a combination of LC3B antibody along with the late endosomal compartments and lysosomes marker LAMP1 antibody (**Figure 2D**). Fusion of LC3B and LAMP1 positive vesicles was observed in ILM, GCL, and INL in OIR and RA neural retinas (**Figure 2E**). Our statistical analysis did not found differences in colocalization quantification in absence of CQ, probably due to the fast flux in the retina (**Figure 2F**). Through the injection of CQ, we could detect an increase of LAMP-1 vesicles, suggesting that lysosomes and late endosomes are following the degradation pathway properly (**Figures 2G,H**). To further examine the lysosomal activity, mice were intravitreally injected with bovine serum albumin derivate DQ-BSA (Frost et al., 2017). Confocal images showed an increased DQ-BSA staining in ECs at the time when the NV peaks in the OIR mice, compared to RA control retinas (**Figure 2I**), correlating with the observed in **Figure 2E**. However, this increase was not observed in the retinal layers where death was increased (**Figure 2I**). Collectively, our results showed an increase in autophagy flux mainly in proliferating ECs, and inner layers of the retina whereas neurons from the ONL did not showed modifications in autophagic flux at P17 OIR.

Rapamycin Promoted Autophagy, Prevented NV and Improved Gliosis in the OIR Mice Model

Rapamycin is a potent inhibitor of the complex mTORC1. One of the functions of this multi-protein complex is to prevent the formation of new autophagosomes by phosphorylation of ATG13. In this sense, Rapamycin acts as an autophagy inductor and its different pharmacological formulations (everolimus, sirolimus, among others) have shown beneficial effects in cancer therapies (Li et al., 2014). On the other hand, mTORC1 phosphorylation increase VEGF synthesis, a trophic factor required for vessel survival, proliferation and migration (Wei et al., 2016). New insights in retinal neurodegeneration pointed Rapamycin as a promising therapy as it could both activate autophagy and decrease angiogenesis (Zhu and Du, 2018). Hence, we decided to evaluate neovascular and neurodegenerative processes in the OIR mouse model after Rapamycin treatment (**Figure 3A**). After a single intraocular injection at P12 OIR, we verified the increase in the autophagy flux 24 h later by Western blot assay (**Figure 3B**). In addition, as Yagasaki et al. (2014) demonstrated previously, Rapamycin decreased the NV in P17 OIR retinas. Quantitative analysis

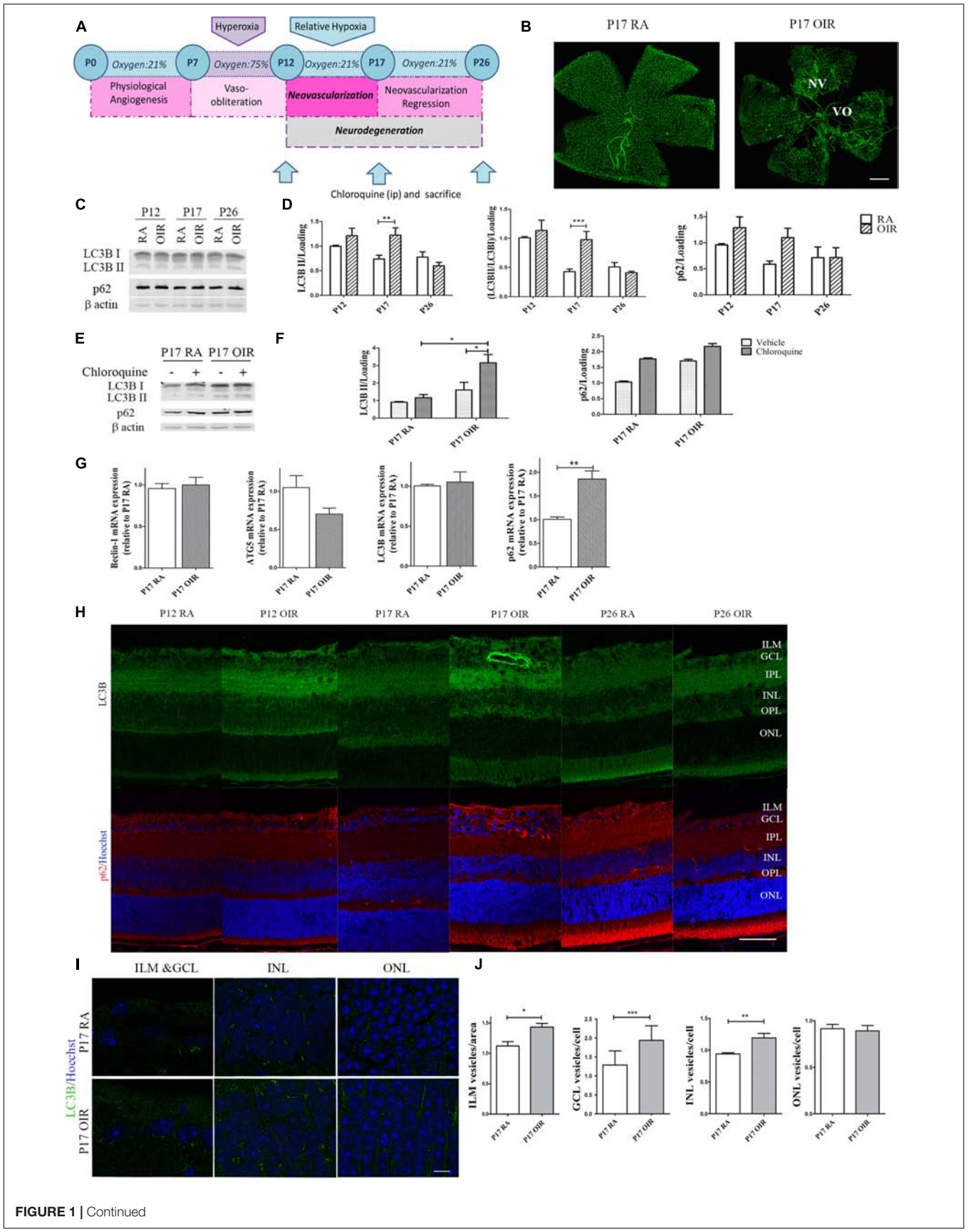

FIGURE 1 | Continued

FIGURE 1 | Effect of hypoxia on the autophagic flux during NV and neurodegeneration in OIR mouse retinas. **(A)** Scheme representing the OIR mouse model with hallmark time points during experimental disease development. Neonatal mice and their nursing mother are kept in room air from birth to P7. At P7, they are exposed to 75% oxygen, which inhibits retinal vessel growth and causes significant VO. Mice are returned to RA at P12; the avascular retina becomes hypoxic, eliciting both normal vessel regrowth and pathological neovascular response. NV reaches its maximum at P17. Shortly thereafter, it spontaneously regresses and the vascular alterations resolve by P25. **(B)** Representative images of flat-mount retinas at P17 showing GSA-IB4 vascular staining in RA and OIR mice. Areas with VO and NV are indicated. Scale bar: 500 μm. **(C,D)** Representative Western blot and quantification data of autophagy markers LC3B II and p62 from neural retinal extracts of RA and OIR at P12, P17, and P26. Mice were injected i.p. with CQ 4 h before sacrifice. β-Actin is shown as a loading control. Graph shows results of three independent experiments. **(E,F)** Representative Western blot and quantification data of autophagy markers, LC3B II and p62, from neural retinal samples of RA and OIR mice injected with vehicle or CQ at P17, and evaluated 4 h after administration. β-Actin is shown as a loading control. Graph shows results of three independent experiments. **(G)** Beclin-1, ATG5, LC3, and p62 mRNA levels were quantified by qRT-PCR in neurosensory retinas of P17 OIR and RA mice. Results were normalized to β-actin and expressed according to the 2-ΔΔCt method using as calibrator the mRNA level obtained from P17 RA mouse retinas. **(H)** Representative immunofluorescence analysis of LC3B (green) and p62 (red) in cryosections of RA and OIR mice injected with CQ at P12, P17, or P26 and evaluated 4 h after administration. Cell nuclei were counterstained with Hoechst 33258 (blue). **(I)** Representative labeling of LC3B (green) in cryosections of RA and OIR mouse retinas at P17, 4 h after CQ administration. Images were taken with oil 60X objective in the best confocal resolution condition. Cell nuclei were counterstained with Hoechst 33258 (blue) Scale bar: 5 μm. **(J)** Quantification of LC3B puncta per area or cell with ImageJ analyze particles software. ILM, inner limiting membrane; GCL, ganglion cell layer; IPL, inner plexiform layer; INL, inner nuclear layer; OPL, outer plexiform layer; ONL, outer nuclear layer. Data are presented as mean ± SEM. $^{*}p < 0.05$, $^{**}p < 0.01$, $^{***}p < 0.001$.

revealed a decrease of more than 75% of retinal NV area. However, the treatment was not able to attenuate other vascular alterations as avascular area, vessel dilatation and tortuosity (**Figures 3C,D**). In line with these observations, our next goal was to determine the protein expression levels of VEGF after Rapamycin treatment. Our results demonstrate that Rapamycin injection at P12 OIR significantly reduced VEGF protein expression in P17, respect to vehicle-injected OIR mouse samples (**Figure 3E**). Pericytes are mesenchymal cells that make important contributions to the microvascular tree in both normal and pathologic tissues (Gerhardt and Betsholtz, 2003). To determine the effect of Rapamycin on pericytes, retinal cryosections at P17 OIR were analyzed by immunofluorescence assay. Confocal microscopy analysis revealed no significant changes in NG-2 (a pericyte marker) staining after Rapamycin injection at P12 among both conditions (**Figure 3F**).

Persistent glial activation is considered a bad prognosis sign, as macroglial reactive cells frequently secrete cytokines and chemokines, contributing to the proinflammatory environment and mediating neuronal death (Subirada et al., 2018). Recently, we have demonstrated that P17 OIR mouse retinas showed the highest neovascular profile and exhibited neuro-glial injury as well as retinal functional loss, which persisted until P26 OIR (Ridano et al., 2017). Herein, we further analyzed if the inhibition of mTORC1 improved gliosis. By Western blot assays we observed comparable protein expression of GFAP in Rapamycin and vehicle-injected P17 OIR retinas (**Figures 4A,B**), which was corroborated by confocal microscopy analysis of flat mounts retinas (**Figure 4C**). However, the quantification at P26 evidenced a significant decrease of the GFAP protein expression after Rapamycin injection at P12. At the same time, we evaluated glial ability to prevent excitotoxicity by analyzing GS protein expression. Quantification of protein levels of the detoxifying enzyme indicated that it was not modified after Rapamycin treatment neither at P17 nor at P26 (**Figures 4A,B**), although a slight increase in the inner layers was detected by immunofluorescence staining (**Figure 4D**).

In retinal neovascular pathologies there is a direct relationship between vascular changes and neuronal dysfunction (Kern, 2014). Thus, we performed ERG studies in both OIR groups (vehicle and Rapamycin) and recorded the intensity (amplitude) and the speed (latency) of the neuronal response after light stimuli. Results demonstrated that neurodegeneration associated to NV was not prevented by the injection at P12 of Rapamycin as ERG signals at P17 and P26 did not show differences after treatment (**Figure 4E**). In line with this result, TUNEL assay (**Figure 4F**) and Western blot quantification of total caspase-3, in retinal extracts of OIR mice (**Figures 4G,H**), were similar in Rapamycin-injected respect to vehicle-injected OIR mouse samples.

We also evaluated changes in autophagy flux at P17 and P26 OIR after Rapamycin treatment. As shown in **Figures 4G,H**, increased levels of LC3B II and p62 expression persisted up to P17. Immunofluorescence assays (**Figure 4I**), were consistent with the Western blot results demonstrating LC3B and p62 staining mainly at GCL and INL. Together, these results indicate that a single injection of Rapamycin was able to prevent the formation of neovessels at P17 OIR by decreasing VEGF protein expression and ameliorate gliosis at P26. By contrast, other vascular and neuronal abnormalities were not reverted.

Anti-VEGF Treatment Increased the Autophagy Flux in OIR Mouse Retinas

In recent years, several studies have shown that VEGF inhibitors can lead to the activation of autophagy, including ranibizumab, bevacizumab, and several other vascular inhibitors (Liang et al., 2015; Lytvynchuk et al., 2015; Liu et al., 2016). Thus, we decided to determine whether the classical anti-angiogenic treatment was able to modulate the autophagic flux. For this purpose, using a similar treatment schedule (**Figure 5A**), we verified the anti-VEGF effect on vascular alteration in flat-mount retinas, where a significant reduction in neovascular and avascular areas was observed (**Figure 5B**). In addition, as expected, the administration of anti-VEGF mAb at P12 significantly reduced VEGF protein expression in P17 respect to vehicle-injected OIR mouse samples (**Figures 5C,D**).

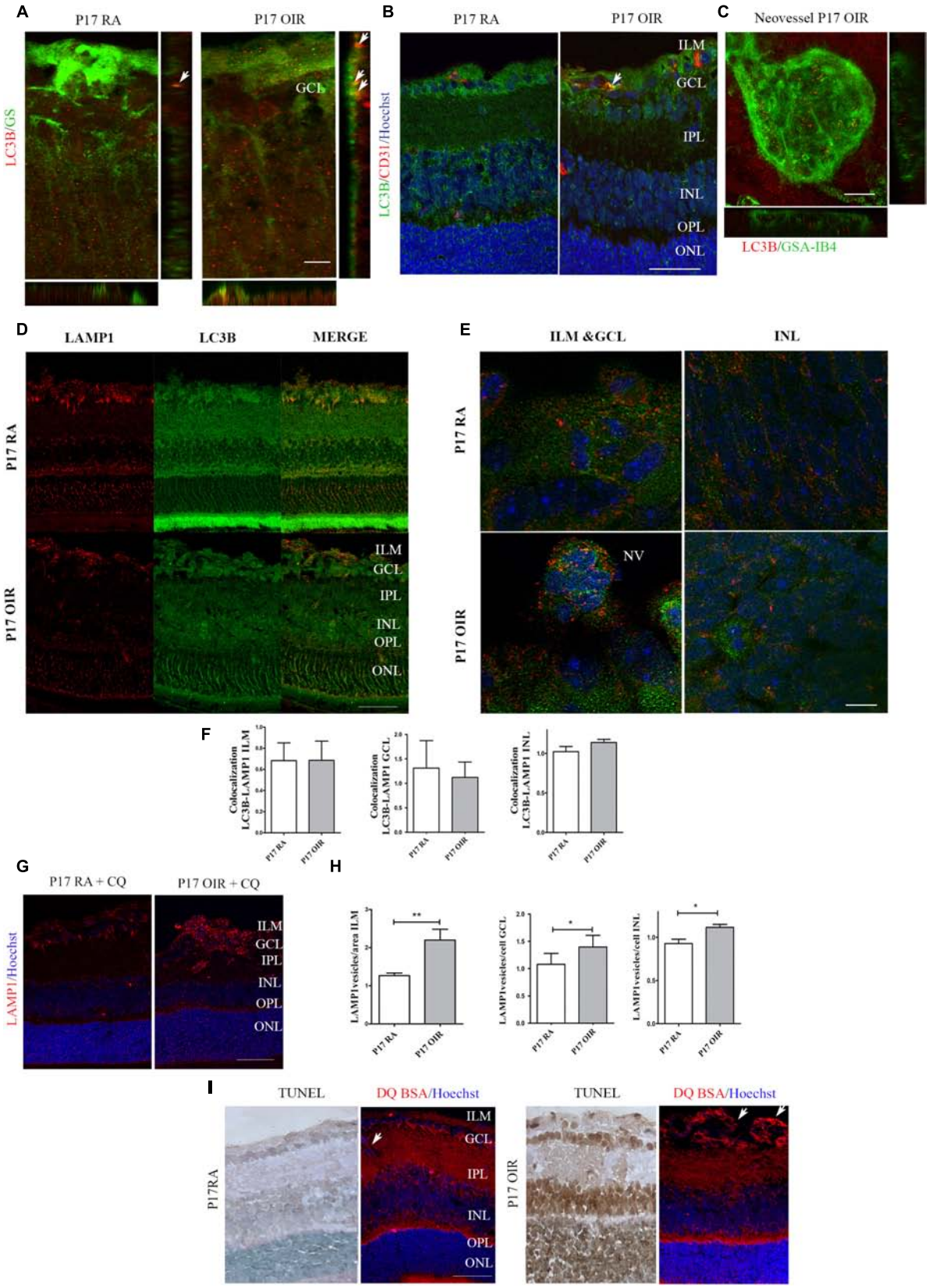

FIGURE 2 | Continued

FIGURE 2 | Effect of hypoxia on LC3B expression and distribution in P17 mouse retinas. Double labeling using: **(A)** a mouse monoclonal antibody for LC3B (red) and a MGC marker, anti-GS (green). Representative merged fluorescence confocal images of entire z-stack (XY) with orthogonal views, XZ and YZ of a mouse retina. Arrows are indicating autophagosomes in MGCs. Scale bar: 5 μm; **(B)** a mouse monoclonal antibody for LC3B (green) and an EC-specific marker, anti-CD31 (red). Cell nuclei were counterstained with Hoechst 33258 (blue). Arrows are indicating autophagosomes in ECs. Scale bar: 50 μm. **(C)** High magnification confocal micrograph of the representative P17 OIR retina showing a typical neovascular tuft (GSA-IB4, green) staining with LC3B (red). Images were taken with oil 60X objective in the best confocal resolution condition. Representative merged fluorescence confocal images of entire z-stack (XY) with orthogonal views, XZ and YZ. Scale bar: 15 μm **(D)** Representative immunofluorescence analysis of LAMP1 (red) and LC3B (green) in cryosections of P17 RA and OIR mice. Scale bar: 50 μm. **(E)** Representative immunofluorescence analysis of LAMP1 (red) and LC3B (green) in cryosections of P17 RA and OIR mice. Images were taken with oil 60X objective and zoom 5x in the best confocal resolution condition. Cell nuclei were counterstained with Hoechst 33258 (blue) Scale bar: 5 μm. **(F)** Quantification of LC3B/LAMP1 vesicles per area (ILM) or cell (GCL and INL) with ImageJ JACoP software. Pearson values were compared statistically. Statistical *t*-test was performed. **(G)** Representative immunofluorescence analysis of LAMP1 (red) in cryosections of RA and OIR mice injected with CQ at P17, and evaluated 4 h after administration. Scale bar: 50 μm. **(H)** Quantification of LAMP1 puncta per area or cell with ImageJ analyze particles software. Data are presented as mean ± SEM. $*p < 0.05$, $**p < 0.01$. **(I)** Representative TUNEL-labeled cryosections of P17 RA and OIR mice and cryosections of mice intravitreally injected with bovine serum albumin derivate DQ-BSA and co stained with anti-LC3B (green). Arrows are indicating DQ-BSA staining in ECs. Scale bar: 50 μm. ILM, inner limiting membrane; GCL, ganglion cell layer; IPL, inner plexiform layer; INL, inner nuclear layer; OPL, outer plexiform layer; ONL, outer nuclear layer; NV, neovascularization.

To determine the effect of anti-VEGF treatment on the autophagic process in the OIR mouse model we first examined the classical autophagy markers by Western blot assays. Quantitative analysis revealed a slight but significantly increase in LC3B II levels at P17 OIR (**Figures 5E,F**). This increase was corroborated by immunofluorescence assays where LC3B was detected mainly in GCL and INL (**Figure 5G**). These findings demonstrated that targeting VEGF prevented vascular alterations and also increased the autophagic flux in P17 OIR retinas.

Spautin-1 Inhibited Autophagy, Reduced NV but Did Not Prevented Neurodegeneration in the OIR Mouse Model

As autophagy seemed a key feature during NV, we next decided to decrease the autophagy flux by a single administration of Spautin-1 at P12 and to evaluate vascular, neuronal, and glial parameters at P17 and P26, respectively (**Figure 6A**). Western blot analysis showed a significant decrease in LC3B II expression at P13 (**Figure 6B**). Quantitative analysis of flat-mounts labeled with GSA-IB4 lectin showed a significant reduction of more than 70% in neovascular area after Spautin-1 treatment. However, other vascular alterations did not improved in OIR Spautin-1 mice, suggesting that autophagy is important for NV and that the activation in the OIR mouse is not mediating physiological revascularization (**Figures 6C,D**). In addition, a slight decrease in NG-2 staining was observed in Spautin-1 mice at P17 OIR (**Figure 6E**).

After Spautin-1 or vehicle treatment, no changes in GFAP levels were detected by Western blot of neural retinas samples (**Figures 7A,B**) or in flat-mount of retinas (**Figure 7C**). Similarly, no statistically differences in the expression of GS protein were found by Western blot (**Figures 7A,B**) or immunofluorescence (**Figure 7D**) after Spautin-1 treatment neither at P17 nor at P26.

In regard to neuronal functionality, the amplitude of the a-wave showed a tendency to decrease in OIR Spautin-1 mice at P17. In accordance, a later response (increased latency) was detected in photoreceptors as well as in inner neurons after autophagy inhibition (**Figure 7E**). Quantitative analysis of a-wave and b-wave amplitudes and latencies evidence no significant changes in neuronal functionality at P26. In line with these results, TUNEL staining showed a slight increase in the number of positive cells in the ONL after Spautin-1 treatment at P17 OIR (**Figure 7F**). Activation of apoptosis, measured by a reduction in total caspase 3 protein levels was not significantly different at both time points evaluated (**Figures 7G,H**). Finally, we evaluated protein expression of LC3B and p62 5 days (P17) or 14 days (P26) after Spautin-1 treatment. Quantitative analysis of Western blot assays (**Figures 7G,H**) and confocal microscopy images (**Figure 7I**) evidenced that both autophagy markers returned to OIR levels. These results showed that the inhibition of autophagy by Spautin-1 was harmful for the functionality and survival of photoreceptors in P17 OIR retinas.

DISCUSSION

Preretinal NV is a common feature in many diseases, including ROP, DR and Sickle cell retinopathy. Even though their pathophysiology is different, this family of retinopathies is characterized by the decrease in oxygen tension at a certain stage. The immediate response is the increase in VEGF synthesis, a trophic factor responsible of the proliferation of ECs that originate fragile and immature vascular tufts (Campochiaro, 2015; Rubio and Adamis, 2016). Simultaneously, other events take place in the retina as gliosis and neurodegeneration, which can be developed by the hypoxic stimulus or another primary injury (Ridano et al., 2017). Coincidentally, proliferative retinopathies treatments are palliative and aim to manage NV. However, ongoing inflammation, neuronal death, and impaired oxygen supply frequently lead to neovascular recurrence. Thus, previous studies indicated that a more appropriate therapy should encompass the normalization of both vascular and non-vascular alterations in proliferative retinopathies (Liang et al., 2012).

Modulation of autophagy flux results an attractive target, as this intracellular process occurs in every cell and has proven relationship with neurodegeneration, angiogenesis, and inflammation (Boya et al., 2016). Several research studies have demonstrated that inhibition or stimulation of the autophagic flux is able to reverse the alterations of multiple chronic or acute pathologies, including visual disturbances (Mitter et al., 2012; Russo et al., 2013; Chinskey et al., 2014;

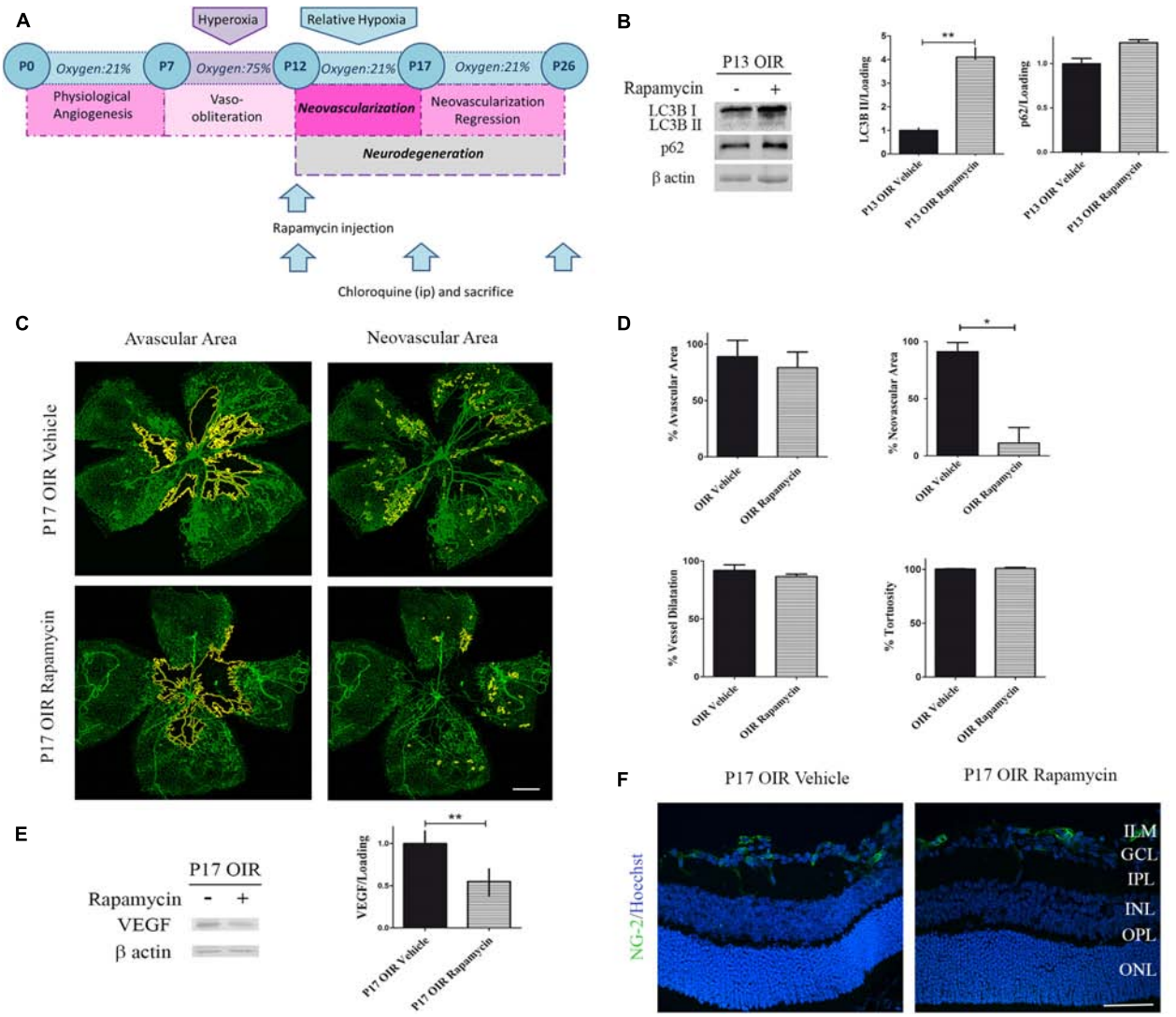

FIGURE 3 | Effect of Rapamycin on the vascular alterations in the OIR mouse retinas. **(A)** Rapamycin treatment schedule. Rapamycin (0,5 μg/ml) or vehicle was intravitreally injected at P12 and evaluated at P13, P17, or P26 after 4 h of CQ administration. **(B)** Representative Western blot and quantification data of autophagy markers, LC3B II and p62, from neural retinal extracts of OIR mice intravitreally injected with vehicle or Rapamycin at P12 and evaluated at P13, 4 h after CQ administration. β-Actin is shown as a loading control. Graph shows results of three independent experiments. **(C)** Representative images of flat-mount retinas at P17 showing GSA-IB4 vascular staining in OIR-vehicle and OIR-Rapamycin mice. Areas with VO and NV are indicated. Scale bar: 500 μm. **(D)** The VO (%) was quantified as the ratio of central avascular area to whole retinal area, the NV (%) was quantified as a percentage of whole retinal area. In mayor vessels of the retina, diameter was quantified by tracing a transversal line to the vessel. The tortuosity was obtained by drawing a line along the vessel and comparing it to a straight line traced from the optic nerve to the first branching point. **(E)** Representative Western blot and quantification data of VEGF from neural retinal extracts in OIR mice intravitreally injected with vehicle or Rapamycin at P12 and evaluated at P17, 4 h after CQ administration. β-Actin is shown as a loading control. Graph shows results of three independent experiments. **(F)** Representative immunofluorescence analysis of NG-2 (green) in cryosections of OIR mice intravitreally injected with vehicle or Rapamycin at P12 and evaluated at P17, 4 h after CQ administration. Scale bar: 50 μm. ILM, inner limiting membrane; GCL, ganglion cell layer; IPL, inner plexiform layer; INL, inner nuclear layer; OPL, outer plexiform layer; ONL, outer nuclear layer. Data are presented as mean ± SEM. $*p < 0.05$, $**p < 0.01$.

Frost et al., 2014; Chai et al., 2016; Rosa et al., 2016; Amato et al., 2018). Rapamycin, rapalogs and CQ are the most habitual choice for experimental design as they have been approved by FDA for a specific treatment (Nalbandian et al., 2015; Kezic et al., 2018) and it would be easier to execute clinical trials for second uses of these drugs.

Therefore, we initially explored changes in the autophagy flux in the OIR mouse model. To note, OIR model very closely recapitulates the pathologic events occurring in ROP and some aspects of proliferative DR (Smith et al., 1994). Treatments were carried out at different postnatal days when pups were still in developmental phase, where autophagy plays a crucial role (Boya et al., 2016). Indeed, Western blot assays in RA showed a decrease of LC3B II and p62 protein levels from P12 to P26, indicating a high autophagy flux early after birth. In contrast, OIR mice showed an increase in LC3B II and p62 protein levels

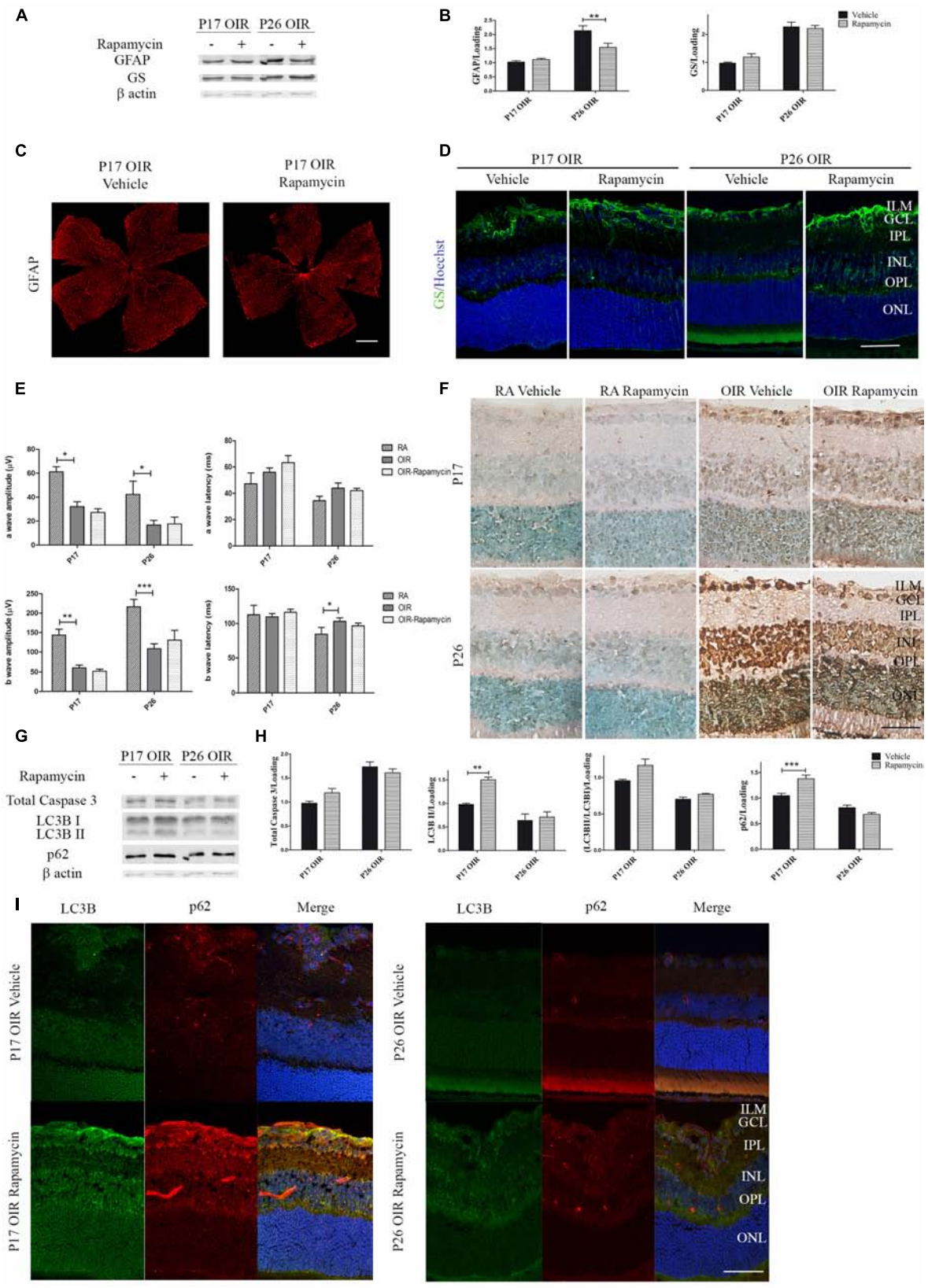

FIGURE 4 | Continued

FIGURE 4 | Effect of Rapamycin on the glial reactivity, neuronal functionality, and autophagy markers in OIR mouse retinas. **(A)** Representative Western blot of GS and GFAP from neural retina extracts of OIR mice intravitreally injected with vehicle or Rapamycin at P12 and evaluated at P17, 4 h after CQ administration. β-Actin is shown as a loading control. **(B)** Levels of GS and GFAP were quantified by densitometry and normalized to β-actin. Graph shows results of three independent experiments. **(C)** Representative images of flat-mount retinas at P17 showing GFAP staining in OIR-vehicle and OIR-Rapamycin mice. Scale bar: 500 μm. **(D)** Representative immunofluorescence analysis of GS (green) in cryosections of OIR mice intravitreally injected with vehicle or Rapamycin at P12 and evaluated at P17, 4 h after CQ administration. Scale bar: 50 μm. **(E)** Amplitudes and latencies of a- and b-waves from scotopic ERG were recorded at P17 and P26 in RA and OIR mice injected at P12 with vehicle or Rapamycin. Data show the average of responses of both eyes with eight mice per condition. **(F)** Representative TUNEL-labeled cryosections of RA and OIR mice injected with vehicle or Rapamycin at P12 and evaluated at P17 and P26. Scale bar: 50 μm. **(G,H)** Representative Western blot and quantification data of total caspase-3, LC3B II and p62 from neural retina samples of OIR mice intravitreally injected with vehicle or Rapamycin at P12 and evaluated at P17 and P26, 4 h after CQ administration. β-Actin is shown as a loading control. Graph shows results of three independent experiments. **(I)** Representative immunofluorescence analysis of LC3B (green) and p62 (red) in cryosections of OIR mice intravitreally injected with vehicle or Rapamycin at P12 and evaluated at P17 and P26, 4 h after CQ administration. Cell nuclei were counterstained with Hoechst 33258 (blue). Scale bar: 50 μm. ILM, inner limiting membrane; GCL, ganglion cell layer; IPL, inner plexiform layer; INL, inner nuclear layer; OPL, outer plexiform layer; ONL, outer nuclear layer. Data are presented as mean ± SEM. $*p < 0.05$, $**p < 0.01$, $***p < 0.001$.

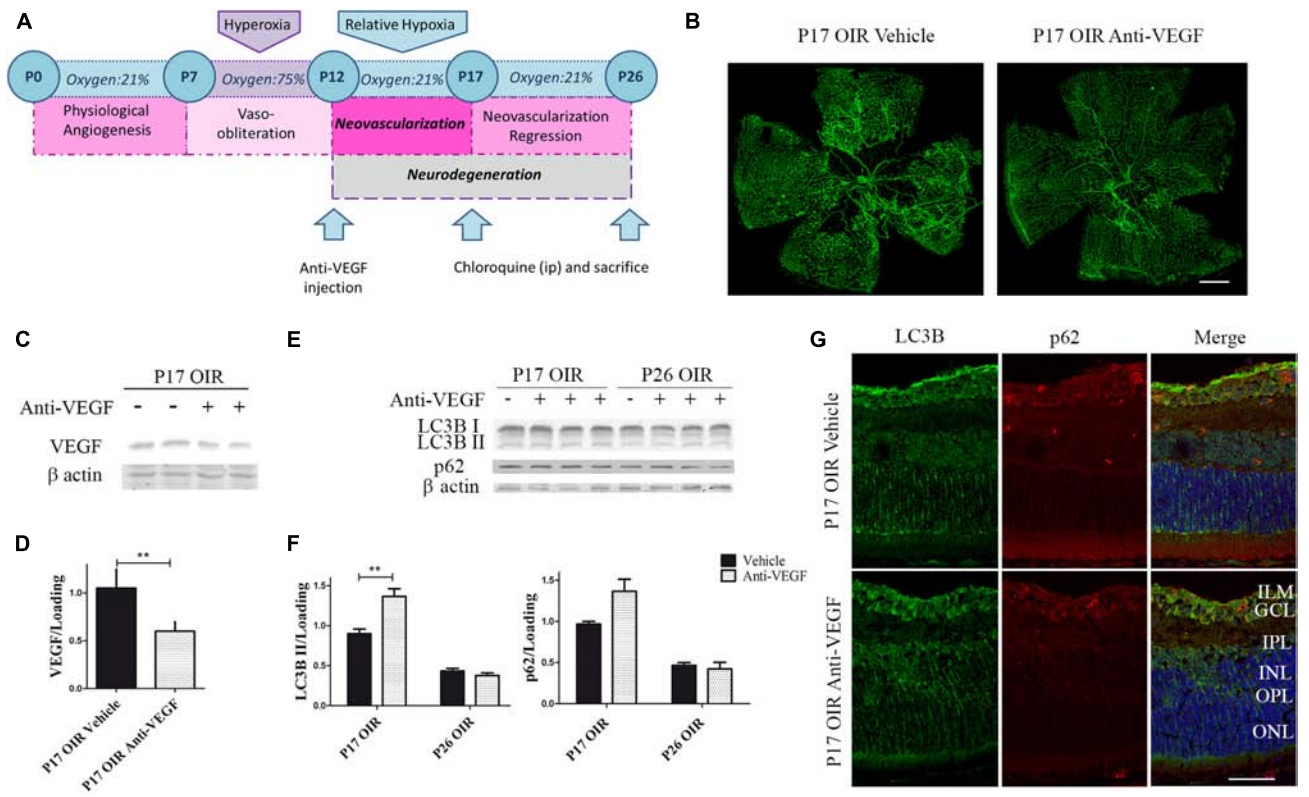

FIGURE 5 | Effect of Anti-VEGF treatment on autophagy markers in the OIR mouse retinas. **(A)** Anti-VEGF mAb treatment schedule. Anti-VEGF mAb (1.25 μg) or vehicle was intravitreally injected at P12 and evaluated a P17 or P26, 4 h after CQ administration. **(B)** Representative images of flat-mount retinas at P17 OIR showing GSA-IB4 vascular staining in vehicle or anti-VEGF-injected eyes. Areas with VO and NV are indicated. Scale bar: 500 μm. **(C)** Representative Western blot of VEGF from P17 neural retinal extracts of OIR mice injected at P12 with vehicle or anti-VEGF mAb. β-Actin is shown as a loading control. **(D)** Levels of VEGF were quantified by densitometry and normalized to β-actin. Graph shows results of three independent experiments. **(E)** Representative Western blot of LC3B II and p62 from neural retina extracts of OIR mice intravitreally injected with vehicle or anti-VEGF mAb at P12 and evaluated at P17 and P26, 4 h after CQ administration. β-Actin is shown as a loading control. **(F)** Levels of LC3B II and p62 were quantified by densitometry and normalized to β-actin. Graph shows results of four independent experiments. **(G)** Representative immunofluorescence analysis of LC3B (green) and p62 (red) in cryosections of OIR mice intravitreally injected with vehicle or anti-VEGF mAb at P12 and evaluated at P17, 4 h after CQ administration. Cell nuclei were counterstained with Hoechst 33258 (blue). Scale bar: 50 μm. ILM, inner limiting membrane; GCL, ganglion cell layer; IPL, inner plexiform layer; INL, inner nuclear layer; OPL, outer plexiform layer; ONL, outer nuclear layer. Data are presented as mean ± SEM. $**p < 0.01$.

at P17 OIR, compared to RA controls demonstrating a rise in autophagosomes in the cytosol of retinal cells. Transcriptional activity of autophagy proteins revealed a significant increase in p62 mRNA levels at P17OIR. Upon induction of the flux, p62 is degraded into the autophagosome and it would be necessary to synthesize more protein. This result would indicate that the increase in p62 protein levels at this time point is a consequence of the increased protein synthesis but not of its accumulation.

Physiological vascularization of the retina completes at P21 in mice, when the provisional hyaloid vasculature is replaced

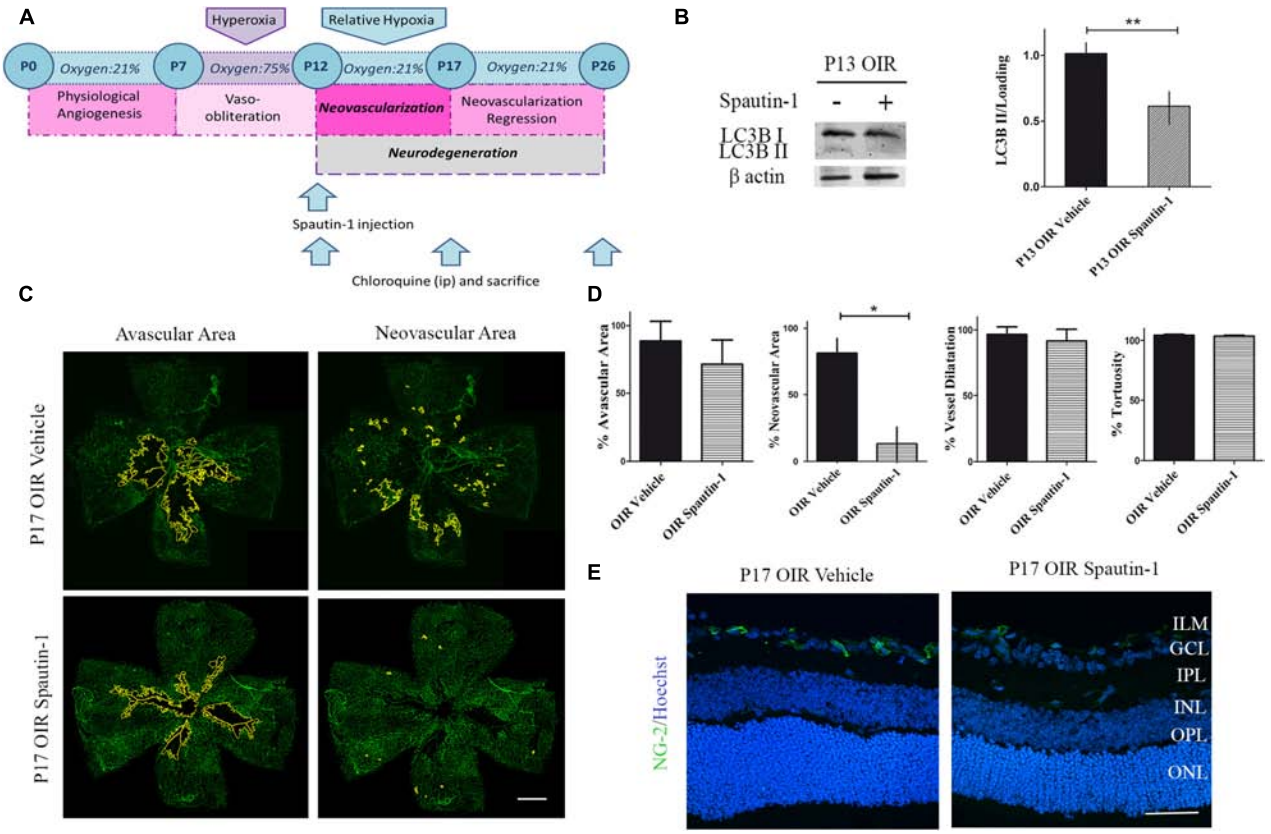

FIGURE 6 | Effect of the Spautin-1 on the NV in OIR mouse retinas. **(A)** Spautin-1 treatment schedule. Spautin-1 (200 μM) or vehicle was intravitreally injected at P12 and evaluated at P17 or P26, 4 h after of CQ administration. **(B)** Representative Western blot and quantification data of autophagy marker LC3B II from neural retinal extracts of OIR mice intravitreally injected with Spautin-1 or vehicle at P12 and evaluated at P13, 4 h after CQ administration. β-Actin is shown as a loading control. Graph shows results of three independent experiments. **(C)** Representative images of flat-mount retinas at P17 showing GSA-IB4 vascular staining in OIR-vehicle and OIR-Spautin-1 mice. Areas with VO and NV are indicated. Scale bar: 500 μm. **(D)** The VO (%) was quantified as the ratio of central avascular area to whole retinal area, the NV (%) was quantified as a percentage of whole retinal area. In mayor vessels of the retina, diameter was quantified by tracing a transversal line to the vessel. The tortuosity was obtained by drawing a line along the vessel and comparing it to a straight line traced from the optic nerve to the first branching point. **(E)** Representative immunofluorescence analysis of NG-2 (green) in cryosections of OIR mice intravitreally injected with vehicle or Spautin-1 at P12 and evaluated at P17, 4 h after CQ administration. Scale bar: 50 μm. ILM, inner limiting membrane; GCL, ganglion cell layer; IPL, inner plexiform layer; INL, inner nuclear layer; OPL, outer plexiform layer; ONL, outer nuclear layer. Data are presented as mean ± SEM. $^{*}p < 0.05$, $^{**}p < 0.01$.

by the definite one following a hypoxic gradient. Firstly, the superficial plexus is formed by the radial sprouting of vessels from the optic nerve. Later, the deep plexus is formed by transversal outgrowth of superficial vessels and the retinal vasculature achieves completion with the formation of the intermediate plexus (Stahl et al., 2010). Due to the fact that there is an irregular oxygen supply in the different layers of the retina, the sensing of the hypoxic stimulus could vary along the neural retina and therefore the cellular response (Rodrigues et al., 2013). Confocal images showed that areas near the vascular plexus, GCs and neurons residing in the INL increased LC3B protein expression in P17 OIR mice, whereas autophagy markers were not modified in ONL neurons. Unchanged autophagic flux in photoreceptors could be explained by the provision of oxygen by the choroid vasculature to rods and cones, preventing severe hypoxia in this layer. Although photoreceptors are damaged in OIR model, a reduced cell death rate is observed (Ridano et al., 2017). Nearby to the ILM, both MGCs and ECs showed an increase in LC3B staining. Interestingly, at P17 OIR, LC3B-positive vesicles were found inside ECs in neovascular tufts, suggesting an increased autophagic flux in proliferating cells.

We further confirmed the activation in autophagy flux at P17 OIR by observing a greater number of LC3B/LAMP1 double labeled vesicles, indicating an increase in amphisomes in the inner layers of the retina compared to control mice. An increase in LAMP1 structures was observed after blockade of the flux with CQ, mainly in the ILM, evidencing that the degradation pathway is activated. In addition, neovessels in the ILM hydrolyzed DQ-BSA in lysosomes in great proportion. By TUNEL assay, we demonstrate that cell viability is reduced in INL and GCL. Indeed, neurons undergoing cell death or high hypoxic stress could activate autophagy flux as a survival mechanism.

Next we wonder if the administration of Rapamycin at P12 could improve vascular, glial, or neuronal alterations in OIR mice. We took into account that mTORC1 inhibition increases autophagy flux, but also modulates multiple intracellular

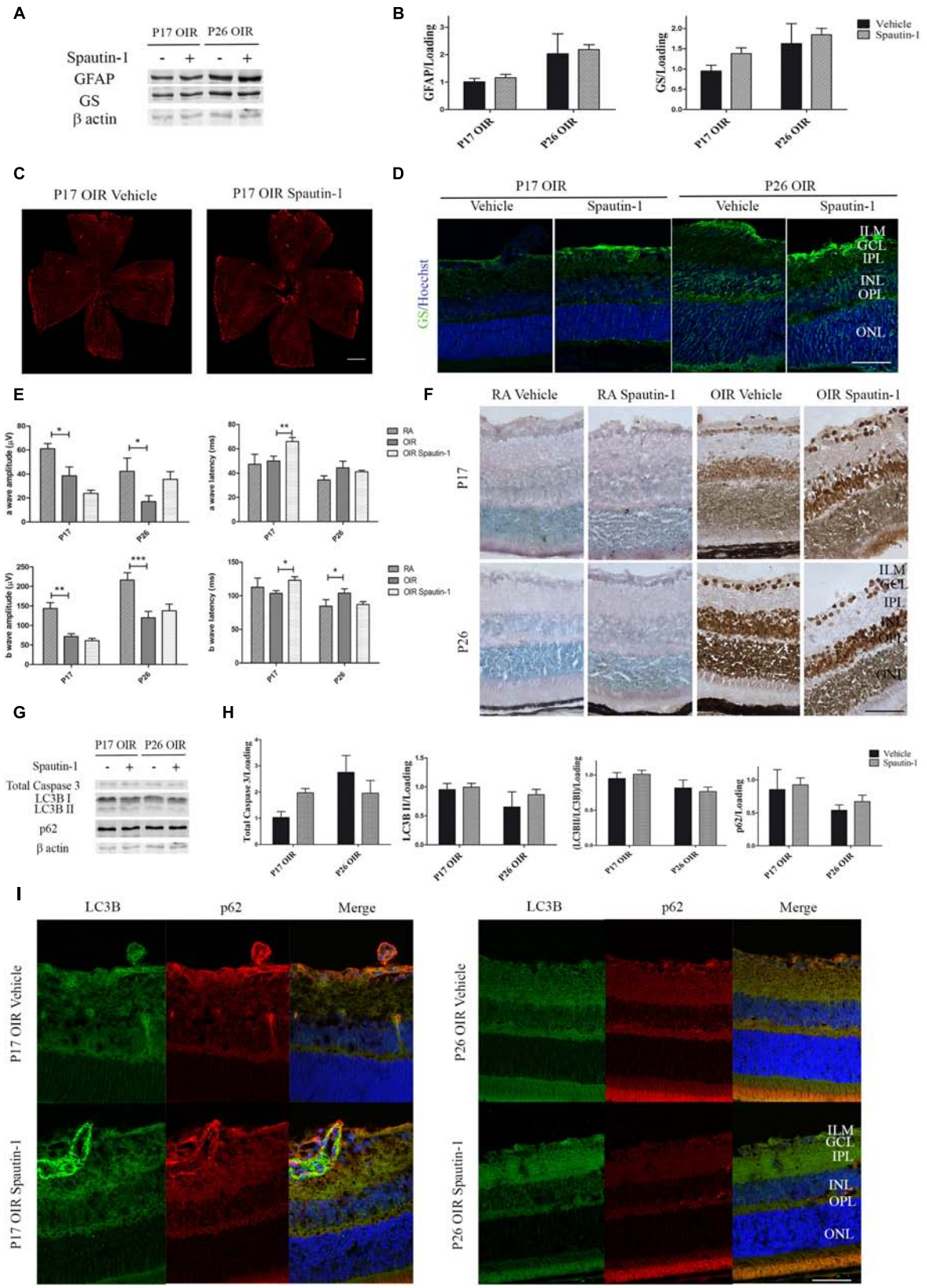

FIGURE 7 | Continued

FIGURE 7 | (A) Effect of Spautin-1 on the glial reactivity, neuronal functionality and autophagy markers in OIR mouse retinas. Representative Western blot of GFAP and GS from neural retina extracts of OIR mice intravitreally injected with Spautin-1 or vehicle at P12 and evaluated at P17, 4 h after CQ treatment. β-Actin is shown as a loading control. **(B)** Levels of GFAP and GS were quantified by densitometry and normalized to β-actin. Graph shows results of four independent experiments. **(C)** Representative images of flat-mount retinas at P17 showing GFAP staining in OIR-vehicle and OIR-Spautin-1 mice. Scale bar: 500 μm. **(D)** Representative immunofluorescence analysis of GS (green) in cryosections of OIR mice intravitreally injected with vehicle or Spautin-1 at P12 and evaluated at P17, 4 h after CQ administration. Scale bar: 50 μm. **(E)** Amplitudes and latencies of a- and b-waves from scotopic ERG were recorded at P17 and P26 in RA and OIR mice injected at P12 with vehicle or Spautin-1. Data show the average of responses in both eyes with eight mice per condition. **(F)** Representative TUNEL-labeled cryosections of RA and OIR mice injected with vehicle or Spautin-1 at P12 and evaluated at P17 and P26. Scale bar: 50 μm. **(G,H)** Representative Western blot and quantification data of total caspase-3, LC3B II and p62 from neural retina samples of OIR mice intravitreally injected with vehicle or Spautin-1 at P12 and evaluated at P17 and P26, 4 h after CQ administration. β-Actin is shown as a loading control. Graph shows results of three independent experiments. **(I)** Representative immunofluorescence analysis of LC3B (green) and p62 (red) in cryosections of OIR mice intravitreally injected with vehicle or Spautin-1 at P12 and evaluated at P17 and P26, 4 h after CQ administration. Cell nuclei were counterstained with Hoechst 33258 (blue). Scale bar: 50 μm. ILM, inner limiting membrane; GCL, ganglion cell layer; IPL, inner plexiform layer; INL, inner nuclear layer; OPL, outer plexiform layer; ONL, outer nuclear layer. Data are presented as mean ± SEM. ns, non-significant, $*p < 0.05$, $**p < 0.01$, $***p < 0.001$.

pathways related to inflammation, angiogenesis and metabolism. A single intraocular injection of Rapamycin decreased the area occupied by neovessels, however the treatment did not promote physiological revascularization (evaluated by avascular area, vessel dilatation, and tortuosity). The normalization of the vascular plexus is essential for the proper irrigation of the retinal tissue and prevents future alterations derived from the turbulence in the blood flow or stasis of blood cells (Liang et al., 2012). The reduction in NV area was supported by the decrease in VEGF levels. It has been described that inhibition of mTORC1 decreases the synthesis of the transcription factor HIF-1α and consequently downregulates the expression of its target genes (Liu et al., 2015). Notably, in the retina VEGF is produced mainly in MGCs, astrocytes, GCs, retinal pigmented epithelium and ECs in a minor proportion (Wang et al., 2010). Then, it is possible that the modulation of the neovascular process is due to the direct effect of Rapamycin on other cells rather than endothelium. In fact, Rapamycin could be a more successful therapeutic strategy because it decreases the synthesis of VEGF, providing an adequate level of the trophic factor. The excessive inhibition of VEGF signaling would be detrimental for neurons. Under certain pathological conditions, increased autophagy flux can also induce cell death (Hirt et al., 2018). In our model, Rapamycin did not alter pericytes viability, one of the most susceptive cells in the vasculature. Persistence of mural cells is a good marker of vascular maturation, indicating that final stage of vasculogenesis is not altered and the newly formed vessels are functional.

Related to gliosis, Rapamycin markedly reduced GFAP expression at P26 OIR, indicating a decrease in the glial response during the neovascular regression stage. This would contribute to the reduction in the persistent pro-inflammatory response that promotes damage in the retinal tissue. Unfortunately, a single dose of Rapamycin was insufficient to increase neuronal functionality. Further studies would be necessary to evaluate if a prolonged administration schedule improves visual function.

Previously, it has been reported that high dose of Rapamycin increases the avascular area (Yagasaki et al., 2014) which could be a result of reduced proliferation or increased cell death of ECs. Here, the induction in autophagy flux did not resulted in an increase of apoptosis, measured by total caspase 3, suggesting that the crosstalk between both pathways is not the responsible of the caspase mediated cell death. Our results showed that the increase in autophagy flux continue up to P17 OIR, indicating that Rapamycin has a relatively long half-life in the vitreous, as previously reported (Nguyen et al., 2018).

In a comparative experiment, we analyzed the effect of the anti-VEGF therapy on the autophagy flux. Western blot analysis revealed a slight induction of the flux at P17 OIR. As confocal images showed an increase in the autophagy proteins, LC3B and p62, in GCL and INL, we consider that the deprivation of the trophic factor VEGF can activate survival mechanisms as autophagy. Previously, we reported that intravitreal administration of anti-VEGF does not improve neuronal functionality and gliosis (Ridano et al., 2017). Thereby, Rapamycin benefits over anti-VEGF therapy rely on the multiplicity of events modulated through the inhibition of mTORC1. Although both treatments reduced NV and activated autophagy, neither of them prevented neurodegeneration in our experimental conditions.

To unravel the role of autophagy in the OIR mouse model, we injected at P12 a single dose of Spautin-1, an inhibitor of the ubiquitin-specific peptidases USP10 and USP13, which target the Beclin-1 subunit of Vps34 complexes (Liu et al., 2011). Remarkably, vascular effects were similar to those observed with Rapamycin. Spautin-1 decreased the neovascular area without modifying other vascular parameters. In this sense, confocal images of neovessels shed light on this result demonstrating that proliferating ECs, highly metabolic cells, showed a fast autophagy flux. Thus, the inhibition of this process would lead to vascular death or a decreased proliferation rate. The interaction between ECs and pericytes is critical for the formation of a structurally sound microvasculature. In this study, we found a reduced NG-2 staining in OIR mice retinas after Spautin-1 treatment indicating an apparent decrease in pericyte density, which may exacerbate vascular alterations.

In regard to non-vascular cells, glial response remained unchanged as no modifications in GS and GFAP levels were detected after Spautin-1 treatment. Electroretinographic recording showed that photoreceptors functionality tend to decrease at P17 OIR in Spautin-1 treated mice. This result reinforces the idea that retinal layers with high autophagy flux at the neovascular peak activate this pathway as a survival mechanism. In this sense, the importance of the autophagic flow

became more evident in the photoreceptors because it is the layer less affected in the OIR. Correlatively, an increase in TUNEL positive staining was observed in the ONL when autophagy was inhibited. Five days after Spautin-1 injection, LC3B II and p62 protein levels returned to OIR control levels, indicating a reduced half-life of the drug in the eye.

Presumably, all retinal cells are intended to activate autophagy flux in hypoxic conditions. However, the ability to respond will depend on the status of the cell as well as the intensity and duration of the stimuli (Boya et al., 2016). Prior to the hypoxic stage in the OIR model, the hyperoxic phase induces several alterations in retinal cells originated by apoptotic events at P12 (Sennlaub et al., 2002; Vecino et al., 2004; Narayanan et al., 2011). Recently, it has been demonstrated that retinas of OIR mice are characterized by increased apoptosis and decreased autophagy from P13 to P15 (Cammalleri et al., 2017). Here, using the same *in vivo* model, we completed the analysis including, in addition to P12 and P17, the vascular regression stage (P26). Overall, our results demonstrate that all treatments of induction or inhibition of the autophagic flux reduced neovascular area but were unable to completely reverse the neuronal damage. Besides, compared to current treatments, rapamycin provides a more promising therapeutic strategy as it reduces both neovascular tufts and persistent gliosis.

ETHICS STATEMENT

C57BL/6J mice were handled according to guidelines of the ARVO Statement for the Use of Animals in Ophthalmic and Vision Research. Experimental procedures were designed and approved by the Institutional Animal Care and Use Committee (CICUAL) of the Faculty of Chemical Sciences, National University of Córdoba (Res. HCD 1216/18). All efforts were made to reduce the number of animals used.

AUTHOR CONTRIBUTIONS

PS and MS designed the experiments. PS, MP, MR, and VL conducted the experiments. PS, MP, MR, VL, and MS interpreted the data. GC and CF contributed new reagents, analytic tools, and analyzed and discussed the available data. PS and MS wrote and edited the manuscript.

FUNDING

This study was funded by the Secretaría de Ciencia y Tecnología, Universidad Nacional de Córdoba (SECyT-UNC) No. 366/16 and the Fondo para la Investigación Científica y Tecnológica (FONCyT), Préstamo BID 2015 PICT No. 1314 (all to MS).

ACKNOWLEDGMENTS

We thank Gustavo Bonacci for advice and Pablo Barcelona for technical assistance. We also thank Carlos Mas, María Pilar Crespo, and Cecilia Sampedro for assistance in confocal microscopy and Soledad Miró and Victoria Blanco for dedicated animal care.

REFERENCES

Amato, R., Catalani, E., Dal Monte, M., Cammalleri, M., Di Renzo, I., Perrotta, C., et al. (2018). Autophagy-mediated neuroprotection induced by octreotide in an ex vivo model of early diabetic retinopathy. *Pharmacol. Res.* 128, 167–178. doi: 10.1016/j.phrs.2017.09.022

Barcelona, P. F., Ortiz, S. G., Chiabrando, G. A., and Sanchez, M. C. (2011). Alpha2-macroglobulin induces glial fibrillary acidic protein expression mediated by low-density lipoprotein receptor-related protein 1 in muller cells. *Invest. Ophthalmol. Vis. Sci.* 52, 778–786. doi: 10.1167/iovs.10-5759

Boya, P., Esteban-Martinez, L., Serrano-Puebla, A., Gomez-Sintes, R., and Villarejo-Zori, B. (2016). Autophagy in the eye: development, degeneration, and aging. *Prog. Retin. Eye Res.* 55, 206–245. doi: 10.1016/j.preteyeres.2016.08.001

Cammalleri, M., Locri, F., Catalani, E., Filippi, L., Cervia, D., Dal Monte, M., et al. (2017). The beta adrenergic receptor blocker propranolol counteracts retinal dysfunction in a mouse model of oxygen induced retinopathy: restoring the balance between apoptosis and autophagy. *Front. Cell. Neurosci.* 11:395. doi: 10.3389/fncel.2017.00395

Campochiaro, P. A. (2015). Molecular pathogenesis of retinal and choroidal vascular diseases. *Prog. Retin. Eye Res.* 49, 67–81. doi: 10.1016/j.preteyeres.2015.06.002

Chai, P., Ni, H., Zhang, H., and Fan, X. (2016). The evolving functions of autophagy in ocular health: a double-edged sword. *Int. J. Biol. Sci.* 12, 1332–1340. doi: 10.7150/ijbs.16245

Chen, S., Zhou, L., Zhang, Y., Leng, Y., Pei, X. Y., Lin, H., et al. (2014). Targeting SQSTM1/p62 induces cargo loading failure and converts autophagy to apoptosis via NBK/Bik. *Mol. Cell. Biol.* 34, 3435–3449. doi: 10.1128/MCB.01383-13

Chinskey, N. D., Besirli, C. G., and Zacks, D. N. (2014). Retinal cell death and current strategies in retinal neuroprotection. *Curr. Opin. Ophthalmol.* 25, 228–233. doi: 10.1097/ICU.0000000000000043

Diabetic Retinopathy Clinical Research Network, Wells, J. A., Glassman, A. R., Ayala, A. R., Jampol, L. M., Aiello, L. P., et al. (2015). Aflibercept, bevacizumab, or ranibizumab for diabetic macular edema. *N. Engl. J. Med.* 372, 1193–1203. doi: 10.1056/NEJMoa1414264

Du, J., Teng, R. J., Guan, T., Eis, A., Kaul, S., Konduri, G. G., et al. (2012). Role of autophagy in angiogenesis in aortic endothelial cells. *Am. J. Physiol. Cell Physiol.* 302, C383–C391. doi: 10.1152/ajpcell.00164.2011

Evans, J. R., Michelessi, M., and Virgili, G. (2014). Laser photocoagulation for proliferative diabetic retinopathy. *Cochrane Database Syst. Rev.* 11, CD011234. doi: 10.1002/14651858.CD011234.pub2

Frost, L. S., Dhingra, A., Reyes-Reveles, J., and Boesze-Battaglia, K. (2017). The use of DQ-BSA to monitor the turnover of autophagy-associated cargo. *Methods Enzymol.* 587, 43–54. doi: 10.1016/bs.mie.2016.09.052

Frost, L. S., Mitchell, C. H., and Boesze-Battaglia, K. (2014). Autophagy in the eye: implications for ocular cell health. *Exp. Eye Res.* 124, 56–66. doi: 10.1016/j.exer.2014.04.010

Gerhardt, H. (2008). VEGF and endothelial guidance in angiogenic sprouting. *Organogenesis* 4, 241–246. doi: 10.4161/org.4.4.7414

Gerhardt, H., and Betsholtz, C. (2003). Endothelial-pericyte interactions in angiogenesis. *Cell Tissue Res.* 314, 15–23. doi: 10.1007/s00441-003-0745-x

Harris, H., and Rubinsztein, D. C. (2011). Control of autophagy as a therapy for neurodegenerative disease. *Nat. Rev. Neurol.* 8, 108–117. doi: 10.1038/nrneurol.2011.200

Hirt, J., Porter, K., Dixon, A., McKinnon, S., and Liton, P. B. (2018). Contribution of autophagy to ocular hypertension and neurodegeneration in the DBA/2J

spontaneous glaucoma mouse model. *Cell. Death Discov.* 4:14. doi: 10.1038/s41420-018-0077-y

Kern, T. S. (2014). Interrelationships between the retinal neuroglia and vasculature in diabetes. *Diabetes Metab. J.* 38, 163–170. doi: 10.4093/dmj.2014.38.3.163

Kezic, A., Popovic, L., and Lalic, K. (2018). mTOR Inhibitor therapy and metabolic consequences: where do we stand? *Oxid. Med. Cell Longev.* 2018:2640342. doi: 10.1155/2018/2640342

Kim, C. B., D'Amore, P. A., and Connor, K. M. (2016). Revisiting the mouse model of oxygen-induced retinopathy. *Eye Brain* 8, 67–79. doi: 10.2147/EB.S94447

Kimura, T., Jia, J., Claude-Taupin, A., Kumar, S., Choi, S. W., Gu, Y., et al. (2017). Cellular and molecular mechanism for secretory autophagy. *Autophagy* 13, 1084–1085. doi: 10.1080/15548627.2017.1307486

Levine, B., Packer, M., and Codogno, P. (2015). Development of autophagy inducers in clinical medicine. *J. Clin. Invest.* 125, 14–24. doi: 10.1172/JCI73938

Li, J., Kim, S. G., and Blenis, J. (2014). Rapamycin: one drug, many effects. *Cell Metab.* 19, 373–379. doi: 10.1016/j.cmet.2014.01.001

Liang, J., Piao, Y., Henry, V., Tiao, N., and de Groot, J. F. (2015). Interferon-regulatory factor-1 (IRF1) regulates bevacizumab induced autophagy. *Oncotarget* 6, 31479–31492. doi: 10.18632/oncotarget.5491

Liang, X., Zhou, H., Ding, Y., Li, J., Yang, C., Luo, Y., et al. (2012). TMP prevents retinal neovascularization and imparts neuroprotection in an oxygen-induced retinopathy model. *Invest. Ophthalmol. Vis. Sci.* 53, 2157–2169. doi: 10.1167/iovs.11-9315

Liu, J., Fan, L., Wang, H., and Sun, G. (2016). Autophagy, a double-edged sword in anti-angiogenesis therapy. *Med. Oncol.* 33, 10. doi: 10.1007/s12032-015-0721-9

Liu, J., Xia, H., Kim, M., Xu, L., Li, Y., Zhang, L., et al. (2011). Beclin1 controls the levels of p53 by regulating the deubiquitination activity of USP10 and USP13. *Cell* 147, 223–234. doi: 10.1016/j.cell.2011.08.037

Liu, N. N., Zhao, N., and Cai, N. (2015). Suppression of the proliferation of hypoxia-Induced retinal pigment epithelial cell by rapamycin through the /mTOR/HIF-1alpha/VEGF/ signaling. *IUBMB Life* 67, 446–452. doi: 10.1002/iub.1382

Lytvynchuk, L., Sergienko, A., Lavrenchuk, G., and Petrovski, G. (2015). Antiproliferative, apoptotic, and autophagic activity of ranibizumab, bevacizumab, pegaptanib, and aflibercept on fibroblasts: implication for choroidal neovascularization. *J. Ophthalmol.* 2015:934963. doi: 10.1155/2015/934963

Mitter, S. K., Rao, H. V., Qi, X., Cai, J., Sugrue, A., Dunn, W. A., et al. (2012). Autophagy in the retina: a potential role in age-related macular degeneration. *Adv. Exp. Med. Biol.* 723, 83–90. doi: 10.1007/978-1-4614-0631-0_12

Mizushima, N., and Komatsu, M. (2011). Autophagy: renovation of cells and tissues. *Cell* 147, 728–741. doi: 10.1016/j.cell.2011.10.026

Nagy, J. A., Benjamin, L., Zeng, H., Dvorak, A. M., and Dvorak, H. F. (2008). Vascular permeability, vascular hyperpermeability and angiogenesis. *Angiogenesis* 11, 109–119. doi: 10.1007/s10456-008-9099-z

Nalbandian, A., Llewellyn, K. J., Nguyen, C., Yazdi, P. G., and Kimonis, V. E. (2015). Rapamycin and chloroquine: the in vitro and in vivo effects of autophagy-modifying drugs show promising results in valosin containing protein multisystem proteinopathy. *PLoS One* 10:e0122888. doi: 10.1371/journal.pone.0122888

Narayanan, S. P., Suwanpradid, J., Saul, A., Xu, Z., Still, A., Caldwell, R. W., et al. (2011). Arginase 2 deletion reduces neuro-glial injury and improves retinal function in a model of retinopathy of prematurity. *PLoS One* 6:e22460. doi: 10.1371/journal.pone.0022460

Nguyen, Q. D., Merrill, P. T., Sepah, Y. J., Ibrahim, M. A., Banker, A., Leonardi, A., et al. (2018). Intravitreal sirolimus for the treatment of noninfectious uveitis: evolution through preclinical and clinical studies. *Ophthalmology* 125, 1984–1993. doi: 10.1016/j.ophtha.2018.06.015

Osaadon, P., Fagan, X. J., Lifshitz, T., and Levy, J. (2014). A review of anti-VEGF agents for proliferative diabetic retinopathy. *Eye* 28, 510–520. doi: 10.1038/eye.2014.13

Ridano, M. E., Subirada, P. V., Paz, M. C., Lorenc, V. E., Stupirski, J. C., Gramajo, A. L., et al. (2017). Galectin-1 expression imprints a neurovascular phenotype in proliferative retinopathies and delineates responses to anti-VEGF. *Oncotarget* 8, 32505–32522. doi: 10.18632/oncotarget.17129

Rodrigues, M., Xin, X., Jee, K., Babapoor-Farrokhran, S., Kashiwabuchi, F., Ma, T., et al. (2013). VEGF secreted by hypoxic Muller cells induces MMP-2 expression and activity in endothelial cells to promote retinal neovascularization in proliferative diabetic retinopathy. *Diabetes* 62, 3863–3873. doi: 10.2337/db13-0014

Rosa, M. D., Distefano, G., Gagliano, C., Rusciano, D., and Malaguarnera, L. (2016). Autophagy in diabetic retinopathy. *Curr. Neuropharmacol.* 14, 810–825. doi: 10.2174/1570159x14666160321122900

Rubio, R. G., and Adamis, A. P. (2016). Ocular Angiogenesis: vascular endothelial growth factor and other factors. *Dev. Ophthalmol.* 55, 28–37. doi: 10.1159/000431129

Russo, R., Berliocchi, L., Adornetto, A., Amantea, D., Nucci, C., Tassorelli, C., et al. (2013). In search of new targets for retinal neuroprotection: is there a role for autophagy? *Curr. Opin. Pharmacol.* 13, 72–77. doi: 10.1016/j.coph.2012.09.004

Russo, R., Varano, G. P., Adornetto, A., Nazio, F., Tettamanti, G., Girardello, R., et al. (2018). Rapamycin and fasting sustain autophagy response activated by ischemia/reperfusion injury and promote retinal ganglion cell survival. *Cell Death Dis.* 9:981. doi: 10.1038/s41419-018-1044-5

Saint-Geniez, M., Maharaj, A. S., Walshe, T. E., Tucker, B. A., Sekiyama, E., Kurihara, T., et al. (2008). Endogenous VEGF is required for visual function: evidence for a survival role on muller cells and photoreceptors. *PLoS One* 3:e3554. doi: 10.1371/journal.pone.0003554

Sanchez, M. C., Barcelona, P. F., Luna, J. D., Ortiz, S. G., Juarez, P. C., Riera, C. M., et al. (2006). Low-density lipoprotein receptor-related protein-1 (LRP-1) expression in a rat model of oxygen-induced retinal neovascularization. *Exp. Eye Res.* 83, 1378–1385. doi: 10.1016/j.exer.2006.07.016

Semenza, G. L. (2012). Hypoxia-inducible factors in physiology and medicine. *Cell* 148, 399–408. doi: 10.1016/j.cell.2012.01.021

Sennlaub, F., Courtois, Y., and Goureau, O. (2002). Inducible nitric oxide synthase mediates retinal apoptosis in ischemic proliferative retinopathy. *J. Neurosci.* 22, 3987–3993. doi: 10.1523/jneurosci.22-10-03987.2002

Smith, L. E., Wesolowski, E., McLellan, A., Kostyk, S. K., D'Amato, R., Sullivan, R., et al. (1994). Oxygen-induced retinopathy in the mouse. *Invest. Ophthalmol. Vis. Sci.* 35, 101–111.

Stahl, A., Connor, K. M., Sapieha, P., Chen, J., Dennison, R. J., Krah, N. M., et al. (2010). The mouse retina as an angiogenesis model. *Invest. Ophthalmol. Vis. Sci.* 51, 2813–2826. doi: 10.1167/iovs.10-5176

Subirada, P. V., Paz, M. C., Ridano, M. E., Lorenc, V. E., Vaglienti, M. V., Barcelona, P. F., et al. (2018). A journey into the retina: muller glia commanding survival and death. *Eur. J. Neurosci.* 47, 1429–1443. doi: 10.1111/ejn.13965

Tah, V., Orlans, H. O., Hyer, J., Casswell, E., Din, N., Sri Shanmuganathan, V., et al. (2015). Anti-VEGF therapy and the retina: an update. *J. Ophthalmol.* 2015:627674. doi: 10.1155/2015/627674

Trachsel-Moncho, L., Benlloch-Navarro, S., Fernandez-Carbonell, A., Ramirez-Lamelas, D. T., Olivar, T., Silvestre, D., et al. (2018). Oxidative stress and autophagy-related changes during retinal degeneration and development. *Cell. Death Dis.* 9:812. doi: 10.1038/s41419-018-0855-8

Vecino, E., Hernandez, M., and Garcia, M. (2004). Cell death in the developing vertebrate retina. *Int. J. Dev. Biol.* 48, 965–974. doi: 10.1387/ijdb.041891ev

Wang, J., Xu, X., Elliott, M. H., Zhu, M., and Le, Y. Z. (2010). Muller cell-derived VEGF is essential for diabetes-induced retinal inflammation and vascular leakage. *Diabetes* 59, 2297–2305. doi: 10.2337/db09-1420

Wei, J., Jiang, H., Gao, H., and Wang, G. (2016). Blocking mammalian target of rapamycin (mtor) attenuates hif-1alpha pathways engaged-vascular endothelial growth factor (vegf) in diabetic Retinopathy. *Cell Physiol. Biochem.* 40, 1570–1577. doi: 10.1159/000453207

Yagasaki, R., Nakahara, T., Ushikubo, H., Mori, A., Sakamoto, K., and Ishii, K. (2014). Anti-angiogenic effects of mammalian target of rapamycin inhibitors in a mouse model of oxygen-induced retinopathy. *Biol. Pharm. Bull.* 37, 1838–1842. doi: 10.1248/bpb.b14-00487

Yang, S., Zhao, J., and Sun, X. (2016). Resistance to anti-VEGF therapy in neovascular age-related macular degeneration: a comprehensive review. *Drug Des. Devel. Ther.* 10, 1857–1867. doi: 10.2147/DDDT.S97653

Yin, Z., Pascual, C., and Klionsky, D. J. (2016). Autophagy: machinery and regulation. *Microb. Cell* 3, 588–596. doi: 10.15698/mic2016.12.546

Zhang, X., Bao, S., Hambly, B. D., and Gillies, M. C. (2009). Vascular endothelial growth factor-A: a multifunctional molecular player in diabetic retinopathy. *Int. J. Biochem. Cell Biol.* 41, 2368–2371. doi: 10.1016/j.biocel.2009.07.011

Zhu, X. R., and Du, J. H. (2018). Autophagy: a potential target for the treatment of intraocular neovascularization. *Int. J. Ophthalmol.* 11, 695–698. doi: 10.18240/ijo.2018.04.26

Conflict of Interest Statement: The authors declare that the research was conducted in the absence of any commercial or financial relationships that could be construed as a potential conflict of interest.

frontiers in Cellular Neuroscience

ORIGINAL RESEARCH
published: 03 July 2019
doi: 10.3389/fncel.2019.00286

MeCP2 Deficiency Disrupts Kainate-Induced Presynaptic Plasticity in the Mossy Fiber Projections in the Hippocampus

Maria Laura Bertoldi[1,2], Maria Ines Zalosnik[1,2], Maria Carolina Fabio[3], Susan Aja[4], German A. Roth[1,2], Gabriele V. Ronnett[4,5†] and Alicia L. Degano[1,2]*

[1] Departamento de Química Biológica Ranwel Caputto, Facultad de Ciencias Químicas, Córdoba, Argentina, [2] Centro de Investigaciones en Química Biológica de Córdoba (CIQUIBIC), CONICET, Universidad Nacional de Córdoba, Córdoba, Argentina, [3] Instituto de Investigaciones Médicas Mercedes y Martin Ferreyra (INIMEC), CONICET, Córdoba, Argentina, [4] Center for Metabolism and Obesity Research, Johns Hopkins Medicine, Baltimore, MD, United States, [5] Department of Neuroscience, The Johns Hopkins University, School of Medicine, Baltimore, MD, United States

OPEN ACCESS

Edited by:
Gabriela Alejandra Salvador, Universidad Nacional del Sur, Argentina

Reviewed by:
Diana Alicia Jerusalinsky, Universidad de Buenos Aires, Argentina
Maurizio Giustetto, University of Turin, Italy

***Correspondence:**
Alicia L. Degano
adegano@fcq.unc.edu.ar; adegano1@gmail.com

†Present address:
Gabriele V. Ronnett, Janssen Research & Development, LLC, Spring House, PA, United States

Specialty section:
This article was submitted to Cellular Neuropathology, a section of the journal Frontiers in Cellular Neuroscience

Received: *30 March 2019*
Accepted: *13 June 2019*
Published: *03 July 2019*

Citation:
Bertoldi ML, Zalosnik MI, Fabio MC, Aja S, Roth GA, Ronnett GV and Degano AL (2019) MeCP2 Deficiency Disrupts Kainate-Induced Presynaptic Plasticity in the Mossy Fiber Projections in the Hippocampus. Front. Cell. Neurosci. 13:286. doi: 10.3389/fncel.2019.00286

Methyl cytosine binding protein 2 (MeCP2) is a structural chromosomal protein involved in the regulation of gene expression. Mutations in the gene encoding MeCP2 result in Rett Syndrome (RTT), a pervasive neurodevelopmental disorder. RTT is one of few autism spectrum disorders whose cause was identified as a single gene mutation. Remarkably, abnormal levels of MeCP2 have been associated to other neurodevelopmental disorders, as well as neuropsychiatric disorders. Therefore, many studies have been oriented to investigate the role of MeCP2 in the nervous system. In the present work, we explore cellular and molecular mechanisms affecting synaptic plasticity events *in vivo* in the hippocampus of MeCP2 mutant mice. While most studies addressed postsynaptic defects in the absence of MeCP2, we took advantage of an *in vivo* activity-paradigm (seizures), two models of MeCP2 deficiency, and neurobiological assays to reveal novel defects in presynaptic structural plasticity in the hippocampus in RTT rodent models. These approaches allowed us to determine that MeCP2 mutations alter presynaptic components, i.e., disrupts the plastic response of mossy fibers to synaptic activity and results in reduced axonal growth which is correlated with imbalanced trophic and guidance support, associated with aberrant expression of brain-derived neurotrophic factor and semaphorin 3F. Our results also revealed that adult-born granule cells recapitulate maturational defects that have been only shown at early postnatal ages. As these cells do not mature timely, they may not integrate properly into the adult hippocampal circuitry. Finally, we performed a hippocampal-dependent test that revealed defective spatial memory in these mice. Altogether, our studies establish a model that allows us to evaluate the effect of the manipulation of specific pathways involved in axonal guidance, synaptogenesis, or maturation in specific circuits and correlate it with changes in behavior. Understanding the mechanisms underlying the neuronal compromise caused by mutations in MeCP2 could provide information on the pathogenic mechanism of autistic spectrum disorders and improve our understanding of brain development and molecular basis of behavior.

Keywords: MeCP2, presynaptic plasticity, neurogenesis, activity-dependent gene expression, autism

INTRODUCTION

Rett syndrome (OMIM #312750) is one of the few ASDs of monogenic origin that results in mental retardation, motor dysfunction, seizures, and features of autism. In 1999, the main cause of RTT was shown to be mutations in the MeCP2 (Amir et al., 1999). This protein is a member of the family of methyl-CpG binding proteins that bind to gene promoters and regulate their expression (Nan et al., 1997). Alterations in this protein have been found in patients with learning disorders and associated neuropathologies, suggesting that this protein plays an important role in the development and maintenance of neuronal circuits. Understanding the pathological mechanisms that lead to this syndrome would be of great importance for knowing the bases of these disorders and for promoting the development of therapies.

Numerous studies in animal models of RTT indicate that MeCP2 contributes to the formation and maintenance of neuronal connectivity; MeCP2 deficiency affects neuronal maturation (Matarazzo et al., 2004; Palmer et al., 2008), axonal and dendritic morphology (Belichenko et al., 2008; Chapleau et al., 2009), axonal guidance events (Degano et al., 2009), regulates synapse formation and function, as well as synaptic plasticity (Asaka et al., 2006). Although RTT is considered a neurodevelopmental disorder, more recent studies have revealed that MeCP2 is also critical for the maintenance of mature neural networks and global cerebral anatomy during stages of postnatal brain development and in the adult brain (Ballas et al., 2012).

Importantly, it has been demonstrated that *in vitro* MeCP2 regulates gene expression induced by neuronal activity; activity increases MeCP2 phosphorylation (Chen et al., 2001; Martinowich et al., 2003), which leads to dynamic interaction with specific co-repressors, for instance NCoR (Lyst et al., 2013), modulating the expression of target genes like BDNF. Although there is strong evidence that MeCP2 mediates activity-dependent responses *in vivo* (Zhou et al., 2006; Ebert et al., 2013), few studies have explored the consequences of MeCP2 mutations on synaptic plasticity, after *in vivo* synaptic stimulation.

Furthermore, the vast majority of the studies in the field have been focused on the consequences of MeCP2 mutation/deficiency on postsynaptic components of neuronal circuitries, i.e., dendritic morphology and arborizations, as well as density and morphology of dendritic spines (Chapleau and Pozzo-Miller, 2008). This was reasonable, as early evidence from post-mortem studies in RTT patients supported the hypothesis that this was a disorder of dendritic refinement (Chahrour and Zoghbi, 2007). Therefore, most efforts have addressed the role of MeCP2 on dendritic function and development, while the implication of MeCP2 on the development and function of presynaptic components (axonal projections), also essential for proper neural connectivity, remains relatively unexplored. To this end, using the olfactory system as a neurodevelopmental model, we previously identified a novel function for MeCP2 in axonal guidance processes during the establishment of neuronal circuits, including axonal trajectory, axon fasciculation, pruning, and axonal targeting (Degano et al., 2009). Moreover, defects in these processes were more evident when synaptic activity was stimulated (in this case, after odorant exposure) (Degano et al., 2014).

The mouse hippocampus, a structure of great relevance in the pathophysiology of RTT (Chahrour and Zoghbi, 2007), displays two main events of presynaptic structural plasticity: adult neurogenesis at the DG, and dynamic changes in the size of the IPT, formed by granule cells MF (**Figure 1A**). Both forms of structural plasticity in the adult hippocampus correlate with improved performance in hippocampal-dependent learning tasks, and they are closely related to each other (Römer et al., 2011). It has been shown that exposure to an enriched environment or the induction of seizures activity favors adult neurogenesis in DG (Parent et al., 1997; Gray and Sundstrom, 1998; Lindvall et al., 2002), as well as the increase in the size of the IPT (Römer et al., 2011). Therefore, we proposed to use mouse models of RTT and a paradigm of seizures induction to investigate the cellular and molecular mechanisms involved in activity-dependent plasticity *in vivo* from the perspective of pre-synaptic components in the hippocampus from MeCP2-mutant mice.

In the present study, we report that inducing seizure activity in MeCP2-mutant animals reveals a novel role for MeCP2 in the structural plasticity of the MF-CA3 circuit. The lack of MeCP2 interferes with activity-dependent structural presynaptic plasticity in the hippocampus, affecting axonal growth/remodeling, the maturation of adult born neurons, as well as BDNF and Sema3F signaling. Likewise, we show that these plasticity defects correlate with a reduced performance in a spatial learning test (Barnes maze).

We propose that this is a model to study the causal relationships between structural alterations in the hippocampus and cognitive alterations present in mouse models of RTT. These studies may lay the foundations to establish a system that allows evaluating the effect of manipulating specific pathways involved in neural connectivity in a specific circuit and correlating it with changes in behavior. Moreover, these results may serve useful for approaching *in vivo*, in real-time studies for understanding the molecular basis of behavior in several neurodevelopmental or neurocognitive disorders.

Abbreviations: ASDs, autism spectrum disorders; BDNF, brain-derived neurotrophic factor; DG, dentate gyrus; GFAP, glial fibrillary acidic protein; IPT, hippocampal infrapyramidal tract; MeCP2; methyl-CpG 2 binding protein 2; MF, mossy fibers; RTT, Rett syndrome; Sema3F, semaphorin 3F; TrkB, tropomyosin-related kinase B.

MATERIALS AND METHODS

Mice

We used two RTT mouse models for these studies. (1) MeCP2-308 model (MUT), these animals carry a premature stop codon at amino acid 308, generating a truncated MeCP2 protein that lacks the C-terminal region (B6.129S-Mecp2 <tm1hzo>/J, Stock 005439, The Jackson Labs) (Shahbazian et al., 2002) and (2) MeCP2-Bird model (KO): these mice carry a conditional deletion in exons 3 and 4 of the Mecp2 gene causing the absence

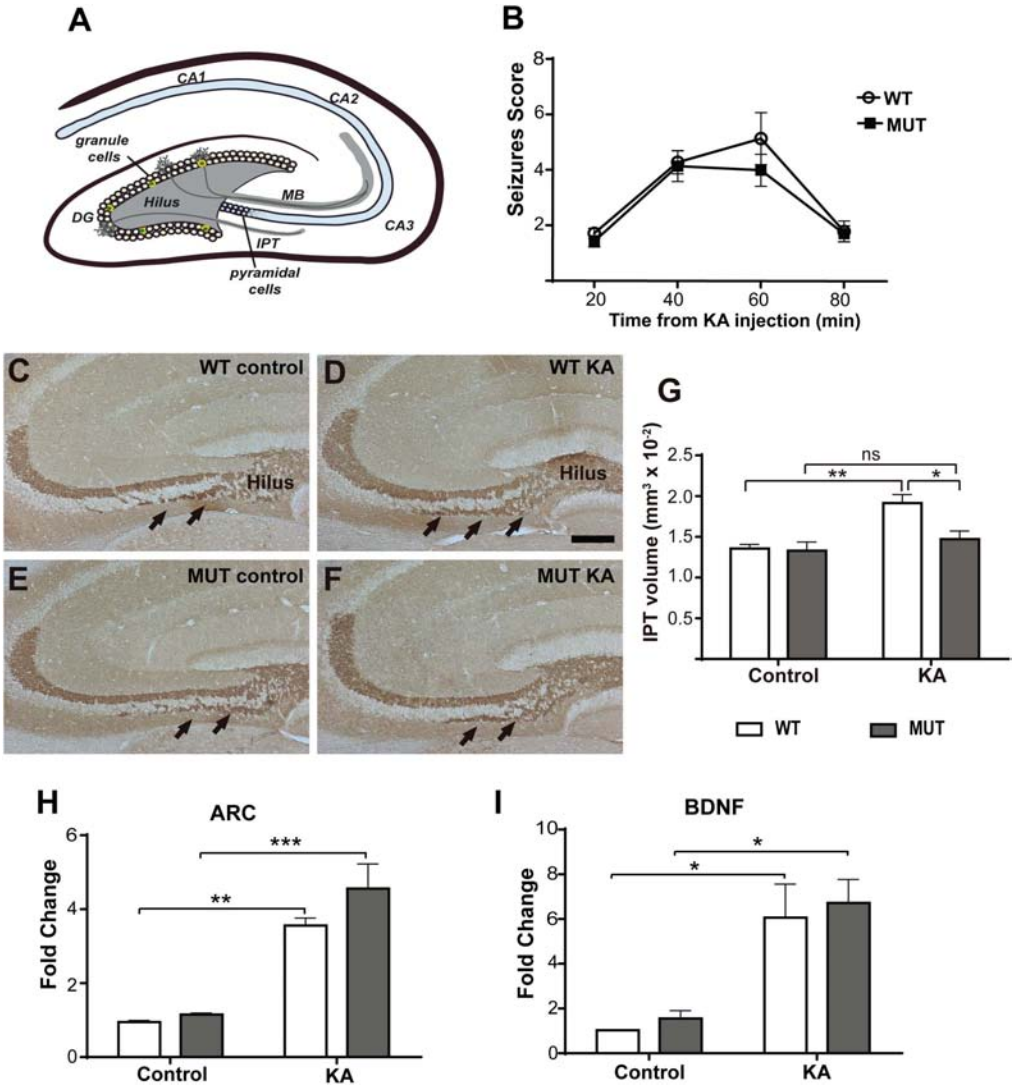

FIGURE 1 | KA-induced seizures failed to increase IPT size in a mouse model of MeCP2-308 mutation. **(A)** Hippocampal MF-CA3 circuit. The MF consist of the axons of the granule cells of the DG that project through the main tract (MT) in the lucid stratum or through the IPT located mainly in the stratum oriens. **(B)** Seizures activity over time after KA administration in MeCP2-308 MUT model. No differences in the development or severity of seizures were observed between WT and MUT mice in response to KA (n = 5 mice per experimental group, two-way ANOVA p = 0.7023, followed by Tukey's HSD test). **(C–F)** Representative images of IPT stained with anti-Synaptoporin in coronal hippocampal sections; IPT is indicated by black arrows. Two weeks after KA injection, WT mice **(D)** but not MUT mice **(F)** showed increased IPT size, in comparison with WT and MUT controls **(C,E)**. Scale bar: 200 μm. **(G)** Quantitative analysis of IPT volume in WT and MeCP2-308 MUT mice. KA-treated WT mice showed an increase in the IPT related to the controls; however, KA-treated MUT mice showed similar IPT size as MUT control. N = 4 mice per experimental group. **(H,I)** KA-induced gene expression: BDNF and Arc expression were determined by real-time RT-PCR from total hippocampus. Six hours after KA injection, a significant increase in the expression of the early activation genes Arc **(H)** and BDNF **(I)** was observed. Fold change was calculated in reference to the WT control group, which was normalized to 1. Results are represented as the ratio between the relative amount of the gene of interest and GAPDH. N = 4 mice per group. cDNA was prepared individually for each mouse and real-time RT-PCR reactions were run in duplicates for each mouse. Data analysis: two-way ANOVA followed by Tukey's HSD test. *$p < 0.05$; **$p < 0.01$; ***$p < 0.001$.

of this protein, starting at embryonic stages (B6.129P2(C)-Mecp2 <tm1.1Bird>/J, Stock 003890, The Jackson Labs) (Guy et al., 2001). Both colonies were maintained in a C57BL/6J background. All the experiments were performed using only hemizygous Mecp2 males (Mecp2 MUT or Mecp2 KO) and their corresponding WT male littermates as control. Animal procedures were fully reviewed and approved by the local animal committee (School of Chemistry, National University of Córdoba, Protocol 2018-832), which follows guidelines from the National Institute of Health.

In vivo Activity Paradigm

Male WT, KO, and MUT mice were genotyped following protocols provided by The Jackson Labs. Each mouse was administered with a single intraperitoneal (i.p.) injection of kainic acid (KA, 20 mg/kg, Sigma). As a control, the same volume

of sterile PBS was injected (McLeod et al., 2013). Considering there are no reports of KA injection in the MUT and in order to provide similar seizure stimulus in WT and MUT mice, we performed several pilot experiments before selecting an adequate age for these experiments. At 6 weeks, the MUT mice were found to be resistant to KA, no convulsions were observed, nor an increase in the expression of activity-induced genes in hippocampus (i.e., BDNF or Arc measured by real-time PCR, data not shown). Conversely, 9-weeks-old MUT males showed similar kinetics and seizure activity as their respective WT littermates (**Figure 1B**). Therefore, since we observed differential sensitivity to KA at different ages in the MeCP2-308 model respect to WT littermates, we decided to use 9-weeks-old MUT males in our experiments for the purpose of using KA exposure as an *in vivo* stimulation paradigm. In the case of the KO, we used 6-weeks-old males, since the response to KA was already reported in the literature (McLeod et al., 2013). It is important to mention that the survival of the two mouse models is very different; male MUT mice live about a year (Shahbazian et al., 2002) while male KO mice survive about 10–12 weeks (Guy et al., 2001).

After KA injection, seizure response was recorded, which became evident after 20 min of injection. From the moment of KA injection, the animals were individually housed in separate boxes and monitored for several hours. The severity of the seizure response was graded according to the following scale: 0, similar to control; 1, increased respiratory rate; 2, in a state of "freezing" and with erratic contractions of the body; 3, straight and stiff tail with or without shaking; 4, the front legs begin to tremble; 5, straight and stiff tail along with tremor of front legs (once); 6, continuously shows straight and stiff tail along with front leg tremor (more than twice); 7, complete clonic tonic seizures, jumps; 8, death [adapted from McLeod et al. (2013)].

Immunohistochemistry

Whole brains were harvested from WT and Mecp2 MUT or KO mice after cardiac perfusion with ice-cold PBS and 4% paraformaldehyde (PFA; Sigma), embedded with Cryoplast (Biopack, Argentina) and serial coronal cryo-sections (20 μm) were obtained. For each brain, 12 numbered slides were used and each one carried six serial sections of the hippocampus. Thus, a fragment of the dorsal region of the hippocampus extending 240 μm along the rostro-caudal axis was represented on each slide (Römer et al., 2011). For BrdU labeling and IPT staining, we used a peroxidase method (ABC System, Vectastain, Vector Laboratories) with biotinylated anti-mouse and anti-rabbit antibodies (1:200; Vector Labs). Fluorescence IHC was performed according to our established protocols (Degano et al., 2009). Primary antibodies include synaptoporin (Synpr; 1:1000; Synaptic Systems), βIII tubulin (TUJ1; Covance; 1:1000), bromodeoxyuridine (BrdU; 1:1000; Roche), GFAP (1:250; Sigma), NeuN (1:1000, LSBio), doublecortin (DCX; 1:200; Santa Cruz), and phospho-TrkB receptor (pTrKB; 1:250; Millipore). Secondary antibodies include biotin donkey anti-rabbit or mouse (1:200, Vector Labs). Cy3 donkey anti-rabbit IgG (1:500), Alexa 545 anti-goat (1:1000), Alexa 488 donkey anti-rabbit, and mouse IgG or chicken (1:1000) were used to facilitate double or triple labeling (Jackson ImmunoResearch). Data were obtained from at least four animals from 3 L per genotype per time point. Images were collected using either a Zeiss Axioskop with a digital camera (Axiocam; Zeiss) or an Olympus FV1000 scanning confocal microscope equipped with a Kr/Ar laser.

Measurement of IPT Volume

Serial coronal sections were stained by IHC, using an antibody against the presynaptic vesicular protein: synaptoporin, enriched in MF (Singec et al., 2002). Images from hippocampus were obtained with an Axioplan microscope (Carl Zeiss) equipped with an Olympus XM10 camera. According to Römer et al. (2011), the IPT area was measured in each section, using the area measurement tool of the FIJI/Image J program (NIH). Then, the IPT volume was obtained for each slide, by multiplying the sum of the areas measured by the inverse of the sampling fraction (12) and by 20 (the thickness of the section in micrometers).

Cell Counts

In order to label proliferating cells, WT and MUT mice were i.p. injected with BrdU (50 mg/kg, Sigma) in 0.01 M PBS. For assessing KA-induced neurogenesis, different cohorts of dividing cells were labeled in a single day. Thus, three doses of BrdU (6 h apart) were injected on the 6th day after KA induction, since it was reported that the highest proliferative activity in DG is detected at 1 week from seizure induction (Burns and Kuan, 2005; Römer et al., 2011). The animals were perfused 2 days after BrdU administration; coronal cryosections were prepared and processed for IHC using anti-BrdU antibodies. Sections were analyzed with an Axioplan microscope (Carl Zeiss) equipped with an Olympus XM10 camera. BrdU-positive cells were analyzed and counted along the rostral–caudal extension of the granule cell layer of DG. The resulting numbers were then multiplied by 12 to obtain the estimated number of total cells per granule cell layer of DG (Römer et al., 2011).

In order to study the maturation of adult-born granule cells of DG, different cohorts of progenitor cells were labeled during 3 consecutive days: 5th, 6th, and 7th days after KA administration (temporal window of high proliferative activity), injecting two doses per day, separated by 7 h. The animals were then perfused 4 weeks after the last BrdU dose, enough time for the new neurons to reach the characteristic morphology of mature granule cells (Burns and Kuan, 2005).

Coronal sections were subjected to triple labeling IHC using: anti-BrdU, to visualize new DG cells and both anti-DCX and anti-neuronal nuclear protein (NeuN) that allows identifying immature and mature neurons, respectively. Triple labeling images (BrdU, DCX, and NeuN) were acquired using Olympus Fluoview 1000 and 1200 confocal microscopes, using a 60× objective. Only BrdU-positive cells located in the granule cell layer of DG were included in the analysis. The markers colocalization was analyzed through the entire *Z*-axis of each BrdU-positive cell (covering the whole cell soma) in single optical planes of 0.7 μm thickness. Total BrdU-positive cells were

counted and their colocalization was analyzed with the neuronal markers in order to calculate the percentage of new mature and immature neurons for each animal.

Real-Time RT-PCR

Total RNA samples were prepared from five to six individual male mice per genotype per condition. Tissues were immediately frozen in liquid nitrogen and homogenized on dry ice. Total RNA was extracted with TRIzol reagent (Invitrogen) according to the manufacturer's protocol. Genomic DNA was digested with 1 unit of DNase I (Invitrogen). cDNA was produced using the mMLV reverse transcriptase (Promega) following standard protocols (Degano et al., 2014). Real-time PCR was carried out on an iCycler (Bio-Rad) by using a reaction mixture with SYBR Green as the fluorescent dye (Applied Biosystems), a 1/10 vol of the cDNA preparation as template, and 250 nM of each primer (Degano et al., 2009, 2014). Primer sequences for BDNF exon IX was obtained from Li et al. (2012). The cycle used for PCR was as follows: 95°C for 180 s (1 time); 95°C for 30 s, 60°C for 30 s, and 72°C for 30 s (40 times); and 95°C for 60 s (1 time). Samples were subjected to a melting-curve analysis to confirm the amplification specificity. The change in fluorescence of SYBR Green dye was monitored in every cycle and the threshold cycle (CT) was calculated above the background for each reaction. For each cDNA sample, a ratio between the relative amounts of target gene and GAPDH was calculated to compensate for variations in quantity or quality of starting mRNA, as well as for differences in reverse transcriptase efficiency. The fold change in the target gene relative to the GAPDH endogenous control gene was determined by: fold change = $2^{-\Delta(\Delta C_T)}$, where $\Delta C_T = C_{T,target} - C_{T,GAPDH}$ and $\Delta(\Delta C_T) = \Delta C_{T,KO} - \Delta C_{T,WT}$. RT-PCRs were run separately for each mouse in triplicate, and data were analyzed for statistical differences by two-way ANOVA using PRISM 6.0 software (GraphPad, San Diego, CA, United States).

Barnes Maze

Barnes maze test was used to evaluate the presence of cognitive deficits in spatial learning and memory of MeCP2 MUT mice in comparison with WT littermates. For this purpose, a Barnes maze for mice was built following the specifications reported by other authors (Rosenfeld and Ferguson, 2014). It consisted of a 92-cm diameter circular platform constructed from a white PVC slab. Twenty holes of 5 cm diameter were made in the perimeter (separated from each other by 7.5 and 2 cm from the edge of the platform). A black exit box 20 cm long, 9 cm high, and 9 cm wide, with a ramp inside it (escape hole), was placed under one of the holes in the platform. The circular platform was located 1 m high from the ground and over it, 1 m away, was illuminated with two white light bulbs of 150 W each. Visual signs consisting of panels with simple colored shapes (squares, triangles, stars) were mounted as visual cues around the room where the test was performed. All of the sessions were recorded using a 12-megapixel camera placed above the platform.

The Barnes maze use is similar to the radial arm and Morris maze but without diet restrictions and with lower physical stress for mice. Inside the maze, mice are motivated to escape from the illuminated and open platform toward a dark, small, and recessed chamber (escape box). In this experiment, we worked with 12 weeks MUT and WT mice, using the protocol of O'Leary and Brown (2013) as reference. The test consists of four steps divided into 4 days:

* Day 1. Habituation – It consisted in making the animal familiar with the environment, the platform, and the escape box. First, the animal was gently introduced into the escape box through the hole in the platform leading to it ("target" hole) and left there for 2 min. Then it was placed in the center of the platform for 30 s covered with a large transparent glass flask. After that period, the animal covered with the flask was guided to the target hole and the flask was located there for 3 min or until the animal enters the escape box. If after 3 min the animal did not enter the escape box, it was guided with the same flask to do so. Once inside the escape box, the animal was left there for 1 min and then it was returned to its usual cage.

* Day 2. Training – Each animal was subjected to three trainings (4 min each), separated from each other by a half-hour break. Every training began with the lights off above the platform and placing the animal in the center of the platform covered by a non-transparent container. Then, the 4-min counting starts, the lights above the platform were turned on and the container that covers the animal removed, allowing it to freely travel the entire platform. When the animal entered the escape box (located in the same hole of the platform in all trainings), the lights were immediately turned off and the mouse was left there for 1 min. In the event that after 4 min the animal has not entered the box, it was guided to it and once inside the box, the lights were turned off again, and the mouse left there for 1 min. In each training we recorded: the percentage of time that the animal spent in each quadrant of the platform, the first quadrant to which the animal was directed when discovered, the number of total explorations of the holes of the platform (considering exploration when the animal pokes its head through one of the holes in the platform), the number of explorations in each quadrant, the number of correct explorations in the target hole, and the latency of entry to the escape box.

* Day 3. Rest.

* Day 4. Memory test – In this case each animal was subjected to a single exposure on the platform that lasted 2 min and in which the escape box was removed. Again, the test started with the lights off and placing the animal in the center of the platform covered by a dark container. When the 2-min count started, lights were turned on and the container covering the animal was removed, allowing it to freely travel the entire platform. Again, the same parameters were recorded here as in the trainings except for the latency of entry to the escape box.

Statistical Analyses

All numerical analyses were performed using PRISM 6.0 software (GraphPad, San Diego, CA, United States). For all comparisons, two-way ANOVA was performed followed by Tukey's *post hoc* test, when appropriate. Differences were considered significantly different at a $p < 0.05$.

RESULTS

Kainic-Induced Seizures Failed to Increase the Size of the IPT in the Absence of MeCP2

To evaluate presynaptic structural plasticity in the absence of MeCP2 (i.e., adult neurogenesis and increase in the size of the IPT), we treated mice with KA to trigger seizures and robust neuronal activity, as shown by other authors (Ebert et al., 2013; Lyst et al., 2013). The animal models we use are from a C57BL6 background, which has a relatively high resistance to excitotoxic insults; therefore, they develop seizures in response to KA and neurogenesis is potentiated without leading to massive neuronal death (Schauwecker and Steward, 1997; Römer et al., 2011).

We generally used the MeCP2-308 mouse model (MUT) for these studies. Some of the experiments were replicated using MeCP2 Bird mouse models. MUT mice and their respective WT littermates were i.p. injected with KA or with sterile PBS (control), so we established four experimental groups: WT control, WT + KA, MUT control, and MUT + KA. In order to provide similar seizure stimulus in WT and MUT mice, we performed several pilot experiments before selecting an adequate developmental stage for this experiments (see the section "Materials and Methods"). A single KA dose was injected in 9-week-old MUT/WT mice, and seizure activity was assessed. **Figure 1** illustrates the average seizure activity at several time points after KA injection. MUT mice (**Figure 1B**) responded to KA with similar seizure activity as the WT, showing comparable kinetics and maximum average scores (MUT: 4 ± 1.29; WT: 5 ± 1.83; $p = 0.702$).

Two weeks after the KA injection, all animals were euthanized and perfused for morphometric analysis, according to Römer et al. (2011). These authors described that during this time window in C57BL/6 mice, the IPT reaches the greatest increase in volume in response to KA-induced seizures. Serial coronal cryosections of the dorsal hippocampus were subjected to IHC for MF labeling and the volume of the IPT was calculated (Römer et al., 2011). As expected, an increase in the IPT size was observed in the WT + KA group comparing with WT controls (**Figures 1C,D,G**). However, no change in the IPT size was observed between MUT control and MUT + KA mice (**Figures 1E–G**). Thus, after KA injection, only WT mice showed a significant increase in the IPT size [$F(1,17) = 4{,}858$; $p = 0.0416$].

To determine whether the lack of IPT growth in response to seizure activity in MeCP2 MUT mice was caused by defective neural activation in response to KA, the expression of activity-induced neuronal genes (Arc and BDNF) was evaluated. For this, new groups of mice from both RTT models were injected with KA and 6 h later, whole hippocampus were dissected from control and KA-injected MUT mice and WT littermates. The expression levels of Arc and BDNF were quantified by real-time RT-PCR. As shown in **Figures 1H,I**, MUT mice showed a significant increase in the expression of Arc and BDNF mRNA after 6 h of KA treatment in comparison with PBS-injected controls. Likewise, WT littermates showed an increase in Arc and BDNF mRNA levels in response to KA. Therefore, no significant differences were recorded between MUT mice and the WTs in terms of expression levels of Arc [$F(1.12) = 1.228$; $p = 0.2895$] and BDNF [$F(1,10) = 0.0034$; $p = 0.9521$] in response to KA stimulation. These results demonstrate that in MUT MeCP2 animals an increase in neuronal activity was induced in response to KA administration, similar in magnitude to that induced in WT animals.

It is important to report that the results shown so far were reproduced using a mouse model of MeCP2 deficiency (MeCP2 Bird model, KO) (**Figure 2**). KO mice responded to KA more severely than WT mice, showing higher seizure scores (KO: 6 ± 0.707; WT: 4 ± 0.316; $p < 0.05$); and the levels of KA-induced Arc and BDNF expression in these animals were similar to the WTs (**Figures 2A,C,D**). Nevertheless, KO mice also failed to show an increase of the IPT after seizure activity (**Figure 2B**).

Kainate-Induced Adult Neurogenesis and Survival of Adult-Born Neurons Are Not Affected in DG of MeCP2 Mutant Mice

It has been shown that the axons of adult-born neurons in DG contribute mainly to the plasticity of the IPT tract (Römer et al., 2011). Likewise, it has been reported that there is a significant rise in the number of new granule cells in the DG after seizure activity (Parent et al., 1997; Gray and Sundstrom, 1998; Scott et al., 1998; Parent and Lowenstein, 2002; Römer et al., 2011), supporting the idea that adult neurogenesis could be related to the increase of the IPT size. Therefore, we quantified the rate of adult neurogenesis in DG after KA administration. Nine-week-old MUT mice and WT littermates received a single i.p. injection of KA or PBS; 6 days later we labeled several cohorts of cell progenitors by i.p. BrdU injections. Animals were sacrificed 2 days later (8 days after KA injection), the dividing cells were labeled by IHC, and BrdU-positive cells were counted along the rostral–caudal extension of the granule cell layer of DG. Eight days after KA injection, a strong increase in the number of BrdU-positive cells was observed in the DG of KA-treated mice compared to the controls (**Figures 3A,B**). However, there were no significant differences in the neurogenic response to KA between the two genotypes [$F(1,8) = 0.2665$; $p = 0.6197$]. A significant increase in the number of dividing cells was observed in both WT and MUT KA-treated mice in comparison with their respective controls (**Figure 3C**). In addition, no significant differences were found between both genotypes in the basal numbers of BrdU-positive cells per DG (WT control: 1464 ± 103, MUT control: 1034 ± 61) ($p = 0.8169$). To confirm that DG dividing cells were neurons, we performed double labeling IHC for BrdU combined with the neuronal marker tubulin β-III (Tuj1) or with an astroglial cell marker (GFAP). Most $BrdU^+$ cells co-localized with the neuronal marker Tuj1, but not with GFAP. **Figures 3E,F** illustrate an example of this control, which was repeated for the samples analyzed. The data suggest that adult neurogenesis in DG is not affected by mutations in MeCP2, since a similar proliferative response was found in MUT and WT mice. However, it is possible that the survival of these new neurons is affected in the absence of MeCP2. For this purpose,

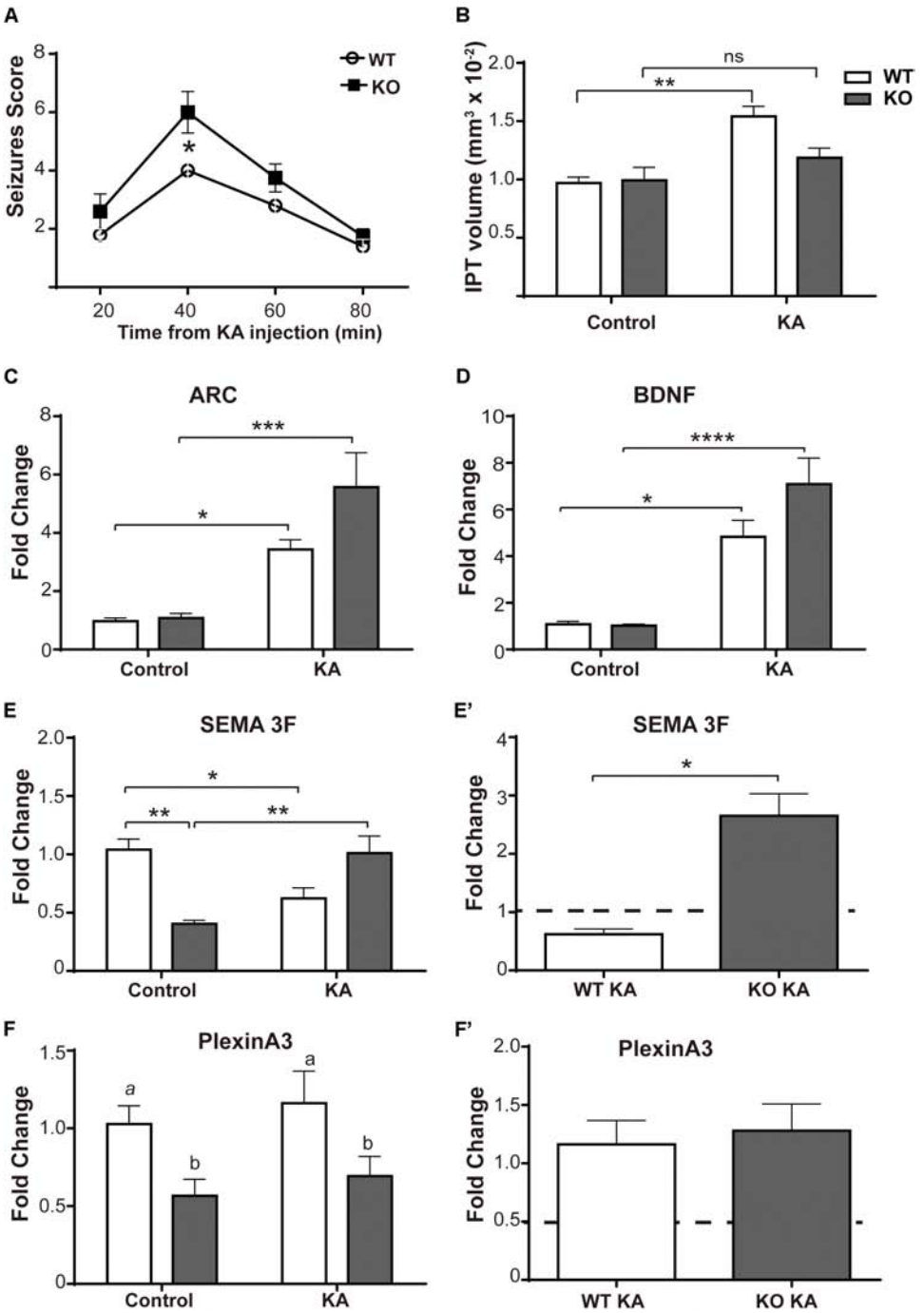

FIGURE 2 | KA-induced seizures failed to increase IPT size in a mouse model of MeCP2 deficiency. **(A)** Seizures activity over time after KA administration. Six-week-old MeCP2-Bird KO mice elicit significantly higher seizures scores than WT littermates, indicative of greater sensitivity to KA. $N = 4–5$ mice per experimental group, two-way ANOVA, followed by Tukey's HSD test, $^*p < 0.05$. **(B)** Quantitative analysis of IPT volume in WT and MeCP2-Bird KO mice. KA-treated WT mice showed an increase in the IPT volume with respect to controls; however, KA-treated KO mice showed similar IPT size as KO control. $N = 4$ mice per experimental group. **(C,D)** KA-induced neuronal gene expression: BDNF and Arc expression were quantified by real-time RT-PCR from total hippocampus. Six hours after KA injection, a significant increase in the expression of the early activation genes Arc **(C)** and BDNF **(D)** was observed. **(E,F)** Sema3F and Plexin A3 expression was assessed by real-time RT-PCR from total hippocampus. Two weeks after KA-seizures induction, a significant decrease in Sema3F was observed in KA-treated WT mice related to WT controls, whereas an opposite response was registered between KA-injected KO mice and KO controls. Basal Sema3F levels in KO mice were significantly lower than in the WT littermates **(E).** Regarding PlxnA3, no changes of expression were observed after KA treatment in WT or KO mice; however, PlxnA3 expression was significantly decreased in KO mice **(F)**. **(C–F)** Fold change was calculated in reference to the WT control group, which was normalized to 1. Results are represented as the ratio between the relative amount of the gene of interest and GAPDH. $N = 5$ mice per experimental group. cDNA was prepared

(Continued)

FIGURE 2 | Continued
individually for each mouse and real-time PCR reactions were run in duplicates for each mouse. Data analysis: two-way ANOVA followed by Tukey's HSD test, $*p < 0.05$; $**p < 0.01$; $***p < 0.001$. **(E′,F′)** In order to better evidence KA effect on each genotype, the expression levels generated by KA were re-calculated in relation to their respective control groups, WT or MUT. The dotted line on the *Y*-axis (*Y* = 1) represents the control values for each genotype. Mann–Whitney *t*-test with 95% confidence intervals, $*p < 0.05$.

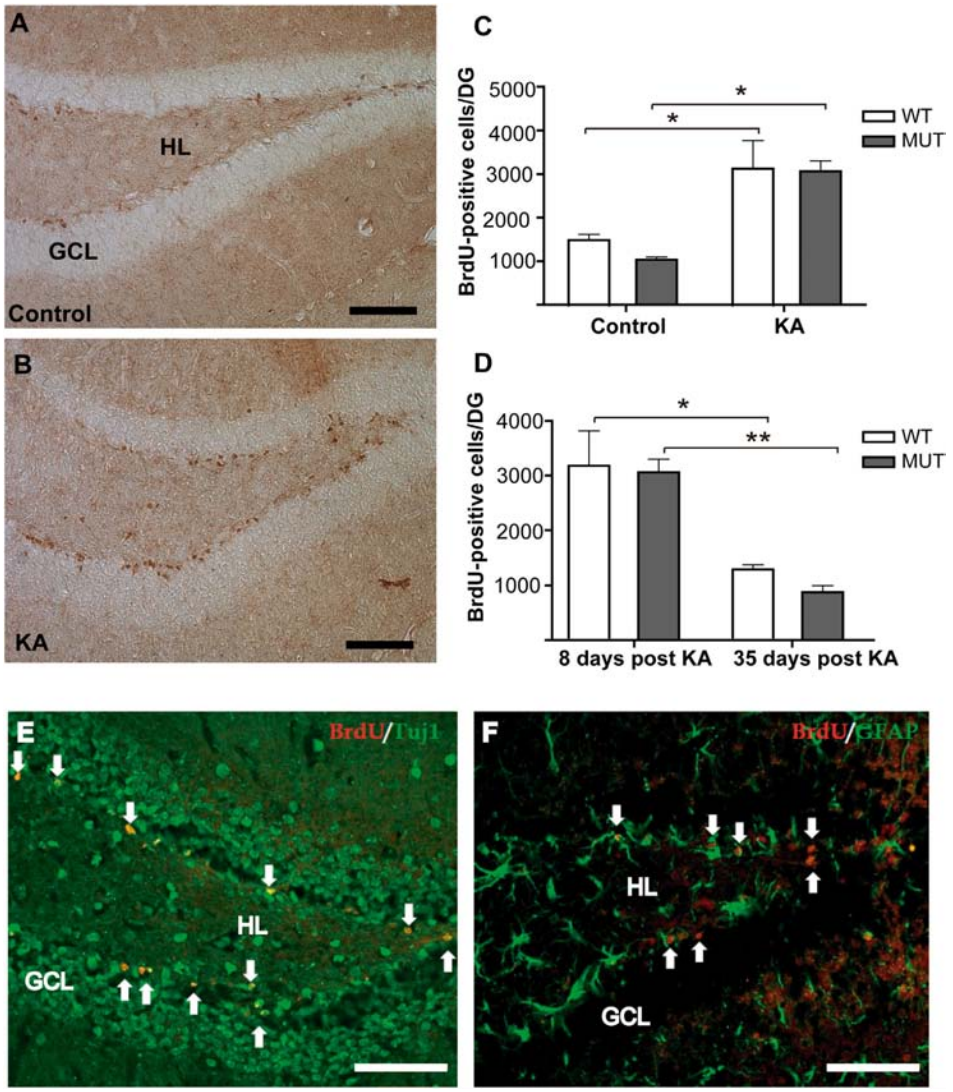

FIGURE 3 | Seizures induce similar rate of adult neurogenesis in WT and MeCP2-308 MUT mice. **(A,B)** IHC for BrDU labeling. Eight days after KA injection, a strong increase in the number of BrDU-positive cells was observed in DG from KA-treated mice **(B)** compared with control littermates **(A)**. Scale bar: 50 μm. GLC, granule cell layer; HL, hilus. **(C)** BrDU-positive cells per DG in KA-treated and controls WT and MUT mice. A single seizure episode induces an increase in the number of BrDU-positive cells that was detected in both WT and MUT mice, respective to their controls. **(D)** Quantification of BrdU-positive cells by DG in WT and MUT mice injected with KA. A similar decrease in the number of BrdU-positive cells was observed in the WT and MUT mice between days 8 and 35 post KA-induced activity. **(E,F)** Double labeling IHC for BrdU and neuronal or astroglial markers in hippocampus 8 days after KA administration. **(E)** Double labeling of newborn DG cells (BrdU in red, white arrows) and Tuj1 (green) a neuronal marker. **(F)** Double labeling of newborn DG cells (BrdU in red, white arrows) and GFAP (in green) labeling astroglial cells in hippocampus. Scale bar: 50 μm. $n = 3$ mice per each experimental group. Data analysis: two-way ANOVA followed by Tukey's HSD test, $*p < 0.05$; $**p < 0.01$.

we evaluated the proportion of KA-induced newborn DG cells ($BrdU^+$) that remained 5 weeks after the induction of seizure activity. **Figure 3D** illustrates the number of $BrdU^+$ cells per DG 8 days and 35 days after KA-induced seizures, when the new DG cells become mature neurons. At 35 days, $BrdU^+$ cells from WT mice decrease about 60% and in MUT 71% respect to day 8; therefore, no significant differences were detected between the genotypes in terms of $BrdU^+$ cell loss [$F(1,9) = 0.2091$;

$p = 0.5883$]. Also, no differences were detected in the absolute number of $BrdU^+$/DG cells between both genotypes at either 8 ($p = 0.9987$) or 35 ($p = 0.8383$) days after KA.

These observations suggest that the survival of the new DG neurons is not affected by MeCP2 mutation; therefore, we conclude that the lack of increase in the size of the IPT, registered 2 weeks after KA injection, was not due to a loss of new DG cells in MUT mice.

Defective Maturation of Adult-Born Granule Neurons Is Recapitulated in Kainate-Treated MeCP2-Mutant Mice

Previous work in the olfactory system and in the hippocampus from MeCP2-KO mice has reported a delay in neuronal maturation during early postnatal development, which is apparently compensated later on (Smrt et al., 2007; Palmer et al., 2008). Given that DG cells undergo adult neurogenesis, we wondered whether the new neurons of the adult organism recapitulate the defects shown in early postnatal development in a model of MeCP2 mutation. Therefore, we evaluated the percentage of maturation of adult born granule cells, taking advantage of the increase in adult neurogenesis induced by seizure activity. Because the numbers of BrdU-positive cells were extremely low in control individuals (injected with PBS), we report only the KA-treated groups. For this study, different cohorts of cell progenitors were marked by BrdU injections when the neurogenesis reached maximum levels (5th, 6th, and 7th day after KA injection), and the animals were perfused 4 weeks from the last BrdU dose. According to the literature, at that time adult-born DG neurons reach the characteristics of mature granule cells (Esposito, 2005). We performed triple immunofluorescence using three markers: anti-BrdU (dividing cells), anti-DCX as a marker of immature neurons, and the nuclear transcription factor NeuN, as a marker for mature granule cells (Esposito, 2005). All the BrdU-positive cells were counted and analyzed per animal sample, and we calculated the percentage of the adult-born neurons that reached maturity ($BrdU^+$ $NeuN^+$), the percentage of immature cells ($BrdU^+$ DCX^+) and at intermediate stage of maturation ($BrdU^+$ DCX^+ $NeuN^+$). **Figure 4A** illustrates examples of double and triple labeling for BrdU-positive cells and the neuronal markers NeuN and DCX. **Figure 4B** shows significant differences between WT and MeCP2 MUT mice [$F(2,21) = 13.73$; $p < 0.001$]; the percentage of new DG cells that reached maturity was significantly lower in MUT mice (MUT_{NeuN}: $86.39 \pm 1.494\%$; WT_{NeuN}: $93.13 \pm 0.762\%$). In addition, MUT mice showed a higher proportion of both immature cells (MUT_{DCX}: $3.85 \pm 0.617\%$; WT_{DCX}: $1.41 \pm 0.481\%$) and cells in transit to maturation ($MUT_{DCX+NeuN+}$: $9.76 \pm 1.521\%$; $WT_{DCX+NeuN+}$: $5.46 \pm 0.537\%$). Thus, MUT adult-born granule cells show abnormal maturation; immature cells accumulate at expense of lower numbers of mature cells.

These results indicate that mice carrying a mutated MeCP2 protein (MUT) show defective neuronal maturation in the adult hippocampus, similar to what was observed during early development in a different mouse model (Smrt et al., 2007).

Altered Expression of Activity-Induced Axon Guidance Molecules in the Context of MeCP2 Mutations

Using the olfactory system and MeCP2-deficient mice, we have demonstrated that axonal guidance defects were accompanied by alterations in the expression of Sema 3F and its receptor complex (PlexinA3 and Neuropilin-2). It has been demonstrated that this axonal guidance molecule regulates axonal growth, guidance, and targeting of hippocampal MF, acting as an inhibitor of axonal growth when combined with its receptor complex present in axons and inducing growth cone collapse (Bagri et al., 2003; Sahay et al., 2003; Riccomagno et al., 2012). Considering this background and the failure of the plastic response of IPT to seizure activity in MeCP2 MUT mice, we explored the Sema 3F pathway in our experimental conditions.

Methyl-CpG 2 binding protein 2 MUT mice and WT littermates were injected with KA or PBS and 2 weeks later the hippocampus of the different experimental groups were dissected. mRNA expression levels of Sema 3F gene and their two receptors (PlxnA3 and Npn-2) were quantified by real-time RT-PCR. **Figure 5** shows the expression levels of the genes analyzed in MUT and WT animals.

Regarding Sema 3F (**Figure 5A**), considerable differences of expression were detected between WT and MUT mice [$F(1,15) = 4.7$; $p < 0.05$]. A significant decrease of Sema3F expression was observed in WT mice + KA compared to WT controls, while in MUT mice no change was registered between controls and KA-treated mice. Likewise, the WT + KA mice presented significantly lower levels of Sema 3F compared to the MUT KA. For PlxnA3 (**Figure 5B**), no significant differences were registered between both genotypes, neither between controls and KA-treated mice [$F(1,14) = 1.327$; $p = 0.2687$]. Although there were no changes in the expression of Npn-2 in response to KA treatment (**Figure 5C**), we found a significant lower expression in the basal levels of Npn-2 in MUT mice [$F(1,14) = 8.072$; $p < 0.05$].

Figures 2E,F show the expression of the Sema 3F and PlxnA3 in KO and WT animals of the MeCP2Bird model after KA-induced seizures. In this animal model, we observed robust differences in Sema 3F expression between WT and KO mice under basal conditions, and also after KA-induced seizures.

Summarizing these observations, the lack of increase in IPT size after KA treatment, in the context of MeCP2 mutations, was accompanied by a deregulation in the expression levels of Sema 3F which, in concert with the receptor complex, exerts an important chemo-repulsive effect on hippocampal axons (Riccomagno et al., 2012).

BDNF Expression Induced by Neuronal Activity Is Deficient in Mecp2 Mutant Mice

In the hippocampus, neurotrophins levels are dynamically regulated by neuronal activity, and the modification of those levels can alter the growth and distribution of projections,

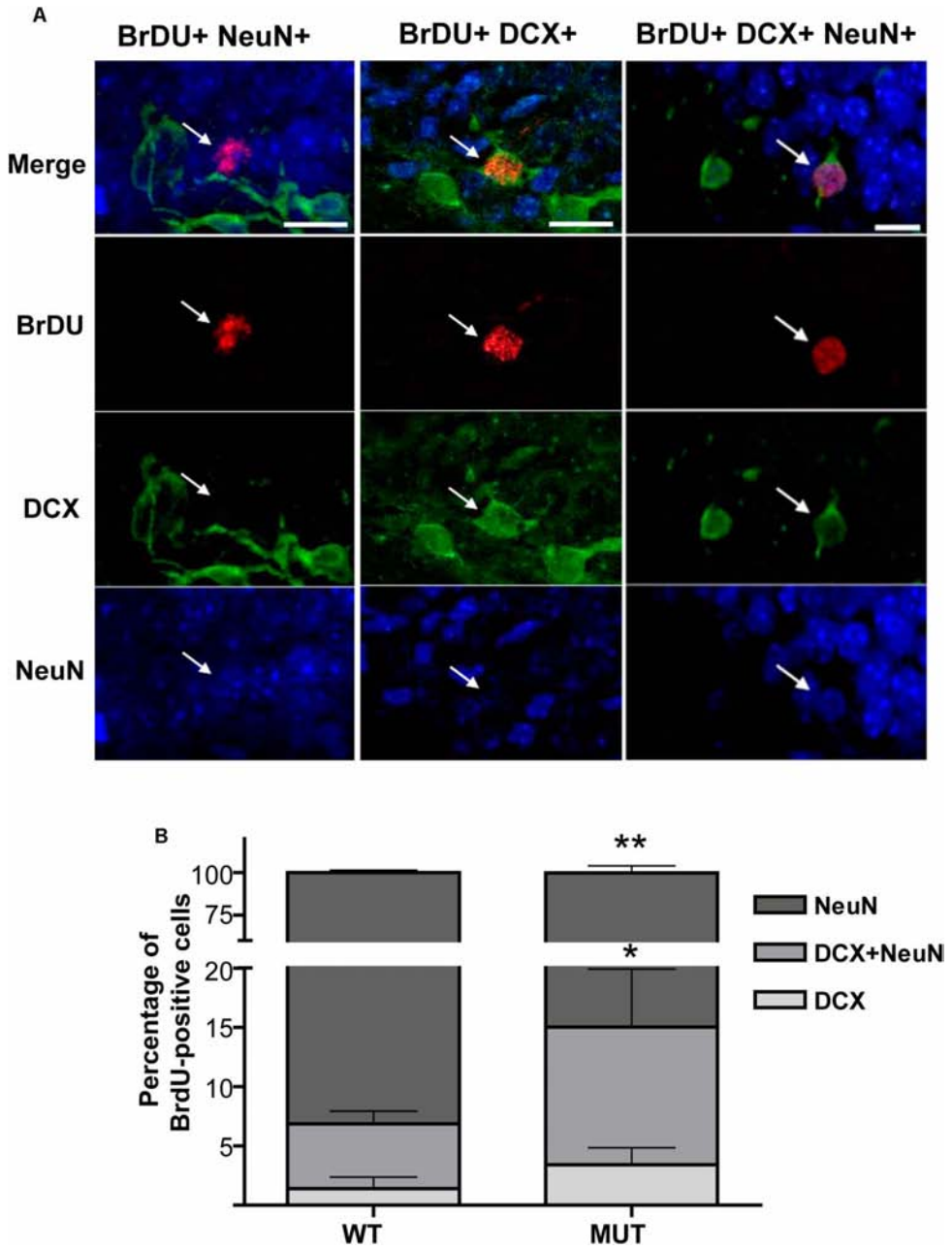

FIGURE 4 | Defective maturation is recapitulated in MeCP2 mutant adult-born granule neurons. **(A)** Triple IHC labeling of BrdU-positive cells and neuronal markers NeuN and DCX. Examples of BrDU-positive neurons in intermediate state of maturation that co-express both NeuN and DCX (right panel). Example of a mature neuron that only expresses NeuN (left panel) and an immature neuron that only expresses DCX (middle panel). The vertical panels are unique optical planes showing the three fluorescence channels separately and their overlapping in the upper panel. Scale bar: 15 μm. **(B)** Percentages of BrdU-positive cells in different stages of maturation in WT and MUT mice exposed to KA. 5 weeks after seizures, WT mice showed a high percentage of mature new granule cells (90%), while MUT mice presented significantly less mature cells and more immature cells. Each bar represents the mean ± standard error (SEM) of BrdU-positive cells co-localizing with the corresponding markers, normalized to the total number of BrdU-positive cells in each mouse. Each bar is subdivided to indicate the mean percentage of BrdU-positive cells at different states of maturation. n = 4–5 mice per experimental group. Data analysis: two-way ANOVA followed by Sidak's test, $^{*}p < 0.05$; $^{**}p < 0.01$.

and MF in particular. BDNF is normally expressed in most hippocampal neurons, including granule cells (Dieni et al., 2012; Isgor et al., 2015). This factor promotes the growth and orientation of granule cell axons *in vitro*, extends innervations of MF into CA3, and regulates its synaptic plasticity (Gómez-Palacio-Schjetnan and Escobar, 2008; Tamura et al., 2009; Römer et al., 2011; Schjetnan and Escobar, 2012). Also, it is now clear that MeCP2 is phosphorylated in response to synaptic activity,

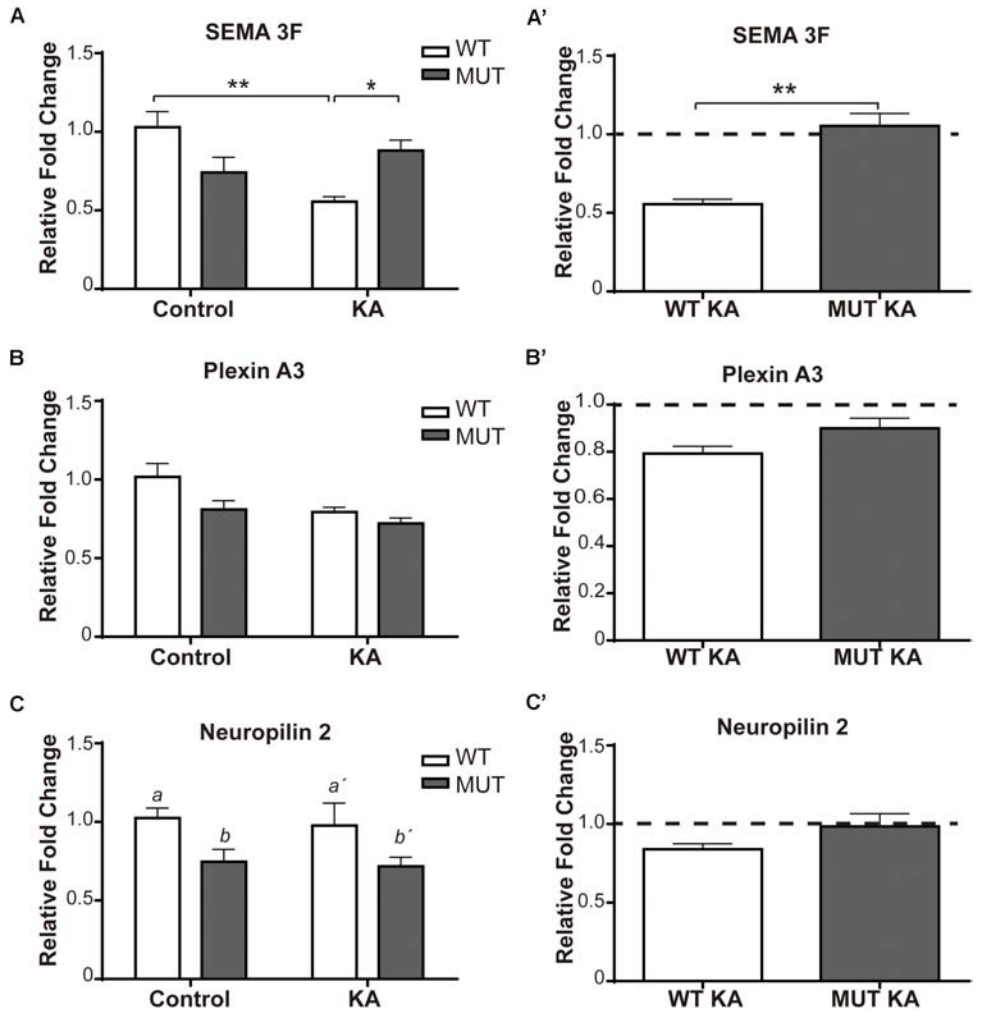

FIGURE 5 | Kainic-induced Sema3F and receptors levels in WT and MeCP2-308 MUT mice. **(A–C)** Sema3F, Plexin A3, and Npn-2 expression were assessed by real-time RT-PCR from total hippocampus. Two weeks after KA-seizures induction, a significant decrease in Sema3F was observed in KA-treated WT mice related to WT controls, whereas no differences were registered between KA-injected MUT and MUT control mice **(A,A')**. Regarding PlxnA3, no changes of expression were observed after KA treatment in WT or MUT mice **(B,B')**; however, Npn-2 expression in MUT mice was significantly lower than WT mice, independently of treatment **(C,C')**. **(A–C)** Fold change was calculated in reference to the WT control group, which was normalized to 1. Results are represented as the ratio between the relative amount of the gene of interest and GAPDH. $N = 5$ mice per experimental group. cDNA was prepared individually for each mouse and real-time PCR reactions were run in duplicates for each mouse. Data analysis: two-way ANOVA followed by Tukey's HSD test, $*p < 0.05$; $**p < 0.01$; $***p < 0.001$. **(A'–C')** In order to better evidence KA effect on each genotype, the expression levels generated by KA were re-calculated in relation to their respective control groups, WT or MUT. The dotted line on the *Y*-axis ($Y = 1$) represents the control values for each genotype. **A'–C':** Mann–Whitney *t*-test with 95% confidence intervals.

and that in this way, activity controls gene expression, i.e., BDNF production (Chen et al., 2001; Martinowich et al., 2003; Zhou et al., 2006). Although we have shown that BDNF levels increased similarly after 6 h of KA injection in both WT and MUT hippocampi (**Figure 1I**), we decided to evaluate BDNF expression after 2 weeks of treatment to determine whether BDNF expression correlates with the increase in IPT volume. As shown in **Figure 6A**, there was a significant difference between both genotypes in terms of BDNF expression [$F(1,13) = 10.61$; $p < 0.01$]. WT animals showed a moderate but significant increase in BDNF expression, 2 weeks after injection with KA. In contrast, in MUT mice BDNF expression remained unchanged between the control and the KA-treated group. Also, BDNF levels in MUT+KA animals were markedly lower than those of WT + KA mice (**Figure 6A**).

Considering that the effects of BDNF are largely mediated through its interaction with and the activation of the TrkB receptor, we proceeded to confirm our result by assessing the number of cells that express the phosphorylated TrkB receptor, as an indicator of BDNF action *in vivo* (Li et al., 2012; Helgager et al., 2014). For this, cryosections from the experimental groups were perfused after 2 weeks of KA treatment, when WT animals showed an increase in BDNF levels and in the size of the IPT in response to KA. Using IHC, we labeled pTrkB-positive cells and it became clear that the area with higher numbers of pTrkB-positive cells was the granule cell layer

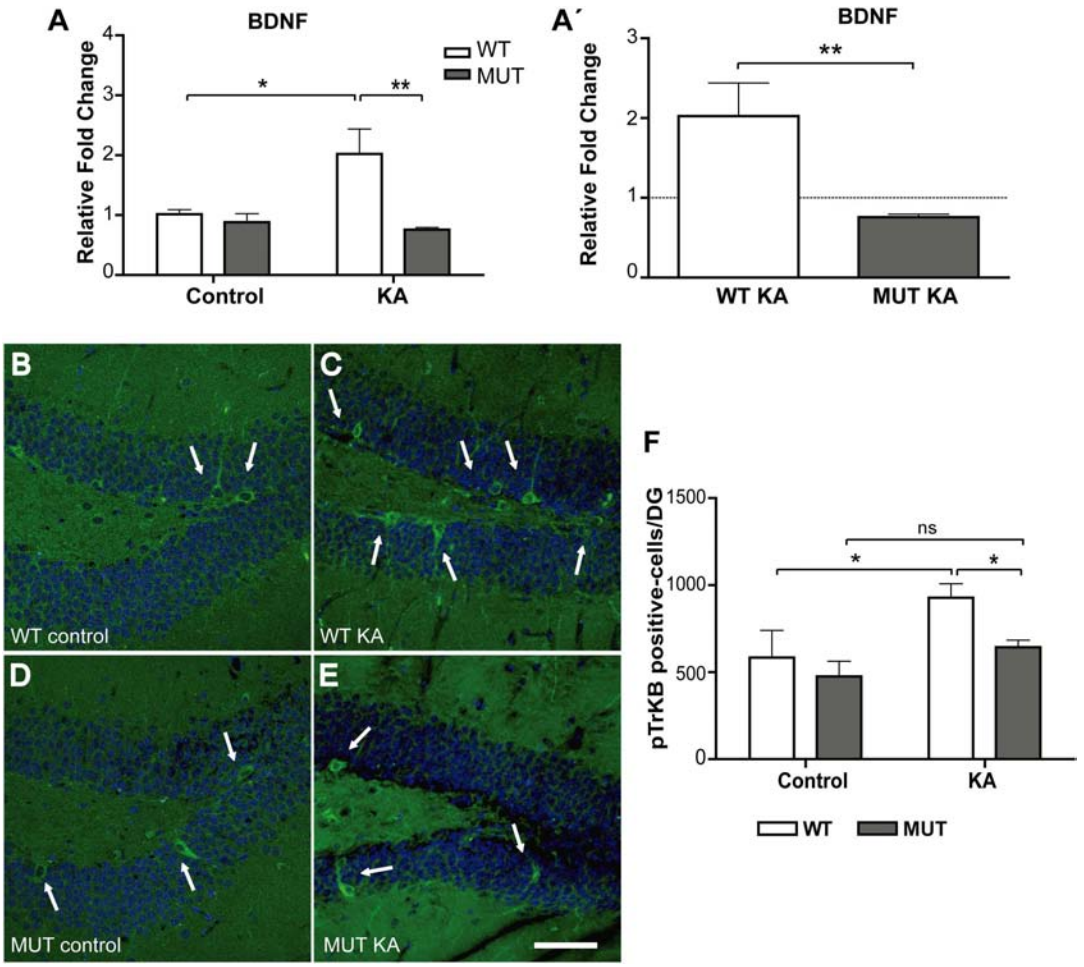

FIGURE 6 | Kainic-induced BDNF expression is deficient in MeCP2-308 MUT mice. **(A,A′)** BDNF expression was assessed by real-time RT-PCR from total hippocampus. **(A)** Two weeks after KA-seizures induction, a significant increase in BDNF was observed in KA-treated WT mice related to WT controls, whereas no differences were registered between KA-injected MUT and MUT control mice. Fold change was calculated in reference to the WT control group, which was normalized to 1. Results are represented as the ratio between the relative amount of the gene of interest and GAPDH. $N = 5$ mice per experimental group. cDNA was prepared individually for each mouse and real-time PCR reactions were run in duplicates for each mouse. **(A′)** In order to better evidence KA effect on each genotype, the expression levels generated by KA were re-calculated in relation to their respective control groups, WT or MUT. The dotted line on the Y-axis ($Y = 1$) represents the control values for each genotype. Data analysis: **(A)** two-way ANOVA followed by Tukey's HSD test, $^{*}p < 0.05$; $^{**}p < 0.01$. **(A′)** Mann–Whitney t-test with 95% confidence intervals, $^{**}p < 0{,}01$. **(B–E)** IHC- and pTrkB-positive cells quantification in DG. Two weeks after KA treatment, an increase in pTrkB-positive cells (white arrows) was observed in WT mice DG injected with KA **(C)** in comparison to KA-injected MUT mice **(E)** or control mice **(B,D)**. IHC labeling pTrkB (green) and Dapi (blue). Scale bar: 50 μm. **(F)** Quantification of pTrkB-positive cells per DG in WT and MUT mice injected with KA and control. A single seizure episode leads to an increase in the number of pTrkB-positive cells, detected 2 weeks after seizure activity only in WT mice. $n = 3$ mice per experimental group. Data analysis: two-way ANOVA followed by Tukey's HSD test, $^{*}p < 0.05$.

of the DG (**Figures 6B–E**). We found a significant difference between WT and MUT mice at 2 weeks after KA administration [$F(1,8) = 11.58$; $p < 0.01$]. While WT + KA showed a significant increase of pTrkB-positive cells in comparison with the controls, no significant differences were observed between treatments in MUT mice (**Figure 6F**). Again, the numbers of pTrkB-positive cells from the WT + KA were significantly higher than those of the MUT + KA.

Altogether, our results indicate that in WT animals, the growth of the IPT, detected at 2 weeks after KA seizure induction, is accompanied by an increase of BDNF expression. Conversely, no increase in the size of IPT is observed in MUT mice, which correlates with deficient BDNF expression in response to KA injection.

Mecp2 Mutant Mice Present Defects in Spatial Memory Evaluated Through the Barnes Maze Test

Given the defects found in activity-dependent plasticity of MF (IPT) in the dorsal region of MeCP2 MUT hippocampus and considering that this circuitry is mainly involved in the processing of spatial memory (Crusio et al., 1987; Crusio and Schwegler, 2005), we decided to assess spatial learning and memory abilities

in these mice through their performance in the Barnes maze. It is estimated that, through successive training sessions, the improvement in performance to locate a hidden box to escape from aversive stimuli allows assessing learning processes and spatial memory in rodents (Rosenfeld and Ferguson, 2014). Considered less stressful for mice than water maze (Morris), the Barnes maze consists of a relatively simple design of a circular platform with several holes equally spaced around the perimeter edge. While one hole leads to an escape cage, the rest are blind. Slightly aversive stimuli (i.e., bright lights) provide the motivation to locate the escape cage, which is also flanked by visual cues (O'Leary and Brown, 2013). Therefore, MUT mice and their WT littermates were evaluated for spatial learning and memory according to their performance in the Barnes maze test.

Learning

The acquisition or learning of the escape box location was assessed by determining the escape latency during three successive training sessions; thus, the acquisition was reflected by lower escape latencies along the trainings. Interestingly, the first thing we noticed was that the percentage of MUT animals that did not learn was almost 20% higher than the WT (WT = 9.52% mice did not learn the task; MUT = 27.3% did not learn the task); "non-learners" were those animals that did not enter the escape box in any of the three training sessions. However, when we evaluated the escape latency of the animals that did learn, no significant differences were found in the acquisition between the groups [$F(6,117) = 0.744$; $p = 0.6150$] (**Figure 7A**). We found that the average escape latency decreased similarly in both groups throughout the successive trainings. This observation suggests that, although a higher percentage of MUT mice failed to learn the task, in the groups that did learn, the learning process was similar to that of the WT littermates.

Memory

Two days after the acquisition phase, we performed a final test of retention or memory, consisting of a single 2-min exposure on the platform, after removal of the escape box. In this spatial preference test the animal that remembers the maze will spend more time in the "target" quadrant, i.e., the quadrant where the escape box was previously located (O'Leary and Brown, 2013). The data showed a significant difference between genotypes [$F(1,36) = 14.81$; $p < 0.001$] (**Figure 7B**). While WT mice spent about 40% of the time in the target quadrant, MUT mice only spent an average of 24% of the total time in that quadrant (**Figure 7B**). Since the average percentage of time that a normal mouse will spend randomly in each quadrant of the platform during the test is about 25%, we can conclude that the MUT mice showed a failure in retaining the task learned during the acquisition phase.

These results were complemented by quantifying the percentage of snouts made by the animals in the target quadrant and in the escape hole with respect to the total snouts in the holes of the platform during the 2 min of the final memory test. The statistics showed a marked difference between WT and MUT MeCP2 [$F(1,38) = 22.7$; $p < 0.0001$]. WT mice explored the target quadrant and the escape hole significantly more than MUT mice (**Figures 7C,D**). Altogether, these results indicate that MeCP2 MUT mice do not show defects in the spatial learning process measured with the Barnes maze; however, they exhibit a marked failure in the spatial memory evaluated by the same test.

DISCUSSION

In the present study, we report that inducing seizure activity in MeCP2 mutant animals reveals a novel role for MeCP2 in the structural plasticity of the MF-CA3 circuit. The lack of MeCP2 interferes with activity-dependent structural presynaptic plasticity in the hippocampus, affecting axonal growth/remodeling, the maturation of adult born neurons, as well as BDNF and Sema3F signaling. Likewise, we show that these plasticity defects correlate with a reduced performance in a spatial learning test (Barnes maze).

Two central events in presynaptic structural plasticity have been described in mice and rat hippocampus: adult neurogenesis and dynamic changes in the size of the IPT, formed by DG granule cell axons. Both the formation of new DG neurons and the anatomy of the IPT are dynamically regulated in response to neurogenic stimuli, such as exposure to an enriched environment or the induction of epileptogenic activity (Parent and Lowenstein, 1997; Gray and Sundstrom, 1998; Lindvall et al., 2002; Belichenko et al., 2008; Römer et al., 2011). Although environmental enrichment may be a better physiological stimulus, it is not possible to ensure that any given animal receive similar stimulation. In the present study, we decided to treat animals with KA in order to trigger seizures and generate robust neuronal activity *in vivo*, as a way to provide controlled stimulation conditions, leading to more homogeneous activity. We based our experimental design on several reports using KA injections in different Rett mouse models, considering that those studies have established most of the activity-dependent responses described in the field (Ebert, 2013).

Most of our studies were developed in the MeCP2-308 (MUT) model which better resembles the human pathology; these mice express a mutated protein, their clinical evolution is progressive, and they survive for over a year. This is important because it permits experiments at more advanced ages and also avoids the results may be masked by near-death physiological conditions, as occurs with most of the studies performed in MeCP2 KO models (survival: 8–11 weeks). The original characterization of this mouse model revealed that MeCP2 MUT animals develop spontaneous seizures from 5 months of age (Moretti et al., 2005). However, there were no reports regarding the induction of seizures activity using this model. Here, we performed KA injection experiments in WT and MUT mice of 6, 9, and 12 weeks of age. Interestingly, 6 weeks old-MUT mice injected with KA did not develop seizures nor showed an increase in the expression of BDNF and Arc, in contrast to their WT littermates (data not shown) and MeCP2-KO mice (**Figure 2A**). Conversely, 12-weeks-old MUT mice were acutely sensitive to the KA doses that were just effective in 12-weeks-old WT mice (data not shown). Lastly, 9-weeks-old WT and MUT mice injected with KA showed similar levels of seizures activity and

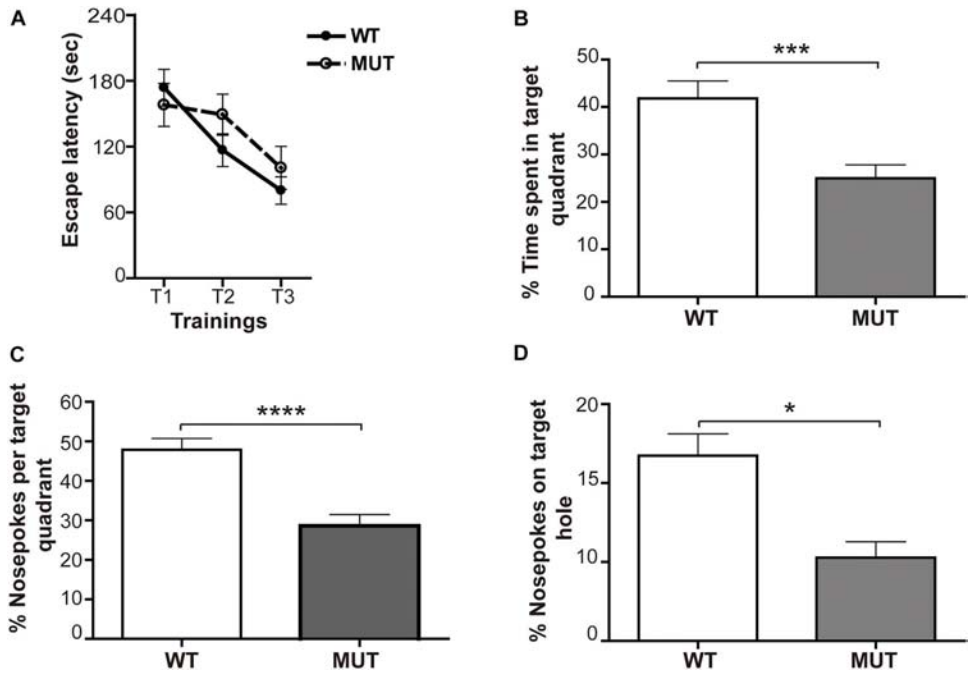

FIGURE 7 | Mecp2-mutant mice show defective spatial memory evaluated through the Barnes maze. **(A)** Learning: the acquisition was reflected by lower escape latencies along the trainings. For both experimental groups, a similar decrease in the escape latency time (measured in seconds) throughout the successive trainings was observed. n = 16-19 mice per experimental group. Data analysis: two-way ANOVA followed by Tukey's HSD test. **(B–D)** Memory: relative percentage of time spent and number of snouts made by the animals in the target quadrant and in the escape hole during the 2 min of the final memory test. **(B)** Percentage of time spent in target quadrant for WT and MUT mice. The analysis shows that WT mice spent significantly more time in the target quadrant than MUT mice. Percentage of snouts in the target quadrant holes **(C)** and in the escape hole **(D)** in relation to the total snouts performed in the holes of the platform in the 2 min of the final memory test. Both the percentage of snouts in the "target" quadrant **(C)** and in the escape hole **(D)** was significantly higher in WT mice when compared with the MUT. n = 16–19 mice per experimental group. Data analysis: Mann–Whitney t-test with 95% confidence interval. *$p < 0.05$; ***$p < 0.001$; ****$p < 0.0001$.

increased expression of BDNF and Arc (**Figures 1B,H,I**). Thus, we found clear age-dependent differences in susceptibility to KA in MUT animals.

However, we observed no change in the IPT volume in 9-week-old MUT mice (**Figure 1G**), even though they showed increased neuronal activity in response to KA, similar in magnitude to that induced in WT animals (**Figures 1B,H,I**). These results suggest that the lack of IPT growth was not due to a defect in early neuronal activation in the hippocampus of MeCP2 MUT mice. We confirmed some of these results using another model MeCP2 Bird mice (KO). MeCP2 KO mice injected at 6 weeks of age showed greater sensitivity to KA than their WT counterparts (**Figure 2A**). This response is consistent with other author reports, using a different KO mouse model of MeCP2 (McLeod et al., 2013). When activity-induced gene expression was quantified after 6 h of KA, both WT and KO mice showed increased expression of BDNF and Arc (**Figures 2C,D**). However, only the WT mice of this model showed a significant increase in IPT size (**Figure 2B**), even though MeCP2 KO animals displayed higher seizures scores. Thus, using two different mouse models we show that even though similar seizure activity was recorded in every KA-injected animal and they show similar levels of hippocampal neural stimulation (measured as levels of activity-induced gene expression), no increase in the size of the IPT was detected in any of the models of MeCP2 deficiency (MUT or KO), indicating a deficit in the plastic IPT response to neuronal activity in the absence of normal MeCP2 function.

Since it has been demonstrated that the IPT size is dynamically influenced by an increase in neurogenesis (Römer et al., 2011), we evaluated adult neurogenesis in DG in response to KA. Our results showed that this process was not affected in MeCP2 MUT mice (**Figures 3A–C**), in agreement with previous work indicating that MeCP2 is not critical for neurogenesis (Smrt et al., 2007). The lack of IPT growth observed in MeCP2 MUT mice in response to KA would not be a consequence of a lower production of new granule cells in DG. However, it is possible that the survival of these new neurons is affected in the absence of MeCP2. In this sense, we observed that the proportion of new cells ($BrdU^+$) that remain 5 weeks in the DG after the induction of seizures activity was similar in WT and MUT mice (**Figure 3D**); therefore, the survival of the new DG neurons seems not to be affected by MeCP2 mutation. These results are also in agreement with older studies that found no signs of neurodegeneration or neuronal death in these models of MeCP2 deficiency (Moretti et al., 2005, 2006).

Interestingly, although neurogenesis was not affected in the absence of MeCP2, the new DG neurons displayed deficits in their ability to transition to a mature state (**Figure 4**). Our results show that mice carrying a mutated MeCP2 protein (MUT) have defects in the maturation of new neurons in adults, in a

manner similar to that observed during early development in other RTT models (Matarazzo et al., 2004; Smrt et al., 2007; Palmer et al., 2008). The increase in adult neurogenesis induced by neuronal activity allowed us to show that this defect is recapitulated in the adult animal. The delay in maturation of DG newborn granule cells in adult animals suggests that, although in response to synaptic activity a similar number of new neurons are generated in the absence of MeCP2, they would not normally integrate into the circuit. This finding could have important implications in hippocampal-dependent learning processes, such as spatial memory tests.

Regarding the structural plasticity of the IPT tract, it has been proposed that this is the result of the coordinated increase of trophic factors and the decrease of chemo-repellant molecules (Bermúdez-Rattoni and Rekart, 2007). The levels of neurotrophins in the hippocampus are regulated dynamically by neuronal activity and the modification of these levels can alter the growth and distribution of the MF. Numerous studies have implicated BDNF as a potent modulator in many aspects of neuronal development (Huang and Reichardt, 2001), as well as in synaptic transmission and plasticity (Poo, 2001; Cowansage et al., 2010; Lu, 2003). BDNF normally expressed in most hippocampal neurons promotes the growth and orientation of the axons of granule cells *in vitro* and regulates the synaptic plasticity of MF (Gómez-Palacio-Schjetnan and Escobar, 2008; Tamura et al., 2009; Schjetnan and Escobar, 2012). In addition, MeCP2 has been shown to be phosphorylated in response to synaptic activity and regulates gene expression, in particular the production of BDNF (Chen et al., 2003; Martinowich et al., 2003). Our results demonstrate that in both WT and MeCP2 MUT animals, BDNF levels increase similarly in response to KA, at 6 h post injection. However, when we determined BDNF expression and pTrKB (an *in situ* indicator of endogenous BDNF protein; Li et al., 2012) at 2 weeks post-KA, we found it remains high in WT animals, but not in the MUT mice (**Figure 6F**). Thus, the IPT growth detected in WT animals was accompanied by an increase in the expression of BDNF; while in MeCP2 MUT mice, the lack of growth correlated with a poor change in BDNF expression. These results indicate that although the signaling events involved in the early neuronal response to seizure activity seems unaffected in the absence of MeCP2 (**Figure 1H**), we do detect a deficit of long-term BDNF support required for driving the axonal growth of MF in response to synaptic activity.

Given the importance of this neurotrophin, and considering that MeCP2 binds to one of BDNF promoters and regulates its expression, many studies have proposed a critical role for BDNF in the pathogenesis of RTT. In this sense, a general reduction in BDNF mRNA levels has been described in MeCP2 KO animal models (complete lack of protein) (Chang et al., 2006; Wang et al., 2006; Kobayashi, 2009; Li and Pozzo-Miller, 2014). However, it is interesting to note that those changes were reported when MeCP2 KO mice were already fully symptomatic (and with a life expectancy of 1–3 more weeks). In this sense, we found no differences in hippocampal BDNF expression between WT and MeCP2 KO 6-weeks-old mice under either basal or KA-treated conditions (**Figure 2D**), suggesting that BDNF expression in the absence of MeCP2 may be either associated to age or secondary to symptoms; this issue has been already noticed in our previous work and also discussed by other authors (Degano et al., 2014; Li and Pozzo-Miller, 2014). In contrast, in the present work, we show that in the MeCP2-308 mouse model, MUT mice in basal conditions show no differences in mRNA levels for BDNF in the hippocampus at either 9 or 11 weeks of age (**Figures 1I**, **6A**). This observation was also reported in older and symptomatic MeCP2-308 MUT animals (Moretti et al., 2006). In addition, we observed that both WT and MUT groups responded with a similar increase in BDNF expression at 6 h post-KA (**Figure 1I**), although this response was not maintained over time in the MUT animals (**Figure 6A**). These results suggest a more complex relationship, and further studies are needed to clarify the role of BDNF in the absence of MeCP2 and in RTT pathogenesis (Li and Pozzo-Miller, 2014). Paradigms of *in vivo* synaptic activation combined with circuit plasticity and molecular tools may help to elucidate these relationships.

On the other hand, a body of evidence suggests that semaphorins are critical determinants of axonal growth and targeting during the development of the nervous system (Pasterkamp, 2012). Mice deficient in Sema 3F, Npn-2, or in PlexinA3 showed robust hypertrophy of the IPT tract (Cheng et al., 2001; Bagri et al., 2003; Riccomagno et al., 2012). Therefore, considering our previous reports revealing axonal guidance and Sema 3F deficits in MeCP2 KO mice (Degano et al., 2009), we focused in evaluating the Sema 3F pathway in the context of MeCP2 mutation. This molecule is involved in the growth, guidance, and target of hippocampal MFs (Bagri et al., 2003; Sahay et al., 2003), acting as an inhibitor of axonal growth and inducing their collapse (Riccomagno et al., 2012). In this sense, the response of WT mice injected with KA (**Figure 5A**) was in line to previous reports, which showed that WT mice exposed to seizure activity (using either KA or pilocarpine) display a decrease in mRNA Sema 3F levels between the 1st and 2nd week after seizures in CA3, CA1, and DG (Barnes et al., 2003; Cai et al., 2016); this decrease overlapped with the formation of new synapses in the MF-CA3 circuitry (Okazaki et al., 1995; Barnes et al., 2003). Thus, the reduction of Sema 3F expression induced by KA in WT animals (low chemo-repulsion) would promote a permissive milieu for MF growth, contributing to the dynamic increase in the size of the IPT registered after KA-induced seizures (Römer et al., 2011). Since both MUT and KO MeCP2 mice failed to show a decrease of Sema3F levels in response to KA (**Figures 2E,E′**, **5A,A′**), we suggest that in these animals a local inhibitory environment for axonal growth is operating, which could account for the lack of IPT volume increase in the absence of normal MeCP2 expression.

It has been suggested that the process of structural plasticity shown by MF in response to synaptic activity involves a tightly regulated balance between growth factors and axonal guidance molecules (Bermúdez-Rattoni and Rekart, 2007). Here we report that an imbalanced expression of those crucial players might be responsible for the lack of MF growth in the absence of MeCP2 (**Figure 8**). Thus, after seizure activity, MeCP2 MUT and KO

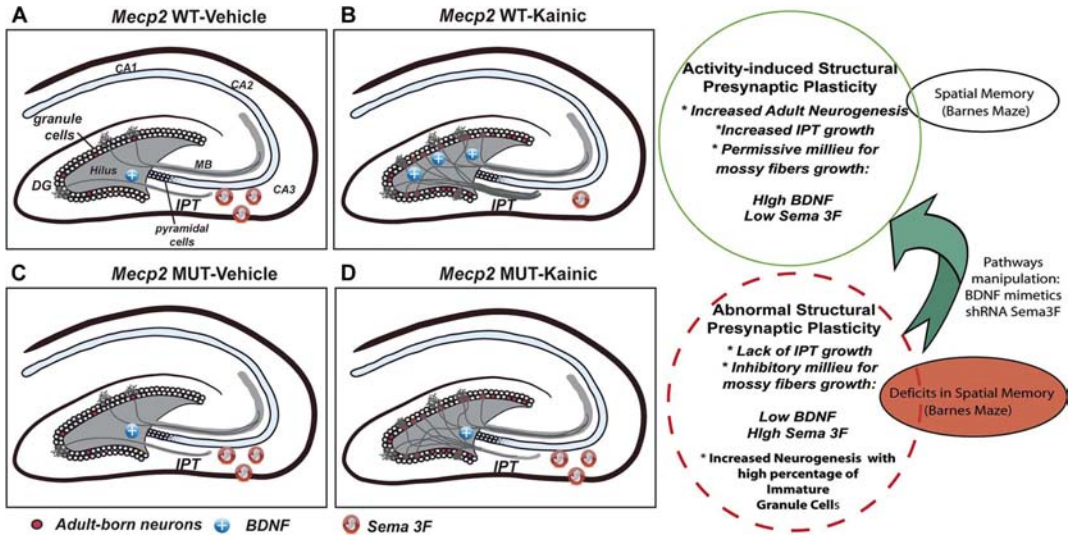

FIGURE 8 | Schematic summary of the activity-induced presynaptic plasticity regulated by MeCP2. In WT mice, seizures activity increases the level of neurogenesis, accompanied with higher levels of BDNF and lower of Sema3F, allowing IPT to grow **(A,B)**. Conversely, MUT animals show abnormal activity-dependent presynaptic plasticity characterized by the lack of IPT growth which correlates with imbalanced trophic and guidance support (BDNF and Sema3F abnormal levels). Although activity do increases the neurogenesis in MUT mice, adult born granule cells show developmental restraining and recapitulate maturational defects **(C,D)**. These results are in line with deficits in spatial memory observed in MUT mice. This study set the basis to establish a model to evaluate the effect of manipulating specific pathways involved in axonal guidance, synaptogenesis, and neuronal maturation to correlate with changes in behavior.

mice display an increase of the chemorepellant Sema 3F, which in concert with a deficient expression of the growth factor BDNF would generate an inhibitory environment for axonal growth.

In this study, we did not analyze the dendritic components of granule DG cells. However, in contrast to postmortem studies in RTT patients (Armstrong et al., 1995), the brains of symptomatic MeCP2-308 MUT mice did not show defects in dendritic arborizations in frontal cortex nor in the density of synapses or dendritic spines in CA1 area of hippocampus (Moretti et al., 2006). In addition, electrophysiological studies suggest that synaptic dysfunction precedes clinical symptoms; these were manifested as an increase in synaptic transmission and decreased LTD in the collateral synapses of Schaffer in this animal model (Moretti et al., 2006). Further studies using this animal model of MeCP2 mutation may define whether axonal components are the main substrate of these synaptic defects.

Presynaptic structural plasticity events have been correlated with improvements of performance in hippocampal-dependent learning tests (Römer et al., 2011). The considerable plasticity of the IPT has been observed early (Schwegler et al., 1990), and abundant evidence demonstrated the positive correlation between IPT size and animal performance in a great variety of behavioral tests of spatial memory (Lipp et al., 1988; Schwegler et al., 1990; Schöpke et al., 1991; Bernasconi-Guastalla et al., 1994; Laghmouch et al., 1997; Crusio and Schwegler, 2005; Delprato et al., 2015). Interestingly, deficits in radial maze performance were also associated with smaller IPT in a mouse model of Fragile-X Syndrome (Mineur et al., 2002). Therefore, we decided to evaluate spatial learning and memory of MeCP2 MUT mice through their ability to navigate the Barnes maze; it is estimated that the improvement in performance to locate an escape box to aversive stimuli, through successive training sessions, allows assessing learning processes and spatial memory in rodents. Previous studies showed that MeCP2-308 MUT mice (>20 weeks of age = fully symptomatic) show learning and memory deficits in several hippocampal-dependent behavior paradigms (Morris water maze, fear contextual conditioning test, and long-term social memory) (Moretti et al., 2005, 2006). Our results indicate that earlier in development (12-weeks-old), 27% of MeCP2-308 MUT mice failed to learn the location of the exit box, compared with 10% of WT littermates. Interestingly, the MUT animals that learned the task had similar performance as the WTs during the trainings. Conversely, these MUT animals displayed clear spatial memory deficits, as they showed a marked failure in the retention of the acquired information evaluated by the same test (**Figures 7B–D**). It is important to emphasize that in this work we also revealed that failure in granule cells maturation recapitulates in each round of neurogenesis in the adult hippocampus, adding to the long-term circuitry dysfunction (**Figure 4**). Although it has not been demonstrated that memory *per se* is altered in patients, cognitive abnormalities are present in individuals with MeCP2 mutations, supporting the concept that the results obtained with the MeCP2-308 animal model would represent a correlate of cognitive deficits in RTT (Moretti et al., 2006).

Alterations of synaptic and axonal refinement have been implicated in the etiology of neurological diseases (Lewis and Levitt, 2002; Johnston, 2004; Pardo and Eberhart, 2007). Likewise, hippocampal MF synapses are important for spatial memory formation and consolidation (Nicoll and Schmitz, 2005; Bischofberger et al., 2006). Spatial learning and environmental enrichment result in an increase in the number, size, and complexity of the MF (Ramírez-Amaya et al., 2001;

Galimberti et al., 2006). In addition, the IPT presents a dramatic reorganization after induction of seizures (Cavazos et al., 1991). While the molecular pathways underlying the activity-dependent remodeling of MFs should still be determined, neurotrophins such as NGF and BDNF may play a role in the remodeling of MF in the normal brain, since their levels are increased with seizures activity (Zafra et al., 1990). Axonal guidance molecules including semaphorins, plexins, and neuropilins can also help to reconfigure MF after changes in activity levels (Holtmaat et al., 2003; Suto et al., 2010).

In light of the present studies, we propose that activity-dependent axonal defects and alterations in neurotrophins and guidance molecules signaling could contribute to the neurological defects present in models of RTT syndrome. Likewise, in this animal model we found a correlation between the structural plasticity of MF and the spatial memory response. This offers a powerful tool for studies on the consequences of MeCP2 mutation, since changes in a relatively simple neural circuit could be connected to changes in spatial memory defined from an animal behavioral test. Based on these studies, we establish a model that would allow to evaluate the effect of the manipulation of specific pathways involved in axonal guidance/synaptogenesis/neuronal maturation in a specific circuit in correlation with changes in spatial memory (**Figure 8**). This strategy may enable a better understanding of the factors that control synaptic activity-dependent remodeling in the normal brain and in disorders of connectivity, such as autism-related disorders.

DATA AVAILABILITY

All datasets generated for this study are included in the manuscript and/or the supplementary files.

ETHICS STATEMENT

Animal procedures were done in accordance with our Institutional Animal Care and Use Committee (IACUC from School of Chemistry, National University of Córdoba), which follows guidelines from the National Institute of Health.

AUTHOR CONTRIBUTIONS

MB, MZ, and MF contributed to the acquisition, analysis, or interpretation of data for the work. SA, GVR, and GAR contributed to key techniques and critically revised the work for important intellectual content. AD contributed to the conception and design of the study, and wrote the first draft of the manuscript. All authors contributed to the manuscript revision, read, and approved the submitted version.

FUNDING

This work was supported by Consejo Nacional de Investigaciones Científicas y Técnicas de la República Argentina (CONICET, to AD), Secretaria de Ciencia y Tecnología-Universidad Nacional de Córdoba (SeCyT-UNC, to AD), Agencia Nacional de Promoción Científica y Técnológica (FONCyT-PICT 2013 No. 106, to AD), International Society for Neurochemistry (ISN-CAEN, to AD and MB), and by a Research with the Daegu Gyeongbuk Institute of Science and Technology (DGIST) Convergence Science Center, funded by grant #10-BD-04 from Korean Ministry of Education, Science, and Technology (to SA and GVR).

REFERENCES

Amir, R. E., Van den Veyver, B. I, Wan, M., Tran, C. Q., Francke, U., and Zoghbi, H. Y. (1999). Rett syndrome is caused by mutations in X-linked MECP2, encoding methyl-CpG-binding protein 2. *Nat. Genet.* 23, 185–188. doi: 10.1038/13810

Armstrong, D., Dunn, J. K., Antalffy, B., and Trivedi, R. (1995). Selective dendritic alterations in the cortex of rett syndrome. *J. Neuropathol. Exp. Neurol.* 54, 195–201. doi: 10.1097/00005072-199503000-199503006

Asaka, Y., Jugloff, D. G. M., Zhang, L., Eubanks, J. H., and Fitzsimonds, R. M. (2006). Hippocampal synaptic plasticity is impaired in the Mecp2-null mouse model of Rett syndrome. *Neurobiol. Dis.* 21, 217–227. doi: 10.1016/j.nbd.2005.07.005

Bagri, A., Cheng, H. J., Yaron, A., Pleasure, S. J., and Tessier-Lavigne, M. (2003). Stereotyped pruning of long hippocampal axon branches triggered by retraction inducers of the semaphorin family. *Cell* 113, 285–299. doi: 10.1016/S0092-8674(03)00267-268

Ballas, N., Mandel, G., Nigam, A., Robinson, J. K., Du, F., Felice, C. A., et al. (2012). MeCP2 is critical for maintaining mature neuronal networks and global brain anatomy during late stages of postnatal brain development and in the mature adult brain. *J. Neurosci.* 32, 10021–10034. doi: 10.1523/jneurosci.1316-12.2012

Barnes, G., Puranam, R. S., Luo, Y., and McNamara, J. O. (2003). Temporal specific patterns of semaphorin gene expression in rat brain after kainic acid-induced status epilepticus. *Hippocampus* 13, 1–20. doi: 10.1002/hipo.10041

Belichenko, N. P., Belichenko, P. V., Li, H. H., Mobley, W. C., and Francke, U. (2008). Comparative study of brain morphology in Mecp2 mutant mouse models of Rett syndrome. *J. Comp. Neurol.* 508, 184–195. doi: 10.1002/cne.21673

Bermúdez-Rattoni, F., and Rekart, J. L. (2007). "SourceNeural Plasticity and Memory: From Genes to Brain Imaging," in *Presynaptic Structural Plasticity and Long-Lasting Memory: Focus on Learning-Induced Redistribution of Hippocampal Mossy Fibers*, ed. F. Bermúdez-Rattoni (Boca Raton FL: CRC Press/Taylor & Francis).

Bernasconi-Guastalla, S., Wolfer, D. P., and Lipp, H. P. (1994). Hippocampal mossy fibers and swimming navigation in mice: correlations with size and left-right asymmetries. *Hippocampus* 4, 53–63. doi: 10.1002/hipo.450040107

Bischofberger, J., Engel, D., Frotscher, M., and Jonas, P. (2006). Timing and efficacy of transmitter release at mossy fiber synapses in the hippocampal network. *Pflugers Arch. Eur. J. Physiol.* 453, 361–372. doi: 10.1007/s00424-006-0093-92

Burns, K. A., and Kuan, C. Y. (2005). Low of bromo- and iododeoxyuridine produce near-saturation labeling of adult proliferative populations in the dentate gyrus. *Eur. J. Neurosci.* 21, 803–807. doi: 10.1111/j.1460-9568.2005.03907.x

Cai, X., Long, L., Yang, L., Chen, Z., Ni, G., Qin, J., et al. (2016). Association between mossy fiber sprouting and expression of semaphorin-3f protein in dentate gyrus of hippocampus in lithium-pilocarpine-induced status epilepticus mouse model. *Neurol. Res.* 6412, 1–6. doi: 10.1080/01616412.2016.1243639

Cavazos, J. E., Golarai, G., and Sutula, T. P. (1991). Mossy fiber synaptic reorganization induced by kindling: time course of development, progression,

and permanence. *J. Neurosci.* 11, 2795–2803. doi: 10.1523/jneurosci.11-09-02795.1991

Chahrour, M., and Zoghbi, H. Y. (2007). The story of rett syndrome: from clinic to neurobiology. *Neuron* 56, 422–437. doi: 10.1016/j.neuron.2007.10.001

Chang, Q., Khare, G., Dani, V., Nelson, S., and Jaenisch, R. (2006). The disease progression of Mecp2 mutant mice is affected by the level of BDNF expression. *Neuron* 49, 341–348. doi: 10.1016/j.neuron.2005.12.027

Chapleau, C. A., Calfa, G. D., Lane, M. C., Albertson, A. J., Larimore, J. L., Kudo, S., et al. (2009). Dendritic spine pathologies in hippocampal pyramidal neurons from Rett syndrome brain and after expression of Rett-associated MECP2 mutations. *Neurobiol. Dis.* 35, 219–233. doi: 10.1016/j.nbd.2009.05.001

Chapleau, C. A., and Pozzo-Miller, L. (2008). "Learning and memory: a comprehensive reference," in *Activity-Dependent Structural Plasticity of Dendritic Spines*, ed J. Byrne (Oxford: Elsevier)

Chen, R. Z., Akbarian, S., Tudor, M., and Jaenisch, R. (2001). Deficiency of methyl-CpG binding protein-2 in CNS neurons results in a Rett-like phenotype in mice. *Nat. Genet.* 27, 327–331. doi: 10.1038/85906

Chen, W. G., Chang, Q., Lin, Y., Meissner, A., West, A. E., Griffith, E. C., et al. (2003). Derepression of BDNF transcription involves calcium-dependent phosphorylation of MeCP2. *Science* 302, 885–889. doi: 10.1126/science.1086446

Cheng, H. J., Bagri, A., Yaron, A., Stein, E., Pleasure, S. J., and Tessier-Lavigne, M. (2001). Plexin-A3 mediates semaphorin signaling and regulates the development of hippocampal axonal projections. *Neuron* 32, 249–263. doi: 10.1016/S0896-6273(01)00478-470

Cowansage, K. K., LeDoux, J. E., and Monfils, M.-H. (2010). Brain-derived neurotrophic factor: a dynamic gatekeeper of neural plasticity. *Curr. Mol. Pharmacol.* 3, 12–29. doi: 10.2174/1874-470211003010012

Crusio, W. E., and Schwegler, H. (2005). Learning spatial orientation tasks in the radial-maze and structural variation in the hippocampus in inbred mice. *Behav. Brain Funct.* 1:3. doi: 10.1186/1744-9081-1-3

Crusio, W. E., Schwegler, H., and Lipp, H. P. (1987). Radial-maze performance and structural variation of the hippocampus in mice: a correlation with mossy fibre distribution. *Brain Res.* 425, 182–185. doi: 10.1016/0006-8993(87)90498-90497

Degano, A. L., Park, M. J., Penati, J., Li, Q., and Ronnett, G. V. (2014). MeCP2 is required for activity-dependent refinement of olfactory circuits. *Mol. Cell. Neurosci.* 59, 63–75. doi: 10.1016/j.mcn.2014.01.005

Degano, A. L., Pasterkamp, R. J., and Ronnett, G. V. (2009). MeCP2 deficiency disrupts axonal guidance, fasciculation, and targeting by altering Semaphorin 3F function. *Mol. Cell Neurosci.* 42, 243–254. doi: 10.1016/j.mcn.2009.07.009

Delprato, A., Bonheur, B., Algéo, M. P., Rosay, P., Lu, L., Williams, R. W., et al. (2015). Systems genetic analysis of hippocampal neuroanatomy and spatial learning in mice. *Genes Brain Behav.* 14, 591–606. doi: 10.1111/gbb.12259

Dieni, S., Matsumoto, T., Dekkers, M., Rauskolb, S., Ionescu, M. S., Deogracias, R., et al. (2012). BDNF and its pro-peptide are stored in presynaptic dense core vesicles in brain neurons. *J. Cell Biol.* 196, 775–788. doi: 10.1083/jcb.201201038

Ebert, D. H. (2013). Activity-dependent neuronal signalling and autism spectrum disorder. *Nature* 493, 327–337. doi: 10.1038/mp.2011.182

Ebert, D. H., Gabel, H. W., Robinson, N. D., Kastan, N. R., Hu, L. S., Cohen, S., et al. (2013). Activity-dependent phosphorylation of MeCP2 threonine 308 regulates interaction with NCoR. *Nature* 499, 341–345. doi: 10.1038/nature12348

Esposito, M. S. (2005). Neuronal differentiation in the adult hippocampus recapitulates embryonic development. *J. Neurosci.* 25, 10074–10086. doi: 10.1523/jneurosci.3114-05.2005

Galimberti, I., Gogolla, N., Alberi, S., Santos, A. F., Muller, D., and Caroni, P. (2006). Long-term rearrangements of hippocampal mossy fiber terminal connectivity in the adult regulated by experience. *Neuron* 50, 749–763. doi: 10.1016/j.neuron.2006.04.026

Gómez-Palacio-Schjetnan, A., and Escobar, M. L. (2008). In vivo BDNF modulation of adult functional and morphological synaptic plasticity at hippocampal mossy fibers. *Neurosci. Lett.* 445, 62–67. doi: 10.1016/j.neulet.2008.08.069

Gray, W. P., and Sundstrom, L. E. (1998). Kainic acid increases the proliferation of granule cell progenitors in the dentate gyrus of the adult rat. *Brain Res.* 790, 52–59. doi: 10.1016/S0006-8993(98)00030-34

Guy, J., Hendrich, B., Holmes, M., Martin, J. E., and Bird, A. (2001). A mouse Mecp2-null mutation causes neurological symptoms that mimic rett syndrome. *Nat. Genet.* 27, 322–326. doi: 10.1038/85899

Helgager, J., Huang, Y., and Mcnamara, J. (2014). Brain-derived neurotrophic factor but not vesicular zinc promotes TrkB activation within mossy fibers of mouse hippocampus in vivo. *J. Comp. Neurol.* 522, 3885–3899. doi: 10.1038/jid.2014.371

Holtmaat, A. J. G. D., Gorter, J. A., De Wit, J., Tolner, E. A., Spijker, S., Giger, R. J., et al. (2003). Transient downregulation of Sema3A mRNA in a rat model for temporal lobe epilepsy: a novel molecular event potentially contributing to mossy fiber sprouting. *Exp. Neurol.* 182, 142–150. doi: 10.1016/S0014-4886(03)00035-39

Huang, E. J., and Reichardt, L. F. (2001). Neurotrophins: roles in neuronal development and function. *Annu. Rev. Neurosci.* 24, 677–736. doi: 10.1146/annurev.neuro.24.1.677

Isgor, C., Pare, C., McDole, B., Coombs, P., and Guthrie, K. (2015). Expansion of the dentate mossy fiber-CA3 projection in the brain-derived neurotrophic factor-enriched mouse hippocampus. *Neuroscience* 288, 10–23. doi: 10.1016/j.neuroscience.2014.12.036

Johnston, M. V. (2004). Clinical disorders of brain plasticity. *Brain Dev.* 26, 73–80. doi: 10.1016/S0387-7604(03)00102-105

Kobayashi, K. (2009). Targeting the hippocampal mossy fiber synapse for the treatment of psychiatric disorders. *Mol. Neurobiol.* 39, 24–36. doi: 10.1007/s12035-008-8049-8045

Laghmouch, A., Bertholet, J. Y., and Crusio, W. E. (1997). Hippocampal morphology and open-field behavior in Mus musculus domesticus and Mus spretus inbred mice. *Behav. Genet.* 27, 67–73. doi: 10.1023/A:1025667426222

Lewis, D. A., and Levitt, P. (2002). Schizophrenia as a disorder of neurodevelopment. *Annu. Rev. Neurosci.* 25, 1–50. doi: 10.1146/annurev.neuro.25.112701.142754

Li, W., Calfa, G., Larimore, J., and Pozzo-Miller, L. (2012). Activity-dependent BDNF release and TRPC signaling is impaired in hippocampal neurons of Mecp2 mutant mice. *Proc. Natl. Acad. Sci. U.S.A.* 109, 17087–17092. doi: 10.1073/pnas.1205271109

Li, W., and Pozzo-Miller, L. (2014). BDNF deregulation in Rett syndrome. *Neuropharmacology* 76, 737–746. doi: 10.1016/j.neuropharm.2013.03.024

Lindvall, O., Elmer, E., Kokaia, Z., Nanobashvili, A., Kokaia, M., and Bengzon, J. (2002). Apoptosis and proliferation of dentate gyrus neurons after single and intermittent limbic seizures. *Proc. Natl. Acad. Sci. U.S.A.* 94, 10432–10437. doi: 10.1073/pnas.94.19.10432

Lipp, H. P., Schwegler, H., Heimrich, B., and Driscoll, P. (1988). Infrapyramidal mossy fibers and two-way avoidance learning: developmental modification of hippocampal circuitry and adult behavior of rats and mice. *J. Neurosci.* 8, 1905–1921. doi: 10.1523/jneurosci.08-06-01905.1988

Lu, B. (2003). Pro-region of neurotrophins: role in synaptic modulation. *Neuron* 39, 735–738. doi: 10.1016/S0896-6273(03)00538-535

Lyst, M. J., Ekiert, R., Ebert, D. H., Merusi, C., Nowak, J., Selfridge, J., et al. (2013). Rett syndrome mutations abolish the interaction of MeCP2 with the NCoR/SMRT co-repressor. *Nat. Neurosci.* 16, 898–902. doi: 10.1038/nn.3434

Martinowich, K., Hattori, D., Wu, H., Fouse, S., He, F., Hu, Y., et al. (2003). DNA methylation-related chromatin remodeling in activity-dependent bdnf gene regulation. *Science* 302, 890–893. doi: 10.1126/science.1090842

Matarazzo, V., Cohen, D., Palmer, A. M., Simpson, P. J., Khokhar, B., Pan, S. J., et al. (2004). The transcriptional repressor Mecp2 regulates terminal neuronal differentiation. *Mol. Cell. Neurosci.* 27, 44–58. doi: 10.1016/j.mcn.2004.05.005

McLeod, F., Ganley, R., Williams, L., Selfridge, J., Bird, A., and Cobb, S. R. (2013). Reduced seizure threshold and altered network oscillatory properties in a mouse model of Rett syndrome. *Neuroscience* 231, 195–205. doi: 10.1016/j.neuroscience.2012.11.058

Mineur, Y. S., Sluyter, F., De Wit, S., Oostra, B. A., and Crusio, W. E. (2002). Behavioral and neuroanatomical characterization of the Fmr1 knockout mouse. *Hippocampus* 12, 39–46. doi: 10.1002/hipo.10005

Moretti, P., Bouwknecht, J. A., Teague, R., Paylor, R., and Zoghbi, H. Y. (2005). Abnormalities of social interactions and home-cage behavior in a mouse model of Rett syndrome. *Hum. Mol. Genet.* 14, 205–220. doi: 10.1093/hmg/ddi016

Moretti, P., Levenson, J. M., Battaglia, F., Atkinson, R., Teague, R., Antalffy, B., et al. (2006). Learning and memory and synaptic plasticity are impaired in a mouse model of rett syndrome. *J. Neurosci.* 26, 319–327. doi: 10.1523/JNEUROSCI.2623-05.2006

Nan, X., Campoy, F. J., and Bird, A. (1997). MeCP2 is a transcriptional repressor with abundant binding sites in genomic chromatin. *Cell* 88, 471–481. doi: 10.1016/S0092-8674(00)81887-81885

Nicoll, R. A., and Schmitz, D. (2005). Synaptic plasticity at hippocampal mossy fibre synapses. *Nat. Rev. Neurosci.* 6, 863–876. doi: 10.1038/nrn1786

Okazaki, M. M., Evenson, D. A., and Victor Nadler, J. (1995). Hippocampal mossy fiber sprouting and synapse formation after status epilepticus in rats: Visualization after retrograde transport of biocytin. *J. Comp. Neurol.* 352, 515–534. doi: 10.1002/cne.903520404

O'Leary, T. P., and Brown, R. E. (2013). Optimization of apparatus design and behavioral measures for the assessment of visuo-spatial learning and memory of mice on the Barnes maze. *Learn. Mem.* 20, 85–96. doi: 10.1101/lm.028076.112

Palmer, A., Qayumi, J., and Ronnett, G. (2008). MeCP2 mutation causes distinguishable phases of acute and chronic defects in synaptogenesis and maintenance, respectively. *Mol. Cell. Neurosci.* 37, 794–807. doi: 10.1016/j.mcn.2008.01.005

Pardo, C. A., and Eberhart, C. G. (2007). Symposium: neurobiology of autism the neurobiology of autism. *Brain Pathol.* 17, 434–447. doi: 10.1111/j.1750-3639.2007.00102.x

Parent, J., and Lowenstein, D. (2002). Seizure-induced neurogenesis: Are more new neurons good for an adult brain? *Prog. Brain Res.* 135, 121–131. doi: 10.1016/S0079-6123(02)35012-X

Parent, J. M., and Lowenstein, D. H. (1997). Mossy fiber reorganization in the epileptic hippocampus. *Curr. Opin. Neurol.* 10, 103–109. doi: 10.1097/00019052-199704000-199704006

Parent, J. M., Yu, T. W., Leibowitz, R. T., Geschwind, D. H., Sloviter, R. S., and Lowenstein, D. H. (1997). Dentate granule cell neurogenesis is increased by seizures and contributes to aberrant network reorganization in the adult rat hippocampus. *J. Neurosci.* 17, 3727–3738. doi: 10.1523/jneurosci.17-10-03727.1997

Pasterkamp, R. J. (2012). Getting neural circuits into shape with semaphorins. *Nat. Rev. Neurosci.* 13, 605–618. doi: 10.1038/nrn3302

Poo, M. M. (2001). Neurotrophins as synaptic modulators. *Nat. Rev. Neurosci.* 2, 24–32. doi: 10.1038/35049004

Ramírez-Amaya, V., Balderas, I., Sandoval, J., Escobar, M. L., and Bermúdez-Rattoni, F. (2001). Spatial long-term memory is related to mossy fiber synaptogenesis. *J. Neurosci.* 21, 7340–7348. doi: 10.1523/jneurosci.21-18-07340.2001

Riccomagno, M. M., Hurtado, A., Wang, H., Macopson, J. G. J., Griner, E. M., Betz, A., et al. (2012). The RacGAP beta-chimaerin selectively mediates stereotyped hippocampal axonal pruning. *Cell* 149, 1594–1606. doi: 10.1016/j.cell.2012.05.018

Römer, B., Krebs, J., Overall, R. W., Fabel, K., Babu, H., Overstreet-Wadiche, L., et al. (2011). Adult hippocampal neurogenesis and plasticity in the infrapyramidal bundle of the mossy fiber projection: I. Co-regulation by activity. *Front. Neurosci.* 5:107. doi: 10.3389/fnins.2011.00107

Rosenfeld, C. S., and Ferguson, S. A. (2014). Barnes maze testing strategies with small and large rodent models. *J. Vis. Exp.* 26:e51194. doi: 10.3791/51194

Sahay, A., Molliver, M. E., Ginty, D. D., and Kolodkin, A. L. (2003). Semaphorin 3F is critical for development of limbic system circuitry and is required in neurons for selective CNS axon guidance events. *J. Neurosci.* 23, 6671–6680. doi: 10.1523/jneurosci.23-17-06671.2003

Schauwecker, P. E., and Steward, O. (1997). Genetic determinants of susceptibility to excitotoxic cell death: implications for gene targeting approaches. *Proc. Natl. Acad. Sci. U.S.A.* 94, 4103–4108. doi: 10.1073/pnas.94.8.4103

Schjetnan, A. G. P., and Escobar, M. L. (2012). In vivo BDNF modulation of hippocampal mossy fiber plasticity induced by high frequency stimulation. *Hippocampus* 22, 1–8. doi: 10.1002/hipo.20866

Schöpke, R., Wolfer, D. P., Lipp, H. -P., and Leisinger-Trigona, M. -C. (1991). Swimming navigation and structural variations of the infrapyramidal mossy fibers in the hippocampus of the mouse. *Hippocampus* 1, 315–328. doi: 10.1002/hipo.450010322

Schwegler, H., Crusio, W. E., and Brust, I. (1990). Hippocampal mossy fibers and radial-maze learning in the mouse: A correlation with spatial working memory but not with non-spatial reference memory. *Neuroscience* 109, 699–713. doi: 10.1016/0306-4522(90)90139-U

Scott, B. W., Wang, S., Burnham, W. M., De Boni, U., and Wojtowicz, J. M. (1998). Kindling-induced neurogenesis in the dentate gyrus of the rat. *Neurosci. Lett.* 248, 73–76. doi: 10.1016/S0304-3940(98)00355-353

Shahbazian, M. D., Young, J. I., Yuva-Paylor, L. A., Spencer, C. M., Antalffy, B. A., Noebels, J. L., et al. (2002). Mice with truncated MeCP2 recapitulate many Rett syndrome features and display hyperacetylation of histone H3. *Neuron* 35, 243–254. doi: 10.1016/S0896-6273(02)00768-767

Singec, I., Knoth, R., Ditter, M., Hagemeyer, C. E., Rosenbrock, H., Frotscher, M., et al. (2002). Synaptic vesicle protein synaptoporin is differently expressed by subpopulations of mouse hippocampal neurons. *J. Comp. Neurol.* 45, 103–203. doi: 10.1002/cne.10371

Smrt, R. D., Eaves-Egenes, J., Barkho, B. Z., Santistevan, N. J., Zhao, C., Aimone, J. B., et al. (2007). Mecp2 deficiency leads to delayed maturation and altered gene expression in hippocampal neurons. *Neurobiol. Dis.* 27, 77–89. doi: 10.1016/j.nbd.2007.04.005

Suto, F., Yoshida, Y., Tawarayama, H., Fujisawa, H., and Mitchell, K. J. (2010). Roles of Semaphorin-6B and Plexin-A2 in lamina-restricted projection of hippocampal mossy fibers. *J. Neurosci.* 30, 7049–7060. doi: 10.1523/jneurosci.0073-10.2010

Tamura, M., Tamura, N., Ikeda, T., Koyama, R., Ikegaya, Y., Matsuki, N., et al. (2009). Influence of brain-derived neurotrophic factor on pathfinding of dentate granule cell axons, the hippocampal mossy fibers. *Mol. Brain.* 2:2. doi: 10.1186/1756-6606-2-2

Wang, Q., Ogier, M., Wang, H., Katz, D. M., Hellard, D., Smith, C., et al. (2006). Dysregulation of brain-derived neurotrophic factor expression and neurosecretory function in Mecp2 null Mice. *J. Neurosci.* 26, 10911–10915. doi: 10.1523/jneurosci.1810-06.2006

Zafra, F., Hengerer, B., Leibrock, J., Thoenen, H., and Lindholm, D. (1990). Activity dependent regulation of BDNF and NGF mRNAs in the rat hippocampus is mediated by non-NMDA glutamate receptors. *EMBO J.* 9, 3545–3550. doi: 10.1038/SJ.BJP.0706310

Zhou, Z., Hong, E. J., Cohen, S., Zhao, W. N., Ho, H. Y., Schmidt, L., et al. (2006). Brain-specific phosphorylation of MeCP2 regulates activity-dependent bdnf transcription, dendritic growth, and spine maturation. *Neuron* 52, 255–269. doi: 10.1016/j.neuron.2006.09.037

Conflict of Interest Statement: GVR is currently employed by company Janssen Research & Development, LLC.

The remaining authors declare that the research was conducted in the absence of any commercial or financial relationships that could be construed as a potential conflict of interest.

frontiers in Cellular Neuroscience

ORIGINAL RESEARCH
published: 11 July 2019
doi: 10.3389/fncel.2019.00311

The Impact of Frequency Scale on the Response Sensitivity and Reliability of Cortical Neurons to 1/f$^{\beta}$ Input Signals

Guojie Qu[†], *Boqiang Fan*[†], *Xin Fu and Yuguo Yu*[*]

State Key Laboratory of Medical Neurobiology, School of Life Science, Human Phenome Institute, Institute of Brain Science, Institute of Science and Technology for Brain-Inspired Intelligence, Fudan University, Shanghai, China

What type of principle features intrinsic inside of the fluctuated input signals could drive neurons with the maximal excitations is one of the crucial neural coding issues. In this article, we examined both experimentally and theoretically the cortical neuronal responsivity (including firing rate and spike timing reliability) to input signals with different intrinsic correlational statistics (e.g., white-type noise, showed 1/f^0 power spectrum, pink noise 1/f, and brown noises 1/f^2) and different frequency ranges. Our results revealed that the response sensitivity and reliability of cortical neurons is much higher in response to 1/f noise stimuli with long-term correlations than 1/f^0 with short-term correlations for a broad frequency range, and also higher than 1/f^2 for all frequency ranges. In addition, we found that neuronal sensitivity diverges to opposite directions for 1/f noise comparing with 1/f^0 white noise as a function of cutoff frequency of input signal. As the cutoff frequency is progressively increased from 50 to 1,000 Hz, the neuronal responsiveness increased gradually for 1/f noise, while decreased exponentially for white noise. Computational simulations of a general cortical model revealed that, neuronal sensitivity and reliability to input signal statistics was majorly dominated by fast sodium inactivation, potassium activation, and membrane time constants.

Keywords: 1/f$^{\beta}$ noise, cortical neurons, patch clamp recording, long-term correlation, Hodgkin-Huxley model, response reliability

OPEN ACCESS

Edited by:
Mario Eduardo Guido, Center for Research in Biological Chemistry Córdoba (CIQUIBIC), Argentina

Reviewed by:
Richardson N. Leão, Federal University of Rio Grande do Norte, Brazil
Thierry Ralph Nieus, Luigi Sacco Hospital, Italy

***Correspondence:**
Yuguo Yu
yuyuguo@fudan.edu.cn

[†]*These authors have contributed equally to this work*

Specialty section:
This article was submitted to Cellular Neurophysiology, a section of the journal Frontiers in Cellular Neuroscience

Received: *22 January 2019*
Accepted: *25 June 2019*
Published: *11 July 2019*

Citation:
Qu G, Fan B, Fu X and Yu Y (2019) The Impact of Frequency Scale on the Response Sensitivity and Reliability of Cortical Neurons to 1/f$^{\beta}$ Input Signals. Front. Cell. Neurosci. 13:311. doi: 10.3389/fncel.2019.00311

INTRODUCTION

For a signal, the inherent frequency structure shown in the Fourier frequency domain characterizes its second-order statistics. The power spectrum of various natural signals typically exhibits the power law 1/f$^{\beta}$ in the frequency domain, with β close to one (Voss and Clarke, 1978; Gilden et al., 1995; Musha and Yamamoto, 1997; De Coensel et al., 2003). Moreover, this 1/f property within a specific frequency range is widely observed in neural activities at all levels, as evidenced in recordings of the membrane potential and current (Diba, 2004; Jacobson et al., 2005; Bédard et al., 2006; Yaron-Jakoubovitch, 2008; El Boustani et al., 2009), EEG (Novikov et al., 1997; Bhattacharya and Petsche, 2001; Bédard et al., 2006; Dehghani et al., 2010; Voytek et al., 2015), MEG (Novikov et al., 1997; Dehghani et al., 2010), LFPs (Bédard and Destexhe, 2009; Bedard et al., 2017; Maex, 2018), and fMRI signals (Bullmore et al., 2001; He, 2011; Ciuciu et al., 2014). In practice, the white

noise (the power law 1/f^0) with generally low cutoff frequencies is widely used to detect neuronal input-and-output functions (Sakai, 1992; Fairhall et al., 2001; Cook et al., 2007; Vilela and Lindner, 2009). Besides, 1/f^2 noise is also observed in neural field potentials (Freeman and Zhai, 2009; Miller et al., 2009; Milstein et al., 2009; He et al., 2010; Halnes et al., 2016) and membrane currents under special conditions (Diba, 2004).

Mammalian sensory neural systems exhibit better responses to naturalistic signals rather than white-type noise signals in a specific frequency domain (Aertsen and Johannesma, 1981; Baddeley et al., 1997; de Ruyter van Steveninck et al., 1997; Yu et al., 2005; Garcia-Lazaro et al., 2006, 2011). It has been speculated that the 1/f property might be the key in shaping the neuronal function preference to the naturalistic input (Yu et al., 2005; Garcia-Lazaro et al., 2006, 2011); this preference may extend to the atomic level of neural organization, namely the single neuronal input-output function (Gal and Marom, 2013).

In addition, white and colored noises with various cutoff frequencies enhance the detection of weak signals by neuronal systems via stochastic resonance (SR) (Nozaki and Yamamoto, 1998,?; Nozaki et al., 1999b; Hutcheon and Yarom, 2000; Jia et al., 2001; Ruszczynski et al., 2001; Chizhov and Graham, 2008; Mino and Durand, 2008; Gutkin et al., 2009; Higgs and Spain, 2009; Sekine et al., 2009; Guo and Li, 2011; Sobie et al., 2011; Duan et al., 2014; Zhao et al., 2017). However, previous studies have regarded the signals with 1/f$^{\beta}$ statistics as mere background noise. In particular, although the signal frequency range has been confirmed to significantly affect neuronal excitability (Nozaki et al., 1999b; Higgs and Spain, 2009), the exact role of the frequency range in neuronal responsiveness to the 1/f$^{\beta}$ statistic remains unclear. As neurons generally encode information according to the rate and/or the precise timing of spikes (Nowak et al., 1997; Reinagel and Reid, 2000; Fellous et al., 2001; Brette and Guigon, 2003; Avissar et al., 2007; Freund and Cerquera, 2012), we sought to examine the neuronal firing rate and spike-timing reliability to input statistics. In this study, we focus on the effects of the signal frequency range to identify the neuronal responsiveness to 1/f$^{\beta}$ ($\beta = 0$, 1, and 2) noises with respect to the firing rate and spike-timing reliability. Specifically, we reveal the mechanism underlying neuronal responsivity to 1/f$^{\beta}$ and the frequency range using theoretical experiments, as this mechanism has not been clearly determined in previous model-based studies (Nozaki and Yamamoto, 1998; Nozaki et al., 1999b; Brunel and Latham, 2003; Mino and Durand, 2008; Sekine et al., 2009; Sobie et al., 2011; Ostojic et al., 2015; Schwalger et al., 2015; Zhao et al., 2017). We conducted *in vitro* whole-cell patch clamp recording experiments on mouse cortical pyramidal neurons to examine the neuronal firing rate and reliability to 1/f, 1/f^0, and 1/f^2 noises with various cutoff frequencies (F_{cut}). We have also carried out a set of computational simulations of a general Hodgkin-Huxley neuronal model (Yu et al., 2012) to reproduce our experimental observations, and revealed the critical factors underlying the neuronal responsiveness to second-order statistics at the cellular level.

METHODS

Signal Production

Input noise stimuli of each type of 1/f$^{\beta}$–white noise (1/f^0), pink noise (1/f), and brown noise (1/f^2) were first generated digitally by computer programming. The noise stimuli were then filtered by different low-pass filter with aimed cutoff frequency range. Each signal intensity [represented by the standard deviation (SD)] was set to the defined value. All the above were done in Matlab R2017a software (Mathworks, USA), and then the signal was loaded to Micro 1401 (CED, UK), where the signals were converted from digital to analog. In the experimental study, a unique set of noise stimuli with designed cutoff frequencies and noise intensities were used as the input signals to recorded neurons. The three signal types have different slopes in PSDs (the white noise has a slope of 0 and 1/f noise has a slope of −1, while 1/f^2 noise has a slope of −2), as shown in **Figure 1A**. The 1/f and 1/f^2 noises have more power in the low frequency components and less power in the high frequency components, while white noise has equal energy at each frequency interval. All three types of signals have equal total power within the examined frequency range.

Brain Slice Preparation

The experimental procedures involving animal experiments in this study were approved by Animal Ethics Committee of Fudan University School of Life Science. Using 0.7% chloral hydrate, 14–28 day-old mice were anesthetized and brain slices prepared by a protective slicing and recovery method reported previously (Ting et al., 2014). Briefly, anesthetized mice were perfused intracardially with ice-cold oxygenated (95% O_2, 5% CO_2) NMDG-based cutting solution containing (in mM) 93 mM NMDG, 2.5 mM KCl, 1.2 mM NaH_2PO_4, 30 mM $NaHCO_3$, 20 mM HEPES, 25 mM glucose, 5 mM sodium ascorbate, 2 mM thiourea, 3 mM sodium pyruvate, 10 mM $MgSO_4$, 2 mM $CaCl_2$, and 12 mM NAC (pH 7.3–7.4, 300–305 mOsm). Brains were carefully removed from the skull and cut coronally at a thickness of 300 μm with a vibratome VT1000S (Leica, Germany) in chilled oxygenated (95% O_2, 5% CO_2) NMDG-based cutting solution. Slices were initially recovered in NMDG-based cutting solution at 32°C for 10 min. Slices were then incubated in oxygenated (95% O_2, 5% CO_2) HEPES-modified solution containing (in mM) 94 mM NaCl, 2.5 mM KCl, 1.2 mM NaH_2PO_4, 30 mM $NaHCO_3$, 20 mM HEPES, 25 mM glucose, 5 mM sodium ascorbate, 2 mM thiourea, 3 mM sodium pyruvate, 2 mM $MgSO_4$, 2 mM $CaCl_2$, and 6 mM NAC (pH 7.3–7.4, 300–305 mOsm) at room temperature for 30 min. Finally, slices were incubated in oxygenated (95% O_2, 5% CO_2) ACSF at room temperature for at least 1 h before recording. The ACSF contained 126 mM NaCl, 2.5 mM KCl, 2 mM $MgSO_4$, 2 mM $CaCl_2$, 26 mM $NaHCO_3$, 1.25 mM NaH_2PO_4, and 12.5 mM dextrose (pH 7.3–7.4, 300–305 mOsm).

Electrophysiological Recordings

Whole-cell slice recordings were performed on the cell body of layer 5 pyramidal neurons in the prefrontal cortex (**Figure 1B**). In total, 12 neurons in 12 slices of six mice were examined.

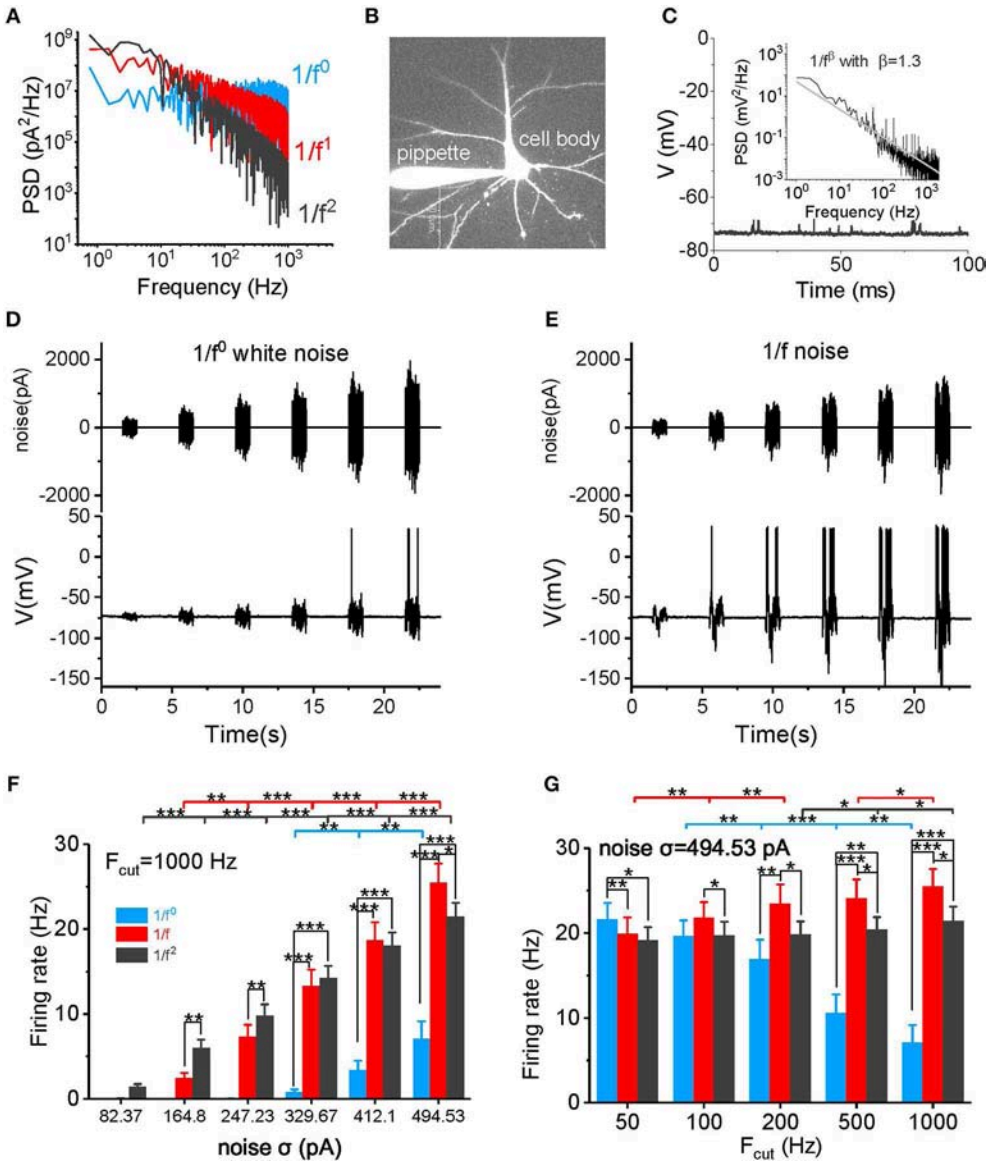

FIGURE 1 | Neuronal firing rate in response to different types of input signal. **(A)** The PSD plots for white noise (blue), 1/f noise (red), and 1/f^2 noise (black) are shown. Noises with a 1,000 Hz cutoff frequency are shown here. **(B)** *In vitro* patch clamp recording of a pyramidal cell. The scale bar indicates 50 μm. **(C)** Plot of the recorded membrane potentials in the resting state vs. time. Inset: The power spectrum density (PSD) plot of the resting potentials shows a 1/f property in a log-log plot. **(D,E)** Representative trace of input 1/f^0 white noise **(D)** and 1/f noise **(E)** with different intensities over time. The signal produced at each intensity lasted for 1 s, followed by a 3 s no-stimulus interval. The bottom panel shows the membrane potential and action potential produced by a recorded pyramidal cell in response to the input signal shown in the top panel. **(F)** Neuronal responsive firing rate for white noise (blue), 1/f (red), and 1/f^2 noise (black) with various intensities (82.37, 164.80, 247.23, 329.67, 412.10, and 494.53 pA) and a cutoff frequency of 1000 Hz. F_{cut}, cutoff frequency. **(G)** Neuronal responsive firing rate for white noise (blue), 1/f (red), and 1/f^2 noise (black) at various cutoff frequencies (50, 100, 200, 500, and 1,000 Hz) with a intensity of 494.53 pA.

Oxygenated (95% O_2, 5% CO_2) ASCF was used as the recording solution. Recordings were conducted on an upright infrared-differential interference contrast (IR-DIC) microscope (Zeiss Axioskop 2 FS plus) with a recording solution temperature of 36 °C. Cortical slices were suspended on a net to allow an oxygenated solution to flow over both the upper and lower surfaces at a rate of 3–4 ml/min. The membrane potential in the whole-cell recordings was corrected for Donnan liquid junction potentials of 15 mV. The temperature was regulated by a Warner Instruments Corporation two channel temperature regulator (Model TC344B).

Whole-cell recordings from the soma were achieved with the help of a Multiclamp 700B amplifier (Axon Instruments, Union City, CA) and Micro 1401 converter. Pipettes had an impedance of 5–6 MΩ and were filled with an intracellular solution that contained 140 mM K-gluconate, 3 mM KCl, 2 mM

$MgCl_2$, 2 mM Na_2ATP, 10 mM HEPES, and 0.2 mM EGTA, and the pH was adjusted to 7.3 with KOH–(270 mOsm). The sample rate of the membrane potential data was 25 kHz for both experiments and computational simulations. Those recorded neurons with input resistance within 100–200 MΩ were saved for analysis in this paper while others were discarded so that the studied neurons have the similar biophysical membrane properties.

Stimulation Mode

To experimentally examine the responsive firing rate to the input signal, the current signal with each intensity (σ = 82.37, 164.80, 247.23, 329.67, 412.10, and 494.53 pA) and each cutoff frequency (F_{cut} = 50, 100, 200, 500, and 1,000 Hz) was injected into neurons three times (**Figures 1D,E**). The signals (σ = 494.53 pA; F_{cut} = 50, 200, 500, and 1,000 Hz) in firing rate detection were also used for spike reliability examination, in which 50 repetitions of signals were injected into neurons. Every neuron in our study received all types of input signal, with its firing rate and reliability for each signal cutoff frequency examined. In the model simulation, the neuron received input signals (σ = 1.5, 3, 4.5, 6, 7.5, 9 μA/cm^2; Fcut = 50, 200, 500, and 1,000 Hz) thrice for firing rate detection. The signal (σ = 9 pA; F_{cut} = 50, 200, 500, and 1,000 Hz) was also injected 50 times for the spike reliability examination. In each test, to simulate the background noise from external or intrinsic fluctuations of the neuron itself, a 1/f noise with 500 Hz cutoff frequency and an intensity of 0.2169 μA/cm^2 was added to the input signal. The duration of stimuli signal of each cutoff frequency and intensity was 1 s.

Firing Rate and Spike Time Reliability

For each neuron under an input signal of each cutoff frequency and intensity, the spike number within the 1s stimuli duration was the firing rate. We averaged the firing rates in the three repetitions to get each neuronal firing rate value. For spike time reliability, 50 repetitions of a 1 s stimuli were injected into neurons, and cross covariance was calculated between all pair-wise combinations of trials (within stimulus size) within each neuron, on binary spike timing trains (with "1" representing an action potential with a 2 ms time bin and "0" representing a non-spiking neuron). The black-covariance function estimates the mean-removed cross-correlation between the two sequences of random processes, thus avoiding the contribution of the mean firing rate to the spike timing reliability. The resulting cross-covariance values at zero-lag (normalized by the average autocovariance function) for each neuron were used to quantify the spike reliability for each input signal statistic (Haider et al., 2010).

Hodgkin-Huxley-Style Cortical Neuronal Model

Three major ionic voltage-dependent currents were used in our cortical model: fast Na^+, I_{Na}, fast K^+, I_K, and a leak current, I_L. The equations describing the voltage and time dependence of the Na^+ and K^+ conductance have been reported in previous publications (McCormick and Huguenard, 1992) and the channel kinetics were modified based on models of cortical neurons (Mainen et al., 1995; Mainen and Sejnowski, 1996; Yu et al., 2008) and experimental studies (Huguenard et al., 1989; Colbert and Pan, 2002; Yu et al., 2008; Schmidt-Hieber and Bischofberger, 2010). The following equations describe the cortical axon single compartment model:

$$
\begin{aligned}
C\frac{\mathrm{dV}}{\mathrm{dt}} &= I_{stim} - g_{Na}^{max}\cdot m^3\cdot h\cdot(V-V_{Na}) \\
&\quad -g_K^{max}\cdot n\cdot(V-V_K) - g_L\cdot(V-V_L), \\
\tau m\frac{dm}{dt} &= -m+m_\infty,\ \ \tau m=\frac{1}{\alpha_m+\beta_m},\ \ m_\infty=\frac{\alpha_m}{\alpha_m+\beta_m} \\
\tau h\frac{dh}{dt} &= -h+h_\infty,\ \ \tau h=\frac{1}{\alpha_h+\beta_h},\ \ h_\infty=\frac{1}{1+e^{(V+60)/6.2}} \\
\tau n\frac{dn}{dt} &= -n+n_\infty,\ \ \tau_n=\frac{1}{\alpha_n+\beta_n},\ \ n_\infty=\frac{\alpha_n}{\alpha_n+\beta_n} \\
\alpha_m(V) &= \varnothing\cdot\frac{0.182\cdot(V+30)}{1-e^{-(V+30)/8}} \\
\beta_m(V) &= -\varnothing\cdot\frac{0.124\cdot(V+30)}{1-e^{(V+30)/8}} \\
\alpha_h(V) &= \varnothing\cdot\frac{0.028\cdot(V+45)}{1-e^{-(V+45)/6}} \\
\beta_h(V) &= -\varnothing\cdot\frac{0.0091\cdot(V+70)}{1-e^{(V+70)/6}} \\
\alpha_n(V) &= \varnothing\cdot\frac{0.01\cdot(V-30)}{1-e^{-(V-30)/9}} \\
\beta_n(V) &= -\varnothing\cdot\frac{0.0005\cdot(V-30)}{1-e^{(V-30)/9}} \\
\varnothing &= Q_{10}{}^{(T-23)/10}
\end{aligned}
$$

where the Q_{10} effect is described by Φ on regulating the temperature dependence of the biochemical reaction rate with Q_{10} = 2.3 (Frankenhaeuser and Moore, 1963; Matteson and Armstrong, 1982). The relationships between temperature and I_{Na} and I_K activation and inactivation are not monotonic and vary in different species (Fohlmeister et al., 2010). The reverse potentials for Na^+ and K^+ currents were adjusted for change in temperature according to the Nernst equation (not shown). Similar results were obtained with a variety of values for Q_{10}. For example, the use of a Q_{10} of 3 yielded similar results for spike efficiency and changes in spike rate with temperature. In our cortical model, Na^+ kinetics were determined based on recent experimental observations (Kole et al., 2008). The parameters used were: membrane capacitance = 0.75 μF/cm^2, g_{Na} = 1950 pS/μm^2, density of g_K = 40 pS/μm^2, and g_{leak} = 0.25 pS/μm^2, based on recent experimental results (Mainen and Sejnowski, 1995; Colbert and Pan, 2002; Kole et al., 2008; Hu et al., 2009; Fleidervish et al., 2010; Schmidt-Hieber and Bischofberger, 2010). The reversal potentials were V_L = −70 mV, V_{Na} = 60 mV, and V_K = −90 mV for leak, sodium, and potassium channels, respectively.

Statistical Analysis

To detect the differential response under various signal intensities, cutoff frequencies, or signal types, we performed

paired *t*-test and Wilcoxon rank sum test. First, Kolmogorov-Smirnov goodness-of-fit hypothesis test was done on the paired difference between the two compared data groups. Depending on whether the normality assumption held for the data, we used a paired *t*-test or the Wilcoxon test for statistical significant comparison. A $p < 0.05$ was considered statistically significant. The data presented in the figures are reported as the mean ± standard error, and the significant level are labeled by $^{*}p < 0.05$, $^{**}p < 0.01$, and $^{***}p < 0.001$, respectively.

RESULTS

Neuronal Responsiveness to Input Stimuli

In the absence of external stimuli, neuronal resting membrane potentials (∼-75 to −70 mV) showed fluctuating synaptic potentials that were received from somatic and dendritic synapses (**Figure 1C**). A power spectrum density (PSD) analysis of resting potentials displayed a typical 1/f property in a log-log plot (see the inset in **Figure 1C**), suggesting that the membrane potentials observed *in vitro* in neurons with synaptic inputs also exhibit a similar statistical property as neurons *in vivo*.

First, we examined the neuronal firing rate in response to the input signal (**Figures 1D,E**). As shown in **Figure 1F** and **Supplementary Figure S1**, the neuronal firing rate increases non-linearly as the noise intensity increases within a firing rate of 0–30 Hz. When the noise cutoff frequency is within 50 Hz, neurons are sensitive to white noise, firing with a high frequency at high noise intensities (**Figure 1G** and **Supplementary Figure S1A**). However, as the cutoff frequency increases, neurons lose their responsiveness to the white noise (**Figure 1G** and **Supplementary Figure S1**) and produce a low firing rate, even at a very high noise intensity levels and when the cutoff frequency is 1,000 Hz (**Figures 1F,G**). The neuronal firing rate increases minimally at a cutoff frequency of 1/f^2 noise (**Figure 1G**). In contrast, the firing rate increases gradually with the cutoff frequency for 1/f noise (**Figure 1G**). When the cutoff frequency is >200 Hz, firing rates for 1/f and 1/f^2 noise are higher than for the white noise (**Figures 1F,G**, and **Supplementary Figures S1C,D**). At low intensities, 1/f noise evokes lower firing rates than the 1/f^2 noise; but at high intensities, 1/f noise evokes higher firing rates than the 1/f^2 noise. The switch in firing rates emerges under various cutoff frequencies (**Figure 1F** and **Supplementary Figure S1**). Notably, at $\sigma = 494.53$ pA and a 1,000 Hz cutoff frequency, 1/f noise evokes the highest firing rate (25.47 ± 2.24 Hz) in all our recordings. Overall, 1/f noise evokes relatively high firing rates under all conditions, particularly at high input intensities, and high cutoff frequencies.

We next examined spike reliability (**Figure 2A**) at four cutoff frequencies (F_{cut} = 50, 200, 500, and 1,000 Hz). The neuronal responses are shown in the post-stimulus time histogram (PSTH) and raster plot (**Figure 2A**). **Figures 2B,C** show the spike-timing reliability, which quantifies the extent of repeatability of spike timing in response to the input signal (Mainen and Sejnowski, 1995; Haider et al., 2010) (calculated from the representative data shown in **Figure 1A**). As the cutoff frequency increases to above 200 Hz, the reliability of the response to white noise decreases significantly (**Figure 2B**). For both the 1/f and 1/f^2 noises, the reliability increases as the cutoff frequency increases (**Figure 2B**). When the cutoff frequency is 50 Hz, the reliability for the 1/f noise is greater than the 1/f^2 noise and less than that for the white noise (**Figure 2B** and **Supplementary Figure S2A**). When the cutoff frequency increases to 200 Hz, the reliability for white noise remains greater than for the 1/f and 1/f^2 noises (**Figure 2B** and **Supplementary Figure S2B**). Interestingly, at 500 and 1,000 Hz, the 1/f noise evokes the greatest reliability (**Figures 2B,C**, and **Supplementary Figure S2C**), suggesting that neurons respond with relatively high reliability to the 1/f property in signals, particularly when the input signal has a high cutoff frequency.

Our data demonstrate that neurons respond to white noise with low sensitivity and reliability, except when the noise is composed of low frequency components only. When the noise intensity is weak, 1/f^2 noise more readily evokes neuronal firing, but high firing rate is difficult to evoke. For the 1/f noise, neurons respond with relatively high sensitivity and high reliability under all conditions. In particular, at high cutoff frequencies or high input intensities, the 1/f noise evokes the highest firing rate and the most reliable neuronal response among all signal types tested. These findings indicate a clear neuronal preference for responses to 1/f noise with high cutoff frequencies.

Computer Simulations of Hodgkin-Huxley Model

A cortical Hodgkin-Huxley-type neuronal model was constructed to study the key factors and dynamic mechanisms underlying neuronal responsiveness to signals with different statistics. We only considered the fast sodium and potassium channels in the model and ignored other subtypes of sodium/potassium and calcium channels to identify the common mechanism underlying the neuronal preference for 1/f statistics.

The model neuron first reproduced the similar responses to input signals with various noise intensities described in our experimental study (**Figure 3A**). For cutoff frequency of 1,000 Hz, the firing rates of neuronal model to white noise is significantly lower than that of 1/f and 1/f^2 noise, and 1/f noise evokes the highest firing rate for the high intensities (**Figures 3B,C**). When the cutoff frequency increases from 50 to 1,000 Hz, the neuronal firing rate of model to input white noise decreases gradually. However, it increases slightly for 1/f noise, while it keeps almost invariant for 1/f^2 noise (**Figure 3C**).

We also evaluated the spike reliability of the model neuron based on the evoked spike trains by repeatedly feeding the model neuron with each type of input signal with the different cutoff frequencies. Neuronal reliability for white noise is high only at a low cutoff frequency, while it decreases significantly with an increase in cutoff frequency (**Figure 3D**). On the contrary, neuronal response reliability to 1/f noise keeps at a much higher reliability level for almost the whole range of cutoff frequency (**Figure 3D**). In addition, the neuronal response reliability to 1/f^2 noise is lower than the other two type of inputs (**Figure 3E**). However, its reliability increases as the cutoff frequency of 1/f^2

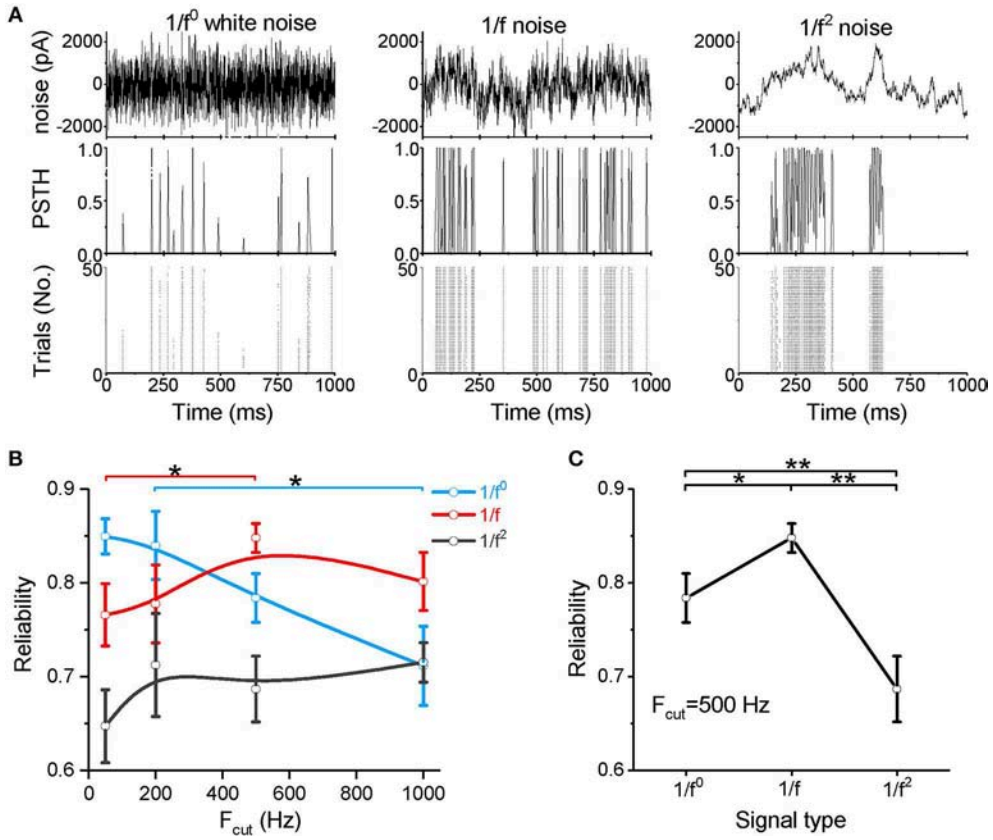

FIGURE 2 | Neuronal spike reliability to different types of input signal. **(A)** Raster plot of the responses from 50 trials (bottom panel) and PSTH (middle panel) for the repeated input stimulus (top panel) reflecting the reliability of cortical neuron firing patterns evoked by white noise (left panel), 1/f noise (middle panel), and 1/f^2 noise (right panel). **(B)** Plot of reliability vs. cutoff frequencies for the three signal types. F_{cut}, cutoff frequency. **(C)** Plot of reliability vs. β for the three types of 1/f$^{\beta}$ input signals with a cutoff frequency of 500 Hz.

noise increases (**Figure 3D**). These model simulation results are consistent with the experimental observations.

Next, we investigated the critical factors of neurons affecting the neuronal preference to 1/f signals. Considering that the responseness of neuronal model is dominated by the sodium and potassium channel kinetics, especially the channel opening velocity constant (e.g., α_m, α_h, α_n) and channel closing velocity constant (e.g., β_m β_h, and β_n) (Yu et al., 2012), we systematically changed the values of these parameters to study their effects on neuronal preference to inputs. We have also varied the values of membrane input resistance R_{input} and the membrane capacitance C_m to understand the effect of the passive membrane property on the neuronal responseness. First we examined the effect of open (α_m) and close (β_m) velocity constants of sodium activation variable. Although neuronal firing rate could be significantly affected by an increase or decrease of the values of α_m and β_m, the changing amount of the firing rate is almost same for all the three signal types (**Supplementary Figures S3A,B**).

However, when the value of α_h is halved, the neuronal firing rate as a function of noise intensity (**Figure 4A1**) or cutoff frequency (**Figure 4A2**) decreases dramatically for both 1/f and 1/f^2 noise, but slightly for white noise. **Figure 4A3** summarizes the contribution effect. When theα_h value increases, the neuronal firing rate increases gradually to a saturation level for both 1/f and 1/f^2 noises while keeps invariant for white noise input. This suggests that α_h plays a role in the neuronal preference to 1/f signals. Next, we varied the value of β_h and observed almost no effect on neuronal firing rate (please see **Supplementary Figure S3C**).

Next, we examined the effect of α_n and β_n for the potassium channel activation variable. When the value of α_n was doubled (**Figures 4B1,B2**), the neuronal firing rate as a function of noise intensity (**Figure 4B1**) or cutoff frequency (**Figure 4B2**) decreased dramatically for both 1/f and 1/f^2 noise, but slightly for white noise. **Figure 4B3** summarizes the contribution effect, and shows that the firing rates of neuronal model decrease gradually when the α_n value increased for both 1/f and 1/f^2 noises while deceased slightly for the white noise input. This suggests that α_n also contributes to the neuronal preference to 1/f signals.

Moreover, when β_n is increased, firing rate for 1/f^2 noise increases greater than for 1/f noise, much more than for white noise, at each noise intensity (**Figure 4C1**) as well as for cutoff frequency (**Figure 4C2**). As a result, in the case of large β_n,

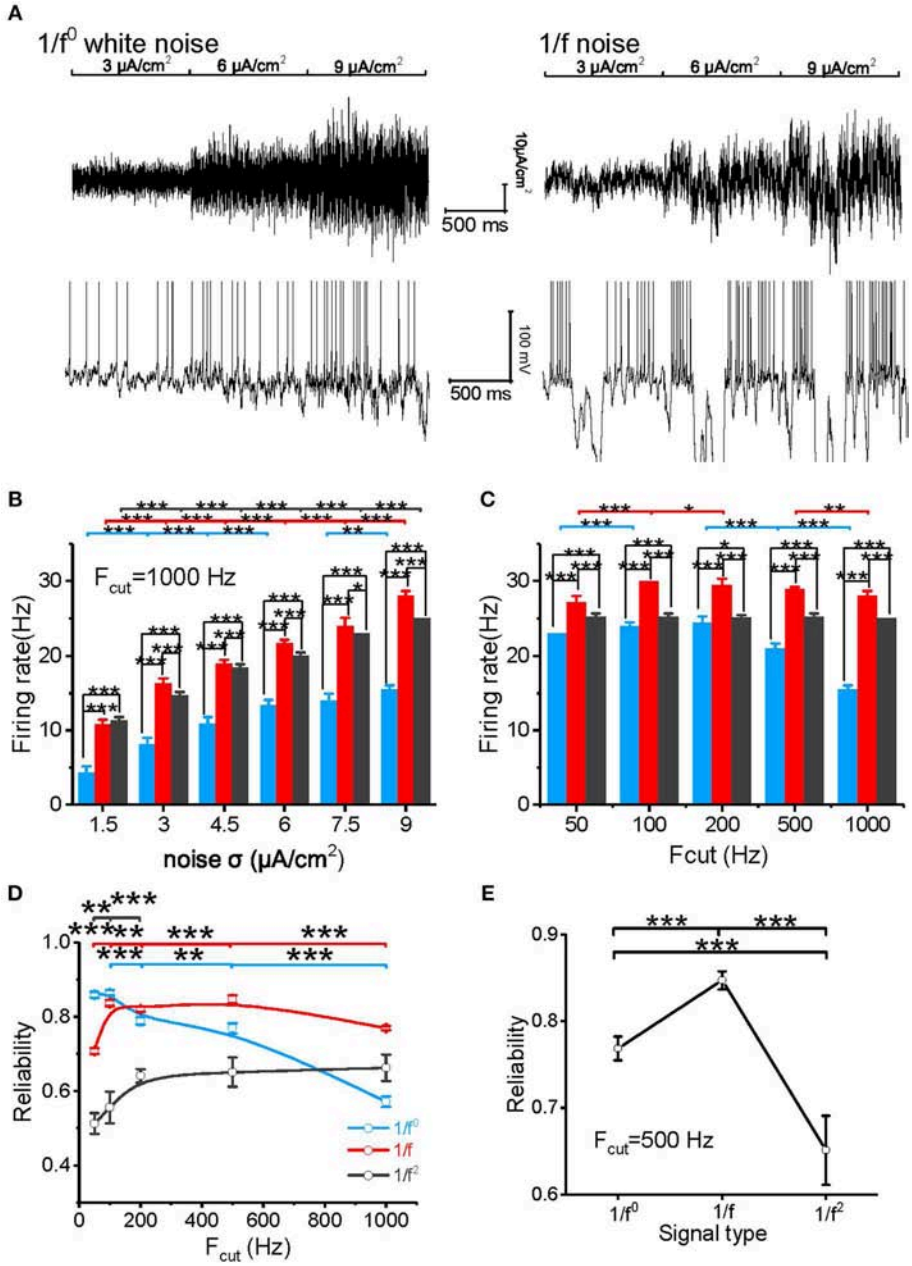

FIGURE 3 | Model neuronal response to different types of input signal. **(A)** The top panel shows white noise (left) and 1/f noise (right) with step-changed variance introduced into the neuronal model. The bottom panel shows the membrane potentials of the model neuron in response to the input. The noise intensity shown here is 3, 6, and 9 μA/cm^2. **(B)** Histogram of the neuronal firing rate vs. input signal SD for white noise (blue), 1/f noise (red), and 1/f^2 noise (black) at the cutoff frequency of 1,000 Hz. **(C)** Histogram of the neuronal firing rate vs. cutoff frequencies (50, 100, 200, 500, and 1,000 Hz) for white noise (blue), 1/f (red), and 1/f^2 noise (black) when the noise SD was 9 μA/cm^2. **(D)** Plot of model neuronal reliability vs. cutoff frequencies (50, 100, 200, 500, and 1,000 Hz) for white noise (blue), 1/f (red), and 1/f^2 noise (black). F$_{cut}$, cutoff frequency. **(E)** Plot of reliability vs. β for the three types of 1/f$^{\beta}$ input signals with a cutoff frequency of 500 Hz.

neuronal firing rate for 1/f^2 noise is larger than 1/f noise, while in the case of small β_n, neuronal firing rate for 1/f^2 noise is lower than 1/f noise (**Figure 4C3**). This indicated that relatively large β_n value may dominate the neuronal preference to 1/f and 1/f^2 noise. For the much small β_n value, neuronal preference to 1/f noise decreases dramatically.

Based on the equation, the membrane time constant $\tau_c = R_{input} * C_m$, τ_c could be changed by either changing R_{input} or C_m. Halved R_{input} increased neuronal firing rate to all the three type of input, and the neuronal sensitivity reached the maximum to white noise in the low cutoff frequency around 200 Hz, which is higher than to 1/f and 1/f^2 noise stimuli (**Figures 5A1,A2**).

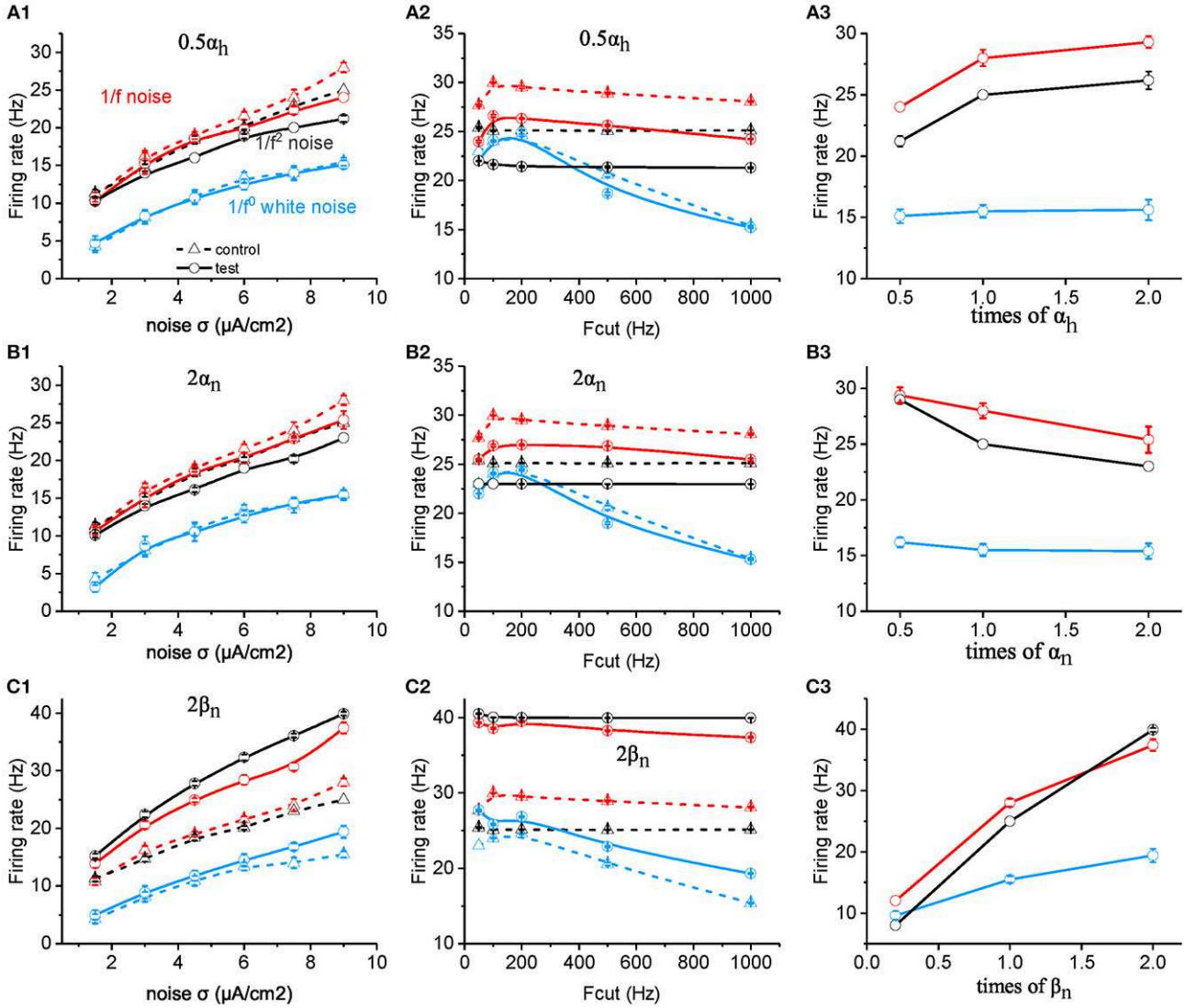

FIGURE 4 | Effects of ionic channel kinetic constants on the responsive firing rate of model neurons. **(A1–C1)** Plots of firing rate vs. intensity for white noise (blue), 1/f (red), and 1/f^2 noise (black) for a normal neuron (dotted line) compared with the results from the model neuron in the case of 0.5 α_h (solid line, **A1**), 2 α_n (solid line, **B1**), 2 β_n (solid line, **C1**). Fcut = 1,000 Hz. **(A2–C2)** Plots of firing rate vs. cutoff frequency for white noise (blue), 1/f (red), and 1/f^2 noise (black) for a normal neuron (dotted line) compared with the results from the model neuron in the case of 0.5 α_h (solid line, **A2**), 2 α_n (solid line, **B2**), 2 β_n (solid line, **C2**). Noise $\sigma = 9$ μA/cm^2. **(A3–C3)** Plots of firing rate vs. times of α_h (solid line, **A3**), α_n (solid line, **B3**), and β_n (solid line, **C3**) for white noise (blue), 1/f (red), and 1/f^2 noise (black) for a normal neuron (dotted line) compared with the results from the model neuron. $F_{cut} = 1{,}000$ Hz. Noise $\sigma = 9$ μA/cm^2.

Doubled C_m decreases the firing rate and makes the neuronal firing rate for 1/f^2 noise larger than for 1/f noise at various noise intensity (**Figure 5B1**) and each cutoff frequency, respectively (**Figure 5B2**). As shown in **Figures 5A,B**, both C_m and R_{input} changed the neuronal firing rate for white noise more than for 1/f noise, while the change for 1/f^2 noise is not that strong. This is contrary to the situation of changing β_n. As β_{nand} R_{input} or C_m have different weighted effect on neuronal response, they may act together to support the neuronal preferential response to 1/f noise with a broad frequency range. So we concluded β_n, R_{input} and C_m play important roles in neuronal responsive firing rate to 1/f$^{\beta}$ noises.

We also examined changes in the spike reliability in response to noises with altered neuronal biophysical parameters. As shown in **Figure 6A**, an increased value ofβ_m results in a significant decreased spike reliability for both 1/f noise (in all frequency range) and white noise (mainly with cutoff frequency higher than 200 Hz). On the contrary, increased β_m results in significantly increased spike reliability for 1/f^2 noise. With doubled α_h, α_n, and β_n (**Figures 6B–D**) and decreased R_{input} (**Figure 6E**), neuronal spike reliability for 1/f^2 noise decreases significantly for most of frequency range. These effects for 1/f^2 noise are stronger than for 1/f noise, and much stronger for white noise. On the contrary, doubled C_m

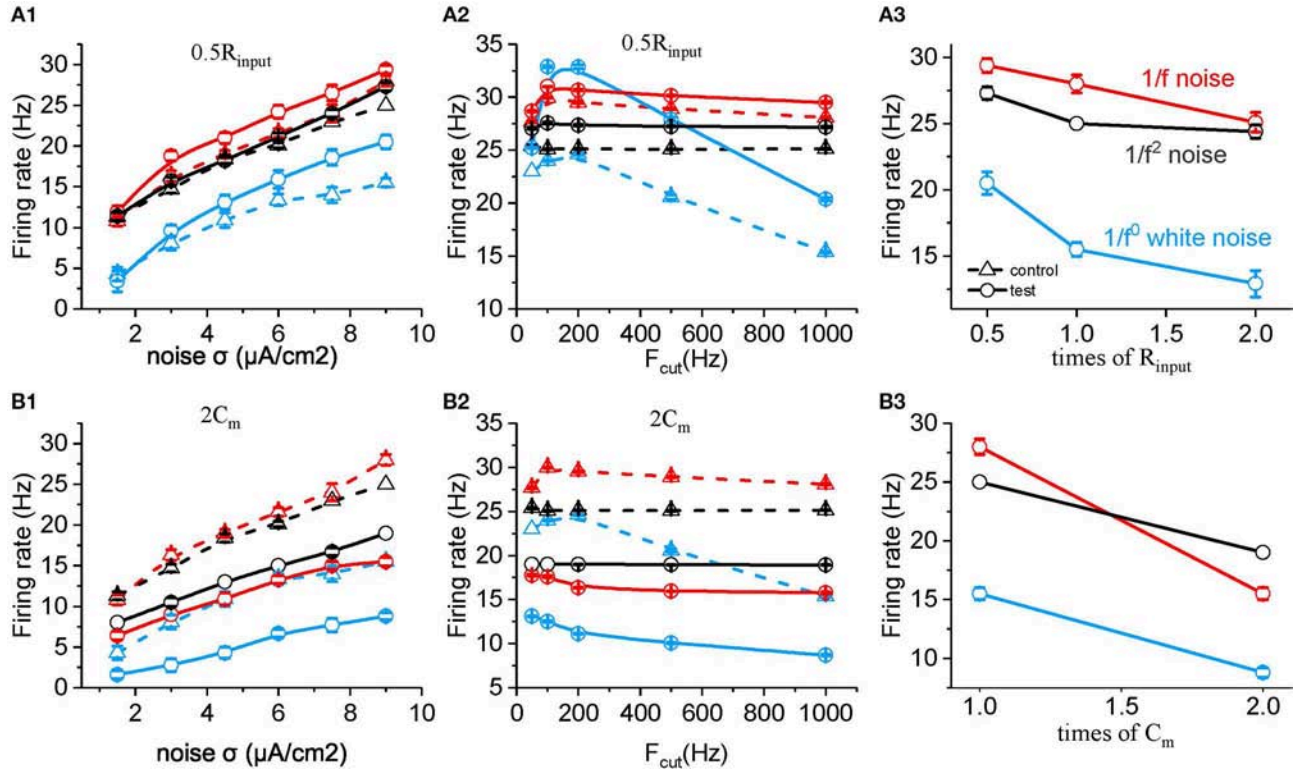

FIGURE 5 | Effects of membrane time constants on the responsive firing rate of model neurons. **(A1,B1)** Plots of firing rate vs. intensity for white noise (blue), 1/f (red), and 1/f^2 noise (black) for a normal neuron (dotted line) compared with the results from the model neuron in the case of 0.5 R_{input} (solid line, **A1**), 2 C_m (solid line, **B1**). Fcut = 1,000 Hz. **(A2,B2)** Plots of firing rate vs. cutoff frequency for white noise (blue), 1/f (red), and 1/f^2 noise (black) for a normal neuron (dotted line) compared with the results from the model neuron in the case of 0.5 R_{input} (solid line, **A2**), 2 C_m (solid line, **B2**). Noise $\sigma = 9$ μA/cm^2. **(A3,B3)** Plots of firing rate vs. times of R_{input} (solid line, **A3**), and C_m (solid line, **B3**) for white noise (blue), 1/f (red), and 1/f^2 noise (black) for a normal neuron (dotted line) compared with the results from the model neuron. $F_{cut} = 1000$ Hz. Noise $\sigma = 9$ μA/cm^2.

decreases the reliability significantly for each type of input, especially for the white noise (**Figure 6F**). Noted here, there is no clear change observed for the other rate constants (i.e., α_m and β_h).

DISCUSSION

Recordings of neuronal membranes exhibit time-dependent voltage fluctuations (Destexhe et al., 2003; El Boustani et al., 2009), which have not been extensively studied in the last few decades due to the lack of a functional understanding of the underlying noise composition. In addition, 1/f$^{\beta}$ noise has mainly been considered as background noise in previous studies (Mainen and Sejnowski, 1995; Nozaki and Yamamoto, 1998; Nozaki et al., 1999b; Jia et al., 2001; Ruszczynski et al., 2001; Richardson et al., 2003; Chizhov and Graham, 2008; Köndgen et al., 2008; Mino and Durand, 2008; Gutkin et al., 2009; Higgs and Spain, 2009; Sekine et al., 2009; Guo and Li, 2011; Sobie et al., 2011; Duan et al., 2014; Zhao et al., 2017). Here, for the first time, we directly examine cortical pyramidal neuronal responsiveness to 1/f$^{\beta}$ ($\beta = 0$, 1, and 2) input signals. Our results shed light on the mechanism by which the statistical structure of input signals affects the dynamics of spike generation in cortical pyramidal cells.

The Effect of the Frequency Range on the 1/f$^{\beta}$ Noise Response

We compared neuronal responses to 1/f^0, 1/f, and 1/f^2 noises with various cutoff frequencies (50–1,000 Hz) and observed that cortical pyramidal cells exhibit a substantial loss of reliability and sensitivity to white noise when the cutoff frequency exceeds 200 Hz. Neuronal responsiveness to 1/f is also better than 1/f^2 at various cutoff frequencies. In previous studies, white noise has been widely utilized to detect neuronal input and output functions (Sakai, 1992; Fairhall et al., 2001; Cook et al., 2007; Vilela and Lindner, 2009). Based on our results, 1/f noise should be a much better probe for determining the response properties of neurons at various input frequency ranges, instead of white noise or 1/f^2 noise, and the signal cutoff frequency should be carefully established in future studies.

Our work suggests that the neuronal firing rate and reliability for 1/f noise are both enhanced with an increase in the cutoff frequency. Thus, each frequency interval has an effect on neuronal responses, and future work should examine the

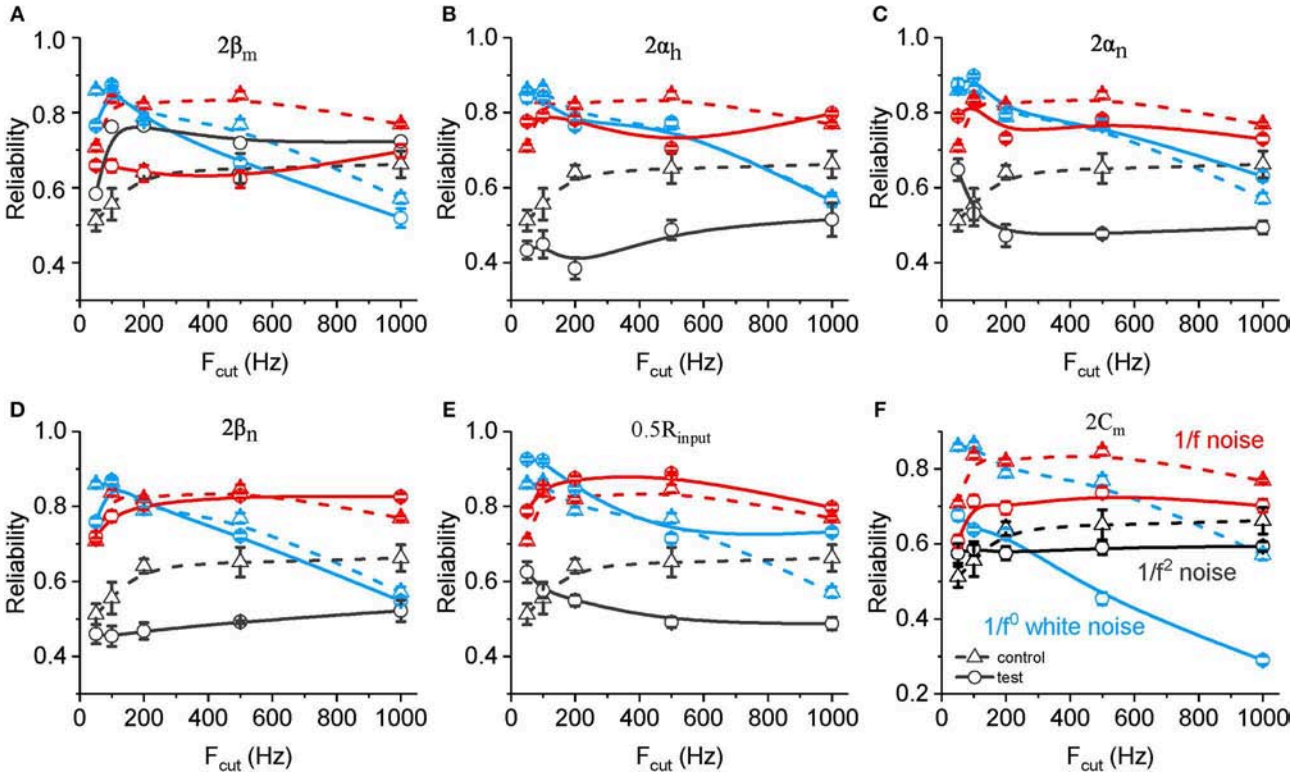

FIGURE 6 | Effects of ionic and membrane time constants on the spike reliability of model neurons. **(A–F)** Plots of reliability vs. cutoff frequency for white noise (blue), 1/f (red) and 1/f^2 noise (black) for a normal neuron (dotted line, **A–F**) compared with the results from the model neuron in the case of 2 β_m (solid line, **A**), 2 α_h (solid line, **B**), 2 α_n (solid line, **C**), 2 β_n (solid line, **D**), 0.5 R_{input} (solid line, **E**), and 2 C_m (solid line, **F**). F_{cut}, cutoff frequency. R_{input}, membrane input resistance. C_m, membrane capacitance.

optimum signal frequency range for neuronal responsiveness and derive the neuronal input-output function for each frequency interval. Although a previous study has found that injecting white noise to the DC component increases neuronal spike reliability (Mainen and Sejnowski, 1995), our findings with zero mean signals imply that neuronal excitability may determine the effects of signal frequency range, and ultimately modulate neuronal response.

Preferential Neuronal Response to 1/f Noise With a Large Frequency Range

The 1/f noise is a common phenomenon in nature (Bak et al., 1987; Gilden et al., 1995; Musha and Yamamoto, 1997; Novikov et al., 1997; De Coensel et al., 2003; Bédard et al., 2006; He, 2014). In the brain, EEG and ECoG recordings reveal that when neuronal populations exhibit the 1/f characteristic, the neural network is capable of highly efficient information processing (Soma et al., 2003; Lin and Chen, 2005; Shew and Plenz, 2013; Wood et al., 2016). At the cellular level, 1/f noise was found to originate from intact network inputs (El Boustani et al., 2009), and can enhance neuronal excitability and the stochastic resonanGarciace effect (Nozaki and Yamamoto, 1998; Nozaki et al., 1999a,b; El Boustani et al., 2009). Based on neuronal sensitivity to low-frequency sine wave signals (Hutcheon et al., 1996; Hunter et al., 1998; Volgushev et al., 1998; Fellous et al., 2001; Yu et al., 2001; Brumberg, 2002; Richardson et al., 2003; Köndgen et al., 2008; Levi et al., 2015), an individual neuron uses signals with a low frequency range to process information. However, recent experiments have observed high frequency components in the recorded membrane potentials of cortical neurons *in vivo* (El Boustani et al., 2009; Bedard et al., 2017).

Our results, for the first time, show that neurons respond preferentially to the 1/f noise in large frequency ranges, with respect to the firing rate and spike timing reliability. Because the rate and temporal encoding are two major encoding methods for neurons (Nowak et al., 1997; Reinagel and Reid, 2000; Fellous et al., 2001; Brette and Guigon, 2003; Avissar et al., 2007; Freund and Cerquera, 2012) and neuronal activities at all levels show 1/f characteristics *in vivo* (Bédard et al., 2006; El Boustani et al., 2009; Freeman and Zhai, 2009; Milstein et al., 2009; Dehghani et al., 2010; He et al., 2010; Ciuciu et al., 2012; Pettersen et al., 2014; Voytek et al., 2015), our results may indicate the positive effects of the 1/f property and large frequency range on the neuronal responses for normal physiological functioning. In addition, since the 1/f type of signal substantially drives neuronal response, our findings suggest new operating rules for synaptic transmission, neuronal plasticity and other activities relying on neuronal firing. It is likely that

future studies of neuronal interactions and network activities will discover additional distinct effects of 1/f probe signals on neural information process and neural computation.

Neuronal Dynamics Underlying the 1/f Preference

Given the low-pass filter property of neuronal membrane, once the signal contain more power in low frequency range, it may induce more neuronal firing, as seen from the neuronal response to 1/f compared with to white noise (Fellous et al., 2001; Brumberg, 2002; Levi et al., 2015). However, this is in contradiction with our finding that 1/f noise evokes higher firing rate than 1/f^2 noise in a large frequency rage. Especially, we observed that neuronal firing rate for 1/f noise increases with the cutoff frequency of 1/f noise increases. In addition, it was reported previously that the refractory period endows neuron with high-pass filtering (Nozaki et al., 1999a), increasing the response complexity. We performed numerical simulations by using the Hodgkin-Huxley model to gain deep insights into the mechanism underlying the neuronal responsive preference for the 1/f noise. We found that β_n, R_{input}, and C_m determine the neuronal preference to input signal with different type of statistics. **Figure 4** shows that the effect of changing β_n on the neuronal firing rate to 1/f^2 is larger to 1/f, much larger than to 1/f^0 noise. On the contrary, the effects of changing R_{input} or C_m on the neuronal firing rate is stronger to 1/f^0 noise than 1/f, even stronger than to 1/f^2 inputs. Here, close rate constant of potassium activation β_n seems to form a high-pass filter effect, while both R_{input} and C_m act as low-pass filter effect. Their appropriately combined action may result in neuronal responsive preference for 1/f noise with a broad frequency range.

In addition, we found the neuronal responsive reliability for 1/f$^{\beta}$ signal types is majorly dominated by several key factors of ion channels and membrane time constants, respectively. Specifically, as shown in results section, the spike reliability for white noise is mainly determined by C_m. Spike reliability for 1/f and 1/f^2 noise is mainly dominated by sodium activation close rate constant (α_m), inactivation open rate constant (α_h) and both open (α_n), and close (β_n) rate constants of potassium channel, as well as membrane time constant. With doubled α_h, α_n, and β_n (**Figures 6B–D**) and decreased R_{input} (**Figure 6E**), neuronal spike reliability for 1/f^2 noise decreases significantly for most of frequency range. These effects for 1/f^2 noise are stronger than for 1/f noise, and much stronger for white noise. These results revealed that the membrane capacitance dominates the neuronal preference to low frequency component, while the combined ion channel kinetics dominates the neuronal preference to high frequency components in the 1/f$^{\beta}$ type noise stimuli.

A prevailing hypothesis in neuronal response is that the stochastic opening and closing of individual ion channels endows cortical neurons an inherent noise. When the correlation time of the external input matches the time scale of the inherent noise, the neuronal responsiveness is maximized. Indeed, previous studies have demonstrated the existence of the optimum time scale of input signals for neuronal spiking reliability (Galán et al., 2008; McGinley et al., 2015). The neuron-preferred 1/f signal in our finding is consistent with this hypothesis.

In addition, cortical neurons are also enriched in other subtypes of sodium, potassium, and calcium channels, which may play important roles in precisely controlling the cellular sensitivity to the input signals with different temporal correlations (Wang et al., 2003). Additionally, a balance between excitatory and inhibitory synaptic inputs may adjust neuronal excitability to different signal statistics (Brunel et al., 2001; Chance et al., 2002; Wang, 2010). The dendritic morphology of the cell may even enhance the neuronal sensitivity to some frequency components within input signals (Eyal et al., 2014; Ostojic et al., 2015). Future studies should examine how the synaptic balance and the interaction between the neuronal intrinsic dynamics and modulations from the recurrent network contribute to the neuronal responses to input signals with various higher order statics and cutoff frequencies.

In summary, as the signal cutoff frequency progressively increases from 50 to 1,000 Hz, the neuronal responsive firing rate and reliability increase for 1/f noise, but decrease for white noise. Ion channel kinetic and membrane time constants endow neurons with a preferential response for 1/f noise with high cutoff frequencies. These results suggest that the 1/f noise is important in determining the computational rules and operating principles of cortical circuits.

AUTHOR CONTRIBUTIONS

YY supervised the research. YY, GQ, and BF designed the research. GQ and XF performed the experimental research. GQ and YY wrote the paper. All authors performed data analysis and reviewed the manuscript.

FUNDING

YY thanks for the support from the National Natural Science Foundation of China (81761128011, 31571070), Shanghai Science and Technology Committee support (16410722600), the program for the Professor of Special Appointment (Eastern Scholar SHH1140004) at Shanghai Institutions of Higher Learning, the Research Fund for the Doctoral Program of Higher Education of China (1322051), and Omics-based precision medicine of epilepsy entrusted by the Key Research Project of the Ministry of Science and Technology of China (Grant No. 2016YFC0904400) for their support.

SUPPLEMENTARY MATERIAL

The Supplementary Material for this article can be found online at: https://www.frontiersin.org/articles/10.3389/fncel.2019.00311/full#supplementary-material

REFERENCES

Aertsen, A. M., and Johannesma, P. I. (1981). A comparison of the spectro-temporal sensitivity of auditory neurons to tonal and natural stimuli. *Biol. Cybern.* 42, 145–156. doi: 10.1007/BF00336732

Avissar, M., Furman, A. C., Saunders, J. C., and Parsons, T. D. (2007). Adaptation reduces spike-count reliability, but not spike-timing precision, of auditory nerve responses. *J. Neurosci.* 27, 6461–6472. doi: 10.1523/JNEUROSCI.5239-06.2007

Baddeley, R., Abbott, L. F., Booth, M. C., Sengpiel, F., Freeman, T., Wakeman, E. A., et al. (1997). Responses of neurons in primary and inferior temporal visual cortices to natural scenes. *Proc. Biol. Sci.* 264, 1775–1783. doi: 10.1098/rspb.1997.0246.

Bak, P., Tang, C., and Wiesenfeld, K., (1987). Self-organized criticality: An explanation of the 1/f noise. *Phys. Rev. Lett.* 59, 381–384. doi: 10.1103/PhysRevLett.59.381

Bédard, C., and Destexhe, A. (2009). Macroscopic models of local field potentials and the apparent 1/f noise in brain activity. *Biophys. J.* 96, 2589–2603. doi: 10.1016/j.bpj.2008.12.3951

Bedard, C., Gomes, J.-M., Bal, T., and Destexhe, A. (2017). A framework to reconcile frequency scaling measurements, from intracellular recordings, local-field potentials, up to EEG and MEG signals. *J. Integr. Neurosci.* 16, 3–18. doi: 10.3233/JIN-160001

Bédard, C., Kröger, H., and Destexhe, A. (2006). Does the 1/f frequency scaling of brain signals reflect self-organized critical states? *Phys. Rev. Lett.* 97:118102. doi: 10.1103/PhysRevLett.97.118102

Bhattacharya, J., and Petsche, H. (2001). Universality in the brain while listening to music. *Proc. Biol. Sci.* 268, 2423–2433. doi: 10.1098/rspb.2001.1802

Brette, R., and Guigon, E. (2003). Reliability of spike timing is a general property of spiking model neurons. *Neural Comput.* 15, 279–308. doi: 10.1162/089976603762552924

Brumberg, J. C. (2002). Firing pattern modulation by oscillatory input in supragranular pyramidal neurons. *Neuroscience* 114, 239–246. doi: 10.1016/S0306-4522(02)00252-X

Brunel, N., Chance, F. S., Fourcaud, N., and Abbott, L. F. (2001). Effects of synaptic noise and filtering on the frequency response of spiking neurons. *Phys. Rev. Lett.* 86, 2186–2189. doi: 10.1103/PhysRevLett.86.2186

Brunel, N., and Latham, P. E. (2003). Firing rate of the noisy quadratic integrate-and-fire neuron. *Neural Comput.* 15, 2281–2306. doi: 10.1162/089976603322362365

Bullmore, E., Long, C., Suckling, J., Fadili, J., Calvert, G., Zelaya, F., et al. (2001). Colored noise and computational inference in neurophysiological (fMRI) time series analysis: resampling methods in time and wavelet domains. *Hum. Brain Mapp.* 12, 61–78. doi: 10.1002/1097-0193(200102)12:23.0.CO;2-W.3.0.CO;2-W

Chance, F. S., Abbott, L. F., and Reyes, A. D. (2002). Gain modulation from background synaptic input. *Neuron* 35, 773–782. doi: 10.1016/S0896-6273(02)00820-6

Chizhov, A. V., and Graham, L. J. (2008). Efficient evaluation of neuron populations receiving colored-noise current based on a refractory density method. *Phys. Rev. E Stat. Nonlin. Soft Matter Phys.* 77:011910. doi: 10.1103/PhysRevE.77.011910

Ciuciu, P., Abry, P., and He, B. J. (2014). Interplay between functional connectivity and scale-free dynamics in intrinsic fMRI networks. *NeuroImage* 95, 248–263. doi: 10.1016/j.neuroimage.2014.03.047

Ciuciu, P., Varoquaux, G., Abry, P., Sadaghiani, S., and Kleinschmidt, A. (2012). Scale-free and multifractal time dynamics of fMRI signals during rest and task. *Front. Physiol.* 3:186. doi: 10.3389/fphys.2012.00186

Colbert, C. M., and Pan, E. (2002). Ion channel properties underlying axonal action potential initiation in pyramidal neurons. *Nat. Neurosci.* 5, 533–538. doi: 10.1038/nn857

Cook, E. P., Wilhelm, A. C., Guest, J. A., Liang, Y., Masse, N. Y., and Colbert, C. M. (2007). The neuronal transfer function: contributions from voltage- and time-dependent mechanisms. *Prog. Brain Res.* 165, 1–12. doi: 10.1016/S0079-6123(06)65001-2

De Coensel, B., Botteldooren, D., De Muer, T. (2003). "1/f noise in rural and urban soundscapes. *Acta Acustica United Acustica* 89, 287–295. doi: 10.1134/1.1560388

de Ruyter van Steveninck, R. R., Lewen, G. D., Strong, S. P., Koberle, R., and Bialek, W. (1997). Reproducibility and variability in neural spike trains. *Science* 275, 1805–1808. doi: 10.1126/science.275.5307.1805

Dehghani, N., Bédard, C., Cash, S. S., Halgren, E., and Destexhe, A. (2010). Comparative power spectral analysis of simultaneous elecroencephalographic and magnetoencephalographic recordings in humans suggests non-resistive extracellular media. *J. Comput. Neurosci.* 29, 405–421. doi: 10.1007/s10827-010-0263-2

Destexhe, A., Rudolph, M., and Paré, D. (2003). The high-conductance state of neocortical neurons *in vivo*. *Nat. Rev. Neurosci.* 4, 739–751. doi: 10.1038/nrn1198

Diba, K. (2004). Intrinsic noise in cultured hippocampal neurons: experiment and modeling. *J. Neurosci.* 24, 9723–9733. doi: 10.1523/JNEUROSCI.1721-04.2004

Duan, F., Chapeau-Blondeau, F., and Abbott, D. (2014). Stochastic resonance with colored noise for neural signal detection. *PLoS ONE* 9:e91345. doi: 10.1371/journal.pone.0091345

El Boustani, S., Marre, O., Béhuret, S., Baudot, P., Yger, P., Bal, T., et al. (2009). Network-state modulation of power-law frequency-scaling in visual cortical neurons. *PLoS Comput. Biol.* 5:e1000519. doi: 10.1371/journal.pcbi.1000519

Eyal, G., Mansvelder, H. D., de Kock, C. P. J., and Segev, I. (2014). Dendrites impact the encoding capabilities of the axon. *J. Neurosci. Off. J. Soc. Neurosci.* 34, 8063–8071. doi: 10.1523/JNEUROSCI.5431-13.2014

Fairhall, A. L., Lewen, G. D., Bialek, W., and de Ruyter Van Steveninck, R. R. (2001). Efficiency and ambiguity in an adaptive neural code. *Nature* 412, 787–792. doi: 10.1038/35090500

Fellous, J. M., Houweling, A. R., Modi, R. H., Rao, R. P., Tiesinga, P. H., and Sejnowski, T. J. (2001). Frequency dependence of spike reliability in cortical pyramidal cells and interneurons. *J. Neurophysiol.* 85, 1782–1787. doi: 10.1152/jn.2001.85.4.1782

Fleidervish, I. A., Lasser-Ross, N., Gutnick, M. J., and Ross, W. N. (2010). Na+ imaging reveals little difference in action potential-evoked Na+ influx between axon and soma. *Nat. Neurosci.* 13, 852–860. doi: 10.1038/nn.2574

Fohlmeister, J. F., Cohen, E. D., and Newman, E. A. (2010). Mechanisms and distribution of ion channels in retinal ganglion cells: using temperature as an independent variable. *J. Neurophysiol.* 103, 1357–1374. doi: 10.1152/jn.00123.2009

Frankenhaeuser, B., and Moore, L. E. (1963). The effect of temperature on the sodium and potassium permeability changes in myelinated nerve fibres of xenopus laevis. *J. Physiol.* 169, 431–437. doi: 10.1113/jphysiol.1963.sp007269

Freeman, W. J., and Zhai, J. (2009). Simulated power spectral density (PSD) of background electrocorticogram (ECoG). *Cogn. Neurodyn.* 3, 97–103. doi: 10.1007/s11571-008-9064-y

Freund, J. A., and Cerquera, A. (2012). How spurious correlations affect a correlation-based measure of spike timing reliability. *Neurocomputing* 81, 97–103. doi: 10.1016/j.neucom.2011.10.014

Gal, A., and Marom, S. (2013). Entrainment of the intrinsic dynamics of single isolated neurons by natural-like input. *J. Neurosci.* 33, 7912–7918. doi: 10.1523/JNEUROSCI.3763-12.2013

Galán, R. F., Ermentrout, G. B., and Urban, N. N. (2008). Optimal time scale for spike-time reliability: theory, simulations, and experiments. *J. Neurophysiol.* 99, 277–283. doi: 10.1152/jn.00563.2007

Garcia-Lazaro, J. A., Ahmed, B., and Schnupp, J. W. (2006). Tuning to natural stimulus dynamics in primary auditory cortex. *Curr. Biol. CB* 16, 264–271. doi: 10.1016/j.cub.2005.12.013

Garcia-Lazaro, J. A., Ahmed, B., and Schnupp, J. W. (2011). Emergence of tuning to natural stimulus statistics along the central auditory pathway. *PLoS ONE* 6:e22584. doi: 10.1371/journal.pone.0022584

Gilden, D. L., Thornton, T., and Mallon, M. W. (1995). 1/f noise in human cognition. *Science* 267, 1837–1839. doi: 10.1126/science.7892611

Guo, D., and Li, C. (2011). Signal propagation in feedforward neuronal networks with unreliable synapses. *J. Comput. Neurosci.* 30, 567–587. doi: 10.1007/s10827-010-0279-7

Gutkin, B. S., Jost, J., and Tuckwell, H. C. (2009). Inhibition of rhythmic neural spiking by noise: the occurrence of a minimum in activity with increasing noise. *Naturwissenschaften* 96, 1091–1097. doi: 10.1007/s00114-009-0570-5

Haider, B., Krause, M. R., Duque, A., Yu, Y., Touryan, J., Mazer, J. A., et al. (2010). Synaptic and network mechanisms of sparse and reliable visual

cortical activity during nonclassical receptive field stimulation. *Neuron* 65, 107–121. doi: 10.1016/j.neuron.2009.12.005

Halnes, G., Mäki-Marttunen, T., Keller, D., Pettersen, K. H., Andreassen, O. A., and Einevoll, G. T. (2016). Effect of ionic diffusion on extracellular potentials in neural tissue. *PLoS Comput. Biol.* 12:e1005193. doi: 10.1371/journal.pcbi.1005193

He, B. J. (2011). Scale-free properties of the functional magnetic resonance imaging signal during rest and task. *J. Neurosci. Off. J. Soc. Neurosci.* 31, 13786–13795. doi: 10.1523/JNEUROSCI.2111-11.2011

He, B. J. (2014). Scale-free brain activity: past, present, and future. *Trends Cogn. Sci.* 18, 480–487. doi: 10.1016/j.tics.2014.04.003

He, B. J., Zempel, J. M., Snyder, A. Z., and Raichle, M. E. (2010). The temporal structures and functional significance of scale-free brain activity. *Neuron* 66, 353–369. doi: 10.1016/j.neuron.2010.04.020

Higgs, M. H., and Spain, W. J. (2009). Conditional bursting enhances resonant firing in neocortical layer 2-3 pyramidal neurons. *J. Neurosci.* 29, 1285–1299. doi: 10.1523/JNEUROSCI.3728-08.2009

Hu, W., Tian, C., Li, T., Yang, M., Hou, H., and Shu, Y. (2009). Distinct contributions of Nav1.6 and Nav1.2 in action potential initiation and backpropagation. *Nat. Neurosci.* 12, 996–1002. doi: 10.1038/nn.2359

Huguenard, J. R., Hamill, O. P., and Prince, D. A. (1989). Sodium channels in dendrites of rat cortical pyramidal neurons. *Proc. Natl. Acad. Sci. U. S. A.* 86, 2473–2477. doi: 10.1073/pnas.86.7.2473

Hunter, J. D., Milton, J. G., Thomas, P. J., and Cowan, J. D. (1998). Resonance effect for neural spike time reliability. *J. Neurophysiol.* 80, 1427–1438. doi: 10.1152/jn.1998.80.3.1427

Hutcheon, B., Miura, R. M., and Puil, E. (1996). Subthreshold membrane resonance in neocortical neurons. *J. Neurophysiol.* 76, 683–697. doi: 10.1152/jn.1996.76.2.683

Hutcheon, B., and Yarom, Y. (2000). Resonance, oscillation and the intrinsic frequency preferences of neurons. *Trends Neurosci.* 23, 216–222. doi: 10.1016/S0166-2236(00)01547-2

Jacobson, G. A., Diba, K., Yaron-Jakoubovitch, A., Oz, Y., Koch, C., Segev, I., et al. (2005). Subthreshold voltage noise of rat neocortical pyramidal neurones. *J. Physiol.* 564, 145–160. doi: 10.1113/jphysiol.2004.080903

Jia, Y., Zheng, X., Hu, X., and Li, J. (2001). Effects of colored noise on stochastic resonance in a bistable system subject to multiplicative and additive noise. *Phys. Rev. E Stat. Nonlin. Soft Matter Phys.* 63:031107. doi: 10.1103/PhysRevE.63.031107

Kole, M. H., Ilschner, S. U., Kampa, B. M., Williams, S. R., Ruben, P. C., and Stuart, G. J. (2008). Action potential generation requires a high sodium channel density in the axon initial segment. *Nat. Neurosci.* 11, 178–186. doi: 10.1038/nn2040

Köndgen, H., Geisler, C., Fusi, S., Wang, X.-J., Lüscher, H.-R., and Giugliano, M. (2008). The dynamical response properties of neocortical neurons to temporally modulated noisy inputs *in vitro*. *Cereb. Cortex* 18, 2086–2097. doi: 10.1093/cercor/bhm235

Levi, R., Akanyeti, O., Ballo, A., and Liao, J. C. (2015). Frequency response properties of primary afferent neurons in the posterior lateral line system of larval zebrafish. *J. Neurophysiol.* 113, 657–668. doi: 10.1152/jn.00414.2014

Lin, M., and Chen, T. (2005). Self-organized criticality in a simple model of neurons based on small-world networks. *Phys. Rev. E Stat. Nonlin. Soft Matter Phys.* 71:016133. doi: 10.1103/PhysRevE.71.016133

Maex, R. (2018). An interneuron circuit reproducing essential spectral features of field potentials. *Neural Comput.* 30, 1296–1322. doi: 10.1162/NECO_a_01068

Mainen, Z. F., Joerges, J., Huguenard, J. R., and Sejnowski, T. J. (1995). A model of spike initiation in neocortical pyramidal neurons. *Neuron* 15, 1427–1439. doi: 10.1016/0896-6273(95)90020-9

Mainen, Z. F., and Sejnowski, T. J. (1995). Reliability of spike timing in neocortical neurons. *Science* 268, 1503–1506. doi: 10.1126/science.7770778

Mainen, Z. F., and Sejnowski, T. J. (1996). Influence of dendritic structure on firing pattern in model neocortical neurons. *Nature* 382, 363–366. doi: 10.1038/382363a0

Matteson, D. R., and Armstrong, C. M. (1982). Evidence for a population of sleepy sodium channels in squid axon at low temperature. *J. Gen. Physiol.* 79, 739–758. doi: 10.1085/jgp.79.5.739

McCormick, D. A., and Huguenard, J. R. (1992). A model of the electrophysiological properties of thalamocortical relay neurons. *J. Neurophysiol.* 68, 1384–1400. doi: 10.1152/jn.1992.68.4.1384

McGinley, M. J., David, S. V., and McCormick, D. A. (2015). Cortical membrane potential signature of optimal states for sensory signal detection. *Neuron* 87, 179–192. doi: 10.1016/j.neuron.2015.05.038

Miller, K. J., Sorensen, L. B., Ojemann, J. G., and den Nijs, M. (2009). Power-law scaling in the brain surface electric potential. *PLoS Comput. Biol.* 5:e1000609. doi: 10.1371/journal.pcbi.1000609

Milstein, J., Mormann, F., Fried, I., and Koch, C. (2009). Neuronal shot noise and Brownian 1/f2 behavior in the local field potential. *PLoS ONE* 4:e4338. doi: 10.1371/journal.pone.0004338

Mino, H., and Durand, D. M. (2008). Stochastic resonance can induce oscillation in a recurrent Hodgkin-Huxley neuron model with added Gaussian noise. *Conf Proc IEEE Eng Med Biol Soc.* 2008, 2457–2460. doi: 10.1109/IEMBS.2008.4649697

Musha, T., and Yamamoto, M. (1997). "1/f fluctuations in biological systems," in *Proceedings of the 19th Annual International Conference of the IEEE Engineering in Medicine and Biology Society. 'Magnificent Milestones and Emerging Opportunities in Medical Engineering' (Cat. No. 97CH36136)*, Vol. 6 (Chicago, IL: IEEE), 2692–2697. doi: 10.1109/IEMBS.1997.756890

Novikov, E., Novikov, A., Shannahoff-Khalsa, D., and Schwartz, B. (1997). Scale-similar activity in the brain. *Phys. Rev.* 56, R2387–R2389. doi: 10.1103/PhysRevE.56.R2387

Nowak, L. G., Sanchez-Vives, M. V., and McCormick, D. A. (1997). Influence of low and high frequency inputs on spike timing in visual cortical neurons. *Cereb. Cortex* 7, 487–501. doi: 10.1093/cercor/7.6.487

Nozaki, D., Collins, J. J., and Yamamoto, Y. (1999a). Mechanism of stochastic resonance enhancement in neuronal models driven by 1/f noise. *Phys. Rev. E Stat. Phys. Plasmas Fluids Relat. Interdiscip. Top.* 60, 4637–4644. doi: 10.1103/PhysRevE.60.4637

Nozaki, D., Marder, D. J., Grigg, P., and Collins, J. J. (1999b). Effects of colored noise on stochastic resonance in sensory neurons. *Phys. Rev. Lett.* 82, 2402–2405. doi: 10.1103/PhysRevLett.82.2402

Nozaki, D., and Yamamoto, Y. (1998). Enhancement of stochastic resonance in a FitzHugh-Nagumo neuronal model driven by colored noise. *Phys. Lett. A* 243, 281–287. doi: 10.1016/S0375-9601(98)00247-3

Ostojic, S., Szapiro, G., Schwartz, E., Barbour, B., Brunel, N., and Hakim, V. (2015). Neuronal morphology generates high-frequency firing resonance. *J. Neurosci. Off. J. Soc. Neurosci.* 35, 7056–7068. doi: 10.1523/JNEUROSCI.3924-14.2015

Pettersen, K. H., Lindén, H., Tetzlaff, T., and Einevoll, G. T. (2014). Power laws from linear neuronal cable theory: power spectral densities of the soma potential, soma membrane current and single-neuron contribution to the EEG. *PLoS Comput. Biol.* 10:e1003928. doi: 10.1371/journal.pcbi.1003928

Reinagel, P., and Reid, R. C. (2000). Temporal coding of visual information in the thalamus. *J. Neurosci. Off. J. Soc. Neurosci.* 20, 5392–5400. doi: 10.1523/JNEUROSCI.20-14-05392.2000

Richardson, M. J., Brunel, N., and Hakim, V. (2003). From subthreshold to firing-rate resonance. *J. Neurophysiol.* 89, 2538–2554. doi: 10.1152/jn.00955.2002

Ruszczynski, P. S., Kish, L. B., and Bezrukov, S. M. (2001). Noise-assisted traffic of spikes through neuronal junctions. *Chaos Woodbury N.* 11, 581–586. doi: 10.1063/1.1379308

Sakai, H. M. (1992). White-noise analysis in neurophysiology. *Physiol. Rev.* 72, 491–505. doi: 10.1152/physrev.1992.72.2.491

Schmidt-Hieber, C., and Bischofberger, J. (2010). Fast sodium channel gating supports localized and efficient axonal action potential initiation. *J. Neurosci. Off. J. Soc. Neurosci.* 30, 10233–10242. doi: 10.1523/JNEUROSCI.6335-09.2010

Schwalger, T., Droste, F., and Lindner, B. (2015). Statistical structure of neural spiking under non-Poissonian or other non-white stimulation. *J. Comput. Neurosci.* 39, 29–51. doi: 10.1007/s10827-015-0560-x

Sekine, M., Mino, H., and Durand, D. M. (2009). Noise induced oscillations in recurrent neural networks. *Conf. Proc. IEEE Eng. Med. Biol. Soc.* 2009, 1521–1524. doi: 10.1109/IEMBS.2009.5333069

Shew, W. L., and Plenz, D. (2013). The functional benefits of criticality in the cortex. *Neuroscientist* 19, 88–100. doi: 10.1177/1073858412445487

Sobie, C., Babul, A., and de Sousa, R. (2011). Neuron dynamics in the presence of 1/f noise. *Phys. Rev. E Stat. Nonlin. Soft Matter Phys.* 83:051912. doi: 10.1103/PhysRevE.83.051912

Soma, R., Nozaki, D., Kwak, S., and Yamamoto, Y. (2003). 1/f noise outperforms white noise in sensitizing baroreflex function in the human brain. *Phys. Rev. Lett.* 91:078101. doi: 10.1103/PhysRevLett.91.078101

Ting, J. T., Daigle, T. L., Chen, Q., and Feng, G. (2014). "Acute brain slice methods for adult and aging animals: application of targeted patch clamp analysis and optogenetics," in *Patch-Clamp Methods and Protocols*, eds. M. Martina and S. Taverna (New York, NY: Springer New York), 221–242. Available online at: http://link.springer.com/10.1007/978-1-4939-1096-0_14 (accessed April 24, 2016). doi: 10.1007/978-1-4939-1096-0_14

Vilela, R. D., and Lindner, B. (2009). Are the input parameters of white noise driven integrate and fire neurons uniquely determined by rate and CV? *J. Theor. Biol.* 257, 90–99. doi: 10.1016/j.jtbi.2008.11.004

Volgushev, M., Chistiakova, M., and Singer, W. (1998). Modification of discharge patterns of neocortical neurons by induced oscillations of the membrane potential. *Neuroscience* 83, 15–25. doi: 10.1016/S0306-4522(97)00380-1

Voss, R. G., and Clarke, J. (1978). "1/f noise"in music: music from 1/f noise. *J. Acoust. Soc. Am.* 63, 258–263. doi: 10.1121/1.381721

Voytek, B., Kramer, M. A., Case, J., Lepage, K. Q., Tempesta, Z. R., Knight, R. T., et al. (2015). Age-related changes in 1/f neural electrophysiological noise. *J. Neurosci. Off. J. Soc. Neurosci.* 35, 13257–13265. doi: 10.1523/JNEUROSCI.2332-14.2015

Wang, X.-J. (2010). Neurophysiological and computational principles of cortical rhythms in cognition. *Physiol. Rev.* 90, 1195–1268. doi: 10.1152/physrev.00035.2008

Wang, X.-J., Liu, Y., Sanchez-Vives, M. V., and McCormick, D. A. (2003). Adaptation and temporal decorrelation by single neurons in the primary visual cortex. *J. Neurophysiol.* 89, 3279–3293. doi: 10.1152/jn.00242.2003

Wood, T., Osredkar, D., Puchades, M., Maes, E., Falck, M., Flatebø, T., et al. (2016). Treatment temperature and insult severity influence the neuroprotective effects of therapeutic hypothermia. *Sci. Rep.* 6:23430. doi: 10.1038/srep 23430

Yaron-Jakoubovitch, A. (2008). A paradoxical isopotentiality: a spatially uniform noise spectrum in neocortical pyramidal cells. *Front. Cell. Neurosci.* 2:3. doi: 10.3389/neuro.03.003.2008

Yu, Y., Hill, A. P., and McCormick, D. A. (2012). Warm body temperature facilitates energy efficient cortical action potentials. *PLoS Comput. Biol.* 8:e1002456. doi: 10.1371/journal.pcbi.1002456

Yu, Y., Liu, F., Wang, J., and Wang, W. (2001). Spike timing precision for a neuronal array with periodic signal. *Phys. Lett.* 282, 23–30. doi: 10.1016/S0375-9601(01)00167-0

Yu, Y., Romero, R., and Lee, T. S. (2005). Preference of sensory neural coding for 1/f signals. *Phys. Rev. Lett.* 94:108103. doi: 10.1103/PhysRevLett.94.108103

Yu, Y., Shu, Y., and McCormick, D. A. (2008). Cortical action potential backpropagation explains spike threshold variability and rapid-onset kinetics. *J. Neurosci.* 28, 7260–7272. doi: 10.1523/JNEUROSCI.1613-08.2008

Zhao, J., Deng, B., Qin, Y., Men, C., Wang, J., Wei, X., et al. (2017). Weak electric fields detectability in a noisy neural network. *Cogn. Neurodyn.* 11, 81–90. doi: 10.1007/s11571-016-9409-x

Conflict of Interest Statement: The authors declare that the research was conducted in the absence of any commercial or financial relationships that could be construed as a potential conflict of interest.

frontiers in Cellular Neuroscience

REVIEW
published: 18 July 2019
doi: 10.3389/fncel.2019.00309

Alzheimer's Disease as a Membrane Disorder: Spatial Cross-Talk Among Beta-Amyloid Peptides, Nicotinic Acetylcholine Receptors and Lipid Rafts

Camila Fabiani[1,2] *and Silvia S. Antollini*[1,2]*

[1] *Instituto de Investigaciones Bioquímicas de Bahía Blanca CONICET-UNS, Bahía Blanca, Argentina,* [2] *Departamento de Biología, Bioquímica y Farmacia, Universidad Nacional del Sur, Bahía Blanca, Argentina*

OPEN ACCESS

Edited by:
Mario Eduardo Guido, Center for Research in Biological Chemistry Córdoba (CIQUIBIC), Argentina

Reviewed by:
Gunter Peter Eckert, University of Giessen, Germany
Aline Stephan, Université de Strasbourg, France
Jacques Fantini, Université Paul Cézanne Aix-Marseille III, France

***Correspondence:**
Silvia S. Antollini
silviant@criba.edu.ar

Specialty section:
This article was submitted to Cellular Neurophysiology, a section of the journal Frontiers in Cellular Neuroscience

Received: *14 February 2019*
Accepted: *25 June 2019*
Published: *18 July 2019*

Citation:
Fabiani C and Antollini SS (2019) Alzheimer's Disease as a Membrane Disorder: Spatial Cross-Talk Among Beta-Amyloid Peptides, Nicotinic Acetylcholine Receptors and Lipid Rafts. Front. Cell. Neurosci. 13:309. doi: 10.3389/fncel.2019.00309

Biological membranes show lateral and transverse asymmetric lipid distribution. Cholesterol (Chol) localizes in both hemilayers, but in the external one it is mostly condensed in lipid-ordered microdomains (raft domains), together with saturated phosphatidyl lipids and sphingolipids (including sphingomyelin and glycosphingolipids). Membrane asymmetries induce special membrane biophysical properties and behave as signals for several physiological and/or pathological processes. Alzheimer's disease (AD) is associated with a perturbation in different membrane properties. Amyloid-β (Aβ) plaques and neurofibrillary tangles of tau protein together with neuroinflammation and neurodegeneration are the most characteristic cellular changes observed in this disease. The extracellular presence of Aβ peptides forming senile plaques, together with soluble oligomeric species of Aβ, are considered the major cause of the synaptic dysfunction of AD. The association between Aβ peptide and membrane lipids has been extensively studied. It has been postulated that Chol content and Chol distribution condition Aβ production and posterior accumulation in membranes and, hence, cell dysfunction. Several lines of evidence suggest that Aβ partitions in the cell membrane accumulate mostly in raft domains, the site where the cleavage of the precursor AβPP by β- and γ- secretase is also thought to occur. The main consequence of the pathogenesis of AD is the disruption of the cholinergic pathways in the cerebral cortex and in the basal forebrain. In parallel, the nicotinic acetylcholine receptor has been extensively linked to membrane properties. Since its transmembrane domain exhibits extensive contacts with the surrounding lipids, the acetylcholine receptor function is conditioned by its lipid microenvironment. The nicotinic acetylcholine receptor is present in high-density clusters in the cell membrane where it localizes mainly in lipid-ordered domains. Perturbations of sphingomyelin or cholesterol composition alter acetylcholine receptor location. Therefore, Aβ processing, Aβ partitioning, and

acetylcholine receptor location and function can be manipulated by changes in membrane lipid biophysics. Understanding these mechanisms should provide insights into new therapeutic strategies for prevention and/or treatment of AD. Here, we discuss the implications of lipid-protein interactions at the cell membrane level in AD.

Keywords: Alzheimer's disease, Aβ peptide, nicotinic acetylcholine receptor, acetylcholinesterase, cell membranes, lipid rafts, cholesterol

INTRODUCTION

Biological membranes were, are, and will be complex, dynamic and controversial. Several different theories/models were postulated until the fluid-mosaic model was proposed by Singer and Nicolson (1972). This description of a biological membrane was very well accepted and gave light about membrane structure and membrane function. Although a lot of new information appeared in the following 40 years, the model was able to survive by absorbing some modifications, as it was emphasized by Nicolson (2014). **Table 1** details and compares the most important features of the original fluid-mosaic model membrane (Singer and Nicolson, 1972) and the current vision of a membrane (Engelman, 2005; Bagatolli, 2010; Goñi, 2014; Nicolson, 2014).

Nowadays, a membrane is thought of as an increasingly complex crowded structure of a great variety of *lipid* and *protein* arrangements with lateral and transverse *asymmetry*, variable *patchiness*, variable *thickness*, and higher *protein* occupancy (Engelman, 2005; Nicolson, 2014). It is universally accepted that biological membranes behave as barriers separating two fluid media and avoiding contact with each other. But being a physical barrier is not its only or main function. Many of the biochemical reactions essential for cell life (metabolic and signaling reactions involving G-protein coupled receptors as the rhodopsin or muscarinic receptor and ion channels as nicotinic, histamine, GABA or glutamate receptors among others transmembrane proteins) occur in the cell membranes, making them a truly important agent in almost all cellular physiological and pathological processes. These reactions imply molecular communication, which involves protein–protein and also protein–lipid interactions. Lipid membranes are not just a "sea" where proteins are embedded, as it was initially postulated by Singer and Nicolson. Lipids (including fatty acids, cholesterol, endocannabinoids, arachidonic acid metabolites as prostaglandins, leukotrienes, and epoxyeicosatrienoic acids, etc.) are active molecules with important implications. Lipids such as chol, cardiolipin, PIP2 and glycolipids condition the function of several transmembrane proteins, a fact reflected in the thousands of research papers that report the effect of these lipids on protein functions (Lee, 2003; Barenholz, 2004; Barrera et al., 2013). Here, we will discuss the implications of lipid-protein interactions at the cell membrane level in AD.

Abbreviations: Aβ, amyloid β protein; ACE, acetylcholinesterase; AD, Alzheimer's disease; APP, amyloid precursor protein; BACE 1, β-site APP-cleaving transmembrane aspartic protease 1; CARC, inversed CRAC; Chol, cholesterol; CRAC, Chol recognition amino acid consensus; DPPC, dipalmitoylphosphatidylcholine; l_d, liquid-disorder domain; LDM, low density membrane domain; l_o, liquid-ordered domain; M1 to M4, nAChR transmembrane segments; MuSK, muscle specific receptor tyrosine kinase; nAChR, nicotinic acetylcholine receptor; NMJ, neuromuscular junction; PA, phosphatidic acid; PC, phosphatidylcholine; PE, phosphatidylethanolamine; PRiMA, proline-rich membrane anchor; PS1, presenilin 1; PUFA, polyunsaturated fatty acid; SM, sphingomyelin.

CROSSTALK OF ALZHEIMER'S DISEASE PATHOGENESIS AND LIPID MEMBRANE

Alzheimer's disease is the most prevalent neurodegenerative disorder in the elderly, and is characterized by progressive cognitive decline. The main pathophysiological characteristics include extracellular accumulation of β-amyloid senile plaques and intracellular accumulation of neurofibrillary tangles (hyperphosphorylated microtubule-associated tau protein) (Feng and Wang, 2012; Kumar et al., 2015). A disruption of the cholinergic pathways that contribute to the cognitive impairment of AD patients is described in the cerebral cortex and in the basal forebrain. AD implicates the formation of extracellular insoluble peptides derived from the action of two transmembrane enzymes, a β-secretase (β-site APP-cleaving transmembrane aspartic protease, BACE 1) and a γ-secretase (an imprecise multimeric protein complex), on the membrane-bound APP. Aβ peptides of different lengths, containing 39–42 amino acid residues, are produced. 1–40 Aβ is produced more frequently while 1–42 Aβ is the predominant species in senile plaques (Iwatsubo et al., 1994). They are amphiphilic peptides with residues 1–28 constituting a hydrophilic domain and residues 29 up to 42 (which correspond to part of the transmembrane domain of APP), a hydrophobic one (Ji et al., 2002). Whereas low concentrations of 1–40 Aβ are related to neurotrophic properties (Yankner et al., 1990; Zou et al., 2002, 2003), 1–42 Aβ, produced in low amounts under physiological conditions, has a much higher tendency to form oligomers, protofibrils and fibrils, which are the ones that constitute AD brain plaques (Jarrett et al., 1993; Gu and Guo, 2013). The structural-activity relation between these assemblies and the differences between 1–40 Aβ and 1–42 Aβ are under continuous investigation and exceed the aim of this review. Alternatively, APP can be cleaved by another membrane enzyme (α-secretase) between amino acids 16 and 17 of the Aβ region, avoiding Aβ peptides generation and producing a neurotrophic and neuroprotective soluble AβPP (sAβPPα) through a non-amyloidogenic pathway (Thornton et al., 2006; Wang et al., 2016). In neurons, amyloidogenic and non-amyloidogenic pathways compete with each other, jumping between neuroprotection and neurodegeneration (Vetrivel and Thinakaran, 2006; Tan and Gleeson, 2019). Furthermore, in normal brains, 1–42 Aβ is produced in low picomolar concentrations and, as it will be explained later, these low,

non-toxic concentrations have physiological implications in synaptic plasticity and memory, among others (Plant et al., 2003; Puzzo et al., 2008, 2011, 2015). In fact, physiological 1–42 Aβ binds to several target molecules as apoE, the receptor for advanced glycosylation end products (RAGE), serpin–enzyme complex receptor (SEC-R) and nicotinic acetylcholine (nACh) receptors (Turner et al., 2003). Thus, although during a person's lifetime there is a continuous formation of all these peptides, the deregulation of the enzymatic equilibrium with the consequent accumulation of insoluble peptides is characteristic of AD. 1–42 Aβ is the most hydrophobic peptide that forms soluble oligomeric intermediates before aggregating as insoluble plaques with cytotoxic properties in the AD brains. It induces iron and cooper reduction in the brain triggering oxidative stress and damage, it causes calcium homeostasis deregulation probably through lipid perturbation at the cell membrane, and it causes oxy-radicals formation and finally neurodegeneration (Butterfield et al., 2013; Fonseca et al., 2015; Cheignon et al., 2018). Amyloidogenic and non-amyloidogenic pathways are thought to occur in different cellular compartments depending

TABLE 1 | Comparison of the main membrane characteristics proposed by the Singer and Nicolson (1972) model and the current cell membrane vision (based on Engelman (2005), Bagatolli (2010), Goñi (2014), Nicolson (2014), and references there in).

Singer and Nicolson (1972)	Today (2019)
The membrane consists of a double layer of lipids (*bilayer*) in a *lamellar liquid-crystalline phase.* (A preliminary deviation of this concept was included in the original model: *"It is therefore not excluded that some significant fraction of the phospholipid (perhaps as much as 30 percent) is physically in a different state from the rest of the lipid."*)	In certain membranes, other phases like *liquid-ordered phases* or *non-lamellar phases* as rhombohedral, tetragonal, inverted hexagonal and cubic phases fulfill physiologically important functions. These phenomena involve membrane phase changes that are possible because of the intrinsic deformability of the membrane. Examples of transient *non-lamellar phases* can be seen during membrane fusion where from two independent bilayers originates only one which involves the coalesce of two bilayers (Chernomordik and Zimmerberg, 1995; Tenchov et al., 2006) or during pore formation by proteins as Bax/colicin family proteins and actinoporins which involves the formation of non-lamellar (semi-toroidal or toroidal) lipidic structures (Gilbert et al., 2014; Gilbert, 2016).
The membrane is considered *flat*.	Membranes are usually *curved*, dynamically modulated by the geometry of both lipids and proteins, and require *asymmetry* between both hemilayers in order to support this membrane curvature (Mouritsen and Bloom, 1984; Epand et al., 1996; Zimmerberg and Gawrisch, 2006; Bagatolli, 2010).
The protein:lipid ratio is 1.5–4, and thus proteins play an important role in the membrane structure. However, lipids and proteins do not interact strongly. They are almost independent entities, without significant perturbation of the bilayer. (A preliminary deviation of this concept was proposed in the original model: *"if it is proposed that, while the largest portion of the phospholipid is in bilayer form and not strongly coupled to proteins in the membrane a small fraction of the lipid is more tightly coupled to protein. With any membrane protein, the tightly coupled lipid might be specific; that is, the interaction might require that the phospholipid contain specific fatty acid chains or particular polar head groups. There is at present, however, no satisfactory direct evidence for such a distinctive lipid fraction".*)	The membrane is full of proteins, leaving no membrane fraction unaffected by their presence. Protein–protein interactions have functional important signaling implications. There are lipids in direct contact with the protein (boundary lipids) that provide a special lipid environment for the proteins. Some of these lipids have a fast exchange with bulk lipids (annular lipids), whereas others (non-annular lipids) are tightly bound to certain membrane proteins stabilizing their conformation and/or function.
Proteins interact with the bilayer in two different forms: as *peripheral or extrinsic proteins* (associated to the lipid bilayer polar headgroups) and as *integral or intrinsic proteins* (associated to the hydrophobic matrix).	There are also other proteins that are only part of the time docked to a membrane (*membrane associated proteins*). They are not involved in the microstructure of the membrane; however, they have important membrane functions and dynamics. For example, protein kinases C and annexins (Bazzi and Nelsestuen, 1996).
The membranes are *fluid*. Lipids and proteins have two of three different modes of motion: *rotational* around an axis perpendicular to the plane of the membrane, and freely *translational* along the plane of the membrane. *Transbilayer* diffusion is forbidden because of the energy barrier presented by the hydrophobic matrix to the polar groups of the lipids and proteins.	The high amount of transmembrane proteins plus peripheral proteins plus protein-protein interactions restricts dramatically the lateral diffusion of proteins. The membranes are seen as "more *mosaic* than *fluid.*"[1] Membrane lipids can also undergo fast transbilayer diffusion (*flip-flop* movements), which can be a protein-helped event or a spontaneous event. Scrambling of lipids contributes to the dynamic transbilayer asymmetry of the membrane; or, contrary to this, to losing the asymmetric condition by triggering a signaling process (i.e., phosphatidylserine flip-flop from the inner to the outer hemilayer and apoptosis).
The two surfaces of membranes are not identical in composition, structure, and distribution of oligosaccharides. This *asymmetry* is based on the forbidden transbilayer diffusion.	Membranes are *asymmetric*. Lipids and proteins are different in each hemilayer, this being a condition that involves lipid transporters or spontaneous lipid movements (Quinn, 2002; Daleke, 2003; van Meer, 2011). Integral proteins are naturally asymmetrical in the membrane after their initial biosynthesis. Asymmetry is essential for cells and its disruption is associated with cell activation or pathological conditions.

(Continued)

TABLE 1 | Continued

Singer and Nicolson (1972)	Today (2019)
The membrane is mainly *homogeneous.* The original model suggested that: *"Such short-range order is probably mediated by specific protein (and perhaps protein-lipid) interactions leading to the formation of stoichiometrically defined aggregates within the membrane. However, in a mosaic membrane with a lipid matrix, the long-range distribution of such aggregates would be expected to be random over the entire surface of the membrane".*	The bilayer is full of uneven *heterogeneous* patches or domains enriched in certain lipids and proteins, which confer irregular thickness in the membrane. This is the result of certain preference of protein-lipid contacts, mismatch between the length of the hydrophobic transmembrane segments of the proteins and the length of the lipid acyl chains, protein–protein contacts, the anchoring of integral proteins to cytoskeletal proteins, the poor miscibility of certain lipids, etc. These domains have very important functional implications. *Membrane rafts* (Simons and Ikonen, 1997) are one type of membrane domains. They are small (10–200 nm), transient and dynamic (short life, ∼200 ms). These domains, which induce lateral order and heterogeneous organization of membranes, are a consequence of the immiscibility of certain lipids of biological membranes, leading to the coexistence of patches with different physical properties and lipid compositions. They also compartmentalize or segregate certain proteins making more efficient a variety of cellular processes. Rafts domains in eukaryotic cell membranes are liquid-ordered domains rich in cholesterol and sphingomyelin. In model membranes, a mixture of lipids that induce a segregation of liquid-ordered (lo) and liquid-disordered phases (ld) is used to study those domains. A *lo phase* is a phase with higher lateral mobility in the bilayer than in a gel phase but with the lipid acyl chains extended and ordered, whereas a *ld phase* is a fluid phase with the acyl chains of the lipids highly disordered and mobile (Simons and van Meer, 1988; Simons and Ikonen, 1997; Brown and London, 2000; London, 2005; Sonnino and Prinetti, 2013).
The membrane is an *isolated system* with no exchange of matter or energy with the environment.	All kind of signals occur in the membrane contacting with the extracellular and intracellular environment, for example molecules reaching and leaving the membrane in response to stimulus (Watson, 2015; Wen et al., 2018).

[1] *Nicolson (2014) said: "I have re-termed the model as the 'Fluid—Mosaic Membrane Model' to highlight the important role of mosaic, aggregate and domain structures in membranes and the restraints on lateral mobility of many if not most membrane protein components."*

on secretases localization. γ-secretase complex is present in multiple compartments: near 6% in the plasma membrane and the rest in intracellular organelles such as endoplasmic reticulum, late Golgi/*trans*-Golgi network and endosomes (Vetrivel et al., 2004; Chyung et al., 2005). However, α- and β-secretases are more compartmentalized. α-cleavage occurs at the cell surface (Parvathy et al., 1999; Haass et al., 2012; Sun and Roy, 2018). APP is released to the plasma membrane through the secretory pathway and stays there for a short time. Therefore, during this short time, APP is proteolytically processed by α-secretase. Anyway, near 70% of APP is internalized by endocytosis. A fraction of this APP is recycled to the cell surface and another one is degraded in lysosomes. BACE 1 is localized late in the Golgi/*trans*-Golgi network and endosomes and cleaves APP during the endocytic/recycling cycle (Koo and Squazzo, 1994); thus, β-cleavage depends on endocytosis (Koo and Squazzo, 1994; Perez et al., 1999; Huse et al., 2000; Daugherty and Green, 2001; Kamal et al., 2001; Ehehalt et al., 2003) and Aβ is produced mainly in the *trans*-Golgi network during the recycling pathway (Vetrivel and Thinakaran, 2006). Additionally, it was suggested that 1–42 Aβ is produced mainly in the endoplasmatic reticulum whereas 1–40 Aβ is produced in the *trans*-Golgi network (Annaert et al., 1999; Greenfield et al., 1999).

APP cleavage by secretases always happens in a membrane, independently of the subcellular compartment. To understand the importance of this fact, it is recommended to read the general commentary by Lukiw (2013) in *Frontiers in Physiology* titled "Alzheimer's disease (AD) as a disorder of the plasma membrane," whereas the author pointed out the implication that the membrane has in the physiopathology of this disease. Several studies postulated that membrane components condition the APP enzymatic processing. Particularly, Chol is a key element in the membrane and it has been related to AD in several ways. Lahdo and De La Fournière-Bessueille (2004) studied the minimum lipid requirements of a monolayer for the insertion of APP. They concluded that APP insertion depends on the Chol content, the Chol/PC and the Chol/SM ratios, and the monolayer membrane order. They identified a critical inflection point at near 30% Chol: at a lower ratio APP localizes in the membrane surface mainly in a β-sheet conformation, whereas as this Chol percentage increases, APP can insert spontaneously into the membrane changing its conformation (Ji et al., 2002; Lahdo and De La Fournière-Bessueille, 2004). Consequently, once APP is confined to the interior of the membrane it can perturb the biophysical properties of this membrane and the activity of several transmembrane or associated-membrane proteins. The Chol concentration and Chol location in brain plasma membranes change throughout a person's life. At early ages, about 87% of the Chol is localized mainly in the inner layer of the brain plasma membrane, but during aging, the percentage of Chol increases in the outer layer losing the initial transmembrane asymmetry and reaching at least 30 mol%, the critical value with respect to APP membrane insertion (Igbavboa et al., 1996; Wood et al., 2002). In another work, it was suggested that modifications of Chol compartmentation and the equilibrium free cholesterol/cholesteryl esters through acyl-coenzyme A:Chol acyltransferase (ACAT) activation, instead of variations of total membrane Chol, are the determinant of Aβ accumulation and cell dysfunction (Puglielli et al., 2001).

The importance of the amount of Chol for APP insertion leads us to think that APP would probably prefer raft domains (Cordy et al., 2006; Reid et al., 2007). Initial studies in the brain showed that both APP and Aβ reside in detergent-insoluble

glycolipid-enriched membrane domains (DIG) (Lee et al., 1998), suggesting that those domains are the place in the membrane where the APP processing occurs. The non-amyloidogenic pathway through α-secretase is thought to occur in non-raft domains (Kojro et al., 2001; Reid et al., 2007). On the other hand, although there is no consensus about the localization of APP and BACE 1, there is agreement that APP cleavage by β- and γ-secretase occurs in raft domains (see **Table 1** for a detailed explanation of raft domains). Experiments in culture cells showed that overexpressed APP and both secretases enzymes localize in Chol-rich domains (Burns and Duff, 2002; Ehehalt et al., 2003), and that Chol depletion by Chol synthesis inhibition or Chol membrane extraction resulted in a reduction of Aβ production (Simons et al., 1998; Fassbender et al., 2001; Ehehalt et al., 2003). Several studies suggest that APP is present in two cellular pools: one in raft domains and another in non-raft domains. Ehehalt et al. (2003) concluded that this APP membrane compartmentation explains how the same protein could be processed in two different ways (generating Aβ in raft domains and being cleaved by α-secretase in non-raft domains). Furthermore, they said that although BACE 1 is present in both raft and non-raft domains it needs to be in raft domains to be functional, outside these domains the enzyme is inactive (**Figure 1a**). That is the reason why, when Chol diminishes, Aβ production also diminishes but increases αCTF (C-terminal fragment) or C83, which is a direct product of α-secretase. Thus, Chol regulates the access of α or β secretase to APP (Ehehalt et al., 2003). On the other hand, immediately after this study, a study in human hippocampal membranes showed that the vast majority of APP is located in non-raft domains, while β-secretase BACE 1 is found in two cellular pools: one in raft domains and another in non-raft domains (Abad-Rodriguez et al., 2004). These authors gave an explanation opposite to the previous one: when Chol diminishes, which is what happens in the membrane from AD patients (Mason et al., 1992; Roth et al., 1995), BACE 1 increases in non-raft domains and then an enhancement of amyloid peptide production occurs. They concluded that BACE 1 in raft domains corresponds to an inactive pool that needs to relocate to non-raft domains to perform its activity, and that it is the Chol which directly conditions APP processing by "allowing" BACE 1 to exit or not from neighboring domains (**Figure 1b**). However, they distinguished between a mild membrane Chol reduction (less than 25%), which results in an increase of APP processing, and a drastic membrane Chol reduction (more than 35%), where an overall disruption of membrane integrity occurs concomitantly with a lower Aβ production. Working with primary cultures of rat hippocampal neurons infected with recombinant Semliki Forest virus (SFV) carrying APP, Simons et al. (1998) arrived to a different conclusion. They showed that depletion of Chol up to 60–70% did not affect the amount of APPsec (the main processed form of APP in neurons obtained by direct α-cleavage), but drastically decreased the amount of Aβ. Therefore, Chol depletion appears to redirect the APP processing from amyloidogenic processing to non-amyloidogenic cleavage. One possible explanation for this is that the small raft-resident pool of APP and BACE 1 is the active one and that it generates C99 to be processed by γ-secretase (Rushworth and Hooper, 2011). Another explanation considers that the amount of both proteins in rafts is so small that the APP processing by BACE 1 is effective once a clustering of raft domains occurs during endocytosis, meanwhile, in the plasma membrane, APP will be mainly cleaved by α-secretase through a non-amyloidogenesis pathway (Ehehalt et al., 2003). Thus, it is possible that APP processing can be altered by membrane lipid composition perturbations. Eckert et al. (2003) showed that Chol depletion decreases the amount of APP in raft domains and, consequently, the production of Aβ. On the other side, Chol increment as in Niemann Pick type C model cells, causes an APP augmentation in raft domains.

A controversial point is where are secretases located, especially β-secretase, and where they function in the membrane. With respect to γ-secretase, however, there is broad consensus. It is postulated that this enzyme is localized in raft domains confirming that the last step in the generation of Aβ occurs in those domains (Vetrivel et al., 2005). These authors postulated that once APP is cleaved by β-secretase, the CTFs (or C99) produced are recruited or sequestered into raft domains where cleavage by γ-secretase takes place. They indicated that ∼20% of BACE 1, less than 5% of APP and more than 70% of CTFs reside in raft domains; and, based on previous work, they assume that all cleavage occurs in these rigid domains (Vetrivel et al., 2005).

By magnetic nuclear resonance of C99, Beel et al. (2010) identified a short sequence of 5 amino acids (VGSNK) between the extracellular segment and the transmembrane domain that interacts with Chol, probably through hydrogen bonds. These authors recognize that although C99 is in raft domains, APP, which has the same loop, localizes mainly in non-raft domains, concluding that one possibility is that APP and C99 have different affinities for Chol. This Chol interaction site is also present in Aβ peptides, thus explaining the reported Chol-Aβ peptides interactions that trigger oligomerization, fibrillization, etc. (Beel et al., 2010) which will be discussed below.

Chol is not only crucial for APP processing in the membrane by compartmentalizing the location of both APP and secretases, but also for modulating the secretases activity. Briefly, Chol positively modulates BACE 1 and γ-secretase activities, and negatively modulates α-secretase (Bodovitz and Klein, 1996; Simons et al., 1998; Frears et al., 1999; Kojro et al., 2001; Wahrle et al., 2002; Ghribi et al., 2006). In lysates from human brain and in cultured cells, a certain amount of Chol stimulated β and γ-secretase activities, but at 20 μM Chol γ-secretase activity was inhibited. It is probable that high Chol can directly stabilize the activities of the enzymes to the maximum level in the correct lipid domain or can reduce enzymes degradation increasing Aβ production (Xiong et al., 2008). Furthermore, APP processing can be modulated by Chol conditioning membrane biophysical properties (Kojro et al., 2001; Fukaya et al., 2007; Kogel et al., 2008; Peters et al., 2009; Yang et al., 2010; Askarova et al., 2011). For example, substitution of Chol by lanosterol or polyunsaturated free fatty acids (PUFAs) induced an increment of membrane fluidity, which was related to an enhancement of α-secretase activity (Kojro et al., 2001; Yang et al., 2010; Askarova et al., 2011).

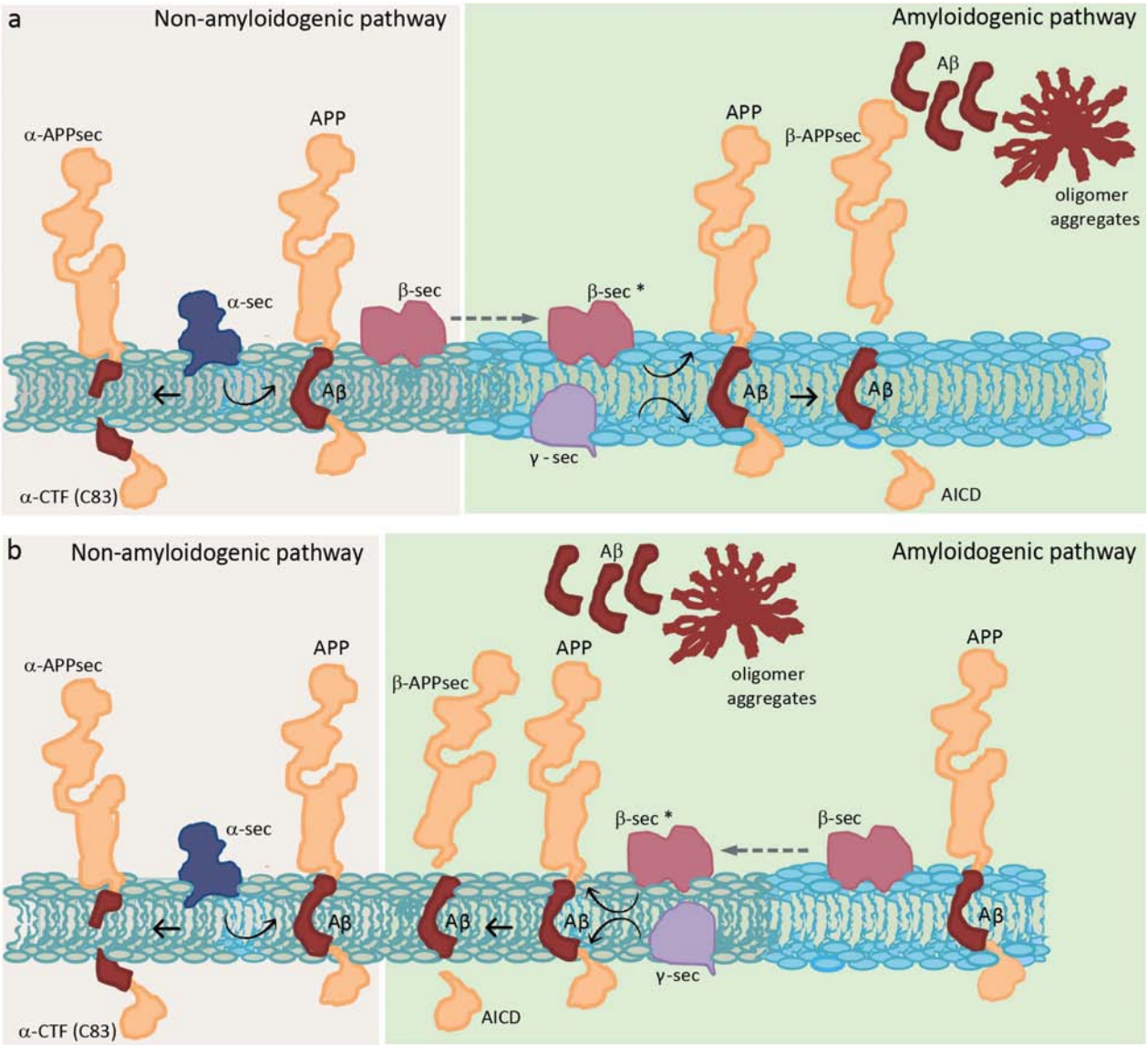

FIGURE 1 | Schematic diagram showing two distinct hypotheses of APP processing, which differ in the membrane location of the whole process. Two different colors are used to represent a raft domain and a liquid-disordered domain (light blue and gray, respectively). **(a)** Hypothesis where β sec is present in both raft and non-raft domains but needs to be in raft domains to be functional (represented as β sec*) (Ehehalt et al., 2003). **(b)** Hypothesis where β sec in raft domains corresponds to an inactive pool that needs to relocate to non-raft domains to be functional (Abad-Rodriguez et al., 2004). APP, amyloid precursor protein; α-CTF, C-terminal fragment obtained by α-secretase; α-APPsec, soluble N-terminal APP fragment obtained by α-secretase; Aβ, amyloid β peptide; β-APPsec, soluble N-terminal APP fragment obtained by β-secretase; AICD, APP intracellular domain obtained by the action of γ-secretase on β-CTF or C99 (intermediate peptide that is not shown and corresponds to Aβ plus AICD, obtained in the first step by the action of β-secretase); α-sec, α-secretase; β-sec, β-secretase; and γ-sec, γ-secretase.

Aβ RELATIONSHIP WITH AND IMPLICATIONS ON CELL MEMBRANE

Chol is also important for Aβ peptide action/effect (Eckert et al., 2003; Wood et al., 2014). Aβ peptide can adopt different conformations: a random-coil conformation in aqueous solution, an antiparallel β-sheet in the core of the amyloid plaques, and an α-helix in membranes containing Chol (Ji et al., 2002). It can exist as monomers, oligomers or as amyloid fibrils (Klein et al., 2004; Reid et al., 2007). Several studies indicate that Chol directly binds to APP as was described above (Beel et al., 2010), and also to C99 and monomeric Aβ peptides (Barrett et al., 2012), to oligomers (Ashley et al., 2006), to aggregates (Avdulov et al., 1997), and to fibrils (Harris, 2008). Considering that the mechanism by which Aβ produces brain dysfunction in AD patients is still unknown, these evidences turned the view of Aβ peptides pathogenesis

from extracellular plaques (the *"amyloid theory"*: extracellular amyloid plaques are the responsible for cell death; Hardy and Higgins, 1992; Haass, 1996; Rushworth and Hooper, 2011; Serrano-Pozo et al., 2011) to Aβ peptides interaction with the plasma membrane (Relini et al., 2014). A more recent explanation indicates that Aβ monomers or small oligomers are responsible of neuronal death rather than amyloid plaques as it was previously thought (Irvine et al., 2008; Shankar et al., 2008). Furthermore, amyloid plaques reduce neuronal death by sequestering the dangerous Aβ monomers/small oligomers (Arbor et al., 2016) (**Figure 2**). This explanation is contrary to a previous one that considered that Aβ aggregation in β-sheet conformation, which will finally end as neurotoxic fibrils, is reduced by Aβ insertion as α-helix after interaction with Chol-containing membranes (Ji et al., 2002). They showed that both 1–40 Aβ and 1–42 Aβ peptides prefer Chol enriched LDM and that while in healthy humans the amount of the former peptide is more than twice the second one, the progression of 1–42 Aβ deposition runs in parallel with an increase of this peptide in LDM domains (Oshima et al., 2001; Ji et al., 2002). The authors concluded that Chol enrichment would be beneficial for reducing fibrils, a membrane condition opposite to the one found in AD brains that show a drastic decrease of membrane Chol content and hence do not have the needed conditions for Aβ insertion, favoring the dangerous pathway of Aβ aggregation (Ji et al., 2002). In the case of AD patients, isolated brain membranes showed a significant decrease in membrane Chol, disfavoring the insertion of Aβ into the membrane (Mason et al., 1992; Roth et al., 1995). Thus, Aβ remains in the membrane surface with a great tendency to aggregation and, ultimately, to plaque formation (Ji et al., 2002). By confocal laser microscopy and fluorescence anisotropy, it was shown that 1–42 Aβ peptides interact with raft domains and that there is an inverse correlation between Chol content and membrane perturbation (Cecchi et al., 2009). It was further indicated that a Chol increment decreases amyloid-induced membrane perturbations at lipid rafts by altering the physicochemical properties of the domain (Cecchi et al., 2009). Specific interactions that induce changes in the lipid bilayer conducing to membrane disruption were described between lipids and Aβ peptides (Qiang et al., 2014). Different kinds of interactions were proposed in the last few years. Vestergaard et al. (2010) performed studies of Aβ interactions with model biomimetic membranes and showed that immediately after peptide addition, membrane fluctuations/morphological changes occur. They suggested that both Chol levels and lipid composition affect how Aβ oligomers interact with the membrane. X-ray diffraction studies of the interaction between a 25–35 Aβ peptide and anionic membranes enabled the identification of immiscible Chol plaques when more than 30 mol% Chol was added. The peptide interacts with the bilayers sequestering more Chol molecules into the plaques and, hence, decreasing the amount of Chol in the membrane (Dies et al., 2014).

Chol is not the only important lipid in the Aβ-membrane interactions, there is also GM1, which is a resident lipid of raft domains (Lin et al., 2008). High Chol levels facilitate gangliosides clustering, which is postulated to modulate Aβ oligomerization. These clusters interact with Aβ peptides in a concentration dependent manner inducing Aβ aggregation in β-sheet rich structures with a high Aβ/ganglioside relationship (McLaurin et al., 1998; Ariga et al., 2001; Kakio et al., 2001, 2002; Matsuzaki, 2007). The binding of Aβ to a GM1 cluster favors a conformation transition that depends on the protein density of the membrane. At low peptide/lipid ratios a transition from random coil to α-helix conformation occurs, whereas at high peptide/lipid ratios a β-sheet rich structure appears, which ends in fibrils formation (Matsuzaki et al., 2010; Fukunaga et al., 2012). Significant alterations in the lipid composition of raft domains in frontal cortex of AD patients were described (Martín et al., 2010; Kosicek and Hecimovic, 2013; Fabelo et al., 2014). A detailed study of the lipid composition of DRM from temporal and frontal cortex of AD brains indicated that there was an increment of GM1 and GM2 in both areas of the brain studied (Molander-Melin et al., 2005). This difference, which was considered an early event in the progression of AD, was not observed between samples from brains of different ages or gender (Molander-Melin et al., 2005). Other studies agree with an age-dependent high-density GM1 clustering in synaptosomes (Gylys et al., 2007; Yamamoto et al., 2008) and specific Aβ peptides and GM1 complexes in early AD brains. GM1-Aβ interactions (GAβ) were described in the brain and associated with AD pathology (Yanagisawa et al., 1995; Choo-Smith et al., 1997; Yanagisawa and Ihara, 1998; Kakio et al., 2001, 2002; Yamamoto et al., 2004, 2005; Wakabayashi et al., 2005). Thus, GM1 is postulated as the seed for the formation of amyloid fibrils (Staneva et al., 2018), and several studies considered raft platforms as the site where these interactions happen. Sasahara et al. (2013) showed that the interaction and aggregation of the peptide enhances lipid phase separation because of the GM1 relation with Aβ aggregates. A two-step phase was postulated to occur in membranes of AD patients: at early stages the proportion of GM1 in raft domains increases accelerating Aβ plaques formation and triggering a gradual raft disruption and perturbation of the cellular function that involves these membrane domains; at a later stage, there is also a decrement in Chol content which prevents Aβ aggregation and increases neurotoxicity (Molander-Melin et al., 2005). A more detailed study of the mechanism of Aβ interaction with GM1 indicates that Aβ oligomers, which have increased hydrophobicity compared to Aβ monomers, primarily bind to GM1 initiating progressive alterations such as membrane biophysical and ion permeability perturbations that end in the well-known synaptotoxic effects of Aβ (Hong et al., 2014).

Although all data points to a direct implication of gangliosides on Aβ oligomerization, a ganglioside-independent Aβ oligomerization mechanism was also observed, suggesting that other lipid components or carbohydrates in raft domains would be also implicated (Kim et al., 2006).

One important consequence of these raft domains/Aβ peptide interaction is the occurrence of Aβ peptide aggregation and Ca^{+2} channels formation in raft domains (Lin et al., 2001). In hippocampal cell membranes this process was related to neurotoxicity (Sepúlveda et al., 2014). Di Scala et al. (2013) identified a Chol binding domain in a 20–35 fragment of 1–42 Aβ, which is also present in other peptides with high

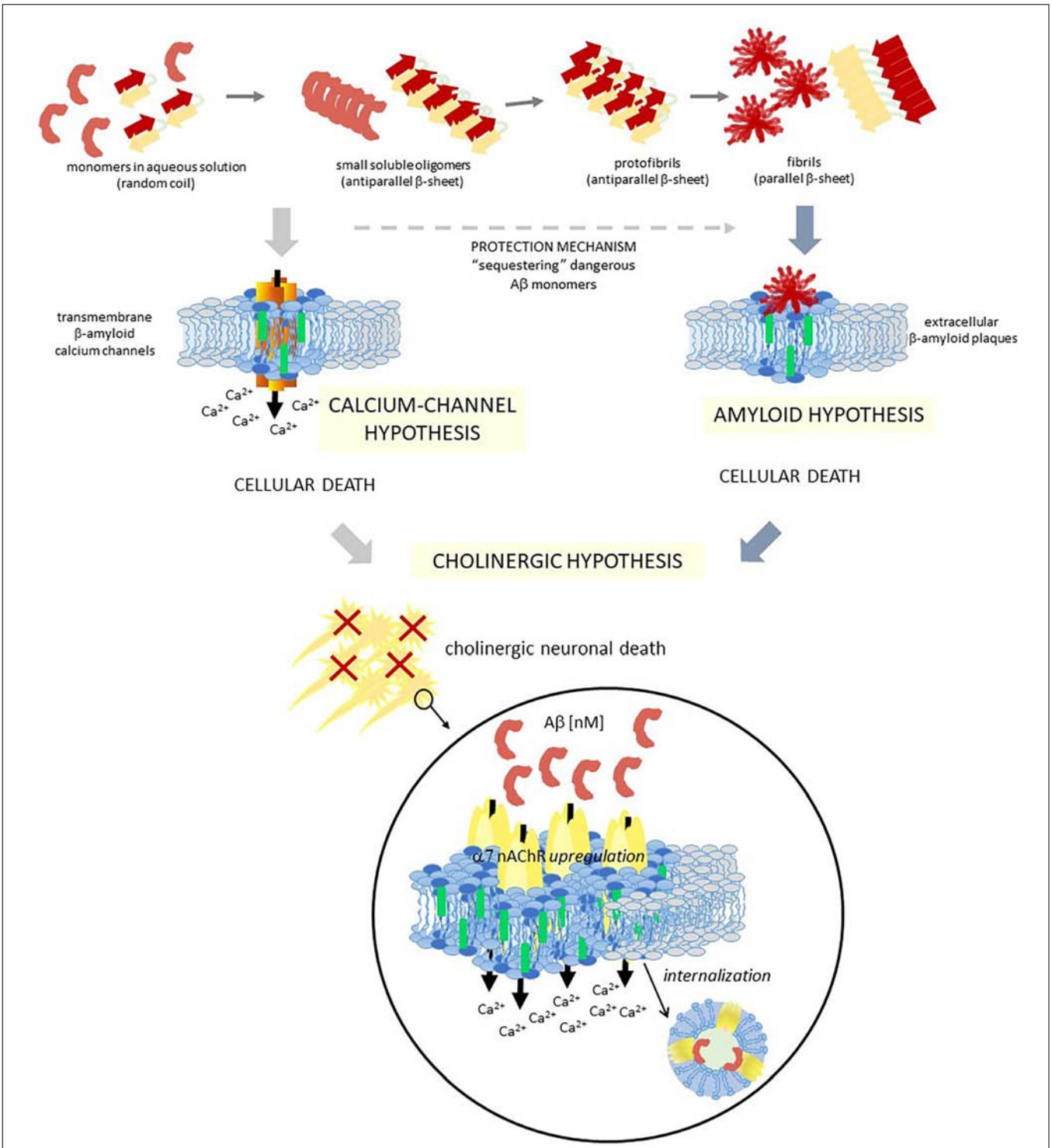

FIGURE 2 | Schematic diagram showing three different hypotheses of AD, which are closely related. Two different colors are used to represent a raft domain and a liquid-disordered domain (light blue and gray, respectively), and also within raft domains, two central lipids are identified for these hypotheses with different colors: chol and GM1 (green and blue, respectively). Aβ, amyloid β peptide; α7 nAChR, α7 nicotinic acetylcholine receptor.

Chol affinity. Interestingly, although both APP and 1–42 Aβ interact with Chol, they have distinct binding domains [17–40 Aβ for APP (Barrett et al., 2012) and 20–35 Aβ for 1–42 Aβ (Di Scala et al., 2013; Fantini et al., 2014)]. By physicochemical and *in silico* experiments, it was demonstrated that this 20–35 Aβ domain forms oligomeric Ca^{2+} channels in the plasma

membrane in a Chol dependent manner (Di Scala et al., 2014). The high interaction with Chol of this 20–35 Aβ domain triggers the helix to an adequate tilted orientation inside the membrane, which allows accurate peptide-peptide interactions and the formation of the circular channel. This oligomeric channel is formed by eight 20–35 Aβ subunits and eight Chol molecules, with a pore size and an external diameter of 1.46 and 4.4 nm, respectively. The formation of these channels could help explain the neurotoxic properties of 1–42 Aβ (**Figure 2**). Similar *in silico* studies performed with 1–40 Aβ showed that the interactions between Chol and peptide are different to those observed with 1–42 Aβ (Di Scala et al., 2013, 2014). Since the initial proposal of the existence of transmembrane ion channels formed by Aβ peptides (Arispe et al., 1993a,b), lots of studies deepened in the "β-*amyloid calcium channel hypothesis*" (Pollard et al., 1995; Kagan et al., 2002; Kawahara, 2010). The first step for this ion channel formation must be the contact between the peptides and the membrane. It was demonstrated that both the lipid composition of the outer membrane and the structural conformation of the Aβ peptide are crucial for this interaction. In solution, it was possible to find Aβ as β-sheet, α-helix or random coil conformations, being the conformational balance dependent on its concentration. It is postulated that the presence of certain lipids can shift the equilibrium to one preferred conformation. Particularly, it was demonstrated that negatively charged lipids take contact with the peptide by specific electrostatic interactions (Hertel et al., 1997; McLaurin and Chakrabartty, 1997; Terzi et al., 1997). Aβ selectively recognizes and accumulates on GM1-rich membrane domains (Yanagisawa et al., 1995; Wakabayashi et al., 2005; Yanagisawa, 2005), and Aβ insertion into the membrane is critically dependent on the Chol/phospholipids ratio (Ji et al., 2002), as it was detailed above. More recent works showed that the formation of Ca^{2+} pores ("annular protofibrils," Lashuel et al., 2002) in the plasma membrane is a mechanism dependent on both gangliosides and Chol. As it was described above, amyloid monomers or soluble oligomers interact with a ganglioside at the cell surface, with a specificity that responds to a ganglioside-binding domain for each amyloid protein (common amino acid residues at specific locations, with specific variations for each ganglioside), being the Ca^{2+} pores significantly diminished in ganglioside deprived cells (Di Scala et al., 2016). Based on this "calcium-channel hypothesis" of the AD, a chimeric peptide formed with a minimal ganglioside-binding domain of α-synuclein and two contiguous His residues as in 1–42 Aβ (Yahi and Fantini, 2014) avoid pore formation by 1–42 Aβ. Treatment of WT 5XFAD mice with a sialic-specific lectin (LFA, Limax flavus agglutinin) significantly reduced amyloid depositions in the brain, probably by interfering with the binding of amyloid peptides to gangliosides (Dukhinova et al., 2019). Furthermore, Cascella et al. (2017) showed that different oligomer conformations can perturb Ca^{2+} cell-permeation by both a channel-independent mechanism as annular protofibrils, or by a channel-dependent one (through NMDA-R and AMPA-R).

Aβ peptides that stay in the membrane surface are in a β-sheet conformation, and once inside the membrane they turn their conformation to an α-helix (Yu and Zheng, 2012). Other studies suggested that 1–40 Aβ interacts with the membrane in two sequential steps. The first one involves the formation of a pore-like structure and membrane permeation, and the second one involves subsequent growth of aggregates with fibril formation and lipid clustering around the fiber which implies lipid extraction, membrane fragmentation, and loss of membrane integrity (Engel et al., 2008; Stefani, 2010; Milanesi et al., 2012; Sciacca et al., 2012; Relini et al., 2013; Kotler et al., 2014).

Recently, Rondelli et al. (2016) described more in detail the interactions between cell membranes and Aβ peptides. Those interactions depend on peptide conformation: structural oligomers are imbibed in the outer hemilayer of the membrane triggering more Aβ addition and further elongation; on the other hand, early labile oligomers in equilibrium with monomers are incorporated as monomers deeply in the membrane coming up to the inner hemilayer, whereas Aβ organization leads to pore formation.

A study of the changes induced by 1–42 Aβ on the morphology and the mechanical stability of model membranes with different Chol content indicates that Chol drives 1–42 Aβ toward rafts domains and that at high Chol concentration the presence of the amyloid peptide did not alter any membrane property, thus assigning a protective effect against membrane destabilization by 1–42 Aβ to the presence of Chol (Seghezza et al., 2014). Recently, Staneva et al. (2018) deepened this idea. They observed that 1–42 Aβ has a higher affinity for liquid-disordered (l_d) than ordered (l_o) phases, confirming previous results (Ahyayauch et al., 2012). They concluded that the fraction of Aβ in l_o domains, probably the functionally important one, might be smaller. While in a l_o phase 1–42 Aβ induces practically no changes in the lipid packing, a significant perturbation of the lipid packing by its presence was observed in a l_d phase. They focus on the presence of GM1 as a crucial lipid. In l_d phases without GM1, the peptide penetrates and messes up the neighboring lipids. However, in the presence of GM1 the peptide interacts with the headgroup of several GM1 promoting a condensing effect and an increased lipid packing and decreases Aβ penetration. The presence of GM1 could affect the line tension between l_o and l_d domains which in turn affects the kinetics of domains formation, growth, shape and size. Thus, although it cannot be discarded that the functional peptide, or at least a minority of it, binds directly to l_o domains, the authors suggested that the fibrillation of Aβ peptides in raft domains is the consequence of a reorganization modulated through Aβ peptides in non-raft domains (Staneva et al., 2018).

Not only specific lipid raft characteristics are necessary for Aβ insertion into the membrane, but also its insertion has consequences on the membrane (Chang et al., 2017). Several studies analyzed the membrane biophysical perturbations caused by Aβ interaction, which could be considered the first step of its biological effect (Kanfer et al., 1999; Chochina et al., 2001; Eckert et al., 2003). A decrease in the fluidity of mouse brain membranes, human lymphocyte membranes and membranes from rat cortex, hippocampus and striatum was observed in the presence of 25–35 Aβ and 1–40 Aβ, and in all cases the effect was dependent on peptide concentration (Müller et al., 1995). Low concentrations of Aβ significantly perturb membrane fluidity by specifically altering the acyl-chain mobility of brain

membranes, an effect dependent on peptide length, with almost no effect at the polar head groups (Müller et al., 2001). Lately, it was observed that monomeric 1–40 Aβ has no effect on membrane fluidity, while oligomeric forms do (Peters et al., 2009). Contrary to these results, by exposition of hippocampal neurons to nanomolar concentrations of Aβ oligomers for 24 h we could not observe changes in membrane fluidity tested with three different fluorescence probes (Uranga et al., 2017). Peters et al. (2009) showed that membrane perturbation by Aβ is a consequence of Aβ complexing with GM1; thus, it is possible that in our experiments the cell membrane did not have the correct GM1/Chol relationship. A previous study of the interaction of 1–42 Aβ with planar bilayers had already demonstrated that the Chol content is directly correlated with Aβ assembly on the membrane surface, that during this process membrane changes occur, and that all this process is governed by lipid bilayer composition (Yip et al., 2002). Thus, membrane lipid environment modulates Aβ production and at the same time Aβ causes a membrane perturbation that positively feedbacks its own production (Peters et al., 2009). Moreover, Aβ insertion into the membrane not only potentiates Aβ production but also unspecifically activates a variety of membrane processes which could eventually end in neuronal cell death (Kanfer et al., 1999). 25–35 Aβ peptide interacts with phospholipids through electrostatic interactions favoring peptide aggregation which causes perturbations at the lipid-water interphase of the membrane (Martínez-Senac et al., 1999). Mass spectroscopy studies showed that Aβ inserts into model membranes containing Chol, but not in the absence of Chol (Ji et al., 2002). This study also indicated that the membrane insertion is initiated by the C-terminus of the Aβ peptide which has the hydrophobic domain.

Brain membranes from middle aged mice were more susceptible to Aβ perturbations than membranes from aged mice; and *in vitro* studies showed that a decrease in membrane Chol content enhanced Aβ effect, while an increase in membrane Chol strongly decreased the perturbation effect (Kirsch et al., 2002), suggesting that Chol protects neuronal membranes from Aβ perturbations and neurotoxicity (Eckert et al., 2003). However, they also observed *in vivo* that a reduction of Chol levels by approx. 30% by treatment with lovastatin (HMG-CoA-reductase inhibitor) resulted in moderated membrane alterations without acyl chain flexibility perturbations and reduced Aβ bulk fluidity perturbation (Kirsch et al., 2002). A possible explanation is that Chol membrane modification involves different membrane Chol pools with different sensitivity for Aβ perturbations whether it is *in vitro* or *in vivo*, with the one at the membrane acyl-chain being the most receptive (Kirsch et al., 2003).

Another important consequence of an enhanced Aβ production linked to lipid membrane is oxidative stress with an excess of lipid peroxidation and increased lipid susceptibility to oxidative damage, which exacerbates Aβ toxicity in the membrane (Behl et al., 1994; Opazo et al., 2002; Cutler et al., 2004; Boyd-Kimball et al., 2005; Wu and Luo, 2005). It is reported that Aβ prefers to interact with membranes with high oxidatively damaged phospholipids (Zampagni et al., 2010), particularly in raft domains, and that these membranes promote misfolding and aggregations of Aβ peptides into fibrils (Shringarpure et al., 2000; Magni et al., 2002; Zhang et al., 2004; Bieschke et al., 2005; Lee et al., 2006; Murray et al., 2007), whereas the misfolded peptides promote more oxidative damage in the membrane, conducing to a positive feedback (Murray et al., 2007). Aβ increases 4-hydroxy-2-nonenal (HNE) production which promotes oxidative damage and also induces Aβ to form β-structure and amyloid fibrils (Mark et al., 1997; Lauderback et al., 2001; Murray et al., 2005, 2007).

Even though it is not a topic of interest for this review, it is important to remember that just as Chol is a crucial lipid molecule for Aβ processing and Aβ membrane effects, the round trip is also valid since Aβ has an impact on Chol homeostasis (Koudinova et al., 2000; Michikawa et al., 2001; Gong et al., 2002; Michikawa, 2003; Koudinov and Koudinova, 2004; Grimm et al., 2005, 2007). This ultimate effect suggests that Aβ down-regulates Chol content and also raft content (Beel et al., 2010). Thus, the peptide behaves as a Chol sensor: when there is high Chol content in a membrane, the amyloidogenic pathway is favored and, thus, an enhancement takes place in Aβ processing, which in turn reduces both Chol uptake and biosynthesis, following up a negative feedback mechanism (Beel et al., 2010).

CROSSTALK BETWEEN AMYLOID HYPOTHESIS AND CHOLINERGIC HYPOTHESIS

The basis of AD pathogenesis is still controversial today, even though several hypotheses try to explain it, such as the Aβ amyloid cascade (Hardy and Allsop, 1991; Hardy and Higgins, 1992), the hyperphosphorylated microtubule-associated tau (Götz et al., 2004), abnormalities of the cholinergic system (Bartus et al., 1982), oxidative stress (Butterfield and Boyd-Kimball, 2005), etc. Even though the amyloid hypothesis is the most popular explanation for the mechanism of AD, it fails to explain several aspects of this multifactorial etiopathology (Herrup, 2015). In addition, until now, the majority of clinical trials conducted to diminish the amount of Aβ did not give good results (Puzzo et al., 2015; Maia and Sousa, 2019). Although these failures are not enough to discard the amyloid hypothesis (see for example Rosenblum, 2014), attention is now focused on the cholinergic hypothesis since it became the main therapeutic strategy for this disease (**Figure 2**). As we will work out in the following paragraphs, these two hypotheses are highly linked.

The cholinergic system involves two families of receptors, nAChR and muscarinic acetylcholine receptors (mAChR). Although both types of receptors are related with cognitive processes (Ghoneim and Mewaldt, 1977; Petersen, 1977; Sarter and Paolone, 2011) and are affected in AD, only the relation between nAChR and AD has been largely studied (Lombardo and Maskos, 2014).

The nAChR is an integral membrane protein that belongs to the Cys-loop superfamily of ligand-gated ion channels (Karlin and Akabas, 1995; Le Novère and Changeux, 1995; Changeux and Edelstein, 1998; Paterson and Nordberg, 2000). The binding of its natural agonist acetylcholine triggers a conformational change

that ends in the opening of a channel and the flux of positive ions across the membrane, causing membrane depolarization and a subsequence intracellular cascade of events (Lindstrom, 2003; Brown, 2006; McKay et al., 2007; Pohanka, 2012). The nAChR presents a pentameric arrangement, with each subunit having a large N-terminal extracellular domain, four transmembrane segments (M1–M4), a small cytoplasmic domain between M3 and M4, and a short C-terminal extracellular domain. To this day, 16 different nAChR subunits (including: α1-7, α9-10, β1-4, γ, δ, and ε) that form homologous and heterologous receptors with distinct structures, functions and locations are known (Champtiaux et al., 2003; Dajas-Bailador and Wonnacott, 2004; Fucile, 2004; Giniatullin et al., 2005; Gotti et al., 2006a, 2007, 2009; Albuquerque et al., 2009; Shen and Yakel, 2009). The muscle-type nAChR of the electric organ of *Torpedo*, first receptor described and still the prototype of the family, is formed by $\alpha 1_2\beta 1\delta\gamma$ (similar to embryonic muscle nAChR of vertebrates, which change to $\alpha 1_2\beta 1\varepsilon\gamma$ in adult). Two receptor subtypes are highly expressed in the central nervous system: the heteropentamer α4β2 nAChR and the homopentamer α7 nAChR (Schmidt and Freeman, 1980; Sargent et al., 1991; Clarke, 1992; Sargent and Garrett, 1995; Cooper et al., 1999; Nashmi et al., 2003; Scholze et al., 2011). The latter is particularly important in AD (Ma and Qian, 2019). It is present in high density in the striatum, thalamus, neocortex, and limbic system suggesting a central role in normal cognition and, hence, in age-related cognitive decline (Bigl et al., 1982; Mesulam et al., 1983; Muir et al., 1993; Sarter and Bruno, 1997; Wenk, 1997; Woolf, 1998; Guillem et al., 2011). It was shown that α7 nAChR is important for growth, development and aging, regulating the plasticity of the neural circuit, neuronal differentiation, proliferation, apoptosis and clearance of aged neurons (Nees, 2015). The levels of this receptor change during development and adult stage, and in AD patients, they decrease significantly (Bowen et al., 1976; Perry et al., 1981, 1985, 1987, 1988; Whitehouse et al., 1981, 1982, 1986; Coyle et al., 1983; Shimohama et al., 1986; Nordberg et al., 1995; Paterson and Nordberg, 2000; Auld et al., 2002; Gotti et al., 2006b; Kim et al., 2013; Ma and Qian, 2019).

Activation of the α7 nAChR opens a high permeability Ca^{++} channel that consequently activates voltage-dependent Ca^{++} channels (Perry et al., 1992; Sharma and Vijayaraghavan, 2001) and triggers an intracellular signaling cascade through activation of a protein kinase. In the case of activation of presynaptic α7 nAChR, the final event is the fusion of vesicles loaded with neurotransmitters (glutamic acid, norepinephrine, acetylcholine, dopamine and GABA) to the presynaptic membrane and the massive release of these neurotransmitters to the synaptic cleft (Wonnacott et al., 2006; Ma and Qian, 2019). Postsynaptic α7 nAChR depolarize the postsynaptic membrane and participate in signal transduction (Messi et al., 1997; Morley and Happe, 2000; Berg and Conroy, 2002). ACE metabolizes acetylcholine after its release to the synaptic cleft ending the cholinergic stimulus (Bowen et al., 1976; Davies and Maloney, 1976; Coyle et al., 1983; Auld et al., 2002).

The cholinergic hypothesis of AD focuses on the fact that in brains of AD patients there is a decrease in the total amount of nAChRs (Whitehouse et al., 1982; Banerjee et al., 2000), which is an outcome of progressive death of forebrain cholinergic neurons with an extended cholinergic presynaptic denervation (Bartus et al., 1982; Court et al., 2000; Graham et al., 2002; Contestabile, 2011; Hampel et al., 2018). This is considered a consequence of enhanced Aβ production (Liu and Wu, 2006). Banerjee et al. (2000) observed that in the remaining cholinergic neurons there was a higher amount of nAChR, which suggests a possible compensatory mechanism. Many efforts were performed to ameliorate this loss. However, current approved pharmacological agents, such as physostigmine, tacrine, donepezil, rivastigmine and galantamine (Martorana et al., 2010), are targeted to inhibit ACE function increasing the amount of acetylcholine at the synapse cleft and ameliorating the clinical symptoms of AD without halting the progress of the disease.

The affinity of α7 nAChR for 1–42 Aβ is in the low picomolar concentration, a range estimated to occur in healthy brains, while the affinity of α4β2 nAChR for 1–42 Aβ is between 100 to 5000 times lower (Wang et al., 2000a); thus, it is expected that both α7 nAChR and 1–42 Aβ could associate under physiological conditions. Puzzo et al. (2015) hypothesized that under physiological conditions a positive feedback mechanism occurs: synaptic activity induces Aβ release that acts as an endogenous ligand and modulates α7 nAChR, which in turn induces release of neurotransmitters and enhances synaptic plasticity and memory. Under pathological conditions, abnormal accumulation of Aβ (nanomolar concentration, Näslund et al., 1994, 2000; Tapiola et al., 2000; Andreasen et al., 2003) induces a negative feedback mechanism which implies inhibition and internalization of α7 nAChR, leading to synaptic dysfunction and memory loss. The Aβ-α7 complex influences tau hyperphosphorylation (Wang et al., 2003) and its internalization leads to plaque formation (Nagele et al., 2003, 2004; Dineley, 2007).

It is thought that the soluble form of Aβ interacts with α7 nAChR with apparently high affinity (Wang et al., 2000a) regulating its function (Dineley et al., 2001; Liu et al., 2001; Pettit et al., 2001). However, there is no consensus about the nature and consequences of this interaction (Farhat and Ahmed, 2017). While several studies propose an agonist-like effect for presynaptic nicotinic receptors (Dineley et al., 2002; Dougherty et al., 2003; Wu et al., 2007; Puzzo et al., 2008; Mehta et al., 2009; Lilja et al., 2011; Arora et al., 2013), others propose an inhibitory action (Dineley et al., 2001; Liu et al., 2001; Pettit et al., 2001; Tozaki et al., 2002; Lee and Wang, 2003; Wu et al., 2004; Wang et al., 2009; Parri et al., 2011), and others a concentration-dependent relationship with a stimulatory effect at picomolar Aβ concentration and an inhibitory effect at high nanomolar Aβ concentration (Puzzo et al., 2008). The variability between all the performed studies is so large in terms of *in vitro* and *in vivo* models, Aβ concentrations and Aβ preparations/conformations, and other conditions, that it is difficult to find a rule for the data obtained. Khan et al. (2010) gave a possible explanation for these inconsistency centered in a different Aβ effect on pre or postsynaptic receptors. Aβ induces a rapid stabilization of an inactive/desensitized state of postsynaptic receptors, resulting in an antagonist effect, and a slower desensitization of presynaptic receptors resulting in an agonist-like effect. The authors pointed

to differences in the lipid microenvironment of the pre and postsynaptic α7 nAChR for these different desensitization rates. Presynaptic terminals have abundance of raft domains, and experimental disruption of these domains dramatically attenuates Aβ evoked α7 nAChR currents (Khan et al., 2010). With respect to the concentration-dependent effect, it is important to take into consideration that in a normal central nervous system 1–42 Aβ is found, although at low picomolar concentrations. Under this condition, it is postulated that Aβ exerts a positive effect on synaptic plasticity and memory formation (Phinney et al., 2003; Plant et al., 2003; Puzzo et al., 2008, 2011, 2015; Puzzo and Arancio, 2013). However, in a pathological condition, Aβ cannot exert its physiological function and hence a feedback mechanism induces more Aβ production, leading to an enhancement of the peptide with the subsequent reduction of α7 nAChR with Aβ removal and synaptic alteration and memory loss (Phinney et al., 2003; Puzzo et al., 2015).

Interaction of Aβ with α7 nAChR increases Aβ internalization (Nagele et al., 2002; D'Andrea and Nagele, 2006) and accumulation in lysosomes causing an excessive intraneuronal 1-42 Aβ accumulation. The majority of the amyloid plaques proceed from the lysis of degenerated, Aβ-overburdened neurons (Wang et al., 2000b; Gyure et al., 2001; Langui et al., 2004; Nunomura et al., 2010; Palop and Mucke, 2010; Li et al., 2011; Deutsch et al., 2014, 2016). Additionally, the formation of the Aβ-α7 nAChR complex may influence the membrane lipid and membrane protein organization (Deutsch et al., 2014, 2016; Ma and Qian, 2019). At the same time, the internalization of the Aβ-α7 nAChR complex triggers an upregulation of the α7 nAChR and magnifies the toxicity of the pathology (Molinari et al., 1998; Xiu et al., 2005; Yu et al., 2005; Liu et al., 2013, 2015; Shen and Wu, 2015) (**Figure 2**). In AD patients and preclinical AD models, a high expression of α7 nAChR was described (Hellström-Lindahl et al., 1999, 2004a,b; Dineley et al., 2002; Jones et al., 2006; Counts et al., 2007; Ikonomovic et al., 2009). Chronic exposure to Aβ enhances the expression of α7 nAChR in neuron and glia cells (Yu et al., 2005; Liu et al., 2013). Also, an age-dependent increase of cell surface α7 nAChR was observed in 5xFAD mice, a model that rapidly develops amyloid pathology (Jin et al., 2015). Several studies contributed to this hypothesis. Treatment of PC12 cells with 1–42 Aβ increased cell surface α7 nAChR, suggesting that the peptide induces translocation of the receptor toward the plasma membrane (Jin et al., 2015). They observed that the agonist nicotine prevented Aβ induced cell death, whereas the competitive antagonist α-bungarotoxin potentiates the peptide effect, indicating that α7 nAChR plays a role in protecting neuronal cells from Aβ 1–42 peptide (Dziewczapolski et al., 2009; Wang et al., 2009; Jin et al., 2015). Contrary to this, Liu et al. (2015) concluded that upregulation of α7 nAChR induced by Aβ is necessary to mediate peptide neurotoxicity, both in hippocampal neurons and differentiated cholinergic SH-SY5Ycells. α7 nAChR function, which is exacerbated by its upregulation, may be necessary for the toxicity of Aβ aggregates; this effect was prevented by α7 nAChR inhibition or deletion. Previous studies showed that the blockade of α7 nAChR significantly ameliorated attentional deficits (Levin et al., 2013; Burke et al., 2014). Likewise, the deletion of α7 nAChR gene was correlated with an improvement in synaptic plasticity and a reduction in cognitive deficiency (Dziewczapolski et al., 2009). Two possible cytotoxic α7 nAChR-mediated mechanisms were proposed: one considers that the α7 nAChR increment in the membrane conduces to a high calcium permeability, which could be the ultimate responsible for cell toxicity, and the other that the high Aβ-α7 nAChR complex internalization and intracellular accumulation leads to neurotoxicity (Liu et al., 2015). Thus, while several studies point to α7 nAChR activation as a beneficial treatment, others suggest that a function inhibition for a beneficial effect is necessary.

A different hypothesis about Aβ and α7 nAChR relationship was postulated by Small et al. (2007). They concluded that Aβ does not bind directly to α7 nAChR but to the lipids of the plasma membrane, and that the perturbation of the structure or fluidity of the lipid microenvironment of the receptor could be the responsible for toxicity through an alteration of the receptor function. Their conclusion is supported by previous evidence that showed that Aβ binds strongly to lipids (Subasinghe et al., 2003; Hou et al., 2005). We will return to this issue later.

We here described the most relevant information about the interaction between Aβ and α7 nAChR, and its final consequences, focusing on the events that occur through the membrane. However, not only the interactions between Aβ and α7 nAChR are important. Other proteins that interact with α7 nAChR including Lynx proteins, NMDA-receptors and the Wnt/β-catenin pathway are important as well. All those interactions that modulate receptor function are specifically altered in AD and can lead to differences in the clinical effect of nAChR ligands in AD (Thomsen et al., 2016). It is also important to take into account that there is an internal cascade of signaling downstream α7 nAChR activation that involves several other active molecules, such as glycogen synthase kinase-3β (GSK-3β), phosphoinosite 3-kinase (PI3K)-Akt, Wnt and the mitogen-activated protein kinase (MAPK) signaling pathway, which are also altered in AD (see Ma and Qian, 2019 for a further explanation).

The last step in cholinergic signaling is the degradation of acetylcholine by the enzyme ACE to end the synaptic transmission. ACE is a globular non-transmembrane protein that can exist in different molecular forms, depending on the splicing of the ACE gene (Henderson et al., 2010). Although all ACE molecular forms and variants have similar catalytic activity, they also have other non-catalytic, non-classical functions, which depend on the multiple molecular forms of this enzyme and on cell types and cellular compartments (Small et al., 1996; Grisaru et al., 1999; Massoulié, 2002; Hicks et al., 2011). In non-neuronal tissues, ACE regulates cell proliferation, differentiation, apoptosis and cell–cell interaction, which is important to take into consideration when ACE inhibitors for AD are designed (Lazarevic-Pasti et al., 2017). ACE_T is the predominant form in central nervous system, which has a C-terminal α-helix peptide of 40 amino acids named T peptide. Through disulphure bondings between these peptides they can be found as homodimers and homotetramers of ACE_T. Also, the T peptide binds to hydrophobic proline-rich domains of

membrane anchoring-proteins (like collagen-like Q subunit in NMJ and proline-rich membrane anchor, PRiMA, in the central nervous system; Massoulié et al., 2005). In the central nervous system, the majority of ACE is found as tetrameric ACE_T (G4) bound to PRiMA (Navaratnam et al., 2000; Perrier et al., 2002; Massoulié et al., 2005), which constitute the functional units at cholinergic synapse (Perrier et al., 2002; Dvir et al., 2010; Henderson et al., 2010; Hicks et al., 2011). PRiMA could bring the membrane-bound ACE together with other proteins in specialized membrane areas, such as raft domains, specifically with α7 nAChR at basal forebrains cholinergic neurons (Henderson et al., 2005; Hicks et al., 2012). A significant proportion of ACE_T is effectively located in raft domains through a Chol-binding domain of 13 amino acids of PRiMA (a CRAC, Chol recognition amino acid consensus, sequence), and Chol depletion or mutations at this domain reduced the lipid raft-PRiMA association (Xie et al., 2010a,b). A diminution of ACE activity in the cerebral cortex and other areas in AD patients was described, being the G4-PRiMA complex the ACE form markedly altered, whereas the ACE monomeric form was almost preserved (Atack et al., 1983; Fishman et al., 1986; Sáez-Valero et al., 1999). Interactions of PRiMA subunit with presenilin 1 (PS1, the catalytic subunit of γ-secretase), which is an aspartyl protease that cleaves substrates inside membrane, were described to occur in raft domains (García-Ayllón et al., 2014). This interaction could explain, in part, the cellular release of ACE through a shedding mechanism that was postulated to involve a metalloprotease (Hicks et al., 2013a). Furthermore, a direct relationship between PS1 and ACE was observed, with an overexpression of ACE related to higher levels of PS1, ACE knockdown leaded to decreased PS1 and a mutated PS1 was related with decreased ACE in the brain (Silveyra et al., 2008, 2012). At the same time, it was also observed that ACE inhibits AβPP processing through γ-secretase (Niu et al., 2012), perhaps, acting as an inhibitor of the secretase by interacting with PS1 (Campanari et al., 2014). In AD, ACE activity is diminished and hence impedes its potentiality to modulate γ-secretase (Campanari et al., 2014).

Interactions of ACE with Aβ are important in AD (Inestrosa et al., 1996; Wang et al., 2000b; Small et al., 2007), as the peptide alters several ACE properties such as its pH optimum and inhibitor sensitivity (Geula and Mesulam, 1989), making Aβ even more neurotoxic (Inestrosa et al., 1996; Alvarez et al., 1998). Moreover, ACE was detected in amyloid plaques evidencing the high affinity between both molecules and suggesting that ACE could promote Aβ aggregation (Morán et al., 1993; Inestrosa et al., 1996). Even more, in some cerebral areas of AD patients almost all ACE is in these complexes. The binding between Aβ and ACE occurs at the ACE peripheral anionic site (PAS); ACE inhibitors that bind to the anionic site (i.e., propidium), as well as antibodies against it, significantly reduce fibril formation (Reyes et al., 1997; Bartolini et al., 2003). Although the ACE catalytic domain does not participate of this interaction (Inestrosa et al., 1996), new compounds with a dual action (blocking PAS and catalytic site) are being designed, looking for the prevention of fibril aggregation with the aim of reversing the progression of the disease and, at the same time, inhibiting acetylcholine degradation to ameliorate the symptomatology (Alptüzün et al., 2010).

Furthermore, a negative relationship between APP and ACE was observed, as an overexpression of APP repressed ACE transcription with reductions of both ACE levels and ACE activity (Hicks et al., 2013b). A similar negative regulation was observed between APP and PRiMA; however, it is not clear if there is a direct downregulation by APP or if this diminution is a consequence of decreased ACE levels (Hicks et al., 2013b; Nalivaeva and Turner, 2016). The authors proposed that this ACE downregulation could be a novel neuroprotective function of APP.

nAChR AND MEMBRANE LIPIDS

As we said in the previous section, there are several nAChR subtypes depending on the individual pentameric arrangement. Summing up, all nAChR have two well defined structural domains: the neurotransmitter-binding site extracellular domain and the transmembrane domain containing the ion pore. Whereas the extracellular domain is the site where the agonists or different activators/inhibitors bind, the transmembrane region, besides having the ion pore, exhibits extensive contacts with the surrounding lipids through structural motifs remarkably conserved along phylogenic evolution (Antollini et al., 2005; Unwin, 2005; Jha et al., 2007; Baenziger and Corringer, 2011; Baenziger and daCosta, 2013; Barrantes, 2015). It is well known that a correct allosteric coupling between both domains is crucial for nAChR function, strongly dependent on its surrounding lipid, which modulates the relative proportion of nAChR in its resting or desensitized states (daCosta et al., 2002; Baenziger et al., 2000, 2008, 2015; daCosta and Baenziger, 2009; Barrantes, 2010; Barrantes et al., 2010; Hénault et al., 2015). The most studied nicotinic receptor is the muscle nAChR, which is not only the paradigm of all other nAChR but also of the entire cys-loop superfamily. In the following paragraphs we will discuss the relationship between distinct lipids or raft domains and the muscle nAChR, knowledge that can be extended to other members of the family, in particular to α7 nAChR.

Several years ago, Marsh and Barrantes (1978) described a layer of immobilized lipids that encircle the muscle nAChR with characteristics different from those of bulk lipids. Subsequent studies assigned an important role to these bounded lipids on muscle nAChR (Criado et al., 1982; Ellena et al., 1983; Ochoa et al., 1983; Sunshine and McNamee, 1992, 1994; Narayanaswami et al., 1993; Fernández-Ballester et al., 1994; Dreger et al., 1997; Barrantes, 2002, 2007; Quesada et al., 2016). The presence of both Chol and negatively charged lipids in the nAChR-lipid microenvironment is necessary to stabilize the nAChR in a functional conformation (Criado et al., 1984; Fong and McNamee, 1986; Butler and McNamee, 1993; Méthot et al., 1995; Antollini et al., 1996). However, there is no consensus about if it is the entity/identity of the lipid itself or the fluidity that each lipid confers to the membrane the responsible of this role. In spite of this controversy, the

importance of a proper lipid microenvironment for muscle nAChR becomes clear when highly hydrophobic molecules, such as free fatty acids or steroids, perturb nAChR function through the membrane localizing at the lipid-nAChR interphase (Andreasen and McNamee, 1980; Villar et al., 1988; Bouzat et al., 1993; Bouzat and Barrantes, 1996; Nurowska and Ruzzier, 1996, 2002; Minota and Watanabe, 1997; Blanton et al., 1999; Garbus et al., 2001, 2002; Antollini and Barrantes, 2002, 2016; Fernández Nievas et al., 2007, 2008). Working with reconstituted *Torpedo* nAChR, Jones and McNamee (1988) distinguished two different populations of lipids in the nAChR-lipid microenvironment region: annular and non-annular lipids. Annular lipids interact with the protein in a relatively less specific manner with a fast rate of exchange with bulk lipids. Contrarily, non-annular lipids are in close contact with the protein, probably in between α-helix transmembrane segments or subunits, and can be associated to lipid binding sites with a slow exchange rate with bulk lipids (Lee, 2003). We identified the same two types of lipids in native *Torpedo* membranes (Antollini and Barrantes, 1998). The entity/identity of non-annular lipids are considered crucial for nAChR function; in the case of annular lipids the biophysical characteristics are more relevant. This is in concordance with other studies that assigned several roles to the lipids in a membrane, two of the main ones being: a collective one, in which they form a viscoelastic lipid "solvent" with the above-mentioned heterogeneities; and an individual one as signaling molecules (Piomelli et al., 2007).

Two annular lipids that are of particular interest are negative lipids and SM. With respect to the requirement of negative lipids, PA is particularly of interest. The segregation of PA domains containing nAChR and the stabilization of a functional conformation of the receptor by PA were described (daCosta et al., 2002, 2004; Poveda et al., 2002, 2008; Wenz and Barrantes, 2005; Dickey and Faller, 2008). SM showed moderated affinity for the nAChR (Bonini et al., 2002) but it is important for proper nAChR stability in the membrane. Its deficit affects the efficiency of the nAChR assembly process and the nAChR targeting to the membrane and increases the rate of turnover (Roccamo et al., 1999; Baier and Barrantes, 2007). Moreover, SM is important for membrane biophysical properties as it is asymmetrically distributed between both membrane hemilayers and it is one of the main actors of lipid raft domains, being both aspects that impact on nAChR (Perillo et al., 2016).

A separate paragraph is for Chol, a key lipid for nAChR (Middlemas and Raftery, 1987). This lipid molecule can be found in every region of a membrane: as a bulk, annular or non-annular lipid. In the first two cases, it probably plays an important function conditioning the physical properties of the environment, mainly because of its participation in raft domain formation and in the maintenance of the asymmetrical membrane condition. As a non-annular lipid, the occurrence of allosteric binding sites is postulated (Addona et al., 1998). It was suggested that the binding domain for Chol is at the nAChR lipid-protein interface, taking contact with the transmembrane subunits αM4, αM1, and γM4 (Corbin et al., 1998); other studies identified interactions of Chol with the transmembrane segments M1, M3, and M4 of each subunit (Hamouda et al., 2006). By fluorescence quenching and energy-transfer measurements of *T. californica* reconstituted membranes, sites accessible to Chol but not to phospholipids were identified (Narayanaswami and McNamee, 1993). Using Molecular Dynamics simulations of the nAChR structure, Brannigan et al. (2008) identified 15 Chol binding sites, large hydrophobic intersubunit and intrasubunit gaps. The location of Chol molecules at these sites improved nAChR stability; and in the case of intrasubunit sites, occupation of these sites by Chol precludes the nAChR from collapsing. A recent study using coarse-grained molecular dynamics simulations suggested that while long n-3 chains (in this case, docosahexaenoic acid, 22:6) have a high propensity for annular and non-annular sites, displacing Chol and occupying sites even deeper within the bundle, shorter n-6 chains do not displace Chol from non-annular sites as efficiently as long n-3 chains (Sharp et al., 2019).

Considering the intimate and close relationship between Chol and the muscle nAChR, studies looking for a consensus about specific Chol domains in the nAChR subunits were performed. A CRAC sequence in a region immediately adjacent to the M1 transmembrane domain of all the subunits of the muscle nAChR was identified (Baier et al., 2011). These sequences are located exiting the membrane bilayer, which suggests that they are probably not good partners for Chol in the hydrophobic membrane environment. However, a novel Chol recognizing domain was identified by *in silico* studies, a sequence opposite to a CRAC one (inverted CRAC or "CARC" sequence) at M1, M3, and M4, which is located inside the membrane and is highly preserved in the evolutionary scale, from prokaryotes to humans (Baier et al., 2011; Di Scala et al., 2017). These *in silico* results were also experimentally confirmed (Fantini et al., 2016). Furthermore, the authors concluded that a CARC sequence generally exhibits more affinity for Chol than a CRAC one (Fantini and Barrantes, 2013), and that it is of high affinity, lipid specific, and saturable (Fantini et al., 2016).

Chol not only conditions nAChR function but also its stability in the plasma membrane. There are some controversies about how the nAChR is organized in the membrane. At the NMJ, supramolecular aggregations of nAChRs (micron-sized two-dimensional clusters) are postulated to occur in Chol-rich lipid microdomains, together with several postsynaptic proteins including rapsyn, MuSK and Src-family kinases. Chol would stabilize NMJ and promote its maturation (Willmann et al., 2006). Depletion of cell-surface Chol produced a marked alteration of the organization of the nAChR (Kellner et al., 2007). One hypothesis for this situation is that after an agrin (extracellular heparan sulfate proteoglycan that aggregates nAChRs on cultured myotubes) stimulus, nAChR and MuSK translocate into raft domains where nAChR clustering occurs, as raft domains concentrate the agrin/MuSK signaling, nAChR and rapsyn. Disruption of these microdomains by Chol depletion inhibits agrin stimulation and formation and maintenance of nAChR clusters (Zhu et al., 2006). A contemporary study suggested that agrin causes the translocation of nAChR into raft domains, which is in agreement with the mentioned hypothesis (Campagna and Fallon, 2006). A slightly different hypothesis

indicates that agrin does not reclute nAChRs into raft domains, as they are already in those domains independently of agrin activation, but it triggers the coalescence of raft domains conducing to nAChR clustering and it is also responsible for its maintenance, as Chol is necessary for all this process (Stetzkowski-Marden et al., 2006a,b; Cartaud et al., 2011). A previous study supports this hypothesis where the authors observed that nAChR subunits and rapsyn are cotargeted in the exocytic pathway to the cell surface inserted in Chol-rich microdomains (Marchand et al., 2002). Furthermore, Chol depletion affects the maintenance of the nAChR in the plasma membrane by several mechanisms. Treatments of cells with methyl-β-cyclodextrin, which extracts Chol from the membrane, enhanced nAChR internalization by endocytosis with a marked decrease of the number of nAChR domains, concomitantly with a gain-of-function of the remaining nAChR (Borroni et al., 2007; Borroni and Barrantes, 2011; Kamerbeek et al., 2013). Furthermore, chronic treatments with mevinolin, an inhibitor of 3-hydroxy-3-methyl-glutaryl-CoA reductase and hence of Chol synthesis, inhibited the trafficking of the receptor toward the membrane surface, which caused low nAChR cell-surface expression, and increased the intracellular nAChR pools (Pediconi et al., 2004). Moreover, Chol conditions muscle nAChR cell-surface diffusion (Baier et al., 2010; Mosqueira et al., 2018) and nAChR stability in confined raft domains (Mosqueira et al., 2018).

Different results of the interaction between muscle nAChR and lipid domains were obtained in model systems. We observed that reconstituted *Torpedo* nAChR in symmetric model membranes with coexistence of liquid-ordered (l_o) and liquid-disordered (l_d) domains was distributed homogeneously, without preference for any domain (Bermúdez et al., 2010). However, similar experiments with a synthetic peptide corresponding to the γM4 peptide showed a marked preference of this peptide for l_o domains (de Almeida et al., 2004; Bermúdez et al., 2010). Thus, although this transmembrane segment could give the nAChR the potentiality to localize in raft domains, it is not sufficient and other conditions must occur which influence nAChR partition profile. One of these mentioned conditions is membrane asymmetry. By increasing SM in the outer hemilayer, we observed an increment of the *Torpedo* nAChR in l_o domains, and the same was observed when specific SM species instead of brain SM were used in symmetric models (Perillo et al., 2016). Recently, by using coarse-grained molecular dynamics simulations of nAChR inserted in a ternary system of DPPC:Chol:PE or PC with PUFA, the authors concluded that nAChR partitioned in l_d domains poor in Chol (Sharp et al., 2019). The simulated membrane, despite having l_o and l_d domains, (a) did not have SM of any species, which is a critical lipid for raft domains in biological membranes, (b) used PUFA which are known to behave as nAChR inhibitors probably by competition with Chol for non-annular sites, as the authors observed in the study, and (c) was symmetric, a condition different to the natural asymmetry of biological membranes. Thus, this work emphasizes that it is not just the presence of an l_o domain, but also its physicochemical characteristics and specific lipid components which condition nAChRs agglomeration.

With respect to neuronal nAChR, it was observed that α7 nAChR is associated with Chol-rich microdomains at somatic spine-rich regions of ciliary neurons and that the

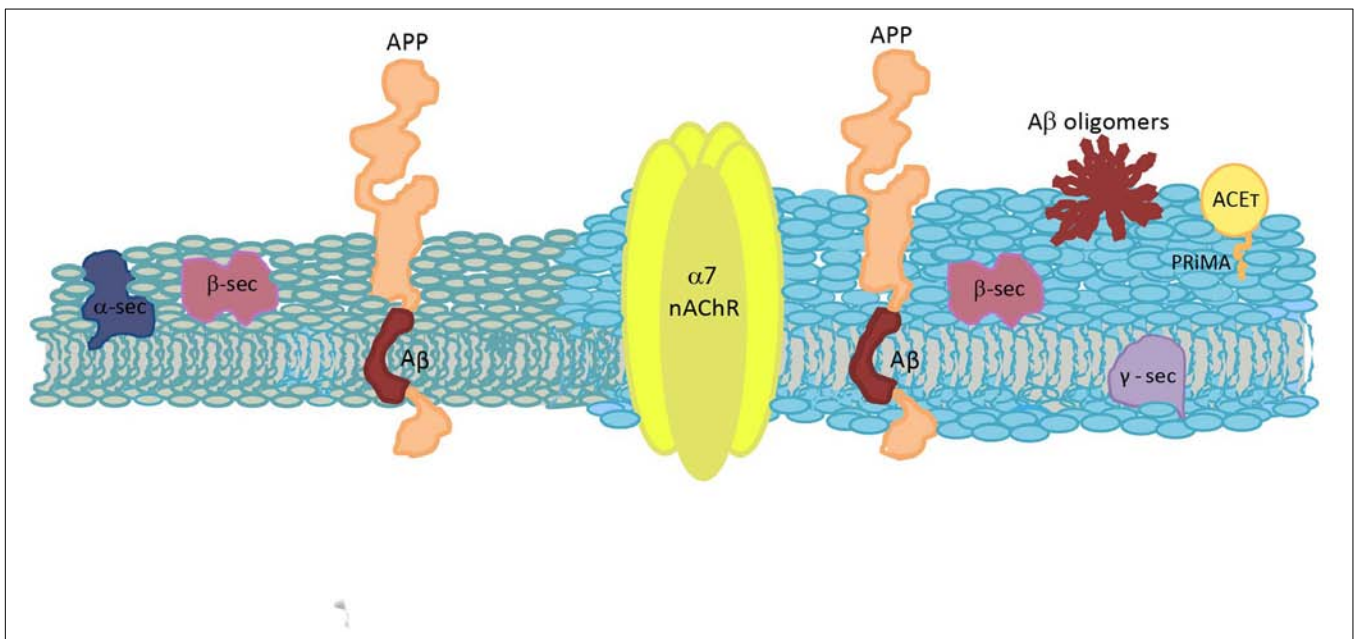

FIGURE 3 | Schematic diagram of a plasma membrane, depicting the spatial relationship between the molecules involved in Aβ synthesis and the cholinergic system. Two different colors are used to represent a raft domain and a liquid-disordered domain (light blue and gray, respectively). APP, amyloid precursor protein; Aβ, amyloid β peptide; α7 nAChR, α7 nicotinic acetylcholine receptor; ACE_T, tetrameric acetylcholinesterase; α-sec, α-secretase; β-sec, β-secretase; γ-sec, γ-secretase; and PRiMA, proline-rich membrane anchor.

maintenance of these receptors within these domains is Chol-dependent (Brusés et al., 2001). Furthermore, in PC-12 cells, a rat pheochromocytoma cell line, α7 nAChR location in raft domains is necessary to regulate cAMP signal through the nicotinic activation, signaling that was altered by Chol depletion (Oshikawa et al., 2003). A similar relation between α7 nAChR location at raft domains and efficiently signaling, with a direct Chol influence, was also observed in CG neurons (Liu et al., 2008). Disruption of raft domains in the same CG neurons increased the mobility of α7 nAChRs in the synaptic space (Fernandes et al., 2010). Disruption of raft domains by removal of Chol and/or SM in rat primary hippocampal neurons slowed the kinetics of α7 nAChR desensitization through increasing the rate of recovery from desensitization and increased the agonist affinity and single-channel conductance (Colón-Sáez and Yakel, 2011). The authors observed the effects of raft domains disruption also on α3β2 nAChRs functionality. These results confirm that, as with muscle nAChR, neuronal nAChR functionality is modulated by its lipid microenvironment with the raft domains integrity a critical factor. On the contrary, α7 nAChR at non-neural tissues, in rat arterial endothelial (RAEC) and human venous endothelial (HUVEC), was found to occur in non-raft subcellular membrane fractions (Peña et al., 2011).

CONCLUSION

Alzheimer's disease is a progressive neurodegenerative condition, the etiopathogenic mechanisms of which are not totally understood. Due to its multifactorial character, the development of new drugs and effective treatments is still a challenge (Dineley, 2007). Here, we intended to focus only in the processes related to this disease that occur in the cell membrane, which allows to observe the multiple crosslinking between specific lipids and the membrane proteins involved in the amyloid process. In a dry human brain, half of its weight corresponds to lipids, molecules with great chemical diversity and complex dynamical heterogeneities (Piomelli et al., 2007). Thus, it is not surprising that through the years more and more biological functions are being related to them. Raft domains are implicated in several of the events involved in AD. Chol is a very important lipid at synaptic membranes (Barrantes, 2007) and it is also a principal author in AD, together with other lipids such as GM1, SM or PA. It is not surprising that APP, Aβ, nAChR and G4-PRiMA all have Chol-recognition amino acid sequences. Although there are still some controversies, there is no doubt that APP processing, Aβ production and Aβ action are intimately related to raft domains, and that the cholinergic system function is highly conditioned by both raft domains and Aβ. A continuous crosstalk between amyloid processing and cholinergic signaling occurs at physiological and pathological conditions, and shifting from one condition to the other is triggered by an imbalance in Aβ synthesis, being Chol homeostasis intimately implicated (**Figure 3**). Currently, the only available treatment for AD is a group of drugs that inhibit ACE. A better understanding of Aβ-α7 nAChR interactions and of the implication of Chol in particular, and membrane heterogeneities in general, could allow for a deepening of the understanding of this neurodegenerative pathology and could help define new therapeutic strategies and potential novel molecular targets.

The World Health Organization (WHO) declared dementia as a public health priority (in *Priority Medicines for Europe and the World "A Public Health Approach to Innovation"* by Saloni Tanna). The number of people worldwide with this condition is in continuous growth: whereas in 2010 this number was estimated to be 35.6 million, it is expected to be near 115.4 million in 2050, in line with the view that this number nearly doubles every 20 years. AD is the most common form of dementia and, hence, it has become a major public health problem because of the continuous increase in the age of the population (in fact, in 2050 it is expected that 22% of the world population will be aged 60 and over). Thus, it is imperative to count with specific biomarkers for early stages of the disease, to improve detection and evaluation and, of course, with effective therapies. At present, the only treatment available is symptomatic: ACE inhibitors, like physostigmine, tacrine, donepezil, rivastigmine, and galantamine. Although new knowledge is continuously emerging, until now and as suggested in this work, there is no consensus among the different coexisting hypotheses around this subject, several of which are antagonistic. This fact clearly contributes to the current situation: there is not a single specific AD treatment commercially available. A great variety of molecular targets were proposed for AD treatment, a few of which were explained here (like β and γ-secretases, α7 nAChR and ACE), and plenty of studies have been conducted on them. Much effort has been invested in this area, but more is still required. Science is facing a huge challenge. Further studies that contribute to the description and explanation of the AD etiopathology will be crucial for a final consensus on AD. Multitarget-drug design is an interesting strategy as AD involves a large number of different molecules. And finally, it should not be forgotten that membrane lipids are not just a "sea" where proteins function but, as explained in detail above, they are necessary for the proper function of these proteins. Chol, GM1, SM, among others, are important lipids for AChR function, conformation and membrane stabilization, and also for Aβ processing and Aβ-membrane insertion. Thus, lipid membrane perturbation, and hence, raft domains alteration and membrane signal perturbation, directly impact in several hot points of AD etiopathology and, for this reason, they can also be considered as interesting molecular targets for AD.

AUTHOR CONTRIBUTIONS

CF and SA contributed to the design, analysis, interpretation, and writing of the manuscript.

FUNDING

This work was supported by grants from the Universidad Nacional del Sur (UNS) and Consejo Nacional de Investigaciones Científicas y Técnicas (CONICET) to SA.

REFERENCES

Abad-Rodriguez, J., Ledesma, M. D., Craessaerts, K., Perga, S., Medina, M., Delacourte, A., et al. (2004). Neuronal membrane cholesterol loss enhances amyloid peptide generation. *J. Cell. Biol.* 167, 953–960. doi: 10.1083/jcb.200404149

Addona, G. H., Sandermann, H., and Kloczewiak, M. A. (1998). Where does cholesterol act during activation of the nicotinic acetylcholine receptor? *Biochim. Biophys. Acta* 1370, 299–309. doi: 10.1016/s0005-2736(97)00280-0

Ahyayauch, H., Raab, M., Busto, J. V., Andraka, N., Arrondo, J. L., Masserini, M., et al. (2012). Binding of β-amyloid (1-42) peptide to negatively charged phospholipid membranes in the liquid-ordered state: modeling and experimental studies. *Biophys. J.* 103, 453–463. doi: 10.1016/j.bpj.2012.06.043

Albuquerque, E. X., Pereira, E. F. R., Alkondon, M., and Rogers, S. W. (2009). Mammalian nicotinic acetylcholine receptors: from structure to function. *Physiol. Rev.* 89, 73–120. doi: 10.1152/physrev.00015.2008

Alptüzün, V., Prinz, M., Hörr, V., Scheiber, J., Radacki, K., Fallarero, A., et al. (2010). Interaction of (benzylidene-hydrazono)-1,4-dihydropyridines with beta-amyloid, acetylcholine, and butyrylcholine esterases. *Bioorg. Med. Chem.* 218, 2049–2059. doi: 10.1016/j.bmc.2010.01.002

Alvarez, A., Alarcón, R., Opazo, C., Campos, E. O., Muñoz, F. J., Calderón, F. H., et al. (1998). Stable complexes involving acetylcholinesterase and amyloid-beta peptide change the biochemical properties of the enzyme and increase the neurotoxicity of Alzheimer's fibrils. *J. Neurosci.* 18, 3213–3223. doi: 10.1523/jneurosci.18-09-03213.1998

Andreasen, N., Sjögren, M., and Blennow, K. (2003). CSF markers for Alzheimer's disease: total tau, phospho-tau and Abeta42. *World J. Biol. Psychiatry* 4, 147–155. doi: 10.1080/15622970310029912

Andreasen, T. J., and McNamee, M. G. (1980). Inhibition of ion permeability control properties of acetylcholine receptor from Torpedo californica by long-chain fatty acids. *Biochemistry* 19, 4719–4726. doi: 10.1021/bi00561a027

Annaert, W. G., Levesque, L., Craessaerts, K., Dierinck, I., Snellings, G., Westaway, D., et al. (1999). Presenilin 1 controls gamma-secretase processing of amyloid precursor protein in pre-golgi compartments of hippocampal neurons. *J. Cell. Biol.* 147, 277–294. doi: 10.1083/jcb.147.2.277

Antollini, S. S., and Barrantes, F. J. (1998). Disclosure of discrete sites for phospholipid and sterols at the protein-lipid interface in native acetylcholine receptor-rich membrane. *Biochemistry* 37, 16653–16662. doi: 10.1021/bi9808215

Antollini, S. S., and Barrantes, F. J. (2002). Unique effects of different fatty acid species on the physical properties of the torpedo acetylcholine receptor membrane. *J. Biol. Chem.* 277, 1249–1254. doi: 10.1074/jbc.M106618200

Antollini, S. S., and Barrantes, F. J. (2016). Fatty Acid Regulation of Voltage- and Ligand-Gated Ion Channel Function. *Front. Physiol.* 28:573. doi: 10.3389/fphys.2016.00573

Antollini, S. S., Soto, M. A., Bonini de Romanelli, I., Gutiérrez-Merino, C., Sotomayor, P., and Barrantes, F. J. (1996). Physical state of bulk and protein-associated lipid in nicotinic acetylcholine receptor-rich membrane studied by laurdan generalized polarization and fluorescence energy transfer. *Biophys. J.* 70, 1275–1284. doi: 10.1016/s0006-3495(96)79684-4

Antollini, S. S., Xu, Y., Jiang, H., and Barrantes, F. J. (2005). Fluorescence and molecular dynamics studies of the acetylcholine receptor gammaM4 transmembrane peptide in reconstituted systems. *Mol. Membr. Biol.* 22, 471–483. doi: 10.1080/09687860500367915

Arbor, S. C., Lafontaine, M., and Cumbay, M. (2016). Amyloid-beta Alzheimer targets -protein processing, lipid rafts, and amyloid-beta pores. *Yale J. Biol. Med.* 89, 5–21.

Ariga, T., Kobayashi, K., Hasegawa, A., Kiso, M., Ishida, H., and Miyatake, T. (2001). Characterization of high-affinity binding between gangliosides and amyloid beta-protein. *Arch. Biochem. Biophys.* 388, 225–230. doi: 10.1006/abbi.2001.2304

Arispe, N., Pollard, H. B., and Rojas, E. (1993a). Giant multilevel cation channels formed by Alzheimer disease amyloid beta-protein [A beta P-(1-40)] in bilayer membranes. *Proc. Natl. Acad. Sci. U.S.A.* 90, 10573–10577. doi: 10.1073/pnas.90.22.10573

Arispe, N., Rojas, E., and Pollard, H. B. (1993b). Alzheimer disease amyloid beta protein forms calcium channels in bilayer membranes: blockade by tromethamine and aluminum. *Proc. Natl. Acad. Sci. U.S.A.* 90, 567–571. doi: 10.1073/pnas.90.2.567

Arora, K., Alfulaij, N., Higa, J. K., Panee, J., and Nichols, R. A. (2013). Impact of sustained exposure to β-amyloid on calcium homeostasis and neuronal integrity in model nerve cell system expressing α4β2 nicotinic acetylcholine receptors. *J. Biol. Chem.* 288, 11175–11190. doi: 10.1074/jbc.M113.453746

Ashley, R. H., Harroun, T. A., Hauss, T., Breen, K. C., and Bradshaw, J. P. (2006). Autoinsertion of soluble oligomers of Alzheimer's Abeta(1-42) peptide into cholesterol-containing membranes is accompanied by relocation of the sterol towards the bilayer surface. *BMC. Struct. Biol.* 6:21. doi: 10.1186/1472-6807-6-21

Askarova, S., Yang, X., and Lee, J. C. (2011). Impacts of membrane biophysics in Alzheimer's Disease: from amyloid precursor protein processing to Aβ peptide-induced membrane changes. *Int. J. Alzheimers Dis.* 2011:134971. doi: 10.4061/2011/134971

Atack, J. R., Perry, E. K., Bonham, J. R., Perry, R. H., Tomlinson, B. E., Blessed, G., et al. (1983). Molecular forms of acetylcholinesterase in senile dementia of Alzheimer type: selective loss of the intermediate (10S) form. *Neurosci. Lett.* 40, 199–204. doi: 10.1016/0304-3940(83)90302-6

Auld, D. S., Kornecook, T. J., Bastianetto, S., and Quirion, R. (2002). Alzheimer's disease and the basal forebrain cholinergic system: relations to beta-amyloid peptides, cognition, and treatment strategies. *Prog. Neurobiol.* 68, 209–245. doi: 10.1016/s0301-0082(02)00079-5

Avdulov, N. A., Chochina, S. V., Igbavboa, U., Warden, C. S., Vassiliev, A. V., and Wood, W. G. (1997). Lipid binding to amyloid beta-peptide aggregates: preferential binding of cholesterol as compared with phosphatidylcholine and fatty acids. *J. Neurochem.* 69, 1746–1752. doi: 10.1046/j.1471-4159.1997.69041746.x

Baenziger, J. E., and Corringer, P. J. (2011). 3D structure and allosteric modulation of the transmembrane domain of pentameric ligand-gated ion channels. *Neuropharmacology* 60, 116–125. doi: 10.1016/j.neuropharm.2010.08.007

Baenziger, J. E., and daCosta, C. J. B. (2013). Molecular mechanisms of acetylcholine receptor-lipid interactions: from model membranes to human biology. *Biophys. Rev.* 5, 1–9. doi: 10.1007/s12551-012-0078-77

Baenziger, J. E., Hénault, C. M., Therien, J. P. D., and Sun, J. (2015). Nicotinic acetylcholine receptor-lipid interactions: mechanistic insight and biological function. *Biochim. Biophys. Acta Biomembr.* 1848, 1806–1817. doi: 10.1016/j.bbamem.2015.03.010

Baenziger, J. E., Morris, M., Darsaut, T. E., and Ryan, S. E. (2000). Effect of membrane lipid composition on the conformational equilibria of the Nicotinic acetylcholine receptor. *J. Biol. Chem.* 275, 777–784. doi: 10.1074/jbc.275.2.777

Baenziger, J. E., Ryan, S. E., Goodreid, M. M., Vuong, N. Q., Sturgeon, R. M., and Corrie, J. B. (2008). Lipid composition alters drug action at the Nicotinic acetylcholine receptor. *Mol. Pharmacol.* 73, 880–890. doi: 10.1124/mol.107.039008

Bagatolli, L. A. (2010). Microscopy imaging of membrane domains. *Biochim. Biophys. Acta* 1798:1285. doi: 10.1016/j.bbamem.2010.05.023

Baier, C. J., and Barrantes, F. J. (2007). Sphingolipids are necessary for nicotinic acetylcholine receptor export in the early secretory pathway. *J. Neurochem.* 101, 1072–1084. doi: 10.1111/j.1471-4159.2007.04561.x

Baier, C. J., Fantini, J., and Barrantes, F. J. (2011). Disclosure of cholesterol recognition motifs in transmembrane domains of the human nicotinic acetylcholine receptor. *Sci. Rep.* 1:69. doi: 10.1038/srep00069

Baier, C. J., Gallegos, C. E., Levi, V., and Barrantes, F. J. (2010). Cholesterol modulation of nicotinic acetylcholine receptor surface mobility. *Eur. Biophys* 39, 213–227. doi: 10.1007/s00249-009-0521-522

Banerjee, C., Nyengaard, J. R., Wevers, A., de Vos, R. A., Jansen Steur, E. N., Lindstrom, J., et al. (2000). Cellular expression of alpha7 Nicotinic Acetylcholine receptor protein in the temporal cortex in Alzheimer's and Parkinson's disease - A stereological approach. *Neurobiol. Dis.* 7, 666–672. doi: 10.1006/nbdi.2000.0317

Barenholz, Y. (2004). Sphingomyelin and cholesterol: from membrane biophysics and rafts to potential medical applications. *Subcell. Biochem.* 37, 167–215. doi: 10.1007/978-1-4757-5806-1_5

Barrantes, F. J. (2002). Lipid matters: nicotinic acetylcholine receptor-lipid interactions. *Mol. Membr. Biol.* 219, 277–284. doi: 10.1080/09687680210166226

Barrantes, F. J. (2007). Cholesterol effects on nicotinic acetylcholine receptor. *Neurochem.* 103, 72–80. doi: 10.1111/j.1471-4159.2007.04719.x

Barrantes, F. J. (2010). Cholesterol effects on nicotinic acetylcholine receptor: cellular aspects. *Subcell. Biochem.* 51, 467–487. doi: 10.1007/978-90-481-8622-8_17

Barrantes, F. J. (2015). Phylogenetic conservation of protein-lipid motifs in pentameric ligand-gated ion channels. *Biochim. Biophys. Acta* 1848, 1796–1805. doi: 10.1016/j.bbamem.2015.03.028

Barrantes, F. J., Borroni, V., and Vallés, S. (2010). Neuronal nicotinic acetylcholine receptor – cholesterol crosstalk in Alzheimer's disease. *FEBS Lett.* 584, 1856–1863. doi: 10.1016/j.febslet.2009.11.036

Barrera, N. P., Zhou, M., and Robinson, C. V. (2013). The role of lipids in defining membrane protein interactions: insights from mass spectrometry. *Trends. Cell. Biol.* 23, 1–8. doi: 10.1016/j.tcb.2012.08.007

Barrett, P. J., Song, Y., Horn, W. D., Van Hustedt, E. J., Johanna, M., Hadziselimovic, A., et al. (2012). The amyloid precursor protein has a flexible transmembrane domain and binds cholesterol. *Science.* 336, 1168–1171. doi: 10.1126/science.1219988

Bartolini, M., Bertucci, C., Cavrini, V., and Andrisano, V. (2003). Beta-Amyloid aggregation induced by human acetylcholinesterase: inhibition studies. *Biochem. Pharmacol.* 65, 407–416. doi: 10.1016/s0006-2952(02)01514-9

Bartus, R. T., Dean, R. L., Beer, B., and Lippa, A. S. (1982). The cholinergic hypothesis of geriatric memory dysfunction. *Science* 1217, 408–414. doi: 10.1126/science.7046051

Bazzi, M. D., and Nelsestuen, G. L. (1996). Extensive segregation of acidic phospholipids in membranes induced by protein kinase C and related proteins. *Biochemistry* 32, 7961–7969. doi: 10.1021/bi00246a013

Beel, A. J., Sakakura, M., Barrett, P. J., and Sanders, C. R. (2010). Direct binding of cholesterol to the amyloid precursor protein: an important interaction in lipid-Alzheimer's disease relationships? *Biochim. Biophys. Acta* 1801, 975–982. doi: 10.1016/j.bbalip.2010.03.008

Behl, C., Davis, J. B., Lesley, R., and Schubert, D. (1994). Hydrogen peroxide mediates amyloid beta protein toxicity. *Cell* 77, 817–827. doi: 10.1016/0092-8674(94)90131-7

Berg, D. K., and Conroy, W. G. (2002). Nicotinic alpha 7 receptors: synaptic options and downstream signaling in neurons. *J. Neurobiol.* 53, 512–523. doi: 10.1002/neu.10116

Bermúdez, V., Antollini, S. S., Nievas, G. A. F., Aveldaño, M. I., and Barrantes, F. J. (2010). Partition profile of the nicotinic acetylcholine receptor in lipid domains upon reconstitution. *J. Lipid Res.* 51, 2629–2641. doi: 10.1194/jlr.M005132

Bieschke, J., Zhang, Q., Powers, E. T., Lerner, R. A., and Kelly, J. W. (2005). Oxidative metabolites accelerate Alzheimer's amyloidogenesis by a two-step mechanism, eliminating the requirement for nucleation. *Biochemistry* 44, 4977–4983. doi: 10.1021/bi0501030

Bigl, V., Woolf, N. J., and Butcher, L. L. (1982). Cholinergic projections from the basal forebrain to frontal, parietal, temporal, occipital, and cingulate cortices: a combined fluorescent tracer and acetylcholinesterase analysis. *Brain Res. Bull.* 8, 727–749. doi: 10.1016/0361-9230(82)90101-0

Blanton, M. P., Xie, Y., Dangott, L. J., and Cohen, J. B. (1999). The steroid promegestone is a noncompetitive antagonist of the Torpedo nicotinic acetylcholine receptor that interacts with the lipid-protein interface. *Mol. Pharmacol.* 55, 269–278. doi: 10.1124/mol.55.2.269

Bodovitz, S., and Klein, W. L. (1996). Cholesterol Modulates alpha-Secretase Cleavage of Amyloid Precursor Protein. *J. Biol. Chem.* 271, 4436–4440. doi: 10.1074/jbc.271.8.4436

Bonini, I. C., Antollini, S. S., Gutiérrez-Merino, C., and Barrantes, F. J. (2002). Sphingomyelin composition and physical asymmetries in native acetylcholine receptor-rich membranes. *Eur. Biophys. J.* 31, 417–427. doi: 10.1007/s00249-002-0230-236

Borroni, V., Baier, C. J., Lang, T., Bonini, I., White, M. M., Garbus, I., et al. (2007). Cholesterol depletion activates rapid internalization of submicron-sized acetylcholine receptor domains at the cell membrane. *Mol. Membr. Biol.* 24, 1–15. doi: 10.1080/09687860600903387

Borroni, V., and Barrantes, F. J. (2011). Cholesterol Modulates the Rate and Mechanism of Acetylcholine Receptor Internalization. *J Biol Chem.* 286, 17122–17132. doi: 10.1074/jbc.M110.211870

Bouzat, C., and Barrantes, F. J. (1996). Modulation of muscle nicotinic acetylcholine receptors by the glucocorticoid hydrocortisone. Possible allosteric mechanism of channel blockade. *J. Biol. Chem.* 271, 25835–25841. doi: 10.1074/jbc.271.42.25835

Bouzat, C. B., Lacorazza, H. D., de Jiménez Bonino, M. B., and Barrantes, F. J. (1993). Effect of chemical modification of extracellular histidyl residues on the channel properties of the nicotinic acetylcholine receptor. *Pflugers. Arch.* 423, 365–371. doi: 10.1007/bf00374929

Bowen, D. M., Smith, C. B., White, P., and Davison, A. N. (1976). Neurotransmitter-related enzymes and indices of hypoxia in senile dementia and other abiotrophies. *Brain* 99, 459–496. doi: 10.1093/brain/99.3.459

Boyd-Kimball, D., Castegna, A., Sultana, R., Poon, H. F., Petroze, R., Lynn, B. C., et al. (2005). Proteomic identification of proteins oxidized by Abeta(1-42) in synaptosomes: implications for Alzheimer's disease. *Brain Res.* 1044, 206–215. doi: 10.1016/j.brainres.2005.02.086

Brannigan, G., Hénin, J., Law, R., Eckenhoff, R., and Klein, M. L. (2008). Embedded cholesterol in the nicotinic acetylcholine receptor. *Proc. Natl. Acad. Sci. U.S.A.* 105, 14418–14423. doi: 10.1073/pnas.0803029105

Brown, D. A. (2006). Acetylcholine. *Br. J. Pharmacol.* 147(Suppl. 1), S120–S126. doi: 10.1038/sj.bjp.0706474

Brown, D. A., and London, E. (2000). Structure and function of sphingolipid- and cholesterol-rich membrane rafts. *J. Biol. Chem.* 275, 17221–17224. doi: 10.1074/jbc.r000005200

Brusés, J. L., Chauvet, N., and Rutishauser, U. (2001). Membrane lipid rafts are necessary for the maintenance of the (alpha)7 nicotinic acetylcholine receptor in somatic spines of ciliary neurons. *J. Neurosci.* 21, 504–512. doi: 10.1523/jneurosci.21-02-00504.2001

Burke, D. A., Heshmati, P., Kholdebarin, E., and Levin, E. D. (2014). Decreasing nicotinic receptor activity and the spatial learning impairment caused by the NMDA glutamate antagonist dizocilpine in rats. *Eur. J. Pharmacol.* 741, 132–139. doi: 10.1016/j.ejphar.2014.07.030

Burns, M., and Duff, K. (2002). Cholesterol in Alzheimer's disease and tauopathy. *Ann. N. Y. Acad. Sci.* 977, 367–375. doi: 10.1111/j.1749-6632.2002.tb04839.x

Butler, D. H., and McNamee, M. G. (1993). FTIR analysis of nicotinic acetylcholine receptor secondary structure in reconstituted membranes. *Biochim. Biophys. Acta* 11150, 17–24. doi: 10.1016/0005-2736(93)90116-h

Butterfield, D. A., and Boyd-Kimball, D. (2005). The critical role of methionine 35 in Alzheimer's amyloid beta-peptide (1-42)-induced oxidative stress and neurotoxicity. *Biochim. Biophys. Acta* 1703, 149–156. doi: 10.1016/j.bbapap.2004.10.014

Butterfield, D. A., Swomley, A. M., and Sultana, R. (2013). Amyloid β-Peptide (1–42)-induced oxidative stress in Alzheimer disease: importance in disease Pathogenesis and Progression. *Antioxid. Redox. Signal.* 19, 823–835. doi: 10.1089/ars.2012.5027

Campagna, J. A., and Fallon, J. (2006). Lipid rafts are involved in C95 (4,8) agrin fragment-induced acetylcholine receptor clustering. *Neuroscience* 138, 123–132. doi: 10.1016/j.neuroscience.2005.11.019

Campanari, M. L., García-Ayllón, M. S., Belbin, O., Galcerán, J., Lleó, A., and Sáez-Valero, J. (2014). Acetylcholinesterase modulates presenilin-1 levels and γ-secretase activity. *J. Alzheimers Dis.* 41, 911–924. doi: 10.3233/JAD-140426

Cartaud, A., Stetzkowski-Marden, F., Maoui, A., and Cartaud, J. (2011). Agrin triggers the clustering of raft-associated acetylcholine receptors through actin cytoskeleton reorganization. *Biol. Cell.* 103, 287–301. doi: 10.1042/BC20110018

Cascella, R., Evangelisti, E., Bigi, A., Becatti, M., Fiorillo, C., Stefani, M., et al. (2017). Soluble oligomers require a ganglioside to trigger neuronal calcium overload. *J. Alzheimers. Dis.* 60, 923–938. doi: 10.3233/JAD-170340

Cecchi, C., Nichino, D., Zampagni, M., Bernacchioni, C., Evangelisti, E., Pensal, A., et al. (2009). A protective role for lipid raft cholesterol against amyloid-induced membrane damage in human neuroblastoma cells. *Biochim. Biophys. Acta* 1788, 2204–2216. doi: 10.1016/j.bbamem.2009.07.019

Champtiaux, N., Gotti, C., Cordero-Erausquin, M., David, D. J., Przybylski, C., Léna, C., et al. (2003). Subunit composition of functional nicotinic receptors in dopaminergic neurons investigated with knock-out mice. *J. Neurosci.* 23, 7820–7829. doi: 10.1523/jneurosci.23-21-07820.2003

Chang, T., Yamauchi, Y., Hasan, M. T., and Chang, C. (2017). Cellular cholesterol homeostasis and Alzheimer's disease. *J. Lipid. Res.* 58, 2239–2254. doi: 10.1194/jlr.R075630

Changeux, J. P., and Edelstein, S. J. (1998). Allosteric receptors after 30 years. *Neuron* 21, 959–980. doi: 10.1016/s0896-6273(00)80616-9

Cheignon, C., Tomas, M., Bonnefont-Rousselot, D., Faller, P., Hureau, C., and Collin, F. (2018). Oxidative stress and the amyloid beta peptide in Alzheimer's disease. *Redox Biol.* 14, 450–464. doi: 10.1016/j.redox.2017.10.014

Chernomordik, L. V., and Zimmerberg, J. (1995). Bending membranes to the task: structural intermediates in bilayer fusion. *Curr. Opin. Struct. Biol.* 5, 541–547. doi: 10.1016/0959-440x(95)80041-7

Chochina, S. V., Avdulov, N. A., Igbavboa, U., Cleary, J. P., O'Hare, E. O., and Wood, W. G. (2001). Amyloid beta-peptide1-40 increases neuronal membrane fluidity: role of cholesterol and brain region. *J. Lipid Res.* 42, 1292–1297.

Choo-Smith, L. P., Garzon-Rodriguez, W., Glabe, C. G., and Surewicz, W. K. (1997). Acceleration of amyloid fibril formation by specific binding of Abeta-(1-40) peptide to ganglioside-containing membrane vesicles. *J. Biol. Chem.* 272, 22987–22990. doi: 10.1074/jbc.272.37.22987

Chyung, J. H., Raper, D. M., and Selkoe, D. J. (2005). Gamma-secretase exists on the plasma membrane as an intact complex that accepts substrates and effects intramembrane cleavage. *J. Biol. Chem.* 280, 4383–4392. doi: 10.1074/jbc.M409272200

Clarke, P. B. (1992). The fall and rise of neuronal alpha-bungarotoxin binding proteins. *Trends Pharmacol. Sci.* 113, 407–413. doi: 10.1016/0165-6147(92)90125-p

Colón-Sáez, J. O., and Yakel, J. L. (2011). The α7 nicotinic acetylcholine receptor function in hippocampal neurons is regulated by the lipid composition of the plasma membrane. *J. Physiol.* 589, 3163–3174. doi: 10.1113/jphysiol.2011.209494

Contestabile, A. (2011). The history of the cholinergic hypothesis. *Behav. Brain Res.* 221, 334–340. doi: 10.1016/j.bbr.2009.12.044

Cooper, S. T., Harkness, P. C., Baker, E. R., and Millar, N. S. (1999). Up-regulation of cell-surface alpha4beta2 neuronal Nicotinic receptors by lower temperature and expression of chimeric subunits. *J. Biol. Chem.* 274, 27145–27152. doi: 10.1074/jbc.274.38.27145

Corbin, J., Wang, H. H., and Blanton, M. P. (1998). Identifying the cholesterol binding domain in the nicotinic acetylcholine receptor with [125I] azido-cholesterol. *Biochim. Biophys. Acta* 1414, 65–74. doi: 10.1016/s0005-2736(98)00153-9

Cordy, J. M., Hooper, N. M., and Turner, A. J. (2006). The involvement of lipid rafts in Alzheimer's disease. *Mol. Membr. Biol.* 23, 111–122. doi: 10.1080/09687860500496417

Counts, S. E., He, B., Che, S., Ikonomovic, M. D., DeKosky, S. T., Ginsberg, S. D., et al. (2007). Alpha7 nicotinic receptor up-regulation in cholinergic basal forebrain neurons in Alzheimer disease. *Arch. Neurol.* 64, 1771–1776. doi: 10.1001/archneur.64.12.1771

Court, J. A., Piggott, M. A., Lloyd, S., Cookson, N., Ballard, C. G., McKeith, I. G., et al. (2000). Nicotine binding in human striatum: elevation in schizophrenia and reductions in dementia with Lewy bodies, Parkinson's disease and Alzheimer's disease and in relation to neuroleptic medication. *Neuroscience* 98, 79–87. doi: 10.1016/s0306-4522(00)00071-3

Coyle, J. T., Price, D. L., and DeLong, M. R. (1983). Alzheimer's disease: a disorder of cortical cholinergic innervation. *Science* 219, 1184–1190. doi: 10.1126/science.6338589

Criado, M., Eibl, H., and Barrantes, F. J. (1984). Functional properties of the acetylcholine receptor incorporated in model lipid membranes. Differential effects of chain length and head group of phospholipids on receptor affinity states and receptor-mediated ion translocation. *J. Biol. Chem.* 259, 9188–9198.

Criado, M., Vaz, W. L., Barrantes, F. J., and Jovin, T. M. (1982). Translational diffusion of acetylcholine receptor (monomeric and dimeric forms) of Torpedo marmorata reconstituted into phospholipid bilayers studied by fluorescence recovery after photobleaching. *Biochemistry* 21, 5750–5755. doi: 10.1021/bi00266a004

Cutler, R. G., Kelly, J., Storie, K., Pedersen, W. A., Tammara, A., Hatanpaa, K., et al. (2004). Involvement of oxidative stress-induced abnormalities in ceramide and cholesterol metabolism in brain aging and Alzheimer's disease. *Proc. Natl. Acad. Sci. U.S.A.* 101, 2070–2075. doi: 10.1073/pnas.0305799101

daCosta, C. J., Ogrel, A. A., McCardy, E. A., Blanton, M. P., and Baenziger, J. E. (2002). Lipid-protein interactions at the nicotinic acetylcholine receptor. A functional coupling between Nicotinic receptors and Phosphatidic acid-containing lipid bilayers. *J. Biol. Chem.* 277, 201–208. doi: 10.1074/jbc.M108341200

daCosta, C. J., Wagg, I. D., McKay, M. E., and Baenziger, J. E. (2004). Phosphatidic acid and phosphatidylserine have distinct structural and functional interactions with the nicotinic acetylcholine receptor. *J. Biol. Chem.* 279, 14967–14974. doi: 10.1074/jbc.M310037200

daCosta, C. J. B., and Baenziger, J. E. (2009). A lipid-dependent uncoupled conformation of the acetylcholine receptor. *J. Biol. Chem.* 284, 17819–17825. doi: 10.1074/jbc.M900030200

Dajas-Bailador, F., and Wonnacott, S. (2004). Nicotinic acetylcholine receptors and the regulation of neuronal signalling. *Trends. Pharmacol. Sci.* 25, 317–324. doi: 10.1016/s0165-6147(04)00118-x

Daleke, D. L. (2003). Regulation of transbilayer plasma membrane phospholipid asymmetry. *J. Lipid Res.* 44, 233–242. doi: 10.1194/jlr.r200019-jlr200

D'Andrea, M. R., and Nagele, R. G. (2006). Targeting the alpha 7 nicotinic acetylcholine receptor to reduce amyloid accumulation in Alzheimer's disease pyramidal neurons. *Curr. Pharm. Des.* 12, 677–684. doi: 10.2174/138161206775474224

Daugherty, B. L., and Green, S. A. (2001). Endosomal sorting of amyloid precursor protein-P-selectin chimeras influences secretase processing. *Traffic* 2, 908–916. doi: 10.1034/j.1600-0854.2001.21206.x

Davies, P., and Maloney, A. J. (1976). Selective loss of central cholinergic neurons in Alzheimer's disease. *Lancet* 2:1403. doi: 10.1016/s0140-6736(76)91936-x

de Almeida, R. F., Loura, L. M., Prieto, M., Watts, A., Fedorov, A., and Barrantes, F. J. (2004). Cholesterol modulates the organization of the gammaM4 transmembrane domain of the muscle nicotinic acetylcholine receptor. *Biophys. J.* 86, 2261–2272. doi: 10.1016/S0006-3495(04)74284-74288

Deutsch, S. I., Burket, J. A., and Benson, A. D. (2014). Targeting the α7 nicotinic acetylcholine receptor to prevent progressive dementia and improve cognition in adults with Down's syndrome. *Prog. Neuropsychopharmacol. Biol. Psychiatry* 254, 131–139. doi: 10.1016/j.pnpbp.2014.05.011

Deutsch, S. I., Burket, J. A., Benson, A. D., and Urbano, M. R. (2016). The 15q13.3 deletion syndrome: Deficient α(7)-containing nicotinic acetylcholine receptor-mediated neurotransmission in the pathogenesis of neurodevelopmental disorders. *Prog. Neuropsychopharmacol. Biol Psychiatry* 64, 09–17. doi: 10.1016/j.pnpbp.2015.08.001

Di Scala, C., Baier, C. J., Evans, L. S., Williamson, P. T. F., Fantini, J., and Barrantes, F. J. (2017). Relevance of CARC and CRAC Cholesterol-Recognition Motifs in the Nicotinic Acetylcholine Receptor and Other Membrane-Bound Receptors. *Curr. Top. Membr.* 80, 3–23. doi: 10.1016/bs.ctm.2017.05.001

Di Scala, C., Chahinian, H., Yahi, N., Garmy, N., and Fantini, J. (2014). Interaction of Alzheimer's β-amyloid peptides with cholesterol: mechanistic insights into amyloid pore formation. *Biochemistry* 53, 4489–4502. doi: 10.1021/bi500373k

Di Scala, C., Yahi, N., Boutemeur, S., Flores, A., Rodriguez, L., Chahinian, H., et al. (2016). Common molecular mechanism of amyloid pore formation by Alzheimer's β-amyloid peptide and α-synuclein. *Sci. Rep.* 29:28781. doi: 10.1038/srep28781

Di Scala, C., Yahi, N., Lelièvre, C., Garmy, N., Chahinian, H., and Fantini, J. (2013). Biochemical identification of a linear cholesterol-binding domain within Alzheimer's β amyloid peptide. *ACS Chem. Neurosci.* 4, 509–517. doi: 10.1021/cn300203a

Dickey, A. N., and Faller, R. (2008). Behavioral differences between Phosphatidic acid and Phosphatidylcholine in the Presence of the Nicotinic Acetylcholine receptor. *Biophys. J.* 95, 5637–5647. doi: 10.1529/biophysj.108.136895

Dies, H., Toppozini, L., and Rheinstädter, M. C. (2014). The interaction between amyloid-β peptides and anionic lipid membranes containing cholesterol and melatonin. *PLoS One* 9:e99124. doi: 10.1371/journal.pone.0099124

Dineley, K. T. (2007). Beta-amyloid peptide–nicotinic acetylcholine receptor interaction: the two faces of health and disease. *Front. Biosci.* 12:5030–5038.

Dineley, K. T., Bell, K. A., Bui, D., and Sweatt, J. D. (2002). Beta -Amyloid peptide activates alpha 7 nicotinic acetylcholine receptors expressed in Xenopus oocytes. *J. Biol. Chem.* 277, 25056–25061. doi: 10.1074/jbc.M200066200

Dineley, K. T., Westerman, M., Bui, D., Bell, K., Ashe, K. H., and Sweatt, J. D. (2001). Beta-amyloid activates the mitogen-activated protein kinase cascade via hippocampal alpha7 nicotinic acetylcholine receptors: in vitro and in vivo mechanisms related to Alzheimer's disease. *J. Neurosci.* 21, 4125–4133. doi: 10.1523/jneurosci.21-12-04125.2001

Dougherty, J. J., Wu, J., and Nichols, R. A. (2003). Beta-amyloid regulation of presynaptic nicotinic receptors in rat hippocampus and neocortex. *J. Neurosci.* 23, 6740–6747. doi: 10.1523/jneurosci.23-17-06740.2003

Dreger, M., Krauss, M., Herrmann, A., and Hucho, F. (1997). Interactions of the Nicotinic acetylcholine receptor Transmembrane segments with the Lipid Bilayer in Native receptor-rich membranes. *Biochemistry* 36, 839–847. doi: 10.1021/bi960666z

Dukhinova, M., Veremeyko, T., Yung, A. W. Y., Kuznetsova, I. S., Lau, T. Y. B., Kopeikina, E., et al. (2019). Fresh evidence for major brain gangliosides as a target for the treatment of Alzheimer's disease. *Neurobiol. Aging* 77, 128–143. doi: 10.1016/j.neurobiolaging.2019.01.020

Dvir, H., Silman, I., Harel, M., Rosenberry, T. L., and Sussman, J. L. (2010). Acetylcholinesterase: from 3D structure to function. *Chem. Biol. Interact.* 187, 10–22. doi: 10.1016/j.cbi.2010.01.042

Dziewczapolski, G., Glogowski, C. M., Masliah, E., and Heinemann, S. F. (2009). Deletion of the alpha 7 nicotinic acetylcholine receptor gene improves cognitive deficits and synaptic pathology in a mouse model of Alzheimer's disease. *J. Neurosci.* 29, 8805–8815. doi: 10.1523/JNEUROSCI.6159-08.2009

Eckert, G. P., Kirsch, C., Leutz, S., Wood, W. G., and Müller, W. E. (2003). Cholesterol Modulates Amyloid Beta-peptide's Membrane Interactions. *Pharmacopsychiatry* 36(Suppl. 2), S136–S143. doi: 10.1055/s-2003-43059

Ehehalt, R., Keller, P., Haass, C., Thiele, C., and Simons, K. (2003). Amyloidogenic processing of the Alzheimer beta-amyloid precursor protein depends on lipid rafts. *J. Cell. Biol.* 160, 113–123. doi: 10.1083/jcb.200207113

Ellena, J. F., Blazing, M. A., and McNamee, M. G. (1983). Lipid-protein interactions in reconstituted membranes containing Acetylcholine receptor. *Biochemistry* 22, 5523–5535. doi: 10.1021/bi00293a012

Engel, M. F., Khemtémourian, L., Kleijer, C. C., Meeldijk, H. J., Jacobs, J., Verkleij, A. J., et al. (2008). Membrane damage by human islet amyloid polypeptide through fibril growth at the membrane. *Proc. Natl. Acad. Sci. U.S.A.* 105, 6033–6038. doi: 10.1073/pnas.0708354105

Engelman, D. M. (2005). Membranes are more mosaic than fluid. *Nature* 438, 578–580. doi: 10.1038/nature04394

Epand, R. F., Kraayenhof, R., Sterk, G. J., Wong Fong Sang, H. W., and Epand, R. M. (1996). Fluorescent probes of membrane surface properties. *Biochim Biophys Acta* 1284, 191–195.

Fabelo, N., Martín, V., Marín, R., Moreno, D., Ferrer, I., and Díaz, M. (2014). Altered lipid composition in cortical lipid rafts occurs at early stages of sporadic Alzheimer's disease and facilitates APP/BACE1 interactions. *Neurobiol. Aging* 35, 1801–1812. doi: 10.1016/j.neurobiolaging.2014.02.005

Fantini, J., and Barrantes, F. J. (2013). How cholesterol interacts with membrane proteins: an exploration of cholesterol-binding sites including CRAC, CARC, and tilted domains. *Front. Physiol.* 4:31. doi: 10.3389/fphys.2013.00031

Fantini, J., Di Scala, C., Evans, L. S., Williamson, P. T. F., and Barrantes, F. J. (2016). Open a mirror code for protein- cholesterol interactions in the two leaflets of biological membranes. *Sci. Rep.* 26:21907. doi: 10.1038/srep21907

Fantini, J., Di Scala, C., Yahi, N., Troadec, J. D., Sadelli, K., and Chahinian, H. (2014). Bxarotene blocks calcium-permeable ion channels formed by neurotoxic Alzheimer's β-amyloid peptides. *ACS Chem. Neurosci.* 5, 216–224. doi: 10.1021/cn400183w

Farhat, S. M., and Ahmed, T. (2017). Neuroprotective and Neurotoxic implications of α7 Nicotinic Acetylcholine receptor and Aβ Interaction: Therapeutic options in Alzheimer's Disease. *Curr. Drug. Targets* 18, 1537–1544. doi: 10.2174/1389450117666161005145143

Fassbender, K., Masters, C., and Beyreuther, K. (2001). Alzheimer's disease: molecular concepts and therapeutic targets. *Naturwissenschaften* 88, 261–267. doi: 10.1007/s001140100237

Feng, Y., and Wang, X. (2012). Antioxidant therapies for Alzheimer's disease. *Oxid. Med. Cell. Longev.* 2012:472932. doi: 10.1155/2012/472932

Fernandes, C. C., Berg, D. K., and Gómez-Varela, D. (2010). Lateral mobility of nicotinic acetylcholine receptors on neurons is determined by receptor composition, local domain, and cell type. *J. Neurosci.* 30, 8841–8851. doi: 10.1523/JNEUROSCI.6236-09.2010

Fernández Nievas, G. A., Barrantes, F. J., and Antollini, S. S. (2007). Conformation-sensitive steroid and fatty acid sites in the transmembrane domain of the nicotinic acetylcholine receptor. *Biochemistry* 46, 3503–3512. doi: 10.1021/bi061388z

Fernández Nievas, G. A., Barrantes, F. J., and Antollini, S. S. (2008). Modulation of nicotinic acetylcholine receptor conformational state by free fatty acids and steroids. *J. Biol. Chem.* 283, 21478–21486. doi: 10.1074/jbc.M800345200

Fernández-Ballester, G., Castresana, J., Fernandez, A. M., Arrondo, J. L., Ferragut, J. A., and Gonzalez-Ros, J. M. (1994). Role of cholesterol as a structural and functional effector of the nicotinic acetylcholine receptor. *Biochem. Soc. Trans.* 122, 776–780. doi: 10.1042/bst0220776

Fishman, E. B., Siek, G. C., MacCallum, R. D., Bird, E. D., Volicer, L., and Marquis, J. K. (1986). Distribution of the molecular forms of acetylcholinesterase in human brain: alterations in dementia of the Alzheimer type. *Ann. Neurol.* 119, 246–252. doi: 10.1002/ana.410190305

Fong, T. M., and McNamee, M. G. (1986). Correlation between acetylcholine receptor function and structural properties of membranes. *Biochemistry* 25, 830–840. doi: 10.1021/bi00352a015

Fonseca, A. C., Moreira, P. I., Oliveira, C. R., Cardoso, S. M., Pinton, P., and Pereira, C. F. (2015). Amyloid-Beta disrupts calcium and redox homeostasis in brain endothelial cells. *Mol. Neurobiol* 51, 610–622. doi: 10.1007/s12035-014-8740-8747

Frears, E. R., Stephens, D. J., Walters, C. E., Davies, H., and Austen, B. M. (1999). The role of cholesterol in the biosynthesis of beta-amyloid. *Neuroreport* 10, 1699–1705. doi: 10.1097/00001756-199906030-00014

Fucile, S. (2004). Ca^{2+} permeability of nicotinic acetylcholine receptors. *Cell. Calcium* 35, 1–8. doi: 10.1016/j.ceca.2003.08.006

Fukaya, T., Gondaira, T., Kashiyae, Y., Kotani, S., Ishikura, Y., Fujikawa, S., et al. (2007). Arachidonic acid preserves hippocampal neuron membrane fluidity in senescent rats. *Neurobiol. Aging* 28, 1179–1186. doi: 10.1016/j.neurobiolaging.2006.05.023

Fukunaga, S., Ueno, H., Yamaguchi, T., Yano, Y., Hoshino, M., and Matsuzaki, K. (2012). GM1 cluster mediates formation of toxic Aβ fibrils by providing hydrophobic environments. *Biochemistry* 51, 8125–8131. doi: 10.1021/bi300839u

Garbus, I., Bouzat, C., and Barrantes, F. J. (2001). Steroids differentially inhibit the nicotinic acetylcholine receptor. *Neuroreport* 12, 227–231. doi: 10.1097/00001756-200102120-00010

Garbus, I., Roccamo, A. M., and Barrantes, F. J. (2002). Identification of threonine 422 in transmembrane domain alpha M4 of the nicotinic acetylcholine receptor as a possible site of interaction with hydrocortisone. *Neuropharmacology* 43, 65–73. doi: 10.1016/s0028-3908(02)00068-0

García-Ayllón, M., Campanari, M., Montenegro, M., Cuchillo-ibáñez, I., Belbin, O., Lleó, A., et al. (2014). Neurobiology of aging Presenilin-1 influences processing of the acetylcholinesterase membrane anchor PRiMA. *Neurobiol. Aging* 35, 1526–1536. doi: 10.1016/j.neurobiolaging.2014.01.147

Geula, C., and Mesulam, M. (1989). Special properties of cholinesterases in the cerebral cortex of Alzheimer's disease. *Brain Res.* 498, 185–189. doi: 10.1016/0006-8993(89)90419-8

Ghoneim, M. M., and Mewaldt, S. P. (1977). Studies on human memory: the interactions of diazepam, scopolamine, and physostigmine. *Psychopharmacology* 52, 1–6. doi: 10.1007/bf00426592

Ghribi, O., Larsen, B., Schrag, M., and Herman, M. M. (2006). High cholesterol content in neurons increases BACE, β -amyloid, and phosphorylated tau levels in rabbit hippocampus. *Exp. Neurol.* 200, 460–467. doi: 10.1016/j.expneurol.2006.03.019

Gilbert, R. J. (2016). Protein-lipid interactions and non-lamellar lipidic structures in membrane pore formation and membrane fusion. *Biochim. Biophys. Acta* 1858, 487–499. doi: 10.1016/j.bbamem.2015.11.026

Gilbert, R. J., Dalla Serra, M., Froelich, C. J., Wallace, M. I., and Anderluh, G. (2014). Membrane pore formation at protein-lipid interfaces. *Trends Biochem. Sci.* 39, 510–516. doi: 10.1016/j.tibs.2014.09.002

Giniatullin, R., Nistri, A., and Yakel, J. L. (2005). Desensitization of nicotinic ACh receptors: shaping cholinergic signaling. *Trends. Neurosci.* 28, 371–378. doi: 10.1016/j.tins.2005.04.009

Gong, J. S., Sawamura, N., Zou, K., Sakai, J., Yanagisawa, K., and Michikawa, M. (2002). Amyloid beta-protein affects cholesterol metabolism in cultured neurons: implications for pivotal role of cholesterol in the amyloid cascade. *Neurosci. Res.* 70, 438–446. doi: 10.1002/jnr.10347

Goñi, F. M. (2014). The basic structure and dynamics of cell membranes?: an update of the Singer - Nicolson model. *Biochim. Biophys. Acta* 1838, 1467–1476. doi: 10.1016/j.bbamem.2014.01.006

Gotti, C., Clementi, F., Fornari, A., Gaimarri, A., Guiducci, S., Manfredi, I., et al. (2009). Structural and functional diversity of native brain neuronal nicotinic receptors. *Biochem. Pharmacol.* 78, 703–711. doi: 10.1016/j.bcp.2009.05.024

Gotti, C., Moretti, M., Gaimarri, A., Zanardi, A., Clementi, F., and Zoli, M. (2007). Heterogeneity and complexity of native brain nicotinic receptors. *Biochem. Pharmacol.* 74, 1102–1111. doi: 10.1016/j.bcp.2007.05.023

Gotti, C., Riganti, L., Vailati, S., and Clementi, F. (2006b). Brain neuronal nicotinic receptors as new targets for drug discovery. *Curr. Pharm. Des.* 12, 407–428. doi: 10.2174/138161206775474486

Gotti, C., Zoli, M., and Clementi, F. (2006a). Brain nicotinic acetylcholine receptors: native subtypes and their relevance. *Trends Pharmacol. Sci.* 27, 482–491. doi: 10.1016/j.tips.2006.07.004

Götz, J., Schild, A., Hoerndli, F., and Pennanen, L. (2004). Amyloid-induced neurofibrillary tangle formation in Alzheimer's disease: insight from transgenic mouse and tissue-culture models. *Int. J. Dev. Neurosci.* 22, 453–465. doi: 10.1016/j.ijdevneu.2004.07.013

Graham, A. J., Martin-Ruiz, C. M., Teaktong, T., Ray, M. A., and Court, J. A. (2002). Human brain nicotinic receptors, their distribution and participation in neuropsychiatric disorders. *Curr. Drug. Targets CNS Neurol. Disord.* 4, 387–397. doi: 10.2174/1568007023339283

Greenfield, J. P., Tsai, J., Gouras, G. K., Hai, B., Thinakaran, G., Checler, F., et al. (1999). Endoplasmic reticulum and trans-Golgi network generate distinct populations of Alzheimer beta-amyloid peptides. *Proc. Natl. Acad. Sci. U.S.A.* 96, 742–747. doi: 10.1073/pnas.96.2.742

Grimm, M. O., Grimm, H. S., and Hartmann, T. (2007). Amyloid beta as a regulator of lipid homeostasis. *Trends. Mol. Med.* 13, 337–344. doi: 10.1016/j.molmed.2007.06.004

Grimm, M. O., Grimm, H. S., Pätzold, A. J., Zinser, E. G., Halonen, R., Duering, M., et al. (2005). Regulation of cholesterol and sphingomyelin metabolism by amyloid- β and presenilin. *Nat. Cell. Biol.* 7, 1118–1123. doi: 10.1038/ncb1313

Grisaru, D., Sternfeld, M., Eldor, A., Glick, D., and Soreq, H. (1999). Structural roles of acetylcholinesterase variants in biology and pathology. *Eur. J. Biochem.* 264, 672–686. doi: 10.1046/j.1432-1327.1999.00693.x

Gu, L., and Guo, Z. (2013). Alzheimer's Aβ42 and Aβ40 peptides form interlaced amyloid fibrils. *J. Neurochem.* 126, 305–311. doi: 10.1111/jnc.12202

Guillem, K., Bloem, B., Poorthuis, R. B., Loos, M., Smit, A. B., Maskos, U., et al. (2011). Nicotinic acetylcholine receptor β2 subunits in the medial prefrontal cortex control attention. *Science* 333, 888–891. doi: 10.1126/science.1207079

Gylys, K. H., Fein, J. A., Yang, F., Miller, C. A., and Cole, G. M. (2007). Increased cholesterol in Abeta-positive nerve terminals from Alzheimer's disease cortex. *Neurobiol. Aging* 28, 8–17. doi: 10.1016/j.neurobiolaging.2005.10.018

Gyure, K. A., Durham, R., Stewart, W. F., Smialek, J. E., and Troncoso, J. C. (2001). Intraneuronal abeta-amyloid precedes development of amyloid plaques in Down syndrome. *Arch. Pathol. Lab. Med.* 125, 489–492.

Haass, C. (1996). The molecular significance of amyloid beta-peptide for Alzheimer's disease. *Eur. Arch. Psychiatry. Clin. Neurosci.* 246, 118–123.

Haass, C., Kaether, C., Thinakaran, G., and Sisodia, S. (2012). Trafficking and Proteolytic Processing of APP. *Cold. Spring. Harb. Perspect. Med.* 2, 1–25. doi: 10.1101/cshperspect.a006270

Hamouda, A. K., Chiara, D. C., Sauls, D., Cohen, J. B., and Blanton, M. P. (2006). Cholesterol interacts with transmembrane alpha-helices M1, M3, and M4 of the Torpedo nicotinic acetylcholine receptor: photolabeling studies using [3H]Azicholesterol. *Biochemistry* 45, 976–986. doi: 10.1021/bi051978h

Hampel, H., Mesulam, M. M., Cuello, A. C., Farlow, M. R., Giacobini, E., and Grossberg, G. T. (2018). The cholinergic system in the pathophysiology and treatment of Alzheimer's disease. *Brain* 141, 1917–1933. doi: 10.1093/brain/awy132

Hardy, J. A., and Allsop, D. (1991). Amyloid deposition as the central event in the aetiology of Alzheimer's disease. *Trends. Pharmacol.* 12, 383–388. doi: 10.1016/0165-6147(91)90609-v

Hardy, J. A., and Higgins, G. A. (1992). Alzheimer's Disease?: the amyloid cascade hypothesis. *Science* 256, 184–185.

Harris, J. R. (2008). Cholesterol binding to amyloid-b fibrils: a TEM study. *Micron* 39, 1192–1196. doi: 10.1016/j.micron.2008.05.001

Hellström-Lindahl, E., Court, J., Keverne, J., Svedberg, M., Lee, M., Marutle, A., et al. (2004a). Nicotine reduces A beta in the brain and cerebral vessels of APPsw mice. *Eur. J. Neurosci.* 19, 2703–2710. doi: 10.1111/j.0953-816X.2004.03377.x

Hellström-Lindahl, E., Mousavi, M., Ravid, R., and Nordberg, A. (2004b). Reduced levels of Abeta 40 and Abeta 42 in brains of smoking controls and Alzheimer's patients. *Neurobiol. Dis.* 15, 351–360. doi: 10.1016/j.nbd.2003.11.024

Hellström-Lindahl, E., Mousavi, M., Zhang, X., Ravid, R., and Nordberg, A. (1999). Regional distribution of nicotinic receptor subunit mRNAs in human brain: comparison between Alzheimer and normal brain. *Brain Res. Mol. Brain. Res.* 661, 94–103. doi: 10.1016/s0169-328x(99)00030-3

Hénault, C. M., Sun, J., Therien, J. P., daCosta, C. J., Carswell, C. L., Labriola, J. M., et al. (2015). The role of the M4 lipid-sensor in the folding, trafficking, and allosteric modulation of nicotinic acetylcholine receptors. *Neuropharmacology* 296, 157–168. doi: 10.1016/j.neuropharm.2014.11.011

Henderson, Z., Boros, A., Janzso, G., Westwood, A. J., Monyer, H., and Halasy, K. (2005). Somato-dendritic nicotinic receptor responses recorded *in vitro* from the medial septal diagonal band complex of the rodent. *J. Physiol. Lond.* 562, 165–182. doi: 10.1113/jphysiol.2004.070300

Henderson, Z., Matto, N., John, D., Nalivaeva, N. N., and Turner, A. J. (2010). Co-localization of PRiMA with acetylcholinesterase in cholinergic neurons of rat brain: an immunocytochemical study. *Brain Res.* 1344, 34–42. doi: 10.1016/j.brainres.2010.05.022

Herrup, K. (2015). The case for rejecting the amyloid cascade hypothesis. *Nat. Neurosci.* 18, 794–799. doi: 10.1038/nn.4017

Hertel, C., Terzi, E., Hauser, N., Jakob-Rotne, R., Seelig, J., and Kemp, J. A. (1997). Inhibition of the electrostatic interaction between beta-amyloid peptide and membranes prevents beta-amyloid-induced toxicity. *Proc. Natl. Acad. Sci. U.S.A.* 94, 9412–9416. doi: 10.1073/pnas.94.17.9412

Hicks, D. A., John, D., Makova, N. Z., Henderson, Z., Nalivaeva, N. N., and Turner, A. J. (2011). Membrane targeting, shedding and protein interactions of brain acetylcholinesterase. *J. Neurochem.* 116, 742–746. doi: 10.1111/j.1471-4159.2010.07032.x

Hicks, D. A., Makova, N. Z., Gough, M., Parkin, E. T., Nalivaeva, N. N., and Turner, A. J. (2013b). The amyloid precursor protein represses expression of acetylcholinesterase in neuronal cell lines. *J. Biol. Chem.* 288, 26039–26051. doi: 10.1074/jbc.M113.461269

Hicks, D. A., Makova, N. Z., Nalivaeva, N. N., and Turner, A. J. (2013a). Chemico-Biological Interactions Characterisation of acetylcholinesterase release from neuronal cells. *Chem. Biol. Interact.* 203, 302–308. doi: 10.1016/j.cbi.2012.09.019

Hicks, D. A., Nalivaeva, N. N., and Turner, A. J. (2012). Lipid rafts and Alzheimer's disease?: protein-lipid interactions and perturbation of signaling. *Front. Physiol.* 3:189. doi: 10.3389/fphys.2012.00189

Hong, S., Ostaszewski, B. L., Yang, T., Malley, T. T. O., Jin, M., Yanagisawa, K., et al. (2014). Soluble Aβ oligomers are rapidly sequestered from brain ISF in vivo and bind GM1 ganglioside on cellular membranes. *Neuron.* 82, 308–319. doi: 10.1016/j.neuron.2014.02.027

Hou, X., Richardson, S. J., Aguilar, M. I., and Small, D. H. (2005). Binding of amyloidogenic transthyretin to the plasma membrane alters membrane fluidity and induces neurotoxicity. *Biochemistry* 44, 11618–11627. doi: 10.1021/bi050700m

Huse, J. T., Pijak, D. S., Leslie, G. J., Lee, V. M., and Doms, R. W. (2000). Maturation and endosomal targeting of beta-site amyloid precursor protein-cleaving enzyme. The Alzheimer's disease beta-secretase. *J. Biol. Chem.* 275, 33729–33737. doi: 10.1074/jbc.M004175200

Igbavboa, U., Avdulov, N. A., Schroeder, F., and Wood, W. G. (1996). Increasing age alters transbilayer fluidity and cholesterol asymmetry in synaptic plasma membranes of mice. *J. Neurochem.* 66, 1717–1725. doi: 10.1046/j.1471-4159.1996.66041717.x

Ikonomovic, M. D., Wecker, L., Abrahamson, E. E., Wuu, J., Counts, S. E., Ginsberg, S. D., et al. (2009). Cortical alpha7 nicotinic acetylcholine receptor and beta-amyloid levels in early Alzheimer disease. *Arch. Neurol.* 66, 646–651. doi: 10.1001/archneurol.2009.46

Inestrosa, N. C., Alvarez, A., and Calderón, F. (1996). Acetylcholinesterase is a senile plaque component that promotes assembly of amyloid beta-peptide into Alzheimer's filaments. *Mol. Psychiatry* 1, 359–361.

Irvine, G. B., El-agnaf, O. M., Shankar, G. M., and Walsh, D. M. (2008). Protein aggregation in the brain: the molecular basis for Alzheimer's and Parkinson' s diseases. *Mol. Med.* 14, 451–464. doi: 10.2119/2007-00100

Iwatsubo, T., Odaka, A., Suzuki, N., Mizusawa, H., Nukina, N., and Ihara, Y. (1994). Visualization of A beta 42(43) and A beta 40 in senile plaques with end-specific

A beta monoclonals: evidence that an initially deposited species is A beta 42(43). *Neuron* 13, 45–53. doi: 10.1016/0896-6273(94)90458-8

Jarrett, J. T., Berger, E. P., and Lansbury, P. T. Jr. (1993). The carboxy terminus of the beta amyloid protein is critical for the seeding of amyloid formation: implications for the pathogenesis of Alzheimer's disease. *Biochemistry* 32, 4693–4697. doi: 10.1021/bi00069a001

Jha, A., Cadugan, D. J., Purohit, P., and Auerbach, A. (2007). Acetylcholine receptor gating at extracellular transmembrane domain interface: the cys-loop and M2-M3 linker. *J. Gen. Physiol.* 130, 547–558. doi: 10.1085/jgp.200709856

Ji, S. R., Wu, Y., and Sui, S. F. (2002). Cholesterol is an important factor affecting the membrane insertion of beta-amyloid peptide (A beta 1-40), which may potentially inhibit the fibril formation. *J. Biol. Chem.* 277, 6273–6279. doi: 10.1074/jbc.M104146200

Jin, Y., Tsuchiya, A., Kanno, T., and Nishizaki, T. (2015). Biochemical and biophysical research communications Amyloid- b peptide increases cell surface localization of a7 ACh receptor to protect neurons from amyloid b -induced damage. *Biochem. Biophys. Res. Commun.* 468, 157–160. doi: 10.1016/j.bbrc.2015.10.141

Jones, I. W., Westmacott, A., Chan, E., Jones, R. W., Dineley, K., and O'Neill, M. J. (2006). Alpha7 nicotinic acetylcholine receptor expression in Alzheimer's disease: receptor densities in brain regions of the APP(SWE) mouse model and in human peripheral blood lymphocytes. *J. Mol. Neurosci.* 30, 83–84. doi: 10.1385/JMN:30:1:83

Jones, O. T., and McNamee, M. G. (1988). Annular and nonannular binding sites for cholesterol associated with the nicotinic acetylcholine receptor. *Biochemistry* 127, 2364–2374. doi: 10.1021/bi00407a018

Kagan, B. L., Hirakura, Y., Azimov, R., Azimova, R., and Lin, M. (2002). The channel hypothesis of Alzheimer's disease: current status. *Peptides* 23, 1311–1315. doi: 10.1016/s0196-9781(02)00067-0

Kakio, A., Nishimoto, S., Yanagisawa, K., Kozutsumi, Y., and Matsuzaki, K. (2002). Interactions of amyloid beta-protein with various gangliosides in raft-like membranes: importance of GM1 ganglioside-bound form as an endogenous seed for Alzheimer amyloid. *Biochemistry* 241, 7385–7390. doi: 10.1021/bi0255874

Kakio, A., Nishimoto, S. I., Yanagisawa, K., Kozutsumi, Y., and Matsuzaki, K. (2001). Cholesterol-dependent formation of GM1 ganglioside-bound amyloid beta-protein, an endogenous seed for Alzheimer amyloid. *J. Biol. Chem.* 276, 24985–24990. doi: 10.1074/jbc.M100252200

Kamal, A., Almenar-Queralt, A., LeBlanc, J. F., Roberts, E. A., and Goldstein, L. S. (2001). Kinesin-mediated axonal transport of a membrane compartment containing beta-secretase and presenilin-1 requires APP. *Nature* 414, 643–648. doi: 10.1038/414643

Kamerbeek, C. B., Borroni, V., Pediconi, M. F., Sato, S. B., Kobayashi, T., and Barrantes, F. J. (2013). Antibody-induced acetylcholine receptor clusters inhabit liquid-ordered and liquid-disordered domains. *Biophys. J.* 150, 1601–1611. doi: 10.1016/j.bpj.2013.08.03

Kanfer, J. N., Sorrentino, G., and Sitar, D. S. (1999). Amyloid beta peptide membrane perturbation is the basis for its biological effects. *Neurochem. Res.* 24, 1621–1630.

Karlin, A., and Akabas, M. H. (1995). Toward a structural basis for the function of nicotinic acetylcholine receptors and their cousins. *Neuron* 15, 1231–1244. doi: 10.1016/0896-6273(95)90004-7

Kawahara, M. (2010). Neurotoxicity of β-amyloid protein: oligomerization, channel formation, and calcium dyshomeostasis. *Curr. Pharm. Des.* 16, 2779–2789. doi: 10.2174/138161210793176545

Kellner, R. R., Baier, C. J., Willig, K. I., Hell, S. W., and Barrantes, F. J. (2007). Nanoscale organization of nicotinic acetylcholine receptors revealed by stimulated emission depletion microscopy. *Neuroscience* 144, 135–143. doi: 10.1016/j.neuroscience.2006.08.071

Khan, G. M., Tong, M., Jhun, M., Arora, K., and Nichols, R. A. (2010). Beta-Amyloid activates presynaptic alpha7 nicotinic acetylcholine receptors reconstituted into a model nerve cell system: involvement of lipid rafts. *Eur. J. Neurosci.* 231, 788–796. doi: 10.1111/j.1460-9568.2010.07116.x

Kim, H.-J., Moon, W.-J., and Han, S.-H. (2013). Differential cholinergic pathway involvement in Alzheimer's disease and subcortical ischemic vascular dementia. *J. Alzheimers Dis.* 35, 129–136. doi: 10.3233/JAD-122320

Kim, S., Yi, J., and Ko, Y. (2006). Amyloid b Oligomerization Is Induced by Brain Lipid Rafts. *J. Cell. Biochem.* 99, 878–889. doi: 10.1002/jcb.20978

Kirsch, C., Eckert, G. P., and Mueller, W. E. (2002). Cholesterol attenuates the membrane perturbing properties of beta-amyloid peptides. *Amyloid* 9, 149–159.

Kirsch, C., Eckert, G. P., and Mueller, W. E. (2003). Statin effects on cholesterol micro-domains in brain plasma membranes. *Biochem. Pharmacol.* 65, 843–856. doi: 10.1016/s0006-2952(02)01654-4

Klein, W. L., Steine, W. B. Jr., and Teplow, D. B. (2004). Small assemblies of unmodified amyloid beta-protein are the proximate neurotoxin in Alzheimer's disease. *Neurobiol. Aging* 25, 569–580. doi: 10.1016/j.neurobiolaging.2004.02.010

Kogel, D., Copanaki, E., Hartig, U., Bottner, S., Peters, I., Muller, W. E., et al. (2008). "Modulation of membrane fluidity by omega 3 fatty acids: enhanced generation of sAPPalpha is required for the neuroprotective effects of DHA," in *The 38th Annual Meeting of the Society for Neuroscience*, Washington, DC, 15–19.

Kojro, E., Gimpl, G., Lammich, S., Marz, W., and Fahrenholz, F. (2001). Low cholesterol stimulates the nonamyloidogenic pathway by its effect on the alpha -secretase ADAM 10. *Proc. Natl. Acad. Sci. U.S.A.* 98, 5815–5820. doi: 10.1073/pnas.081612998

Koo, E. H., and Squazzo, S. L. (1994). Evidence that production and release of amyloid beta-protein involves the endocytic pathway. *J. Biol. Chem.* 269, 17386–17389.

Kosicek, M., and Hecimovic, S. (2013). Phospholipids and Alzheimer's disease: alterations, mechanisms and potential biomarkers. *Int. J. Mol. Sci.* 214, 1310–1322. doi: 10.3390/ijms14011310

Kotler, S. A., Walsh, P., Brender, J. R., and Ramamoorthy, A. (2014). Differences between amyloid-β aggregation in solution and on the membrane: insights into elucidation of the mechanistic details of Alzheimer's disease. *Chem. Soc. Rev.* 19, 6692–6700. doi: 10.1039/c3cs60431d

Koudinov, A. R., and Koudinova, N. V. (2004). Cholesterol homeostasis failure as a unifying cause of synaptic degeneration. *J. Neurol. Sci.* 229-230, 233–240. doi: 10.1016/j.jns.2004.11.036

Koudinova, N. V., Koudinov, A. R., and Yavin, E. (2000). Alzheimer's Abeta1-40 peptide modulates lipid synthesis in neuronal cultures and intact rat fetal brain under normoxic and oxidative stress conditions. *Neurochem. Res.* 25, 653–660.

Kumar, A., Singh, A., and Ekavali. (2015). A review on Alzheimer's disease pathophysiology and its management: an update. *Pharmacol. Rep.* 67, 195–203. doi: 10.1016/j.pharep.2014.09.004

Lahdo, R., and De La Fournière-Bessueille, L. (2004). Insertion of the amyloid precursor protein into lipid monolayers: effects of cholesterol and apolipoprotein E. *Biochem. J.* 382, 987–994. doi: 10.1042/BJ20040777

Langui, D., Girardot, N., El, Hachimi KH, Allinquant, B., Blanchard, V., Pradier, L., et al. (2004). Subcellular topography of neuronal Abeta peptide in APPxPS1 transgenic mice. *Am. J. Pathol.* 165, 1465–1477. doi: 10.1016/s0002-9440(10)63405-0

Lashuel, H. A., Hartley, D., Petre, B. M., Walz, T., and Lansbury, P. T. Jr. (2002). Neurodegenerative disease: amyloid pores from pathogenic mutations. *Nature* 418:291. doi: 10.1038/418291a

Lauderback, C. M., Hackett, J. M., Keller, J. N., Varadarajan, S., Szweda, L., Kindy, M., et al. (2001). Vulnerability of synaptosomes from apoE knock-out mice to structural and oxidative modifications induced by A beta(1-40): implications for Alzheimer's disease. *Biochemistry* 240, 2548–2554. doi: 10.1021/bi002312k

Lazarevic-Pasti, T., Leskovac, A., Momic, T., Petrovic, S., and Vasic, V. (2017). Modulators of Acetylcholinesterase activity: from Alzheimer's disease to anti-cancer drugs. *Curr. Med. Chem.* 24, 3283–3309. doi: 10.2174/0929867324666170705123509

Le Novère, N., and Changeux, J. P. (1995). Molecular evolution of the nicotinic acetylcholine receptor: an example of multigene family in excitable cells. *J Mol. Evol.* 40, 155–172. doi: 10.1007/bf00167110

Lee, A. G. (2003). Lipid - protein interactions in biological membranes: a structural perspective. *Biochim. Biophys. Acta* 1612, 1–40. doi: 10.1016/S0005-2736(03)00056-57

Lee, D. H. S., and Wang, H.-Y. (2003). Differential physiologic responses of α7 nicotinic acetylcholine receptors to β-amyloid$_{1-40}$ and β-amyloid$_{1-42}$. *J. Neurobiol.* 55, 25–30. doi: 10.1002/neu.10203

Lee, E. B., Leng, L. Z., Zhang, B., Kwong, L., Trojanowski, J. Q., Abel, T., et al. (2006). Targeting amyloid-β peptide (Aβ) oligomers by passive immunization with a conformation-selective monoclonal antibody improves learning and

memory in Aβ precursor protein (APP) transgenic mice. *J. Biol. Chem.* 281, 4292–4299. doi: 10.1074/jbc.M511018200

Lee, S. J., Liyanage, U., Bickel, P. E., Xia, W., Lansbury, P. T. Jr., and Kosik, K. S. (1998). A detergent-insoluble membrane compartment contains A beta in vivo. *Nat. Med.* 4, 730–734. doi: 10.1038/nm0698-730

Levin, E. D., Cauley, M., and Rezvani, A. H. (2013). Improvement of attentional function with antagonism of nicotinic receptors in female rats. *Eur. J. Pharmacol.* 702, 269–274. doi: 10.1016/j.ejphar.2013.01.056

Li, L., Cheung, T., Chen, J., and Herrup, K. (2011). A comparative study of five mouse models of Alzheimer's disease: cell cycle events reveal new insights into neurons at risk for death. *Int. J. Alzheimers Dis.* 2011:171464. doi: 10.4061/2011/171464

Lilja, A. M., Porras, O., Storelli, E., Nordberg, A., and Marutle, A. (2011). Functional interactions of fibrillar and oligomeric amyloid-β with alpha7 nicotinic receptors in Alzheimer's disease. *J. Alzheimers Dis.* 23, 335–347. doi: 10.3233/JAD-2010-101242

Lin, H., Bhatia, R., and Lal, R. (2001). Amyloid beta protein forms ion channels: implications for Alzheimer's diseases pathophysiology. *FASEB J.* 15, 2433–2444. doi: 10.1096/fj.01-0377com

Lin, M. S., Chen, L. Y., Wang, S. S., Chang, Y., and Chen, W. Y. (2008). Examining the levels of ganglioside and cholesterol in cell membrane on attenuation the cytotoxicity of beta-amyloid peptide. *Colloids Surf. B. Biointerfaces* 65, 172–177. doi: 10.1016/j.colsurfb.2008.03.012

Lindstrom, J. M. (2003). Nicotinic acetylcholine receptors of muscles and nerves: comparison of their structures, functional roles, and vulnerability to pathology. *Ann. N.Y. Acad. Sci.* 998, 41–52. doi: 10.1196/annals.1254.007

Liu, Q., Kawai, H., and Berg, D. K. (2001). Beta -Amyloid peptide blocks the response of alpha 7-containing nicotinic receptors on hippocampal neurons. *Proc. Natl. Acad. Sci. U.S.A.* 98, 4734–4739. doi: 10.1073/pnas.081553598

Liu, Q., and Wu, J. (2006). Neuronal nicotinic acetylcholine receptors serve as sensitive targets that mediate beta-amyloid neurotoxicity. *Acta. Pharmacol. Sin.* 27, 1277–1286. doi: 10.1111/j.1745-7254.2006.00430.x

Liu, Q., Xie, X., Emadi, S., Sierks, M. R., and Wu, J. (2015). A novel nicotinic mechanism underlies b -amyloid-induced neurotoxicity. *Neuropharmacology* 97, 457–463. doi: 10.1016/j.neuropharm.2015.04.025

Liu, Q., Xie, X., Lukas, R. J., St John, P. A., and Wu, J. (2013). A novel nicotinic mechanism underlies β-amyloid-induced neuronal hyperexcitation. *J. Neurosci.* 33, 7253–7263. doi: 10.1523/JNEUROSCI.3235-12.2013

Liu, R., Gu, R., Qi, X., Zhang, T., Zhao, Y., and He, Y. (2008). Decreased Nicotinic receptors and cognitive deficit in rats intracerebroventricularly injected with beta-amyloid peptide (1-42) and fed a high-cholesterol diet. *J. Neurosci. Res.* 86, 183–193. doi: 10.1002/jnr.21463

Lombardo, S., and Maskos, U. (2014). Neuropharmacology Role of the nicotinic acetylcholine receptor in Alzheimer's disease pathology and treatment. *Neuropharmacology* 96, 255–262. doi: 10.1016/j.neuropharm.2014.11.018

London, E. (2005). How principles of domain formation in model membranes may explain ambiguities concerning lipidraft formation in cells. *Biochim. Biophys. Acta* 30, 203–220. doi: 10.1016/j.bbamcr.2005.09.002

Lukiw, W. J. (2013). Alzheimer's disease (AD) as a disorder of the plasma membrane. *Front. Physiol.* 4:24. doi: 10.3389/fphys.2013.00024

Ma, K., and Qian, Y. (2019). Neuropeptides Alpha 7 nicotinic acetylcholine receptor and its effects on Alzheimer's disease. *Neuropeptides* 73, 96–106. doi: 10.1016/j.npep.2018.12.003

Magni, F., Galbusera, C., Tremolada, L., Ferrarese, C., and Kienle, M. G. (2002). Characterisation of adducts of the lipid peroxidation product 4-hydroxy-2-nonenal and amyloid beta-peptides by liquid chromatography/electrospray ionisation mass spectrometry. *Rapid. Commun. Mass. Spectrom.* 16, 1485–1493. doi: 10.1002/rcm.743

Maia, M. A., and Sousa, E. (2019). BACE-1 and γ-secretase as therapeutic targets for Alzheimer's disease. *Pharmaceuticals* 12:41. doi: 10.3390/ph12010041

Marchand, S., Devillers-thie, A., Pons, S., Changeux, J., and Cartaud, J. (2002). Rapsyn escorts the Nicotinic Acetylcholine receptor along the exocytic pathway via association with lipid rafts. *J. Neurosci.* 22, 8891–8901. doi: 10.1523/jneurosci.22-20-08891.2002

Mark, R., Lovell, M. A., Markesbery, W., Koiiuchida, I., and Mattson, P. (1997). A role for 4-Hydroxynonenal, an aldehydic product of lipid peroxidation, in disruption of ion homeostasis and neuronal death induced by amyloid-beta peptide. *J. Neurochem.* 68, 255–264. doi: 10.1046/j.1471-4159.1997.68010255.x

Marsh, D., and Barrantes, F. J. (1978). Immobilized lipid in acetylcholine receptor-rich membranes from Torpedo marmorata. *Proc. Natl. Acad. Sci. U.S.A.* 75, 4329–4333. doi: 10.1073/pnas.75.9.4329

Martín, V., Fabelo, N., Santpere, G., Puig, B., Marín, R., Ferrer, I., et al. (2010). Lipid alterations in lipid rafts from Alzheimer's disease human brain cortex. *J. Alzheimers. Dis.* 19, 489–502. doi: 10.3233/JAD-2010-1242

Martínez-Senac, M., Villalaín, J., and Gómez-Fernández, J. C. (1999). Structure of the Alzheimer beta-amyloid peptide (25-35) and its interaction with negatively charged phospholipid vesicles. *Eur. J. Biochem.* 265, 744–753. doi: 10.1046/j.1432-1327.1999.00775.x

Martorana, A., Esposito, Z., and Koch, G. (2010). Beyond the cholinergic hypothesis: do current drugs work in Alzheimer's disease? *CNS Neurosci. Ther.* 16, 235–245. doi: 10.1111/j.1755-5949.2010.00175.x

Mason, R. P., Shoemaker, W. J., Shajenko, L., Chambers, T. E., and Herbette, L. G. (1992). Evidence for changes in the Alzheimer's disease brain cortical membrane structure mediated by cholesterol. *Neurobiol. Aging* 13, 413–419. doi: 10.1016/0197-4580(92)90116-f

Massoulié, J. (2002). The origin of the molecular diversity and functional anchoring of cholinesterases. *Neurosignals* 11, 130–143. doi: 10.1159/000065054

Massoulié, J., Bon, S., Perrier, N., and Falasca, C. (2005). The C-terminal peptides of acetylcholinesterase: cellular trafficking, oligomerization and functional anchoring. *Chem. Biol. Interact.* 157-158, 3–14. doi: 10.1016/j.cbi.2005.10.002

Matsuzaki, K. (2007). Physicochemical interactions of amyloid β -peptide with lipid bilayers. *Biochim. Biophys. Acta* 1768, 1935–1942. doi: 10.1016/j.bbamem.2007.02.009

Matsuzaki, K., Kato, K., and Yanagisawa, K. (2010). Abeta polymerization through interaction with membrane gangliosides. *Biochim. Biophys. Acta* 1801, 868–877. doi: 10.1016/j.bbalip.2010.01.008

McKay, B. E., Placzek, A. N., and Dani, J. A. (2007). Regulation of synaptic transmission and plasticity by neuronal nicotinic acetylcholine receptors. *Biochem. Pharmacol.* 74, 1120–1133. doi: 10.1016/j.bcp.2007.07.001

McLaurin, J., and Chakrabartty, A. (1997). Characterization of the interactions of Alzheimer beta-amyloid peptides with phospholipid. *Eur. J. Biochem.* 1245, 355–363. doi: 10.1111/j.1432-1033.1997.t01-2-00355.x

McLaurin, J., Franklin, T., Fraser, P. E., and Chakrabartty, A. (1998). Structural transitions associated with the interaction of Alzheimer beta-amyloid peptides with gangliosides. *J. Biol. Chem.* 273, 4506–4515. doi: 10.1074/jbc.273.8.4506

Mehta, T. K., Dougherty, J. J., Wu, J., Choi, C. H., Khan, G. M., and Nichols, R. A. (2009). Defining pre-synaptic nicotinic receptors regulated by beta amyloid in mouse cortex and hippocampus with receptor null mutants. *J. Neurochem.* 109, 1452–1458. doi: 10.1111/j.1471-4159.2009.06070.x

Messi, M. L., Renganathan, M., Grigorenko, E., and Delbono, O. (1997). Activation of alpha7 nicotinic acetylcholine receptor promotes survival of spinal cord motoneurons. *FEBS Lett.* 411, 32–38. doi: 10.1016/s0014-5793(97)00600-5

Mesulam, M. M., Mufson, E. J., Levey, A. I., and Wainer, B. H. (1983). Cholinergic innervation of cortex by the basal forebrain: cytochemistry and cortical connections of the septal area, diagonal band nuclei, nucleus basalis (substantia innominata), and hypothalamus in the rhesus monkey. *J. Comp. Neurol.* 20, 170–197. doi: 10.1002/cne.902140206

Méthot, N., Demers, C. N., and Baenziger, J. E. (1995). Structure of both the ligand- and lipid-dependent channel-inactive states of the nicotinic acetylcholine receptor probed by FTIR spectroscopy and hydrogen exchange. *Biochemistry* 34, 15142–15149. doi: 10.1021/bi00046a021

Michikawa, M. (2003). The role of cholesterol in pathogenesis of Alzheimer's disease: dual metabolic interaction between amyloid β-protein and cholesterol. *Mol. Neurobiol.* 27, 1–12. doi: 10.1385/MN:27:1:1

Michikawa, M., Gong, J. S., Fan, Q. W., Sawamura, N., and Yanagisawa, K. (2001). A novel action of alzheimer's amyloid beta-protein (Abeta): oligomeric Abeta promotes lipid release. *J. Neurosci.* 218, 7226–7235.

Middlemas, D. S., and Raftery, M. A. (1987). Identification of Subunits of Acetylcholine Receptor That Interact with a Cholesterol Photoaffinity Probe. *Biochemistry* 126, 1219–1223. doi: 10.1021/bi00379a003

Milanesi, L., Sheynis, T., Xue, W. F., Orlova, E. V., Hellewell, A. L., Jelinek, R., et al. (2012). Direct three-dimensional visualization of membrane disruption by amyloid fibrils. *Proc. Natl. Acad. Sci. U.S.A.* 109, 20455–20460. doi: 10.1073/pnas.1206325109

Minota, S., and Watanabe, S. (1997). Inhibitory effects of arachidonic acid on nicotinic transmission in bullfrog sympathetic neurons. *J. Neurophysiol.* 178, 2396–2401. doi: 10.1152/jn.1997.78.5.2396

Molander-Melin, M., Blennow, K., Bogdanovic, N., Dellheden, B., and Fredman, P. (2005). Structural membrane alterations in Alzheimer brains found to be associated with regional disease development; increased density of gangliosides GM1 and GM2 and loss of cholesterol in detergent- resistant membrane domains. *J. Neurochem.* 92, 171–182. doi: 10.1111/j.1471-4159.2004.02849.x

Molinari, E. J., Delbono, O., Messi, M. L., Renganathan, M., Arneric, S. P., Sullivan, J. P., et al. (1998). Up-regulation of human alpha7 nicotinic receptors by chronic treatment with activator and antagonist ligands. *Eur. J. Pharmacol.* 347, 131–139. doi: 10.1016/s0014-2999(98)00084-3

Morán, M. A., Mufson, E. J., and Gómez-Ramos, P. (1993). Colocalization of cholinesterases with beta amyloid protein in aged and Alzheimer's brains. *Acta Neuropathol.* 85, 362–369. doi: 10.1007/bf00334445

Morley, B. J., and Happe, H. K. (2000). Cholinergic receptors: dual roles in transduction and plasticity. *Hear. Res.* 147, 104–112. doi: 10.1016/s0378-5955(00)00124-6

Mosqueira, A., Camino, P. A., and Barrantes, F. J. (2018). Cholesterol modulates acetylcholine receptor diffusion by tuning confinement sojourns and nanocluster stability. *Sci. Rep.* 8:11974. doi: 10.1038/s41598-018-30384

Mouritsen, O. G., and Bloom, M. (1984). Mattress model of lipid-protein interactions in membranes. *Biophys J.* 46, 141–153. doi: 10.1016/s0006-3495(84)84007-2

Muir, J. L., Page, K. J., Sirinathsinghji, D. J., Robbins, T. W., and Everitt, B. J. (1993). Excitotoxic lesions of basal forebrain cholinergic neurons: effects on learning, memory and attention. *Behav. Brain Res.* 157, 123–131. doi: 10.1016/0166-4328(93)90128-d

Müller, W. E., Kirsch, C., and Eckert, G. P. (2001). Membrane-disordering effects of beta-amyloid peptides. *Biochem. Soc. Trans.* 29, 617–623. doi: 10.1042/bst0290617

Müller, W. E., Koch, S., Eckert, A., Hartmann, H., and Scheuer, K. (1995). β-amyloid peptide decreases membrane fluidity. *Brain Res.* 674, 133–136. doi: 10.1016/0006-8993(94)01463-R

Murray, I. V. J., Liu, L., Komatsu, H., Uryu, K., Xiao, G., John, A., et al. (2007). Membrane-mediated amyloidogenesis and the promotion of oxidative lipid damage by amyloid beta proteins. *J. Biol. Chem.* 282, 9335–9345. doi: 10.1074/jbc.M608589200

Murray, J. K., Farooqi, B., Sadowsky, J. D., Scalf, M., Freund, W. A., Smith, L. M., et al. (2005). Efficient synthesis of a beta-peptide combinatorial library with microwave irradiation. *J. Am. Chem. Soc.* 127, 13271–13280. doi: 10.1021/ja052733v

Nagele, R. G., D'Andrea, M. R., Anderson, W. J., and Wang, H. Y. (2002). Intracellular accumulation of beta-amyloid(1-42) in neurons is facilitated by the alpha 7 nicotinic acetylcholine receptor in Alzheimer's disease. *Neuroscience* 110, 199–211. doi: 10.1016/s0306-4522(01)00460-2

Nagele, R. G., D'Andrea, M. R., Lee, H., Venkataraman, V., and Wang, H. Y. (2003). Astrocytes accumulate A beta 42 and give rise to astrocytic amyloid plaques in Alzheimer disease brains. *Brain Res.* 971, 197–209. doi: 10.1016/s0006-8993(03)02361-8

Nagele, R. G., Wegiel, J., Venkataraman, V., Imaki, H., Wang, K.-C., and Wegiel, J. (2004). Contribution of glial cells to the development of amyloid plaques in Alzheimer's disease. *Neurobiol. Aging* 25, 663–674. doi: 10.1016/j.neurobiolaging.2004.01.007

Nalivaeva, N. N., and Turner, A. J. (2016). Chemico-Biological Interactions AChE and the amyloid precursor protein (APP) -Cross-talk in Alzheimer's disease. *Chem. Biol. Interact.* 259, 301–306. doi: 10.1016/j.cbi.2016.04.009

Narayanaswami, V., Kim, J., and McNamee, M. G. (1993). Protein-lipid interactions and *Torpedo californica* nicotinic acetylcholine receptor function. 1. Spatial disposition of cysteine residues in the γ subunit analyzed by fluorescence-quenching and energy-transfer measurements. *Biochemistry* 32, 12413–12419. doi: 10.1021/bi00097a020

Narayanaswami, V., and McNamee, M. G. (1993). Protein-lipid interactions and Torpedo californica nicotinic acetylcholine receptor function. 2. Membrane fluidity and ligand-mediated alteration in the accessibility of gamma subunit cysteine residues to cholesterol. *Biochemistry* 123, 12420–12427. doi: 10.1021/bi00097a021

Nashmi, R., Dickinson, M. E., McKinney, S., Jareb, M., Labarca, C., Fraser, S. E., et al. (2003). Assembly of alpha4beta2 nicotinic acetylcholine receptors assessed with functional fluorescently labeled subunits: effects of localization, trafficking, and nicotine-induced upregulation in clonal mammalian cells and in cultured midbrain neurons. *J. Neurosci.* 23, 11554–11567. doi: 10.1523/jneurosci.23-37-11554.2003

Näslund, J., Haroutunian, V., Mohs, R., Davis, K. L., Davies, P., Greengard, P., et al. (2000). Correlation between elevated levels of amyloid beta-peptide in the brain and cognitive decline. *JAMA* 283, 1571–1577.

Näslund, J., Schierhorn, A., Hellman, U., Lannfelt, L., Roses, A. D., Tjernberg, L. O., et al. (1994). Relative abundance of Alzheimer A beta amyloid peptide variants in Alzheimer disease and normal aging. *Proc. Natl. Acad. Sci. U.S.A.* 91, 8378–8382. doi: 10.1073/pnas.91.18.8378

Navaratnam, D. S., Fernando, F. S., Priddle, J. D., Giles, K., Clegg, S. M., Pappin, D. J., et al. (2000). Hydrophobic protein that copurifies with human brain acetylcholinesterase: amino acid sequence, genomic organization, and chromosomal localization. *J. Neurochem.* 74, 2146–2153. doi: 10.1046/j.1471-4159.2000.0742146.x

Nees, F. (2015). The nicotinic cholinergic system function in the human brain. *Neuropharmacology* 96, 289–301. doi: 10.1016/j.neuropharm.2014.10.021

Nicolson, G. L. (2014). The fluid-mosaic model of membrane structure?: still relevant to understanding the structure, function and dynamics of biological membranes after more than 40 years. *Biochim. Biophys. Acta.* 1838, 1451–1466. doi: 10.1016/j.bbamem.2013.10.019

Niu, X., Zhang, X., Xie, J., and Zhang, X. (2012). Acetylcholinesterase blocks cleavage of APP by γ-secretase in 293 cells and mouse brain. *Mol. Neurodegener.* 7(Suppl. 1):S11. doi: 10.1186/1750-1326-7-S1-S11

Nordberg, A., Lundqvist, H., Hartvig, P., Lilja, A., and Långström, B. (1995). Kinetic analysis of regional (S)(-)11C-nicotine binding in normal and Alzheimer brains–in vivo assessment using positron emission tomography. *Alzheimer Dis. Assoc. Disord.* 9, 21–27. doi: 10.1097/00002093-199505000-00006

Nunomura, A., Tamaoki, T., Tanaka, K., Motohashi, N., Nakamura, M., and Hayashi, T. (2010). Intraneuronal amyloid beta accumulation and oxidative damage to nucleic acids in Alzheimer disease. *Neurobiol. Dis.* 37, 731–737. doi: 10.1016/j.nbd.2009.12.012

Nurowska, E., and Ruzzier, F. (1996). Corticosterone modifies the murine muscle acetylcholine receptor channel kinetics. *Neuroreport* 8, 77–80. doi: 10.1097/00001756-199612200-00016

Nurowska, E., and Ruzzier, F. (2002). Modulation of acetylcholine receptor channel kinetics by hydrocortisone. *Biochim. Biophys. Acta* 1564, 14–20. doi: 10.1016/s0005-2736(02)00356-5

Ochoa, E. L., Dalziel, A. W., and McNamee, M. G. (1983). Reconstitution of acetylcholine receptor function in lipid vesicles of defined composition. *Biochim. Biophys. Acta* 1727, 151–162. doi: 10.1016/0005-2736(83)90379-6

Opazo, C., Huang, X., Cherny, R. A., Moir, R. D., Roher, A. E., White, A. R., et al. (2002). Metalloenzyme-like activity of Alzheimer's disease beta-amyloid. Cu-dependent catalytic conversion of dopamine, cholesterol, and biological reducing agents to Neurotoxic H(2)O(2). *J. Biol. Chem.* 277, 40302–40308. doi: 10.1074/jbc.M206428200

Oshikawa, J., Toya, Y., Fujita, T., Egawa, M., Kawabe, J., Umemura, S., et al. (2003). Nicotinic acetylcholine receptor alpha 7 regulates cAMP signal within lipid rafts. *Am. J. Physiol. Cell. Physiol.* 285, C567–C574.

Oshima, N., Morishima-kawashima, M., Yamaguchi, H., Yoshimura, M., Schenk, D., and Ihara, Y. (2001). Accumulation of amyloid beta - protein in the low - density membrane domain accurately reflects the extent of beta -amyloid deposition in the Brain. *Am. J. Pathol.* 158, 2209–2218. doi: 10.1016/s0002-9440(10)64693-7

Palop, J. J., and Mucke, L. (2010). Amyloid-beta-induced neuronal dysfunction in Alzheimer's disease: from synapses toward neural networks. *Nat. Neurosci.* 13, 812–818. doi: 10.1038/nn.2583

Parri, H. R., Hernandez, C. M., and Dineley, K. T. (2011). Research update: Alpha7 nicotinic acetylcholine receptor mechanisms in Alzheimer's disease. *Biochem. Pharmacol.* 82, 931–942. doi: 10.1016/j.bcp.2011.06.039

Parvathy, S., Hussain, I., Karran, E. H., Turner, A. J., and Hooper, N. M. (1999). Cleavage of Alzheimer's amyloid precursor protein by alpha. -secretase occurs

at the surface of neuronal cells. *Biochemistry* 38, 9728–9734. doi: 10.1021/bi9906827

Paterson, D., and Nordberg, A. (2000). Neuronal nicotinic receptors in the human brain. *Prog. Neurobiol.* 61, 75–111. doi: 10.1016/s0301-0082(99)00045-3

Pediconi, M. F., Gallegos, C. E., and Barrantes, F. J. (2004). Metabolic cholesterol depletion hinders cell-surface trafficking of the nicotinic acetylcholine receptor. *Neuroscience* 128, 239–249. doi: 10.1016/j.neuroscience.2004.06.007

Peña, V. B., Bonini, I. C., Antollini, S. S., Kobayashi, T., and Barrantes, F. J. (2011). A7-Type Acetylcholine Receptor Localization and Its Modulation By Nicotine and Cholesterol in Vascular Endothelial Cells. *J. Cell. Biochem.* 112, 3276–3288. doi: 10.1002/jcb.23254

Perez, R. G., Soriano, S., Hayes, J. D., Ostaszewski, B., Xia, W., Selkoe, D. J., et al. (1999). Mutagenesis identifies new signals for beta-amyloid precursor protein endocytosis, turnover, and the generation of secreted fragments, including Abeta42. *J. Biol. Chem.* 274, 18851–18856. doi: 10.1074/jbc.274.27.18851

Perillo, V. L., Peñalva, D. A., Vitale, A. J., Barrantes, F. J., and Antollini, S. S. (2016). Transbilayer asymmetry and sphingomyelin composition modulate the preferential membrane partitioning of the nicotinic acetylcholine receptor in Lo domains. *Arch. Biochem. Biophys.* 591, 76–86. doi: 10.1016/j.abb.2015.12.003

Perrier, A. L., Massoulié, J., and Krejci, E. (2002). PRiMA: the membrane anchor of acetylcholinesterase in the brain. *Neuron.* 33, 275–285.

Perry, E. K., Blessed, G., Tomlinson, B. E., Perry, R. H., Crow, T. J., Cross, A. J., et al. (1981). Neurochemical activities in human temporal lobe related to aging and Alzheimer-type changes. *Neurobiol. Aging* 2, 251–266.

Perry, E. K., Curtis, M., Dick, D. J., Candy, J. M., Atack, J. R., Bloxham, C. A., et al. (1985). Cholinergic correlates of cognitive impairment in Parkinson's disease: comparisons with Alzheimer's disease. *J. Neurol. Neurosurg. Psychiatry* 48, 413–421.

Perry, E. K., Johnson, M., Kerwin, J. M., Piggott, M. A., Court, J. A., Shaw, P. J., et al. (1992). Convergent cholinergic activities in aging and Alzheimer's disease. *Neurobiol. Aging* 13, 393–400. doi: 10.1016/0197-4580(92)90113-c

Perry, E. K., Perry, R. H., Smith, C. J., Dick, D. J., Candy, J. M., Edwardson, J. A., et al. (1987). Nicotinic receptor abnormalities in Alzheimer's and Parkinson's diseases. *J. Neurol. Neurosurg. Psychiatry* 50, 806–809.

Perry, G., Lipphardt, S., Mulvihill, P., Kancherla, M., Mijares, M., Gambetti, P., et al. (1988). Amyloid precursor protein in senile plaques of Alzheimer disease. *Lancet* 2, 746–751.

Peters, I., Igbavboa, U., Schütt, T., Haidari, S., Hartig, U., Rosello, X., et al. (2009). The interaction of beta-amyloid protein with cellular membranes stimulates its own production. *Biochim. Biophys. Acta* 1788, 964–972. doi: 10.1016/j.bbamem.2009.01.012

Petersen, R. C. (1977). Scopolamine induced learning failures in man. *Psychopharmacology* 52, 283–289. doi: 10.1007/BF00426713

Pettit, D. L., Shao, Z., and Yakel, J. L. (2001). Beta-Amyloid(1-42) peptide directly modulates nicotinic receptors in the rat hippocampal slice. *J. Neurosci.* 21:RC120.

Phinney, A. L., Horne, P., Yang, J., Janus, C., Bergeron, C., and Westaway, D. (2003). Mouse models of Alzheimer's disease: the long and filamentous road. *Neurol. Res.* 25, 590–600. doi: 10.1179/016164103101202020

Piomelli, D., Astarita, G., and Rapaka, R. (2007). A neuroscientist's guide to lipidomics. *Nat. Rev. Neurosci.* 8, 743–754. doi: 10.1038/nrn2233

Plant, L. D., Boyle, J. P., Smith, I. F., Peers, C., and Pearson, H. A. (2003). The production of amyloid beta peptide is a critical requirement for the viability of central neurons. *J. Neurosci.* 23, 5531–5535. doi: 10.1523/jneurosci.23-13-05531.2003

Pohanka, M. (2012). Alpha7 nicotinic acetylcholine receptor is a target in pharmacology and toxicology. *Int. J. Mol. Sci.* 13, 2219–2238. doi: 10.3390/ijms13022219

Pollard, H. B., Arispe, N., and Rojas, E. (1995). Ion Channel Hypothesis for Alzheimer Amyloid Peptide Neurotoxicity. *Cell. Mol. Neurobiol.* 15, 513–526. doi: 10.1007/bf02071314

Poveda, J. A., Encinar, J. A., Fernández, A. M., Mateo, C. R., Ferragut, J. A., and González-Ros, J. M. (2002). Segregation of phosphatidic acid-rich domains in reconstituted acetylcholine receptor membranes. *Biochemistry* 41, 12253–12262. doi: 10.1021/bi0200099

Poveda, J. A., Fernández, A. M., and Encinar, J. A. (2008). Protein-promoted membrane domains. *Biochim. Biophys. Acta* 1778, 1583–1590. doi: 10.1016/j.bbamem.2008.01.021

Puglielli, L., Konopka, G., Pack-Chung, E., Ingano, L. A. M., Berezovska, O., Hyman, B. T., et al. (2001). Acyl-coenzyme A: cholesterol acyltransferase modulates the generation of the amyloid β-peptide. *Nat. Cell. Biol.* 3, 905–912. doi: 10.1038/ncb1001-905

Puzzo, D., and Arancio, O. (2013). Amyloid-β peptide: Dr. Jekyll or Mr. Hyde? *J. Alzheimers Dis.* 33, S111–S120.

Puzzo, D., Gulisano, W., Arancio, O., and Palmeri, A. (2015). The keystone of Alzheimer pathogenesis might be sought in Aβ physiology. *Neuroscience* 307, 26–36. doi: 10.1016/j.neuroscience.2015.08.039

Puzzo, D., Privitera, L., Fa', M., Staniszewski, A., Hashimoto, G., Aziz, F., et al. (2011). Endogenous amyloid-β is necessary for hippocampal synaptic plasticity and memory. *Ann. Neurol.* 69, 819–830. doi: 10.1002/ana.22313

Puzzo, D., Privitera, L., Leznik, E., Fà, M., Staniszewski, A., Palmeri, A., et al. (2008). Picomolar amyloid-beta positively modulates synaptic plasticity and memory in hippocampus. *J. Neurosci.* 28, 14537–14545. doi: 10.1523/JNEUROSCI.2692-08.2008

Qiang, W., Yau, W. M., and Schulte, J. (2014). Fibrillation of β amyloid peptides in the presence of phospholipid bilayers and the consequent membrane disruption. *Biochim. Biophys. Acta* 1848, 266–276. doi: 10.1016/j.bbamem.2014.04.011

Quesada, O., González-Freire, C., Ferrer, M. C., Colón-Sáez, J. O., Fernández-García, E., Mercado, J., et al. (2016). Uncovering the lipidic basis for the preparation of functional nicotinic acetylcholine receptor detergent complexes for structural studies. *Sci. Rep.* 19:32766. doi: 10.1038/srep32766

Quinn, P. J. (2002). Plasma membrane phospholipid asymmetry. *Subcell Biochem.* 36, 39–60. doi: 10.1007/0-306-47931-1_3

Reid, P. C., Urano, Y., Kodama, T., and Hamakubo, T. (2007). Alzheimer's Disease?: cholesterol, membrane rafts, isoprenoids and statins. *J. Cell. Mol. Med.* 11, 383–392. doi: 10.1111/j.1582-4934.2007.00054.x

Relini, A., Marano, N., and Gliozzi, A. (2013). Misfolding of amyloidogenic proteins and their interactions with membranes. *Biomolecules* 27, 20–55. doi: 10.3390/biom4010020

Relini, A., Marano, N., and Gliozzi, A. (2014). Probing the interplay between amyloidogenic proteins and membranes using lipid monolayers and bilayers. *Adv. Colloid Interface Sci.* 207, 81–92. doi: 10.1016/j.cis.2013.10.015

Reyes, A. E., Perez, D. R., Alvarez, A., Garrido, J., Gentry, M. K., and Doctor, B. P. (1997). A monoclonal antibody against acetylcholinesterase inhibits the formation of amyloid fibrils induced by the enzyme. *Biochem. Biophys. Res. Commun.* 232, 652–655. doi: 10.1006/bbrc.1997.6357

Roccamo, A. M., Pediconi, M. F., Aztiria, E., Zanello, L., Wolstenholme, A., and Barrantes, F. J. (1999). Cells defective in sphingolipids biosynthesis express low amounts of muscle nicotinic acetylcholine receptor. *Eur. J. Neurosci.* 11, 1615–1623. doi: 10.1046/j.1460-9568.1999.00574.x

Rondelli, V., Brocca, P., Motta, S., Messa, M., Colombo, L., Salmona, M., et al. (2016). Amyloid - β Peptides in interaction with raft-mime model membranes: a neutron reflectivity insight. *Sci. Rep*. 16:20997. doi: 10.1038/srep20997

Rosenblum, W. I. (2014). Why Alzheimer trials fail: removing soluble oligomeric beta amyloid is essential, inconsistent, and difficult. *Neurobiol. Aging* 35, 969–974. doi: 10.1016/j.neurobiolaging.2013.10.085

Roth, G. S., Joseph, J. A., and Mason, R. P. (1995). Membrane alterations as causes of impaired signal transduction in Alzheimer's disease and aging. *Trends. Neurosci.* 18, 203–206. doi: 10.1016/0166-2236(95)93902-a

Rushworth, J. V., and Hooper, N. M. (2011). Lipid rafts: linking Alzheimer's Amyloid- β production, aggregation, and toxicity at neuronal membranes. *Int. J. Alzheimers Dis.* 2011:603052. doi: 10.4061/2011/603052

Sáez-Valero, J., Sberna, G., McLean, C. A., and Small, D. H. (1999). Molecular isoform distribution and glycosylation of acetylcholinesterase are altered in brain and cerebrospinal fluid of patients with Alzheimer's disease. *J. Neurochem.* 72, 1600–1608. doi: 10.1046/j.1471-4159.1999.721600.x

Sargent, P. B., Bryan, G. K., Streichert, L. C., and Garrett, E. N. (1991). Denervation does not alter the number of neuronal bungarotoxin binding sites on autonomic neurons in the frog cardiac ganglion. *J. Neurosci.* 11, 3610–3623. doi: 10.1523/jneurosci.11-11-03610.1991

Sargent, P. B., and Garrett, E. N. (1995). The characterization of alpha-bungarotoxin receptors on the surface of parasympathetic neurons in the frog heart. *Brain Res.* 680, 99–107. doi: 10.1016/0006-8993(95)00250-t

Sarter, M., and Bruno, J. P. (1997). Cognitive functions of cortical acetylcholine: toward a unifying hypothesis. *Brain Res.* 23, 28–46. doi: 10.1016/s0165-0173(96)00009-4

Sarter, M., and Paolone, G. (2011). Deficits in attentional control: cholinergic mechanisms and circuitry-based treatment approaches. *Behav. Neurosci.* 125, 825–835. doi: 10.1037/a0026227

Sasahara, K., Morigaki, K., and Shinya, K. (2013). Effects of membrane interaction and aggregation of amyloid β-peptide on lipid mobility and membrane domain structure. *Phys. Chem. Chem. Phys.* 15, 8929–8939. doi: 10.1039/c3cp44517h

Schmidt, J. T., and Freeman, J. A. (1980). Electrophysiologic evidence that retinotectal synaptic transmission in the goldfish is nicotinic cholinergic. *Brain Res.* 187, 129–142. doi: 10.1016/0006-8993(80)90499-0

Scholze, P., Ciuraszkiewicz, A., Groessl, F., Orr-Urtreger, A., McIntosh, J. M., and Huck, S. (2011). α4β2 nicotinic acetylcholine receptors in the early postnatal mouse superior cervical ganglion. *Dev. Neurobiol.* 71, 390–399. doi: 10.1002/dneu.20870

Sciacca, M. F., Kotler, S. A., Brender, J. R., Chen, J., Lee, D. K., and Ramamoorthy, A. (2012). Two-step mechanism of membrane disruption by Aβ through membrane fragmentation and pore formation. *Biophys. J.* 103, 702–710. doi: 10.1016/j.bpj.2012.06.045

Seghezza, S., Diaspro, A., Canale, C., and Dante, S. (2014). Cholesterol drives aβ(1-42) interaction with lipid rafts in model membranes. *Langmuir* 30, 13934–13941. doi: 10.1021/la502966m

Sepúlveda, F. J., Fierro, H., Fernandez, E., Castillo, C., Peoples, R. W., Opazo, C., et al. (2014). Nature of the neurotoxic membrane actions of amyloid-β on hippocampal neurons in Alzheimer's disease. *Neurobiol. Aging* 5, 472–481. doi: 10.1016/j.neurobiolaging.2013.08.035

Serrano-Pozo, A., Frosch, M. P., Masliah, E., and Hyman, B. T. (2011). Neuropathological alterations in Alzheimer disease. *Cold. Spring. Harb. Perspect. Med.* 1:a006189. doi: 10.1101/cshperspect.a006189

Shankar, G. M., Li, S., Mehta, T. H., Garcia-Munoz, A., Shepardson, N. E., Smith, I., et al. (2008). Amyloid-beta protein dimers isolated directly from Alzheimer's brains impair synaptic plasticity and memory. *Nat. Med.* 14, 837–842. doi: 10.1038/nm1782

Sharma, G., and Vijayaraghavan, S. (2001). Nicotinic cholinergic signaling in hippocampal astrocytes involves calcium-induced calcium release from intracellular stores. *Proc. Natl. Acad. Sci. U.S.A.* 98, 4148–4153. doi: 10.1073/pnas.071540198

Sharp, L., Salari, R., and Brannigan, G. (2019). Boundary lipids of the nicotinic acetylcholine receptor: spontaneous partitioning via coarse-grained molecular dynamics simulation. *Biochim. Biophys. Acta. Biomembr.* 1861, 887–896. doi: 10.1016/j.bbamem.2019.01.005

Shen, J., and Wu, J. (2015). Nicotinic cholinergic mechanisms in Alzheimer's disease. *Int. Rev. Neurobiol.* 124, 275–292. doi: 10.1016/bs.irn.2015.08.00

Shen, J. X., and Yakel, J. L. (2009). Nicotinic acetylcholine receptor-mediated calcium signaling in the nervous system. *Acta Pharmacol. Sin.* 30, 673–680. doi: 10.1038/aps.2009.64

Shimohama, S., Taniguchi, T., Fujiwara, M., and Kameyama, M. (1986). Changes in nicotinic and muscarinic cholinergic receptors in Alzheimer-type dementia. *J. Neurochem.* 46, 288–293. doi: 10.1111/j.1471-4159.1986.tb12960.x

Shringarpure, R., Grune, T., Sitte, N., and Davies, K. J. (2000). 4-Hydroxynonenal-modified amyloid-beta peptide inhibits the proteasome: possible importance in Alzheimer's disease. *Cell. Mol. Life Sci.* 57, 1802–1809. doi: 10.1007/pl00000660

Silveyra, M. X., Evin, G., Montenegro, M. F., Vidal, C. J., Martínez, S., and Culvenor, J. G. (2008). Presenilin 1 interacts with acetylcholinesterase and alters its enzymatic activity and glycosylation. *Mol. Cell. Biol.* 28, 2908–2919. doi: 10.1128/MCB.02065-2067

Silveyra, M. X., García-Ayllón, M. S., Serra-Basante, C., Mazzoni, V., García-Gutierrez, M. S., and Manzanares, J. (2012). Changes in acetylcholinesterase expression are associated with altered presenilin-1 levels. *Neurobiol. Aging* 33, 627–637. doi: 10.1016/j.neurobiolaging.2011.04.006

Simons, K., and Ikonen, E. (1997). Functional rafts in cell membranes. *Nature* 387, 569–572. doi: 10.1038/42408

Simons, K., and van Meer, G. (1988). Lipid sorting in epithelial cells. *Biochemistry* 23, 6197–6202. doi: 10.1021/bi00417a001

Simons, M., Keller, P., De Strooper, B., Beyreuther, K., Dotti, C. G., and Simons, K. (1998). Cholesterol depletion inhibits the generation of beta-amyloid in hippocampal neurons. *Proc. Natl. Acad. Sci. U.S.A.* 95, 6460–6464. doi: 10.1073/pnas.95.11.6460

Singer, A. S. J., and Nicolson, G. L. (1972). The Fluid Mosaic Model of the Structure of Cell Membranes. *Science* 175, 720–731. doi: 10.1126/science.175.4023.720

Small, D. H., Maksel, D., Kerr, M. L., Ng, J., Hou, X., Chu, C., et al. (2007). The b -amyloid protein of Alzheimer's disease binds to membrane lipids but does not bind to the a 7 nicotinic acetylcholine receptor. *J. Neurochem.* 101, 1527–1538. doi: 10.1111/j.1471-4159.2006.04444.x

Small, D. H., Michaelson, S., and Sberna, G. (1996). Non-classical actions of cholinesterases: role in cellular differentiation, tumorigenesis and Alzheimer's disease. *Neurochem. Int.* 28, 453–483. doi: 10.1016/0197-0186(95)00099-2

Sonnino, S., and Prinetti, A. (2013). Membrane domains and the "lipid raft" concept. *Curr Med Chem.* 20, 4–21. doi: 10.2174/0929867311320010003

Staneva, G., Puff, N., Stanimirov, S., Tochev, T., Angelova, M. I., and Seigneuret, M. (2018). The Alzheimer's disease amyloid-β peptide affects the size-dynamics of raft-mimicking Lo domains in GM1-containing lipid bilayers. *Soft. Matter.* 14, 9609–9618. doi: 10.1039/c8sm01636d

Stefani, M. (2010). Biochemical and biophysical features of both oligomer/fibril and cell membrane in amyloid cytotoxicity. *FEBS J.* 277, 4602–4613. doi: 10.1111/j.1742-4658.2010.07889.x

Stetzkowski-Marden, F., Gaus, K., Recouvreur, M., Cartaud, A., and Cartaud, J. (2006a). Agrin elicits membrane lipid condensation at sites of acetylcholine receptor clusters in C2C12 myotubes. *J. Lipid. Res.* 47, 2121–2133. doi: 10.1194/jlr.M600182-JLR200

Stetzkowski-Marden, F., Recouvreur, M., Camus, G., Cartaud, A., Marchand, S., and Cartaud, J. (2006b). Rafts are required for acetylcholine receptor clustering. *J. Mol. Neurosci.* 30, 37–38. doi: 10.1385/JMN:30:1:37

Subasinghe, S., Unabia, S., Barrow, C. J., Mok, S. S., Aguilar, M. I., and Small, D. H. (2003). Cholesterol is necessary both for the toxic effect of Abeta peptides on vascular smooth muscle cells and for Abeta binding to vascular smooth muscle cell membranes. *J. Neurochem.* 84, 471–479. doi: 10.1046/j.1471-4159.2003.01552.x

Sun, J., and Roy, S. (2018). The physical approximation of APP and BACE-1: a key event in alzheimer's disease pathogenesis. *Dev. Neurobiol.* 78, 340–347. doi: 10.1002/dneu.22556

Sunshine, C., and McNamee, M. G. (1992). Lipid modulation of nicotinic acetylcholine receptor function: the role of neutral and negatively charged lipids. *Biochim. Biophys. Acta* 1108, 240–246. doi: 10.1016/0005-2736(92)90031-g

Sunshine, C., and McNamee, M. G. (1994). Lipid modulation of nicotinic acetylcholine receptor function: the role of membrane lipid composition and fluidity. *Biochim. Biophys. Acta* 1191, 59–64. doi: 10.1016/0005-2736(94)90233-X

Tan, J. Z. A., and Gleeson, P. A. (2019). The role of membrane trafficking in the processing of amyloid precursor protein and production of amyloid peptides in Alzheimer's disease. *BBA - Biomembr.* 1861, 697–712. doi: 10.1016/j.bbamem.2018.11.013

Tapiola, T., Pirttilä, T., Mehta, P. D., Alafuzofff, I., Lehtovirta, M., and Soininen, H. (2000). Relationship between apoE genotype and CSF beta-amyloid (1-42) and tau in patients with probable and definite Alzheimer's disease. *Neurobiol. Aging* 21, 735–740. doi: 10.1016/s0197-4580(00)00164-0

Tenchov, B. G., MacDonald, R. C., and Siegel, D. P. (2006). Cubic phases in phosphatidylcholine-cholesterol mixtures: cholesterol as membrane "fusogen". *Biophys. J.* 91, 2508–2516. doi: 10.1529/biophysj.106.083766

Terzi, E., Hölzemann, G., and Seelig, J. (1997). Interaction of Alzheimer beta-amyloid peptide(1-40) with lipid membranes. *Biochemistry* 36, 14845–14852. doi: 10.1021/bi971843e

Thomsen, M. S., Andreasen, J. T., Arvaniti, M., and Kohlmeier, K. A. (2016). Nicotinic Acetylcholine receptors in the pathophysiology of Al zheimer's disease: the role of protein-protein interactions in current and future treatment. *Curr. Pharm. Des.* 22, 2015–2034. doi: 10.2174/1381612822666160127112357

Thornton, E., Vink, R., Blumbergs, P. C., and Van Den Heuvel, C. (2006). Soluble amyloid precursor protein alpha reduces neuronal injury and improves functional outcome following diffuse traumatic brain injury in rats. *Brain Res.* 1094, 38–46. doi: 10.1016/j.brainres.2006.03.107

Tozaki, H., Matsumoto, A., Kanno, T., Nagai, K., Nagata, T., Yamamoto, S., et al. (2002). The inhibitory and facilitatory actions of amyloid-beta peptides on

nicotinic ACh receptors and AMPA receptors. *Biochem. Biophys. Res. Commun.* 294, 42–45. doi: 10.1016/S0006-291X(02)00429-421

Turner, P. R., O'Connor, K., Tate, W. P., and Abraham, W. C. (2003). Roles of amyloid precursor protein and its fragments in regulating neural activity, plasticity and memory. *Prog Neurobiol.* 70, 1–32. doi: 10.1016/s0301-0082(03)00089-3

Unwin, N. (2005). Refined structure of the nicotinic acetylcholine receptor at 4A resolution. *J. Mol. Biol.* 346, 967–989. doi: 10.1016/j.jmb.2004.12.031

Uranga, R. M., Alza, N. P., Conde, M. A., Antollini, S. S., and Salvador, G. A. (2017). Phosphoinositides: two-path signaling in neuronal response to Oligomeric amyloid β peptide. *Mol. Neurobiol.* 54, 3236–3252. doi: 10.1007/s12035-016-9885-9883

van Meer, G. (2011). Dynamic transbilayer lipid asymmetry. *Cold Spring Harb. Perspect. Biol.* 3:004671. doi: 10.1101/cshperspect.a004671

Vestergaard, M., Hamada, T., Morita, M., and Takagi, M. (2010). Cholesterol, Lipids, Amyloid Beta, and Alzheimer' s. *Curr. Alzheimer Res.* 7, 262–270. doi: 10.2174/156720510791050821

Vetrivel, K. S., Cheng, H., Kim, S., Chen, Y., Barnes, N. Y., Parent, A. T., et al. (2005). Spatial segregation of gamma-secretase and substrates in distinct membrane domains. *J. Biol. Chem.* 280, 25892–25900. doi: 10.1074/jbc.M503570200

Vetrivel, K. S., Cheng, H., Lin, W., Sakurai, T., Li, T., Nukina, N., et al. (2004). Association of γ-secretase with lipid rafts in post-Golgi and endosome membranes. *J. Biol. Chem.* 279, 44945–44954. doi: 10.1074/jbc.M407986200

Vetrivel, K. S., and Thinakaran, G. (2006). Amyloidogenic processing of beta-amyloid precursor protein in intracellular compartments. *Neurology* 66, 69–73. doi: 10.1212/01.wnl.0000192107.17175.39

Villar, M. T., Artigues, A., Ferragut, J. A., and Gonzalez-Ros, J. M. (1988). Phospholipase A2 hydrolysis of membrane phospholipids causes structural alteration of the nicotinic acetylcholine receptor. *Biochim. Biophys. Acta* 938, 35–43. doi: 10.1016/0005-2736(88)90119-8

Wahrle, S., Das, P., Nyborg, A. C., Mclendon, C., Shoji, M., Kawarabayashi, T., et al. (2002). Cholesterol-dependent gamma-secretase activity in buoyant cholesterol-rich membrane microdomains. *Neurobiol. Dis.* 9, 11–23. doi: 10.1006/nbdi.2001.0470

Wakabayashi, M., Okada, T., Kozutsumi, Y., and Matsuzaki, K. (2005). GM1 ganglioside-mediated accumulation of amyloid beta-protein on cell membranes. *Biochem. Biophys. Res. Commun.* 328, 1019–1023. doi: 10.1016/j.bbrc.2005.01.060

Wang, H.-Y., Lee, D. H., Davis, C. B., and Shank, R. P. (2000a). Amyloid peptide Abeta(1-42) binds selectively and with picomolar affinity to alpha7 nicotinic acetylcholine receptors. *J. Neurochem.* 75, 1155–1161. doi: 10.1046/j.1471-4159.2000.0751155.x

Wang, H.-Y., Lee, D. H. S., D'Andrea, M. R., Peterson, P. A., Shank, R. P., and Reitz, A. B. (2000b). β-amyloid$_{1-42}$ binds to α7 nicotinic acetylcholine receptor with high affinity. Implications for Alzheimer's disease pathology. *J. Biol. Chem.* 275, 5626–5632. doi: 10.1074/jbc.275.8.5626

Wang, H. Y., Li, W., Benedetti, N. J., and Lee, D. H. (2003). Alpha 7 nicotinic acetylcholine receptors mediate beta-amyloid peptide-induced tau protein phosphorylation. *J. Biol. Chem.* 278, 1547–1553. doi: 10.1074/jbc.M212532200

Wang, H. Y., Stucky, A., Liu, J., Shen, C., Trocme-Thibierge, C., and Morain, P. (2009). Dissociating beta-amyloid from alpha 7 nicotinic acetylcholine receptor by a novel therapeutic agent, S 24795, normalizes alpha 7 nicotinic acetylcholine and NMDA receptor function in Alzheimer's disease brain. *J. Neurosci.* 229, 10961–10973. doi: 10.1523/JNEUROSCI.6088-08.2009

Wang, Y., Qu, D., and Wang, K. (2016). Therapeutic approaches to Alzheimer's disease through stimulating of non-amyloidogenic processing of amyloid precursor protein. *Eur. Rev. Med. Pharmacol. Sci.* 20, 2389–2403.

Watson, H. (2015). Biological membranes. *Essays Biochem.* 59, 43–69. doi: 10.1042/bse0590043

Wen, P.-C., Mahinthichaichan, P., Trebesch, N., Jiang, T., Zhao, Z., Shinn, E., et al. (2018). Microscopic view of lipids and their diverse biological functions. *Curr. Opin. Struct. Biol.* 51, 177–186. doi: 10.1016/j.sbi.2018.07.003

Wenk, G. L. (1997). The nucleus basallis magnocellularis cholinergic system: one hundred years of progress. *Neurobiol. Learn. Mem.* 67, 85–95. doi: 10.1006/nlme.1996.3757

Wenz, J. J., and Barrantes, F. J. (2005). Nicotinic acetylcholine receptor induces lateral segregation of phosphatidic acid and phosphatidylcholine in reconstituted membranes. *Biochemistry* 44, 398–410. doi: 10.1021/bi048026g

Whitehouse, P. J., Martino, A. M., Antuono, P. G., Lowenstein, P. R., Coyle, J. T., Price, D. L., et al. (1986). Nicotinic acetylcholine binding sites in Alzheimer's disease. *Brain Res.* 371, 146–151. doi: 10.1016/0006-8993(86)90819-x

Whitehouse, P. J., Price, D. L., Clark, A. W., Coyle, J. T., and DeLong, M. R. (1981). Alzheimer disease: evidence for selective loss of cholinergic neurons in the nucleus basalis. *Ann. Neurol.* 10, 122–126. doi: 10.1002/ana.410100203

Whitehouse, P. J., Struble, R. G., Clark, A. W., and Price, D. L. (1982). Alzheimer disease: plaques, tangles, and the basal forebrain. *Ann. Neurol.* 12:494. doi: 10.1002/ana.410120517

Willmann, R., Pun, S., Sadasivam, G., Santos, A. F., Caroni, P., and Fuhrer, C. (2006). Cholesterol and lipid microdomains stabilize the postsynapse at the neuromuscular junction. *EMBO J.* 25, 4050–4060. doi: 10.1038/sj.emboj.7601288

Wonnacott, S., Barik, J., Dickinson, J., and Jones, I. W. (2006). Nicotinic receptors modulate transmitter cross talk in the CNS: Nicotinic modulation of transmitters. *J. Mol. Neurosci.* 30, 137–140. doi: 10.1385/JMN:30:1:137

Wood, W. G., Li, L., Müller, W. E., and Eckert, G. P. (2014). Cholesterol as a causative factor in Alzheimer disease: a debatable hypothesis. *J.Neurochem.* 129, 559–572. doi: 10.1111/jnc.12637

Wood, W. G., Schroeder, F., Igbavboa, U., Avdulov, N. A., and Chochina, S. V. (2002). Brain membrane cholesterol domains, aging and amyloid beta-peptides. *Neurobiol. Aging* 23, 685–694. doi: 10.1016/s0197-4580(02)00018-0

Woolf, N. J. (1998). A structural basis for memory storage in mammals. *Prog. Neurobiol.* 55, 59–77. doi: 10.1016/s0301-0082(97)00094-4

Wu, J., Khan, G. M., and Nichols, R. A. (2007). Dopamine release in prefrontal cortex in response to beta-amyloid activation of alpha7 nicotinic receptors. *Brain Res.* 1182, 82–89. doi: 10.1016/j.brainres.2007.08.079

Wu, J., Kuo, Y. P., George, A. A., Xu, L., Hu, J., and Lukas, R. J. (2004). Beta-Amyloid directly inhibits human alpha4beta2-nicotinic acetylcholine receptors heterologously expressed in human SH-EP1 cells. *J. Biol. Chem.* 279, 37842–37851. doi: 10.1074/jbc.M400335200

Wu, Y., and Luo, Y. (2005). Transgenic C. *elegans as a model in Alzheimer's research*. *Curr. Alzheimer. Res.* 2, 37–45. doi: 10.2174/1567205052772768

Xie, H. Q., Leung, K. W., Chen, V. P., Chan, G. K. L., Xu, S. L., Guo, A. J. Y., et al. (2010a). Chemico-Biological Interactions PRiMA directs a restricted localization of tetrameric AChE at synapses. *Chem. Biol. Interact.* 187, 78–83. doi: 10.1016/j.cbi.2010.02.018

Xie, H. Q., Liang, D., Leung, K. W., Chen, V. P., Zhu, K. Y., Chan, W. K. B., et al. (2010b). Targeting Acetylcholinesterase to Membrane Rafts a function mediated by the proline-rich membrane anchor (PRiMA) in neurons. *J. Biol. Chem.* 285, 11537–11546. doi: 10.1074/jbc.M109.038711

Xiong, H., Callaghan, D., Jones, A., Walker, D. G., Lue, L. F., and Beach, T. G. (2008). Cholesterol retention in Alzheimer's brain is responsible for high beta- and gamma-secretase activities and Abeta production. *Neurobiol. Dis.* 29, 422–437. doi: 10.1016/j.nbd.2007.10.005

Xiu, J., Nordberg, A., Zhang, J. T., and Guan, Z. Z. (2005). Expression of nicotinic receptors on primary cultures of rat astrocytes and up-regulation of the alpha7, alpha4 and beta2 subunits in response to nanomolar concentrations of the beta-amyloid peptide(1-42). *Neurochem. Int.* 47, 281–290. doi: 10.1016/j.neuint.2005.04.023

Yahi, N., and Fantini, J. (2014). Deciphering the glycolipid code of Alzheimer's and Parkinson's amyloid proteins allowed the creation of a universal ganglioside-binding peptide. *PLoS One.* 9:e104751. doi: 10.1371/journal.pone.0104751

Yamamoto, N., Hasegawa, K., Matsuzaki, K., Naiki, H., and Yanagisawa, K. (2004). Environment- and mutation-dependent aggregation behavior of Alzheimer amyloid beta-protein. *J. Neurochem.* 90, 62–69. doi: 10.1111/j.1471-4159.2004.02459.x

Yamamoto, N., Matsubara, T., Sato, T., and Yanagisawa, K. (2008). Age-dependent high-density clustering of GM1 ganglioside at presynaptic neuritic terminals promotes amyloid β -protein fi brillogenesis. *Biochim. Biophys. Acta* 1778, 2717–2726. doi: 10.1016/j.bbamem.2008.07.028

Yamamoto, N., Matsuzaki, K., and Yanagisawa, K. (2005). Cross-seeding of wild-type and hereditary variant-type amyloid beta-proteins in the presence of gangliosides. *J. Neurochem.* 95, 1167–1176. doi: 10.1111/j.1471-4159.2005.03444.x

Yanagisawa, K. (2005). GM1 ganglioside and the seeding of amyloid in Alzheimer's disease: endogenous seed for Alzheimer amyloid. *Neuroscientist* 11, 250–260. doi: 10.1177/1073858405275177

Yanagisawa, K., and Ihara, Y. (1998). GM1 ganglioside-bound amyloid beta-protein in Alzheimer's disease brain. *Neurobiol. Aging* 19(1 Suppl.), S65–S67. doi: 10.1177/1073858405275177

Yanagisawa, K., Odaka, A., Suzuki, N., and Ihara, Y. (1995). GM1 ganglioside-bound amyloid beta-protein (A beta): a possible form of preamyloid in Alzheimer's disease. *Nat. Med.* 1, 1062–1066. doi: 10.1038/nm1095-1062

Yang, X., Askarova, S., and Lee, J. C.-M. (2010). Membrane biophysics and mechanics in Alzheimer's disease. *Mol. Neurobiol.* 41, 138–148. doi: 10.1007/s12035-010-8121-9

Yankner, B. A., Duffy, L. K., and Kirschner, D. A. (1990). Neurotrophic and neurotoxic effects of amyloid beta protein: reversal by tachykinin neuropeptides. *Science* 250, 279–282. doi: 10.1126/science.2218531

Yip, C. M., Darabie, A. A., and McLaurin, J. (2002). Abeta42-peptide assembly on lipid bilayers. *J. Mol. Biol.* 318, 97–107. doi: 10.1016/s0022-2836(02)00028-1

Yu, W. F., Guan, Z. Z., Bogdanovic, N., and Nordberg, A. (2005). High selective expression of alpha7 nicotinic receptors on astrocytes in the brains of patients with sporadic Alzheimer's disease and patients carrying Swedish APP 670/671 mutation: a possible association with neuritic plaques. *Exp. Neurol.* 2192, 215–225. doi: 10.1016/j.expneurol.2004.12.015

Yu, X., and Zheng, J. (2012). Cholesterol promotes the interaction of Alzheimer β-amyloid monomer with lipid bilayer. *J. Mol. Biol.* 421, 561–571. doi: 10.1016/j.jmb.2011.11.006

Zampagni, M., Evangelisti, E., Cascella, R., Liguri, G., Becatti, M., Pensalfini, A., et al. (2010). Lipid rafts are primary mediators of amyloid oxidative attack on plasma membrane. *J. Mol. Med.* 88, 597–608. doi: 10.1007/s00109-010-0603-608

Zhang, Q., Powers, E. T., Nieva, J., Huff, M. E., Dendle, M. A., Bieschke, J., et al. (2004). Metabolite-initiated protein misfolding may trigger Alzheimer's disease. *Proc. Natl. Acad. Sci. U.S.A.* 101, 4752–4757. doi: 10.1073/pnas.0400924101

Zhu, D., Xiong, W. C., and Mei, L. (2006). Lipid rafts serve as a signaling platform for Nicotinic Acetylcholine receptor clustering. *J. Neurosci.* 26, 4841–4851. doi: 10.1523/JNEUROSCI.2807-05.2006

Zimmerberg, J., and Gawrisch, K. (2006). The physical chemistry of biological membranes. *Nat. Chem. Biol.* 2, 564–567. doi: 10.1038/nchembio1106-564

Zou, K., Gong, J. S., Yanagisawa, K., and Michikawa, M. (2002). A novel function of monomeric amyloid beta-protein serving as an antioxidant molecule against metal-induced oxidative damage. *J. Neurosci.* 22, 4833–4841. doi: 10.1523/jneurosci.22-12-04833.2002

Zou, K., Kim, D., Kakio, A., Byun, K., Gong, J. S., Kim, J., et al. (2003). Amyloid beta-protein (Abeta)1-40 protects neurons from damage induced by Abeta1-42 in culture and in rat brain. *J. Neurochem.* 87, 609–619. doi: 10.1046/j.1471-4159.2003.02018.x

Conflict of Interest Statement: The authors declare that the research was conducted in the absence of any commercial or financial relationships that could be construed as a potential conflict of interest.

frontiers in Cellular Neuroscience

ORIGINAL RESEARCH
published: 25 July 2019
doi: 10.3389/fncel.2019.00334

A Defective Crosstalk Between Neurons and Müller Glial Cells in the *rd1* Retina Impairs the Regenerative Potential of Glial Stem Cells

Yanel A. Volonté[1], Harmonie Vallese-Maurizi[1†], Marcos J. Dibo[1†], Victoria B. Ayala-Peña[1], Andrés Garelli[1], Samanta R. Zanetti[1], Axel Turpaud[1], Cheryl Mae Craft[2,3], Nora P. Rotstein[1], Luis E. Politi[1] and Olga L. German[1]**

[1] Instituto de Investigaciones Bioquímicas de Bahía Blanca, Departamento de Biología, Bioquímica y Farmacia, Universidad Nacional del Sur – National Research Council of Argentina (CONICET), Bahía Blanca, Argentina, [2] Department of Ophthalmology, USC Roski Eye Institute, Keck School of Medicine of the University of Southern California, Los Angeles, CA, United States, [3] Department of Integrative Anatomical Sciences, Keck School of Medicine of the University of Southern California, Los Angeles, CA, United States

OPEN ACCESS

Edited by:
Mario Eduardo Guido, Center for Research in Biological Chemistry Córdoba (CIQUIBIC), Argentina

Reviewed by:
Antje Grosche, Ludwig-Maximilians-Universität München, Germany
Hugo Guerrero-Cazares, Mayo Clinic, United States

***Correspondence:**
Luis E. Politi
inpoliti@criba.edu.ar
Olga L. German
olgerman@criba.edu.ar

[†] These authors have contributed equally to this work

Specialty section:
This article was submitted to Cellular Neuropathology, a section of the journal Frontiers in Cellular Neuroscience

Received: 28 January 2019
Accepted: 08 July 2019
Published: 25 July 2019

Citation:
Volonté YA, Vallese-Maurizi H, Dibo MJ, Ayala-Peña VB, Garelli A, Zanetti SR, Turpaud A, Craft CM, Rotstein NP, Politi LE and German OL (2019) A Defective Crosstalk Between Neurons and Müller Glial Cells in the rd1 Retina Impairs the Regenerative Potential of Glial Stem Cells. Front. Cell. Neurosci. 13:334. doi: 10.3389/fncel.2019.00334

Müller glial cells (MGC) are stem cells in the retina. Although their regenerative capacity is very low in mammals, the use of MGC as stem cells to regenerate photoreceptors (PHRs) during retina degenerations, such as in retinitis pigmentosa, is being intensely studied. Changes affecting PHRs in diseased retinas have been thoroughly investigated; however, whether MGC are also affected is still unclear. We here investigated whether MGC in *retinal degeneration 1* (*rd1*) mouse, an animal model of retinitis pigmentosa, have impaired stem cell properties or structure. *rd1* MGC showed an altered morphology, both in culture and in the whole retina. Using mixed neuron-glial cultures obtained from newborn mice retinas, we determined that proliferation was significantly lower in *rd1* than in *wild type (wt)* MGC. Levels of stem cell markers, such as *Nestin* and *Sox2*, were also markedly reduced in *rd1* MGC compared to *wt* MGC in neuron-glial cultures and in retina cryosections, even before the onset of PHR degeneration. We then investigated whether neuron-glial crosstalk was involved in these changes. Noteworthy, *Nestin* expression was restored in *rd1* MGC in co-culture with *wt* neurons. Conversely, *Nestin* expression decreased in *wt* MGC in co-culture with *rd1* neurons, as occurred in *rd1* MGC in *rd1* neuron-glial mixed cultures. These results imply that MGC proliferation and stem cell markers are reduced in *rd1* retinas and might be restored by their interaction with "healthy" PHRs, suggesting that alterations in *rd1* PHRs lead to a disruption in neuron-glial crosstalk affecting the regenerative potential of MGC.

Keywords: Müller glial cells, stem cells, retinal degeneration, retinal regeneration, photoreceptors

INTRODUCTION

Retinitis pigmentosa constitutes a group of inherited diseases that have as a common feature the degeneration and loss of rod and cone photoreceptors (PHRs). Although the genetic mutations leading to this disease are well-established, it has still no cure or effective treatments. The use of stem cells to replace neuronal loss in the injured retina is now being actively investigated as a promising

new treatment for this disease. The discovery that Müller glial cells (MGC) can regenerate retina neurons following diverse insults (Karl et al., 2008) makes these cells potentially useful candidates for replacement therapies. MGC have multiple key roles in the retina, such as providing nutrients and trophic factors required for PHR survival (Bringmann et al., 2009; Vecino et al., 2016). Fischer and Reh (Fischer and Reh, 2003) have shown that MGC are stem cells that effectively regenerate the eye in fish and lower vertebrates. However, their regenerative potential is extremely low in vertebrates; generation of a few novel neurons in the murine retina was only possible because of the use of multiple exogenous stimuli (Fischer and Reh, 2003). *Notch* and *Wnt* signaling have been proposed to regulate the mechanisms by which MGC promote retina regeneration (Das et al., 2006). We previously showed that MGC express several stem cell markers and can transform PHR progenitor cells into multipotent stem cells, which in turn differentiate as functional PHRs (Insua et al., 2008; Simón et al., 2012). Nevertheless, MGC are inefficient in regenerating the retina in humans, such as in patients suffering from retinitis pigmentosa, and in the *rd1* mice, a frequently used animal model for this disease.

About 100 gene mutations have been identified to cause PHR cell death in retinitis pigmentosa (Hartong et al., 2006; Huang et al., 2017), most of them affecting PHRs. In the *rd1* mice, the occurrence of a mutation in the beta-subunit of rod cGMP phosphodiesterase gene, which mainly affects PHRs, is responsible for the disease (Pittler and Baehr, 1991). By contrast, only a few mutations causing the disease have been found in MGC; one of them, affecting a gene encoding CRALBP in an autosomal recessive form of retinitis pigmentosa, may disturb Vitamin A metabolism (Maw et al., 1997). Little is known regarding the role of MGC in this disease. Following neuronal damage in the injured retina, MGC show a reactive gliosis, characterized by an increase in glial cell proliferation, preceded by downregulation of the cell cycle blocker, p27 ^{kip1} (Dyer and Cepko, 2000; Bringmann et al., 2006). Defects in MGC have been reported in another ocular disorder, Retinal Telangiectasia; a mutation in *Crb1* gene delocalizes the cellular connections at retinal MGC/PHR junctions (Zhao et al., 2015). Even when these alterations in MGC may not be the main cause of retinal degenerations, they might disrupt the normal crosstalk between MGC and PHRs, thus contributing to the degenerative process (Dong et al., 2017).

Retinal degeneration in the *rd1* mice occurs much faster than in humans. In the healthy mouse retina, most PHRs are "born" between PN days (PND) 0 and 2; soon after, their progenitors exit the cell cycle and begin their differentiation; a small peak in their apoptosis is detected by PND 7 and 8, and no cell death is detectable thereafter (Young, 1984). In the *rd1* retina, significant PHR cell death starts by PND 11, peaking by PND 15 and 16 (Lolley et al., 1994; Portera-Cailliau et al., 1994); after 4 weeks, while in the healthy mice PHRs become differentiated and functional, in the *rd1* mice the PHR cell layer completely disappears (Farber and Lolley, 1974; Politi and Adler, 1988).

The finding of the group of Canto Soler that human induced pluripotent stem cells (iPS) differentiate into retinal progenitors that originate retinal tissue containing the major retinal cell types, including functional PHRs (Zhong et al., 2014), underscores the therapeutic potential of stem cells. However, whether MGC are adequate sources of stem cells for retina regeneration in mammals remains to be established. In particular, alterations in PHRs in retinitis pigmentosa might change their normal interactions with MGC, disturbing neuron-glial crosstalk; in turn, this would lead to a deficient release of survival factors by MGC and contribute to a generalized retinal damage. Hence, understanding the significance of the alterations in MGC and in neuron-glial crosstalk during retina degeneration is particularly relevant when considering the use of MGC as a source of stem cells in regenerative therapies.

To establish whether MGC isolated from diseased retinas are a viable option for replacement therapies it is necessary to ascertain if these cells differ in their regenerative potential and in their cellular interactions with PHRs in healthy and degenerating retinas. For this purpose, we first analyzed stem cell characteristics of MGC in whole retinas and neuron-glial cultures from *rd1* and *wt* animals. Then, we separately prepared pure neuronal and MGC cultures to obtain co-cultures and investigated the interactions of *rd1* MGC with either *rd1* or *wt* neurons. We determined that proliferation and the levels of stem cell markers decreased in *rd1* MGC compared to their *wt* counterparts, and that these markers were partially restored when *rd1* MGC were co-cultured with *wt* neurons, suggesting that an impaired neuron-glial crosstalk affects the stem cell potential of *rd1* MGC.

MATERIALS AND METHODS

Materials

Two-day-old C57BL/6J (*wt)* or C57BL/6J-Pde6brd1-2J/J (*rd1)* mice bred in our own colony were used in all experiments. All proceedings concerning animal use were in accordance with the guidelines published in the NIH *Guide for the care and use of laboratory animals* and following the protocols approved by the Institutional Committee for the Care of Laboratory Animals from the Universidad Nacional del Sur (Argentina). Plastic 35-mm-diameter and 60-mm-diameter culture dishes were purchased from Greiner Bio-One (GBO). Fetal bovine serum (FBS) was from Natocor (Córdoba, Argentina). Dulbecco's modified Eagle's medium (DMEM) was purchased from Life Technologies (Grand Island, NY, United States). Trypsin, trypsin inhibitor, transferrin, hydrocortisone, putrescine, insulin, polyornithine, selenium, gentamycin, 4,6-diamidino-2-phenylindole (DAPI), poly-ornithine, paraformaldehyde (PF) and primers for RQ-PCR were from Sigma (St. Louis, MO, United States). Fluorescein-conjugated secondary antibodies were from Jackson InmunoResearch (West Grove, PA, United States). Type 2 collagenase was purchased from Invitrogen. Monoclonal antibodies against BrdU (clone G3G4) and VIMENTIN (clone 40E-C) were from DSHB (developed under the auspices of the NICHD and maintained by the University of Iowa, Department of Biological Sciences), NESTIN was from DSHB and from ABCAM (clone Rat-401), anti-Glutamine Synthetase (GS) and anti-SOX2 (SRY, sex determing region Y-box 2) were

from ABCAM. Polyclonal goat anti-SOX2 (Santa Cruz # sc-17320) was a generous gift from Valeria Levi and Alejandra Guberman (University of Buenos Aires, Argentina). Polyclonal rabbit anti-CRX was from Cheryl M. Craft's laboratory (Zhu and Craft, 2000). CellTracer® Green CMFDA Dye, Alexa Fluor™ 555 Phalloidin, TO-PRO™-3 Iodide, terminal deoxynucleotidyl transferase (Tdt), BrdUTP (5-Bromo-2′-Deoxyuridine 5′-Triphosphate) and TdT Buffer were from Molecular Probes, Invitrogen (Carlsbad, CA, United States). Quick-zol RNA Isolation Reagent was from Kalium technologies (Embiotec). The Moloney Murine Leukemia Virus Reverse Transcriptase (M-MLV RT) and RNasin® Ribonuclease Inhibitors were from Promega. KAPPA SYBRs FAST qPCR Kit were from Biosystems S.A. (Buenos Aires, Argentina). The IntraStain, Two-step fixation and permeabilization for Flow Cytometry was from Agilent Dako. OCT Embedding Compound Cryoplast® was from Biopack®. Solvents were HPLC grade, and all other reagents were analytical grade.

Retina Cultures

Müller Glial Cell Cultures

Purified cultures of Müller glial cells were prepared following protocols previously described (Hicks and Courtois, 1990). Briefly, newborn mouse eyes were excised and incubated overnight in DMEM at room temperature and then treated with trypsin (1 mg/ml) and type 2 collagenase (2 mg/ml). Retinas were then dissected, chopped into small pieces, and seeded onto 35-mm-diameter plastic dishes, in culture medium supplemented with 10% FBS. The medium was routinely replaced every 3–4 days. After 8–10 days, pure Müller glial cells became confluent and were used for neuron-glial co-cultures (**Figures 1a–e**).

Neuronal Cultures

Neuronal cultures from 2-day mouse retinas were obtained following previously described procedures, with slight modifications (Politi et al., 1996; Rotstein et al., 1996, 1997). In brief, after dissection and dissociation of the retinas, the cells were resuspended in a chemically defined medium (Politi et al., 1988) and seeded onto 35-mm-diameter plastic dishes, pretreated with poly-ornithine and schwannoma-conditioned medium (Adler, 1982). Cultures were incubated at 36°C in a humidified atmosphere of 5% CO_2. Immediately after seeding, nearly all cells were undifferentiated retinal progenitor cells, which were still in the cell cycle; many of them underwent their last mitotic division during the first day *in vitro*. Soon after exiting the cell cycle, cells began to differentiate into PHRs and amacrine neurons (**Figures 1f–j**).

Mixed Neuron–Glial Cultures

To analyze the interactions between MGC and neurons from either *wt* or *rd1* retinas, we obtained long-term mixed cultures of MGC and retina neurons, following previously described protocols (Politi et al., 1996; Simón et al., 2012), with slight modifications. Briefly, retinas from 2-day-old mice were chemically and mechanically dissociated with trypsin [250 μl of 0.25% trypsin in 6 ml of calcium- and magnesium-free Hanks (CMF)] for 6 min. Cells were then resuspended in DMEM medium supplemented with 10% FBS and seeded onto 35-mm-diameter plastic dishes with no previous treatment. Analysis of

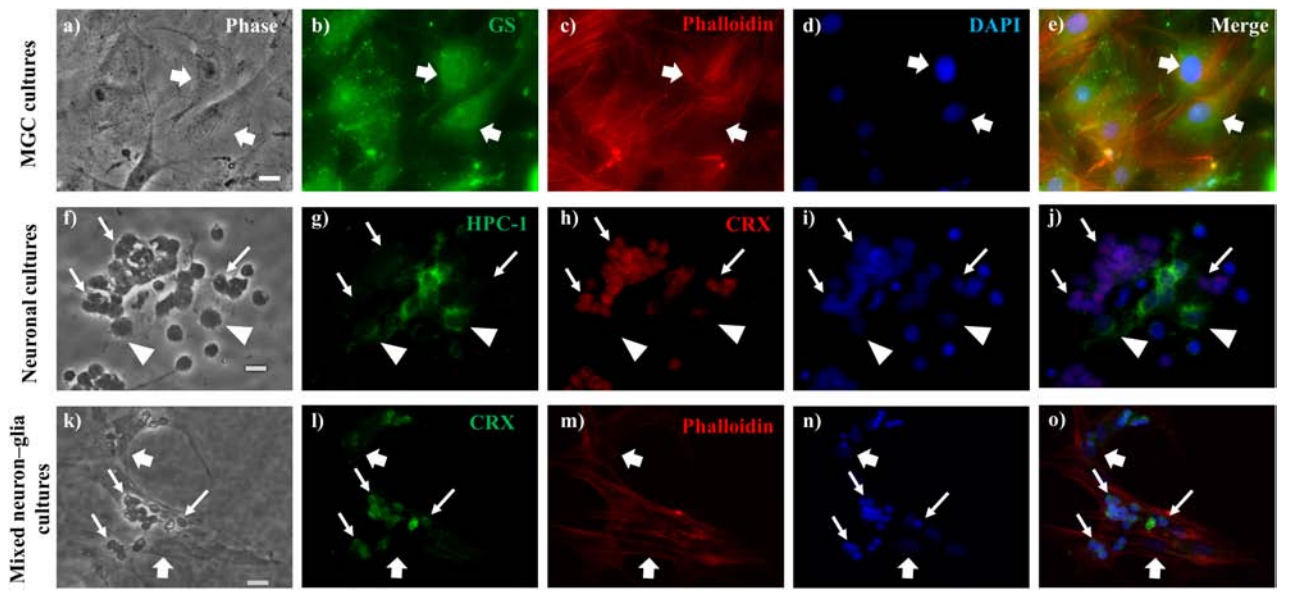

FIGURE 1 | Identification of neurons and Müller glial cells (MGC) in glial, neuronal and mixed neuron-glial cultures. Phase **(a,f,k)** and fluorescence **(b–e,g–j,l–o)** photomicrographs of *wt* MGC culture **(a–e)**, 2-day *wt* neuronal cultures **(f–j)** and 6-day *wt* mixed neuron-glial cultures **(k–o)**, showing MGC (thick arrows) identified by their anti-Glutamine Synthase (GS) labeling **(b)**, with their actin cytoskeleton visualized by phalloidin labeling **(c,m)**; photoreceptors (thin arrows) labeled with anti-CRX **(h,l)** and amacrine neurons (arrowheads) labeled with HPC-1 **(g)** antibodies. Cell nuclei were visualized with the DNA probe DAPI **(d,i,n)**. Note that cell nuclei were markedly smaller in neurons than in MGC **(n)**. Merge images **(e,j,o)**. Scale bars: 20 μm.

MGC began at day 6, since only after this time *in vitro*, MGC are clearly recognizable and begin to express most of their markers. This time *in vitro* is equivalent to 8 days *in vivo*, when the retina has a maximum of gliogenic factors and cues that signal and stabilize glial fate (Nelson et al., 2011; **Figures 1k–o**).

Neuron-Glial Co-cultures

To investigate whether the crosstalk between neurons and glial cells might modulate the stem cell potential of MGC, we prepared neuron-glial co-cultures combining *rd1* and *wt* neurons with either *rd1* or *wt* MGC. Pure neuronal cultures from *wt* or *rd1* retinas were initially labeled with the fluorescent dye CellTracer® following the manufacturer's specifications and after 3 days *in vitro* they were co-cultured with unlabeled *rd1* or *wt* MGC for 24 h. For this purpose, confluent (8−10 days) *rd1* or *wt* MGC were detached from their substrata and reseeded over the pre-labeled pure neuronal cultures. As the dye fluorescence persists during the whole culture time, even after mitosis, unlabeled MGC and their newly generated daughter cells were easily recognized from the pre-labeled neurons. Cells were then fixed and analyzed by immunocytochemical methods and RQ-PCR.

In the diverse cellular culture protocols described above, the number of cells seeded in each culture dish was standardized; in each experiment we seeded about 700,000 cells per dish (700,979 cells/dish; +/−49,755), so the starting points were comparable.

Immunocytochemical and Immunohistochemical Methods

To prepare retina cryosections, PND 9, PND 14 and PND30 (adult) *wt* and *rd1* mice were sacrificed, their eyes were enucleated, and then fixed for 3 h. in PBS-2% PF at 4°C. After lens removal, eyes were immersed in PBS-30% sucrose until sunk, mounted in OCT blocks, frozen first at −20°C and then stored at −70°C until they were cut with a Leica CM1860 cryostat. Cultures were fixed for 1 h. with PBS-4%PF, followed by permeation with 0.1% Triton X-100. The cultures and slices were then stained at room temperature for 10 min with DAPI, TOPRO-3, to visualize nuclei, or for 30 min with phalloidin, to label the actin cytoskeleton. Alternatively, immunohistological staining of cells was carried out using an anti-CRX rabbit antibody (1:800), anti-NESTIN mouse antibody (1:100), anti-GS rabbit antibody (1:100), anti-BrdU mouse antibody (1:00), and anti-opsin (Rho4D2) mouse antibody (1:100). Secondary antibodies, conjugated with Cy2 or Cy3 (1:200 dilution) were then used. Background labeling was removed by washing with PBS prior to microscopy.

Cell Identification

Müller glial cells were identified by their flat and irregular morphology and by immunocytochemistry, with polyclonal antibodies against GS (Simón et al., 2012, 2015; **Figures 1a–e,k–o** and **Supplementary Figures S1f–j**). PHRs and amacrine cells were the two main neuronal types present in neuronal cultures; they represented more than 98% of the cells and were identified by their morphology using phase-contrast microscopy, and by immunocytochemistry with monoclonal antibodies against CRX and syntaxin (HPC-1), respectively. Controls for immunocytochemistry were done by omitting the primary or secondary antibodies. PHRs have a round cell body of about 5−10 μm, and a short and single axon, which usually ends in a conspicuous synaptic "spherule"; sometimes these cells display a connecting cilium at the opposite end, but they fail to develop their characteristic outer segments (**Figures 1f–j,k–o** and **Supplementary Figures S1a–e**, **S2b,f**); all of them express CRX, the PHR specific transcription factor, and were identified by using a CRX antibody (Cheryl M. Craft's laboratory; University of Southern California, Los Angeles, CA, United States), (Garelli et al., 2006; **Figures 1h,l**). Amacrine cells are larger than PHRs (10–30 μm) and have multiple neurites; they all show anti-syntaxin immunoreactivity (Barnstable, 1980), which starts at early stages of development, and is retained even after undergoing degenerative changes that alter their morphology (Politi et al., 2001; **Figure 1g**).

Evaluation of Cell Proliferation

To identify cells that were replicating their DNA, mixed neuron-glial cultures were incubated with 50 μM BrdU (final concentration in culture) for the final 24 h. before fixation, at days 6 and 11 in culture. After fixation, BrdU uptake was analyzed by immunocytochemistry using an anti- BrdU monoclonal antibody.

Flow Cytometry

For quantitative evaluation of NESTIN expression, MGC from 11-day neuron–glial mixed cultures were analyzed by flow cytometry. Single cell suspensions, previously filtered using a 32-μm pore-size nylon mesh, were fixed and then permeated with solutions A and B from Dako IntraStain kit. Cells were then successively stained with primary (NESTIN 1/100) and secondary (Cy2 anti-mouse 1/200) antibodies. Flow cytometry analyses were done with a FACSCalibur flow cytometer (BD Biosciences). Quantification of NESTIN-positive MGC by FACS was performed using FACSComp. A minimum of 10,000 events was analyzed for each sample.

Real-Time Quantitative Polymerase Chain Reaction (RQ-PCR)

Wild type and *rd1* mice were sacrificed at PND 0 (birth), PND 2, PND 4, PND 8, PND 10 (when all cell types have been generated and early signs of degeneration appear), PND 20 (progressive stages of PHR degeneration), PND 40 (complete loss of PHR), and PND 180. Retinas from three different mice were used for each stage. Retinas were dissected, and total RNA was extracted with Quick-Zol reagent (Kalium Technologies), according to the manufacturer's instructions. The amount of RNA was measured by spectrophotometry. Reverse transcription of total RNA was performed using the High-Capacity cDNA Reverse Transcription Kit. Quantitative PCR was done by SYBR Green real-time PCR methods. The relative mRNA expression was calculated using the quantification cycle method (Cq-method) (Bustin et al., 2009), with *Eef2* (Eukaryotic elongation factor) for normalization. All experimental conditions were processed in triplicate.

RQ-PCR primers were specifically designed to amplify the following cDNAs:

m-*Bax* F(5′TACTCCCGTCCTACCTCAGC 3′) R(5′CGCGG GTACTAAATGAACGC 3′),
m-*Nes* F(5′CCCTTAGTCTGGAAGTGGCTAC 3′) R(5′GTGC TGGTCCTCTGGTATCC 3′),
m-*Sox2* F(5′TGGATAACTGTTCAGCCACCAA 3′) R(5′GGC GCAGTATCTCATCTGCT 3′),
m-*Vim* F(5′ATGCTTCTCTGGCACGTCTT 3′) R(5′AGCCA CGCTTTCATACTGCT 3′),
m-*Eef2* F(5′GACTCTGAGAATCCGTCGCC 3′) R(5′CACAC AAGGGAGTCGGTCAG 3′).

The efficiency was about 90% for each pair of primers.

Quantitative Image Analysis

After performing immunocytochemical labeling, cultures and tissue cryosections were analyzed by phase contrast and epifluorescence microscopy, using a Nikon Eclipse E600 microscope with a C-C Phase Contrast Turret Condenser and a Y-FL Epi-Fluorescence Attachment or with a laser scanning confocal microscope (Leica DMIRE2) with a 63X-water objective. Phase photomicrographs were processed using the XnView image processor to give a differential interference contrast effect. Fluorescence intensities of the 8- or 16-bit image were analyzed after manually outlining regions of interest (ROI) with the software Fiji-Image J (NIH, Bethesda, MD, United States) (Schindelin et al., 2012). The average fluorescence intensity of a given ROI was measured within the stained positive regions of the cell, and the average fluorescence intensity of an area of the same size positioned over a region outside the cell was subtracted. In cryosections, the measurements were carried out on randomly chosen cells, selected from phase-contrast images obtained from three PND 14 mice per each condition. We then calculated the *Corrected Total Cell Fluorescence* (CTCF) as *Integrated Density - (Area of selected cells x Mean fluorescence of background readings.* To evaluate morphological changes of radial processes of MGC during the time course of the degeneration, we measured and compared the thickness of NESTIN-immunolabeled radial processes in both *wt* and *rd1* mice at PND 14. Ten measurements were performed for each condition. Data were evaluated by Student's *t*-test and differences were considered significant at $p < 0.05$.

Statistical Analysis

The results represent the average of at least three experiments (± SEM), unless specifically indicated, and each experiment was performed in triplicate. For cytochemical studies, 10 fields per sample, randomly chosen, were analyzed in each case. Each value represents the average of at least three experiments, with three or four dishes for each condition ± SEM, unless otherwise indicated. Statistical significance was determined by Student's two-tailed *t*-test or by ANOVA followed by Tukey's test with $p < 0.05$ considered significant.

RESULTS

The Course of *rd1* Neuronal Death Was Similar *in vivo* and *in vitro*

We first compared the structure of *rd1* and *wt* retinas, at 9, 14, and 30 days of development *in vivo*. As expected, at PND 9 the outer nuclear layer (ONL) of both *wt* and *rd1* retinas had almost the same width and showed a similar pattern of opsin labeling (**Figures 2Aa–f**). In contrast, by PND 14 the ONL in *rd1* retinas was significantly reduced and showed a decrease in opsin labeling, which was below detectable levels after 4 weeks of development (Adult). In contrast, ONL width and opsin labeling were preserved in *wt* retinas (**Figures 2Ag–r**).

To investigate interactions between neurons and MGC, we prepared neuron-glial cultures (**Figures 2Ba–h**). Analysis of CRX labeling at 6 and 11 days *in vitro* revealed that most neurons in these mixed cultures were PHRs. In mixed *wt* cultures, PHRs amounted to 96 ± 29% and 94 ± 18.5%, respectively, of total neurons; similarly, in *rd1* cultures, these values were 94.5 ± 37% and 96 ± 20%, respectively, **Supplementary Figure S2**). The course of PHR death in mixed neuro-glial cultures was in close correspondence with the observed in whole retinas. By day 11 in culture (equivalent to 13 days *in vivo*), a marked increase in the amount of TUNEL-positive neurons (**Figures 2Bb,f**) and of pyknotic nuclei (**Figures 2Bc,g**, white arrowheads) was observed in *rd1* compared to *wt* neuronal cultures. Whereas at day 6 in culture (equivalent to 8 days *in vivo*) both *wt* and *rd1* cultures had similar percentages of pyknotic or fragmented neuronal nuclei, by day 11 the percentage of fragmented nuclei remained at 18 ± 3% in *wt* cultures but increased to 32.5 ± 1.7% in *rd1* cultures (**Figure 2Bi**). Consistently, the percentages of TUNEL-positive PHRs by day 11 were 7.5 ± 3.8% and 23.9 ± 5.4% in *wt* and *rd1*cultures, respectively (**Figure 2Bj**). In contrast, no TUNEL-positive MGC were observed at either time in culture; in addition, MGC had intact nuclei in the *rd1* and in the *wt* cultures (**Figures 2Bb,c,f,g** empty arrowheads). Quantitative analysis showed that the percentage of surviving *rd1* and *wt* MGC in each case was 100% ± 0.0%; (**Figure 2Bk**). We then evaluated the expression level of the Bcl-2 pro-apoptotic protein BAX in mixed neuron-glia cultures. The translocation of this protein to the outer mitochondrial membrane is crucial for triggering the intrinsic apoptotic pathway. Analysis of *Bax* mRNA levels by RQ-PCR showed they significantly increased (in arbitrary units) in *rd1* compared to *wt* cultures, with a 3.7 ± 0.4 fold-increase at day 6 and 1.3 ± 0.2 fold-increase at day 11 (**Figure 2Bl**).

Cell Cycle Progression Decreased in *rd1* MGC

Since one of the hallmarks of stem cells is their proliferative capacity, we evaluated whether it was affected in *rd1* MGC in mixed neuron-glial cultures (**Figures 3a–j**). Evaluation of BrdU uptake in mixed cultures showed that this uptake was lower in *rd1* than in *wt* MGC. By day 11, less BrdU-labeled MGC were visible in *rd1* than in *wt* cultures (**Figures 3a,f**). Quantitative analysis established that the percentages of BrdU-labeled MGC were significantly lower in *rd1* than in *wt* MGC (**Figure 3k**), both

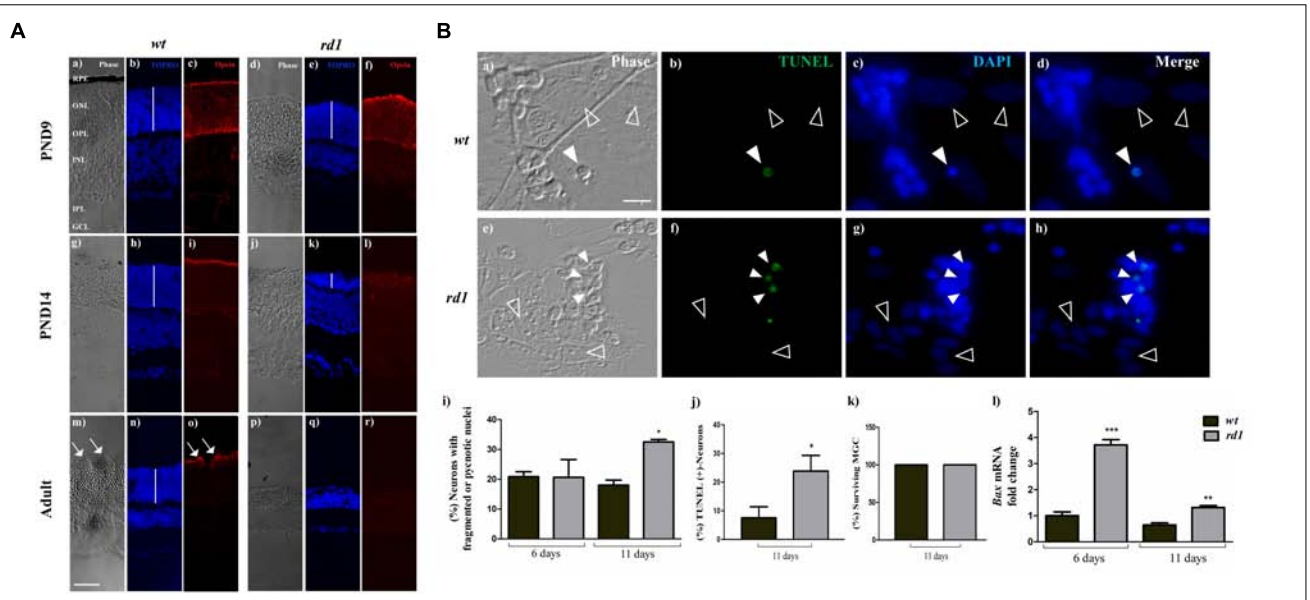

FIGURE 2 | Selective degeneration of photoreceptors in the *rd1* mice retina and in mixed *rd1* neuron-glial cultures. Panel **(A)** phase **(a,d,g,j,m,p)** and fluorescence **(b,c,e,f,h,i,k,l,n,o,q,r)** photomicrographs of retinal cryosections from *wt* PND 9 **(a–c)**, PND 14 **(g–i)** and Adult (**m–o**, PND30); and *rd1* PND 9 **(d–f)**, PND 14 **(j–l),** and Adult **(p–r)**. Photoreceptors were labeled with an anti-opsin, Rho4-D2, antibody **(c,f,i,l,o,r)** and cell nuclei were stained with the nuclear probe TOPRO-3 **(b,e,h,k,n,q)**. White vertical bars show the thickness of the Outer Nuclear Layer (ONL) in *wt* and *rd1* retinas. Opsin immunolabeling was evident in *wt* and *rd1* retinas at PND 9 **(c,f)**, and concentrated in photoreceptor outer segments of *wt* retinas at PND 14 and 30 **(i,o)**; in contrast, it was barely visible in *rd1* retinas at PND 14 **(l)** and completely disappeared by PND 30 **(r)**. White arrows in **(m,o)** show outer segments in *wt* photoreceptors at PND 30. Panel **(B)** phase **(a,e)** and fluorescence **(b–d,f–h)** photomicrographs of mixed neuron-glial cultures from *wt* **(a–d)** and *rd1* **(e–h)** mice after 11 days in culture showing apoptotic neurons (white arrowheads) detected by TUNEL labeling **(b,f)**. Nuclei were stained with DAPI **(c,g).** Note that MGC nuclei (empty arrowheads in **a–h**) remained intact in *wt* and *rd1* cultures. Bars in **(i)** show the percentage of neurons with fragmented or pyknotic nuclei, **(j)** depict the percentage of TUNEL-positive neurons, **(k)** show the percentage of surviving MGC and **(l)** represent the fold-change in Bax mRNA levels relative to these levels in wt cultures at day 6. In Panel **(A)** scale bar: 50 μm. In Panel **(B)** scale bar: 5 μm. Results represent the mean ± SEM of three experiments ($n = 3$). Statistical analysis was performed using a two-tailed Student *t*-test [Panel **(B) j,k**] and a One-way ANOVA with a *post hoc* Tukey test [Panel **(B) i,l**]. *$p < 0.05$, **$p < 0.01$, ***$p < 0.001$.

after 6 and 11 days in culture. By day 11, when *wt* cultures still had 37.36 ± 5.4% BrdU-positive cells, this percentage was only 5.2 ± 1.7% in *rd1* cultures (**Figure 3k**).

A reduction in proliferation in *rd1* MGC would lead to a progressive decrease in their number. Quantification of *rd1* and *wt* MGC evidenced that the number of *rd1* MGC was approximately half of that observed in *wt* cultures by day 6 (**Table 1**). This difference decreased with time in culture and tended to disappear by day 11; this might be a consequence of the cells reaching confluence in *wt* cultures, which posed additional restrictions to their proliferation. As a whole, the above results suggest that proliferation, a critical parameter of stem cells, was reduced in *rd1* MGC.

TABLE 1 | Number of MGC per dish.

	MGC/dish	
Days in culture	***wt***	***rd1***
6	32375 ± 7249	16720 ± 1747*
11	104110 ± 15110	95297 ± 14693

*Number of rd1 and wt MGC per 35 mm dish after 6 and 11 in vitro. One-tailed Student t-test, *p < 0.05.*

Stem Cell Markers Decreased in *rd1* MGC

To investigate whether the stem cell potential of MGC in *rd1* retinas was affected, we evaluated the expression of *Nestin*, a neuroectodermal stem cell marker that is expressed in many different, mitotically active cell types during development (Lendahl et al., 1990; Park et al., 2010). By day 11, nearly all MGC in *wt* neuron-glial cultures had an intense NESTIN labeling, with a widespread, radial distribution toward the edges of the cells; by contrast, *rd1* MGC showed weaker NESTIN labeling, which remained close to the nucleus or formed fiber bundles (**Figures 4Aa–h**). Further analysis of NESTIN expression by flow cytometry showed that at day 11 the number of MGC expressing NESTIN was similar in both *wt* and *rd1* cultures (**Figure 4Ai**); however, evaluation of mean fluorescence intensity (MFI) evidenced that this intensity, i.e., NESTIN expression, was lower in *rd1* than in *wt* MGC (**Figures 4Aj,k**). This implies that although the amount of MGC expressing NESTIN remained similar in *rd1* and *wt* cultures, individual *rd1* MGC expressed less NESTIN than their *wt* counterparts.

We then evaluated the levels of *Nestin* mRNA in *rd1* and *wt* mixed neuron-glial cultures at days 6 and 11. At day 6, *Nestin* mRNA levels were similar in *rd1* and *wt* cultures; however, by

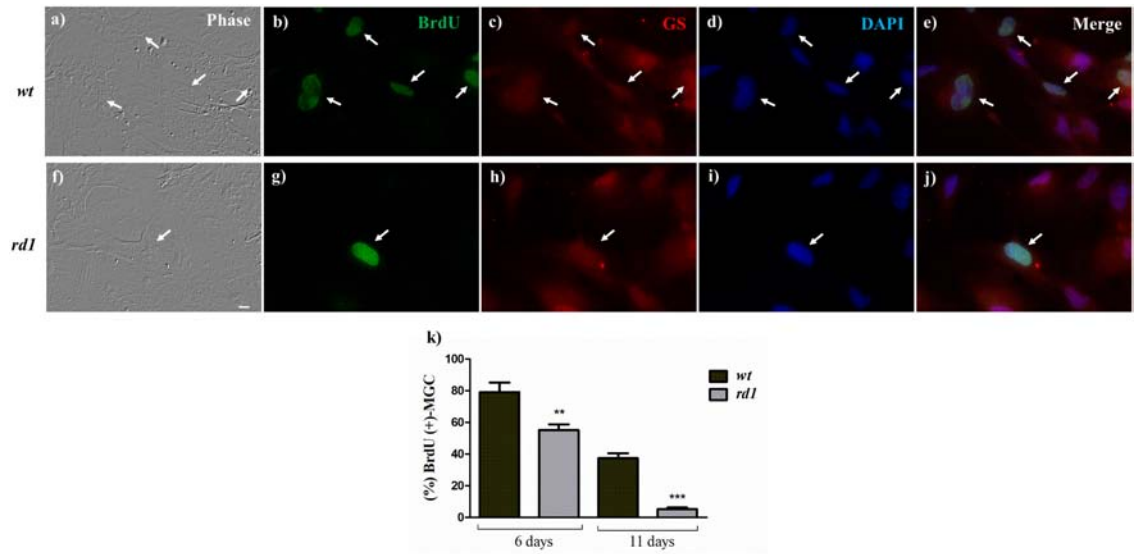

FIGURE 3 | Decreased proliferation of *rd1* Müller glial cells in neuron-glial cultures. Phase **(a,f)** and fluorescence photomicrographs of 11-day *wt* **(a–e)** and *rd1* **(f–j)** mixed neuron-glial cultures showing BrdU uptake by MGC, determined with a monoclonal anti-BrdU antibody (**b,g**, arrows). MGC were identified by their labeling with an anti-GS antibody **(c,h)**. Nuclei were labeled with DAPI **(d,i)**. Merge **(e,j)**. Bars in **(k)** represent the percentage of BrdU-positive at days 6 and 11. Scale bar: 30 μm. Results represent the mean ± SEM of three experiments ($n = 3$). Statistical analysis was performed using a One-way ANOVA with a *post hoc* Tukey test. $^{**}p < 0.01$, $^{***}p < 0.001$.

day 11, they were significantly reduced in *rd1* compared with *wt* cultures (**Figure 4Al**).

Since NESTIN participates in the organization of intermediate filaments (Boraas et al., 2016), we also analyzed the expression of *Vimentin*, a type III intermediate filament protein. *Vimentin* mRNA levels showed a significant fold-reduction in *rd1* neuron-glial cultures compared with *wt* cultures, both by days 6 and 11 (**Figure 4Am**).

Similar changes in NESTIN expression were observed in MGC *in vivo*. Since the reduction in NESTIN expression was more evident at day 11 *in vitro,* we analyzed NESTIN distribution in cryosections from *wt* and *rd1* retinas at PND 14, an equivalent time of development *in vivo*. MGC showed an intense NESTIN labeling throughout the *wt* retina, which overlapped with GS labeling (**Figures 4Ba–d**). In contrast, NESTIN labeling was reduced and lost its fibrillary pattern in MGC in *rd1* retinas (**Figures 4Be–h**), and the number of NESTIN-labeled MGC per area decreased in *rd1* compared to *wt* retinas (**Figure 4Bk**). Quantitative analysis of fluorescence intensity evidenced a remarkable decrease in NESTIN immunolabeling in *rd1* retinas, which was reduced to half of that observed in *wt* retinas (**Figure 4Bl**). Conspicuous morphological changes were also evident in MGC in *rd1* retinas. The basal regions of MGC projections were thicker in *rd1* than in *wt* retinas, as observed when analyzing equivalent areas and positions in retinal sections (**Figures 4Bi,j,m**).

A maximum peak of mitosis occurs in newborn mice between PND 0 to PND 3 (Livesey and Cepko, 2001). As NESTIN has been proposed to play a role in the transition from proliferating stem cells to postmitotic neurons (Zimmerman et al., 1994), *Nestin* expression would be expected to increase at PND 3, the timepoint at which most proliferating stem cells in the retina become postmitotic and begin to differentiate as neurons (Livesey and Cepko, 2001). Analysis of the changes in *Nestin* mRNA levels in *wt* and *rd1* retinas at different developmental times evidenced that in *wt* retinas *Nestin* mRNA increased 4.1 ± 2.1 and 6.3 ± 0.01 fold at PND 2 and PND 4, respectively, compared to PND 0 (**Figure 4Bn**). By contrast, in *rd1* retinas *Nestin* mRNA at PND 2 remained at PND 0 levels, and by PND 4, its fold increase was lower than that observed in *wt* retinas (**Figure 4Bn**). By PND 8, the fold change in *Nestin* levels was below PND0 levels, both in *rd1* and *wt,* and remained lower than PND0 levels from PND 10 to adulthood.

Expression of *Sox2,* a transcription factor involved in self-renewal of stem cells was also affected in *rd1* retinas. In *wt* retinas, *Sox2* mRNA levels peaked at PND 2, rapidly decreased at PND 4 and were below PND 0 levels beyond PND 8 (**Figure 5h**) whereas in *rd1* retinas, *Sox2* mRNA levels were significantly lower than in *wt* retinas at PND 2 and 4 (**Figure 5h**).

When PND 14 retina cryosections were analyzed, SOX2 expression was reduced in *rd1* compared to *wt* retinas (**Figures 5a–f**, arrowheads). At this time of development, *rd1* retinas had fewer SOX2-positive nuclei than *wt* retinas (**Figure 5g**). Whereas *wt r*etinas had SOX2-positive cells in the ganglion cell layer, virtually no SOX2-positive cells were detectable in this layer in *rd1* retinas.

Interaction With *wt* Neurons Restored *Nestin* Expression in *rd1* MGC

As a whole, the above results show that proliferation and stem cell markers were decreased in *rd1* MGC, even before the

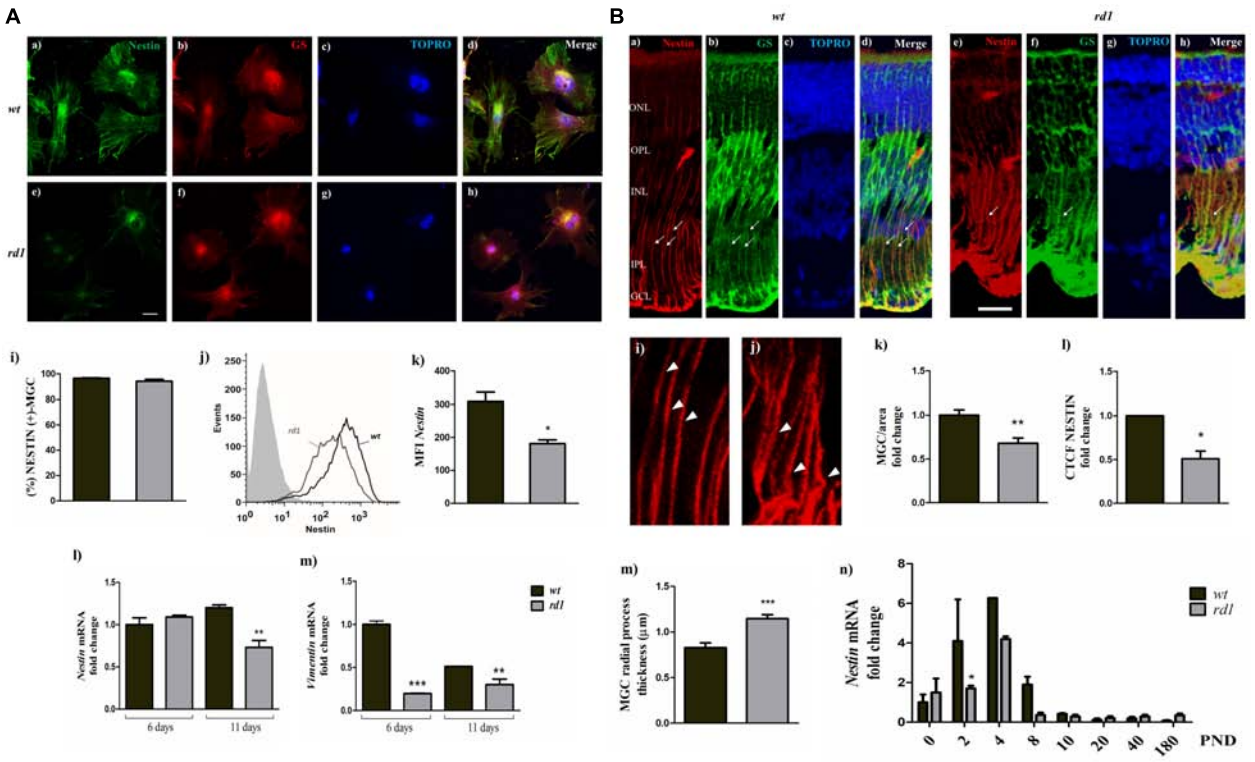

FIGURE 4 | *Nestin* expression decreased in *rd1* retinas. Panel **(A)** fluorescence photomicrographs of 11-day *wt* **(a–d)** and *rd1* **(e–h)** mixed neuron-glial cultures showing NESTIN **(a,e)**; GS **(b,f)** and TOPRO-3 **(c,g)** labeling. Merge pictures are shown in **(d,h)**. Bars in **(i)** depict the percentage of NESTIN-expressing MGC, determined by flow cytometry. The histogram **(j)** shows the distribution of the intensity of NESTIN expression in MGC and bars in **(k)** show the medium fluorescence intensity of NESTIN labeling in *wt* and *rd1* MGC. Bars represent the fold-change in *Nestin* **(l)** and *Vimentin* mRNA levels **(m)** in *rd1* and *wt* cultures, relative to their levels in *wt* cultures at day 6. Scale bar: 40 μm. Results represent the mean ± SEM of three experiments ($n = 3$). Panel **(B)** Fluorescence photomicrographs of *wt* **(a–d)** and *rd1* **(e–h)** PND 14 retina cryosections showing MGC labeling with NESTIN **(a,e)** and GS **(b,f)**; MGC projections are indicated with thin arrows. Nuclei were stained with TOPRO-3 **(c,g)**. Merge pictures are shown in **(d,h)**. Confocal optical sections of retinas show the regular nestin filament distribution in MGC radial processes in *wt* retinas (**i**, arrowheads) and the conspicuous thickening and disorganization of radial processes at their basal ends in the *rd1* retinas (**j**, arrowheads). Bars in **(k)** show the fold change in the number of NESTIN-expressing MGC per area. Bars **(l)** depict the *Corrected Total Cell Fluorescence* (CTCF) as *Integrated Density− (Area of selected cells x Mean fluorescence of background readings,* analyzed after manually outlining regions of interest (ROI) with the software Fiji-Image J (see section "Materials and Methods"). Bars in **(m)** depict the thickness of MGC radial processes in *wt* and *rd1* retinas [shown with thin arrows in Panel **(B) a,b,d,e,f,h**; arrowheads in **i,j**]. Bars in **(n)** represent the fold changes in *Nestin* mRNA levels at PND 0-180 in *rd1* and *wt* mice retinas relative to their levels at PND 0 in *wt* retinas. Scale bar: 20 μm. Results in **k–m** represents the mean ± SEM of ten separate measures. Results in **(n)** represent the mean ± SEM of three mice per condition at each PND day analyzed. Statistical analysis was performed using a two-tailed Student *t*-test [Panels **(A) i,k** and **(B) k–m]** and a One-way ANOVA with a *post hoc* Tukey test [Panels **(A) l,m and (B) n]**. $^{*}p < 0.05$, $^{**}p < 0.01$, $^{***}p < 0.001$.

PHR degeneration peak, suggesting a deficiency in the stem cell potential of these cells. We reasoned that the alterations in *rd1* neurons might impair neuron-glial crosstalk and affect the normal functions of *rd1* MGC, thus contributing to this deficiency. If this was the case, the interaction of healthy *wt* neurons with *rd1* MGC would, at least partially, reestablish their stem cell potential. Our culture systems allow us to prepare purified neuronal and MGC cultures, from developing *rd1* or *wt* retinas, and then seed them together to obtain co-cultures with different combinations of *rd1* and *wt* cells. To investigate the influence of neuronal cells on the stem cell capability of MGC, we separately cultured pure *rd1* and *wt* retinal neurons, labeled them with CellTracer® for 3 days and then seeded unlabeled *wt* or *rd1* MGC over these neuronal cultures, to analyze NESTIN expression in the different neuron-glial co-cultures. *rd1* MGC co-cultured with *rd1* neurons had a faint NESTIN labeling (**Figures 6Aa–d**). Noteworthy, interaction with *wt* neurons (**Figures 6Ae–h**) increased NESTIN expression in *rd1* MGC. Quantitative analysis evidenced that NESTIN-positive *rd1* MGC significantly increased in *rd1* MGC-*wt* neuron co-cultures compared to *rd1* pure MGC cultures; in contrast, no significant change was observed in *rd1* MGC-*rd1* neuron co-cultures compared to *rd1* pure MGC cultures (**Figure 6Ai**). To further assess the effect of neuron-glial interactions on *Nestin* levels, we analyzed the levels of *Nestin* mRNA. In *rd1* MGC-*wt* neuron co-cultures, *Nestin* mRNA levels increased almost 50-fold relative to *rd1* pure MCG cultures; in contrast, no increase was observed in *rd1* MGC- *rd1* neuron co-cultures (**Figure 6Aj**).

If neuron-glial interactions were responsible for modulating the levels of stem cell markers such as *Nestin*, *rd1* neurons

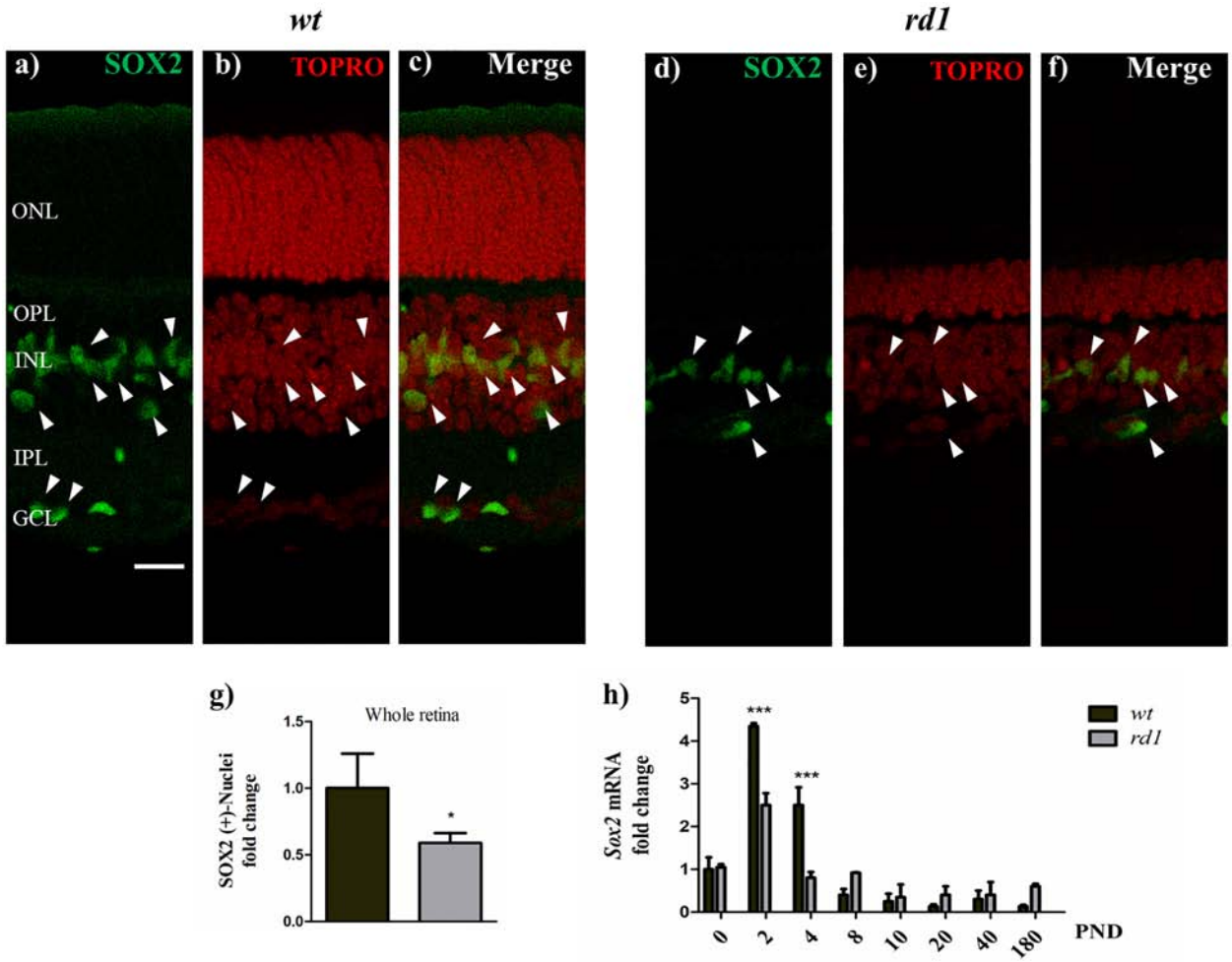

FIGURE 5 | SOX2 expression decreased in *rd1* retinas. Fluorescence photomicrographs show SOX2 expression (**a,d**, arrowheads) in retina cryosections obtained from *wt* **(a–c)** and *rd1* **(d–f)** mice at PND14, determined with an anti-SOX2 polyclonal antibody. Nuclei were stained with DAPI **(b,e)** and merge pictures are shown in **(c,f)**. Bars **(g)** show the fold change of total SOX2-positive nuclei in *rd1* retinas relative to *wt* retinas. Bars **(h)** represent the fold changes in *Sox2* mRNA levels at PND 0-180 in *rd1* and *wt* mice retinas relative to their levels at PND 0 in *wt* retinas. Scale bar: 20 μm. Results in **(g)** represent the mean ± SEM of ten measures. Results in **(h)** represent the mean ± SEM of three mice per condition. Statistical analysis was performed using a two-tailed Student *t*-test **(g)**, and a One-way ANOVA with a *post hoc* Tukey test **(h)**. $^{*}p < 0.05$, $^{***}p < 0.001$.

would downregulate these levels in *wt* MGC in co-culture. This reduction in NESTIN expression was evident when *wt* MGC were co-cultured with *rd1* neurons. Whereas *wt* MGC showed a bright NESTIN expression when co-cultured with *wt* neurons (**Figures 6Ba–d**), their NESTIN expression was noticeably reduced when co-cultured with *rd1* neurons (**Figures 6Be–h**). The fold change in NESTIN-positive *wt* MGC, relative to their number in *wt* pure MGC cultures, was reduced by half when co-cultured with *rd1* neurons; in contrast, NESTIN positive-*wt* MGC were the same in pure *wt* MGC cultures and in co-culture with *wt* neurons (**Figure 6Bi**). Noteworthy, the levels of *Nestin* mRNA were dramatically reduced in *wt* MGC-*rd1* neuron co-cultures relative to pure *wt* MGC cultures, and significantly increased, up to nearly 3.3 ± 1 times in *wt* MGC-*wt* neuron co-cultures (**Figure 6Bj**).

As a whole, these results suggest that the crosstalk between neurons and MGC is crucial for regulating Nestin expression in MGC, and interactions with *wt* neurons can restore this expression in *rd1* MGC.

MGC Had a Distorted Morphology and Were Overloaded With Neurons in *rd1* Cultures

We finally analyzed whether the changes in the levels of intermediate filaments, as NESTIN and VIMENTIN, in *rd1* MGC correlated with changes in MGC morphology. Analysis of their actin cytoskeleton revealed that *rd1* MGC had remarkable alterations in their morphology. By day 6, *wt* cultures had many MGC, which exhibited an extended actin cytoskeleton (**Figures 7a,b,d**). In contrast, *rd1* cultures showed fewer

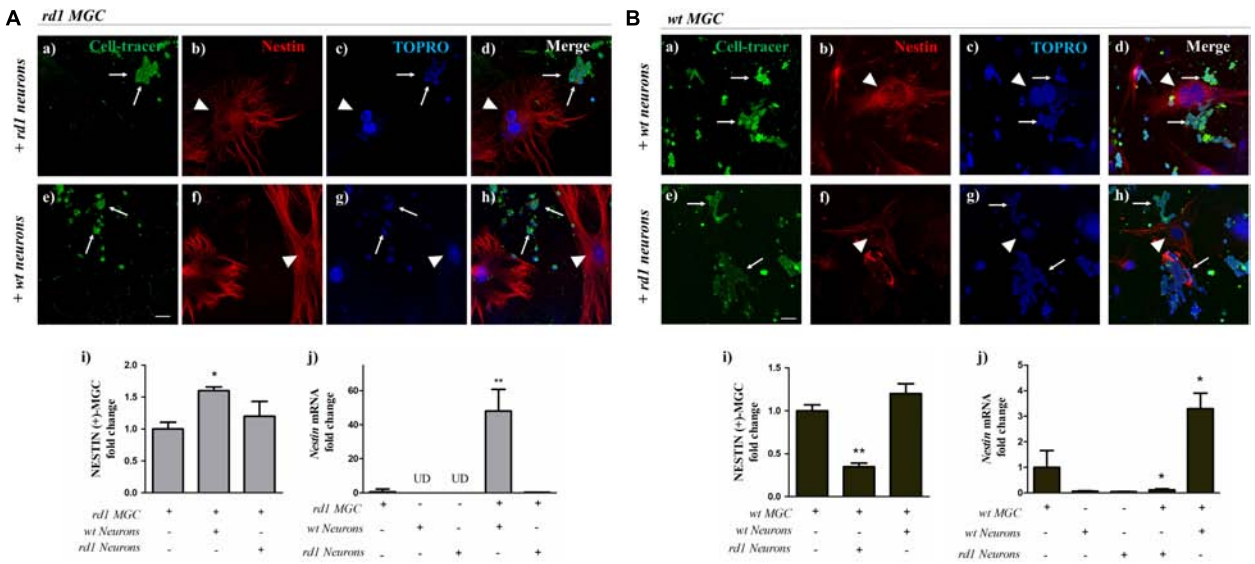

FIGURE 6 | Changes in *Nestin* expression in MGC when co-cultured with *wt* or *rd1* neurons. Neuron-glial co-cultures were prepared seeding unlabeled *rd1* MGC (Panel **A**) or *wt* MGC (Panel **B**) over 3-day cultures of either *rd1* or *wt* neurons labeled with the green fluorescent CellTracer probe (thin arrows), and were then incubated for 24 h. Fluorescence photomicrographs show Cell-Trace labeled neurons (green in **a,e**) and NESTIN-labeled MGC (red in **b,f**, arrowheads); nuclei were stained with TOPRO-3 (blue in **c,g**). Merge pictures are shown in **(d,h)**. Bars in Panels **A (i)** and **B (i)** show the fold change in NESTIN-positive *rd1 MGC* (Panel **A**) *or wt MGC* (Panel **B**) when co-cultured with either *wt* neurons or *rd1* neurons, relative to pure *rd1* or *wt* MGC cultures, respectively. Bars in Panels **A (j)** and **B (j)** depict the fold change *in Nestin* mRNA levels in *rd1* MGC (Panel **A**) or *wt* MGC (Panel **B**) when co-cultured with either *wt* or *rd1* neurons, relative to pure *rd1 or wt* MGC cultures, respectively. Scale bar: 40 μm. Results represent the mean ± SEM of three experiments ($n = 3$). UD, undetected. Statistical analysis was performed using a One-way ANOVA with a *post hoc* Tukey test. $^*p < 0.05$, $^{**}p < 0.01$.

MGC, which evidenced a marked retraction in their actin cytoskeleton and almost a complete loss of their lamellipodia, leading to a decrease in cell body size and a distorted morphology (**Figures 7e,f,h**).

In addition, the neuron:MGC ratio was markedly different in *wt* and *rd1* neuro-glial cultures. Whereas in *wt* cultures few neurons were observed growing on MGC (**Figures 7a–d**), their number markedly increased in *rd1* cultures by day 6 (**Figures 7e–h**). This difference might result from the reduction in the number of MGC in *rd1* cultures compared with *wt* cultures at this time of development, due to the decrease in their proliferation, as described above (**Table 1**). Quantitative analysis showed that the ratio of neurons per glial cell at day 6 was almost three-fold higher in *rd1* than in *wt* cultures (**Table 2**). This implies that individual *rd1* MGC supported significantly more neurons than their *wt* counterparts.

TABLE 2 | MGC: neuron ratio.

	G:N	
Days in culture	***wt***	***rd1***
6	1 : 2.3 ± 0.5	1 : 6.6 ± 2.5*
11	1 : 1 ± 0.3	1 : 2 ± 0.5

*MGC: neuron ratios in wt and rd1 mixed neuron-glial cultures at 6 and 11 days in vitro. One-way ANOVA with a post hoc Tukey test, *p < 0.05.*

DISCUSSION

The major conclusions from the present work are that *rd1* MGC have a significant decrease in their stem cell markers even before the degeneration of PHR started in *rd1* retinas. Furthermore, at least one of their stem cell characteristics was restored by their interaction with *wt* neurons in co-culture, suggesting that a defective cross talk between neurons and MGC is at least partially responsible for this decrease.

The mechanisms regulating the neurogenic potential of MGC remain enigmatic. Their regenerative capacity is remarkably dissimilar among vertebrates. Although in the zebrafish, MGC can efficiently regenerate the retina after different lesions (Sherpa et al., 2008, 2014; Lenkowski and Raymond, 2014; Ranski et al., 2018), these cells are unable to function as retinal progenitors in mammals (Goldman, 2014). Intriguingly, cumulative evidence suggests that mammalian MGC have the molecular mechanisms to accomplish retina regeneration. Different injuries trigger their proliferation; activation of MGC following oxidative damage induces their dedifferentiation and re-entry in the cell cycle (Abrahan et al., 2009); neurotoxic damage promotes proliferation and the expression of progenitor markers in retina MGC (Ooto et al., 2004), which differentiate as specific neuronal types (Das et al., 2006). A human embryonic stem cell line (hESC) can differentiate into retinal amacrine neurons and ganglion cells, and integration of the hESC-derived retinal progenitors with a degenerated mouse retina increases the expression of specific PHR markers (Lamba et al., 2006). Human induced

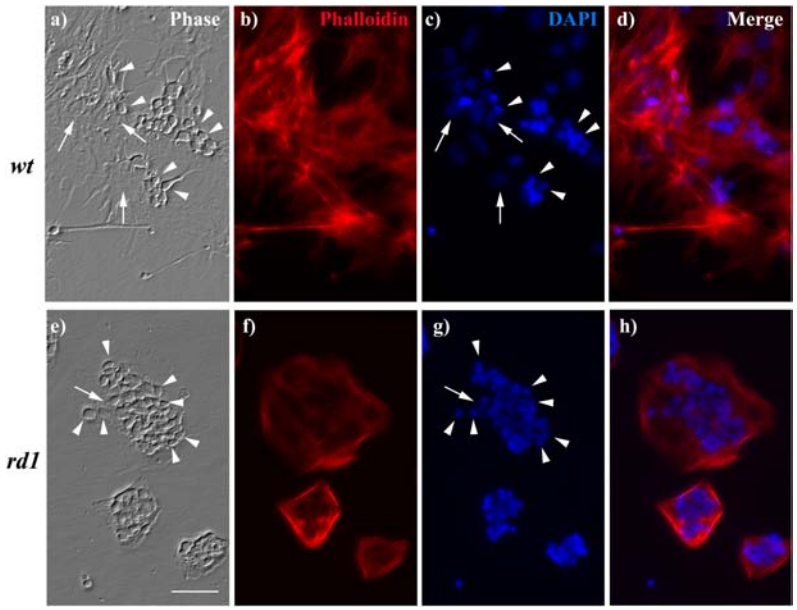

FIGURE 7 | MGC morphology and neuron:glial ratio was altered in *rd1* mixed neuron-glial cultures. Phase **(a,e)** and fluorescence photomicrographs **(b–d,f–h)** of 6-day *wt* **(a–d)** and *rd1* **(e–h)** mixed neuron glial cultures showing neuronal cells (arrowheads) growing on top of MGC (arrows). Actin cytoskeleton was stained with phalloidin **(b,f)** and nuclei with DAPI **(c,g)**. Merge pictures are shown in **(d,h)**. Scale bar: 50 μm.

pluripotent stem cells (hiPSC) have been shown to differentiate into retinal progenitors and recapitulate retinal development to form three-dimensional retina cups containing major retinal cell types, including PHR with an advanced differentiation and photosensitivity (Zhong et al., 2014), implying that the generation of functional PHR from stem cells is feasible in mammals. Stem cells in mammalian retinas, such as MGC, can be assumed to replace neurons lost during the life span of healthy retinas. However, the substantial differences in the genetic setup of hiPSCs and mature MGC likely contribute to the incapacity of the latter to regenerate PHRs during retina degeneration. The inability of MGC to regenerate the retina has been suggested to result from either intrinsic features of mammalian MGC or extrinsic properties of their "niche," which interfere with the reprograming process of these cells (Xia and Ahmad, 2016). Analysis of cultured MGC from *rd1* retinas revealed that their cell cycle was downregulated, compared to *wt* MGC. By day 6, prior to the onset of PHR degeneration, the number of *rd1* MGC was about half of that of *wt* MGC in mixed neuron-glial cultures and their BrdU-uptake was markedly reduced; this uptake was virtually negligible at day 11 *in vitro* in *rd1* MGC, whereas *wt* MGC still retained their proliferative capacity at this time in culture. This is in close agreement with previous findings showing that there are significantly less MGC in the *rd1* retinas than in the corresponding *wt* retinas (Chua et al., 2013). The significant reduction in the mitotic cycle in *rd1* MGC might further diminish the already limited regenerative capacity of healthy MGC.

Expression of stem cell markers was also reduced in *rd1* MGC. NESTIN is a well-established stem cell marker; its levels increase in most stem cells in the central nervous system (Lendahl et al., 1990) and it is downregulated upon differentiation (Sahlgren et al., 2006). The levels and distribution of NESTIN were affected in *rd1* MGC compared to *wt* MGC. *Nestin* was down regulated in *rd1* MGC, which had lower mRNA levels than *wt* MGC by day 11. Even when a similar number of MGC expressed NESTIN in *rd1* and *wt* neuron-glial cultures, the level of NESTIN expression was significantly lower in *rd1* cultures. This was consistent with the significant reduction in NESTIN-positive MGC in whole *rd1* retinas compared to *wt* retinas by PND 14. Early during development, the rodent retina is enriched in NESTIN-expressing progenitors, which later differentiate as neuronal progenitors and, further during development, as MGC. PND 2 is a critical point in development, corresponding with the highest mitotic peak of PHR progenitors and with the onset of MGC differentiation, which reaches its maximum levels between PND 5 and 8 (Cepko et al., 1996; Nelson et al., 2011). Interestingly, the largest difference in the level of *Nestin* mRNA between *rd1* and *wt* retinas was visible at PND2, suggesting a reduction in the number of progenitors in *rd1* retinas. SOX2 is a critical transcription factor for reprograming MGC toward a proliferative mode, for inducing their transformation into pluripotent stem cells and for the maintenance of neural stem cells (Favaro et al., 2009; Gorsuch et al., 2017). *Sox2* was also downregulated in *rd1* retinas; the levels of *Sox2* mRNA were lower in *rd1* than in *wt* retinas early during development. *Sox2* changes were similar to those described for *Nestin*. In *wt* retinas, the fold changes in *Sox2* mRNA levels relative to PND 0 showed a peak at PND 2, and rapidly decreased thereafter. In the *rd1* retinas the pattern of changes in *Sox2* mRNA was similar to the observed in *wt* retinas, but their increase at PND 2 and 4 was significantly lower than in *wt* retinas. Consistently, *rd1* retinas had remarkably less SOX2-expressing nuclei than *wt* retinas by PND 14. VIMENTIN is

also considered a stem cell marker, although less specific than *Nestin*, since its expression has been found not only in developing tissues, but also in differentiated tissues (Traub et al., 1985; Lendahl et al., 1990). *Vimentin* is expressed in human stem cells when cultured on mouse PA6 stromal cells (Gong et al., 2008), and in cells derived from stem cell spheres when acquiring a Müller glial phenotype (Coles et al., 2004). VIMENTIN is closely linked to NESTIN, which is required for its polymerization (Park et al., 2010); in turn, NESTIN, along with the mitosis promoting factor (MPF), are important for the phosphorylation-mediated disassembly of VIMENTIN during mitosis (Chou et al., 2003). Noteworthy, *Vimentin* mRNA levels were significantly lower in *rd1* than in *wt* neuron-glial cultures by days 6 and 11 in culture. As a whole, our present findings that *wt* MGC expressed stem cell markers like *Nestin*, *Sox2* and *Vimentin*, and proliferated in culture are consistent with previous work from our laboratory evidencing that cultured rat MGC proliferate actively and express PAX6 and NESTIN (Insua et al., 2008; Simón et al., 2012). Our results also suggest that the regenerative capacity still preserved by MGC in *wt* retinas was further decreased in *rd1* retinas. *Nestin*, *Sox2* and *Vimentin* levels were reduced in *rd1* retinas, particularly in MGC, and these cells also evidenced a decreased proliferation rate. These findings support a decline in the stem cell potential of MGC in *rd1* retinas.

Little is known regarding the alterations that *rd1* MGC undergo during retinal degeneration (Roesch et al., 2012). Most studies on retinitis pigmentosa, including those using the *rd1* mice, focus mainly on the alterations affecting PHRs, such as genetic mutations, cell death, or abnormal development or functionality (Pittler and Baehr, 1991; Arikawa et al., 1992; Chen et al., 1996). Moreover, among the over 100 mutations leading to retinitis pigmentosa, most affect PHRs. Only a few reported mutations are known to affect MGC, such as a mutation in *Cralbp*, altering retinoid association/dissociation to its ligand binding pocket, and consequently the visual cycle (Golovleva et al., 2003), and no evidences of mutations affecting the regenerative capacity of MGC have been reported for this pathology. Our data strongly suggests that a defective neuron-glial crosstalk is responsible for the impaired stem cell capacity of *rd1* MGC. *Nestin* levels dramatically increased when *rd1* MGC were co-cultured with *wt* neurons. In contrast, when *wt* MGC were co-cultured with *rd1* neurons, *Nestin* levels were markedly reduced. These experiments strongly suggest that the crosstalk with neurons regulates *Nestin* expression in MGC and the interaction with healthy PHR progenitors is crucial for regulating MGC stem cell potential. To our knowledge, this is the first report highlighting the relevance of neuron-glial crosstalk in supporting the stem cell potential of MGC. This is consistent with the hypothesis that the "niche," i.e., the environment surrounding MGC, might be modified in the retina during neurodegenerative diseases. MGC and neurons are known to maintain an active crosstalk, or "molecular dialogue" in the retina. The occurrence of gliosis in MGC in the beta-PDE model, *rd10* mice, before the beginning of retinal degeneration, suggests this crosstalk between PHR and MGC starts very early during development (Dong et al., 2017). Many of the factors involved in this "dialogue" have been identified; MGC release several molecules, such as FGF, GDNF, DHA, and LIF, that rescue PHRs in different models of retinal degeneration (Faktorovich et al., 1990, 1992; LaVail et al., 1992, 1998; Rotstein et al., 1996; Cayouette et al., 1998; Chong et al., 1999; Frasson et al., 1999; Harada et al., 2002; Miranda et al., 2009; German et al., 2013). MGC also release molecular cues that regulate their own regenerative responses, reducing proliferation (Fischer et al., 2004; Zhao et al., 2014). In turn, PHRs regulate MGC functions, even while undergoing degeneration. PHR degeneration modulates the expression of *Neurotrophin* receptor genes in retinal MGC (Harada et al., 2000). PHRs have also been reported to release stress signals, the damage-associated molecular patterns (DAMPs) during degenerative processes of the retina, that orchestrate a broad neuroprotective response in MGC, including release of Leukemia Inhibitory Factor (LIF), a critical PHR survival factor (Hooper et al., 2018). A further putative signal might be glutamate, which PHRs release as a neurotransmitter; activation of NMDA receptors has been shown to increase proliferation and differentiation of hippocampal neural progenitor cells (Joo et al., 2007) and might have a similar effect on retinal MGC. The progressive degeneration of PHRs in the *rd1* mice might lead to a shortage of glutamate, among other factors, which might affect MGC stem cell capability. Further research is required to establish how neuron-glial crosstalk is regulated and modified along development or after retinal injuries to regulate MGC regenerative capacity.

CONCLUSION

Replacement therapies using stem cells are currently intensely investigated for retina neurodegenerations and establishing the most adequate source of these stem cells is crucial for these therapies. Our results imply that the limited capacity of mammalian MGC for restoring lost PHRs is further impaired in degenerated retinas. This capacity might be improved by their crosstalk with "healthy" PHR partners, suggesting that it is possible to manipulate these stem cells to recover their proliferative potential by creating an adequate "niche." Identifying the molecular cues required for this manipulation is an exciting challenge that deserves further investigation.

ETHICS STATEMENT

All procedures concerning animal use were carried out in strict accordance with the National Institutes of Health Guide for the Care and Use of Laboratory Animals and the protocols approved by the Institutional Committee for the Care of Laboratory Animals from the Universidad Nacional del Sur (Argentina) (Protocols CICUAE-UNS: 058/2015, 059/2015, and 060/2015).

AUTHOR CONTRIBUTIONS

All authors contributed intellectually to the manuscript. YV, HV-M, MD, OG, VA-P, SZ, and AG performed the experiments and analyzed the data. YV involved in the all experiments. YV, OG, HV-M, and AT performed the cultures. HV-M and AT involved in the immunocytochemistry imaging. MD involved in

the immunohistochemistry and image processing. VA-P involved in the RQ-PCR assays. SZ and MD involved in the Flow Cytometry assays. AG involved in the preparation of retina cryosections. CC interpreted and analyzed the data and reviewed the manuscript. YV, OG, and LP elaborated strategies for the experiments. YV, OG, NR, and LP interpreted the data and elaborated the manuscript. LP and OG conducted the research and wrote the manuscript.

FUNDING

This work was supported by the National Research Council of Argentina (CONICET) (PIP 11220-1101–00827, to LP); the National Agency for Science and Technology (ANPCYT), (PICT-201-0475 to OG, PICT-2016-0353 to LP); from the Secretary of Science and Technology, UNS (24/ZB68 to OG, 24-B190 to LP); from P30EY029220 from the NIH and unrestricted Grant to the Department of Ophthalmology, Keck School of Medicine of USC from the Research to Prevent Blindness, New York, NY, United States to CC.

ACKNOWLEDGMENTS

YV has a postdoctoral fellowship from the Argentina National Research Council (CONICET). HV-M, MD, and AT have doctoral fellowships from the CONICET. VA-P and SZ are assistant researchers, OG and AG are adjunct researchers and NR and LP are principal researchers from the CONICET. We thank Beatriz De los Santos and Edgardo Buzzi for their excellent technical assistance. We are very grateful to Valeria Levi and Alejandra Guberman (Facultad de Ciencias Exactas y Naturales, Universidad de Buenos Aires, Buenos Aires, Argentina) for the kind gift of anti-SOX2.

SUPPLEMENTARY MATERIAL

The Supplementary Material for this article can be found online at: https://www.frontiersin.org/articles/10.3389/fncel.2019.00334/full#supplementary-material

FIGURE S1 | Specificity of photoreceptors and glial markers in culture. Phase **(a,f)** and fluorescence **(b–e,g–j)** photomicrographs of *wt* neuronal cultures **(a–e)**, showing photoreceptors labeled with an anti-CRX antibody **(c,h)**, and of *rd1* MGC cultures **(f–j)**, showing MGC labeled with an anti-GS antibody **(b,g)**. Nuclei were visualized with DAPI **(d,i)**. Merge images **(e,j)**. Scale bar: 20 μm.

FIGURE S2 | CRX-positive neurons in mixed neuron-glial cultures. Phase **(a,e)** and fluorescence **(b–d,f–h)** photomicrographs of 6-day mixed *wt* **(a–d)** and *rd1* **(e–h)** neuron-glial cultures showing photoreceptors labeled with anti-CRX antibody **(b f)**. Cell nuclei were visualized with DAPI **(c,g)**. Merge images **(d,h)**. Bars in **(i)** represent the percentage of CRX-positive neurons (photoreceptors) at days 6 and 11 in *wt* and *rd1* mixed neuron-glial cultures. Scale bar: 20 μm. Statistical analysis was performed using a One-way ANOVA with a *post hoc* Tukey test. No significant differences were observed between conditions.

REFERENCES

Abrahan, C. E., Insua, M. F., Politi, L. E., German, O. L., and Rotstein, N. P. (2009). Oxidative stress promotes proliferation and dedifferentiation of retina glial cells in vitro. *J. Neurosci. Res.* 87, 964–977. doi: 10.1002/jnr.21903

Adler, R. (1982). Regulation of neurite growth in purified retina neuronal cultures: effects of PNPF, a substratum-bound, neurite-promoting factor. *J. Neurosci. Res.* 8, 165–177. doi: 10.1002/jnr.490080207

Arikawa, K., Molday, L. L., Molday, R. S., and Williams, D. S. (1992). Localization of peripherin/rds in the disk membranes of cone and rod photoreceptors: relationship to disk membrane morphogenesis and retinal degeneration. *J. Cell Biol.* 116, 659–667. doi: 10.1083/jcb.116.3.659

Barnstable, C. J. (1980). Monoclonal antibodies which recognize different cell types in the rat retina. *Nature* 286, 231–235. doi: 10.1038/286231a0

Boraas, L. C., Guidry, J. B., Pineda, E. T., and Ahsan, T. (2016). Cytoskeletal expression and remodeling in pluripotent stem cells. *PLoS One* 11:e0145084. doi: 10.1371/journal.pone.0145084

Bringmann, A., Pannicke, T., Biedermann, B., Francke, M., Iandiev, I., Grosche, J., et al. (2009). Role of retinal glial cells in neurotransmitter uptake and metabolism. *Neurochem. Int.* 54, 143–160. doi: 10.1016/j.neuint.2008.10.014

Bringmann, A., Pannicke, T., Grosche, J., Francke, M., Wiedemann, P., Skatchkov, S. N., et al. (2006). Müller cells in the healthy and diseased retina. *Prog. Retin. Eye Res.* 25, 397–424. doi: 10.1016/j.preteyeres.2006.05.003

Bustin, S. A., Benes, V., Garson, J. A., Hellemans, J., Huggett, J., Kubista, M., et al. (2009). The MIQE guidelines: minimum information for publication of quantitative real-time PCR experiments. *Clin. Chem.* 55, 611–622. doi: 10.1373/clinchem.2008.112797

Cayouette, M., Behn, D., Sendtner, M., Lachapelle, P., and Gravel, C. (1998). Intraocular gene transfer of ciliary neurotrophic factor prevents death and increases responsiveness of rod photoreceptors in the retinal degeneration slow mouse. *J. Neurosci* 18, 9282–9293. doi: 10.1523/jneurosci.18-22-09282.1998

Cepko, C. L., Austin, C. P., Yang, X., Alexiades, M., and Ezzeddine, D. (1996). Cell fate determination in the vertebrate retina. *Proc. Natl. Acad. Sci. U.S.A.* 93, 589–595.

Chen, J., Flannery, J. G., LaVail, M. M., Steinberg, R. H., Xu, J., and Simon, M. I. (1996). bcl-2 overexpression reduces apoptotic photoreceptor cell death in three different retinal degenerations. *Proc. Natl. Acad. Sci. U.S.A.* 93, 7042–7047. doi: 10.1073/pnas.93.14.7042

Chong, N. H., Alexander, R. A., Waters, L., Barnett, K. C., Bird, A. C., and Luthert, P. J. (1999). Repeated injections of a ciliary neurotrophic factor analogue leading to long-term photoreceptor survival in hereditary retinal degeneration. *Invest. Ophthalmol. Vis. Sci.* 40, 1298–1305.

Chou, Y.-H., Khuon, S., Herrmann, H., and Goldman, R. D. (2003). Nestin promotes the phosphorylation-dependent disassembly of vimentin intermediate filaments during mitosis. *Mol. Biol. Cell* 14, 1468–1478. doi: 10.1091/mbc.E02-08-0545

Chua, J., Nivison-Smith, L., Fletcher, E. L., Trenholm, S., Awatramani, G. B., and Kalloniatis, M. (2013). Early remodeling of Müller cells in the rd/rd mouse model of retinal dystrophy. *J. Comp. Neurol.* 521, 2439–2453. doi: 10.1002/cne.23307

Coles, B. L. K., Angénieux, B., Inoue, T., Del Rio-Tsonis, K., Spence, J. R., McInnes, R. R., et al. (2004). Facile isolation and the characterization of human retinal stem cells. *Proc. Natl. Acad. Sci. U.S.A.* 101, 15772–15777. doi: 10.1073/pnas.0401596101

Das, A. V., Mallya, K. B., Zhao, X., Ahmad, F., Bhattacharya, S., and Thoreson, W. B. (2006). Neural stem cell properties of Müller glia in the mammalian retina: regulation by Notch and Wnt signaling. *Dev. Biol.* 299, 283–302. doi: 10.1016/j.ydbio.2006.07.029

Dong, E., Bachleda, A., Xiong, Y., Osawa, S., and Weiss, E. R. (2017). Reduced phosphoCREB in Müller glia during retinal degeneration in rd10 mice. *Mol. Vis.* 23, 90–102.

Dyer, M. A., and Cepko, C. L. (2000). Control of Müller glial cell proliferation and activation following retinal injury. *Nat. Neurosci.* 3, 873–880. doi: 10.1038/78774

Faktorovich, E. G., Steinberg, R. H., Yasumura, D., Matthes, M. T., and LaVail, M. M. (1990). Photoreceptor degeneration in inherited retinal dystrophy delayed by basic fibroblast growth factor. *Nature* 347, 83–86. doi: 10.1038/347083a0

Faktorovich, E. G., Steinberg, R. H., Yasumura, D., Matthes, M. T., and LaVail, M. M. (1992). Basic fibroblast growth factor and local injury protect photoreceptors from light damage in the rat. *J. Neurosci* 12, 3554–3567. doi: 10.1523/jneurosci.12-09-03554.1992

Farber, D. B., and Lolley, R. N. (1974). Cyclic guanosine monophosphate: elevation in degenerating photoreceptor cells of the C3H mouse retina. *Science* 186, 449–451. doi: 10.1126/science.186.4162.449

Favaro, R., Valotta, M., Ferri, A. L. M., Latorre, E., Mariani, J., Giachino, C., et al. (2009). Hippocampal development and neural stem cell maintenance require Sox2-dependent regulation of Shh. *Nat. Neurosci.* 12, 1248–1256. doi: 10.1038/nn.2397

Fischer, A. J., and Reh, T. A. (2003). Potential of Müller glia to become neurogenic retinal progenitor cells. *Glia* 43, 70–76. doi: 10.1002/glia.10218

Fischer, A. J., Schmidt, M., Schmidt, M., Omar, G., and Reh, T. A. (2004). BMP4 and CNTF are neuroprotective and suppress damage-induced proliferation of Müller glia in the retina. *Mol. Cell. Neurosci.* 27, 531–542. doi: 10.1016/j.mcn.2004.08.007

Frasson, M., Picaud, S., Léveillard, T., Simonutti, M., Mohand-Said, S., Dreyfus, H., et al. (1999). Glial cell line-derived neurotrophic factor induces histologic and functional protection of rod photoreceptors in the rd/rd mouse. *Invest. Ophthalmol. Vis. Sci.* 40, 2724–2734.

Garelli, A., Rotstein, N. P., and Politi, L. E. (2006). Docosahexaenoic acid promotes photoreceptor differentiation without altering Crx expression. *Investig. Ophthalmol. Vis. Sci.* 47, 3017–3027. doi: 10.1167/iovs.05-1659

German, O. L., Monaco, S., Agnolazza, D. L., Rotstein, N. P., and Politi, L. E. (2013). Retinoid X receptor activation is essential for docosahexaenoic acid protection of retina photoreceptors. *J. Lipid Res.* 54, 2236–2246. doi: 10.1194/jlr.M039040

Goldman, D. (2014). Müller glial cell reprogramming and retina regeneration. *Nat. Rev. Neurosci.* 15, 431–442. doi: 10.1038/nrn3723

Golovleva, I., Bhattacharya, S., Wu, Z., Shaw, N., Yang, Y., Andrabi, K., et al. (2003). Disease-causing mutations in the cellular retinaldehyde binding protein tighten and abolish ligand interactions. *J. Biol. Chem.* 278, 12397–12402. doi: 10.1074/jbc.M207300200

Gong, J., Sagiv, O., Cai, H., Tsang, S. H., and Del Priore, L. V. (2008). Effects of extracellular matrix and neighboring cells on induction of human embryonic stem cells into retinal or retinal pigment epithelial progenitors. *Exp. Eye Res.* 86, 957–965. doi: 10.1016/j.exer.2008.03.014

Gorsuch, R. A., Lahne, M., Yarka, C. E., Petravick, M. E., Li, J., and Hyde, D. R. (2017). Sox2 regulates Müller glia reprogramming and proliferation in the regenerating zebrafish retina via Lin28 and Ascl1a. *Exp. Eye Res.* 161, 174–192. doi: 10.1016/j.exer.2017.05.012

Harada, T., Harada, C., Kohsaka, S., Wada, E., Yoshida, K., Ohno, S., et al. (2002). Microglia-Müller glia cell interactions control neurotrophic factor production during light-induced retinal degeneration. *J. Neurosci* 22, 9228–9236. doi: 10.1523/jneurosci.22-21-09228.2002

Harada, T., Harada, C., Nakayama, N., Okuyama, S., Yoshida, K., Kohsaka, S., et al. (2000). Modification of glial-neuronal cell interactions prevents photoreceptor apoptosis during light-induced retinal degeneration. *Neuron* 26, 533–541. doi: 10.1016/s0896-6273(00)81185-x

Hartong, D. T., Berson, E. L., and Dryja, T. P. (2006). Retinitis pigmentosa. *Lancet* 368, 1795–1809. doi: 10.1016/S0140-6736(06)69740-7

Hicks, D., and Courtois, Y. (1990). The growth and behaviour of rat retinal Müller cells in vitro. 1. An improved method for isolation and culture. *Exp. Eye Res.* 51, 119–129. doi: 10.1016/0014-4835(90)90063-z

Hooper, M. J., Wang, J., Browning, R., and Ash, J. D. (2018). Damage-associated molecular pattern recognition is required for induction of retinal neuroprotective pathways in a sex-dependent manner. *Sci. Rep.* 8, 9115. doi: 10.1038/s41598-018-27479-x

Huang, L., Zhang, Q., Huang, X., Qu, C., Ma, S., Mao, Y., et al. (2017). Mutation screening in genes known to be responsible for retinitis pigmentosa in 98 small han chinese families. *Sci. Rep.* 7:1948. doi: 10.1038/s41598-017-00963-6

Insua, M. F., Simón, M. V., Garelli, A., de los Santos, B., Rotstein, N. P., and Politi, L. E. (2008)). Trophic factors and neuronal interactions regulate the cell cycle and Pax6 expression in Müller stem cells. *J. Neurosci. Res.* 86, 1459–1471. doi: 10.1002/jnr.21606

Joo, J.-Y., Kim, B.-W., Lee, J.-S., Park, J.-Y., Kim, S., Yun, Y.-J., et al. (2007). Activation of NMDA receptors increases proliferation and differentiation of hippocampal neural progenitor cells. *J. Cell Sci.* 120, 1358–1370. doi: 10.1242/jcs.002154

Karl, M. O., Hayes, S., Nelson, B. R., Tan, K., Buckingham, B., and Reh, T. A. (2008). Stimulation of neural regeneration in the mouse retina. *Proc. Natl. Acad. Sci.* 105, 19508–19513. doi: 10.1073/pnas.0807453105

Lamba, D. A., Karl, M. O., Ware, C. B., and Reh, T. A. (2006). Efficient generation of retinal progenitor cells from human embryonic stem cells. *Proc. Natl. Acad. Sci. U.S.A.* 103, 12769–12774. doi: 10.1073/pnas.0601990103

LaVail, M. M., Unoki, K., Yasumura, D., Matthes, M. T., Yancopoulos, G. D., and Steinberg, R. H. (1992). Multiple growth factors, cytokines, and neurotrophins rescue photoreceptors from the damaging effects of constant light. *Proc. Natl. Acad. Sci. U.S.A.* 89, 11249–11253. doi: 10.1073/pnas.89.23.11249

LaVail, M. M., Yasumura, D., Matthes, M. T., Lau-Villacorta, C., Unoki, K., Sung, C. H., et al. (1998). Protection of mouse photoreceptors by survival factors in retinal degenerations. *Invest. Ohthalmol. Vis. Sci.* 39, 592–602.

Lendahl, U., Zimmerman, L. B., and McKay, R. D. (1990). CNS stem cells express a new class of intermediate filament protein. *Cell* 60, 585–595. doi: 10.1016/0092-8674(90)90662-x

Lenkowski, J. R., and Raymond, P. A. (2014). Müller glia: stem cells for generation and regeneration of retinal neurons in teleost fish. *Prog. Retin. Eye Res.* 40, 94–123. doi: 10.1016/j.preteyeres.2013.12.007

Livesey, F. J., and Cepko, C. L. (2001). Vertebrate neural cell-fate determination: lessons from the retina. *Nat. Rev. Neurosci.* 2, 109–118. doi: 10.1038/35053522

Lolley, R. N., Rong, H., and Craft, C. M. (1994). Linkage of photoreceptor degeneration by apoptosis with inherited defect in phototransduction. *Invest. Ophthalmol. Vis. Sci.* 35, 358–362.

Maw, M. A., Kennedy, B., Knight, A., Bridges, R., Roth, K. E., Mani, E. J., et al. (1997). Mutation of the gene encoding cellular retinaldehyde-binding protein in autosomal recessive retinitis pigmentosa. *Nat. Genet.* 17, 198–200. doi: 10.1038/ng1097-198

Miranda, G. E., Abrahan, C. E., Politi, L. E., and Rotstein, N. P. (2009). Sphingosine-1-phosphate is a key regulator of proliferation and differentiation in retina photoreceptors. *Invest. Ophthalmol. Vis. Sci.* 50, 4416–4428. doi: 10.1167/iovs.09-3388

Nelson, B. R., Ueki, Y., Reardon, S., Karl, M. O., Georgi, S., Hartman, B. H., et al. (2011). Genome-wide analysis of Müller glial differentiation reveals a requirement for Notch signaling in postmitotic cells to maintain the glial fate. *PLoS One* 6:e22817. doi: 10.1371/journal.pone.0022817

Ooto, S., Akagi, T., Kageyama, R., Akita, J., Mandai, M., Honda, Y., et al. (2004). Potential for neural regeneration after neurotoxic injury in the adult mammalian retina. *Proc. Natl. Acad. Sci. U.S.A.* 101, 13654–13659. doi: 10.1073/pnas.0402129101

Park, D., Xiang, A. P., Mao, F. F., Zhang, L., Di, C. G., Liu, X. M., et al. (2010). Nestin is required for the proper self-renewal of neural stem cells. *Stem Cells* 28, 2162–2171. doi: 10.1002/stem.541

Pittler, S. J., and Baehr, W. (1991). Identification of a nonsense mutation in the rod photoreceptor cGMP phosphodiesterase beta-subunit gene of the rd mouse. *Proc. Natl. Acad. Sci. U.S.A.* 88, 8322–8326. doi: 10.1073/pnas.88.19.8322

Politi, L., and Adler, R. (1988). Selective failure of long-term survival of isolated photoreceptors from both homozygous and heterozygous rd (retinal degeneration) mice. *Exp. Eye Res.* 47, 269–282. doi: 10.1016/0014-4835(88)90010-3

Politi, L. E., Bouzat, C., de los Santos, E. B., and Barrantes, F. J. (1996). Heterologous retinal cultured neurons and cell adhesion molecules induce clustering of acetylcholine receptors and polynucleation in mouse muscle BC3H-1 clonal cell line. *J. Neurosci. Res.* 43, 639–651. doi: 10.1002/(sici)1097-4547(19960315)43:6<639::aid-jnr1>3.0.co;2-f

Politi, L. E., Lehar, M., and Adler, R. (1988). Development of neonatal mouse retinal neurons and photoreceptors in low density cell culture. *Invest. Ophthalmol. Vis. Sci.* 29, 534–543.

Politi, L. E., Rotstein, N. P., and Carri, N. G. (2001). Effect of GDNF on neuroblast proliferation and photoreceptor survival: additive protection with docosahexaenoic acid. *Invest. Ophthalmol. Vis. Sci.* 42, 3008–3015.

Portera-Cailliau, C., Sung, C. H., Nathans, J., and Adler, R. (1994). Apoptotic photoreceptor cell death in mouse models of retinitis pigmentosa. *Proc. Natl. Acad. Sci. U.S.A.* 91, 974–978. doi: 10.1073/pnas.91.3.974

Ranski, A. H., Kramer, A. C., Morgan, G. W., Perez, J. L., and Thummel, R. (2018). Characterization of retinal regeneration in adult zebrafish following multiple rounds of phototoxic lesion. *PeerJ* 6:e5646. doi: 10.7717/peerj.5646

Roesch, K., Stadler, M. B., and Cepko, C. L. (2012). Gene expression changes within Müller glial cells in retinitis pigmentosa. *Mol. Vis.* 18, 1197–1214.

Rotstein, N. P., Aveldaño, M. I., Barrantes, F. J., and Politi, L. E. (1996). Docosahexaenoic acid is required for the survival of rat retinal photoreceptors in vitro. *J. Neurochem.* 66, 1851–1859. doi: 10.1046/j.1471-4159.1996.66051851.x

Rotstein, N. P., Aveldaño, M. I., Barrantes, F. J., Roccamo, A. M., and Politi, L. E. (1997). Apoptosis of retinal photoreceptors during development in vitro: protective effect of docosahexaenoic acid. *J. Neurochem.* 69, 504–513. doi: 10.1046/j.1471-4159.1997.69020504.x

Sahlgren, C. M., Pallari, H.-M., He, T., Chou, Y.-H., Goldman, R. D., and Eriksson, J. E. (2006). A nestin scaffold links Cdk5/p35 signaling to oxidant-induced cell death. *EMBO J.* 25, 4808–4819. doi: 10.1038/sj.emboj.7601366

Schindelin, J., Arganda-Carreras, I., Frise, E., Kaynig, V., Longair, M., Pietzsch, T., et al. (2012). Fiji: an open-source platform for biological-image analysis. *Nat. Methods* 9, 676–682. doi: 10.1038/nmeth.2019

Sherpa, T., Fimbel, S. M., Mallory, D. E., Maaswinkel, H., Spritzer, S. D., Sand, J. A., et al. (2008). Ganglion cell regeneration following whole-retina destruction in zebrafish. *Dev. Neurobiol.* 68, 166–181. doi: 10.1002/dneu.20568

Sherpa, T., Lankford, T., McGinn, T. E., Hunter, S. S., Frey, R. A., Sun, C., et al. (2014). Retinal regeneration is facilitated by the presence of surviving neurons. *Dev. Neurobiol.* 74, 851–876. doi: 10.1002/dneu.22167

Simón, M. V., De Genaro, P., Abrahan, C. E., de los Santos, B., Rotstein, N. P., and Politi, L. E. (2012). Müller glial cells induce stem cell properties in retinal progenitors in vitro and promote their further differentiation into photoreceptors. *J. Neurosci. Res.* 90, 407–421. doi: 10.1002/jnr.22747

Simón, M. V., Prado Spalm, F. H., Politi, L. E., and Rotstein, N. P. (2015). Sphingosine-1-phosphate is a crucial signal for migration of retina müller glial cells. *Investig. Ophthalmol. Vis. Sci.* 56, 5808–5815. doi: 10.1167/iovs.14-16195

Traub, P., Perides, G., Scherbarth, A., and Traub, U. (1985). Tenacious binding of lipids to vimentin during its isolation and purification from Ehrlich ascites tumor cells. *FEBS Lett.* 193, 217–221. doi: 10.1016/0014-5793(85)80155-1

Vecino, E., Rodriguez, F. D., Ruzafa, N., Pereiro, X., and Sharma, S. C. (2016). Glia–neuron interactions in the mammalian retina. *Prog. Retin. Eye Res.* 51, 1–40. doi: 10.1016/j.preteyeres.2015.06.003

Xia, X., and Ahmad, I. (2016). Unlocking the neurogenic potential of mammalian Müller Glia. *Int. J. stem cells* 9, 169–175. doi: 10.15283/ijsc16020

Young, R. W. (1984). Cell death during differentiation of the retina in the mouse. *J. Comp. Neurol.* 229, 362–373. doi: 10.1002/cne.902290307

Zhao, M., Andrieu-Soler, C., Kowalczuk, L., Paz Cortés, M., Berdugo, M., Dernigoghossian, M., et al. (2015). A new CRB1 rat mutation links Müller glial cells to retinal telangiectasia. *J. Neurosci.* 35, 6093–6106. doi: 10.1523/JNEUROSCI.3412-14.2015

Zhao, X.-F., Wan, J., Powell, C., Ramachandran, R., Myers, M. G., and Goldman, D. (2014). Leptin and IL-6 family cytokines synergize to stimulate Müller Glia reprogramming and retina regeneration. *Cell Rep.* 9, 272–284. doi: 10.1016/j.celrep.2014.08.047

Zhong, X., Gutierrez, C., Xue, T., Hampton, C., Vergara, M. N., Cao, L.-H., et al. (2014). Generation of three-dimensional retinal tissue with functional photoreceptors from human iPSCs. *Nat. Commun.* 5:4047. doi: 10.1038/ncomms5047

Zhu, X., and Craft, C. M. (2000).). Modulation of CRX transactivation activity by phosducin isoforms. *Mol. Cell. Biol.* 20, 5216–5226. doi: 10.1128/mcb.20.14.5216-5226.2000

Zimmerman, L., Parr, B., Lendahl, U., Cunningham, M., McKay, R., Gavin, B., et al. (1994). Independent regulatory elements in the nestin gene direct transgene expression to neural stem cells or muscle precursors. *Neuron* 12, 11–24. doi: 10.1016/0896-6273(94)90148-1

Conflict of Interest Statement: The authors declare that the research was conducted in the absence of any commercial or financial relationships that could be construed as a potential conflict of interest.

frontiers in Cellular Neuroscience

MINI REVIEW
published: 30 July 2019
doi: 10.3389/fncel.2019.00350

Protein Misfolding, Signaling Abnormalities and Altered Fast Axonal Transport: Implications for Alzheimer and Prion Diseases

Emiliano Zamponi[1] *and Gustavo F. Pigino*[2*†]

[1] *Department of Molecular, Cellular, and Developmental Biology, University of Colorado Boulder, Boulder, CO, United States,*
[2] *Laboratorio de Neuropatología Experimental, Instituto de Investigación Médica Mercedes y Martín Ferreyra, INIMEC-CONICET-Universidad Nacional de Córdoba, Córdoba, Argentina*

OPEN ACCESS

Edited by:
Mario Eduardo Guido, Center for Research in Biological Chemistry Córdoba (CIQUIBIC), Argentina

Reviewed by:
Alessio Cardinale, Bambino Gesù Children's Hospital (IRCCS), Italy
Sergio T. Ferreira, Federal University of Rio de Janeiro, Brazil
Gerardo Morfini, The University of Illinois at Chicago, United States

***Correspondence:**
Gustavo F. Pigino
pigino@immf.uncor.edu;
pigino@uic.edu

†Present address:
Gustavo F. Pigino, Department of Anatomy and Cell Biology, The University of Illinois at Chicago, Chicago, IL, United States

Specialty section:
This article was submitted to Cellular Neuropathology, a section of the journal Frontiers in Cellular Neuroscience

Received: *15 January 2019*
Accepted: *15 July 2019*
Published: *30 July 2019*

Citation:
Zamponi E and Pigino GF (2019) Protein Misfolding, Signaling Abnormalities and Altered Fast Axonal Transport: Implications for Alzheimer and Prion Diseases. Front. Cell. Neurosci. 13:350. doi: 10.3389/fncel.2019.00350

Histopathological studies revealed that progressive neuropathies including Alzheimer, and Prion diseases among others, include accumulations of misfolded proteins intracellularly, extracellularly, or both. Experimental evidence suggests that among the accumulated misfolded proteins, small soluble oligomeric conformers represent the most neurotoxic species. Concomitant phenomena shared by different protein misfolding diseases includes alterations in phosphorylation-based signaling pathways synaptic dysfunction, and axonal pathology, but mechanisms linking these pathogenic features to aggregated neuropathogenic proteins remain unknown. Relevant to this issue, results from recent work revealed inhibition of fast axonal transport (AT) as a novel toxic effect elicited by oligomeric forms of amyloid beta and cellular prion protein PrP^{C}, signature pathological proteins associated with Alzheimer and Prion diseases, respectively. Interestingly, the toxic effect of these oligomers was fully prevented by pharmacological inhibitors of casein kinase 2 (CK2), a remarkable discovery with major implications for the development of pharmacological target-driven therapeutic intervention for Alzheimer and Prion diseases.

Keywords: fast axonal transport, kinesin-1, casein kinase 2, signaling, synaptic dysfuction, protein misfolding, prion protein

INTRODUCTION

Adult-onset misfolding diseases are among the most challenging disorders faced by modern molecular medicine. A pathogenic feature common to these diseases includes the accumulation of aggregated proteinaceous entities. By mid 20th century, it became clear that protein aggregates were the culprit of misfolding diseases, including Alzheimer's (AD) and prion diseases (PrDs) (Hardy and Selkoe, 2002; Colby and Prusiner, 2011). More recently, the "amyloid cascade hypothesis" was proposed, suggesting that a cascade of pathological events associated with extracellular accumulation of amyloid precursor protein (APP) fragments underlies AD (Hardy and Higgins, 1992). This hypothesis was later extended to other misfolding diseases, leading to a modified hypothesis that included the notion that smaller, oligomeric intraneuronal aggregates may play a

more relevant pathological role in AD and PrDs, (Takahashi et al., 2002; Forloni et al., 2016; Cline et al., 2018; Ono, 2018). As these disorders associated with small soluble aggregates (oligomers ranging from 4 to 200 kDa), the term "oligomeropathies" was coined to emphasize this notion (Forloni et al., 2016). Still, after many decades of intense research, mechanisms linking oligomeric protein aggregates to disease pathogenesis remain elusive.

Synaptic disfunction and axonal pathology are common early pathological features shared by neurons affected in protein misfolding diseases (Selkoe, 2002; Senatore et al., 2013; Chiesa, 2015; Soto and Pritzkow, 2018), suggesting that pathological misfolded proteins, including amyloid beta (Aβ) and PrP^C, may alter cellular processes critical for synaptic and axonal function. One such process involves fast axonal transport (AT) a cellular process crucial for homeostatic maintenance of pre and postsynaptic compartments underlying functional neuronal connectivity (Ermolayev et al., 2009a,b; Pigino et al., 2009; Zamponi et al., 2017). In this mini-review, we discuss how two unrelated pathogenic proteins bearing oligomeric conformation, amyloid beta (oAβ-42) and cellular prion protein ($oPrP^C$), inhibit AT by altering a common signaling pathways important for AT regulation. Implications of these in the Conclusion section.

EARLY SYNAPTIC DYSFUNCTION AND NEURITIC PATHOLOGY IN PROTEIN MISFOLDING DISEASES

Decades of research revealed neuronal synaptic terminals as primary targets in many protein misfolded diseases (Jeffrey et al., 2000; Selkoe, 2002; Conforti et al., 2007; Siskova et al., 2009). Accordingly, recent studies determined that abnormally folded tau and oligomeric amyloid beta, hallmarks AD proteins, inhibit synaptic transmission through a mechanism involving aberrant activation of the proteins kinases GSK3β and CK2, respectively (Moreno et al., 2009, 2016). Early synaptic dysfunction and axonal pathology represent common pathological events to all these disorders, preceding months or even years before any signs of overt neuronal cell death (Moreno and Mallucci, 2010; Adalbert and Coleman, 2013). Cumulative evidence indicates that deficits in neuronal connectivity associated with synaptic disfunction and axonal degeneration, rather than the loss of specific population of vulnerable neurons, underlies the clinical manifestation of each disease (Chiesa et al., 2005; Brady and Morfini, 2010; Coleman, 2011). Accordingly, therapeutic strategies based on preventing neuronal apoptosis failed to alter the progression of clinical symptoms in different animal models of protein misfolding diseases, including PrDs, amyotrophic lateral sclerosis (ALS) and PD (Chiesa et al., 2005; Gould et al., 2006; Waldmeier et al., 2006). Remarkably, eliminating cellular prion protein on mice infected with prions that normally develop the classic prion pathology and clinical signs of neurodegeneration (Mallucci et al., 2007; White et al., 2008) recovered synaptic dysfunction, which further prevented neuronal loss (Moreno and Mallucci, 2010). Therefore, the available information strongly suggests that preserving neuronal connectivity may represent an effective therapeutic strategy (Lingor et al., 2012). However, the development of such approaches requires the knowledge of pathogenic mechanism underlying loss of neuritic connectivity in all these unrelated neurological disorders (Luo and O'Leary, 2005; Conforti et al., 2007; Gerdts et al., 2016).

The development of mouse models for misfolding disorders was a major breakthrough that allowed an evaluation of hypothesis-driven disease mechanisms (Suter and Scherer, 2003). However, a major obstacle has been the scarcity of appropriate experimental systems that allow a direct evaluation of aggregation-dependent effects of neuropathogenic proteins. Within this context, the isolated squid axoplasm and squid giant synapse preparation represents unique experimental systems (Song et al., 2016). Isolated squid giant axon is independent of any nuclear or synaptic activity contributions, which cannot be achieved when working with mammalian neurons either *in vitro* or *in vivo* (Grant et al., 2006; Kanaan et al., 2012; Song et al., 2016). One putative limitation for the squid giant axon, as well as other invertebrate model such as *Drosophila melanogaster* and *Caenorhabditis elegans*, could be the state of conservation on regulatory mechanisms for AT between mammalian and invertebrate neurons. In this regard, we and others have shown that every specific axonal activity explored in the squid *Loligo pealeii* is conserved from cephalopods to humans. The *Loligo pealeii* was a pioneering animal model that provided fundamental insights into nerve cell excitability (Schwiening, 2012). Furthermore, it was instrumental for the discovery of kinesin-1 (Brady, 1985; Vale et al., 1985) and its regulatory mechanisms (Brady and Morfini, 2017), as well as the determination of the specific molecular mechanisms involved in synaptic transmission (Llinas et al., 1980).

OLIGOMERIC FORMS OF Aβ-42 AND PRP^C PROMOTE ABERRANT ACTIVATION OF THE PROTEIN KINASES GSK3β AND CK2

A common pathological feature displayed by many adult onset aggregopathies is aberrant patterns of protein phosphorylation, which indirectly reflects alterations in the activity of phosphotransferases (Walaas and Greengard, 1991; Baskaran and Velmurugan, 2018). Cytoskeletal components of the axonal compartment, including the microtubule-associated protein tau and neurofilaments, are the most widely reported neuronal proteins aberrantly phosphorylated in AD and PrDs (Stoothoff and Johnson, 2005; Holmgren et al., 2012; Rudrabhatla, 2014).

In the last two decades of pharmacological research working with multiple cellular and animal models, it has become clear that GSK3-β kinase plays a key role in AD and PrDs pathology (Llorens-Martin et al., 2014). Significantly, GSK3β activity has been shown to be abnormally activated by the AD associated oligomeric Aβ-42 peptide (oAβ-42) and by PrP (Perez et al., 2003; Pigino et al., 2009; Decker et al., 2010; Tang et al., 2012; Simon et al., 2014). In addition, extracellular fibrillar Aβ-42 (fAβ) and either extracellular or intracellular oAβ-42 were found to

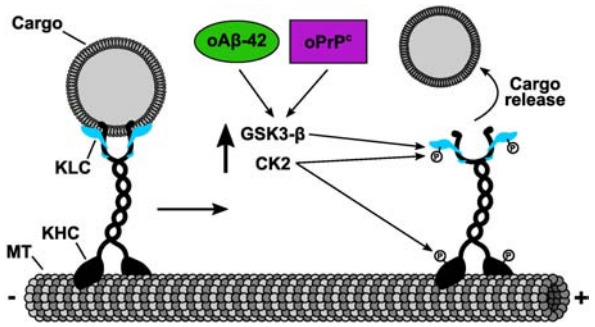

FIGURE 1 | Common molecular mechanism of fast axonal transport inhibition shared by $oPrP^C$ and oAβ-42. Cellular and pharmacological data determined that both $oPrP^C$ and oAβ-42 induced fast axonal transport inhibition. The inhibitory mechanism was mediated by the activation of endogenous CK2 and GSK3β that in turn phosphorylated KLCs. Phosphorylation of KLCs (letter P on KLCs) promoted the detachment of conventional kinesin from its transported vesicular cargoes. We and others have shown that CK2 can also phosphorylate kinesin-1 heavy chains (KHCs) (letter P on KHCs). Based on our previous results working with KHCs phosphorylation, we predict an additional mechanism of fast axonal transport inhibition induced by CK2 phosphorylation on KHCs which in turn will promote a reduction of kinesin-1 association to microtubules (MTs).

activate CK2 both *in vivo* and *in vitro* (Chauhan et al., 1993; De Felice et al., 2009; Pigino et al., 2009; Tang et al., 2012; Ramser et al., 2013). Making this even more compelling, PrP reportedly associates with and activates CK2 (Meggio et al., 2000; Chen et al., 2008; Zamponi et al., 2017). Together these experimental evidences strongly indicates that oAβ-42 and oPrP promote activation of neuronal GSK3β and CK2 kinases (Pigino et al., 2009; Zamponi et al., 2017), a discovery bearing major implications for both AD and PrP pathogenesis.

Since most kinases have many different neuronal substrates, they could potentially affect a wide variety of cellular processes, including gene transcription (Whitmarsh, 2007; Thapar and Denmon, 2013; Gao and Roux, 2015), cytoskeleton organization (Rudrabhatla, 2014), protein degradation and mitochondrial function, among others. However, the precise molecular events linking these processes to synaptic dysfunction and axonal pathology have yet to be discovered. On the other hand, we do know AT is a process of utmost importance for maintaining normal axonal and synaptic function (Gibbs et al., 2015; Zamponi et al., 2017). In support, loss of function mutations in specific subunits of kinesin-1 and cytoplasmic dynein, major motor proteins responsible for the execution of AT, cause neuropathologies featuring synaptic dysfunction and axonal pathology early in the course of disease (Reid, 2003; Brady and Morfini, 2010).

FAST AXONAL TRANSPORT ALTERATIONS IN ALZHEIMER AND PRION DISEASES

In the last decade, genetic evidences have shown that alterations in kinesin and cytoplasmic dynein motor functions underlie a group of neuropathies (Brady and Morfini, 2010, 2017). Interestingly, all of these disorders display synaptic dysfunction and l axonopathy, signature pathogenic events associated with dying-back degeneration of neurons (Brady and Morfini, 2010). Although these neuropathies are associated with functional mutations in molecular motors, it became apparent that many more adult onset aggregopathies present defects in AT, including AD, and PrDs (Gibbs et al., 2015; Brady and Morfini, 2017; Zamponi et al., 2017). However, AT failure in these neuropathies was a result of alterations in phosphotransferase activities that regulate kinesin and dynein motor functions, rather than through mutation-based loss of motor activities (Brady and Morfini, 2017). Our recent results showed that cellular PrP can activate endogenous axonal CK2 activity and induce a dramatic inhibit AT of various membrane-bound organelles including synaptic vesicles and mitochondria (Zamponi et al., 2017). Abnormally activated CK2 in turn phosphorylates light chains subunits of kinesin-1, inducing a dissociation of this motor protein with its transported cargoes (**Figure 1**). Consistent with this molecular mechanism, inhibition of endogenous CK2 activity by specific pharmacological CK2 inhibitors prevented oPrP-induced AT inhibition in both isolated squid axoplasm and mammalian neurons (Zamponi et al., 2017). Remarkably, we and others have shown previously the same mechanism of AT inhibition induced by the AD related peptide oAβ-42 (Pigino et al., 2009; Tang et al., 2012). These important discoveries represent a message of hope for the development of therapies to treat aggregopathies involving compromised AT. In particular, these insights would be crucial for treating disorders that are induced by aggregated misfolded proteins capable of altering phosphotransferases important for regulating AT, a vitally important neuronal process that sustain normal axon functions and synaptic activities.

CONCLUSION

For many decades the research on pathological mechanisms associated to adult onset neurological disorders such as AD and other aggregopathies, was focused almost exclusively on preventing neuronal cell death. The development of animal models, specifically focusing on these devastating diseases, has helped in the formulation of new hypothesis driven pathological mechanisms. Many research programs have developed effective ways of preserving neurons affected in these animal models, however, little or no progress was achieved in stopping or slowing the progression of these diseases. Indeed, cardinal research programs aimed to genetically prove the direct involvement of apoptosis, a pathological component of AD, PD, PrD, and ALS, determined that although apoptosis plays an important role in these diseases, preserving affected neurons did not prevent the clinical symptoms or synaptic dysfunction and loss (Chiesa et al., 2005; Gould et al., 2006).

The discovery that functional mutations in kinesin-1 and cytoplasmic dynein, the main molecular motors responsible for neuronal AT, suffice to promote dying back neuropathies was

a major step forward (Brady and Morfini, 2010). However, mutations in molecular motors are rare, usually embryonic lethal, and only account for a small proportion of neurological disorders. It has become established in recent years, that deficiencies in AT are associated to a larger group of misfolding diseases including AD, PD, and PrDs. And, current research indicates that AT deficiencies observed in these diseases are induced by altered kinases involved in regulation of AT (Gibbs et al., 2015; Brady and Morfini, 2017). Altogether, this molecular and pharmacological information will set the basis for developing novel target-driven pharmacological interventions specific for each disease. These interventions will in turn ameliorate neuronal AT and therefore prevent or slow down the dying back progression of axonal degeneration and loss (Brady and Morfini, 2017).

AUTHOR CONTRIBUTIONS

GP wrote the original manuscript. EZ designed and draw the figure.

FUNDING

This work was supported by the Alzheimer's Association (Grant # NIRGD-11-206379).

ACKNOWLEDGMENTS

The authors thank Brittan Hlista for editing this manuscript.

REFERENCES

Adalbert, R., and Coleman, M. P. (2013). Review: axon pathology in age-related neurodegenerative disorders. *Neuropathol. Appl. Neurobiol.* 39, 90–108. doi: 10.1111/j.1365-2990.2012.01308.x

Baskaran, R., and Velmurugan, B. K. (2018). Protein phosphatase 2A as therapeutic targets in various disease models. *Life Sci.* 210, 40–46. doi: 10.1016/j.lfs.2018.08.063

Brady, S., and Morfini, G. (2010). A perspective on neuronal cell death signaling and neurodegeneration. *Mol. Neurobiol.* 42, 25–31. doi: 10.1007/s12035-010-8128-2

Brady, S. T. (1985). A novel brain ATPase with properties expected for the fast axonal transport motor. *Nature* 317, 73–75. doi: 10.1038/317073a0

Brady, S. T., and Morfini, G. A. (2017). Regulation of motor proteins, axonal transport deficits and adult-onset neurodegenerative diseases. *Neurobiol. Dis.* 105, 273–282. doi: 10.1016/j.nbd.2017.04.010

Chauhan, A., Chauhan, V. P., Murakami, N., Brockerhoff, H., and Wisniewski, H. M. (1993). Amyloid beta-protein stimulates casein kinase I and casein kinase II activities. *Brain Res.* 629, 47–52. doi: 10.1016/0006-8993(93)90479-7

Chen, J., Gao, C., Shi, Q., Wang, G., Lei, Y., Shan, B., et al. (2008). Casein kinase II interacts with prion protein in vitro and forms complex with native prion protein in vivo. *Acta Biochim. Biophys. Sin* 40, 1039–1047. doi: 10.1111/j.1745-7270.2008.00486.x

Chiesa, R. (2015). The elusive role of the prion protein and the mechanism of toxicity in prion disease. *PLoS Pathog.* 11:e1004745. doi: 10.1371/journal.ppat.1004745.

Chiesa, R., Piccardo, P., Dossena, S., Nowoslawski, L., Roth, K. A., Ghetti, B., et al. (2005). "Bax deletion prevents neuronal loss but not neurological symptoms in a transgenic model of inherited prion disease. *Proc. Natl. Acad. Sci. U.S.A.* 102, 238–243. doi: 10.1073/pnas.0406173102

Cline, E. N., Bicca, M. A., Viola, K. L., and Klein, W. L. (2018). The amyloid-beta oligomer hypothesis: beginning of the third decade. *J. Alzheimers. Dis.* 64, S567–S610. doi: 10.3233/JAD-179941

Colby, D. W., and Prusiner, S. B. (2011). "Prions."cold spring harb. *Perspect. Biol.* 3, a006833. doi: 10.1101/cshperspect.a006833

Coleman, M. (2011). Molecular signaling how do axons die? *Adv. Genet.* 73, 185–217. doi: 10.1016/B978-0-12-380860-8.00005-7

Conforti, L., Adalbert, R., and Coleman, M. P. (2007). Neuronal death: where does the end begin? *Trends Neurosci.* 30, 159–166. doi: 10.1016/j.tins.2007.02.004

De Felice, F. G., Vieira, M. N., Bomfim, T. R., Decker, H., Velasco, P. T., Lambert, M. P., et al. (2009). "Protection of synapses against Alzheimer's-linked toxins: insulin signaling prevents the pathogenic binding of Abeta oligomers."*Proc. Natl. Acad. Sci. U.S.A.* 106, 1971–1976. doi: 10.1073/pnas.0809158106

Decker, H., Lo, K. Y., Unger, S. M., Ferreira, S. T., and Silverman, M. A. (2010). Amyloid-beta peptide oligomers disrupt axonal transport through an NMDA receptor-dependent mechanism that is mediated by glycogen synthase kinase 3beta in primary cultured hippocampal neurons. *J. Neurosci.* 30, 9166–9171. doi: 10.1523/JNEUROSCI.1074-10.2010

Ermolayev, V., Cathomen, T., Merk, J., Friedrich, M., Hartig, W., Harms, G. S., et al. (2009a). Impaired axonal transport in motor neurons correlates with clinical prion disease. *PLoS Pathog.* 5:e1000558. doi: 10.1371/journal.ppat.1000558

Ermolayev, V., Friedrich, M., Nozadze, R., Cathomen, T., Klein, M. A., Harms, G. S., et al. (2009b). "Ultramicroscopy reveals axonal transport impairments in cortical motor neurons at prion disease."*Biophys. J.* 96, 3390–3398. doi: 10.1016/j.bpj.2009.01.032

Forloni, G., Artuso, V., La Vitola, P., and Balducci, C. (2016). Oligomeropathies and pathogenesis of Alzheimer and Parkinson's diseases. *Mov. Disord.* 31, 771–781. doi: 10.1002/mds.26624

Gao, B., and Roux, P. P. (2015). "Translational control by oncogenic signaling pathways. *Biochim. Biophys. Acta* 1849, 753–765. doi: 10.1016/j.bbagrm.2014.11.006

Gerdts, J., Summers, D. W., Milbrandt, J., and DiAntonio, A. (2016). axon self-destruction: new links among SARM1, MAPKs, and NAD+ metabolism. *Neuron* 89, 449–460. doi: 10.1016/j.neuron.2015.12.023

Gibbs, K. L., Greensmith, L., and Schiavo, G. (2015). Regulation of axonal transport by protein kinases. *Trends Biochem. Sci.* 40, 597–610. doi: 10.1016/j.tibs.2015.08.003

Gould, T. W., Buss, R. R., Vinsant, S., Prevette, D., Sun, W., Knudson, C. M., et al. (2006). Complete dissociation of motor neuron death from motor dysfunction by Bax deletion in a mouse model of ALS. *J. Neurosci.* 26, 8774–8786. doi: 10.1523/jneurosci.2315-06.2006

Grant, P., Zheng, Y., and Pant, H. C. (2006). Squid (*Loligo pealei*) giant fiber system: a model for studying neurodegeneration and dementia? *Biol. Bull.* 210, 318–333. doi: 10.2307/4134568

Hardy, J., and Selkoe, D. J. (2002). The amyloid hypothesis of Alzheimer's disease: progress and problems on the road to therapeutics. *Science* 297, 353–356. doi: 10.1126/science.1072994

Hardy, J. A., and Higgins, G. A. (1992). Alzheimer's disease: the amyloid cascade hypothesis. *Science* 256, 184–185.

Holmgren, A., Bouhy, D., and Timmerman, V. (2012). Neurofilament phosphorylation and their proline-directed kinases in health and disease. *J. Peripher. Nerv. Syst.* 17, 365–376. doi: 10.1111/j.1529-8027.2012.00434.x

Jeffrey, M., Halliday, W. G., Bell, J., Johnston, A. R., MacLeod, N. K., Ingham, C., et al. (2000). "Synapse loss associated with abnormal PrP precedes neuronal degeneration in the scrapie-infected murine hippocampus." *Neuropathol. Appl. Neurobiol.* 26, 41–54. doi: 10.1046/j.1365-2990.2000.00216.x

Kanaan, N. M., Pigino, G. F., Brady, S. T., Lazarov, O., Binder, L. I., and Morfini, G. A. (2012). Axonal degeneration in Alzheimer's disease: when signaling abnormalities meet the axonal transport system. *Exp. Neurol.* 246, 44–53. doi: 10.1016/j.expneurol.2012.06.003

Lingor, P., Koch, J. C., Tonges, L., and Bahr, M. (2012). Axonal degeneration as a therapeutic target in the CNS. *Cell Tissue Res.* 349, 289–311. doi: 10.1007/s00441-012-1362-3

Llinas, R., Steinberg, I. Z., and Walton, K. (1980). Transmission in the squid giant synapse: a model based on voltage clamp studies. *J. Physiol.* 76, 413–418.

Llorens-Martin, M., Jurado, J., Hernandez, F., and Avila, J. (2014). GSK-3beta, a pivotal kinase in Alzheimer disease. *Front. Mol. Neurosci.* 7:46. doi: 10.3389/fnmol.2014.00046

Luo, L., and O'Leary, D. D. (2005). Axon retraction and degeneration in development and disease. *Annu. Rev. Neurosci.* 28, 127–156. doi: 10.1146/annurev.neuro.28.061604.135632

Mallucci, G. R., White, M. D., Farmer, M., Dickinson, A., Khatun, H., Powell, A. D., et al. (2007). Targeting cellular prion protein reverses early cognitive deficits and neurophysiological dysfunction in prion-infected mice. *Neuron* 53, 325–335. doi: 10.1016/j.neuron.2007.01.005

Meggio, F., Negro, A., Sarno, S., Ruzzene, M., Bertoli, A., Sorgato, M. C., et al. (2000). Bovine prion protein as a modulator of protein kinase CK2. *Biochem. J.* 352(Pt 1), 191–196. doi: 10.1042/bj3520191

Moreno, H., Morfini, G., Buitrago, L., Ujlaki, G., Choi, S., Yu, E., et al. (2016). Tau pathology-mediated presynaptic dysfunction. *Neuroscience* 325, 30–38. doi: 10.1016/j.neuroscience.2016.03.044

Moreno, H., Yu, E., Pigino, G., Hernandez, A. I., Kim, N., Moreira, J. E., et al. (2009). Synaptic transmission block by presynaptic injection of oligomeric amyloid beta. *Proc. Natl. Acad. Sci. U.S.A.* 106, 5901–5906. doi: 10.1073/pnas.0900944106

Moreno, J. A., and Mallucci, G. R. (2010). Dysfunction and recovery of synapses in prion disease: implications for neurodegeneration. *Biochem. Soc. Trans.* 38, 482–487. doi: 10.1042/BST0380482

Ono, K. (2018). Alzheimer's disease as oligomeropathy. *Neurochem. Int.* 119, 57–70. doi: 10.1016/j.neuint.2017.08.010

Perez, M., Rojo, A. I., Wandosell, F., Diaz-Nido, J., and Avila, J. (2003). Prion peptide induces neuronal cell death through a pathway involving glycogen synthase kinase 3. *Biochem. J.* 372(Pt 1), 129–136. doi: 10.1042/bj20021596

Pigino, G., Morfini, G., Atagi, Y., Deshpande, A., Yu, C., Jungbauer, L., et al. (2009). Disruption of fast axonal transport is a pathogenic mechanism for intraneuronal amyloid beta. *Proc. Natl. Acad. Sci. U.S.A.* 106, 5907–5912. doi: 10.1073/pnas.0901229106

Ramser, E. M., Gan, K. J., Decker, H., Fan, E. Y., Suzuki, M. M., Ferreira, S. T., et al. (2013). Amyloid-beta oligomers induce tau-independent disruption of BDNF axonal transport via calcineurin activation in cultured hippocampal neurons. *Mol. Biol. Cell* 24, 2494–2505. doi: 10.1091/mbc.E12-12-0858

Reid, E. (2003). Science in motion: common molecular pathological themes emerge in the hereditary spastic paraplegias. *J. Med. Genet.* 40, 81–86. doi: 10.1136/jmg.40.2.81

Rudrabhatla, P. (2014). Regulation of neuronal cytoskeletal protein phosphorylation in neurodegenerative diseases. *J. Alzheimers. Dis.* 41, 671–684. doi: 10.3233/JAD-130794

Schwiening, C. J. (2012). A brief historical perspective: hodgkin and huxley. *J. Physiol.* 590, 2571–2575. doi: 10.1113/jphysiol.2012.230458

Selkoe, D. J. (2002). Alzheimer's disease is a synaptic failure. *Science* 298, 789–791.

Senatore, A., Restelli, E., and Chiesa, R. (2013). Synaptic dysfunction in prion diseases: a trafficking problem? *Int. J. Cell Biol.* 2013, 543803. doi: 10.1155/2013/543803

Simon, D., Herva, M. E., Benitez, M. J., Garrido, J. J., Rojo, A. I., Cuadrado, A., et al. (2014). Dysfunction of the PI3K-Akt-GSK-3 pathway is a common feature in cell culture and in vivo models of prion disease. *Neuropathol. Appl. Neurobiol.* 40, 311–326. doi: 10.1111/nan.12066

Siskova, Z., Page, A., O'Connor, V., and Perry, V. H. (2009). Degenerating synaptic boutons in prion disease: microglia activation without synaptic stripping. *Am. J. Pathol.* 175, 1610–1621. doi: 10.2353/ajpath.2009.090372

Song, Y., Kang, M., Morfini, G., and Brady, S. T. (2016). Fast axonal transport in isolated axoplasm from the squid giant axon. *Methods Cell Biol.* 131, 331–348. doi: 10.1016/bs.mcb.2015.07.004

Soto, C., and Pritzkow, S. (2018). Protein misfolding, aggregation, and conformational strains in neurodegenerative diseases. *Nat. Neurosci.* 21, 1332–1340. doi: 10.1038/s41593-018-0235-9

Stoothoff, W. H., and Johnson, G. V. (2005). Tau phosphorylation: physiological and pathological consequences. *Biochim. Biophys. Acta* 1739, 280–297. doi: 10.1016/j.bbadis.2004.06.017

Suter, U., and Scherer, S. S. (2003). Disease mechanisms in inherited neuropathies. *Nat. Rev. Neurosci.* 4, 714–726. doi: 10.1038/nrn1196

Takahashi, R. H., Milner, T. A., Li, F., Nam, E. E., Edgar, M. A., Yamaguchi, H., et al. (2002). Intraneuronal Alzheimer abeta42 accumulates in multivesicular bodies and is associated with synaptic pathology. *Am. J. Pathol.* 161, 1869–1879. doi: 10.1016/s0002-9440(10)64463-x

Tang, Y., Scott, D. A., Das, U., Edland, S. D., Radomski, K., Koo, E. H., et al. (2012). Early and selective impairments in axonal transport kinetics of synaptic cargoes induced by soluble amyloid beta-protein oligomers. *Traffic* 13, 681–693. doi: 10.1111/j.1600-0854.2012.01340.x

Thapar, R., and Denmon, A. P. (2013). Signaling pathways that control mRNA turnover. *Cell. Signal.* 25, 1699–1710. doi: 10.1016/j.cellsig.2013.03.026

Vale, R. D., Reese, T. S., and Sheetz, M. P. (1985). Identification of a novel force-generating protein, kinesin, involved in microtubule-based motility. *Cell* 42, 39–50. doi: 10.1016/s0092-8674(85)80099-4

Walaas, S. I., and Greengard, P. (1991). Protein phosphorylation and neuronal function. *Pharmacol. Rev.* 43, 299–349.

Waldmeier, P., Bozyczko-Coyne, D., Williams, M., and Vaught, J. L. (2006). Recent clinical failures in Parkinson's disease with apoptosis inhibitors underline the need for a paradigm shift in drug discovery for neurodegenerative diseases. *Biochem. Pharmacol.* 72, 1197–1206. doi: 10.1016/j.bcp.2006.06.031

White, M. D., Farmer, M., Mirabile, I., Brandner, S., Collinge, J., and Mallucci, G. R. (2008). Single treatment with RNAi against prion protein rescues early neuronal dysfunction and prolongs survival in mice with prion disease. *Proc. Natl. Acad. Sci. U.S.A.* 105, 10238–10243. doi: 10.1073/pnas.0802759105

Whitmarsh, A. J. (2007). Regulation of gene transcription by mitogen-activated protein kinase signaling pathways. *Biochim. Biophys. Acta* 1773, 1285–1298. doi: 10.1016/j.bbamcr.2006.11.011

Zamponi, E., Buratti, F., Cataldi, G., Caicedo, H. H., Song, Y., Jungbauer, L. M., et al. (2017). Prion protein inhibits fast axonal transport through a mechanism involving casein kinase 2. *PLoS One* 12:e0188340. doi: 10.1371/journal.pone.0188340.

Conflict of Interest Statement: The authors declare that the research was conducted in the absence of any commercial or financial relationships that could be construed as a potential conflict of interest.

The reviewer, GM, declared a past co-authorship with one of the authors, GP, to the handling Editor.

frontiers in Pharmacology

BRIEF RESEARCH REPORT
published: 07 August 2019
doi: 10.3389/fphar.2019.00883

Ambroxol Hydrochloride Improves Motor Functions and Extends Survival in a Mouse Model of Familial Amyotrophic Lateral Sclerosis

Alexandra Bouscary[1,2], Cyril Quessada[1,2], Althéa Mosbach[1,2], Noëlle Callizot[3], Michael Spedding[4], Jean-Philippe Loeffler[1,2]* and Alexandre Henriques[1,2,4]*†*

[1] Université de Strasbourg, UMR_S 1118, Fédération de Médecine Translationnelle, Strasbourg, France, [2] INSERM, U1118, Mécanismes Centraux et Périphériques de la Neurodégénérescence, Strasbourg, France, [3] Neuro-sys SAS, Gardanne, France, [4] Spedding Research Solutions SAS, Le Vesinet, France

OPEN ACCESS

Edited by:
Mario Eduardo Guido, Center for Research in Biological Chemistry Córdoba (CIQUIBIC), Argentina

Reviewed by:
Alberto Ferri, Institute of Traslational Pharmacology (CNR), Italy
Mariano Soiza-Reilly, CONICET Instituto de Fisiología, Argentina

***Correspondence:**
Michael Spedding
michael@speddingresearchsolutions.fr
Jean-Philippe Loeffler
loeffler@unistra.fr
Alexandre Henriques
alexandre.henriques@neuro-sys.com

†Present address:
Alexandre Henriques
Neuro-sys SAS, Gardanne, France

Specialty section:
This article was submitted to Neuropharmacology, a section of the journal Frontiers in Pharmacology

Received: *21 February 2019*
Accepted: *15 July 2019*
Published: *07 August 2019*

Citation:
Bouscary A, Quessada C, Mosbach A, Callizot N, Spedding M, Loeffler J-P and Henriques A (2019) Ambroxol Hydrochloride Improves Motor Functions and Extends Survival in a Mouse Model of Familial Amyotrophic Lateral Sclerosis. Front. Pharmacol. 10:883. doi: 10.3389/fphar.2019.00883

Amyotrophic lateral sclerosis (ALS) is a multifactorial and fatal neurodegenerative disease. Growing evidence connects sphingolipid metabolism to the pathophysiology of ALS. In particular, levels of ceramides, glucosylceramides, and gangliosides are dysregulated in the central nervous system and at the neuromuscular junctions of both animal models and patients. Glucosylceramide is the main precursor of complex glycosphingolipids that is degraded by lysosomal (GBA1) or non-lysosomal (GBA2) glucocerebrosidase. Here, we report that GBA2, but not GBA1, activity is markedly increased in the spinal cord, of SOD1^{G86R} mice, an animal model of familial ALS, even before disease onset. We therefore investigated the effects of ambroxol hydrochloride, a known GBA2 inhibitor, in SOD1^{G86R} mice. A presymptomatic administration of ambroxol hydrochloride, in the drinking water, delayed disease onset, protecting neuromuscular junctions, and the number of functional spinal motor neurons. When administered at disease onset, ambroxol hydrochloride delayed motor function decline, protected neuromuscular junctions, and extended overall survival of the SOD1^{G86R} mice. In addition, ambroxol hydrochloride improved motor recovery and muscle re-innervation after transient sciatic nerve injury in non-transgenic mice and promoted axonal elongation in an *in vitro* model of motor unit. Our study suggests that ambroxol hydrochloride promotes and protects motor units and improves axonal plasticity, and that this generic compound is a promising drug candidate for ALS.

Keywords: ambroxol, GBA2, glucocerebrosidase, ALS, neuromuscular junction, glucosylceramide

INTRODUCTION

Amyotrophic lateral sclerosis (ALS) is a fatal neurodegenerative disease characterized by a loss of cortical motor neurons in the motor cortex and spinal motor neurons located in the brainstem and in the spinal cord with denervation. Considered to be the most common motor neuron disease in adults, ALS leads to progressive paralysis, muscle atrophy, fasciculation, and spasticity and affects the central nervous system and peripheral organs (Schmitt et al., 2014). ALS is associated with sporadic forms (90%) and familial form (10%). Mutations on genes encoding superoxide dismutase 1 (SOD1), TAR DNA-binding protein of 43 kDa (TDP-43) and fused in sarcoma (FUS), and repeat expansions in chromosome 9 open reading frame 72 (C9ORF72) (Lattante et al., 2015) are now documented. It is

reported that lipid metabolism in ALS patient has a major impact on the disease severity. A high incidence of dyslipidemia and hypermetabolism is present in ALS patients (Desport et al., 2001; Funalot et al., 2009) and hypermetabolism and high low-density lipoprotein (LDL)/high-density lipoprotein (HDL) ratios or high body mass index are associated with better prognosis and slower disease progression (Dupuis et al., 2008; Paganoni et al., 2011; Jésus et al., 2018). The causes of the metabolic dysfunctions in ALS remain unknown and could result from central pathologies combined with peripheral alterations.

Metabolomic studies have now shown that recent human evolution has marked changes in lipid metabolism in muscle and brain to support increased metabolic activity (Noakes and Spedding, 2012; Bozek et al., 2014). Beyond their role in energy metabolism, lipids and particularly sphingolipids are modulators of cellular signaling pathways and participate in the maintenance and repair of the various components of the motor axis such as neurons and muscles. Our transcriptomic studies on muscle biopsies in ALS patients showed a significant increase in the expression of the UGCG gene (UDP-glucose ceramide glucosyltransferase), encoding the sphingolipid metabolism enzyme that synthesizes glucosylceramide (GlcCer) (Henriques et al., 2015; Dodge, 2017; Henriques et al., 2017). It has been shown in ALS that GlcCer and ceramide levels are deregulated (Cutler et al., 2002; Dodge et al., 2015; Henriques et al., 2015; Henriques et al., 2018). These data suggest that GlcCer plays a key role in the pathophysiology of ALS. We performed a lipidomic analysis of different tissues of SOD1^{G86R} mice, an animal model of ALS, and we observed a complete rearrangement of the main lipid classes, including sphingolipids like GlcCer and ceramides in the muscles and spinal cords of SOD1^{G86R} mice, before the onset of the disease. Inhibition of GlcCer synthesis by administration of a UGCG inhibitor (AMP-DMN) significantly delays functional recovery after sciatic nerve injury (Henriques et al., 2015; Henriques et al., 2018). GlcCer is the precursor of gangliosides, and this hydrolysis is performed by GBA1 and GBA2, two beta-glucocerebrosidases (GCases).

Our previous results have shown a beneficial effect for SOD1^{G86R} mice after inhibition of GlcCer degradation (Henriques et al., 2017). Partial inhibition of GlcCer degradation with a low dose of conduritol B epoxide (CBE) (10 mg/kg/d) delays disease onset and improves motor functions in presymptomatic and in symptomatic SOD1^{G86R} mice. Pharmacological inhibition of GCase by CBE preserves motor neuron number and the neuromuscular junctions (NMJs) in SOD1^{G86R} mice. Furthermore, CBE promotes recovery after sciatic nerve injury *in vivo* (Henriques et al., 2017). Conversely, a high dose CBE (100 mg/kg/d) induced neuronal toxicity and can be used to inhibit the lysosomal GCase to induce a chemical model of Gaucher's diseases (Kanfer et al., 1975; Vardi et al., 2016). Indeed, CBE is an inhibitor of lysosomal GCase (GBA1) and, less potently, of the non-lysosomal GCase (GBA2) (Ridley et al., 2013). Moreover, loss-of-function mutations of GBA1 are a major cause of hereditary Parkinson's Disease (PD), while the activation of beta-GCase increases alpha-synuclein clearance and lysosomal function in dopaminergic neurons (Schapira, 2015; Mazzulli et al., 2016; Stojkovska et al., 2018); thus, there may be a risk of PD with GBA1 inhibitors.

GBA2 is localized at the plasma membrane and as a membrane-associated protein at the Golgi apparatus and at the endoplasmic reticulum (Woeste and Wachten, 2017). Loss of function of GBA2 is associated with hereditary spastic paraplegia suggesting that the regulation of GlcCer at the plasma membrane and/or at intracellular organelles is important for the maintenance of motor functions, even if the role of GBA2 in the central nervous system remains poorly understood.

Our approach was therefore to inhibit the non-lysosomal GBA2 without inhibiting GBA1. Among the safe molecules able to cross the blood–brain barrier (BBB), ambroxol hydrochloride (AMB) has been extensively studied (Albin and Dauer, 2014; McNeill et al., 2014; Ambrosi et al., 2015; Migdalska-Richards et al., 2016b; Migdalska-Richards et al., 2017; O'Regan et al., 2017). In our study, we confirmed that AMB inhibited GBA2 activity. We have then investigated the effects of AMB *in vivo,* in a transgenic model of ALS and on non-transgenic mice to determine whether it could improve the lifespan of SOD1^{G86R} mice and stimulate the plasticity of the neuromuscular junctions (NMJs).

RESULTS

GBA2 Activity Is Increased in Pre-Symptomatic SOD1^{G86R} Mice

GlcCer is a precursor of complex glycosphingolipids. It is synthetized from ceramide by the GlcCer synthase and degraded by GBA1 or GBA2, two GCases. We previously reported that inhibition of GCase activity by a low dose of CBE is neuroprotective in the SOD1^{G86R} mice (Henriques et al., 2017). CBE has inhibitory activities on lysosomal and GBA2 activity (Ridley et al., 2013).

Here, we sought to measure GCase activities at specific pH, and in presence or absence of detergent, to determine whether GBA1 (pH = 4.6, with detergent) and GBA2 (pH = 5.8, no detergent) activities are dysregulated in tissues of SOD1^{G86R} mice (Witte et al., 2010). At a symptomatic disease stage, characterized by moderate motor dysfunctions, GBA1 activity was not significantly altered in SOD1^{G86R} when compared to control non-transgenic mice (**Figure 1A**). However, GBA2 activity was strongly increased in the spinal cord of SOD1^{G86R} mice at 105d (symptomatic) but not in muscle or in liver. This increase in GBA2 activity was also observed in presymptomatic SOD1^{G86R} mice (**Supplementary Figure 1A**). The GBA1 activity was not changed at either time point. GBA1 and GBA2 share common enzymatic activity but differ in structure, thus allowing the use of specific inhibitors. The effects of AMB on GCase activities *in vitro* have been compared to those of CBE. As previously reported (Ridley et al., 2013), CBE had a strong inhibitory effect on the GBA1 activity being 10-fold less potent on GBA2 activity (**Figure 1B**). AMB has been reported to inhibit the GBA2 activity (Maegawa et al., 2009), which was confirmed in a dose-dependent manner (**Figure 1C**). Taken together, these results show that GBA2 activity is increased in SOD1^{G86R} mice, already

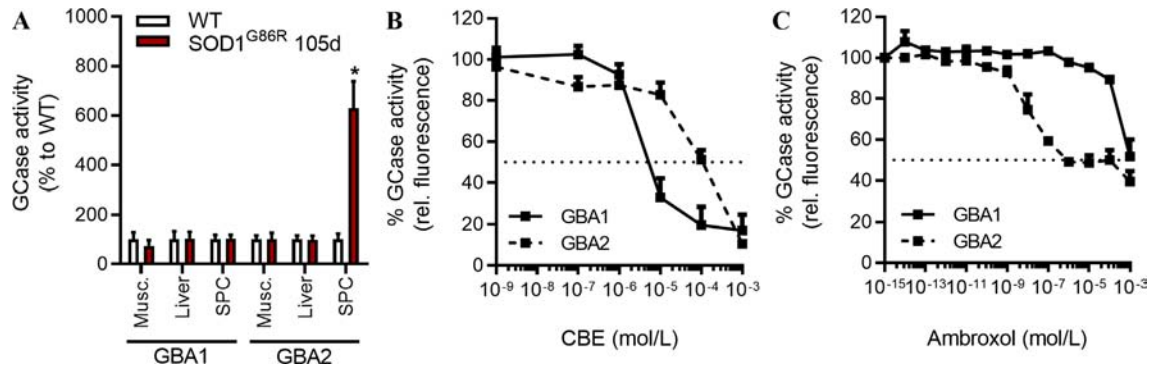

FIGURE 1 | GCase activities in symptomatic SOD1^{G86R} mice. **(A)** GCase activity in different tissues of SOD1^{G86R} and wild type (WT) mice at 105d (n = 5–9/tissues, $^*p < 0.05$). **(B)** GCase [glucocerebrosidase (GBA)] activity after conduritol B epoxide (CBE) dose-response (n = 6/group). **(C)** GCase (GBA) activity after ambroxol hydrochloride (AMB) dose-response in liver tissue (n = 4/group).

at pre-symptomatic disease stage, and that AMB can inhibit its activity.

Ambroxol Hydrochloride Delays Disease Onset, Preserve the Integrity of Motor Units, and Increases Survival of SOD1^{G86R} Mice

AMB was administrated to presymptomatic SOD1^{G86R} mice, to determine whether it could influence disease onset and loss of motor functions in a preventive manner. Grip strength was used as an indicator of muscle strength. SOD1^{G86R} mice were treated from 75 days to 95 days of age, and body mass and muscle strength were evaluated every other day (**Figure 2**). In the first cohort of presymptomatic SOD1^{G86R} mice, AMB had no significant effects on the body mass of treated mice (**Figure 2A**); however, it strongly improved the muscle strength of SOD1^{G86R} mice and significantly delayed of disease onset, defined as a drop of more than 20% of the mouse maximal strength (**Figure 2B**). These results were replicated in a separate cohort of SOD1^{G86R} mice, using the same experimental conditions (**Supplementary Figure 2**). Indeed, an improved muscle strength and a delayed disease onset were observed after AMB administration in the second cohort.

At 95 days of age, neurodegeneration of motor neurons is detected in the lumbar region of the spinal cord of SOD1^{G86R} mice (Henriques et al., 2017). As compared to the WT mice, 40% of motor neurons (MNs) are lost at this time point. The number of MNs in the lumbar region of the spinal cord was significantly higher in SOD1^{G86R} mice treated with AMB (**Figures 2C**, **D**), suggesting that presymptomatic administration of AMB delays neurodegeneration. In order to determine whether the spared MNs have axonal projection to hind limb muscles, fluorogold, a retrograde tracer, has been injected in gastrocnemius and tibialis anterior muscles. SOD1^{G86R} mice treated with AMB had more MNs-positive for fluorogold (**Figures 2E**, **F**).

Muscle strength is dependent on the innervation status of muscles. The integrity of NMJs was assessed by immunohistochemistry with the overlapping of post-synaptic cluster of nicotinic acetylcholine receptors (nAChR) and the axonal markers neurofilament and synaptophysin. AMB has significantly protected muscle innervation in SOD1^{G86R} mice, as they had almost two times more NMJs than the vehicle group, at 95 days of age (**Figure 2G**, **H**). These results suggest that presymptomatic administration of AMB delays disease onset by improving the integrity of the motor units.

Next, we sought to determine whether a later administration of AMB, at disease onset, could slow down disease progression and improve survival of SOD1^{G86R} mice. AMB was administrated to SOD1^{G86R} mice and wild-type littermates, starting at 95 days of age. From 95 days of age, motor symptoms progress rapidly in SOD1^{G86R} mice, and they reach disease end stage around 110 days of age. Body mass, muscle strength, and overall survival were monitored to follow the progression of ALS symptoms (**Figure 3**). After administration of AMB, the decline in body mass was limited, and SOD1^{G86R} mice were heavier, although this effect was transient (**Figure 3A**). A clear improvement of muscle strength was observed, starting from day 101, in SOD1^{G86R} mice treated with AMB when compared to the SOD1^{G86R} vehicle group (**Figure 3B**). Most importantly, survival of SOD1^{G86R} mice was significantly increased by 6 days after administration of AMB (**Figure 3C**).

Altogether, these results show that AMB delays disease progression when the treatment is initiated at disease onset.

Ambroxol Hydrochloride Improves Motor Recovery After Sciatic Nerve Injury in Non-Transgenic Mice

We have previously demonstrated that partial inhibition of GCase activity with CBE improves axonal elongation *in vitro* and *in vivo* recoveries after sciatic nerve injury (Henriques et al., 2017).

We hypothesized that AMB could exert similar pro-regenerative effects. First, we investigated whether AMB could enhance axonal elongation and the formation of NMJs, in an *in vitro* model of motor units, based on a co-culture of myoblasts and spinal cord explants (Combes et al., 2015). This *in vitro* model allows the maturation of axons and the formation of NMJs, as

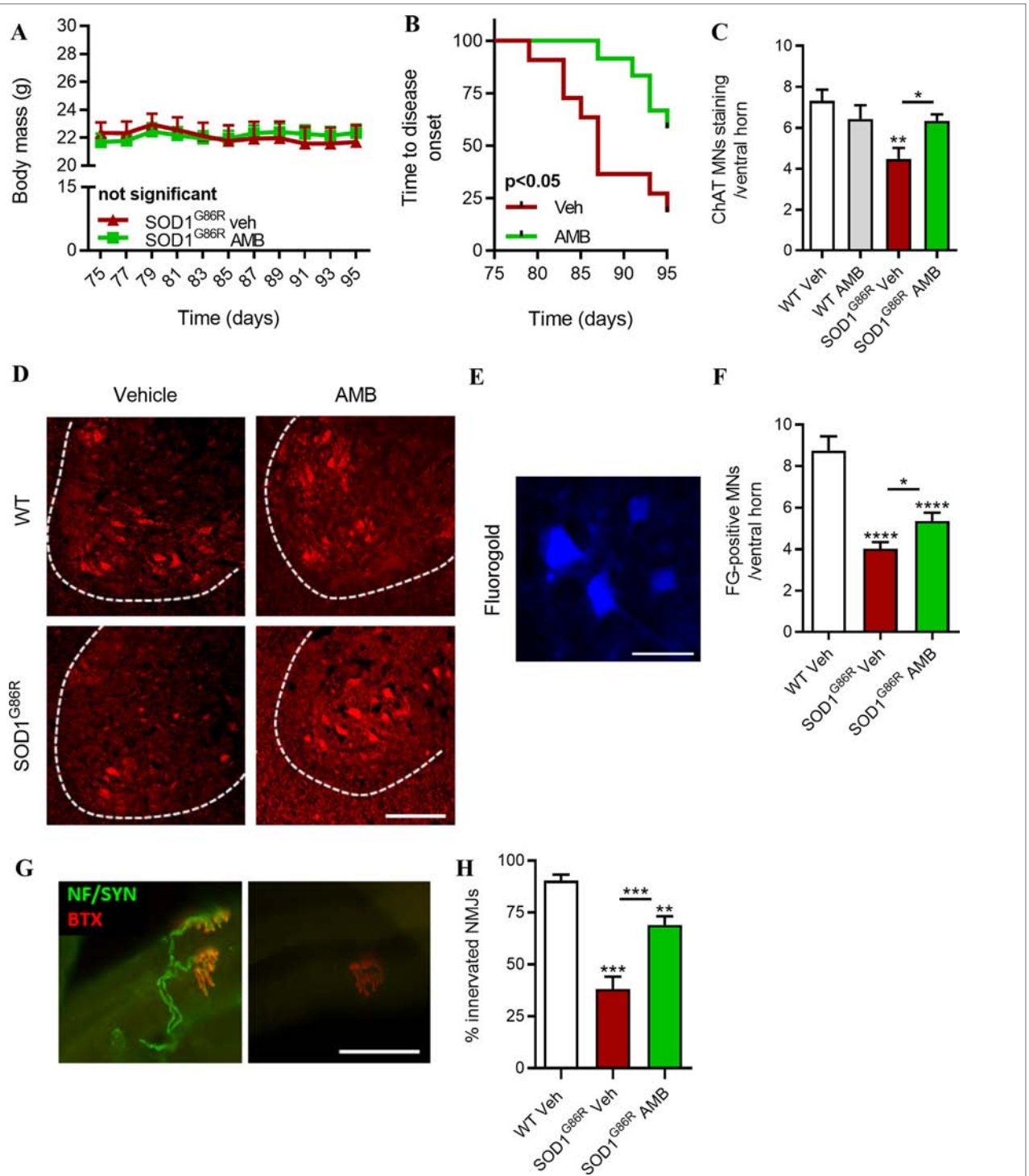

FIGURE 2 | AMB improves motor functions and preserves neuromuscular junction and the functional motor neurons (MNs) in pre-symptomatic SOD1^{G86R} mice. **(A)** Body mass evolution in SOD1^{G86R} mice after AMB treatment (not significant, n = 11–12/group). **(B)** Kaplan–Meier showing time to onset of muscle strength loss in SOD1^{G86R} mice ($p < 0.05$, n = 11–12/group). **(C)** Quantification of choline acetyl transferase (ChAT)-positive cells located in the ventral horn of the spinal cord and having a size bigger than 400 µm^2 (n = 5/group). **(D)** Representative pictures of the ventral horn of the L1–L3 lumbar area, after immunostaining with ChAT (red), a marker specific for spinal motor neurons. Ventral horns are delimited by dashed lines. Scale bar = 100 µm. **(E)** Representative picture of retrogradely labeled spinal MNs after fluorogold (FG) injection in hindlimb muscles. Scale bar = 50 µm. **(F)** Quantification of FG-positive MNs in ventral horn of the spinal cord (n = 10/group, $^*p < 0.05$; $^{****}p < 0.00001$, one-way ANOVA test). **(G)** Representative pictures of innervated (left panel) and denervated (right panel) of neuromuscular junctions in SOD1^{G86R} mice (bungarotoxin, BTX, red; neurofilament and synaptophysin, green). Scale bar = 50 µm. **(H)** Neuromuscular junctions (NMJ) integrity in tibialis anterior muscle ($^{**}p < 0.01$; $^{***}p < 0.001$).

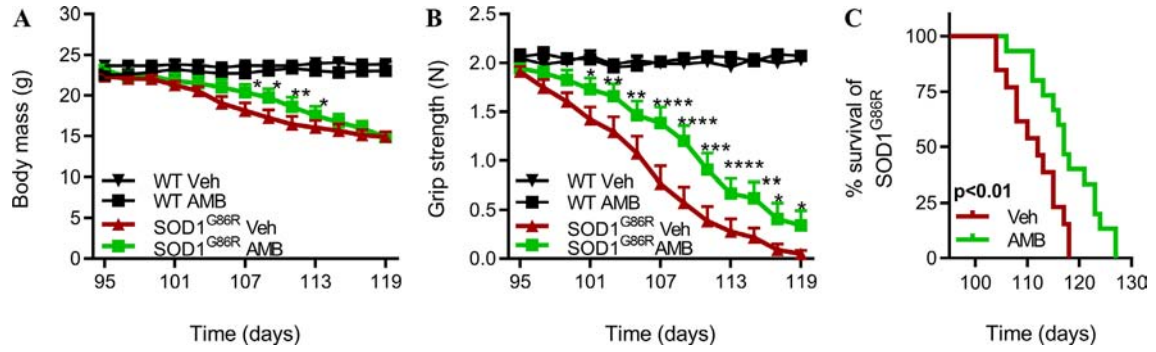

FIGURE 3 | AMB delays disease onset and improves motor functions in symptomatic SOD1^{G86R} mice. **(A)** Body mass evolution in SOD1^{G86R} and WT mice (n = 12–15/group). **(B)** Muscle strength evolution in SOD1^{G86R} and WT (n = 12–15/group). **(C)** Kaplan–Meier analysis of SOD1^{G86R} mice survival (n = 13–15/group, $^{*}p < 0.05$; $^{**}p < 0.01$; $^{***}p < 0.001$; $^{****}p < 0.0001$).

observed by muscle contraction triggered by the application of acetylcholine. The presence of NMJs was confirmed by the colocalization of the axonal neurofilament and the presence of post-synaptic nicotinic acetylcholine receptors (**Figure 4A**, **Supplementary Figure 3**).

The neurite network was significantly longer in presence of the highest dose of AMB (100 μM) (**Figure 4B**). This effect corresponds to a +45% increase when compared to the vehicle group. Lower doses of AMB did not promote neurite elongation.

AMB was able to significantly increase the number of *in vitro* NMJs, determined by the number clusterized nAChRs, in a linear dose-dependent manner, at doses ranging from 10 to 100 μM. The effect of AMB was therefore stronger on the formation of NMJs than on the elongation of axons, in this model (**Figure 4C**).

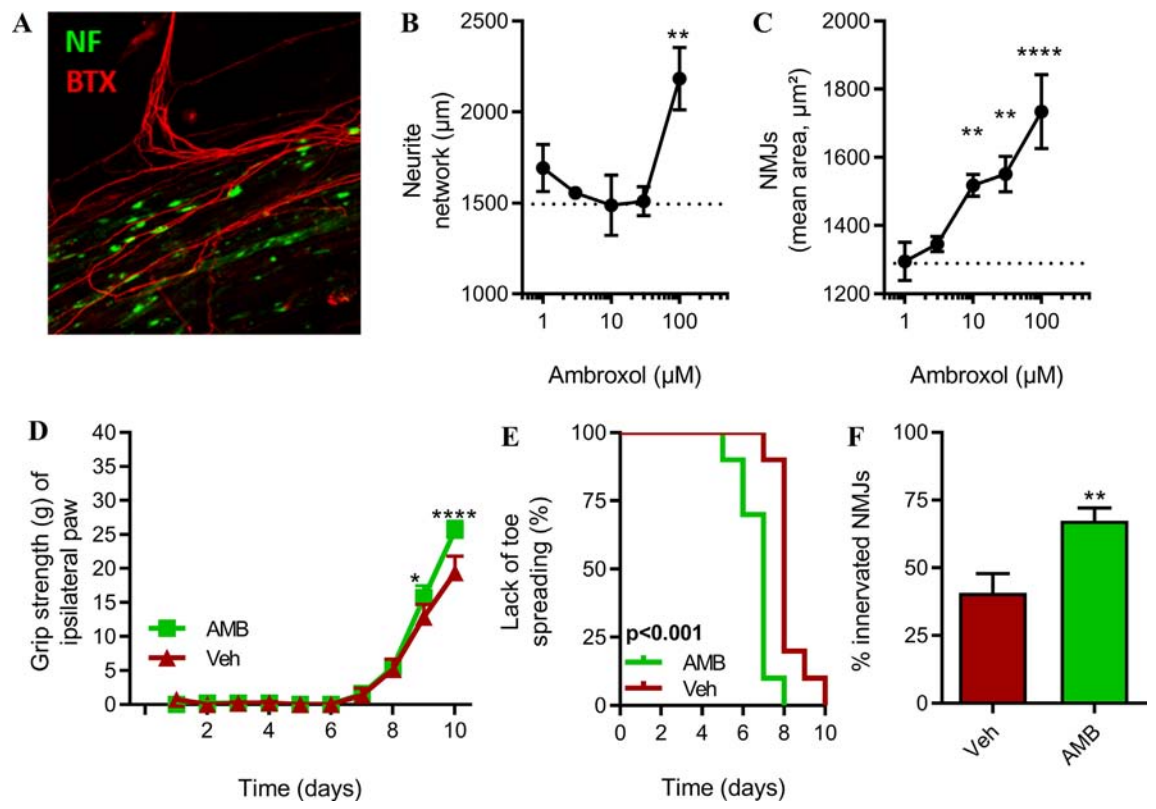

FIGURE 4 | Inhibition of GlcCer degradation by AMB improves *in vivo* axonal plasticity and nerve regeneration after sciatic nerve crush study in non-transgenic mice. **(A)** Representative picture of *in vitro* neuromuscular junctions (NMJs). **(B)** Total length of neurofilament-positive neurites and **(C)** total area NMJs (n = 5/group). **(D)** Muscle strength of ipsilateral hind paws (n = 10/group, $^{*}p < 0.05$; $^{****}p < 0.0001$). **(E)** Kaplan–Meier showing time to observable toe spreading after sciatic nerve injury (n = 10/group, $p < 0.001$). **(F)** NMJ integrity in tibialis anterior muscle (n = 10/group, $^{**}p < 0.01$).

To further evaluate the pro-regenerative effect of AMB on the motor units, we have subjected non-transgenic mice to peripheral nerve injury, to follow-up functional recovery, such as muscle strength and toe spreading, and the number of functional NMJs after treatment with AMB. Upon treatment, mice recovered significantly faster when compared to the control group. Indeed, on days 9 and 10, muscle strength of the injured hindlimb was statistically higher after application of AMB (**Figure 4D**). In a second and independent cohort, we have confirmed the beneficial effect of AMB (3 mM) on functional recovery after sciatic injury. The regenerative effect of AMB was also observed at a dose of 1 mM in this model (**Supplementary Figure 4**). Spontaneous toe spreading is lost after hindlimb muscle denervation. The recovery of toe spreading is a proxy for early sign of reinnervation and was monitored every day. AMB caused a modest but significant effect, as the mice recovered between 1 to 2 days earlier as compared to the control group (**Figure 4E**). Most importantly, 10 days after injury, the number of innervated neuromuscular junctions was 70% greater after application of AMB, suggesting that AMB promotes the formation of new NMJs, which may strongly participate in the pro-regenerative effect of this compound (**Figure 4F**).

DISCUSSION

Glycosphingolipids and Motor Axis

Dysregulation of GlcCer and other glycosphingolipids (e.g., GM1a) was previously reported by us and others in ALS patients and in animal models (Dodge et al., 2015; Henriques et al., 2015; Dodge, 2017; Henriques et al., 2017; Henriques et al., 2018).

GlcCer is degraded by GBA1 or GBA2 beta-GCases. Growing evidence suggests a tight connection between GBA2 activity and motor functions, as full loss of function of GBA2 is a cause of hereditary spastic paraplegia type 46 (SPG46) (Woeste and Wachten, 2017; Woeste et al., 2019). Conversely, pharmacological inhibition of GBA2 activity has been shown to improve the motor phenotype (e.g., motor coordination) of an animal model of Niemann's Pick disease (Marques et al., 2015). Moreover, GM1a, a downstream metabolite of GlcCer, is detected on the cell surface of motor axons and at nerve endings in NMJs. The presence of anti-GM1 autoantibodies has been associated with multifocal motor neuropathy and the acute motor axonal form of Guillain-Barré, suggesting a key role for glycosphingolipids in the maintenance of motor axons and possibly NMJs.

We have shown that inhibition of GCase by CBE causes a concentration-dependent increase in GlcCer, and in the downstream glycosphingolipid GM1a, which was associated with pro-survival and pro-regenerative effects. Treatment with CBE fully prevented loss of GM1a/CTB staining at NMJs in tibialis anterior muscle of SOD1^{G86R} mice, associated with delayed loss in grip strength (Henriques et al., 2017). Interestingly, the inhibition of GlcCer synthase (GCS) accelerates functional decline. Inhibition of GCS also delays the recovery to spinal crush in non-transgenic mice. Thus, a coherent picture emerges in ALS where inhibiting GCase activity and increasing the pool of glycosphingolipids, presumably at the NMJs, are beneficial.

Ambroxol Improved Motor Function in SOD1^{G86R} Mice

Our results showed that GBA2 activity is increased in the spinal cord of SOD1^{G86R} mice, even at the presymptomatic disease stage, which could impair the metabolism of glycosphingolipids and later contribute to the development of motor dysfunctions. Here, we propose ambroxol as a drug candidate for ALS. Ambroxol is known to inhibit of GBA2 activity, mainly catalyzed by GBA2. By inhibiting GBA2, we aimed to prevent the hydrolysis of GlcCer located outside the lysosome, mainly at the plasma membrane, the endoplasmic reticulum, and/or at the Golgi apparatus (Maegawa et al., 2009; Shanmuganathan and Britz-McKibbin, 2011). Our study showed that ambroxol delayed the decline of motor functions and protected motor neurons from degeneration in a transgenic animal model of ALS. Most importantly, ambroxol was able to maintain the functionality of spinal motor neurons in the SOD1^{G86R} mice. For these promising pre-clinical effects, ambroxol has recently been given orphan drug status for ALS by the European Medical Agency.

Clinical Relevance of Ambroxol for ALS

Ambroxol is marketed as an expectorant and mucolytic for lung diseases and for sore throat, with local anesthetic effects. In the CNS, ambroxol is potentially an inhibitor of sodium (Nav1.8) and calcium channels, with claimed anti-glutamatergic properties. Evidence suggests that ambroxol has direct anti-oxidative properties which could translate into beneficial effects in ALS (reviewed by Weiser, 2008).

In addition to its effects on GBA2, ambroxol is also known to bind the enzyme GBA1 in the cytosol and to correct enzyme folding and to improve its addressing to the acidic environment of the lysosome where the drug dissociates, thereby increasing GBA1 activity. The chaperone effect on ambroxol on GBA1 is combined with a positive modulation of GBA1 expression level (Magalhaes et al., 2018). It cannot be excluded that ambroxol could stimulate lysosomal-dependent pathway of protein clearance in ALS (Boland et al., 2018), as ambroxol reduces the alpha-synucleinopathy in an *in vivo* model of PD (Migdalska-Richards et al., 2016b).

Gaucher's disease is caused by genetic mutations of GBA1, resulting in the loss of GBA1 activity (Kanfer et al., 1975; Vardi et al., 2016). In addition, mutations on GBA1 and/or reduced expression of the protein are an important risk factor of PD (Barrett et al., 2013).

Recently, high dose of ambroxol was able to decrease the severity of neurological symptoms of patients with the neuropathic form of Gaucher's disease, suggesting that oral administration of ambroxol successfully target the metabolism of glycosphingolipids in the central nervous system (Narita et al., 2016). Two other clinical trials are currently investigating the effects of ambroxol in PD (NCT02941822; NCT02914366).

Ambroxol Improved the Plasticity of Motor Units

We have also shown that ambroxol hastened functional recovery in a non-transgenic animal model of sciatic nerve injury. Given the modest effect on the kinetic of recovery, the effects of ambroxol are most likely due to an increased ability to rebuilt NMJs. Indeed, in presence of ambroxol, the percentage of re-innervated NMJs was twice higher than that in the vehicle group. Moreover, the *in vitro* co-culture model of motor units provided similar results as ambroxol strongly increased the formation of NMJs but modestly promoted axonal elongation. It indicates that ambroxol was able to stimulate the formation of NMJs. This effect could explain the beneficial outcomes in the SOD1^{G86R} mice through motor axonal sprouting and muscle re-innervation.

Altogether, our results further connected the glycosphingolipid metabolism to the pathophysiology of ALS and indicated that inhibition of GBA2 may be a novel target for ALS.

METHODS

Animal Care and Maintenance

FVB/N non-transgenic female mice derived from Charles River were used to perform nerve sciatic injury experiment.

For others' experiments, FVB/N female mice, overexpressing the SOD1^{G86R} (Ripps et al., 1995), were generated and maintained in our animal facility at 23°C with 12-h light/dark cycle. They had water and regular A04 rodent chow *ad libitum*. AMB (3 mM, Sigma-Aldrich) was given by drinking water for mice treated, and vehicle mice was treated with animal facility water. For the presymptomatic stage study, the treatment started at 75 days of age and stopped at 95 days of age. For the symptomatic stage study (survival experiment), the treatment started to 95 days of age and stopped when mice were euthanized. Mice showing strong motor dysfunction at 93 days of age were not included in the symptomatic cohort. Mice were euthanized when animals were paralyzed and unable to roll over within 5 s after being pushed on their back. For euthanasia, mice were intracardially perfused with PBS 1X at 4°C after intraperitoneal injection with Dolethal (120 mg/kg).

Motor Assessment

Body mass was analyzed on a daily basis. Muscle strength (mean of three tests, grip test, Bioseb, Chaville, France) and the inverted grid test to assess the motor performance and coordination of mice were analyzed every 2 days. Onset of muscle strength loss was defined as a drop of more than 10% of the mouse maximal strength.

Sciatic Nerve Injury

Peripheral nerve injury was performed in order to induce muscle denervation and axonal regeneration. Wild-type mice were anesthetized with ketamine chlorohydrate (100 mg/kg) and xylazine (5 mg/kg). The sciatic nerve was exposed at mid-thigh level and lesioned with fine forceps for 30 s. The skin incision was sutured, and mice were allowed to recover. The hind limb, contralateral to the lesion, served as control. Mice were treated with AMB (3 mM) for 13 days, starting the day before surgery. Mice were followed on a daily basis. Mice were sacrificed by intraperitoneal injection with Doléthal (120 mg/kg) and intracardially perfused with PBS at 4°C.

Retrograde Labeling

Mice were treated with AMB (3 mM in drinking water) or with the vehicle solution (regular drinking water) from 75d of age at 95d of age. Mice were anesthetized at 94 days of age with ketamine chlorohydrate (100 mg/kg) and xylazine (5 mg/kg), and their hind limb muscles were injected with fluorogold (hydroxystilbamidine bis[methanesulfonate], Sigma-Aldrich; 10 mg/ml in PBS, 10% DMSO) FG with Hamilton seringue (26 gauge, 10 μl), and tissues were collected 24 h after injection.

Motor Neurons Counting

Tissues were fixed paraformaldehyde 4% and stored in PBS at 4°C until further use. Lumbar segments L1–L3 fixed in paraformaldehyde 4% were used for studying the number of motor neurons innervating hind limb muscle. After cryoprotection in 30% sucrose, coronal sections 16 μm thick from L1–L3 spinal segment were realized with a cryostat and were either stained with an anti-choline acetylcholine transferase (1/100, Millipore, France) and an alexa594-conjugated goat (1/200, Jackson ImmunoResearch, Suffolk, UK) antibodies, either mount on slides for Fluorogold counting. All neurons located in the ventral horn, which were >400 μm^2 in size and ChAT-positive, were considered as alpha motor neurons. 10 sections of spinal cord were counted, and cell area of motor neurons was measured with ApoTome 2 (Zeiss) microscope.

Neuromuscular Junction Labeling

Tissues were fixed paraformaldehyde 4% and stored in PBS at 4°C until further use. Under a binocular microscope, tibialis anterior muscle fibers were prepared into thin bundles. Neuromuscular junction morphology was studied by labeling of the acetylcholine receptors with rhodamine-conjugated α-bungarotoxin (1/400, Sigma-Aldrich), and labeling of nerve terminals was performed with a rabbit polyclonal anti-synaptophysin antibody diluted 1/50 (Abcam, Cambridge, UK), and anti-neurofilament diluted 1/50. For immunofluorescence of terminal nerve, Alexa-conjugated goat anti-rabbit IgG diluted 1/500 (Jackson ImmunoResearch, Suffolk, UK) was used. Muscle bundles were mounted into slides, prior to fluorescence microscopy (ApoTome 2, Zeiss). NMJs were considered as denervated when the presynaptic nerve terminal was absent from the postsynaptic region.

Beta-Glucosidase Activity

Tissues were snap frozen in liquid nitrogen and stored at −80°C until further use. Frozen tissues were lysed with a TissuLyser (Qiagen, CA) and suspended in phosphate potassium (pH7) buffer extraction. After centrifugation (12,000 rpm for 15 min at 4°C), the supernatants were transferred to new tubes and stored at −80°C. The bicinchoninic acid assay (BCA) method, a colorimetric assay method, was used to measured protein level with a BCA range (Interchim). A GBA buffer was used and adapted according

to the enzymatic activity desired (McIlvaine buffer, 150 mM). For GBA1, enzymatic reaction was carried out with the GBA buffer pH4.6 and adding 0.1% triton and 0.1% BSA. For GBA2, enzymatic reaction was carried out with the GBA buffer pH5.8 and adding 0.1% BSA. After inhibitor addition and fluorescent agent 4-methylumbelliferone addition (4-MU, Sigma-Aldrich), samples were incubated 2 h at 37°C. For reading results, excitation was carried out at 360-nm excitation, and absorbance was measured at 445 nm emission (TriStar LB 941, Berthold Technologies).

Co-Culture of Spinal Cord Explants and Myoblasts

The rat spinal cord–human muscle co-culture was performed as described previously (Combes et al., 2015). Human myoblast was grown on 96-well plate in a mix of MEM and M199 medium, supplemented with glutamine 2 mM, insulin, epidermal growth factor, basic fibroblast growth factor, fetal bovine serum 10%, and penicillin/streptomycin. Spinal cord explants with dorsal roots of 13-day-old Wistar rat embryos (Janvier, Le Genest-St-IsIe, France) were dissected and grown on the muscle monolayer. The co-cultures were maintained in a mix medium (MEM/M199), with 5% fetal calf serum, insulin, glutamine, and penicillin streptomycin. Ambroxol treatment was initiated when the spinal cord explants were added to the muscle monolayer and lasted 27 days. The treatment was renewed every other day during medium change. A total of 10 wells per conditions have been initiated. *In vitro* NMJs and neurite network were identified by immunostaining with alpha-bungarotoxin coupled with Alexa 488 and with a primary antibody against neurofilament 200 kD from mouse revealed with an anti-mouse Alexa 568. Sixty pictures have been automatically taken using same acquisition parameter with ImageXpress (Molecular Device) at 10× magnification and were analyzed with MetaXpress (Molecular Device). After segmentation of the pictures (**Supplementary Figure 3**), the total length of the neurite network and the total area of clustered nAChR were measured.

Statistical Analysis

Data are expressed as the mean ± SEM and were analyzed with GraphPad Prism version 6.0 software. Student's *t* test was used to compare two groups, and ANOVA followed by Fisher's LSD test was applied to compare more than two groups. Grip strength curves were analyzed with two-way ANOVA, and survival curves were analyzed with log-rank test. Differences with *p*-values of <0.05 were considered significant.

DATA AVAILABILITY

The raw data supporting the conclusions of this manuscript will be made available by the authors, without undue reservation, to any qualified researcher.

ETHICS STATEMENT

Experiments were performed by authorized investigator after approval by the ethic committee of the University of Strasbourg and by the ministry of higher education and research (APAFIS #4555; #7146; #8828; #17157). They followed current European Union regulations (Directive 2010/63/EU).

AUTHOR CONTRIBUTIONS

Conceived and designed the experiments: AB, J-PL, AH; Performed the experiments: AB, CQ, AM, AH; Analysis and interpretation of the data: AB, NC, MS, J-PL, AH; Contributed reagents/materials/analysis tools: MS, J-PL; Wrote, discussed and approved the final version of the manuscript: AB, CQ, AM, NC, MS, J-PL, AH.

FUNDING

The work was funded by "Association pour la Recherche et le Développement de Moyens de Lutte contre les Maladies Neurodégénératives" (AREMANE, J.P.L.), the "Association française contre les myopathies" (AFM, JPL). SRS contributed with salary and reagents. J-PL and MS are currently receiving funds from Fight MND foundation.

ACKNOWLEDGEMENTS

We thank Annie Picchinenna for her help in the project.

SUPPLEMENTARY MATERIAL

The Supplementary Material for this article can be found online at: https://www.frontiersin.org/articles/10.3389/fphar.2019.00883/full#supplementary-material

REFERENCES

Albin, R. L., and Dauer, W. T. (2014). Magic shotgun for Parkinson's disease? *Brain* 137, 1274–1275. doi: 10.1093/brain/awu076

Ambrosi, G., Ghezzi, C., Zangaglia, R., Levandis, G., Pacchetti, C., and Blandini, F. (2015). Ambroxol-induced rescue of defective glucocerebrosidase is associated with increased LIMP-2 and saposin C levels in GBA1 mutant Parkinson's disease cells. *Neurobiol. Dis.* 82, 235–242. doi: 10.1016/j.nbd.2015.06.008

Barrett, M. J., Giraldo, P., Capablo, J. L., Alfonso, P., Irun, P., Garcia-Rodriguez, B., et al. (2013). Greater risk of parkinsonism associated with non-N370S GBA1 mutations. *J. Inherit. Metab. Dis.* 36, 575–580. doi: 10.1007/s10545-012-9527-5

Boland, B., Yu, W. H., Corti, O., Mollereau, B., Henriques, A., Bezard, E., et al. (2018). Promoting the clearance of neurotoxic proteins in neurodegenerative disorders of ageing. *Nat. Rev. Drug Discov.* 17, 660–688. doi: 10.1038/nrd.2018.109

Bozek, K., Wei, Y., Yan, Z., Liu, X., Xiong, J., Sugimoto, M., et al. (2014). Exceptional evolutionary divergence of human muscle and brain metabolomes parallels human cognitive and physical uniqueness. *PLoS Biol.* 12, e1001871. doi: 10.1371/journal.pbio.1001871

Combes, M., Poindron, P., and Callizot, N. (2015). Glutamate protects neuromuscular junctions from deleterious effects of β-amyloid peptide and conversely: an in vitro study in a nerve-muscle coculture. *J. Neurosci. Res.* 93, 633–643. doi: 10.1002/jnr.23524

Cutler, R. G., Pedersen, W. A., Camandola, S., Rothstein, J. D., and Mattson, M. P. (2002). Evidence that accumulation of ceramides and cholesterol esters mediates oxidative stress–induced death of motor neurons in amyotrophic lateral sclerosis. *Ann. Neurol.* 52, 448–457. doi: 10.1002/ana.10312

Desport, J. C., Preux, P. M., Magy, L., Boirie, Y., Vallat, J. M., Beaufrère, B., et al. (2001). Factors correlated with hypermetabolism in patients with amyotrophic lateral sclerosis. *Am. J. Clin. Nutr.* 74, 328–334. doi: 10.1093/ajcn/74.3.328

Dodge, J. C. (2017). Lipid involvement in neurodegenerative diseases of the motor system: insights from lysosomal storage diseases. *Front. Mol. Neurosci.* 10 (356), 1–14. doi: 10.3389/fnmol.2017.00356

Dodge, J. C., Treleaven, C. M., Pacheco, J., Cooper, S., Bao, C., Abraham, M., et al. (2015). Glycosphingolipids are modulators of disease pathogenesis in amyotrophic lateral sclerosis. *Proc. Natl. Acad. Sci.* 112, 8100–8105. doi: 10.1073/pnas.1508767112

Dupuis, L., Corcia, P., Fergani, A., Gonzalez De Aguilar, J. L., Bonnefont-Rousselot, D., Bittar, R., et al. (2008). Dyslipidemia is a protective factor in amyotrophic lateral sclerosis. *Neurology* 70 (13), 1004–1009. doi: 10.1212/01.wnl.0000285080.70324.27

Funalot, B., Desport, J.-C., Sturtz, F., Camu, W., and Couratier, P. (2009). High metabolic level in patients with familial amyotrophic lateral sclerosis. *Amyotroph. Lateral Scler.* 10, 113–117. doi: 10.1080/17482960802295192

Henriques, A., Croixmarie, V., Bouscary, A., Mosbach, A., Keime, C., Boursier-Neyret, C., et al. (2018). Sphingolipid metabolism is dysregulated at transcriptomic and metabolic levels in the spinal cord of an animal model of amyotrophic lateral sclerosis. *Front. Mol. Neurosci.* 10 (433), 1–14. doi: 10.3389/fnmol.2017.00433

Henriques, A., Croixmarie, V., Priestman, D. A., Rosenbohm, A., Dirrig-Grosch, S., D'Ambra, E., et al. (2015). Amyotrophic lateral sclerosis and denervation alter sphingolipids and up-regulate glucosylceramide synthase. *Hum. Mol. Genet.* 24, 7390–7405. doi: 10.1093/hmg/ddv439

Henriques, A., Huebecker, M., Blasco, H., Keime, C., Andres, C. R., Corcia, P., et al. (2017). Inhibition of β-glucocerebrosidase activity preserves motor unit integrity in a mouse model of amyotrophic lateral sclerosis. *Sci. Rep.* 7 (5235), 1–15. doi: 10.1038/s41598-017-05313-0

Jésus, P., Fayemendy, P., Nicol, M., Lautrette, G., Sourisseau, H., Preux, P.-M., et al. (2018). Hypermetabolism is a deleterious prognostic factor in patients with amyotrophic lateral sclerosis. *Eur. J. Neurol.* 25, 97–104. doi: 10.1111/ene.13468

Kanfer, J. N., Legler, G., Sullivan, J., Raghavan, S. S., and Mumford, R. A. (1975). The Gaucher mouse. *Biochem. Biophys. Res. Commun.* 67, 85–90. doi: 10.1016/0006-291X(75)90286-7

Lattante, S., Ciura, S., Rouleau, G. A., and Kabashi, E. (2015). Defining the genetic connection linking amyotrophic lateral sclerosis (ALS) with frontotemporal dementia (FTD). *Trends Genet.* 31, 263–273. doi: 10.1016/j.tig.2015.03.005

Maegawa, G. H. B., Tropak, M. B., Buttner, J. D., Rigat, B. A., Fuller, M., Pandit, D., et al. (2009). Identification and characterization of ambroxol as an enzyme enhancement agent for gaucher disease. *J. Biol. Chem.* 284, 23502–23516. doi: 10.1074/jbc.M109.012393

Magalhaes, J., Gegg, M. E., Migdalska-Richards, A., and Schapira, A. H. (2018). Effects of ambroxol on the autophagy-lysosome pathway and mitochondria in primary cortical neurons. *Sci. Rep.* 8, 1385. doi: 10.1038/s41598-018-19479-8

Marques, A. R. A., Aten, J., Ottenhoff, R., van Roomen, C. P. A. A., Herrera Moro, D., Claessen, N., et al. (2015). Reducing GBA2 activity ameliorates neuropathology in niemann-pick Type C mice. *PLoS One* 10, e0135889. doi: 10.1371/journal.pone.0135889

Mazzulli, J. R., Zunke, F., Tsunemi, T., Toker, N. J., Jeon, S., Burbulla, L. F., et al. (2016). Activation of -glucocerebrosidase reduces pathological -synuclein and restores lysosomal function in parkinson's patient midbrain neurons. *J. Neurosci.* 36, 7693–7706. doi: 10.1523/JNEUROSCI.0628-16.2016

McNeill, A., Magalhaes, J., Shen, C., Chau, K.-Y., Hughes, D., Mehta, A., et al. (2014). Ambroxol improves lysosomal biochemistry in glucocerebrosidase mutation-linked Parkinson disease cells. *Brain* 137, 1481–1495. doi: 10.1093/brain/awu020

Migdalska-Richards, A., Daly, L., Bezard, E., and Schapira, A. H. V. (2016b). Ambroxol effects in glucocerebrosidase and α-synuclein transgenic mice: ambroxol in transgenic mice. *Ann. Neurol.* 80, 766–775. doi: 10.1002/ana.24790

Migdalska-Richards, A., Ko, W. K. D., Li, Q., Bezard, E., and Schapira, A. H. V. (2017). Oral ambroxol increases brain glucocerebrosidase activity in a nonhuman primate. *Synapse* 71, e21967. doi: 10.1002/syn.21967

Narita, A., Shirai, K., Itamura, S., Matsuda, A., Ishihara, A., Matsushita, K., et al. (2016). Ambroxol chaperone therapy for neuronopathic Gaucher disease: a pilot study. *Ann. Clin. Transl. Neurol.* 3, 200–215. doi: 10.1002/acn3.292

Noakes, T., and Spedding, M. (2012). Olympics: run for your life. *Nature* 487, 295–296. doi: 10.1038/487295a

O'Regan, G., deSouza, R.-M., Balestrino, R., and Schapira, A. H. (2017). Glucocerebrosidase Mutations in Parkinson Disease. *J. Park. Dis.* 7, 411–422. doi: 10.3233/JPD-171092

Paganoni, S., Deng, J., Jaffa, M., Cudkowicz, M. E., and Wills, A.-M. (2011). Body mass index, not dyslipidemia, is an independent predictor of survival in amyotrophic lateral sclerosis. *Muscle Nerve* 44, 20–24. doi: 10.1002/mus.22114

Ridley, C. M., Thur, K. E., Shanahan, J., Thillaiappan, N. B., Shen, A., Uhl, K., et al. (2013). β-Glucosidase 2 (GBA2) Activity and Imino Sugar Pharmacology. *J. Biol. Chem.* 288, 26052–26066. doi: 10.1074/jbc.M113.463562

Ripps, M. E., Huntley, G. W., Hof, P. R., Morrison, J. H., and Gordon, J. W. (1995). Transgenic mice expressing an altered murine superoxide dismutase gene provide an animal model of amyotrophic lateral sclerosis. *Proc. Natl. Acad. Sci.* 92, 689–693. doi: 10.1073/pnas.92.3.689

Schapira, A. H. V. (2015). Glucocerebrosidase and Parkinson disease: recent advances. *Mol. Cell. Neurosci.* 66, 37–42. doi: 10.1016/j.mcn.2015.03.013

Schmitt, F., Hussain, G., Dupuis, L., Loeffler, J.-P., and Henriques, A. (2014). A plural role for lipids in motor neuron diseases: energy, signaling and structure. *Front. Cell. Neurosci.* 8 (52), 1–10. doi: 10.3389/fncel.2014.00025

Shanmuganathan, M., and Britz-McKibbin, P. (2011). Inhibitor screening of pharmacological chaperones for lysosomal β-glucocerebrosidase by capillary electrophoresis. *Anal. Bioanal. Chem.* 399, 2843–2853. doi: 10.1007/s00216-011-4671-6

Stojkovska, I., Krainc, D., and Mazzulli, J. R. (2018). Molecular mechanisms of α-synuclein and GBA1 in Parkinson's disease. *Cell Tissue Res.* 373, 51–60. doi: 10.1007/s00441-017-2704-y

Vardi, A., Zigdon, H., Meshcheriakova, A., Klein, A. D., Yaacobi, C., Eilam,R., et al. (2016). Delineating pathological pathways in a chemically induced mouse model of Gaucher disease. *J. Pathol.* 239, 496–509. doi: 10.1002/path.4751

Weiser, T. (2008). Ambroxol: a CNS drug? *CNS Neurosci. Ther.* 14, 17–24. doi: 10.1111/j.1527-3458.2007.00032.x

Witte, M. D., Kallemeijn, W. W., Aten, J., Li, K.-Y., Strijland, A., Donker-Koopman, W. E., et al. (2010). Ultrasensitive in situ visualization of active glucocerebrosidase molecules. *Nat. Chem. Biol.* 6, 907–913. doi: 10.1038/nchembio.466

Woeste, M. A., and Wachten, D. (2017). The Enigmatic Role of GBA2 in controlling locomotor function. *Front. Mol. Neurosci.* 10 (386), 1–9. doi: 10.3389/fnmol.2017.00386

Woeste, M. A., Stern, S., Raju, D. N., Grahn, E., Dittmann, D., Gutbrod, K., et al. (2019). Species-specific differences in non-lysosomal glucosylceramidase GBA2 function underlie locomotor dysfunction arising from loss-of-function mutations. *J. Biol. Chem.* 294 (11), 3853–3871. doi: 10.1074/jbc.RA118.006311

Conflict of Interest Statement: MS, J-PL, and AH hold a patent entitled 'Inhibitors of GlcCer degradation in the treatment of diseases of the motor units', and the European Medicines Agency has granted AMB orphan designation for the therapy of amyotrophic lateral sclerosis to Spedding Research Solutions SAS. AH worked for part of the period of this work for Spedding Research Solutions SAS, where MS is president. AH and NC are currently employed by Neuro-sys SAS.

The remaining authors declare that the research was conducted in the absence of any commercial or financial relationships that could be construed as a potential conflict of interest.

frontiers in Cellular Neuroscience

ORIGINAL RESEARCH
published: 16 August 2019
doi: 10.3389/fncel.2019.00376

Expression of Non-visual Opsins Opn3 and Opn5 in the Developing Inner Retinal Cells of Birds. Light-Responses in Müller Glial Cells

Maximiliano N. Rios[1,2†], Natalia A. Marchese[1,2†] and Mario E. Guido[1,2]*

[1] Centro de Investigaciones en Química Biológica de Córdoba (CIQUIBIC), CONICET, Facultad de Ciencias Químicas, Universidad Nacional de Córdoba, Córdoba, Argentina, [2] Departamento de Química Biológica "Ranwel Caputto," Facultad de Ciencias Químicas, Universidad Nacional de Córdoba, Córdoba, Argentina

OPEN ACCESS

Edited by:
Dieter Wicher,
Max Planck Institute for Chemical Ecology, Germany

Reviewed by:
Victoria P. Connaughton,
American University, United States
Marian Henryk Lewandowski,
Jagiellonian University, Poland

***Correspondence:**
Mario E. Guido
mguido@fcq.unc.edu.ar

[†] These authors have contributed equally to this work

Specialty section:
This article was submitted to Cellular Neurophysiology, a section of the journal Frontiers in Cellular Neuroscience

Received: 11 June 2019
Accepted: 02 August 2019
Published: 16 August 2019

Citation:
Rios MN, Marchese NA and Guido ME (2019) Expression of Non-visual Opsins Opn3 and Opn5 in the Developing Inner Retinal Cells of Birds. Light-Responses in Müller Glial Cells. Front. Cell. Neurosci. 13:376. doi: 10.3389/fncel.2019.00376

The avian retina is composed of different types of photoreceptors responsible for image and non-image forming tasks: the visual photoreceptor cells (cones and rods), the melanopsin-expressing intrinsically photoresponsive retinal ganglion cells (ipRGCs) and horizontal cells. Furthermore, the non-visual opsins Opn3 (encephalopsin/panaopsin) and Opn5 (neuropsin) have been shown to be expressed in the vertebrate inner retina, responding to blue (BL) and UV light, respectively. Here we investigated the expression and localization of Opn3 and Opn5 in the developing chick retina at different embryonic days (E) as well as in primary cultures of retinal Müller glial cells (MCs). Opn3 and Opn5 mRNAs and proteins appeared as early as E10 although traces of Opn3- and Opn5-like proteins were seen earlier by E7 in the forming RGC layer and in glial cells extending throughout the developing nuclear layer. Later on, at postnatal days 1–10 (PN1–10) a significant expression of Opn3 was observed in inner retinal cells and processes in plexiform layers, together with expression of the glial markers glutamine synthetase (GS) and the glial fibrillary acidic protein (GFAP). Opn3 and Opn5 were found to be expressed in primary MC cultures prepared at E8 and kept for 2 weeks. In addition, significant effects of BL exposure on Opn3 expression and subcellular localization were observed in MCs as BL significantly increased its levels and modified its nuclear location when compared with dark controls, through a mechanism dependent on protein synthesis. More importantly, a subpopulation of MCs responded to brief BL pulses by increasing intracellular Ca^{2+} levels; whereas light-responses were completely abolished with the retinal bleacher hydroxylamine pretreatment. Taken together, our findings show that these two opsins are expressed in inner retinal cells and MCs of the chicken retina at early developmental phases and remain expressed in the mature retina at PN days. In addition, the novel photic responses seen in MCs may suggest another important role for the glia in retinal physiology.

Keywords: retina, opsin, Müller cells, blue light, retinal ganglion cells, calcium, development

INTRODUCTION

Opsins are photosensitive pigments that bind a retinaldehyde chromophore to form a light-sensitive G protein-coupled receptor able to sense specific wavelength ranges. The vertebrate retina contains a number of different opsins responsible for the photoreception involved in visual functions such as image- and non-image forming tasks (Guido et al., 2010; Meister and Tessier-Lavigne, 2013; Diaz et al., 2016). Classical photoreceptor cells (PRCs) – cones and rods – are responsible for color (diurnal) and black and white (nocturnal) vision, respectively (Meister and Tessier-Lavigne, 2013). PRCs connect through the outer plexiform layer (OPL) to the inner nuclear layer (INL), comprising horizontal cells (HCs), bipolar and amacrine cells, and the INL cells connect with the retinal ganglion cells (RGCs) through the inner plexiform layer (IPL). RGC axons form the optic nerve and send visual information to the brain (Meister and Tessier-Lavigne, 2013). The retina contains diverse types of glial cells, the most abundant being the Müller glial cells (MCs) that extend throughout the inner retina. MCs are responsible for several important physiological activities, both during and after development, significantly contributing to homeostasis and even to more complex processes such as neuronal regeneration (Jorstad et al., 2017; Subirada et al., 2018).

In recent decades, a subpopulation of RGCs expressing the non-visual photopigment melanopsin (Opn4) (Provencio et al., 1998, 2000) was characterized as intrinsically photosensitive RGCs (ipRGCs) in the rodent retina (Hattar et al., 2002). These cells projecting to different brain areas were shown to be involved in setting the biological clock, controlling pupillary light reflexes, suppressing pineal melatonin and other activities (Berson, 2003; Guido et al., 2010; Ksendzovsky et al., 2017; Lazzerini Ospri et al., 2017). It was reported that ipRGCs are also present in chick retina (Contin et al., 2006, 2010; Diaz et al., 2014, 2017) and that they may participate in the regulation of diverse non-visual functions, as observed in blind chicks (Valdez et al., 2012, 2013, 2015). In birds, as well as in other non-mammalian vertebrates, there are two Opn4 genes, the *Xenopus* (Opn4x) and the mammalian (Opn4m) orthologs (Bellingham et al., 2006). Both proteins are expressed in RGCs of chicks very early in development at embryonic day (E) 8 (Verra et al., 2011) while Opn4x is also strongly expressed in HCs by E15 and at later stages (Verra et al., 2011; Morera et al., 2016). Opn4x confers photosensitivity on these HCs (Morera et al., 2016), likely contributing to lateral interaction with PRCs and cooperating with ipRGCs in non-visual activities.

A number of other non-visual opsins/photoisomerases have been reported to be present in the inner retina of mammals such as neuropsin (Opn5) (Tarttelin et al., 2003; Kojima et al., 2011; Nieto et al., 2011) and encephalospin/panaopsin (Opn3) (Halford et al., 2001b). Both opsins are also present in the post-hatching chick retina and brain, specifically in HCs, hypothalamus, and cerebellum (Yamashita et al., 2010; Kato et al., 2016). Furthermore, the putative photoisomerase retinal G protein-coupled receptor (RGR) was shown to be expressed in the inner retina of birds and particularly in Opn4x (+) ipRGCs to modulate retinaldehyde levels in the light, thus maintaining the balance of inner retinal retinoid pools (Diaz et al., 2017).

The goal of the current work was to investigate the onset of expression of the non-visual opsins Opn3 and Opn5 during development in the embryonic chick retina and in primary cultures of MCs. To this end, we first examined the expression of Opn3 and Opn5 at the mRNA and protein levels in whole developing retina at different embryonic (E) stages and in primary MC cultures of E8 retinas. Finally, we evaluated the effect of light exposure on Opn3 expression in retinal cells and the potential photic responses of MCs in culture by Ca^{+2} fluorescence imaging.

MATERIALS AND METHODS

Animal Handling

For the different studies performed, chicken embryos (*Gallus gallus domesticus*) (Avico) at different E and at postnatal day 1 (PN1) were used as previously described in Diaz et al. (2016). Eggs were incubated at 37°C with 60% of humid atmosphere (Yonar®Incubators). Chickens were sacrificed by decapitation. All experiments were performed in accordance with the Use of Animals in Ophthalmic and Vision Research of ARVO, approved by the local animal care committee (School of Chemistry, National University of Córdoba; Exp.15-99-39796) and CICUAL (Institutional Committee for the Care and Use of Experimental Animals).

Retinal Fixation and Sectioning

After enucleation, eyes were hemisected equatorially and the gel vitreous was removed from the posterior eyecup. Samples were fixed for 30 min at 20°C in 4% paraformaldehyde plus 3% sucrose in 0.1 M phosphate buffer, pH 7.4, as described in Diaz et al. (2016). Fixed samples were washed three times in phosphate-buffered saline (PBS; 0.05 M phosphate buffer, 195 mM NaCl, pH 7.4), cryo-protected in PBS plus 30% sucrose, soaked in embedding medium (O.C.T. Compound, Tissue-Tek) for 10 min, and freeze-mounted onto aluminium sectioning blocks. Transverse sections nominally 14 μm thick were cut consistently from the posterior pole of the eye, near the dorsal portion of the pecten, and thaw-mounted on Super-Frost glass slides (Fisher Scientific). Sections were air-dried and stored at −20°C until use.

Primary Cultures of Müller Glial Cells

Primary cultures of MCs were purified from neural chick E8 retinas dissected in ice-cold Ca^{+2}–Mg^{+2}-free Tyrode's buffer containing 25 mM glucose as previously reported (Loiola and Ventura, 2011; Lopez-Colome et al., 2012; Diaz et al., 2014, 2016; Freitas et al., 2016). Briefly, cells were treated with papain (P3125 Sigma–Aldrich) for 25 min at 37°C and deoxyribonuclease I (18047-019 Invitrogen) and rinsed with fetal bovine serum (FBS) 10% and Dulbecco's modified Eagle's medium (DMEM). After dissociation, the cells in suspension were seeded in Petri dishes and grown in DMEM supplemented with 10% FBS for at least 1 week; then, cultures were replicated using trypsin in new

Petri dishes and allowed to grow for another week in DMEM supplemented with 10% FBS at 37°C under constant 5% CO_2-air flow in a humid atmosphere.

Light Treatment in Primary Cultures of Retinal Cells

Primary cultures of MCs were pre-incubated with 9-*cis*-retinal 0.6 μM for 1 h in DMEM. Cultures were then divided into three groups: darkness control (dark), blue light (BL) stimulation (470–490 nm, peak at 480 nm) for 1 h (BL 1 h, LED of 68 μW/cm^2), and darkness condition for 1 h after the BL stimulation (1 h post-BL). In some experiments, cells were treated with 50 μg/mL cycloheximide (CHD) (Sigma–Aldrich) to inhibit protein synthesis, for 1 h before BL stimulation or at the beginning of the BL stimulus for the 1 h post-BL group. Cells were used for immunocytochemistry and protein purification.

Immunohistochemistry

Retinal sections were fixed with 4% paraformaldehyde, washed in PBS for 10 min, and permeabilized with Triton 100 0.1% for 15 min according to Diaz et al. (2016) with modifications. Samples were subsequently treated with blocking buffer [PBS supplemented with 3% bovine serum albumin (BSA) 0.1% Tween 20, and 0.1% $NaNO_3$] for 40 min and incubated overnight at 4°C with the respective antibodies as indicated in **Supplementary Table 1**. The retinal sections were rinsed three times in washing buffer (PBS with Tween 20 0.1%) and finally incubated with secondary antibodies (Jackson Dylight™ 488-conjugated AffiniPure Donkey Anti-Mouse or Dylight™ 549-conjugated AffiniPure Donkey Anti-Rabbit at 1:1000 dilution) for 1 h at room temperature (RT). The samples were also incubated with 4′,6-diamidino-2-phenylindole (DAPI) stain (3 μM). Coverslips were finally washed thoroughly and visualized by confocal microscopy (FV1200; Olympus, Tokyo, Japan).

Western Blot

Homogenates of chick embryonic retinas and primary MCs cultures were resuspended in RIPA buffer [50 mM Tris–HCl, pH 8.0, with 150 mM sodium chloride, 1.0% Igepal (NP-40), 0.5% sodium-deoxycholate, and 0.1% sodium dodecyl sulfate] containing protease inhibitors (Sigma–Aldrich) and processed for western blot (WB) according to Verra et al. (2011) and Nieto et al. (2011). Homogenates were resuspended in sample buffer and separated by SDS-gel electrophoresis on 12% polyacrylamide gels (50 mg total protein/lane), transferred onto Polyvinylidenefluoride (PVDF) membranes, blocked for 1 h at RT with 5% BSA in PBS, and then incubated overnight at 4°C with specific antibodies (**Supplementary Table 1**) in the incubation buffer (3% BSA, 0.1% Tween 20, 1% glycine, 0.02% sodium azide in PBS). Membranes were washed three times for 15 min each in washing buffer (0.1% Tween 20 in PBS) and incubated with the corresponding secondary antibody in the incubation buffer during 1 h at RT followed by three washes with washing buffer for 15 min each. Membranes were scanned using an Odyssey IR Imager (LI-COR Biosciences). After incubation with the specific antibodies, membranes were stripped with NaOH 1 M for 5 min and incubated in blocking buffer containing α-tubulin antibody.

Immunocytochemistry

Cultured cells were fixed for 15 min in 4% paraformaldehyde in PBS and washed in PBS, treated with blocking buffer (3% BSA, 0.1% Tween 20, 1% glycine, 0.02% sodium azide in PBS), and incubated overnight with the primary antibodies (**Supplementary Table 1**). They were then rinsed in PBS and incubated with secondary antibodies from Jackson (1:1000) for 1 h at RT. Samples were incubated with DAPI (3 μM). Coverslips were finally washed thoroughly and visualized by confocal microscopy (FV1200; Olympus, Tokyo, Japan) (Morera et al., 2012).

RNA Isolation and RT-PCR

Total RNA from whole retina and MC cultures was extracted following the method of Chomczynski and Sacchi using the TRIzol™ kit for RNA isolation (Invitrogen). RNA integrity was checked and quantified by UV spectrophotometry (Epoch Microplate Spectrophotometer, Biotek). Finally, 2 μg of total RNA was treated with DNAse (Promega) to eliminate contaminating genomic DNA. cDNA was synthesized with M-MLV (Promega) using Random Primers (Promega) as previously described in Diaz et al. (2016).

The oligonucleotide sequences used for PCR from the *G. gallus* sequences were as follows:

Opn3:

Forward GCCTCTTCGGGATCGTTTCA
Reverse ATGTGATAGCCCGCCAAGAC

Opn5:

Forward GACTTAAAGCTGCGGTGCTC
Reverse TCCCAGAGTTGAAAGAATCCCAAT

TATA-binding protein (*TBP*):

Forward TGGCACACGAGTAACAAGAG
Reverse CCTTGAGCGTCAGGGAAATAG

Polymerase Chain Reaction

Initial denaturation step of 1 min at 94°C, 35 cycles of 60 s at 94°C, 50 s at 60–65°C, 90 s at 72°C, and a final 5 min elongation step at 72°C. Amplification products were separated by 2% agarose gel electrophoresis and visualized by ethidium bromide or sybersafe (Invitrogen™) staining.

Calcium Imaging by Calcium Orange AM Fluorescence Microscopy

Cells were grown in an 8-well Lab-Tek recording chamber (Nunc™, NY, United States) in a colorless DMEM (GIBCO). On the day of the experiment, MCs were incubated with 0.1% of pluronic acid F-127 and the Ca^{2+} indicator dye

Calcium Orange AM 5 μM (Invitrogen–Molecular Probes) in a colorless DMEM for 1 h at 37°C, under darkness condition. The fluorescence imaging technique was performed by using the Ca^{2+}-sensitive indicator excited at 543 nm with a laser coupled to a confocal microscope (Olympus FluoView-1000). The emitted fluorescence was captured every 2 s, using a PlanApo N 60 × Uplan SApo oil-immersion objective (NA: 1.42; Olympus). The 12 bit 4 × 4 binned fluorescence images for each photo were used to quantify fluorescence levels in the cells using ImageJ; the mean fluorescence intensity in each cell was background-corrected by subtracting the mean fluorescence of an area with no cells (only cells showing positive fluorescence pre-stimuli were considered for the analysis). The mean intensity of individual cells was measured in each captured image series. Changes in fluorescence levels were quantified as the ratio between each relative intensity level measured after a BL stimulus of 68 μW/cm^2 for 20 s (F) and the mean of intensities of serial pictures before stimulation (F_o), the same measurements were quantified in the background to correct F/F_o for each cell, as described in Morera et al. (2016). Fluorescence intensities during stimulation were not considered for the analyses and are shown as arbitrary values of F/F_o = 1. In some experiments, MC cultures were treated with 30 mM hydroxylamine (Taurus) for 1 h in DMEM to block the retinal binding to opsins or treated with 2 μM Ionomycin (Sigma–Aldrich) as positive control. HEK-293 cells, that do not express non-visual opsins, were used as negative controls and stimulated with a BL pulse or Ionomycin. Values of F/F_o are not linearly related to changes in $[Ca^{+2}]_i$ but are intended to provide a qualitative indication of variations in $[Ca^{+2}]_i$. No significant vehicle effects or changes in focus were detected. Responses were considered significant when the ratio at the peak differed from the baseline levels by at least 20%.

MTT Assay

Mcs enriched cultures were replicated in 96-well plates and grown for 4 days at 37°C. Cells were divided into two groups: dark and BL for 1 h. Cells in darkness were used as basal controls. After treatment, the medium was removed and replaced by 10% FBS in DMEM and cells were kept in darkness for 24 h at 37°C. Then, 10 μL of MTT reagent (5 mg/mL; Sigma) was added to each well, plates were further incubated for 2 h at 37°C as described by Wagner et al. (2018) followed by addition of 100 μL of DMSO:isopropanol (1:1, v/v) and incubation for a few minutes at RT, protected from light. Samples were analyzed at a wavelength of 570 nm with a reference at 650 nm in an Epoch Microplate Spectrophotometer.

Statistics

Statistical analyses involved a t-test or one-way analysis of variance (ANOVA) followed by Bonferroni *post hoc* comparison when appropriate. Otherwise, when normal distribution or homogeneity of residuals was infringed, Mann–Whitney (M–W) or Kruskal–Wallis (K–W) tests were used with pairwise comparisons performed by the Dunn's test when appropriate. In all cases significance was considered at $p < 0.05$.

RESULTS

To investigate expression of Opn3 and Opn5 in the developing retina of chickens, we evaluated their expression at different embryonic stages in the whole retina and in primary cultures of MCs at early embryonic days. BL-driven responses in MCs were assessed by WB, immunochemistry, and Ca^{+2} fluorescence imaging.

Expression of Opn3 and Opn5 in the Developing Retina

Figures 1, **2** show that Opn3 and Opn5 mRNAs (**Figure 1A**) and proteins (**Figures 1B–F**, **2D**) from samples of the whole developing retina collected at different embryonic days appeared as early as E10. However, traces of Opn3- and Opn5-like proteins were also seen earlier by E7 mainly in the first-appearing cells in the RGC layer and extending throughout the developing nuclear layer (**Figures 1E,F**, **2D**). A significant effect of developmental time for Opn3 expression along the embryonic stages up to PN1 was found ($p < 0.05$ by K–W test) (**Figure 1C**) whereas *post hoc* comparisons indicated that levels of Opn3 protein at PN1 differed from those at E10. By contrast, no significant differences were observed in Opn5 expression across time examined from E10 to PN1 (**Figure 1D**). Controls of antibody specificity against Opn3 and Opn5 proteins are shown in **Supplementary Figures 1**, **2**, respectively.

In later stages (PN10), positive immunoreactivity for Opn3-like protein was observed in inner retinal cells and plexiform layers in close proximity to the glial marker glutamine synthetase (GS) (**Figure 2D**). As shown in **Figure 2**, the glial fibrillary acidic protein (GFAP) marker was detectable by WB in samples of the whole retina as early as E10 whereas GS was visualized at a later stage (E15 and later on); nevertheless, GS-like protein was observed as early as E7 by IHC (**Figure 2D**), when Opn3 and Opn5 were also visualized.

A significant temporal effect on GS expression along development was visualized ($p < 0.05$ by K–W test) with the highest GS levels at PN1 ($p < 0.01$) compared with those at E10 (**Figure 2B**). Also, there was a significant temporal effect for GFAP expression along the embryonic days ($p < 0.05$ by K–W test). Pairwise comparisons revealed that GFAP levels at PN1 ($p < 0.0001$) differed from those at E10 (**Figure 2C**).

Expression of Opn3 and Opn5 in Müller Glial Cell Primary Cultures. Light Effects

We next investigated expression of Opn3 and Opn5 early in development, in primary cultures highly enriched in MCs prepared at E8 and kept for 2 weeks. Glial cell cultures exhibited the typical glial morphology and expressed higher levels of the characteristic glial marker GFAP by WB [median value, in arbitrary units, 1.20 vs. 0.89 in MCs and total retina (TR) cultures, respectively, **Figure 3A**], and showed positive

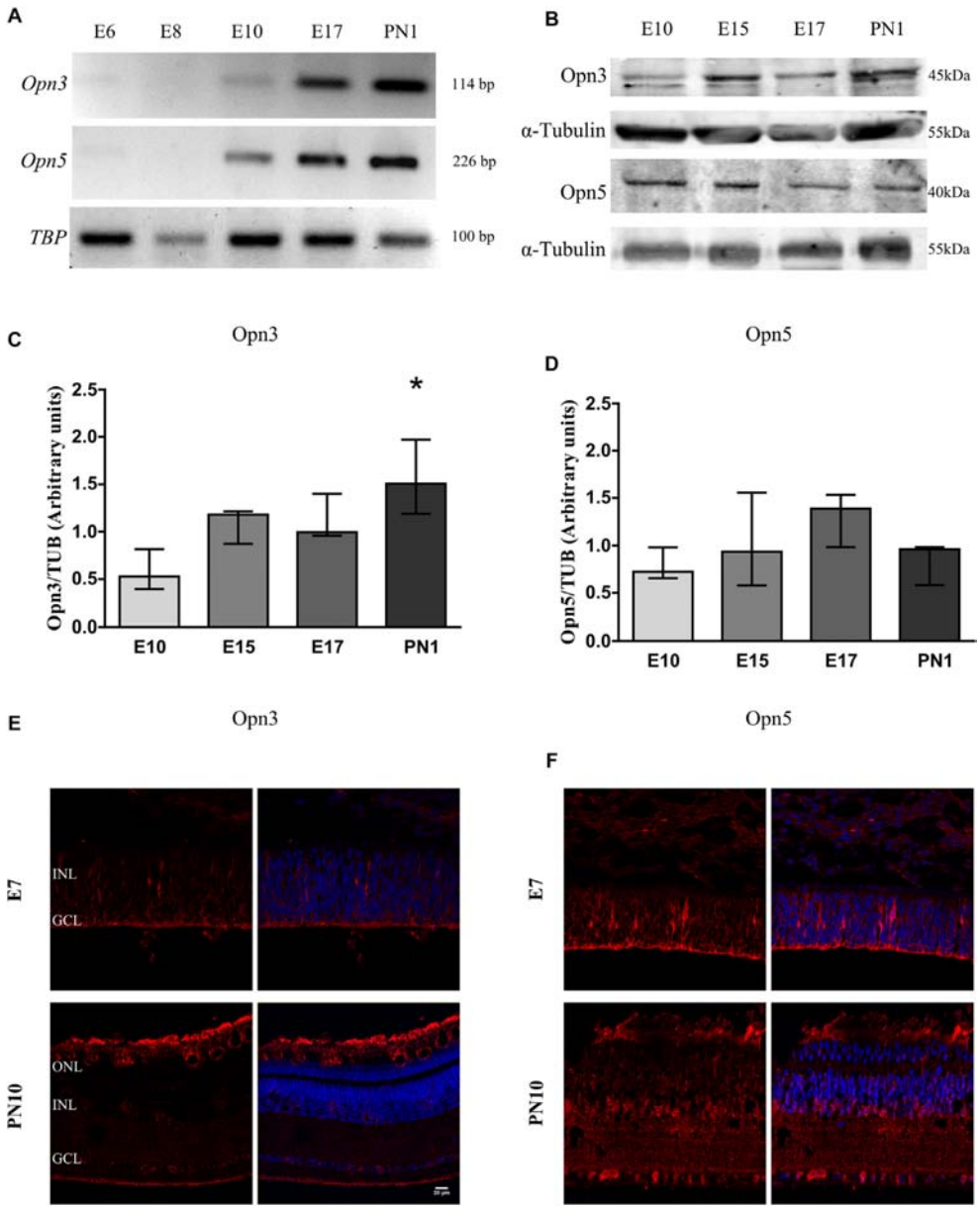

FIGURE 1 | Temporal profiles of Opn3 and Opn5 expression in the developing chicken retina. **(A)** Analysis of *Opn3* and *Opn5* mRNA expression (with *TBP* as housekeeping gene) in the whole chicken retina from embryonic day 6 (E6) to post-natal day 1 (PN1). **(B–D)** Analysis of protein expression of Opn3 and Opn5 in the whole chicken retina from E10 to PN1 by WB. **(B)** Immunoblots show two bands of ∼43–45 kDa for Opn3 protein, whereas a single band was observed at ∼40 kDa for Opn5 protein. **(C)** The histogram shows the median with range for Opn3 levels in the whole chicken retina from E10 to PN1. The K–W test revealed a significant effect of developmental stage [$H_{(3)} = 8.13$, $^*p < 0.05$], *Values at PN1 differ from those at E10 stage ($n = 3$/group). **(D)** The graph shows the median with range for Opn5 levels in the whole chicken retina from E10 to PN1. The K–W test revealed no significant effect of development [$H_{(3)} = 3.97$, $p > 0.05$ ($n = 3$/group)]. **(E,F)** Immunohistochemical labeling of Opn3- and Opn5-like proteins, respectively, in retinal sections at E7 and PN10. Opn3- and Opn5-like proteins are stained in red and DAPI in blue. Retinal sections were visualized by confocal microscopy at 60× magnification. Scale bar = 20 μm.

immunoreactivity for the glial markers GS and Vimentin by ICC (**Figures 3B**, **4C**). Double immunolabeling for Opn3- and Opn5-like proteins together with the glial marker GS was observed in MCs cultures (**Figure 3B**). It is noteworthy that both opsins exhibited a particular subcellular pattern of labeling in GS (+) MCs (merge). Immunoreactivity for the two photopigments was seen in the whole cell with some nuclear staining; similar subcellular distribution has been reported in different cell lines as described in The Human Protein Atlas[1].

In another series of experiments, MCs cultures were exposed to BL of 68 μW/cm^2 for 1 h (BL), other cultures were later returned to the dark for 1 h (1 h post-BL), and controls

[1]https://www.proteinatlas.org/ENSG00000054277-OPN3/cell#human

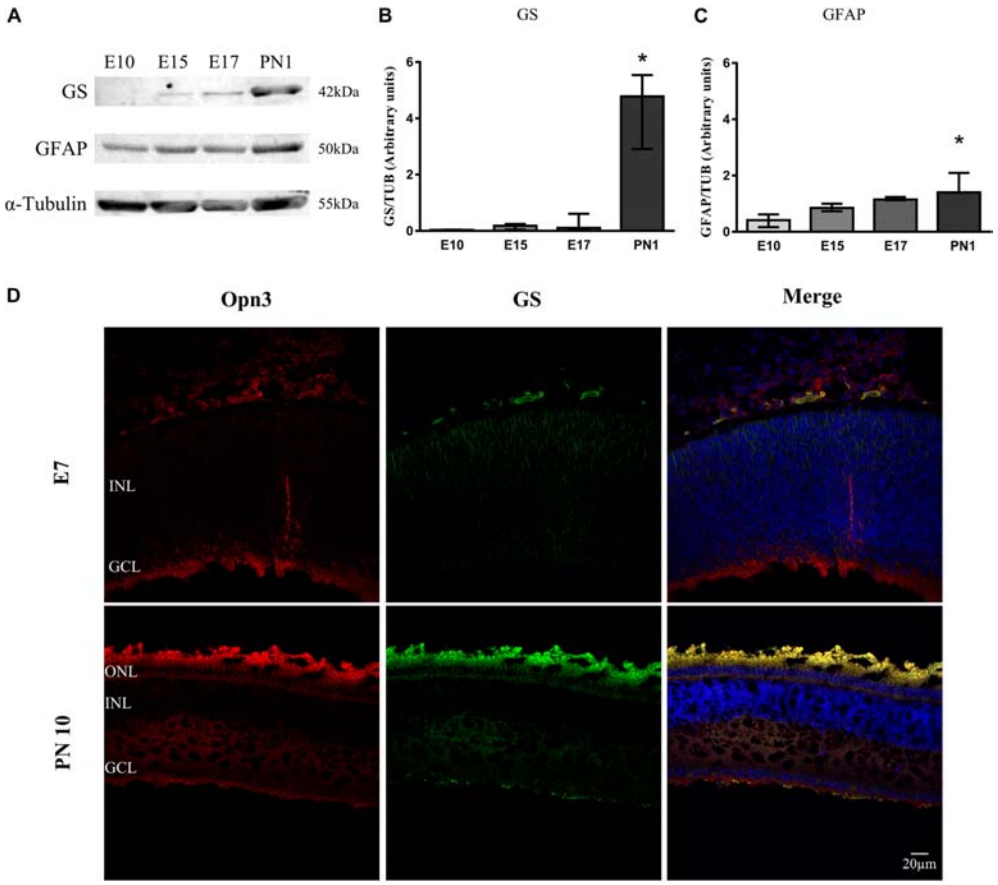

FIGURE 2 | Temporal profile of Müller glial cells markers in the developing chicken retina. **(A)** Analysis of glutamine synthetase (GS) and glial fibrillary acidic protein (GFAP) levels of whole chicken retinas from embryonic day 10 (E10) to post-natal day 1 (PN1) assessed by WB; immunoblots show bands at ∼42 and 50 kDa, respectively. **(B,C)** The histograms show the median with range of GS and GFAP levels in the whole chicken retina from E10 to PN1. The K–W test revealed a significant effect of development on glial markers' protein expression [$H_{(3)} = 9.36$, $p < 0.001$ for GS and $H_{(3)} = 10.38$, $p < 0.0001$ for GFAP]. PN1 values differ from those at E10 stage (*$p < 0.05$, $n = 3$/group). **(D)** Immunohistochemistry showing co-localization of Opn3- (red) and GS-like proteins (green) in the chicken retina at E7 and PN10. At E7 Opn3-like protein is localized mainly in the ganglion cell layer (GCL) with low GS expression. In the PN10 stage, Opn3-like protein shows a more ubiquitous localization in the inner nuclear layer (INL) and an increase in the expression with GS at the GCL. Retina sections were visualized by confocal microscopy at 60× magnification. Scale bar = 20 μm.

maintained in the dark for different pharmacological treatments (**Figure 4** and **Supplementary Figure 3**). As shown in **Figure 4**, BL exposure significantly increased the levels of Opn3 protein in the MCs cultures (**Figures 4A,B**) as seen in 1 h BL or 1 h post-BL cultures compared with dark controls. The one-way ANOVA revealed a significant effect of light condition on Opn3 levels (dark, BL 1 h, and 1 h post-BL) ($p < 0.01$). *Post hoc* comparisons indicated that Opn3 levels for 1 h BL and 1 h post-BL conditions differed from controls maintained in the dark ($p < 0.05$).

In addition, BL exposure caused a notable change in the intracellular localization of this opsin as shown in **Figure 4C**. As denoted with white arrowheads and further magnified in the insets (**Figure 4C**), immunoreactivity associated to Opn3 was distributed all through the cellular body and nuclei of both dark conditions (dark control and 1 h dark post-BL) whereas for BL-treated cultures, a diminished nuclear localization and a higher immunoreactivity in processes resembling proto-end feet were visualized.

In further experiments carried out in the presence of the protein synthesis inhibitor CHD shown in **Supplementary Figure 3**, it was demonstrated that if protein synthesis is blocked, no light induction is observed in 1 h BL- or 1 h post-BL-treated cultures with similar protein levels to those found in the dark (**Supplementary Figures 3A,B**). Results strongly suggest that such mechanism depends on the *de novo* synthesis of protein. The K–W test revealed that there was no significant effect on Opn3 expression under the different light conditions examined with CHD pretreatment. In addition, **Supplementary Figure 3C** shows that Opn3 immunolabeling remained concentrated in nuclear compartments and all through the cell body in cultures treated with CHD, even after BL exposure (**Supplementary Figure 3C**) and no re-localization of Opn3-like

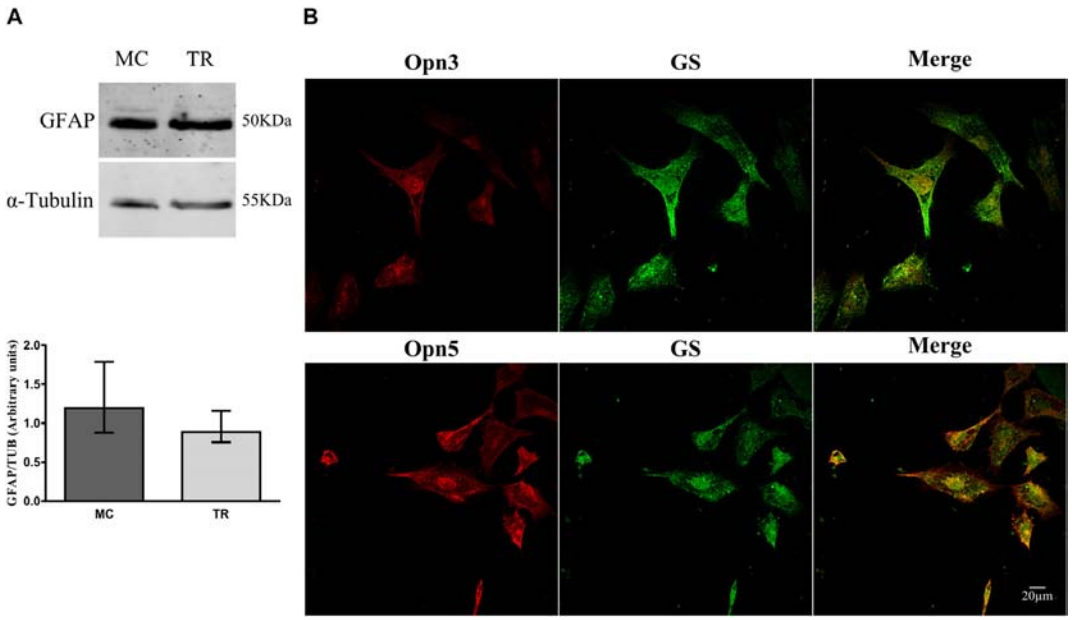

FIGURE 3 | Characterization of primary cultures of Müller glial cells. **(A)** Analysis of GFAP levels by WB in primary cultures of Müller glial cells and of total retina (TR) prepared at E8, immunoblots show bands at ∼50 kDa. The histograms show the median with range for GFAP levels in primary cultures of MC and TR (n = 4/group). Primary cultures were highly enriched in Müller glial cells as defined by morphological cell identification (non-neuron-like morphology) and glial marker expression. **(B)** Primary cultures of Müller cells were labeled for Opn3- or Opn5- (red) and GS-like proteins (green) and visualized by confocal microscopy. Müller cells showed ubiquitous and generalized localization of Opn3 and Opn5. Scale bar = 20 μm.

immunofluorescence was observed in any illumination condition (dark, BL, or 1 h post-BL).

In another series of control experiments, and to discard any deleterious effect of bright BL exposure in retinal cell cultures, cell viability by MTT in dark or photic-exposed cells to BL for 1 h was assessed 24 h after the stimulus (**Supplementary Figure 4**). No significant differences were found in cell viability according to MTT absorbance of MCs cultures between dark and 1 h BL conditions.

Light Responses in Primary Müller Glial Cell Cultures

For all retinal photoreceptors characterized, a common feature found leading to intrinsic photosensitivity is related to significant changes in intracellular Ca^{2+} levels differentially causing cell hyperpolarization or depolarization, respectively (Qiu et al., 2005; Sekaran et al., 2005; Contin et al., 2010; Nieto et al., 2011; Morera et al., 2016; Diaz et al., 2017). Taking these observations into consideration, and in order to test whether primary MCs cultures expressing non-visual opsins (shown in **Figures 3**, **4** and **Supplementary Figure 3**) may respond to BL, we assessed changes in intracellular Ca^{2+} levels by fluorescent imaging with calcium orange in cell cultures after photic stimulation. At first, when MCs cultures were exposed to brief light pulses of white (1000 lux), red or BL of 68 μWatt for 10 s, no responses were evoked (data not shown); however, a BL pulse of 20 s was able to promote significant increases (>20%) in relative intracellular Ca^{2+} levels in individual MCs (**Figures 5A,B**). Moreover, **Figure 5C** shows the light-evoked responses in Ca^{2+} fluorescence for the subpopulation displaying ≥20% increase responses, with the dark blue recording representing the average of all evoked responses. In this subset of glial cells, positive light responses to a 20 s BL pulse persisted for several minutes, ranging from 100 to 300 s. In addition, the Ca^{+2} ionophore ionomycin (2 μM) was used as a positive control in MCs, promoting an acute and transient peak of Ca^{+2} increase as indicated in the inset of **Figure 5C**. As shown in **Figures 5E,F**, 41.40% of cells in the culture did not respond to BL stimulation at the intensity applied (**Figure 5E**, black circles); however, 58.60% of cells left did respond according to the following distribution: 14% of cells did respond, showing a 10–20% increase in Ca^{2+} fluorescence levels over the basal threshold (**Figures 5E,F**, green squares), while another subpopulation of cells (∼44.80%) responded with an increase in Ca^{2+} levels >20% (**Figures 5E,F**, blue triangles). It is known that most opsin photopigments identified used a vitamin A-derivative retinaldehyde as chromophore (Diaz et al., 2016). To further investigate the specificity of the BL responses observed in MCs cultures, in other series of control experiments, we proceeded to bleach the retinaldehyde by pretreating cultures with hydroxylamine before BL stimulation. As shown in **Figure 5D**, light-responses associated to changes in intracellular Ca^{2+} were completely abolished with the retinal bleacher hydroxylamine (30 mM) pretreatment, resulting in 87.5% of non-responding cells. Relative fluorescent Ca^{2+} levels (ΔF) analysis indicates significant different responses of the higher than 20% increase subpopulation and ionomycin stimulated group compared with

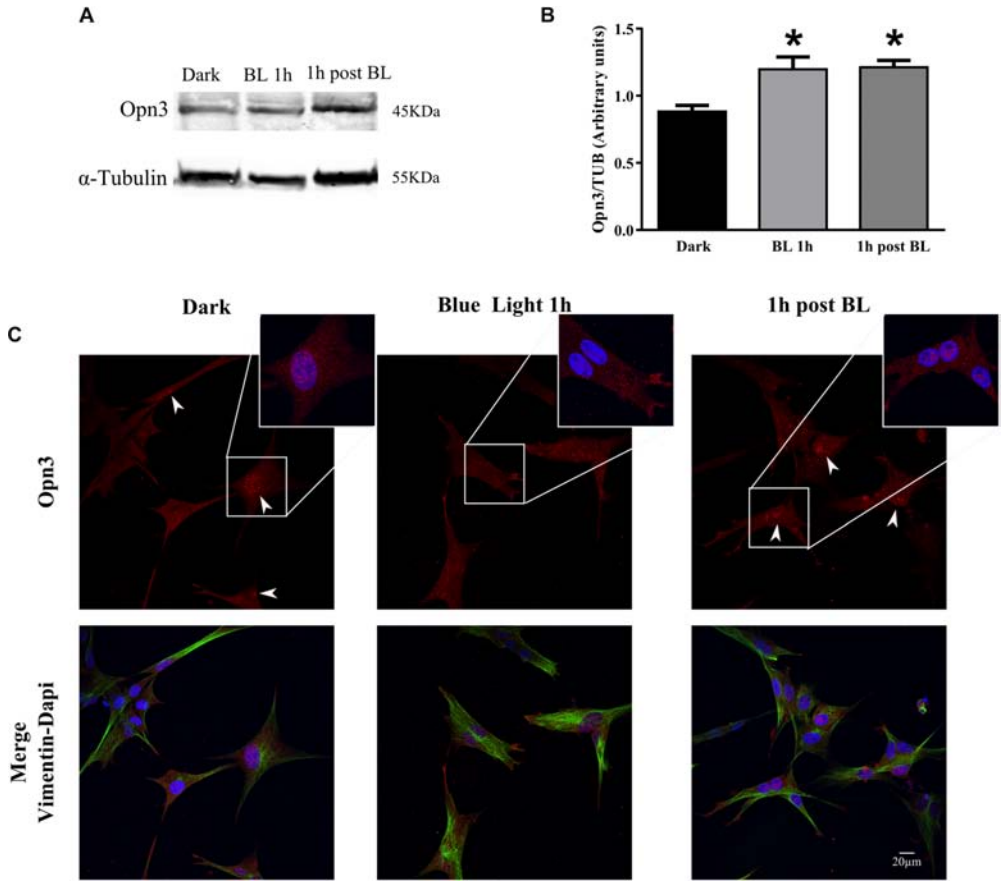

FIGURE 4 | Effect of blue light on Opn3 protein in primary cultures of Müller glial cells. **(A)** Analysis of Opn3 protein in Müller cells at different light conditions by WB. Immunoblots show two bands of ∼43–45 kDa for Opn3 protein in the three experimental conditions: dark, blue light for 1 h (BL 1 h), and 1 h post-BL. **(B)** The histograms show the media ± SEM of Opn3 levels in the three illumination conditions. Increased Opn3 protein levels in Müller glial cells cultures were observed for 1 h of BL stimulation and 1 h after BL exposure over the dark control [$*p < 0.01$ by one-way ANOVA $F_{(2,9)} = 8.48$, $n = 3$–5/group]. **(C)** Localization of Opn3 immunoreactivity in Müller cell cultures by ICC for Opn3 (red), the intermedium filament marker Vimentin (green), and DAPI (blue), further magnified in the insets. Opn3-like protein was localized in inner cellular membranes with a strong labeling surrounding the nucleus in darkness and 1 h post-BL conditions, where nuclear accumulations were detected (see insets for higher magnification). By contrast, cell cultures exposed to BL for 1 h did not show substantial nuclear-like accumulation of Opn3 immunofluorescence. Scale bar = 20 μm.

fluorescence values in non-responding retinal MCs ($p < 0.0001$ by ANOVA, **Figure 5E**).

Although not all glial cells in the cultures responded to light in the experimental conditions tested, other controls were carried out to assess the specificity of the observed photic responses, by assessing Ca^{2+} fluorescence imaging in HEK-293 cells exposed to bright BL (68 $\mu W/cm^2$) (**Supplementary Figure 5**). No BL responses were found in any cell of the cultures exposed to different intensities and durations (data not shown). HEK-293 cells not expressing Opn3 and Opn5 [our results, Yamashita et al. (2010) and Sugiyama et al. (2014) were unable to respond to BL under the experimental conditions tested (light blue lines; average: dark blue) but did so in the presence of 2 μM ionomycin (orange lines, average: red) (**Supplementary Figure 5A**)]. This pharmacological treatment, known to promote the intracellular mobilization of Ca^{+2}, did elicit significant increases in the Ca^{2+} indicator fluorescence (**Supplementary Figure 5B**).

DISCUSSION

In addition to the cone and rod photopigments (Opn1 and Opn2) involved in purely visual functions relating to day/night vision and image forming processes, a wide range of non-visual opsins has been characterized in vertebrates over the last decades whose functions are not fully known (Peirson et al., 2009; Guido et al., 2010; Nagata et al., 2010; Terakita and Nagata, 2014; Leung and Montell, 2017; Dalesio et al., 2018); among these, Opn3, Opn4, and Opn5 are the most recently identified. In addition to mammals and other vertebrates (Bertolesi et al., 2014), ipRGCs expressing Opn4x and Opn4m were also shown to be present in chick retina (Contin et al., 2006, 2010; Diaz et al., 2014, 2016), appearing very early in development at E8 (Verra et al., 2011). Opn4x is also strongly expressed in HCs by E15 and at later stages (Verra et al., 2011; Morera et al., 2016), conferring photosensitivity on these HCs through a photocascade involving the Gq protein, activation

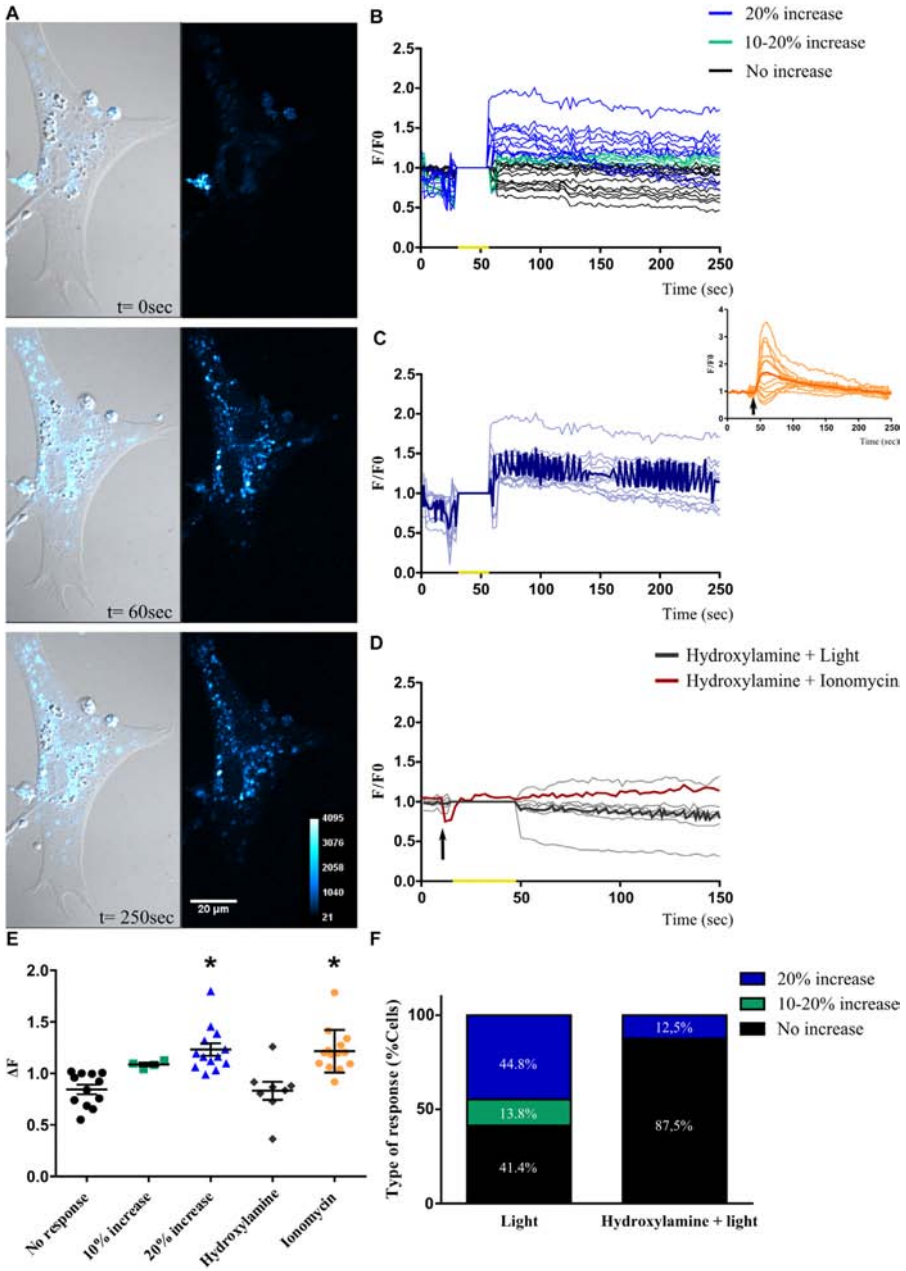

FIGURE 5 | Blue light-induced changes in intracellular Ca^{2+} levels in Müller glial cells. **(A)** Representative Müller glial cells kept in culture for 2 weeks loaded with Calcium Orange AM and displaying a significant increase in intracellular Ca^{2+} fluorescence levels after a blue light pulse (BL) of 20 s and visualized at 60 and 250 s (left panels). The Ca^{2+} response is shown in a pseudo color scale with the highest response in white (right panels). Scale bar = 20 μm. **(B)** Graphical representation showing the F/F_o ratio for different Ca^{2+} responses in Müller glial cells when exposed to a single brief BL pulse of 68 μW/cm^2 for 20 s (yellow mark). Responses are divided into: (i) cells that did not respond to BL (black lines); (ii) cells that responded with fluorescence increase between 10–20% to BL (green lines); (iii) cells that responded with an increase in fluorescence >20% to BL (blue lines). **(C)** Graphical representation of the F/F_o ratio for changes in fluorescence levels in cells that responded with 20% increase in fluorescence to the BL stimulus (yellow mark). The dark blue line represents the average response of photosensitive cells. Inset shows Müller glial cells responses to ionomycin stimulation (2 μM) (arrow). **(D)** Graphical representation indicating the F/F_o ratio for the changes in fluorescence levels in cells pre-treated with the retinal bleacher hydroxylamine (30 mM) and stimulated with BL pulse (yellow mark; gray lines) and the ionophore ionomycin (2 μM) (arrow; red line). **(E)** Graphical representation of relative fluorescent Ca^{2+} levels (ΔF) in Müller glial cells when exposed to a single brief BL pulse: black, cells that did not respond to BL; green, cells that responded with a fluorescence increase between 10 and 20% to BL; blue, cells that responded with an increase in fluorescence >20% to BL; gray, cells pre-treated with the retinal bleacher hydroxylamine (30 mM); and orange, cells stimulated with ionomycin (2 μM). The graph shows individual values with the media ± SEM. A one-way ANOVA revealed a significant effect of treatment of light or ionomycin [$F_{(4,46)} = 10.63$, $^*p < 0.0001$) compared with the no-increase in Ca^{2+} levels group (51 cells from eight independent experiments). **(F)** Graphical representation for the percentage of each type of response in Müller glial cells pre-treated or not with hydroxylamine. The Ca^{2+} increase triggered by the brief BL pulse is abolished with the retinal bleacher, suggesting an opsin-mediated response.

of phospholipase C, Ca^{2+} mobilization, and GABA release (Morera et al., 2016).

Here, we demonstrate that the non-visual opsins Opn3 and Opn5 are expressed in inner retinal cells of chick retina at early phases of development and remain expressed in the mature retina at PN1 and PN10. Moreover, our results indicate that these opsins are expressed particularly in glial cells, considering the similar expression pattern of the glial marker GS and Opn3 in the developing and mature retina and their expression in enriched MCs cultures.

Opn3 was originally designated as encephalopsin and then as panopsin, since it was found to be expressed within the retina and in extra-retinal tissues such as brain, testis, liver, and lung (Blackshaw and Snyder, 1999; Halford et al., 2001a,b; Tarttelin et al., 2003). In the human retina, Opn3 protein is expressed in the different neural layers including the GCL (Halford et al., 2001a); in the chick, it was more recently shown that two Opn3-related proteins (cOpn3 and cTMT) are present in PN retinal HCs, hypothalamus, and cerebellum (Kato et al., 2016). Here, we found that Opn3 mRNA and protein were detected in the whole chick retina at early stages around E7–10 up to PN1 and PN10 (**Figures 1**, **2**). Opn3 expression was localized at first in cells of the forming GCL and extending throughout the inner developing retina; whereas later on, Opn3 immunoreactivity was also visualized in INL and their plexiform layers (IPL and OPL) of retinal sections (**Figures 1**, **2**).

Remarkably, Opn3 and glial markers show matching expression curves along the embryonic stages. Our present results indicate a gradual increase of the glial structural marker GFAP expression up to the PN1; whereas at this point a substantial increase in GS expression was found which correlates with a functional visual retina (**Figure 2**; Thanos and Mey, 2001). In fact, GS at PN10 is observed as a ubiquitous immunolabeling at the ONL, IPL, and GCL where glutamate transmission is essential for retinal activity (Meister and Tessier-Lavigne, 2013). In this sense, MCs are fully specified near the last stages of development, along which these cells are becoming mature by establishing their polarity and functional domains throughout the retinal layers (MacDonald et al., 2017). It has been proposed that synaptic activity plays a crucial role in shaping these functional domains, as Ca^{+2} responses in MCs vary from acetylcholine- to glutamate-dependent activities across the developmental stages (Rosa et al., 2015; MacDonald et al., 2017). Interestingly, we observed similar distribution patterns of Opn3 and GS in the chicken strongly predicting non-visual opsin expression by MCs. In fact, this was later confirmed in primary cultures of MCs, prepared at E8 and kept for 2 weeks, showing co-expression of GS/vimentin and Opn3/Opn5 (**Figures 3**, **4**).

The presence of Opn3 in extra ocular tissue has been related to the light-driven regulation of different functions (Koyanagi et al., 2013) such as wound healing responses (Castellano-Pellicena et al., 2018) and pigmentation of melanocytes (Regazzetti et al., 2018). Although the precise role of Opn3 in the developing and mature retina of birds is still unknown, it is noteworthy that levels of Opn3 protein and its intracellular localization are highly regulated by light in MCs (**Figure 4** and **Supplementary Figure 3**), neurons (data not shown), and melanocytes (Ozdeslik et al., 2019). Particularly, Opn3 protein levels in MCs were significantly induced by light exposure (1 h BL or 1 h post-BL) with a marked modification in protein pattern location, in which the immunolabeling associated to Opn3 substantially decreased in the cellular nuclei in the light condition and it was recovered 1 h later in the dark after BL exposure (**Figure 4**). In addition, it is important to remark that this mechanism of light induction and protein intracellular re-localization of Opn3 protein is dependent on *de novo* synthesis of protein as clearly observed after treatment with CHD (**Supplementary Figure 3**).

Opn5 mRNA was found to be expressed in mouse testis, brain, and eye, as well as in human retina and brain (Tarttelin et al., 2003). Whereas in the rat, Opn5 mRNA and protein are clearly expressed in the retina, specifically in INL and GCL cells and in IPL processes (Nieto et al., 2011); moreover, within the human and mice retina Opn5 is particularly seen in a subset of non-rod/non-cone retinal neurons and in the epidermal and muscle cells of the outer ears (Kojima et al., 2011). In the chicken, it was shown to be expressed in the pineal gland and in neurons of the INL and GCL of the retina of post-hatching chicks at PN14 (Yamashita et al., 2010), reflecting a similar retinal distribution in mammalian and non-mammalian retinas. Here we demonstrated that Opn5 mRNA and protein appeared very early in the developing retina at around E7–10, particularly in cells of the forming GCL and cells extending throughout the immature inner retina, resembling glial morphology (**Figure 1**). Moreover, primary cultures of MCs clearly exhibited a positive immunoreactivity for Opn5-like protein, further supporting the idea that this opsin is also expressed in retinal cells and MC cultures at early developmental stages (**Figure 3**). In fact, this opsin plays a key role during eye development in mice mediating light-dependent vascularization by a dopamine pathway (Nguyen et al., 2019). In the mature retina at PN10, Opn5-like protein is visualized in the GCL, INL, and processes concentrated at the IPL and OPL. These results allow us to hypothesize that Opn5 may play a key role in sensing UV light in the inner retina. Indeed, this opsin constitutes a functional UV-sensitive Gi-coupled bistable photopigment with maximal efficiency ∼420 nm, capable of conferring light-induced Ca^{2+} responses, cyclic AMP decrease, and MAPK phosphorylation after heterologous expression in HEK-293 cells (Sugiyama et al., 2014). In birds, apart from its potential role in the retina, Opn5 is involved in the photoreception required for seasonal reproduction, presumably acting as a deep brain photoreceptor molecule (Nakane et al., 2010; Yamashita et al., 2010). In mammals, Opn5 has been reported to be directly and specifically involved in the photic synchronization of the retinal clock (Buhr et al., 2015) and more recently to be associated with photoentrainment and phase shifting to UV light (Ota et al., 2018). However, in triple knockout mice lacking essential components of phototransduction signaling for rods, cones, and ipRGCs, minimal responses were observed following UV light stimulation, suggesting a very limited role for Opn5 in driving excitatory photic responses within the mouse retina (Hughes et al., 2016).

In order to have an active opsin photopigment, the PRC requires a vitamin A derivative available to work as chromophore since it is known that for most photopigments characterized such chromophores are retinoids that can be recycled in the retina itself or in the adjacent retinal pigment epithelium (Diaz et al., 2016, 2017; Morera et al., 2016). In this connection, the putative photoisomerase RGR found to be expressed in the inner chicken retina (Bailey and Cassone, 2004) and particularly in ipRGCs early in development is likely to be used by the different opsins (Opn3, 4, and 5) for the purpose of modulating retinaldehyde levels in light and thus keeping the balance of inner retinal retinoid pools (Diaz et al., 2016). Initially identified in bovine retinal pigment epithelium (Jiang et al., 1993), RGR was subsequently found within the retina in RGCs and/or MCs (Pandey et al., 1994; Hao and Fong, 1996, 1999; Chen et al., 2001a,b; Maeda et al., 2003; Bailey and Cassone, 2004; Wenzel et al., 2005; Diaz et al., 2017). It thus appears more likely that RGR enhances the classical and ipRGC visual cycles rather than forming part of an alternative photic visual cycle (Wenzel et al., 2005; Radu et al., 2008; Diaz et al., 2017).

Retinal Müller Glial Cells as Light-Sensors: Ca^{2+} Responses Triggered by Light Stimulation

Here we show for the first time that primary cultures of embryonic MCs expressing typical markers for glia also display the expression of Opn3- and Opn5-like proteins (**Figure 3**). Similar results were observed in retinal sections having double immunolabeling for Opn3 and the glial marker GS (**Figure 2**). Additionally Opn3 levels and cellular localization are modified by BL stimulation by a mechanism dependent on protein synthesis (**Figure 4** and **Supplementary Figure 3**). The question arising from these observations is whether these opsin-expressing glial cells respond to light. One known characteristic of vertebrate photosensitivity to PRCs, ipRGCs, and Opn4x-expressing HCs is the change in intracellular Ca^{2+} levels after light exposure, differentially causing cell hyperpolarization or depolarization, respectively, in avian and mammalian retinal cells (Qiu et al., 2005; Sekaran et al., 2005; Contin et al., 2010; Nieto et al., 2011; Meister and Tessier-Lavigne, 2013; Morera et al., 2016; Diaz et al., 2017). MCs primary cultures showed distinct and specific increases in somatic Ca^{+2} responses to a brief light stimulus for at least 20 s at the blue range wavelength (∼480 nm) (**Figure 5**) compared with basal values at dark conditions or cultures subject to shorter light exposure times and different wavelengths (red, white) (data not shown). Furthermore, three different subpopulations of cells were observed in the MCs primary cultures in terms of responses to BL: 41% of the population showed no response, whereas the 59% remaining displayed detectable BL responses; most of them responding with a >20% average increase in fluorescence. This latter segment of the population exhibited lasting responses to brief light pulses of at least 20 s, persisting for at least 100–300 s. In agreement with this, the photic responses involving Ca^{+2} mobilization were lost when cells were pretreated with hydroxylamine a retinaldehyde bleacher as previously shown in intrinsically photosensitive HCs strongly indicating that this phenomenon requires an active chromophore (Morera et al., 2016). Even though most cells expressed Opn3, only ∼60% of them responded to light with Ca^{+2} increase, the remaining percentage may not have functional opsins in their membrane; need longer time of exposure, higher BL intensities, or might be activating a different signaling pathway, i.e., related to cyclic nucleotides as it has been previously described by Koyanagi et al. (2013). Indeed, in *ex vivo* conditions there is only a percentage of MCs that show Ca^{+2} increase in response to the neuronal activation observed after light or electric stimulation (Newman, 2005). In line with our results the human MCs line MIO-M1 was shown to express a number of different opsins and to respond to repetitive stimulation with 480 nm light (Hollborn et al., 2011). In isolated rat retina, Ca^{+2} increases in glial cells were evoked by light-induced neuronal activity, suggesting a neuron-to-glia signaling in the retina mediated by ATP release (Newman, 2005). In MCs of the adult guinea pig retina, light stimulation evoked two differential Ca^{+2} responses (Rillich et al., 2009) probably an indication that retinal light stimulation causes glial activation by alterations in both the membrane potential and ATP-mediated mechanisms. However, our results clearly show direct Ca^{+2} responses to BL stimulation by MCs in primary cultures free of other types of retinal cells. Since Opn3 responds specifically to BL in a wavelength range peaking at 480 nm whereas Opn5 has been reported to respond to UV stimulation at 380 nm in the dark, we assumed that Opn5 would not be selectively activated by the experimental conditions applied (BL in dark adapted cells) (Kojima et al., 2011; Yamashita et al., 2014). Nevertheless, we cannot discard that the edges of the action spectra for lights centered at 480 nm could stimulate Opn5 in the violet/UV range as reported. Further experiments will be required to fully understand the role of retinal glial cells under physiological conditions and photic stimulation in the context of the entire retina. In this connection, Ca^{+2} increase in MCs has been linked to ATP release (Newman, 2003), extracellular H^+ flux (Tchernookova et al., 2018), and potentially D-serine release (Metea and Newman, 2006), to regulate retinal neurotransmission. In addition, MCs may play a role in non-visual processes regulated by light such as the setting of the biological clock as well as in optical and visual functions acting as living optic fibers or enhancers of human vision acuity (MacDonald et al., 2017). Along these lines it has recently been demonstrated that a cell-autonomous clock present in SCN astrocytes may drive circadian behavior in mammals (Brancaccio et al., 2019).

Overall, we show that the two studied non-visual opsins are present in the inner retina of chicks from very early developmental stages to PN before there is any sign of vision. Their expression was found to be present in inner retinal cells including MCs kept in culture for several days. It is therefore likely that these opsins contribute with Opn4m and x to the detection of light and thus to regulation of the diverse activities required for the adequate development of the eye and functioning of the avian retina. Moreover, we demonstrated that MCs were affected by BL stimulation in terms of Opn3 protein and its intracellular localization as previously reported for the immunoreactivity of Opn4 and Opn5 in the retina of rats exposed

to continuous light of low intensity (Benedetto et al., 2017). In addition, similar results were found in primary cultures of Opn3 (+) retinal neurons of chick embryos exposed to BL and displaying marked changes in protein levels and intracellular localization (data not shown). More important, MCs expressing non-visual opsins appear to be able to sense BL in the inner retina by increasing intracellular levels of Ca^{2+}, novel events that presumably affect cell to cell interaction and glia to neuron communication, while increasing levels of Opn3 in the whole cell, thus preparing the inner retina and its circuits for the light exposure times.

DATA AVAILABILITY

The datasets generated for this study are available on request to the corresponding author.

ETHICS STATEMENT

All experiments were performed in accordance with the Use of Animals in Ophthalmic and Vision Research of ARVO, approved by the local animal care committee (School of Chemistry, National University of Córdoba; Exp. 15-99-39796) and CICUAL (Institutional Committee for the Care and Use of Experimental Animals).

AUTHOR CONTRIBUTIONS

MR, NM, and MG designed the research, and analyzed and discussed the data. MR and NM performed the research. MG contributed to the new reagents, analytic tools and wrote the manuscript.

FUNDING

This work was supported by the Agencia Nacional de Promoción Científica y Técnica (FONCyT, PICT 2013 No. 021 and PICT 2016 No. 187), the Consejo Nacional de Investigaciones Científicas y Tecnológicas de la República Argentina (CONICET) (PIP 2014), and the Secretaría de Ciencia y Tecnología de la Universidad Nacional de Córdoba (SeCyT-UNC).

SUPPLEMENTARY MATERIAL

The Supplementary Material for this article can be found online at: https://www.frontiersin.org/articles/10.3389/fncel.2019.00376/full#supplementary-material

REFERENCES

Bailey, M. J., and Cassone, V. M. (2004). Opsin photoisomerases in the chick retina and pineal gland: characterization, localization, and circadian regulation. *Invest. Ophthalmol. Vis. Sci.* 45, 769–775.

Bellingham, J., Chaurasia, S. S., Melyan, Z., Liu, C., Cameron, M. A., Tarttelin, E. E., et al. (2006). Evolution of melanopsin photoreceptors: discovery and characterization of a new melanopsin in nonmammalian vertebrates. *PLoS Biol.* 4:e254. doi: 10.1371/journal.pbio.0040254

Benedetto, M. M., Guido, M. E., and Contin, M. A. (2017). Non-Visual photopigments effects of constant light-emitting diode light exposure on the inner retina of wistar rats. *Front. Neurol.* 8:417. doi: 10.3389/fneur.2017.00417

Berson, D. M. (2003). Strange vision: ganglion cells as circadian photoreceptors. *Trends Neurosci.* 26, 314–320. doi: 10.1016/S0166-2236(03)00130-9

Bertolesi, G. E., Hehr, C. L., and McFarlane, S. (2014). Wiring the retinal circuits activated by light during early development. *Neural Dev.* 9:3. doi: 10.1186/1749-8104-9-3

Blackshaw, S., and Snyder, S. H. (1999). Encephalopsin: a novel mammalian extraretinal opsin discretely localized in the brain. *J. Neurosci.* 19, 3681–3690. doi: 10.1523/jneurosci.19-10-03681.1999

Brancaccio, M., Edwards, M. D., Patton, A. P., Smyllie, N. J., Chesham, J. E., Maywood, E. S., et al. (2019). Cell-autonomous clock of astrocytes drives circadian behavior in mammals. *Science* 363, 187–192. doi: 10.1126/science.aat4104

Buhr, E. D., Yue, W. W., Ren, X., Jiang, Z., Liao, H. W., Mei, X., et al. (2015). Neuropsin (OPN5)-mediated photoentrainment of local circadian oscillators in mammalian retina and cornea. *Proc. Natl. Acad. Sci. U.S.A.* 112, 13093–13098. doi: 10.1073/pnas.1516259112

Castellano-Pellicena, I., Uzunbajakava, N. E., Mignon, C., Raafs, B., Botchkarev, V. A., and Thornton, M. J. (2018). Does blue light restore human epidermal barrier function via activation of opsin during cutaneous wound healing? *Lasers Surg. Med.* 51, 370–382. doi: 10.1002/lsm.23015

Chen, P., Hao, W., Rife, L., Wang, X. P., Shen, D., Chen, J., et al. (2001a). A photic visual cycle of rhodopsin regeneration is dependent on Rgr. *Nat. Genet.* 28, 256–260. doi: 10.1038/90089

Chen, P., Lee, T. D., and Fong, H. K. (2001b). Interaction of 11-cis-retinol dehydrogenase with the chromophore of retinal g protein-coupled receptor opsin. *J. Biol. Chem.* 276, 21098–21104. doi: 10.1074/jbc.M01044 1200

Contin, M. A., Verra, D. M., and Guido, M. E. (2006). An invertebrate-like phototransduction cascade mediates light detection in the chicken retinal ganglion cells. *FASEB J.* 20, 2648–2650. doi: 10.1096/fj.06-6133fje

Contin, M. A., Verra, D. M., Salvador, G., Ilincheta, M., Giusto, N. M., and Guido, M. E. (2010). Light activation of the phosphoinositide cycle in intrinsically photosensitive chicken retinal ganglion cells. *Invest. Ophthalmol. Vis. Sci.* 51, 5491–5498. doi: 10.1167/iovs.10-5643

Dalesio, N. M., Barreto Ortiz, S. F., Pluznick, J. L., and Berkowitz, D. E. (2018). Olfactory, taste, and photo sensory receptors in non-sensory organs: it just makes sense. *Front. Physiol.* 9:1673. doi: 10.3389/fphys.2018.01673

Diaz, N. M., Morera, L. P., and Guido, M. E. (2016). Melanopsin and the non-visual photochemistry in the inner retina of vertebrates. *Photochem. Photobiol.* 92, 29–44. doi: 10.1111/php.12545

Diaz, N. M., Morera, L. P., Tempesti, T., and Guido, M. E. (2017). The visual cycle in the inner retina of chicken and the involvement of retinal g-protein-coupled receptor (RGR). *Mol. Neurobiol.* 54, 2507–2517. doi: 10.1007/s12035-016-9830-35

Diaz, N. M., Morera, L. P., Verra, D. M., Contin, M. A., and Guido, M. E. (2014). Early appearance of nonvisual and circadian markers in the developing inner retinal cells of chicken. *Biomed. Res. Int.* 2014:646847. doi: 10.1155/2014/646847

Freitas, H. R., Ferraz, G., Ferreira, G. C., Ribeiro-Resende, V. T., Chiarini, L. B., do Nascimento, J. L., et al. (2016). Glutathione-induced calcium shifts in chick retinal glial cells. *PLoS One* 11:e0153677. doi: 10.1371/journal.pone.0153677

Guido, M. E., Garbarino-Pico, E., Contin, M. A., Valdez, D. J., Nieto, P. S., Verra, D. M., et al. (2010). Inner retinal circadian clocks and non-visual

photoreceptors: novel players in the circadian system. *Prog. Neurobiol.* 92, 484–504. doi: 10.1016/j.pneurobio.2010.08.005

Halford, S., Bellingham, J., Ocaka, L., Fox, M., Johnson, S., Foster, R. G., et al. (2001a). Assignment of panopsin (OPN3) to human chromosome band 1q43 by in situ hybridization and somatic cell hybrids. *Cytogenet. Cell Genet.* 95, 234–235. doi: 10.1159/000059351

Halford, S., Freedman, M. S., Bellingham, J., Inglis, S. L., Poopalasundaram, S., Soni, B. G., et al. (2001b). Characterization of a novel human opsin gene with wide tissue expression and identification of embedded and flanking genes on chromosome 1q43. *Genomics* 72, 203–208. doi: 10.1006/geno.2001.6469

Hao, W., and Fong, H. K. (1996). Blue and ultraviolet light-absorbing opsin from the retinal pigment epithelium. *Biochemistry* 35, 6251–6256. doi: 10.1021/bi952420k

Hao, W., and Fong, H. K. (1999). The endogenous chromophore of retinal G protein-coupled receptor opsin from the pigment epithelium. *J. Biol. Chem.* 274, 6085–6090. doi: 10.1074/jbc.274.10.6085

Hattar, S., Liao, H. W., Takao, M., Berson, D. M., and Yau, K. W. (2002). Melanopsin-containing retinal ganglion cells: architecture, projections, and intrinsic photosensitivity. *Science* 295, 1065–1070. doi: 10.1126/science.1069609

Hollborn, M., Ulbricht, E., Rillich, K., Dukic-Stefanovic, S., Wurm, A., Wagner, L., et al. (2011). The human muller cell line MIO-M1 expresses opsins. *Mol. Vis.* 17, 2738–2750.

Hughes, S., Rodgers, J., Hickey, D., Foster, R. G., Peirson, S. N., and Hankins, M. W. (2016). Characterisation of light responses in the retina of mice lacking principle components of rod, cone and melanopsin phototransduction signalling pathways. *Sci. Rep.* 6:28086. doi: 10.1038/srep28086

Jiang, M., Pandey, S., and Fong, H. K. (1993). An opsin homologue in the retina and pigment epithelium. *Invest. Ophthalmol. Vis. Sci.* 34, 3669–3678.

Jorstad, N. L., Wilken, M. S., Grimes, W. N., Wohl, S. G., VandenBosch, L. S., Yoshimatsu, T., et al. (2017). Stimulation of functional neuronal regeneration from muller glia in adult mice. *Nature* 548, 103–107. doi: 10.1038/nature23283

Kato, M., Sugiyama, T., Sakai, K., Yamashita, T., Fujita, H., Sato, K., et al. (2016). Two opsin 3-related proteins in the chicken retina and brain: a TMT-Type opsin 3 is a blue-light sensor in retinal horizontal cells, hypothalamus, and cerebellum. *PLoS One* 11:e0163925. doi: 10.1371/journal.pone.0163925

Kojima, D., Mori, S., Torii, M., Wada, A., Morishita, R., and Fukada, Y. (2011). UV-sensitive photoreceptor protein OPN5 in humans and mice. *PLoS One* 6:e26388. doi: 10.1371/journal.pone.0026388

Koyanagi, M., Takada, E., Nagata, T., Tsukamoto, H., and Terakita, A. (2013). Homologs of vertebrate Opn3 potentially serve as a light sensor in nonphotoreceptive tissue. *Proc. Natl. Acad. Sci. U.S.A.* 110, 4998–5003. doi: 10.1073/pnas.1219416110

Ksendzovsky, A., Pomeraniec, I. J., Zaghloul, K. A., Provencio, J. J., and Provencio, I. (2017). Clinical implications of the melanopsin-based non-image-forming visual system. *Neurology* 88, 1282–1290. doi: 10.1212/WNL.0000000000003761

Lazzerini Ospri, L., Prusky, G., and Hattar, S. (2017). Mood, the circadian system, and melanopsin retinal ganglion cells. *Annu. Rev. Neurosci.* 40, 539–556. doi: 10.1146/annurev-neuro-072116-31324

Leung, N. Y., and Montell, C. (2017). Unconventional roles of opsins. *Annu. Rev. Cell Dev. Biol.* 33, 241–264. doi: 10.1146/annurev-cellbio-100616-2

Loiola, E. C., and Ventura, A. L. (2011). Release of ATP from avian muller glia cells in culture. *Neurochem. Int.* 58, 414–422. doi: 10.1016/j.neuint.2010.12.019

Lopez-Colome, A., Martinez-Lozada, Z., Guillem, A. M., Lopez, E., and Ortega, A. (2012). Glutamate transporter-dependent mTOR phosphorylation in muller glia cells. *ASN Neuro.* 4:e00095. doi: 10.1042/AN20120022

MacDonald, R. B., Charlton-Perkins, M., and Harris, W. A. (2017). Mechanisms of muller glial cell morphogenesis. *Curr. Opin. Neurobiol.* 47, 31–37. doi: 10.1016/j.conb.2017.08.005

Maeda, T., Van Hooser, J. P., Driessen, C. A., Filipek, S., Janssen, J. J., and Palczewski, K. (2003). Evaluation of the role of the retinal G protein-coupled receptor (RGR) in the vertebrate retina in vivo. *J. Neurochem.* 85, 944–956. doi: 10.1046/j.1471-4159.2003.01741.x

Meister, M., and Tessier-Lavigne, M. (2013). "Low-level visual processing: the retina," in *Principles of Neural Science*, 5th Edn, eds J. H. S. Eric, R. Kandel, T. M. Jessell, S. A. Siegelbaum, and A. J. Hudspeth (New York, NY: The McGraw-Hill Companies Inc.).

Metea, M. R., and Newman, E. A. (2006). Calcium signaling in specialized glial cells. *Glia* 54, 650–655. doi: 10.1002/glia.20352

Morera, L. P., Diaz, N. M., and Guido, M. E. (2012). A novel method to prepare highly enriched primary cultures of chicken retinal horizontal cells. *Exp. Eye Res.* 101, 44–48. doi: 10.1016/j.exer.2012.05.010

Morera, L. P., Diaz, N. M., and Guido, M. E. (2016). Horizontal cells expressing melanopsin x are novel photoreceptors in the avian inner retina. *Proc. Natl. Acad. Sci. U.S.A.* 113, 13215–13220. doi: 10.1073/pnas.1608901113

Nagata, T., Koyanagi, M., and Terakita, A. (2010). "Molecular evolution and functional diversity of opsin-based photopigments," in *Photobiological Sciences Online*, eds J. Lee, and K. Smith (Osaka: Osaka City University).

Nakane, Y., Ikegami, K., Ono, H., Yamamoto, N., Yoshida, S., Hirunagi, K., et al. (2010). A mammalian neural tissue opsin (opsin 5) is a deep brain photoreceptor in birds. *Proc. Natl. Acad. Sci. U.S.A.* 107, 15264–15268. doi: 10.1073/pnas.1006393107

Newman, E. A. (2003). Glial cell inhibition of neurons by release of ATP. *J. Neurosci.* 23, 1659–1666. doi: 10.1523/jneurosci.23-05-01659.2003

Newman, E. A. (2005). Calcium increases in retinal glial cells evoked by light-induced neuronal activity. *J. Neurosci.* 25, 5502–5510. doi: 10.1523/JNEUROSCI.1354-05.2005

Nguyen, M. T., Vemaraju, S., Nayak, G., Odaka, Y., Buhr, E. D., Alonzo, N., et al. (2019). An opsin 5-dopamine pathway mediates light-dependent vascular development in the eye. *Nat. Cell Biol.* 21, 420–429. doi: 10.1038/s41556-019-0301-x

Nieto, P. S., Valdez, D. J., Acosta-Rodriguez, V. A., and Guido, M. E. (2011). Expression of novel opsins and intrinsic light responses in the mammalian retinal ganglion cell line RGC-5. presence of OPN5 in the rat retina. *PLoS One* 6:e26417. doi: 10.1371/journal.pone.0026417

Ota, W., Nakane, Y., Hattar, S., and Yoshimura, T. (2018). Impaired circadian photoentrainment in Opn5-null mice. *Science* 6, 299–305. doi: 10.1016/j.isci.2018.08.010

Ozdeslik, R. N., Olinski, L. E., Trieu, M. M., Oprian, D. D., and Oancea, E. (2019). Human nonvisual opsin 3 regulates pigmentation of epidermal melanocytes through functional interaction with melanocortin 1 receptor. *Proc. Natl. Acad. Sci. U.S.A.* 116, 11508–11517. doi: 10.1073/pnas.1902825116

Pandey, S., Blanks, J. C., Spee, C., Jiang, M., and Fong, H. K. (1994). Cytoplasmic retinal localization of an evolutionary homolog of the visual pigments. *Exp. Eye Res.* 58, 605–613. doi: 10.1006/exer.1994.1055

Peirson, S. N., Halford, S., and Foster, R. G. (2009). The evolution of irradiance detection: melanopsin and the non-visual opsins. *Philos. Trans. R. Soc. Lond. B Biol. Sci.* 364, 2849–2865. doi: 10.1098/rstb.2009.0050

Provencio, I., Jiang, G., De Grip, W. J., Hayes, W. P., and Rollag, M. D. (1998). Melanopsin: an opsin in melanophores, brain, and eye. *Proc. Natl. Acad. Sci. U.S.A.* 95, 340–345. doi: 10.1073/pnas.95.1.340

Provencio, I., Rodriguez, I. R., Jiang, G., Hayes, W. P., Moreira, E. F., and Rollag, M. D. (2000). A novel human opsin in the inner retina. *J. Neurosci.* 20, 600–605. doi: 10.1523/jneurosci.20-02-00600.2000

Qiu, X., Kumbalasiri, T., Carlson, S. M., Wong, K. Y., Krishna, V., Provencio, I., et al. (2005). Induction of photosensitivity by heterologous expression of melanopsin. *Nature* 433, 745–749. doi: 10.1038/nature03345

Radu, R. A., Hu, J., Peng, J., Bok, D., Mata, N. L., and Travis, G. H. (2008). Retinal pigment epithelium-retinal G protein receptor-opsin mediates light-dependent translocation of all-trans-retinyl esters for synthesis of visual chromophore in retinal pigment epithelial cells. *J. Biol. Chem.* 283, 19730–19738. doi: 10.1074/jbc.M801288200

Regazzetti, C., Sormani, L., Debayle, D., Bernerd, F., Tulic, M. K., De Donatis, G. M., et al. (2018). Melanocytes sense blue light and regulate pigmentation through opsin-3. *J. Invest. Dermatol.* 138, 171–178. doi: 10.1016/j.jid.2017.07.833

Rillich, K., Gentsch, J., Reichenbach, A., Bringmann, A., and Weick, M. (2009). Light stimulation evokes two different calcium responses in muller glial cells of the guinea pig retina. *Eur. J. Neurosci.* 29, 1165–1176. doi: 10.1111/j.1460-9568.2009.06682.x

Rosa, J. M., Bos, R., Sack, G. S., Fortuny, C., Agarwal, A., Bergles, D. E., et al. (2015). Neuron-glia signaling in developing retina mediated by neurotransmitter spillover. *eLife* 4:e09590. doi: 10.7554/eLife.09590

Sekaran, S., Lupi, D., Jones, S. L., Sheely, C. J., Hattar, S., Yau, K. W., et al. (2005). Melanopsin-dependent photoreception provides earliest light detection in the mammalian retina. *Curr. Biol.* 15, 1099–1107. doi: 10.1016/j.cub.2005.05.053

Subirada, P. V., Paz, M. C., Ridano, M. E., Lorenc, V. E., Vaglienti, M. V., Barcelona, P. F., et al. (2018). A journey into the retina: muller glia commanding survival and death. *Eur. J. Neurosci.* 47, 1429–1443. doi: 10.1111/ejn.13965

Sugiyama, T., Suzuki, H., and Takahashi, T. (2014). Light-induced rapid Ca(2)(+) response and MAPK phosphorylation in the cells heterologously expressing human OPN5. *Sci. Rep.* 4:5352. doi: 10.1038/srep05352

Tarttelin, E. E., Bellingham, J., Hankins, M. W., Foster, R. G., and Lucas, R. J. (2003). Neuropsin (Opn5): a novel opsin identified in mammalian neural tissue. *FEBS Lett.* 554, 410–416. doi: 10.1016/s0014-5793(03)01212-2

Tchernookova, B. K., Heer, C., Young, M., Swygart, D., Kaufman, R., Gongwer, M., et al. (2018). Activation of retinal glial (Muller) cells by extracellular ATP induces pronounced increases in extracellular H+ flux. *PLoS One* 13:e0190893. doi: 10.1371/journal.pone.0190893

Terakita, A., and Nagata, T. (2014). Functional properties of opsins and their contribution to light-sensing physiology. *Zoolog. Sci.* 31, 653–659. doi: 10.2108/zs140094

Thanos, S., and Mey, J. (2001). Development of the visual system of the chick. II. mechanisms of axonal guidance. *Brain Res. Brain Res. Rev.* 35, 205–245.

Valdez, D. J., Garbarino-Pico, E., Diaz, N. M., Silvestre, D. C., and Guido, M. E. (2012). Differential regulation of arylalkylamine N-acetyltransferase activity in chicken retinal ganglion cells by light and circadian clock. *Chronobiol. Int.* 29, 1011–1020. doi: 10.3109/07420528.2012.707160

Valdez, D. J., Nieto, P. S., Della Costa, N. S., Schurrer, C., and Guido, M. E. (2015). Circadian control of the pupillary light responses in an avian model of blindness, the GUCY1* chickens. *Invest. Ophthalmol. Vis. Sci.* 56, 730–737. doi: 10.1167/iovs.14-15481

Valdez, D. J., Nieto, P. S., Diaz, N. M., Garbarino-Pico, E., and Guido, M. E. (2013). Differential regulation of feeding rhythms through a multiple-photoreceptor system in an avian model of blindness. *FASEB J.* 27, 2702–2712. doi: 10.1096/fj.12-222885

Verra, D. M., Contin, M. A., Hicks, D., and Guido, M. E. (2011). Early onset and differential temporospatial expression of melanopsin isoforms in the developing chicken retina. *Invest. Ophthalmol. Vis. Sci.* 52, 5111–5120. doi: 10.1167/iovs.11-75301

Wagner, P. M., Sosa Alderete, L. G., Gorne, L. D., Gaveglio, V., Salvador, G., Pasquare, S., et al. (2018). Proliferative glioblastoma cancer cells exhibit persisting temporal control of metabolism and display differential temporal drug susceptibility in chemotherapy. *Mol. Neurobiol.* 56, 1276–1292. doi: 10.1007/s12035-018-1152-3

Wenzel, A., Oberhauser, V., Pugh, E. N. Jr., Lamb, T. D., Grimm, C., Samardzija, M., et al. (2005). The retinal G protein-coupled receptor (RGR) enhances isomerohydrolase activity independent of light. *J. Biol. Chem.* 280, 29874–29884. doi: 10.1074/jbc.M503603200

Yamashita, T., Ohuchi, H., Tomonari, S., Ikeda, K., Sakai, K., and Shichida, Y. (2010). Opn5 is a UV-sensitive bistable pigment that couples with Gi subtype of G protein. *Proc. Natl. Acad. Sci. U.S.A.* 107, 22084–22089. doi: 10.1073/pnas.1012498107

Yamashita, T., Ono, K., Ohuchi, H., Yumoto, A., Gotoh, H., Tomonari, S., et al. (2014). Evolution of mammalian Opn5 as a specialized UV-absorbing pigment by a single amino acid mutation. *J. Biol. Chem.* 289, 3991–4000. doi: 10.1074/jbc.M113.514075

Conflict of Interest Statement: The authors declare that the research was conducted in the absence of any commercial or financial relationships that could be construed as a potential conflict of interest.

frontiers in Cellular Neuroscience

ORIGINAL RESEARCH
published: 30 August 2019
doi: 10.3389/fncel.2019.00391

The *WWOX* Gene Influences Cellular Pathways in the Neuronal Differentiation of Human Neural Progenitor Cells

Katarzyna Kośla, Elżbieta Płuciennik, Ewa Styczeń-Binkowska, Magdalena Nowakowska, Magdalena Orzechowska and Andrzej K. Bednarek*

Department of Molecular Carcinogenesis, Medical University of Łódź, Łódź, Poland

The brain is the most functionally organized structure of all organs. It manages behavior, perception and higher cognitive functions. The *WWOX* gene is non-classical tumor suppressor gene, which has been shown to have an impact on proliferation, apoptosis and migration processes. Moreover, genetic aberrations in *WWOX* induce severe neuropathological phenotypes in humans and rodents. The aim of the present study was to investigate in detail the impact of *WWOX* on human neural progenitor cell (hNPC) maintenance and how depletion of *WWOX* disturbs signaling pathways playing a pivotal role in neuronal differentiation and central nervous system (CNS) organogenesis. hNPC with a silenced *WWOX* gene exhibited lowered mitochondrial redox potential, enhanced adhesion to fibronectin and extracellular matrix protein mixture, downregulation of MMP2/9 expression and impaired 3D growth. Global transcriptome analysis using cap analysis of gene expression (CAGE) found that *WWOX* downregulation significantly changes the expression of multiple genes engaged in cytoskeleton organization, adhesion, cell signaling and chromatin remodeling. The massive changes in gene expression caused by *WWOX* silencing may strongly affect the differentiation and migration of neurons in organogenesis, brain injury, cancerogenesis or neurodifferentiation. *WWOX* gene appears to be an important regulator of neural tissue architecture and function.

Keywords: *WWOX*, neural progenitor cells, neuronal differentiation, neurodegeneration, WOREE, SCAR, CAGE

OPEN ACCESS

Edited by:
Mario Eduardo Guido, Center for Research in Biological Chemistry Córdoba (CIQUIBIC), Argentina

Reviewed by:
Gourav Roy Choudhury, University of Pennsylvania, United States
Silvina Varónica Sonzogni, University of Buenos Aires, Argentina

****Correspondence:***
Katarzyna Kośla
katarzyna.kosla@umed.lodz.pl

Specialty section:
This article was submitted to Cellular Neuropathology, a section of the journal Frontiers in Cellular Neuroscience

Received: *15 February 2019*
Accepted: *08 August 2019*
Published: *30 August 2019*

Citation:
Kośla K, Płuciennik E, Styczeń-Binkowska E, Nowakowska M, Orzechowska M and Bednarek AK (2019) The WWOX Gene Influences Cellular Pathways in the Neuronal Differentiation of Human Neural Progenitor Cells. Front. Cell. Neurosci. 13:391. doi: 10.3389/fncel.2019.00391

INTRODUCTION

The *WWOX* gene is an important transcription regulator. It is known to regulate the activity of a number of transcription factors, including Jun, AP2gamma, NFkappaB, ErbB4 (Aqeilan et al., 2004a, 2005; Gaudio et al., 2006; Chen et al., 2013). It has been found to have tumor suppressor activity, and recent studies have investigated its potential new physiological roles in DNA repair and glucose metabolism (Aqeilan et al., 2005; Abu-Remaileh and Aqeilan, 2014; Iatan et al., 2014). In addition to steroid-hormone regulated tissues like those in the testis, ovary and breast, the *WWOX* gene also shows high expression in the brain and cerebellum (Nunez et al., 2006). Loss of correct *WWOX* expression is a common event associated with cancer promotion, progression and resistance to treatment (Płuciennik et al., 2006, 2014; Dias et al., 2007; Donati et al., 2007; Wang et al., 2011; Lan et al., 2012; Sun et al., 2017; Seabra et al., 2018). Unlike classic suppressor genes, the loss of functionality of only one *WWOX* allele is sufficient to increase the chance of cancerogenesis (haploinsufficiency).

WWOX has also been found to play a significant role in glioblastoma (GBM), the most malignant brain tumor. It has been shown that loss of heterozygosity, a relatively frequent occurrence in GBM, along with promoter methylation may decrease the expression of the *WWOX* gene. Our experiment also revealed a correlation between the expression of *WWOX* and that of *Bcl2*, *Ki67*, and *ErbB4* in this type of cancer (Kosla et al., 2011). Further investigations have found *WWOX* expression to modulate the global profile of gene expression in the GBM T98G cell line, and increased *WWOX* expression makes its phenotype less malignant. Cells with ectopically expressed *WWOX* demonstrate significantly different transcription profiles among almost 3000 genes, with WNT, TGFβ, Notch and Hedgehog being the main cellular pathways affected; all of these are involved both in GBM carcinogenesis and neural differentiation. Moreover, the *WWOX*-transfected GBM cells presented greatly altered biological characteristics, lowered proliferation, adhesion and impaired 3D growth (Kośla et al., 2014).

Recent evidence suggests that *WWOX* may play a regulatory role in central nervous system (CNS) development and functioning (Chen et al., 2004; Lo et al., 2008; Suzuki et al., 2009; Tabarki et al., 2015a; Liu et al., 2018; Shaukat et al., 2018; Hussain et al., 2019). Complete loss of WWOX protein function in knock-out mice results in epilepsy and balance disturbances. The animals show progressive susceptibility to spontaneous and audiogenic tonic-clonic epilepsy, which is indicative of a neurodegenerative process (Mallaret et al., 2014). Suzuki et al. (2009) report the presence of a spontaneous homozygous 13-bp deletion in exon 9 of the *WWOX* gene that has also been found in *Ide/Ide* rats. This deletion results in a frameshift in the C-terminus of the WWOX protein and may influence protein stability, since WWOX protein was undetectable in the hippocampus of the *Ide/Ide* rats. In addition to various abnormalities, such as dwarfism, postnatal lethality and male hypogonadism, the animals also display a high incidence of epilepsy, ataxic gait, audiogenic seizures and many vacuoles in the hippocampus and amygdala, indicating the progression of neurodegeneration (Suzuki et al., 2009). There is a strong overlap between the symptoms present in KO *WWOX* rodent models and those observed in humans. The genetic aberrations in the *WWOX* locus has been linked with two human neuropathological phenotypes: Spinocerebellar ataxia, autosomal recessive 12 (SCAR12, MIM 614322) and WWOX-Related Epileptic Encephalopathy/Early Infantile Epileptic Encephalopathy 28 (WOREE/EIEE28, MIM 616211). All known patients suffering from SCAR12 carry a homozygous missense mutation in *WWOX* coding region (139C > A or 1114G > C) that causes a partial loss of gene function, with the resulting substitutions placed in the WW1 protein–protein interaction domain and in the SDR (short-chain dehydrogenase/reductase) domain, respectively. These mutations affect the ability of the protein to bind to its cellular partners and may reduce its catalytic activity. The WOREE patients exhibiting more severe neurological disorders harbor nonsense/frameshift mutations and/or robust deletions of whole exons of *WWOX* gene (Mignot et al., 2015; Tabarki et al., 2015b; Elsaadany et al., 2016; Piard et al., 2018).

Overall, reports describing neural aberrations connected with disruption of *WWOX locus* in humans and animals indicate that germline loss-of-function of *WWOX* leads to serious developmental deficiency in the neural system.

The *WWOX* gene was found to be also involved in neurodegenerative Alzheimer's disease. The level of WWOX protein is much lower in the hippocampal neurons of those suffering from Alzheimer's disease in comparison to healthy individuals (Sze et al., 2004; Teng et al., 2012). Moreover, *in vitro* studies of *WWOX* silencing in neuronal cells have resulted in spontaneous Tau phosphorylation and accumulation of neurofibrillary tangles (NFTs). It has been confirmed that WWOX interacts with GSK3β, ERK and other kinases inhibiting the phosphorylation of Tau and preventing NFTs formation and cell death. The role of WWOX as a Tau phosphorylation regulator is important not only in the context of neurodegeneration, but also neuronal differentiation, where the Tau protein takes part in microtubule assembly and neurite outgrowth. The level of *WWOX* expression was shown to decrease with age and is significantly lower in middle-aged individuals (Sze et al., 2004; Wang et al., 2012).

To date, WWOX has been experimentally shown to act as a regulator of several transcription factors, including p73 (considered as one of the main regulators of CNS organogenesis), ErbB4, Met, c-Jun, Gli1, and AP-2 (Aqeilan et al., 2004a,b, 2005; Gaudio et al., 2006; Matteucci et al., 2009; Xiong et al., 2014). The shared mechanism of regulation is based on partner protein sequestration in the cytoplasm. Upon binding to WWOX, the locked transcription factors are unable to translocate to the nucleus and activate their target genes. A set of 240 proteins thought to be able to bind with WWOX has been given by Abu-Odeh et al. (2014). An analysis of potential WWOX partners shows that the protein can affect pathways critical for neuronal differentiation, such as Notch, Hippo, Wnt, and TGFβ, which are also disturbed in the course of brain cancer.

So far, the molecular mechanism by which WWOX regulates nerve cell functioning is largely unknown. It has been suggested that *WWOX* may influence the CNS by regulating the proteins taking part in neuronal differentiation, through negative regulation of GSK3β, and apoptosis, probably via the mitochondrial pathway by downregulating apoptotic inhibitors Bcl2 and Bcl-xL. WWOX has also been shown to influence the action of such neural pathways as Wnt (Dvl-2), TGFβ (TIAF1, SMAD3, and SMAD7), Hedgehog (Gli1) by interacting with their constituent proteins (Bouteille et al., 2009; Ferguson et al., 2013; Xiong et al., 2014; Chiang et al., 2015; Hsu et al., 2016). A recent study on WWOX KO mice by Hussain et al. (2019) found that lack of the protein leads to a reduction of GABA-ergic hippocampal neurons and a lowered level of GABA synthesis.

The described neuropathological phenotypes arising from genetic aberrations of the *WWOX* locus demonstrates the importance of the gene in CNS development and functioning. Although *WWOX* mutations found in SCAR12 or WOREE are very rare, possibly because of intrauteral lethality, changes in its expression are very common in pathological states like Alzheimer's disease or GBM.

The development of the CNS is a highly organized process consisting of neurogenesis, neuron migration, synaptogenesis and gliogenesis, which is controlled at multiple levels. It is likely that the WWOX protein is involved in at least some of these steps. Briefly, the process of cytoskeleton reorganization requires a complex configuration of intrinsic and extrinsic cues involving the action of membrane and ECM proteins, which triggers specific signaling pathways. Its details are still poorly understood and await further investigation. Our findings indicate that the silencing of WWOX in human neural progenitors results in significant changes in the regulation of genes encoding membrane/ECM, cell signaling, chromatin condensation and cytoskeleton proteins.

The study examines which specific genes and cellular pathways are influenced by WWOX in human neural progenitor cells (hNPC) and how *WWOX* affects their biological properties and differentiation. *WWOX* expression was silenced in the hNPC line, and the cells were tested for their ECM adhesion ability, mitochondrial potential and 3D growth; in addition, a global gene expression analysis was conducted with next generation sequencing (NGS).

MATERIALS AND METHODS

Cell Line and Culture Conditions

The human neural stem cells (hNSC, Thermo Fisher Scientific) are derived from H9 embryonic stem cells (hESC). According to manufacturer description they have the potential to differentiate into neurons, astrocytes and oligodendrocytes. The cells were cultured as an adherent culture in vessels coated with ECM protein mixture (Geltrex, Thermo Fisher Scientific). The cells were maintained in KnockOut^{TM} DMEM/F-12 Medium supplemented with 20 ng/ml EGF, FGFb, StemPro Neural Supplement (Thermo Fisher Scientific) and Antibiotic-Antimycotic (Gibco) and handled according to the supplier recommendations.

Spontaneous differentiation of the cells was triggered by culturing in medium without the addition of EGF and FGFb growth factors for 14 days. Although the supplier claims that the cells are able to differentiate into neurons, astrocytes and oligodendrocytes upon growth factor removal, in our conditions all the cells were found to undergo differentiation into neurons, which was confirmed by immunocytochemistry. All differentiated cells were found to be positive for neuronal markers MAP2 and TUJ1 and negative for astrocytes – GFAP or oligodendrocytes – GalC markers (**Supplementary Figure S2**). This suggests that the cells lose their multipotence and instead of being neural stem cells are rather a neural progenitors (hNPC) and were regarded in this study as such.

The 2D differentiation assays were conducted on Geltrex coated vessels, and neuron maturity was assessed by immunocytochemistry with antibodies against neuronal marker MAP2. For a 3D culture assay, 16,000, 25,000, and 35,000 cells were seeded on a solidified 2 mm layer of growth factor-reduced Geltrex basement membrane matrix (Thermo Fisher Scientific).

In every conducted experiment the cells from both experimental variants were in the same, low passage number.

WWOX Gene Silencing

The *WWOX* gene was silenced by a shRNA lentiviral delivery system (Santa Cruz Biotechnology). The control cells were transduced with the same type of vector harboring scrambled shRNA sequence instead of targeting investigated gene. Target cells were seeded at a density of 5×10^4 cells/cm^2, and the next day, were infected with the virus suspension in culturing medium supplemented with polybrene 5 μg/ml (Sigma-Aldrich). After 24 h, the transduction mixture was removed and replaced with regular medium. The stable transductants were selected with 0.4 μg/ml puromycin. The gene silencing efficiency was assessed with Western blot.

Western Blot

The cellular proteins were extracted with RIPA buffer supplemented with protease inhibitor cocktail, PMSF and Na-orthovanadate (Santa Cruz Biotechnology). Briefly, 60 μg of protein was resolved on SDS-PAGE and transferred to PVDF membrane. After blocking in 5% non-fat milk, membranes were incubated overnight in 4°C with a primary antibody, anti-WWOX (Thermo Fisher Scientific). After 1-h incubation with a suitable secondary antibody conjugated with alkaline phosphatase (Sigma-Aldrich), the membranes were developed with Novex AP Chromogenic Substrate (Thermo Fisher Scientific). The ImageJ software was used for densitometric analysis of protein amount, adjusted to GAPDH as a reference protein.

Immunocytochemistry

The cells were fixed with ice cold ethanol:acetic acid (95:5) solution for 10 min. After a double wash with DPBS, unspecific antibody binding was blocked with blocking buffer (2% BSA, 1% donkey serum, and 0.1% Triton-X100). Next step was incubation with the primary antibodies (Millipore, Thermo Fisher Scientific) 1:200 solution in 5% donkey serum, 4°C, overnight. After double washing with DPBS, the cells were incubated with secondary antibodies (donkey, Alexa Fluor 488/594 conjugated), diluted 1:1000. The nuclei were counterstained with DAPI and the cells were imagined with FLoid Cell Imaging System (Thermo Fisher Scientific).

Adhesion Assays

The cells were seeded on 96-well plate coated with Geltrex (Gibco) at a density of 17,500 cells/well. The adhesion to fibronectin was assessed on 48-well fibronectin-coated plate (BD). The cells were seeded at a density of 100,000 cells/well. The cells were incubated for 90 min at 37°C. Next the cells were washed with PBS and adherent cells were stained with Cell Stain Solution (Cell Biolabs, Inc.). The stain was dissolved in Extraction Solution (Cell Biolabs, Inc.) and the absorbance was read with a plate reader (BioTek), $\lambda = 570$ nm.

Zymography

The level of metalloproteinase 2 and 9 was examined by gelatin zymography. The cells were cultured on a six-well plate for 48 h and the culture medium was collected for protein analysis. Protein concentration was measured with a Qubit Protein Assay with Qubit 2.0 fluorometer (Thermo Fisher Scientific). A total of 2 μg protein extracts was loaded and separated on 10% SDS-PAGE gel prepared with addition of 2 mg/ml gelatin. The gel was washed with Triton X-100 and incubated in a developing buffer (0.5 M Tris–HCl, 2 M NaCl, 50 mM CaCl 2, pH 7.5) at 37°C for 18 h. Next, it was stained with Coomassie Brilliant Blue R-250 and incubated in destaining buffer (methanol: acetic acid: water, 3:1:6) to visualize white bands on a blue background where gelatinolytic metalloproteinases were active. The active or inactive form of MMP2 and 9 was identified according to protein marker separated on the same gel. The amount of the proteins was assessed with ImageJ software, based on the area of the clear band.

Redox Assay

The mitochondrial metabolic activity was measured using PrestoBlue reagent (resazurin based, Thermo Fisher Scientific). Cells were seeded on 96-well white, clear-bottom 96-well plate at a density of 20,000 cells/well. PrestoBlue was added to fresh medium 18 h post seeding and the cells were incubated in 37°C. The fluorescence of resorufin obtained by reduction of resazurin in mitochondria was measured in intervals for 5 h with Victor X4 plate reader (PerkinElmer), excitation $\lambda = 550$ nm.

Statistical Analysis of Biological Assays

The results of the adhesion, mitochondrial redox potential and zymography procedures are presented as means. The normality of data distribution was verified with Shapiro–Wilk Normality Test and the statistical relevance was evaluated with unpaired *t*-test. The results are described as significant when $p < 0.05$.

CAGE Gene Expression Analysis

The gene expression profile of 2D cultured undifferentiated and differentiated cells were analyzed with cap analysis of gene expression (CAGE) technique.

The libraries for sequencing were prepared according to Carnici, described in detail elsewhere (Takahashi et al., 2012). Briefly, polyadenylated and non-polyadenylated RNA was reverse transcribed into cDNA with the use of a random prime-containing *Eco*P15I sequence. The next step was biotinylation of the cap site and the 3′ ends of the hybridized RNAs. Non-hybridized ssRNAs were digested and the 5′ complete cDNAs hybridized to biotin-tagged, cap-containing RNAs were separated on streptavidin-coated magnetic beads. cDNA was released from RNA and a double-stranded 5′ linker with a barcode and *Eco*P15I sequences was ligated. Subsequently, using the biotinylated 2nd SOL primer, a second strand cDNA was synthetized. The digestion with *Eco*P15I allowed 27 bp fragments to be cleaved inside the 5′ end of the cDNA. At the 3′ end of the cDNA, a 3′ linker with 3′ Illumina primer sequence was ligated. Following this, the constructed CAGE tags were amplified and purified. The prepared libraries were sequenced on an Illumina HiSeq System. The data was then analyzed in-house. The raw data from CAGE experiment are deposited in NCBI Gene Expression Omnibus (GEO) Database with accession number GSE126075.

Data Processing

The obtained CAGE data was processed by the MOIRAI system (Hasegawa et al., 2014), a GUI-based workflow system allowing quality control and further data transformation into multiple file formats for subsequent expression analyses. Briefly, raw input was split by barcode, following which, sequences of low quality (with base N) were removed and processed via BWA to output BAM files. Primarily, the GRCh37/hg19 assembly was used as a reference human genome; however, the data was reprocessed through UCSC liftOver tool (Kuhn et al., 2013) to convert the genomic coordinates of CAGE peaks into current GRCh38/hg38 assembly and make the data meaningful for the recent genome version. Subsequently, CAGE output was analyzed with CAGEr (Haberle et al., 2015), a Bioconductor package enabling preprocessing, identification and normalization of transcription start sites (TSS) and downstream analysis of the promoterome based upon CAGE sequencing with the BSgenome.Hsapiens.UCSC.hg38 package as a referent genome (Pagés, 2018). Analysis was performed according to Haberle and Plessy[1]. In brief, raw CAGE tag counts were normalized with simple TPM method, TSS were clustered into tag clusters corresponding to individual promoters using paraclu clustering algorithm and mapped to known promoters using CAGE peaks identified as true TSS by TSS classifier available at FANTOM5 repository (Lizio et al., 2015) (GRCh38/hg38 assembly).

Global Biological Differentiation – Gene Set Enrichment Analysis

Global differences between hNPC with silenced *WWOX* expression and controls before and after differentiation were determined in terms of gene ontology (GO), such as biological processes (BP), by applying the gene set enrichment analysis (GSEA) algorithm. Enrichment analysis was performed for 9427 genes between shWWOX and shScrambled, classified as phenotype labels separately for hNPC and neurons through *t*-test with a weighted scoring scheme and a permutation type regarding phenotype. Significance threshold was set as FDR < 0.25.

Protein–Protein Interaction Analysis

The interaction relationships of the proteins encoded by the differentially expressed genes were searched and visualized with the Search Tool for the Retrieval of Interacting Genes (STRING) Plug-in (version 1.4.0)[2] in Cytoscape software (version 3.6.1)[3]. All the parameters were set as default values, and the confidence (combined score) ≥ 0.4 was used as the cut off criterion.

[1]http://bioconductor.org/packages/release/bioc/vignettes/CAGEr/inst/doc/CAGEexp.html

[2]http://www.string-db.org

[3]http://www.cytoscape.org

Principle Component Analysis

Dimensional grouping investigating hNPC phenotypes according to a set of selected genes was performed using principle component analysis (PCA). The analysis involved 362 genes of several oxidative stress response/antioxidant defense/oxygen species activity connected groups form The Molecular Signatures Database (MSigDB)[4], a collection of annotated gene sets. The PCA was conducted to determine the contribution of particular genes into partitioning of cell genotype across first and second dimensions (dim1 and dim2) with the oxidative gene set as an active variable. All analyses were performed using FactoMineR and Factoextra R packages.

RESULTS

An analysis of NGS data deposited in the RIKEN Fantom5 Project data repository[5] indicates that the level of *WWOX* expression in the human brain varies according to location (**Figure 1**). The highest levels are observed in the corpus callosum and medulla oblongata, and the lowest in the postcentral and paracentral gyrus. Moreover, adults display greater *WWOX* expression in the brain as a whole than 20–33 weeks fetuses, 17.7 TPM RLE (tags per million, relative log expression) vs. 9.2 TPM RLE.

In the present study, the hNPC cells were transduced with lentiviral shRNA vector. After confirmation of *WWOX* gene silencing by Western blot (**Supplementary Figure S1**) the hNPC/shWWOX cells and control hNPC/shScrambled were cultured either as a 2D monolayer culture using plates coated with a thin layer of diluted Geltrex or as a 3D culture in a thick (2–3 mm) Geltrex scaffold. Next, the cells were used in a number of biological experiments, and global analysis of transcriptome was performed using CAGE.

[4]http://software.broadinstitute.org/gsea/msigdb/index.jsp

[5]http://fantom.gsc.riken.jp/

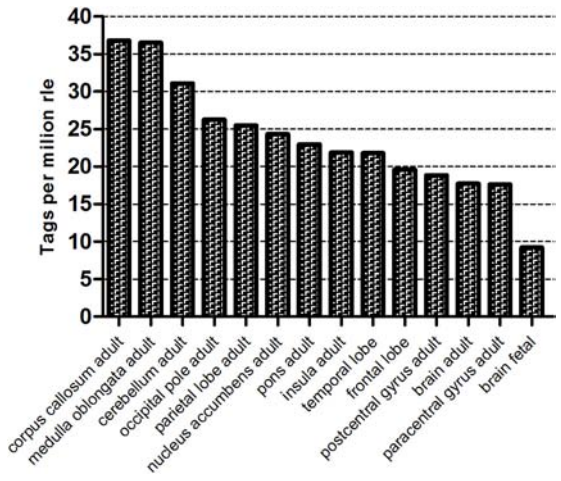

FIGURE 1 | The *WWOX* gene expression level in different human brain compartment (Fantom 5, Zenbu, Riken). The counts were normalized as TPM (tags per million) after scaling by normalization factors calculated by RLE (relative log expression) method.

WWOX Depletion Alters the Main Biological Functions of hNPC

A number of biological differences were observed between the hNPC cells with silenced *WWOX* and controls.

WWOX silencing reduced the mitochondrial redox activity of the cells (**Figure 2**) and strongly affected their adhesion to ECM proteins. The hNPC cells with silenced *WWOX* demonstrated considerably stronger adhesion to the ECM protein mixture ($p = 0.0626$) and to fibronectin alone ($p < 0.05$) (**Figure 3**).

It was also found that downregulation of *WWOX* lowered pro-MMP2 and pro-MMP9 metalloproteinase secretion (**Figure 4**).

Most striking was that in 3D culture, the hNPC with silenced *WWOX* remained as isolated, single cells that did not proliferate nor differentiate, while cells with unaltered *WWOX* expression differentiated and exhibited extensive network formation (**Figures 5**, **6**). This observation was confirmed in three separate experiments and was not influenced by the seeding density (data not shown). No such phenomenon was observed when the cells were cultured in 2D as a monolayer (**Figure 7**).

Functional Enrichment Analysis

The global gene expression was assessed in the hNPC with the silenced *WWOX* expression and the control group before and after differentiation by CAGE. Whole transcriptome sequencing revealed global changes in the regulation of a number of pivotal cellular pathways and functions. It was found that 2282 genes were differentially expressed between hNPC/shScrambled and hNPC/sh*WWOX* (log2 FC $> \pm 1$, $p < 0.05$) and 7392 differed between differentiated neurons/shScrambled and neurons/sh*WWOX*. To identify global biological changes between cells with different *WWOX* status, enrichment analysis was performed within GO BP using a GSEA algorithm. The top five most altered BP classified according to GO terms are presented in **Table 1** and includes adhesion, neural migration and differentiation. Significantly greater numbers of enriched gene sets was found for undifferentiated cells (44 for hNPC/shScrambled and 109 for hNPC/sh*WWOX*, FDR < 0.25) than for differentiated neurons (no gene sets for neurons/shScrambled and four sets in neurons/sh*WWOX*). The

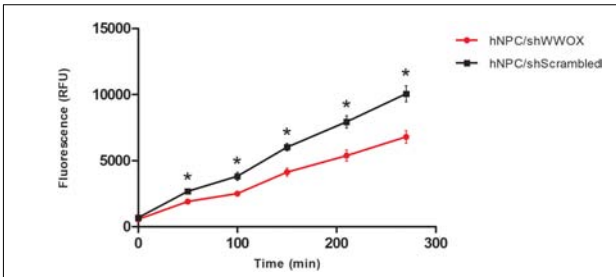

FIGURE 2 | Mitochondrial redox activity tested by PrestoBlue®assay based on colorimetric measurement of resofurin, $*p < 0.05$.

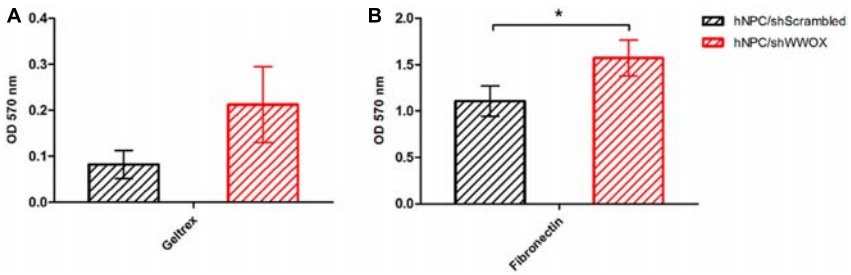

FIGURE 3 | Adhesion of *WWOX* silenced hNPC cells to ECM protein mixture (Geltrex, **A**), the tendency not reaching the statistical significance (0.0626) and to fibronectin **(B)**, $*p < 0.05$.

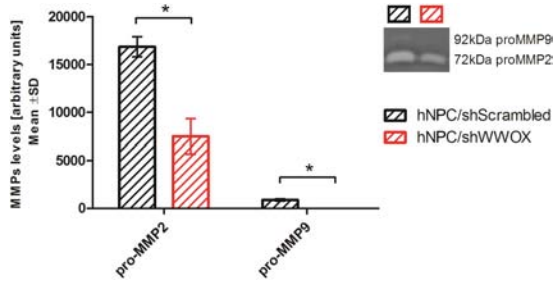

FIGURE 4 | Gelatin zymography analysis showing the level of pro-MMP2 (72 kDa) and pro-MMP9 (92 kDa) secreted by control and WWOX-silenced hNPC, $*p < 0.05$.

detailed results are available as **Supplementary Tables S2, S3**. Enrichment plots for selected gene sets are given in **Figure 8**.

The GSEA showed that *WWOX* silencing causes substantial gene expression reorganization. We found dualistic enrichment of GO_Stem_Cell_Differentiation gene set in both phenotypes (**Figure 8B**). In the hNPC/shScrambled the leading edge subset (considered as the most upregulated and promising genes) included LOXL3, JAG1, SOX21, ERBB4, KITLG, GPM6A, EFNB1, FGF10, NRG1, WWTR1, RUNX2, LAMA5, MSI2, SEMA4D, BCHE, FOXC1, SMAD4, SEMA5A, SEMA5B, SEMA6C, SEMA3A, SEMA6A, SEMA3C, GSK3B, BMP7, SFRP1, SEMA4F, and SEMA4B, whereas the hNPC/sh*WWOX* leading edge subset included HHEX, FGFR2, GBX2, SNAI1, GREM1, MSX2, and MSX1.

Protein–Protein Interaction Network Analysis

Based on information from the STRING database, the protein–protein global interaction network was constructed with Log2 fold change of differentially expressed genes belonging to gene sets related to membrane proteins, cytoskeleton and cell signaling. The selected genes encode proteins that play an important role in the steps of CNS development –

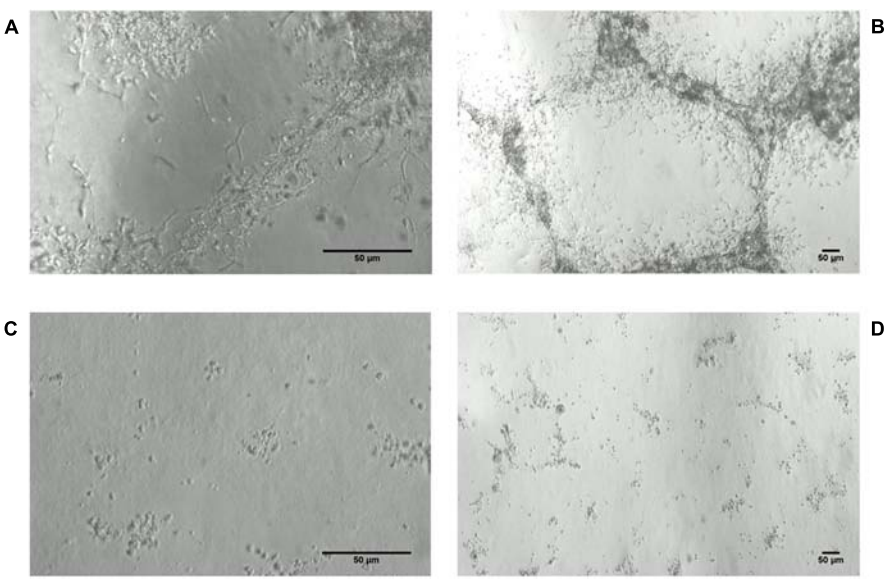

FIGURE 5 | hNPC cells cultured for 8 days in thick 3D Geltrex (ECM protein mixture) layer. **(A,B)** hNPC/shScrambled, 200× and 40×, respectively. **(C,D)** hNPC/shWWOX, 200× and 40×, respectively.

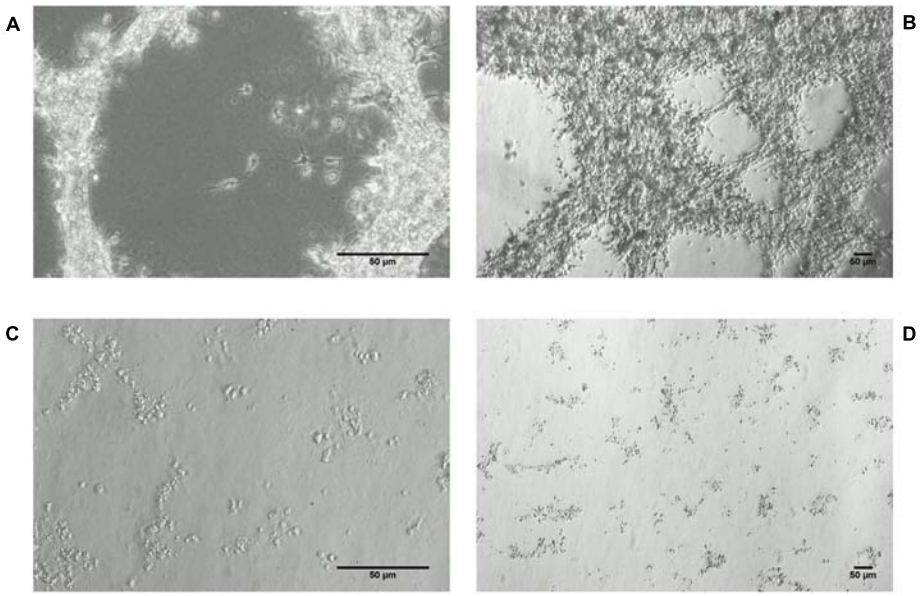

FIGURE 6 | hNPC cells cultured for 19 days in thick 3D Geltrex (ECM protein mixture) layer. **(A,B)** hNPC/shScrambled, 200× and 40×, respectively. **(C,D)** hNPC/shWWOX, 200× and 40×, respectively.

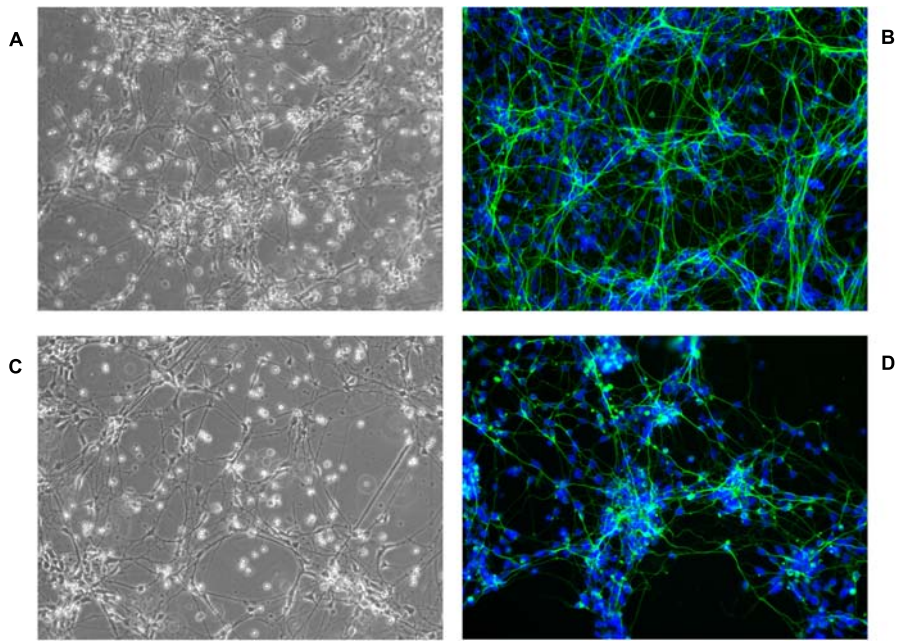

FIGURE 7 | hNPC cells cultured for 18 days in 2D ECM protein mixture coated vessels, 200×. **(A,B)** hNPC/shScrambled, **(C,D)** hNPC/shWWOX, green MAP2 neuronal marker, blue DAPI nucleus counterstain.

neurogenesis, neuron migration, and synaptogenesis. The constructed network comprised of 198 nodes and 1113 edges (**Figure 9**; for details see **Supplementary Figure S3**). **Figure 10** presents protein–protein interaction networks of genes which are differentially expressed between undifferentiated hNPC (A) and differentiated neurons (B). In hNPC, the most significantly upregulated genes (Log2 fold change $> \pm 1$, $p < 0.05$) are associated with signaling and chromatin remodeling.

Principle Component Analysis

Principle component analysis employing the oxidative gene set served to identify genes of the highest contribution to spatial partitioning of the genotypes and selection of

TABLE 1 | Top gene sets enriched in hNPC with native *WWOX* expression level.

Gene set name	Gene number	Enrichment score
GO_neural_crest_cell_differentiation	33	0.622
GO_neural_crest_cell_migration	21	0.677
GO_homophilic_cell_adhesion_via_plasma_membrane_adhesion_molecules	53	0.511
GO_cell_cell_adhesion_via_plasma_membrane_adhesion_molecules	69	0.428
GO_negative_regulation_of_axon_extension	21	0.578

FDR q-value < 0.25.

genes differentiating hNPC/shScrambled, hNPC/shWWOX, neurons/shScrambled and neurons/shWWOX in the most significant manner. As expected, we obviously found clear partitioning of hNPC and neuronal genotypes across the first dimension with a total variance of 77.7%. However, we also observed a clear partitioning across the dim2 with a total variance of 14.6%. The dim2 differentiates shScrambled and shWWOX variants indicating changes in oxidation-related genes induced by *WWOX* depletion (**Figure 11**). PCA analysis showed that among oxidative catabolism and oxidative stress genes that expression differentiates between *WWOX* expressing and *WWOX* depleted hNPC as well as neurons are those important for energy and redox metabolism. Examples of genes mostly involved in such differentiation are: Hexokinase 2 (HK2), Pyruvate Dehydrogenase Kinase 1 (PDK1), Lactate Dehydrogenase A (LDHA), Ferredoxin Reductase (FDXA), Cytochrome C (CYCS), Superoxide Dismutase 1 and 2 (SOD1 and SOD2), and Peroxiredoxin 2 (PRDX2), see **Supplementary Table S1** for all involved genes.

DISCUSSION

The *WWOX* tumor suppressor gene has been recently recognized as a global modulator of transcription and an important regulator of brain differentiation and maintenance. Aberrations in *WWOX* expression lead to severe developmental neuropathologies as well as metabolic insufficiency and premature death (Shaukat et al., 2018). Public data from the Fantom 5 Project of the Riken Database (Robinson et al., 2010; Lizio et al., 2015) indicate that in human brain, *WWOX* expression is strongly dependent on the brain compartment as well as the age of the organism. In our study, we aimed to clarify the molecular basis of *WWOX* actions in neural tissue by analyzing the changes in phenotype and gene expression in hNPC with silenced *WWOX*.

The process of brain development is highly organized and its precise orchestration is vital to ensure the perfect construction of such a complex organ. Neurons and glial cells must be created in accurate numbers, locations and timing. The differentiation of neural stem cells into neurons, as well as the maintenance of the pool of undifferentiated neural progenitors, is governed by intra and extracellular signaling and involves mainly Notch, Wnt, and Hedgehog signaling pathways (Jiang and Nardelli, 2016). Our analysis of the functional networks of the differentially expressed genes revealed that *WWOX* expression in hNPC is associated with transcription regulation of genes of neural differentiation that take part in such pathways as Notch, PI3K kinase, PDGF, Cadherin, Hedgehog, and Endothelin signaling pathway.

The migration of the newborn neurons to their destination sites requires several major changes in cell polarity and motility. Young neurons leaving the SVZ exhibit multipolarity, and those on their way to target site typically display a bipolar morphology (Marín et al., 2006). This elaborate process is guided by intricate intra and extracellular signals. The pivotal role in migration is played by cytoskeleton components such as actin filaments and microtubules, as well as motor proteins like dyneins and kinesins, which undergo strictly controlled rearrangements to facilitate directional movement (Jiang and Nardelli, 2016). We showed that *WWOX* silencing in neural progenitor cells significantly changed expression of a large set of genes connected to cytoskeleton organization, e.g., MAP2/4/6, DCLK, NEFM, and NEFL that are engaged in microtubule and neurofilament assembly. Spalice et al. (2009) showed that impairment in the function of cytoskeletal genes, such as those associated with tubulins, causes severe disturbances in gyrification and lissencephaly, i.e., lack of brain folds and grooves (Liu, 2011). This emphasize the importance of migration process in cortex development.

During synaptogenesis the targets identification by the protruding ends of the outgrowing axons is mediated by cell adhesion molecules, e.g., NCAMs, N-cadherin and integrins, as well as extracellular matrix proteins (Dickson, 2002). Repulsive or attractive cues triggers signalization leading to reorganization of cytoskeleton facilitating directional movement. A number of cell-adhesion proteins is also involved in pre- and postsynaptic specialization (Li and Sheng, 2003). In our study, the lack of *WWOX* expression resulted in significant changes in cellular adhesion to ECM proteins. The hNPC/sh*WWOX* cells demonstrated increased ability to adhere to fibronectin ($p < 0.05$) and to the ECM protein mixture ($p = 0.0626$). Previous studies conducted on various cancer cell lines also identified a negative correlation between *WWOX* expression level and adherence ability (Zhang et al., 2009; Paige et al., 2010; Kośla et al., 2014). Our data indicates that WWOX is an important regulator of the tissue architecture. The changes in *WWOX* expression influence the levels of a number of pivotal adherence proteins, e.g., CDH2 (expression doubled in hNPC/shScrambled in compare to hNPC/sh*WWOX*) and ITGβ1 (expression lowered twice in hNPC/shScrambled in compare to hNPC/sh*WWOX*). The amount of secreted metalloproteinases (pro-MMP2 and pro-MMP9) was also significantly lowered in *WWOX* depleted cells. Metalloproteinases play a major role in the process of migration for neural progenitor cells and neural crest cells (Wang et al., 2006; Monsonego-Ornan et al., 2012). The interaction between ECM proteins and neural stem/progenitor cells is essential for the process of neurodifferentiation and functional maturation (Li et al., 2014). In addition to differentiation, the biochemical and biomechanical interaction with the extracellular microenvironment is also crucial for neural cell migration during the development of the nervous system, as well as in the case of brain injury (Joo et al., 2015). The precise nature of the effect of

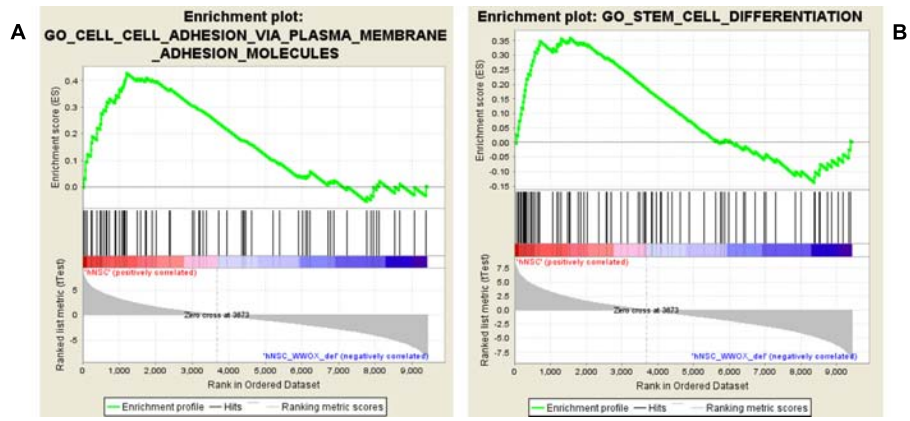

FIGURE 8 | GSEA enrichment plots presenting adhesion **(A)** and differentiation **(B)** gene sets enriched in hNPC cells.

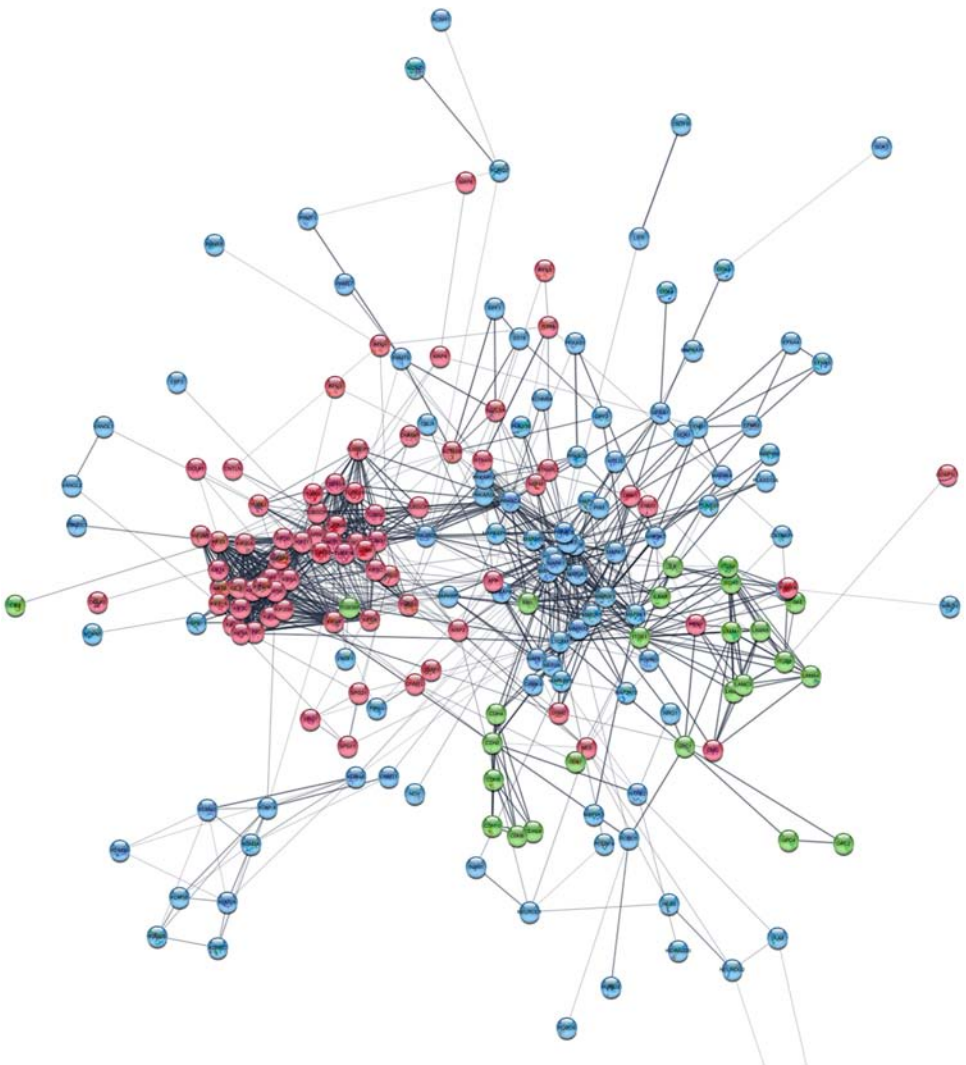

FIGURE 9 | Protein–protein interaction network of differentially expressed genes involved in neuron migration. Cytoskeleton and ER are red; membrane and ECM proteins are green; cell signaling and chromatin remodeling are blue. High resolution figure with legible gene names available in **Supplementary Figure S3**.

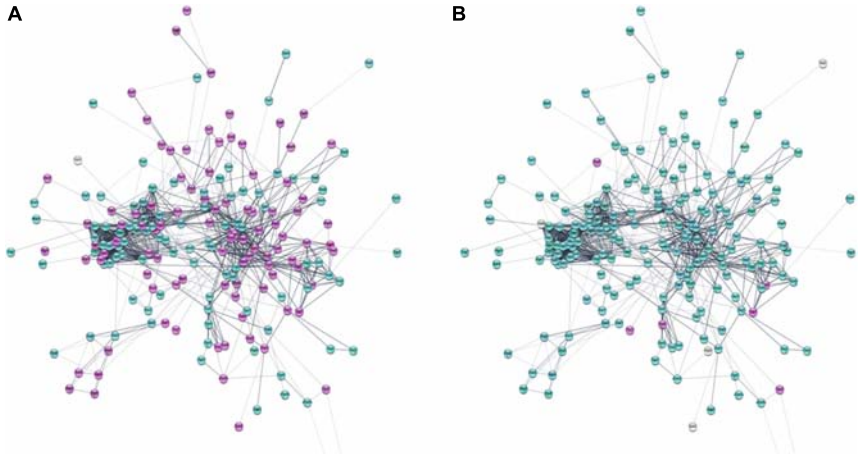

FIGURE 10 | Protein–protein interaction network of differentially expressed genes involved in neuron migration. **(A)** Log2 fold change of gene expression in hNPC/shWWOX vs. hNPC/shScrambled. **(B)** Log2 fold change of gene expression in neurons/shWWOX vs. neurons/shScrambled. Significantly upregulated genes are magenta; significantly downregulated genes are turquoise (Log2 fold change $> \pm 1$, $p < 0.05$). High resolution figure with legible gene names available in **Supplementary Figures S4, S5**.

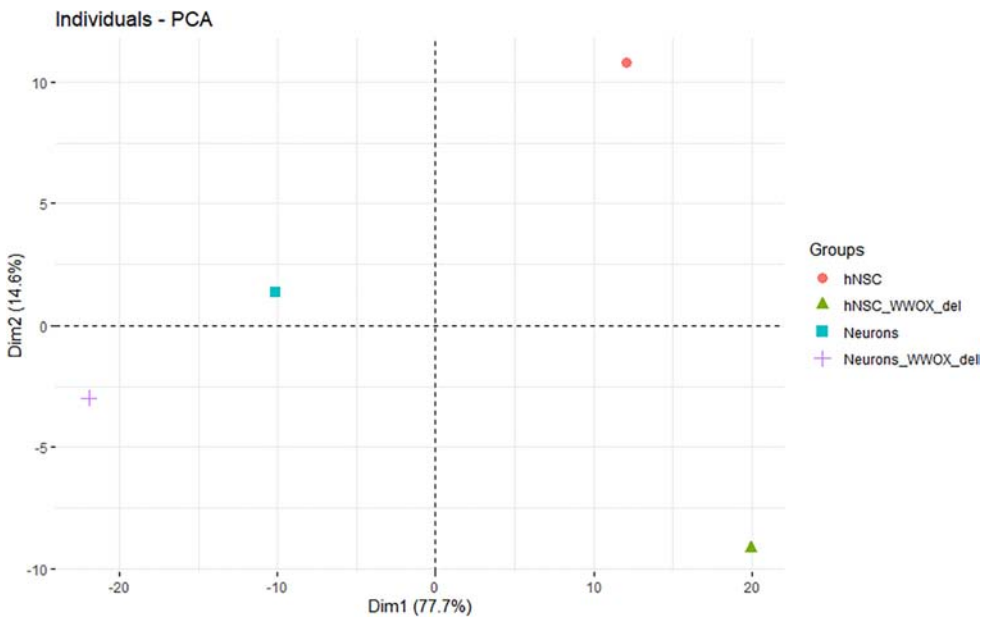

FIGURE 11 | The principle component analysis employing the gene set of oxidative gene set for identification of genes of the highest contribution to spatial partitioning of the genotypes and selection of genes differentiating hNPC/shScrambled, hNPC/shWWOX, neurons/shScrambled and neurons/shWWOX in the most significant manner. The partitioning of hNPC and neuron genotypes across the first dimension. The partitioning of shScrambled control and shWWOX genotypes across the second dimension.

WWOX on cell adhesion to ECM proteins remain unclear, but aberrations in WWOX protein level or functionality may disturb this physiologically relevant interactions.

The other main change observed in hNPC phenotype concerned mitochondrial redox potential. A number of papers have presented data suggesting that WWOX is capable of modulating cell metabolism (O'Keefe et al., 2011; Dayan et al., 2013; Abu-Remaileh et al., 2014; Choo et al., 2015). In the presented study, hNPC with silenced *WWOX* exhibit significantly lowered mitochondrial redox potential. Reactive oxygen species levels and mitochondrial metabolic state strongly contribute to neurogenesis and neuron maturation. The balance in this processes is critical for maintaining cellular homeostasis and accurate source, timing and localization of ROS synthesis is crucial for neuron physiology (Beckervordersandforth, 2017; Wilson et al., 2018). In our study, the transcriptome of investigated cells was analyzed to look for a confirmation of the observed decrease of the redox potential in *WWOX* depleted

hNPC. A PCA with an oxidative stress response/antioxidant defense gene set was employed. The analysis clearly shows that in the terms of the resultant effect of the considered genes' expression, the control and *WWOX*-depleted genotypes are completely different (**Figure 11**). This is true both for undifferentiated hNPC and differentiated neurons. Amongst the genes with the highest contribution to differentiation between *WWOX* high/low variants are several important players participating in basic metabolism and reactive oxygen species control (**Supplementary Table S1**). Therefore, we conclude that *WWOX* might have considerable impact on neurons through modulation of oxygen metabolism and mitochondria functioning.

The specific mechanisms that underlie the individual stages of brain development process are far from being understood. Even so, our findings suggest that the WWOX protein might be an important regulator of neuronal migration and synaptogenesis. Its expression downregulation is significantly associated with changes in the level of expression of the genes involved in cell motility and adhesion, regulation of chromatin condensation and global cell signaling. The gene expression alternations identified in the CAGE analysis are consistent with phenotypical changes including cell adhesion, motility and ability for 3D growth.

The most striking observation in hNPC phenotype was noted when the cells were cultured in a three dimensional scaffold formed of ECM protein mixture. Under these conditions, the hNPC/sh*WWOX* cells lost their potential for 3D growth. They remained as single cells that did neither proliferate nor differentiate, whereas hNPC/shScrambled controls formed extensive cellular networks. This effect of *WWOX* depletion was observed irrespective of seeding density. This observation, along with changes in cellular adhesion, suggests that *WWOX* deprivation may lead to deficiency in cytoskeleton organization, interactions between cells and extracellular matrix proteins that impair correct tissue formation. In fact, human individuals known to possess dysfunctional *WWOX* variants present physical abnormalities in brain structure, *inter alia* global atrophy and hypoplasia of the corpus callosum (Abdel-Salam et al., 2014; Elsaadany et al., 2016; Johannsen et al., 2018). Similarly, Abdeen et al. (2013) report that silencing *WWOX* expression in MCF-10A normal breast cell line caused impairment of 3D growth and increases levels of fibronectin. In our previous report we demonstrated that differentiation of *WWOX* expression influences the 3D growth of the GBM T98G cell line, with upregulation of its expression disturbing the growth and spread of cancer cells in an ECM matrix (Kośla et al., 2014). This inability to perform 3D growth might by implied by massive gene expression deregulation triggered by *WWOX* depletion.

To identify which specific pathways may be influenced by WWOX protein in hNPC, the transcription profiles of undifferentiated hNPC cells and hNPC differentiated into neurons were compared between *WWOX* high and *WWOX* low variants and analyzed ontologically to match the differentially expressed genes with the BP. The global analysis showed enrichment in 14 gene sets related to neuronal development and differentiation (e.g., neuronal progenitor cell population maintenance, regulation of neuron migration, neural crest cell differentiation) (**Supplementary Table S2**). It was found that the gene sets were enriched in hNPC/shScrambled cells versus hNPC/sh*WWOX*, indicating that WWOX-induced transcription downregulation severely interferes with CNS developmental processes. Our results shows that beside adhesion membrane proteins, *WWOX* expression also influences a significant set of genes engaged in cytoskeleton structure and intracellular signaling. This can directly imply the observed disability for 3D growth and differentiation. *In vivo* the change in cell polarity and morphology is needed to allow migration from neurogenic niches to the final localization, and *WWOX* silencing appears to cause deregulation of the genes crucial for microtubule and neurofilament assembly as well as motor proteins.

The other large functional groups emerging from the ontological analysis were the gene sets connected with cellular adhesion and neurotransmitter management. It was shown recently that in a murine model, *WWOX* knockout may lower GABA synthesis (Hussain et al., 2019).

The multiplicity of molecular changes caused by *WWOX* depletion highlights its importance for the neural differentiation process. Aberration of its expression and/or protein functionality may disturb the delicate balance of this complicated net of connections and consequently lead to severe neuropathological conditions. WWOX has been postulated to act as linker in various protein crosstalk, an important multifunctional node that connects numerous proteins in many pathways, what may nicely explain the versatile effects of its silencing.

CONCLUSION

Our findings indicate that appropriate *WWOX* expression is required for hNPC maintenance and differentiation. The silencing of *WWOX* expression results in global transcriptional changes, with the upregulation of some group of genes and simultaneous downregulation of others. Hence, it appears that the WWOX protein may be one of the master expression regulators in neural tissue.

DATA AVAILABILITY

The datasets generated for this study can be found in NCBI GEO Database, GSE126075.

AUTHOR CONTRIBUTIONS

KK planned and performed the experiments, bioinformatic analysis, and wrote the manuscript. EP contributed to the interpretation of the results. ES-B and MN participated in performing the biological experiments. MO performed the statistical and bioinformatic analysis. AB conceived the idea, performed the bioinformatic analysis of CAGE results, and contributed to writing of the manuscript.

FUNDING

This study was supported by the National Science Centre, Poland, grant no. 2015/17/D/NZ2/01989 and the Medical University of Łódź grant no. 503/0-078-02/503-01-004.

SUPPLEMENTARY MATERIAL

The Supplementary Material for this article can be found online at: https://www.frontiersin.org/articles/10.3389/fncel.2019.00391/full#supplementary-material

REFERENCES

Abdeen, S. K., Salah, Z., Khawaled, S., and Aqeilan, R. I. (2013). Characterization of WWOX inactivation in murine mammary gland development. *J. Cell. Physiol.* 228, 1391–1396. doi: 10.1002/jcp.24310

Abdel-Salam, G., Thoenes, M., Afifi, H. H., Körber, F., Swan, D., and Bolz, H. J. (2014). The supposed tumor suppressor gene WWOX is mutated in an early lethal microcephaly syndrome with epilepsy, growth retardation and retinal degeneration. *Orphanet J. Rare Dis.* 9:12. doi: 10.1186/1750-1172-9-12

Abu-Odeh, M., Bar-Mag, T., Huang, H., Kim, T., Salah, Z., Abdeen, S. K., et al. (2014). Characterizing WW domain interactions of tumor suppressor WWOX reveals its association with multiprotein networks. *J. Biol. Chem.* 289, 8865–8880. doi: 10.1074/jbc.M113.506790

Abu-Remaileh, M., and Aqeilan, R. I. (2014). Tumor suppressor WWOX regulates glucose metabolism via HIF1α modulation. *Cell Death Differ.* 21, 1805–1814. doi: 10.1038/cdd.2014.95

Abu-Remaileh, M., Seewaldt, V. L., and Aqeilan, R. I. (2014). WWOX loss activates aerobic glycolysis. *Mol. Cell. Oncol.* 2:e965640. doi: 10.4161/23723548.2014.965640

Aqeilan, R. I., Donati, V., Palamarchuk, A., Trapasso, F., Kaou, M., Pekarsky, Y., et al. (2005). WW domain-containing proteins, WWOX and YAP, compete for interaction with ErbB-4 and modulate its transcriptional function. *Cancer Res.* 65, 6764–6772. doi: 10.1158/0008-5472.CAN-05-1150

Aqeilan, R. I., Palamarchuk, A., Weigel, R. J., Herrero, J. J., Pekarsky, Y., and Croce, C. M. (2004a). Physical and functional interactions between the Wwox tumor suppressor protein and the AP-2gamma transcription factor. *Cancer Res.* 64, 8256–8261. doi: 10.1158/0008-5472.CAN-04-2055

Aqeilan, R. I., Pekarsky, Y., Herrero, J. J., Palamarchuk, A., Letofsky, J., Druck, T., et al. (2004b). Functional association between Wwox tumor suppressor protein and p73, a p53 homolog. *Proc. Natl. Acad. Sci. U.S.A.* 101, 4401–4406. doi: 10.1073/pnas.0400805101

Beckervordersandforth, R. (2017). Mitochondrial metabolism-mediated regulation of adult neurogenesis. *Brain Plast.* 3, 73–87. doi: 10.3233/BPL-170044

Bouteille, N., Driouch, K., Hage, P. E., Sin, S., Formstecher, E., Camonis, J., et al. (2009). Inhibition of the Wnt/beta-catenin pathway by the WWOX tumor suppressor protein. *Oncogene* 28, 2569–2580. doi: 10.1038/onc.2009.120

Chen, S.-J., Huang, S.-S., and Chang, N.-S. (2013). Role of WWOX and NF-kappaB in lung cancer progression. *Transl. Respir. Med.* 1:15. doi: 10.1186/2213-0802-1-15

Chen, S. T., Chuang, J. I., Wang, J. P., Tsai, M. S., Li, H., and Chang, N.-S. (2004). Expression of WW domain-containing oxidoreductase WOX1 in the developing murine nervous system. *Neuroscience* 124, 831–839. doi: 10.1016/j.neuroscience.2003.12.036

Chiang, M.-F., Chen, H.-H., Chi, C.-W., Sze, C.-I., Hsu, M.-L., Shieh, H.-R., et al. (2015). Modulation of sonic hedgehog signaling and WW domain containing oxidoreductase WOX1 expression enhances radiosensitivity of human glioblastoma cells. *Exp. Biol. Med.* 240, 392–399. doi: 10.1177/1535370214565989

Choo, A., O'Keefe, L. V., Lee, C. S., Gregory, S. L., Shaukat, Z., Colella, A., et al. (2015). Tumor suppressor WWOX moderates the mitochondrial respiratory complex. *Genes Chromosomes Cancer* 54, 745–761. doi: 10.1002/gcc.22286

Dayan, S., O'Keefe, L. V., Choo, A., and Richards, R. I. (2013). Common chromosomal fragile site FRA16D tumor suppressor WWOX gene expression and metabolic reprograming in cells. *Genes Chromosomes Cancer* 52, 823–831. doi: 10.1002/gcc.22078

Dias, E. P., Pimenta, F. J., Sarquis, M. S., Dias Filho, M. A., Aldaz, C. M., Fujii, J. B., et al. (2007). Association between decreased WWOX protein expression and thyroid cancer development. *Thyroid* 17, 1055–1059. doi: 10.1089/thy.2007.0232

Dickson, B. J. (2002). Molecular mechanisms of axon guidance. *Science* 298, 1959–1964. doi: 10.1126/science.1072165

Donati, V., Fontanini, G., Dell'Omodarme, M., Prati, M. C., Nuti, S., Lucchi, M., et al. (2007). WWOX expression in different histologic types and subtypes of non-small cell lung cancer. *Clin. Cancer Res.* 13, 884–891. doi: 10.1158/1078-0432.CCR-06-2016

Elsaadany, L., El-Said, M., Ali, R., Kamel, H., and Ben-Omran, T. (2016). W44X mutation in the WWOX gene causes intractable seizures and developmental delay: a case report. *BMC Med. Genet.* 17:53. doi: 10.1186/s12881-016-0317-z

Ferguson, B. W., Gao, X., Zelazowski, M. J., Lee, J., Jeter, C. R., Abba, M. C., et al. (2013). The cancer gene WWOX behaves as an inhibitor of SMAD3 transcriptional activity via direct binding. *BMC Cancer* 13:593. doi: 10.1186/1471-2407-13-593

Gaudio, E., Palamarchuk, A., Palumbo, T., Trapasso, F., Pekarsky, Y., Croce, C. M., et al. (2006). Physical association with WWOX suppresses c-Jun transcriptional activity. *Cancer Res.* 66, 11585–11589. doi: 10.1158/0008-5472.CAN-06-3376

Haberle, V., Forrest, A. R. R., Hayashizaki, Y., Carninci, P., and Lenhard, B. (2015). *CAGEr*: precise TSS data retrieval and high-resolution promoterome mining for integrative analyses. *Nucleic Acids Res.* 43:e51. doi: 10.1093/nar/gkv054

Hasegawa, A., Daub, C., Carninci, P., Hayashizaki, Y., and Lassmann, T. (2014). MOIRAI: a compact workflow system for CAGE analysis. *BMC Bioinformatics* 15:144. doi: 10.1186/1471-2105-15-144

Hsu, L.-J., Chiang, M.-F., Sze, C.-I., Su, W.-P., Yap, Y. V., Lee, I.-T., et al. (2016). HYAL-2-WWOX-SMAD4 signaling in cell death and anticancer response. *Front. Cell Dev. Biol.* 4:141. doi: 10.3389/fcell.2016.00141

Hussain, T., Kil, H., Hattiangady, B., Lee, J., Kodali, M., Shuai, B., et al. (2019). Wwox deletion leads to reduced GABA-ergic inhibitory interneuron numbers and activation of microglia and astrocytes in mouse hippocampus. *Neurobiol. Dis.* 121, 163–176. doi: 10.1016/j.nbd.2018.09.026

Iatan, I., Choi, H. Y., Ruel, I., Reddy, M. V. P. L., Kil, H., Lee, J., et al. (2014). The WWOX gene modulates high-density lipoprotein and lipid metabolism. *Circ. Cardiovasc. Genet.* 7, 491–504. doi: 10.1161/CIRCGENETICS.113.000248

Jiang, X., and Nardelli, J. (2016). Cellular and molecular introduction to brain development. *Neurobiol. Dis.* 92, 3–17. doi: 10.1016/j.nbd.2015.07.007

Johannsen, J., Kortüm, F., Rosenberger, G., Bokelmann, K., Schirmer, M. A., Denecke, J., et al. (2018).). A novel missense variant in the SDR domain of the WWOX gene leads to complete loss of WWOX protein with early-onset epileptic encephalopathy and severe developmental delay. *Neurogenetics* 19, 151–156. doi: 10.1007/s10048-018-0549-545

Joo, S., Kim, J. Y., Lee, E., Hong, N., Sun, W., and Nam, Y. (2015). Effects of ECM protein micropatterns on the migration and differentiation of adult neural stem cells. *Sci. Rep.* 5:13043. doi: 10.1038/srep13043

Kośla, K., Nowakowska, M., Pospiech, K., and Bednarek, A. K. (2014). WWOX modulates the gene expression profile in the T98G glioblastoma cell line rendering its phenotype less malignant. *Oncol. Rep.* 32, 1362–1368. doi: 10.3892/or.2014.3335

Kosla, K., Pluciennik, E., Kurzyk, A., Jesionek-Kupnicka, D., Kordek, R., Potemski, P., et al. (2011). Molecular analysis of WWOX expression correlation with proliferation and apoptosis in glioblastoma multiforme. *J. Neurooncol.* 101, 207–213. doi: 10.1007/s11060-010-0254-251

Kuhn, R. M., Haussler, D., and Kent, W. J. (2013). The UCSC genome browser and associated tools. *Brief. Bioinform.* 14, 144–161. doi: 10.1093/bib/bbs038

Lan, C., Chenggang, W., Yulan, B., Xiaohui, D., Junhui, Z., and Xiao, W. (2012). Aberrant expression of WWOX protein in epithelial ovarian cancer: a clinicopathologic and immunohistochemical study. *Int. J. Gynecol. Pathol.* 31, 125–132. doi: 10.1097/PGP.0b013e3182297fd2

Li, Y., Liu, M., Yan, Y., and Yang, S.-T. (2014). Neural differentiation from pluripotent stem cells: the role of natural and synthetic extracellular matrix. *World J. Stem Cells* 6, 11–23. doi: 10.4252/wjsc.v6.i1.11

Li, Z., and Sheng, M. (2003). Some assembly required: the development of neuronal synapses. *Nat. Rev. Mol. Cell Biol.* 4, 833–841. doi: 10.1038/nrm1242

Liu, C.-C., Ho, P.-C., Lee, I.-T., Chen, Y.-A., Chu, C.-H., Teng, C.-C., et al. (2018). WWOX phosphorylation, signaling, and role in neurodegeneration. *Front. Neurosci.* 12:563. doi: 10.3389/fnins.2018.00563

Liu, J. S. (2011). Molecular genetics of neuronal migration disorders. *Curr. Neurol. Neurosci. Rep.* 11, 171–178. doi: 10.1007/s11910-010-0176-175

Lizio, M., Harshbarger, J., Shimoji, H., Severin, J., Kasukawa, T., Sahin, S., et al. (2015). Gateways to the FANTOM5 promoter level mammalian expression atlas. *Genome Biol.* 16:22. doi: 10.1186/s13059-014-0560-566

Lo, C.-P., Hsu, L.-J., Li, M.-Y., Hsu, S.-Y., Chuang, J.-I., Tsai, M.-S., et al. (2008). MPP+-induced neuronal death in rats involves tyrosine 33 phosphorylation of WW domain-containing oxidoreductase WOX1. *Eur. J. Neurosci.* 27, 1634–1646. doi: 10.1111/j.1460-9568.2008.06139.x

Mallaret, M., Synofzik, M., Lee, J., Sagum, C. A., Mahajnah, M., Sharkia, R., et al. (2014). The tumour suppressor gene WWOX is mutated in autosomal recessive cerebellar ataxia with epilepsy and mental retardation. *Brain J. Neurol.* 137, 411–419. doi: 10.1093/brain/awt338

Marín, O., Valdeolmillos, M., and Moya, F. (2006). Neurons in motion: same principles for different shapes? *Trends Neurosci.* 29, 655–661. doi: 10.1016/j.tins.2006.10.001

Matteucci, E., Bendinelli, P., and Desiderio, M. A. (2009). Nuclear localization of active HGF receptor met in aggressive MDA-MB231 breast carcinoma cells. *Carcinogenesis* 30, 937–945. doi: 10.1093/carcin/bgp080

Mignot, C., Lambert, L., Pasquier, L., Bienvenu, T., Delahaye-Duriez, A., Keren, B., et al. (2015). WWOX-related encephalopathies: delineation of the phenotypical spectrum and emerging genotype-phenotype correlation. *J. Med. Genet.* 52, 61–70. doi: 10.1136/jmedgenet-2014-102748

Monsonego-Ornan, E., Kosonovsky, J., Bar, A., Roth, L., Fraggi-Rankis, V., Simsa, S., et al. (2012). Matrix metalloproteinase 9/gelatinase B is required for neural crest cell migration. *Dev. Biol.* 364, 162–177. doi: 10.1016/j.ydbio.2012.01.028

Nunez, M. I., Ludes-Meyers, J., and Aldaz, C. M. (2006). WWOX protein expression in normal human tissues. *J. Mol. Histol.* 37, 115–125. doi: 10.1007/s10735-006-9046-9045

O'Keefe, L. V., Colella, A., Dayan, S., Chen, Q., Choo, A., Jacob, R., et al. (2011). Drosophila orthologue of WWOX, the chromosomal fragile site FRA16D tumour suppressor gene, functions in aerobic metabolism and regulates reactive oxygen species. *Hum. Mol. Genet.* 20, 497–509. doi: 10.1093/hmg/ddq495

Pagés, H., (2018). *BSgenome: Software Infrastructure for Efficient Representation of Full Genomes and Their SNPs. R Package Version 1.48.0*. Available at: http://bioconductor.riken.jp/packages/3.7/bioc/html/BSgenome.html

Paige, A. J. W., Zucknick, M., Janczar, S., Paul, J., Mein, C. A., Taylor, K. J., et al. (2010). WWOX tumour suppressor gene polymorphisms and ovarian cancer pathology and prognosis. *Eur. J. Cancer* 46, 818–825. doi: 10.1016/j.ejca.2009.12.021

Piard, J., Hawkes, L., Milh, M., Villard, L., Borgatti, R., Romaniello, R., et al. (2018). The phenotypic spectrum of WWOX-related disorders: 20 additionalcases of WOREE syndrome and review of the literature. *Genet. Med.* 21, 1308–1318. doi: 10.1038/s41436-018-0339-3

Płuciennik, E., Kusińska, R., Potemski, P., Kubiak, R., Kordek, R., and Bednarek, A. K. (2006). WWOX–the FRA16D cancer gene: expression correlation with breast cancer progression and prognosis. *Eur. J. Surg. Oncol.* 32, 153–157. doi: 10.1016/j.ejso.2005.11.002

Płuciennik, E., Nowakowska, M., Stępien, A., Wołkowicz, M., Stawiński, A., Różański, W., et al. (2014). Alternating expression levels of WWOX tumor suppressor and cancer-related genes in patients with bladder cancer. *Oncol. Lett.* 8, 2291–2297. doi: 10.3892/ol.2014.2476

Robinson, M. D., McCarthy, D. J., and Smyth, G. K. (2010). edgeR: a bioconductor package for differential expression analysis of digital gene expression data. *Bioinformatics* 26, 139–140. doi: 10.1093/bioinformatics/btp616

Seabra, M. A. L., Cândido, E. B., Vidigal, P. V. T., Lamaita, R. M., Rodrigues, A. N., and Silva Filho, A. L. D. (2018). Immunohistochemical WWOX expression and association with angiogenesis, p53 expression, cell proliferation and clinicopathological parameters in cervical cancer. *Rev. Bras. Ginecol. Obstet.* 40, 79–85. doi: 10.1055/s-0037-1618597

Shaukat, Q., Hertecant, J., El-Hattab, A. W., Ali, B. R., and Suleiman, J. (2018). West syndrome, developmental and epileptic encephalopathy, and severe CNS disorder associated with WWOX mutations. *Epileptic Disord.* 20, 401–412. doi: 10.1684/epd.2018.1005

Spalice, A., Parisi, P., Nicita, F., Pizzardi, G., Del Balzo, F., and Iannetti, P. (2009). Neuronal migration disorders: clinical, neuroradiologic and genetics aspects. *Acta Paediatr.* 98, 421–433. doi: 10.1111/j.1651-2227.2008.01160.x

Sun, W., Dou, J., Zhang, L., Qiao, L., Shen, N., and Gao, W. (2017). Expression of CD133, E-cadherin and WWOX in colorectal cancer and related analysis. *Pak. J. Med. Sci.* 33, 425–429. doi: 10.12669/pjms.332.11687

Suzuki, H., Katayama, K., Takenaka, M., Amakasu, K., Saito, K., and Suzuki, K. (2009). A spontaneous mutation of the Wwox gene and audiogenic seizures in rats with lethal dwarfism and epilepsy. *Genes Brain Behav.* 8, 650–660. doi: 10.1111/j.1601-183X.2009.00502.x

Sze, C.-I., Su, M., Pugazhenthi, S., Jambal, P., Hsu, L.-J., Heath, J., et al. (2004). Down-regulation of WW domain-containing oxidoreductase induces tau phosphorylation in vitro. A potential role in Alzheimer's disease. *J. Biol. Chem.* 279, 30498–30506. doi: 10.1074/jbc.M401399200

Tabarki, B., Al Mutairi, F., and Al Hashem, A. (2015a). The fragile site WWOX gene and the developing brain. *Exp. Biol. Med.* 240, 400–402. doi: 10.1177/1535370214561952

Tabarki, B., AlHashem, A., AlShahwan, S., Alkuraya, F. S., Gedela, S., and Zuccoli, G. (2015b). Severe CNS involvement in WWOX mutations: description of five new cases. *Am. J. Med. Genet. A.* 167, 3209–3213. doi: 10.1002/ajmg.a.37363

Takahashi, H., Lassmann, T., Murata, M., and Carninci, P. (2012). 5' end-centered expression profiling using cap-analysis gene expression and next-generation sequencing. *Nat. Protoc.* 7, 542–561. doi: 10.1038/nprot.2012.005

Teng, C.-C., Yang, Y.-T., Chen, Y.-C., Kuo, Y.-M., and Sze, C.-I. (2012). Role of WWOX/WOX1 in Alzheimer's disease pathology and in cell death signaling. *Front. Biosci.* 4:1951–1965. doi: 10.2741/e516

Wang, H.-Y., Juo, L.-I., Lin, Y.-T., Hsiao, M., Lin, J.-T., Tsai, C.-H., et al. (2012). WW domain-containing oxidoreductase promotes neuronal differentiation via negative regulation of glycogen synthase kinase 3β. *Cell Death Differ.* 19, 1049–1059. doi: 10.1038/cdd.2011.188

Wang, L., Zhang, Z. G., Zhang, R. L., Gregg, S. R., Hozeska-Solgot, A., LeTourneau, Y., et al. (2006). Matrix metalloproteinase 2 (MMP2) and MMP9 secreted by erythropoietin-activated endothelial cells promote neural progenitor cell migration. *J. Neurosci.* 26, 5996–6003. doi: 10.1523/JNEUROSCI.5380-05.2006

Wang, X., Chao, L., Ma, G., Chen, L., Zang, Y., and Sun, J. (2011). The prognostic significance of WWOX expression in patients with breast cancer and its association with the basal-like phenotype. *J. Cancer Res. Clin. Oncol.* 137, 271–278. doi: 10.1007/s00432-010-0880-881

Wilson, C., Muñoz-Palma, E., and González-Billault, C. (2018). From birth to death: a role for reactive oxygen species in neuronal development. *Semin. Cell Dev. Biol.* 80, 43–49. doi: 10.1016/j.semcdb.2017.09.012

Xiong, A., Wei, L., Ying, M., Wu, H., Hua, J., and Wang, Y. (2014). Wwox suppresses breast cancer cell growth through modulation of the hedgehog-GLI1 signaling pathway. *Biochem. Biophys. Res. Commun.* 443, 1200–1205. doi: 10.1016/j.bbrc.2013.12.133

Zhang, J., Li, L., Song, H., Paige, A., and Gabra, H. (2009). [Effect of WWOX gene on the attachment and adhesion of ovarian cancer cells]. *Zhonghua Fu Chan Ke Za Zhi* 44, 529–532.

Conflict of Interest Statement: The authors declare that the research was conducted in the absence of any commercial or financial relationships that could be construed as a potential conflict of interest.

frontiers in Cellular Neuroscience

ORIGINAL RESEARCH
published: 04 September 2019
doi: 10.3389/fncel.2019.00403

Normal and Pathological Tau Uptake Mediated by M1/M3 Muscarinic Receptors Promotes Opposite Neuronal Changes

*Viktoriya Morozova[1,2], Leah S. Cohen[1], Ali El-Hadi Makki[1], Alison Shur[1,2], Guillermo Pilar[3], Abdeslem El Idrissi[1,2] and Alejandra D. Alonso[1,2]**

[1] Department of Biology and Center for Developmental Neuroscience, College of Staten Island, The City University of New York, Staten Island, NY, United States, [2] Biology Program, The Graduate Center, The City University of New York, New York, NY, United States, [3] Department of Neurosciences, Case Western Reserve University, Cleveland, OH, United States

The microtubule associated protein tau is mainly found in the cell's cytosol but recently it was also shown in the extracellular space. In neurodegenerative diseases, like Alzheimer's disease (AD), pathological tau spreads from neuron to neuron enhancing neurodegeneration. Here, we show that HEK293 cells and neurons in culture uptake extracellular normal and pathological Tau. Muscarinic receptor antagonists atropine and pirenzepine block 80% this uptake. CHO cells do not express these receptors therefore cannot uptake tau, unless transfected with M1 and/or M3 receptor. These results strongly suggest that muscarinic receptors mediate this process. Uptake of normal tau in neurons enhances neuronal process formation but a pseudophosphorylated form of tau (pathological human tau, PH-Tau) disrupts them and accumulates in the somatodendritic compartment. AD hyperphosphorylated tau (AD P-Tau) has similar effects as PH-Tau on cultured neurons. Addition of either PH-Tau or AD P-tau to neuronal cultures induced microglial activation. In conclusion, uptake of extracellular tau is mediated by muscarinic receptors with opposite effects: normal tau stabilizes neurites; whereas pathological tau disrupts this process leading to neurodegeneration.

Keywords: tau, muscarinic receptors, uptake, neurodegeneration, Alzheimer's disease

OPEN ACCESS

Edited by:
Thomas Fath, Macquarie University, Australia

Reviewed by:
Hermona Soreq, The Hebrew University of Jerusalem, Israel
Carlos J. Rodriguez-Ortiz, University of California, Irvine, United States

***Correspondence:**
Alejandra D. Alonso
Alejandra.Alonso@csi.cuny.edu

Specialty section:
This article was submitted to Cellular Neuropathology, a section of the journal Frontiers in Cellular Neuroscience

Received: *11 June 2019*
Accepted: *19 August 2019*
Published: *04 September 2019*

Citation:
Morozova V, Cohen LS, Makki AE-H, Shur A, Pilar G, El Idrissi A and Alonso AD (2019) Normal and Pathological Tau Uptake Mediated by M1/M3 Muscarinic Receptors Promotes Opposite Neuronal Changes. Front. Cell. Neurosci. 13:403. doi: 10.3389/fncel.2019.00403

INTRODUCTION

Tau is a neuronal cytosolic microtubule associated phospho-protein whose function can be influenced by post-translational modifications. Abnormally phosphorylated tau is a common denominator in several types of dementia, including Alzheimer's disease (AD) and other tauopathies (Goedert et al., 2010; Beharry et al., 2014).

Unlike normal tau, soluble hyperphosphorylated tau taken from AD patients (AD P-tau) does not promote microtubule assembly. Instead, AD P-tau binds normal tau, sequestering it from interactions with tubulin and producing bundles of filaments observed by electron microscopy (Alonso et al., 1996). This suggests that differences in tau phosphorylation states could affect its conformation and subsequently alter protein-protein interactions and tau biological function. Seeding activity into self-assembled aggregates can lead to the development of neurofibrillary

tangles. We have shown previously that pseudophosphorylation at Ser199, Thr212, Thr231, and Ser262 with inclusion of the FTDP-17 R406W mutation (Pathological Human Tau, PH-Tau) results in a protein that mimics the effect of AD P-tau in culture (Alonso et al., 2010). This protein has been studied in mammalian cell culture, Drosophila, and mouse models. The expression of PH-Tau induced microtubule disruption in all systems, and resulted in cognitive and behavior impairment in Drosophila and mice (Alonso et al., 2010; Beharry et al., 2013; Di et al., 2016).

In AD, the initial neurodegenerative lesions are in the transentorhinal cortex spreading slowly to the hippocampus and neocortex (Hyman et al., 1984; Braak and Braak, 1991; Goedert et al., 2010), leading to cognitive decline. It was proposed that pathological tau is spread from cell to cell in a prion-like fashion (Holmes and Diamond, 2014; Mudher et al., 2017). The seeding and propagation of filamentous structures by hyperpshosphorylated tau has been a central point in AD research (Alonso et al., 2016; Hu et al., 2016; Iqbal et al., 2016; Mudher et al., 2017; Shafiei et al., 2017). Cells in culture take up tau aggregates ranging in size from oligomers and short filaments (neuronal cells) to fibrils (non-neuronal cells) through endocytosis (Frost et al., 2009; Nonaka et al., 2010; Guo and Lee, 2011; Wu et al., 2013; Sanders et al., 2014; Wu et al., 2016). Recently, it has been shown that monomeric tau can enter neurons (Evans et al., 2018) and based on the kinetics of tau uptake, it was suggested that this might be a receptor-mediated process (Evans et al., 2018). Furthermore, intracerebral injections of abnormal tau showed that tau pathology propagates away from the injection site, to neighboring brain regions indicating that tau can be transferred from cell to cell (Bolmont et al., 2007; Clavaguera et al., 2009; Lasagna-Reeves et al., 2012; Clavaguera et al., 2013; Iba et al., 2013; Wu et al., 2013; Ahmed et al., 2014; Clavaguera et al., 2014). Taken together, these results have led to the tau propagation hypothesis in which tau is released from one neuron into the intra-neuronal space, and taken up by other neurons transferring tau toxicity in a similar fashion as prion proteins (as reviewed in Takeda, 2019).

In this study we demonstrate that addition of recombinant tau protein to the culture media of Human Embryonic Kidney cells (HEK293) and primary cerebellar neuronal culture results in the uptake of tau and PH-Tau. Chinese Hamster Ovary (CHO) cells are unable to uptake tau unless they are transfected with M1- and M3-type muscarinic receptors. Furthermore, uptake into both HEK293 cells and cerebellar neurons is blocked by atropine, a muscarinic receptor antagonist, and uptake in cerebellar neurons is blocked by pirenzepine, an M1 antagonist, but not AF-DX116, an M2 antagonist, or pertussis toxin (PTX), an M2/M4 antagonist. Neuronal cultures incubated with wild-type tau for 7 days show an abundant and well-organized neuritic arbor. Similar cultures exposed to PH-Tau and AD P-tau show accumulation of tau in the somatodendritic neuronal compartment and disruption of neuronal processes. Our experimental results suggest that both tau and pathogenic tau are taken up in mammalian cells and neurons in a muscarinic receptor-mediated uptake mechanism that facilitates long-term neuronal changes.

MATERIALS AND METHODS

Antibodies

The primary antibodies used in this work are as follows: tau-13 (mouse, 1:1,000,000 for Western blot, 1:1000 for immunohistochemistry), CHRM1 (rabbit, 1:1000, Invitrogen, Cat#711098), βactin (1:2500, Santa Cruz, Cat#SC4778), β-III tubulin (chicken, 1:1000, Abcam, Cat#AB107216), GFAP (rabbit, 1:1000, Invitrogen Cat#PA3-16-727), IbaI (rabbit, 1:1000, Wako Cat#019-19741). The secondary antibodies used in this work are as follows: anti-mouse IgG-HRP (1:2000, Santa Cruz, Cat#SC-516102), anti-mouse Alexa 488 (1:1000, Invitrogen, Cat#A21202), anti-chicken Alexa 555 (1:1000, Invitrogen, Cat#A21437), anti-rabbit Alexa 594 (1:1000, Invitrogen, Cat#A21203). Tau-13 antibodies were a gift from Dr. Nicholas Kanaan at Michigan State University (originally created by Dr. Lester Binder at Northwestern University).

Recombinant Protein Expression and Purification

GST-tagged proteins were transformed into BL21(DE3)pLysS cells and purified using glutathione-sepharose beads (GE Healthcare) as described (Cevher et al., 2010).

Protein Quantitation, PAGE, and Western Blot Analysis

Quantitation of protein samples was performed by either the Bradford assay or by UV quantitation. The Bradford assay was performed on recombinant proteins and cell and neuronal lysates as described by the BioRad manual. Recombinant protein was also determined by UV spectroscopy at 280 nm using the extinction coefficients of 50685 $M^{-1}cm^{-1}$ for GST-tau, 56185 $M^{-1}cm^{-1}$ for GST-PH-Tau, and 43110 $M^{-1}cm^{-1}$ for GST. Recombinant proteins (10 μg per lane), cell and neuronal lysates (7 μg per lane) were analyzed by SDS-PAGE and Western blot as described with some modifications (Grundke-Iqbal et al., 1984).

Cell Culture and Transfection

HEK293 cells were grown in DMEM cell media supplemented with 10% Fetal Bovine Serum (FBS), sodium pyruvate, Glutamax, and Antibiotic-Antimitotic. CHO cells were grown in FK12 media with 10% FBS, sodium pyruvate, Glutamax and Antibiotic-Antimitotic. Media components were from Gibco or Thermo Fisher Scientific.

Chinese Hamster Ovary cells were plated on glass coverslips overnight. Transfections were performed using LipofectamineTM 2000 (Invitrogen, Carlsbad, CA, United States), according to the manufacturer's instructions. Briefly, transfections were performed in serum-free media OptiMEM using 3 μg of total DNA and 3 μl of Lipofectamine^{TM} 2000 per 35 mm dish. Cells were incubated in transfection media for 4 h and then replaced with fresh cell media.

Preparation of Mixed Cerebellar Neuronal Culture

Cerebellar granule cells were prepared from PN7 CD1 mice. The cerebellum was removed and single cell suspension was prepared by trypsinization and trituration in 1% trypsin in Ca^{2+}, Mg^{2+} free isotonic phosphate buffer (CMF-PBS). Cells were washed in CMF-PBS and resuspended in minimum essential culture medium supplemented with 0.25% glucose, 2 mM GlutaMax, 10% Horse Serum, 5% FBS, and 25 U/ml both penicillin and streptomycin. Cells were seeded into PDL-coated dishes and incubated at 37°C, 5% CO_2. Twenty-four hours after neuronal isolation, culture media was changed to media containing 15% of N2 supplement (R&S system) and 10 μM KCl. This media was changed every 2 days. Media components were from Gibco, Sigma, or Corning.

Protein Addition to Cultures

GST, GST-tau, and GST-PH-Tau (0.4 μg/ml final concentration) were added to the cell media of HEK293 cells, CHO cells and primary neuronal cultures. HEK293 and CHO cells were incubated with proteins for 2–4 h and washed with PBS. After additional incubation for 48 h, cells were fixed, processed for immunocytochemistry and viewed by confocal microscopy. M1/M3 transfected CHO cells were incubated for 48 h, then tau or PH-tau was added to the cells as described, incubated for 4 h, then media was changed and cells were grown for another 24 h and then processed for western blot.

Neuronal cultures were incubated for 24 h in the presence of tau or PH-Tau and were either fixed and processed for immunochemistry (DIV8) or incubated for longer time periods. For longer incubation times, half of the media was removed after 24 h and replaced with fresh media. The cultures were fixed and processed at DIV10, DIV12, or DIV14.

Blocking of Muscarinic Receptors

HEK293 cells and neuronal cultures were treated with 100 μM Atropine sulfate salt monohydrate (Sigma), 10 μM Pirenzepine Dichloride (Alfa Aesar), 40 ng/ml Pertussis toxin (Enzo), or 10 μM AF-DX116 (Toriks Biochemicals) in the culture media for 10 min prior to protein addition. After pre-treatment, half of the media was removed, replaced with fresh media and tau, PH-Tau or AD P-tau were added immediately to the cultures and incubated as described above.

Immunocytochemistry of Cell and Neuronal Cultures

HEK293 and CHO cells were fixed with cold methanol at −20°C for 5 min. Fixed cells were washed with PBS three times for 5 min and then blocked with 5% Donkey serum in PBS for 1 h at room temperature. Tau-13 was added to blocking buffer and cells were incubated overnight at 4°C with agitation. Cells were washed three times for 5 min each and incubated with anti-mouse Alexa 488 in blocking buffer (1:1000 dilution) for 2 h. Finally, cells were washed three times with PBS and the coverslips were mounted on the slides using Vectashield mounting media containing DAPI (Vector Laboratories, Inc.) and viewed by confocal microscopy.

Neuronal cultures were fixed with warm 4% paraformaldehyde for 10 min at room temperature, washed with PBS three times for 5 min and permeabilized with 100% methanol at −20°C for 10 min. Permeabilized cells were washed again with PBS three times for 5 min and blocked with 5% BSA, 1% Donkey serum, 0.2% TritonX-100 in PBS for 1 h at room temperature. Tau-13, β-III tubulin, GFAP, or IbaI were added to blocking buffer and cultures were incubated overnight at 4°C. Cultures were washed with 0.2% TritonX-100 in PBS (PBS-T) three times 5 min each and incubated with anti-mouse Alexa 488, anti-chicken Alexa 555, or anti-rabbit Alexa 594 in blocking buffer for 2 h at room temperature. Cultures were washed with PBS-T and then with PBS. Coverslips were mounted as described above.

LIVE/DEAD Imaging

Neuronal cultures (DIV 14) cultured in 24-well plates were treated with reagents from the LIVE/DEAD Cell Imaging Kit (488/570) (Invitrogen) as described by the manufacturer's protocol. Analysis was performed using a Zeiss-Axio Observer Z1 Live Imager.

Stereotaxic Injections

Five-month-old CD-1 mice were anesthetized with 100 mg/kg ketamine and mounted onto a stereotaxic apparatus, and kept anesthetized under isofluorane throughout the procedure. A midsagittal incision was made and a hole was drilled using a Circuit Medic Micro Drill System into the cranium according to the following coordinates set from bregma: AP: + 2.18 mm, ML: + 2.85 mm, DV: −2.5 mm. The mice were injected with 2 μL of 2 μg/mL of either aCSF, tau, or PH-Tau with the use of a Hamilton syringe at a rate of 0.5 μL/min for 4 min of total injection time with a KD Scientific Syringe Infusion Pump. The incision was treated with garamycin and closed with surgical staples, and the mice were placed onto a heating pad while they recovered from the procedure. The mice were sacrificed after 45 days.

Cryosectioning and H&E Staining

Mice were anesthetized with 0.3 mL urethane (1 g/mL) and transcardially perfused with 0.1 M phosphate buffered saline (PBS) and 4% paraformaldehyde (PFA) in 0.1 M PBS then stored in PFA followed by 30% sucrose at 4°C. Brains were cryosectioned in sagittal vibratome sections (50 μm) and mounted onto microscope slides. Tissue sections were then incubated in the following order: PBS for 5 min, dH_2O for 1 min, hematoxylin for 4 min, running tap water for 3–5 min, dH_2O for 1 min, eosin for 2 min, 70% alcohol for 2 min, 95% alcohol for 2 min, 100% alcohol for 2 min, and xylene for 2 min. The tissue sections were covered in a Permount/xylene solution and coverslipped. The staining was observed with an EVOS PLc light microscope at 20×.

Confocal Image Acquisition, Measurements, and Statistical Analysis

Images for each set of analysis were observed under a LEICA TGS SP5 confocal laser scaning microscope (Leica Microsystems CMSGmbH, Mannheim, Germany) and obtained using the same gain, laser intensity and pinhole size. Confocal images were analyzed using ImageJ software. Images were split onto blue (DAPI), green and red channels. The same threshold was assigned to all pictures for each channel. Mean gray value was calculated from each channel and divided by the number of the nuclei. The results were graphed and compared using Excel 2010.

All experiments were performed at least three times and at least 10 images from each experiment were analyzed. Statistics were performed using Microsoft Excel 2010. Two-Sample *t*-Test assuming equal variances was used to compare samples. The data reported as mean values. An alpha level of 0.05 was used for all statistical tests. The significance was determined based on two-tailed *P* values.

RESULTS

Tau Uptake Into Cells Is Receptor Mediated

Propagation of abnormal tau in AD and other tauopathies has been proposed to occur through cell-to-cell transfer (as reviewed in Takeda, 2019). To better understand the mechanism of uptake, culture media spiked with recombinant proteins GST-tau, or GST-PH-Tau, 400 ng/mL (**Supplementary Figure S1**) was added to HEK293 or CHO cells and incubated for 4 h. After replacing the culture media, the cells were incubated in normal media for 2 days. Cells were washed to remove all extracellular tau, fixed and labeled with an anti-human tau antibody, counterstained with DAPI to observe the nuclei, and analyzed by confocal microscopy. Tau and PH-Tau were taken up into the HEK293 cells, but no uptake was observed in CHO cells (**Figure 1A**). GST alone was not detected in both cell lines (data not shown). These results indicate that tau, independent of phosphorylation state, can be uptaken in a cell-specific manner.

To determine if similar uptake can be observed in neuronal cells, primary mixed cerebellar neuronal cultures were prepared at Day 7 after birth (DIV1). Tau and PH-Tau, each at 400 ng/mL, were added to the media at DIV7 and incubated for 24 h. After incubation, the cultures were washed as above, fixed, processed for immunochemistry and double-labeled with anti-human tau and β-III tubulin (**Figure 1B**). DAPI was used as a counterstain to observe the nuclei. Both Tau and PH-Tau were taken up by neurons and accumulated at similar levels around the cell nucleus (**Figure 1B**, ROI). Uptake was observed without changes in neuritic morphology or neuronal numbers when comparing to control. Similar experiments were performed with human tau without a GST-tag and uptake was observed indicating that the uptake was due to tau and not the GST-tag (**Supplementary Figure S2**).

The different responses between HEK293 and CHO might be because HEK cells were generated from human embryonic kidney having properties similar to immature neurons and CHO cells are an epithelial cell line derived from ovaries of Chinese hamster (Shaw et al., 2002; Shafer and Williams, 2004; Lin et al., 2014). Similar to neurons, HEK293 cells express muscarinic receptors, while CHO cells do not. Neuronal muscarinic receptors have been shown to interact with tau (Gomez-Ramos et al., 2008; Gomez-Ramos et al., 2009; Avila et al., 2015). Western blot analysis of these cell lines shows that both HEK293 cells express about eight-fold higher M1 receptors (CHRM1) while primary cerebellar neuronal cultures express more than 20-fold higher M1 muscarinic receptors when compared to CHO cells (**Figure 1D**, left). Pre-treatment of cells with the muscarinic receptor antagonist atropine resulted in reduced uptake of both recombinant tau proteins in HEK293 cells and neuronal cultures (**Figure 1A**, bottom, **Figure 1B**, last column). Quantitative analysis shows that tau uptake in the neuronal cultures was reduced up to 80% of that without atropine (**Figure 1C**). Taken together these results implicate the involvement of muscarinic receptors in the uptake of tau into HEK293 cells and neurons.

Muscarinic Receptor Subtypes M1 and M3 Are Involved in the Uptake of Tau

Given that tau is uptaken by HEK293 cells and neurons but not CHO cells, and uptake is blocked by atropine, we wanted to further analyze which of the five main subtypes of muscarinic receptors were involved. Primary cerebellar cultures were treated with pirenzepine, an M1 antagonist, AF-DX116, a selective M2 antagonist, and pertussis toxin (PTX), which blocks downstream processes of G_i G protein-coupled receptors (including M2/M4) (**Figure 1C**). Pirenzepine blocked the uptake of tau and PH-Tau about 80% which is similar to atropine. Conversely, both AF-DX116 and PTX did not block the uptake of either tau protein significantly. These results further implicate the M1 muscarinic receptor but not M2/M4 in the uptake of tau into the cells.

To further examine the role of muscarinic receptor subtypes in uptake into cells, CHO cells were transiently transfected with M1-HA, M3-HA, or both. The transfected cells were cultured for 48 h and then media containing the recombinant proteins was added as described above. The cells were collected after 24 h, washed, lysed and analyzed by immunoblot using anti-human tau. In CHO cells transfected with M1 or M3 there is ∼19-fold increase tau uptake (**Figure 1D**, right) compared to non-transfected CHO cells. When the cells were transfected with both M1 and M3 at the same time, the level of tau uptake increased by 31.5-fold. CHO cells transfected with either M1 or M3 appear to uptake tau at similar levels as HEK293 cells. When both receptors are present the uptake increases significantly. These results imply that both M1 and M3 are involved in the uptake of tau into cells.

Consequences of Tau Exposure in Neuronal Processes

To observe changes in neurons due to the uptake of tau or PH-Tau we performed the experiments as described above, where the neurons were exposed to tau for 24 h and cultures were allowed to grow and differentiate for up to seven more

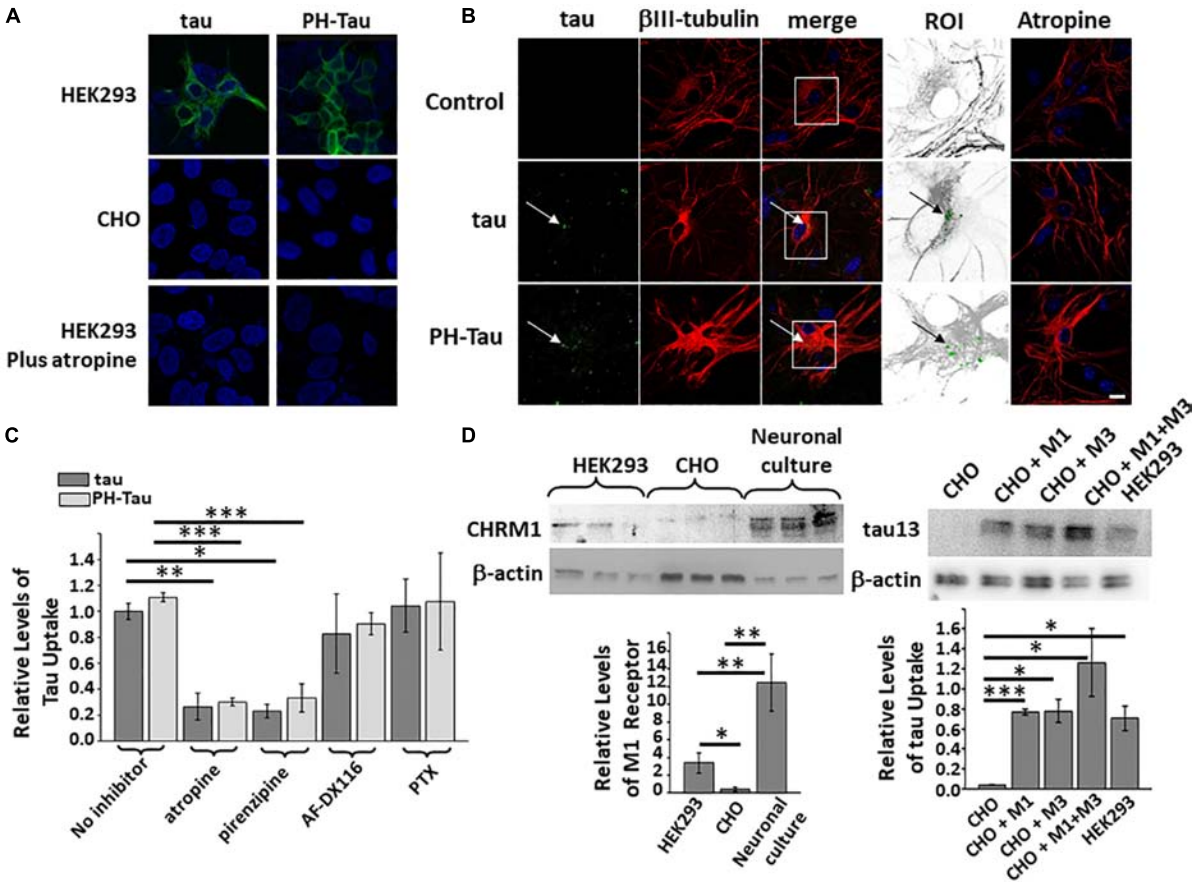

FIGURE 1 | Uptake of tau is cell-type specific. Recombinant tau and PH-Tau (400 ng/mL) were added to HEK293 and CHO cells **(A)** and to primary neuronal cultures **(B)**. Confocal analysis indicated that uptake occurred in HEK293 and neuronal cultures (white arrows) but not CHO cells and was blocked by pre-treatment with atropine. In the neuronal images, the boxed areas were zoomed 2.5× and converted (βIII-tubulin, gray; tau, green). **(C)** Quantitation of tau uptake into neuronal cultures indicates that both tau (dark bars) and PH-Tau (light bars) are uptaken at similar levels. Pre-treatment with antagonists atropine and pirenzepine block the uptake of both proteins by about 80%. Conversely, AF-DX116 and PTX do not block uptake. **(D)** Left: Western blot analysis of cultured cells and neurons to analyze the presence of the M1 muscarinic receptor. Quantitation indicated that both HEK293 and neuronal cultures have a large amount of M1 muscarinic receptors compared to CHO cells. Right: Western blot analysis of HEK293 cells transfected with M1, M3, or M1/M3 muscarinic receptors to determine tau uptake. The introduction of the muscarinic receptors resulted in the significant uptake of tau into CHO cells. Scale bar: 20 μm. All experiments were performed three times with 10 images analyzed per experiment. (*$p < 0.05$, **$p < 0.01$, ***$p < 0.001$).

days *in vitro* (**Figure 2A**). βIII-tubulin intensity at DIV10 appears to be higher in all cultures to which tau was added when compared to the control cultures. After this point, the cultures treated with PH-Tau, showed decreasing intensity of βIII-tubulin. DIV12 neurons treated with PH-Tau began to lose neurites, a feature indicative of neurodegeneration. Interestingly, the few neurons in cultures treated with pathogenic tau, which are still present at DIV14, appear more similar to neuronal processes treated with wild-type tau than those in the control. Conversely, there was an increase in βIII-tubulin intensity in cultures treated with normal tau. DIV14 neurons treated with tau appear to bundle together and to be straighter than neurons in the control samples. Levels of βIII-tubulin in culture were quantitated at DIV14 based on the confocal acquired fluorescence (**Figure 2A**, graph). The quantitative analysis confirms that by DIV14, βIII-tubulin levels increased upon addition of tau and decreased when PH-Tau was added. Based on the observed changes in βIII-tubulin for each sample, it appears that the uptake of tau reinforces neuritic growth, while the uptake of PH-Tau triggers the loss of neurites and result in neurodegeneration similar to that observed in AD pathology.

As seen in **Figure 1**, the initial uptake of tau was blocked by atropine and when these cultures were allowed to incubate for 7 days, the neurons appeared similar to cultures without tau addition (**Figure 2A**, bottom images). Quantitative analysis of cultures at DIV14 of the exposed to tau with and without atropine pre-treatment show a significant decrease in βIII-tubulin intensity when atropine was present. The neudegeneration that was induced by exposure to PH-Tau was significantly inhibited by pre-treatment with atropine (**Figure 2A**, graph). These results indicate that muscarinic receptors play a role in the uptake of tau and that blocking them can control the uptake and therefore the overall condition of the neurons.

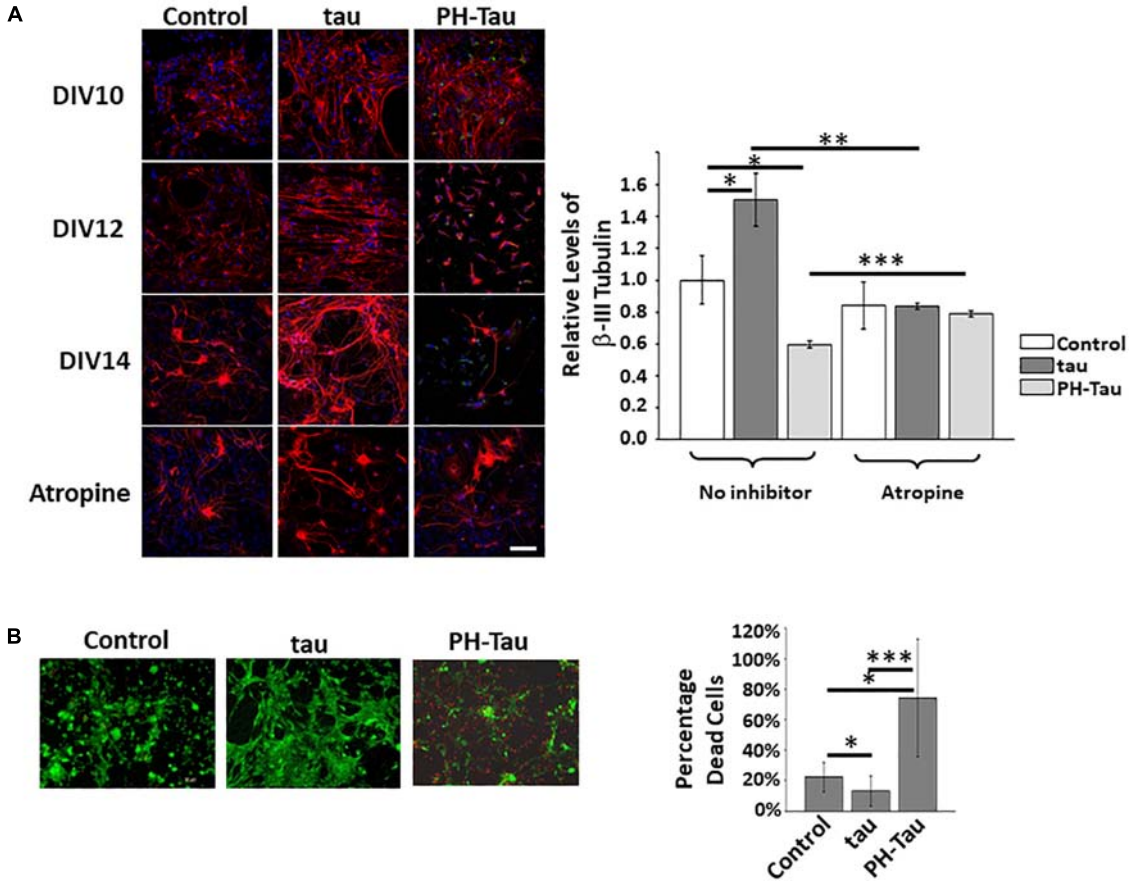

FIGURE 2 | Uptake of tau affects the neuritic morphology of neurons in culture. **(A)** Proteins were added to the neuronal culture media as described. Over a period of 7 days, the neurons were fixed and studied by confocal microscopy. The addition of WT tau appears to stabilize and organize the neuronal processes whereas PH-Tau triggers a loss if neurites over time. Pre-treatment with atropine appears to block the uptake of tau and reduces changes in neuritic morphology. Graph: Quantitation of β-III tubulin indicates that tau (dark bars) increases protein levels whereas PH-Tau (light bars) decreases the levels indicating a loss of neuritic morphology. **(B)** LIVE/DEAD Imaging of neuronal cultures after treatment with tau or PH-Tau. The number of dead cells increases significantly in cultures treated with PH-Tau. Scale bar: 20 μm. All experiments were performed three times with 10 images analyzed per experiment. (*$p < 0.05$, **$p < 0.01$, ***$p < 0.001$).

Addition of PH-Tau Results in Increased Cell Death in Neuronal Cultures

To determine if this neuronal loss was due to cell death, neuronal cultures were prepared as described and were analyzed using the LIVE/DEAD Cell Imaging Invitrogen kit (**Figure 2B**). Live neurons stain green whereas cell death is indicated by red staining. There is a significant increase in the number of red cells in the neuronal cultures treated with PH-Tau when compared to the tau-treated and control cultures. Additionally, the cells (red or green) look mostly rounded, due to a loss of neuritic projections which is consistent with the results seen above when analyzing βIII-tubulin in treated cells. The percentage of dead cells in the neuronal cultures treated with wild-type tau is decreased 50% compared to control mixed primary neuronal cultures. This may be correlated to the increase in βIII-tubulin observed above. These results indicate that the addition of wild-type tau may play a role in strengthening the health of the neurons. Conversely, addition of PH-tau results in loss of neuritic projections and induction of cellular death which is similar to phenotypes seen in neurons of AD patients.

Microglial Activation Is Triggered by the Presence of PH-Tau

An important component of inflammation seen in brains of patients with AD other tauopathies is microglia activation. Therefore we investigated if in our experiments there was a microglia modification. The neuronal cultures analyzed contain a mixture of cells including neurons, microglia, and astrocytes (**Supplementary Table S1**). Primary cerebellar neuronal cultures were treated as described above and then washed and fixed at DIV14. Immunohistochemistry was performed with antibodies against GFAP, an astrocyte marker, and Iba1, a marker for activated microglia. It is important to note that other subpopulations of microglia may stain for Iba-1 (Ito et al., 1998), however, we are looking at relative changes upon addition of tau. No significant changes were found in the levels of astrocytes as judged by the levels of GFAP

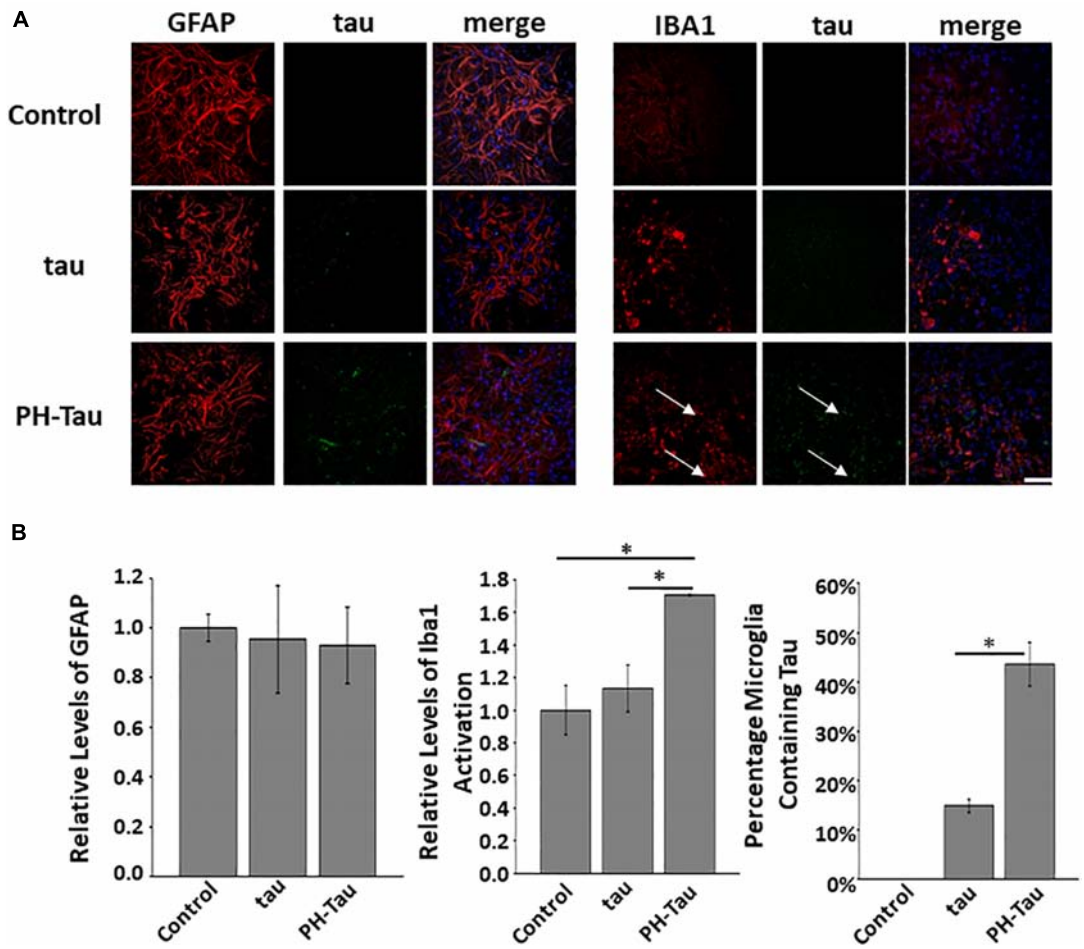

FIGURE 3 | Uptake of tau affects the microglia but not astrocytes in neuronal culture. **(A)** Proteins were added to the neuronal culture media and analyzed after 7 days. There is no significant change in the amount of GFAP fluorescence in cultures challenged with either tau or PH-Tau when compared to control. The addition of the PH-Tau but not tau appears to activate the microglia which is correlated with the uptake of tau into the cells (white arrows). Scale Bar: 20 μm. **(B)** Left: Quantitation of the GFAP levels indicates that there is no change after addition of tau to cultures. Middle: Iba1 activation indicates that PH-Tau significantly activates the microglial response. Right: This activation correlates with the amount of tau uptaken by the microglia in culture. All experiments were performed three times with 10 images analyzed per experiment. (*$p < 0.05$).

in the cultured neurons (**Figure 3A**, top). However, there was a significant increase in the activation of microglia in the cultures treated with PH-Tau when compared to control and tau-treated cultures (**Figure 3A** bottom, and **Figure 3B** left graph).

Further analysis of these cultures indicated that tau uptake into the microglia was dependent on the conformation of tau as PH-Tau was taken up to a much higher extent than the wild-type form (**Figure 3B**, right graph). The increase in microglial activation was directly correlated to the amount of tau uptake in the Iba1 active cells (**Figure 3B**, compare left and right graphs). In cultures treated with PH-Tau, 43% of activated microglia were also positive for human tau. Cultures treated with tau had significantly lower proportion of tau containing microglia which correlates to an insignificant level of Iba1 activation (**Figure 3B**, graphs). An increased microglial response could be indicative of conditions that may lead to inflammation, similar to that found in patients with AD.

PH-Tau Effectively Mimics AD P-Tau Taken From Human Brain Tissue

Alzheimer's disease P-tau, soluble, hyperphosphorylated tau extracted from the brains of human patients was used in similar experiments to those described above. The uptake of AD P-tau was shown to be similar to tau and PH-Tau and is also blocked by atropine (**Figure 4A** top and top graph). Cultures treated with PH-Tau followed a similar pattern of neurodegeneration compared to the addition of AD P-tau, showing increased βIII-tubulin at DIV10 followed by a decrease compared to control (**Figure 4A** bottom and bottom graph). Furthermore, pre-treatment with atropine resulted in very little loss of βIII-tubulin compared to control. Finally, in cultures treated with AD P-tau,

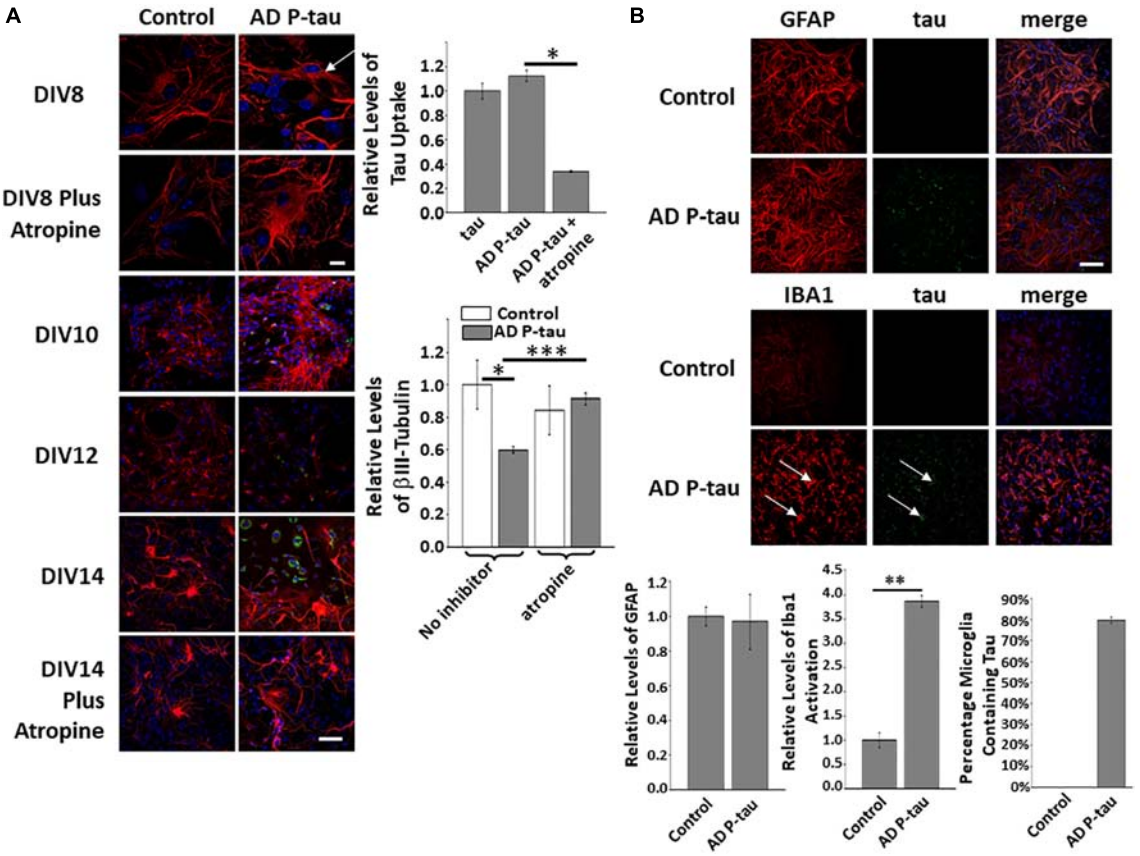

FIGURE 4 | AD P-tau addition to neuronal cultures has similar effects as PH-Tau. **(A)** AD P-tau is uptaken after incubation of 24 h and atropine blocks this uptake. The white arrow indicates where tau (green) is localized near the nucleus. No tau is observed in neurons pre-treated with atropine. Quantitation of uptake is observed in the top graph on the right. At DIV10, β-III tubulin appears to increase compared to control followed by a sharp decrease over time, see DIV12 and DIV14. The pre-treatment with atropine blocks the decrease in β-III tubulin levels. These changes are observed by confocal microscopy (images) and by quantitation of tau uptake (bar graph, top right) or β-III tubulin fluorescence (bar graph, bottom right). **(B)** Activation of microglia is observed upon addition of AD P-tau and this activation is correlated with the uptake of protein (indicated by the white arrows). GFAP levels are observed in the top row and activation of microglia is observed by an increase in fluorescence of Iba1. Bar graphs show levels of GFAP fluorescence (left), quantiation of Iba1 activation (middle) and AD P-tau uptake (right) Scale bar: 20 μm. All experiments were performed three times with 10 images analyzed per experiment. (*$p < 0.05$, **$p < 0.01$, ***$p < 0.001$).

no change was observed in GFAP staining, but microglia were activated almost four-fold more than control cells and almost 80% of these activated microglia were also positive for human tau. Taken together, these results confirm the validity of PH-Tau as a good mimic for AD P-tau and can be used as a surrogate in future studies.

Histological Evaluation of Neurodegeneration in CA3 Region of the Hippocampus

Mice received a stereotaxic intracranial injection of pure artificial cerebral spinal fluid (aCSF) or either tau or PH-Tau dissolved in aCSF. Forty-five days post injection, mice were perfused with 4% paraformaldehyde and brains were dissected and post fixed for 2 h. Coronal cryosections were stained with Haemotoxylin and Eosin (H&E). These images are representative of the (A) aCSF-injected, (B) tau-injected, and (C) PH-Tau-injected mice (**Figure 5**). The arrow indicates the injection site and the box represents the imaged area shown on the right panels. The aCSF and wild-type tau injected mice show relatively healthy neurons as demonstrated by the light appearance of neurons and their morphological integrity. Whereas the PH-Tau injected mice show relatively unhealthy neurons as evident from nuclear condensation based on intense staining and the irregular shape of the cell body.

DISCUSSION

In this study, we have observed that recombinant tau and pathological tau can be taken up from the culture media into cell lines, microglia, and neurons and that this uptake activity involves muscarinic receptors. The addition of normal tau to neurons promotes neuritic extension, while PH-Tau leads to the disruption of neuritic processes and accumulation in the somatodendritic compartment. These findings suggest a novel mechanism for the pathogenesis of hyperphosphorylated tau

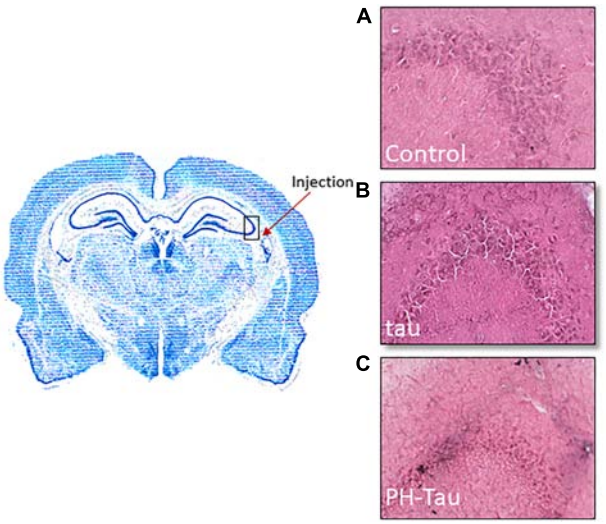

FIGURE 5 | Neurodegeneration observed in the CA3 region of the hippocampus. Stereotaxic intracranial injections were performed using **(A)** aCSF, **(B)** tau, and **(C)** PH-Tau. After 45 days, the brains were harvested and prepared by cryosectioning after fixation. The arrow indicates the injection site and the box represent the imaged area shown on the right panel. H&E staining was performed to follow changes in nerons in the CA3 region. Healthy neurons were observed in the aCSF and wild-type tau injections whereas condensed nuclei and changes in cellular morphology was observed when PH-Tau was injected.

and demonstrate additional functions for normal tau. We have further confirmed our previous study which showed that PH-Tau mimics AD P-Tau in cultured neurons. Both forms of tau caused the disruption of neuritic processes and accumulation of tau aggregates in the somatodendritic compartment.

The addition of tau to cell and neuronal cultures has been previously studied (Frost et al., 2009; Nonaka et al., 2010; Guo and Lee, 2011; Wu et al., 2013; Sanders et al., 2014; Wu et al., 2016; Evans et al., 2018). Research has indicated that the minimal unit for uptake is trimeric tau (Mirbaha et al., 2015). These tau trimers also appear to be the minimal tau toxic unit in both AD and PSP (Shafiei et al., 2017). Native gel electrophoresis indicates that the tau and PH-Tau that we are using are both mixtures of oligomeric states but that PH-Tau appears to be composed of a greater number of higher order complexes (**Supplementary Figure S3**). Furthermore, when seeded with AD P-tau the number of higher oligomeric complexes increases indicating the seeding ability of pathological tau. Our experiments show that normal tau is taken up similarly to PH-Tau. However, only PH-Tau exhibited a toxic effect indicating that it may not be the size of the aggregate that is toxic, but the phosphorylation state of tau.

To determine the importance of muscarinic receptors in intracellular uptake of tau, we added normal tau or PH-Tau to the culture media of HEK293 cells or CHO cells. Uptake of tau was only observed in HEK293 cells. Unlike HEK293 cells, CHO cells do not naturally express muscarinic receptors. Transfection of CHO cells with either M1, M3, or M1/M3 muscarinic receptors indicated that the presence of these receptors was necessary for tau uptake (**Figure 1D**). To further investigate the role of muscarinic receptors, cell cultures were pre-treated with atropine, a known muscarinic receptor antagonist, prior to the addition of tau. Atropine blocked tau uptake in HEK293 cells, indicating that the presence of muscarinic receptors is correlated with tau uptake. It is known that cortical neurons, including hippocampal cells have M1 and M3 muscarinic receptors and so do glial cells (Levey et al., 1994). Neuronal cultures were used to determine if both forms of tau could be uptaken in the brain. Tau, PH-Tau, and AD P-tau were all uptaken at similar levels and this uptake was blocked up to 80% by atropine (**Figures 1B,C**, **4**). The M1 anatagonist pirenzepine blocked uptake in a similar fashion as atropine, but AF-DX116 and pertussis toxin, were both unable to block uptake. These results implicate M1 receptors in the uptake of tau (**Figure 1C**). Interestingly, a cholinesterase inhibitor is one of the medications prescribed to ameliorate some of the cognitive deficits of AD (Birks, 2006; Soukup et al., 2017). The present findings that atropine blocked the PH-Tau uptake could provide an explanation for the limited efficacy of this therapeutic intervention. Acetylcholine is one of the transmitters in the cortical and hippocampal circuits, and because PH-Tau transfer to other neurons may be blocked, other, non-effected neurons, could maintain the synaptic transmission prolonging persistence of acetylcholine in the synaptic cleft. Complementary to this cholinergic mechanism was the study of Schmitz et al. (2016), patients with early stages of AD, clinically silent, have abnormal degeneration of cholinergic neurons.

From our experimental evidence, neurons treated with wild-type tau that were cultured until DIV14 were more organized and had many more aligned neuritic processes compared to the untreated neurons (**Figure 2**). These findings suggest that extra-neuronal tau might be a physiological signal. Although the presence of tau in the extracellular space is described, there is no consensus about physiological function for this localization of tau (Chai et al., 2012; Magnoni et al., 2012; Karch et al., 2013; Bright et al., 2015; Kanmert et al., 2015). Tau increases the electrical activity of iPSC-derived or primary cortical neurons, in line with the finding that tau leads to intracellular calcium increase (Gomez-Ramos et al., 2008; Bright et al., 2015). As such, extracellular tau may play an important neuromodulatory role for cognition. In agreement with our results, Biundo et al. (2018) have shown that tau depletion in a mouse model led to age-dependent deficits in memory and synaptic plasticity, correlating with levels of normal tau expression. Considering the potential beneficial role of normal tau with respect to the electrophysiological functioning and morphology of neurons, our study further explored the effects of pathological tau. Addition of PH-Tau or AD P-tau to the culture medium induced a retraction of the neuritic processes (**Figures 2**, **4**). This retraction by PH-Tau is noticeable 5 days (DIV12) after exposure (**Figure 2**). Similarly, at 45 days post injection of mice injected with PH-Tau, the neuronal nuclei began to condense and the cell bodies did not appear rounded (**Figure 5**). Though uptake of wild-type tau and PH-Tau both appear to be mediated via similar muscarinic receptors, the effects on neurons and microglia are opposite in nature. The downstream effects of each of these proteins should be further investigated.

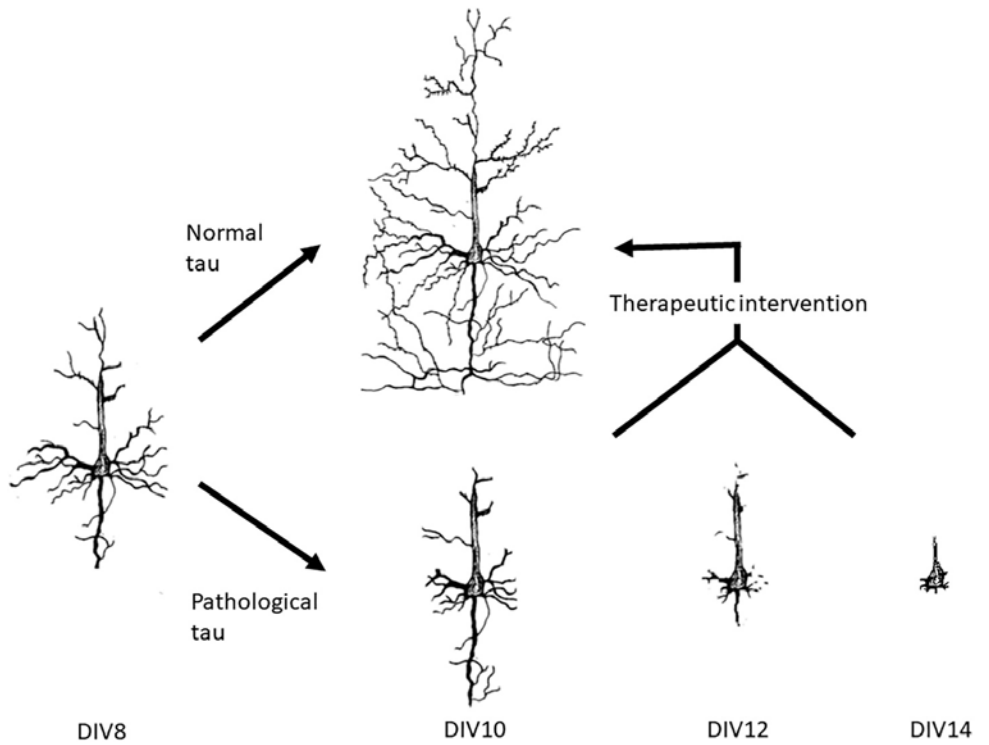

FIGURE 6 | Neuronal culture model system for the development of therapeutic interventions. We have shown that the neuronal culture system that we use can mimic neurodegeneration within 2 weeks of preparation. At DIV7, tau proteins are added to the culture medium for 24 h before exchanging the media to tau free media. Uptake of the proteins can be observed at DIV8. By DIV10, no tau is observed in the normal tau cultures, but the levels of βIII-tubulin increase. Cultures treated with pathogenic tau began to degenerate by DIV10 with significant loss of βIII-tubulin by DIV14. This system can be used to try out novel therapeutics to either halt degeneration and/or return the neurons to their original form.

Microglia activation, as indicated by an increase in Iba1 staining in cultures, after treatment with PH-Tau and ADP-Tau, while astrocytes were left unchanged (**Figures 3**, **4**). This may indicate a response to the presence of pathological tau. Microglia are capable of taking up extracellular tau and have the ability to degrade the protein to remove it from the matrix (Bolós et al., 2016). Murine microglial cells from young mice have been used to clear tau from brain slices of P301S mice and from AD patients (Luo et al., 2015). Other studies have shown that microglia cluster in tau-rich regions indicating that they may play a role in the clearance of pathogenic tau (Bolós et al., 2016; Davies et al., 2017). Interestingly, there is a report of an increase in microglia that express muscarinic receptors, in particular M3, in AD mouse models (Pannell et al., 2016). Tau has been shown to bind to M1 and M3 mucarinic receptors (Gomez-Ramos et al., 2008). Therefore, activation of microglial cells that express M1 and M3 muscarinic receptors in the presence of extracellular tau for clearance further supports our findings that these specific receptor subtypes are important for tau uptake.

In this report, novel function and pathophysiology of tau in the extracellular space were investigated and neurons treated with pathological tau mimic the neurodegeneration observed in AD (**Figure 6**). This versatile model allows for the potential development of high throughput screening of novel therapeutics against tau-induced neurodegeneration. We showed that the uptake of tau is correlated with microtubule stabilization, and that the uptake of wild-type tau can increase stabilization and organization of microtubules whereas uptake of PH-Tau causes destabilization leading to neurite retraction. With these neuronal cultures therapeutic interventions can be tried at varying points of neurodegeneration with the hope of allowing the neurites to regenerate over time. Further analysis is necessary to understand the mechanisms of tau propagation, nucleation of oligomerization and induction of neurodegeneration.

With the present findings we hypothesize that under normal physiological conditions, tau is released in the extracellular space, uptaken by other neuronal cells in a muscarinic-receptor mediated pathway, and the connectivity of the neurons is reinforced. Early onset of AD progression begins with the appearance of pathological tau in a subset of neurons that can be secreted in the microenvironment, spreading its toxicity to the neighboring cells. Tau can be released as a naked pathological tau aggregates or in vesicles or exosomes. Pathological tau uptake by microglial cells induces activation, initiating an inflammatory response. Pathological tau exhibits a prion-like behavior inducing conformational changes in normal tau, disrupting microtubules or through other pathways, causing neurodegeneration. This sequence of events suggests a mechanism of propagation that exacerbates pathological conditions and that it could be a target for therapeutic intervention.

DATA AVAILABILITY

The datasets generated for this study are available on request to the corresponding author.

ETHICS STATEMENT

Animal Subjects: The animal study was reviewed and approved by the College of Staten Island (CSI) Office for the Protection of Research subjects *via* the Institutional Animal Care and Use Committee.

AUTHOR CONTRIBUTIONS

All authors contributed in the critical discussion of the experimental designs, results, and writing of the manuscript. VM performed the protein purifications, cell and primary neuronal culture, and immunocytochemistry and confocal imaging. LC performed the native gel electrophoresis and participated in the recombinant protein purification. AE-HM, AS, and AEL participated in the *in vivo* recombinant tau and PH-Tau stereotactic injection. GP participated in the design of the pharmacological inhibition of muscarinic receptors experiments. AA supervised the research project.

FUNDING

This study was supported at least in part by the private donation by Jeff Lin, as well as grants from the NIH (1R15AG058197-01 to AA) and PSC CUNY (60290-00 48 to AA).

ACKNOWLEDGMENTS

We are grateful to Drs. Robert Marraccino, Fred Naider, and Marta Hallak for their critical editing of the manuscript and Dr. Frida Kleiman for providing the GST expression plasmids. Tau 12 and Tau 13 antibodies were a gift from Dr. Nicholas Kanaan at the Michigan State University (originally created by Dr. Lester Binder at the Northwestern University). We are also grateful to Dr. Khalid Iqbal for providing the isolated AD P-tau and his expert opinion on drug discovery.

SUPPLEMENTARY MATERIAL

The Supplementary Material for this article can be found online at: https://www.frontiersin.org/articles/10.3389/fncel.2019.00403/full#supplementary-material

REFERENCES

Ahmed, Z., Cooper, J., Murray, T. K., Garn, K., McNaughton, E., Clarke, H., et al. (2014). A novel in vivo model of tau propagation with rapid and progressive neurofibrillary tangle pathology: the pattern of spread is determined by connectivity, not proximity. *Acta Neuropathol.* 127, 667–683. doi: 10.1007/s00401-014-1254-6

Alonso, A. D., Beharry, C., Corbo, C. P., and Cohen, L. S. (2016). Molecular mechanism of prion-like tau-induced neurodegeneration. *Alzheimers Dement.* 12, 1090–1097. doi: 10.1016/j.jalz.2015.12.014

Alonso, A. D., Di Clerico, J., Li, B., Corbo, C. P., Alaniz, M. E., Grundke-Iqbal, I., et al. (2010). Phosphorylation of tau at Thr212. *J. Biol. Chem.* 285, 30851–30860. doi: 10.1074/jbc.M110.110957

Alonso, A. D., Grundke-Iqbal, I., and Iqbal, K. (1996). Alzheimer's disease hyperphosphorylated tau sequesters normal tau into tangles of filaments and disassembles microtubules. *Nat. Med.* 2, 783–787. doi: 10.1038/nm0796-783

Avila, J., Gomez-Ramos, A., and Bolos, M. (2015). AD genetic risk factors and tau spreading. *Front. Aging Neurosci.* 7:99. doi: 10.3389/fnagi.2015.00099

Beharry, C., Alaniz, M. E., and Alonso, A. D. (2013). Expression of Alzheimer-like pathological human tau induces a behavioral motor and olfactory learning deficit in Drosophila melanogaster. *J. Alzheimers. Dis.* 37, 539–550. doi: 10.3233/JAD-130617

Beharry, C., Cohen, L. S., Di, J., Ibrahim, K., Briffa-Mirabella, S., and Alonso, A. D. (2014). Tau-induced neurodegeneration: mechanisms and targets. *Neurosci. Bull.* 30, 346–358. doi: 10.1007/s12264-013-1414-z

Birks, J. (2006). Cholinesterase inhibitors for Alzheimer's disease. *Cochrane Database Syst. Rev.* 25:CD005593.

Biundo, F., Del Prete, D., Zhang, H., Arancio, O., and D'Adamio, L. (2018). A role for tau in learning, memory and synaptic plasticity. *Sci. Rep.* 8:184. doi: 10.1038/s41598-018-21596-3

Bolmont, T., Clavaguera, F., Meyer-Luehmann, M., Herzig, M. C., Radde, R., Staufenbiel, M., et al. (2007). Induction of tau pathology by intracerebral infusion of amyloid-beta -containing brain extract and by amyloid-beta deposition in APP x Tau transgenic mice. *Am. J. Pathol.* 171, 2012–2020. doi: 10.2353/ajpath.2007.070403

Bolós, M., Llorens-Martín, M., Jurado-Arjona, J., Hernández, F., Rábano, A., and Avila, J. (2016). Direct evidence of internalization of tau by microglia in vitro and in vivo. *J. Alzheimers Dis.* 50, 77–87. doi: 10.3233/JAD-150704

Braak, H., and Braak, E. (1991). Neuropathological stageing of Alzheimer-related changes. *Acta Neuropathol.* 82, 239–259. doi: 10.1007/bf00308809

Bright, J., Hussain, S., Dang, V., Wright, S., Cooper, B., Byun, T., et al. (2015). Human secreted tau increases amyloid-beta production. *Neurobiol. Aging* 36, 693–709. doi: 10.1016/j.neurobiolaging.2014.09.007

Cevher, M. A., Zhang, X., Fernandez, S., Kim, S., Baquero, J., Nilsson, P., et al. (2010). Nuclear deadenylation/polyadenylation factors regulate 3' processing in response to DNA damage. *EMBO J.* 29, 1674–1687. doi: 10.1038/emboj.2010.59

Chai, X., Dage, J. L., and Citron, M. (2012). Constitutive secretion of tau protein by an unconventional mechanism. *Neurobiol. Dis.* 48, 356–366. doi: 10.1016/j.nbd.2012.05.021

Clavaguera, F., Akatsu, H., Fraser, G., Crowther, R. A., Frank, S., Hench, J., et al. (2013). Brain homogenates from human tauopathies induce tau inclusions in mouse brain. *Proc. Natl. Acad. Sci. U.S.A.* 110, 9535–9540. doi: 10.1073/pnas.1301175110

Clavaguera, F., Bolmont, T., Crowther, R. A., Abramowski, D., Frank, S., Probst, A., et al. (2009). Transmission and spreading of tauopathy in transgenic mouse brain. *Nat. Cell Biol.* 11, 909–913. doi: 10.1038/ncb1901

Clavaguera, F., Grueninger, F., and Tolnay, M. (2014). Intercellular transfer of tau aggregates and spreading of tau pathology: implications for therapeutic strategies. *Neuropharmacology* 76(Pt A), 9–15. doi: 10.1016/j.neuropharm.2013.08.037

Davies, D. S., Ma, J., Jegathees, T., and Goldsbury, C. (2017). Microglia show altered morphology and reduced arborization in human brain during aging and Alzheimer's disease. *Brain Pathol.* 27, 795–808. doi: 10.1111/bpa.12456

Di, J., Cohen, L. S., Corbo, C. P., Phillips, G. R., El Idrissi, A., and Alonso, A. D. (2016). Abnormal tau induces cognitive impairment through two different mechanisms: synaptic dysfunction and neuronal loss. *Sci. Rep.* 6:20833. doi: 10.1038/srep20833

Evans, L. D., Wassmer, T., Fraser, G., Smith, J., Perkinton, M., Billinton, A., et al. (2018). Extracellular monomeric and aggregated tau efficiently enter human neurons through overlapping but distinct pathways. *Cell Rep.* 22, 3612–3624. doi: 10.1016/j.celrep.2018.03.021

Frost, B., Jacks, R. L., and Diamond, M. I. (2009). Propagation of tau misfolding from the outside to the inside of a cell. *J. Biol. Chem.* 284, 12845–12852. doi: 10.1074/jbc.M808759200

Goedert, M., Clavaguera, F., and Tolnay, M. (2010). The propagation of prion-like protein inclusions in neurodegenerative diseases. *Trends Neurosci.* 33, 317–325. doi: 10.1016/j.tins.2010.04.003

Gomez-Ramos, A., Diaz-Hernandez, M., Rubio, A., Diaz-Hernandez, J. I, and Miras-Portugal, M. (2009). Characteristics and consequences of muscarinic receptor activation by tau protein. *Eur. Neuropsychopharmacol.* 19, 708–717. doi: 10.1016/j.euroneuro.2009.04.006

Gomez-Ramos, A., Diaz-Hernandez, M., Rubio, A., Miras-Portugal, M. T., and Avila, J. (2008). Extracellular tau promotes intracellular calcium increase through M1 and M3 muscarinic receptors in neuronal cells. *Mol. Cell. Neurosci.* 37, 673–681. doi: 10.1016/j.mcn.2007.12.010

Grundke-Iqbal, I., Iqbal, K., Tung, Y. C., and Wisniewski, H. M. (1984). Alzheimer paired helical filaments: immunochemical identification of polypeptides. *Acta Neuropathol.* 62, 259–267. doi: 10.1007/bf00687607

Guo, J. L., and Lee, V. M. (2011). Seeding of normal Tau by pathological Tau conformers drives pathogenesis of Alzheimer-like tangles. *J. Biol. Chem.* 286, 15317–15331. doi: 10.1074/jbc.M110.209296

Holmes, B. B., and Diamond, M. I. (2014). Prion-like properties of Tau protein: the importance of extracellular Tau as a therapeutic target. *J. Biol. Chem.* 289, 19855–19861. doi: 10.1074/jbc.R114.549295

Hu, W., Zhang, X., Xie, S., Chen, Y. H., Liu, F., and Iqbal, K. (2016). Hyperphosphorylation determines both the spread and the morphology of tau pathology. *Alzheimer's Dement.* 12, 1066–1077. doi: 10.1016/j.jalz.2016.01.014

Hyman, B. T., Van Hoesen, G. W., Damasio, A. R., and Barnes, C. L. (1984). Alzheimer's disease: cell-specific pathology isolates the hippocampal formation. *Science* 225, 1168–1170. doi: 10.1126/science.6474172

Iba, M., Guo, J. L., McBride, J. D., Zhang, B., Trojanowski, J. Q., and Lee, V. M. (2013). Synthetic tau fibrils mediate transmission of neurofibrillary tangles in a transgenic mouse model of Alzheimer's-like tauopathy. *J. Neurosci.* 33, 1024–1037. doi: 10.1523/jneurosci.2642-12.2013

Iqbal, K., Liu, F., and Gong, C. X. (2016). Tau and neurodegenerative disease: the story so far. *Nat. Rev. Neurol.* 12, 15–27. doi: 10.1038/nrneurol.2015.225

Ito, D., Imai, Y., Ohsawa, K., Nakajima, K., Fukuuchi, Y., and Kohsaka, S. (1998). Microglia-specific localisation of a novel calcium binding protein. Iba1. *Brain Res. Mol. Brain Res.* 57, 1–9. doi: 10.1016/s0169-328x(98)00040-0

Kanmert, D., Cantlon, A., Muratore, C. R., Jin, M., O'Malley, T. T., Lee, G., et al. (2015). C-terminally truncated forms of tau, but not full-length tau or its c-terminal fragments, are released from neurons independently of cell death. *J. Neurosci.* 35, 10851–10865. doi: 10.1523/JNEUROSCI.0387-15.2015

Karch, C. M., Jeng, A. T., and Goate, A. M. (2013). Calcium phosphatase calcineurin influences tau metabolism. *Neurobiol. Aging* 34, 374–386. doi: 10.1016/j.neurobiolaging.2012.05.003

Lasagna-Reeves, C. A., Castillo-Carranza, D. L., Sengupta, U., Sarmiento, J., Troncoso, J., Jackson, G. R., et al. (2012). Identification of oligomers at early stages of tau aggregation in Alzheimer's disease. *FASEB J.* 26, 1946–1959. doi: 10.1096/fj.11-199851

Levey, A. I., Edmunds, S. M., Heilman, C. J., Desmond, T. J., and Frey, K. A. (1994). Localization of muscarinic m3 receptor protein and M3 receptor binding in rat brain. *Neuroscience* 63, 207–221. doi: 10.1016/0306-4522(94)90017-5

Lin, Y. C., Boone, M., Meuris, L., Lemmens, I., Van Roy, N., Soete, A., et al. (2014). Genome dynamics of the human embryonic kidney 293 lineage in response to cell biology manipulations. *Nat. Commun.* 5:4767. doi: 10.1038/ncomms5767

Luo, W., Liu, W., Hu, X., Hanna, M., Caravaca, A., and Paul, S. M. (2015). Microglial internalization and degradation of pathological tau is enhanced by an anti-tau monoclonal antibody. *Sci. Rep.* 5:11161. doi: 10.1038/srep11161

Magnoni, S., Esparza, T. J., Conte, V., Carbonara, M., Carrabba, G., Holtzman, D. M., et al. (2012). Tau elevations in the brain extracellular space correlate with reduced amyloid-beta levels and predict adverse clinical outcomes after severe traumatic brain injury. *Brain* 135(Pt 4), 1268–1280. doi: 10.1093/brain/awr286

Mirbaha, H., Holmes, B. B., Sanders, D. W., Bieschke, J., and Diamond, M. I. (2015). Tau Trimers are the minimal propagation unit spontaneously internalized to seed intracellular aggregation. *J. Biol. Chem.* 290, 14893–14903. doi: 10.1074/jbc.M115.652693

Mudher, A., Colin, M., Dujardin, S., Medina, M., Dewachter, I., Alavi Naini, S. M., et al. (2017). What is the evidence that tau pathology spreads through prion-like propagation? *Acta Neuropathol. Commun.* 5:99. doi: 10.1186/s40478-017-0488-7

Nonaka, T., Watanabe, S. T., Iwatsubo, T., and Hasegawa, M. (2010). Seeded aggregation and toxicity of {alpha}-synuclein and tau: cellular models of neurodegenerative diseases. *J. Biol. Chem.* 285, 34885–34898. doi: 10.1074/jbc.m110.148460

Pannell, M., Meier, M. A., Szulzewsky, F., Matyash, V., Endres, M., Kronenberg, G., et al. (2016). The subpopulation of microglia expressing functional muscarinic acetylcholine receptors expands in stroke and Alzheimer's disease. *Brain Struct. Funct.* 221, 1157–1172. doi: 10.1007/s00429-014-0962-y

Sanders, D. W., Kaufman, S. K., DeVos, S. L., Sharma, A. M., Mirbaha, H., Li, A., et al. (2014). Distinct tau prion strains propagate in cells and mice and define different tauopathies. *Neuron* 82, 1271–1288. doi: 10.1016/j.neuron.2014.04.047

Schmitz, T. W., Nathan Spreng, R., and Alzheimer's Disease Neuroimaging, I. (2016). Basal forebrain degeneration precedes and predicts the cortical spread of Alzheimer's pathology. *Nat. Commun.* 7:13249. doi: 10.1038/ncomms13249

Shafer, S. H., and Williams, C. L. (2004). Elevated Rac1 activity changes the M3 muscarinic acetylcholine receptor-mediated inhibition of proliferation to induction of cell death. *Mol. Pharmacol.* 65, 1080–1091. doi: 10.1124/mol.65.5.1080

Shafiei, S. S., Guerrero-Munoz, M. J., and Castillo-Carranza, D. L. (2017). Tau oligomers: cytotoxicity, propagation, and mitochondrial damage. *Front Aging Neurosci.* 9:83. doi: 10.3389/fnagi.2017.00083

Shaw, G., Morse, S., Ararat, M., and Graham, F. L. (2002). Preferential transformation of human neuronal cells by human adenoviruses and the origin of HEK 293 cells. *FASEB J.* 16, 869–871. doi: 10.1096/fj.01-0995fje

Soukup, O., Winder, M., Killi, U. K., Wsol, V., Jun, D., Kuca, K., et al. (2017). Acetylcholinesterase inhibitors and drugs acting on muscarinic receptors- potential crosstalk of cholinergic mechanisms during pharmacological treatment. *Curr. Neuropharmacol.* 15, 637–653. doi: 10.2174/1570159X14666160607212615

Takeda, S. (2019). Progression of Alzheimer's disease, tau propagation, and its modifiable risk factors. *Neurosci. Res.* 141, 36–42. doi: 10.1016/j.neures.2018.08.005

Wu, J. W., Herman, M., Liu, L., Simoes, S., Acker, C. M., Figueroa, H., et al. (2013). Small misfolded Tau species are internalized via bulk endocytosis and anterogradely and retrogradely transported in neurons. *J. Biol. Chem.* 288, 1856–1870. doi: 10.1074/jbc.M112.394528

Wu, J. W., Hussaini, S. A., Bastille, I. M., Rodriguez, G. A., Mrejeru, A., Rilett, K., et al. (2016). Neuronal activity enhances tau propagation and tau pathology in vivo. *Nat. Neurosci.* 19, 1085–1092. doi: 10.1038/nn.4328

Conflict of Interest Statement: The authors declare that the research was conducted in the absence of any commercial or financial relationships that could be construed as a potential conflict of interest.

frontiers in Cellular Neuroscience

REVIEW
published: 20 September 2019
doi: 10.3389/fncel.2019.00428

Novel Cellular Functions of Very Long Chain-Fatty Acids: Insight From ELOVL4 Mutations

Ferenc Deák[1,2,3], *Robert E. Anderson*[1,2,4,5,6], *Jennifer L. Fessler*[6] *and David M. Sherry*[2,6,7]*

[1] *Department of Geriatric Medicine, Reynolds Oklahoma Center on Aging, University of Oklahoma Health Sciences Center, Oklahoma City, OK, United States,* [2] *Oklahoma Center for Neurosciences, University of Oklahoma Health Sciences Center, Oklahoma City, OK, United States,* [3] *Harold Hamm Diabetes Center, University of Oklahoma Health Sciences Center, Oklahoma City, OK, United States,* [4] *Dean McGee Eye Institute, University of Oklahoma Health Sciences Center, Oklahoma City, OK, United States,* [5] *Department of Ophthalmology, University of Oklahoma Health Sciences Center, Oklahoma City, OK, United States,* [6] *Department of Cell Biology, University of Oklahoma Health Sciences Center, Oklahoma City, OK, United States,* [7] *Department of Pharmaceutical Sciences, University of Oklahoma Health Sciences Center, Oklahoma City, OK, United States*

OPEN ACCESS

Edited by:
Gabriela Alejandra Salvador, Universidad Nacional del Sur, Argentina

Reviewed by:
Marta I. Aveldaño, CONICET Bahía Blanca, Argentina
Oscar Monroig, Spanish National Research Council (CSIC), Spain

***Correspondence:**
David M. Sherry
david-sherry@ouhsc.edu

Specialty section:
This article was submitted to Cellular Neuropathology, a section of the journal Frontiers in Cellular Neuroscience

Received: *28 March 2019*
Accepted: *06 September 2019*
Published: *20 September 2019*

Citation:
Deák F, Anderson RE, Fessler JL and Sherry DM (2019) Novel Cellular Functions of Very Long Chain-Fatty Acids: Insight From ELOVL4 Mutations. Front. Cell. Neurosci. 13:428. doi: 10.3389/fncel.2019.00428

Elongation of Very Long chain fatty acids-4 (ELOVL4) protein is a member of the ELOVL family of fatty acid elongases that is collectively responsible for catalyzing formation of long chain fatty acids. ELOVL4 is the only family member that catalyzes production of Very Long Chain Saturated Fatty Acids (VLC-SFA) and Very Long Chain Polyunsaturated Fatty Acids (VLC-PUFA) with chain lengths ≥28 carbons. ELOVL4 and its VLC-SFA and VLC-PUFA products are emerging as important regulators of synaptic signaling and neuronal survival in the central nervous system (CNS). Distinct sets of mutations in *ELOVL4* cause three different neurological diseases in humans. Heterozygous inheritance of one set of autosomal dominant *ELOVL4* mutations that leads to truncation of the ELOVL4 protein causes Stargardt-like macular dystrophy (STGD3), an aggressive juvenile-onset retinal degeneration. Heterozygous inheritance of a different set of autosomal dominant *ELOVL4* mutations that leads to a full-length protein with single amino acid substitutions causes spinocerebellar ataxia 34 (SCA34), a late-onset neurodegenerative disease characterized by gait ataxia and cerebellar atrophy. Homozygous inheritance of a different set of *ELOVL4* mutations causes a more severe disease with infantile onset characterized by seizures, spasticity, intellectual disability, ichthyosis, and premature death. ELOVL4 is expressed widely in the CNS and is found primarily in neurons. ELOVL4 is expressed in cell-specific patterns within different regions of the CNS that are likely to be related to disease symptoms. In the retina, ELOVL4 is expressed exclusively in photoreceptors and produces VLC-PUFA that are incorporated into phosphatidylcholine and enriched in the light sensitive membrane disks of the photoreceptor outer segments. VLC-PUFA are enzymatically converted into "elovanoid" compounds that appear to provide paracrine signals that promote photoreceptor and neuronal survival. In the brain, the main ELOVL4 products are VLC-SFA that are incorporated into sphingolipids and enriched in synaptic vesicles,

where they regulate kinetics of presynaptic neurotransmitter release. Understanding the function of ELOVL4 and its VLC-SFA and VLC-PUFA products will advance our understanding of basic mechanisms in neural signaling and has potential for developing novel therapies for seizure and neurodegenerative diseases.

Keywords: very long chain-fatty acids, seizure, neurodegeneration, spinocerebellar ataxia, Stargardt's-like macular dystrophy

INTRODUCTION

Lipids are critical biochemical components of the central nervous system (CNS) that are essential for proper CNS function. The lipid composition of the brain is unique and exceedingly diverse (Sastry, 1985; Bozek et al., 2015; Hopiavuori et al., 2017; Hopiavuori et al., 2018). Aberrant lipid composition, metabolism, and signaling in the CNS is associated with neuropsychiatric and neurodegenerative diseases. Aging also is known to alter lipid composition in the brain (see Sebastiao et al., 2013; Muller et al., 2015; Lauwers et al., 2016; Spassieva et al., 2016). In general, lipids are known as key participants in membrane structures and for their role in cell signaling (Bazinet and Laye, 2014; Sanchez-Alegria et al., 2018). Recently, lipids also have been suggested to serve as regulators of synaptic transmission (Marza et al., 2008; Brodde et al., 2012; Sebastiao et al., 2013; Carta et al., 2014; Lauwers et al., 2016), and a number of lipid metabolism enzymes have been localized to synaptic terminals where they would be positioned to provide local regulation of synaptic transmission (Cremona et al., 1999; Di Paolo et al., 2004; Rohrbough et al., 2004). However, these studies focused primarily on lipids with fatty acid chains of 16–22 carbons in length. Our understanding of the functions of fatty acids with longer chain lengths in the nervous system is more limited.

Recent studies have revealed novel functions for Very Long Chain-Fatty Acids (VLC-FA), defined by a chain length of 28 or more carbons, in neural signaling (Bennett et al., 2014a,b; Bhattacharjee et al., 2017; Jun et al., 2017; Hopiavuori et al., 2018). This review will discuss the seven known members of the Elongation of Very Long Chain-Fatty Acids (ELOVL) family of enzymes responsible for elongation of saturated and polyunsaturated fatty acids (**Figure 1**). In particular, we will focus on ELOVL4 and the role of its Very Long Chain-Saturated Fatty Acids (VLC-SFA) and Very Long Chain-PolyUnsaturated Fatty Acids (VLC-PUFA) products in neurological disease, synaptic transmission, and neuronal survival in the CNS. By convention, *ELOVL4* refers to the human gene, *Elovl4* to the non-human mammalian gene, and *elovl4* to non-mammalian gene. ELOVL4 refers to the protein in all species.

The ELOVL Family of Fatty Acid Elongases

The ELOVL family of enzymes in mammals is comprised of seven members that all reside in the endoplasmic reticulum (ER) and are thought to form a multimeric complex (Okuda et al., 2010). Together, the ELOVL family is responsible for the elongation of saturated and unsaturated fatty acids (Guillou et al., 2010; Kihara, 2012; Yu et al., 2012). ELOVL4, specifically, is essential for the biosynthesis of VLC-SFA and VLC-PUFA (Agbaga et al., 2008). Each member of the ELOVL family is a multi-pass transmembrane protein containing a large ELO domain with a high degree of homology to a family of fatty acid elongases in yeast (Zhang et al., 2003), an N-linked glycosylation near the N-terminus, a catalytic histidine motif (HXXHH) that is essential for the elongase function (Logan et al., 2014), and a di-lysine ER-retention motif (KXKXX) located in the C-terminus domain that is required for proper localization to the ER (Logan et al., 2013). The initial topological model of ELOVL protein structure, based on ELOVL4, predicted five transmembrane domains (SOUSI model; **Figure 2A**; Zhang et al., 2001; Molday and Zhang, 2010). More recent modeling, using a variety of bioinformatics tools (MEMSAT-SVM, MEM-SAT3; ENSEMBLE, Phobius, and TMHMM2 models; **Figure 2B**), predicts seven transmembrane domains (Ozaki et al., 2015). In both models, the N-terminus and N-linked glycosylation site are located in the ER lumen, and the C-terminus ER-retention motif is located on the cytoplasmic side of the ER membrane. A key difference between the 5- and 7-membrane spanning topologies is the placement of the catalytic histidine motif. The five transmembrane spanning topology places this motif in or near the ER lumen close to the start of the third transmembrane domain. The seven transmembrane spanning topology places this motif near the beginning of the fourth transmembrane domain on the cytoplasmic side of the ER membrane. The precise structure of the ELOVL proteins remains unresolved as no crystal structures of any full-length ELOVL proteins are available to date.

Fatty acid elongation occurs by cycling through a four step process (condensation, reduction, dehydration, and reduction), with two carbon atoms added through each cycle. Members of the ELOVL family catalyze the first step, a condensation reaction between a fatty acyl-CoA and malonyl-CoA (Pereira et al., 2004; Jakobsson et al., 2006). The second and fourth reduction steps are catalyzed by 3-ketoacyl-CoA and trans-2,3-enoyl-CoA reductases (KAR and TER), respectively, the third dehydration step is catalyzed by 3-hydroxyacyl-CoA dehydratases (HACD1-4) (**Figure 3**; Moon and Horton, 2003; Konishi et al., 2010). The ELOVL family proteins are thought to form hetero-oligomeric complexes in the ER (Okuda et al., 2010).

Complexing of ELOVL proteins is important to their function (Okuda et al., 2010; Logan et al., 2014). ELOVL4 is known to homodimerize, with dimerization of WT and STDG3 mutant ELOVL4 causing mislocalization of the complex away from the ER (Grayson and Molday, 2005; Molday and Zhang, 2010) and exerting a dominant negative effect on enzyme function

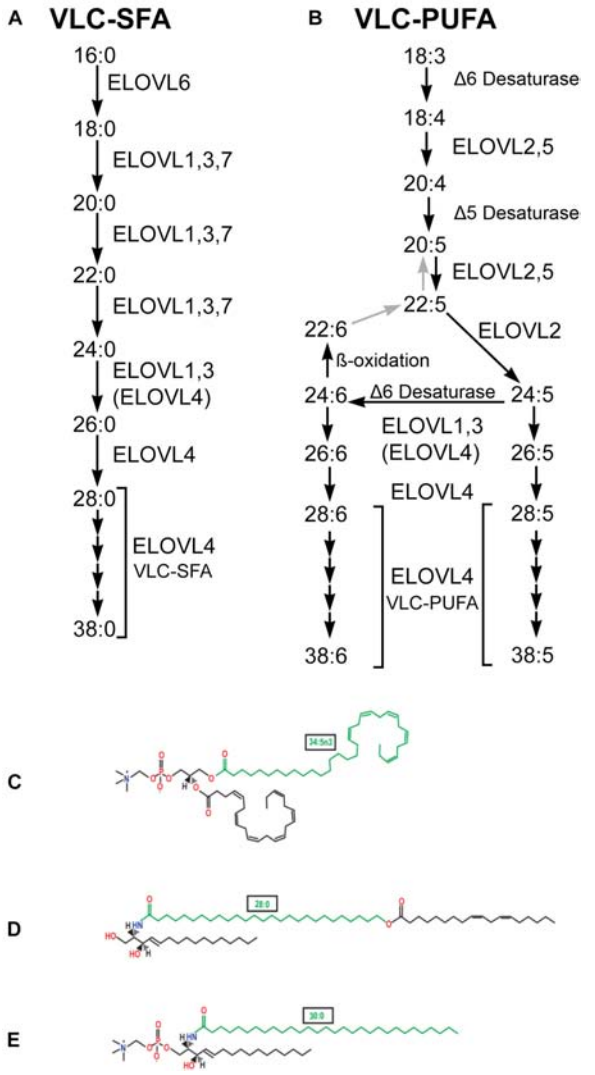

FIGURE 1 | VLC-SFA and VLC-PUFA elongation pathways. **(A)** VLC-SFA biosynthesis pathway. Elongation steps are performed by ELOVL1-7. Although some ELOVL family members catalyze specific steps in VLC-SFA synthesis, others are multifunctional and may catalyze multiple steps. Elongation of C24 substrates also may be performed by ELOVL4 (ELOVL4). **(B)** VLC-PUFA biosynthesis pathway. Desaturation and elongation steps are performed by ELOVL1-5, Δ5 Desaturase (fatty acid desaturase-1, FADS1), and Δ6 desaturase (fatty acid desaturase-2, FADS2) as indicated. Although some ELOVL family members catalyze specific steps in VLC-PUFA synthesis, others are multifunctional and may catalyze multiple steps. Elongation of C24 substrates also may be performed by ELOVL4 (ELOVL4). **(C)** VLC-PUFA are incorporated into phosphatidylcholine in the retina. Example shown contains the VLC-PUFA, 34:5n3 (green), and the long chain-PUFA, 22:6n3 (DHA). **(D)** VLC-SFA are incorporated into ω-O-acylceramides in the skin. Example shown contains the VLC-SFA, 28:0 (green) ω-O-linked with 18:2n3. **(E)** VLC-SFA are incorporated into sphingolipids in the brain. Example shown shows sphingomyelin containing the VLC-SFA, 30:0 (green) (panels C–E from Hopiavuori et al., 2019, used with permission).

(Logan et al., 2014). In addition, ELOVL4 can hetero-oligomerize with other ELOVL family members and also can complex with other enzymes associated with VLC-FA elongation (Okuda et al., 2010). Furthermore, STDG3 mutants of ELOVL4 interact with other ELOVL family elongases and other VLC-FA-associated enzymes more strongly that WT ELOVL4, suggesting that mutant forms of ELOVL4 also might affect synthesis of other fatty acid species in addition to VLC-FA (Okuda et al., 2010).

The ELOVL family of elongases is involved in elongation of many different lipid species. Importantly, some ELOVL family elongases show distinct substrate selectivity and mediate very specific elongation reactions, while other members of the family show broader substrate selectivity and can show functional redundancy (Guillou et al., 2010; Kihara, 2012; Yu et al., 2012). Thus, the ELOVL family mediates a wide range of fatty acid elongation reactions leading to a diverse array of PUFA and SFA products.

ELOVL4 mediates elongation of long chain PUFA and SFA to form VLC-PUFA and VLC-SFA of 28 carbon chain length, respectively (**Figure 1**). ELOVL4 can then further elongate VLC-PUFA and VLC-SFA of 28 carbon chain length to produce VLC-PUFA and VLC-SFA species with chain lengths up to 38 carbons (Agbaga et al., 2008, 2010b). With respect to formation of VLC-PUFA, both 20:5n3 (eicosapentaenoic acid, EPA) and 22:5n3 (docosapentaenoic acid, DPA) precursors support downstream synthesis of VLC-PUFA (Agbaga et al., 2008). EPA is preferred as a substrate for elongation to VLC-PUFA over 20:4n6 (arachidonic acid, AA) and 22:6n3 (docosahexaenoic acid, DHA) (Yu et al., 2012). Importantly, ELOVL4 does not elongate shorter chain polyunsaturated fatty acids to DHA (Agbaga et al., 2010a). Formation of VLC-SFA is accomplished by ELOVL4-mediated elongation of 26:0–28:0, which can then be elongated further by ELOVL4 to produce VLC-SFA with longer carbon chains (Guillou et al., 2010; Kihara, 2012). The major VLC-SFA products of ELOVL4 in the brain are 28:0 and 30:0 (Hopiavuori et al., 2018).

The extreme length of the VLC-SFA and VLC-PUFA confers unique properties to the complex lipids and membranes into which they are incorporated. The very long, linear carbon chain of VLC-SFA confers a high melting temperature and would increase membrane stiffness through Van der Waals interactions between adjacent alkyl chains. Furthermore, the linear structure of VLC-SFA would be of sufficient length to span across the leaflets of the lipid bilayer, further affecting membrane properties (Hopiavuori et al., 2018, discussed further below). In contrast, VLC-PUFA, due to their length and multiple methylene interrupted *cis* double bonds, lead to locally disordered phospholipid packing in the membrane, increased fluidity, and potentially affect membrane curvature (Antonny et al., 2015; Lauwers et al., 2016).

The VLC-PUFA and VLC-SFA products of ELOVL4 are generated in a tissue-specific manner and are incorporated into more complex lipids in a tissue-specific manner. In the skin, the major products of ELOVL4 are VLC-SFA, as shown by the fact that epidermal fatty acids longer than C26 are virtually absent in newborn mice lacking a functional Elovl4 protein (Cameron et al., 2007). The molecular species of skin ceramides and glucosylceramides (GlcCer) contain VLC-SFA in non-hydroxy, α-hydroxy, and ω-hydroxy forms, the latter occurring in non-esterified and esterified forms (mostly with

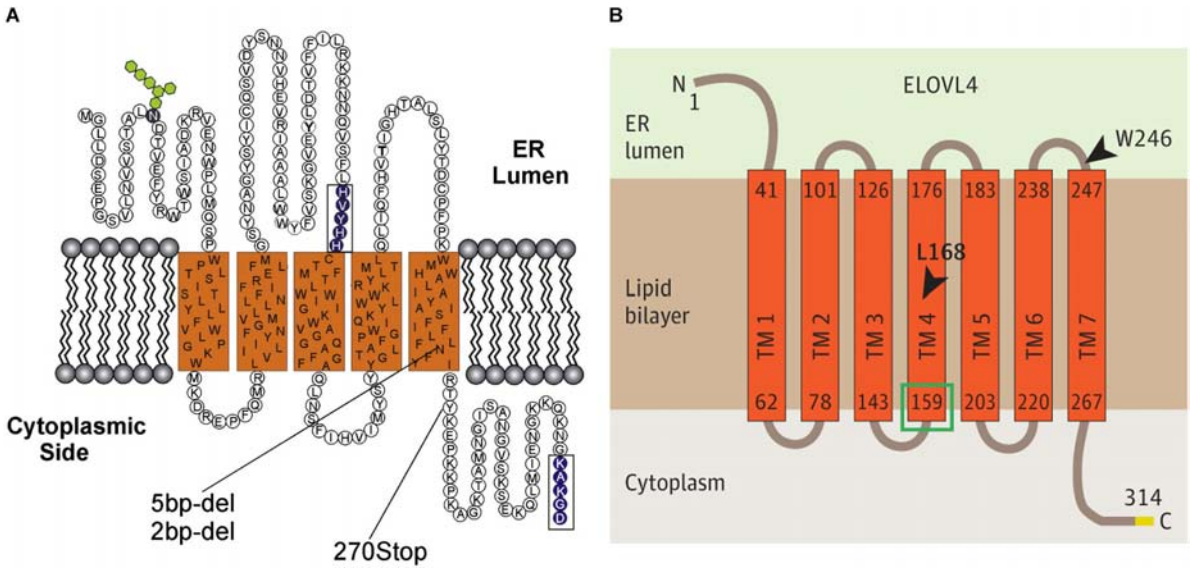

FIGURE 2 | Predicted transmembrane topology for ELOVL4. **(A)** Predicted five transmembrane-spanning topology for ELOVL4 (Zhang et al., 2001; Molday and Zhang, 2010). **(B)** Predicted seven transmembrane-spanning topology for ELOVL4 (Ozaki et al., 2015; figures used with permission).

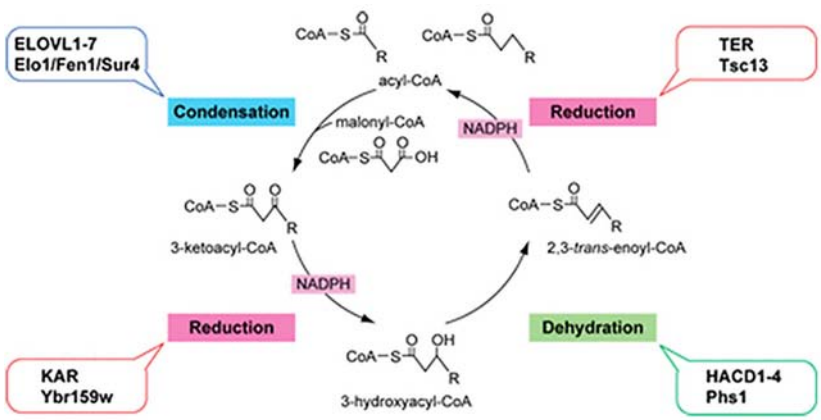

FIGURE 3 | Fatty acid elongation by the ELOVL family of enzymes. Diagram of the four-step fatty acid elongation cycle indicating the mammalian (ALL CAPITALS) and the yeast enzymes involved in each step. The ELOVL family elongasaes catalyze the initial condensation reaction (Kihara, 2012; figure used with permission).

18:2) (**Figure 1**). Strikingly, the skin of Elovl4$^{-/-}$ mice is devoid of the epidermal unique ω-O-acylceramides (> C30) (McMahon et al., 2007; Vasireddy et al., 2007). Part of the ω-hydroxy-Ceramide and GlcCer species are esterified to specific skin proteins (Amen et al., 2013), and are critical to establishing the extremely hydrophobic extracellular lipid lamellae of the stratum corneum that serves as the water barrier for the skin. Similarly, ELOVL4 in the Meibomian gland also generates VLC-SFA that are incorporated into ω-O-acylceramides, which are essential components of the lipid layer that covers the aqueous tear film and prevents evaporation (McMahon et al., 2014). In the testes, ELOVL4 produces VLC-PUFA (Santiago Valtierra et al., 2018), which are incorporated into sphingolipid products via ceramide synthase 3 (CerS3) (Rabionet et al., 2008). Conditional deletion of CerS3 leads to the absence of virtually all of sphingolipid products that contain VLC-PUFA, and infertility due to enhanced apoptosis during meiosis and spermatogenic arrest (Rabionet et al., 2015). VLC-PUFA are likely to be important to human fertility, as decreased VLC-PUFA levels in sperm are associated with decreased sperm quantity and quality (Craig et al., 2019).

In the CNS, ELOVL4 produces both VLC-SFA and VLC-PUFA in a region-specific manner. In the brain, the main ELOVL4 products are VLC-SFA, which are incorporated in sphingolipids that are enriched in synaptic vesicles and regulate presynaptic release (Hopiavuori et al., 2018). In retina, the main ELOVL4 products are VLC-PUFA (Agbaga et al., 2008, 2010b), which are incorporated into phosphatidylcholine and enriched in the light sensitive photoreceptor outer segments

(Aveldano, 1987). VLC-PUFA are critical to photoreceptor health and survival (Agbaga et al., 2008, 2010b; Bennett et al., 2014a,b; Bhattacharjee et al., 2017; Jun et al., 2017). VLC-PUFA have been reported previously in the brain (Poulos et al., 1988; Robinson et al., 1990). Although VLC-PUFA are present in the brain only in trace amounts in health, phosphatidylcholine species containing VLC-PUFA were reported previously in the brain of newborn children affected with Zellweger disease (Poulos et al., 1988), a rare peroxisomal biogenesis disorder in which in the oxidation of VLC-FA is impaired. Such PC species also were detected in the brain of healthy newborn rats in small amounts, decreasing substantially from postnatal days 1 to 16 and being virtually absent at 60 days (Robinson et al., 1990). Recent exhaustive lipidomic studies of healthy wildtype adult mouse brain did not detect these species (Hopiavuori et al., 2017).

The Function of the Mammalian ELOVL Elongase Family in Health and Disease

The mammalian ELOVL family of elongases has a number of important functions in the body and, as a group, are particularly important to CNS function, the epidermal water barrier, systemic metabolic functions, and also are likely to be important to fertility. Mutations affecting *ELOVL1*, *-4*, *-5,* and *-7* are associated with neurological disease. Importantly, the diseases caused by these mutations have some shared characteristics that suggest fatty acid elongation in general is particularly critical to the health of the CNS. No disease causing mutations in *ELOVL2*, *-3*, or *-6* have been reported to date. The synthetic activities and functions of each ELOVL family member are summarized below.

ELOVL1

ELOVL1 elongates SFA with chain lengths of 18–24 carbons and shows functional redundancy with ELOVL3 and ELOVL7 (**Figure 1**; Guillou et al., 2010; Ohno et al., 2010; Kihara, 2012). Deletion of *Elovl1* in mice causes disruption of the lamellae in the stratum corneum of the skin and disrupts the water barrier of the skin leading to perinatal lethality (Sassa et al., 2013). *Elovl1* mutant mice also show deficiency of VLC-SFA and VLC-mono-unsaturated fatty acids in the tear film (Sassa et al., 2018). *ELOVL1* is expressed at moderate levels in the brain (Tvrdik et al., 2000). An autosomal dominant mutation in human *ELOVL1* has recently been reported that produces ichthyosis, hypomyelination, spastic paraplegia, partial deafness, and optic atrophy (Mueller et al., 2019). This syndrome shares some symptoms with the neuro-ichtyotic syndrome caused by autosomal recessive mutations in *ELOVL4* (Aldahmesh et al., 2011; Mir et al., 2014; discussed below).

ELOVL2

ELOVL2 elongates PUFA with 20–22 carbon and SFA with 18–20 carbon chains (**Figure 1**; Guillou et al., 2010; Zadravec et al., 2011; Kihara, 2012)and has low expression in the brain (Tvrdik et al., 2000). Knockout studies in mice indicate that *Elovl2* is essential for normal lipid homeostasis (Pauter et al., 2014). No human diseases arising from *ELOVL2* mutations have been reported to date, although polymorphisms with genetic linkage to autism have been reported recently (Sun et al., 2018). Interestingly, human epigenetic screening indicates that the *ELOVL2* gene shows a progressive increase in methylation that begins at an early stage of life and is a promising biomarker for aging in all tissues (Garagnani et al., 2012; Gopalan et al., 2017; Slieker et al., 2018; Jung et al., 2019) that can be used for forensic age determination (Spolnicka et al., 2018).

ELOVL3

ELOVL3 elongates SFA with chain lengths of 18–24 carbons and can be functionally redundant with ELOVL1 and ELOVL7 (**Figure 1**; Westerberg et al., 2004; Guillou et al., 2010; Kihara, 2012). Knockout of *Elovl3* in mice disrupts the water barrier of the skin and causes hyperplasia of the sebaceous glands and hair loss (Westerberg et al., 2004; Kihara, 2012). No linkage to CNS disease in humans has been reported for ELOVL3.

ELOVL4

ELOVL4 elongates long-chain PUFA and long-chain SFA of 24 carbon length to VLC-PUFA and VLC-SFA ($\geq$26 carbons; **Figure 1**; Agbaga et al., 2008, 2010b; Guillou et al., 2010; Kihara, 2012). ELOVL4 also can further elongate VLC-PUFA and VLC-SFA up to 38 carbons in length. No other ELOVL family member performs this function. Thus, there is no compensation for mutations that compromise the ability of ELOVL4 to synthesize VLC-PUFA or VLC-SFA. Mutations in *ELOVL4* cause three different human diseases with tissue-specific characteristics: Stargardt-like macular dystrophy (STGD3), spinocerebellar ataxia 34 (SCA34), and a neuro-ichthyotic syndrome. All of these diseases have profound effects on the CNS and are discussed in more detail in several sections below.

ELOVL5

ELOVL5 mediates elongation of long chain-PUFA and long chain-SFA between 18 and 22 carbons in length (**Figure 1**; Leonard et al., 2002; Guillou et al., 2010; Kihara, 2012). Two different mutations in *ELOVL5* cause spinocerebellar ataxia 38 (SCA38) in humans, which is characterized by gait ataxia, nystagmus, anosmia, and cerebellar atrophy (Di Gregorio et al., 2014). In the cerebellum, ELOVL5 is highly expressed in Purkinje cells, which provide the sole output from the cerebellar cortex, and in some cells of unidentified type located in the granule cell layer (Di Gregorio et al., 2014; Hoxha et al., 2017).

ELOVL6

ELOVL6 has been suggested to mediate the first, rate-limiting step in fatty acid elongation of saturated and unsaturated/polyunsaturated fatty acids with chain length of 16 carbons, and is expressed at high levels in the liver, adipose tissue, and brain (**Figure 1**; Moon et al., 2001; Guillou et al., 2010; Kihara, 2012; Moon et al., 2014). *Elovl6* knockout mice are insulin resistant and develop obesity and hepatosteatosis when fed a high fat diet (Matsuzaka et al., 2007), indicating that ELOVL6 is important to normal metabolic regulation. The activity of ELOVL6 can also regulate thermogenic activity in brown fat adipocytes (Tan et al., 2015) and chondrocyte growth (Kikuchi et al., 2016). No direct causal linkage of *ELOVL6* mutations to human disease has been established.

ELOVL7

ELOVL7 elongates SFA with chain lengths of 18–22 carbons and shows some functional redundancy with ELOVL1 and ELOVL3 (Guillou et al., 2010; Naganuma et al., 2011; Kihara, 2012). No direct causal relationship between ELOVL7 and human disease has been established. However, association of single nucleotide polymorphisms in *ELOVL7* with early onset Parkinson's disease has been reported (Li et al., 2018). A case of apparent mitochondrial encephalomyopathy arising from homozygous deletion of the contiguous *NDUFAF2*, *ERCC8*, and *ELOVL7* genes on chromosome 5 has been reported (Janssen et al., 2009). No changes in fatty acid synthesis were found, suggesting that deletion of *ELOVL7* is unlikely to be the root cause of the disease.

Non-mammalian ELOVL Family Fatty Acid Elongases

ELOVL family fatty acid elongases in fish also have been of particular interest because of their function as source of polyunsaturated fatty acids. As indicated above, ELOVL family elongases are highly conserved across eukaryotes, and homologs of mammalian ELOVL2, ELOVL4, and ELOVL5 have been identified and characterized functionally in several species of teleost fish, including zebrafish, Salmon, cobia, and Chu's croaker (Hastings et al., 2004; Morais et al., 2009; Monroig et al., 2010, 2011; Carmona-Antonanzas et al., 2011; Lin et al., 2018). For more detailed discussion of ELOVL gene evolution (see Castro et al., 2016). A single isoform of ELOVL2 has been identified in fish (Morais et al., 2009). ELOVL5 is expressed in a single isoform in some fish species (i.e., Chu's croaker, Lin et al., 2018), while other species express two functionally similar isoforms (ELOVL5a and b) (i.e., Atlantic salmon, Hastings et al., 2004; Morais et al., 2009). ELOVL2 and ELOVL5 are functionally redundant with one another and serve functions similar to their mammalian homologs: ELOVL2 elongates C20 and C22 PUFA to C24 PUFA; ELOVL5a and 5b elongate C18 and C20 PUFA to C22 PUFA (Carmona-Antonanzas et al., 2011).

Similar to mammals, ELOVL4 in fish is highly expressed in brain, retina, and gonads and is essential for formation of VLC-SFA and VLC-PUFA (Monroig et al., 2010, 2011; Carmona-Antonanzas et al., 2011). However, ELOVL4 in fish can be expressed in a single isoform (i.e., Atlantic salmon, cobia Carmona-Antonanzas et al., 2011; Monroig et al., 2011) or two isoforms (ELOVL4a and b) that are encoded by separate genes (i.e., zebrafish, Monroig et al., 2010). ELOVL4a and ELOVL4b show very distinct substrate specificities: ELOVL4b readily elongates both VLC-SFA and VLC-PUFA, but ELOVL4a elongates only VLC-SFA (Monroig et al., 2010). In fish that express only a single ELOVL4 isoform, ELOVL4 shows activity similar to zebrafish ELOVL4b and elongates both VLC-SFA and VC-PUFA (Monroig et al., 2010; Carmona-Antonanzas et al., 2011). Fish ELOVL4 also can elongate C20 and C22 substrates, making it functionally redundant with ELOVL2 and to a lesser extent ELOVL5 (Carmona-Antonanzas et al., 2011), in contrast to mammalian ELOVL4. Importantly, this broad substrate selectivity could allow fish ELOVL2 and ELOVL4 to participate in the synthesis of DHA, as these enzymes can catalyze synthesis of 24:5n-3 from 22:5n-3, allowing for subsequent desaturation and β-oxidation to form DHA (Hastings et al., 2004; Monroig et al., 2010, 2011; Carmona-Antonanzas et al., 2011).

Distribution of the ELOVL Family in the CNS

Several members of the ELOVL family are expressed in the CNS (ELOVL1, -3, -4, -5, and -6), but their expression levels differ across brain regions (Tvrdik et al., 2000; Lein et al., 2007; Hoxha et al., 2017; Sherry et al., 2017). ELOVL2 and ELOVL7 are expressed at very low levels in mammalian brain, if at all (Tvrdik et al., 2000; Lein et al., 2007), although ELOVL2 is expressed highly in the brain of non-mammals (Oboh et al., 2016). The best characterized ELOVL family members in the mammalian brain are ELOVL4 and ELOVL5 (Hoxha et al., 2017; Sherry et al., 2017; Hopiavuori et al., 2018). Mutations in either *ELOVL4* or *ELOVL5* cause neurological disease in humans (see below and **Table 1**). Interestingly, zebrafish ELOVL4a, which catalyzes formation of VLC-SFA only, is highly expressed in brain, and ELOVL4b, which catalyzes production of VLC-PUFA as well as VLC-SFA, is highly expressed in retina (Monroig et al., 2010; Carmona-Antonanzas et al., 2011). This distribution of ELOVL4 isoforms would result in similar patterns of VLC-SFA and VLC-PUFA production in the brains and retinae of teleost fish and mammals. ELOVL5 also is expressed at high levels in the fish brain (Kohlhardt, 1989), similar to mammalian brain.

ELOVL4 Distribution in the Brain

ELOVL4 is the most highly expressed and widely distributed member of the ELOVL family in the brain as shown by immunolabeling and *in situ* hybridization (see **Figure 4**). ELOVL4 expression varies in a region- and cell type-specific manner (Lein et al., 2007; Sherry et al., 2017; Hopiavuori et al., 2018) which is likely to be related to the dysfunctions observed in diseases arising from *Elovl4* mutations. Expression of ELOVL4 is especially prominent in the olfactory bulb, hippocampus, cerebral cortex, thalamus, and cerebellum, although most other brain regions also show substantial levels of ELOVL4. An exception to this pattern is the basal ganglia, which show very little ELOVL4 expression (Sherry et al., 2017). At the cellular level, ELOVL4 expression is primarily neuronal, although small ELOVL4-positive cells have been observed in brain white matter suggesting potential expression in oligodendrocytes (Sherry et al., 2017). Among neurons, ELOVL4 expression is present in glutamatergic as well as GABAergic neurons (Sherry et al., 2017), and also may occur in neurons that utilize other neurotransmitters.

Within a region, ELOVL4 expression is cell-specific (**Figure 5**). In the retina, ELOVL4 is expressed exclusively by photoreceptor cells (Agbaga et al., 2008), consistent with the photoreceptor degeneration associated with ELOVL4 mutations that cause Stargardt's-like macular dystrophy (STGD3) (Bernstein et al., 2001; Edwards et al., 2001; Zhang et al., 2001; Maugeri et al., 2004; Bardak et al., 2016; Donato et al., 2018). In the cerebellum, ELOVL4 levels are extremely high in granule cells, moderate in basket and stellate cells, and low in Purkinje cells (Sherry et al., 2017). These cell-specific differences

TABLE 1 | Summary of human disease-causing *ELOVL4* mutations.

Human disease	Inheritance	Genomic mutation	Protein mutation/structure /function	Retinal symptoms	Other CNS symptoms	Skin symptoms	Onset/Progression	References
Wildtype ELOVL4.	Homozygous	Wildtype (no mutation)	Wildtype. Intrinsic endoplasmic reticulum membrane protein. 314 AA length	–	–	–	–	Edwards et al., 2001; Zhang et al., 2001
Stargardt's-like macular dystrophy (STGD3)	Autosomal dominant	790–794 del AACTT "5 bp deletion"	Exon 6, N264Lfs10X	Macular degeneration	None reported	None	Juvenile onset. Rapid progression.	Edwards et al., 2001; Zhang et al., 2001
Stargardt's-like macular dystrophy (STGD3)	Autosomal dominant	789 del T *plus* 794 del T "2 bp deletion"	Exon 6, N264Tfs9X	Macular degeneration	None reported	None	Juvenile onset. Rapid progression.	Bernstein et al., 2001
Stargardt's-like macular dystrophy (STGD3)	Autosomal dominant	c.810C > G	Exon 6, Y270X	Macular degeneration	None reported	None	Juvenile onset. Rapid progression.	Maugeri et al., 2004
Stargardt's-like macular dystrophy (STGD3)	Autosomal dominant	c.814G > C	Exon 6, E272Q	Macular degeneration	None reported	None reported	Juvenile onset. Rapid progression.	Bardak et al., 2016
Stargardt's-like macular dystrophy (STGD3)	Autosomal dominant	c.895A > G	Exon 6, M299V	Macular degeneration	None reported	None reported	Juvenile onset. Rapid progression.	Bardak et al., 2016
Stargardt's-like macular dystrophy (STGD3)	Autosomal dominant	c.-90 G > C	Promoter, rs62407622	Macular degeneration	None reported	None reported	Juvenile onset. Rapid progression.	Donato et al., 2018
Stargardt's-like macular dystrophy (STGD3)	Autosomal dominant	c.-236 C > T	Promoter, rs240307	Macular degeneration	None reported	None reported	Juvenile onset. Rapid progression.	Donato et al., 2018
Spinocerebellar ataxia (SCA34)	Autosomal dominant	c.504G > C	Exon 4, L168F Full-length protein	Not reported	Gait and limb ataxia. Dysarthria. Nystagmus and eye movement deficits. Abnormal tendon reflexes. No autonomic disturbance. Cerebellar and pontine atrophy.	Erythrokerato-dermia Variabilis	Avg. onset: 51 years of age. Onset in 4th to 5th decade. Slow progression.	Cadieux-Dion et al., 2014

(Continued)

TABLE 1 | Continued

Human disease	Inheritance	Genomic mutation	Protein mutation/structure /function	Retinal symptoms	Other CNS symptoms	Skin symptoms	Onset/Progression	References
Spinocerebellar ataxia (SCA34)	Autosomal dominant	c.736T > G	Exon 4, W246G Full-length protein	Normal	Gait and limb ataxia. Dysarthria. Nystagmus and eye movement deficits. Abnormal tendon reflexes. Babinski reflex may be present. Autonomic disturbance sometimes present. Cerebellar and pontine atrophy.	None	Avg. onset: 34 years of age (range: 2nd–6th decade). Slow progression.	Ozaki et al., 2015
Spinocerebellar ataxia (SCA34)	Autosomal dominant	c.539A > C	Exon 4, Q180P Full length protein	None reported	Gait ataxia more pronounced than limb ataxia. Dysarthria. Nystagmus and eye movement deficits. Moderate cerebellar and pontine atrophy.	Erythrokerato-dermia Variabilis	Onset in middle 20 s (1 case known). Progression unclear at present	Bourassa et al., 2015
Spinocerebellar ataxia (SCA34)	Autosomal dominant	c698C > T	Exon 4, T233M Full length protein	None reported	Gait ataxia (no limb ataxia). No dysarthria. No nystagmus, but abnormal eye movements present. Hyporeflexia. Mild cerebellar and pontine atrophy.	Erythrokerato-dermia Variabilis	15 years of age (1 case known). Slow progression	Bourque et al., 2018
ELOVL4 Neuro-ichthyotic syndrome	Homozygous recessive	c.689delT	Exon 6, I230MfsX22	Normal fundus and flicker ERG	Seizures, intellectual disability, spastic quadriplegia	Ichthyosis	Infancy (Gestation?) Developmental delay	Aldahmesh et al., 2011
ELOVL4 Neuro-ichthyotic syndrome	Homozygous recessive	c.646C > T	Exon 5, R216X	Not reported	Seizures, intellectual disability, spastic quadriplegia	Ichthyosis	Infancy (Gestation?) Developmental delay	Aldahmesh et al., 2011
ELOVL4 Neuro-ichthyotic syndrome	Homozygous recessive	c.78C > G	Exon 1, Y26X	Not reported	Seizures, intellectual disability, spastic quadriplegia	Ichthyosis	Infancy (Gestation?) Developmental delay	Mir et al., 2014

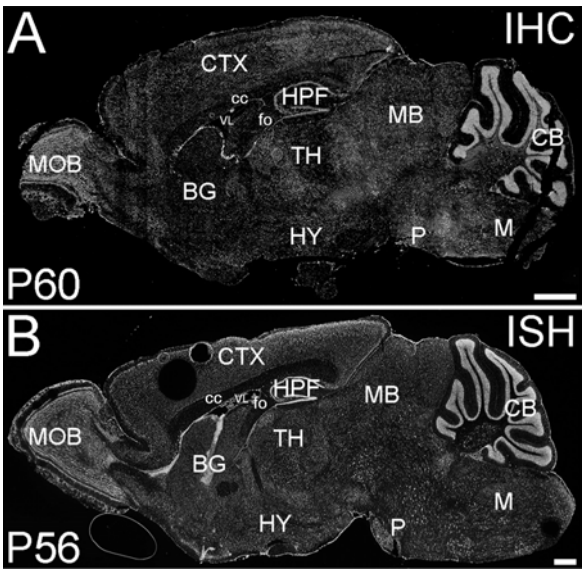

FIGURE 4 | ELOVL4 protein and mRNA distribution in the adult mouse brain. **(A)** Immunofluorescent labeling for ELOVL4 in the postnatal day 60 mouse brain is widely distributed, but shows cell-specific distribution in different regions of the brain. **(B)** *In situ* hybridization (ISH) for *Elovl4* mRNA in the mouse brain at P56 shows distribution similar to that of ELOVL4 protein. (Image from: Allen Institute for Brain Science Allen Mouse Brain Atlas for the P56 mouse brain, image number 69059903_134; http://mouse.brain-map.org). CB, cerebellum; BG, basal ganglia; CTX, cerebral cortex; HPF, hippocampal formation; HY, hypothalamus; M, medulla; MB, midbrain; MOB, main olfactory bulb; P, pons; cc, corpus callosum; fo, fornix; VL, lateral ventricle. Scale bars = 1 mm (figure from Sherry et al., 2017). Used with open access under the Creative Commons attribution license CC-BY, version 4.0; http://creativecommons.org/licenses/by/4.0/).

in ELOVL4 expression may be related to the symptoms and progression of spinocerebellar ataxia-34 (SCA34), which is caused by human *ELOVL4* mutations (Cadieux-Dion et al., 2014; Bourassa et al., 2015; Ozaki et al., 2015; Bourque et al., 2018). In the hippocampus, the highest levels of ELOVL4 in neurons in the CA3 and CA4 regions, with low expression in CA1 and dentate gyrus (Sherry et al., 2017; Hopiavuori et al., 2018), consistent with the severe, spontaneous epileptiform bursting and seizure activity observed in mice homozygous for the 5bp deletion STGD3 mutant *ELOVL4* alleles (Hopiavuori et al., 2018). This phenotype is also consistent with the seizure activity reported in the recessive human *ELOVL4* neuro-ichthyotic syndrome (Aldahmesh et al., 2011; Mir et al., 2014).

Expression of ELOVL4 in the brain is developmentally regulated, with *Elovl4* mRNA expression levels peaking around the time of birth and then steadily falling as the brain matures, reaching a steady state level by about postnatal day 30 in mice (Mandal et al., 2004). Immunolabeling studies of the developing mouse brain between embryonic day 18 (E18) and postnatal day 60 (P60) show that ELOVL4 is very highly expressed in regions such as the subventricular zone, the dentate gyrus of the hippocampus, and the internal and external granular layers of the cerebellum during periods of neurogenesis (Sherry et al., 2017). ELOVL4 expression in these regions declines as neurogenesis declines, suggesting some role for ELOVL4 and its VLC-FA products in neurogenesis.

ELOVL5 Distribution in the Brain

ELOVL5 distribution has been characterized in the cerebellum, using immunolabeling of wildtype mouse cerebellum (Di Gregorio et al., 2014) and β-galactosidase reporter labeling in transgenic *Elovl5* knockout mice (Hoxha et al., 2017). ELOVL5 is expressed in cerebellar Purkinje cells, stellate and basket cells in the molecular layer, and at lower levels in a sparse, unidentified cell population in the granule cell layer of the cerebellar cortex and in cells in the deep cerebellar nuclei (Di Gregorio et al., 2014; Hoxha et al., 2017). Two different missense mutations in *ELOVL5* (c.214C > G, p.Leu72Val and c.689G > T, p.Gly230Val) cause SCA38, which is characterized by gait ataxia, dysarthria, abnormal eye movements, and cerebellar atrophy with onset in the third or fourth decade (Di Gregorio et al., 2014). ELOVL5 expression also was noted in small cells located in the white matter, most likely representing myelin-producing oligodendrocytes (Hoxha et al., 2017). Elsewhere in the brain, ELOVL5 is expressed by the mitral cells of the olfactory bulb, consistent with the anosmia (loss of the sense of smell) reported in *Elovl5* knockout mice, and in various sites in the brainstem (Hoxha et al., 2017). ELOVL5 also is expressed in other regions of the brain, but this has not been characterized in detail.

Thus, ELOVL4 and ELOVL5, and possibly other ELOVL enzyme family members, are expressed in a region- and cell-specific manner in the CNS, which would lead to cell-specific profiles of fatty acid synthesis and incorporation into complex lipids (Agbaga et al., 2018). This suggests that the effects of mutations on the enzymatic activity of ELOVL4, ELOVL5, and other lipid metabolizing enzymes are likely to be key determinants of the neurological symptoms associated with specific mutations in these enzymes. Developing a better understanding of the lipid profiles of specific cell types in the CNS will be important to advancing our mechanistic understanding of the role of VLC-FA in the healthy CNS and in neurological disease.

Diseases Associated With ELOVL4

Several disease-causing mutations in the human *ELOVL4* gene have been identified to date (Bernstein et al., 2001; Edwards et al., 2001; Zhang et al., 2001; Maugeri et al., 2004; Aldahmesh et al., 2011; Cadieux-Dion et al., 2014; Mir et al., 2014; Bourassa et al., 2015; Ozaki et al., 2015; Bardak et al., 2016; Bourque et al., 2018; Donato et al., 2018; **Table 1** and **Figure 6**). Mutations in *ELOVL4* cause three distinct neurodegenerative diseases that depend on the specific mutation and its pattern of inheritance: Stargardt-like macular dystrophy (STGD3), spinocerebellar ataxia-34 (SCA34) with or without erythrokeratodermia variabilis (EKV), and a severe neuro-ichthyotic syndrome. Each disease is discussed below.

STGD3

Six different heterozygous mutations in *ELOVL4* cause autosomal dominant STGD3, an aggressive degeneration striking the macular region of the retina with juvenile onset and rapid

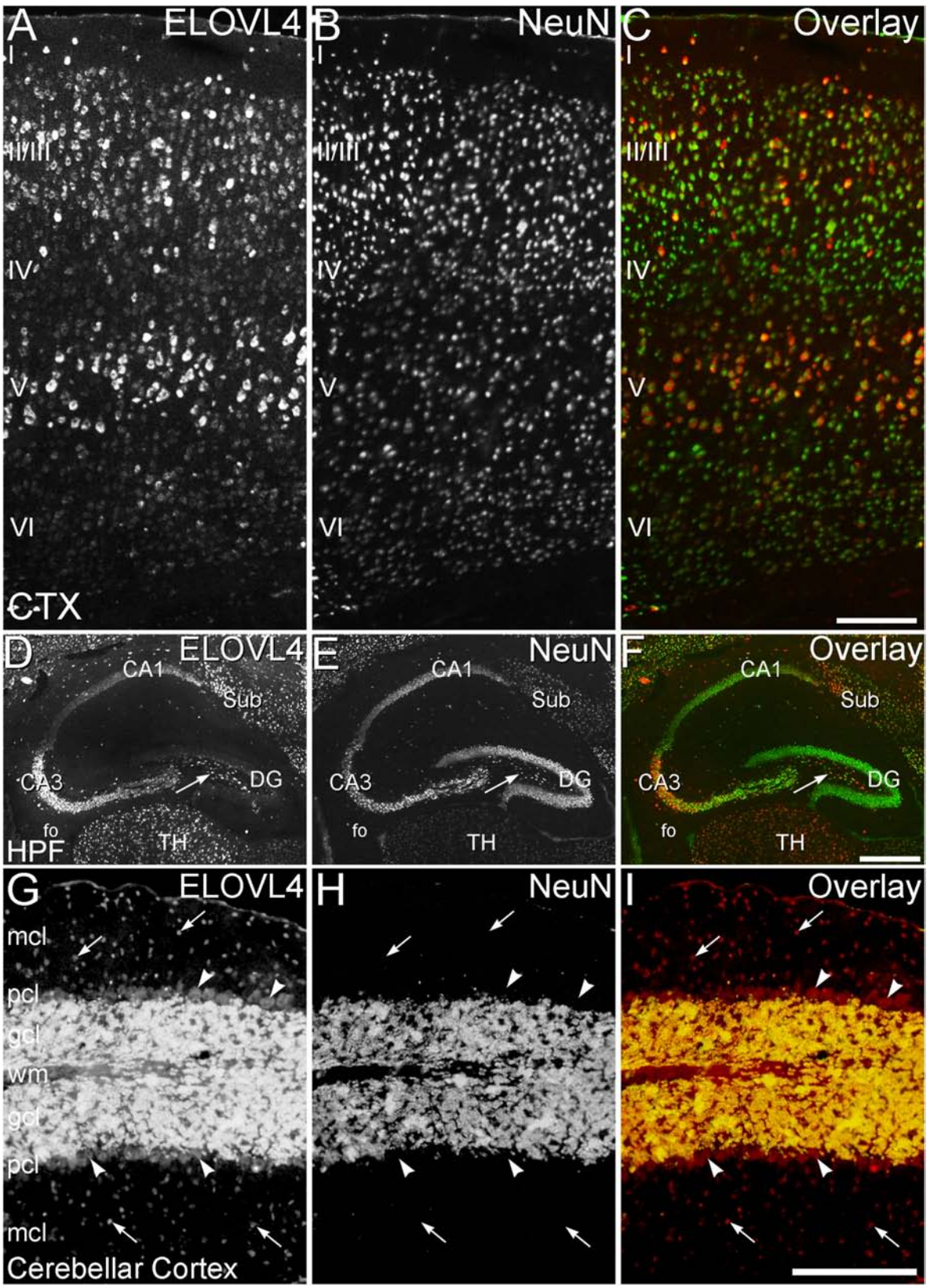

FIGURE 5 | Continued

FIGURE 5 | Cell-specific expression of ELOVL4 in isocortex, hippocampus and cerebellum. **(A–C)** Cerebral Cortex (CTX). **(A)** Labeling for ELOVL4 is present in all layers of the cerebral cortex (CTX). Cells in the pyramidal layers (II/III and V) are most prominently labeled, but ELOVL4-positive cells also are present in the molecular layer (I), layer 4 (IV) and layer 6 (VI). **(B)** Labeling for the neuronal marker, NeuN. **(C)** Overlay of panels A and B shows close correspondence of ELOVL4 (red) and NeuN labeling (green). **(D–F)** Hippocampal formation (HPF). **(D)** Labeling for ELOVL4 is present in the cellular layers of the HPF, including the Cornu Ammonis, with field 1 (CA1) showing less prominent labeling than field 3 (CA3). Prominent ELOVL4 labeling also is present in the subiculum (sub) and interneurons in the polymorph layer (arrow). Cells along the inner margin of the dentate gyrus (DG) show moderate ELOVL4 labeling, but most dentate granule cells show little ELOVL4 labeling. **(E)** Labeling for the neuronal marker, NeuN. **(F).** Overlay of **(D,E)** shows close correspondence of ELOVL4 (red) and NeuN (green) labeling. TH, Thalamus. **(G–I)** Cerebellar cortex. **(G)** Cross section through a cerebellar folium showing ELOVL4 expression in the cerebellar cortex. Neurons (arrows) in the molecular cell layer (mcl) show strong ELOVL4 labeling, but the Purkinje cells (arrowheads) in the Purkinje cell layer (pcl) show only moderate levels of ELOVL4 labeling. The densely packed cells of the granule cell layer (gcl) show very intense labeling. **(H)** Labeling for the neuronal marker, NeuN, strongly labels neurons in the gcl, but not Purkinje cells, as appropriate. **(I)** Overlay of **(G,H)** shows close correspondence of intense ELOVL4 (red) and NeuN (green) labeling resulting in an orange color in the gcl. wm, white matter of the arbor vitae. Scale bars = 200 μm for **(A–C,G–I)**; 500 μm for **(D–F)** (figure from Sherry et al., 2017; used with open access under the Creative Commons attribution license CC-BY, version 4.0; http://creativecommons.org/licenses/by/4.0/).

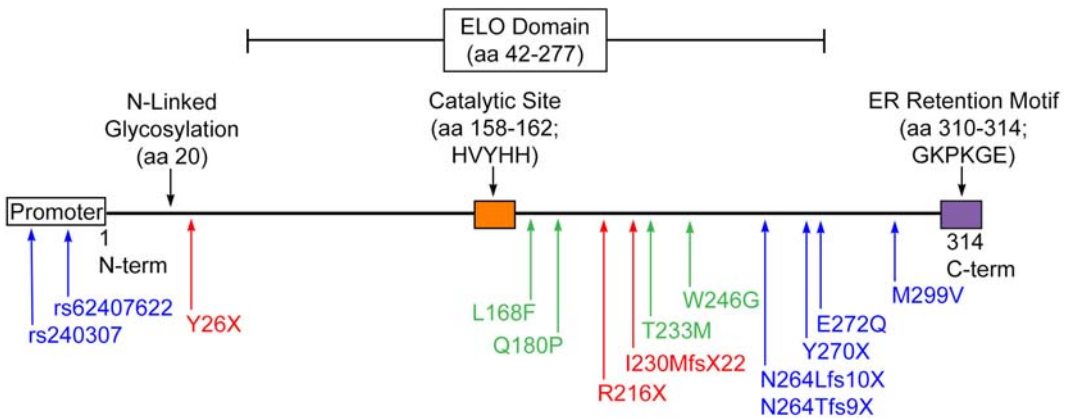

FIGURE 6 | Disease-causing mutations in ELOVL4. STGD3-causing mutations (blue) result in early truncation of ELOVL4 and the loss of the C-terminal ER retention motif or, in the case of the promoter mutations, severely suppress *ELOVL4* expression. SCA34-causing mutations (green) result in amino acid substitutions but still produce a full-length protein. ELOVL4 Neuro-ichthyosis-causing mutations (red) cause very early termination of the protein that would truncate substantial portions of transmembrane domains in either the 5-transmembrane or 7-transmembrane models of ELOVL4 topology in addition to deleting the ER retention motif.

progression (Bernstein et al., 2001; Edwards et al., 2001; Zhang et al., 2001; Maugeri et al., 2004; Bardak et al., 2016; Donato et al., 2018). Symptoms associated with STGD3 are limited to the retina, as STGD3 patients show no additional CNS disease or skin abnormalities (Bernstein et al., 2001; Edwards et al., 2001; Zhang et al., 2001). Importantly, STGD3-causing *ELOVL4* mutations result in a loss of function. STGD3 arises from several different mutations in exon 6 that result in premature termination of the protein and cause the loss of the C-terminal ER retention motif (Bernstein et al., 2001; Edwards et al., 2001; Zhang et al., 2001; Maugeri et al., 2004; Bardak et al., 2016). The 5 bp deletion STDG3 mutant form of ELOVL4 exerts a dominant-negative effect on the enzyme and leads to mislocalization of ELOVL4 away from the ER (Logan et al., 2013; Logan et al., 2014). Two additional STGD3-causing mutations in the *ELOVL4* promoter that suppress *ELOVL4* expression have been identified recently (Donato et al., 2018).

SCA34

Four different heterozygous mutations in the *ELOVL4* gene cause autosomal dominant spinocerebellar ataxia-34 (SCA34), a late-onset degenerative disease of the cerebellum that may present with or without erythrokeratodermia variabilis (EKV; red thickened skin) (Cadieux-Dion et al., 2014; Bourassa et al., 2015; Ozaki et al., 2015; Bourque et al., 2018). The gait ataxia and cerebellar degeneration that are characteristic of the disease appear in the second to sixth decade of life, with symptom onset varying according to the specific mutation. Other CNS symptoms also may be present, including dysarthria (difficulty speaking), abnormal eye movements, and abnormal tendon reflexes. Patients with SCA34 do not show any clinical retinal deficits. All of the known mutations that cause SCA34 are mutations in exon 4 that result in a single amino acid substitution and produce a full-length protein. The presence of neural deficits and degeneration in the brain appear in the absence of retinal symptoms in SCA34 patients, suggesting that SCA34-causing mutations in *ELOVL4* may preferentially affect synthesis of VLC-SFA, rather than VLC-PUFA. A recent study suggests that SCA34 patients with the p.T233M SCA34 mutation also may experience multi-system neurodegeneration beyond the cerebellum, neuropsychiatric disturbances, and dementia, in addition to the known motor deficits of SCA34 (Ozaki et al., 2019).

ELOVL4 Neuro-Ichthyotic Syndrome

Three different homozygous mutations in the *ELOVL4* gene cause a severe neuro-ichthyotic syndrome (Aldahmesh et al., 2011; Mir et al., 2014). The neural components of this syndrome

include severe seizures, intellectual disability, spasticity, and neurodegeneration in the brain. These neurological impairments are accompanied by ichthyosis (a scaly thickening of the skin), developmental delay, and premature death. Mutations that cause this severe syndrome may be associated with truncation of the protein, whether affecting just the first few amino acids at the N-terminal (Mir et al., 2014), or the last C-terminal third of the protein (Aldahmesh et al., 2011), which includes the critical ER retention motif of ELOVL4. Interestingly, homozygous inheritance of STDG3 alleles in transgenic mice in which ELOVL4 has been rescued in the skin to prevent perinatal death due to dehydration, causes a syndrome characterized by severe seizures and early death about postnatal days 20–21 (Hopiavuori et al., 2018). No cases of homozygous inheritance of STGD3 or SCA34 *ELOVL4* alleles in humans have been reported to date.

Neurophysiological Role of ELOVL4, Its Products, and Their Functions in the CNS and at the Synapse

Despite the obvious importance of ELOVL4 to the health and function of the CNS, the precise role and mechanisms of action of its main fatty acid products, VLC-PUFA and VLC-SFA, are incompletely understood. Recent evidence suggests that specific lipid species that contain each of these types of very-long acyl chains may have important roles, with VLC-PUFA serving as precursors of metabolites involved in homeostatic signals and VLC-SFA serving as modulators of synaptic transmission.

VLC-PUFA as Homeostatic Survival Signals

Recently, elegant studies of VLC-PUFA by the Bazan laboratory identified a new class of bioactive fatty acids they named "elovanoids" (Bhattacharjee et al., 2017; Jun et al., 2017; Bazan, 2018). These compounds, hydroxylated derivatives of 32:6n-3 and 34:6n-3 produced by a form of lipoxygenase, were described as neuroprotective in the retina., The primary products of ELOVL4 in the retina are VLC-PUFA that are incorporated into phosphatidylcholine and enriched in the disc membranes of the light-sensitive photoreceptor outer segments (Aveldano, 1987). Each morning, photoreceptors shed a portion of the discs at the distal tip of the outer segment, which are phagocytosed by the overlying retinal pigmented epithelium (RPE) and degraded. The VLC-PUFA in the shed outer segment membranes serve as the precursors for production of oxygenated elovanoid derivatives in RPE cells. Elovanoids then provide a neuroprotective feedback signal to enhance expression of pro-survival proteins by the photoreceptors to compensate for high levels of oxidative stress (Jun et al., 2017). In good agreement with these findings, elovanoids also have been shown to have protective effects in neurons subjected to oxygen and glucose deprivation or to induced excitotoxicity in culture, and in an animal model of ischemic stroke (Bhattacharjee et al., 2017). Together, these data revealed a novel pro-homeostatic and neuroprotective lipid-signaling mechanism that helps to sustain the integrity of neuronal cells. For more information on omega-3 and omega-6 unsaturated fatty acids, DHA, docosanoids, elovanoids and their biological functions, we refer to an excellent recent review from Bazan (2018).

VLC-SFA as Modulators of Synaptic Function

An emerging understanding suggests that VLC-SFA are important for normal synaptic function and that VLC-SFA deficiency arising from ELOVL4 mutations impairs synaptic transmission and causes synaptopathy. Recent studies performed using mice homozygous for the 5 bp deletion STDG3 mutation, which effectively renders ELOVL4 inactive, showed that VLC-SFA are important, novel modulators of presynaptic release kinetics (Hopiavuori et al., 2018). Of the potential roles that VLC-SFA may play in the CNS, we will consider two major areas below: as structural elements and as signaling molecule and signal modifiers. We also provide thoughts on future research directions to better understand the function of VLC-FA and their potential clinical relevance.

Structural Role of VLC-SFA

Although much remains unknown about the role of ELOLV4 and its VLC-SFA products in neurophysiology, we suggest that VLC-SFA incorporated into sphingolipids in the synaptic vesicle membrane may potentially serve as membrane stabilizers, anchor points for proteins, and lipid raft-like components.

Potential Role for VLC-SFA in Membrane Fusion

One of the most precisely regulated membrane fusion events known occurs during neurotransmission in the synaptic terminal (Südhof, 2004; Südhof and Rothman, 2009). Membrane fusion is a fundamental step in neurotransmitter release when synaptic vesicles (SV) fuse with the plasma membrane at the active zone to release their neurotransmitter content into the synaptic cleft. Receptors on the postsynaptic side bind the transmitter and relay the signal to the next neuron. This process, which is the basis for information processing in the brain, has received considerable attention in human cognitive research and in neurodegenerative diseases such as Alzheimer's and Parkinson's diseases (Dickson, 1997; Selkoe, 2001, 2002; Petersen, 2004; Nguyen et al., 2006). The core machinery required for action potential evoked synchronized transmitter release and the molecular components needed for neurotransmission are now identified. This core complex contains three SNARE (soluble NSF attachment protein -SNAP- receptor) proteins (Sollner et al., 1993): the synaptic vesicle protein, synaptobrevin (also known as VAMP, Vesicle Associated Membrane Protein), and the target membrane bound syntaxin and SNAP-25 proteins. The coiled motifs of these three proteins form a four helical complex structure, thus bringing the membranes in close proximity (McNew et al., 2000; Melia et al., 2002). During action potentials, the fusion of the vesicular and active zone membranes is triggered by binding of calcium ions to synaptotagmin1, another vesicular protein, which binds preferentially to phospholipids (Perin et al., 1990; Fernandez-Chacon et al., 2001). Recently, an array of synaptic proteins (Munc13, Munc18, Rabphilin, and Complexin) that interact with the core complex and assist in the precise regulation of synaptic release have been discovered (Hata et al., 1993; Rizo and Sudhof, 2002; Deák et al., 2006b;

Deák et al., 2009; Südhof and Rothman, 2009). Recently, the exact stoichiometry of these and other SV proteins and SV lipids was reported, and biophysical characterization of SV membranes was performed (Takamori et al., 2006; Hopiavuori et al., 2017; Hopiavuori et al., 2018). Regarding lipids, these authors showed that an average 40 nm diameter SV contains some 7000 phospholipid and 5-6000 cholesterol molecules. Together, the glycerophospholipids phosphatidylcholine, phosphatidylethanolamine, and phosphatidylserine comprise more than 90% of the phospholipid content, part of the rest being phosphatidylinositol, sphingomyelin, and hexosylceramide (Takamori et al., 2006). The most abundant VLC-SFA components of the SV membrane lipid were 28:0 and 30:0 incorporated into sphingolipids (Hopiavuori et al., 2018).

During exocytosis, the membrane lipid bilayers merge in a stepwise process. First, the membrane leaflets exposed to the cytoplasm make contact each other and then, if forced with sufficient energy, will merge. Only after this process is initiated, and at least partially completed, can the other membrane leaflets – in the case of synaptic neurotransmission, the luminal leaflet of the synaptic vesicle and the extracellular leaflet of the plasma membrane – contact each other. Thus, an intermediate state – called hemifusion – exists when the outer leaflets of the vesicle and plasma membrane form a temporary new bilayer. After these outer leaflets merge, the vesicular lumen and the synaptic cleft remain separate. Next, after a fusion pore is formed, the release of neurotransmitter is initiated (**Figure 7**).

VLC-SFA potentially could change the structure of the lipid bilayer and its biophysical properties, thereby affecting the process of membrane fusion. The SV membrane contains 28:0 and 30:0 as components of sphingolipids (Hopiavuori et al., 2018). These very long saturated acyl chains are of sufficient length to traverse both leaflets of the SV lipid bilayer. We hypothesize that the hydrophobic van der Walls interactions between these very long chains stabilize the SV lipid bilayer, hindering the separation of the two leaflets during hemifusion and fusion pore formation. The enrichment of VLC-SFA in SV membranes, therefore, would increase the energy required to initiate vesicular fusion, stabilizing the membranes and reducing random spontaneous fusion events unrelated to action-potential mediated synaptic release. According to this model, acyl-acyl hydrophobic interactions across the lipid bilayer would increase the van der Waals forces within the bilayer, thereby stabilizing the membrane and inhibiting fusion with other membranes. Assuming that the energy source driving membrane fusion is constant, the vesicular release process would be slowed in SVs with high VLC-SFA content. The VLC-SFA in the vesicle membrane could thereby provide a biophysical resistance to the activation of SNARE complexes, which is essential for Ca^{2+}-regulated exocytosis of synaptic vesicles (Deák et al., 2006a, 2009; Südhof and Rothman, 2009; Südhof and Rizo, 2011; Imig et al., 2014; Shen et al., 2015), slowing SV fusion. We suggest that this increased barrier may help to regulate the timing of vesicular release. *Elovl4* mutations that cause seizures (STDG3 and ELOVL4 neuro-ichthyotic syndrome) effectively eliminate the enzymatic function of ELOVL4 and, thus, lead to SVs that lack VLC-SFA. The absence of the van der Waals forces generated by the VLC-SFA within the SV lipid bilayer would therefore be expected to increase the probability of spontaneous release events by removing a barrier to fusion. In this case, the precise timing of synaptic release would be compromised, leading to bursting activity and seizures, as seen in the hippocampus of knock-in mice homozygous for the 5bp deletion STGD3 *ELOVL4* mutation (**Figure 8**; Hopiavuori et al., 2018). Consistent with this hypothesis, hippocampal neurons cultured from mice homozygous for the 5bp deletion STGD3 *ELOVL4* mutation show accelerated synaptic release kinetics (Hopiavuori et al., 2018). Critically, supplementation of a mixture of 28:0 and 30:0 VLC-SFA to these neurons via the culture medium restored normal synaptic release kinetics (**Figure 9**; Hopiavuori et al., 2018).

The length and saturation of VLC-SFA also may enable them to sterically inhibit protein-protein interactions in the vesicular release machinery. However, interactions between VLC-SFA and the vesicle fusion machinery remain unknown at present. VLC-SFA interactions are also likely to keep the membrane bilayers highly ordered and stable, thus hindering the effects of synaptobrevin juxta- and trans-membrane regions in disturbing outer leaflet lipid ordering and changing curvature of membrane (Tarafdar et al., 2015). It is also plausible for charged phospholipids (e.g., sphingolipids) containing VLC-SFA to interact with the release proteins via a strongly charged segment in synaptobrevin/VAMP located next to its transmembrane domain outside of the SV (Quetglas et al., 2000).

What other functional consequences might result from the presence of VLC-SFA in the SV membrane? It is well established that the SNARE protein syntaxin1A forms clusters in the active zone (Takamori et al., 2006; Khuong et al., 2013). Interestingly, the syntaxin1A clusters are dispersed in the absence of $PI(3,4,5)P_3$ at *Drosophila* larval neuromuscular junction (Khuong et al., 2013). Could VLC-SFA containing sphingolipids, similarly, cluster synaptobrevin/VAMPs, the vesicular SNARE binding partners of syntaxins in the SV membrane? Although an intriguing possibility, it is unlikely that islands of VLC-SFA in the membrane would serve as anchoring points for vesicular SNAREs, as the expected effect of VLC-SFA deficiency would be to disorganize the VAMPs, which would lead to slower release. Exactly the opposite of the observed effect of VLC-SFA deficiency in the mouse model (Hopiavuori et al., 2018). The presence of VLC-SFA could impose some ordering of proteins at the fusion site beyond the SNARE proteins, though, as many accessory or modulatory vesicular proteins have transmembrane domains (e.g., Synaptotagmins) or membrane anchoring lipid modifications. Interestingly, the role of VLC-SFA in synaptic release is markedly different from that described for cholesterol, which facilitates synchronized evoked transmitter release (Wasser et al., 2007; Linetti et al., 2010; Teixeira et al., 2012). Miniature synaptic potentials arise from single SV release in the absence of action potentials (Katz and Miledi, 1979; Sara et al., 2005). Therefore, these events are useful direct indicators of membrane fusion dynamics; future studies could address the effect of VLC-SFA on miniature release.

Alternatively, the effect of VLC-SFA anchoring points should be considered for vesicular events that do not complete

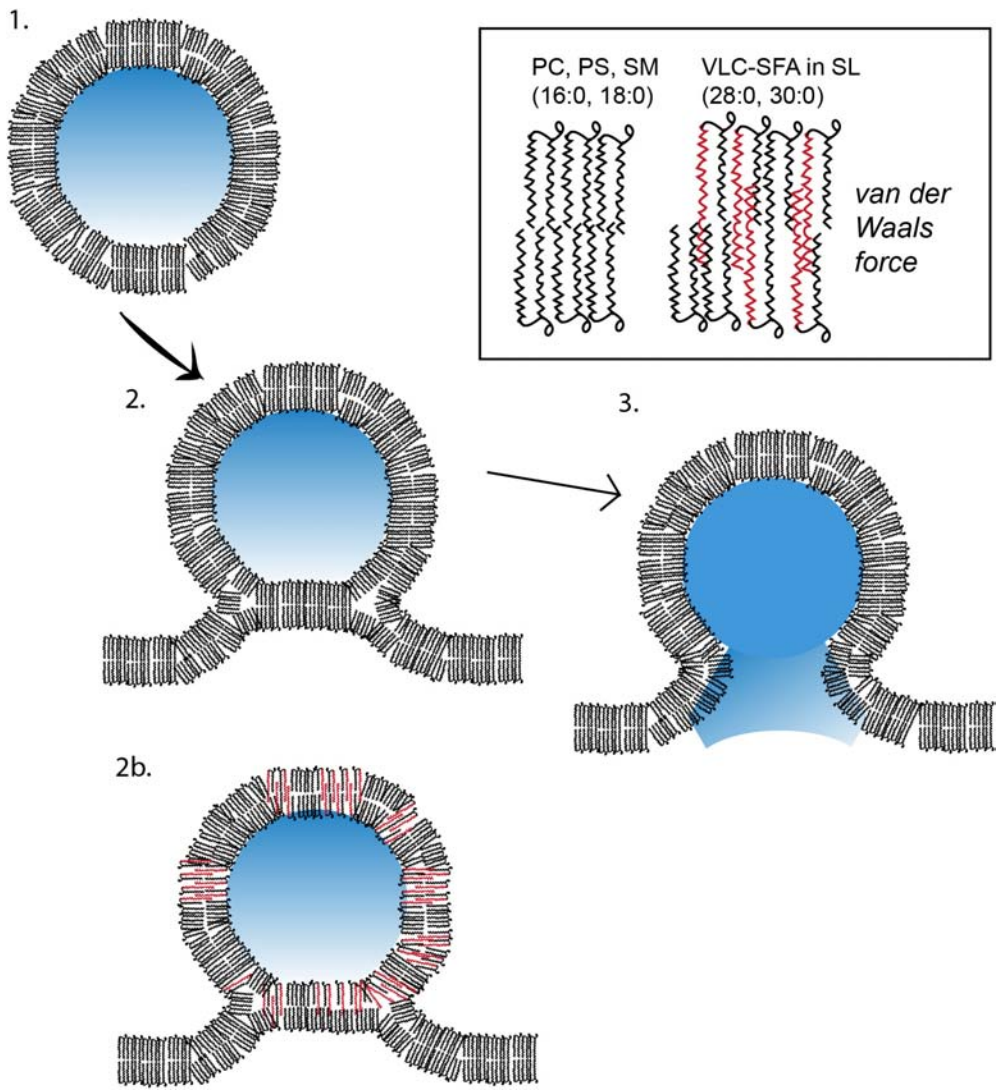

FIGURE 7 | Model of membrane fusion between a VLC-SFA-rich synaptic vesicle and presynaptic active zone membrane. In this cartoon, a synaptic vesicle (SV) containing lipids with common fatty acids (phosphatidylcholine or phosphatidylserine molecules with palmitic, 16:0, and stearic acids, 18:0) is used as a model to illustrate the three stages of synaptic vesicular exocytosis, namely, (1) undocked vesicle; (2) docked and hemifused vesicle stage, with deformation tilt of the membranes and stalk formation; and (3) membrane fusion and contents release stage. In (2b), an SV is depicted with lipids containing, in addition, VLC-SFA (typically 28:0 or 30:0 fatty acid chains, see inset). We have shown that the normal presence of these fatty acids in the SV membrane renders it more stable than do the shorter LC fatty acids, thereby fusing and releasing at comparatively lower rates (Hopiavuori et al., 2018) (PS, phosphatidylserine; PC, phosphatidylcholine; SM, sphingomyelin; SL, sphingolipids; see text for more details).

fusion and intermixing of vesicular membrane with the plasma membrane. Neurophysiologists call such partial fusion events as "Kiss and run" (Fesce et al., 1994; Stevens and Williams, 2000) when the fusion pore is reversibly closed and the vesicle escapes intact without merging fully into the active zone membrane (Gandhi and Stevens, 2003; Südhof and Rizo, 2011). It remains to be tested whether VLC-SFA alter the preference for the fusion mode from total exocytosis to kiss-and-run events.

Another intriguing question is whether VLC-SFA are components of lipid rafts. Lipid rafts are specific microdomains of the plasma membrane, which differ in their composition from the rest of the plasma membrane (Jacobson et al., 2007). Formation of rafts requires cholesterol, and these cholesterol- and sphingolipid-rich plasma membrane microdomains play important roles in compartmentalization of cellular functions. Lipid rafts, which range in size from 10 to 200 nm in diameter, comprise various fractions of the plasma membrane depending on the cell type, and provide a mechanism for ordering clusters of proteins within them (Hao et al., 2001). The detergent-insoluble lipid rafts contain proteins that are modified posttranslationally by acylation or glycosylphosphatidylinositol (GPI) modification. Some as yet unidentified interactions between VLC-SFA and other components of the lipid rafts could increase the stability of the raft domains. Alternatively, the long acyl chain length of

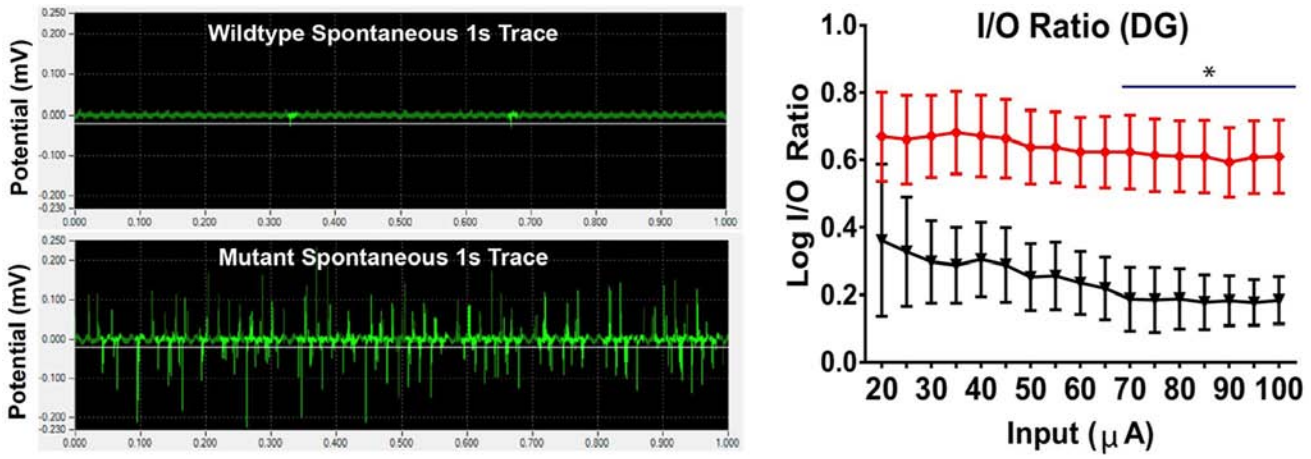

FIGURE 8 | Seizure activity resulting from STGD3 deletion. **Left:** Spontaneous bursting activity in hippocampal slices from $S^{+}Elovl4^{mut/mut}$ mice with knock-in of the 5 bp STGD3 mutation and skin-specific rescue of wildtype (WT) *ELOVL4* function to prevent perinatal lethality, and $S^{+}Elovl4^{wt/wt}$ control mice expressing the WT *ELOVL4* gene under baseline conditions. Representative traces of field potentials from postnatal day 19 $S^{+}Elovl4^{wt/wt}$ **(upper trace)** and $S^{+}Elovl4^{mut/mut}$ mice **(lower trace)**. Each trace represents the first 1 s of a single channel chosen from a 10 min recording taken using a 64 channel multi-electrode array. The $S^{+}Elovl4^{mut/mut}$ slice shows a dramatic increase in spontaneous neuronal activity compared to WT littermates. **Right:** Stepwise increased stimulations to perforant path synapses in dentate gyrus (DG) revealed a markedly enhanced input/output (I/O) ratio indicating a boost in synaptic strength in the main input pathway from the entorhinal cortex of $S^{+}Elovl4^{mut/mut}$ mice (red) compared to $S^{+}Elovl4^{wt/wt}$ control mice (statistics: two-way RM ANOVA, $*p < 0.05$ from 70 to 100 μA). Reproduced from Hopiavuori et al. (2018) with the permission under the Creative Commons Attribution 4.0 International License (link to the Creative Commons license; http://creativecommons.org/licenses/by/4.0/).

VLC-SFA are suited perfectly to the increased width of the lipid bilayer in the rafts.

VLC-PUFA also are potential modulators of synaptic function. Due to their polyunsaturated structure and large size, VLC-PUFA could regulate membrane fluidity and curvature by disrupting phospholipid packing of the lipid bilayer of synaptic membranes, similarly, to DHA and other PUFA (Antonny et al., 2015; Lauwers et al., 2016). The retina provides one example for such a role of VLC-PUFA: depletion of VLC-PUFA from mouse photoreceptors by conditional knockout of *Elovl4* reduced photoreceptor synaptic vesicle diameter compared to synaptic vesicle diameter in wildtype photoreceptors (Bennett et al., 2014b). This change in diameter potentially could affect vesicle fusion or transmitter content. Consistent with this notion, the amplitude of signals in the electroretinogram that reflect transmission of rod photoreceptor signals to the inner retina, also was reduced in the conditional *Elovl4* knockout mice (Bennett et al., 2014a). For more detailed insight on VLC-FA function in the retina and vision, we refer to our colleague's most recent review (Hopiavuori et al., 2019).

Potential Signaling Functions of VLC-SFA and VLC-PUFA

VLC-SFA and VLC-PUFA potentially also might tune synaptic transmission through inter-neuronal interactions. As discussed above, elegant studies by the Bazan laboratory identified a new class of bioactive oxygenated VLC-PUFA derivatives they named elovanoids, including mono-hydroxy 32:6n3, the stable derivative of the hydroperoxy precursor of elovanoid-N32, which has neuroprotective activity in the retina (**Figure 10**; Jun et al., 2017). Alternatively, VLC-SFA or VLC-PUFA could potentially serve as an initial substrate for novel messenger pathways to provide either intracellular or trans-synaptic signals that would modulate synaptic function. For example, endocannabinoids provide retrograde signals to modulate presynaptic function via receptor-mediated signaling (Wilson and Nicoll, 2002; Fan and Yazulla, 2004). Another example to be considered is intracellular signaling via the PLC-PIP2-IP3/DAG pathway.

Proper intracellular membrane trafficking depends on the phosphatidylinositol-phosphate (PIP) system. Although PIPs are a minor fraction of the membrane lipids, they are essential for proper targeting of vesicular traffic and for synaptic endocytosis (Di Paolo et al., 2004; Zoncu et al., 2007). The cytoplasmic side of cellular membranes acquires an asymmetrical PIP profile through an elaborate regulatory system of selective PI kinases, including PIPKgamma (Wenk et al., 2001), PIPK4 (Guo et al., 2003), and phosphatases. Importantly, PIPs also interact with various ion channels. For instance, modulation of transient receptor potential (TRP) channels by phosphoinositides, especially PIP_2, is well established (Rohacs and Nilius, 2007; Rohacs, 2015). Whether VLC-FA can exert similar effects on integral membrane proteins such as ion channels is a fascinating untested question.

Open Questions, Future Directions

Trafficking of VLC-SFA-Containing Membranes From Endoplasmic Reticulum (ER) to SV

Although there is abundant information on ER trafficking from yeast and other single cell organisms (Novick and Schekman, 1979; Balch et al., 1984; Kaiser and Schekman, 1990), the details of

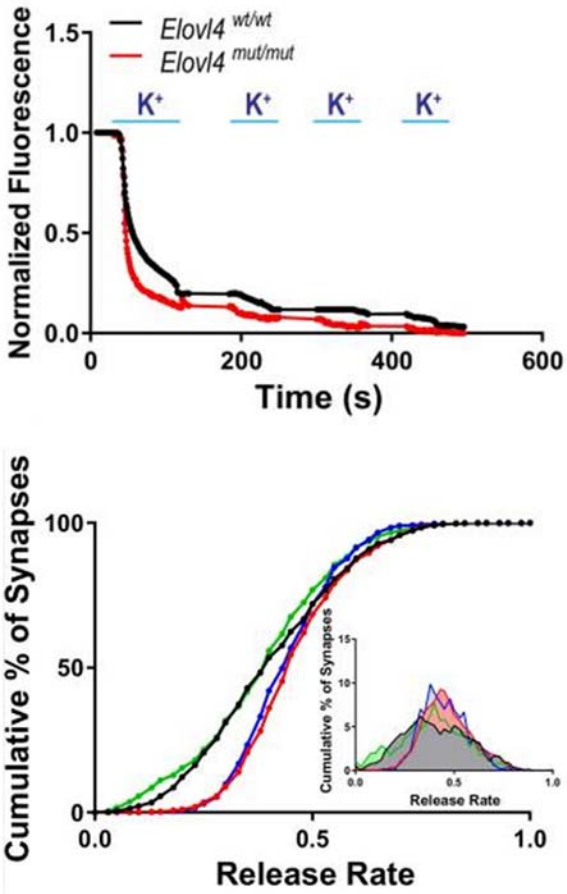

FIGURE 9 | Accelerated synaptic vesicle release in *Elovl4* mutant neurons and its rescue by VLC-SFA. **Top panel:** Faster synaptic release in Elovl4$^{mut/mut}$ hippocampal synapses (red) compared to WT control synapses (black), as detected with FM1-43 dye. Representative traces of average synaptic release activated by four rounds of high K^+ depolarization. **Bottom panel:** Cumulative graph depicts the fraction of total releasable synaptic vesicle pool exocytosed after 15 s depolarization (WT = black line). Vesicle release kinetics was recorded by FM1-43 fluorescence from 900 to 1200 synapses. Note the robust right shift of the cumulative distribution for *Elovl4*$^{mut/mut}$ synapses (red), which is rescued by supplementation with 28:0 and 30:0 SFAs (green) but not by 24:0 (blue). Inset: Frequency distribution of responses with slowest responding synapses on the left, and the fastest on the right on the curve. Reproduced from Hopiavuori et al. (2018) with permission under the Creative Commons Attribution 4.0 International License (link to the Creative Commons license; http://creativecommons.org/licenses/by/4.0/).

SV formation are incompletely understood. Because the enzymes that elongate fatty acids, including ELOVL4, localize to the ER, questions arise about how lipids containing the VLC-SFA get selectively incorporated into synaptic vesicles, during the step of vesicle budding and fusion that precedes the release of vesicles from the ER. Before vesicle budding, v-SNARE and transmembrane cargo proteins from the ER membrane collect into the ER budding zone and recruit the proximal and distal coat assembly, leading to a vesicle bound by a neck to the ER membrane (Bonifacino and Glick, 2004). The cargo then becomes concentrated, membrane curvature increases, and vesicle scission occurs. It is tempting to speculate that there may be interaction between lipids containing VLC-SFA and specific transmembrane cargo proteins of the ER. It may also be envisaged that specific proteins of the proximal coat assembly, which regulate the coordinated sorting of vesicles, play a role in selectively trapping the lipids with VLC-SFA into vesicle populations destined to become SVs.

Targeting of vesicles to different organelles requires highly coordinated modification of the PIPs in their membranes. For instance, PIPK4 phosphorylates PIP_2 in SV (Guo et al., 2003). Interestingly, contact sites between virtually every organelle and the ER have been identified, and the functional importance of these small, specialized membrane domains is increasingly recognized. Recent developments have highlighted the role of PI-4-P gradients as critical determinants of the non-vesicular transport of various lipids from the ER to other organelles such as the Golgi or plasma membrane (Balla, 2018).

In addition to the ER at the soma, a well-developed smooth ER (SER) in neuronal axons has been known for nearly half a century (Droz et al., 1975). The axonal ER has important biosynthetic functions including synthesis of axonal proteins and nerve ending components (Luarte et al., 2018). An interesting possibility is that the lipid composition of SVs originating from the somatic ER might be modified at the axonal SER during their axonal transport. One can also hypothesize that VLC-SFA may be synthesized there and added to sphingosine (by one of the Cer synthases) or exchanged with an ordinary (16:0) FA-containing sphingolipid at the SER by lipid remodeling. It is clear that most ELOVL4 is localized to the somatic SER, but the possibility that a small fraction of ELOVL4 might be present in axonal SER outposts cannot be ruled out.

Further Clinical Implications of VLC-FA

Epilepsy and Ketogenic Diet

Epilepsy patients are prescribed a ketogenic diet – a fat-rich diet that is low in sugars – when all anti-convulsive drugs fail to reduce seizures (Cervenka et al., 2013; Sharma and Tripathi, 2013). The clinical effectiveness of the ketogenic diet (including medium-chain triglyceride diet) has been confirmed in a number of clinical trials carried out mainly on children (Liu, 2008; Kayyali et al., 2014; Kossoff et al., 2018), but its application may be limited by the number of early (gastrointestinal distress, acidosis, hypoglycaemia, dehydration and lethargy), and late adverse effects (hyperuricemia, hyperlipidaemia, kidney stones, easy bruising, and decreases in height and weight) (Ballaban-Gil et al., 1998; Kang et al., 2004; Ulamek-Koziol et al., 2016). With strict monitoring and adapting the diet to the needs of the individual patient according to recently updated guidelines (Kossoff et al., 2018), it is possible to avoid most of these complications. The mechanism by which the ketogenic diet helps to control seizures remains unknown (Kayyali et al., 2014). Assessing changes of VLC-FA levels in the CNS associated with ketogenic diet and seizure disorders could provide valuable insight into the pathophysiology of epilepsy and help to develop more effective therapies.

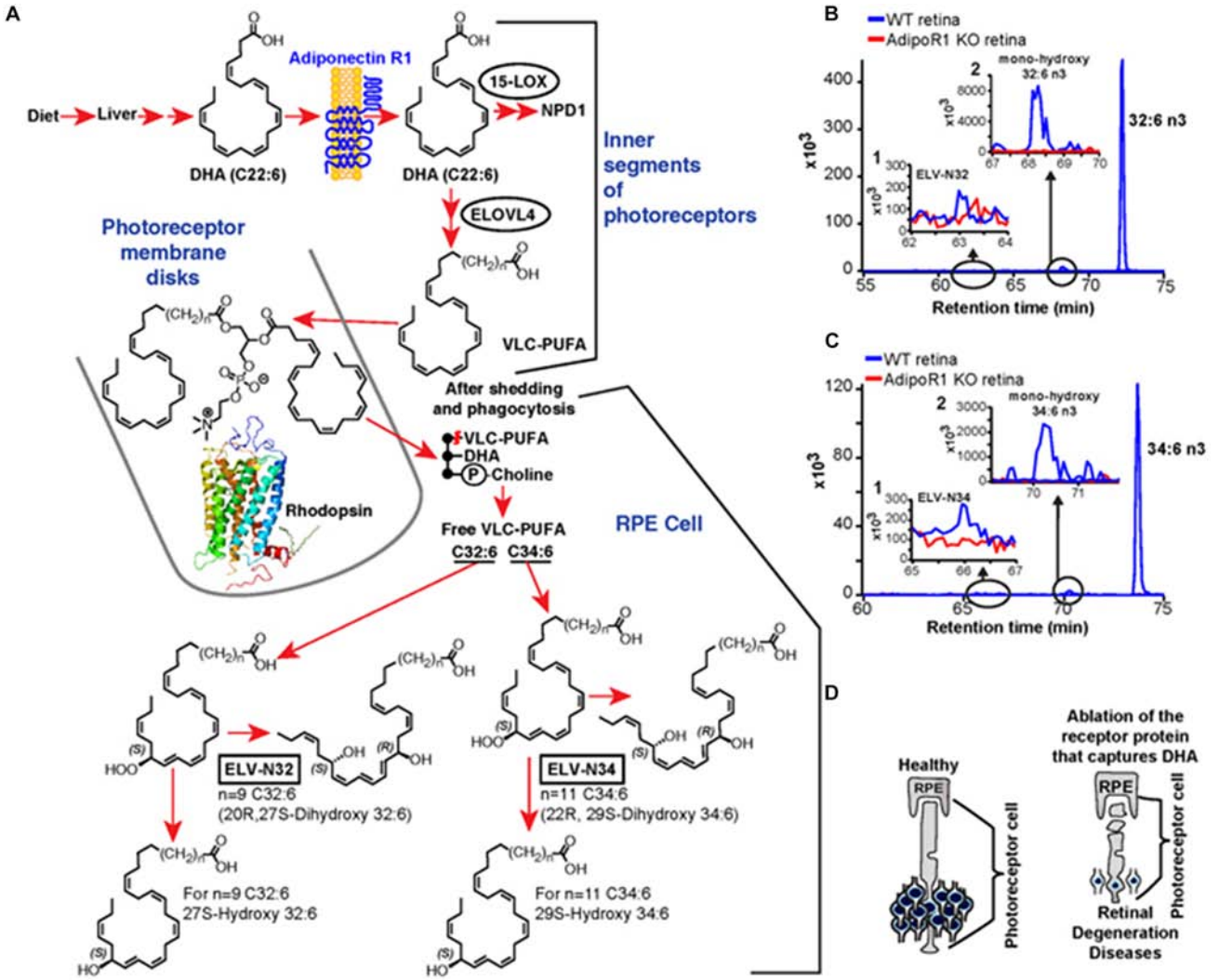

FIGURE 10 | Elovanoid signaling derivatives of VLC-PUFA. Genetic ablation of adiponectin receptor 1 leads to depletion of VLC-PUFAs and its derivatives in retina. **(A)** Dietary DHA, or that derived from dietary 18:3n3, is supplied by the liver and captured by adiponectin receptor 1 (AdipoR1), followed by elongation in the inner segment of PRC by ELOVL4 to VLC-PUFA and incorporation into phosphatidylcholine molecular species, which also contains DHA. During daily PRC outer segment renewal, these phosphatidylcholine molecular species interact with rhodopsin and, after shedding and phagocytosis, become part of RPE cells. UOS or other disruptors of homeostasis trigger the release of VLC-PUFAs. 32:6n3 and 34:6n3 are depicted generating hydroperoxy forms, and then ELV-N32 or ELV-N34, respectively. **(B)** The pool size of free 32:6n3 in retinas of AdipoR1 knockout (KO) mice (red) is decreased as compared with that in wild type (WT) (blue). Insert (1) shows ELV-N32 in KO (red) and WT (blue); insert (2) shows mono-hydroxy 32:6n3, the stable derivative of the hydroperoxy precursor of ELV-N32, in WT (blue) and lack of detectable signal in the KO (red). **(C)** Similarly, the pool size of free 34:6n3 in retinas of AdipoR1 KO mice (red) is decreased as compared with that in WT (blue). Insert (1) shows ELV-N32 in KO (red) and WT (blue); insert (2) shows mono-hydroxy 34:6n3, the stable derivative of the hydroperoxy precursor of ELV-N34, in WT (blue) and lack of detectable signal in the KO (red). **(D)** RPE cells sustain PRC functional integrity (left); right, the ablation of AdipoR1 switches off DHA availability, and PRC degeneration ensues. Reproduced from Jun et al. (2017) with permission under the Creative Commons Attribution 4.0 International License (link to the Creative Commons license; http://creativecommons.org/licenses/by/4.0/).

Dementia and Alzheimer's Disease

There is tremendous interest in nutritional interventions to prevent cognitive impairment in the elderly, including the potential of fatty acids to prevent or slow cognitive impairment (Bazan et al., 2002; Sinn et al., 2010; Calon, 2011; Jiao et al., 2014; Burckhardt et al., 2016; Rangel-Huerta and Gil, 2018). Change in cell membrane lipid composition has been suggested to be associated with cognitive impairment in Alzheimer's disease (Drolle et al., 2017; Diaz et al., 2018; Penke et al., 2018). Moreover, association between beta-amyloid (Aβ), a main pathological hallmark of Alzheimer's, and arachidonic acid in erythrocyte membrane was found to be specific to Apolipoprotein E ε4 non-carrier patients (Hooper et al., 2017). Treatments with DHA or other PUFAs have not provided significant protection from cognitive decline in the elderly thus far (Carrie et al., 2009; Dacks et al., 2013; Jiao et al., 2014; Phillips et al., 2015;

Nishihira et al., 2016; Zhang et al., 2016), however, assessment of treatments including lipids with longer fatty acids than DHA have started only recently. Ongoing massive clinical trials, like the Cognitive Ageing, Nutrition, and Neurogenesis (CANN) trial, are presently testing potential benefits of combined dietary intervention with long-chain n-3 PUFA and flavonoids on cognition in older adults with mild cognitive impairment or subjective memory impairment (Irvine et al., 2018). The studies summarized in this review pose a number of stimulating questions and open future research directions to explore the potential applicability of VLC-FA to the treatment of specific human brain and retina diseases, like cognitive impairment, epileptic seizures and macular degeneration.

IN SUMMARY

Recent studies reveal novel functional roles for ELOVL4 and its VLC-FA products in the CNS, including retina and brain, in health and disease. VLC-PUFA play vital functions in the CNS as precursors of compounds that serve newly recognized roles in homeostatic signaling and regulation of neuronal survival. Most recently it was shown that VLC-SFA have essential functions in synaptic transmission, with disruption of VLC-SFA synthesis leading to seizures and neurodegeneration both in patients lacking ELOVL4 and in mouse models of ELOVL4 mutations. A better understanding of VLC-SFA and VLC-PUFA metabolism and their functions in the CNS holds great promise for development of new therapeutic avenues for treatment of seizures and neurodegenerative diseases.

AUTHOR CONTRIBUTIONS

FD, RA, JF, and DS contributed to the writing and editing of the manuscript.

FUNDING

This work was supported by a Presbyterian Health Foundation Team Science grant to FD, RA, and DS and NIH grant P30AG050911-04S1. FD was supported by a bridge grant from the Presbyterian Health Foundation and NIH grant P30AG050911-04S1. JF was supported by the OUHSC Department of Cell Biology and a Presbyterian Health Foundation Seed Grant to DS. RA was supported by the NIH grants R01EY04149, P30EY021725, and R21NS090117.

ACKNOWLEDGMENTS

The authors are thankful to Dr. Martin-Paul Agbaga, Dr. Blake Hopiavuori, Dr. Raghavendra Y. Nagaraja, Gyening Yeboah, Richard Brush, Megan Stiles, and Dr. Feng Li for their insights and discussion.

REFERENCES

Agbaga, M. P., Brush, R. S., Mandal, M. N., Elliott, M. H., Al-Ubaidi, M. R., and Anderson, R. E. (2010a). Role of ELOVL4 protein in the biosynthesis of docosahexaenoic acid. *Adv. Exp. Med. Biol.* 664, 233–242. doi: 10.1007/978-1-4419-1399-9-27

Agbaga, M. P., Mandal, M. N., and Anderson, R. E. (2010b). Retinal very long-chain PUFAs: new insights from studies on ELOVL4 protein. *J. Lipid Res.* 51, 1624–1642. doi: 10.1194/jlr.R005025

Agbaga, M. P., Brush, R. S., Mandal, M. N., Henry, K., Elliott, M. H., and Anderson, R. E. (2008). Role of Stargardt-3 macular dystrophy protein (ELOVL4) in the biosynthesis of very long chain fatty acids. *Proc. Natl. Acad. Sci. U.S.A.* 105, 12843–12848. doi: 10.1073/pnas.0802607105

Agbaga, M. P., Merriman, D. K., Brush, R. S., Lydic, T. A., Conley, S. M., Naash, M. I., et al. (2018). Differential composition of DHA and very-long-chain PUFAs in rod and cone photoreceptors. *J. Lipid Res.* 59, 1586–1596. doi: 10.1194/jlr.M082495

Aldahmesh, M. A., Mohamed, J. Y., Alkuraya, H. S., Verma, I. C., Puri, R. D., Alaiya, A. A., et al. (2011). Recessive mutations in ELOVL4 cause ichthyosis, intellectual disability, and spastic quadriplegia. *Am. J. Hum. Genet.* 89, 745–750. doi: 10.1016/j.ajhg.2011.10.011

Amen, N., Mathow, D., Rabionet, M., Sandhoff, R., Langbein, L., Gretz, N., et al. (2013). Differentiation of epidermal keratinocytes is dependent on glucosylceramide:ceramide processing. *Hum. Mol. Genet.* 22, 4164–4179. doi: 10.1093/hmg/ddt264

Antonny, B., Vanni, S., Shindou, H., and Ferreira, T. (2015). From zero to six double bonds: phospholipid unsaturation and organelle function. *Trends Cell Biol.* 25, 427–436. doi: 10.1016/j.tcb.2015.03.004

Aveldano, M. I. (1987). A novel group of very long chain polyenoic fatty acids in dipolyunsaturated phosphatidylcholines from vertebrate retina. *J. Biol. Chem.* 262, 1172–1179.

Balch, W. E., Dunphy, W. G., Braell, W. A., and Rothman, J. E. (1984). Reconstitution of the transport of protein between successive compartments of the Golgi measured by the coupled incorporation of N-acetylglucosamine. *Cell* 39(2 Pt 1), 405–416. doi: 10.1016/0092-8674(84)90019-9

Balla, T. (2018). Ca(2+) and lipid signals hold hands at endoplasmic reticulum-plasma membrane contact sites. *J. Physiol.* 596, 2709–2716. doi: 10.1113/JP274957

Ballaban-Gil, K., Callahan, C., O'Dell, C., Pappo, M., Moshe, S., and Shinnar, S. (1998). Complications of the ketogenic diet. *Epilepsia* 39, 744–748.

Bardak, H., Gunay, M., Ercalik, Y., Bardak, Y., Ozbas, H., Bagci, O., et al. (2016). Analysis of ELOVL4 and PRPH2 genes in turkish stargardt disease patients. *Genet. Mol. Res.* 15, 1–6. doi: 10.4238/gmr15048774

Bazan, N. G. (2018). Docosanoids and elovanoids from omega-3 fatty acids are pro-homeostatic modulators of inflammatory responses, cell damage and neuroprotection. *Mol. Aspects Med.* 64, 18–33. doi: 10.1016/j.mam.2018.09.003

Bazan, N. G., Colangelo, V., and Lukiw, W. J. (2002). Prostaglandins and other lipid mediators in Alzheimer's disease. *Prostaglandins Other Lipid Mediat.* 6, 197–210. doi: 10.1016/s0090-6980(02)00031-x

Bazinet, R. P., and Laye, S. (2014). Polyunsaturated fatty acids and their metabolites in brain function and disease. *Nat. Rev. Neurosci.* 15, 771–785. doi: 10.1038/nrn3820

Bennett, L. D., Brush, R. S., Chan, M., Lydic, T. A., Reese, K., Reid, G. E., et al. (2014a). Effect of reduced retinal VLC-PUFA on rod and cone photoreceptors. *Invest. Ophthalmol. Vis. Sci.* 55, 3150–3157. doi: 10.1167/iovs.14-13995

Bennett, L. D., Hopiavuori, B. R., Brush, R. S., Chan, M., Van Hook, M. J., Thoreson, W. B., et al. (2014b). Examination of VLC-PUFA-deficient photoreceptor terminals. *Invest Ophthalmol. Vis. Sci.* 55, 4063–4072. doi: 10.1167/iovs.14-13997

Bernstein, P. S., Tammur, J., Singh, N., Hutchinson, A., Dixon, M., Pappas, C. M., et al. (2001). Diverse macular dystrophy phenotype caused by a novel complex mutation in the ELOVL4 gene. *Invest. Ophthalmol. Vis. Sci.* 42, 3331–3336.

Bhattacharjee, S., Jun, B., Belayev, L., Heap, J., Kautzmann, M. A., Obenaus, A., et al. (2017). Elovanoids are a novel class of homeostatic lipid mediators that protect neural cell integrity upon injury. *Sci. Adv.* 3:e1700735. doi: 10.1126/sciadv.1700735

Bonifacino, J. S., and Glick, B. S. (2004). The mechanisms of vesicle budding and fusion. *Cell* 116, 153–166. doi: 10.1016/s0092-8674(03)01079-1

Bourassa, C. V., Raskin, S., Serafini, S., Teive, H. A., Dion, P. A., and Rouleau, G. A. (2015). A new ELOVL4 mutation in a case of spinocerebellar ataxia with erythrokeratodermia. *JAMA Neurol.* 72, 942–943. doi: 10.1001/jamaneurol.2015.0888

Bourque, P. R., Warman-Chardon, J., Lelli, D. A., LaBerge, L., Kirshen, C., Bradshaw, S. H., et al. (2018). Novel ELOVL4 mutation associated with erythrokeratodermia and spinocerebellar ataxia (SCA 34). *Neurol. Genet.* 4:e263. doi: 10.1212/NXG.0000000000000263

Bozek, K., Wei, Y., Yan, Z., Liu, X., Xiong, J., Sugimoto, M., et al. (2015). Organization and evolution of brain lipidome revealed by large-scale analysis of human, chimpanzee, macaque, and mouse tissues. *Neuron* 85, 695–702. doi: 10.1016/j.neuron.2015.01.003

Brodde, A., Teigler, A., Brugger, B., Lehmann, W. D., Wieland, F., Berger, J., et al. (2012). Impaired neurotransmission in ether lipid-deficient nerve terminals. *Hum. Mol. Genet.* 21, 2713–2724. doi: 10.1093/hmg/dds097

Burckhardt, M., Herke, M., Wustmann, T., Watzke, S., Langer, G., and Fink, A. (2016). Omega-3 fatty acids for the treatment of dementia. *Cochrane Database Syst. Rev.* 4:CD009002. doi: 10.1002/14651858.CD009002.pub3

Cadieux-Dion, M., Turcotte-Gauthier, M., Noreau, A., Martin, C., Meloche, C., Gravel, M., et al. (2014). Expanding the clinical phenotype associated with ELOVL4 mutation: study of a large french-canadian family with autosomal dominant spinocerebellar ataxia and erythrokeratodermia. *JAMA Neurol.* 71, 470–475. doi: 10.1001/jamaneurol.2013.6337

Calon, F. (2011). Omega-3 polyunsaturated fatty acids in Alzheimer's disease: key questions and partial answers. *Curr. Alzheimer Res.* 8, 470–478. doi: 10.2174/156720511796391881

Cameron, D. J., Tong, Z., Yang, Z., Kaminoh, J., Kamiyah, S., Chen, H., et al. (2007). Essential role of Elovl4 in very long chain fatty acid synthesis, skin permeability barrier function, and neonatal survival. *Int. J. Biol. Sci.* 3, 111–119. doi: 10.7150/ijbs.3.111

Carmona-Antonanzas, G., Monroig, O., Dick, J. R., Davie, A., and Tocher, D. R. (2011). Biosynthesis of very long-chain fatty acids (C>24) in atlantic salmon: cloning, functional characterisation, and tissue distribution of an Elovl4 elongase. *Comp. Biochem. Physiol. B Biochem. Mol. Biol.* 159, 122–129. doi: 10.1016/j.cbpb.2011.02.007

Carrie, I., Abellan Van Kan, G., Rolland, Y., Gillette-Guyonnet, S., and Vellas, B. (2009). PUFA for prevention and treatment of dementia? *Curr. Pharm. Des.* 15, 4173–4185. doi: 10.2174/138161209789909764

Carta, M., Lanore, F., Rebola, N., Szabo, Z., Da Silva, S. V., Lourenco, J., et al. (2014). Membrane lipids tune synaptic transmission by direct modulation of presynaptic potassium channels. *Neuron* 81, 787–799. doi: 10.1016/j.neuron.2013.12.028

Castro, L. F., Tocher, D. R., and Monroig, O. (2016). Long-chain polyunsaturated fatty acid biosynthesis in chordates: insights into the evolution of Fads and Elovl gene repertoire. *Prog. Lipid Res.* 62, 25–40. doi: 10.1016/j.plipres.2016.01.001

Cervenka, M. C., Henry, B., Nathan, J., Wood, S., and Volek, J. S. (2013). Worldwide dietary therapies for adults with epilepsy and other disorders. *J. Child Neurol.* 28, 1034–1040. doi: 10.1177/0883073813488671

Craig, L. B., Brush, R. S., Sullivan, M. T., Zavy, M. T., Agbaga, M. P., and Anderson, R. E. (2019). Decreased very long chain polyunsaturated fatty acids in sperm correlates with sperm quantity and quality. *J. Assist. Reprod. Genet.* 36, 1379–1385. doi: 10.1007/s10815-019-01464-3

Cremona, O., Di Paolo, G., Wenk, M. R., Luthi, A., Kim, W. T., Takei, K., et al. (1999). Essential role of phosphoinositide metabolism in synaptic vesicle recycling. *Cell* 99, 179–188. doi: 10.1016/s0092-8674(00)81649-9

Dacks, P. A., Shineman, D. W., and Fillit, H. M. (2013). Current evidence for the clinical use of long-chain polyunsaturated n-3 fatty acids to prevent age-related cognitive decline and Alzheimer's disease. *J. Nutr. Health Aging* 17, 240–251. doi: 10.1007/s12603-012-0431-3

Deák, F., Shin, O. H., Kavalali, E. T., and Sudhof, T. C. (2006a). Structural determinants of synaptobrevin 2 function in synaptic vesicle fusion. *J. Neurosci.* 26, 6668–6676. doi: 10.1523/JNEUROSCI.5272-05.2006

Deák, F., Shin, O. H., Tang, J., Hanson, P., Ubach, J., Jahn, R., et al. (2006b). Rabphilin regulates SNARE-dependent re-priming of synaptic vesicles for fusion. *EMBO J.* 25, 2856–2866. doi: 10.1038/sj.emboj.7601165

Deák, F., Xu, Y., Chang, W. P., Dulubova, I., Khvotchev, M., Liu, X., et al. (2009). Munc18-1 binding to the neuronal SNARE complex controls synaptic vesicle priming. *J. Cell Biol.* 184, 751–764. doi: 10.1083/jcb.200812026

Di Gregorio, E., Borroni, B., Giorgio, E., Lacerenza, D., Ferrero, M., Lo Buono, N., et al. (2014). ELOVL5 mutations cause spinocerebellar ataxia 38. *Am. J. Hum. Genet.* 95, 209–217. doi: 10.1016/j.ajhg.2014.07.001

Di Paolo, G., Moskowitz, H. S., Gipson, K., Wenk, M. R., Voronov, S., Obayashi, M., et al. (2004). Impaired PtdIns(4,5)P2 synthesis in nerve terminals produces defects in synaptic vesicle trafficking. *Nature* 431, 415–422. doi: 10.1038/nature02896

Diaz, M., Fabelo, N., Ferrer, I., and Marin, R. (2018). "Lipid raft aging" in the human frontal cortex during nonpathological aging: gender influences and potential implications in Alzheimer's disease. *Neurobiol. Aging* 67, 42–52. doi: 10.1016/j.neurobiolaging.2018.02.022

Dickson, D. W. (1997). The pathogenesis of senile plaques. *J. Neuropathol. Exp. Neurol.* 56, 321–339. doi: 10.1097/00005072-199704000-00001

Donato, L., Scimone, C., Rinaldi, C., Aragona, P., Briuglia, S., D'Ascola, A., et al. (2018). Stargardt phenotype associated with two ELOVL4 promoter variants and ELOVL4 downregulation: new possible perspective to etiopathogenesis? *Invest. Ophthalmol. Vis. Sci.* 59, 843–857. doi: 10.1167/iovs.17-22962

Drolle, E., Negoda, A., Hammond, K., Pavlov, E., and Leonenko, Z. (2017). Changes in lipid membranes may trigger amyloid toxicity in Alzheimer's disease. *PLoS One* 12:e0182194. doi: 10.1371/journal.pone.0182194

Droz, B., Rambourg, A., and Koenig, H. L. (1975). The smooth endoplasmic reticulum: structure and role in the renewal of axonal membrane and synaptic vesicles by fast axonal transport. *Brain Res.* 93, 1–13. doi: 10.1016/0006-8993(75)90282-6

Edwards, A. O., Donoso, L. A., and Ritter, R. (2001). A novel gene for autosomal dominant Stargardt-like macular dystrophy with homology to the SUR4 protein family. *Invest. Ophthalmol. Vis. Sci.* 42, 2652–2663.

Fan, S. F., and Yazulla, S. (2004). Inhibitory interaction of cannabinoid CB1 receptor and dopamine D2 receptor agonists on voltage-gated currents of goldfish cones. *Vis. Neurosci.* 21, 69–77. doi: 10.1017/s0952523804041070

Fernandez-Chacon, R., Konigstorfer, A., Gerber, S. H., Garcia, J., Matos, M. F., Stevens, C. F., et al. (2001). Synaptotagmin I functions as a calcium regulator of release probability. *Nature* 410, 41–49. doi: 10.1038/35065004

Fesce, R., Grohovaz, F., Valtorta, F., and Meldolesi, J. (1994). Neurotransmitter release: fusion or 'kiss-and-run'? *Trends Cell Biol.* 4, 1–4. doi: 10.1016/0962-8924(94)90025-6

Gandhi, S. P., and Stevens, C. F. (2003). Three modes of synaptic vesicular recycling revealed by single-vesicle imaging. *Nature* 423, 607–613. doi: 10.1038/nature01677

Garagnani, P., Bacalini, M. G., Pirazzini, C., Gori, D., Giuliani, C., Mari, D., et al. (2012). Methylation of ELOVL2 gene as a new epigenetic marker of age. *Aging Cell* 11, 1132–1134. doi: 10.1111/acel.12005

Gopalan, S., Carja, O., Fagny, M., Patin, E., Myrick, J. W., McEwen, L. M., et al. (2017). Trends in DNA methylation with age replicate across diverse human populations. *Genetics* 206, 1659–1674. doi: 10.1534/genetics.116.195594

Grayson, C., and Molday, R. S. (2005). Dominant negative mechanism underlies autosomal dominant stargardt-like macular dystrophy linked to mutations in ELOVL4. *J. Biol. Chem.* 280, 32521–32530. doi: 10.1074/jbc.M503411200

Guillou, H., Zadravec, D., Martin, P. G., and Jacobsson, A. (2010). The key roles of elongases and desaturases in mammalian fatty acid metabolism: insights from transgenic mice. *Prog. Lipid Res.* 49, 186–199. doi: 10.1016/j.plipres.2009.12.002

Guo, J., Wenk, M. R., Pellegrini, L., Onofri, F., Benfenati, F., and De Camilli, P. (2003). Phosphatidylinositol 4-kinase type IIalpha is responsible for the phosphatidylinositol 4-kinase activity associated with synaptic vesicles. *Proc. Natl. Acad. Sci. U.S.A.* 100, 3995–4000. doi: 10.1073/pnas.0230488100

Hao, M., Mukherjee, S., and Maxfield, F. R. (2001). Cholesterol depletion induces large scale domain segregation in living cell membranes. *Proc. Natl. Acad. Sci. U.S.A.* 98, 13072–13077. doi: 10.1073/pnas.231377398

Hastings, N., Agaba, M. K., Tocher, D. R., Zheng, X., Dickson, C. A., Dick, J. R., et al. (2004). Molecular cloning and functional characterization of fatty acyl desaturase and elongase cDNAs involved in the production of eicosapentaenoic and docosahexaenoic acids from alpha-linolenic acid in Atlantic salmon (salmo salar). *Mar. Biotechnol.* 6, 463–474. doi: 10.1007/s10126-004-3002-8

Hata, Y., Slaughter, C. A., and Sudhof, T. C. (1993). Synaptic vesicle fusion complex contains unc-18 homologue bound to syntaxin. *Nature* 366, 347–351. doi: 10.1038/366347a0

Hooper, C., De Souto Barreto, P., Payoux, P., Salabert, A. S., Guyonnet, S., Andrieu, S., et al. (2017). Cross-sectional associations of cortical beta-amyloid with erythrocyte membrane long-chain polyunsaturated fatty acids in older adults with subjective memory complaints. *J. Neurochem.* 142, 589–596. doi: 10.1111/jnc.14062

Hopiavuori, B. R., Agbaga, M. P., Brush, R. S., Sullivan, M. T., Sonntag, W. E., and Anderson, R. E. (2017). Regional changes in CNS and retinal glycerophospholipid profiles with age: a molecular blueprint. *J. Lipid Res.* 58, 668–680. doi: 10.1194/jlr.M070714

Hopiavuori, B. R., Anderson, R. E., and Agbaga, M. P. (2019). ELOVL4: very long-chain fatty acids serve an eclectic role in mammalian health and function. *Prog. Retin. Eye Res.* 69, 137–158. doi: 10.1016/j.preteyeres.2018.10.004

Hopiavuori, B. R., Deak, F., Wilkerson, J. L., Brush, R. S., Rocha-Hopiavuori, N. A., Hopiavuori, A. R., et al. (2018). Homozygous expression of mutant ELOVL4 leads to seizures and death in a novel animal model of very long-chain fatty acid deficiency. *Mol. Neurobiol.* 55, 1795–1813. doi: 10.1007/s12035-017-0824-8

Hoxha, E., Gabriele, R. M. C., Balbo, I., Ravera, F., Masante, L., Zambelli, V., et al. (2017). Motor deficits and cerebellar atrophy in Elovl5 knock out mice. *Front. Cell Neurosci.* 11:343. doi: 10.3389/fncel.2017.00343

Imig, C., Min, S. W., Krinner, S., Arancillo, M., Rosenmund, C., Sudhof, T. C., et al. (2014). The morphological and molecular nature of synaptic vesicle priming at presynaptic active zones. *Neuron* 84, 416–431. doi: 10.1016/j.neuron.2014.10.009

Irvine, M. A., Scholey, A., King, R., Gillings, R., Vauzour, D., Demichele, S. J., et al. (2018). The cognitive ageing, nutrition and neurogenesis (CANN) trial: design and progress. *Alzheimers Dement.* 4, 591–601. doi: 10.1016/j.trci.2018.08.001

Jacobson, K., Mouritsen, O. G., and Anderson, R. G. (2007). Lipid rafts: at a crossroad between cell biology and physics. *Nat. Cell Biol.* 9, 7–14. doi: 10.1038/ncb0107-7

Jakobsson, A., Westerberg, R., and Jacobsson, A. (2006). Fatty acid elongases in mammals: their regulation and roles in metabolism. *Prog. Lipid Res.* 45, 237–249. doi: 10.1016/j.plipres.2006.01.004

Janssen, R. J., Distelmaier, F., Smeets, R., Wijnhoven, T., Ostergaard, E., Jaspers, N. G., et al. (2009). Contiguous gene deletion of ELOVL7, ERCC8 and NDUFAF2 in a patient with a fatal multisystem disorder. *Hum. Mol. Genet.* 18, 3365–3374. doi: 10.1093/hmg/ddp276

Jiao, J., Li, Q., Chu, J., Zeng, W., Yang, M., and Zhu, S. (2014). Effect of n-3 PUFA supplementation on cognitive function throughout the life span from infancy to old age: a systematic review and meta-analysis of randomized controlled trials. *Am. J. Clin. Nutr.* 100, 1422–1436. doi: 10.3945/ajcn.114.095315

Jun, B., Mukherjee, P. K., Asatryan, A., Kautzmann, M. A., Heap, J., Gordon, W. C., et al. (2017). Elovanoids are novel cell-specific lipid mediators necessary for neuroprotective signaling for photoreceptor cell integrity. *Sci. Rep.* 7:5279. doi: 10.1038/s41598-017-05433-7

Jung, S. E., Lim, S. M., Hong, S. R., Lee, E. H., Shin, K. J., and Lee, H. Y. (2019). DNA methylation of the ELOVL2, FHL2, KLF14, C1orf132/MIR29B2C, and TRIM59 genes for age prediction from blood, saliva, and buccal swab samples. *Forensic. Sci. Int. Genet.* 38, 1–8. doi: 10.1016/j.fsigen.2018.09.010

Kaiser, C. A., and Schekman, R. (1990). Distinct sets of SEC genes govern transport vesicle formation and fusion early in the secretory pathway. *Cell* 61, 723–733. doi: 10.1016/0092-8674(90)90483-u

Kang, H. C., Chung, D. E., Kim, D. W., and Kim, H. D. (2004). Early- and late-onset complications of the ketogenic diet for intractable epilepsy. *Epilepsia* 45, 1116–1123. doi: 10.1111/j.0013-9580.2004.10004.x

Katz, B., and Miledi, R. (1979). Estimates of quantal content during 'chemical potentiation' of transmitter release. *Proc. R. Soc. Lond. B Biol. Sci.* 205, 369–378. doi: 10.1098/rspb.1979.0070

Kayyali, H. R., Gustafson, M., Myers, T., Thompson, L., Williams, M., and Abdelmoity, A. (2014). Ketogenic diet efficacy in the treatment of intractable epileptic spasms. *Pediatr. Neurol.* 50, 224–227. doi: 10.1016/j.pediatrneurol.2013.11.021

Khuong, T. M., Habets, R. L., Kuenen, S., Witkowska, A., Kasprowicz, J., Swerts, J., et al. (2013). Synaptic PI(3,4,5)P3 is required for syntaxin1a clustering and neurotransmitter release. *Neuron* 77, 1097–1108. doi: 10.1016/j.neuron.2013.01.025

Kihara, A. (2012). Very long-chain fatty acids: elongation, physiology and related disorders. *J. Biochem.* 152, 387–395. doi: 10.1093/jb/mvs105

Kikuchi, M., Shimada, M., Matsuzaka, T., Ishii, K., Nakagawa, Y., Takayanagi, M., et al. (2016). Crucial role of Elovl6 in chondrocyte growth and differentiation during growth plate development in mice. *PLoS One* 11:e0159375. doi: 10.1371/journal.pone.0159375

Kohlhardt, M. (1989). Insensitivity of the open state of (-)-DPI-modified cardiac Na+ channels to the blocking effects of the (+) enantiomer. *Eur. J. Pharmacol.* 168, 115–118. doi: 10.1016/0014-2999(89)90642-0

Konishi, H., Okuda, A., Ohno, Y., and Kihara, A. (2010). Characterization of HACD1 K64Q mutant found in arrhythmogenic right ventricular dysplasia patients. *J. Biochem.* 148, 617–622. doi: 10.1093/jb/mvq092

Kossoff, E. H., Zupec-Kania, B. A., Auvin, S., Ballaban-Gil, K. R., Christina Bergqvist, A. G., Blackford, R., et al. (2018). Optimal clinical management of children receiving dietary therapies for epilepsy: updated recommendations of the International ketogenic diet study group. *Epilepsia Open* 3, 175–192. doi: 10.1002/epi4.12225

Lauwers, E., Goodchild, R., and Verstreken, P. (2016). Membrane lipids in presynaptic function and disease. *Neuron* 90, 11–25. doi: 10.1016/j.neuron.2016.02.033

Lein, E. S., Hawrylycz, M. J., Ao, N., Ayres, M., Bensinger, A., Bernard, A., et al. (2007). Genome-wide atlas of gene expression in the adult mouse brain. *Nature* 445, 168–176. doi: 10.1038/nature05453

Leonard, A. E., Kelder, B., Bobik, E. G., Chuang, L. T., Lewis, C. J., Kopchick, J. J., et al. (2002). Identification and expression of mammalian long-chain PUFA elongation enzymes. *Lipids* 37, 733–740. doi: 10.1007/s11745-002-0955-6

Li, G., Cui, S., Du, J., Liu, J., Zhang, P., Fu, Y., et al. (2018). Association of GALC, ZNF184, IL1R2 and ELOVL7 with parkinson's disease in southern chinese. *Front. Aging Neurosci.* 10:402. doi: 10.3389/fnagi.2018.00402

Lin, Z., Huang, Y., Zou, W., Rong, H., Hao, M., and Wen, X. (2018). Cloning, tissue distribution, functional characterization and nutritional regulation of a fatty acyl Elovl5 elongase in chu's croaker Nibea coibor. *Gene* 659, 11–21. doi: 10.1016/j.gene.2018.03.046

Linetti, A., Fratangeli, A., Taverna, E., Valnegri, P., Francolini, M., Cappello, V., et al. (2010). Cholesterol reduction impairs exocytosis of synaptic vesicles. *J. Cell Sci.* 123(Pt 4), 595–605. doi: 10.1242/jcs.060681

Liu, Y. M. (2008). Medium-chain triglyceride (MCT) ketogenic therapy. *Epilepsia* 49(Suppl. 8), 33–36. doi: 10.1111/j.1528-1167.2008.01830.x

Logan, S., Agbaga, M. P., Chan, M. D., Brush, R. S., and Anderson, R. E. (2014). Endoplasmic reticulum microenvironment and conserved histidines govern ELOVL4 fatty acid elongase activity. *J. Lipid Res.* 55, 698–708. doi: 10.1194/jlr.M045443

Logan, S., Agbaga, M. P., Chan, M. D., Kabir, N., Mandal, N. A., Brush, R. S., et al. (2013). Deciphering mutant ELOVL4 activity in autosomal-dominant stargardt macular dystrophy. *Proc. Natl. Acad. Sci. U.S.A.* 110, 5446–5451. doi: 10.1073/pnas.1217251110

Luarte, A., Cornejo, V. H., Bertin, F., Gallardo, J., and Couve, A. (2018). The axonal endoplasmic reticulum: one organelle-many functions in development, maintenance, and plasticity. *Dev. Neurobiol.* 78, 181–208. doi: 10.1002/dneu.22560

Mandal, M. N., Ambasudhan, R., Wong, P. W., Gage, P. J., Sieving, P. A., and Ayyagari, R. (2004). Characterization of mouse orthologue of ELOVL4: genomic organization and spatial and temporal expression. *Genomics* 83, 626–635. doi: 10.1016/j.ygeno.2003.09.020

Marza, E., Long, T., Saiardi, A., Sumakovic, M., Eimer, S., Hall, D. H., et al. (2008). Polyunsaturated fatty acids influence synaptojanin localization to regulate synaptic vesicle recycling. *Mol. Biol Cell.* 19, 833–842. doi: 10.1091/mbc.e07-07-0719

Matsuzaka, T., Shimano, H., Yahagi, N., Kato, T., Atsumi, A., Yamamoto, T., et al. (2007). Crucial role of a long-chain fatty acid elongase, Elovl6, in obesity-induced insulin resistance. *Nat. Med.* 13, 1193–1202. doi: 10.1038/nm1662

Maugeri, A., Meire, F., Hoyng, C. B., Vink, C., Van Regemorter, N., Karan, G., et al. (2004). A novel mutation in the ELOVL4 gene causes autosomal dominant Stargardt-like macular dystrophy. *Invest. Ophthalmol. Vis. Sci.* 45, 4263–4267. doi: 10.1167/iovs.04-0078

McMahon, A., Butovich, I. A., Mata, N. L., Klein, M., Ritter, R. III, Richardson, J., et al. (2007). Retinal pathology and skin barrier defect in mice carrying a stargardt disease-3 mutation in elongase of very long chain fatty acids-4. *Mol. Vis.* 13, 258–272.

McMahon, A., Lu, H., and Butovich, I. A. (2014). A role for ELOVL4 in the mouse meibomian gland and sebocyte cell biology. *Invest. Ophthalmol. Vis. Sci.* 55, 2832–2840. doi: 10.1167/iovs.13-13335

McNew, J. A., Weber, T., Parlati, F., Johnston, R. J., Melia, T. J., Sollner, T. H., et al. (2000). Close is not enough: SNARE-dependent membrane fusion requires an active mechanism that transduces force to membrane anchors. *J. Cell Biol.* 150, 105–117.

Melia, T. J., Weber, T., McNew, J. A., Fisher, L. E., Johnston, R. J., Parlati, F., et al. (2002). Regulation of membrane fusion by the membrane-proximal coil of the t-SNARE during zippering of SNAREpins. *J. Cell Biol.* 158, 929–940. doi: 10.1083/jcb.200112081

Mir, H., Raza, S. I., Touseef, M., Memon, M. M., Khan, M. N., Jaffar, S., et al. (2014). A novel recessive mutation in the gene ELOVL4 causes a neuro-ichthyotic disorder with variable expressivity. *BMC Med. Genet.* 15:25. doi: 10.1186/1471-2350-15-25

Molday, R. S., and Zhang, K. (2010). Defective lipid transport and biosynthesis in recessive and dominant stargardt macular degeneration. *Prog. Lipid Res.* 49, 476–492. doi: 10.1016/j.plipres.2010.07.002

Monroig, O., Rotllant, J., Cerda-Reverter, J. M., Dick, J. R., Figueras, A., and Tocher, D. R. (2010). Expression and role of Elovl4 elongases in biosynthesis of very long-chain fatty acids during zebrafish danio rerio early embryonic development. *Biochim. Biophys. Acta* 1801, 1145–1154. doi: 10.1016/j.bbalip.2010.06.005

Monroig, Ó, Webb, K., Ibarra-Castro, L., Holt, G. J., and Tocher, D. R. (2011). Biosynthesis of long-chain polyunsaturated fatty acids in marine fish: characterization of an Elovl4-like elongase from cobia rachycentron canadum and activation of the pathway during early life stages. *Aquaculture* 312, 145–153. doi: 10.1016/j.aquaculture.2010.12.024

Moon, Y. A., and Horton, J. D. (2003). Identification of two mammalian reductases involved in the two-carbon fatty acyl elongation cascade. *J. Biol. Chem.* 278, 7335–7343. doi: 10.1074/jbc.M211684200

Moon, Y. A., Ochoa, C. R., Mitsche, M. A., Hammer, R. E., and Horton, J. D. (2014). Deletion of ELOVL6 blocks the synthesis of oleic acid but does not prevent the development of fatty liver or insulin resistance. *J. Lipid Res.* 55, 2597–2605. doi: 10.1194/jlr.M054353

Moon, Y. A., Shah, N. A., Mohapatra, S., Warrington, J. A., and Horton, J. D. (2001). Identification of a mammalian long chain fatty acyl elongase regulated by sterol regulatory element-binding proteins. *J. Biol. Chem.* 276, 45358–45366. doi: 10.1074/jbc.M108413200

Morais, S., Monroig, O., Zheng, X., Leaver, M. J., and Tocher, D. R. (2009). Highly unsaturated fatty acid synthesis in Atlantic salmon: characterization of ELOVL5- and ELOVL2-like elongases. *Mar. Biotechnol.* 11, 627–639. doi: 10.1007/s10126-009-9179-0

Mueller, N., Sassa, T., Morales-Gonzalez, S., Schneider, J., Salchow, D. J., Seelow, D., et al. (2019). De novo mutation in ELOVL1 causes ichthyosis, acanthosis nigricans, hypomyelination, spastic paraplegia, high frequency deafness and optic atrophy. *J. Med. Genet.* 56, 164–175. doi: 10.1136/jmedgenet-2018-105711

Muller, C. P., Reichel, M., Muhle, C., Rhein, C., Gulbins, E., and Kornhuber, J. (2015). Brain membrane lipids in major depression and anxiety disorders. *Biochim. Biophys. Acta* 1851, 1052–1065. doi: 10.1016/j.bbalip.2014.12.014

Naganuma, T., Sato, Y., Sassa, T., Ohno, Y., and Kihara, A. (2011). Biochemical characterization of the very long-chain fatty acid elongase ELOVL7. *FEBS Lett.* 585, 3337–3341. doi: 10.1016/j.febslet.2011.09.024

Nguyen, J. H., Yamamoto, S., Steers, J., Sevlever, D., Lin, W., Shimojima, N., et al. (2006). Matrix metalloproteinase-9 contributes to brain extravasation and edema in fulminant hepatic failure mice. *J. Hepatol.* 44, 1105–1114. doi: 10.1016/j.jhep.2005.09.019

Nishihira, J., Tokashiki, T., Higashiuesato, Y., Willcox, D. C., Mattek, N., Shinto, L., et al. (2016). Associations between serum omega-3 fatty acid levels and cognitive functions among community-dwelling octogenarians in okinawa, Japan: the KOCOA study. *J. Alzheimers Dis.* 51, 857–866. doi: 10.3233/JAD-150910

Novick, P., and Schekman, R. (1979). Secretion and cell-surface growth are blocked in a temperature-sensitive mutant of *Saccharomyces cerevisiae*. *Proc. Natl. Acad. Sci. U.S.A.* 76, 1858–1862. doi: 10.1073/pnas.76.4.1858

Oboh, A., Betancor, M. B., Tocher, D. R., and Monroig, O. (2016). Biosynthesis of long-chain polyunsaturated fatty acids in the African catfish *Clarias gariepinus*: molecular cloning and functional characterisation of fatty acyl desaturase (fads2) and elongase (elovl2) cDNAs7. *Aquaculture* 462, 70–79. doi: 10.1016/j.aquaculture.2016.05.018

Ohno, Y., Suto, S., Yamanaka, M., Mizutani, Y., Mitsutake, S., Igarashi, Y., et al. (2010). ELOVL1 production of C24 acyl-CoAs is linked to C24 sphingolipid synthesis. *Proc. Natl. Acad. Sci. U.S.A.* 107, 18439–18444. doi: 10.1073/pnas.1005572107

Okuda, A., Naganuma, T., Ohno, Y., Abe, K., Yamagata, M., Igarashi, Y., et al. (2010). Hetero-oligomeric interactions of an ELOVL4 mutant protein: implications in the molecular mechanism of stargardt-3 macular dystrophy. *Mol. Vis.* 16, 2438–2445.

Ozaki, K., Ansai, A., Nobuhara, K., Araki, T., Kubodera, T., Ishii, T., et al. (2019). Prevalence and clinicoradiological features of spinocerebellar ataxia type 34 in a Japanese ataxia cohort. *Parkinsonism Relat. Disord.* doi: 10.1016/j.parkreldis.2019.05.019 [Epub ahead of print].

Ozaki, K., Doi, H., Mitsui, J., Sato, N., Iikuni, Y., Majima, T., et al. (2015). A Novel Mutation in ELOVL4 leading to spinocerebellar ataxia (SCA) with the hot cross bun sign but lacking erythrokeratodermia: a broadened spectrum of SCA34. *JAMA Neurol.* 72, 797–805. doi: 10.1001/jamaneurol.2015.0610

Pauter, A. M., Olsson, P., Asadi, A., Herslof, B., Csikasz, R. I., Zadravec, D., et al. (2014). Elovl2 ablation demonstrates that systemic DHA is endogenously produced and is essential for lipid homeostasis in mice. *J. Lipid Res.* 55, 718–728. doi: 10.1194/jlr.M046151

Penke, B., Paragi, G., Gera, J., Berkecz, R., Kovacs, Z., Crul, T., et al. (2018). The role of lipids and membranes in the pathogenesis of Alzheimer's disease: a comprehensive view. *Curr. Alzheimer Res.* 15, 1191–1212. doi: 10.2174/1567205015666180911151716

Pereira, S. L., Leonard, A. E., Huang, Y. S., Chuang, L. T., and Mukerji, P. (2004). Identification of two novel microalgal enzymes involved in the conversion of the omega3-fatty acid, eicosapentaenoic acid, into docosahexaenoic acid. *Biochem. J.* 384(Pt 2), 357–366. doi: 10.1042/BJ20040970

Perin, M. S., Fried, V. A., Mignery, G. A., Jahn, R., and Sudhof, T. C. (1990). Phospholipid binding by a synaptic vesicle protein homologous to the regulatory region of protein kinase C. *Nature* 345, 260–263. doi: 10.1038/345260a0

Petersen, R. C. (2004). Mild cognitive impairment as a diagnostic entity. *J. Intern. Med.* 256, 183–194. doi: 10.1111/j.1365-2796.2004.01388.x

Phillips, M. A., Childs, C. E., Calder, P. C., and Rogers, P. J. (2015). No effect of omega-3 fatty acid supplementation on cognition and mood in individuals with cognitive impairment and probable alzheimer's disease: a randomised controlled trial. *Int. J. Mol. Sci.* 16, 24600–24613. doi: 10.3390/ijms161024600

Poulos, A., Sharp, P., Johnson, D., and Easton, C. (1988). The occurrence of polyenoic very long chain fatty acids with greater than 32 carbon atoms in molecular species of phosphatidylcholine in normal and peroxisome-deficient (Zellweger's syndrome) brain. *Biochem. J.* 253, 645–650. doi: 10.1042/bj2530645

Quetglas, S., Leveque, C., Miquelis, R., Sato, K., and Seagar, M. (2000). Ca2+-dependent regulation of synaptic SNARE complex assembly via a calmodulin- and phospholipid-binding domain of synaptobrevin. *Proc. Natl. Acad. Sci. U.S.A.* 97, 9695–9700. doi: 10.1073/pnas.97.17.9695

Rabionet, M., Bayerle, A., Jennemann, R., Heid, H., Fuchser, J., Marsching, C., et al. (2015). Male meiotic cytokinesis requires ceramide synthase 3-dependent sphingolipids with unique membrane anchors. *Hum. Mol. Genet.* 24, 4792–4808. doi: 10.1093/hmg/ddv204

Rabionet, M., van der Spoel, A. C., Chuang, C. C., von Tumpling-Radosta, B., Litjens, M., Bouwmeester, D., et al. (2008). Male germ cells require polyenoic sphingolipids with complex glycosylation for completion of meiosis: a link to ceramide synthase-3. *J. Biol. Chem.* 283, 13357–13369. doi: 10.1074/jbc.M800870200

Rangel-Huerta, O. D., and Gil, A. (2018). Effect of omega-3 fatty acids on cognition: an updated systematic review of randomized clinical trials. *Nutr. Rev.* 76, 1–20. doi: 10.1093/nutrit/nux064

Rizo, J., and Sudhof, T. C. (2002). Snares and munc18 in synaptic vesicle fusion. *Nat. Rev. Neurosci.* 3, 641–653. doi: 10.1038/nrn898

Robinson, B. S., Johnson, D. W., and Poulos, A. (1990). Unique molecular species of phosphatidylcholine containing very-long-chain (C24-C38) polyenoic fatty acids in rat brain. *Biochem. J.* 265, 763–767. doi: 10.1042/bj2650763

Rohacs, T. (2015). Phosphoinositide regulation of TRPV1 revisited. *Pflugers Arch.* 467, 1851–1869. doi: 10.1007/s00424-015-1695-3

Rohacs, T., and Nilius, B. (2007). Regulation of transient receptor potential (TRP) channels by phosphoinositides. *Pflugers Arch.* 455, 157–168. doi: 10.1007/s00424-007-0275-6

Rohrbough, J., Rushton, E., Palanker, L., Woodruff, E., Matthies, H. J., Acharya, U., et al. (2004). Ceramidase regulates synaptic vesicle exocytosis and trafficking. *J. Neurosci.* 24, 7789–7803. doi: 10.1523/JNEUROSCI.1146-04.2004

Sanchez-Alegria, K., Flores-Leon, M., Avila-Munoz, E., Rodriguez-Corona, N., and Arias, C. (2018). PI3K signaling in neurons: a central node for the control of multiple functions. *Int. J. Mol. Sci.* 19, E3725. doi: 10.3390/ijms19123725

Santiago Valtierra, F. X., Penalva, D. A., Luquez, J. M., Furland, N. E., Vasquez, C., Reyes, J. G., et al. (2018). Elovl4 and Fa2h expression during rat spermatogenesis: a link to the very-long-chain PUFAs typical of germ cell sphingolipids. *J. Lipid Res.* 59, 1175–1189. doi: 10.1194/jlr.M081885

Sara, Y., Virmani, T., Deak, F., Liu, X., and Kavalali, E. T. (2005). An isolated pool of vesicles recycles at rest and drives spontaneous neurotransmission. *Neuron* 45, 563–573. doi: 10.1016/j.neuron.2004.12.056

Sassa, T., Ohno, Y., Suzuki, S., Nomura, T., Nishioka, C., Kashiwagi, T., et al. (2013). Impaired epidermal permeability barrier in mice lacking elovl1, the gene responsible for very-long-chain fatty acid production. *Mol. Cell Biol.* 33, 2787–2796. doi: 10.1128/MCB.00192-13

Sassa, T., Tadaki, M., Kiyonari, H., and Kihara, A. (2018). Very long-chain tear film lipids produced by fatty acid elongase ELOVL1 prevent dry eye disease in mice. *FASEB J.* 32, 2966–2978. doi: 10.1096/fj.201700947R

Sastry, P. S. (1985). Lipids of nervous tissue: composition and metabolism. *Prog. Lipid Res.* 24, 69–176. doi: 10.1016/0163-7827(85)90011-6

Sebastiao, A. M., Colino-Oliveira, M., Assaife-Lopes, N., Dias, R. B., and Ribeiro, J. A. (2013). Lipid rafts, synaptic transmission and plasticity: impact in age-related neurodegenerative diseases. *Neuropharmacology* 64, 97–107. doi: 10.1016/j.neuropharm.2012.06.053

Selkoe, D. J. (2001). Alzheimer's disease: genes, proteins, and therapy. *Physiol. Rev.* 81, 741–766.

Selkoe, D. J. (2002). Alzheimer's disease is a synaptic failure. *Science* 298, 789–791.

Sharma, S., and Tripathi, M. (2013). Ketogenic diet in epileptic encephalopathies. *Epilepsy Res. Treat.* 2013:652052. doi: 10.1155/2013/652052

Shen, D. N., Zhang, L. H., Wei, E. Q., and Yang, Y. (2015). Autophagy in synaptic development, function, and pathology. *Neurosci. Bull.* 31, 416–426. doi: 10.1007/s12264-015-1536-6

Sherry, D. M., Hopiavuori, B. R., Stiles, M. A., Rahman, N. S., Ozan, K. G., Deak, F., et al. (2017). Distribution of ELOVL4 in the developing and adult mouse brain. *Front. Neuroanat.* 11:38. doi: 10.3389/fnana.2017.00038

Sinn, N., Milte, C., and Howe, P. R. (2010). Oiling the brain: a review of randomized controlled trials of omega-3 fatty acids in psychopathology across the lifespan. *Nutrients* 2, 128–170. doi: 10.3390/nu2020128

Slieker, R. C., Relton, C. L., Gaunt, T. R., Slagboom, P. E., and Heijmans, B. T. (2018). Age-related DNA methylation changes are tissue-specific with ELOVL2 promoter methylation as exception. *Epigenetics Chromatin* 11:25. doi: 10.1186/s13072-018-0191-3

Sollner, T., Whiteheart, S. W., Brunner, M., Erdjument-Bromage, H., Geromanos, S., Tempst, P., et al. (1993). SNAP receptors implicated in vesicle targeting and fusion. *Nature* 362, 318–324. doi: 10.1038/362318a0

Spassieva, S. D., Ji, X., Liu, Y., Gable, K., Bielawski, J., Dunn, T. M., et al. (2016). Ectopic expression of ceramide synthase 2 in neurons suppresses neurodegeneration induced by ceramide synthase 1 deficiency. *Proc. Natl. Acad. Sci. U.S.A.* 113, 5928–5933. doi: 10.1073/pnas.1522071113

Spolnicka, M., Pospiech, E., Peplonska, B., Zbiec-Piekarska, R., Makowska, Z., Pieta, A., et al. (2018). DNA methylation in ELOVL2 and C1orf132 correctly predicted chronological age of individuals from three disease groups. *Int. J. Legal. Med.* 132, 1–11. doi: 10.1007/s00414-017-1636-0

Stevens, C. F., and Williams, J. H. (2000). "Kiss and run" exocytosis at hippocampal synapses. *Proc. Natl. Acad. Sci. U.S.A.* 97, 12828–12833. doi: 10.1073/pnas.230438697

Südhof, T. C. (2004). The synaptic vesicle cycle. *Annu. Rev. Neurosci.* 27, 509–547. doi: 10.1146/annurev.neuro.26.041002.131412

Südhof, T. C., and Rizo, J. (2011). Synaptic vesicle exocytosis. *Cold Spring Harb. Perspect. Biol.* 3:a005637. doi: 10.1101/cshperspect.a005637

Südhof, T. C., and Rothman, J. E. (2009). Membrane fusion: grappling with SNARE and SM proteins. *Science* 323, 474–477. doi: 10.1126/science.1161748

Sun, C., Zou, M., Wang, X., Xia, W., Ma, Y., Liang, S., et al. (2018). FADS1-FADS2 and ELOVL2 gene polymorphisms in susceptibility to autism spectrum disorders in Chinese children. *BMC Psychiatr.* 18:283. doi: 10.1186/s12888-018-1868-7

Takamori, S., Holt, M., Stenius, K., Lemke, E. A., Gronborg, M., Riedel, D., et al. (2006). Molecular anatomy of a trafficking organelle. *Cell* 127, 831–846. doi: 10.1016/j.cell.2006.10.030

Tan, C. Y., Virtue, S., Bidault, G., Dale, M., Hagen, R., Griffin, J. L., et al. (2015). Brown adipose tissue thermogenic capacity is regulated by Elovl6. *Cell Rep.* 13, 2039–2047. doi: 10.1016/j.celrep.2015.11.004

Tarafdar, P. K., Chakraborty, H., Bruno, M. J., and Lentz, B. R. (2015). Phosphatidylserine-dependent catalysis of stalk and pore formation by synaptobrevin JMR-TMD peptide. *Biophys. J.* 109, 1863–1872. doi: 10.1016/j.bpj.2015.08.051

Teixeira, G., Vieira, L. B., Gomez, M. V., and Guatimosim, C. (2012). Cholesterol as a key player in the balance of evoked and spontaneous glutamate release in rat brain cortical synaptosomes. *Neurochem. Int.* 61, 1151–1159. doi: 10.1016/j.neuint.2012.08.008

Tvrdik, P., Westerberg, R., Silve, S., Asadi, A., Jakobsson, A., Cannon, B., et al. (2000). Role of a new mammalian gene family in the biosynthesis of very long chain fatty acids and sphingolipids. *J. Cell Biol.* 149, 707–718. doi: 10.1083/jcb.149.3.707

Ulamek-Koziol, M., Pluta, R., Bogucka-Kocka, A., and Czuczwar, S. J. (2016). To treat or not to treat drug-refractory epilepsy by the ketogenic diet? that is the question. *Ann. Agric. Environ. Med.* 23, 533–536. doi: 10.5604/12321966.1226841

Vasireddy, V., Uchida, Y., Salem, N. Jr., Kim, S. Y., Mandal, M. N., Reddy, G. B., et al. (2007). Loss of functional ELOVL4 depletes very long-chain fatty acids (> or =C28) and the unique omega-O-acylceramides in skin leading to neonatal death. *Hum. Mol. Genet.* 16, 471–482. doi: 10.1093/hmg/ddl480

Wasser, C. R., Ertunc, M., Liu, X., and Kavalali, E. T. (2007). Cholesterol-dependent balance between evoked and spontaneous synaptic vesicle recycling. *J. Physiol.* 579(Pt 2), 413–429. doi: 10.1113/jphysiol.2006.123133

Wenk, M. R., Pellegrini, L., Klenchin, V. A., Di Paolo, G., Chang, S., Daniell, L., et al. (2001). PIP kinase Igamma is the major PI(4,5)P(2) synthesizing enzyme at the synapse. *Neuron* 32, 79–88. doi: 10.1016/s0896-6273(01)00456-1

Westerberg, R., Tvrdik, P., Unden, A. B., Mansson, J. E., Norlen, L., Jakobsson, A., et al. (2004). Role for ELOVL3 and fatty acid chain length in development of hair and skin function. *J. Biol. Chem.* 279, 5621–5629. doi: 10.1074/jbc.M310529200

Wilson, R. I., and Nicoll, R. A. (2002). Endocannabinoid signaling in the brain. *Science* 296, 678–682. doi: 10.1126/science.1063545

Yu, M., Benham, A., Logan, S., Brush, R. S., Mandal, M. N., Anderson, R. E., et al. (2012). ELOVL4 protein preferentially elongates 20:5n3 to very long chain PUFAs over 20:4n6 and 22:6n3. *J. Lipid Res.* 53, 494–504. doi: 10.1194/jlr.M021386

Zadravec, D., Tvrdik, P., Guillou, H., Haslam, R., Kobayashi, T., Napier, J. A., et al. (2011). ELOVL2 controls the level of n-6 28:5 and 30:5 fatty acids in testis, a prerequisite for male fertility and sperm maturation in mice. *J. Lipid Res.* 52, 245–255. doi: 10.1194/jlr.M011346

Zhang, K., Kniazeva, M., Han, M., Li, W., Yu, Z., Yang, Z., et al. (2001). A 5-bp deletion in ELOVL4 is associated with two related forms of autosomal dominant macular dystrophy. *Nat. Genet.* 27, 89–93. doi: 10.1038/83817

Zhang, X. M., Yang, Z., Karan, G., Hashimoto, T., Baehr, W., Yang, X. J., et al. (2003). Elovl4 mRNA distribution in the developing mouse retina and phylogenetic conservation of Elovl4 genes. *Mol. Vis.* 9, 301–307.

Zhang, Y., Chen, J., Qiu, J., Li, Y., Wang, J., and Jiao, J. (2016). Intakes of fish and polyunsaturated fatty acids and mild-to-severe cognitive impairment risks: a dose-response meta-analysis of 21 cohort studies. *Am. J. Clin. Nutr.* 103, 330–340. doi: 10.3945/ajcn.115.124081

Zoncu, R., Perera, R. M., Sebastian, R., Nakatsu, F., Chen, H., Balla, T., et al. (2007). Loss of endocytic clathrin-coated pits upon acute depletion of phosphatidylinositol 4,5-bisphosphate. *Proc. Natl. Acad. Sci. U.S.A.* 104, 3793–3798. doi: 10.1073/pnas.0611733104

Conflict of Interest: RA has a United States Patent (No. 8,021,874) entitled "Very Long Chain Polyunsaturated Fatty Acids, Methods of Production, and Uses."

The remaining authors declare that the research was conducted in the absence of any commercial or financial relationships that could be construed as a potential conflict of interest.

frontiers in Cellular Neuroscience

BRIEF RESEARCH REPORT
published: 29 October 2019
doi: 10.3389/fncel.2019.00487

Processing Bodies Oscillate in Neuro 2A Cells

Melisa Malcolm[1,2], *Lucía Saad*[1,2], *Laura Gabriela Penazzi*[1,2] *and Eduardo Garbarino-Pico*[1,2]*

[1] *Departamento de Química Biológica Ranwel Caputto, Facultad de Ciencias Químicas, Universidad Nacional de Córdoba (UNC), Córdoba, Argentina,* [2] *CONICET-UNC, Centro de Investigaciones en Química Biológica de Córdoba (CIQUIBIC), Córdoba, Argentina*

Circadian rhythms are biological variables that oscillate with periods close to 24 h that are generated internally by biological clocks. Depending on the tissue/cell type, about 5–20% of genes are expressed rhythmically. Unexpectedly, the correlation between the oscillations of messengers and the proteins they encode is low. We hypothesize that these discrepancies could be because in certain phases of the circadian cycle some messengers could be translationally silenced and stored. Processing bodies (PBs) are membraneless organelles formed by ribonucleoprotein aggregates located in the cytoplasm. They contain silenced messengers and factors involved in mRNA processing. A previous work showed that the number of cells containing these mRNA granules varies when comparing two time-points in U2OS cell cultures and that these differences disappear when an essential clock gene is silenced. Here we evaluate whether PBs oscillate in Neuro2A cells. We analyzed in cell cultures synchronized with dexamethasone the variations in the number, the signal intensity of the markers used (GE-1/HEDLS and DDX6), and the area of PBs between 8 and 68 h post-synchronization. All three parameters oscillated with periods compatible with a circadian regulated process. The most robust rhythm was the number of PBs. These rhythms could be generated by oscillations in proteins that have been involved in the nucleation of these foci such as LSM1, TTP, and BRF1. The described phenomenon would allow to explain the differences observed in the temporal profiles of some messengers and their proteins and to understand how circadian clocks can control post-transcriptionally cellular functions.

Keywords: processing bodies, circadian rhythms, Neuro 2A, RNA granules, GE1/Hedls, DDX6/P54/RCK, membraneless organelles

OPEN ACCESS

Edited by:
Alejandra Alonso, College of Staten Island, United States

Reviewed by:
Rachid El Fatimy, Brigham and Women's Hospital, Harvard Medical School, United States
Steven Lanier McKnight, UT Southwestern Medical Center, United States

***Correspondence:**
Eduardo Garbarino-Pico
egarbarino@unc.edu.ar

Specialty section:
This article was submitted to Cellular Neurophysiology, a section of the journal Frontiers in Cellular Neuroscience

Received: *31 March 2019*
Accepted: *14 October 2019*
Published: *29 October 2019*

Citation:
Malcolm M, Saad L, Penazzi LG and Garbarino-Pico E (2019) Processing Bodies Oscillate in Neuro 2A Cells. Front. Cell. Neurosci. 13:487. doi: 10.3389/fncel.2019.00487

INTRODUCTION

Throughout evolution, living beings have developed mechanisms capable of measuring time and controlling numerous functions in a cyclic manner. Most of these oscillations have a period of 1 day in natural environments and close to 24 h in constant conditions. These mechanisms are called biological clocks and the functions they control circadian rhythms.

They are believed to confer adaptative advantages by predicting the cyclic changes in the environment caused by the rotation of the Earth (e.g., light/dark and temperature cycles) and temporarily organizing physiology (Schibler et al., 2015; Bass and Lazar, 2016; Takahashi, 2017). Examples of circadian rhythms are cycles of sleep/wakefulness, locomotor activity or body temperature. In neurons, rhythms have been described in firing rate, gene expression, the activity of enzymes and channels and even in synaptic plasticity, among others. The molecular clockwork consists of a group of genes that mutually regulate each other through interconnected transcription-translation negative feedback loops (TTFLs) (Takahashi, 2017). These circuits rhythmically regulate the abundance of messengers encoded by ∼5–20% of genes in different tissues/organs and about 50% of mRNAs oscillate in at least some tissue (Zhang et al., 2014). Importantly, post-transcriptional regulation also plays a very important role in the generation of rhythms in protein abundance (Green, 2018). This is reflected in the poor correlation that exists between variations in the abundance of transcripts and their corresponding proteins (Reddy et al., 2006; Mauvoisin et al., 2014; Robles et al., 2014).

In the last two decades, new types of intracellular compartments characterized by not being delimited by membranes have been described in eukaryotic cells, collectively called membraneless organelles or RNA granules. They are condensed liquid-like droplets of ribonuleoprotein complexes (Courchaine et al., 2016; Sfakianos et al., 2016; Shin and Brangwynne, 2017). In cytosol, these subcompartments include processing bodies (PBs), stress granules, germ granules and neuronal granules. PBs are constitutively present, contain translationally silent mRNAs and factors involved in messengers $5'\rightarrow3'$ degradation, repression of translation, and RNA interference (Decker and Parker, 2012; Ivanov et al., 2018; Standart and Weil, 2018). Because of this, and other indirect evidence, it has been proposed that these foci would play a role in mRNA degradation (Sheth and Parker, 2003). However, it was also demonstrated that some messengers localizing in PBs can be translated again, consequently they would also serve as storage places (Brengues et al., 2005). Recently, it was possible to purify PBs and determine the identity of many of the proteins and mRNAs that compose them (Hubstenberger et al., 2017). From these studies it was proposed that PBs would store mRNA regulons, that is groups of transcripts coding for proteins with regulatory functions of specific pathways, while messengers with basic functions are virtually excluded (for example, transcripts coding for histone methylases but not for histones were found in PBs) (Hubstenberger et al., 2017; Standart and Weil, 2018). Thus, PBs have a role in the post-transcriptional regulation of gene expression, remarkably they would store silenced the mRNAs of groups of genes that modulate specific functions.

Since it is proposed that PBs store silenced messengers, if these structures were to oscillate, this would help to explain (at least partially) the discrepancies observed when analyzing the mRNA and protein profiles corresponding to a number of genes (Reddy et al., 2006; Mauvoisin et al., 2014; Robles et al., 2014). That is, if the messengers of a particular gene are mostly located in PBs, no matter how abundant, this will not be reflected in their protein levels or translation rate. If it is also considered that these foci contain fundamentally transcripts of regulatory factors (Hubstenberger et al., 2017; Standart and Weil, 2018), changes in their abundance and/or size would contribute to understanding the pathways by which many rhythmic cellular processes are regulated. In fact, Jang et al. (2015) have demonstrated changes in the number of cells containing PBs in cultures of U2OS cells (human osteosarcoma cell line). They decided to study this because previously, by ribosome profiling, they had found that the translation of *Lsm1* was circadian modulated into U2OS cells. LSM1 is a marker of PBs (Ingelfinger et al., 2002; Kedersha and Anderson, 2007). They also demonstrated that silencing a fundamental clock gene in the circadian clock molecular mechanism abrogates those differences (Jang et al., 2015). Given that this work analyzes only two time-points post-synchronization with dexamethasone (4 and 16 h), and that one of these is very close to the addition of this synchronizing agent that dramatically affects cellular physiology, we decided to analyze whether the number and size of PBs varies for 68 h in a neuroblastoma cell line. In this Brief Research Report we show that these two parameters oscillate cyclically in cultures of Neuro 2A cells.

MATERIALS AND METHODS

Cell Culture

Mouse Albino neuroblastoma (Neuro 2a) cells (ATCC) were cultured in Minimum Essential Medium (MEM, Gibco) supplemented with 10% fetal bovine serum (FBS, Internegocios S.A, Argentina), in a 37°C incubator with 5% CO_2 according ATCC recommendations. These cells have been used before for studying circadian rhythms in cell cultures (Chilov et al., 2001; Margadant et al., 2007; Repouskou et al., 2010; Chang and Guarente, 2013). Cells were grown on coverslips in a 24-well plate until they reached ∼70% of confluence, and then maintained in serum starvation conditions (0.25%, see below) to prevent the progression of the cell cycle. This is important to ensure that changes observed over time are regulated by the circadian clock and not by the cell cycle. Initially we tried to completely eliminate serum from the medium, but cells did not survive the 68 h that the experiment required. Subsequently we tested for 96 h different serum concentrations: 0, 0.1, 0.25, and 0.5%. Cells died at serum concentration lower than 0.25% and proliferate at 0.5% FBS; thus we chose 0.25% FBS, a concentration in which the number of cells did not vary during the 96 h analyzed. To control that the cells were not proliferating, we analyzed cultures grown in the same conditions by flow cytometry with propidium iodide. Indeed, when the cultures contained only 0.25% FBS in the medium, the cells were arrested. For circadian clock synchronization (i.e., to entrain the cell population to the same circadian phase), cells were treated for 1 h with 100 nM dexamethasone (Balsalobre et al., 2000; Nagoshi et al., 2005; Repouskou et al., 2010); then culture medium was replaced with fresh 0.25% FBS-MEM.

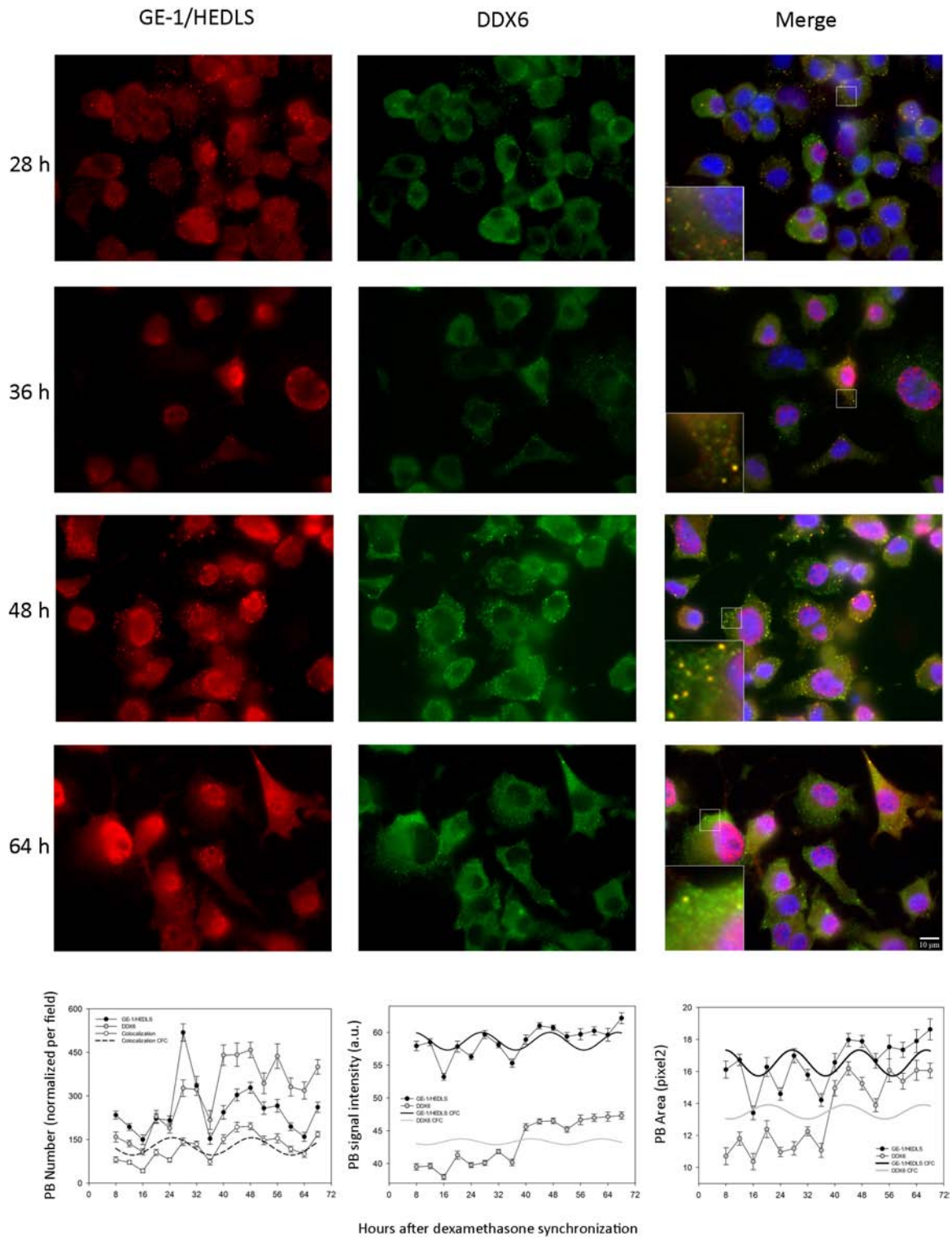

FIGURE 1 | Processing Bodies oscillate cyclically in synchronized cultures of Neuro 2A cells. When the cultures reached 60–70% confluence, the medium was replaced with a fresh one containing only 0.25% serum, condition in which the cell cycle is arrested (see M&M). The following day they were synchronized with dexamethasone and fixed every 4 h between 8 and 68 h post-synchronization. The cells fixed on cover slips were treated with two antibodies by ICC, anti-GE-1/HEDLS (red) and anti-DDX6 (green), recognized PB markers. In addition, the nuclei were stained with dapi (blue). Then they were analyzed by epifluorescence microscopy and pictures were taken with a CCD camera. On the left are shown the post-synchronization time-points that are illustrated and on top the names of the markers. The images were analyzed with ImageJ and three parameters were quantified: number (per field, it was normalized considering that the

(Continued)

FIGURE 1 | Continued
field was completely covered with cells), average signal intensity and the average area of the PBs. These quantifications are shown in the right panel. The Kruskall–Wallis test followed by Dunn's multiple comparison test was used to determine whether the changes over time were statistically significant. MetaCycle was used to assess whether the time series of data showed rhythmicity. These analyses are presented in **Table 1** and **Supplementary Tables S5–S10**, all three parameters showed cyclic changes with the two markers. With the period, phase and amplitude values obtained by MetaCycle, the data were adjusted to a cosine-fitted curve (CFC). In the case of the PB number, the curve obtained when considering the PBs detected with the two antibodies (colocalization) is also shown.

Cells were fixed every 4 h for 68 h post-synchronization for immunocytochemistry analysis.

Immunocytochemistry

Immunocytochemistry (ICC) was achieved according a protocol described by Kedersha and colleagues for analyzing PBs (Kedersha and Anderson, 2007). Briefly, Neuro 2a cells were washed twice with PBS, fixed with paraformaldehyde 4% for 15 min., permeabilized with -20°C methanol for 10 min., and incubated 1 h in blocking solution (5% Horse serum-PBS). These steps were carried out at room temperature (RT). Then cells were incubated with a mouse monoclonal antibody against p70 S6 kinase α (H-9) (Santa Cruz Biotechnology), diluted 1:1000 in blocking solution, in a humidified chamber overnight at RT. This antibody recognizes p70 S6 kinase α in the nucleus and GE-1/HEDLS/EDC4 in cytoplasm, a known marker for PBs and has been widely used for studying this foci [reviewed in 20]. Then, cells were rinsed three times with PBS, followed by incubation with a polyclonal DyLight 549-AffiniPure donkey anti-mouse IgG secondary antibody (1:2000, Jackson ImmunoResearch Labs), diluted in the same blocking solution, 30 min at RT. Nuclei were stained with Dapi. Cells were rinsed three times with PBS and mounted on slices with mowiol (Sigma-Aldrich). In addition to anti-GE-1/HEDLS, anti-DDX6/P54/RCK (Bethyl Laboratories, 1:500 in blocking solution) was used in double immunolabeling experiments. This is another recognized PB marker (Kedersha and Anderson, 2007).

Image Detection and Analysis

Slices were visualized using an BX61 Fluorescence Microscope (Olympus) equipped with a UPLSAPO 60XO oil objective lens (NA 1.35) and U-T31 000v2 specific DAPI/Hoechs, U-TSP101para FITC, and U-T31014 Wide-band excitation set for Elphidium Bromide TRITC, Phenothrin Dil Chroma Filters. The images were acquired with a JAI® CV-M4+CL monochrome camera controlled by Cytovision® (Leica Biosystems). PBs were quantified according the procedure developed by Nissan and Parker (2008) for stress granules with modifications. The entire procedure was conducted using algorithms that guarantee an unbiased treatment of all pictures. Digital images of 1376 × 1038 pixels and 8 bits were processed with the ImageJ program as follow: *1)* Process menu > "Filters" > "Gaussian Blur" sigma radius 0.8 pix. *2)* Process menu > "Subtract background" (Rolling ball radius: 5 pix). *3)* Image > "Adjust" > "Threshold" 40 (red channel) or 35 (green channel). *4)* Analyze menu > "Analyze particles" > size 3–300 pix2, circularity 0.7-1. Importantly, the same threshold value was used in the analysis of all the images within each experiment, to ensure an unbiased comparison between time-points. P- bodies are considered circular, ∼300–500 nm in diameter (Cougot et al., 2012), for this reason we exclude particles without a circularity <0.7 (1 correspond to a perfect circle) or out of 3–300 pix^2 range. This pixel size range allows quantifying particles with a diameter of 200–2000 nm. The PBs observed in Neuro 2a cells presented an average diameter of 476 nm with this procedure. We were able to decrease the upper limit to a value closer to the largest particle found, even though it would not have affected the results. P-body number was normalized by area covered by cells, for that purpose, masks were created with Fiji ImageJ, and area occupied in each microphotograph was measured.

Statistical Analysis

Statistical analysis was performed using GraphPad Prism version 5.00 for Windows (GraphPad Software). Values are shown as mean ± SEM, unless otherwise indicated. The Kolmogorov-Smirnov's test was used to check for normality, and Barlett's test to check homogeneity of variances. Because non-normal distribution or homogeneity of variances were found, Kruskal–Wallis's test was used instead of ANOVA, followed by Dunn's multiple comparisons test; p-values ≤ 0.05 were considered as statistically significant. To evaluate periodicity in time-series data we employed MetaCycle (Wu et al., 2016), which is a R package that runs and integrates three algorithms: ARSER (Yang and Su, 2010), JTK_CYCLE (Hughes et al., 2010), and Lomb-Scargle (Glynn et al., 2006). The statistics applied with this analysis allow us to determine whether the data are periodic and, if so, their period, amplitude and phase. These parameters were applied to a Cosine function to plot the adjusted curves shown in the graph.

RESULTS

As mentioned in the Introduction, Jang and collaborators had shown important evidence that the number of PBs is regulated by the circadian clock (Jang et al., 2015). However, this study was limited to only two time-points, insufficient to describe a rhythm. Importantly, one of the time-points at which the number of PBs was analyzed was too close to synchronization (4 h), when the culture – and therefore the phenomenon studied – are still under the effect of the synchronizing agent (dexamethasone in this case). It is usual to start measuring at least 8 h after synchronization to analyze the rhythms independent of the effect of the agent used. We have also found, by using a database of circadian gene expression

TABLE 1 | PB temporal oscillations in Neuro 2a cells. PB number (normalized per field).

DDX6			GE-1/HEDLS			DDX6			GE-1/HEDLS		
t(h)	**Mean**	**SEM**	**Mean**	**SEM**	***n***	**t(h)**	**Mean**	**SEM**	**Mean**	**SEM**	***n***
8	158.50	78.03	233.90	61.24	20	40	440.14	440.14	243.39	117.03	20
12	135.88	55.14	193.19	57.38	24	44	441.96	441.96	303.24	91.81	20
16	107.21	44.95	149.42	71.50	18	48	458.20	458.20	328.19	89.84	20
20	228.78	95.91	222.16	77.44	21	52	343.16	343.16	257.67	86.02	16
24	188.79	77.82	215.81	66.44	20	56	436.80	436.80	265.86	102.40	20
28	326.62	125.14	518.41	129.08	19	60	330.72	330.72	194.10	66.05	25
32	322.07	93.82	334.35	150.35	20	64	318.47	318.47	159.11	69.52	20
36	217.18	142.59	152.55	82.95	19	68	399.98	399.98	260.99	73.01	17

Statistical analysis

Kruskall-Wallis DDX6		Kruskall-Wallis GE-1/HEDLS	
P	**H**	***P***	**H**
P < 0.0001	171.50	P < 0.0001	132.30

MetaCycle (meta2d)1 DDX6				MetaCycle (meta2d)1GE-1/HEDLS			
P	**Period**	**Phase**	**Amp**	***P***	**Period**	**Phase**	**Amp**
5.32E-04	23.33	1.17	41.12	0.00	23.57	647	57.79

Signal intensity (a.u.)

DDX6			GE-1/HEDLS			DDX6			GE-1/HEDLS		
t(h)	**Mean**	**SEM**	**Mean**	**SEM**	***n***	**t(h)**	**Mean**	**SEM**	**Mean**	**SEM**	***n***
8	39.48	2.18	57.93	3.20	20	40	45.56	2.60	58.90	3.59	20
12	39.61	2.02	58.50	2.62	24	44	46.41	1.73	61.00	2.15	20
16	37.94	1.63	53.21	2.19	15	48	46.49	2.02	60.72	1.91	20
20	41.27	2.86	57.84	3.83	21	52	45.19	1.78	59.37	2.54	16
24	39.75	1.70	56.28	2.01	20	56	46.64	3.46	59.72	3.96	20
28	40.08	1.66	59.68	2.63	19	60	46.97	2.78	60.23	3.12	25
32	41.83	1.52	58.10	2.02	20	64	47.14	3.13	59.63	4.29	20
36	40.15	2.19	55.31	2.76	19	68	47.31	2.28	62.19	3.42	17

Satistical analysis

Kruskall-Wallis DDX6		Kruskall-Wallis GE-1/HEDLS	
P	**H**	***P***	**H**
P < 0.0001	232.70	P < 0.0001	113.30

MetaCycle (meta2d)1 DDX6				MetaCycle (meta2d)1 GE-1/HEDLS			
P	**Period**	**Phase**	**Amp**	***P***	**Period**	**Phase**	**Amp**
1.85E-06	20.60	0.44	0.44	341E-07	19.93	7.22	1.34

Area (pixel^2)

DDX6			GE-1/HEDLS			DDX6			GE-1/HEDLS		
t(h)	**Mean**	**SEM**	**Mean**	**SEM**	***n***	**t(h)**	**Mean**	**SEM**	**Mean**	**SEM**	***n***
8	10.70	2.36	16.12	2.38	20	40	14.95	2.41	16.56	2.81	20
12	11.80	2.02	16.72	1.75	24	44	16.19	1.84	17.97	1.83	20
16	10.37	2.15	13.41	1.82	15	48	15.25	1.86	17.88	1.80	20

(Continued)

TABLE 1 | Continued

DDX6			GE-1/HEDLS			DDX6			GE-1/HEDLS		
t(h)	**Mean**	**SEM**	**Mean**	**SEM**	***n***	**t(h)**	**Mean**	**SEM**	**Mean**	**SEM**	***n***
20	12.39	2.44	16.28	2.73	21	52	13.89	1.65	16.67	1.84	16
24	10.97	1.30	14.60	1.74	20	56	16.07	3.37	17.53	3.46	20
25	11.19	1.81	16.98	1.90	19	60	15.39	2.47	17.35	2.38	25
32	12.25	1.27	15.78	1.56	20	64	16.07	2.79	17.90	3.19	20
36	11.07	1.92	14.21	1.74	19	68	16.05	1.90	18.63	2.73	17

Satistical analysis	**Kruskall-Wallis DDX6**		**Kruskall-Wallis GE-1/HEDLS**	
	P	**H**	***P***	**H**
	$P < 0.0001$	182.50	$P < 0.0001$	91.06

MetaCycle (meta2d)1 DDX6				**MetaCycle (meta2d)1 GE-1/HEDLS**			
P	**Period**	**Phase**	**Amp**	***p***	**Period**	**Phase**	**Amp**
141E-06	22.74	20.52	144	0.00	19.72	7.87	0.80

Note that the mean was calculated as the mean of the means of each micmphotograph. N indicates the number of microphotographs per time analyzed. Each picture contain an average of 23 cells per field.

[CircaDB, Pizarro et al., 2013], that two proteins involved in the nucleation of PBs, Tristetraprolin (TTP) and BRF-1 (Franks and Lykke-Andersen, 2007), present oscillations in the levels of their messengers in murine liver (**Supplementary Figures S1**, **S2**, from CircaDB). All this together led us to analyze whether PBs show oscillations over time.

In this work we analyze whether PBs present rhythms in cultures of Neuro 2A cells, which have already been used for circadian studies (Chilov et al., 2001; Margadant et al., 2007; Repouskou et al., 2010; Chang and Guarente, 2013). These cells were established from mouse neuroblastoma, so they grow continuously and do not stop dividing under normal culture conditions (10% FBS-MEM). For this reason we first test with which serum concentration the cells stop dividing and thus prevent the progress of the cell cycle from interfering with the determinations of the analyzed variables (see section "Materials and Methods"). When the cultures reached 60–70% confluence, the cell population was synchronized with dexamethasone for 1 h and subsequently maintained at 0.25% FBS-MEM until they were fixed at the indicated time-points. PBs were detected by ICC with an antibody recognizing the GE-1/HEDLS marker. Microphotographs were taken and the PBs were quantified with ImageJ (see section "Materials and Methods"). The number of PBs showed oscillations over time (**Supplementary Figure S3**). The determinations were made between 8 and 68 h post-synchronization, in that lapse two peaks and two valleys can be observed in the three parameters analyzed. In **Supplementary Figure S3A** are shown representative pictures of these time-points (left panel) and the same photos with the mask that was obtained with the quantification procedure used (right panel). **Supplementary Figure S3B** shows the result of quantifying the number of PBs normalized by the area occupied by cells, the average intensity of the signal obtained after subtracting the background, and the average area of the granules at the different times analyzed. The three variables analyzed showed a similar profile. All three parameters showed significant changes over time (Kruskall–Wallis test, **Supplementary Table S1** and **Supplementary Tables S2–S4** show Dunn's multiple comparison tests for the three parameters). The MetaCycle R package was used to determine whether the time series of data were rhythmic (Wu et al., 2016). This package applies statistical tests that determined that the parameters cycle with periods compatible with circadian rhythms, in addition to estimating amplitude and phase of oscillations (**Supplementary Table S1**). The number of PBs was the rhythm that showed the greatest amplitude. When the experiment was repeated, similar results were obtained. While the period of oscillations in signal intensity and area were comparable in the two experiments (signal intensity 24.17 vs. 22.81; area 23.34 vs. 22.46), the period of the number of PBs showed differences (30.52 vs. 23.15). In any case, taking into account that the variable is not being measured continuously and the sampling frequency (every 4 h), it is to be expected that the period cannot be determined precisely and the differences that are observed in the period estimations.

In order to corroborate with another marker the existence of the oscillations described in PBs, we performed double immunostaining experiments analyzing DDX6 [also known as P54/RCK, another recognized PB marker (Kedersha and Anderson, 2007)] together with GE-1/HEDLS. The cultures were synchronized and the same time-points were taken as in **Supplementary Figure S1**, although in this case two antibodies were used in the ICC. **Figure 1** and **Table 1** show that the number, signal intensity and area of PBs showed relatively similar profiles with both markers. All three variables, with both antibodies, showed statistically significant changes over time in the form of periodic oscillations of at least two cycles (Kruskall–Wallis test and MetaCycle, **Table 1**; **Supplementary Tables S5–S10**,

Dunn's multiple comparison tests. n = 16–24 pictures per time-point). In each microphotography there were 23.6 ± 9.1 nuclei (average ± SD); that is, between 378 and 566 cells were analyzed at each time-point. Remarkably, all three parameters showed higher levels in the second cycle when PBs were detected with anti-DDX6 (**Figure 1** and **Table 1**). The PB number was the variable that showed the greatest amplitude with the two markers. It was normalized by the surface occupied by the cells since several of them were not completely included in the pictures. Considering this, when the PB number was divided by the number of nuclei, on average this coefficient was between 2.3 and 7.9 per cell when GE-1/HEDLS was used and between 2.7 and 10.8 with DDX6. The period estimated with the two antibodies was very similar, 23.57 h with anti-GE-1/HEDLS and 23.33 h with anti-DDX6. When only granules marked with both markers were considered, as expected the number decreased. Even so the behavior over time remained rhythmic (Fig. 1. p = 2.19E-11 by MetaCycle). When the signal intensity was analyzed, the overall values were different with each antibody, this is to be expected since they are different antibodies and fluorophores, although the time pattern was relatively similar but with greater amplitude for GE-1/HEDLS (**Figure 1** and **Table 1**). In the case of the PB area, as anticipated, the values were reduced since in general the overlap of the signal was not complete, which means that not all the pixels recognized with one antibody as a PB matched exactly with those detected by the other. However, the temporal behavior also showed to be statistically rhythmic (p = 5.3E-4). This experiment was repeated and showed similar results; therefore, these oscillations were demonstrated in 4 independent experiments with anti-GE-1/HEDLS and in 2 with anti-DDX6. In these repetitions minor changes in the phase and amplitude of the rhythms are observed, this is expected since the measurements were not made in a continuous way but with intervals of 4 h and taking different samples in each time-point; nevertheless the temporal profiles are similar in all the cases.

CONCLUSION

This work shows for the first time oscillations in the dynamics of PBs. These rhythms were evidenced both in the number, intensity levels of the marker used, and the area of these cytoplasmic ribonucleoprotein granules with two different markers. A previous study had shown differences in the number of PBs when comparing two time-points in U2OS cells, as well as that this difference disappeared by silencing a clock gene essential for the functioning of the circadian clock molecular mechanism (Jang et al., 2015). Taken together, these works indicate that PBs are modulated by circadian clocks. Interestingly, both we (manuscript submitted) and another group (Wang et al., 2019), have found that other type of mRNA granules, the stress granules, also have temporal variations in their number.

In this brief report we limit ourselves to presenting the phenomenon, we have not explored the mechanisms by which the rhythms described in PBs are generated. A plausible hypothesis is that the circadian clock control the levels of factors that can induce the formation of PBs. In fact, changes in the rate of translation of a marker of these foci, LSM1, suggested to Jang and colleagues that PBs could be controlled by the circadian clock (Jang et al., 2015). We searched the CircaDB database (Pizarro et al., 2013) for messengers of two other of these proteins, TTP and BRF1 (Franks and Lykke-Andersen, 2007), that oscillated in their levels, and in fact do so (**Supplementary Figures S1**, **S2**). Other proteins that induce the formation of PBs may also participate in the generation of the observed rhythms. In addition to changes in the concentration of these proteins, post-translational modifications that induce the phase transitions that form PBs have also been described. If any of these modifications are rhythmically controlled, this could also contribute to the phenomenon described.

It is currently postulated that PBs are membrane-free compartments where transcripts are stored (Hubstenberger et al., 2017; Standart and Weil, 2018). They have also been involved in translation silencing and mRNA degradation [discussed in Decker and Parker (2012), Ivanov et al. (2018)]. Since at the beginning of the century technologies were available to analyze the transcriptome and the proteome globally, circadian experiments were performed that demonstrated a significant number of genes (∼50%) showed, contrary to expectations, a poor correlation between the abundance rhythms of their mRNA and protein (Reddy et al., 2006; Mauvoisin et al., 2014; Robles et al., 2014). The presence of many of these messengers in PBs, instead of in polysomes, could explain that even being abundant, their corresponding proteins would not be present in the same magnitude.

Considering the evidence suggesting that PBs store groups of messengers that participate in the regulation of specific pathways [mRNA regulons (Hubstenberger et al., 2017)], the fact that these foci are rhythmically regulated would contribute to understand how clocks can control a number of circadian rhythms at a post-transcriptional level.

DATA AVAILABILITY STATEMENT

All datasets generated for this study are included in the article/**Supplementary Material**.

AUTHOR CONTRIBUTIONS

MM, LS, and LP: acquisition, analysis and interpretation of data, making of the figures, revising the work, and design critically. EG-P: conception and design of the work, and manuscript writing. All authors contributed to the manuscript revision, and read and approved the submitted version.

FUNDING

The authors would like to acknowledge the support of the Agencia Nacional de Promoción Científica y Tecnológica (PICT

2013-2680), the Consejo Nacional de Investigaciones Científicas y Técnicas (CONICET), and the Universidad Nacional de Córdoba of Argentina for providing facilities and grants to carry out the research.

ACKNOWLEDGMENTS

The authors appreciate the technical assistance of Drs. Alejandra Trenchi, Susana Deheza, Gabriela Schachener, and the members of the "Centro de Microscopia Óptica y Confocal Avanzada de Coìrdoba (CEMINCO)", integrated to the "Sistema Nacional de Microscopia (SNM-MINCyT)" for microscopy assistant.

SUPPLEMENTARY MATERIAL

The Supplementary Material for this article can be found online at: https://www.frontiersin.org/articles/10.3389/fncel.2019.00487/full#supplementary-material

REFERENCES

Balsalobre, A., Brown, S. A., Marcacci, L., Tronche, F., Kellendonk, C., and Reichardt, H. M. (2000). Resetting of circadian time in peripheral tissues by glucocorticoid signaling. *Science* 289, 2344–2347. doi: 10.1126/science.289.5488.2344

Bass, J., and Lazar, M. A. (2016). Circadian time signatures of fitness and disease. *Science* 354, 994–999. doi: 10.1126/science.aah4965

Brengues, M., Teixeira, D., and Parker, R. (2005). Movement of eukaryotic mRNAs between polysomes and cytoplasmic processing bodies. *Science* 310, 486–489. doi: 10.1126/science.1115791

Chang, H. C., and Guarente, L. (2013). SIRT1 mediates central circadian control in the SCN by a mechanism that decays with aging. *Cell* 153, 1448–1460. doi: 10.1016/j.cell.2013.05.027

Chilov, D., Hofer, T., Bauer, C., Wenger, R. H., and Gassmann, M. (2001). Hypoxia affects expression of circadian genes PER1 and CLOCK in mouse brain. *FASEB J.* 15, 2613–2622. doi: 10.1096/fj.01-0092com

Cougot, N., Cavalier, A., Thomas, D., and Gillet, R. (2012). The dual organization of P-bodies revealed by immunoelectron microscopy and electron tomography. *J. Mol. Biol.* 420, 17–28. doi: 10.1016/j.jmb.2012.03.027

Courchaine, E. M., Lu, A., and Neugebauer, K. M. (2016). Droplet organelles? *EMBO J.* 35, 1603–1612. doi: 10.15252/embj.201593517

Decker, C. J., and Parker, R. (2012). P-bodies and stress granules: possible roles in the control of translation and mRNA degradation. *Cold Spring Harb. Perspect. Biol.* 4:a012286. doi: 10.1101/cshperspect.a012286

Franks, T. M., and Lykke-Andersen, J. (2007). TTP and BRF proteins nucleate processing body formation to silence mRNAs with AU-rich elements. *Genes Dev.* 21, 719–735. doi: 10.1101/gad.1494707

Glynn, E. F., Chen, J., and Mushegian, A. R. (2006). Detecting periodic patterns in unevenly spaced gene expression time series using Lomb-Scargle periodograms. *Bioinformatics* 22, 310–316. doi: 10.1093/bioinformatics/bti789

Green, C. B. (2018). Circadian posttranscriptional regulatory mechanisms in mammals. *Cold Spring Harb. Perspect. Biol.* 10:a030692. doi: 10.1101/cshperspect.a030692

Hubstenberger, A., Courel, M., Benard, M., Souquere, S., Ernoult-Lange, M., and Chouaib, R. (2017). P-Body purification reveals the condensation of repressed mRNA regulons. *Mol. Cell* 68, 144.e5–157.e5. doi: 10.1016/j.molcel.2017.09.003

Hughes, M. E., Hogenesch, J. B., and Kornacker, K. (2010). JTK-CYCLE: an efficient nonparametric algorithm for detecting rhythmic components in genome-scale data sets. *J. Biol. Rhythms* 25, 372–380. doi: 10.1177/0748730410379711

Ingelfinger, D., Arndt-Jovin, D. J., Luhrmann, R., and Achsel, T. (2002). The human LSm1-7 proteins colocalize with the mRNA-degrading enzymes Dcp1/2 and Xrnl in distinct cytoplasmic foci. *RNA* 8, 1489–1501.

Ivanov, P., Kedersha, N., and Anderson, P. (2018). Stress granules and processing bodies in translational control. *Cold Spring Harb. Perspect. Biol.* 11:a032813. doi: 10.1101/cshperspect.a032813

Jang, C., Lahens, N. F., Hogenesch, J. B., and Sehgal, A. (2015). Ribosome profiling reveals an important role for translational control in circadian gene expression. *Genome Res.* 25, 1836–1847. doi: 10.1101/gr.191296.115

Kedersha, N., and Anderson, P. (2007). Mammalian stress granules and processing bodies. *Methods Enzymol.* 431, 61–81. doi: 10.1016/s0076-6879(07)31005-7

Margadant, C., van Opstal, A., and Boonstra, J. (2007). Focal adhesion signaling and actin stress fibers are dispensable for progression through the ongoing cell cycle. *J. Cell Sci.* 120, 66–76. doi: 10.1242/jcs.03301

Mauvoisin, D., Wang, J., Jouffe, C., Martin, E., Atger, F., and Waridel, P. (2014). Circadian clock-dependent and -independent rhythmic proteomes implement distinct diurnal functions in mouse liver. *Proc. Natl. Acad. Sci. U.S.A.*111, 167–172. doi: 10.1073/pnas.1314066111

Nagoshi, E., Brown, S. A., Dibner, C., Kornmann, B., and Schibler, U. (2005). Circadian gene expression in cultured cells. *Methods Enzymol.* 393, 543–557. doi: 10.1016/s0076-6879(05)93028-0

Nissan, T., and Parker, R. (2008). Analyzing P-bodies in *Saccharomyces cerevisiae*. *Methods Enzymol.* 448, 507–520. doi: 10.1016/S0076-6879(08)02625-6

Pizarro, A., Hayer, K., Lahens, N. F., and Hogenesch, J. B. (2013). CircaDB: a database of mammalian circadian gene expression profiles. *Nucleic Acids Res.* 41, D1009–D1013. doi: 10.1093/nar/gks1161

Reddy, A. B., Karp, N. A., Maywood, E. S., Sage, E. A., Deery, M., and O'Neill, J. S. (2006). Circadian orchestration of the hepatic proteome. *Curr. Biol.* 16, 1107–1115. doi: 10.1016/j.cub.2006.04.026

Repouskou, A., Sourlingas, T. G., Sekeri-Pataryas, K. E., and Prombona, A. (2010). The circadian expression of c-MYC is modulated by the histone deacetylase inhibitor trichostatin A in synchronized murine neuroblastoma cells. *Chronobiol. Int.* 27, 722–741. doi: 10.3109/07420521003786800

Robles, M. S., Cox, J., and Mann, M. (2014). In-vivo quantitative proteomics reveals a key contribution of post-transcriptional mechanisms to the circadian regulation of liver metabolism. *PLoS Genet.* 10:e1004047. doi: 10.1371/journal.pgen.1004047

Schibler, U., Gotic, I., Saini, C., Gos, P., Curie, T., Emmenegger, Y., et al. (2015). Clock-talk: interactions between central and peripheral circadian oscillators in mammals. *Cold Spring Harb. Symp. Quant. Biol.* 80, 223–232. doi: 10.1101/sqb.2015.80.027490

Sfakianos, A. P., Whitmarsh, A. J., and Ashe, M. P. (2016). Ribonucleoprotein bodies are phased in. *Biochem. Soc. Trans.* 44, 1411–1416. doi: 10.1042/bst20160117

Sheth, U., and Parker, R. (2003). Decapping and decay of messenger RNA occur in cytoplasmic processing bodies. *Science* 300, 805–808. doi: 10.1126/science.1082320

Shin, Y., and Brangwynne, C. P. (2017). Liquid phase condensation in cell physiology and disease. *Science* 357:eaaf4382. doi: 10.1126/science.aaf4382

Standart, N., and Weil, D. (2018). P-Bodies: cytosolic droplets for coordinated mRNA storage. *Trends Genet.* 34, 612–626. doi: 10.1016/j.tig.2018.05.005

Takahashi, J. S. (2017). Transcriptional architecture of the mammalian circadian clock. *Nat. Rev. Genet.* 18, 164–179. doi: 10.1038/nrg.2016.150

Wang, R., Jiang, X., Bao, P., Qin, M., and Xu, J. (2019). Circadian control of stress granules by oscillating EIF2alpha. *Cell Death Dis.* 10:215. doi: 10.1038/s41419-019-1471-y

Wu, G., Anafi, R. C., Hughes, M. E., Kornacker, K., and Hogenesch, J. B. (2016). MetaCycle: an integrated R package to evaluate periodicity in large scale data. *Bioinformatics* 32, 3351–3353. doi: 10.1093/bioinformatics/btw405

Yang, R., and Su, Z. (2010). Analyzing circadian expression data by harmonic regression based on autoregressive spectral estimation. *Bioinformatics* 26, i168–i174. doi: 10.1093/bioinformatics/btq189

Zhang, R., Lahens, N. F., Ballance, H. I., Hughes, M. E., and Hogenesch, J. B. (2014). A circadian gene expression atlas in mammals: implications for biology and medicine. *Proc. Natl. Acad. Sci. U.S.A.* 111, 16219–16224. doi: 10.1073/pnas.1408886111

Conflict of Interest: The authors declare that the research was conducted in the absence of any commercial or financial relationships that could be construed as a potential conflict of interest.

frontiers in Neuroscience

MINI REVIEW
published: 12 November 2019
doi: 10.3389/fnins.2019.01226

Stress, Dietary Patterns and Cardiovascular Disease: A Mini-Review

Luis Pedro Morera[1], Georgina Noel Marchiori[2,3], Leonardo Adrián Medrano[1,4] and María Daniela Defagó[2,3]*

[1] Instituto de Organizaciones Saludables, Universidad Siglo 21, Córdoba, Argentina, [2] Instituto de Investigaciones en Ciencias de la Salud (INICSA), CONICET, Universidad Nacional de Córdoba, Córdoba, Argentina, [3] Escuela de Nutrición, Facultad de Ciencias Médicas, Universidad Nacional de Córdoba, Córdoba, Argentina, [4] Department of Pyschology, Pontificia Universidad Católica Madre y Maestra, Santiago de los Caballeros, Dominican Republic

According to the World Health Organization, an unhealthy diet and insufficient physical activity are the leading global risks to health. Dietary behavior is a modifiable factor in cardiovascular disease (CVD) prevention. Furthermore, the fact that cardiovascular events and stress-related emotional disorders share a common epidemiology may indicate the existence of pathways linking these two diseases (Chauvet-Gelinier and Bonin, 2017). Psychosocial stress can lead to changes in dietary patterns (DP) and under chronic stress conditions, high caloric and hyperpalatable foods are preferred. The interplay between these two factors impacts on several biological pathways: for example, it can prime the hippocampus to produce a potentiated neuroinflammatory response, generating memory deficits; it can also affect gut microbiota composition, ultimately influencing behavior and brain health and creating a predisposition to the development of diseases such as obesity, CVD, diabetes and metabolic syndrome. Though both cognition and emotion can be heavily affected by caloric intake, diet composition and stress, the molecular pathways involved remain elusive (Spencer et al., 2017). In this review, we describe the interplay between stress and DP at a molecular level, and how these factors relate to brain health and mental fitness. Finally, we show how these findings could give rise to novel therapeutic targets for chronic diseases.

Keywords: stress, cardiovascular disease, dietary patterns, nutrition, microbiome

OPEN ACCESS

Edited by:
Gabriela Alejandra Salvador, Universidad Nacional del Sur, Argentina

Reviewed by:
Marcelo Sergio Vatta, Universidad de Buenos Aires, Argentina
Sara Pauwels, KU Leuven, Belgium

****Correspondence:***
Luis Pedro Morera
luis.p.morera@gmail.com

Specialty section:
This article was submitted to Neuroendocrine Science, a section of the journal Frontiers in Neuroscience

Received: *15 January 2019*
Accepted: *29 October 2019*
Published: *12 November 2019*

Citation:
Morera LP, Marchiori GN, Medrano LA and Defagó MD (2019) Stress, Dietary Patterns and Cardiovascular Disease: A Mini-Review. Front. Neurosci. 13:1226. doi: 10.3389/fnins.2019.01226

INTRODUCTION

Cardiovascular disease (CVD), is the leading cause of mortality and disability worldwide. According to the Global Burden of Disease study, ischemic heart disease and stroke accounted for 25% of total deaths worldwide in 2013 (Rubinstein et al., 2010; GBD 2013 Mortality and Causes of Death Collaborators, 2015).

The current epidemic of CVD is largely explained by several modifiable risk factors associated with lifestyle, feasible to modify. In this sense, an unbalanced diet, excessive alcohol and tobacco consumption, hypercholesterolemia, diabetes mellitus, high blood pressure, visceral obesity, physical inactivity and psychosocial stress increase the risk of future CVD events and are responsible for an estimated 90% of the population-attributable risk fraction of

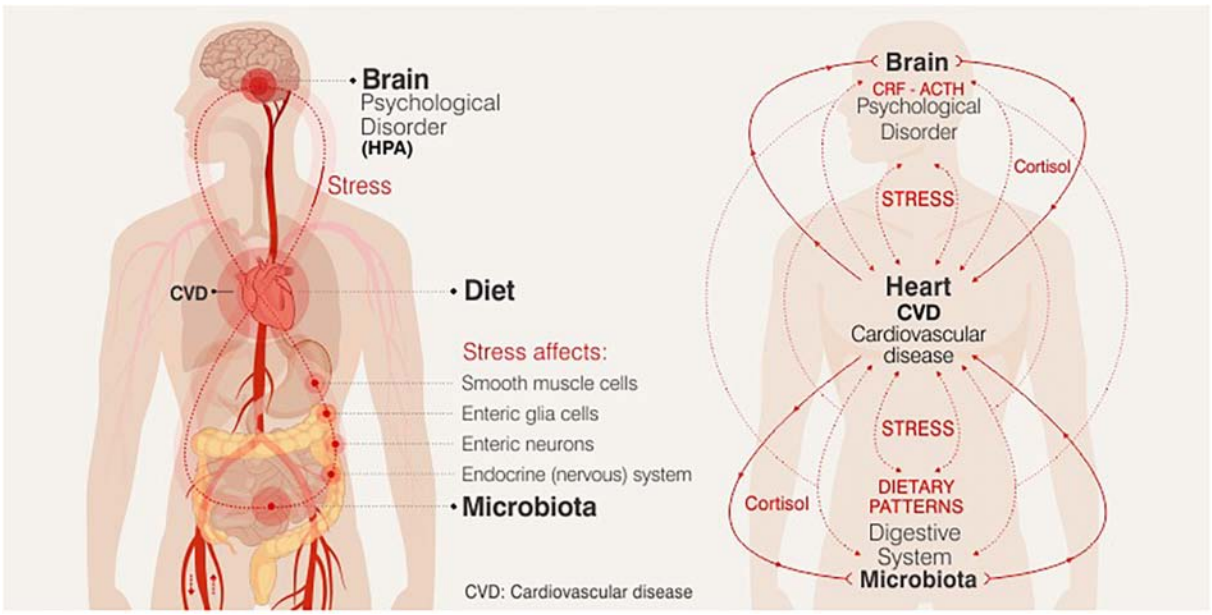

FIGURE 1 | Relationship between nutritional changes and emotional state and brain health.

ischemic heart disease and stroke worldwide (Schächinger et al., 2000; O'Donnell et al., 2010; Uthman et al., 2014; Karmali et al., 2017). Even more stress-related psychological disorders such as depression show a higher prevalence in patients with coronary artery disease or heart failure compared with the general population (Lane et al., 2002; Ruo et al., 2003; Rutledge et al., 2006).

Chronic or acute exposure to stress (defined as an ongoing or anticipated threat to homeostasis or well-being) favors to the destabilization of the dynamic balance of the organism, and its response promotes the release of chemical mediators that affect the metabolic and behavioral state in humans. Stress-induced activation of the neuroendocrine hypothalamic-pituitary-adrenal axis (HPA), upon exposure to a stressor cortisol is expected to exert widespread metabolic effects, which is mostly necessary to maintain or restore homeostasis. Stress, perhaps, is the trigger in the cascade of neuroendocrine effects that drive the development of the visceral distribution of adipose tissue, resistance to insulin and the consequent hyperinsulinemia, thus leading to the accumulation of cardiovascular risk factors (Serrano Ríos, 2005). Since glucocorticoids favor increased adiposity, mainly, abdominal fat, they can lead to increased appetite, affecting the quantity and quality of the diet (increased sweet and high fat food intake), and body weight gain. Thus, exposure to stress can modify eating behavior. These stress-induced alterations in food intake and energy balance then interacting with emotional state and health cardiovascular, **Figure 1** (Epel et al., 2001; Groesz et al., 2012). Though a relationship between nutritional changes and emotional state and brain health is already known to exist, the exact nature of this relationship has not been established. Research over the last decade has focused on bidirectional communication between gut and brain, termed the gut-brain axis. Dysbiosis and inflammation of the gut have been linked to several mental illnesses including anxiety and depression, although the molecular pathways involved have not yet been elucidated (Clapp et al., 2017).

The aim of this mini-review is to summarize the findings in the literature on how stress influences the molecular pathways affecting behavior, dietary patterns (DP) and their impact on health, and the synergistic effects of this cycle.

Figure 1 The potential biological mechanisms that connect the observed relationships between DP, stress and mental health could be modulated by the immune and endocrine systems, brain plasticity and the microbiome-gut-brain axis, being key targets for nutritional therapy in future research.

METHODS

The authors conducted a literature search of available sources describing issues relating to stress, DP and behavior. Research studies were selected based on research topics found in globally acknowledged databases such as Web of Science, PubMed, Springer, and Scopus, from 2010 up to the present time and classified according to their relevancy. The information provided in the selected studies was carefully evaluated and is described and discussed in the following sections.

NUTRITION AND CARDIOVASCULAR DISEASE

Diet is one of the most studied factors in the pathogenesis of CVD since it affects diverse cardiometabolic risk factors such

as obesity, lipid blood profile, blood pressure, glucose-insulin homeostasis, endothelial health, adipocyte metabolism, cardiac function, metabolic expenditure, weight regulation, visceral adiposity, and the microbiome (Mozaffarian, 2016).

Dietary patterns refers to the habitual combinations of foods and meals consumed on a daily basis (Hu, 2002). Several DP have been related to beneficial cardiovascular effects. For example, the Mediterranean DP -characterized by moderate energy intake, high consumption of olive oil, fish, legumes, nuts, fruits, and vegetables; fewer red meats and processed (sodium-preserved) meats; and a regular and moderate consumption of red wine- is associated with low CVD incidence and mortality (Shen et al., 2015; Sanches Machado d'Almeida et al., 2018). This DP and others such as Prudent, DASH or Healthy DP are high in fiber, vitamins, antioxidants, minerals, phenolics, and unsaturated fats, and low in glycemic index, glycemic load, salt, and *trans* fat (Esmaillzadeh et al., 2007; Mozaffarian et al., 2011). The Western DP on the other hand, characterized by a high intake of red meats, fat dairy products, refined grains and sugars, has been positively correlated with higher concentrations of markers of endothelial dysfunction, the first step in CVD: fasting insulin, C peptide, leptin, C reactive protein, homocysteine, tissue plasminogen activator antigen, interleukin 6 (IL-6), E-selectin, intercellular adhesion molecule 1 (sICAM-1) and vascular cells of molecular adhesion 1 (sVCAM-1) (Defagó et al., 2014; Rodríguez-Monforte et al., 2015; Marchiori et al., 2017).

In the long term, not only the quality but also the quantity of nutrients consumed can influence the neural circuits that regulate motivation, emotion and mood. Evidence can be found in literature about the relationship between saturated, *trans* fat intake and the risk of mental disorders (Barnard et al., 2014). Chronic exposure to a high-fat diet may affect the underlying neurobiological pathways of emotion and reward via its action on energy metabolism, endocrine function and immunity. Saturated and *trans* fatty acids favor central fat deposition and have been related with cardiometabolic and neurological diseases (Micha and Mozaffarian, 2008). The omega-3 polyunsaturated fatty acids (PUFAs) participate in modulation inflammation and immunospecific response, cell growth and tissue repair. Omega-3 plays a role in neuronal membrane fluidity and receptor function and lower levels of these PUFAs have been associated with common mental disorders such as depression and generalized anxiety, also with accelerated neurodegeneration (Grant and Guest, 2016).

Acute stress exposure (short term exposure) may shut down appetite by corticotropin-releasing hormone action and epinephrine liberation. However, if the stressor agent persists, the increased cortisol increases appetite and the motivation to eat (Razzoli et al., 2017). Experimental studies have demonstrated how chronic stress exposure increases susceptibility to diet-induced obesity, with induced spontaneous binging and hyperphagia and a preference for highly-palatable food, rich in calories, *trans* fat, salt and sugar (Packard et al., 2014; Ulrich-Lai et al., 2015). Research on human behavior shows a strong link between exposure to stress and binge eating disorder, often associated with development the overweight and obesity. Stress-induced non-nutritive food selection, is often referred to as eating "comfort food" or highly palatable food (Leigh et al., 2018).

NUTRITION, MICROBIOME AND CARDIOVASCULAR DISEASE

The human gut microbiome contains 10^{14} resident micro-organisms, among which bacteria are the most well-studied group, predominated by gram positive *Firmicutes* and gram negative *Bacteroidetes* (Cresci and Bawden, 2015). The collective genome of the microbiome contains millions of genes compared to the approximately 25,000 genes of the human genome and thus contributes to a wide range of biochemical and metabolic functions, such as nutrient acquisition, the harvesting of energy and large numbers of host metabolic pathways.

Inflammatory related diseases has been related to intestinal microbiome composition (bowel and skin diseases, autoimmune arthritis, type 2 diabetes, and atherosclerosis among others) (Buford, 2017). Specifically, an abnormal change in gut flora has been linked to a range of CVD risk factors, including obesity and diabetes. The first analyses on human intestinal microbiota reported a lower amount of *Bacteroidetes* than *Firmicutes* in obese individuals, however, these findings have not been consistently demonstrated in all subsequent metagenomic studies on obesity in humans (Ley, 2010). A lower abundance of butyrate-producing bacteria, in particular *Faecalibacterium prausnitzii,* a major member of the *Firmicutes phylum,* in individuals with obesity-related metabolic disturbances and diabetes has been observed. Furthermore, the presence of this bacterium is inversely correlated with the intake of dietary fat. Other studies have identified increased abundance of *Bifidobacteria* species in healthy individuals compared with individuals with obesity and diabetes (Martín et al., 2017). Dysbiosis has also been linked to CVD and metabolic diseases such as a lower ratio of *Bacteroidetes* to *Firmicutes* in obesity and hypertension, or increased *Collinsella* in atherosclerosis (Brahe et al., 2016).

Several DP have been studied for their ability to modulate the intestinal microbiota. In general terms, a Western DP led to a marked decrease in numbers of total bacteria and beneficial *Bifidobacterium* and *Eubacterium* species, whereas Mediterranean and Prudent DP have been linked to increases in *Lactobacillus, Bifidobacterium,* and *Prevotella*, and decreases in *Clostridium (*Koloverou et al., 2016; Singh et al., 2017*)*. However, dietary manipulation to modify gut microbiome is still at the incipient stage It has been detected that dietary fiber including prebiotics has a beneficial effect on gut microbiota and host health, improving insulin sensitivity, low-grade chronic inflammation, and lipid metabolism (Ahmadmehrabi and Tang, 2017). Prebiotics are non-digestible dietary compounds that stimulate growth or activity of autochthonous microorganisms, resulting in health benefits. They are basically oligo- or polysaccharides of fructose or galactose and also lactulose and lactitol; they promote the development of *bifidobacteria*, which

are capable of degrading various complex carbohydrates. Many *Firmicutes* and in particular *Bacteroides* are also able to carry out this function (Suárez, 2013). Prebiotics are naturally present in foods such as wheat, garlic, onion, asparagus, leek, beet, chicory root, and artichoke, among others; they can also be added to products such as milk, yogurt and breakfast cereals. In this regard, adherence to a DP rich in fruits, vegetables and whole grains may modulate the gut microbiome and thus favorably impact on human health.

GUT BRAIN AXIS AND STRESS

The mechanisms underlying microbiota-gut-brain axis communication involves neuro-immune-endocrine mediators. This interconnected network includes the central nervous system (CNS), the autonomic nervous system, the enteric nervous system and the HPA (Farzi et al., 2018).

In an organism exposed to stress, the hypothalamus stimulates the pituitary by releasing corticotropin-releasing factor (CRF). In the anterior pituitary, CRF causes the release of the adrenocorticotropic hormone (ACTH), which in turn stimulates the adrenals to cause an increased rate of synthesis and release of cortisol (cortisol in humans and corticosterone in rodents) (Foster et al., 2017). Cortisol serves to maintain homeostasis during normal states of activity (regulating cellular function and metabolism) and during periods of stress (Christiansen et al., 2007).

Chronically elevated cortisol levels can disturb brain function, affecting cognition, emotion and motivation, short and long-term memory; sustained HPA axis activation also impairs the immune system response, as has been demonstrated particularly in early life stress (Shirtcliff et al., 2009). Cortisol exerts it's effects trough the interaction with two corticoid receptors, high affinity mineralocorticoid receptors (MR) and low affinity glucocorticoid receptors (GR). A persistently activated HPA axis will eventually lead to a compensatory downregulation of the expression of GR signaling through epigenetic modifications (Weaver et al., 2004). In addition, glucocorticoids increase intestinal permeability, and negatively affects the gut microbiota composition.

Stress-related changes could be also mediated by neuroendocrine hormones, such as norepinephrine (NE) and dopamine (DA); it has long been known that these catecholamines can increase the growth rate of Gram-negative bacteria (Lyte and Ernst, 1992).

In turn, changes in gut microbiome composition has been already related to cognitive disorders and mental illness. There is strong evidence linking major depression and microbiome, and preclinical evidence related to anxiety disorders (Foster and McVey Neufeld, 2013; Malan-Muller et al., 2017).

LINKING MICROBIOME AND NEURONAL SIGNALING: MECHANISTIC EVIDENCE

Further research is required to elucidate the exact mechanisms and mediators involved in brain-microbiota communication. A central issue that remains unresolved is which mediators the microbiota uses to communicate with the brain and how this network ultimately influences behavior and health.

There are three major systems along with their mediators playing a role in inter-talk between the microbiota and the brain: neuronal communication, endocrine signaling mediators and the immune system mediators. Together, these systems create an integrated molecular network that impact both in gut and brain function.

The gut communicates with the brain through a systemic, central route. The vagus nerve sends information to the brain, where it is processed in the nucleus tractus solitarius; this nucleus then projects to the parabrachial nucleus, which in turns projects to the prefrontal cortex (PFC) and amygdala. These latter are key loci that control anxiety and fear responses. It has been reported that both regions display irregularities in germ free animals (GF), including hypermyelination in the PFC.

Previous papers have shown that the *N*-methyl-D-aspartate (NMDA) receptor subunit (NMDArec2B) has reduced expression in the amygdala of GF animals (Neufeld et al., 2011). Furthermore, it has been demonstrated that feeding prebiotics to these animals elevates their levels of brain-derived neurotrophic factor (BDNF), NMDA receptor subunits, and D-serine in the brain. Moreover, GABA receptor and serotonin 1A receptor are upregulated in the amygdala and hippocampus, respectively, upon supplementing GF animals with a Lactobacillus strain, ultimately regulating behavior in mice (Bravo et al., 2011).

TABLE 1 | Molecular signaling pathways linking the microbiome with stress-related health outcomes.

Pathway	Mediator	Microbiome	Health outcome	References
Neural pathways	Serotonin	GF vs. specific pathogen-free animals (SPF)	Anxiety-like behavior	Neufeld et al., 2011; Clarke et al., 2012
	GABA	*Bacteroides*, *Parabacteroides* and *Escherichia* species	Depression	Strandwitz et al., 2018
	miRNA	GF vs. GF colonized animals	Anxiety- and fear-related behavior	Hoban et al., 2017
	c-FOS	*Campylobacter jejuni*	Anxiety-like behavior	Lyte et al., 2006; Goehler et al., 2008
	BDNF	GF animals	Brain development	Diaz Heijtz et al., 2011
Endocrine pathways	Cortisol	*Lactobacillus helveticus, Bifidobacteria*	Anxiety-like behavior	Foster et al., 2017
Immune signaling	TNF-α	*Lactobacillus plantarum* PS128	Improved anxiety-like behavior	Liu et al., 2016
	IL-6	*Lactobacillus*	Inflammation, overweight, obesity.	Cooper et al., 2016
	IL-1β	*Akkermansia* spp. and *Blautia* spp.	Depression	Marc et al., 2014; Wong et al., 2016

The biogenic amine Serotonin [5-hydroxytryptamine (5-HT)] exerts its function in the brain and in the ENS. Most of 5-HT is synthetized by gut mucosal enterochromaffin cells and ENS neurons. Peripherally, 5-HT is involved in gastrointestinal function, smooth muscle contraction and relaxation, and in pain perception. In the brain it is involved in regulating mood and cognition (Yano et al., 2015). Serotonin synthesis depends on the availability of tryptophan, an essential amino acid that must be supplied in the diet, and microbiota plays a central role in the regulation and synthesis of this amine.

Together these findings reinforce the concept that DP can have either a positive or a negative impact on the CNS by regulating critical neurotransmitters implicated in psychiatric disorders, such as depression (Wallace and Milev, 2017; Zalar et al., 2018).

Finally, the immune system plays an important intermediary role between the brain and the gut. Gut-associated lymphoid tissue is the main component of mucosal-associated lymphoid tissue and corresponds to almost 70% of the entire immune system (Vighi et al., 2008). Dysbiosis of the gut microbiota is linked to abnormal immune responses, which are accompanied by irregular cytokine synthesis and release. It has been reported that TNFα and IFNγ production capacity appears to be influenced by the microbiome, whereas cytokines such as IL-1β, IL-6, and Th17-derived IL-17, and IL-22 display fewer, but more specific, associations with the gut microbiota (Schirmer et al., 2016).

Table 1 Mechanistic pathways, mediators and main microbiome modifications associated with stress related psychological disorders. Molecular signaling pathways linking the microbiome with stress-related health outcomes.

Several studies related to preclinical models of bacterial infections, probiotics treatment and analysis of germ-free (GF) animals suggest that the microbiota can influence the CNS and consequently behavior. Stress-related disorders such as anxiety and depression are among the main psychiatric conditions associated with microbiome changes (Desbonnet et al., 2010, 2015; Bravo et al., 2011).

CONCLUSION

The treatment of multidimensional diseases such as CVD require multidimensional approaches. Nutritional psychiatry is a growing field of research seeking to provide clinically relevant interventions for multifactorial diseases. This emerging line of inquiry has assembled data on biological pathways such as gastrointestinal microbiota and inflammation, on DP and on how these are modulated by the environment. It has become clear that this intertwined network of environmental factors (such as stress and DP) interacting with the above-mentioned pathways combines to modulate behavior.

Some trending foods and (controversial) diets have brought lasting changes to traditional diets, however, in most cases neither these nor dietary supplements have been subjected to adequate clinical trials to test their safety and efficacy. A better understanding of the interplay between diet, stress, neuronal signaling, phenotypes, and the microbiome will provide important insights into the utility of scientific evidence-based nutrition. Future studies are imperative to proactively avoid cardiovascular events in patient population.

AUTHOR CONTRIBUTIONS

All authors equally contributed to the drafting, analyses the final version of the manuscript, and read and approved the final version of the manuscript.

FUNDING

This work was supported by the Ministry of Science and Technology of Córdoba grant GRFT 2017, Universidad Siglo 21 and SECyT Secretary of Science and Technology of the National University of Córdoba (SECyT).

REFERENCES

Ahmadmehrabi, S., and Tang, W. H. W. (2017). Gut microbiome and its role in cardiovascular diseases. *Curr. Opin. Cardiol.* 32, 761–766. doi: 10.1097/HCO.0000000000000445

Barnard, N. D., Bunner, A. E., and Agarwal, U. (2014). Saturated and trans fats and dementia: a systematic review. *Neurobiol. Aging* 35, S65–S73. doi: 10.1016/j.neurobiolaging.2014.02.030

Brahe, L. K., Astrup, A., and Larsen, L. H. (2016). Can we prevent obesity-related metabolic diseases by dietary modulation of the gut microbiota? *Adv. Nutr.* 7, 90–101. doi: 10.3945/an.115.010587

Bravo, J. A., Forsythe, P., Chew, M. V., Escaravage, E., Savignac, H. M., Dinan, T. G., et al. (2011). Ingestion of *Lactobacillus* strain regulates emotional behavior and central GABA receptor expression in a mouse via the vagus nerve. *Proc. Natl. Acad. Sci. U.S.A.* 108, 16050–16055. doi: 10.1073/pnas.1102999108

Buford, T. W. (2017). Dis trust your gut: the gut microbiome in age-related inflammation, health, and disease. *Microbiome* 5:80. doi: 10.1186/s40168-017-0296-0

Chauvet-Gelinier, J.-C., and Bonin, B. (2017). Stress, anxiety and depression in heart disease patients: a major challenge for cardiac rehabilitation. *Ann. Phys. Rehabil. Med.* 60, 6–12. doi: 10.1016/j.rehab.2016.09.002

Christiansen, J. J., Djurhuus, C. B., Gravholt, C. H., Iversen, P., Christiansen, J. S., Schmitz, O., et al. (2007). Effects of cortisol on carbohydrate, lipid, and protein metabolism: studies of acute cortisol withdrawal in adrenocortical failure. *J. Clin. Endocrinol. Metab.* 92, 3553–3559. doi: 10.1210/jc.2007-0445

Clapp, M., Aurora, N., Herrera, L., Bhatia, M., Wilen, E., and Wakefield, S. (2017). gut microbiota's effect on mental health: the gut-brain axis. *Clin. Pract.* 7:987.

Clarke, G., Grenham, S., Scully, P., Fitzgerald, P., Moloney, R. D., Shanahan, F., et al. (2012). The microbiome-gut-brain axis during early life regulates the hippocampal serotonergic system in a sex-dependent manner. *Mol. Psychiatry* 18, 666–673. doi: 10.1038/mp.2012.77

Cooper, D., Kim, E. B., Marco, M., Rust, B., Welch, L., Horn, W., et al. (2016). Relationship between human gut microbiota and interleukin 6 levels in overweight and obese adults. *FASEB J.* 30:146.

Cresci, G. A., and Bawden, E. (2015). Gut microbiome: what we do and don't know. *Nutr. Clin. Pract.* 30, 734–746.

Defagó, M. D., Elorriaga, N., Irazola, V. E., and Rubinstein, A. L. (2014). Influence of food patterns on endothelial biomarkers: a systematic review. *J. Clin. Hypertens.* 16, 907–913. doi: 10.1111/jch.12431

Desbonnet, L., Clarke, G., Traplin, A., O'sullivan, O., Crispie, F., Moloney, R. D., et al. (2015). Gut microbiota depletion from early adolescence

in mice: implications for brain and behaviour. *Brain Behav. Immun.* 48, 165–173. doi: 10.1016/j.bbi.2015.04.004

Desbonnet, L., Garrett, L., Clarke, G., Kiely, B., Cryan, J. F., and Dinan, T. G. (2010). Effects of the probiotic Bifidobacterium infantis in the maternal separation model of depression. *Neuroscience* 170, 1179–1188. doi: 10.1016/j.neuroscience.2010.08.005

Diaz Heijtz, R., Wang, S., Anuar, F., Qian, Y., Björkholm, B., Samuelsson, A., et al. (2011). Normal gut microbiota modulates brain development and behavior. *Proc. Natl. Acad. Sci. U.S.A.* 108, 3047–3052. doi: 10.1073/pnas.1010529108

Epel, E., Lapidus, R., Mcewen, B., and Brownell, K. (2001). Stress may add bite to appetite in women: a laboratory study of stress-induced cortisol and eating behavior. *Psychoneuroendocrinology* 26, 37–49. doi: 10.1016/s0306-4530(00)00035-4

Esmaillzadeh, A., Kimiagar, M., Mehrabi, Y., Azadbakht, L., Hu, F. B., and Willett, W. C. (2007). Dietary patterns and markers of systemic inflammation among iranian women. *J. Nutr.* 137, 992–998. doi: 10.1093/jn/137.4.992

Farzi, A., Fröhlich, E. E., and Holzer, P. (2018). Gut Microbiota and the Neuroendocrine System. *Neurotherapeutics* 15, 5–22. doi: 10.1007/s13311-017-0600-5

Foster, J. A., and McVey Neufeld, K.-A. (2013). Gut-brain axis: how the microbiome influences anxiety and depression. *Trends Neurosci.* 36, 305–312. doi: 10.1016/j.tins.2013.01.005

Foster, J. A., Rinaman, L., and Cryan, J. F. (2017). Stress & the gut-brain axis: regulation by the microbiome. *Neurobiol. Stress* 7, 124–136.

Goehler, L. E., Park, S. M., Opitz, N., Lyte, M., and Gaykema, R. P. A. (2008). Campylobacter jejuni infection increases anxiety-like behavior in the holeboard: possible anatomical substrates for viscerosensory modulation of exploratory behavior. *Brain Behav. Immun.* 22, 354–366. doi: 10.1016/j.bbi.2007.08.009

Grant, R., and Guest, J. (2016). "Role of omega-3 PUFAs in neurobiological health," in *The Benefits of Natural Products for Neurodegenerative Diseases*, eds M.M. Essa, M. Akbar, and G. Guillemin (Cham: Springer International Publishing), 247–274. doi: 10.1007/978-3-319-28383-8_13

Groesz, L. M., Mccoy, S., Carl, J., Saslow, L., Stewart, J., Adler, N., et al. (2012). What is eating you? Stress and the drive to eat. *Appetite* 58, 717–721. doi: 10.1016/j.appet.2011.11.028

Hoban, A. E., Stilling, R. M., Moloney, G., Moloney, R. D., Shanahan, F., Dinan, T. G., et al. (2017). Microbial regulation of microRNA expression in the amygdala and prefrontal cortex. *Microbiome* 5:102. doi: 10.1186/s40168-017-0321-3

Hu, F. B. (2002). Dietary pattern analysis: a new direction in nutritional epidemiology. *Curr. Opin. Lipidol.* 13, 3–9. doi: 10.1097/00041433-200202000-00002

Karmali, K. N., Persell, S. D., Perel, P., Lloyd-Jones, D. M., Berendsen, M. A., and Huffman, M. D. (2017). Risk scoring for the primary prevention of cardiovascular disease. *Cochrane Database Syst. Rev.* 3:CD006887

Koloverou, E., Panagiotakos, D. B., Pitsavos, C., Chrysohoou, C., Georgousopoulou, E. N., Grekas, A., et al. (2016). Adherence to Mediterranean diet and 10-year incidence (2002–2012) of diabetes: correlations with inflammatory and oxidative stress biomarkers in the ATTICA cohort study. *Diabetes Metab. Res. Rev.* 32, 73–81. doi: 10.1002/dmrr.2672

Lane, D., Carroll, D., Ring, C., Beevers, D. G., and Lip, G. Y. H. (2002). The prevalence and persistence of depression and anxiety following myocardial infarction. *Br. J. Health Psychol.* 7, 11–21. doi: 10.1348/135910702169321

Leigh, S. J., Lee, F., and Morris, M. J. (2018). Hyperpalatability and the generation of obesity: roles of environment, stress exposure and individual difference. *Curr. Obes. Rep.* 7, 6–18. doi: 10.1007/s13679-018-0292-0

Ley, R. E. (2010). Obesity and the human microbiome. *Curr. Opin. Gastroenterol.* 26, 5–11. doi: 10.1097/mog.0b013e328333d751

Liu, W.-H., Chuang, H.-L., Huang, Y.-T., Wu, C.-C., Chou, G.-T., Wang, S., et al. (2016). Alteration of behavior and monoamine levels attributable to *Lactobacillus plantarum* PS128 in germ-free mice. *Behav. Brain Res.* 298, 202–209. doi: 10.1016/j.bbr.2015.10.046

Lyte, M., and Ernst, S. (1992). Catecholamine induced growth of gram negative bacteria. *Life Sci.* 50, 203–212. doi: 10.1016/0024-3205(92)90273-r

Lyte, M., Li, W., Opitz, N., Gaykema, R. P. A., and Goehler, L. E. (2006). Induction of anxiety-like behavior in mice during the initial stages of infection with the agent of murine colonic hyperplasia citrobacter rodentium. *Physiol. Behav.* 89, 350–357. doi: 10.1016/j.physbeh.2006.06.019

Malan-Muller, S., Valles-Colomer, M., Raes, J., Lowry, C. A., Seedat, S., and Hemmings, S. M. J. (2017). The gut microbiome and mental health: implications for anxiety- and trauma-related disorders. *J. Int. Biol.* 22, 90–107. doi: 10.1089/omi.2017.0077

Marc, U., Jose, M.-E., Lucile, C., Ricard, N., Magi, F., Eduard, V., et al. (2014). Cytokine-induced depression: current status and novel targets for depression therapy. *CNS Neurol. Disord. Drug Targets* 13, 1066–1074. doi: 10.2174/1871527313666140612121921

Marchiori, G. N., González, A. L., Perovic, N. R., and Defagó, M. D. (2017). Una mirada global sobre la influencia de los patrones alimentarios en las enfermedades cardiovasculares. *Perspect. Nutr. Humana.* 19, 79–92. doi: 10.17533/udea.penh.v19n1a07

Martín, R., Miquel, S., Benevides, L., Bridonneau, C., Robert, V., Hudault, S., et al. (2017). Functional characterization of novel *Faecalibacterium prausnitzii* strains isolated from healthy volunteers: a step forward in the use of f. prausnitzii as a next-generation probiotic. *Front. Microbiol.* 8:1226. doi: 10.3389/fmicb.2017.01226

Micha, R., and Mozaffarian, D. (2008). Trans fatty acids: effects on cardiometabolic health and implications for policy. *Prostaglandins Leukot. Essent. Fatty Acids* 79, 147–152. doi: 10.1016/j.plefa.2008.09.008

GBD 2013 Mortality and Causes of Death Collaborators, (2015). Global, regional, and national age-sex specific all-cause and cause-specific mortality for 240 causes of death, 1990-2013: a systematic analysis for the Global Burden of Disease study 2013. *Lancet* 385, 117–171. doi: 10.1016/s0140-6736(14)61682-2

Mozaffarian, D. (2016). Dietary and policy priorities for cardiovascular disease, diabetes, and obesity: a comprehensive review. *Circulation* 133, 187–225. doi: 10.1161/CIRCULATIONAHA.115.018585

Mozaffarian, D., Appel, L. J., and Horn, L. V. (2011). Components of a cardioprotective diet. *Circulation* 123, 2870–2891. doi: 10.1161/circulationaha.110.968735

Neufeld, K. M., Kang, N., Bienenstock, J., and Foster, J. A. (2011). Reduced anxiety-like behavior and central neurochemical change in germ-free mice. *Neurogastroenterol. Motil.* 23, 255–264. doi: 10.1111/j.1365-2982.2010.01620.x

O'Donnell, M. J., Xavier, D., Liu, L., Zhang, H., Chin, S. L., Rao-Melacini, P., et al. (2010). Risk factors for ischaemic and intracerebral haemorrhagic stroke in 22 countries (the INTERSTROKE study): a case-control study. *Lancet* 376, 112–123. doi: 10.1016/s0140-6736(10)60834-3

Packard, A. E. B., Ghosal, S., Herman, J. P., Woods, S. C., and Ulrich-Lai, Y. M. (2014). Chronic variable stress improves glucose tolerance in rats with sucrose-induced prediabetes. *Psychoneuroendocrinology* 47, 178–188. doi: 10.1016/j.psyneuen.2014.05.016

Razzoli, M., Pearson, C., Crow, S., and Bartolomucci, A. (2017). Stress, overeating, and obesity: insights from human studies and preclinical models. *Neurosci. Biobehav. Rev.* 76, 154–162. doi: 10.1016/j.neubiorev.2017.01.026

Rodríguez-Monforte, M., Flores-Mateo, G., and Sánchez, E. (2015). Dietary patterns and CVD: a systematic review and meta-analysis of observational studies. *Br. J. Nut.* 114, 1341–1359. doi: 10.1017/s0007114515003177

Rubinstein, A., Colantonio, L., Bardach, A., Caporale, J., Garcia Marti, S., Kopitowski, K., et al. (2010). Estimación de la carga de las enfermedades cardiovasculares atribuible a factores de riesgo modificables en Argentina. *Rev. Panam. Salud. Publica* 27, 237–245 doi: 10.1590/s1020-49892010000400001

Ruo, B., Rumsfeld, J. S., Hlatky, M. A., Liu, H., Browner, W. S., and Whooley, M. A. (2003). Depressive symptoms and health-related quality of life: the heart and soul study. JAMA 290, 215–221.

Rutledge, T., Reis, V. A., Linke, S. E., Greenberg, B. H., and Mills, P. J. (2006). Depression in heart failure: a meta-analytic review of prevalence, intervention effects, and associations with clinical outcomes. *J. Am. College Cardiol.* 48, 1527–1537.

Sanches Machado d'Almeida, K., Ronchi Spillere, S., Zuchinali, P., and Corrêa Souza, G. (2018). Mediterranean diet and other dietary patterns in primary prevention of heart failure and changes in cardiac function markers: a systematic review. *Nutrients* 10:58. doi: 10.3390/nu10010058

Schächinger, V., Britten, M. B., and Zeiher, A. M. (2000). Prognostic impact of coronary vasodilator dysfunction on adverse long-term outcome of coronary heart disease. *Circulation* 101, 1899–1906. doi: 10.1161/01.cir.101.16.1899

Schirmer, M., Smeekens, S. P., Vlamakis, H., Jaeger, M., Oosting, M., Franzosa, E. A., et al. (2016). Linking the human gut microbiome to inflammatory cytokine production capacity. *Cell* 167, 1125–1136.e8. doi: 10.1016/j.cell.2016.10.020

Serrano Ríos, M. (2005). El síndrome metabólico: ¿ una versión moderna de la enfermedad ligada al estrés? *Rev. Esp. Cardiol.* 58, 768–771.

Shen, J., Wilmot, K. A., Ghasemzadeh, N., Molloy, D. L., Burkman, G., Mekonnen, G., et al. (2015). Mediterranean dietary patterns and cardiovascular health. *Ann. Rev. Nut.* 35, 425–449.

Shirtcliff, E. A., Coe, C. L., and Pollak, S. D. (2009). Early childhood stress is associated with elevated antibody levels to herpes simplex virus type 1. *Proc. Natl. Acad. Sci. U.S.A.* 106, 2963–2967. doi: 10.1073/pnas.0806660106

Singh, R. K., Chang, H.-W., Yan, D., Lee, K. M., Ucmak, D., Wong, K., et al. (2017). Influence of diet on the gut microbiome and implications for human health. *J. Transl. Med.* 15:73.

Spencer, S. J., Korosi, A., Layé, S., Shukitt-Hale, B., and Barrientos, R. M. (2017). Food for thought: how nutrition impacts cognition and emotion. *npj Science of Food* 1:7.

Strandwitz, P., Kim, K. H., Terekhova, D., Liu, J. K., Sharma, A., Levering, J., et al. (2018). GABA-modulating bacteria of the human gut microbiota. *Nat. Microbiol.* 4, 396–403 doi: 10.1038/s41564-018-0307-3

Suárez, J. E. (2013). Microbiota autóctona, probióticos y prebióticos. *Nutr. Hosp.* 28, 38–41.

Ulrich-Lai, Y. M., Fulton, S., Wilson, M., Petrovich, G., and Rinaman, L. (2015). Stress exposure, food intake and emotional state. *Stress* 18, 381–399.

Uthman, O., Hartley, L., Rees, K., Taylor, F., Volmink, J., Ebrahim, S., et al. (2014). Multiple risk factor interventions for primary prevention of cardiovascular disease in low- and middle-income countries. *Cochrane Database Syst. Rev.* 8:CD011163

Vighi, G., Marcucci, F., Sensi, L., Di Cara, G., and Frati, F. (2008). Allergy and the gastrointestinal system. *Clin. Exp. Immunol.* 153, 3–6. doi: 10.1111/j.1365-2249.2008.03713.x

Wallace, C. J. K., and Milev, R. (2017). The effects of probiotics on depressive symptoms in humans: a systematic review. *Ann. Gen. Psychiatry* 16:14. doi: 10.1186/s12991-017-0138-2

Weaver, I. C. G., Cervoni, N., Champagne, F. A., D'alessio, A. C., Sharma, S., Seckl, J. R., et al. (2004). Epigenetic programming by maternal behavior. *Nat. Neurosci.* 7, 847–854.

Wong, M. L., Inserra, A., Lewis, M. D., Mastronardi, C. A., Leong, L., Choo, J., et al. (2016). Inflammasome signaling affects anxiety- and depressive-like behavior and gut microbiome composition. *Mol. Psychiatry* 21, 797–805. doi: 10.1038/mp.2016.46

Yano, J. M., Yu, K., Donaldson, G. P., Shastri, G. G., Ann, P., Ma, L., et al. (2015). Indigenous bacteria from the gut microbiota regulate host serotonin biosynthesis. *Cell* 161, 264–276. doi: 10.1016/j.cell.2015.02.047

Zalar, B., Haslberger, A., and Peterlin, B. (2018). The role of microbiota in depression - a brief review. *Psychiatr. Danub.* 30, 136–141 doi: 10.24869/psyd.2018.136

Conflict of Interest: The authors declare that the research was conducted in the absence of any commercial or financial relationships that could be construed as a potential conflict of interest.

frontiers in Cellular Neuroscience

ORIGINAL RESEARCH
published: 05 May 2020
doi: 10.3389/fncel.2020.00106

Function of P2X4 Receptors Is Directly Modulated by a 1:1 Stoichiometric Interaction With 5-HT$_3$A Receptors

*Paola Soto, Pablo S. Gaete, Christian Fuentes, Benjamin Lozano, Pamela A. Naulin, Xavier F. Figueroa and Nelson Patricio Barrera**

Department of Physiology, Faculty of Biological Sciences, Pontificia Universidad Católica de Chile, Santiago, Chile

Interacting receptors at the neuronal plasma membrane represent an additional regulatory mode for intracellular transduction pathways. P2X4 receptor triggers fast neurotransmission responses *via* a transient increase in intracellular Ca^{2+} levels. It has been proposed that the P2X4 receptor interacts with the 5-HT$_3$A receptor in hippocampal neurons, but their binding stoichiometry and the role of P2X4 receptor activation by ATP on this crosstalking system remains unknown. *Via* pull-down assays, total internal reflection fluorescence (TIRF) microscopy measurements of the receptors colocalization and expression at the plasma membrane, and atomic force microscopy (AFM) imaging, we have demonstrated that P2X4/5-HT$_3$A receptor complexes can interact with each other in a 1:1 stoichiometric manner that is preserved after ATP binding. Also, macromolecular docking followed by 100 ns molecular dynamics (MD) simulations suggested that the interaction energy of the P2X4 receptor with 5-HT$_3$A receptor is similar at the *holo* and the *apo* state of the P2X4 receptor, and the interacting 5-HT$_3$A receptor decreased the ATP binding energy of P2X4 receptor. Finally, the P2X4 receptor-dependent Ca^{2+} mobilization is inhibited by the 5-HT$_3$A interacting receptor. Altogether, these findings provide novel molecular insights into the allosteric regulation of P2X4/5-HT$_3$A receptor complex in lipid bilayers of living cells *via* stoichiometric association, rather than accumulation or unspecific clustering of complexes.

Keywords: receptor-receptor interaction, atomic force microscopy, stoichiometry, P2X4 receptor, 5-HT$_3$A receptor, intracellular Ca^{2+}, ATP

OPEN ACCESS

Edited by:
Gabriela Alejandra Salvador, Universidad Nacional del Sur, Argentina

Reviewed by:
Ralf Hausmann, RWTH Aachen University, Germany
Jeremias Corradi, Instituto de Investigaciones Bioquímicas de Bahía Blanca (INIBIBB), Argentina

****Correspondence:***
Nelson P. Barrera
nbarrera@bio.puc.cl

Specialty section:
This article was submitted to Cellular Neurophysiology, a section of the journal Frontiers in Cellular Neuroscience

Received: *02 April 2019*
Accepted: *07 April 2020*
Published: *05 May 2020*

Citation:
Soto P, Gaete PS, Fuentes C, Lozano B, Naulin PA, Figueroa XF and Barrera NP (2020) Function of P2X4 Receptors Is Directly Modulated by a 1:1 Stoichiometric Interaction With 5-HT$_3$A Receptors. Front. Cell. Neurosci. 14:106. doi: 10.3389/fncel.2020.00106

INTRODUCTION

Receptor-receptor interaction has been an extensive research area with enormous implications in neuronal crosstalking transduction mechanisms, which usually provide new molecular ways to tune and regulate the receptor function (Barrera et al., 2005b; Ferre et al., 2007). Ionotropic receptors located at the central nervous system, such as those belonging to the cys loop family,

have been found to form macromolecular complexes composed by two or more different receptors (Ferre et al., 2007). In particular, P2X2 and 5-HT$_3$A receptors are co-expressed at the plasma membrane and physically interact with each other in myenteric neurons and heterologous systems. This interaction depends on the second intracellular loop of the 5-HT3A subunit and an unknown region of the P2X2 receptor that was initially thought to be the C-term tail (Boué-Grabot et al., 2003). As a functional consequence, the inhibition of the additive responses attained with serotonin and ATP was observed. Similar receptor-receptor interactions and inhibitory crosstalking have been observed between P2X and nicotinic acetylcholine (nACh) receptors (Barajas-López et al., 1998) and between P2X and GABA receptors (Jo et al., 2011). Recently, Emerit et al. (2016) showed that the 5-HT$_3$A receptor can colocalize with the P2X4 receptor at the plasma membrane of hippocampal neurons. Nevertheless, it remains unknown the stoichiometry of these interacting receptors, whether the interaction is controlled by the agonist binding and the functional role of this regulatory mechanism.

P2X4 receptor is also regulated by direct interactions with phospholipids. In this context, phosphoinositides PI(4,5)P2 (PIP$_2$) and PI(3,4,5)P3 (PIP$_3$) can modulate P2X4 activity, apparently, by direct interactions with the proximal C-terminal domain of the receptor (C360–V375), which was shown to be required for the development of full receptor function, since depletion of PIP$_2$ and PIP$_3$ dramatically inhibits the P2X4-mediated Ca^{2+} signal activated by ATP (Bernier et al., 2008). Therefore, as it has been proposed that 5-HT$_3$A receptor may interact with the C-term tail of P2X receptors (e.g., P2X2 receptor), the potential interaction between this receptor and P2X4 receptor may also represent a relevant control mechanism of the phospholipids-mediated P2X4 regulation.

A variety of methods have been continuously developed to tackle the molecular architecture of interacting membrane proteins, from high resolution, such as x-ray crystallography, to complementary biophysical approaches, including cryo-electron microscopy, mass spectrometry and atomic force microscopy (AFM). Based on the surface scanning of the sample, AFM has already been used to characterize the molecular architecture of individual P2X and 5-HT3 receptors (Barrera et al., 2005a,c, 2007; Antonio et al., 2011), among others.

Herein, *via* pull-down assay of interacting receptors, AFM imaging, macromolecular docking, molecular dynamics (MD) simulations, and total internal reflection fluorescence (TIRF) microscopy analysis, we propose that P2X4 receptor physically interacts in a 1:1 stoichiometric manner with 5-HT$_3$A receptor, which is maintained after ATP binding. By measurements of intracellular Ca^{2+} levels, we further confirmed that the interacting 5-HT$_3$A receptor inhibits the response to ATP of the P2X4 receptor. Altogether, these findings provide insights into the inhibitory responses triggered *via* stoichiometric binding of interacting receptors, which consequently support the notion that interacting receptors in specific numbers rather than receptor aggregation are involved in crosstalking neuronal responses.

MATERIALS AND METHODS

Expression of P2X4/5-HT$_3$A Receptor Complexes on tsA201 Cells

tsA201 cells (Sigma–Aldrich, St. Louis, MO, USA. Cat. # 96121229-1VL) were grown in DMEM medium (Gibco, Grand Island, NY, USA), supplemented with 10% fetal bovine serum (FBS, Gibco, Grand Island, NY, USA), 100 unit/ml penicillin (Sigma–Aldrich, St. Louis, MO, USA) and 100 μg/ml streptomycin (Sigma–Aldrich, St. Louis, MO, USA). Cells were maintained at 37°C in a humidified 5% CO_2–95% air atmosphere incubator. To induce the expression of P2X4 and 5-HT$_3$A receptors, tsA201 cells with a confluence of 40–60% were transfected with the pDNAs of P2X4 and 5-HT$_3$A receptors using polyethyleneimine (PEI, Sigma–Aldrich, St. Louis, MO, USA) as transfection reagent. Briefly, 10 ml of DMEM without serum were mixed with 275 μl of 1 mg/ml PEI alone (mock transfection) or plus pDNAs for P2X4 and/or 5-HT$_3$A (25 μg each) and left for 15 min at room temperature. Then, cells were incubated with this mixture for 24 h at 37°C. For transfection, the following constructs were used; rat P2X4 (*Rattus norvegicus*, GenBank: U47031.1) with a C-terminal hemagglutinin (HA) tag and human 5-HT$_3$A (*Homo sapiens*, GenBank: AK304630.1) with a C-terminal MYC/His-6 epitope tag, subcloned into the vector pcDNA3.1 (Invitrogen). Immunofluorescence analysis and Ca^{2+} measurements were performed using cells seeded onto sterile glass coverslips.

Measurements of Intracellular Ca^{2+} Levels

Ca^{2+} measurements were performed using the fluorescent Ca^{2+} indicator, Fluo 4, as described recently by Lillo et al. (2018). To upload Fluo 4, cells were incubated with 5 μM Fluo 4-AM for 45 min in a MOPS-buffered solution (composition in mM: 118 NaCl; 5.4 KCl; 2.5 $CaCl_2$; 1.2 KH_2PO_4; 1.2 $MgSO_4$; 11.1 glucose and 5 MOPS) adjusted to pH 7.4. The fluorescent indicator was washed out and the experiments started after 15 min of equilibration. Cells were visualized using an Olympus BX50 WI microscope and the fluorescent signal was recorded using an intensified CCD camera (Retiga Fast 1394, QImaging) and IPLab software. Images were acquired every 2 s at basal conditions and during 2 min of stimulation. Changes in intracellular Ca^{2+} levels were expressed as the variations of the fluorescence intensity along the time (F/F_0), where F is the fluorescence detected during the recording and F_0 is the basal fluorescence, or the maximum net fluorescence observed after stimulation ($\Delta F/F_0$). Three concentrations of ATP (1, 10 and 100 μM) were tested and, to confirm the activation of P2X4 receptors, 30 μM PPADS was preincubated during 15 min before the ATP application. Both reagents were poured over the cultured cells.

Confocal and Epifluorescence Microscopy

Cells were fixed with 1% formaldehyde and then washed with PBS solution (composition in mM: 136.9 NaCl; 2.68 KCl;

10.44 NaH_2PO_4; 1.76 KH_2PO_4) adjusted to pH 7.4. Nonspecific protein binding sites were blocked with PBS containing 0.1% FBS. Cells were incubated overnight with an anti-MYC monoclonal antibody to detect 5-HT$_3$A receptor (1:250, Thermo Fisher Scientific, Cat. # PA1-981, Rockford, IL, USA) and an anti-HA monoclonal antibody to label P2X4 receptor (1:250 Thermo Fisher Scientific, Cat. # 26183, Rockford, IL, USA). Cells were washed three times for 10 min with PBS and then incubated for 1 h with a secondary antibody conjugated to Alexa Fluor®555 for anti-MYC (1:500, Cat. #A-21424, Molecular Probes, Eugene, OR, USA) or Alexa Fluor®488 for anti-HA (1:500, Cat. # A-11029, Molecular Probes, Eugene, OR, USA). Then, cells were washed and mounted with Fluoromount-G (Electron Microscopy Sciences, Cat. # 17984-25, Hatfield, PA, USA). The fluorescent signal was examined using either an Olympus IX81 confocal inverted microscope coupled with an ORCA R2 Hamamatsu CCD camera or an Olympus BX41 WI microscope coupled with a Jenoptik ProgRes C5 CCD camera. As a negative control, primary antibodies were omitted.

TIRF Microscopy

TIRF microscopy imaging was performed using a NIKON Eclipse Ti2-E microscope with the module NIKON H-TIRF with a 100X magnification and up to 100 nm sample depth. Sample preparation was similar to the confocal experiments except for using PBS as mounting protocol and secondary antibodies conjugated to Alexa Fluor®555 and Alexa Fluor®488 to identify anti-HA and anti-MYC primary antibodies, respectively.

Quantification of P2X4 Receptor Expression and Colocalization of P2X4/5-HT$_3$A Receptor Complexes

Fluorescence intensity of P2X4 receptor expression attained by TIRF and epi microscopies were quantified using the ImageJ software (Schneider et al., 2012). Window and level parameters were optimized to select the Regions of Interest (ROIs) and exclude background noise. Fluorescence intensity was measured as the mean intensity of each ROI in raw images ± SE. For the colocalization analysis of P2X4/5-HT$_3$A receptor complexes, coloc2 plug-in implemented in ImageJ allowed to evaluate the correlation between the pixel's intensity on each channel *via* Pearson's R coefficient. Note that protein colocalization and expression experiments were performed using the same instrumental acquisition parameters such as light intensity and exposure time for all the images.

Purification of P2X4/5-HT$_3$A Receptor Complexes

Cells (five flasks of 150 cm^2 for each condition) were washed with HBS solution (composition in mM: 50 HEPES; 100 NaCl; 2 EDTA) adjusted to pH 7.6, and then, removed by shaking. Cells were collected in falcon tubes and centrifuged at 6,500 g at 4°C for 5 min. The pellet was resuspended in a solubilization solution (9 ml, composition in mM: 10 Tris-HCl; 100 NaCl; 5 EDTA, adjusted to pH 7.6), 1% Triton X-100 (Sigma–Aldrich, Cat. # 9002-93-1), a protease inhibitor mixture (complete, EDTA-Free, Roche) and 10 μl PMSF. The sample was incubated on a rotating wheel for 1 h at 4°C. The supernatant was placed in a Beckman centrifuge tube and subjected to ultracentrifugation at 50,000 *g* at 4°C for 1 h. The supernatant, corresponding to the positive control for the plasma membrane protein and named MEMBRANE fraction in Western blot analysis, was mixed with pre-washed anti-HA agarose beads (Thermo Fisher Scientific) and incubated for 3 h at 4°C. Beads were washed with 10 ml washing buffer (solubilization buffer containing 1% w/v Triton X-100) and centrifuged at 6,500 *g* three times. One last washing step was performed including a solution of 0.1% CHAPS (3-[(3-Cholamidopropyl)dimethylammonio]-1-propanesulfonate; Cat. # 220201, Calbiochem). Finally, proteins were eluted from beads by incubating them with 200 μl of 0.1% CHAPS plus 6 μl HA peptide (Thermo Fisher Scientific). An identical purification protocol was followed when tsA201 cells were expressing only P2X4 receptors. The ELUTION fraction (200 μl), representing the purified receptor or complex, was stored to perform Western blot analysis and AFM imaging. Five independent purification series were performed for the complex. Note that 100 μM ATP was applied in the eluted sample in solution during 30 min at room temperature, before protein adsorption (50 μl) onto mica.

When P2X4/5-HT$_3$A receptor complexes were pulled down *via* His6 tag, the purification procedure was similar to that used with the HA tag, except that in this case HisPur Ni-NTA agarose beads were used (Thermo Fisher Scientific) to carry out the extraction of His6 tagged proteins. Later, beads bound to the 5-HT$_3$A-MYC/His6 receptors were deposited in purification columns (Cat. # 450015, Invitrogen), and 200 mM imidazole was used for elution. An identical protocol was followed in tsA201 cells expressing only 5-HT$_3$A receptors. Five independent purification series were performed for each receptor.

Western Blot Analysis

Purified proteins were separated by 10% SDS-PAGE and transferred onto a nitrocellulose membrane (BioRad, CA, USA). Primary antibodies: anti-MYC (1:500, Thermo Fisher Scientific, Cat. # PA1-981, Rockford, IL, USA), or anti-HA (1:500 Thermo Fisher Scientific, Cat. # 26183, Rockford, IL, USA) were incubated overnight in a PBS solution containing 4% milk at 4°C. HRP-labeled secondary antibodies (1:1,000, Cat. # 621040, Molecular Probes, Eugene, OR, USA) were incubated at room temperature for 1 h in a PBS solution containing 4% milk. The SuperSignal® West Femto chemiluminescent substrate (Thermo Fisher Scientific) was used to detect protein bands. Molecular mass was estimated with prestained markers (Bio-Rad Laboratories, Hercules, CA, USA). The MyECL™ Imager (Thermo Fisher Scientific) was used to reveal the membrane.

AFM Imaging

Purified protein samples (50 μl from eluted samples) were placed on muscovite micas (Electron Microscopy Sciences, Cat. # 71855-01, Hatfield, PA, USA) to be adsorbed. After incubation for 15 min at room temperature, the mica was washed with Milli-Q water and dried with nitrogen gas. Images of dry samples were acquired in an AFM (MFP-3D-SA Asylum Research, CA, USA) using the intermittent contact mode. Cantilever was used with a drive frequency of ∼300 kHz and a spring constant of 40 N/m.

The force applied to obtain the images was kept as low as possible. The target amplitude was ∼0.5 V and amplitude setpoint ∼0.4 V. Each image (4 μm^2) was obtained in 15 min and 50 images were analyzed. The molecular volumes of the adsorbed receptor and complex particles were determined from the height and radius of the particle obtained by AFM (Barrera et al., 2008). The molecular volume was calculated from the equation:

$$Vm = (\pi h/6)(3r^2+h^2) \quad (1)$$

where h is the height of the particle and r is the radius at half the height. The equation considers the protein molecule as a sphere. Histograms of molecular volumes were fit by Gaussian distribution.

To calculate the individual receptor or complex concentration for the analyzed samples, the following equation was used:

$$M = \frac{\text{total mica area } (\mu m^2) \times \text{particle number per scanning area } (\frac{particle}{\mu m^2}) \times 10^6 (\frac{\mu l}{L})}{\text{elution volume in mica } (\mu l) \times \text{Avogadro Number } (\frac{particle}{mol})} \quad (2)$$

where M represents the molarity of the purified particle sample obtained from AFM imaging. For P2X4 receptors, 5-HT$_3$A receptors and P2X4/5-HT$_3$A receptor complexes, molecular volume cut-offs corresponding to their peaks were 403 and 431 (Antonio et al., 2011), 726 and 788 (Barrera et al., 2005a), and 991 and 1209 (**Figure 3**), respectively. Calculated values are derived from five independent purification processes for each sample, where all the samples were adsorbed in the same mica type surface during 15 min.

Molecular Docking and Molecular Dynamics Simulations of the P2X4/5-HT$_3$A Receptor Complex

The amino acid sequence of rat P2X4 subunit was obtained from UNIPROT (entry P51577) and aligned against the sequence of the zebrafish crystallized structures of P2X4 receptor (Hattori and Gouaux, 2012; PDB codes 4DW0 for the *apo* structure and 4DW1 for the *holo*-structure) by using MultAlin (Corpet, 1988). One hundred homology models for the *apo* and *holo*-structures were generated by using Modeller 9.18 (Webb and Sali, 2017) and the one having lowest DOPE score for each case was selected and verified by using the web servers MolProbity (Chen et al., 2010) and ProSA (Wiederstein and Sippl, 2007) to evaluate both stereochemical and energetics of each model. From the two final models, N and C-term tails were cut from MET 1 to VAL 28 and from LEU 358 to GLU 388, respectively.

The amino acid sequence of the human 5-HT3A subunit was obtained from UNIPROT (entry P46098) and aligned against the sequence of mouse 5-HT$_3$A receptor structure (Basak et al., 2018; PDB code 6BE1). One hundred homology models for the *apo* structures were generated by using Modeller 9.18 (Webb and Sali, 2017) and the one having the lowest DOPE were selected and verified by using the web servers MolProbity and ProSA to evaluate both stereochemical and energetics. From the final model, the N-term tail was cut from MET 1 to THR 30 and the intracellular loop consisting from CYS 356 to ALA 411 was cut as well.

Docking of ATP into the P2X4 receptor was performed in AutoDock (Morris et al., 2008). Binding pockets had volumes of 22.5 × 22.5 × 22.5 Å^3 and the center of each box was placed as the ligand is seen in the crystal structure. The 100 best conformations were saved and grouped in clusters of root mean square displacement (RMSD) less than 2 Å. Selected dockings for each binding pocket had a negative binding energy and a similar spatial orientation as the crystallized bound ATP.

Due to pentameric and trimeric symmetry of both 5-HT$_3$A and P2X4 receptors, respectively (Hattori and Gouaux, 2012; Basak et al., 2018), there are several possible combinations depending upon their interaction surface. However, we used two experimental evidence to take an appropriate orientation for the receptor complex: (1) choosing the minimal distance between both receptors at the second intracellular loop of the 5-HT$_3$A receptor, which has been postulated as a domain involved in the physical P2X2/5-HT$_3$A receptor interaction (Emerit et al., 2016); and (2) rotating, in the perpendicular plane of the bilayer, all possible conformations of the complex until the largest interaction surface was found since it has been shown that bigger interaction surfaces are more energetically favorable between macromolecular complexes (Casuso et al., 2012). To have a similar comparison between the two dockings, the P2X4 receptor *apo* structure was aligned to the first resulting docking of the P2X4 *holo*/5-HT$_3$A receptor complex.

The homology model of the P2X4 receptor in its *holo* state was combined with three ATP molecules in their binding pocket. Later both *apo* and *holo*-structures in the designed position were merged with the structure of the 5-HT$_3$A receptor and were protonated accordingly to the physiological pH. Both complexes were inserted in a pre-equilibrated POPC bilayer (of size 204 × 124 Å^2) created using the Visual Molecular Dynamics suite (VMD; Humphrey et al., 1996). To do this, both the bilayer and the receptor complex were aligned and all overlapped lipids (nearer than 0.8 Å) and water molecules (nearer than 3 Å) were deleted. The complex of receptor-bilayer was solvated by using the TIP3 water model and NaCl was added to both neutralize and provide a physiological concentration of salt. Simulations were performed using NAMD 2.12 with the temperature at 310 K and pressure at 1 atm with periodic boundary conditions (PBC). The first step was to minimize the energy by simulating 10,000 steps in the NVT ensemble, and then, the NPT ensemble was simulated. One hundred ns MD simulations for both P2X4 *apo*/5-HT$_3$A and P2X4 *holo*/5-HT$_3$A receptor complexes were carried out, which correspond to a similar simulation time already applied in our group to study allosteric regulation of P2X4 receptor by ivermectin (Latapiat et al., 2017). To maintain temperature and pressure constant, Langevin dynamics and Nosé–Hoover Langevin piston methods were used for temperature and pressure coupling. To calculate electrostatic interactions, Ewald sums were used with a grid density of 1 Å. Ligand parameterization (ATP) was done using the SwissParam webserver (Zoete et al., 2011) and the CHARMM27 forcefield was used for lipids and protein. Electrostatic and van der Waals interactions between both

receptors (or between P2X4 receptor and ATP molecules) within 12 Å cut off, corresponding to the total interaction energy, were measured by using VMD plugin "NAMDEnergy" every 40 ps during the simulation.

Reagents

MOPS, ATP and all chemicals of analytical grade were obtained from Sigma–Aldrich (St. Louis, MO, USA). Fluo 4-AM was purchased in Life Technologies (Eugene, OR, USA) and pyridoxalphosphate-6-azophenol-2′,4′ disulfonic acid (PPADS) in Tocris Bioscience (Ellisville, MO, USA). ATP and PPADS were dissolved in water. Fluo 4-AM was dissolved in DMSO.

Statistical Analysis

Values are represented as means ± SE. Comparisons between groups were made using unpaired student's *t*-test or 1-way ANOVA plus Newman–Keuls *post hoc* test, as appropriate. A value of $p < 0.05$ was considered significant.

RESULTS

First, the P2X4 receptor function in transfected tsA201 cells was evaluated by measuring the changes in free intracellular Ca^{2+} concentration observed in response to ATP application. Stimulation with 100 μM ATP evoked a Ca^{2+} signal that showed two components: a first fast-transient component that peaked at ∼12 s and decreased thereafter, and a second slow component that starts after ∼60 s (**Figures 1A,B**). In tsA201 cells co-transfected with P2X4 and 5-HT$_3$A receptors, the transient increase in intracellular Ca^{2+} was blunted (**Figure 1B**) whereas the time course of the second component was similar to that observed in P2X4 transfected cells. Although the Ca^{2+} response was evaluated at a range of ATP concentrations (1–100 μM), the most striking difference in the initial Ca^{2+} signaling (first 60 s) between cells transfected with P2X4 receptor alone or co-transfected with P2X4 and 5-HT$_3$A receptors was attained with 100 μM ATP (**Figure 1C**). As expected, the intracellular Ca^{2+} concentration was not affected by ATP in non-transfected cells (mock, **Figures 1B,C**). Consistent with the activation of P2X4 receptors, the response induced by ATP was almost completely blocked (∼85%) by 15 min pre-incubation with the preferential P2X receptor antagonist PPADS (**Figure 1D**; Lê et al., 1998). Interestingly, the response of co-transfected cells was inhibited by PPADS in the same proportion to that observed in cells transfected with P2X4 alone. As PPADS blocks access to the orthosteric ATP-binding pocket (Huo et al., 2018), these results suggest that the Ca^{2+} influx *via* transfected P2X4 receptors is inhibited by the presence of 5-HT$_3$A receptors without interfering with the ATP binding site through direct steric interaction or *via* a downstream effect.

To test whether or not both P2X4 and 5-HT$_3$A receptors interact with each other, tsA201 cells co-expressing P2X4 and 5-HT$_3$A receptors were identified by confocal, TIRF and epifluorescence analysis using anti-HA and anti-MYC antibodies. As shown in **Figures 2A–C**, confocal imaging revealed that both receptors colocalize in the same cell at the plasma and intracellular membranes. Then, the colocalization of P2X4 and 5-HT$_3$A receptor complexes at the plasma membrane was quantified using TIRF microscopy (**Figures 2D–F**) analysis, which showed a significant colocalization Pearson R index of 0.88 ± 0.09 (**Figure 2G**).

To evaluate a potential direct interaction, P2X4 or 5-HT$_3$A receptors were purified with HA or Ni^{2+} bound agarose beads from tsA201 cells expressing only one type of receptor. The success and specificity of the purification process was confirmed by Western blot analysis against HA or MYC tag epitopes for P2X4 or 5-HT$_3$A receptors, respectively (**Figures 2J,L**). Electrophoretic migration for each subunit (55 kDa for 5-HT$_3$A and 70 kDa for P2X4) reached a similar molecular weight of that previously published (Barrera et al., 2005a) for 5-HT$_3$A (55kDa) and slightly larger of that reported (Antonio et al., 2011) for P2X4 (65kDa). The difference observed in the electrophoretic migration of P2X4 subunit could correspond to a bigger glycosylation state, which is a posttranslational modification commonly observed for P2X receptors (Barrera et al., 2005c; Ormond et al., 2006; Antonio et al., 2011), since, according to its primary sequence, P2X4 subunit should have a molecular weight of 43.5 kDa. Once both P2X4 and 5-HT$_3$A receptors were co-expressed in tsA201 cells, the purification process was based on pull-down experiments targeting the HA tag epitope in the P2X4 receptor. As a negative control, 5-HT$_3$A receptors expressed alone were not detected in pull-down experiments using the HA-based purification protocol (data not shown). Western blot analysis demonstrated the presence of the P2X4 receptor in the eluted samples, but also a band corresponding to the 5-HT3A subunit was detected by anti-MYC antibody binding, demonstrating that both P2X4 and 5-HT$_3$A receptors interact each other in cells co-expressing both receptors (**Figure 2K**). A similar finding was observed after pulling down the complex by targeting the His6 tag epitope in the 5-HT$_3$A receptor, where a band corresponding to the P2X4 subunit was detected by anti-HA antibody binding (**Figure 2M**). To analyze the stoichiometry of the interaction, complexes formed by interacting P2X4/5-HT$_3$A receptors were recorded by AFM imaging (**Figures 3A–D**). The molecular volumes of the purified samples showed 2 peaks at 489 ± 24 nm^3 and 1100 ± 109 nm^3, which are consistent with the detection of P2X4 alone (417 nm^3; Antonio et al., 2011) and a P2X4/5-HT$_3$A receptor complex with a stoichiometry 1:1; this is 417 nm^3 and 757 nm^3 (Barrera et al., 2005a; **Figure 3B**). After stimulation of the purified sample with 100 μM ATP in solution before adsorption onto mica for AFM imaging, the proportion of the complex marginally increased from 42% to 51% (area under the double Gaussian curve fit, cut off 800 nm^3) with no change on the peak values (505 ± 15 nm^3 and 1236 ± 62 nm^3; $p > 0.05$; **Figure 3D**). All the peaks at histograms were derived from non-linear Gaussian distributions and were elected those that presented the best fits, R^2 values corresponding to 0.9307 and 0.9126 for the P2X4/5-HT$_3$A receptor complexes in the absence and presence of ATP, respectively.

To determine the protein concentration of the purified samples obtained from cells transfected with P2X4 or P2X4/5-HT$_3$A receptor complexes, we used the number of protein particles adsorbed into mica, as an indicator of the concentration

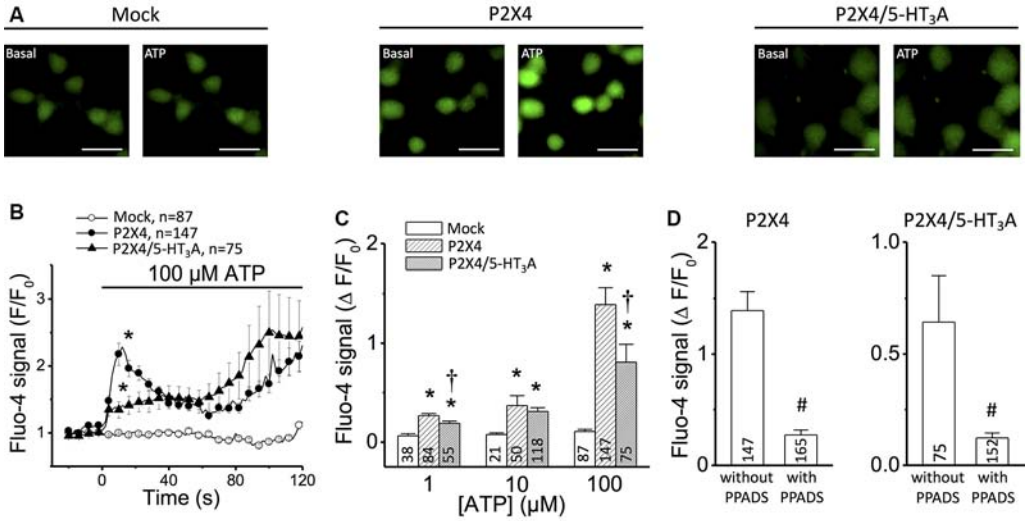

FIGURE 1 | Ca^{2+} measurements in tsA201 cells expressing P2X4 receptor alone or P2X4/5-HT_3A receptor complexes. **(A)** Representative images of Ca^{2+} measurements in mock-transfected cells, cells transfected with P2X4 receptor alone and cells co-transfected with P2X4 plus 5-HT_3A receptors. Changes in intracellular Ca^{2+} concentration were detected using the Ca^{2+} indicator Fluo-4. Images were captured before (Basal) and 20 s after the addition of 100 μM ATP. Scale bars represent 30 μm. **(B)** Time course of Fluo-4 fluorescence signal in cells stimulated with 100 μM ATP. The horizontal bar indicates the stimulation period. **(C)** Analysis of the maximum increase in intracellular Ca^{2+} levels observed after stimulation with 1–100 μM ATP. **(D)** Analysis of the maximum increase in intracellular Ca^{2+} levels observed in cells transfected with P2X4 receptor alone (left) or co-transfected with P2X4 and 5-HT_3A receptors (right) after application of 100 μM ATP in the absence or presence of 30 μM PPADS, an inhibitor of P2X receptors. Three independent Ca^{2+} measurements were carried out for each condition from different batches of cells. Numbers inside bars indicate the number of cells analyzed. Values are the mean ± SE. $^{*}p < 0.05$ vs. Mock by 1-way ANOVA plus Newman–Keuls *post hoc* test; $^{\dagger}p < 0.05$ vs. P2X4 by 1-way ANOVA plus Newman–Keuls *post hoc* test; $^{\#}p < 0.05$ vs. without PPADS by unpaired student's *t*-test.

determined by the Avogadro Number relationship (equation 2). This analysis showed that P2X4 receptors from single transfected cells and P2X4/5-HT_3A receptor complexes from cotransfected cells had a similar concentration of 3.3 ± 0.6 pM and 3.7 ± 1.3 pM ($p > 0.05$), respectively. However, AFM imaging of purified samples from cotransfected cells also presented an abundant peak at approximately the volume of individual P2X4 receptors, which suggests that pulling down the HA-tagged protein (P2X4 receptor) from the plasma membrane purified the complexes as well as P2X4 receptors alone and, therefore, increased the overall P2X4 expression at the plasma membrane. This correlates well with the TIRF microscopy analysis, where the P2X4 receptor expression in the cotransfected tsA201 cells was approximately two-fold higher than that observed on single transfected cells (**Figure 2H**). Interestingly, according to the analysis of epifluorescence imaging, the total cellular P2X4 receptor expression in tsA201 cells was similar in single and cotransfection experiments (**Figure 2I**), indicating a cellular redistribution of P2X4 receptors depending upon the presence of 5-HT_3A receptors.

To calculate interaction energy between P2X4 and 5-HT_3A receptors, macromolecular dockings for the interacting receptors were followed by 100 ns MD simulations, considering domains involved in the physical crosstalking between P2X and 5-HT_3 receptors (Boué-Grabot et al., 2003; Emerit et al., 2016), and the larger interaction energy between membrane protein complexes observed through larger subunit interfaces (Casuso et al., 2012; **Figures 3E,F**). Total interaction energy (van der Waals and electrostatic energies) of P2X4 receptor at the *apo* state with 5-HT_3A receptor was −301 ± 9 kcal/mol (mean ± SE; **Figure 3E**), which was not statistically different ($p > 0.05$) from that observed with P2X4 receptor at *holo* state (−278 ± 12 kcal/mol; **Figure 3F**). Also, the binding interaction energy of 3 ATP molecules to P2X4 receptor *holo* (−310 ± 12 kcal/mol) was significantly larger than that observed in the presence of interacting 5-HT_3A receptor (−168 ± 3 kcal/mol, $p < 0.05$), suggesting that the inhibitory effect of 5-HT_3A receptor could be allosteric, reducing the ATP affinity of the P2X4 receptor.

DISCUSSION

The P2X4 receptor activation by ATP binding triggered an initial transient increase in intracellular Ca^{2+} level that was followed by a slow component, where only the transient increase was strongly inhibited by the 5-HT_3A receptor, which could correlate well with a reduced Ca^{2+} influx through P2X receptors. Our data brings a novel outcome for the P2X4/5-HT_3A receptor complex interaction. A functional cross-inhibition has been demonstrated between P2X2 and 5-HT_3A receptors (Boué-Grabot et al., 2003), but that study was based on simultaneous activation of the receptors by parallel stimulation with ATP and 5-HT. This current report demonstrates that the mere presence of the 5-HT_3A interacting receptor in the complex, independent of its agonist, is sufficient to inhibit the P2X4 receptor. A similar inhibitory response has been observed for the mGlu5a

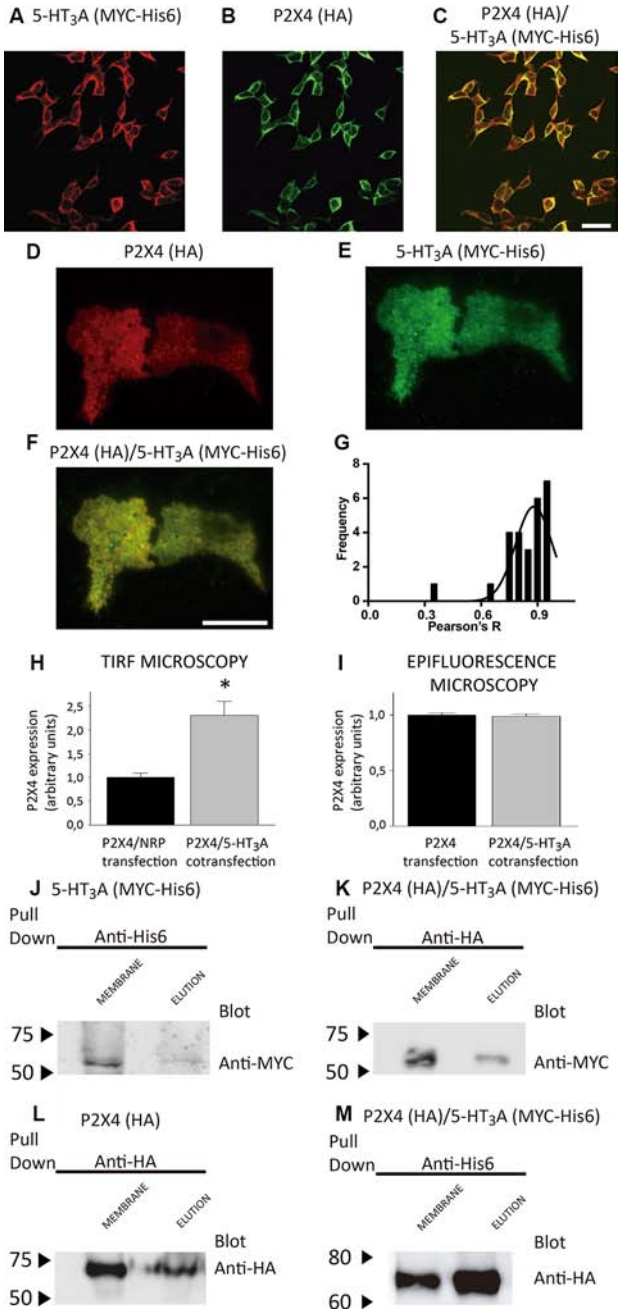

FIGURE 2 | Expression and purification of P2X4/5-HT$_3$A receptor complexes. **(A,B)** Detection of co-expressed 5-HT$_3$A **(A)** and P2X4 **(B)** receptors by confocal immunofluorescence in tsA201 cells *via* anti-MYC (1:250) and anti-HA (1:250) antibodies, followed by their corresponding secondary antibodies conjugated to Alexa Fluor®555 and Alexa Fluor®488, respectively. The merge of panels **(A,B)** is shown in **(C)**, where scale bar represents 30 μm. **(D,E)** Analysis by total internal reflection fluorescence (TIRF) microscopy of co-expressed P2X4 **(D)** and 5-HT$_3$A **(E)** receptors individually and merge images **(F)** in tsA201 cells *via* anti-HA (1:250) and anti-MYC (1:250) antibodies, followed by their corresponding secondary antibodies conjugated to Alexa Fluor®555 and Alexa Fluor®488, respectively. Scale bar in **(F)** represents 3 μm. **(G)** Colocalization analysis of the P2X4/5-HT$_3$A receptor complexes in tsA201 cells (n = 26 from two

(*Continued*)

FIGURE 2 | Continued
independent experiments). **(H,I)** P2X4 receptor expression analysis in tsA201 cells through TIRF (**H**, n = 26 for P2X4/NRP and P2X4/5-HT$_3$A transfections from two independent experiments) and epifluorescence (**I**, n = 273 for P2X4 and 254 for P2X4/5-HT$_3$A transfections from two independent experiments) measurements. Non-related plasmid (NRP) corresponds to pDNA IRES-GFP (0.5 μg each well) used in the same amount as the other receptor plasmids. Data are shown as mean ± SE. $^*p < 0.05$ vs. P2X4/NRP expression by unpaired t-test. **(J,L)** Western blot analysis of the purified samples from tsA201 cells expressing only 5-HT$_3$A **(J)** or P2X4 **(L)** receptors identified by anti-MYC or anti-HA antibodies, respectively. Specific bands in plasma membrane enriched fraction (MEMBRANE) and purified (ELUTION) samples were observed at 55 kDa **(J)** for 5-HT3A and 70 kDa **(L)** for P2X4 subunits. **(K,M)** Western blot analysis of purified samples from tsA201 cells co-expressing 5-HT$_3$A and P2X4 receptors after pulling down the complexes with either the HA-tag purification **(K)** or His6-tag purification **(M)** method. Bands corresponding to 5-HT3A (anti-MYC antibody; **K**) and P2X4 subunits (anti-HA antibody; **M**) were detected at similar molecular weights compared to those present after single transfection. Arrowheads indicate molecular mass markers in kDa.

receptor agonist-independent effect on the NMDA receptor (Perroy et al., 2008). Nevertheless, it remains to be determined whether the activation of the 5-HT$_3$A receptor can further inhibit the P2X4 receptor-dependent ATP response or the P2X4 receptor *apo* could be able to inhibit the activated 5-HT$_3$A receptor, which would enlighten the whole mechanistic scenario of these ionotropic receptors' interaction.

Our data are consistent with the notion that P2X4/5-HT$_3$A receptor interaction results in an allosteric inhibition of ATP-induced P2X4 activation. To further support this proposal, we performed additional experiments to reach the saturation of the concentration-response curve elicited by ATP in cells transfected with P2X4 receptor alone or co-transfected with P2X4 and 5-HT$_3$A receptors. However, stimulation with 1 mM ATP induced an increase in intracellular Ca^{2+} concentration in non-transfected cells (mock cells), which precluded the direct comparison of the response observed at different ATP concentrations (data not shown), and then, the analysis of the Emax and EC50 observed in response to ATP, as required to confirm the presence of an allosteric interaction of 5-HT$_3$A receptors with P2X4 receptors.

An alternative explanation to the inhibitory action of 5-HT$_3$A receptors on the P2X4 receptor-triggered Ca^{2+} increase would be a reduction of the expression of P2X4 receptors at the plasma membrane in cotransfected cells. Conversely, we found a similar total expression of the P2X4 receptor between transfected tsA201 cells containing P2X4 and P2X4/5-HT3A subunits. Furthermore, the expression of P2X4 receptors specifically at the plasma membrane, revealed by TIRF microscopy analysis, indicated a two-fold increase of the purinergic receptor in cotransfected cells. Interestingly, a redistribution of P2X4 receptor from intracellular locations to the cell surface without changing total cellular expression has been demonstrated after activation of the C-C chemokine receptor type 2 in microglial cells, which is mediated by delivery of lysosomal P2X4 receptor to the plasma membrane (Toyomitsu et al., 2012). Besides, the P2X4 receptor has been shown to colocalize with the 5-HT$_3$A receptor at the cell surface of

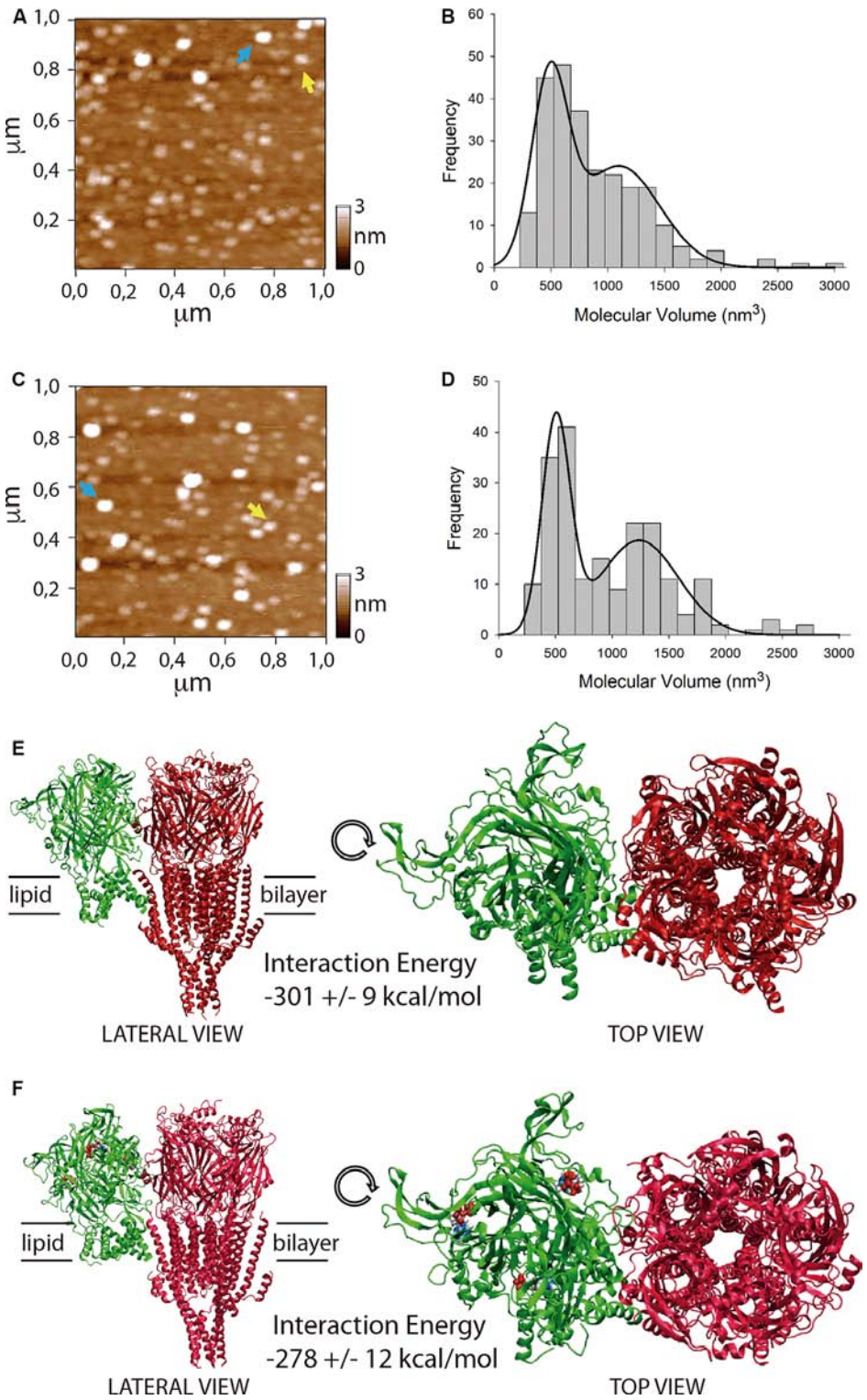

FIGURE 3 | Stoichiometry and interaction energy on P2X4/5-HT$_3$A receptor complexes. **(A–D)** Atomic force microscopy (AFM) imaging of purified P2X4/5-HT$_3$A receptor complexes in the absence **(A,B)** and presence **(C,D)** of 100 μM ATP. Yellow and blue arrows indicate molecular volumes of 493 nm^3 and 1,194 nm^3 **(A)** and 486 nm^3 and 1,125 nm^3 **(C)**. Histogram of molecular volumes of particles fitted by double Gaussian peaks in the absence **(B)** and presence **(D)** of 100 μM ATP. **(E)** Molecular docking of the complex formed between P2X4 receptor *apo* (green) and 5-HT$_3$A receptor (red). **(F)** Molecular docking of the complex formed between P2X4 receptor *holo* (green) and 5-HT$_3$A receptor (red). ATP molecules are depicted as colored blobs. Interaction energy values for both complexes are indicated as mean ± SE after 100 ns molecular dynamics (MD) simulations.

hippocampal neurons when its internalization motif is replaced by a FLAG epitope (Emerit et al., 2016). Our results have shown that this mutation is not needed for a significant plasma membrane expression of both receptors; however, it has yet to be determined whether the physical interaction between P2X4 and 5-HT$_3$A receptors is enough to trigger the protein trafficking or requires intracellular signaling pathway. Remarkably, the expression pattern of purified P2X4/5-HT$_3$A receptor complexes vs. the P2X4 receptor alone, revealed by AFM imaging, resembles relatively well to that observed on the plasma membrane in living cells. Almost half of the particles of the purified samples from tsA201 cells coexpressing P2X4 and 5-HT$_3$A receptors correspond to the assembled complex and present an identical concentration to that from cells expressing only P2X4 receptors. If we consider the other half of particles that match the molecular volume of free P2X4 receptors, then the total purinergic receptor should increase almost twice, reinforcing our notion that the purification process is highly enriched in the plasma membrane fraction.

Our AFM results demonstrate for the first time that the P2X4/5-HT$_3$A receptor complex is formed with a stoichiometry 1:1, which is maintained by the presence of the P2X4 receptor agonist. To propose a molecular way for the allosteric inhibition of 5-HT$_3$A receptor on P2X4 receptor function, we embarked on testing a docking between both receptors, considering the postulated domains for physical crosstalking (Boué-Grabot et al., 2003; Emerit et al., 2016), and interfaces with larger surfaces that maintain a trimeric/pentameric symmetry, which has been already postulated as variables energetically favorable for interacting macromolecules (Casuso et al., 2012). After 100 ns MD simulations, no differences in interaction energy between the P2X4 receptor *apo* or P2X4 receptor *holo* complexed with 5-HT$_3$A receptors were found. Also, the presence of the interacting 5-HT$_3$A receptor decreased the ATP binding interaction energy of ATP molecules to the P2X4 receptor, which is consistent with a negative allosteric effect of 5-HT$_3$A receptors that preserves the 1:1 stoichiometric interaction between both receptors. Nevertheless, further bioinformatic analysis should be performed to corroborate these findings, in particular, to explore extensively other receptor-receptor surface dockings *via*, for example, coarse-grained approaches, which would result in the same or additional conformations of the receptor complex.

Crosstalking mechanisms lead to more complex neuronal signaling by providing additional regulatory roles of agonists and receptors. Taken together, we have shown here that the P2X4 receptor is inhibited by a physical interaction with the 5-HT$_3$A receptor in a 1:1 stoichiometry and ATP maintains this complex. As 5-HT$_3$A receptor can interact with other P2X receptors subtypes such as P2X2 and P2X3 (Emerit et al., 2016), it remains to be solved if the same stoichiometry and steric mechanism participate in the functional regulation of these receptors. Furthermore, as P2X4 receptors can be modulated by membrane phosphoinositides (Bernier et al., 2008), it could be further explored whether or not the 5-HT$_3$A receptor and phospholipids can coexist to control the P2X4 receptor function *via* modifications of the stoichiometric binding.

DATA AVAILABILITY STATEMENT

All datasets generated for this study are included in the article.

AUTHOR CONTRIBUTIONS

PS performed AFM experiments and data analysis, immunofluorescence and western blot experiments. PG performed Ca^{2+} measurements and helped writing the article. CF performed homology modeling, molecular docking, and data analysis. BL performed western blot and TIRF experiments, followed by a quantitative analysis of immunofluorescence images. PN performed western blot and TIRF experiments. XF supervised Ca^{2+} measurements and helped writing the article. NB designed and supervised the investigation, analyzed the data and wrote the article.

FUNDING

Millennium Scientific Initiative ICM P10-035F, Newton Picarte PCI-DPI Conicyt grant 20140080 and FONDECYT grant 1181326 funded NB. FONDECYT grants 1150530 and 3160348 funded XF and PG, respectively. PS holds a PhD scholarship from Pontificia Universidad Católica de Chile. CF holds an MSc scholarship from CONICYT. This work was supported in part by the Advanced Microscopy Facility UMA-UC.

ACKNOWLEDGMENTS

To Prof. Michael Edwardson (University of Cambridge, UK) for providing the P2X4 and 5-HT$_3$A receptor constructs and scientific feedback on the experimental design, analysis, and procedure.

REFERENCES

Antonio, L. S., Stewart, A. P., Xu, X. J., Varanda, W. A., Murrell-Lagnado, R. D., and Edwardson, J. M. (2011). P2X4 receptors interact with both P2X2 and P2X7 receptors in the form of homotrimers. *Br. J. Pharmacol.* 163, 1069–1077. doi: 10.1111/j.1476-5381.2011.01303.x

Barrera, N. P., Ge, H., Henderson, R. M., Fitzgerald, W. J., and Edwardson, J. M. (2008). Automated analysis of the architecture of receptors, imaged by atomic force microscopy. *Micron* 39, 101–110. doi: 10.1016/j.micron.2006.12.006

Barrera, N. P., Henderson, R. M., Murrell-Lagnado, R. D., and Edwardson, J. M. (2007). The stoichiometry of $P2X_{2/6}$ receptor heteromers depends on relative subunit expression levels. *Biophys. J.* 93, 505–512. doi: 10.1529/biophysj.106.101048

Barrera, N. P., Herbert, P., Henderson, R. M., Martin, I. L., and Edwardson, J. M. (2005a). Atomic force microscopy reveals the stoichiometry and subunit arrangement of 5-HT3 receptors. *Proc. Natl. Acad. Sci. U S A* 102, 12595–12600. doi: 10.1073/pnas.0503253102

Barrera, N. P., Morales, B., Torres, S., and Villalon, M. (2005b). Principles: mechanisms and modeling of synergism in cellular responses. *Trends Pharmacol. Sci.* 26, 526–532. doi: 10.1016/j.tips.2005.08.003

Barrera, N. P., Ormond, S. J., Henderson, R. M., Murrell-Lagnado, R. D., and Edwardson, J. M. (2005c). Atomic force microscopy imaging demonstrates that

$P2X_2$ receptors are trimers but that $P2X_6$ receptor subunits do not oligomerize. *J. Biol. Chem.* 280, 10759–10765. doi: 10.1074/jbc.m412265200

Basak, S., Gicheru, Y., Samanta, A., Molugu, S. K., Huang, W., Fuente, M., et al. (2018). Cryo-EM structure of 5-HT3A receptor in its resting conformation. *Nat. Commun.* 9:514. doi: 10.1038/s41467-018-02997-4

Bernier, L. P., Ase, A. R., Chevallier, S., Blais, D., Zhao, Q., Boué-Grabot, E., et al. (2008). Phosphoinositides regulate P2X4 ATP-gated channels through direct interactions. *J. Neurosci.* 28, 12938–12945. doi: 10.1523/JNEUROSCI.3038-08.2008

Barajas-López, C., Espinosa-Luna, R., and Zhu, Y. (1998). Functional interactions between nicotinic and P2X channels in short-term cultures of guinea-pig submucosal neurons. *J. Physiol.* 513, 671–683. doi: 10.1111/j.1469-7793.1998.671ba.x

Boué-Grabot, E., Barajas-López, C., Chakfe, Y., Blais, D., Bélanger, D., Emerit, M. B., et al. (2003). Intracellular cross talk and physical interaction between two classes of neurotransmitter-gated channels. *J. Neurosci.* 23, 1246–1253. doi: 10.1523/JNEUROSCI.23-04-01246.2003

Casuso, I., Khao, J., Chami, M., Paul-Gilloteaux, P., Husain, M., Duneau, J. P., et al. (2012). Characterization of the motion of membrane proteins using high-speed atomic force microscopy. *Nat. Nanotechnol.* 7, 525–529. doi: 10.1038/nnano.2012.109

Chen, V. B., Arendall, W. B. III., Headd, J. J., Keedy, D. A., Immormino, R. M., Kapral, G. J., et al. (2010). MolProbity: all-atom structure validation for macromolecular crystallography. *Acta Crystallogr. D Biol. Crystallogr.* 66, 12–21. doi: 10.1107/S0907444909042073

Corpet, F. (1988). Multiple sequence alignment with hierarchical clustering. *Nucleic Acids Res.* 16, 10881–10890. doi: 10.1093/nar/16.22.10881

Emerit, M. B., Baranowski, C., Diaz, J., Martinez, A., Areias, J., Alterio, J., et al. (2016). A new mechanism of receptor targeting by interaction between two classes of ligand-gated ion channels. *J. Neurosci.* 36, 1456–1470. doi: 10.1523/JNEUROSCI.2390-15.2016

Ferre, S., Ciruela, F., Woods, A. S., Lluis, C., and Franco, R. (2007). Functional relevance of neurotransmitter receptor heteromers in the central nervous system. *Trends Neurosci.* 30, 440–446. doi: 10.1016/j.tins.2007.07.001

Hattori, M., and Gouaux, E. (2012). Molecular mechanism of ATP binding and ion channel activation in P2X receptors. *Nature* 485, 207–212. doi: 10.1038/nature11010

Humphrey, W., Dalke, A., and Schulten, K. (1996). VMD: visual molecular dynamics. *J. Mol. Graph.* 14, 33–38, 27–38. doi: 10.1016/0263-7855(96)00018-5

Huo, H., Fryatt, A. G., Farmer, L. K., Schmid, R., and Evans, R. J. (2018). Mapping the binding site of the P2X receptor antagonist PPADS reveals the importance of orthosteric site charge and the cysteine-rich head region. *J. Biol. Chem.* 293, 12820–12831. doi: 10.1074/jbc.ra118.003737

Jo, Y. H., Donier, E., Martinez, A., Garret, M., Toulme, E., and Boue-Grabot, E. (2011). Cross-talk between P2X4 and γ-aminobutyric acid, type A receptors determines synaptic efficacy at a central synapse. *J. Biol. Chem.* 286, 19993–20004. doi: 10.1074/jbc.m111.231324

Latapiat, V., Rodríguez, F. E., Godoy, F., Montenegro, F. A., Barrera, N. P., and Huidobro-Toro, J. P. (2017). P2X4 receptor *in silico* and electrophysiological approaches reveal insights of ivermectin and zinc allosteric modulation. *Front. Pharmacol.* 8:918. doi: 10.3389/fphar.2017.00918

Lê, K. T., Babinski, K., and Séguéla, P. (1998). Central P2X4 and P2X6 channel subunits coassemble into a novel heteromeric ATP receptor. *J. Neurosci.* 18, 7152–7159. doi: 10.1523/JNEUROSCI.18-18-07152.1998

Lillo, M. A., Gaete, P. S., Puebla, M., Ardiles, N. M., Poblete, I., Becerra, A., et al. (2018). Critical contribution of Na^+-Ca^{2+} exchanger to the Ca^{2+}-mediated vasodilation activated in endothelial cells of resistance arteries. *FASEB J.* 32, 2137–2147. doi: 10.1096/fj.201700365rr

Morris, G. M., Huey, R., and Olson, A. J. (2008). Using AutoDock for ligand-receptor docking. *Curr. Protoc. Bioinformatics* 24, 8:8.14.1–8.14.40. doi: 10.1002/0471250953.bi0814s24

Ormond, S. J., Barrera, N. P., Qureshi, O. S., Henderson, R. M., Edwardson, J. M., and Murrell-Lagnado, R. D. (2006). An uncharged region within the N terminus of the $P2X_6$ receptor inhibits its assembly and exit from the endoplasmic reticulum. *Mol. Pharmacol.* 69, 1692–1700. doi: 10.1124/mol.105.020404

Perroy, J., Raynaud, F., Homburger, V., Rousset, M. C., Telley, L., Bockaert, J., et al. (2008). Direct interaction enables cross-talk between ionotropic and group I metabotropic glutamate receptors. *J. Biol. Chem.* 283, 6799–6805. doi: 10.1074/jbc.M705661200

Schneider, C. A., Rasband, W. S., and Eliceiri, K. W. (2012). NIH Image to ImageJ: 25 years of image analysis. *Nat. Methods* 9, 671–675. doi: 10.1038/nmeth.2089

Toyomitsu, E., Tsuda, M., Yamashita, T., Tozaki-Saitoh, H., Tanaka, Y., and Inoue, K. (2012). CCL2 promotes P2X4 receptor trafficking to the cell surface of microglia. *Purinergic Signal.* 8, 301–310. doi: 10.1007/s11302-011-9288-x

Webb, B., and Sali, A. (2017). Protein structure modeling with MODELLER. *Methods Mol. Biol.* 1654, 39–54. doi: 10.1007/978-1-4939-7231-9_4

Wiederstein, M., and Sippl, M. J. (2007). ProSA-web: interactive web service for the recognition of errors in three-dimensional structures of proteins. *Nucleic Acids Res.* 35, W407–W410. doi: 10.1093/nar/gkm290

Zoete, V., Cuendet, M. A., Grosdidier, A., and Michielin, O. (2011). SwissParam: a fast force field generation tool for small organic molecules. *J. Comput. Chem.* 32, 2359–2368. doi: 10.1002/jcc.21816

Conflict of Interest: The authors declare that the research was conducted in the absence of any commercial or financial relationships that could be construed as a potential conflict of interest.

Advantages of publishing in Frontiers

OPEN ACCESS
Articles are free to read for greatest visibility and readership

FAST PUBLICATION
Around 90 days from submission to decision

HIGH QUALITY PEER-REVIEW
Rigorous, collaborative, and constructive peer-review

TRANSPARENT PEER-REVIEW
Editors and reviewers acknowledged by name on published articles

Frontiers
Avenue du Tribunal-Fédéral 34
1005 Lausanne | Switzerland

Visit us: www.frontiersin.org
Contact us: info@frontiersin.org | +41 21 510 17 00

REPRODUCIBILITY OF RESEARCH
Support open data and methods to enhance research reproducibility

DIGITAL PUBLISHING
Articles designed for optimal readership across devices

FOLLOW US
@frontiersin

IMPACT METRICS
Advanced article metrics track visibility across digital media

EXTENSIVE PROMOTION
Marketing and promotion of impactful research

LOOP RESEARCH NETWORK
Our network increases your article's readership